Dissertation zur Erlangung des Doktorgrades
der Fakultät für Chemie und Pharmazie
der Ludwig-Maximilians-Universität München

Molecular Machinery and Uncommon Isomerization Reactions Driven by Light

Aaron Gerwien

aus

Bremen, Deutschland

2020

Erklärung
Diese Dissertation wurde im Sinne von § 7 der Promotionsordnung vom 28. November 2011 von Herrn Prof. Dr. Henry Dube betreut.

Eidesstattliche Versicherung
Diese Dissertation wurde eigenständig und ohne unerlaubte Hilfe erarbeitet.

München, den 13.11.2020

.....
Aaron Gerwien

Dissertation eingereicht am	13.11.2020
1. Gutachter: Prof. Dr. Henry Dube	
2. Gutachter: Dr. Oliver Thorn-Seshold	
Mündliche Prüfung am	14.12.2020

Danksagung

Zuerst möchte ich mich bei Prof. Dr. Henry Dube bedanken, dass er es mir ermöglicht hat meine Doktorarbeit auf dem Bereich der Photochemie und molekularen Motoren anzufertigen. Besonders bedanken möchte ich mich für die Möglichkeit immer alles (teilweise sehr lautstark) diskutieren zu können. Diese offene Arbeitsatmosphäre habe ich sehr geschätzt. Es war eine schöne Zeit, in der ich immer gerne zur Arbeit (die sich für mich fast nie, wie Arbeit angefühlt hat) gegangen bin.

Bei Dr. Oliver Thorn-Seshold bedanke ich mich für die Übernahme des Koreferats.

Bei meinen lieben Kollegen Dr. Sandra Wiedbrauk, Dr. Ludwig Huber, Dr. Monika Schildhauer, Dr. Christian Petermayer, Stefan Thumser, Thomas Bartelmann, Nicolai Bach, Kerstin Grill (Hoffmann), Laura Köttner, Benjamin Regen-Pregizer und Edgar Uhl möchte ich mich besonders bedanken, da ihr einfach ein tolles Team seid, mit dem man immer Spaß haben konnte, sei es im Labor, auf Gruppenausflügen oder auf mal wieder ausgefallenen Weihnachtsfeiern.

Besonders bedanken möchte ich mich dabei bei Dr. Monika Schildhauer, die durch die Betreuung meiner Masterarbeit mir klar gemacht hat, wie schön es im AK Dube ist. Außerdem bei Stefan (Esteban) Thumser für das Beibringen von Gaussian und allem anderen was zum Rechnen auf den Uni-Clustern dazu gehört. Sowie bei Thomas Bartelmannn für die Einführung in Blender, das geilste Programm überhaupt. Bei Christian Petermayer möchte ich mich bedanken, dass er der beste Schrottbastler nach MacGyver ist, und so unsere Gruppe immer funktionierende Geräte zu Verfügung hatte.

Edgar Uhl, Dr. Monika Schildhauer und Till Reinhardt, es war immer großartig mit euch zu Wandern.

Vielen Dank an Dr. Peter Mayer für die hervorragende Arbeit bei weit über 100 Kristallstrukturen und bei allen Mitarbeitern des Departements. Besonderer Dank gilt Dr. David Stephenson (jetzt kommen wir endlich nicht mehr wieder), Brigitte Breitenstein, Sonja Kosak, Claudia Ober, Petra Keilholz, Susanne Ebert, Robert Eicher, Heidi Buchholz und Michael Gayer.

Des Weiteren möchte ich mich bei allen Kooperationspartnern bedanken. Vor allem bei Dr. Lars Heinke, Dr. Susanne Gerndt, Roland Wilcken für die erfolgreichen Projekte aber auch bei Tobias Fischer und Prof. Dr. Josef Wachtveitl als auch bei Willibald Stockerl und Prof. Ruth M. Gschwind für die Kooperation bei aktuellen Projekten, die hoffentlich ebenso erfolgreich zu Ende gehen.

Außerdem möchte ich mich bei allen Praktikanten und Masteranden bedanken, die ich hoffentlich nicht zu sehr geschunden habe: Sebastian König, Ferdinand Lajos Kiss Michaela Colling-Kaltenegger, Till Nicolas Reinhardt, Lukas Horndasch, Benjamin Gabriel Jehle, Marvin Maria Irmler, Fabien Kohl. Ihr habt alle tolle Arbeit geleistet.

Von ganzem Herzen möchte ich mich bei meiner Familie bedanken. Ohne eure Unterstützung wäre ich nie so weit gekommen.

Am Ende möchte ich mich ganz Besonders bei meiner Freundin Dr. Desirée Heerdegen bedanken, die mich über die ganze Doktorarbeit ausgehalten und unterstützt hat. Schön, dass es dich gibt.

Publications

A. Gerwien, T. Reinhardt, P. Mayer, H. Dube, *Org. Lett.* **2018**, *1*, 232-235. Synthesis of Double-Bond Substituted Hemithioindigo Photoswitches.

A. Gerwien, M. Schildhauer, S. Thumser, P. Mayer, H. Dube, *Nat. Commun.* **2018**, *9*, 2510. Direct Evidence for Hula Twist and Single-Bond Rotation Photoproducts.

A. Gerwien, P. Mayer, H. Dube, *J. Am. Chem. Soc.* **2018**, *140*, 16442-16445. Photon-Only Molecular Motor with Reverse Temperature-Dependent Efficiency.

A. Gerwien, P. Mayer, H. Dube, *Nat. Commun.* **2019**, *10*, 4449. Green Light Powered Molecular State Motor Enabling Eight-Shaped Unidirectional Rotation.

A. Gerwien, B. Jehle, M. Irmler, P. Mayer, H. Dube, in preparation. An 8-state molecular sequential switch featuring the unprecedented “double single-bond rotation” photoreaction.

Publications as coauthor not included in this thesis

A. B. Kanj, A. Chandresh, A. Gerwien, S. Grosjean, S. Bräse, Y. Wang, H. Dube, L. Heinke *Chem. Sci*. **2020**, *11*, 1404-1410. Proton-Conduction Photomodulation in Spiropyran-Functionalized MOFs with Large On-Off ratio.

M. Müller; S. Gerndt; Y.-K. Chao; T. Zisis; O. N. P. Nguyen; A. Gerwien; N. Urban; C. Müller; F. A. Gegenfurtner; F. Geisslinger; C. Ortler; S. Zahler; M. Biel; M. Schäfer; C. Grimm; F. Bracher; A. M. Vollmar; K. Bartel, *Cell Chem. Biol.* **2020**, accepted. Gene editing and synthetically accessible inhibitors reveal role for TPC2 in cancer cell proliferation and tumor growth.

R. Wilcken, A. Gerwien, L. Huber, H. Dube, E. Riedle, in preparation. Quantitative in-situ NMR-illumination for excitation and kinetics of molecular motor intermediates.

Contribution of colleagues

[I] Monika Schildhauer	Pioneering work on sterically hindered HTI derivatives and low temperature UV-Vis measurements.
[II] Kerstin Grill	Pioneering work on sterically hindered HTI derivatives.
[III] Stefan Thumser	Theoretical assessment and assistance for many investigated systems.
[IV] Dr. Peter Mayer	Measurement and identification of all structures in the crystalline state

Contribution of students

[V] Ferdinand Lajos Kiss	Synthesis and investigation of HTI derivatives with large paddle-like substituents (not included in this thesis).
[VI] Michaela Colling-Kaltenegger	Synthesis and investigation of HTI derivatives with large paddle-like substituents (not included in this thesis).
[VII] Sebastian König	Synthesis and investigation of HTI derivatives with intramolecular hydrogen bonds (not included in this thesis).
[VIII] Till Nicolas Reinhardt	Synthesis of many fourfold substituted HTI derivatives.
[IX] Lukas Horndasch	Investigation the photochemical properties of fourfold substituted HTI derivatives (not included in this thesis).
[X] Benjamin Gabriel Jehle	Synthesis and investigation of eight-state HTI derivatives.
[XI] Marvin Maria Irmler	Synthesis and investigation of eight-state HTI derivatives.
[XII] Fabien Kohl	Synthesis and investigation HTI photoswitches with several states and new isomerization mechanisms (not included in this thesis).

Table of contents

1. Summary

The main part of this thesis consists of the design of hemithioindigo (HTI) photoswitches with increasing complexity leading to new generations of photoswitches with unprecedented properties and reaction mechanisms. The development of a synthetic protocol for the introduction of a fourth substituent to the HTI double bond (Figure 1, 2nd from left), allowed the synthesis of in total 30 HTIs with almost all desired substitution patterns. The synthesis is the cornerstone of all further designed HTIs in this work as it can deliver sterically overcrowded derivatives with high internal rotation barriers. The fourfold substituted HTIs behave like traditional HTI photoswitches and possess at least two stable states with *E* and *Z* configured central double bond at ambient temperatures with - in some cases - significant performance increases like absorptions up to 625 nm.[1]

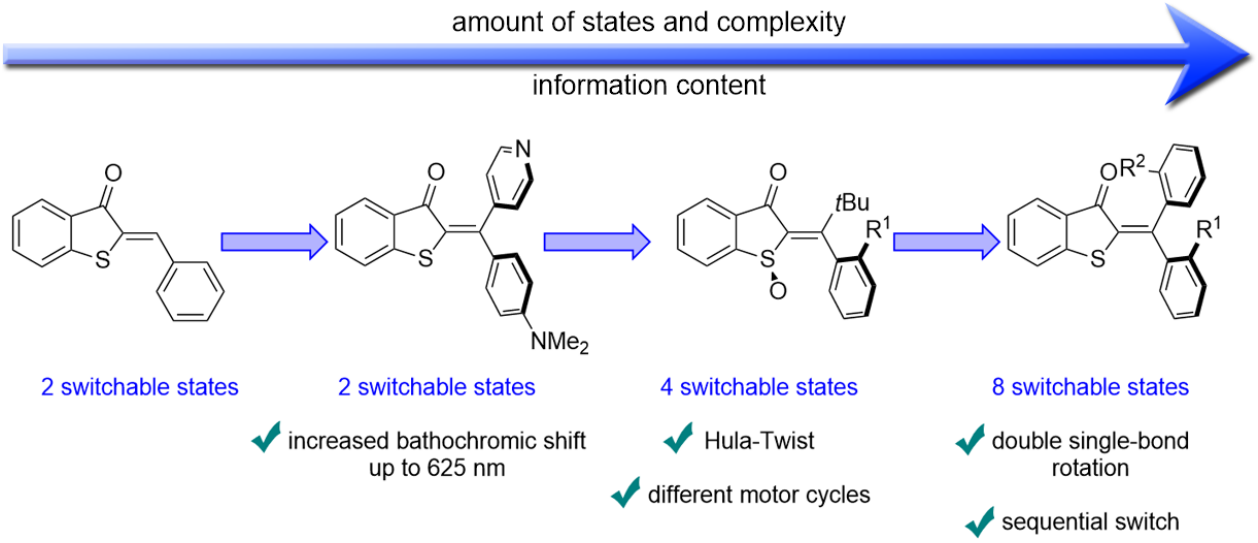

Figure 1: HTI photoswitches developed in this work. With increasing amounts of states, the complexity of the system rises and more information can be stored and extracted from the molecule. This enables the determination of the mechanism and direction of the photoisomerization.

With the introduction of one nonsymmetric substitution pattern at the stilbene part and oxidation of the sulfur, four diastereomeric states could be obtained within a single HTI switch (Figure 1, 3rd from left). The atropisomers are generally stable at ambient temperature due to large steric demand of the tertiary butyl group, enabling the investigation of each isomer individually. In these four state photoswitches, every isomer can be interconverted by three different photoreactions: Double-bond isomerization (DBI), single-bond rotation (SBR) and Hula-Twist (HT). The existence of the Hula-Twist photoreaction was unambiguously proven by this approach for the first time. In total, 20 derivatives were synthesized and their photoreactions explored. The outstanding derivatives are presented separately in this summary below.

By introducing a second nonsymmetric aryl substituent (Figure 1, right) the static sulfoxide stereocenter is exchanged by a flexible stereoinformation, which leads to four diastereomeric states. In this new class of multi-state HTI switches, all chiral stereoinformations can be switched by light, enabling also the eight enantiomers to be converted into each other. This results in new possible photoreactions connecting these eight enantiomers leading to new type of photoswitch in which the isomers are converted in a sequential manner. However, these photoswitches are not molecular motors as the directional movement is reversed in each rotation sequence. The best performing derivative as sequential switch is presented separately below.

Direct evidence for the Hula-Twist photoreaction

HTI **1** is a photoswitch with four stable states at ambient temperatures, which are separable by column chromatography. The structures of all four isomers could be unambiguously proven by X-ray analysis in the crystalline state and assigned to their respective NMR spectra. Subsequently, the photoreactions of the isomers were followed by NMR spectroscopy at room temperature and quantum yields for each isomer interconversion could be determined individually. It could be shown that isomer **B** is directly converted to isomer **C** with a quantum yield of 8%. For this interconversion the double bond and the adjacent single bond rotate at the same time. This isomerization was proposed earlier as Hula-Twist reaction but could never be unambiguously proven. HTI **1** and its quantum yields are shown in Figure 2.[2]

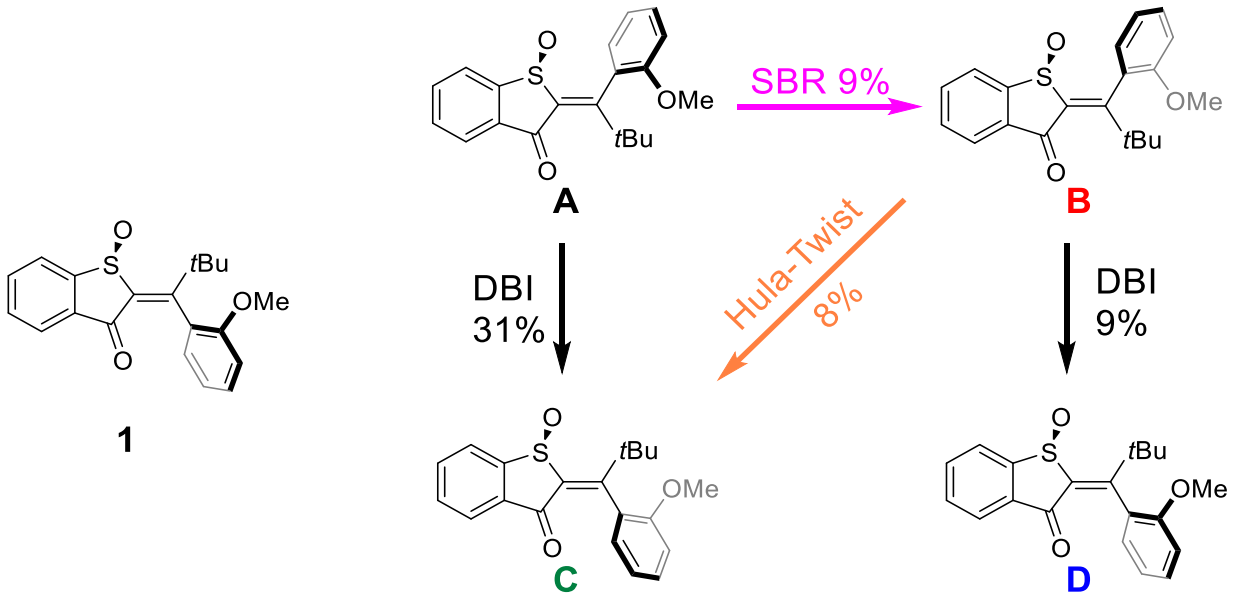

Figure 2: HTI **1**, the first derivative that enabled a direct experimental evidence of the Hula-Twist photoreaction. The quantum yields for isomer interconversion were measured in benzene-d_6 with 405 nm illumination at 23°C.[2]

The ratio between the three possible photoreactions strongly depends on the surrounding medium and it was possible to control, which photoreaction is performed from nearly exclusive DBI of isomer **B** in solid organic ices to about 80% HT in CD_2Cl_2 solution at -80°C.[2]

Photon-only driven molecular motor

By introducing a second methoxy substituent the quantum yields of the *E* isomers of HTI **2** increase substantially and become reliably measurable. Thus, a more significant backwards reaction from the former photochemical sink isomer **C** to isomer **A** of derivative **2** is introduced (Figure 3). With the already known SBR from **A** to **B** and HT from **B** to **C** a complete rotation cycle is performed from HTI **2** in which the chiral sulfoxide dictates the rotation direction.[3]

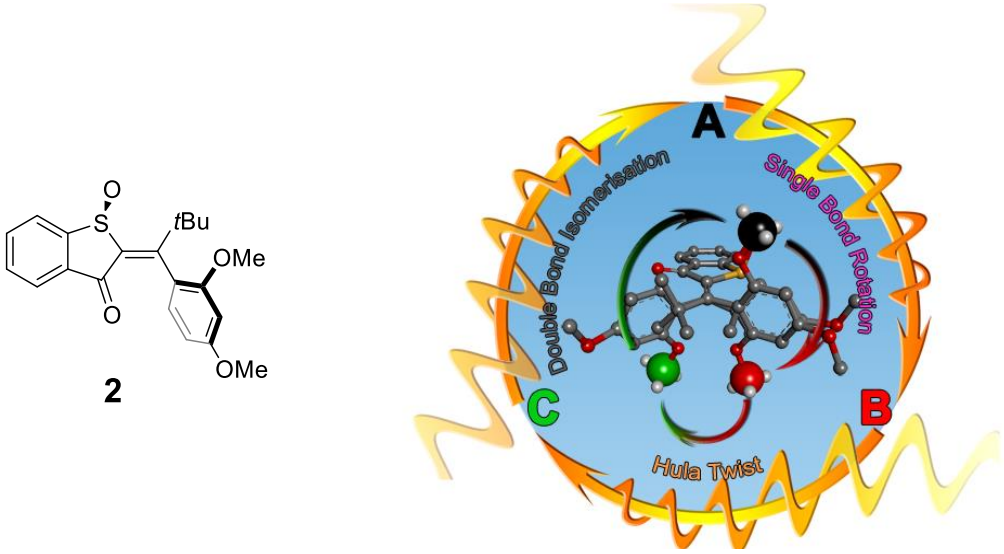

Figure 3: First light-only driven molecular motor **2**. A complete rotation is performed by consecutive SBR from **A** to **B** followed by HT to **C** and DBI back to the starting point **A**.[3]

HTI **2** is the first light-only driven molecular motor. All other known light driven molecular motors need thermal ratcheting steps for their unidirectional rotation, reducing their rotation speed at lower temperature and turning them into simple switches if the energy barriers of their thermally induced motions cannot be overcome. HTI **2** behaves differently, as no thermal steps are involved in the rotation process in the ground state. Indeed, the rotation speed increases with lower temperatures as the selectivity for the photoreactions needed for the rotation increases.[3]

Eight-shape molecular motor

By introducing the strong electron donating group julolidine it was possible to induce a hitherto unknown thermal Hula-Twist isomerization. Combined with two photochemical double-bond isomerizations an eight-shape motor trajectory was achieved. One further highlight of this molecular motor besides being powered by green light is the fluorescence of two states, enabling a direct optical readout of the current state of the motor.[4]

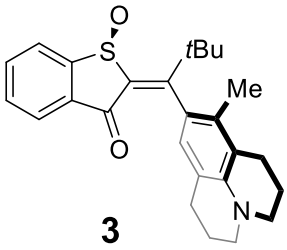

3

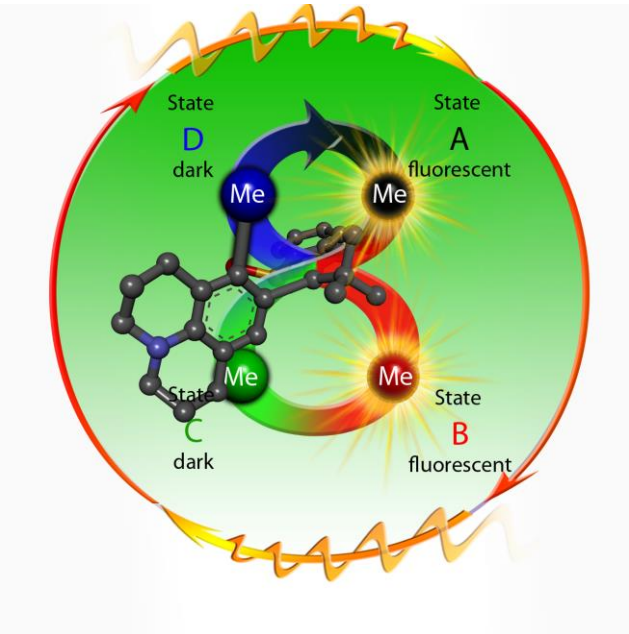

Figure 4: Eight-shape rotation of molecular motor **3**. A complete rotation is performed by consecutive photoinduced DBI from isomer **A** to **C** followed by thermal HT to **B**, which is converted photochemically via DBI to isomer **D** isomerizing thermally via another HT back to the starting point **A**. As the double bond rotates two times by 360° until the starting point is reached again, the rotation trajectory mimics an 8 shape. [4]

Eight-state sequential switch

By introducing a second flexible chiral element at the central double bond and omitting the sulfoxide a photoswitch with eight states (four of which are enantiomeric) is obtained. In contrast to the before presented systems the two enantiomeric structural spaces are not separated anymore but can be interconverted. In case of HTI **4** the photoreactions as well as thermal reactions of the respective isomers are selectively converting only one isomer into another. The exception is isomer **B**, which is converted to isomer **D** by photochemical HT reaction or alternatively to isomer **B'** in a completely new photoreaction in which both single bonds rotate at the same time. From this branching point an eight-step or a five-step cycle can be performed by this system. By changing the temperature and solvent it can be controlled, which cycle is performed.

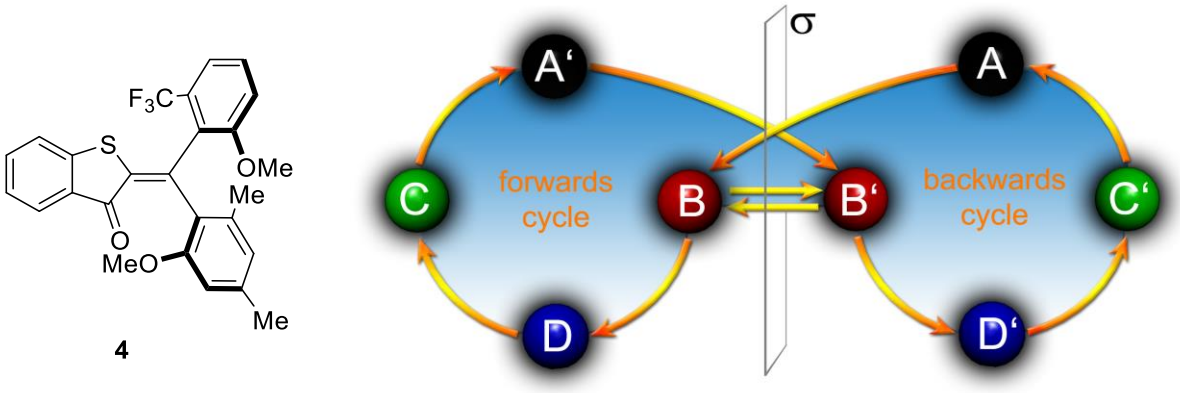

Figure 5: Eight-state sequential switch **4**. Both enantiomeric structural half spaces are connected, which results in consecutive forwards and backwards cycles. By changing the irradiation conditions at the branching point **B**, a switching between an 8-step cycle and a 5-step cycle is possible.

As both enantiomeric structural half spaces are interconnected **4** is not a motor but a special kind of switch as one forward rotation cycle must follow one backward cycle continuously. This is also different from a normal switch performing the forwards and backwards rotation randomly. Therefore, we called **4** a sequential switch.

In summary, in this thesis concepts for new and refined molecular tools like molecular motors and multistate switches driven by different isomerization reactions are presented. A focus was also the investigation of uncommon isomerization reactions like the elusive Hula-Twist reaction or the hitherto unknown dual single-bond isomerization. Variation of the irradiation conditions allowed the control over the different photoreactions and switching between different isomerization cycles could be obtained, varying the illumination conditions. Introduction of the Hula-Twist photoreaction and the dual single-bond isomerization considerably expands the scope of photochemical isomerization reactions. The construction of new molecular motor systems with these uncommon photoreactions demonstrates not only application examples but also new design principles for molecular machines in general.

2. Introduction

2.1. Photoswitches

Photoswitches react to the presence of light by switching between at least two distinct states. Typically, small organic molecules are used as photoswitches, but also inorganic complexes can be utilized. Light input leads to the generation of a new isomeric species with different chemical and physical properties that can trigger a measurable response such as conductance change or binding to another molecule. With this property they constitute a major column of modern nanotechnology.[5-7]

In general, photoswitches are photochromic compounds with different absorption spectra in each state. Therefore, UV-Vis spectroscopy is used in most cases to follow the change of isomer composition from the initial isomer **A** to the photogenerated isomer **B**. The photochromism of a photoswitch is one core property, which determines the performance of the switch. It enables easier readout of the states and more selective irradiation of one state yielding larger amounts of the desired photoproduct in the photostationary state (PSS). Other core properties are the quantum yield, which determines how efficient the photoreaction takes place after absorbing photons and the thermal stability of the individual isomers. An idealized photoswitch is shown in Figure 6.[5-7]

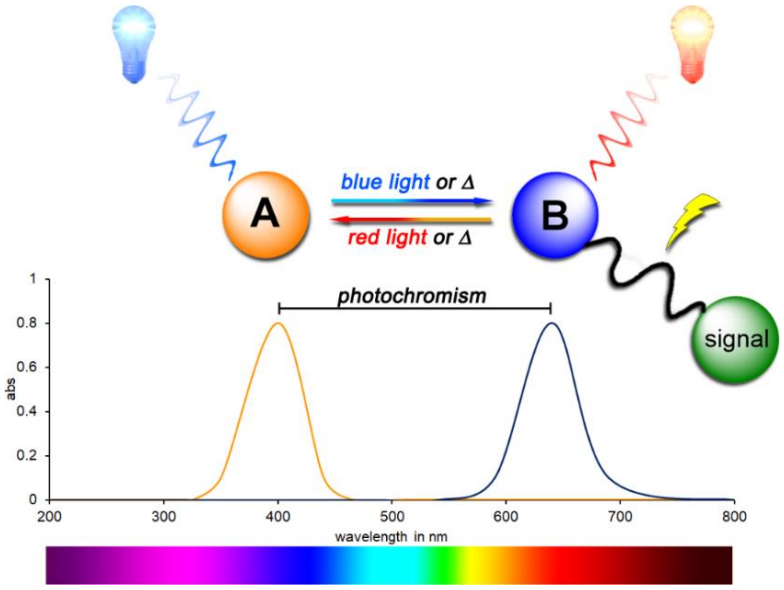

Figure 6: Properties of an idealized photoswitch with two isomers **A** (orange) and **B** (blue). Isomer **A** absorbing blue light (about 400 nm) appears as yellow/orange chromophore. Upon light absorption, it is converted into isomer **B**, that appears as blue chromophore as it absorbs light of the wavelengths 600 – 700 nm. By irradiation with these wavelengths **B** can be turned back into isomer **A**. The isomerization can be also triggered thermally and the activation barrier for this reaction determines the thermal stability of the photoswitch. Ideally only one isomer (here **B**) triggers the desired signal, which can be physically (e.g. fluorescence or absorbance) or chemically (e.g. pH modulation or binding to another molecule).

The most common photoswitches are shown in Figure 7 with their respective absorption spectra in each state. They can be roughly divided into two groups: photoswitches that undergo photocyclization reactions and *E*/*Z* isomerization photoswitches.

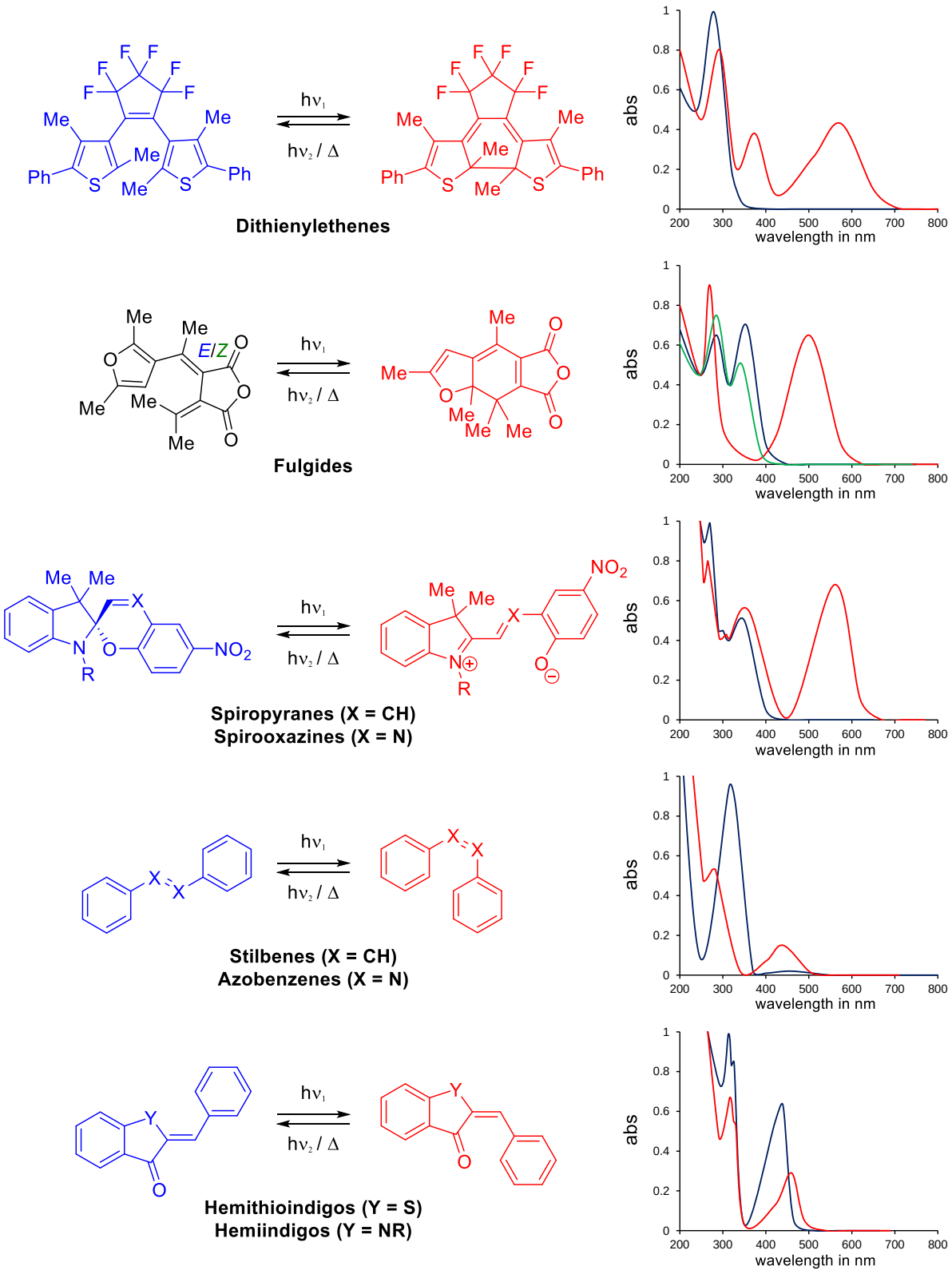

Figure 7: Common organic photoswitches with their respective absorption spectra of each isomer. Only one derivative for each photoswitch class is shown with typical or no substitution pattern. The absorptions of the photoswitches were measured in the following solvents: dithienylethene (cyclohexane)[8], fulgide (ethanol)[9], spiropyran (acetonitrile)[10], azobenzene (methanol)[11], hemithioindigo (dichloromethane) and the absorption of one isomer was normalized to 1.

Diarylethenes,[8, 12-16] here shown as dithienylethenes, and fulgides[9, 17, 18] undergo 4n+2 conrotatory ring closing and opening reactions upon illumination. The initial state can also be recovered thermally with in general relatively low thermal barriers, resulting in ring opening at ambient temperatures. These photoswitches are therefore positively photochromic meaning that the bathochromic (red shifted) absorbing state is the thermodynamically less stable form. Due to the large electronic changes between both states, they possess one of the largest photochromism of all switches. Therefore, huge efforts in the development of diarylethenes were invested in the past decades to enhance their thermal stability and fatigue resistance. Especially their property to switch effectively in solid state[19] combined with the large photochromism make them promising candidates for optical data storage applications.[15, 16] However, due to minor geometrical changes upon switching, the use for molecular machines and photoswitchable drugs are limited.

Spiropyrans have similar properties to diarylethenes but photoswitching typically takes place by a combination of DBI, nucleophilic addition, and heterolytic bond cleavage. Another difference to diarylethenes is that the closed form (spiropyran) is colorless, and the open zwitterionic state (merocyanine) is deeply colored, typically purple to blue.[20, 21] Both states are relatively equal in their relative energies and the energy differences are largely dependent on the surrounding medium and substitution pattern, enabling the use of spiropyrans as positively and negatively photochromic switches. Typically, in organic solvents the spiropyran state is most stable and a positively photochromic switch is obtained, but with the correct substitution pattern and in polar solvents such as water the merocyanine form becomes more stable turning the spiropyran into a negatively photochromic switch.[22] Due to the large change in the polarity and electronics upon switching, spiropyrans are employed in various applications[10, 23, 24] using these changes to switch the solubility of polymers or nanoparticles,[25] aggregation to defined structures,[26] photocontrolled metal ion complexation[27, 28] and conductance switching.[29, 30] Spiropyrans, especially spirooxazines are one of the most stable photoswitches towards photobleaching enabling their usage in self coloring lenses with several thousand switching cycles without loss of efficiency.[31, 32]

Other photoswitches with photocyclization are norbornadienes, that switch only in the UV-region, but with up to 36 kcal·mol^{-1} energy difference between both states. They are discussed as solar energy storage systems.[33-35] Dihydroazulenes, switching via a 10 π-electron rearrangement, are discussed in the same regard but show worse properties.[36-38] Another type of photocyclization switches are the negatively photochromic DASAs (donor-acceptor Stenhouse adducts), which show similar good photochromism and properties as spiropyrans, but structural diversity is limited. Similar applications as for spiropyrans are imaginable, but as relatively new photoswitches they provide less examples in the literature.[39-42]

Another class of photoswitches are *E*/*Z* isomerisation switches. In general, this class shows only small photochromism between the states due to marginal changes in the electronics but large and well-defined geometrical changes upon switching. This property makes these kind of switches the ideal base for

photopharmacology and molecular machines. The most common switches in this class are by far stilbenes and azobenzenes.[43, 44] While unsubstituted azobenzenes are yellow chromophores absorbing blue light, unsubstituted stilbenes absorb exclusively UV-light.[43, 45] As these energy rich light types are harmful to cells and tissue penetration is very shallow, many attempts were made to shift the absorption into the biooptical window (650 – 1350 nm).[46] The use of strong donor-acceptor substitution patterns, boron adducts, and bridged derivatives lead to successful shifted absorption in the red to near infrared region, but all of these attempts show also downsides like low thermal stability of the isomers.[44] Stilbenes[43] were used as basis for the development of the first light driven molecular motors[47] by Ben Feringa, rewarded with the Nobel Prize in 2016.[48]

Another class of *E*/*Z* isomerization photoswitches are indigoid photoswitches like hemithioindigos (HTIs) and hemiindigos (HIs), derived from the parent chromophores thioindigo and indigo.[49] Their properties are similar to stilbene and azobenzene photoswitches but as one side of the double bond is fixated in a heterocycle only a few degrees of freedom are left in the system, making these photoswitches an ideal rigid framework for molecular devices such as photon powered motors.[49, 50] The majority of the developed systems in this work is based on HTIs and the evolution of indigoid photoswitches and their applications are presented in detail in chapter 2.3.

Other *E*/*Z* photoisomerization photoswitches are for example imines/hydrazones[51] or biological photoswitches like retinal,[52] or previtamine D_3.[53]

There are also molecular switches, which do not operate under light control, but can be addressed by other inputs like acid/base, redox control, or chemical transformations. These are typical switching modes for rotaxane based shuttles[54] but also double- and single-bonds can be switched by these transformations.[55] Rotaxane based switches are the foundation of many of the most progressive artificial machines, for which Fraser Stoddart[56] and Pierre Sauvage[57] were rewarded with the Nobel Prize 2016 for this kind of molecular machines.

2.2. Photon absorption and relaxation

The presented photoswitches change their constitution or stereochemistry after irradiation with light, but how does this transformation work? The molecule must be able to absorb photons like a chromophore to reach an electronically excited state from which it decays to another ground state configuration unlike a classical chromophore, which decays exclusively back to the starting isomer. Therefore, first the absorption of a molecule is important. Absorption is mainly characterized by interaction of molecules with the electric field vector of the electromagnetic radiation. Interactions with the oscillating magnetic field of the light wave are of minor importance, since transitions generated by the magnetic field are much weaker than electric dipole transitions in molecules.[58]

The mathematical description of the absorption of a photon by a molecule is given by the time dependent perturbation theory, in which the Schrödinger equation (eq. 1) is extended by the perturbation operator, which includes the effect of the electromagnetic field on the molecule. The obtained new equation describes the wavefunction also as a factor of time and is therefore called time dependent Schrödinger equation[59] (eq. 2).

$$\hat{H}_o \Psi_i = E \Psi_i \qquad \text{(eq. 1)}$$

$$(\hat{H}_o + \hat{H}')\Psi_{(x,t)} = E\Psi_{(x,t)} \qquad \text{(eq. 2)}$$

The new time dependent wave function can be derived from the initial wave function by introducing a time dependent coefficient $a_f(t)$. This coefficient is directly proportional to the transition moment (TM) of the absorption and therefore determines the absorption strength of a molecule. After applying the Born-Oppenheimer approximation[60] (nuclei are fixed), and the Condon approximation[61] (nuclei have the same position after excitation), the wave function can be grouped into the product of an electron function, a spin function and a vibrational function (eq. 3):

$$TM = \underbrace{\int \phi_i \hat{\mu}\, \phi_f d\tau_e}_{\text{Electronic transition moment}} \underbrace{\int S_i\, S_f d\tau_S}_{\text{Spin overlap integral}} \underbrace{\int \theta_i \theta_f d\tau_N}_{\text{Overlap integral of vibration}} \qquad \text{(eq. 3)}$$

The first term is called electronic transition moment, which is defined by the overlap and symmetry of the orbitals before and after excitation. The spin overlap integral takes into account the spin state of the initial and final orbital. The last term describes the overlap integral of the vibrational modes of the participating orbital. The TM can be transformed to the Einstein coefficient A_{ik}, which is the probability for the transition between the states i and k by eq. 4:

$$A_{ik} = \frac{3}{4} \frac{\omega_{ik}^3}{4\,\pi\,\varepsilon\,\hbar\,c^3} \, |TM_{ik}|^2 \qquad \text{(eq. 4)}$$

Therefore, the strength of absorption or emission is dependent on the TM and the transition rules that defines whether a transition is allowed (high probability) or forbidden (low probability) can be derived from the TM. There are many transition rules and only the most important and easiest should be discussed here. For example, the overlap of the molecular orbitals is part of one transition rule and if the ground state orbital does not match with the excited state orbital the transition is forbidden (first integral in eq. 3). Thus $n \rightarrow \pi^*$

transitions are forbidden and generally show weak intensities, whereas π→ π* transitions are allowed and exhibit high absorption intensities. Another rule says that the spins of the electrons must be unchanged during the excitation or emission (second integral in eq. 3). Therefore, a transition is spin forbidden if the multiplicity of the ground and excited state changes e.g. from singlet to triplet. Another transition rule is the Laporte rule, which states that the parity of the orbitals must change during the transition. However, as all of these equations are only approximations, even forbidden transitions still have small intensities or probabilities as vibrationally induced distortion of the molecular symmetry as well as minor influences like magnetic interactions or the spin-orbit interaction are present in reality. The latter is the reason for observable singlet-triplet transitions for heavier atoms.

A description of the transition between two states is provided by the Franck-Condon principle,[62] which takes into account that the energy of a molecule is quantized and dependent on the electronic and vibrational mode. In Figure 8 an energy diagram of a molecule with two electronic states (S_0 and S_1) is shown.

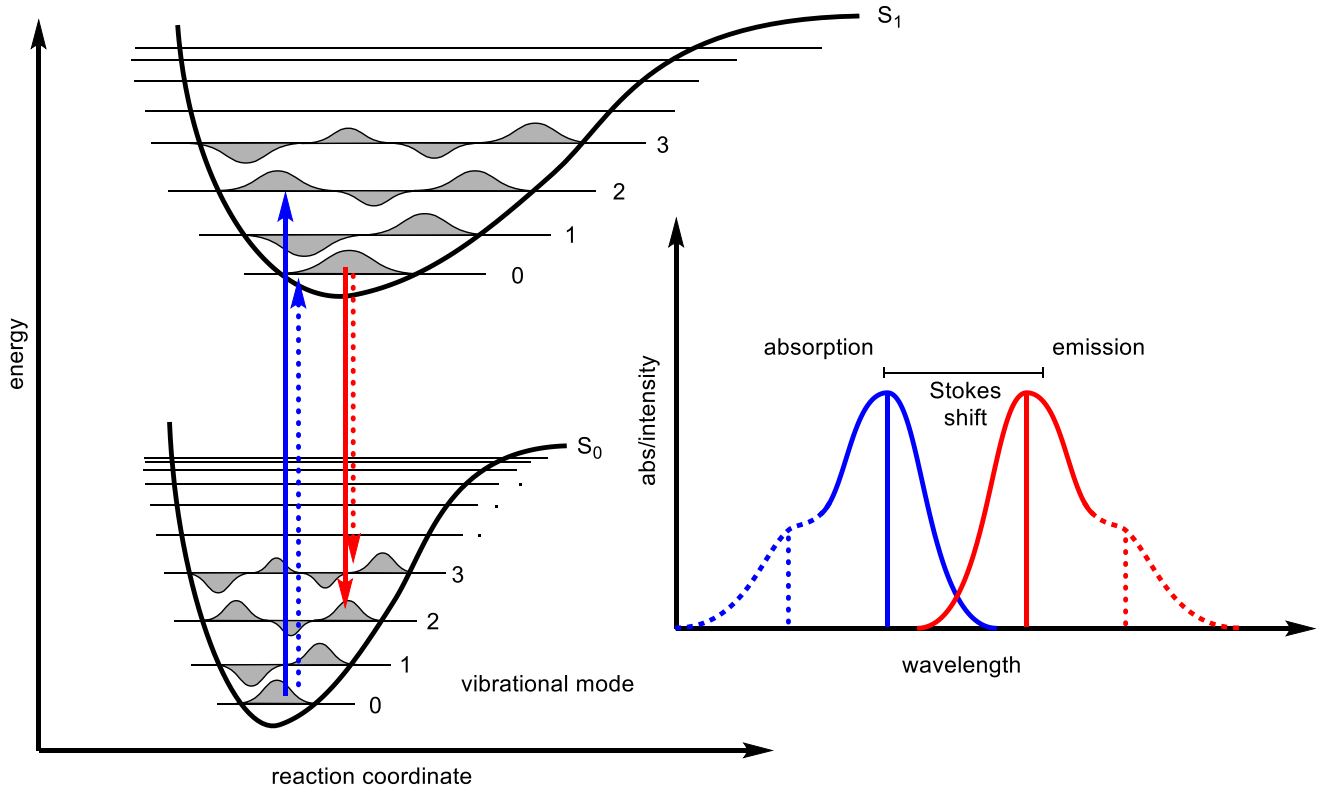

Figure 8: Absorption and emission following the Franck-Condon principle. Energy diagram of a molecule with two electronic states (S_0 and S_1, left). The reaction coordinate describes the movement of atomic nuclei. Each electronic state is divided in different vibrational states. Excitation (blue) and emission (red) takes place from the lowest vibrational state of each electronic state. The transition probabilities lead to the simplified spectrum on the right. The spectrum is mirrored as emission spectrum (red, fluorescence). The excitation/deexcitation in different vibrational modes leads to broadening of the absorption bands or "shoulders". Only at lower temperatures the excitation/deexcitation into different vibrational modes are separated as different bands.[63]

Each electronic state (S_0 and S_1 in Figure 3) is divided in different vibrational states. In the Franck-Condon model excitation (blue) and emission (red) takes place from the lowest vibrational state of each electronic state, respectively. As the electrons are much smaller than nuclei the change of the electronic state is much faster than the nuclei movement and the transitions are described as vertical processes in which no nuclear motion occurs.[61] Transitions are more likely, if the overlap of the wavefunction (grey) of the initial vibrational state and the final vibrational state is maximal (third integral in eq. 3). The transition probabilities lead to the simplified spectrum on the right side of Figure 3. The 0→2 transition (blue, straight) is more likely and requires less energy than the 0→3 transition (blue, dotted). After excitation, the molecule relaxes very quickly under energy transfer as heat to the lowest vibrational mode (internal conversion) from which emission can occur. This order of events is also known as Kasha's rule in cases where fluorescence is the main deexcitation pathway. Thus, the absorption spectrum is mirrored as emission spectrum (red, fluorescence) and red-shifted as a little bit of energy was already transferred as heat. The difference in the maxima between both spectra is called Stokes shift. In theory, the Franck-Condon principle would lead to clear sharp bands in the spectrum but by interaction with other molecules in proximity every molecule has slightly different energy differences between the states and the bands are broadened.[63]

One mechanism of deexcitation is therefore the emission but Figure 8 shows that the emission does not yield any alteration to the initial molecules structure. To obtain a photoproduct the nuclei must rearrange to a more stable position in the excited state, before deexcitation takes place. From the new most stable form in the excited state the molecule can return into its ground state by emission with the nuclei coordinates being different and may forming a photoproduct, which is separated by a thermal barrier from the starting point in the ground state. This type of photochemical reaction is called adiabatic and is shown on the left in Figure 9.

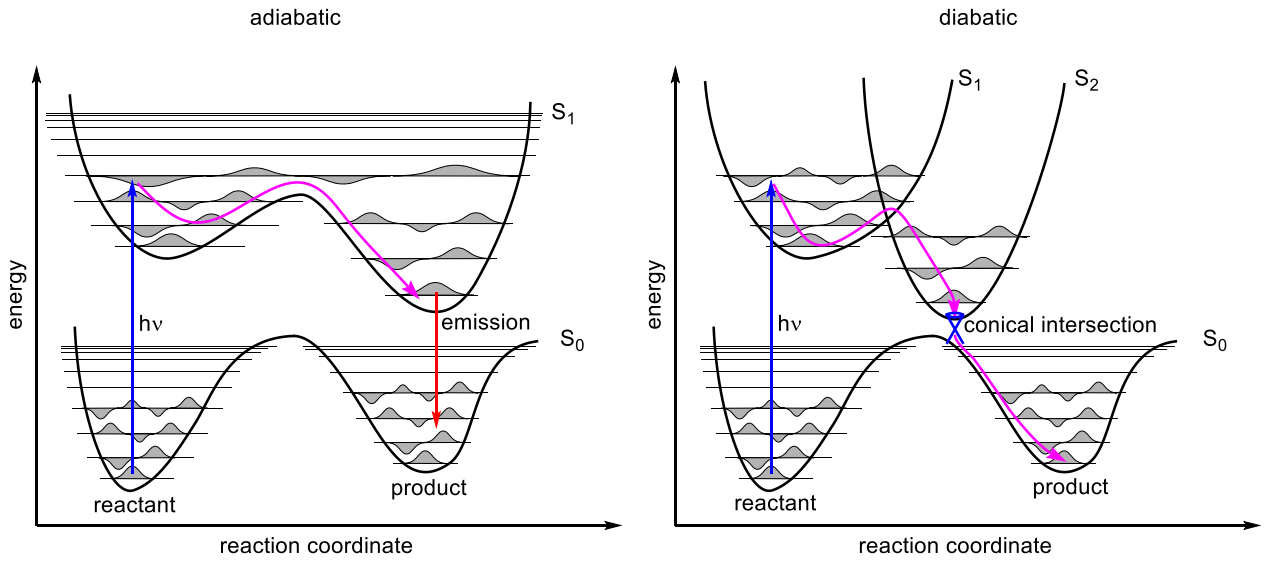

Figure 9: Comparison between adiabatic (left) and diabatic (right) photoreactions. In an adiabatic photoreaction the product is formed without crossing of the electronic states. In a diabatic photoreaction the product is formed after or during deexcitation through a conical intersection at the crossing point of the excited and the ground state.[64]

Adiabatic photoreactions are very rare.[64] They only occur if no crossing between the different electronic states is present and the excited state surface has a minimum at the product side of the reaction, which is reachable before the deexcitation – mostly by emission – occurs. This is possible if the geometrical changes during the reaction are small and the electronic surfaces are relatively flat, so no crossing can occur. Examples for adiabatic photoreactions are the photoinduced reaction from Dewar benzene to benzene[65, 66] or the intermolecular hydrogen transfer of 1,7-diazaindene from the pyrrole ring to the pyridine ring.[67, 68]

Diabatic photoreactions are more common. In diabatic photoreactions a crossing between the electronic states is present and the molecular motions follow the common energy surface until the minimum energy is reached. This process is very fast, and the molecule has no time to explore the whole excited energy surface and to develop equilibria in the excited state but follows the "easiest" way downwards. This principle is called NEER (non-equilibration of excited rotamers).[69] The crossing point of the excited state with the ground state is called conical intersection.[70] If a conical intersection is available for a molecule it will always deexcite diabatically, as this process is much faster than the deexcitation by emission. Photoswitches react in general diabatically for example dithienylethenes[71], azobenzenes[72, 73], or HTIs.[74-76]

In both general photoreaction mechanisms, a special case can occur, in which the light energy is used to overcome barriers in the ground state through internal heating. This type of reaction is called "hot ground state" mechanism. The energy diagram for a hot ground state reaction is shown in Figure 10.

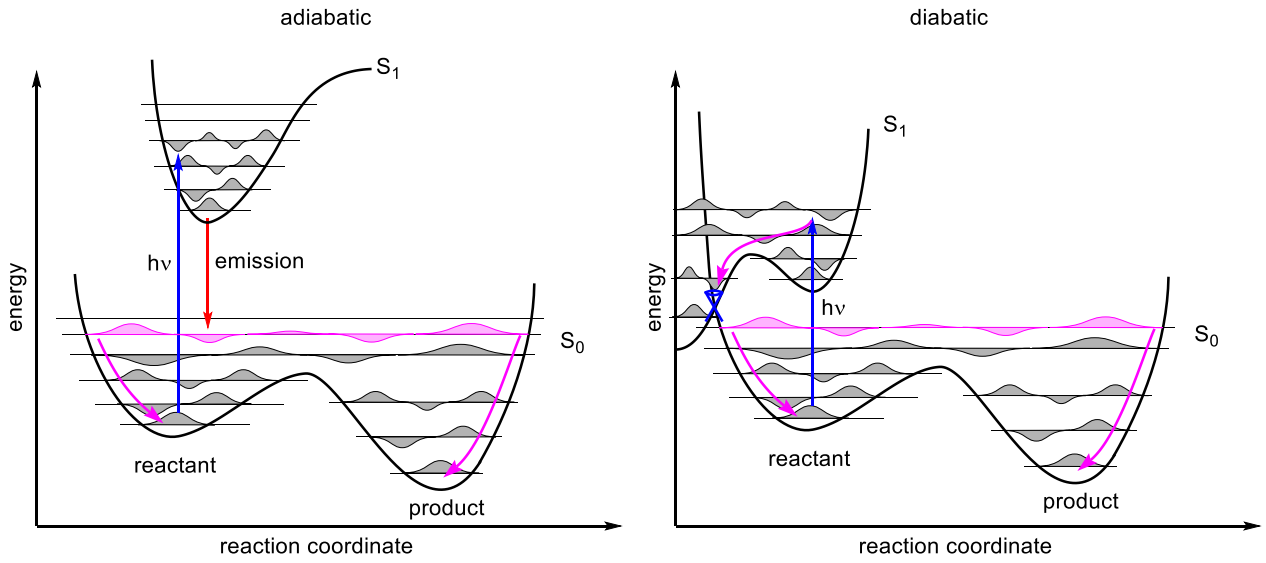

Figure 10: Energy diagrams for adiabatic and diabatic hot ground state reactions. As the probability at the edges of the wavefunctions is higher than in the middle, the molecules “cool down” from the edges of the potential well to the minimum structures.[64]

The hot ground state reaction can occur if the ground state surface is relatively flat and if the energy of the system cannot be transferred to the surrounding medium for example in vacuum. Accordingly, examples for hot ground state reactions are rare but one very vivid study of the ring opening of cyclohexadiene following the reaction after excitation by transient ultrafast electron diffraction illustrates this type of reaction. Directly after ring opening a mixture of all rotational isomers of hexatriene is observable as one very broad species containing the largest population of the most unstable isomers as they are near the potential well walls. After internal cooling all three possible isomers are obtained.[77]

2.3. Azobenzenes

Azobenzenes are one of the most used photoswitches, especially for materials and photopharmacology applications e.g. as photoswitchable antibiotics[78], ion channel switches[79] and much more[44]. Therefore, huge effort in the development of red-shifted derivatives was invested to enable photoswitching at the biooptical window (650 – 1350 nm)[46]. The most successful approaches are shown in Figure 11 with their most redshifted absorbance maxima in the *E* state.

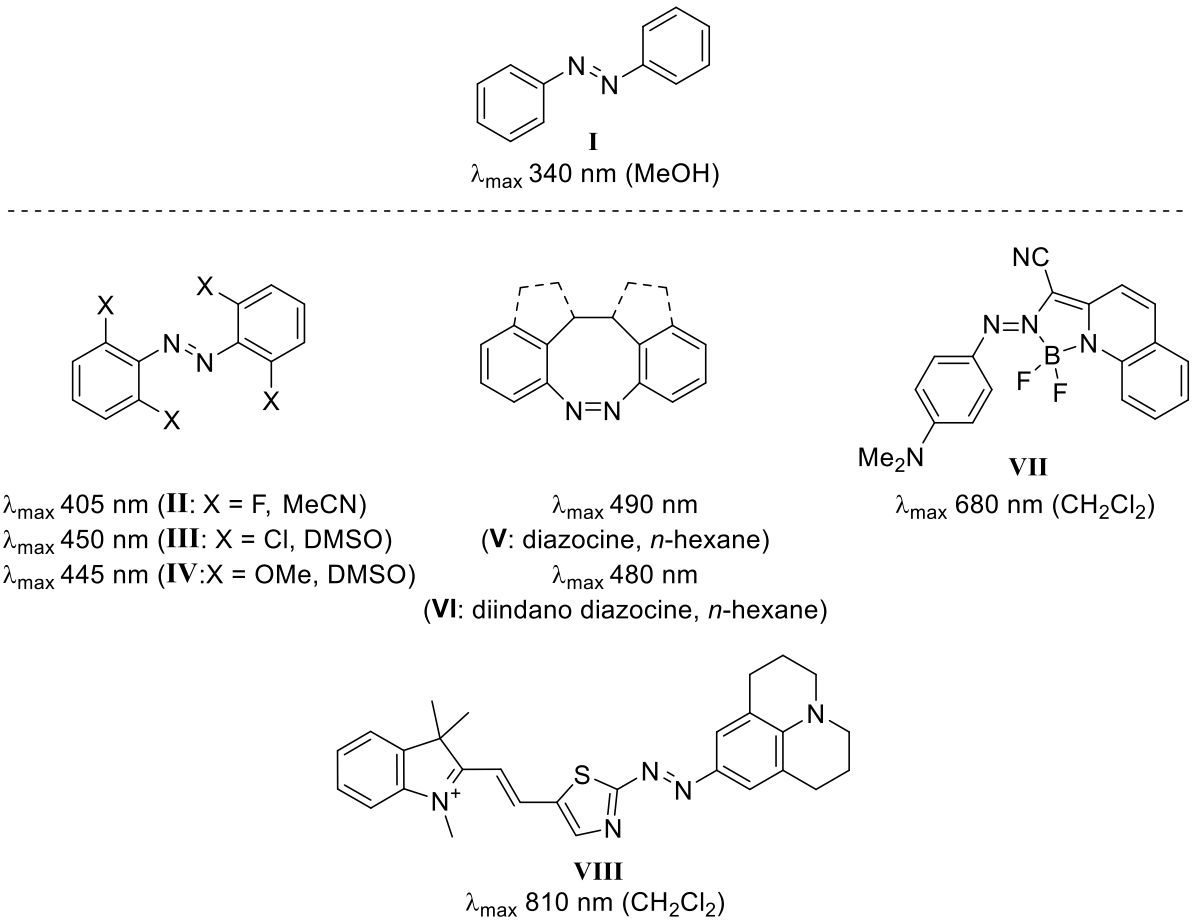

Figure 11: Comparison between different azobenzenes I[11], II[80], III[81], IV[82], V[83, 84], VI [85], VII[86], VIII[87].

Recently, fourfold *ortho*-substituted azobenzenes **II**-**IV**[80-82] gained attention as they enable a redshift of the azobenzenes in combination with increased energy barriers for thermal interconversions. In addition, methoxy azobenzenes like **IV** can be easily protonated at relatively high pH of 5-7 to azonium ions, with subsequent absorption shift to 600 nm. In general, the thermal stability of azonium switches is extremely low making it impossible to generate the *Z* isomer at ambient temperatures in appreciable amounts. The methoxy groups stabilize the azonium ion by an intramolecular hydrogen bond increasing the thermal

stability into the seconds regime.[82] Thermal stabilities in this regime are desired in photopharmacology, as they ensure that the photoswitch returns to its inactive thermal stable state after diffusing out of the irradiation area.[44, 88]

In another approach by Herges and coworkers[83, 84] both benzene rings were linked with an ethylene bridge. This leads to reversed thermal properties, with the *Z* isomer as the most stable isomer. With a photochromism of about 100 nm, very high quantum yields of $\phi_{(Z\rightarrow E)}$ = 72% and $\phi_{(E\rightarrow Z)}$ = 50%, and isomer enrichment in the PSS >90% in both switching directions these azobenzenes are nearly perfect photoswitches. In addition, the reported thermal half-lives of 4.5 h are also satisfactory for azobenzenes. The only drawbacks are the cumbersome synthesis of these derivatives, the low molar absorption coefficients, and smaller geometric changes upon switching.[44, 85, 89, 90]

In 2014 Aprahamian and coworkes reported azobenzene BF_2 adducts **VI**, which absorb near infrared light and switch with extremely high quantum yields up to 95%. Thermal stabilities are comparable with other azobenzene switches and are in a range of seconds to a few hours, but in protic solvents the BF_2 adducts are not stable and decompose to hydrazones.[51]

It is also possible to bathochromicly shift the absorbance of azobenzenes by incorporating a push-pull effect[91], like in every other dye. This can lead to a tremendous redshift even into the infrared region as azobenzene **VII** demonstrates.[87] However, the push-pull approach lowers the activation barrier for thermal *Z*/*E* isomerization. Therefore, photoswitching is not observable anymore in strong push-pull substituted azobenzenes, as the thermal back reaction is much faster than the photoswitching.[87]

In general, both azobenzenes substituted with a variety of (hetero)-aromatics[92-95] at the diazo group and azobenzenes with aliphatic substitutions at the phenyl group are photoswitches.[96, 97] However, in comparison to the diarylazobenzenes only a few applications are reported. This might trace back to the known homolytic decomposition of diazenes which are used as radical initiators like AIBN. A study of White and coworkers combined the photoswitching and radical initiator properties for the synthesis of graft polymers.[98]

2.4. Indigoid photoswitches

Indigoid photoswitches are derived from the dye indigo[99] and can be divided into indigos, thioindigos, hemiindigos (HIs) and hemithioindigos (HTIs), which are shown in Figure 12. Although they have been known as chromophores for a long time, their photoswitching properties were discovered much later.[100] Main developments for this class of photoswitches were just made recently. Therefore, indigoid photoswitches are less explored than other photoswitches like azobenzene or spiropyrans and provide great research potential.[49, 50]

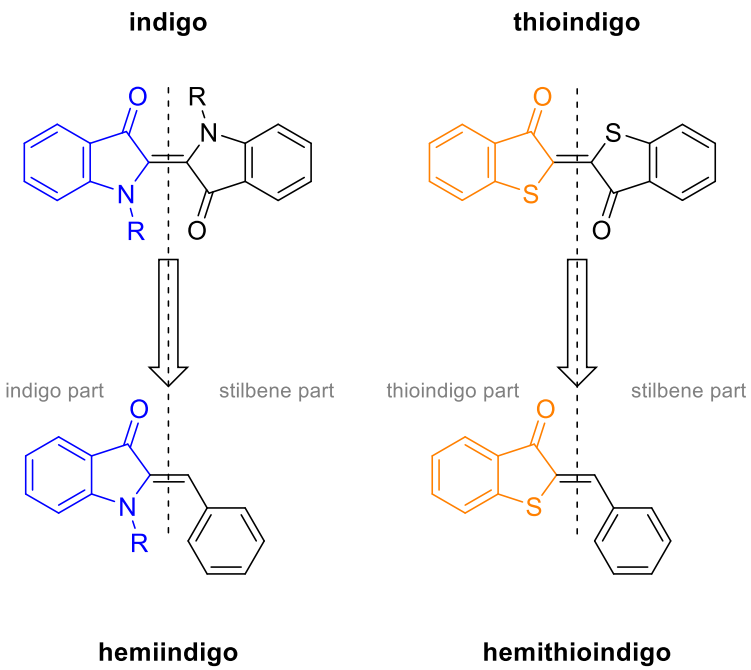

Figure 12: Indigoid photoswitches. The parent chromophores of this class of photoswitches are indigo and thioindigo from which the more commonly used photoswitches hemiindigo and hemithioindigo are derived.

Although the indigo chromophore is the parent chromophore of indigoid photoswitches, only few photoswitches based on the indigo core itself were discovered.[101, 102] In indigo, another deexcitation pathway than switching is possible by intramolecular proton transfer. This intramolecular proton transfer in the excited state (ESPT) is presumed to be the reason for the outstanding photostability of indigo dyes and outcompetes every other photoreaction like the *E*/*Z* isomerization.[103-108] A similar ESPT was introduced to thioindigo by addition of hydroxy groups at the 4 position by which the fluorescence and *E*/*Z* isomerization could be suppressed completely.[109] By removing the "labile" hydrogen atoms from indigo by substitution with carbon based residues indigo can be transformed into a photoswitch with preservation of the indigoid chromophores typical blue color as shown in Figure 13.[110-113] This was shown first by *Wyman in 1956.* [114] However, efficient photoswitches with long half-lives of the thermally unstable *Z* isomer can only be obtained by aryl substitution.[101, 102] Later our group reported indigo photoswitches with only one aromatic residue[115]. Their thermal half-lives are extremely dependent on the concentration of water in the solvent, which limit their application in biological systems but may be used in sensors or smart materials.

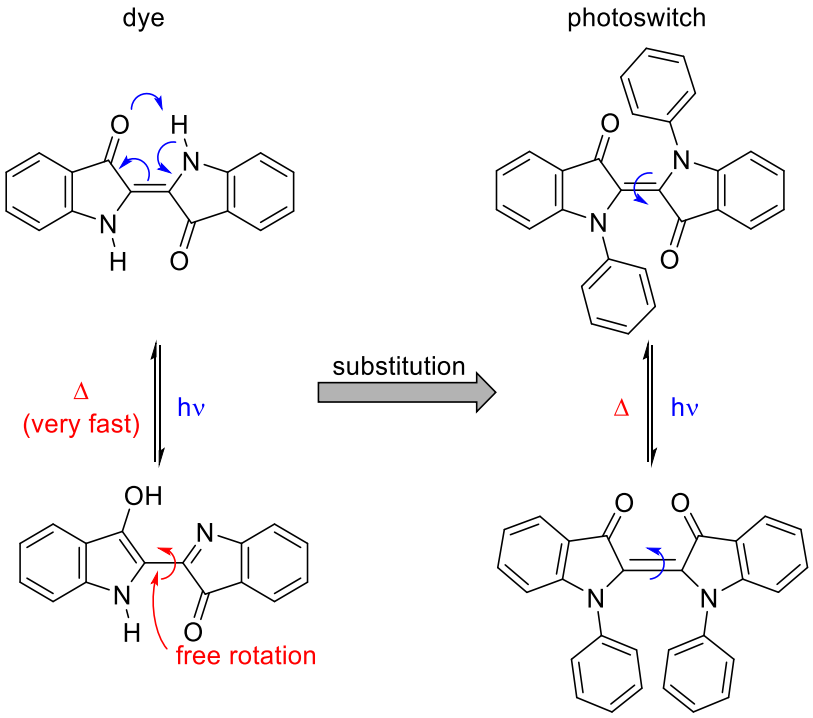

Figure 13: From the dye indigo to the photoswitch. In the parent chromophore fast intramolecular proton transfer in the excited state (ESPT) leads to a suppression of the *E*/*Z* photoisomerization.

Thioindigo photoswitches were extensively studied in the 1950's to 1970's but nowadays receive only limited attention.[103, 116-122] This may be caused by the complicated photochemistry involving significant fluorescence[119] and triplet state formation,[118, 120] which prevent photoswitching under certain conditions. In addition, the solubility of thioindigo is low in almost every solvent and often aggregation is observed. However, with the right substitution pattern good photoswitching can be obtained even in water.[123]

Hemiindigo (HI) was first synthetized by Adolf von Baeyer in 1883.[49] The synthesis consists of a condensation of indoxyl acetate with an aldehyde and is shown in Figure 14. Despite the straightforward synthesis, HIs were not considered as good photoswitches as first investigations showed [2+2] cycloadditions[124, 125] and triplet state formation[125] besides *E*/*Z* isomerization. Except of a very early example by Mostoslavskii reported in 1970[126] and one example of pyrrole-substituted HIs published in 1999[127] by the group of Ikegami, HI photoswitches were not further investigated until our group 2017 showed that HIs can be turned into excellent photoswitches by substitution with electron donating groups.[128] By further substitution with axially chiral groups at the indoxyl nitrogen atom, HI photoswitches show strong ECD signals in the *Z* isomer and weak ECD signals in the *E* isomeric form and can therefore be used as ECD on/off switches as our group reported in 2018.[129]

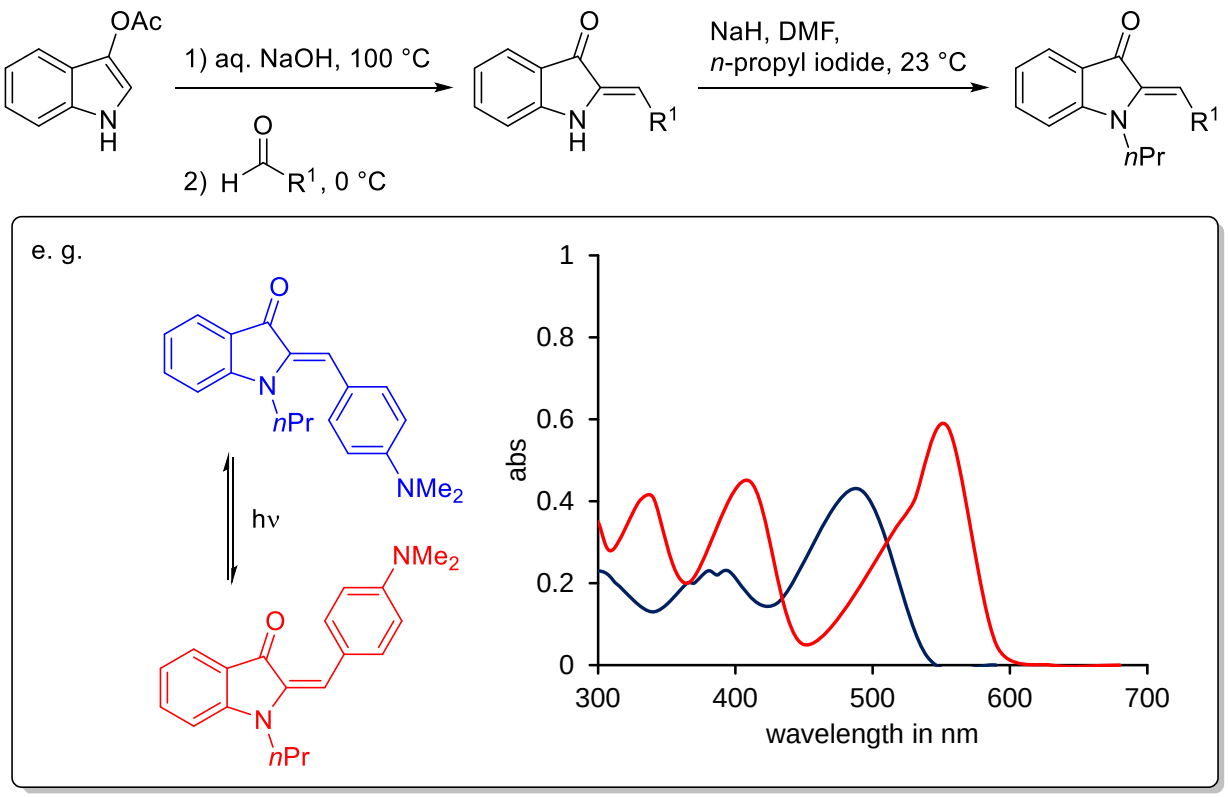

Figure 14: Synthesis of HI photoswitches and exemplary UV-Vis spectra illustrating their photochromism.[128]

Hemithioindigos (HTIs) can be prepared like HIs by condensation of an aldehyde with benzothiophenone. They were first synthesized by Friedländer in 1906 as presented in route A in Figure 15.[130] Nowadays, benzothiophenones are synthesized most often by Friedel-Crafts acylation (route B, Figure 15).[131, 132] If the thiol is not commercially available, it is also possible to deprotonate in *ortho* position of an aromatic amide. Subsequent reaction with dimethylsulfide yields the methylthioether which can be deprotonated with LDA and undergoes ring closure to the benzothiophenone (route C, Figure 15).[133] The drawback of HTI synthesis by condensation is the short shelf life of the benzothiophenone, which is converted by light or oxygen to thioindigo. Thioindigo is also often a side product of the condensation reaction and difficult to separate from the HTI. Therefore, other synthesis approaches were developed like the iodine mediated ring closure shown in route D (Figure 15)[134] or the Umpolung of the sulfur in route E (Figure 15) followed by nucleophilic attack of the double bond also yielding the thiophenone ring.[135] It is also possible to use cascade reactions like in route F (Figure 15) to yield HTI photoswitches. Interestingly, intermediate formation of benzothiophenon could not be observed in this reaction but the reaction proceeds via the disulfide.[136] Many other synthetic routes were published, but due to too many steps or low product yields they are not commonly used.[137-147]

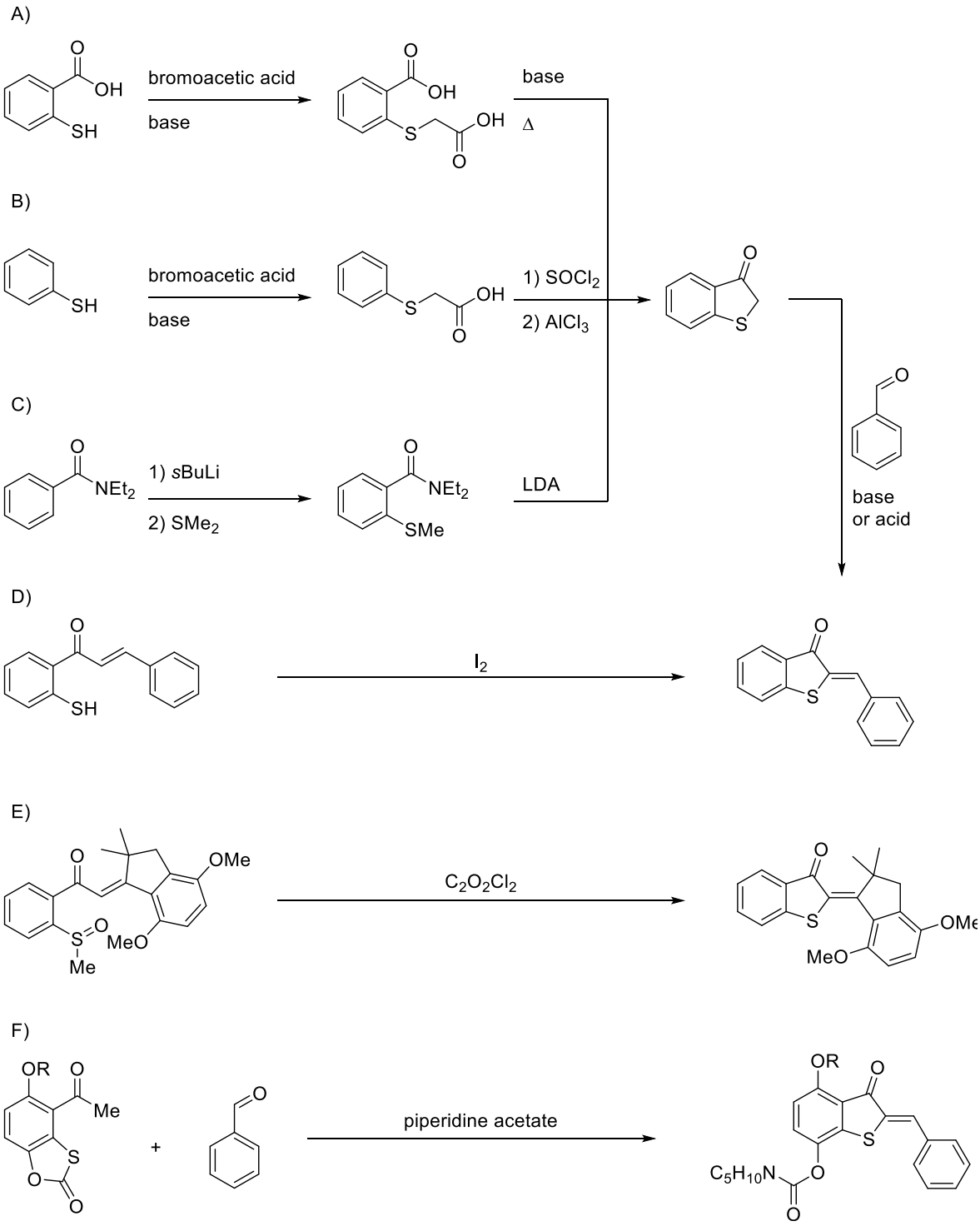

Figure 15: Different synthetic approaches towards HTI. A) Friedländer's original synthesis[130], B) improved synthesis by Friedel-Crafts acylation[131], C) synthesis by Mukherjee[133], D) synthesis by Zheng[134], E) synthesis by Huber[135], F) tandem reaction by Konieczny[136].

Compared to other photoswitches HTIs have only mediocre quantum yields and photochromism. However, they possess many advantages like visible light responsiveness in both switching directions, remarkably

high thermal stabilities of individual switching states, easy synthesis, many substitution possibilities, and a very rigid framework. In the last decades, many HTIs were intensively studied becoming by far the most used photoswitches in the indigoid photoswitch family. As for every other photoswitch different attempts to bathochromically shift the absorption to obtain a large photochromism were conducted. This is possible by introduction of push-pull substitution as well as by intramolecular hydrogen bonds. As HTIs already contain a pull substituent with the keto group only an electron rich substituent needs to be added. If the push-pull substituents are conjugated over the central double bond a large redshift can be observed but the thermal stability of the metastable isomers is drastically lowered.[148] Additionally, if the stilbene part is slightly twisted, these photoswitches show different photochemistry, as by formation of a twisted intramolecular charge transfer (TICT) state in polar solvents the *E*/*Z* isomerization is completely suppressed (Figure 16, left).[149] To avoid these drawback effects the electron rich substituent can also be introduced at the thioindigo part of the molecule (Figure 16, center).[148] By introducing a pyrrole an intramolecular hydrogen bond is formed in the *E* isomer, which also enhances the photochemical properties (Figure 16, right).[150]

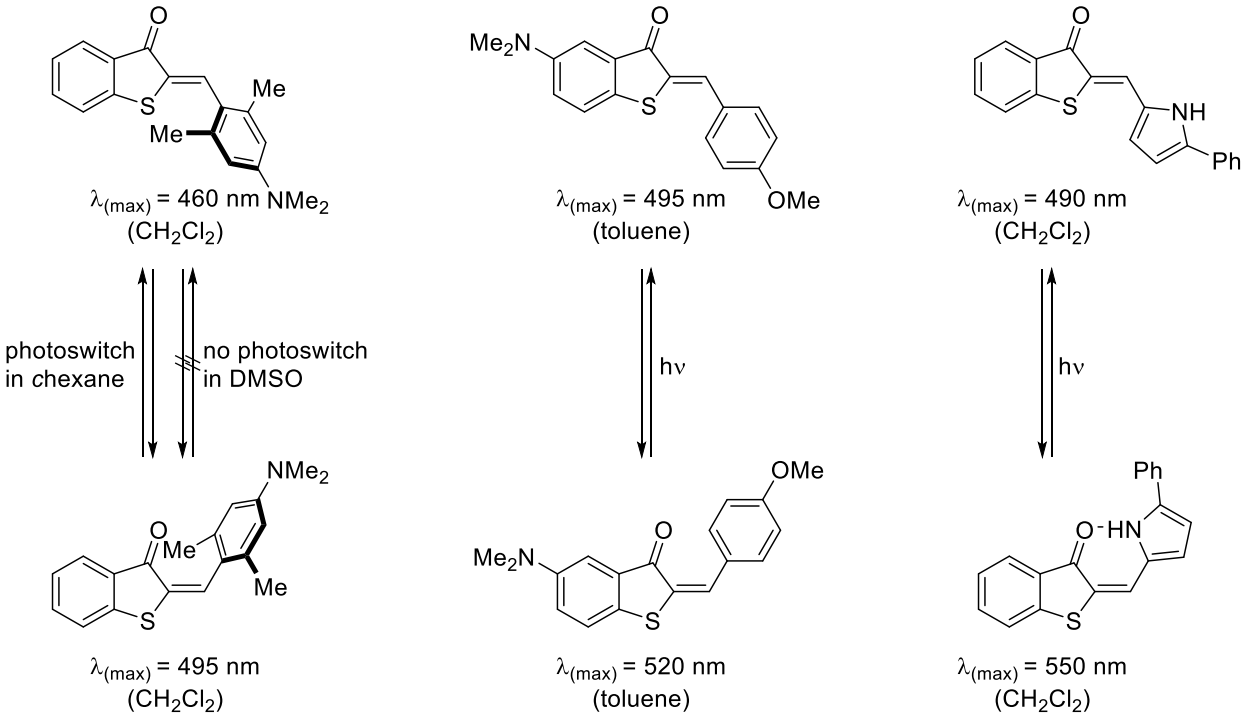

Figure 16: HTI photoswitches with extraordinary properties. Left: By introducing an electron rich substituent and twisting around the stilbene fragments single-bond another deexcitation pathway in polar solvents via a TICT state is accessible leading to no photoswitching.[149] Center: By introducing the electron donating substituent at the thioindigo part a redshift without loss of thermal stability is obtained.[148] Right: An intramolecular hydrogen bond leads to a larger redshift and better photochromism.[150]

Hemithioindigos were used in photopharmacology, e.g. as a photoswitchable lipoxygenase LOX-12/15 inhibitor[151], to control the endogenous cytoskeleton structure[152, 153], in β-hairpin peptides[154], in supramolecular chemistry as shuttles[155], guest molecules in capsules[156, 157], and as photoswitchable receptors.[158, 159]

2.5. Unusual photoswitching types in nature and in artificial systems

In nature a variety of photoswitches are present, for example retinal[160-164] (Figure 17), previtamine D_3[165-167], or *p*-coumaric acid.[168, 169] These photoswitches are in general much more complicated than their artificial analogs due to the variety of possible photoreactions. However, by embedding the photoswitch into an enzyme the photochemistry is controlled. Thus, all mammals use retinal as photoreceptor molecule, which is embedded within different mutations of the rhodopsin enzyme so that different colors can be seen with this single photoswitch.[170-178]

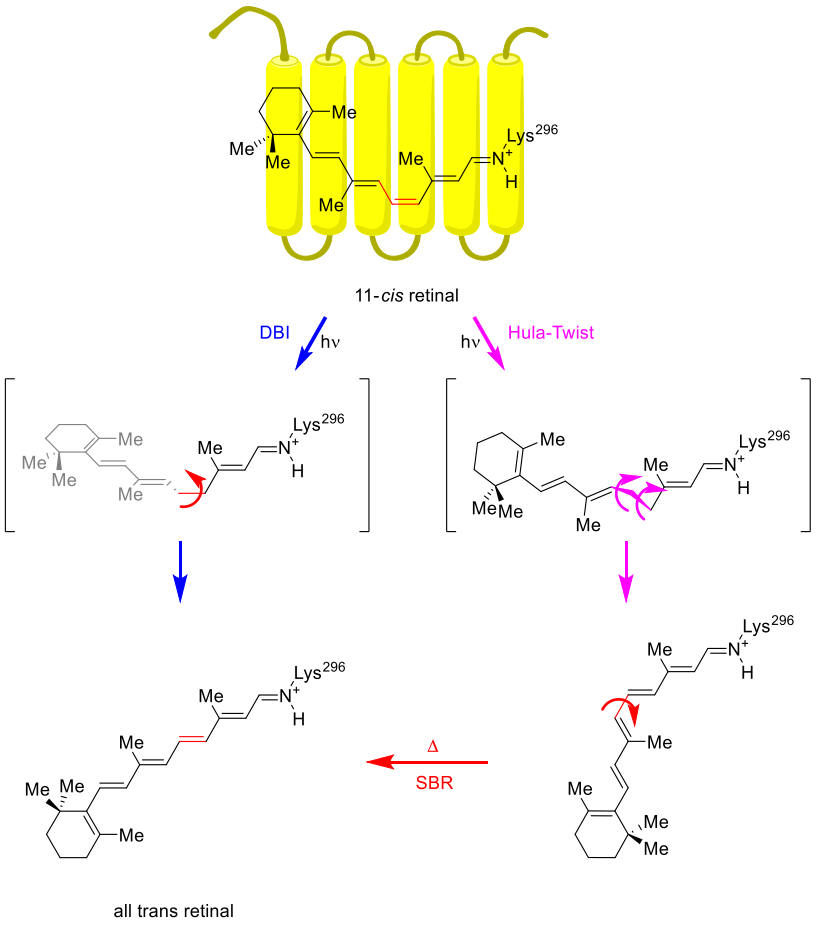

Figure 17: Hula-Twist (HT), single-bond rotation (SBR), and double-bond isomerization (DBI) as possible photoreactions of retinal.

In 1985, Liu and Asato proposed the Hula-Twist (HT) mechanism for the isomerization of retinal to explain how retinal can undergo extremely fast and efficient photoswitching despite being embedded in a confined protein environment. They argued that the normal DBI requires a large motion out of the plane, which can be circumvented by the HT mechanism in which the adjacent single bond rotates at the same time as the double bond. By this rotation only the CH group has to move out of the molecular plane. The HT reaction would lead to a thermally unstable rotamer, which is converted by fast thermal single-bond rotation to the final product.[179]

The HT reaction was subsequently discussed for various photoreactions[53, 166, 180-185] but as the primary photoproduct in all these examples is extremely unstable, their structures could never be unambiguously proven, which led to numerous discussions how the obtained spectral data (predominantly UV-Vis absorption and fluorescence) should be interpreted in terms of geometry.[165, 186, 187] This is also the case for the isomerization mechanism of retinal, although at the current state the HT mechanism can almost surely be excluded by time resolved Raman spectroscopy analysis[188] and femtosecond X-ray crystal structural analysis[52] revealing that a DBI with a twisting along the whole retinal backbone is more likely. For the fast and efficient photoisomerization, a special vibration of the hydrogen atoms at the isomerizable double-bond called HOOP is held responsible, in which both hydrogens move in opposite directions.[188-190] Based on the HOOP model, an artificial *E*/*Z* photoswitch inspired by retinal was designed by Olivucci and coworkers. However, the performance of the artificial switch is comparable to other artificial switches and does not reach the high quantum yield and fast photoisomerization properties of retinal.[191]

Sole single-bond rotations can also be induced by light, but only a few examples are reported and to the best of my knowledge no photoswitches based on different atropisomers are used so far.[192-195]

2.6. Multi-state photoswitches

Most photoswitches, except a few cases like fulgides, undergo reversible changes in conformation or configuration alternating between two different states upon irradiation with light. This property is typically used for on/off switching of a myriad of applications allowing the control of different events at the molecular scale, which were already described above.[196-205] Fulgides can undergo *E*/*Z* photoisomerization as well as photo-electrocyclization and therefore possess three switching states (Figure 18). They are an example for how to surpass the binary behavior of typical photoswitches. However, fulgides are not typical multi-switch systems, in most cases multiple individual photoswitches are combined into a single molecule. In these cases, either the same or different types of photochromic switches are linked covalently or through coordination to metal centers.[206-211] These approaches were realized with the well-known photoswitches azobenzene[212-220], diarylethene[221-227], and spiropyrane[228] and also with the hemithioindigo (HTI) chromophore.[229] In Figure 18 examples for multi-switching photoswitches are shown.

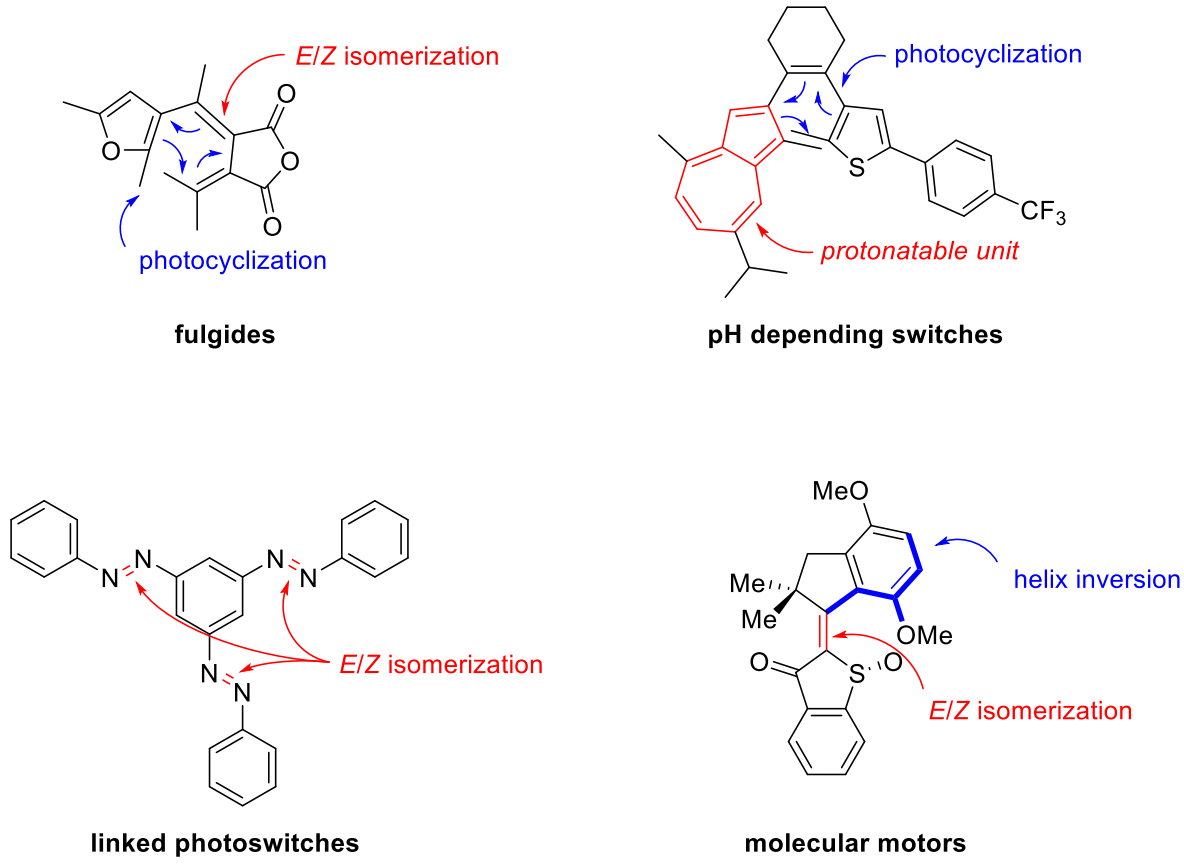

Figure 18: Examples for multi-state switches. Fulgides with three states. A diarylethene pH-gated switch with four states, a triple azobenzene with four states and an HTI motor as an example for molecular motors with four states.

As in fulgides and linked photoswitches the trigger for every switching event is light, it is problematic to design orthogonal switching systems, in which different defined isomerization states are obtained in the PSS

at different wavelengths. Thus, other triggers are used in many cases to enable the realization of multiple states. The most common orthogonal trigger to light is pH modulation. In Figure 18 a pH-sensitive diarylethene switch is shown. In the deprotonated form (shown in Figure 18) the cyclization quantum yield is low, upon protonation a new state is obtained, which can undergo efficient photocyclization. The cyclic form can be deprotonated again to reach the fourth state. Also, other photoswitches like spiropyrans and HTIs can be turned into multi-state switches by protonation and deprotonation.[230, 231] Photon driven molecular motors[47, 48], usually with four different diastereomeric states, are multi-state switches as well and often used in the latter regard and not in their unique capacity to move unidirectionally.[232, 233] For example, the Feringa group used an molecular motor as a molecular receptor for chloride ions in enantioselective catalysis with the different states of the motor as shown in Figure 19.[234] While in the open *E* form the substitution reaction of a chloride with a protected enolate is catalyzed with no enantioselectivity, the *Z-M* conformation catalyzes the formation of the *R*-product and the *Z-P* conformation favors the formation of the *S*-product.[234] The advantage in applications of this type of multi-state switches over the linked multi-switches is unequivocally the precise spatial control as the central double bond is the only modifiable part. However, as the helix inversion is a thermal ratcheting step, the isomerization is only possible in one way. This advantageous behavior with regard to unidirectional movement may therefore restrict motor applications as multi-state switches as the different isomers cannot be populated in an arbitrary order. Rotaxanes[54, 235-238] are another example for multi-state switches with precise spatial control, but as they represent large multicomponent assemblies they are not be discussed in this introduction.

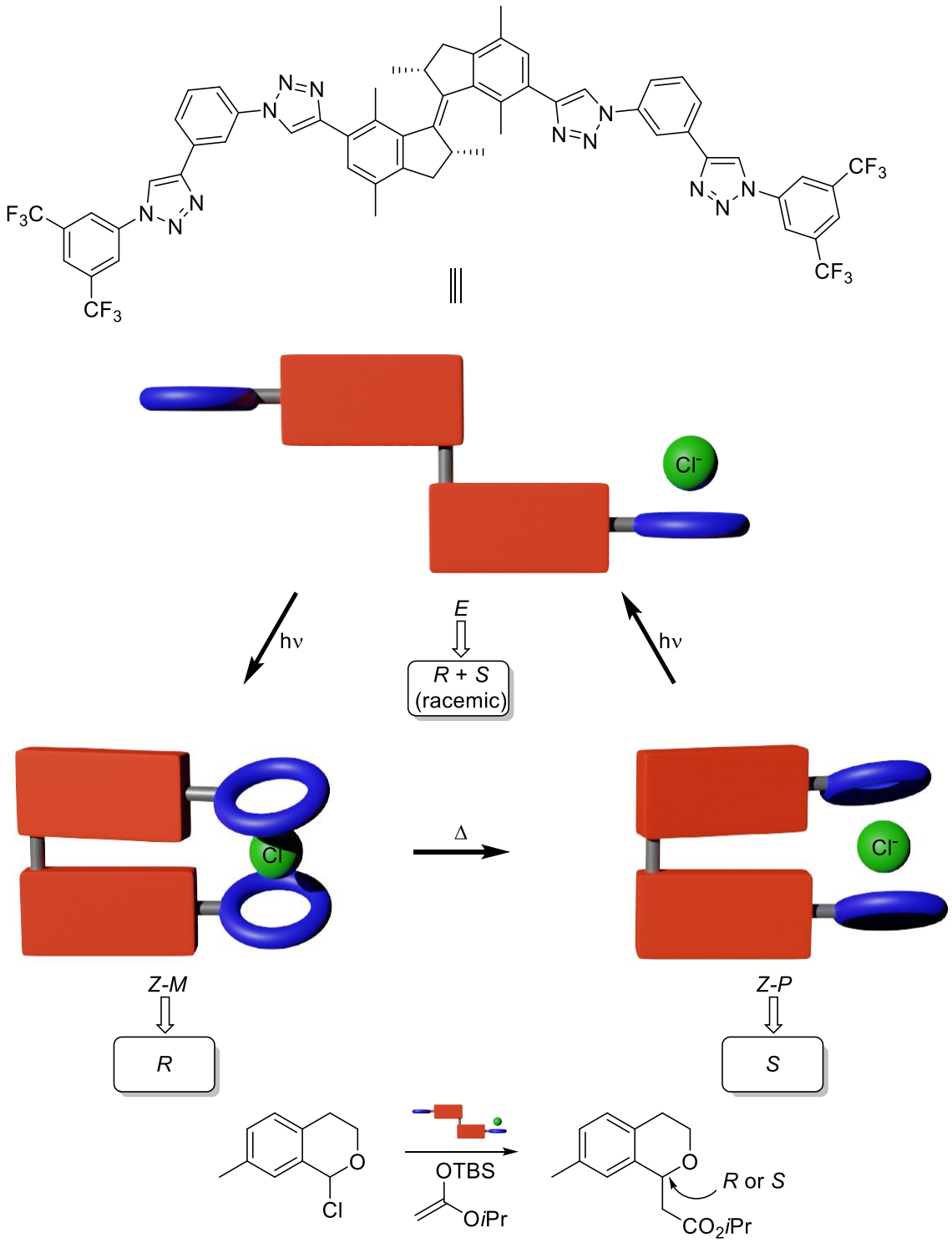

Figure 19: Stereodivergent catalysis of a substitution reaction with a molecular motor with three states.[234]

2.7. Molecular Motors

A special form of multi-state photoswitches are molecular motors, in which the states are populated in a fixed order resulting in a directional movement. In contrast to switches, a molecular motor does not undo its work by switching backwards to its original state. Therefore, molecular motors are able to provide a constant energy output and are a main research field in the development of molecular machinery. In 2016 Ben L. Feringa[239], Jean-Pierre Sauvage[57] and Fraser J. Stoddart[56] were rewarded with the Nobel Prize for their pioneering research in molecular machinery.

2.7.1. Design principles of molecular motors

The history of molecular motors dates back to Richard Feynman who presented in 1959 ideas for the development of molecular machines in an innovative lecture.[240] The "thought machine" called Smoluchowski-Feynman ratchet was inspired by a macroscopic heat engine that has to obey the same laws of physics (Figure 20).[241, 242]

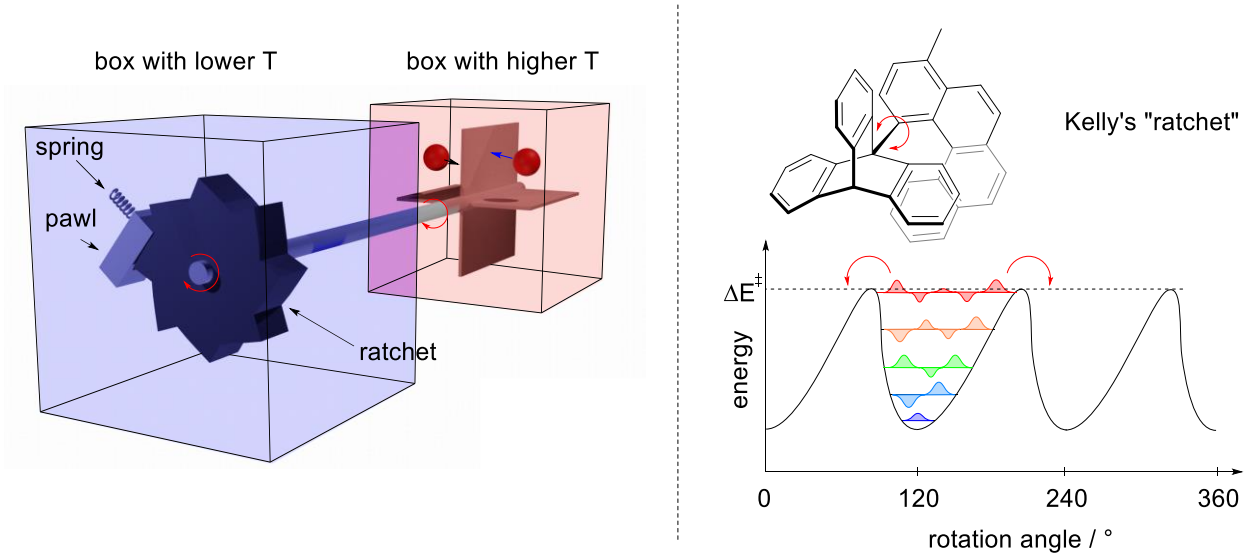

Figure 20: Smoluchowski-Feynman ratchet (left) and Kelly's ratchet (right). In the Smoluchowski-Feynman "thought machine" a ratchet in one box (blue) is connected by an axle to vanes in another box with higher temperature (red). Random Brownian motion leads to collision of molecules with the paddle wheels. If a molecule hits the paddles from the back (black arrow) the ratchet can rotate clockwise. If a molecule hits the paddles from the front (blue arrow) the pawl blocks the counterclockwise rotation. By the unidirectional rotation, the heat from the red box is transferred to the blue box until both boxes have the same temperature and the unidirectional rotation stops. [241, 242] Kelly tried to construct a molecular ratchet based on a macroscopic ratchet (right). But as molecules follow the laws of quantum mechanics, it is impossible to construct a thermal ratchet as the shape of the energy barriers is irrelevant and only the activation energy determines the rotation direction.[243]

The Smoluchowski-Feynman obeys the laws of classical mechanics, especially the second law of thermodynamics, and is therefore functioning theoretically. A few rules for the construction of molecular motors can be derived from this thought experiment: A constant energy supply is necessary to power the rotation, all other degrees of freedom should be suppressed, and an asymmetry is necessary to determine the

rotation direction. However, construction of the Smoluchowski-Feynman ratchet on a molecular level is not possible. Molecules follow the rules of quantum mechanics rather than classical mechanics and a construction of a ratchet, which blocks the rotation in one way without external manipulation of the system is impossible. To illustrate this, Kelly designed the "ratchet" molecule, which is shown in Figure 20.[243] Although the shape of energy barriers is asymmetric, rotation occurs in both directions with the same probability as the energy barriers have overall the same height.

The design of barriers alone is therefore not suitable to create a molecular motor. A more successful approach is the design of the energy minima, as molecules will always preferably populate the state with the lowest energy according to the Boltzmann distribution.[244] However, to build up a gradient an external energy input is necessary. In general, this is done in two ways: the molecules are "lifted" in a higher state on another way than the thermal decay or the energy surface is modulated in the desired way to enable unidirectional movement. Both possibilities are shown in Figure 21.

Molecules will always follow the thermodynamic gradient to their most stable state, if the activation barriers to reach this state can be overcome at the surrounding temperature. But after the equilibrium is reached, the forward and backward reactions have the same speed and no net flux is observed anymore. To bring the system out of equilibrium again an energy supply is necessary to increase the population of the less stable state again. To not undo the movement of the thermal decay, the population of the unstable state must take place by another way. Therefore, another energy input than heat is needed, which could be light or chemical energy. The modulation of the population is the design principle of motors, which rotate around one bond and use - in most cases - light as fuel.

Another way to obtain a molecular motor is to modulate the energy surface while the movement takes place, so the molecule always follows the thermal decay to the next most stable state. This is the general design principle of rotaxane or catenane based motors. By stepwise modulation of the binding areas (Figure 21, marked in red) of the macrocycle (Figure 21, marked in blue) an unidirectional movement of the macrocycle is obtained. Alternatively, the barriers to reach the next binding areas can be modulated. Typically, the changes in the energy surface are introduced chemically but also light as a trigger can be used.

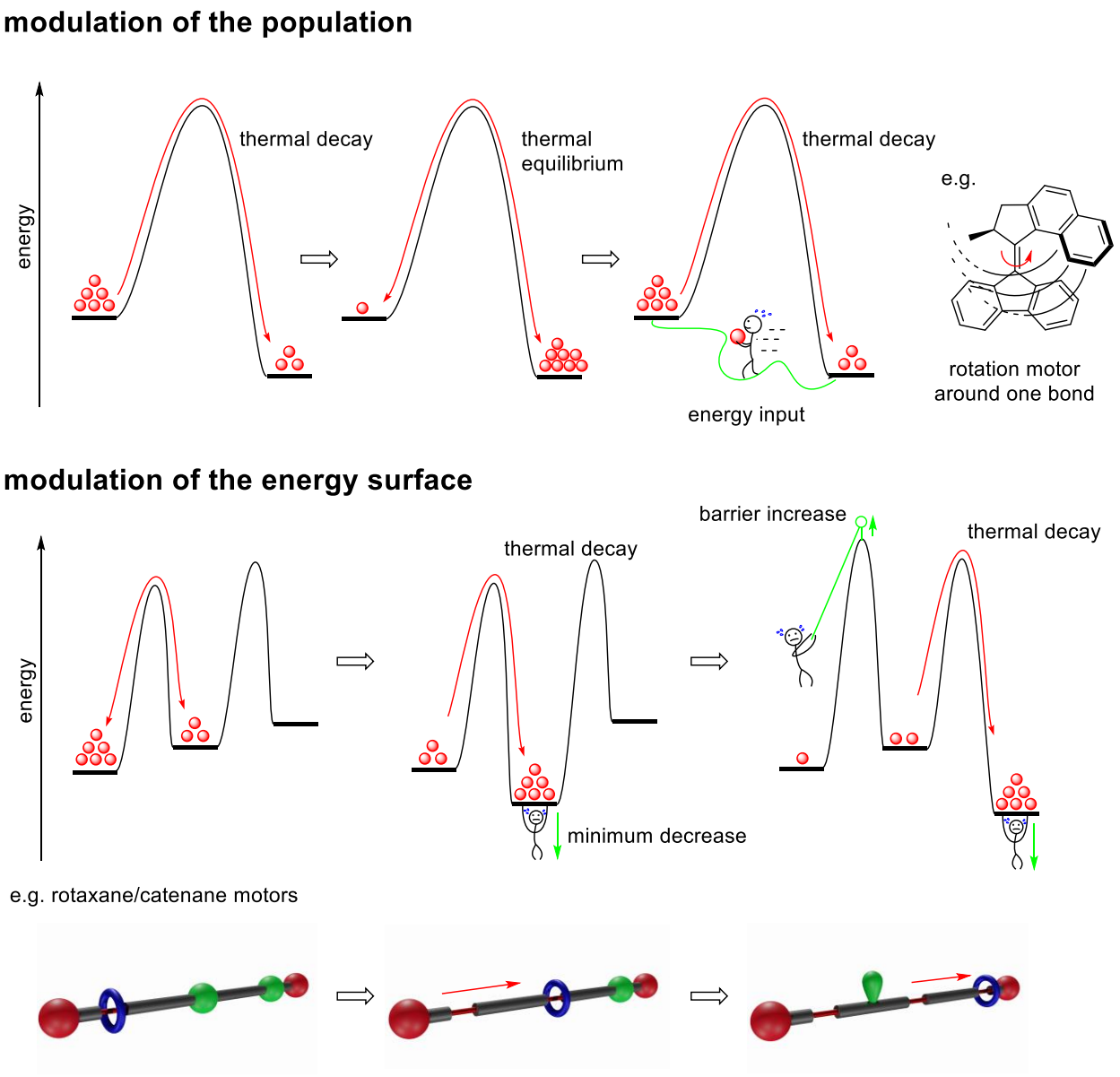

Figure 21: Design principles for molecular motors. External stimuli are illustrated by stickmen and green colors. Thermal processes are shown in red and take place by Brownian motion.

2.7.2. Feringa motors

In 1999 Feringa and coworkers reported the first light driven molecular motor, which exhibits the discussed design principles presented above. The molecular motor is shown in Figure 22 with its rotation cycle. It is based on a stilbene photoswitch with two stereocenters and a sterically induced helicity. The carbon stereocenters are permanent and do not change during the rotation. They are responsible for the rotation direction. The *E*/*Z* configuration as well as the helix configuration is flexible and therefore the molecule can exist in four different diastereomers. Isomer **A** can be photoisomerized to isomer **B** by *E*/*Z* photoisomerization. As the rotation is less than 180° an unstable helical geometry is formed. Subsequently

isomer **B** is transformed by a thermal helix inversion (THI) step to the more stable isomer **C**. As isomer **B** is thermally decaying it cannot undergo a photochemical backwards reaction to isomer **A**, thus the nonsymmetric energy surface is responsible for the sequential population of the isomers. A second light induced isomerization from **C** to **D** also delivers an unstable helical geometry, which is again converted by a thermal step into the most stable starting isomer **A**.[47]

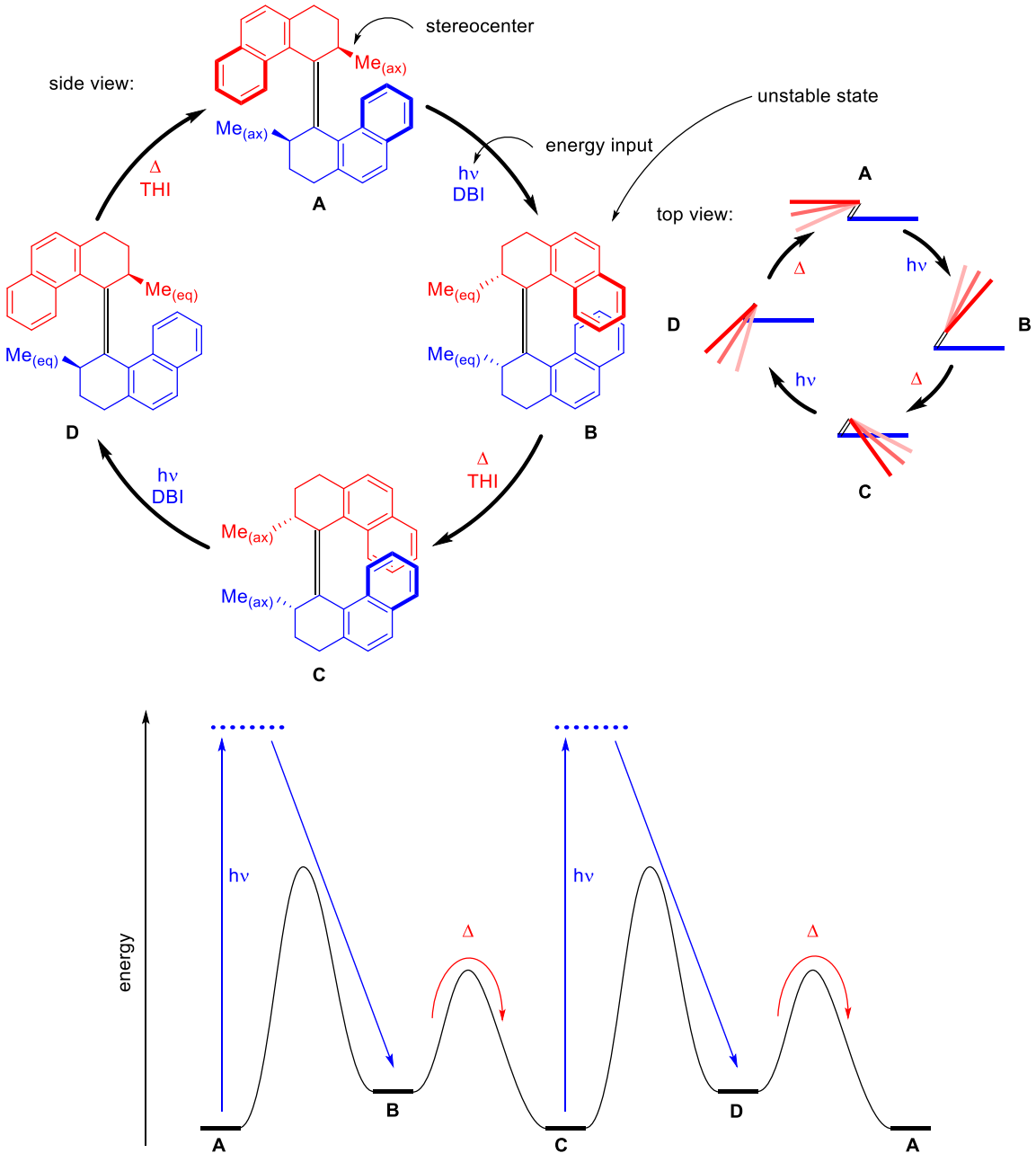

Figure 22: First light driven molecular motor by Feringa and coworkers.[47] The motor can adopt four possible diastereomeric states, which are populated consecutively by alternating thermal and photochemical steps. To visualize the rotational movement the motor is shown from the top with rotating rotor part in red. The movement of the rotor part is indicated by fading color. The prerequisites for a molecular motor are shown: the presence of a permanent stereoinformation and the energy input to reach a thermodynamically unstable state. At the bottom the sketched energy profile of the motor is shown. DBI = double bond isomerization, THI = thermal helix inversion.

The directionality is controlled in every step by the permanent carbon stereocenters. They dictate which helix is the most stable and by the induced pre-twist of the central double bond the photoisomerization direction is determined. The energy barriers for the THI steps for the first Feringa motor are relatively high and helix inversion proceeds slowly at temperatures above 60°C. But without helix inversion the motor turns into a switch as **B** cannot further isomerize to **C** but photochemically returns back to **A** again. The speed and efficiency of the motor is therefore very dependent on the operating temperature. In addition, harmful UV-light is necessary to power the motor. Therefore, in the following years a lot of improvements for the Feringa motor were published to lower the energy barriers for THIs [245, 246] and to obtain derivatives with redshifted absorption.[247, 248] They are classified in three generations, which are distinguished by differences in the installed stereoinformation.[249-251]

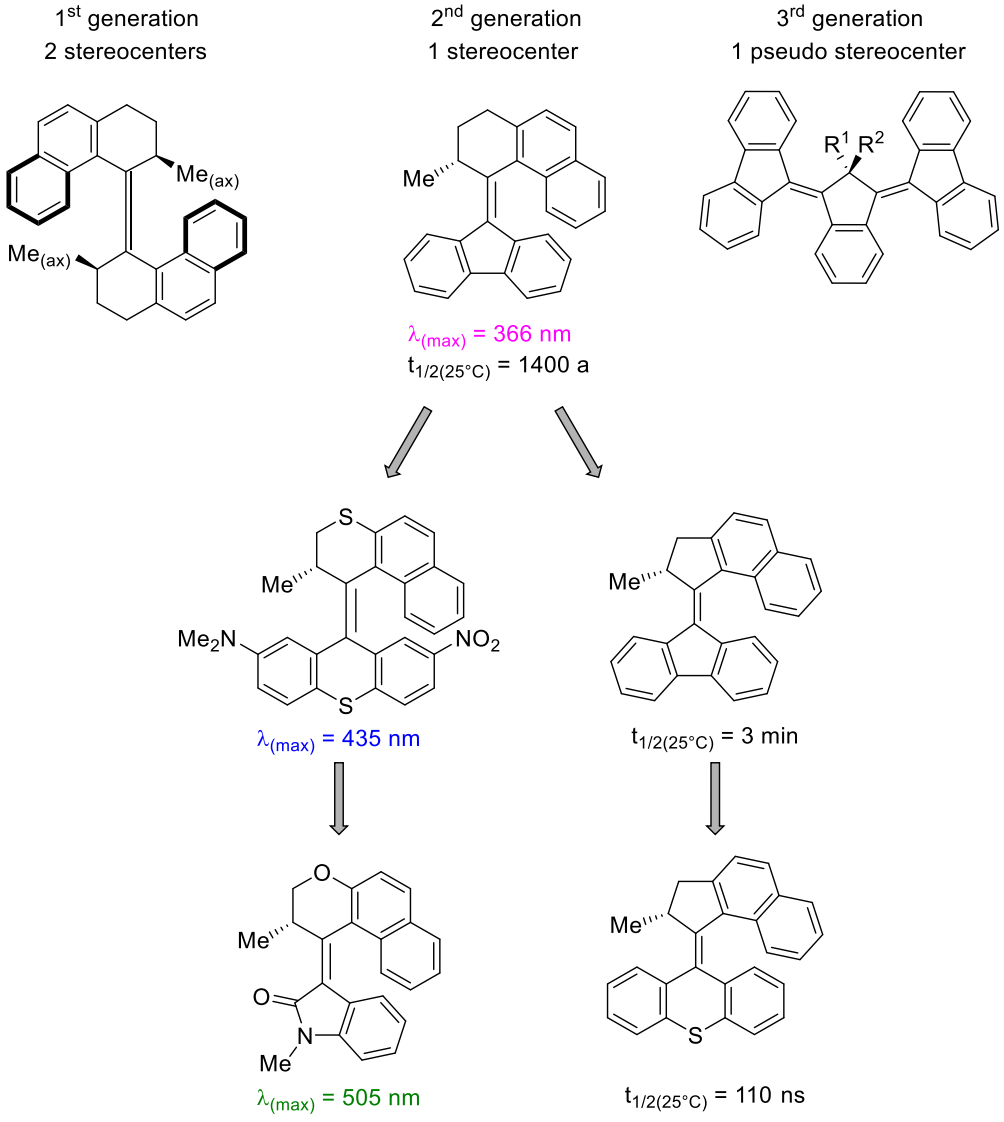

Figure 23: Development of Feringa light driven motors. The generations are distinguished by the type of introduced stereoinformation. The most common version is the 2nd generation with a lot of examples and improvements like the redshift of absorption or the tuning of thermal half-lives, which are shown for a few examples.[245-251]

By lowering the THI energy barriers, thermal half lives in the nanosecond regime at room temperature could be obtained. Therefore, rotation speeds in the MHz regime were suggested to be possible.[246] However, these rotation speeds are hard to achieve practically as the required light intensities for such rotation speeds would likely evaporate the sample. Therefore, for motors with fast thermal steps the light induced steps become the rate limiting component, with realistically obtainable rotation speeds in the low Hz regime.[252] To control the energy barriers of THI steps directly during operation, derivatives which can bind metal ions were used.[253, 254] In a similar approach the binding of an ammonium ion to a crown ether was employed to stop the rotation completely.[255] To obtain control of the rotation direction the stereocenter could be switched during operation with an amide derivative after deprotonation.[256] Another approach to dictate the rotation direction is the use of a symmetric photoswitch, which is turned into a motor by complexation of a chiral ligand. Therefore, the configuration of the ligand dictates the rotation direction.[257]

Transfer of the motor motion to other molecular parts or to macroscopically visible effects is extremely challenging and only a few first examples are reported. In 2017 the Feringa group reported a motor system in which a naphthyl rotor is attached near the isomerizable double bond (Figure 24). During the motor operation the naphthalene rotor rotates as well to always face the same side of the motor.[258] Also the Dube group reported a molecular system allowing to remotely drive the rotation of a biaryl. This system is presented in Chapter 2.7.4.

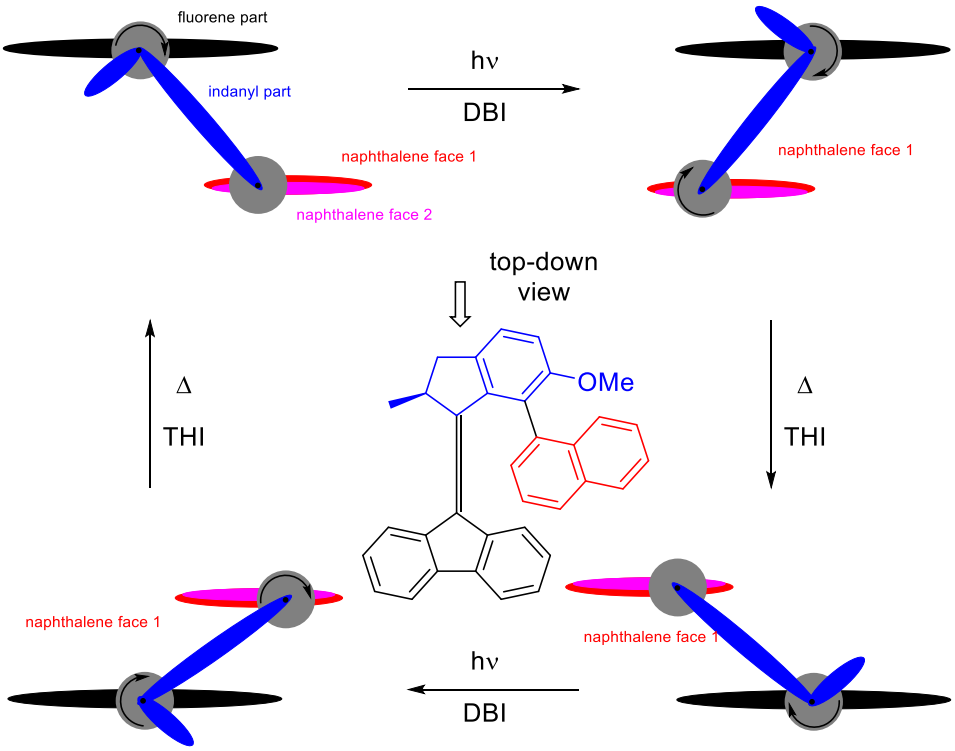

Figure 24: Locked synchronous motion of a molecular motor with a naphthalene rotor by the Feringa group. DBI = double bond isomerization, THI = thermal helix inversion.[258]

Transfer of the rotation of molecular motors to macroscopically visible effects were also investigated by the Feringa group. Molecular motors were added as dopant to liquid crystal films with a little glass rod mounted in the film. Under irradiation, rearrangement of the crystal film was observable, and the glass rod started to rotate. However, after reaching the PSS the rotation stops and the same effect was observable by using a chiral photoswitch as dopant.[259, 260] Therefore, the unidirectional rotation of the motor seems not to be important for the observed rotation of the rod but the chiral reorganization after photoswitching of the liquid crystal. The group of Guiseppone successfully used the unidirectionality of the motor to shrink a macroscopic gel. They connected PEG chains to the motor were winded up by rotation of the motor, resulting in a macroscopically visible shrinking of the PEG gel.[261-263]

2.7.3. Lehn's imine motors

In 2014 the group of Jean-Marie Lehn reported a new class of molecular motors based on imines. The first derivative (shown in Figure 25) follows a similar working mechanism as Feringa's motors with alternating photochemical DBI and thermal helix inversion.[264]

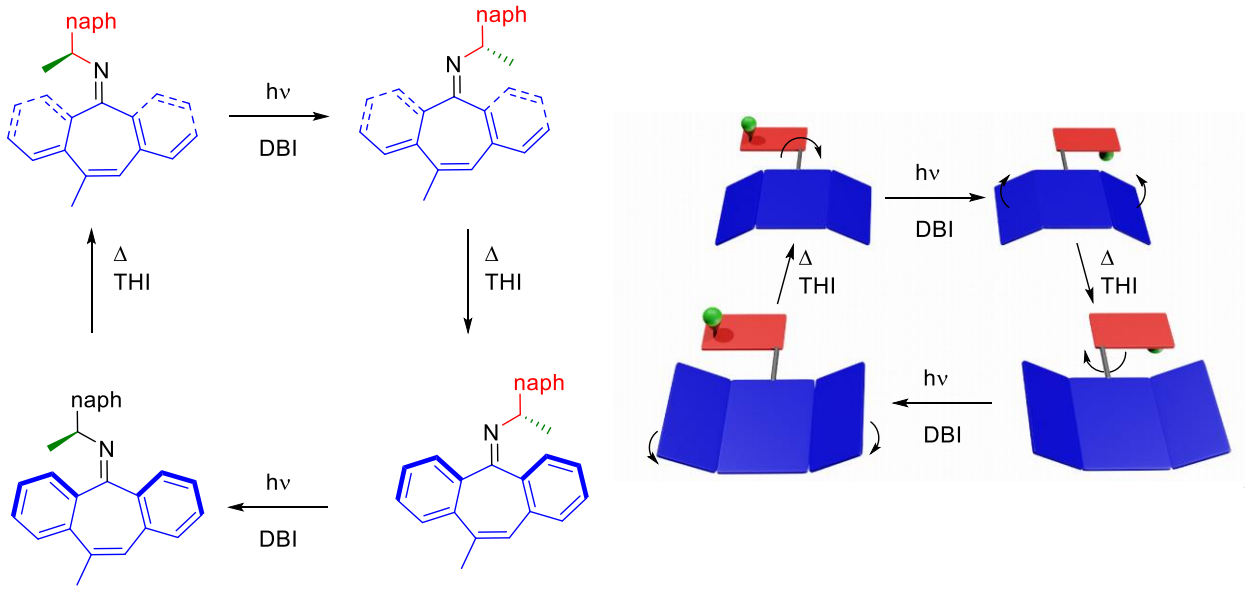

Figure 25: Imine based molecular motor by Greb and Lehn. Left: Lewis structures of the rotation cycle. Right: Simplified visualization to follow the rotation. The color code represents the different parts of the motor. DBI = double bond isomerization, THI = thermal helix inversion.[264]

The second reported derivative has a very high barrier for the THI, which cannot be overcome under the experimental conditions. Instead, a thermal imine bond isomerization occurs. Quantum chemical calculations reveal that this isomerization proceeds via an N-inversion pathway. As the photoisomerization occurs by rotation of the C-N double bond and a large motion out of the plane is necessary, the

photoisomerization motion and the thermal motion do not cancel each other out and a two-step motor with a new working mechanism was obtained. This motor is shown in Figure 26 with the ellipsoid shape rotation around the central CN double-bond.[264]

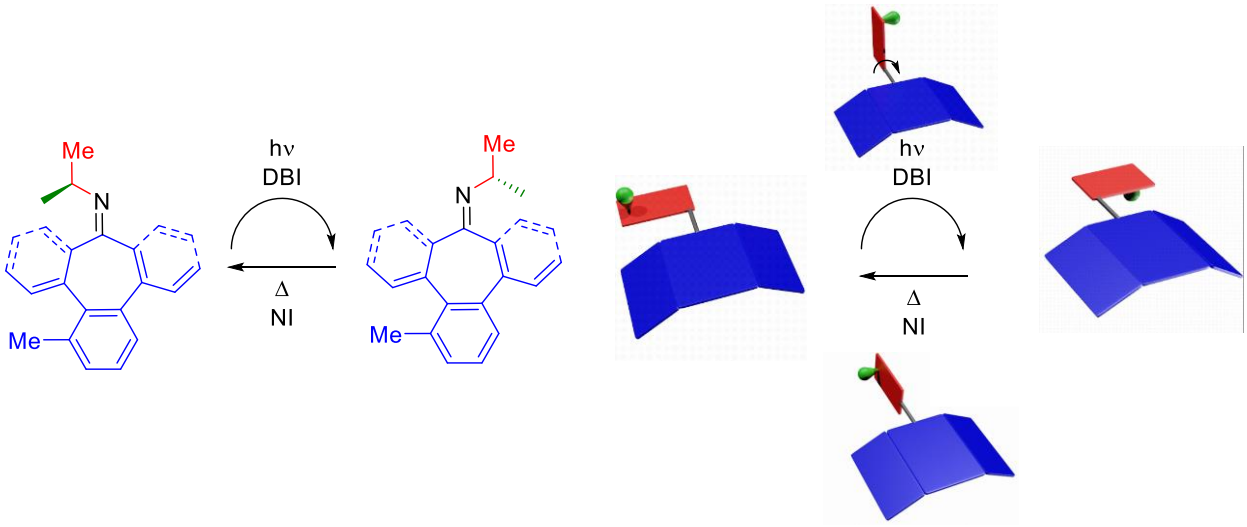

Figure 26: Two-step motor by Greb and Lehn. Left: Lewis structures of the rotation cycle. Right: Simplified visualization to follow the rotation. The color code represents the different parts of the motor. DBI = double bond isomerization, NI = nitrogen inversion.[264]

In 2015 other imine-based motors with camphorquinone scaffolds working with the same rotation mechanism were reported. The rotation cycle of these derivatives could be unambiguously proven by trapping experiments of the transition states.[265] In comparison to the Feringa motors, imine-based motors are much easier to synthesize, but they also require UV-light for isomerization and the chemical stability of imines is generally not very high.

2.7.4. Dube's HTI motors

In 2015 our group reported an HTI based molecular motor operating with the same alternating DBI and THI rotation mechanism as Feringa's motors.[266] The HTI framework offers many interesting possibilities. The chromophore itself is already absorbing visible light, the synthesis is relatively simple and straightforward introduction of the permanent stereoinformation is possible at the late stage by oxidation of the sulfur. The HTI motor with its rotation cycle and energy profile is shown in Figure 27.

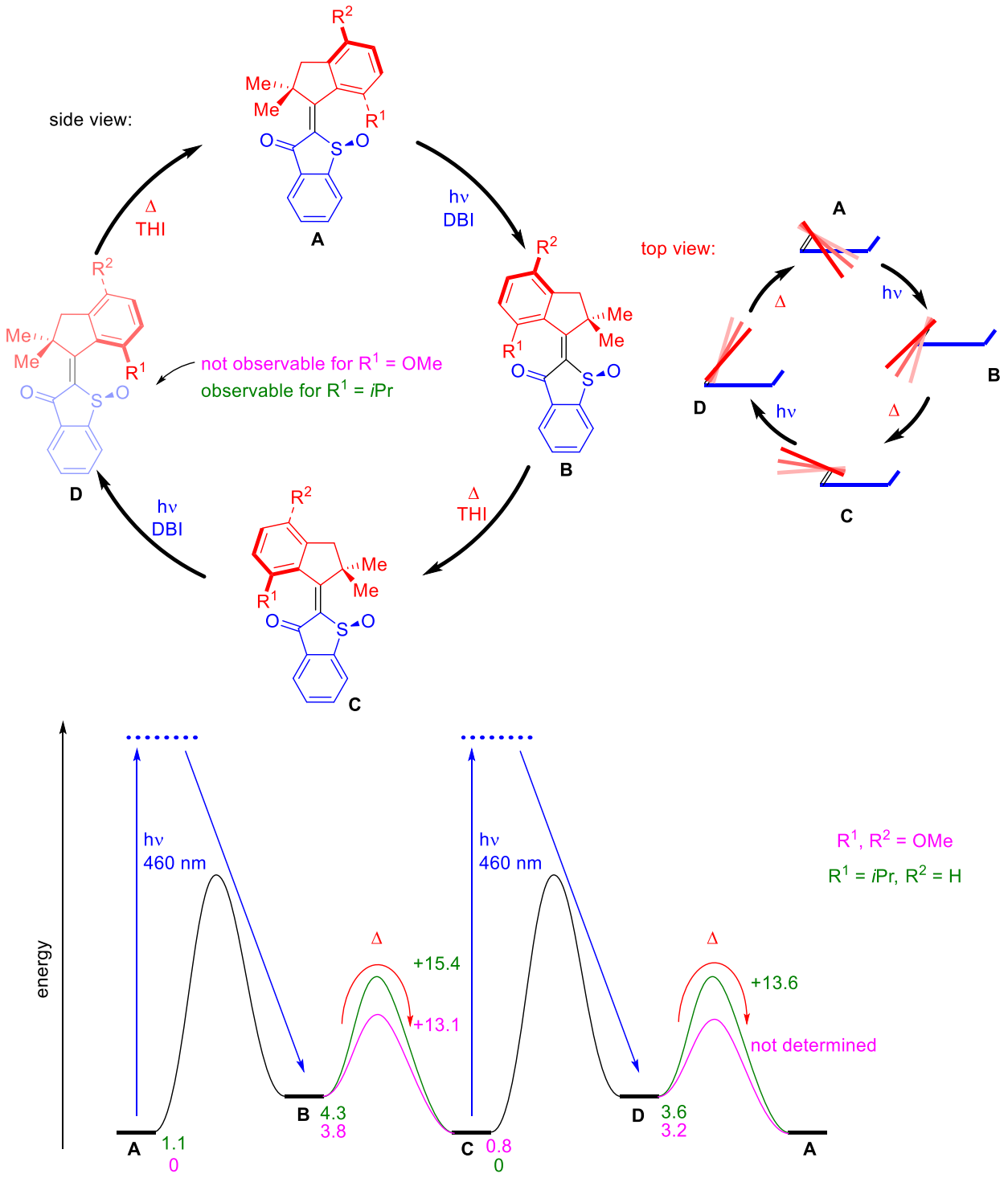

Figure 27: HTI-based motors by the Dube group. The rotation cycle is shown as Lewis structures and as top-down view. The movement of the rotor part is indicated by fading color. For the first motor derivative bearing two methoxy groups as R^1 and R^2 (pink) state **D** could not be observed experimentally as the THI from **D** to **A** has such a low barrier that **D** is converted immediately to isomer **A** even at -90°C. For a derivative with R^1 = *i*Pr and R^2 = H (green) the barrier was increased and isomer **D** was observed. Therefore, the unidirectionality of the motor was proven. In the lower part, the energy profile of both derivatives is shown. The minimum energy values were obtained on the MPW1K/6-311G(d,p) level of theory, the activation energies for THI were obtained experimentally. All values are given in kcal·mol^{-1}.[266]

The first HTI motor bearing two methoxy groups as R^1 and R^2 (see Figure 27) show very low activation barriers for the HTIs, resulting in very fast thermal steps (faster than 1 ms at 25 °C). Thus, already the first derivative possessed similar thermal properties as the fastest Feringa motors (chapter 2.7.2) and a tuning of the thermal steps for better motor performance was not necessary.[266] However, the extremely fast THI from isomer **D** to **A** prevented the observation of isomer **D** and the whole unidirectional rotation cycle could not be elucidated fully experimentally. In 2017 a new version of the motor was presented with R^1 = *i*Pr and R^2 = H substitution. The larger *i*Pr group increases the energy barrier for the THI allowing the observation of the **D** isomer and therefore the unidirectional rotation of this class of HTI based motors was directly proven.[135] Later the unidirectional rotation cycle was also confirmed for the original HTI motor by quantum chemical calculations of the excited state and ultrafast transient absorption measurements.[76]

For the next stage our group focused on the development of applications for the HTI motors, like the attachment on a gold surface.[267] A breakthrough in the transduction of the work from a molecular motor was the unidirectional acceleration of a biaryl rotation by connecting the biaryl into a macrocycle with the motor.[268, 269] The system is depicted in Figure 28.[268] The cycle starts at state **A**, which isomerizes under irradiation in a DBI to state **B**. **B** undergoes THI to state **C** and the motor therefore performs a 180° rotation as already presented for the plain motor derivative. In state **C** the macrocycle is stretched as the biaryl is not directly following the THI. Therefore, state **C** represents a tense state with "spring loaded" macrocycle. The subsequent thermal biaryl rotation (TBR) of the remote biaryl releases the strain and establishes state **D** and does so with significantly faster kinetics as compared to the control compound lacking the macrocyclic structure Thus, the biaryl rotates around 180° in the same direction as the motor in an actively accelerated fashion. State **D** is again photoisomerized to state **E**, which is converted by THI to state **F**. **F** is again a tense state with "spring loaded" macrocycle, which releases the strain by TBR to reach the starting point **A** again. Hence, a complete rotation of the motor and the biaryl in the same direction is completed. The energy profile reveals, why the transduction of the motor motion to the biaryl is possible. The photochemically obtained states **B** and **E** are highest in energies and by THI to **C** and **F**, respectively, the energy is lowered although this results in a strained macrocycle. By TBR this strain is released, and the energetically favored states **A** and **D** are formed. If the strain of the macrocycle or the energy of the TBR product would be higher than the energy of the photoproduct, the further unidirectional rotation would not be possible as the thermal sink states **A** and **D** would not be populated. This would result in a stop of the rotation as isomers **A** and **B** as well as isomers **D** and **E** would be in photo equilibrium without thermal follow up reactions. The maximum force the motor can transmit before the rotation stops is therefore the energy difference between the helix states. In this case 72%, corresponding to about 1.5 kcal/mol of the motor power is used to enable the unidirectional rotation of the biaryl.

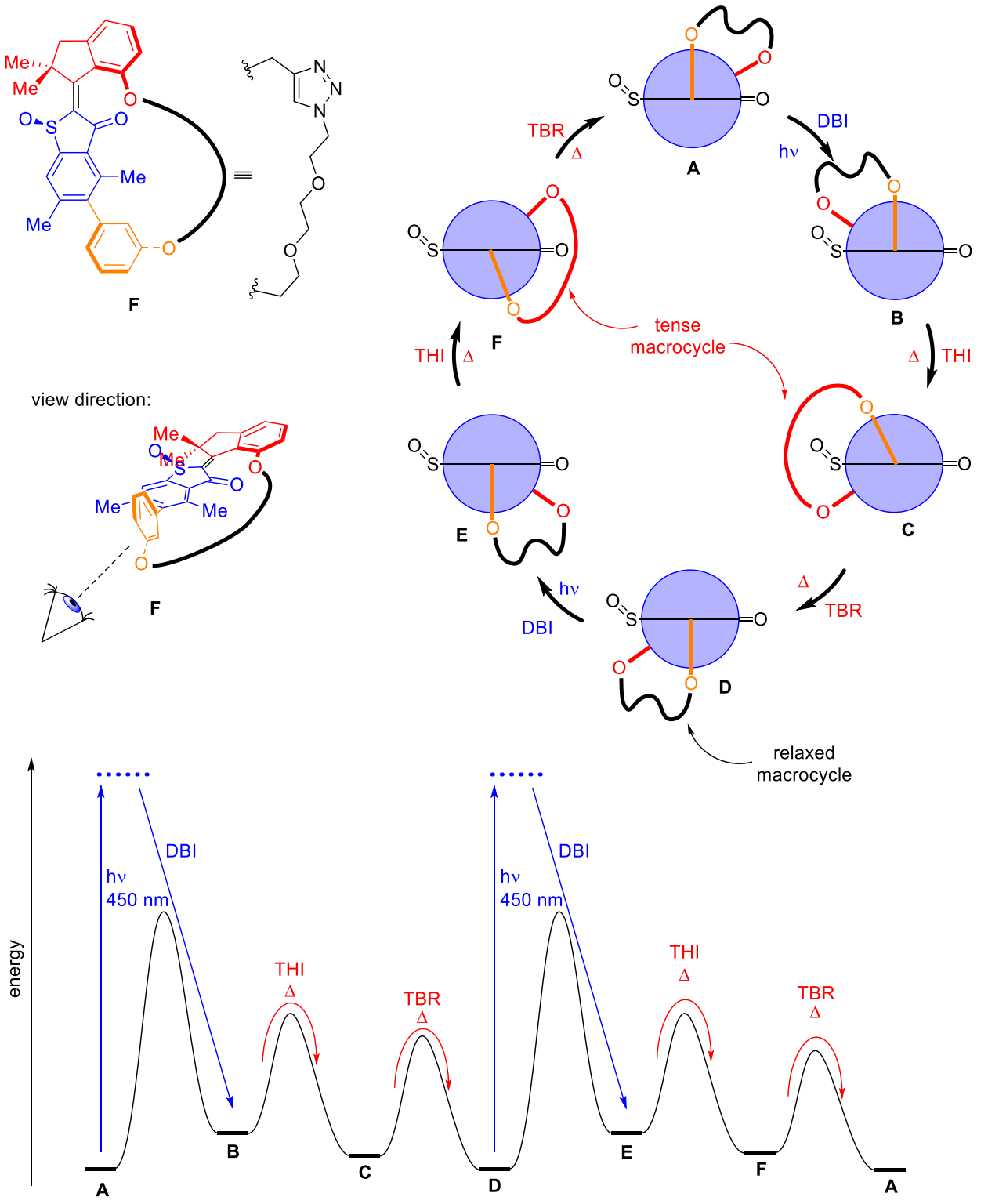

Figure 28: Motor system, which accelerates the biphenyl rotation around a remote axis. The motor system is depicted in the **F** state as Lewis structure. The rotation cycle is visualized by an edge-on-view along the central HTI axis. From state **A** a photochemical double bond isomerization (DBI) to state **B** occurs. **B** undergoes thermal helix inversion (THI) to state **C**. In state **C** the macrocycle is stretched, which results in an accelerated thermal biaryl rotation (TBR) to release the strain. This is repeated for another 180° to reach the starting point. In the lower part, the energy profile is depicted. The TBR is possible as by release of the macrocycle strain the TBR product (**D** and **A**) are lower in energy than the strained states (**C** and **F**).[268]

3. Objective

In the introduction several multi-state molecular switch and molecular motor architectures are presented. However, they are usually based on the simple combination of different switches that are covalently bound together. The aim of this thesis is the development of multi-state switches and motors in which the switchable bonds are as close together as possible to obtain simple and small nanoscale devices. The development of the switches is shown in Figure 29.

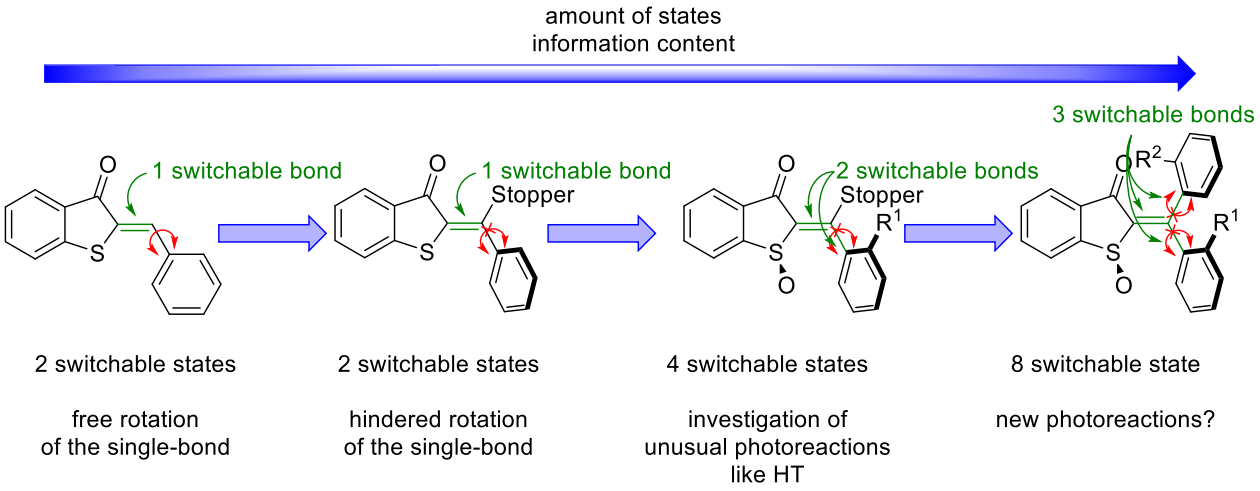

Figure 29: Design of multi-state switches based on HTI, by introducing steric hindrance, atropisomers and sulfoxidation. HT = Hula Twist.

By increasing the steric hindrance of the single-bond directly adjacent to a double-bond the rotation of this single-bond at ambient conditions is suppressed. It is thus possible to use single bond rotation for the establishment of geometrical changes in the molecule by e.g. atropisomerizations. Therefore, two switching pathways are obtained: the double-bond rotation and the single-bond rotation, which together enable a "high-density multi-state switch". However, these switching pathways are not necessarily independent from each other, they can switch in a consecutive as well as simultaneous manner. The simultaneous switching of a double-bond and the adjacent single-bond was already discussed for some naturally occurring photoswitches like retinal or previtamin D_3 and is called Hula-Twist (HT). But as these natural switches encounter very low energy barriers for their thermal SBRs, the HT photoproduct could not be unambiguously proven. HTIs are the ideal photoswitches to obtain the described bonding situation – one rotatable double bond with one adjacent rotatable single bond – as two single-bonds adjacent to the double-bond are locked in the benzothiophenone ring. This leaves the single bond connecting to the stilbene fragment as option to introduce switching capacity via its rotation. This is most straightforwardly done by introducing a chiral aromatic moiety, which establishes the single bond as a chiral axis and

atropisomerization as switching mechanism. If the atropisomization energy barrier is high enough both atropisomers are stable at room temperature and as a result four different states – two different atropisomer per *E* or *Z* configuration of the double bond result within a single small switching architecture. If additionally, the sulfur is oxidized to obtain a permanent stereocenter the atropisomers become diastereomers and can be spectroscopically distinguished. With the obtained four-state photoswitch the investigation of the HT photoreaction compared to simple double-bond isomerization (DBI) and single-bond rotation (SBR) should be possible. By introducing the chiral sulfoxide, the obtained four-state switches could also be the basis for new molecular motors with unprecedented rotation mechanisms. If the number of states is further increased to eight states by introducing another dynamic chiral element even more information could be stored and obtained from these photoswitches. In such eight-state switch more different and unprecedented photoreactions would be possible.

4. Synthesis of fourfold-double-bond-substituted HTI photoswitches

To obtain HTI photoswitches with four switchable states as presented in the objective, a high energy barrier for the single-bond rotation is necessary to obtain stable atropisomers at ambient conditions. By introducing large groups in *ortho*-position of the stilbene part of HTIs but leaving hydrogen as fourth "substituent" of the double bond, it was not possible to increase the energy barriers high enough as Monika Schildhauer showed in previous studies. Also, the introduction of a methyl group at the double bond by reacting the HTI with diazomethane was not enough as early studies of Kerstin Grill (née Hoffmann) and this author in the Dube group demonstrated. Therefore, larger groups as fourth substituents at the HTI double-bond are required, but no synthetic protocol for the introduction of a fourth substituent at this position was available. Therefore, a versatile synthesis allowing the introduction of sterically demanding groups at this position was to be developed. As key step of building up the steric hindrance a cross-coupling reaction was envisioned as these reactions are known to be very efficient in the synthesis of sterically hindered biphenyls. To enable the cross-coupling a halogen atom at the double-bond was required, which could be obtained from the corresponding enol by chlorination under *Vilsmeier-Haack* conditions. The synthesis of the enol has already been described in the literature and is possible by a substitution reaction of thiosalicylic acid with an α-bromoketone and subsequent cyclisation. The synthesis of fourfold-substituted HTI by this method revealed to be very versatile and high yielding. Thus, 30 HTI derivatives were prepared, from which some show remarkably better photoswitching properties than unsubstituted HTIs like absorptions up to 625 nm. In addition, the synthesis of the chlorides is possible in multi-gram scales with cheap starting materials and the purification is possible by crystallization without the need of chromatography. All following HTI photoswitches presented in this thesis are prepared by this method. The synthetic methodology was developed first during the master thesis of this author in the *Dube* group.

License

Organic LETTERS

Letter

Cite This: Org. Lett. 2018, 20, 232–235

pubs.acs.org/OrgLett

Synthesis of Double-Bond-Substituted Hemithioindigo Photoswitches

Aaron Gerwien, Till Reinhardt, Peter Mayer, and Henry Dube*

Ludwig-Maximilians-Universität München, Department für Chemie and Munich Center for Integrated Protein Science CIPSM, 81377 Munich, Germany

Supporting Information

ABSTRACT: A very short, high yielding, and convergent synthesis with broad substrate scope, enabling access to a very diverse range of hemithioindigos with 4-fold substituted double-bonds, is presented. With this method, carbon as well as nitrogen, oxygen, or sulfur based substituents can easily be introduced, delivering a wide array of novel structural motifs. Irradiation studies with visible light demonstrate proficient photoswitching properties of these chromophores at wavelengths up to 625 nm.

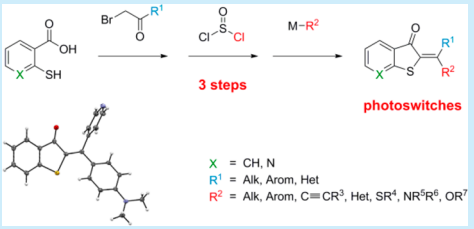

Hemithioindigo (HTI) is a chromophore[1] of very high current interest because of its efficient photoswitching properties[2] in the visible part of the electromagnetic spectrum. For this reason, HTI has attracted increasing attention for applications in biological,[3] supramolecular,[4] or medicinal chemistry[5] as well as in the realms of molecular machines[6] or molecular computing.[7] HTIs consist of a central double-bond, which bears a thioindigo moiety at one end and a so-called stilbene fragment at the other end (Figure 1). The central

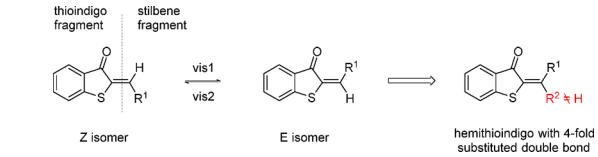

Figure 1. Hemithioindigo chromophore and derivatives with 4-fold substituted double-bond.

double-bond undergoes photoisomerization after irradiation with a suitable wavelength, usually from the thermodynamically stable *Z* to the metastable *E* configuration. The complementary *E* to *Z* photoisomerization takes place after irradiation with longer wavelengths (positive photochromism).

A number of different synthetic schemes are available to obtain HTI chromophores.[8] However, the overwhelmingly prevalent structural motive contains a stilbene fragment with only one, and typically aromatic, substituent. HTIs bearing instead two substituents at that side of the double-bond (i.e., an overall 4-fold substituted double-bond) are known in the literature, but only limited and (in most cases) cumbersome syntheses are available for this scarcely explored class of potential photoswitches. We have used HTIs with 4-fold-substituted double-bonds in the context of light driven molecular motors[6a] and also recently presented a new synthesis to access sterically more hindered derivatives, which showcases the importance of this substitution pattern for advanced functions.[6b]

For the introduction of two carbon-based substituents R^1 and R^2 at the stilbene fragment, most published synthetic schemes rely on condensation reactions between benzothiophenone and either ketones and analogues,[9] electron-poor double-bonds bearing a leaving group,[10] or reverse condensations between oxidized benzothiophenones and enolates or enols.[11] Additionally, very limited and few examples are described employing Friedel–Crafts acylations,[12] ring contraction reactions,[13] rearrangement reactions of *N*-tosylsulfilimines[14] or thiochromanone sulfoxides,[15] addition of diazomethane,[16] or Grignard addition to ketone-substituted hydroxyl-benzothiophenone.[17] However, in all hitherto described cases many synthetic steps are usually required, yields are low, and the scope as well as the functional group tolerance is very limited. The situation is similarly restricted for the introduction of one carbon-based substituent in combination with a heteroatom-substituent, e.g., amine[18] or thioether[18e,19] groups.

In the present work, we describe a short, modular, and high yielding synthesis for 4-fold double-bond substituted HTIs, which provides a vast range of highly interesting substitution patterns. The convergent nature of this synthesis allows facile generation of a multitude of new HTI chromophores and photoswitches with group variation at both molecular fragments. This protocol also allows the easy generation of precursor HTI structures ready for further late-stage functionalization via, e.g., cross-coupling chemistry or peptide conjugation. Apart from carbon-based substituents, introduction of heteroatoms such as oxygen, sulfur, or nitrogen at the central double-bond is also possible in a very convenient and straightforward way (Scheme 1).

Our synthesis commences with inexpensive commercially available starting materials, i.e., different thiosalicylic acids (for introduction of different thioindigo fragments) and α-bromoketones (Scheme 2). A nucleophilic substitution reaction

Received: November 20, 2017
Published: December 15, 2017

DOI: 10.1021/acs.orglett.7b03574
Org. Lett. 2018, 20, 232–235

Scheme 1. Synthesis of HTIs with 4-Fold Substituted Double-Bonds

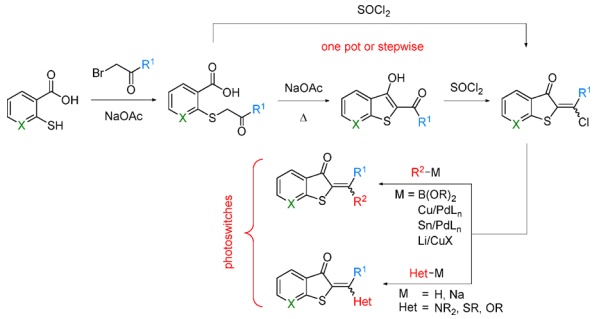

Scheme 2. Synthesis of Chlorinated HTIs 10 to 14

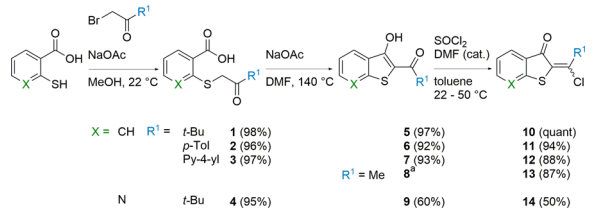

[a]Prepared according to ref 22. All yields are isolated yields.

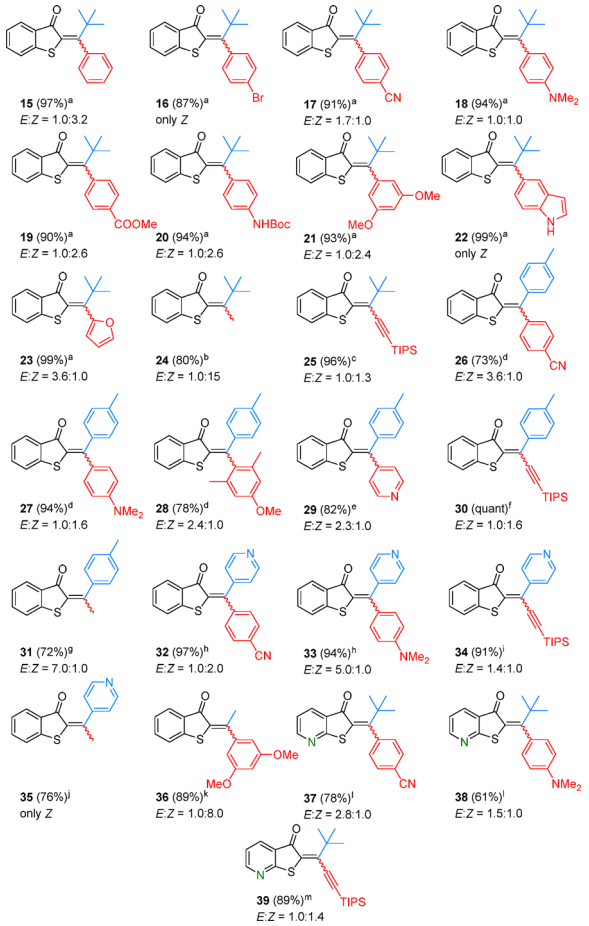

Figure 2. Prepared substituted HTIs **15**–**39**. Conditions: (a) **10**, various boronic acids, $Pd(PPh_3)_4$, K_2CO_3, dioxane/H_2O, 80 °C; (b) **10**, MeLi, CuI, THF, −78 → 23 °C; (c) **10**, (triisopropylsilyl)acetylene, CuI, $PdCl_2(PPh_3)_2$, NEt_3, THF, 60 °C; (d) **11**, various boronic acids, $Pd(PPh_3)_4$, K_2CO_3, dioxane/H_2O, 80 °C; (e) **11**, 4-(tributylstannyl)-pyridine, $Pd(PPh_3)_4$, CsF, CuI, dioxane, 100 °C; (f) **11**, (triisopropylsilyl)acetylene, CuI, $PdCl_2(PPh_3)_2$, NEt_3, THF, 60 °C; (g) **11**, MeLi, CuI, THF, −78 → 23 °C; (h) **12**, various boronic acids, $Pd(PPh_3)_4$, K_2CO_3, dioxane/H_2O, 80 °C; (i) **12**, (triisopropylsilyl)-acetylene, CuI, $PdCl_2(PPh_3)_2$, NEt_3, THF, 60 °C; (j) **12**, MeLi, CuI, THF, −78 → 23 °C; (k) **13**, potassium (3,5-dimethoxyphenyl)-trifluoroborate, APhos Pd G3, dioxane/H_2O, 80 °C; (l) **14**, various boronic acids, $Pd(PPh_3)_4$, K_2CO_3, dioxane/H_2O, 80 °C; (m) **14**, (triisopropylsilyl)acetylene, CuI, $PdCl_2(PPh_3)_2$, NEt_3, THF, 60 °C. All reported yields are isolated yields.

replaces the bromine with the thiol group and provides the corresponding thioethers in excellent yields. In this reaction, the first substituent (R^1) is introduced and can be varied between aliphatic or aromatic character. Addition of NaOAc in DMF leads to facile ring closure and formation of the corresponding 3-hydroxybenzothiophenyl-ketone, a reaction that has been described before for related benzothiophenyl-ketones.[20] Reaction with thionyl chloride readily establishes the HTI chromophore structure with a chloride as the fourth substituent at the double-bond, again in excellent yields. Interestingly, the corresponding regioisomer with the chloride at the benzothiophene ring is not observed under these conditions. These two steps can also be realized in a one-pot reaction without the need to isolate the benzothiophenyl-ketone products while maintaining high yields of the products (e.g., 92% for **10**). The chlorinated HTIs are stable and easy to handle compounds and were, to the best of our knowledge, not described so far. The only related structures bear a carboxylic acid or ester function as R^1 group and could only be obtained under low yielding and harsh reaction conditions.[21]

With chloride as the fourth substituent at the double-bond, the HTIs are now set up for introduction of various substituents R^2 via nucleophilic substitution reactions or cross-coupling chemistry. We exemplify the broad scope of this step by installing a variety of aliphatic, aromatic, acetylenic, or heterocyclic substituents with different electronic and steric character using Suzuki, Sonogashira, or Stille cross-coupling reactions (Figure 2).

As can be seen in Figure 2, these palladium-catalyzed reactions give very high yields, usually beyond 90%, without interference of the particular electronics at the metalated species. Typically mixtures of *E* and *Z* isomers are obtained, which are most likely a result of the thermal- and light-induced isomerizability. Thus, pharmaceutically interesting heterocycle motives such as pyridines (HTIs **29**, **32**, **33**, **34**, and **35**), indole (HTI **22**), or furane (HTI **23**) can be introduced as well as ordinary aromatics bearing nitriles (HTIs **17**, **26**, **32**, and **37**), amines (HTIs **18**, **27**, **33**, and **38**), or methoxy groups (HTIs **21**, **28**, and **36**). Of special interest is the straightforward introduction of protected carboxylic acid and amine functionalities (HTIs **19** and **20**) as they can be used directly for further peptide coupling or other bioconjugation chemistry. Substitution with silyl-protected acetylene (HTIs **25**, **30**, **34**, and **39**) provides a different possibility for further functional group elaboration via, e.g., click-chemistry or cross-coupling reactions. Another interesting aspect is the selectivity of cross-coupling reactions as exemplified by the high yielding introduction of a brominated aromatic substituent in HTI **16**. Apparently the chlorinated precursor HTI **10** is a considerably better electrophile and undergoes oxidative addition faster than the bromide-bearing coupling partner. This allows introducing another halogen functional group with reactivity orthogonal to amide chemistry for further and late-stage cross-coupling chemistry. For chlorinated HTI **10** as well as

DOI: 10.1021/acs.orglett.7b03574
Org. Lett. 2018, 20, 232−235

HTIs **19**, **29**, **33**, and **37**, crystal structures were obtained (shown in Figure 4a) facilitating assignment of the double-bond configuration in solution by extrapolating ^{1}H NMR shifts (see Supporting Information). Introduction of aliphatic groups is also straightforward starting from the HTI chlorides by reacting them with, e.g., methyl-cuprates. The corresponding methyl-substituted derivatives are obtained in good yields (HTIs **24**, **31**, and **35** in Figure 2). For the introduction of heteroatom-substituents at the double-bond, the HTI chlorides can be reacted with amines (HTIs **40**, **43**, and **44** in Figure 3), alcohols (HTI **41** in

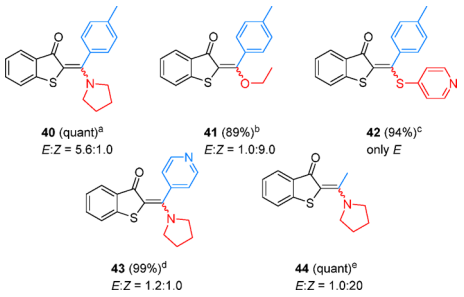

Figure 3. Prepared heteroatom substituted HTIs **40**–**44**. Conditions: (a) **11**, pyrrolidine, dioxane, 23 °C; (b) **11**, NaOEt, EtOH, 23 °C; (c) **11**, pyridine-4-thiol, K_2CO_3, THF, 23 °C; (d) **12**, pyrrolidine, dioxane, 23 °C; (e) **13**, pyrrolidine, dioxane, 23 °C. All yields are isolated yields.

Figure 3), or thiols (HTI **42** in Figure 3). In each case, high yields of the corresponding products are obtained. Crystal structural data were obtained for HTIs **40**, **42**, and **44** (Figure 4a).

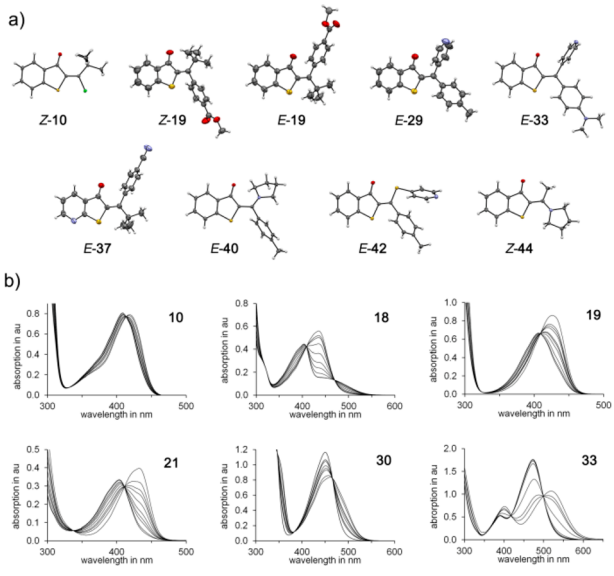

Figure 4. (a) Structures in the crystalline state of HTIs *Z*-**10**, *Z*-**19**, *E*-**19**, *E*-**29**, *E*-**33**, *E*-**37**, *E*-**40**, *E*-**42**, and *Z*-**44**. (b) Absorption changes at different time points during photoisomerization of HTIs **10**, **18**, **19**, **21**, **30**, and **33** in toluene solution.

To showcase the potential of this method to generate actual photoswitches, we have examined the photoswitching properties of all HTIs presented in this work. Apart from a few exceptions (HTIs **23**, **24**, **35**, **40**, **43**, and **44**), all derivatives show good photoswitching properties in the visible part of the spectrum. This can be clearly seen by the spectral changes upon photoirradiation and the clean isosbestic points that are observed (see Figure 4b for the photoswitching of HTIs **10**, **18**, **19**, **21**, **30**, and **33** in toluene as example). First, trends can be established: all HTIs bearing strong electron donating substituents show pronounced red shifts of their absorptions and typically considerable photochromism. If both substituents are electron withdrawing, then photoswitching is not efficient because of the strongly reduced photochromism. Heteroatom substituents also seem to inhibit photoisomerization in most cases.

In summary, we present a novel, concise, and highly efficient method to synthesize HTI photoswitches with 4-fold substituted double-bonds. This method possesses a very broad substrate scope and delivered more than 30 new photoswitches with very different structures and electronic properties. Incorporation of aromatic, heterocyclic, aliphatic, or acetylenic carbon based substituents is similarly straightforward as the introduction of nitrogen, oxygen, or sulfur based residues as the fourth substituent. We also provide a variety of prefunctionalized HTIs for further synthetic elaboration, i.e., brominated and acetylene-substituted derivatives for late stage cross-coupling or click-chemistry reactions and aminated as well as carboxylated derivatives for amide formation or peptide conjugation chemistry. The photoswitching properties under visible light irradiations were examined for all derivatives showing that efficient photoisomerizations take place in almost all cases. A full photophysical and -chemical assessment of these structures is currently underway in our laboratory.

■ ASSOCIATED CONTENT

Supporting Information

The Supporting Information is available free of charge on the ACS Publications website at DOI: 10.1021/acs.orglett.7b03574.

Synthetic procedures as well as a full set of characterization data including melting points, ^{1}H NMR, ^{13}C NMR, IR, and (HR)MS, structural analysis in solution and in the crystal, and photophysical data including extinction coefficients and absorption changes during light irradiation (PDF)

Accession Codes

CCDC 1586002–1586010 contain the supplementary crystallographic data for this paper. These data can be obtained free of charge via www.ccdc.cam.ac.uk/data_request/cif, or by emailing data_request@ccdc.cam.ac.uk, or by contacting The Cambridge Crystallographic Data Centre, 12 Union Road, Cambridge CB2 1EZ, UK; fax: +44 1223 336033.

■ AUTHOR INFORMATION

Corresponding Author

*E-mail: heduch@cup.uni-muenchen.de.

ORCID

Henry Dube: 0000-0002-5055-9924

Notes

The authors declare no competing financial interest.

■ ACKNOWLEDGMENTS

H.D. thanks the "Fonds der Chemischen Industrie" for a Liebig fellowship and the DFG for an Emmy–Noether fellowship. We further thank the collaborative research center SFB749 and the Cluster of Excellence "Center for Integrated Protein Science Munich (CiPSM)" for financial support.

DOI: 10.1021/acs.orglett.7b03574
Org. Lett. 2018, 20, 232–235

REFERENCES

(1) Friedländer, P. *Ber. Dtsch. Chem. Ges.* **1906**, *39*, 1060−1066.

(2) (a) Izmail'skii, V. A.; Mostoslavskii, M. A. *Ukr. Khem. Zh.* **1961**, *27*, 234−237. (b) Reamonn, L. S. S.; O'Sullivan, W. I. *J. Chem. Soc., Perkin Trans. 1* **1977**, 1009−1012. (c) Ichimura, K.; Seki, T.; Tamaki, T.; Yamaguchi, T. *Chem. Lett.* **1990**, *9*, 1645−1646. (d) Yamaguchi, T.; Seki, T.; Tamaki, T.; Ichimura, K. *Bull. Chem. Soc. Jpn.* **1992**, *65*, 649−656. (e) Cordes, T.; Schadendorf, T.; Priewisch, B.; Rück-Braun, K.; Zinth, W. *J. Phys. Chem. A* **2008**, *112*, 581−588. (f) Cordes, T.; Schadendorf, T.; Rück-Braun, K.; Zinth, W. *Chem. Phys. Lett.* **2008**, *455*, 197−201. (g) Nenov, A.; Cordes, T.; Herzog, T. T.; Zinth, W.; de Vivie-Riedle, R. *J. Phys. Chem. A* **2010**, *114*, 13016−13030. (h) Maerz, B.; Wiedbrauk, S.; Oesterling, S.; Samoylova, E.; Nenov, A.; Mayer, P.; de Vivie-Riedle, R.; Zinth, W.; Dube, H. *Chem. - Eur. J.* **2014**, *20*, 13984−13992. (i) Wiedbrauk, S.; Maerz, B.; Samoylova, E.; Reiner, A.; Trommer, F.; Mayer, P.; Zinth, W.; Dube, H. *J. Am. Chem. Soc.* **2016**, *138*, 12219−12227. (j) Wiedbrauk, S.; Maerz, B.; Samoylova, E.; Mayer, P.; Zinth, W.; Dube, H. *J. Phys. Chem. Lett.* **2017**, *8*, 1585−1592. (k) Wang, J.; Rueck-Braun, K. *ChemPhotoChem.* **2017**, *1*, 493−498. (l) Zweig, J. E.; Newhouse, T. R. *J. Am. Chem. Soc.* **2017**, *139*, 10956−10959.

(3) (a) Eggers, K.; Fyles, T. M.; Montoya-Pelaez, P. J. *J. Org. Chem.* **2001**, *66*, 2966−2977. (b) Lougheed, T.; Borisenko, V.; Hennig, T.; Rück-Braun, K.; Woolley, G. A. *Org. Biomol. Chem.* **2004**, *2*, 2798−2801. (c) Seki, T.; Tamaki, T.; Yamaguchi, T.; Ichimura, K. *Bull. Chem. Soc. Jpn.* **1992**, *65*, 657−663. (d) Herre, S.; Steinle, W.; Rück-Braun, K. *Synthesis* **2005**, 3297−3300. (e) Cordes, T.; Weinrich, D.; Kempa, S.; Riesselmann, K.; Herre, S.; Hoppmann, C.; Rück-Braun, K.; Zinth, W. *Chem. Phys. Lett.* **2006**, *428*, 167−173. (f) Regner, N.; Herzog, T. T.; Haiser, K.; Hoppmann, C.; Beyermann, M.; Sauermann, J.; Engelhard, M.; Cordes, T.; Rück-Braun, K.; Zinth, W. *J. Phys. Chem. B* **2012**, *116*, 4181−4191. (g) Kitzig, S.; Thilemann, M.; Cordes, T.; Rück-Braun, K. *ChemPhysChem* **2016**, *17*, 1252−1263.

(4) (a) Tanaka, K.; Kohayakawa, K.; Iwata, S.; Irie, T. *J. Org. Chem.* **2008**, *73*, 3768−3774. (b) Dube, H.; Rebek, J., Jr. *Angew. Chem., Int. Ed.* **2012**, *51*, 3207−3210. (c) Guentner, M.; Uhl, E.; Mayer, P.; Dube, H. *Chem. - Eur. J.* **2016**, *22*, 16433−16436.

(5) (a) Fullbeck, M.; Michalsky, E.; Jaeger, I. S.; Henklein, P.; Kuhn, H.; Rück-Braun, K.; Preissner, R. *Genome Inform* **2006**, *17*, 141−151. (b) Herre, S.; Schadendorf, T.; Ivanov, I.; Herrberger, C.; Steinle, W.; Rück-Braun, K.; Preissner, R.; Kuhn, H. *ChemBioChem* **2006**, *7*, 1089−1095.

(6) (a) Guentner, M.; Schildhauer, M.; Thumser, S.; Mayer, P.; Stephenson, D.; Mayer, P. J.; Dube, H. *Nat. Commun.* **2015**, *6*, 8406. (b) Huber, L. A.; Hoffmann, K.; Thumser, S.; Böcher, N.; Mayer, P.; Dube, H. *Angew. Chem., Int. Ed.* **2017**, *56*, 14536−14539.

(7) Kink, F.; Collado, M. P.; Wiedbrauk, S.; Mayer, P.; Dube, H. *Chem. - Eur. J.* **2017**, *23*, 6237−6243.

(8) (a) Konieczny, M. T.; Konieczny, W. *Heterocycles* **2005**, *65*, 451−464. (b) Wiedbrauk, S.; Dube, H. *Tetrahedron Lett.* **2015**, *56*, 4266−4274.

(9) (a) Fraleoni, A.; Zanirato, P. *J. Chem. Res., Synop.* **1999**, *542*−*543*, 2401−2420. (b) Schönberg, A.; Junghans, K. *Chem. Ber.* **1966**, *99*, 1241−1244. (c) Oksengendler, G. M.; Kiprianov, A. I. *Ukr. Khem. Zh.* **1950**, *16*, 383−393.

(10) Brooker, L. G. S.; White, F. L. Nonionized cyanine dyes. US2739964, 1956.

(11) (a) Varvanina, G. V.; Stepanov, B. I. *Tr. Inst. - Mosk. Khim.-Tekhnol. Inst. im. D. I. Mendeleeva* **1963**, 53−56. (b) Mostoslavskii, M. A.; Izmail'skii, V. A.; Shevchuk, I. N. *Zh. Obshch. Khim.* **1962**, *32*, 660.

(12) Boykin, D. W.; Parham, W. E. *J. Org. Chem.* **1979**, *44*, 424−428.

(13) Gabbutt, C. D.; Hepworth, J. D.; Heron, B. M.; Kanjia, M. *Tetrahedron* **1994**, *50*, 827−834.

(14) (a) Tamura, Y.; Takebe, Y.; Bayomi, S. M. M.; Mukai, C.; Ikeda, M.; Murase, M.; Kise, M. *J. Chem. Soc., Perkin Trans. 1* **1981**, 1037−1040. (b) Bayomi, S. M. M.; Takebe, Y.; Ikeda, M. *Egypt. J. Pharm. Sci.* **1984**, *23*, 355−363.

(15) Still, I. W. J.; Thomas, M. T. *Tetrahedron Lett.* **1970**, *48*, 4225−4228.

(16) Levai, A.; Patonay, T. *J. Heterocycl. Chem.* **1999**, *36*, 747−753.

(17) Awad, S. B.; Abdul-Malik, N. F. *Aust. J. Chem.* **1975**, *28*, 601−605.

(18) (a) Chuev, I. I.; Aldoshin, S. M.; Bren, V. A.; Shepelenko, E. N. *Izv. Akad. Nauk, Ser. Khim.* **1995**, 104−106. (b) Shepelenko, E. N.; Dubonosov, A. D.; Bushkov, A. Y.; Sitkina, L. M.; Bren, V. A.; Lyubarskaya, A. E.; Minkin, V. I. *Zh. Org. Khim.* **1990**, *26*, 1540−1543. (c) Shepelenko, E. N.; Bren, V. A.; Dubonosov, A. D.; Lyubarskaya, A. E.; Minkin, V. I. *Khim. Geterotsikl. Soedin.* **1989**, 591−595. (d) Shepelenko, E. N.; Bren, V. A.; Andreichikova, G. E. *Khim. Geterotsikl. Soedin.* **1987**, 1043−1046. (e) Tominaga, Y.; Hidaki, S.; Matsuda, Y.; Kobayashi, G.; Sakemi, K. *Yakugaku Zasshi* **1984**, *104*, 134−141.

(19) Tominaga, M.; Morita, Y.; Matsuda, Y.; Kobayashi, G. *Chem. Pharm. Bull.* **1975**, *23*, 2390−2396.

(20) Moinet, G.; Leriche, C.; Kergoat, M. Preparation of benzofuran and benzothiophene derivatives as antidiabetic agents. FR2862646A1, 2005.

(21) Buehler, N.; Bosshard, H. Halobenzothiophenecarboxylic acids. DE2804842A1, 1978.

(22) Chan, S. L.-F.; Low, K.-H.; Yang, C.; Cheung, S. H.-F.; Che, C.-M. *Chem. - Eur. J.* **2011**, *17*, 4709−4714.

DOI: 10.1021/acs.orglett.7b03574
Org. Lett. 2018, 20, 232−235

Synthesis of Double-Bond-Substituted Hemithioindigo Photoswitches

*Aaron Gerwien, Till Reinhardt, Peter Mayer, and Henry Dube**

Corresponding Author

*heduch@cup.uni-muenchen.de

Supporting Information

Table of contents

Synthesis

General Experimental

Reagents and solvents were obtained from *abcr, Acros, Fluka, Merck, Sigma-Aldrich* or *TCI* in the qualities *puriss., p.a., or purum* and used as received. Technical solvents were distilled on a rotary evaporator (*vacuubrand* CVC 3000) before use for column chromatography and extraction. Reactions were monitored on *Merck* Silica 60 F254 TLC plates. Detection was done by irradiation with UV light (254 nm or 366 nm). Following reagents were prepared following literature procedures: 1-(3-Hydroxybenzo[*b*]thien-2-yl)ethanone (**8**)[1], potassium trifluoro-2-furanylborate[2], potassium (3,5-dimethoxyphenyl)trifluoroborate[3].

Column chromatography was performed with silica gel 60 (*Merck*, particle size 0.063- 0.200 mm) and distilled technical solvents (*i*Hex refers to a solvent mixture of all isomers of hexane except for *n*hexane with 2-methylpentane as main component and also including methylcyclopentane as additional component).

^{1}H-NMR and ^{13}C-NMR spectra were measured on a *Varian Mercury 200 VX, Varian 300, Inova 400, Varian 600 NMR or Bruker Avance III HD 800 MHz* spectrometer at 23 °C. Chemical shifts (δ) are given relative to tetramethylsilane as external standard. Residual solvent signals in the ^{1}H- and ^{13}C-NMR spectra were used as internal reference. Deuterated solvents were obtained from *Cambridge Isotope Laboratories* or *Eurisotop* and used without further purification. For ^{1}H-NMR: $CDCl_3$ = 7.26 ppm, CD_2Cl_2 = 5.32 ppm, toluene-d_8 = 2.08 ppm, cyclohexane-d_{12} = 1.38 ppm, $(CD_3)_2SO$ = 2.50 ppm, THF-d_8 = 1.72, 3.58 ppm. For ^{13}C-NMR: $CDCl_3$ = 77.16 ppm, CD_2Cl_2 = 53.84 ppm, toluene-d_8 = 20.43, cyclohexane-d_{12} = 26.43 ppm, THF-d_8 = 67.57, 23.37 ppm. The resonance multiplicity is indicated as *s* (singlet), *d* (doublet), *t* (triplet), *q* (quartet) and *m* (multiplet) and *br* (broad signal). The abbreviation 'app' stands for apparent (e.g. 'app t' = apparent triplet). The chemical shifts are given in parts per million (ppm) on the delta scale (δ), and the coupling constant values (*J*) are given in hertz (Hz).

Electron Impact (EI) mass spectra were measured on a *Finnigan MAT95Q* or on a *Finnigan MAT90* mass spectrometer. **Electronspray ionisation (ESI) mass spectra** were measured on a *Thermo Finnigan LTQ-FT*. The most important signals are reported in *m/z* units with *M* as the molecular ion.

Elemental analyses were performed in the micro analytical laboratory of the LMU department of chemistry on an *Elementar Vario EL* apparatus.

Infrared spectra were recorded on a *Perkin Elmer Spectrum BX-FT-IR* instrument equipped with a *Smith DuraSamplIR II ATR*-device. Transmittance values are described qualitatively by wavenumber (cm^{-1}) as very strong (vs), strong (s), medium (m) and weak (w).

Isomerization experiments: The irradiation of the solutions was conducted in the NMR tubes with concentrations of the HTIs of $1x10^{-3}$ mol/L in deuterated solvents or in the UV-Vis cuvettes in *spectroscopy grade* solvents. For irradiation LED-diodes from *Roithner Lasertechnik GmbH* (365 nm, 385 nm, 405 nm, 420 nm, 435 nm, 470 nm, 505 nm, 515 nm, 530 nm, 590 nm) and *Lumex* (565 nm) were used.

UV-Vis spectra were measured on a *Varian Cary 5000* spectrophotometer. The spectra were recorded in a quartz cuvette (1 cm). Solvents for spectroscopy were obtained from *VWR* and *Merck*. Absorption wavelength (λ) are reported in nm and the extinction coefficients (ε) $L \cdot mol^{-1} \cdot cm^{-1}$ in brackets. Shoulders are declared as sh.

Fluorescence spectra were recorded on a *Varian Cary Eclips* spectrofluorometer at different excitation wavelengths, the emission recordings were set to 0.5 increments at a wavelength range of 350 nm to 850 nm.

Melting points (M.p.) were measured on a *Büchi B-540* melting point apparatus in open capillaries and are not corrected.

Typical Procedures

Preparation of Thioethers 1-4 (TP 1) adopting a published protocol[4]: Thiosalicylic acid (1.0 equiv) or 2-mercaptonicotinic acid (1.0 equiv) and sodium acetate (2.0 equiv) were added to the *in situ* generated alpha-bromination products of the corresponding ketones (1.0 equiv) in methanol (1 M solution) and the solution was stirred at 23 °C. After 30 minutes the reaction solution was poured into ice water and the reaction product was filtered off, washed with water and hexanes and dried *in vacuo*.

Preparation of (3-hydroxybenzo[*b*]thiophen-2-yl)methanones 5-7 and 9 (TP 2) adopting a published protocol[4]: Thioethers **1-4** were dissolved in DMF to receive a 1 M solution, sodium acetate (3.0 equiv) was added and the solution was heated to 140 °C for 4 hours under continuous stirring. After the mixture cooled down to 22 °C, water (50 ml) was added and the product was extracted with dichloromethane (3 x 50 ml). The solvent was removed *in vacuo* and the product was purified by column chromatography over a short plug of silica or crystallization.

Preparation of vinyl chlorides 10-14 (TP 3): (3-hydroxybenzo[*b*]thiophen-2-yl)methanones **5-7** and **9** were dissolved in toluene to receive a 1 M solution thionyl chloride (2.0 equiv) and DMF (0.1 equiv) were added and the solution was stirred at 50 °C for 3 hours. Saturated sodium carbonate solution was added until the solution was neutralized and the product was extracted with dichloromethane (3 x 50 mL). The solvent was removed *in vacuo* and the product was purified by column chromatography over a short plug of silica or by crystallization.

Typical Procedure for *Suzuki-Miyaura* Reactions (TP 4): Chlorides **10-14** were dissolved in dioxane to receive a 1 M solution. Corresponding boronic acids (1.5 equiv), potassium carbonate (2.0 equiv) and water (10 vol %) were added and the solution was degassed before $Pd(PPh_3)_4$ (5 mol %) was added. The reaction was heated to 80 °C under continuous stirring for 0.5 to 24 hours, subsequently 5 mL of a saturated aq. sodium carbonate solution was added and the product was extracted with dichloromethane (3 x 10 ml). The solvent was removed *in vacuo* and the product was purified by column chromatography and if possible by crystallization.

Typical Procedure for *Sonogashira-Hagihara* Reactions (TP 5): Chlorides **10-14** (1.0 equiv) were dissolved in dry THF (1 M solution) in a flame-dried flask. (Triisopropylsilyl)acetylene (1.2 equiv), triethyl amine (2.5 equiv) and copper(I) iodide (0.2 equiv) were added under argon counter-flow. After purging of the solution with argon, $PdCl_2(PPh_3)_2$ (0.1 equiv) was added and the reaction was heated to 60 °C for 2 – 12 hours. Subsequently, the reaction was quenched with sat. aq. ammonium chloride solution (5 mL) and ammonia (25% solution in H_2O, 5 mL). The aqueous phase was extracted with dichloromethane (3 x 20 mL), the combined organic phases dried over Na_2SO_4 and the solvent was removed *in vacuo*. The crude product was purified by column chromatography.

Typical procedure for *Stille* reactions (TP 6): Chlorides **10-14** (1.0 equiv) were dissolved in dry 1,4-dioxane (1 M solution) in a flame-dried flask and 4-(tributylstannyl)pyridine (2.0 equiv), cesium fluoride (3.0 equiv) and copper(I) iodide (0.1 equiv) were added under argon counter-flow. After purging of the solution with argon, $Pd(PPh_3)_4$ (0.05 equiv) was added and the reaction was heated to 100 °C for 3 – 12 hours. Subsequently, the reaction was quenched with sat. aq. $NaHCO_3$ (10 mL), the aqueous phase was extracted with dichloromethane (3 x 20 mL), the combined organic phases dried over Na_2SO_4 and the solvent was removed *in vacuo*. The crude product was purified by column chromatography.

Typical procedure for amination reactions (TP 7): Chlorides **10-14** (1.0 equiv) were dissolved in 1,4-dioxane (1 M solution) and pyrrolidine (2.0 equiv) was added. The reaction mixture was stirred at 22 °C for 0.5 – 1 h. Subsequently, sat. aq. $NaHCO_3$ (10 mL) was added, the aqueous phase was extracted with dichloromethane (3 x 20 mL), the combined organic phases dried over Na_2SO_4 and the solvent was removed *in vacuo*. The crude product was purified by column chromatography.

Building Block Synthesis

2-((3,3-Dimethyl-2-oxobutyl)thio)benzoic acid (**1**)

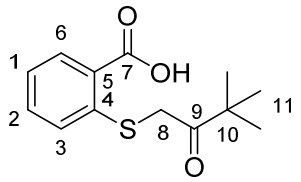

2-((3,3-Dimethyl-2-oxobutyl)thio)benzoic acid (**1**) was prepared following **TP 1** from 1-bromo-3,3-dimethylbutan-2-one (50 mmol), sodium acetate (100 mmol) and thiosalicylic acid (50 mmol). The title compound (**1**) was isolated as colorless solid (12.4 g, 49 mmol, 98%).

HR-MS (EI^+), [M^+]: *m/z* calcd: 252.0815 for $[C_{13}H_{16}O_3S]^+$, found: 252.0815.

^{1}H-NMR (400 MHz, $CDCl_3$) δ (ppm) = 8.08 (dd, ^3J(H,H) = 8.0 Hz, ^4J(H,H) = 1.6 Hz, 1H, H-C(6)), 7,47 (ddd, ^3J(H,H) = 8.0 Hz, ^3J(H,H) = 7.8 Hz, ^4J(H,H) = 1.6 Hz, 1H, H-C(2)), 7,34 (dd, ^3J(H,H) = 7.8 Hz, ^4J(H,H) = 1,6 Hz, 1H, H-C(3)), 7.25 (app td, ^3J(H,H) = 8.0 Hz, ^4J(H,H) = 1.6 Hz, 1H, H-C(1)), 4.02 (s, 2H, H-C(8)), 1.24 (s, 9H, H-C(11)).

^{13}C-NMR (101 MHz, $CDCl_3$) δ (ppm) = 209.9 (C(9)), 170.9 (C(7)), 140.1 (C(4)), 133.2 (C(2)), 132.4 (C(6)), 128.3 (C(5)), 127.7 (C(3)), 125.4 (C(1)), 44.7 (C(8)), 39.3 (C(10)), 26.8 (C(11)).

IR $\tilde{\nu}$ (cm^{-1}) = 2969 (w), 2643 (w), 1684 (vs), 1583 (w), 1561 (w), 1472 (w), 1460 (m), 1404 (m), 1395 (m), 1367 (w), 1314 (m), 1289 (m), 1255 (vs), 1151 (w), 1058 (m), 1050 (m), 1044 (s), 917 (s), 815 (w), 803 (w), 793 (w), 734 (vs), 703 (m), 686 (w).

Melting Point: 161 °C.

R_f (SiO_2, *i*Hex/EtOAc = 50/50) = 0.12.

2-((2-Oxo-2-(*p*-tolyl)ethyl)thio)benzoic acid (**2**)

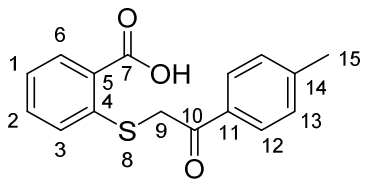

2-((2-Oxo-2-(*p*-tolyl)ethyl)thio)benzoic acid (**2**) was prepared according to **TP 1** from 2-bromo-1-(*p*-tolyl)ethan-1-one (7.45 mmol) and thiosalicylic acid (7.45 mmol). The title compound was isolated as colorless solid after recrystallization from dichloromethane/*n*heptane (2.04 g, 7.13 mmol, 96%) and removing the solvent *in vacuo*.

HR-MS (EI) for $C_{16}H_{14}O_3{}^{32}S^{\cdot+}$, $[M]^{\cdot+}$, calcd. 286.0658, found 286.0663.

^{1}H NMR ($CDCl_3$, 600 MHz): δ (ppm) = 8.05 (dd, ^3J(H,H) = 7.9, ^4J(H,H) = 1.2 Hz, 1H, H-C(6)), 7.91 (d, ^3J(H,H) = 8.2 Hz, 2H, H-C(12)), 7.52 – 7.50 (m, 1H, H-C(3)), 7.48 (app t, ^3J(H,H) = 7.5 Hz, 1H, H-C(2)), 7.28 (d, ^3J(H,H) = 8.5 Hz, 2H, H-C(13)), 7.26 – 7.23 (m, 1H, H-C(1)), 4.38 (s, 2H, H-C(9)), 2.42 (s, 3H, H-C(15)).

^{13}C NMR ($CDCl_3$, 150 MHz): δ (ppm) = 194.1 (C(10)), 169.4 (C(7)), 145.1 (C(14)), 139.7 (C(4)), 133.3 (C(2)), 132.9 (C(11)), 132.4(C(6)), 129.7 (C(13)), 129.1 (C(12)), 128.2 (C(5)), 128.0 (C(3)), 125.6 (C(1)), 40.3 (C(9)), 21.9 (C(15)).

IR: $\tilde{\upsilon}$/cm^{-1} = 2982 (w), 2875 (w), 2656 (w), 2564 (w), 1670 (vs), 1606 (m), 1586 (w), 1566 (m), 1468 (m), 1426 (m), 1415 (m), 1318 (m), 1273 (s), 1262 (s), 1184 (m), 1160 (w), 1116 (w), 1064 (w), 1045 (w), 1014 (w), 954 (w), 893 (m), 838 (w), 812 (w), 764 (m), 740 (s), 707 (w), 697 (m), 686 (w).

Melting point: 173 – 176 °C.

R_f (SiO_2, hexanes:EtOAc = 1:1) = 0.12.

2-((2-Oxo-2-(pyridin-4-yl)ethyl)thio)benzoic acid (**3**)

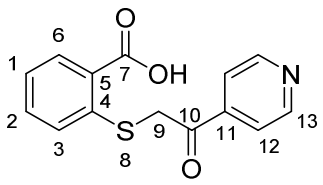

2-((2-Oxo-2-(pyridin-4-yl)ethyl)thio)benzoic acid (**3**) was prepared according to **TP 1** from 2-bromo-1-(pyridin-4-yl)ethan-1-one hydrobromid (15.87 mmol) and thiosalicylic acid (15.87 mmol). The title compound was isolated as colorless crystals (4.22 g, 15.43 mmol, 97%) after recrystallization from *n*heptane/dichloromethane and removing the solvent *in vacuo*.

HR-MS (EI) for $C_{14}H_{11}NO_3{}^{32}S^{\cdot+}$, $[M]^{\cdot+}$, calcd. 273.0454, found 273.0452.

^{1}H NMR (DMSO-d_6, 400 MHz): δ (ppm) = 13.10 (s, 1H, OH)), 8.83 (d, ^3J(H,H) = 6.1 Hz, 1H, H-C(13)), 7.91 (d, ^3J(H,H) = 6.1 Hz, 1H, H-C(12)), 7.89 (dd, ^3J(H,H) = 7.8, ^4J(H,H) = 1.6 Hz, 1H, H-C(6)), 7.50 (app td, ^3J(H,H) = 8.6, ^4J(H,H) = 1.6 Hz, 1H, H-C(2)), 7.44 (dd, ^3J(H,H) = 8.3, ^4J(H,H) = 1.2 Hz, 1H, H-C(3)), 7.23 (app td, ^3J(H,H) = 8.6, ^4J(H,H) = 1.6 Hz, 1H, H-C(1)), 4.73 (s, 2H, H-C(9)).

^{13}C NMR (DMSO-d_6, 100 MHz): δ (ppm) = 194.8 (C(10)), 167.4 (C(7)), 150.8 (C(13)), 141.5 (C(11)), 139.4 (C(4)), 132.3 (C(2)), 130.9 (C(6)), 128.2 (C(5)), 126.1 (C(3)), 124.4 (C(1)), 121.6 (C(12)), 38.9 (C(9)).

IR: $\tilde{\upsilon}$/cm^{-1} = 2426 (b), 1844 (b), 1698 (s), 1670 (m), 1603 (w), 1587 (w), 1559 (w), 1465 (w), 1410 (m), 1393 (m), 1331 (w), 1314 (m), 1297 (m), 1271 (w), 1243 (s), 1229 (s), 1200 (vs), 1153 (s), 1093 (w), 1059 (m), 1044 (m), 1004 (s), 988 (w), 963 (w), 810 (s), 798 (m), 735 (vs), 703 (m), 689 (m).

Melting point: 197 °C.

2-((3,3-Dimethyl-2-oxobutyl)thio)nicotinic acid (**4**)

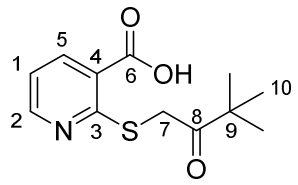

2-((3,3-Dimethyl-2-oxobutyl)thio)nicotinic acid (**4**) was prepared according to **TP 1** from 1-bromo-3,3-dimethylbutan-2-one (11.6 mmol) and 2-mercaptonicotinic acid (11.6 mmol). The title compound was isolated divergently from the **TP 1** by extraction of the aqueous phase with $CHCl_3$/*iso*-propanol (3:1, 4 x 100 mL) and removal of the solvent *in vacuo* as colorless solid (2.81 g, 11.1 mmol, 95%).

HR-MS (EI) for $C_{12}H_{15}O_3N^{32}S^{\cdot+}$, $[M]^{\cdot+}$, calcd. 253.0767, found 253.0760.

^{1}H NMR ($CDCl_3$, 599 MHz): δ (ppm) = 8.47 (dd, ^3J(H,H) = 4.7 Hz, ^4J(H,H) = 1.8 Hz, 1H, H-C(2)), 8.31 (dd, ^3J(H,H) = 7.8 Hz, ^4J(H,H) = 1.8 Hz, 1H, H-C(5)), 7.08 (dd, ^3J(H,H) = 7.8 Hz, ^3J(H,H) = 4.7 Hz, 1H, H-C(1)), 4.19 (s, 2H, H-C(7)), 1.30 (s, 9H, H-C(10)).

^{13}C NMR ($CDCl_3$, 151 MHz): δ (ppm) = 170.2 (C(6)), 161.8 (C(3)), 152.2 (C(2)), 140.1 (C(5)), 122.2 (C(4)), 118.7 (C(1)), 44.7 (C(9)), 36.6 (C(7)), 27.1 (C(10)).

C(8) could not be found in the ^{13}C spectrum, but was observable in the HMBC spectrum at approx. 209 ppm.

IR: $\tilde{\upsilon}$/cm^{-1} = 2962 (m), 2901 (m), 2867 (m), 1656 (w), 2562 (w), 1706 (s), 1672 (vs), 1576 (m), 1553 (s), 1477 (w), 1466 (w), 1449 (m), 1426 (s), 1393 (s), 1362 (m), 1294 (vs), 1264 (m), 1250 (m), 1234 (m), 1154 (m), 1134 (m), 1071 (s), 1054 (s), 1024 (w), 1009 (m), 997 (m), 918 (s), 871 (w), 831 (m), 820 (m), 762 (s), 748 (m), 720 (s).

Melting point: 160 – 161 °C.

R_f (SiO_2, EtOAc = 100%) = 0.28.

1-(3-Hydroxybenzo[*b*]thiophen-2-yl)-2,2-dimethylpropan-1-one (**5**)

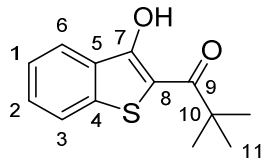

1-(3-Hydroxybenzo[*b*]thiophen-2-yl)-2,2-dimethylpropan-1-one (**5**) was prepared following **TP 2** from 2-((3,3-dimethyl-2-oxobutyl)thio)benzoic acid (**1**) (40 mmol) and sodium acetate (117 mmol). The title compound (**5**) was isolated after crystallization from hexanes/dichloromethane as light yellow crystals (9.1 g, 39 mmol, 97%).

HR-MS (EI^+), [M^+]: *m/z* calcd: 234.0715 for $[C_{13}H_{14}O_2S]^+$, found: 234.0716.

^{1}H-NMR (400 MHz, $CDCl_3$) δ (ppm) = 13.51 (s, 1H, H-O), 8.06 (d, ^3J(H,H) = 9.1 Hz, 1H, H-C(6)), 7.70 (d, ^3J(H,H) = 8.1 Hz, 1H, H-C(3)), 7.52 (app t, ^3J(H,H) = 8.1 Hz, 1H, H-C(2)), 7.38 (app t, ^3J(H,H) = 8.1 Hz, 1H, H-C(1)), 1.43 (s, 9H, H-C(11)).

^{13}C-NMR (101 MHz, $CDCl_3$) δ (ppm) = 206.1 (C(9)), 165.3 (C(7)), 139.6 (C(4)), 130.4 (C(5)), 130.3 (C(2)), 124.9 (C(1)), 124.0 (C(6)), 123.0 (C(3)), 107.9 (C(8)), 44.0 (C(10)), 27.6 (C(11)).

IR $\tilde{\nu}$ (cm^{-1}) = 2969 (w), 2643 (w), 1684 (vs), 1583 (w), 1561 (w), 1472 (w), 1460 (m), 1404 (m), 1395 (m), 1367 (w), 1314 (m), 1289 (m), 1255 (vs), 1151 (w), 1058 (m), 1050 (m), 1044 (s), 917 (s), 815 (w), 803 (w), 793 (w), 734 (vs), 703 (m), 686 (w).

Melting Point: 161 °C.

R_f (SiO_2, *i*Hex/EtOAc = 98/2) = 0.56.

(3-Hydroxybenzo[*b*]thiophen-2-yl)(*p*-tolyl)methanone (**6**)

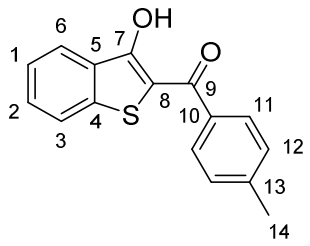

(3-Hydroxybenzo[*b*]thiophen-2-yl)(*p*-tolyl)methanone (**6**) was prepared according to **TP 2** from 2-((2-oxo-2-(*p*-tolyl)ethyl)thio)benzoic acid (**2**) (4.48 mmol). The title compound was purified by FCC (SiO_2, *i*Hex:EtOAc = 9:1) and isolated as yellow solid (1113 mg, 4.12 mmol, 92%).

HR-MS (EI) for $C_{16}H_{12}O_2{}^{32}S^{\cdot+}$, $[M]^{\cdot+}$, calcd. 268.0553, found 268.0552.

^{1}H NMR ($CDCl_3$, 600 MHz): δ (ppm) = 13.56 (s, 1H, H-O), 8.07 (d, ^3J(H,H) = 8.1 Hz, 1H, H-C(6)), 7.98 (d, ^3J(H,H) = 7.9 Hz, 2H, H-C(11)), 7.74 (d, ^3J(H,H) = 8.1 Hz, 1H, H-C(3)), 7.55 (ddd, ^3J(H,H) = 8.1 Hz, ^3J(H,H) = 7.0 Hz, ^4J(H,H) = 1.2 Hz, 1H, H-C(2)), 7.44 (ddd, ^3J(H,H) = 7.5 Hz, ^3J(H,H) = 7.1 Hz, ^4J(H,H) = 0.9 Hz, 1H, H-C(1)), 7.35 (d, ^3J(H,H) = 7.9 Hz, 2H, H-C(12)), 2.46 (s, 3H, H-C(14)).

^{13}C NMR ($CDCl_3$, 150 MHz): δ (ppm) = 191.6 (C(9)), 165.5 (C(7)), 143.7 (C(13)), 140.8 (C(4)), 135.7 (C(10)), 130.5 (C(5)), 130.2 (C(2)), 129.6 (C(12)), 128.7 (C(11)), 124.8 (C(1)), 124.1 (C(6)), 123.1 (C(3)), 109.7 (C(8)), 21.9 (C(14)).

IR: $\tilde{\upsilon}/cm^{-1}$ = 3062 (w), 3030 (w), 2918 (w), 1927 (w), 1818 (w), 1710 (w), 1582 (s), 1554 (s), 1512 (vs), 1456 (s), 1428 (s), 1403 (s), 1337 (s), 1302 (s), 1271 (vs), 1231 (vs), 1184 (m), 1171 (s), 1120 (s), 1092 (s), 1065 (m), 1040 (m), 1016 (m), 988 (w), 968 (s), 844 (m), 811 (s), 780 (m), 768 (m), 744 (s), 726 (vs), 698 (m).

Melting point: 95 – 98 °C.

R_f (SiO_2, *i*Hex:EtOAc = 9:1) = 0.70.

(3-Hydroxybenzo[*b*]thiophen-2-yl)(pyridin-4-yl)methanone (**7**)

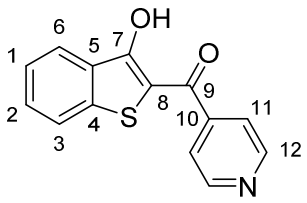

(3-Hydroxybenzo[*b*]thiophen-2-yl)(pyridin-4-yl)methanone (**7**) was prepared according to **TP 2** from 2-((2-oxo-2-(pyridin-4-yl)ethyl)thio)benzoic acid (**3**) (12.05 mmol). The title compound was purified by column chromatography (SiO_2, *i*Hex:EtOAc = 9:1) and isolated as yellow solid (2.99 g, 11.17 mmol, 93%).

HR-MS (EI) for $C_{14}H_9NO_2{}^{32}S^{\cdot+}$, $[M]^{\cdot+}$, calcd. 255.0349, found 255.0349.

^{1}H NMR ($CDCl_3$, 600 MHz): δ (ppm) = 13.10 (s, 1H,H-O), 8.86 (d, ^3J(H,H) = 6.0 Hz, 2H, H-C(12)), 8.08 (dd, ^3J(H,H) = 8.1 Hz, ^4J(H,H) = 0.5 Hz, 1H, H-C(6)), 7.83 (d, ^3J(H,H) = 6.0 Hz, 2H, H-C(11)), 7.74 (dd, ^3J(H,H) = 8.2 Hz, ^4J(H,H) = 0.8 Hz, 1H, H-C(3)), 7.59 (ddd, ^3J(H,H) = 8.3 Hz, ^3J(H,H) = 7.0 Hz, ^4J(H,H) = 1.3 Hz, 1H, H-C(2)), 7.46 (ddd, ^3J(H,H) = 8.0 Hz, ^3J(H,H) = 7.0 Hz, ^4J(H,H) = 1.0 Hz, 1H, H-C(1)).

^{13}C NMR ($CDCl_3$, 150 MHz): δ (ppm) = 189.9 (C(9)), 166.5 (C(7)), 150.9 (C(12)), 144.7 (C(10)), 141.2 (C(4)), 131.0 (C(2)), 130.1 (C(5)), 125.2 (C(1)), 124.4 (C(6)), 123.3 (C(3)), 121.7 (C(11)), 109.5 (C(8)).

IR: $\tilde{\upsilon}/cm^{-1}$ = 1583 (m), 1506 (s), 1412 (s), 1340 (w), 1309 (m), 1280 (w), 1264 (w), 1220 (m), 1173 (m), 1116 (w), 1095 (w), 1067 (m), 1017 (w), 992 (w), 975 (w), 960 (w), 947 (w), 860 (m), 851 (m), 823 (s), 778 (m), 742 (vs), 731 (vs), 718 (s), 699 (vs), 687 (vs), 664 (w).

Melting point: 143 °C.

R_f (SiO_2, *i*Hex:EtOAc = 95:5) = 0.11.

1-(3-Hydroxythieno[2,3-*b*]pyridin-2-yl)-2,2-dimethylpropan-1-one (**9**)

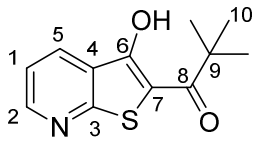

1-(3-Hydroxythieno[2,3-*b*]pyridin-2-yl)-2,2-dimethylpropan-1-one (**9**) was prepared according to **TP 2** from 2-((3,3-dimethyl-2-oxobutyl)thio)nicotinic acid (**4**) (10.4 mmol). The title compound was purified by FCC (SiO_2, *i*Hex:EtOAc = 9:1 to 1:1) and isolated as yellow oil (1.48 g, 6.30 mmol, 60%).

HR-MS (EI) for $C_{12}H_{13}O_2N^{32}S^{\cdot+}$, $[M]^{\cdot+}$, calcd. 235.0662, found 235.0661.

^{1}H NMR ($CDCl_3$, 599 MHz): δ (ppm) = 13.47 (s, 1H, H-O), 8.74 (dd, ^3J(H,H) = 4.6 Hz, ^4J(H,H) = 1.7 Hz, 1H, H-C(2)), 8.25 (dd, ^3J(H,H) = 8.1 Hz, ^4J(H,H) = 1.7 Hz, 1H, H-C(5)), 7.34 (dd, ^3J(H,H) = 8.1 Hz, ^3J(H,H) = 4.6 Hz, 1H, H-C(1)), 1.44 (s, 9H, H-C(10)).

^{13}C NMR ($CDCl_3$, 151 MHz): δ (ppm) = 206.5 (C(8)), 162.3 (C(6)), 160.2 (C(3)), 152.4 (C(2)), 131.7 (C(5)), 124.3 (C(4)), 119.9 (C(1)), 107.5 (C(7)), 44.0 (C(9)), 27.3 (C(10)).

IR: $\tilde{\upsilon}/cm^{-1}$ = 2973 (m), 2933 (w), 2870 (w), 1587 (s), 1562 (s), 1502 (s), 1476 (m), 1456 (s), 1416 (m), 1394 (m), 1367 (m), 1303 (s), 1258 (s), 1233 (m), 1201 (vs), 1116 (s), 1074 (s), 992 (s), 939 (w), 844 (m), 796 (s), 763 (m), 750 (s), 727 (m).

R_f (SiO_2, *i*Hex:EtOAc = 9:1) = 0.44.

(*Z*)-2-(1-Chloro-2,2-dimethylpropylidene)benzo[*b*]thiophen-3(2*H*)-one (**10**)

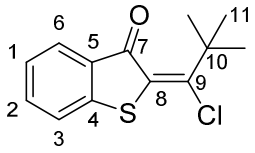

From **5**:

(*Z*)-2-(1-Chloro-2,2-dimethylpropylidene)benzo[*b*]thiophen-3(2H)-one (**10**) was prepared following **TP 3** from 1-(3-hydroxybenzo[*b*]thiophen-2-yl)-2,2-dimethylpropan-1-one (**5**) (8.5 mmol). The title compound (**10**) was isolated after column chromatography (SiO_2, *i*Hex/EtOAc = 99/1 → 95/5) and crystallization from *n*heptane as light yellow solid (2.15 g, 8.5 mmol, quant.).

From **1**:

2-(1-Chloro-2,2-dimethylpropylidene)benzo[*b*]thiophen-3(2H)-one (**10**) was prepared following **TP 3** directly from 2-((3,3-dimethyl-2-oxobutyl)thio)benzoic acid (**1**) (0.42 mmol). The title compound (**10**) was isolated after column chromatography (SiO_2, *i*Hex/EtOAc = 99/1 → 95/5) as light yellow solid (96.5 mg, 0.38 mmol, 92%).

HR-MS (EI^+), [M^+]: *m/z* calcd. 252.0370 for $[C_{13}H_{13}O^{35}Cl^{32}S]^+$, found 252.0361.

^{1}H-NMR (400 MHz, CD_2Cl_2) δ (ppm) = 7.75 (dd, ^3J(H,H) = 7.8 Hz, ^4J(H,H) = 1.4 Hz, 1H, H-C(6)), 7.55 (ddd, ^3J(H,H) = 7.9 Hz, ^3J(H,H) = 7.2 Hz, ^4J(H,H) = 1.3 Hz, 1H, H-C(2)), 7.39 (dd, ^3J(H,H) = 7.9 Hz, ^4J(H,H) = 0.9 Hz, 1H, H-C(3)), 7.25 (ddd, ^3J(H,H) = 8.1 Hz, ^3J(H,H) = 7.3 Hz, ^4J(H,H) = 1.0 Hz, 1H, H-C(1)), 1.49 (s, 9H, H-C(11)).

^{13}C-NMR (101 MHz, CD_2Cl_2) δ (ppm) = 184.0 (C(7)), 159.3 (C(9)), 144.9 (C(4)), 135.5 (C(2)), 134.3 (C(8)), 134.3 (C(5)), 127.3 (C(6)), 125.8 (C(1)), 123.5 (C(3)), 42.1 (C(10)), 28.8 (C(11)).

IR $\tilde{\nu}$ (cm^{-1}) = 2975 (w), 1583 (vs), 1509 (s), 1477 (m), 1461 (w), 1400 (w), 1390 (w), 1366 (m), 1334 (m), 1304 (s), 1288 (m), 1275 (m), 1239 (m), 1205 (vs), 1172 (m), 1129 (w), 1095 (s), 1063 (m), 999 (vs), 940 (w), 856 (w), 821 (m), 774 (s), 750 (s), 735 (vs).

Melting Point: 51 °C.

R_f (SiO_2, *i*Hex/EtOAc = 98/2) = 0.51.

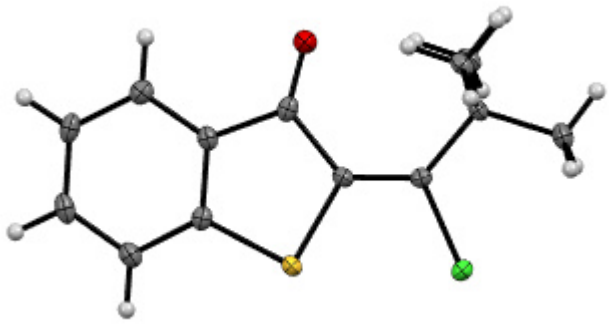

Figure 1: MERCURY-picture of the *Z*-isomeric structure of **10** in the crystalline state**.** Crystal structural data are given in the appendix.

2-(Chloro(*p*-tolyl)methylene)benzo[*b*]thiophen-3(2*H*)-one (**11**)

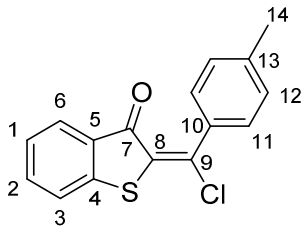

2-(Chloro(*p*-tolyl)methylene)benzo[*b*]thiophen-3(2*H*)-one (**11**) was prepared according to **TP 3** from (3-hydroxybenzo[*b*]thiophen-2-yl)(*p*-tolyl)methanone (**6**) (0.61 mmol) and thionyl chloride (3.1 mmol). The title compound was purified by FCC (SiO_2, *i*Hex:EtOAc = 98:2 to 95:5) and isolated as orange solid (165 mg, 0.575 mmol, 94%). The product was obtained as a mixture of *E*- and *Z*-isomers (*E*:*Z* = 4.6:1.0).

HR-MS (EI) for $C_{16}H_{10}O^{35}Cl^{32}S^{\cdot+}$, $[M]^{\cdot+}$, calcd. 285.0135, found 285.0142.

^{1}H NMR ($CDCl_3$, 600 MHz): δ (ppm) = 7.94 (dd, ^3J(H,H) = 7.8 Hz, ^4J(H,H) = 1.4 Hz, 1H, H-C(6)$_Z$), 7.72 (dd, ^3J(H,H) = 7.7 Hz, ^4J(H,H) = 1.4 Hz, 1H, H-C(6)$_E$), 7.61 (d, ^3J(H,H) = 8.2 Hz, 2H, H-C(11)$_Z$), 7.58 – 7.53 (m, 2H, H-C(2$_E$, 2$_Z$)), 7.47 (d, ^3J(H,H) = 8.1 Hz, 2H, H-C(11)$_E$), 7.44 (d, ^3J(H,H) = 7.8 Hz, 1H, H-C(3)$_E$), 7.36 (d, ^3J(H,H) = 7.9 Hz, 1H, H-C(3)$_Z$), 7.31 – 7.27 (m, 3H, H-C(12$_Z$, 1$_Z$), 7.26 – 7.22 (m, 3H, H-C(12$_E$, 1$_E$), 2.43 (s, 3H, H-C(14)$_Z$), 2.42 (s, 3H, H-C(14)$_E$).

^{13}C NMR ($CDCl_3$, 151 MHz): δ (ppm) = 185.7 (C(7)$_Z$), 183.7 (C(7)$_E$), 144.3 (C(4)$_Z$), 144.2 (C(4)$_E$), 143.7 (C(9)$_E$), 141.3 (C(9)$_Z$), 141.2 (C(13)$_E$), 136.4 (C(13)$_Z$), 136.3 (C(10)$_Z$), 135.5 (C(2)$_E$), 135.2 (C(2)$_Z$), 133.1 (C(5)$_E$), 133.0 (C(10)$_E$), 132.4 (C(8)$_E$), 132.1 (C(5)$_Z$), 129.5 (C(12)$_Z$), 129.3 (C(11)$_E$), 129.1 (C(8)$_Z$), 129.0 (C(12)$_E$), 128.9 (C(11)$_Z$), 127.4 (C(6)$_Z$), 127.3 (C(6)$_E$), 125.7 (C(1)$_E$), 125.5 (C(1)$_Z$), 123.6 (C(3)$_Z$), 123.1 (C(3)$_E$), 21.8 (C(14)$_Z$), 21.7 (C(14)$_E$).

IR: $\tilde{\upsilon}$/cm^{-1} = 3334 (br, m), 3027 (w), 2974 (m), 2918 (m), 1923 (w), 1812 (w), 1730 (w), 1675 (vs), 1591 (s), 1582 (s), 1545 (s), 1502 (m), 1447 (s), 1312 (m), 1278 (s), 1234 (m), 1211 (m), 1185 (m), 1156 (m), 1117 (w), 1088 (w), 1071 (m), 1046 (s), 1019 (s), 868 (m), 836 (w), 814 (m), 780 (m), 761 (m), 736 (vs), 710 (m), 683 (m).

Melting point: 187 – 188 °C.

R_f (SiO_2, *i*Hex:EtOAc = 95:5) = 0.70.

2-(Chloro(pyridin-4-yl)methylene)benzo[*b*]thiophen-3(2*H*)-one (**12**)

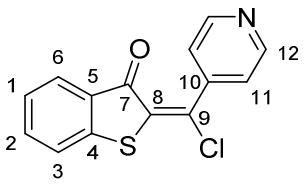

2-(Chloro(pyridin-4-yl)methylene)benzo[*b*]thiophen-3(2*H*)-one (**12**) was prepared according to **TP 3** from (3-hydroxybenzo[*b*]thiophen-2-yl)(pyridin-4-yl)methanone (**7**) (4.15 mmol) and thionyl chloride (20.7 mmol). The title compound was purified by FCC (SiO_2, *i*Hex:EtOAc = 98:2 to 95:5) and isolated as orange solid (772 mg, 3.68 mmol, 88%). The product was obtained as pure *Z*-isomer.

HR-MS (EI) for $C_{16}H_8ON^{35}Cl^{32}S^{\cdot+}$, $[M]^{\cdot+}$, calcd. 273.0010, found 273.0017.

^{1}H NMR ($CDCl_3$, 600 MHz): δ (ppm) = 8.72 (d, ^3J(H,H) = 6.2 Hz, 2H, H-C(12)), 7.74 – 7.70 (m, 1H, H-C(6)), 7.59 (ddd, ^3J(H,H) = 8.0 Hz, ^3J(H,H) = 7.2 Hz, ^4J(H,H) = 1.3 Hz, 1H, H-C(2)), 7.44 (dd, ^3J(H,H) = 7.9 Hz, ^4J(H,H) = 0.8 Hz, 1H, H-C(3)), 7.41 (d, ^3J(H,H) = 6.1 Hz, 2H, H-C(11)), 7.29 – 7.24 (m, 1H, H-C(1)).

^{13}C NMR ($CDCl_3$, 150 MHz): δ (ppm) = 183.7 (C(7)), 150.1 (C(12)), 143.9 (C(9)), 143.5 (C(10)), 138.2 (C(4)), 136.1 (C(2)), 134.9 (C(5)), 132.4 (C(8)), 127.4 (C(6)), 126.1 (C(1)), 123.8 (C(3)), 123.1 (C(11)).

IR: $\tilde{\upsilon}/cm^{-1}$ = 1679 (vs), 1602 (w), 1585 (s), 1564 (m), 1545 (m), 1533 (m), 1488 (w), 1474 (w), 1448 (s), 1407 (s), 1325 (w), 1314 (w), 1281 (s), 1235 (m), 1219 (m), 1209 (m), 1155 (w), 1120 (w), 1092 (w), 1067 (w), 1050 (s), 1024 (m), 991 (w), 977 (w), 950 (w), 876 (w), 862 (w), 816 (s), 787 (w), 769 (s), 742 (vs), 706 (w), 685 (m), 666 (w).

Melting point: 183 °C.

R_f (SiO_2, *i*Hex:EtOAc = 95:5) = 0.10.

2-(1-Chloroethylidene)benzo[*b*]thiophen-3(2*H*)-one (**13**)

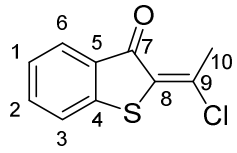

2-(1-Chloroethylidene)benzo[*b*]thiophen-3(2*H*)-one (**13**) was prepared following **TP 3** from 1-(3-hydroxybenzo[*b*]thiophen-2-yl)ethan-1-one (2.6 mmol). The title compound (**13**) was isolated after column chromatography (SiO_2, *i*Hex/EtOAc = 99/1 → 95/5) as light yellow solid (472 mg, 2.25 mmol, 87%).

HR-MS (EI) for $C_{10}H_7{}^{35}ClO^{32}S^{\cdot+}$, $[M]^{\cdot+}$, calcd. 209.9901, found 209.9908.

^{1}H NMR ($CDCl_3$, 600 MHz): δ (ppm) = 7.82 (dd, ^3J(H,H) = 7.8 Hz, ^4J(H,H) = 1.4 Hz, 1H, H-C(6)), 7.56 (ddd, ^3J(H,H) = 7.9 Hz, ^4J(H,H) = 7.2 Hz, ^3J(H,H) = 1.3 Hz, 1H, H-C(2)), 7.42 (dd, ^3J(H,H) = 8.0 Hz, ^4J(H,H) = 0.8 Hz, 1H, H-C(3)), 7.26 (ddd, ^3J(H,H) = 8.0 Hz, ^3J(H,H) = 7.2 Hz, ^4J(H,H) = 0.9 Hz, 1H, H-C(1)), 2.87 (s, 3H, H-C(10)).

^{13}C NMR ($CDCl_3$, 150 MHz): δ (ppm) = 185.8 (C(7)), 146.0 (C(9)), 144.4 (C(4)), 135.4 (C(2)), 132.9 (C(5)), 131.8 (C(8)), 127.2 (C(6)), 125.5 (C(1)), 123.6 (C(3)), 23.9 (C(10)).

IR: $\tilde{\upsilon}/cm^{-1}$ = 1676 (s), 1616 (w), 1591 (s), 1563 (s), 1507 (w), 1471 (w), 1448 (m), 1422 (m), 1383 (w), 1370 (m), 1311 (w), 1281 (s), 1215 (m), 1161 (w), 1139 (s), 1097 (w), 1081 (w), 1062 (w), 1030 (w), 997 (w), 997 (m), 956 (w). 865 (w), 788 (w), 757 (m), 740 (vs), 683 (m).

Melting point: 104 °C decomposition.

R_f (SiO_2, *i*Hex:EtOAc = 95:5) = 0.79.

2-(1-Chloro-2,2-dimethylpropylidene)thieno[2,3-*b*]pyridin-3(2*H*)-one (**14**)

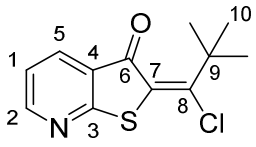

2-(1-Chloro-2,2-dimethylpropylidene)thieno[2,3-*b*]pyridin-3(2*H*)-one (**14**) was prepared according to **TP 3** from 1-(3-hydroxythieno[2,3-*b*]pyridin-2-yl)-2,2-dimethylpropan-1-one (**9**) (4.25 mmol) and thionyl chloride (21.2 mmol). The title compound was purified by FCC (SiO_2, *i*Hex:EtOAc = 9:1 to 6:4) and isolated as orange solid (542 mg, 2.14 mmol, 50%). The product was obtained as a mixture of *E*- and *Z*-isomers (*E*:*Z* = 3.8:1.0).

HR-MS (EI) for $C_{12}H_{12}ON^{35}Cl^{32}S^{\cdot+}$, $[M]^{\cdot+}$, calcd. 253.0323, found 253.0318.

^{1}H NMR ($CDCl_3$, 400 MHz): δ (ppm) = 8.70 (dd, ^3J(H,H) = 4.8 Hz, ^4J(H,H) = 1.8 Hz, 1H, H-C(2)$_Z$), 8.67 (dd, ^3J(H,H) = 4.8 Hz, ^4J(H,H) = 1.8 Hz, 1H, H-C(2)$_E$), 8.11 (dd, ^3J(H,H) = 7.7 Hz, ^4J(H,H) = 1.8 Hz, 1H, H-C(5)$_Z$), 8.02 (dd, ^3J(H,H) = 7.8 Hz, ^4J(H,H) = 1.8 Hz, 1H, H-C(5)$_E$), 7.25 (dd, ^3J(H,H) = 7.7 Hz, ^3J(H,H) = 4.8 Hz, 1H, H-C(1)$_Z$), 7.22 (dd, ^3J(H,H) = 7.8, ^3J(H,H) = 4.8 Hz, 1H, H-C(1)$_E$), 1.53 (s, 9H, H-C(10)$_Z$), 1.51 (s, 9H, H-C(10)$_E$).

^{13}C NMR ($CDCl_3$, 101 MHz): δ (ppm) = 185.1 (C(6)$_Z$), 182.3 (C(6)$_E$), 166.5 (C(3)$_E$), 165.3 (C(3)$_Z$), 161.2 (C(8)$_E$), 156.0 (C(2)$_Z$), 155.7 (C(2)$_E$), 152.6 (C(8)$_Z$), 134.6 (C(5)$_Z$), 134.6 (C(5)$_E$), 133.5 (C(7)$_E$), 128.2 (C(4)$_E$), 125.9 (C(7)$_Z$), 125.3 (C(4)$_Z$), 120.6 (C(1)$_Z$), 120.6 (C(1)$_E$), 42.7 (C(9)$_Z$), 42.0 (C(9)$_E$), 29.5 (C(10)$_Z$), 28.6 (C(10)$_E$).

IR: $\tilde{\upsilon}$/cm^{-1} = 2970 (m), 2930 (m), 1678 (vs), 1573 (vs), 1524 (vs), 1524 (vs), 1484 (m), 1455 (m), 1398 (vs), 1365 (s), 1283 (s), 1263 (m), 1206 (m), 1128 (m), 1093 (s), 1074 (s), 1044 (m), 986 (w), 949 (m), 936 (m), 904 (m), 814 (m), 803 (m), 763 (vs), 714 (w).

Melting point: 78 – 82 °C.

R_f (SiO_2, *i*Hex:EtOAc = 95:5) = 0.41, 0.30.

tert-Butyl Substituted HTIs

2-(2,2-Dimethyl-1-phenylpropylidene)benzo[*b*]thiophen-3(2*H*)-one (**15**)

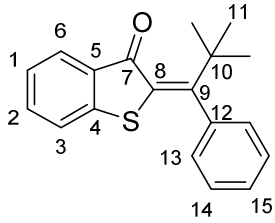

2-(2,2-Dimethyl-1-phenylpropylidene)benzo[*b*]thiophen-3(2*H*)-one (**15**) was prepared according to **TP 4** from chloride (**10**) (0.40 mmol) and phenylboronic acid (0.60 mmol). The title compound was purified by FCC (SiO_2, *i*Hex:EtOAc = 95:5) and isolated as yellow solid (114 mg, 0.39 mmol, 97%, *E*:*Z* = 1.0:3.2).

HR-MS (EI) for $C_{19}H_{18}OS^{\cdot+}$, $[M]^{\cdot+}$, calcd. 294.1073, found 294.1071.

***Z*-isomer:**

^{1}H NMR ($CDCl_3$, 599 MHz): δ (ppm) = 7.81 (dd, ^3J(H,H) = 7.8 Hz, ^4J(H,H) = 1.3 Hz, 1H, H-C(6)), 7.45 (ddd, ^3J(H,H) = 7.9 Hz, ^3J(H,H) = 7.2 Hz, ^4J(H,H) = 1.3 Hz, 1H, H-C(2)), 7.43 – 7.37 (m, 3H, H-C(14), H-C(15)), 7.21 – 7.17 (m, 2H, H-C(1), H-C(3)), 7.14 – 7.11 (m, 2H, H-C(13)), 1.36 (s, 9H, H-C(11)).

^{13}C NMR ($CDCl_3$, 151 MHz): δ (ppm) = 186.9 (C(7)), 165.1 (C(9)), 145.8 (C(4)), 144.5 (C(12)), 134.7 (C(2)), 133.9 (C(8)), 133.4 (C(5)), 128.3 (C(14)), 127.8 (C(15)), 126.9 (C(6)), 126.7 (C(13)), 124.8 (C(3)), 122.8 (C(1)), 38.6 (C(10)), 29.3 (C(11)).

IR: $\tilde{\upsilon}/cm^{-1}$ = 3052 (w), 2969 (w), 2914 (w), 2862 (w), 1661 (s), 1586 (m), 1536 (s), 1487 (m), 1450 (m), 1395 (w), 1359 (m), 1314 (w), 1280 (s), 1218 (m), 1116 (w), 1071 (s), 1037 (w), 1018 (w), 951 (m), 930 (w), 897 (m), 810 (w), 798 (w), 787 (w), 742 (vs), 714 (m), 698 (s), 671 (m).

Melting point: 88 – 89 °C.

R_f (SiO_2, *i*Hex:EtOAc = 95:5) = 0.72.

***E*-isomer:**

^{1}H NMR ($CDCl_3$, 400 MHz): δ (ppm) = 7.63 (dd, ^{3}J(H,H) = 7.7 Hz, ^{4}J(H,H) = 1.3 Hz, 1H, H-C(6)), 7.51 (ddd, ^{3}J(H,H) = 8.3 Hz, ^{3}J(H,H) = 7.2 Hz, ^{4}J(H,H) = 1.3 Hz, 1H, H-C(2)), 7.46 – 7.33 (m, 4H, H-C(14), H-C(15), H-C(3)), 7.16 (ddd, ^{3}J(H,H) = 8.0 Hz, ^{3}J(H,H) = 7.2 Hz, ^{4}J(H,H) = 1.0 Hz, 1H, H-C(1)), 7.02 – 6.96 (m, 2H, H-C(13)), 1.31 (s, 9H, H-C(11)).

^{13}C NMR ($CDCl_3$, 101 MHz): δ (ppm) = 188.0 (C(7)), 161.5 (C(9)), 144.4 (C(4)), 141.7 (C(12)), 135.0 (C(2)), 131.6 (C(5)), 128.6 (C(8)), 128.4 (C(14)), 126.9 (C(15)), 126.9 (C(6)), 126.4 (C(13)), 125.0 (C(1)), 123.0 (C(3)), 38.4 (C(10)), 29.6 (C(11)).

C(6) and C(15) could not be assigned distinctively and could be interchanged.

IR: $\tilde{\upsilon}/cm^{-1}$ = 3054 (w), 1956 (m), 2927 (m), 2864 (w), 1676 (s), 1588 (s), 1544 (s), 1488 (w), 1473 (m), 1448 (s), 1394 (w), 1364 (m), 1313 (w), 1281 (s), 1212 (m), 1157 (w), 1075 (m), 1053 (s), 1016 (m), 998 (w), 928 (w), 870 (w), 844 (w), 823 (w), 782 (m), 734 (vs), 700 (s), 668 (m).

Melting point: 84 – 87 °C.

R_f (SiO_2, *i*Hex:EtOAc = 95:5) = 0.53.

2-(1-(4-Bromophenyl)-2,2-dimethylpropylidene)benzo[*b*]thiophen-3(2*H*)-one (**16**)

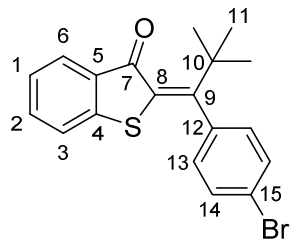

2-(1-(4-Bromophenyl)-2,2-dimethylpropylidene)benzo[*b*]thiophen-3(2*H*)-one (**16**) was prepared according to **TP 4** from chloride (**16**) (0.40 mmol) and (4-bromophenyl)boronic acid (0.60 mmol). The title compound was purified by FCC (SiO_2, hexanes:EtOAc = 95:5 to 9:1) and isolated as yellow solid (131 mg, 0.35 mmol, 87%, only *Z*-isomer).

HR-MS (EI) for $C_{18}H_{16}O^{79}Br^{32}S^{\cdot+}$, $[M]^{\cdot+}$, calcd. 372.0178, found 372.0187.

^{1}H NMR ($CDCl_3$, 400 MHz): δ (ppm) = 7.81 (dd, ^3J(H,H) = 7.8 Hz, ^3J(H,H) = 1.3 Hz, 1H, H-C(6)), 7.55 (d, ^3J(H,H) = 8.4 Hz, 1H, H-C(14)), 7.46 (ddd, ^3J(H,H) = 7.8 Hz, ^3J(H,H) = 7.3 Hz, ^4J(H,H) = 1.4 Hz, 1H, H-C(2)), 7.24 – 7.16 (m, 2H, H-C(1), H-C(3)), 7.01 (d, ^3J(H,H) = 8.4 Hz, 1H, H-C(13)), 1.34 (s, 9H, H-C(11)).

^{13}C NMR ($CDCl_3$, 100 MHz): δ (ppm) = 186.8 (C(7)), 163.4 (C(9)), 145.6 (C(4)), 143.1 (C(12)), 134.9 (C(2)), 134.1 (C(8)), 133.2 (C(5)), 131.6 (C(14)), 128.5 (C(13)), 127.0 (C(6)), 125.0 (C(1)), 122.8 (C(3)), 122.0 (C(15)), 38.5 (C(10)), 29.4 (C(11)).

IR: $\tilde{\upsilon}/cm^{-1}$ = 1662 (s), 1636 (w), 1585 (m), 1558 (w), 1533 (m), 1506 (w), 1477 (m), 1450 (m), 1387 (w), 1358 (w), 1313 (w), 1280 (s), 1219 (m), 1095 (w), 1071 (s), 1009 (s), 950 (w), 929 (w), 897 (w), 828 (w), 809 (m), 765 (w), 745 (vs), 685 (w), 673 (m).

Melting point: 169 °C.

R_f (SiO_2, *i*Hex:EtOAc = 95:5) = 0.65.

4-(2,2-Dimethyl-1-(3-oxobenzo[*b*]thiophen-2(3*H*)-ylidene)propyl)benzonitrile (**17**)

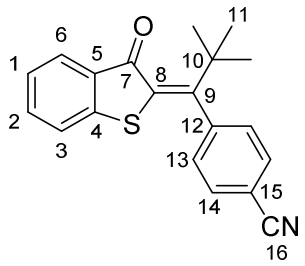

4-(2,2-Dimethyl-1-(3-oxobenzo[*b*]thiophen-2(3*H*)-ylidene)propyl)benzonitrile (**17**) was prepared according to **TP 4** from chloride (**10**) (0.40 mmol) and (4-cyanophenyl)boronic acid (0.60 mmol). The title compound was purified by FCC (SiO_2, *i*Hex:EtOAc = 95:5 to 9:1) and isolated as yellow solid (116 mg, 0.364 mmol, 91%, *Z*:*E* = 1.0:1.7).

***Z*-isomer:**

HR-MS (EI) for $C_{20}H_{17}ON^{32}S^{\cdot+}$, $[M]^{\cdot+}$, calcd. 319.1025, found 319.1027.

^{1}H NMR ($CDCl_3$, 400 MHz): δ (ppm) = 7.83 (d, ^3J(H,H) = 7.7 Hz, 1H, H-C(6)), 7.75 (d, ^3J(H,H) = 8.4 Hz, 2H, H-C(13)), 7.50 (ddd, ^3J(H,H) = 7.8 Hz, ^3J(H,H) = 7.3 Hz, ^4J(H,H) = 1.4 Hz, 1H, H-C(2)), 7.27 (d, ^3J(H,H) = 7.4 Hz, 2H, H-C(14)), 7.25 – 7.18 (m, 2H, H-C(1), H-C(3)), 1.36 (s, 9H, H-C(11)).

^{13}C NMR ($CDCl_3$, 100 MHz): δ (ppm) = 186.7 (C(7)), 162.0 (C(9)), 148.6 (C(15)), 145.2 (C(4)), 135.2 (C(2)), 133.9 (C(8)), 132.9 (C(5)), 132.3 (C(13)), 127.8 (C(14)), 127.1 (C(6)), 125.2 (C(3)), 122.9 (C(1)), 118.6 (C(12)), 112.0 (C(16)), 38.6 (C(10)), 29.5 (C(11)).

IR: $\tilde{\upsilon}$/cm^{-1} = 2963 (w), 2233 (m), 1656 (s), 1603 (w), 1585 (s), 1532 (m), 1498 (m), 1448 (s), 1392 (w), 1360 (w), 1314 (w), 1276 (s), 1215 (s), 1156 (w), 1106 (w), 1066 (s), 1018 (m), 950 (m), 926 (w), 896 (w), 857 (w), 838 (m), 818 (w), 771 (w), 747 (vs), 699 (w), 676 (m).

Melting point: 198 °C.

R_f (SiO_2, *i*Hex:EtOAc = 95:5) = 0.34.

***E*-isomer:**

HR-MS (EI) for $C_{20}H_{17}ON^{32}S^{\cdot+}$, $[M]^{\cdot+}$, calcd. 319.1025, found 319.1027.

^{1}H NMR ($CDCl_3$, 400 MHz): δ (ppm) = 7.70 (d, ^3J(H,H) = 8.5 Hz, 1H, H-C(13)), 7.65 – 7.59 (m, 1H, H-C(6)), 7.54 (ddd, ^3J(H,H) = 8.0 Hz, ^3J(H,H) = 7.2 Hz, ^4J(H,H) = 1.3 Hz, 1H, H-C(2)), 7.44 (d, ^3J(H,H) = 7.9 Hz, 1H, H-C(3)), 7.19 (ddd, ^3J(H,H) = 7.9 Hz, ^3J(H,H) = 7.2 Hz, ^4J(H,H) = 1.0 Hz, 1H, H-C(1)), 7.11 (d, ^3J(H,H) = 8.5 Hz, 1H, H-C(14)), 1.30 (s, 9H, H-C(11)).

^{13}C NMR ($CDCl_3$, 100 MHz): δ (ppm) = 188.0 (C(7)), 158.5 (C(9)), 147.1 (C(15)), 144.5 (C(4)), 135.5 (C(2)), 132.3 (C(13)), 131.0 (C(5)), 129.3 (C(8)), 127.6 (C(14)), 126.9 (C(6)), 125.4 (C(1)), 123.2 (C(3)), 119.2 (C(12)), 110.9 (C(16)), 38.2 (C(10)), 29.6 (C(11)).

IR: $\tilde{\upsilon}/cm^{-1}$ = 2972 (w), 2226 (m), 1676 (s), 1623 (w), 1603 (w), 1584 (s), 1540 (s), 1506 (w), 1497 (w), 1475 (w), 1447 (s), 1397 (m), 1363 (m), 1312 (w), 1281 (s), 1210 (m), 1177 (w), 1155 (m), 1108 (w), 1073 (m), 1051 (s), 1022 (w), 1009 (m), 980 (w), 955 (w), 934 (w), 869 (w), 849 (m), 827 (s), 767 (m), 768 (w), 750 (vs), 724 (w), 700 (w), 673 (w).

Melting point: 210 °C.

R_f (SiO_2, *i*Hex:EtOAc = 95:5) = 0.52.

2-(1-(4-(Dimethylamino)phenyl)-2,2-dimethylpropylidene)benzo[*b*]thiophen-3(2*H*)-one (**18**)

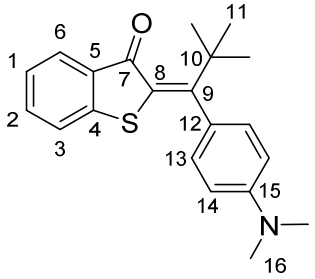

2-(1-(4-(Dimethylamino)phenyl)-2,2-dimethylpropylidene)benzo[*b*]thiophen-3(2*H*)-one (**18**) was prepared according to **TP 4** from chloride (**10**) (0.40 mmol) and (4-*N*,*N*-dimethylaminophenyl)boronic acid (0.60 mmol). The title compound was purified by FCC (SiO_2, *i*Hex:EtOAc = 95:5 to 9:1) and isolated as orange solid (128 mg, 0.38 mmol, 94%, mixture of *Z*:*E* = 1:1).

HR-MS (EI) for $C_{21}H_{23}ON^{32}S^{\cdot+}$, $[M]^{\cdot+}$, calcd. 337.1495, found 337.1499.

^{1}H NMR ($CDCl_3$, 400 MHz): δ (ppm) = 7.81 (dd, ^3J(H,H) = 8.0 Hz, ^4J(H,H) = 1.1 Hz, 1H, H-C(6)$_Z$), 7.65 (dd, ^3J(H,H) = 7.7 Hz, ^4J(H,H) = 1.3 Hz, 1H, H-C(6)$_E$), 7.49 (ddd, ^3J(H,H) = 8.3 Hz, ^3J(H,H) = 7.1 Hz, ^4J(H,H) = 1.3 Hz, 1H, H-C(2)$_E$),7.46 – 7.39 (m, 2H, H-C(2)$_Z$, H-C(3)$_E$), 7.21 – 7.12 (m, 3H, H-C(1)$_Z$, H-C(3)$_Z$, H-C(1)$_E$), 6.98 (d, ^3J(H,H) = 8.7 Hz, 2H, H-C(13)$_Z$), 6.84 (d, ^3J(H,H) = 8.8 Hz, 2H, H-C(13)$_E$), 6.78 (d, ^3J(H,H) = 8.8 Hz, 2H, H-C(14)$_E$), 6.73 (d, ^3J(H,H) = 8.7 Hz, 2H, H-C(14)$_Z$), 3.01 (s, 6H, H-C(16)$_Z$), 3.00 (s, 6H, H-C(16)$_E$), 1.35 (s, 9H, H-C(11)$_Z$), 1.31 (s, 9H, H-C(11)$_E$).

^{13}C NMR ($CDCl_3$, 100 MHz): δ (ppm) = 188.0 (C(7)$_E$), 186.6 (C(7)$_Z$), 166.6 (C(9)$_Z$), 163.0 (C(9)$_E$), 149.8 (C(15)$_Z$), 149.4 (C(15)$_E$), 146.2 (C(4)$_Z$), 144.3 (C(4)$_E$), 134.7 (C(2)$_E$), 134.4 (C(2)$_Z$), 133.8 (C(5)$_Z$), 133.0 (C(12)$_Z$), 131.9 (C(5)$_E$), 129.5 (C(12)$_E$), 128.5 (C(8)$_E$), 127.6 (C(13)$_Z$), 127.3 (C(13)$_E$), 126.9 (C(6)$_E$), 126.8 (C(6)$_Z$), 124.8 (C(1)$_E$), 124.5 (C(1)$_Z$), 122.9 (C(3)$_E$), 122.7 (C(3)$_Z$), 112.2 (C(14)$_E$), 111.3 (C(14)$_Z$), 40.6 (C(16)$_E$), 40.4 (C(16)$_Z$), 39.0 (C(10)$_E$), 38.9 (C(10)$_Z$), 29.7 (C(11)$_E$), 29.3 (C(11)$_Z$).

C(8)$_Z$ could not be found and might superimpose with another signal.

IR: $\tilde{\upsilon}$/cm^{-1} = 1684 (w), 1659 (m), 1607 (m), 1587 (m), 1516 (s), 1478 (w), 1449 (m), 1392 (w), 1356 (s), 1314 (w), 1281 (m), 1221 (m), 1189 (m), 1166 (m), 1122 (w), 1069 (m), 1053 (w), 1019 (w), 990 (w), 955 (m), 944 (w), 930 (w), 899 (m), 870 (w), 812 (m), 768 (m), 742 (vs), 713 (m), 675 (m).

Melting point: 175 °C.

R_f (SiO_2, *i*Hex:EtOAc = 95:5) = 0.53.

Methyl 4-(2,2-dimethyl-1-(3-oxobenzo[*b*]thiophen-2(3*H*)-ylidene)propyl)benzoate (**19**)

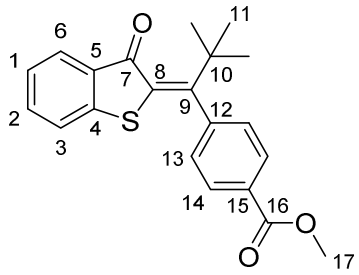

Methyl 4-(2,2-dimethyl-1-(3-oxobenzo[*b*]thiophen-2(3*H*)-ylidene)propyl)benzoate (**19**) was prepared according to **TP 4** from chloride (**10**) (0.40 mmol) and (4-(methoxycarbonyl)phenyl)boronic acid (0.60 mmol). The title compound was purified by FCC (SiO_2, *i*Hex:EtOAc = 95:5) and isolated as yellow solid (127 mg, 0.36 mmol, 90%, *E*:*Z* = 1.0:2.6).

HR-MS (EI) for $C_{21}H_{20}O_3{}^{32}S^{\cdot+}$, $[M]^{\cdot+}$, calcd. 352.1128, found 352.1127.

***Z*-isomer:**

^{1}H NMR ($CDCl_3$, 400 MHz): δ (ppm) = 8.10 (d, ^3J(H,H) = 8.4 Hz, 2H, H-C(14)), 7.81 (dd, ^3J(H,H) = 7.8 Hz, ^4J(H,H) = 1.2 Hz, 1H, H-C(6)), 7.46 (ddd, ^3J(H,H) = 7.8 Hz, ^3J(H,H) = 7.3 Hz, ^4J(H,H) = 1.3 Hz, 1H, H-C(1)), 7.23 – 7.15 (m, 4H, H-C(13), H-C(3), H-C(2)), 3.95 (s, 3H, H-C(17)), 1.35 (s, 9H, H-C(11)).

^{13}C NMR ($CDCl_3$, 101 MHz): δ (ppm) = 186.8 (C(7)), 166.8 (C(16)), 163.6 (C(9)), 148.8 (C(12)), 145.5 (C(4)), 134.9 (C(1)), 133.6 (C(8)), 133.0 (C(5)), 129.7 (C(14)), 129.6 (C(15)), 127.0 (C(6)), 126.9 (C(13)), 125.0 (C(3)), 122.8 (C(2)), 52.5 (C(17)), 38.6 (C(10)), 29.4 (C(11)).

IR: $\tilde{\upsilon}$/cm^{-1} = 3006 (w), 2972 (w), 1722 (s), 1662 (s), 1604 (m), 1585 (s), 1535 (s), 1808 (w), 1450 (m), 1437 (m), 1394 (m), 1360 (w), 1302 (m), 1280 (vs), 1271 (vs), 1219 (s), 1195 (m), 1171 (m), 1114 (s), 1071 (s), 1033 (w), 1013 (m), 952 (m), 929 (w), 856 (w), 832 (w), 802 (w), 788 (w), 751 (s), 744 (s), 722 (m), 703 (m).

Melting point: 170 – 172 °C.

R_f (SiO_2, *i*Hex:EtOAc = 95:5) = 0.40.

***E*-isomer:**

^{1}H NMR ($CDCl_3$, 400 MHz): δ (ppm) = 8.10 (d, ^{3}J(H,H) = 8.7 Hz, 2H, H-C(14)), 7.61 (dd, ^{3}J(H,H) = 7.7 Hz, ^{4}J(H,H) = 1.2 Hz, 1H, H-C(6)), 7.53 (ddd, ^{3}J(H,H) = 8.5 Hz, ^{3}J(H,H) = 7.2 Hz, ^{4}J(H,H) = 1.3 Hz, 1H, H-C(2)), 7.43 (d, ^{3}J(H,H) = 7.8 Hz, 1H, H-C(3)), 7.17 (ddd, ^{3}J(H,H) = 8.0 Hz, ^{3}J(H,H) = 7.2 Hz, ^{4}J(H,H) = 1.0 Hz, 1H, H-C(1)), 7.07 (d, ^{3}J(H,H) = 8.7 Hz, 2H, H-C(13)), 3.93 (s, 3H, H-C(17)), 1.30 (s, 9H, H-C(11).

^{13}C NMR ($CDCl_3$, 101 MHz): δ (ppm) = 188.0 (C(7)), 167.1 (C(16)), 160.0 (C(9)), 147.0 (C(12)), 144.4 (C(4)), 135.2 (C(2)), 131.2 (C(5)), 129.9 (C(14)), 128.8 (C(8)), 128.7 (C(15)), 126.9 (C(6)), 126.6 (C(13)), 125.2 (C(1)), 123.1 (C(3)), 52.2 (C(17)), 38.2 (C(10)), 29.6 (C(11)).

IR: $\tilde{\upsilon}/cm^{-1}$ = 2968 (w), 1710 (s), 1673 (s), 1607 (m), 1585 (m), 1540 (m), 1504 (w), 1448 (m), 1434 (m), 1398 (w), 1368 (w), 1312 (w), 1276 (vs), 1220 (m), 1180 (m), 1158 (w), 1102 (s), 1074 (m), 1051 (m), 1022 (m), 997 (m), 964 (w), 932 (w), 872 (w), 860 (w), 810 (w), 785 (w), 749 (s), 712 (w), 702 (w), 672 (w).

Melting point: 165 – 167 °C.

R_f (SiO_2, *i*Hex:EtOAc = 95:5) = 0.22.

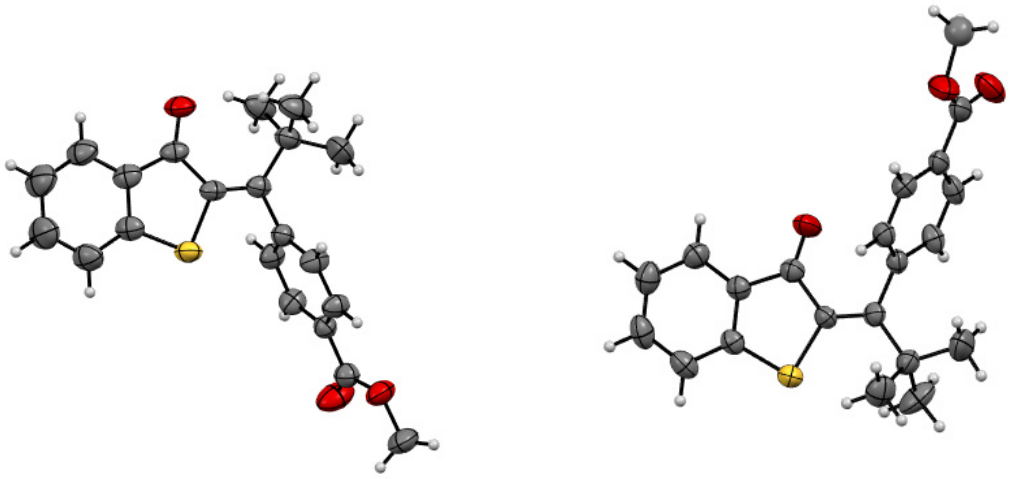

Figure 2: MERCURY-picture of the *Z*- (left) and *E*- (right) isomeric structures of **19** in the crystalline state**.** Crystal structural data are given in the appendix.

tert-Butyl (4-(2,2-dimethyl-1-(3-oxobenzo[*b*]thiophen-2(3*H*)-ylidene)propyl)phenyl)carbamate (**20**)

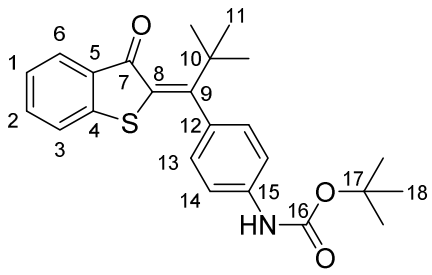

tert-Butyl(4-(2,2-dimethyl-1-(3-oxobenzo[*b*]thiophen-2(3*H*)-ylidene)propyl)phenyl)carbamate (**20**) was prepared according to **TP 4** at a reduced temperature of 60 °C from chloride (**10**) (0.40 mmol) and (4-((tert-butoxycarbonyl)amino)phenyl)boronic acid (0.60 mmol). The title compound was purified by FCC (SiO_2, *i*Hex:EtOAc = 95:5 to 9:1) and isolated as yellow solid (152 mg, 0.371 mmol, 94%, *E*:*Z* = 1.0:2.6).

HR-MS (EI) for $C_{24}H_{27}O_3N^{32}S^{\cdot+}$, $[M]^{\cdot+}$, calcd. 409.1706, found 409.1714.

***Z*-isomer:**

^{1}H NMR ($CDCl_3$, 600 MHz): δ (ppm) = 7.80 (d, ^{3}J(H,H) = 7.9 Hz, 1H, H-C(6)), 7.47 – 7.40 (m, 3H, H-C(2), H-C(14)), 7.21 – 7.16 (m, 2H, H-C(1), H-C(3)), 7.04 (d, ^{3}J(H,H) = 8.4 Hz, 2H, H-C(13)), 6.56 (s, 1H, H-N), 1.54 (s, 9H, H-C(18)), 1.34 (s, 9H, H-C(11)).

^{13}C NMR ($CDCl_3$, 151 MHz): δ (ppm) = 186.8 (C(7)), 165.0 (C(9)), 152.7 (C(16)), 145.9 (C(4)), 139.2 (C(12)), 138.1 (C(15)), 134.7 (C(2)), 134.4 (C(8)), 133.5 (C(5)), 127.5 (C(13)), 126.9 (C(6)), 124.7 (C(1)), 122.8 (C(3)), 117.9 (C(14)), 80.9 (C(17)), 38.7 (C(10)), 29.3 (C(11)), 28.5 (C(18)).

IR: $\tilde{\upsilon}/cm^{-1}$ = 3406 (w), 3002 (w), 2969 (w), 1703 (s), 1670 (s), 1610 (m), 1686 (s), 1515 (s), 1502 (s), 1483 (m), 1451 (m), 1402 (m), 1392 (m), 1364 (m), 1313 (s), 1280 (s), 1256 (m), 1226 (s), 1155 (vs), 1114 (m), 1068 (s), 1056 (s), 1029 (m), 1016 (m), 953 (w), 937 (w), 896 (m), 825 (s), 796 (w), 770 (m), 761 (m), 741 (vs), 701 (w), 673 (m), 663 (m).

Melting point: 180 – 183 °C.

R_f (SiO_2, *i*Hex:EtOAc = 95:5) = 0.27.

***E*-isomer:**

^{1}H NMR ($CDCl_3$, 600 MHz): δ (ppm) = 7.63 (dd, ^{3}J(H,H) = 7.7 Hz, ^{4}J(H,H) = 1.2 Hz, 1H, H-C(6)), 7.50 (ddd, ^{3}J(H,H) = 7.9 Hz, ^{3}J(H,H) = 7.1 Hz, ^{4}J(H,H) = 1.3 Hz, 1H, H-C(2)), 7.45 – 7.39 (m, 3H, H-C(3), H-C(14)), 7.15 (ddd, ^{3}J(H,H) = 7.9 Hz, ^{3}J(H,H) = 7.2 Hz, ^{4}J(H,H) = 1.0 Hz, 1H, H-C(1)), 6.90 (d, ^{3}J(H,H) = 8.6 Hz, 2H, H-C(13)), 6.52 (s, 1H, H-N), 1.52 (s, 9H, H-C(18)), 1.30 (s, 9H, H-C(11)).

^{13}C NMR ($CDCl_3$, 151 MHz): δ (ppm) = 188.0 (C(7)), 161.4 (C(9)), 152.8 (C(16)), 144.3 (C(4)), 137.3 (C(15)), 136.3 (C(12)), 135.0 (C(2)), 131.7 (C(5)), 128.8 (C(8)), 127.1 (C(13)), 126.9 (C(6)), 125.0 (C(1)), 123.0 (C(3)), 118.4 (C(14)), 80.5 (C(17)), 38.5 (C(10)), 29.6 (C(11)), 28.5 (C(18)).

IR: $\tilde{\upsilon}/cm^{-1}$ = 3342 (m), 2973 (w), 1720 (s), 1661 (s), 1612 (w), 1590 (s), 1521 (s), 1477 (m), 1452 (m), 1404 (m), 1364 (m), 1315 (s), 1284 (s), 1228 (s), 1184 (m), 1077 (m), 1048 (s), 1017 (s), 940 (w), 902 (w), 870 (m), 833 (s), 815 (m), 768 (m), 744 (vs), 726 (m), 674 (m).

Melting point: 210 – 213 °C.

R_f (SiO_2, hexanes:EtOAc = 95:5) = 0.09.

2-(1-(3,5-Dimethoxyphenyl)-2,2-dimethylpropylidene)benzo[*b*]thiophen-3(2*H*)-one (**21**)

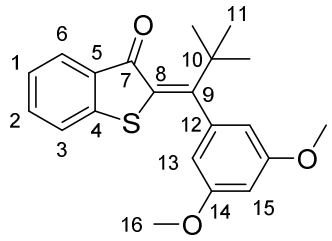

0.40 mmol Scale:

2-(1-(3,5-Dimethoxyphenyl)-2,2-dimethylpropylidene)benzo[*b*]thiophen-3(2*H*)-one (**21**) was prepared according to **TP 4** from chloride (**10**) (0.40 mmol) and (3,5-dimethoxyphenyl)boronic acid (0.60 mmol). The title compound was purified by FCC (SiO_2, *i*Hex:EtOAc = 95:5 to 9:1) and isolated as yellow solid (133 mg, 0.376 mmol, 93%, *E*:*Z* = 1.0:2.4).

1.20 mmol Scale:

2-(1-(3,5-Dimethoxyphenyl)-2,2-dimethylpropylidene)benzo[*b*]thiophen-3(2*H*)-one (**21**) was prepared according to **TP 4** from chloride (**10**) (1.20 mmol) and (3,5-dimethoxyphenyl)boronic acid (1.80 mmol). The title compound was purified by FCC (SiO_2, *i*Hex:EtOAc = 9:1) and isolated as yellow solid (419 mg, 1.18 mmol, 98%, *E*:*Z* = 1.0:3.8).

HR-MS (EI) for $C_{21}H_{22}O_3{}^{32}S^{\cdot+}$, $[M]^{\cdot+}$, calcd. 354.1284, found 354.1282.

***Z*-isomer:**

^{1}H NMR ($CDCl_3$, 400 MHz): δ (ppm) = 7.83 – 7.78 (m, 1H, H-C(6)), 7.54 – 7.38 (m, 1H, H-C(2)), 7.23 – 7.13 (m, 2H, H-C(1), H-C(3)), 6.46 (m, 1H, H-C(15)), 6.26 (d, ^4J(H,H) = 2.2 Hz, 2H, H-C(13)), 3.82 (s, 6H, H-C(16)), 1.37 (s, 9H, H-C(11)).

^{13}C NMR ($CDCl_3$, 101 MHz): δ (ppm) = 186.9 (C(7)), 164.9 (C(9)), 160.7 (C(14)), 146.1 (C(12)), 146.0 (C(4)), 134.7 (C(2)), 133.6 (C(8)), 133.3 (C(5)), 126.9 (C(6)), 124.7 (C(3)), 122.8 (C(1)), 105.2 (C(13)), 99.4 (C(15)), 55.6 (C(16)), 38.6 (C(10)), 29.2 (C(11)).

C(4) and C(12) could not be assigned distinctively and could be interchanged. The correct signalsof the *Z*-isomer were found by subtraction of the *E*-isomer signals determined from the isomeric pure NMR sample of the *E*-isomer.

IR: $\tilde{\upsilon}/cm^{-1}$ = 2976 (w), 2949 (w), 1670 (s), 1583 (vs), 1538 (s), 1450 (s), 1419 (s), 1393 (w), 1361 (m), 1342 (m), 1314 (w), 1296 (m), 1281 (s), 1203 (vs), 1155 (vs), 1066 (s), 1048 (s), 986 (w), 924 (m), 900 (w), 868 (w), 846 (s), 827 (m), 796 (w), 772 (m), 744 (s), 705 (m), 691 (m).

Melting point: 107 – 110 °C.

R_f (SiO_2, *i*Hex:EtOAc = 9:1) = 0.66.

***E*-isomer:**

^{1}H NMR ($CDCl_3$, 400 MHz): δ (ppm) = 7.65 (dd, ^3J(H,H) = 7.7 Hz, ^4J(H,H) = 1.4 Hz, 1H, H-C(6)), 7.51 (ddd, ^3J(H,H) = 7.9 Hz, ^3J(H,H) = 7.2 Hz, ^4J(H,H) = 1.3 Hz, 1H, H-C(2)), 7.42 (d, ^3J(H,H) = 7.9 Hz, 1H, H-C(3)), 7.16 (ddd, ^3J(H,H) = 8.0 Hz, ^3J(H,H) = 7.1 Hz, ^4J(H,H) = 1.0 Hz, 1H, H-C(1)), 6.46 (t, ^4J(H,H) = 2.3 Hz, 1H, H-C(15)), 6.13 (d, ^4J(H,H) = 2.3 Hz, 2H, H-C(13)), 3.79 (s, 6H, H-C(16)), 1.32 (s, 9H, H-C(11)).

^{13}C NMR ($CDCl_3$, 101 MHz): δ (ppm) = 187.5 (C(7)), 161.0 (C(9)), 161.0 (C(14)), 144.3 (C(4)), 143.6 (C(12)), 134.9 (C(2)), 131.6 (C(5)), 128.4 (C(8)), 126.9 (C(6)), 125.0 (C(1)), 123.1 (C(3)), 104.8 (C(13)), 98.5 (C(15)), 55.4 (C(16)), 38.3 (C(10)), 29.5 (C(11)).

C(9) and C(14) could not be assigned distinctively and could be interchanged.

IR: $\tilde{\upsilon}/cm^{-1}$ = 3003 (w), 2977 (m), 2929 (w), 2838 (w), 1679 (s), 1609 (m), 1585 (vs), 1544 (s), 1449 (s), 1428 (s), 1395 (w), 1364 (m), 1321 (s), 1279 (s), 1254 (m), 1223 (m), 1204 (s), 1161 (vs), 1074 (s), 1059 (m), 1046 (s), 1019 (m), 999 (m), 943 (m), 925 (m), 835 (s), 794 (w), 768 (w), 741 (s), 704 (m), 689 (w).

Melting point: 143 – 146 °C.

R_f (SiO_2, *i*Hex:EtOAc = 9:1) = 0.54.

2-(1-(1*H*-Indol-5-yl)-2,2-dimethylpropylidene)benzo[*b*]thiophen-3(2*H*)-one (**22**)

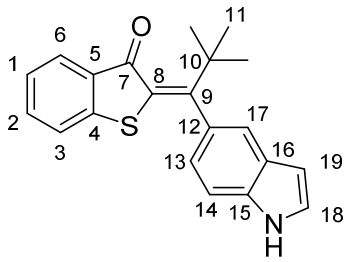

2-(1-(1*H*-Indol-5-yl)-2,2-dimethylpropylidene)benzo[*b*]thiophen-3(2*H*)-one (**22**) was prepared according to **TP 4** from chloride (**22**) (0.40 mmol) and (6-indolyl)boronic acid (0.60 mmol). The title compound was purified by FCC (SiO_2, *i*Hex:EtOAc = 95:5 to 9:1) and isolated as yellow solid (133 mg, 0.40 mmol, 99%, only the *Z*-isomer was obtained).

HR-MS (EI) calcd. for $C_{21}H_{19}ON^{32}S^{\cdot+}$, $[M]^{\cdot+}$, 333.1182, found 333.1180.

^{1}H NMR ($CDCl_3$, 600 MHz): δ (ppm) = 8.28 (s, 1H, H-N), 7.82 (d, ^3J(H,H) = 7.9 Hz, 1H, H-C(6)), 7.44 (d, ^3J(H,H) = 8.2 Hz, 1H, H-C(14)), 7.43 – 7.40 (m, 1H, H-C(2)), 7.40 (d, ^4J(H,H) = 0.9 Hz, 1H, H-C(17)), 7.28 (dd, ^3J(H,H) = 3.1 Hz, ^3J(H,H) = 2.5 Hz, 1H, H-C(18)), 7.18 (ddd, ^3J(H,H) = 8.0 Hz, ^3J(H,H) = 7.1 Hz, ^4J(H,H) = 0.9 Hz, 1H, H-C(1)), 7.13 (dd, ^3J(H,H) = 7.9 Hz, ^4J(H,H) = 0.7 Hz, 1H, H-C(3)), 6.96 (dd, ^3J(H,H) = 8.3 Hz, ^4J(H,H) = 1.7 Hz, 1H, H-C(13)), 6.60 (app td, ^3J(H,H) = 2.1 Hz, ^4J(H,H) = 1.0 Hz, 1H, H-C(19)), 1.39 (s, 9H, H-C(11)).

^{13}C NMR ($CDCl_3$, 150 MHz): δ (ppm) = 186.8 (C(7)), 167.2 (C(9)), 146.2 (C(4)), 136.7 (C(12)), 135.1 (C(15)), 134.6 (C(8)), 134.5 (C(2)), 133.7 (C(5)), 127.4 (C(16)), 126.9 (C(6)), 125.1 (C(18)), 124.5 (C(1)), 122.8 (C(3)), 121.0 (C(13)), 118.9 (C(17)), 110.8 (C(14)), 103.3 (C(19)), 39.0 (C(10)), 29.3 (C(11)).

IR: $\tilde{\upsilon}$/cm^{-1} = 1653 (s), 1585 (m), 1558 (w), 1527 (m), 1507 (w), 1464 (m), 1447 (m), 1414 (w), 1389 (w), 1357 (w), 1311 (w), 1280 (s), 1241 (w), 1220 (m), 1153 (w) 1118 (w), 1093 (w), 1069 (s), 1033 (w), 1017 (w), 970 (m), 931 (w), 910 (w), 890 (w), 877 (m), 801 (w), 760 (s), 744 (vs), 732 (vs), 677 (m), 665 (s).

Melting point: 180 °C.

R_f (SiO_2, *i*Hex:EtOAc = 95:5) = 0.28.

2-(1-(Furan-2-yl)-2,2-dimethylpropylidene)benzo[*b*]thiophen-3(2*H*)-one (**23**)

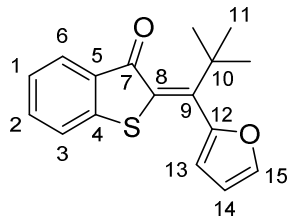

2-(1-(Furan-2-yl)-2,2-dimethylpropylidene)benzo[*b*]thiophen-3(2*H*)-one (**23**) was prepared according to **TP 4** from chloride (**23**) (0.40 mmol) and potassium 2-furantrifluoroborate (0.60 mmol). The title compound was purified by FCC (SiO_2, *i*Hex:EtOAc = 98:2 to 95:5) and isolated as orange solid (113 mg, 0.397 mmol, 99%, *E*:*Z* = 3.6:1.0).

HR-MS (EI) for $C_{17}H_{16}O_2{}^{32}S^{\cdot+}$, $[M]^{\cdot+}$, calcd. 284.0866, found 284.0848.

NMR spectra were only recorded for the major *E*-isomer, as too less material of the minor *Z*-isomer was obtained.

***Z*-isomer:**

IR: $\tilde{\upsilon}/cm^{-1}$ = 2976 (w), 2956 (w), 2865 (w), 1680 (s), 1589 (s), 1544 (m), 1488 (m), 1464 (m), 1452 (s), 1398 (w), 1362 (w), 1313 (w), 1279 (s), 1219 (s), 1151 (s), 1066 (m), 1056 (s), 1010 (s), 994 (m), 929 (m), 883 (w), 858 (w), 808 (w), 784 (m), 766 (s), 735 (vs).

Melting point: 115 – 118 °C.

R_f (SiO_2, *i*Hex:EtOAc = 95:5) = 0.64.

***E*-isomer:**

^{1}H NMR ($CDCl_3$, 400 MHz): δ (ppm) = 7.71 (dd, ^3J(H,H) = 7.7 Hz, ^4J(H,H) = 1.3 Hz, 1H, H-C(6)), 7.56 (dd, ^3J(H,H) = 1.8 Hz, ^4J(H,H) = 0.8 Hz, 1H, H-C(15)), 7.52 (ddd, ^3J(H,H) = 7.9 Hz, ^3J(H,H) = 7.2 Hz, ^4J(H,H) = 1.4 Hz, 1H, H-C(2)), 7.41 (d, ^3J(H,H) = 8.0 Hz, 1H, H-C(3)), 7.19 (ddd, ^3J(H,H) = 8.0 Hz, ^3J(H,H) = 7.0 Hz, ^4J(H,H) = 0.9 Hz, 1H, H-C(1)), 6.51 (dd, ^3J(H,H) = 3.3 Hz, ^3J(H,H) = 1.8 Hz, 1H, H-C(14)), 6.09 (dd, ^3J(H,H) = 3.3 Hz, ^4J(H,H) = 0.8 Hz, 1H, H-C(13)), 1.33 (s, 9H, H-C(11)).

^{13}C NMR ($CDCl_3$, 101 MHz): δ (ppm) = 187.7 (C(7)), 151.1 (C(12)), 148.2 (C(9)), 144.3 (C(4)), 142.0 (C(15)), 135.2 (C(2)), 133.4 (C(8)), 130.9 (C(5)), 127.1 (C(6)), 125.3 (C(1)), 123.1 (C(3)), 110.9 (C(14)), 107.1 (C(13)), 38.7 (C(10)), 29.0 (C(11)).

IR: $\tilde{\upsilon}/cm^{-1}$ = 2955 (w), 2362 (w), 1680 (s), 1588 (m), 1542 (m), 1488 (m), 1451 (m), 1397 (w), 1362 (w), 1279 (m), 1219 (s), 1151 (m), 1055 (m), 1010 (s), 928 (m), 858 (w), 784 (w), 766 (m), 734 (vs).

Melting point: 119 – 121 °C.

R_f (SiO_2, *i*Hex:EtOAc = 95:5) = 0.40.

2-(3,3-Dimethylbutan-2-ylidene)benzo[*b*]thiophen-3(2*H*)-one (**24**)

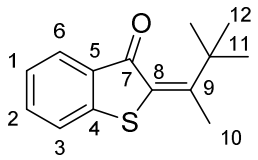

Copper iodine (0.2 mmol, 1.0 equiv) was suspensed in dry THF (1 mL) in a flame-dried flask and cooled to -78 °C. Methyl lithium (1.5 M in diethylether, 0.27 mL, 0.4 mmol, 2.0 equiv) was added under argon atmosphere. The solution was warmed slowly to 22 °C until the suspension became clear. Subsequently, the reaction mixture was added slowly to another flame-dried flask containing a 0.1 M solution of chloride **13** (0.2 mmol, 1.0 equiv) in dry THF under argon atmosphere at -78 °C. The reaction was warmed slowly to 22 °C over 3 hours and quenched with sat. aq. NH_4Cl (10 mL). The aqueous phase was extracted with dichloromethane (3 x 20 mL), the combined organic phases were dried over Na_2SO_4 and the solvent was removed *in vacuo.* The title compound was purified by FCC (SiO_2, *i*Hex:EtOAc = 95:5) and isolated as light yellow oil (37.2 mg, 0.16 mmol, 80%, *E*:*Z* = 1:15).

HR-MS (EI) for $C_{14}H_{16}O^{32}S^{\cdot+}$, $[M]^{\cdot+}$, calcd. 232.0916, found 232.0912.

NMR spectra are only stated for the *Z*-isomer due to the low concentration of the *E*-isomer.

^{1}H NMR ($CDCl_3$, 600 MHz): δ (ppm) = 7.83 (d, ^3J(H,H) = 7.8 Hz, 1H, H-C(6)), 7.51 (d, ^3J(H,H) = 8.0 Hz, 1H, H-C(2)), 7.40 (d, ^3J(H,H) = 7.9 Hz, 1H, H-C(3)), 7.22 (d, ^3J(H,H) = 7.7 Hz, 1H, H-C(1)), 2.58 (s, 3H, H-C(10)), 1.38 (s, 9H, H-C(12)).

^{13}C NMR ($CDCl_3$, 150 MHz): δ (ppm) = 190.1 (C(7)), 163.8 (C(9)), 144.5 (C(4)), 134.5 (C(2)), 132.2 (C(5)), 126.7 (C(6)), 126.5 (C(8)), 124.7 (C(1)), 122.8 (C(3)), 39.9(C(11)), 29.1 (C(12)), 18.6 (C(10)).

IR: $\tilde{\upsilon}$/cm^{-1} = 2963 (m), 1806 (w), 1762 (m), 1686 (m), 1588 (s), 1514 (w), 1476 (w), 1461 (m), 1449 (m), 1393 (m), 1333 (w), 1302 (w), 1280 (s), 1219 (m), 1203 (m), 1178 (w), 1160 (w), 1125 (w), 1095 (w), 1067 (s), 1037 (w), 1014 (w), 991 (m), 974 (m), 931 (w), 890 (w), 843 (w), 744 (vs), 730 (vs), 693 (w), 675 (w).

R_f (SiO_2, *i*Hex:EtOAc = 95:5) = 0.65.

2-(4,4-Dimethyl-1-(triisopropylsilyl)pent-1-yn-3-ylidene)benzo[*b*]thiophen-3(2*H*)-one (**25**)

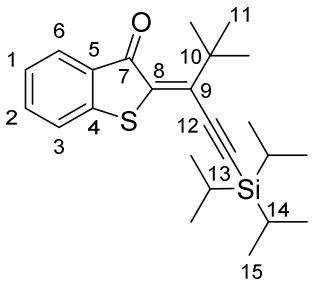

2-(4,4-Dimethyl-1-(triisopropylsilyl)pent-1-yn-3-ylidene)benzo[*b*]thiophen-3(2*H*)-one (**25**) was prepared according to **TP 5** from chloride (**10**) (0.40 mmol) and (triisopropylsilyl)acetylene (0.48 mmol). The title compound was purified by FCC (SiO_2, *i*Hex:EtOAc = 95:5) and isolated as reddish-brown oil (151 mg, 0.379 mmol, 96%). The product was obtained as a mixture of *E*- and *Z*-isomers (*E*:*Z* = 1.0:1.3).

HR-MS (EI) for $C_{24}H_{34}O^{32}S^{28}Si^{\cdot+}$, $[M]^{\cdot+}$, calcd. 398.2094, found 398.2095.

^{1}H NMR ($CDCl_3$, 600 MHz): δ (ppm) = 7.89 (dd, ^3J(H,H) = 7.7 Hz, ^4J(H,H) = 1.4 Hz, 1H, H-C(6)$_Z$), 7.78 (dd, ^3J(H,H) = 7.8 Hz, ^4J(H,H) =1.4 Hz, 1H, H-C(6)$_E$), 7.53 – 7.48 (m, 2H, H-C(2$_Z$, 2$_E$)), 7.39 – 7.36 (m, 2H, H-C(3$_Z$, 3$_E$)), 7.25 – 7.19 (m, 2H, H-C(1$_Z$, 1$_E$)), 1.47 (s, 9H, H-C(11)$_E$), 1.45 (s, 9H, H-C(11)$_Z$), 1.23 – 1.15 (m, 42H, H-C(14$_Z$, 14$_E$), H-C(15$_E$, 15$_Z$)).

^{13}C NMR ($CDCl_3$, 151 MHz): δ (ppm) = 186.4 (C(7)$_Z$), 184.8 C(7)$_E$), 145.3 (C(4)$_E$), 144.5 (C(9)$_E$), 142.7 (C(4)$_Z$), 140.9 (C(8)$_E$), 138.9 (C(9)$_Z$), 137.1 (C(8)$_Z$), 134.8 (C(2)$_E$), 134.8 (C(2)$_Z$), 133.8 (C(5)$_E$), 131.2 (C(5)$_Z$), 127.1 (C(6)$_Z$), 127.1 (C(6)$_E$), 125.2 (C(1)$_Z$), 125.0 (C(1)$_E$), 123.2 (C(3)$_E$), 122.8 (C(3)$_Z$), 112.4 (C(13)$_E$), 109.1 (C(13)$_Z$), 107.8 (C(12)$_E$), 105.1 (C(12)$_Z$), 38.0 (C(10)$_Z$), 37.5 (C(10)$_E$), 29.6 (C(11)$_Z$), 29.0 (C(11)$_E$), 18.9 (C(15)$_Z$), 18.9 (C(15)$_E$), 11.7 (C(14)$_Z$), 11.5 (C(14)$_E$).

C(8)$_Z$ and C(8)$_E$ could not be assigned distinctively and could be interchanged.

IR: $\tilde{\upsilon}$/cm^{-1} = 3069 (w), 2942 (s), 2864 (s), 2126 (w), 1681 (m), 1666 (s), 1587 (s), 1497 (s), 1451 (s), 1394 (w), 1363 (m), 1312 (w), 1280 (s), 1246 (m), 1220 (m), 1150 (m), 1072 (s), 1055 (m), 1008 (s), 997 (s), 956 (s), 910 (m), 882 (s), 860 (s), 847 (m), 792 (w), 774 (w), 740 (vs), 679 (vs).

R_f (SiO_2, *i*Hex:EtOAc = 95:5) = 0.53, 0.58.

p-Tolyl Substituted HTIs

4-((3-Oxobenzo[*b*]thiophen-2(3*H*)-ylidene)(*p*-tolyl)methyl)benzonitrile (**26**)

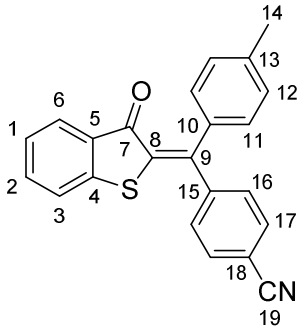

4-((3-Oxobenzo[*b*]thiophen-2(3*H*)-ylidene)(*p*-tolyl)methyl)benzonitrile (**26**) was prepared according to **TP 4** from chloride (**11**) (0.40 mmol) and (4-cyanophenyl)boronic acid (0.60 mmol). The title compound was purified by FCC (SiO_2, *i*Hex:EtOAc = 9:1 to 8:2) and isolated as orange solid (104 mg, 0.294 mmol, 73%). The product was obtained as a mixture of *E*- and *Z*-isomers (*E*:*Z* = 3.6:1.0)

HR-MS (EI) for $C_{23}H_{14}NOS^{\cdot+}$, $[M\text{-}H]^{\cdot+}$, calcd. 353.0791, found 352.0798.

^{1}H NMR ($CDCl_3$, 600 MHz): δ (ppm) = 7.78 (dd, *J* = 7.8 Hz, 1.3 Hz, 1H), 7.75 (ddd, *J* = 7.7 Hz, 1.3 Hz, 0.7 Hz, 1H), 7.70 – 7.67 (m, 3H), 7.56 – 7.52 (m, 2H), 7.40 (dt, *J* = 7.9 Hz, 0.8 Hz, 1H), 7.39 – 7.36 (m, 2H), 7.29 (dt, *J* = 8.2 Hz, 1.8 Hz, 2H), 7.26 – 7.20 (m, 2H), 7.15 (ddd, *J* = 10.0 Hz, 8.2 Hz, 6.4 Hz, 2H), 2.40 (s, 6H).

^{13}C NMR ($CDCl_3$, 151 MHz): δ (ppm) = 187.0, 186.7, 148.5, 147.9, 146.8, 145.8, 145.0, 144.9, 140.5, 139.7, 137.9, 135.5, 135.3, 132.4, 132.4, 132.2, 132.1, 132.1, 131.7, 130.6, 130.3, 129.8, 129.7, 129.6, 129.3, 127.3, 127.2, 125.6, 125.5, 123.6, 123.5, 119.0, 118.5, 112.9, 112.1, 21.7, 21.6.

The signals could not be assigned distinctively due to many superimpositions.

IR: $\tilde{\upsilon}/cm^{-1}$ = 2921 (w), 2228 (w), 1668 (s), 1604 (m), 1588 (s), 1531 (m), 1497 (m), 1450 (m), 1404 (w), 1315 (w), 1281 (s), 1219 (m), 1191 (w), 1156 (w), 1117 (w), 1072 (m), 1048 (s), 1017 (m), 952 (m), 867 (w), 847 (m), 824 (s), 770 (m), 742 (vs), 689 (w).

Melting point: 153 – 155 °C.

R_f (SiO_2, *i*Hex:EtOAc = 95:5) = 0.18, 0.15.

2-((4-(Dimethylamino)phenyl)(*p*-tolyl)methylene)benzo[*b*]thiophen-3(2*H*)-one (**27**)

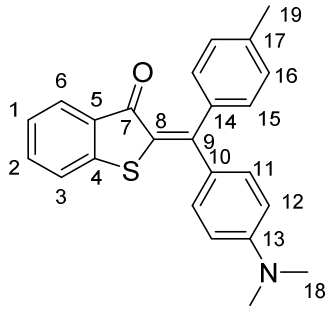

2-((4-(Dimethylamino)phenyl)(*p*-tolyl)methylene)benzo[*b*]thiophen-3(2*H*)-one (**27**) was prepared according to **TP 4** from chloride (**11**) (0.40 mmol) and (4-*N*,*N*-dimethylaminophenylboronic acid (0.60 mmol). The title compound was purified by FCC (SiO_2, *i*Hex:EtOAc = 95:5 to 9:1) and isolated as dark red solid (139.89 mg, 0.38 mmol, 94%, *E*:*Z* = 1:1.6).

HR-MS (EI) for $C_{24}H_{21}N^{32}S^{\cdot+}$, $[M]^{\cdot+}$, calcd. 371.1338, found 371.1336.

The signals could not be assigned distinctively due to many superimpositions.

^{1}H NMR ($CDCl_3$, 400 MHz): δ (ppm) = 7.84 (d, *J* = 7.7 Hz, 1H), 7.79 (d, *J* = 7.7 Hz, 1H), 7.51 – 7.45 (m), 7.44 – 7.35 (m), 7.35 – 7.25 (m), 7.24 – 7.14 (m), 3.03 (s, 12H), 2.42 (s, 6H).

^{13}C NMR ($CDCl_3$, 100 MHz): δ (ppm) = 186.6, 186.0, 153.8, 152.7, 151.5, 151.1, 145.9, 145.7, 140.5, 139.5, 138.6, 137.6, 134.0, 134.0, 133.9, 133.4, 132.8, 132.5, 130.7, 130.0, 129.1, 129.0, 128.0, 126.9, 126.4, 124.7, 124.6, 123.3, 123.2, 111.2, 110.8, 40.3, 40.2, 21.6, 21.6.

IR: $\tilde{\upsilon}/cm^{-1}$ = 1653 (m), 1601 (s), 1585 (m), 1548 (w), 1515 (s), 1501 (s), 1449 (m), 1410 (w), 1365 (m), 1323 (w), 1310 (w), 1280 (s), 1221 (w), 1199 (s), 1180 (w), 1155 (w), 1111 (w), 1069 (w), 1051 (vs), 1018 (m), 1002 (w), 959 (m), 949 (w), 866 (w), 815 (s), 800 (w), 768 (m), 746 (vs), 730 (w), 692 (w), 665 (w).

Melting point: 168 °C.

R_f (SiO_2, *i*Hex:EtOAc = 95:5) = 0.34.

2-((4-Methoxy-2,6-dimethylphenyl)(*p*-tolyl)methylene)benzo[*b*]thiophen-3(2*H*)-one (**28**)

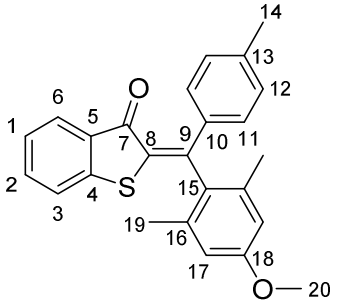

2-((4-Methoxy-2,6-dimethylphenyl)(*p*-tolyl)methylene)benzo[*b*]thiophen-3(2*H*)-one (**28**) was prepared according to **TP 4** from chloride (**11**) (0.40 mmol) and 4-methoxy-2,5-dimethylphenylboronic acid (0.60 mmol). The title compound was purified by FCC (SiO_2, *i*Hex:EtOAc = 95:5 to 8:2) and isolated as orange solid (121 mg, 0.313 mmol, 78%, *E*:*Z* = 2.4:1.0).

HR-MS (EI) for $C_{25}H_{22}O_2{}^{32}S^{\cdot+}$, $[M]^{\cdot+}$, calcd. 386.1335, found 386.1334.

NMR spectra were only recorded for one isomer due to insufficient material of the second isomer.

***Z*-isomer:**

IR: $\tilde{\upsilon}/cm^{-1}$ = 3002 (w), 2965 (w), 2841 (w), 1660 (vs), 1604 (s), 1585 (s), 1538 (s), 1508 (m), 1467 (m), 1446 (s), 1374 (w), 1218 (vs), 1278 (s), 1210 (m), 1194 (m), 1173 (s), 1144 (s), 1118 (w), 1072 (m), 1052 (vs), 1020 (s), 966 (m), 955 (m), 930 (w), 854 (m), 840 (m), 825 (m), 776 (m), 752 (vs), 724 (w), 695 (w), 656 (w).

Melting point: 161 – 164 °C.

R_f (SiO_2, hexanes:EtOAc = 95:5) = 0.45.

***E*-isomer:**

^{1}H NMR ($CDCl_3$, 599 MHz): δ (ppm) = 7.76 (dd, ^3J(H,H) = 7.8 Hz, ^4J(H,H) = 1.4 Hz, 1H, H-C(6)), 7.52 (ddd, ^3J(H,H) = 7.9 Hz, ^3J(H,H) = 7.1 Hz, ^4J(H,H) = 1.3 Hz, 1H, H-C(2)), 7.46 (d, ^3J(H,H) = 8.2 Hz, 2H, H-C(11)), 7.44 (d, ^3J(H,H) = 7.9 Hz, 1H, H-C(3)), 7.23 – 7.19 (m, 3H, H-C(12), H-C(1)), 6.69 (s, 2H, H-C(17)), 3.82 (s, 3H, H-C(20)), 2.38 (s, 3H, H-C(14)), 2.06 (s, 6H, H-C(19)).

^{13}C NMR ($CDCl_3$, 151 MHz): δ (ppm) = 187.1 (C(7)), 158.9 (C(18)), 149.1 (C(9)), 146.0 (C(4)), 140.0 (C(13)), 137.1 (C(10)), 136.4 (C(16)), 134.7 (C(2)), 132.4 (C(15)), 132.1 (C(5)), 130.2 (C(8)), 129.7 (C(11)), 129.4 (C(12)), 127.1 (C(6)), 125.1 (C(1)), 123.5 (C(3)), 113.5 (C(17)), 55.1 (C(20)), 21.6 (C(14)), 20.4 (C(19)).

IR: $\tilde{\upsilon}/cm^{-1}$ = 3002 (w), 2965 (w), 2840 (w), 1664 (s), 1603 (m), 1584 (s), 1537 (s), 1506 (m), 1466 (m), 1446 (s), 1373 (w), 1318 (s), 1280 (s), 1216 (m), 1188 (m), 1174 (m), 1143 (s), 1066 (vs), 1052

(s), 1018 (m), 956 (m), 936 (m), 851 (m), 842 (m), 828 (m), 799 (m), 775 (m), 751 (s), 726 (m), 696 (w), 656 (w).

Melting point: 191 – 193 °C.

R_f (SiO_2, hexanes:EtOAc = 95:5) = 0.32.

2-(Pyridin-4-yl(*p*-tolyl)methylene)benzo[*b*]thiophen-3(2*H*)-one (**29**)

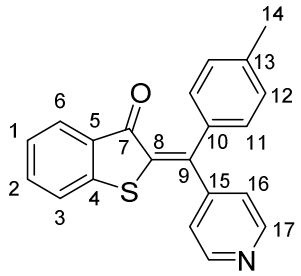

2-(Pyridin-4-yl(*p*-tolyl)methylene)benzo[*b*]thiophen-3(2*H*)-one (**29**) was prepared according to **TP 6** from chloride (**11**) (0.40 mmol) and 4-(tributylstannyl)pyridine (0.80 mmol). The title compound was purified by FCC (SiO_2, *i*Hex:EtOAc = 8:2 to 6:4) and isolated as orange solid (108 mg, 0.328 mmol, 82%, *Z*:*E* = 1.0:2.3).

HR-MS (EI) for $C_{21}H_{14}ON^{32}S^{\cdot+}$, $[M\text{-}H]^{\cdot+}$, calcd. 329.0791, found 328.0790.

***Z*-isomer:**

^{1}H NMR ($CDCl_3$, 400 MHz): δ (ppm) = 8.69 (bs, 2H, H-C(17)), 7.78 (d, ^3J(H,H) = 8.3 Hz, 1H, H-C(6)), 7.55 (app t, ^3J(H,H) = 8.2 Hz, 1H, H-C(2)), 7.38 (d, ^3J(H,H) = 7.9 Hz, 1H, H-C(3)), 7.33 (d, ^3J(H,H) = 4.7 Hz, 2H, H-C(16)), 7.28 – 7.24 (m, 1H, H-C(1)), 7.24 – 7.19 (m, 2H, H-C(12)), 7.17 (d, ^3J(H,H) = 8.2 Hz, 2H, H-C(11)), 2.40 (s, 3H, H-C(14)).

^{13}C NMR ($CDCl_3$, 100 MHz): δ (ppm) = 186.7 (C(7)), 150.2 (C(17)), 149.9 (C(15)), 147.4 (C(9)), 145.1 (C(4)), 139.6 (C(13)), 135.3 (C(2)), 135.2 (C(10)), 132.3 (C(5)), 132.2 (C(8)), 129.5 (C(11)), 129.3 (C(12)), 127.3 (C(6)), 125.6 (C(1)), 124.0 (C(16)), 123.5 (C(3)), 21.6 (C(14)).

IR: $\tilde{\upsilon}/cm^{-1}$ = 3031 (w), 1670 (s), 1603 (m), 1585 (s), 1541 (s), 1508 (m), 1486 (m), 1449 (s), 1406 (m), 1311 (w), 1282 (s), 1218 (m), 1190 (m), 1161 (m), 1121 (w), 1070 (m), 1048 (s), 1020 (m), 989 (m), 960 (m), 866 (w), 832 (m), 821 (m), 794 (w), 767 (m), 746 (vs), 712 (m), 694 (w), 672 (w).

Melting point: 174 – 178 °C.

R_f (SiO_2, *i*Hex:EtOAc = 7:3) = 0.46.

***E*-isomer:**

^{1}H NMR ($CDCl_3$, 600 MHz): δ (ppm) = 8.67 (s, 2H, H-C(17)), 7.76 (dd, ^3J(H,H) = 7.7 Hz, ^4J(H,H) = 1.3 Hz, 1H, H-C(6)), 7.54 (ddd, ^3J(H,H) = 8.4 Hz, ^3J(H,H) = 7.3 Hz, ^4J(H,H) = 1.3 Hz, 1H, H-C(2)), 7.39 (d, ^3J(H,H) = 7.9 Hz, 1H, H-C(3)), 7.30 (d app t, ^3J(H,H) = 8.2 Hz, ^4J(H,H) = 1.9 Hz, 2H, H-C(11)), 7.26 – 7.21 (m, 3H, H-C(12), H-C(1)), 7.20 – 7.17 (m, 2H, H-C(16)), 2.40 (s, 3H, H-C(14)).

^{13}C NMR ($CDCl_3$, 151 MHz): δ (ppm) = 187.0 (C(7)), 149.9 (C(17)), 148.4 (C(15)), 146.7 (C(9)), 145.8 (C(4)), 140.4 (C(13)), 137.6 (C(10)), 135.3 (C(2)), 132.0 (C(8)), 131.7 (C(5)), 129.7 (C(11)),

129.6 (C(12)), 127.2 (C(6)), 125.5 (C(1)), 124.0 (C(16)), 123.6 (C(3)), 21.6 (C(14)).

IR: $\tilde{\upsilon}/cm^{-1}$ = 3022 (w), 2361 (w), 1920 (w), 1668 (vs), 1606 (w), 1586 (vs), 1529 (s), 1508 (s), 1487 (m), 1446 (s), 1407 (m), 1320 (m), 1295 (m), 1279 (s), 1217 (m), 1192 (m), 1176 (m), 1152 (m), 1122 (w), 1070 (m), 1050 (s), 1018 (m), 988 (m), 966 (m), 954 (m), 868 (w), 823 (s), 806 (m), 766 (m), 737 (vs), 723 (s), 690 (w).

Melting point: 183 – 185 °C.

R_f (SiO_2, *i*Hex:EtOAc = 7:3) = 0.35.

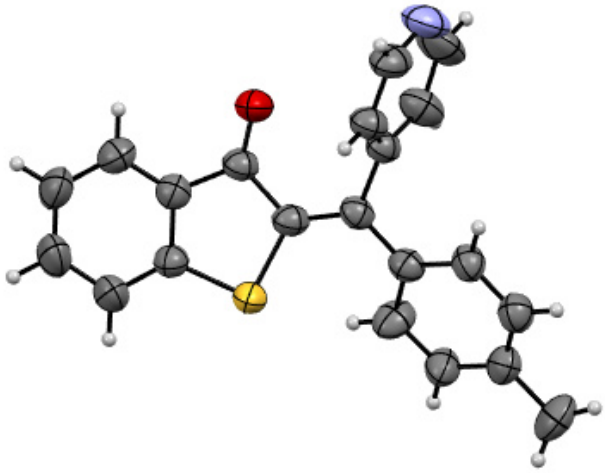

Figure 3: MERCURY-picture of the *E*-isomeric structure of **29** in the crystalline state**.** Crystal structural data are given in the appendix.

2-(1-(*p*-Tolyl)-3-(triisopropylsilyl)prop-2-yn-1-ylidene)benzo[*b*]thiophen-3(2*H*)-one (**30**)

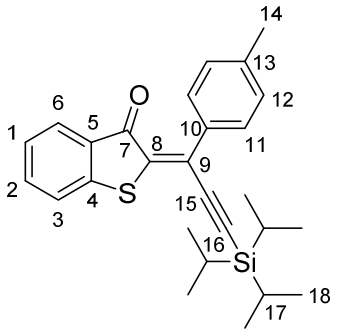

2-(1-(*p*-Tolyl)-3-(triisopropylsilyl)prop-2-yn-1-ylidene)benzo[*b*]thiophen-3(2*H*)-one (**30**) was prepared according to **TP 5** from chloride (**11**) (0.40 mmol) and (Triisopropylsilyl)acetylene (0.48 mmol). The title compound was purified by FCC (SiO_2, *i*Hex:EtOAc = 98:2 to 95:5) and isolated as reddish-brown oil (184 mg, 0.400 mmol, quant.). The product was obtained as a mixture of *E*- and *Z*-isomers (*E*:*Z* = 1.0:1.6).

HR-MS (EI) for $C_{27}H_{32}O^{32}S^{28}Si^{\cdot+}$, $[M]^{\cdot+}$, calcd. 432.1938, found 432.1933.

^{1}H NMR ($CDCl_3$, 600 MHz): δ (ppm) = 7.95 (dd, ^3J(H,H) = 7.8 Hz, ^4J(H,H) = 1.4 Hz, 1H, H-C(6)$_E$), 7.74 (dd, ^3J(H,H) = 7.7 Hz, ^4J(H,H) = 1.4 Hz, 1H, H-C(6)$_Z$), 7.67 (d app t, ^3J(H,H) = 8.1 Hz, ^4J(H,H) = 2.3 Hz, ^5J(H,H) = 1.9 Hz, 2H, H-C(11)$_E$), 7.58 (d app t, ^3J(H,H) = 8.1 Hz, ^4J(H,H) = 2.3 Hz, ^5J(H,H) = 1.8 Hz, 2H, H-C(11)$_Z$), 7.55 – 7.50 (m, 2H, H-C(2$_E$, 2$_Z$), 7.44 (d, ^3J(H,H) = 7.9 Hz, 1H, H-C(3)$_Z$), 7.36 (d, ^3J(H,H) = 7.9 Hz, 1H, H-C(3)$_E$), 7.28 – 7.24 (m, 3H, H-C(12$_E$, 1$_E$), 7.23 – 7.19 (m, 3H, H-C(1$_Z$, 12$_Z$), 2.41 (s, 3H, H-C(14)$_E$), 2.40 (s, 3H, H-C(14)$_Z$), 1.23 – 1.14 (m, 42H, H-C(18$_E$, 18$_Z$, 17$_E$, 17$_Z$)).

^{13}C NMR ($CDCl_3$, 151 MHz): δ (ppm) = 185.7 (C(7)$_E$), 185.0 (C(7)$_Z$), 144.6 (C(4)$_Z$), 144.0 (C(4)$_E$), 140.0 (C(9)$_Z$), 139.9 (C(13)$_E$), 138.9 (C(8)$_E$), 138.5 (C(8)$_Z$), 136.6 (C(10)$_E$), 135.1 (C(2)$_Z$), 134.8 (C(2)$_E$), 133.3 (C(5)$_Z$), 132.2 (C(13)$_Z$), 131.9 (C(5)$_E$), 131.2 (C(10)$_Z$), 129.6 (C(11)$_Z$), 129.3 (C(12)$_E$), 129.1 (C(11)$_E$), 128.6 (C(12)$_Z$), 127.8 (C(9)$_E$), 127.3 (C(6)$_E$), 127.1 (C(6)$_Z$), 125.4 (C(1)$_E$), 125.3 (C(1)$_Z$), 123.7 (C(3)$_Z$), 123.3 (C(3)$_E$), 108.9 (C(16)$_Z$), 107.6 (C(15)$_Z$), 107.1 (C(16)$_E$), 105.9 (C(15)$_E$), 21.7 (C(14)$_Z$), 21.6 (C(14)$_E$), 18.9 (C(18)$_E$), 18.9 (C(18)$_Z$), 11.6 (C(17)$_E$), 11.4 (C(17)$_Z$).

IR: $\tilde{\upsilon}$/cm^{-1} = 2942 (s), 2891 (m), 2864 (s), 2060 (w), 1669 (s), 1586 (s), 1520 (m), 1503 (s), 1450 (s), 1383 (w), 1312 (w), 1280 (vs), 1260 (m), 1217 (m), 1186 (w), 1159 (w), 1110 (w), 1065 (s), 1050 (s), 1018 (s), 995 (s), 918 (w), 900 (m), 881 (vs), 834 (m), 818 (s), 772 (m), 740 (vs), 727 (m), 693 (m), 679 (s).

R$_f$ (SiO_2, *i*Hex:EtOAc = 95:5) = 0.47, 0.35.

2-(1-(*p*-Tolyl)ethylidene)benzo[*b*]thiophen-3(2*H*)-one (**31**)

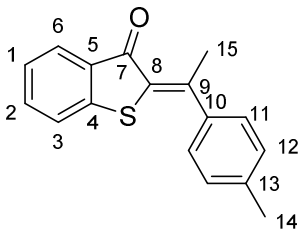

Copper iodine (0.2 mmol, 1.0 equiv) was suspensed in dry THF (1 mL) in a flame-dried flask and cooled to -78 °C. Methyl lithium (1.5 M in diethylether, 0.27 mL, 0.4 mmol, 2.0 equiv) was added under argon atmosphere. The solution was warmed slowly to 22 °C until the suspension became clear. Subsequently, the reaction mixture was added slowly to another flame-dried flask containing a 0.1 M solution of chloride **11** (0.2 mmol, 1.0 equiv) in dry THF under argon atmosphere. The reaction was warmed slowly to 22 °C over 3 hours and quenched with sat. aq. NH_4Cl (10 mL). The aqueous phase was extracted with dichloromethane (3 x 20 mL), the combined organic phases were dried over Na_2SO_4 and the solvent was removed *in vacuo*. The title compound was purified by FCC (SiO_2, hexanes:EtOAc = 95:5) and isolated as yellow solid (49.3 mg, 0.15 mmol, 72%, as a mixture of *E*:*Z* = 7:1).

HR-MS (EI) for $C_{17}H_{13}O^{32}S^{\cdot+}$, $[M]^{\cdot+}$, calcd. 266.0754, found 266.0764.

NMR spectra are only stated for the *Z*-isomer due to the low concentration of the *E*-isomer.

^{1}H NMR ($CDCl_3$, 600 MHz): δ (ppm) = 7.88 (d, ^3J(H,H) = 7.8 Hz, 1H, H-C(6)), 7.50 (d, ^3J(H,H) = 7.9 Hz, 1H, H-C(2)), 7.38 (d, ^3J(H,H) = 8.1 Hz, 2H, H-C(11)), 7.34 (d, ^3J(H,H) = 7.9 Hz, 1H, H-C(3)), 7.26 (d, ^3J(H,H) = 8.5 Hz, 2H, H-C(12)), 7.23 (app t, ^3J(H,H) = 8.4 Hz, 1H, H-C(1)), 2.82 (s, 3H, H-C(15)), 2.41 (s, 3H, H-C(14)).

^{13}C NMR ($CDCl_3$, 150 MHz): δ (ppm) = 188.7 (C(7)), 151.7 (C(9)), 146.1 (C(4)), 140.9 (C(10)), 139.2 (C(13)), 134.6 (C(2)), 132.9 (C(5)), 129.9 (C(8), 129.4 (C(12)), 127.5 (C(11)), 126.9 (C(6)), 124.8 (C(1)), 123.3 (C(3)), 22.0 (C(15)), 21.5 (C(14)).

IR: $\tilde{\upsilon}$/cm^{-1} =1666 (vs), 1591 (vs), 1557 (m), 1508 (m), 1449 (s), 1368 (m), 1312 (m), 1283 (s), 1217 (w), 1186 (w), 1158 (w), 1106 (w), 1078 (w), 1019 (w), 976 (m), 908 (w), 817 (m), 791 (w), 741 (s), 721 (w), 658 (w).

Melting point: 96 °C.

R_f (SiO_2, *i*Hex:EtOAc = 95:5) = 0.55.

4-Pyridinyl Substituted HTIs

4-((3-Oxobenzo[*b*]thiophen-2(3*H*)-ylidene)(pyridin-4-yl)methyl)benzonitrile (**32**)

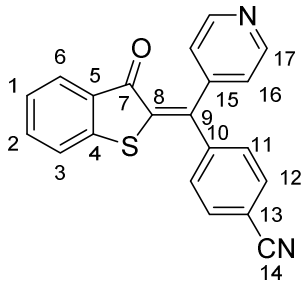

4-((3-Oxobenzo[*b*]thiophen-2(3*H*)-ylidene)(pyridin-4-yl)methyl)benzonitrile (**32**) was prepared according to **TP 4** from chloride (**12**) (0.20 mmol) and 4-cyanophenylboronic acid (0.30 mmol). The title compound was purified by FCC (SiO_2, *i*Hex:EtOAc = 95:5 to 9:1) and isolated as yellow solid (66.7 mg, 0.20 mmol, 97%, *Z*:*E* = 2:1).

***Z*-Isomer:**

HR-MS (EI) for $C_{21}H_{11}ON_2{}^{32}S^{\cdot+}$, $[M]^{\cdot+}$, calcd. 340.0665, found 340.0635.

^{1}H NMR ($CDCl_3$, 600 MHz): δ (ppm) = 8.72 (bs, 2H, H-C(17)), 7.80 – 7.74 (m, 1H, H-C(6)), 7.73 – 7.69 (m, 2H, H-C(12)), 7.59 (ddd, ^3J(H,H) = 7.9 Hz, ^3J(H,H) = 7.3 Hz, ^4J(H,H) = 1.4 Hz, 1H, H-C(2)), 7.41 (d, ^3J(H,H) = 7.9 Hz, 1H, H-C(3)), 7.39 – 7.35 (m, 1H, H-C(11)), 7.32 – 7.26 (m, 3H, H-C(1), H-C(16)).

^{13}C NMR ($CDCl_3$, 150 MHz): δ (ppm) = 186.9 (C(7)), 150.5 (C(17)), 148.2 (C(15)), 144.9 (C(4)), 143.6 (C(9)), 143.1 (C(10)), 136.0 (C(2)), 134.2 (C(8)), 132.5 (C(12)), 131.5 (C(5)), 130.1 (C(11)), 127.5 (C(6)), 126.0 (C(1)), 123.8 (C(3)), 123.6 (C(16)), 118.6 (C(14)), 112.7 (C(13)).

IR: ϑ̃/cm^{-1} = 2227 (m), 1683 (s), 1653 (w), 1603 (w), 1583 (s), 1561 (w), 1538 (w), 1506 (w) 1497 (w), 1490 (w), 1448 (m), 1409 (m), 1326 (w), 1311 (w), 1280 (s), 1223 (m), 1216 (w), 1197 (w), 1183 (w), 1158 (w), 1109 (w), 1068 (m), 1047 (s), 1019 (m), 989 (w), 979 (w), 967 (m), 952 (w), 891 (w), 869 (w), 851 (m), 836 (w), 825 (m), 794 (m), 751 (vs), 742 (s), 725 (m), 708 (m), 693 (m), 676 (m), 656 (m).

Melting point: 215 °C.

R_f (SiO_2, hexanes:EtOAc = 1:1) = 0.22.

***E*-Isomer:**

HR-MS (EI) for $C_{21}H_{11}ON_2{}^{32}S^{\cdot+}$, $[M]^{\cdot+}$, calcd. 340.0665, found 340.0635.

^{1}H NMR ($CDCl_3$, 400 MHz): δ (ppm) = 8.69 (d, ^3J(H,H) = 5.5 Hz, 1H, H-C(17)), 7.77 (d, ^3J(H,H) = 7.3 Hz, 1H, H-C(6)), 7.72 (d, ^3J(H,H) = 8.5 Hz, 1H, H-C(12)), 7.59 (app td, ^3J(H,H) = 7.1 Hz, ^4J(H,H) = 1.2 Hz, 1H, H-C(2)), 7.53 (d, ^3J(H,H) = 8.5 Hz, 1H, H-C(11)), 7.40 (d, ^3J(H,H) = 7.9 Hz, 1H, H-C(3)), 7.28 (t, ^3J(H,H) = 7.5 Hz, 1H, H-C(1)), 7.17 (d, ^3J(H,H) = 6.0 Hz, 1H, H-C(16)).

^{13}C NMR ($CDCl_3$, 100 MHz): δ (ppm) = 186.7 (C(7)), 150.2 (C(17)), 147.0 (C(15)), 144.9 (C(4)), 144.8 (C(10)), 143.4 (C(9)), 135.9 (C(2)), 134.2 (C(8)), 132.7 (C(12)), 131.5 (C(5)), 130.2 (C(11)), 127.5 (C(6)), 126.0 (C(1)), 123.8 (C(16)), 123.7 (C(3)), 118.2 (C(14)), 113.4 (C(13)).

IR: $\tilde{\upsilon}/cm^{-1}$ = 2227 (m), 1670 (s), 1636 (w), 1586 (s), 1558 (m), 1533 (m), 1497 (w), 1451 (m), 1404 (m), 1310 (w), 1283 (s), 1219 (w), 1182 (w), 1164 (w), 1115 (w), 1068 (w), 1052 (s), 1016 (m), 993 (w), 966 (w), 953 (w), 867 (w), 839 (s), 828 (s), 806 (w), 792 (w), 752 (vs), 752 (s), 691 (s).

Melting point: 215 °C.

R_f (SiO_2, *i*Hex:EtOAc = 1:1) = 0.14.

2-((4-(Dimethylamino)phenyl)(pyridin-4-yl)methylene)benzo[*b*]thiophen-3(2*H*)-one (**33**)

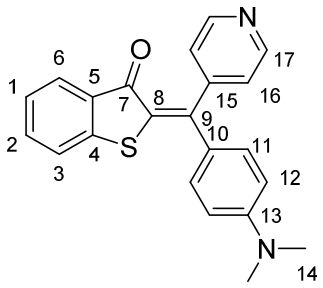

2-((4-(Dimethylamino)phenyl)(pyridin-4-yl)methylene)benzo[*b*]thiophen-3(2*H*)-one (**33**) was prepared according to **TP 4** from chloride (**12**) (0.20 mmol) and (4-*N*,*N*-dimethylaminophenylboronic acid (0.40 mmol). The title compound was purified by FCC (SiO_2, *i*Hex:EtOAc = 95:5 to 9:1) and isolated as dark red solid (64.1 mg, 0.19 mmol, 94%, mixture of *E*:*Z* = 5:1).

HR-MS (EI) for $C_{22}H_{18}ON_2{}^{32}S^{\cdot+}$, $[M]^{\cdot+}$, calcd. 358.1134, found 358.1132.

NMR spectra are only stated for the *E*-isomer due to the low concentration of the *Z*-isomer.

^{1}H NMR ($CDCl_3$, 600 MHz): δ (ppm) = 8.67 (d, ^3J(H,H) = 6.0 Hz, 1H, H-C(17)), 7.75 (d, ^3J(H,H) = 7.1 Hz, 1H, H-C(6)), 7.52 (app td, ^3J(H,H) = 8.2 Hz, ^4J(H,H) = 1.4 Hz, 1H, H-C(2)), 7.43 (d, ^3J(H,H) = 7.9 Hz, 1H, H-C(3)), 7.33 (d, ^3J(H,H) = 9.1 Hz, 2H, H-C(11)), 7.22 (app td, ^3J(H,H) = 7.8 Hz, ^4J(H,H) = 0.9 Hz, 1H, H-C(1)), 7.18 (d, ^3J(H,H) = 6.0 Hz, 1H, H-C(16)), 6.67 (d, ^3J(H,H) = 9.1 Hz, 2H, H-C(12)), 3.04 (s, 6H, H-C(14)).

^{13}C NMR ($CDCl_3$, 150 MHz): δ (ppm) = 186.8 (C(7)), 151.2 (C(13)), 149.9 (C(17)), 149.4 (C(15)), 147.7 (C(9)), 145.8 (C(4)), 134.6 (C(2)), 132.6 (C(8)), 132.5 (C(5)), 132.1 (C(11)), 127.0 (C(6)), 126.7 (C(10)), 125.2 (C(1)), 124.3 (C(16)), 123.4 (C(3)), 111.4 (C(12)), 40.2 (C(14)).

IR: $\tilde{\upsilon}$/cm^{-1} = 1658 (m), 1602 (s), 1593 (s), 1585 (s), 1547 (w), 1513 (vs), 1487 (s), 1449 (m), 1407 (m), 1368 (s), 1313 (m), 1279 (s), 1230 (w), 1217 (w), 1204 (s), 1184 (w), 1161 (m), 1060 (s), 1017 (w), 1001 (w), 989 (w), 964 (m), 951 (m), 884 (w), 821 (s), 802 (w), 792 (w), 745 (s), 732 (w) 692 (w), 671 (w).

Melting point: 241 °C.

R_f (SiO_2, *i*Hex:EtOAc = 1:1) = 0.11.

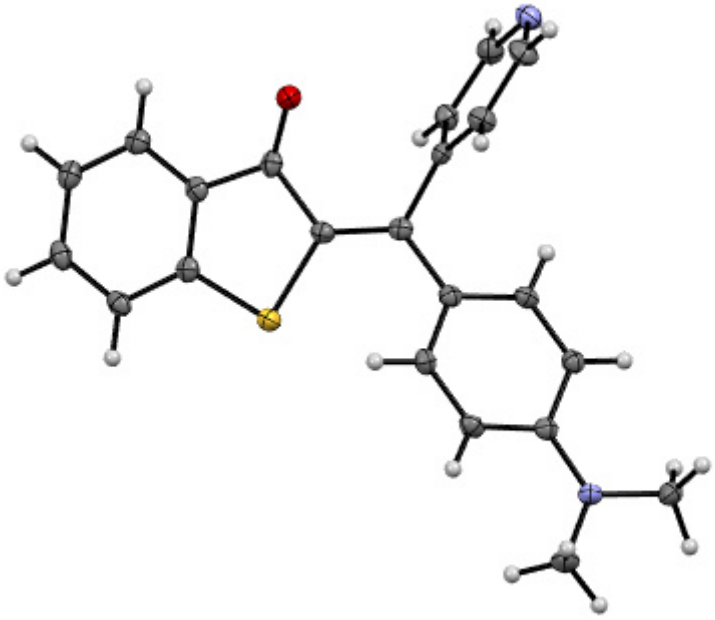

Figure 4: MERCURY-picture of the *E*-isomeric structure of **33** in the crystalline state**.** Crystal structural data are given in the appendix.

2-(1-(Pyridin-4-yl)-3-(triisopropylsilyl)prop-2-yn-1-ylidene)benzo[*b*]thiophen-3(2*H*)-one (**34**)

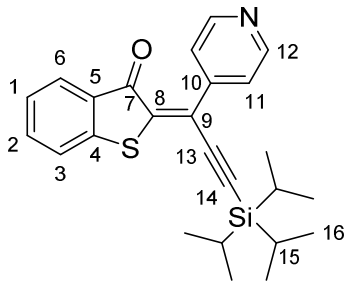

2-(1-(Pyridin-4-yl)-3-(triisopropylsilyl)prop-2-yn-1-ylidene)benzo[*b*]thiophen-3(2*H*)-one (**34**) was prepared according to **TP 5** from chloride (**12**) (0.20 mmol) and (triisopropylsilyl)acetylene (0.25 mmol). The title compound was purified by FCC (SiO_2, *i*Hex:EtOAc = 8:2 to 7:3) and isolated as orange oil (77 mg, 0.183 mmol, 91%, *E*:*Z* = 1.4:1.0).

HR-MS (EI) for $C_{25}H_{29}NO^{32}S^{28}Si^{\cdot+}$, $[M]^{\cdot+}$, calcd. 419.1734, found 419.1736.

***E*-isomer:**

^{1}H NMR ($CDCl_3$, 400 MHz): δ (ppm) = 8.72 (dd, ^{3}J(H,H) = 6.1 Hz, ^{4}J(H,H) = 1.6 Hz, 2H, H-C(12)), 7.95 (d, ^{3}J(H,H) = 7.7 Hz, 1H, H-C(6)), 7.62 (dd, ^{3}J(H,H) = 6.2 Hz, ^{4}J(H,H) = 1.7 Hz, 2H, H-C(11)), 7.55 (ddd, ^{3}J(H,H) = 8.4, Hz, ^{3}J(H,H) = 7.6 Hz, ^{4}J(H,H) = 1.2 Hz, 1H, H-C(2)), 7.37 (d, ^{3}J(H,H) = 7.9 Hz, 1H, H-C(3)), 7.29 (app t, ^{3}J(H,H) = 7.5 Hz, 1H, H-C(1)), 1.21 – 1.14 (m, 21H, H-C(15), H-C(16)).

^{13}C NMR ($CDCl_3$, 101 MHz): δ (ppm) = 185.6 (C(7)), 150.4 (C(12)), 146.9 (C(10)), 143.2 (C(4)), 141.1 (C(8)), 135.4 (C(2)), 131.3 (C(5)), 127.5 (C(6)), 125.9 (C(1)), 124.0 (C(9)), 123.5 (C(3)), 123.0 (C(11)), 108.4 (C(14)), 104.7 (C(13)), 18.8 (C(16)), 11.5 (C(15)).

IR: ϑ/cm^{-1} = 2941 (m), 2889 (m), 2863 (m), 1680 (s), 1586 (s), 1550 (m), 1523 (m), 1488 (m), 1450 (s), 1407 (m), 1384 (w), 1327 (w), 1312 (m), 1280 (s), 1216 (m), 1158 (w), 1123 (m), 1069 (m), 999 (vs), 988 (s), 954 (m), 918 (m), 881 (s), 828 (m), 800 (m), 740 (s), 721 (w), 683 (m), 670 (m).

R_f (SiO_2, *i*Hex:EtOAc = 7:3) = 0.53.

***Z*-isomer:**

^{1}H NMR ($CDCl_3$, 400 MHz): δ (ppm) = 8.67 (d, ^{3}J(H,H) = 6.0 Hz, 2H, H-C(12)), 7.73 (d, ^{3}J(H,H) = 8.3 Hz, 1H, H-C(6)), 7.57 (app t, ^{3}J = 8.3 Hz, 1H, H-C(2)), 7.48 (d, ^{3}J = 6.1 Hz, 2H, H-C(11)), 7.45 (d, ^{3}J = 7.9 Hz, 1H, H-C(3)), 7.25 (app t, ^{3}J = 7.5 Hz, 2H, H-C(1)), 1.21 – 1.11 (m, 21H, H-C(15), H-C(16)).

^{13}C NMR ($CDCl_3$, 100 MHz): δ (ppm) = 185.2 (C(7)), 149.7 (C(12)), 144.3 (C(4)), 143.2 (C(10)), 141.2 (C(8)), 135.8 (C(2)), 132.5 (C(5)), 127.3 (C(6)), 126.8 (C(9)), 125.8 (C(1)), 123.9 (C(3)), 123.5 (C(11)), 110.5 (C(14)), 106.4 (C(13)), 18.8 (C(16)), 11.3 (C(15)).

IR: $\tilde{\upsilon}/cm^{-1}$ = 2942 (s), 2889 (m), 2863 (s), 1675 (s), 1586 (s), 1552 (m), 1522 (m), 1488 (m), 1451 (s), 1407 (m), 1284 (w), 1282 (vs), 1218 (m), 1159 (w), 1111 (w), 1064 (s), 1018 (m), 998 (s), 955 (w), 905 (m), 881 (m), 816 (s), 742 (s), 727 (m), 684 (s).

R_f (SiO_2, hexanes:EtOAc = 7:3) = 0.48.

2-(1-(Pyridin-4-yl)ethylidene)benzo[*b*]thiophen-3(2*H*)-one (**35**)

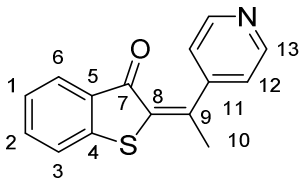

Copper iodine (0.2 mmol, 1.0 equiv) was suspensed in dry THF (1 mL) in a flame-dried flask and cooled to -78 °C. Methyl lithium (1.5 M in diethylether, 0.27 mL, 0.4 mmol, 2.0 equiv) was added under argon atmosphere. The solution was warmed slowly to 22 °C until the suspension became clear. Subsequently, the reaction mixture was added slowly to another flame-dried flask containing a 0.1 M solution of chloride **12** (0.2 mmol, 1.0 equiv) in dry THF under argon atmosphere. The reaction was warmed slowly to 22 °C over 3 hours and quenched with sat. aq. NH_4Cl (10 mL). The aqueous phase was extracted with dichloromethane (3 x 20 mL), the combined organic phases were dried over Na_2SO_4 and the solvent was removed *in vacuo*. The title compound was purified by FCC (SiO_2, *i*Hex:EtOAc = 95:5) and isolated as yellow oil (38.5 mg, 0.15 mmol, 76%, *E*:*Z* = only the *Z*-isomer was obtained).

HR-MS (EI) for $C_{15}H_{11}NO^{32}S^{\cdot+}$, $[M]^{\cdot+}$, calcd. 253.0555, found 253.0551.

^{1}H NMR ($CDCl_3$, 600 MHz): δ (ppm) = 8.73 (bs, 2H, H-C(13)), 7.89 (dd, ^3J(H,H) = 7.7 Hz, ^4J(H,H) = 1.4 Hz, 1H, H-C(6)), 7.57 – 7.51 (m, 1H, H-C(2)), 7.37 (d, ^3J(H,H) = 6.0 Hz, 2H, H-C(12)), 7.35 (d, ^3J(H,H) = 7.9 Hz, 1H, H-C(3)), 7.28 (app t, ^3J(H,H) = 7.3 Hz, 1H, H-C(1)), 2.80 (s, 3H, H-C(10)).

^{13}C NMR ($CDCl_3$, 150 MHz): δ (ppm) = 188.8 (C(7)), 151.4 (C(11)), 150.2 (C(13)), 146.7 (C(9)), 145.4 (C(4)), 135.2 (C(2)), 132.2 (C(5)), 131.2 (C(8)), 127.1 (C(6)), 125.4 (C(1)), 123.5 (C(3)), 122.0 (C(12)), 21.1 (C(10)).

IR: $\tilde{\upsilon}/cm^{-1}$ = 1668 (vs), 1590 (vs), 1555 (m), 1509 (m), 1448 (s), 1369 (m), 1311 (m), 1284 (s), 1217 (w), 1186 (w), 1158 (w), 1106 (w), 1078 (w), 1019 (w), 976 (m), 908 (w), 817 (m), 791 (w), 741 (s), 721 (w), 660 (w).

R_f (SiO_2, *i*Hex:EtOAc = 7:3) = 0.26.

Methyl Substituted HTI

2-(1-(3,5-Dimethoxyphenyl)ethylidene)benzo[*b*]thiophen-3(2*H*)-one (**36**)

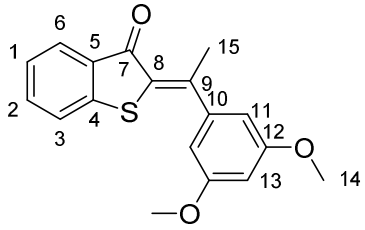

2-(1-(3,5-Dimethoxyphenyl)ethylidene)benzo[*b*]thiophen-3(2*H*)-one (**36**) was prepared according to **TP 4** from chloride (**13**) (0.20 mmol) and potassium (4-methoxyphenyl)trifluoroborate (0.30 mmol), but without a base and with APhos Pd G3 (5 mol%) as catalyst. The title compound was purified by FCC (SiO_2, *i*Hex:EtOAc = 95:5 to 9:1) and isolated as yellow oil (55.8 mg, 0.18 mmol, 89%, mixture of *E*:*Z* = 1:8).

HR-MS (EI) for $C_{18}H_{16}O_3{}^{32}S^{\cdot+}$, $[M]^{\cdot+}$, calcd. 312.0815, found 312.0816.

NMR spectra are only stated for the *Z*-isomer due to the low concentration of the *E*-isomer.

^{1}H NMR ($CDCl_3$, 600 MHz): δ (ppm) = 7.88 (dd, ^3J(H,H) = 7.8 Hz, ^4J(H,H) = 1.2 Hz, 1H, H-C(6)), 7.50 (app t, ^3J(H,H) = 7.2 Hz, 1H, H-C(2)), 7.34 (d, ^3J(H,H) = 7.9 Hz, 1H, H-C(3)), 7.25 (app t, ^3J(H,H) = 7.8 Hz, 1H, H-C(1)), 6.59 (d, ^4J(H,H) = 2.3 Hz, 2H, H-C(11)), 6.49 (t, ^4J(H,H) = 2.2 Hz, 1H, H-C(13)), 3.83 (s, 6H, H-C(14)), 2.81 (s, 3H, H-C(15)).

^{13}C NMR ($CDCl_3$, 150 MHz): δ (ppm) = 188.8 (C(7)), 161.0 (C(12)), 151.2 (C(9)), 146.1 (C(4)), 145.6 (C(10)), 134.7 (C(2)), 132.8 (C(5)), 130.2 (C(8)), 126.9 (C(6)), 124.9 (C(1)), 123.4 (C(3)), 105.5 (C(11)), 101.0 (C(13)), 55.6 (C(14)), 21.8 (C(15)).

IR: $\tilde{\upsilon}/cm^{-1}$ = 1667 (m), 1589 (vs), 1566 (m), 1450 (m), 1421 (w), 1350 (w), 1282 (m), 1205 (m), 1156 (s), 1112 (w), 1083 (w), 1061 (m), 988 (w), 926 (w), 926 (w), 742 (m), 699 (w).

R_f (SiO_2, *i*Hex:EtOAc = 95:5) = 0.38.

Nicotinic-Acid Derived HTIs

4-(2,2-Dimethyl-1-(3-oxothieno[2,3-*b*]pyridin-2(3*H*)-ylidene)propyl)benzonitrile (**37**)

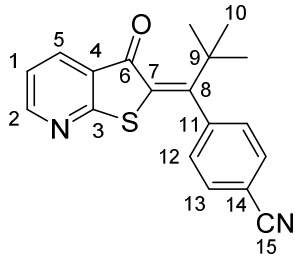

4-(2,2-Dimethyl-1-(3-oxothieno[2,3-*b*]pyridin-2(3*H*)-ylidene)propyl)benzonitrile (**37**) was prepared according to **TP 4** from chloride (**37**) (0.20 mmol) and (4-cyanophenyl)boronic acid (0.30 mmol). The title compound was purified by FCC (SiO_2, hexanes:EtOAc = 9:1 to 7:3) and isolated as pale yellow solid (51 mg, 0.160 mmol, 78%, *Z*:*E* = 1.0:2.8).

Analytic data were only recorded for one isomer due to insufficient material of the *Z*-isomer.

***E*-isomer:**

HR-MS (EI) for $C_{19}H_{16}ON_2S^{\cdot+}$, $[M]^{\cdot+}$, calcd. 320.0978, found 320.0973.

^{1}H NMR ($CDCl_3$, 600 MHz): δ (ppm) = 8.67 (dd, ^3J(H,H) = 4.9 Hz, ^4J(H,H) = 1.8 Hz, 1H, H-C(2)), 7.83 (dd, ^3J(H,H) = 7.6 Hz, ^3J(H,H) = 1.8 Hz, 1H, H-C(5)), 7.73 – 7.70 (m, 2H, H-C(13)), 7.17 (dd, ^3J(H,H) = 7.7 Hz, ^3J(H,H) = 4.8 Hz, 1H, H-C(1)), 7.13 – 7.10 (m, 2H, H-C(12)), 1.31 (s, 9H, H-C(10)).

^{13}C NMR ($CDCl_3$, 151 MHz): δ (ppm) = 186.5 (C(6)), 166.8 (C(3)), 160.3 (C(8)), 156.1 (C(2)), 146.9 (C(15)), 134.4 (C(5)), 132.4 (C(13)), 129.2 (C(7)), 127.3 (C(12)), 125.3 (C(4)), 120.6 (C(1)), 119.0 (C(11)), 111.1 (C(14)), 38.4 (C(9)), 29.6 (C(10)).

IR: $\tilde{\upsilon}$/cm^{-1} = 3355 (w), 3276 (w), 2972 (m), 2225 (s), 1679 (vs), 1603 (s), 1575 (s), 1545 (s), 1512 (m), 1497 (m), 1458 (m), 1395 (vs), 1368 (m), 1284 (s), 1252 (m), 1216 (s), 1172 (m), 1133 (m), 1090 (m), 1058 (s), 1021 (m), 933 (w), 856 (w), 828 (s), 781 (m), 761 (s), 701 (w), 683 (w).

Melting point: 197 – 199 °C.

R_f (SiO_2, *i*Hex:EtOAc = 8:2) = 0.29.

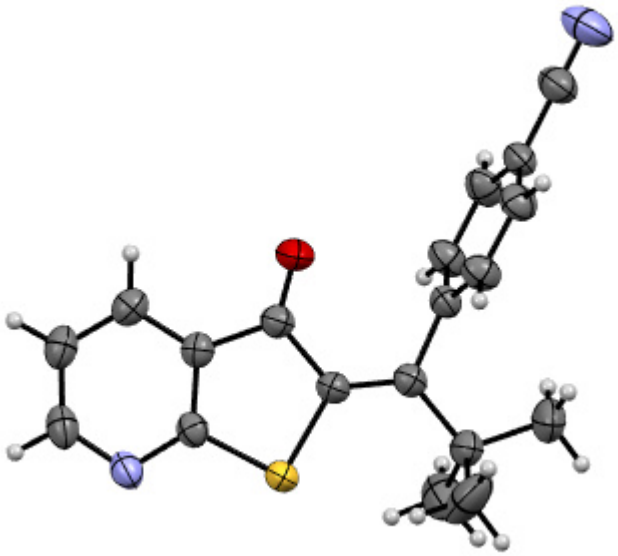

Figure 5: MERCURY-picture of the *E*-isomeric structure of **37** in the crystalline state**.** Crystal structural data are given in the appendix.

2-(1-(4-(Dimethylamino)phenyl)-2,2-dimethylpropylidene)thieno[2,3-*b*]pyridin-3(2*H*)-one (**38**)

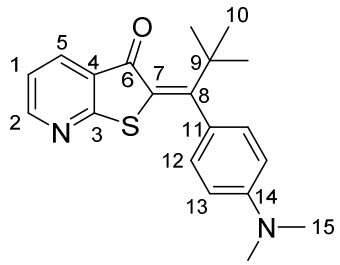

2-(1-(4-(Dimethylamino)phenyl)-2,2-dimethylpropylidene)thieno[2,3-*b*]pyridin-3(2*H*)-one (**38**) was prepared according to **TP 4** from chloride (**14**) (0.20 mmol) and (4-(dimethylamino)phenyl)boronic acid (0.30 mmol). The title compound was purified by FCC (SiO_2, *i*Hex:EtOAc = 9:1 to 8:2) and isolated as red solid (42 mg, 0.125 mmol, 61%). The product was obtained as a mixture of *E*- and *Z*-isomers (*Z*:*E* = 1.0:1.5).

HR-MS (EI) for $C_{20}H_{22}ON_2S^{\cdot+}$, $[M]^{\cdot+}$, calcd. 338.1447, found 338.1441.

^{1}H NMR ($CDCl_3$, 599 MHz): δ (ppm) = 8.62 (dd, ^3J(H,H) = 4.7 Hz, ^4J(H,H) = 1.8 Hz, 1H, H-C(2)$_E$), 8.57 (dd, ^3J(H,H) = 4.8 Hz, ^4J(H,H) = 1.8 Hz, 1H, H-C(2)$_Z$), 8.01 (dd, ^3J(H,H) = 7.7 Hz, ^4J(H,H) = 1.8 Hz, 1H, H-C(5)$_Z$), 7.84 (dd, ^3J(H,H) = 7.7 Hz, ^4J(H,H) = 1.8 Hz, 1H, H-C(5)$_E$), 7.12 (m, 2H, H-C(1$_E$, 1$_Z$), 6.97 (d app t, ^3J(H,H) = 8.7 Hz, ^4J(H,H) = 3.0 Hz, 2H, H-C(12)$_Z$), 6.84 (d, ^3J(H,H) = 8.2 Hz, 2H, H-C(12)$_E$), 6.77 (d, ^3J(H,H) = 7.3 Hz, 2H, H-C(13)$_Z$), 6.72 (d, ^3J(H,H) = 8.5 Hz, 2H, H-C(13)$_E$), 3.01 (s, 6H, H-C(15)$_Z$), 3.00 (s, 6H, H-C(15)$_E$), 1.34 (s, 9H, H-C(10)$_Z$), 1.32 (s, 9H, H-C(10)$_E$).

^{13}C NMR ($CDCl_3$, 151 MHz): δ (ppm) = 186.5 (C(6)$_E$), 185.2 (C(6)$_Z$), 168.6 (C(8)$_E$), 167.8 (C(3)$_Z$), 166.7 (C(3)$_E$), 164.9 (C(8)$_Z$), 155.6 (C(2)$_E$), 155.4 (C(2)$_Z$), 149.9 (C(14)$_Z$), 149.5 (C(14)$_E$), 134.4 (C(5)$_Z$), 134.2 (C(5)$_E$), 132.5 (C(11)$_Z$), 129.3 (C(11)$_E$), 128.5 (C(7)$_E$), 128.0 (C(4)$_Z$), 127.5 (C(12$_Z$)), 127.1 (C(12)$_E$), 126.1 (C(4)$_E$), 120.2 (C(1)$_E$), 119.8 (C(1)$_Z$), 112.1 (C(13)$_E$), 111.5 (C(13)$_Z$), 40.5 (C(15)$_E$), 40.5 (C(15)$_Z$), 39.2 (C(9)$_Z$), 39.1 (C(9)$_E$), 29.7 (C(10)$_E$), 29.2 (C(10)$_Z$).

C(7)$_Z$ could not be found and might superimpose with the signal of C(7)$_E$.

IR: $\tilde{\upsilon}$/cm^{-1} = 2889 (w), 2807 (w), 1661 (s), 1607 (s), 1573 (s), 1536 (m), 1511 (s), 1478 (m), 1455 (m), 1395 (s), 1349 (s), 1285 (s), 1256 (m), 1216 (m), 1192 (m), 1166 (m), 1126 (m), 1094 (m), 1073 (m), 1010 (w), 953 (m), 944 (m), 894 (w), 812 (s), 772 (vs), 733 (w), 700 (w), 690 (w).

Melting point: 218 – 221 °C.

R$_f$ (SiO_2, *i*Hex:EtOAc = 8:2) = 0.46.

2-(4,4-Dimethyl-1-(triisopropylsilyl)pent-1-yn-3-ylidene)thieno[2,3-*b*]pyridin-3(2*H*)-one (**39**)

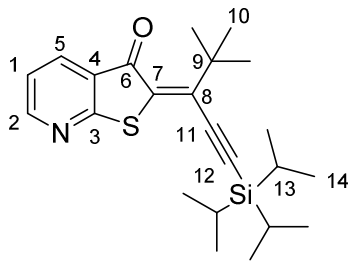

2-(4,4-Dimethyl-1-(triisopropylsilyl)pent-1-yn-3-ylidene)thieno[2,3-*b*]pyridin-3(2*H*)-one (**39**) was prepared according to **TP 5** from chloride (**14**) (0.20 mmol) and (triisopropylsilyl)acetylene (0.25 mmol). The title compound was purified by FCC (SiO_2, *i*Hex:EtOAc = 95:5 to 9:1) and isolated as orange oil (73 mg, 0.183 mmol, 89%, *E*:*Z* = 1.0:1.4).

HR-MS (EI) for $C_{23}H_{33}ON^{32}S^{28}Si^{\cdot+}$, $[M]^{\cdot+}$, calcd. 399.2047, found 399.2043.

***E*-isomer:**

^{1}H NMR ($CDCl_3$, 400 MHz): δ (ppm) = 8.62 (dd, ^{3}J(H,H) = 4.8 Hz, ^{4}J(H,H) = 1.8 Hz, 1H, H-C(2)), 7.99 (dd, ^{3}J(H,H) = 7.7 Hz, ^{3}J(H,H) = 1.8 Hz, 1H, H-C(5)), 7.17 (dd, ^{3}J(H,H) = 7.7 Hz, ^{3}J(H,H) = 4.8 Hz, 1H, H-C(1)), 1.46 (s, 9H, H-C(10)), 1.19 – 1.14 (m, 21H, H-C(13), H-C(14)).

^{13}C NMR ($CDCl_3$, 101 MHz): δ (ppm) = 183.2 (C(6)), 167.2 (C(3)), 155.4 (C(2)), 146.5 (C(8)), 140.2 (C(7)), 134.4 (C(5)), 128.1 (C(4)), 120.3 (C(1)), 114.3 (C(11)), 107.5 (C(12)), 37.7 (C(9)), 28.9 (C(10)), 18.8 (C(14)), 11.5 (C(13)).

C(11) and C(12) could not be assigned distinctively and could be interchanged.

IR: $\tilde{\upsilon}/cm^{-1}$ = 2942 (s), 2865 (s), 1669 (vs), 1572 (s), 1495 (s), 1458 (m), 1398(vs), 1363 (m), 1281 (m), 1253 (w), 1215 (m), 1152 (w), 1125 (m), 1092 (m), 1061 (m), 1012 (m), 996 (m), 957 (w), 910 (w), 882 (m), 861 (m), 779 (w), 763 (m), 748 (w), 680 (vs).

R_f (SiO_2, *i*Hex:EtOAc = 9:1) = 0.66.

***Z*-isomer:**

^{1}H NMR ($CDCl_3$, 400 MHz): δ (ppm) = 8.64 (dd, ^{3}J(H,H) = 4.8 Hz, ^{4}J(H,H) = 1.8 Hz, 1H, H-C(2)), 8.10 (dd, ^{3}J(H,H) = 7.7 Hz, ^{4}J(H,H) = 1.8 Hz, 1H, H-C(5)), 7.19 (dd, ^{3}J(H,H) = 7.7 Hz, ^{3}J(H,H) = 4.8 Hz, 1H, H-C(1)), 1.46 (s, 9H, H-C(10)), 1.19 – 1.16 (m, 21H, H-C(13), H-C(14)).

^{13}C NMR ($CDCl_3$, 101 MHz): δ (ppm) = 184.7 (C(6)), 165.3 (C(3)), 155.6 (C(2)), 140.6 (C(8)), 136.7 (C(7)), 134.4 (C(5)), 125.3 (C(4)), 120.4 (C(1)), 110.1 (C(11)), 105.1 (C(12)), 38.2 (C(9)), 29.6 (C(10)), 18.9 (C(14)), 11.6 (C(13)).

C(11) and C(12) could not be assigned distinctively and could be interchanged.

IR: $\tilde{\upsilon}/cm^{-1}$ = 2941 (s), 2864 (s), 2127 (w), 1682 (s), 1571 (s), 1509 (m), 1456 (s), 1397 (vs), 1365 (m), 1282 (s), 1257 (m), 1214 (m), 1151 (m), 1125 (m), 1092 (m), 1062 (w), 1045 (m), 1009 (s), 956 (s), 919 (w), 881 (s), 861 (m), 848 (m), 782 (w), 762 (s), 721 (m), 679 (s).

R_f (SiO_2, *i*Hex:EtOAc = 9:1) = 0.47.

Heteroatom Substituted HTIs

2-(Pyrrolidin-1-yl(*p*-tolyl)methylene)benzo[*b*]thiophen-3(2*H*)-one (**40**)

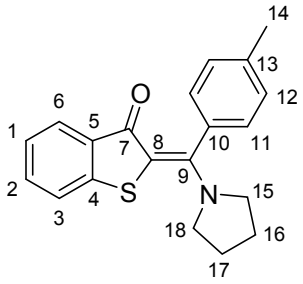

2-(Pyrrolidin-1-yl(*p*-tolyl)methylene)benzo[*b*]thiophen-3(2*H*)-one (**40**) was prepared according to **TP 7** from chloride (**11**) (0.40 mmol) and pyrrolidine (1.6 mmol). The title compound was purified by FCC (SiO_2, EtOAc = 100%) and isolated as orange solid (128 mg, 0.40 mmol, quant). The product was obtained as a mixture of *E*- and *Z*-isomers (*Z*:*E* = 1.0:5.6).

HR-MS (EI) for $C_{20}H_{19}ON^{32}S^{\cdot+}$, $[M]^{\cdot+}$, calcd. 321.1182, found 321.1184.

NMR signal could only be assigned for the major *E*-isomer.

^{1}H NMR ($CDCl_3$, 599 MHz): δ (ppm) = 7.92 (d, ^3J(H,H) = 7.8 Hz, 1H, H-C(6)), 7.40 – 7.34 (m, 2H, H-C(2), H-C(3)), 7.29 (s, 4H, H-C(12), H-C(11)), 7.24 (ddd, ^3J(H,H) = 8.0 Hz, ^3J(H,H) = 6.6 Hz, ^4J(H,H) =1.4 Hz, 1H, H-C(1)), 4.00 (s, 2H, H-C(15 or 18)), 3.40 (s, 2H, H-C(15 or 18)), 2.44 (s, 3H, H-C(14)), 2.02 (m, 4H, H-C(16, 17)).

^{13}C NMR ($CDCl_3$, 151 MHz): δ (ppm) = 178.7 (C(7)), 158.1 (C(9)), 143.6 (C(4)), 140.6 (C(13)), 136.1 (C(5)), 134.8 (C(10)), 130.5 (C(2)), 129.7 (C(12)), 128.8 (C(11)), 125.3 (C(6)), 123.6 (C(1)), 122.8 (C(3)), 105.1 (C(8)), 54.8 (C(15 or 18)), 52.9 (C(15 or 18)), 26.0 (C(16 or 17)), 25.7 (C(16 or 17)), 21.7 (C(14)).

Proton and carbon signals of 15, 18 and 17, 16, respectively, are interchangeable and could not be assigned distinctively.

IR: $\tilde{\upsilon}/cm^{-1}$ = 3062 (w), 2926 (w), 2871 (w), 1922 (w), 1599 (s), 1584 (s), 1562 (m), 1484 (s), 1443 (vs), 1326 (s), 1280 (s), 1250 (m), 1228 (m), 1154 (m), 1110 (m), 1074 (s), 1030 (m), 1018 (m), 978 (w), 951 (w), 919 (w), 861 (w), 828 (m), 788 (w), 772 (w), 739 (s), 702 (w), 665 (w).

Melting point: 180 – 183 °C.

R_f (SiO_2, EtOAc = 100%) = 0.27.

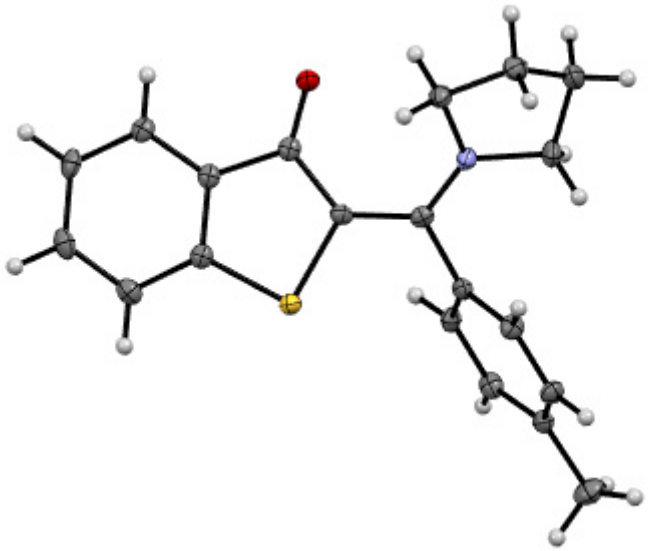

Figure 6: MERCURY-picture of the *E*-isomeric structure of **40** in the crystalline state**.** Crystal structural data are given in the appendix.

2-(Ethoxy(*p*-tolyl)methylene)benzo[*b*]thiophen-3(2*H*)-one (**41**)

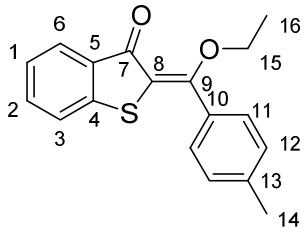

Chloride **11** (0.40 mmol, 1.0 equiv) was dissolved in dry EtOH (5 mL) in a flame-dried flask and sodium ethoxide (0.44 mmol, 1.0 equiv) was added under argon atmosphere. After 1 hour sat. aq. NH_4Cl (10 mL) was added and the aqueous phase was extracted with dichloromethane (3 x 20 mL), the combined organic phases were dried over Na_2SO_4 and the solvent was removed *in vacuo.* The title compound was purified by FCC (SiO_2, *i*Hex:EtOAc = 95:5) and isolated as yellow solid (105.2 mg, 0.35 mmol, 89%, *E*:*Z* = 1:9).

Analytical data was only recorded for the major *Z*-isomer.

HR-MS (EI) for $C_{18}H_{16}O_2{}^{32}S^{\cdot+}$, $[M]^{\cdot+}$, calcd. 296.0866, found 296.0864.

^{1}H NMR ($CDCl_3$, 600 MHz): δ (ppm) = 7.72 (d, ^3J(H,H) = 7.7 Hz, 1H, H-C(6)), 7.50 (app t, ^3J(H,H) = 6.9 Hz, 1H, H-C(2)), 7.46 (d, ^3J(H,H) = 7.9 Hz, 1H, H-C(3)), 7.35 (d, ^3J(H,H) = 8.1 Hz, 2H, H-C(11)), 7.32 (d, ^3J(H,H) = 8.1 Hz, 2H, H-C(12)), 7.18 (app t, ^3J(H,H) = 7.3 Hz, 1H, H-C(1)), 3.93 (q, ^3J(H,H) = 7.0 Hz, 2H, H-C(15)), 2.44 (s, 3H, H-C(14)), 1.30 (t, ^3J(H,H) = 7.1 Hz, 3H, H-C(16)).

^{13}C NMR ($CDCl_3$, 150 MHz): δ (ppm) = 186.0 (C(7)), 164.9 (C(9)), 144.6 (C(4)), 140.8 (C(13)), 134.3 (C5)), 134.0 (C(2)), 129.5 (C(12)), 129.1 (C(11)), 128.3 (C(10)), 126.2 (C(6)), 124.6 (C(1)), 123.7 (C(3)), 114.1 (C(8)), 66.4 (C(15)), 21.8 (C(14)), 15.5 (C(16)).

IR: $\tilde{\upsilon}$/cm^{-1} =1667 (m), 1583 (m), 1554 (s), 1507 (m), 1472 (w), 1448 (m), 1404 (w), 1337 (w), 1291 (s), 1284 (s), 1261 (s), 1223 (m), 1183 (w), 1169 (m), 1144 (m), 1117 (w), 1091 (w), 1078 (w), 1061 (s), 997 (m), 969 (w), 950 (w), 913 (m), 885 (m), 821 (m), 780 (w), 769 (w), 742 (vs), 727 (m), 694 (w), 662 (w).

Melting point: 66 °C.

R_f (SiO_2, *i*Hex:EtOAc = 90:10 = 0.43.

2-((Pyridin-4-ylthio)(*p*-tolyl)methylene)benzo[*b*]thiophen-3(2*H*)-one (**42**)

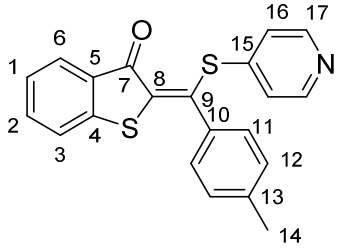

Chloride **11** (0.40 mmol, 1.0 equiv) was dissolved in THF (5 mL), potassium carbonate (0.60 mmol, 1.5 equiv) and pyridine-4-thiol (0.44 mmol, 1.1 equiv) were added and the solution was stirred for 12 hours. Subsequently, sat. aq. NH_4Cl (10 mL) was added and the aqueous phase was extracted with dichloromethane (3 x 20 mL), the combined organic phases were dried over Na_2SO_4 and the solvent was removed *in vacuo*. The title compound was purified by FCC (SiO_2, *i*Hex:EtOAc = 1:1) and isolated as yellow solid (136.6 mg, 0.38 mmol, 94%, only the *E*-isomer was obtained).

HR-MS (EI) for $C_{21}H_{15}ON^{32}S^{\cdot+}$, $[M]^{\cdot+}$, calcd. 361.0590, found 361.0584.

^{1}H NMR ($CDCl_3$, 400 MHz): δ (ppm) = 8.28 (d, ^3J(H,H) = 4.0 Hz, 2H, H-C(17)), 7.96 (d, ^3J(H,H) = 8.9 Hz, 1H, H-C(6)), 7.52 (ddd, ^3J(H,H) = 8.4 Hz, ^3J(H,H) = 7.3 Hz, ^4J(H,H) = 1.3 Hz, 1H, H-C(2)), 7.36 (d, ^3J(H,H) = 7.9 Hz, 1H, H-C(3)), 7.29 (app t, ^3J(H,H) = 7.5 Hz, 1H, H-C(1)), 7.13 (d, ^3J(H,H) = 8.2 Hz, 2H, H-C(11)), 7.09 (d, ^3J(H,H) = 6.0 Hz, 2H, H-C(16)), 7.03 (d, ^3J(H,H) = 7.9 Hz, 2H, H-C(12)), 2.27 (s, 3H, H-C(14)).

^{13}C NMR ($CDCl_3$, 100 MHz): δ (ppm) = 186.5 (C(7)), 149.4 (C(17)), 148.3 (C(9)), 145.6 (C(4)), 143.2 (C(15)), 139.8 (C(13)), 134.5 (C(2)), 134.0 (C(10)), 132.1 (C(5)), 129.4 (C(11)), 129.3 (C(12)), 128.9 (C(8)), 128.2 (C(16)), 126.9 (C(6)), 125.2 (C(1)), 123.4 (C(3)), 21.5 (C(14)).

IR: $\tilde{\upsilon}/cm^{-1}$ = 1644 (s), 1606 (w), 1582 (m), 1569 (m), 1548 (w), 1528 (m) 1495 (s), 1456 (w), 1445 (m), 1402 (s), 1379 (w), 1313 (w), 1283 (s), 1241 (w), 1231 (w), 1213 (m), 1159 (w), 1111 (w), 1098 (m), 1063 (m), 1038 (w), 1017 (m), 987 (w), 960 (m), 865 (m), 824 (w), 811 (m), 791 (s), 762 (m), 741 (vs), 704 (w), 690 (m).

Melting point: 198 °C.

R_f (SiO_2, *i*Hex:EtOAc = 1:1) = 0.36.

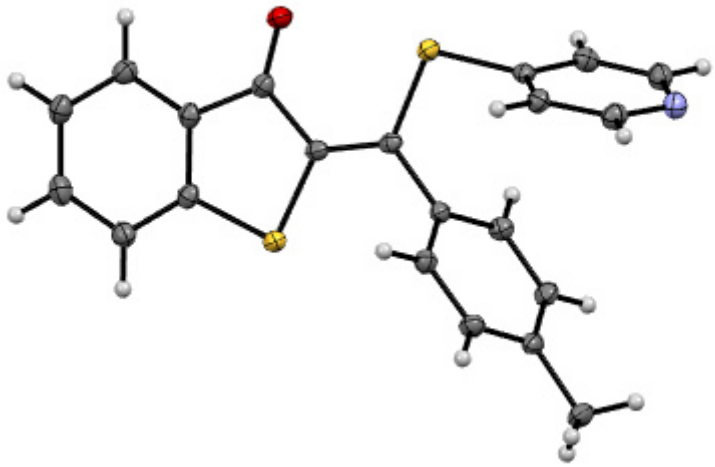

Figure 7: MERCURY-picture of the *E*-isomeric structure of **42** in the crystalline state**.** Crystal structural data are given in the appendix.

2-(Pyridin-4-yl(pyrrolidin-1-yl)methylene)benzo[*b*]thiophen-3(2*H*)-one (**43**)

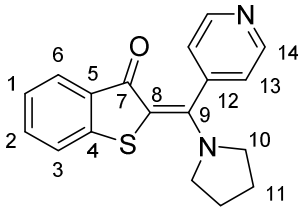

2-(Pyridin-4-yl(pyrrolidin-1-yl)methylene)benzo[*b*]thiophen-3(2*H*)-one (**43**) was prepared according to **TP 7** from chloride (**12**) (0.20 mmol) and pyrrolidine (0.4 mmol). The title compound was purified by crystallization from *n*heptane/methylenchloride and isolated as orange solid (61.2 mg, 0.20 mmol, 99%, mixture of *Z*:*E* = 1:1.2).

HR-MS (EI) for $C_{18}H_{16}ON_2{}^{32}S^{\cdot+}$, $[M]^{\cdot+}$, calcd. 308.0978, found 308.0967.

^{1}H NMR ($CDCl_3$, 400 MHz): δ (ppm) = 8.78 (d, ^3J(H,H) = 5.9 Hz, 1H, H-C(14)$_E$), 8.75 (d, ^3J(H,H) = 5.8 Hz, 2H, H-C(14)$_Z$), 7.90 (d, ^3J(H,H) = 7.9 Hz, 1H, H-C(6)$_E$), 7.72 (d, ^3J(H,H) = 7.8 Hz, 1H, H-C(6)$_Z$), 7.48 (d, ^3J(H,H) = 7.8 Hz, 1H, H-C(3)$_Z$), 7.44 (app t, ^3J(H,H) = 6.9 Hz, 1H, H-C(2)$_Z$), 7.41 (app t, ^3J(H,H) = 7.1 Hz, 1H, H-C(2)$_E$), 7.36 (d, ^3J(H,H) = 7.9 Hz, 1H, H-C(3)$_E$), 7.31 (d, ^3J(H,H) = 5.9 Hz, 1H, H-C(13)$_E$), 7.26 (app t, ^3J(H,H) = 4.8 Hz, 1H, H-C(1)$_E$), 7.22 (d, ^3J(H,H) = 6.0 Hz, 1H, H-C(13)$_Z$), 7.18 (app t, ^3J(H,H) = 7.4 Hz, 1H, H-C(1)$_Z$), 3.91 (bs, 2H, H-C(10)$_E$), 3.61 (bs, 4H, H-C(10)$_Z$), 3.36 (bs, 2H, H-C(10)$_E$), 2.03 (bs, 4H, H-C(11)$_E$), 1.96 (bs, 4H, H-C(11)$_Z$).

^{13}C NMR ($CDCl_3$, 100 MHz): δ (ppm) = 184.2 (C(7)$_Z$), 179.7 (C(7)$_E$), 155.1 (C(9)$_Z$), 154.0 (C(9)$_E$), 150.9 (C(14)$_E$), 150.8 (C(14)$_Z$), 146.4 (C(12)$_Z$), 145.0 (C(12)$_E$), 143.4 (C(4)$_E$), 142.8 (C(4)$_Z$), 135.4 (C(5)$_E$), 134.2 (C(5)$_Z$), 132.2 (C(2)$_Z$), 131.2 (C(2)$_E$), 125.9 (C(6)$_Z$), 125.5 (C(6)$_E$), 124.2 (C(1)$_Z$), 124.0 (C(1)$_E$), 122.8 (C(3,13)$_E$), 122.7 (C(3)$_Z$), 122.4 (C(13)$_Z$), 104.4 (C(8)$_E$), 101.8 (C(8)$_Z$), 51.7 (C(10)$_Z$), 25.6 (C(11)$_Z$).

(C(10)$_E$) and (C(11)$_E$) could not be found, because of line broadening from pseudo rotation around the amine nitrogen atom.

IR: $\tilde{\upsilon}$/cm^{-1} = 1624 (w), 1596 (m) 1584 (m), 1490 (vs), 1473 (s), 1444 (vs), 1405 (m), 1325 (s), 1285 (m), 1251 (w), 1229 (w), 1214 8w), 1160 (w), 1093 (w), 1071 (s), 1029 (w), 1018 (w), 993 (w), 952 (w), 931 (m), 894 (w), 869 (w), 858 (w), 831 (w), 785 (m), 737 (s), 726 (m), 690 (w), 671 (w).

Melting point: 198 °C.

R_f (SiO_2, EtOAc) = 0.06.

2-(1-(Pyrrolidin-1-yl)ethylidene)benzo[*b*]thiophen-3(2*H*)-one (**44**)

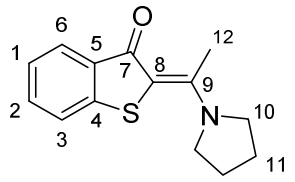

2-(1-(Pyrrolidin-1-yl)ethylidene)benzo[*b*]thiophen-3(2*H*)-one (**44**) was prepared according to **TP 7** from chloride (**13**) (0.47 mmol) and pyrrolidine (0.94 mmol). The title compound was purified by crystallization from *n*heptane/dichloromethane and isolated as orange solid (116.8 mg, 0.47 mmol, quant, *E*:*Z* = 1:20).

HR-MS (EI) for $C_{14}H_{15}ON^{32}S^{\cdot+}$, $[M]^{\cdot+}$, calcd. 245.0869, found 245.0871.

NMR spectra are only stated for the *Z*-isomer due to the low concentration of the *E*-isomer.

^{1}H NMR ($CDCl_3$, 400 MHz): δ (ppm) = 7.91 (bs, 1H, H-C(6)), 7.47 (bs, 1H, H-C(3)), 7.42 (app t, ^{3}J(H,H) = 7.4 Hz, 1H, H-C(2)), 7.25 (app t, ^{3}J(H,H) = 7.8 Hz, 1H, H-C(1)), 3.80 (bs, 4H, H-C(10)), 2.92 (bs, 2H, H-C(12)), 2.45 (bs, 1H, H-C(12)), 2.00 (bs, 4H, H-C(11)).

^{13}C NMR ($CDCl_3$, 100 MHz): δ (ppm) = 184.2 (C(7)), 161.1 (C(9)), 141.6 (C(4)), 131.2 (C(2)), 125.7 (C(6)), 123.7 (C(1)), 123.4 (C(5)), 122.8 (C(3)), 51.3 (C(10)), 25.5 (C(11)), 23.3 (C(12)), 19.1 (C(12)).

The Signal of C(8) could not be found due to line broadening and very weak signals in the ^{13}C-NMR caused by the pseudo rotation around the nitrogen atom.

IR: $\tilde{\upsilon}$/cm^{-1} = 1585 (m), 1560 (w), 1520 (vs), 1445 (m), 1391 (m), 1366 (m), 1345 (w), 1335 (s), 1320 (w), 1303 (w), 1282 (m), 1262 (w), 1223 (w), 1170 (w), 1113 (m), 1074 (m), 1033 (m), 1016 (m), 988 (w), 964 (w), 952 (w), 925 (w), 902 (m), 863 (w), 878 (w), 777 (w), 733 (vs), 691 (w), 681 (m).

Melting point: 177 °C.

R_f (SiO_2, EtOAc) = 0.09.

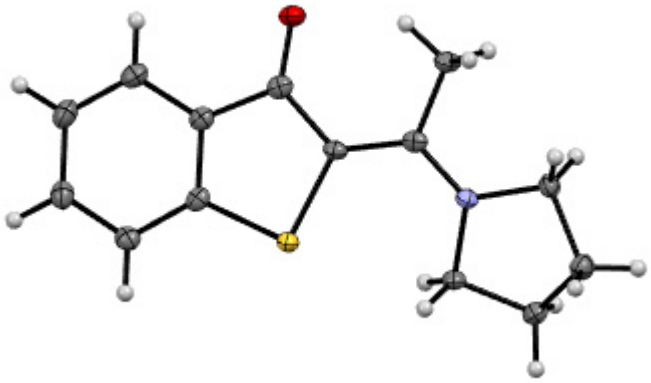

Figure 8: MERCURY-picture of the *Z*-isomeric structure of **44** in the crystalline state**.** Crystal structural data are given in the appendix.

Determination of *E*/*Z* Stereochemistry

It was not possible to obtain crystal structure information for all HTIs, due to high cost and time effort. Therefore, crystal structures were only recorded for some selected HTIs to determine their stereochemistry. Correlation between these crystal structures and the corresponding ^{1}H-NMR shows very characteristic chemical shift differences of certain protons in *E*- or *Z*-conformation. The differences between these shifts are shown in Scheme 1 and are marked with ↑ for a downfield shift of a proton (higher ppm) or ↓ for an upfield shift of a proton (lower ppm).

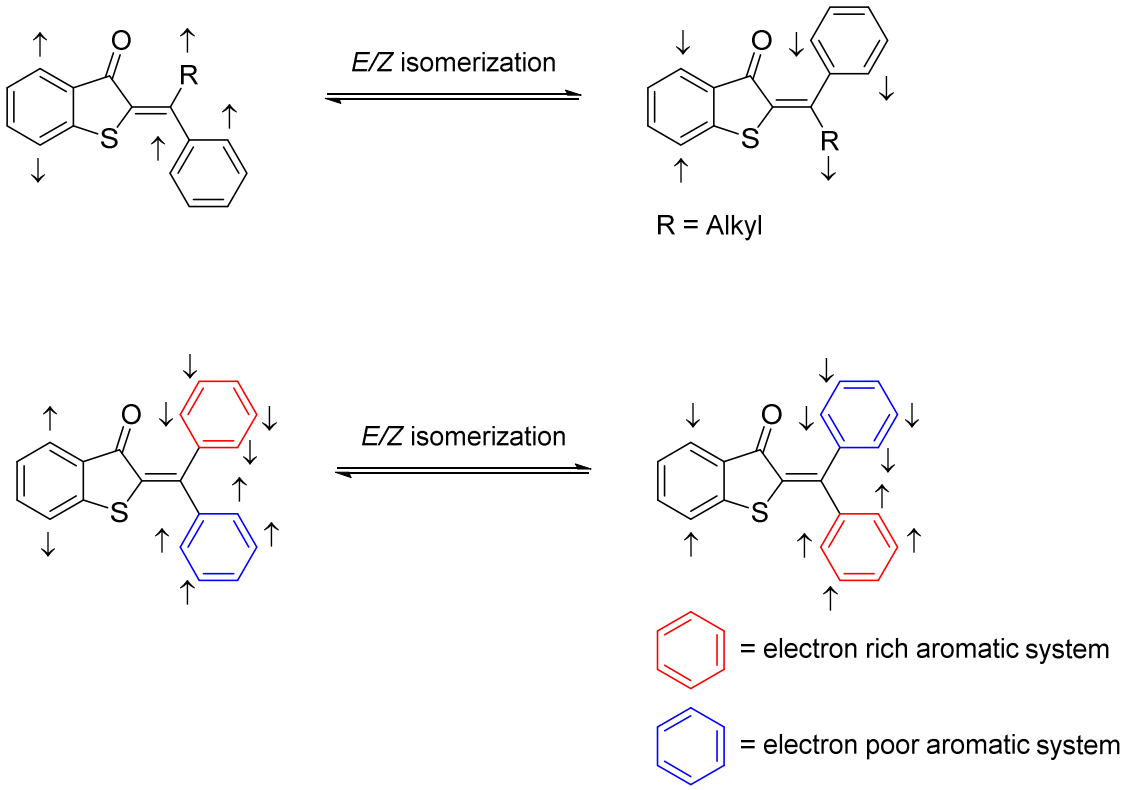

Scheme 1: Differences between chemical shifts in ^{1}H-NMR spectra of characteristic protons in *E*- or *Z*-conformation. The difference between these shifts is marked with ↑ for a downfield shift of a proton (higher ppm) or ↓ for an upfield shift of a proton (lower ppm).

These shifts can be explained by the ring current effect of the stilbene part, shown as an example in Scheme 2 for the red proton and the distance in relation to the carbonyl group.

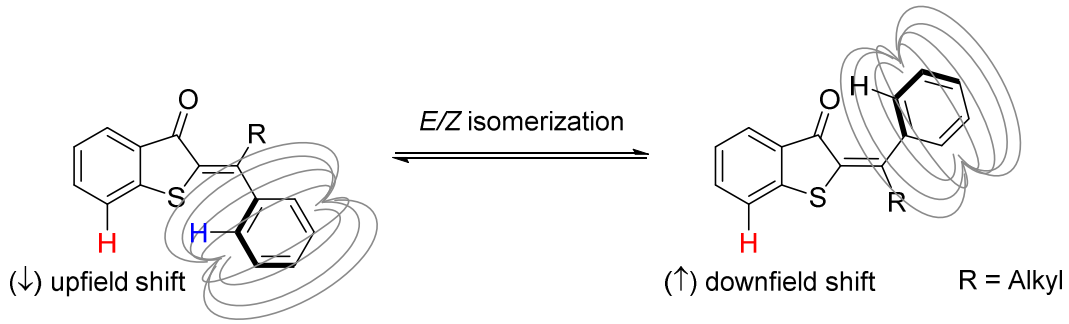

Scheme 2: Chemical shift difference for the red proton in the *E*- or *Z*-conformation.

Determination of Photophysical Properties

General

Determination of the UV-vis spectra of pure *E*- and *Z*-isomers

The UV-vis spectra of the pure *E*- or *Z*-isomers could only in some cases be obtained directly from isomerically pure material. If the *E*- or *Z*-isomer could not be separated purely, the UV-vis spectra of pure *E*- and *Z*-isomers were obtained by subtraction of a *E*/*Z*-mix spectrum with known composition (previously determined by integration of ^{1}H NMR signals) from a second *E*/*Z*-mix spectrum with different but also known isomer composition and a subsequent multiplication with an upkeep factor. Weighting is done by multiplying the first *E*/*Z*-mix spectrum with the *Z*- (or *E*-) isomer percentages of the second *E*/*Z*-mixture (determined via ^{1}H NMR spectroscopy) and *vice versa*. The obtained absorption spectrum of the respective pure isomer is multiplied by compensation factors to match the absorption values of the isosbestic points.

Extinction coefficients

Extinction coefficients were determined by charging a 10 mL volumetric flask with 0.1000 - 0.6000 mg (weighted on a *Sartorius Cubis* ® MSE2.7S balance) of the respective hemithioindigo and the desired solvent (spectroscopic grade) to obtain defined solutions of chromophores. From the known positions of the isosbestic points and the previously determined UV-vis spectra of the pure isomers, the extinction coefficients could be determined using the *Lambert-Beer* law.

UV-Vis-Spectra

2-(1-chloro-2,2-dimethylpropylidene)benzo[*b*]thiophen-3(2*H*)-one (**10**)

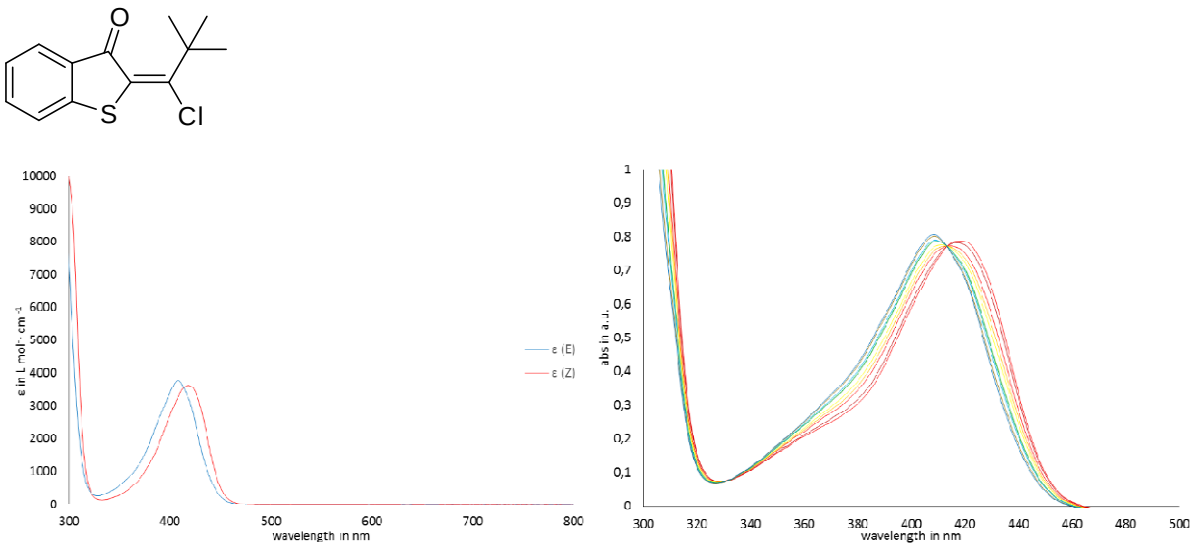

Figure 9: Calculated extinction coefficients for both isomers (left) and corresponding absorption changes during irradiation with 420 and 435 nm (right) of **10** in toluene.

2-(chloro(*p*-tolyl)methylene)benzo[*b*]thiophen-3(2*H*)-one (**11**)

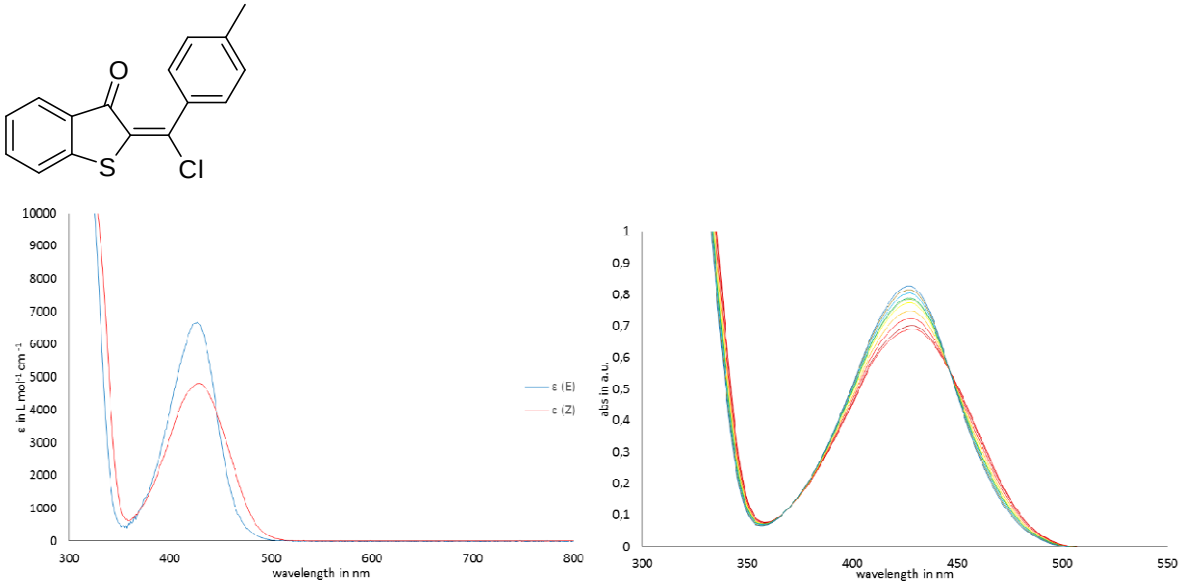

Figure 10: Calculated extinction coefficients for both isomers (left) and corresponding absorption changes during irradiation with 435 nm and 470 nm (right) of **11** in toluene.

2-(chloro(pyridin-4-yl)methylene)benzo[*b*]thiophen-3(2*H*)-one (**12**)

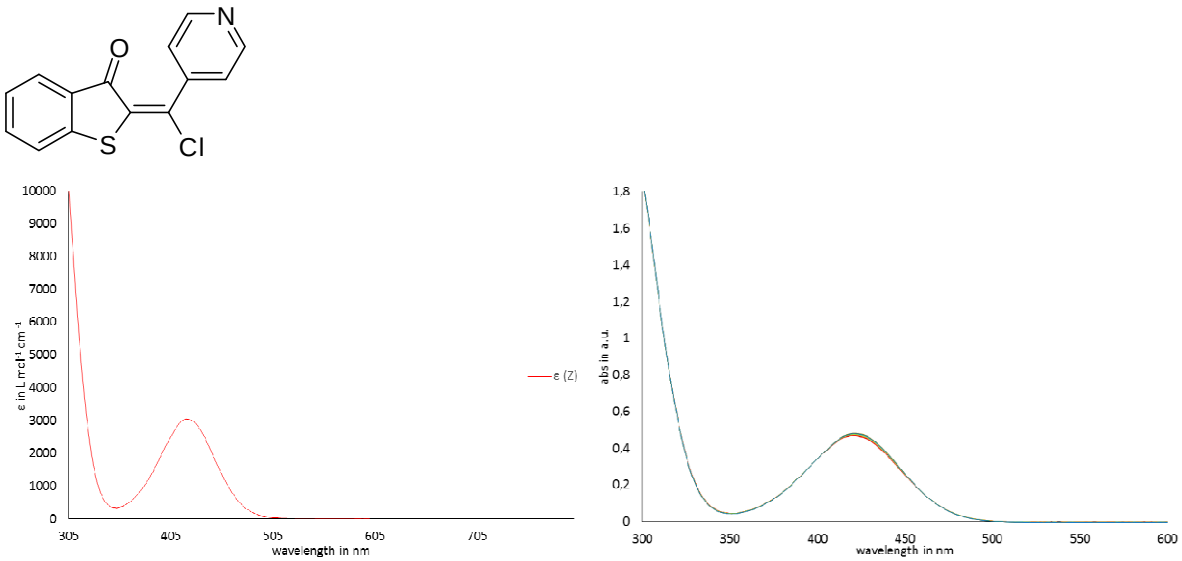

Figure 11: Extinction coefficients for the *Z*-isomer of HTI **12** (left) and corresponding absorption changes during irradiation with 405, 420, 435 and 450 nm (right) of **12** in toluene. It was not possible to generate enough *E*-isomer to calculate its extinction coefficients.

2-(1-chloroethylidene)benzo[*b*]thiophen-3(2*H*)-one (**13**)

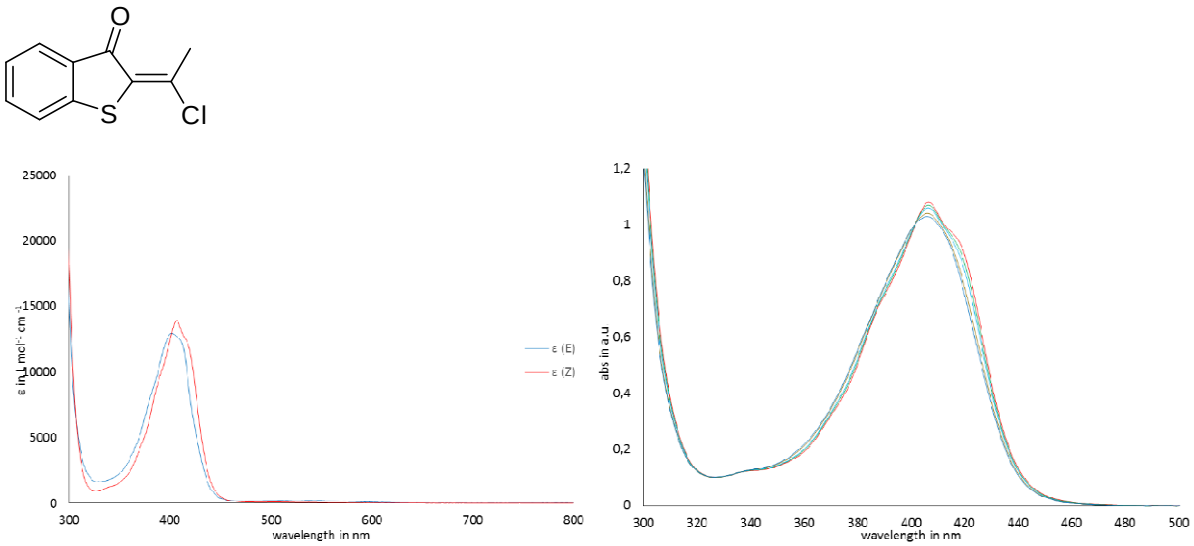

Figure 12: Calculated extinction coefficients for both isomers (left) and corresponding absorption changes during irradiation with 435 nm (right) of **13** in toluene.

2-(1-chloro-2,2-dimethylpropylidene)thieno[2,3-*b*]pyridin-3(2*H*)-one (**14**)

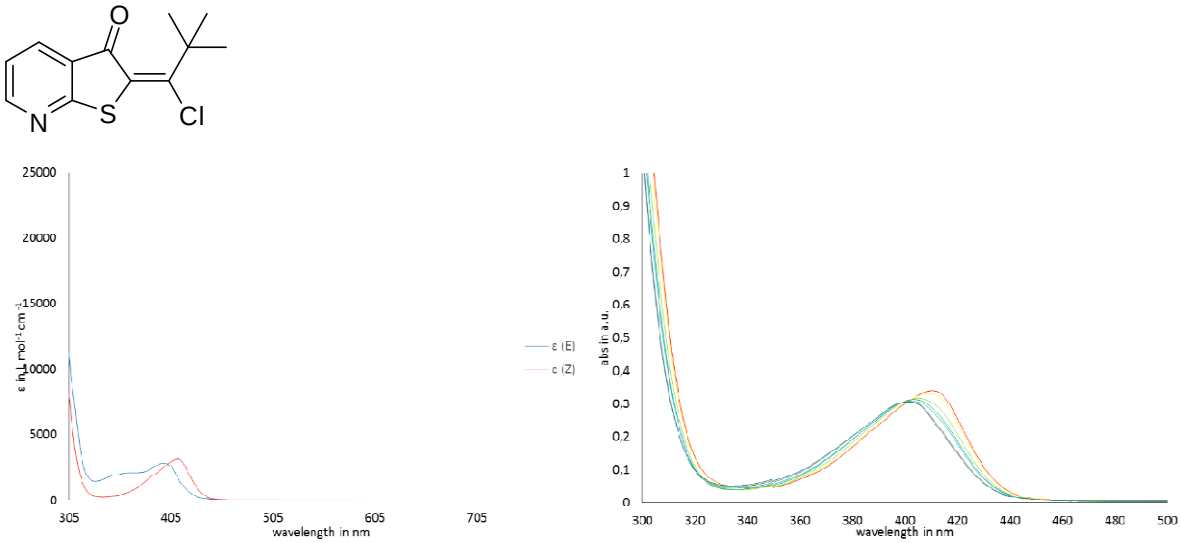

Figure 13: Calculated extinction coefficients for both isomers (left) and corresponding absorption changes during irradiation with 405, 435 and 450 nm (right) of **14** in toluene.

2-(2,2-dimethyl-1-phenylpropylidene)benzo[*b*]thiophen-3(2*H*)-one (**15**)

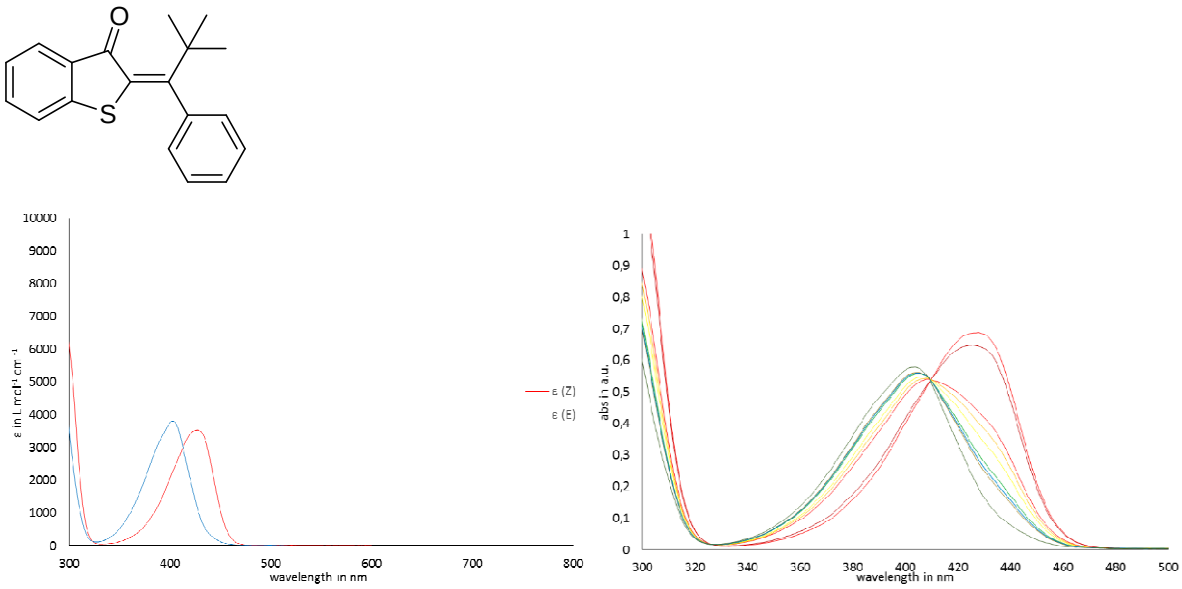

Figure 14: Extinction coefficients for both isomers (left) and corresponding absorption changes during irradiation with 420 nm and 470 nm (right) of **15** in toluene.

2-(1-(4-bromophenyl)-2,2-dimethylpropylidene)benzo[*b*]thiophen-3(2*H*)-one (**16**)

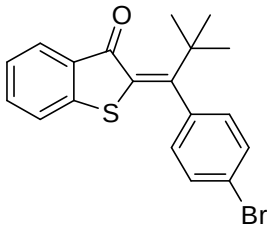

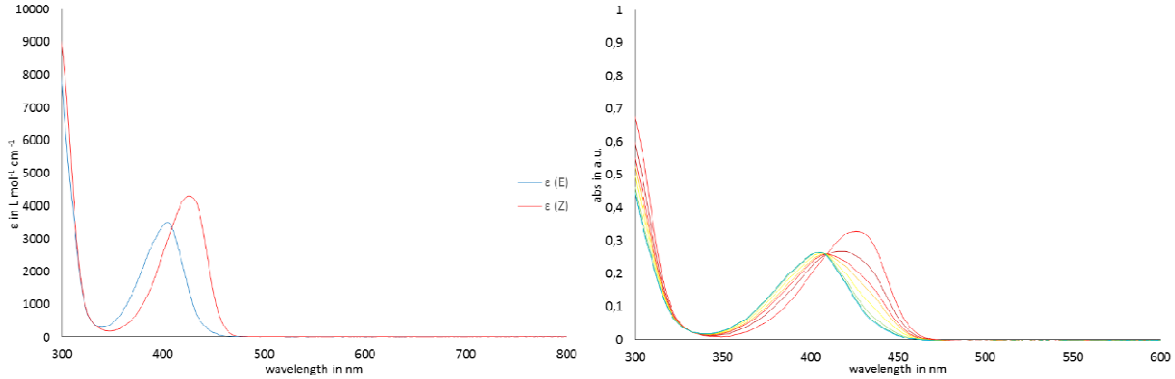

Figure 15: Calculated extinction coefficients for both isomers of HTI **16** (left) and corresponding absorption changes during irradiation with 435 and 450 nm (right) of **16** in toluene.

4-(2,2-dimethyl-1-(3-oxobenzo[*b*]thiophen-2(3*H*)-ylidene)propyl)benzonitrile (**17**)

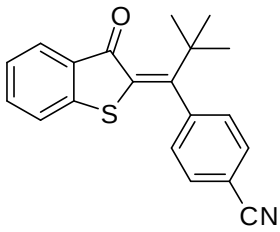

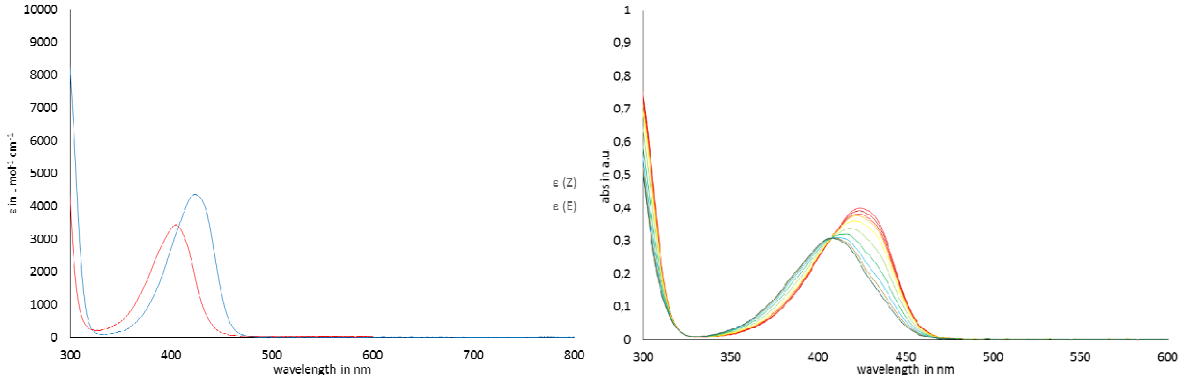

Figure 16: Extinction coefficients for both isomers of HTI **17** (left) and corresponding absorption changes during irradiation with 435 nm (right) of **17** in toluene.

2-(1-(4-(dimethylamino)phenyl)-2,2-dimethylpropylidene)benzo[*b*]thiophen-3(2*H*)-one (**18**)

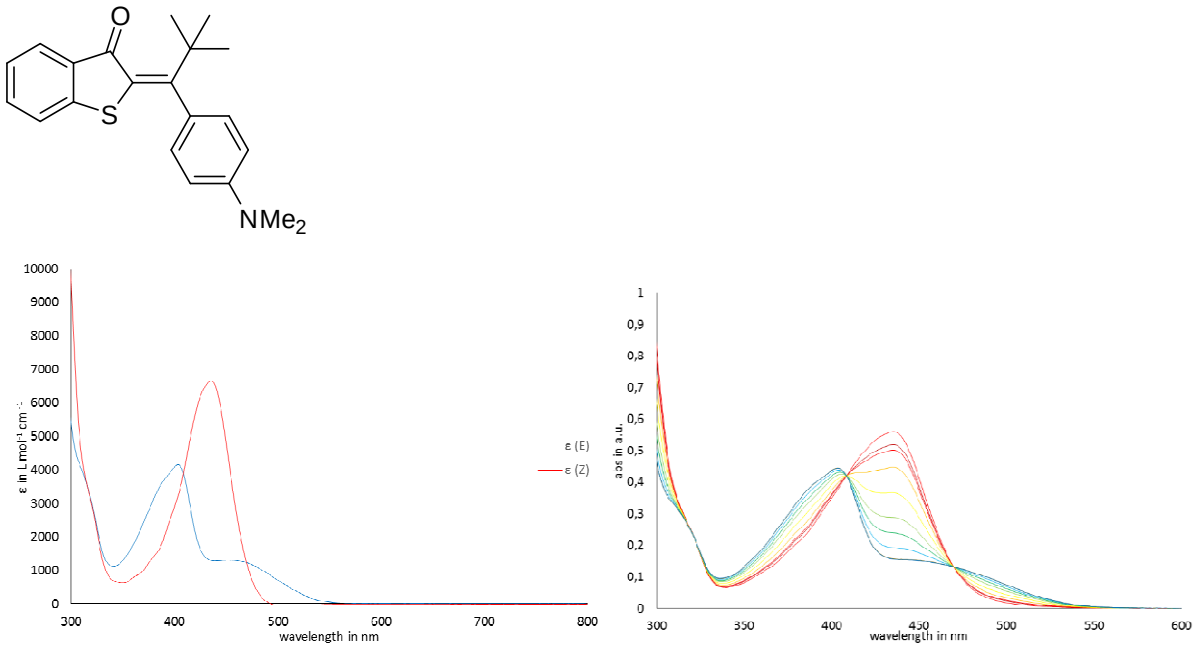

Figure 17: Calculated extinction coefficients for both isomers of HTI **18** (left) and corresponding absorption changes during irradiation with 450 and 530 nm (right) of **18** in toluene.

methyl 4-(2,2-dimethyl-1-(3-oxobenzo[*b*]thiophen-2(3*H*)-ylidene)propyl)benzoate (**19**)

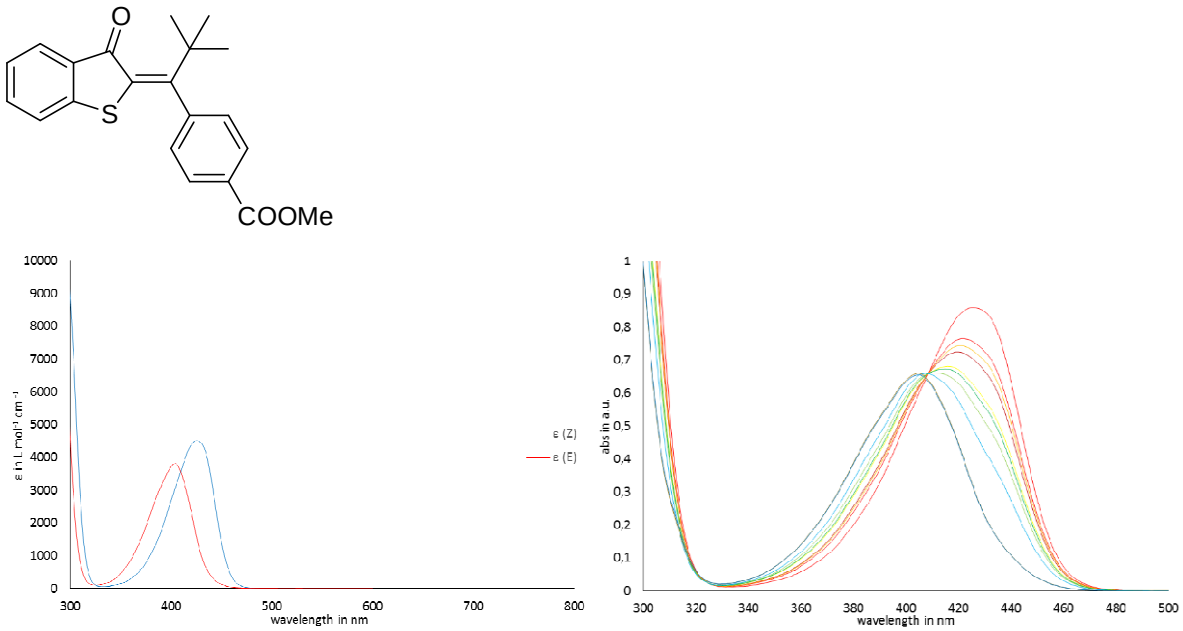

Figure 18: Extinction coefficients for both isomers (left) and corresponding absorption changes during irradiation with 435 nm (right) of **19** in toluene.

tert-butyl (4-(2,2-dimethyl-1-(3-oxobenzo[*b*]thiophen-2(3*H*)-ylidene)propyl)phenyl)carbamate (**20**)

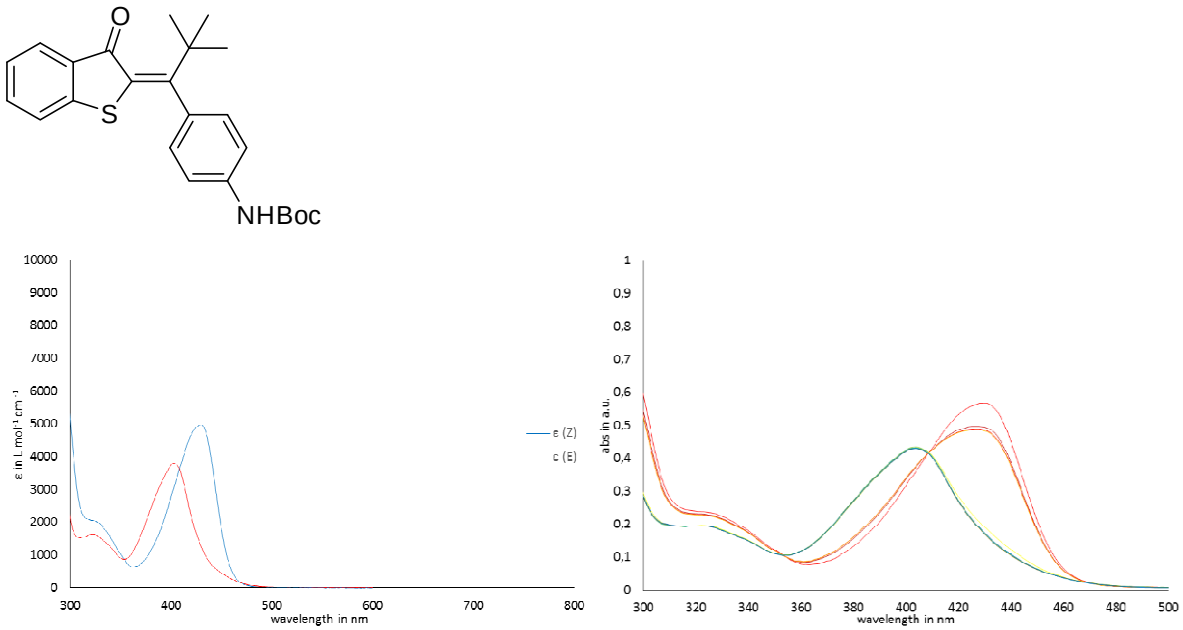

Figure 19: Extinction coefficients for both isomers of HTI **20** (left) and corresponding absorption changes during irradiation with 405, 435, 450, 470 nm (right) of **20** in toluene.

2-(1-(3,5-dimethoxyphenyl)-2,2-dimethylpropylidene)benzo[*b*]thiophen-3(2*H*)-one (**21**)

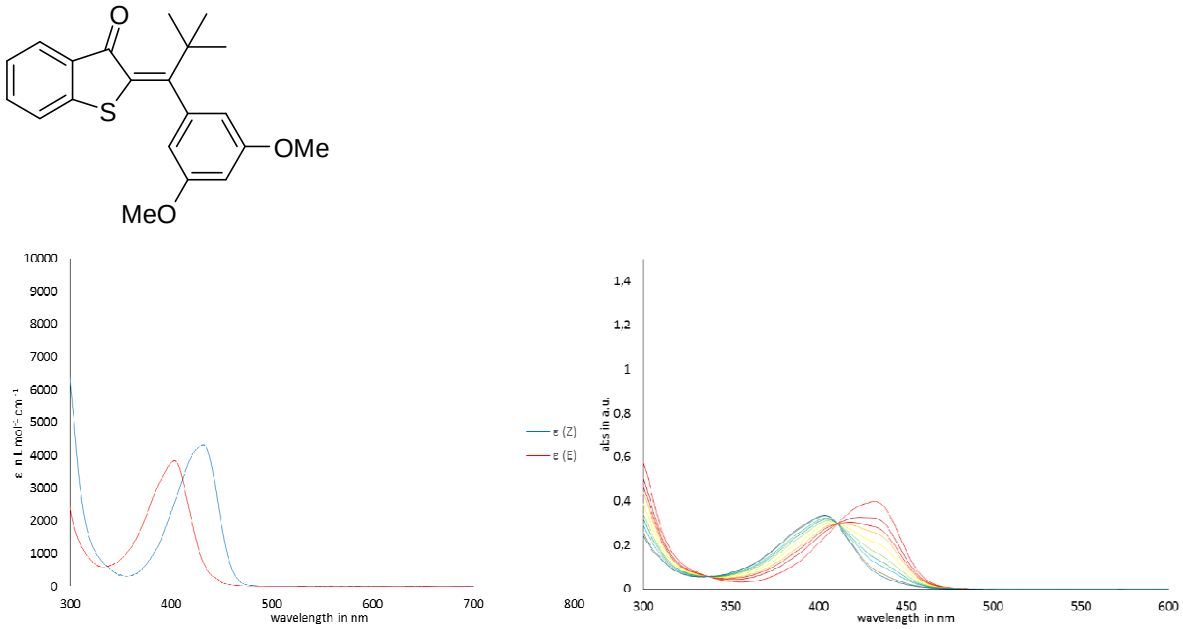

Figure 20: Extinction coefficients for both isomers of HTI **21** (left) and corresponding absorption changes during irradiation with 365, 435 and 450 nm (right) of **21** in toluene.

2-(1-(1*H*-indol-5-yl)-2,2-dimethylpropylidene)benzo[*b*]thiophen-3(2*H*)-one (**22**)

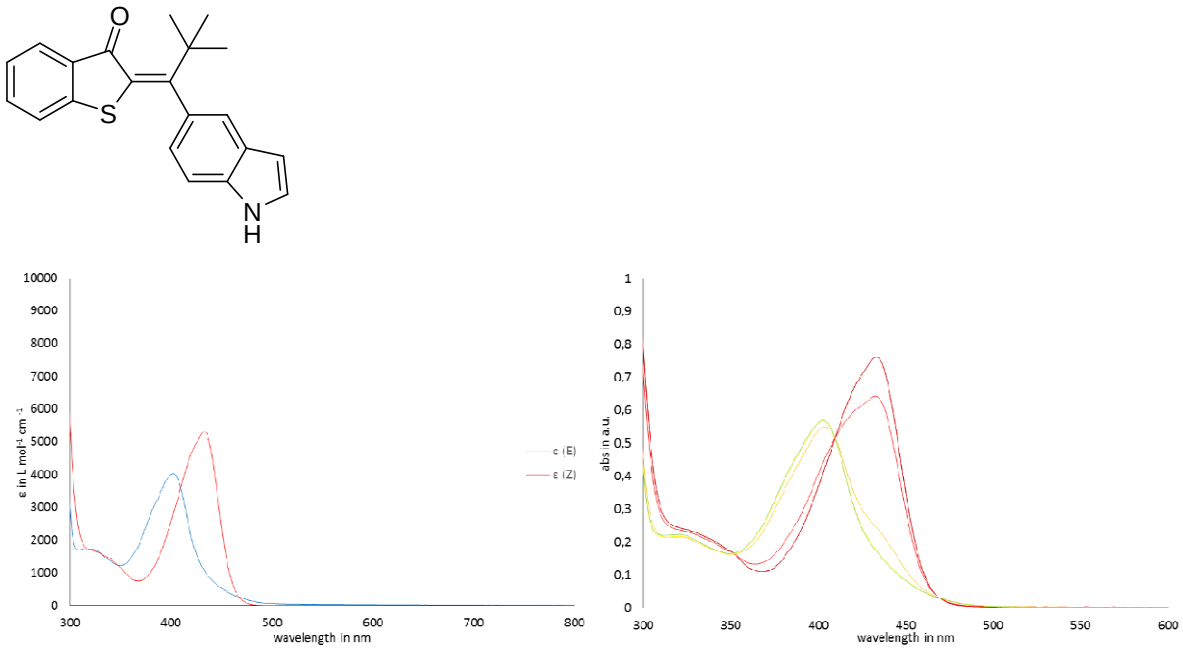

Figure 21: Calculated extinction coefficients for both isomers of HTI **22** (left) and corresponding absorption changes during irradiation with 435 nm (right) of **22** in toluene.

2-(1-(furan-2-yl)-2,2-dimethylpropylidene)benzo[*b*]thiophen-3(2*H*)-one (**23**)

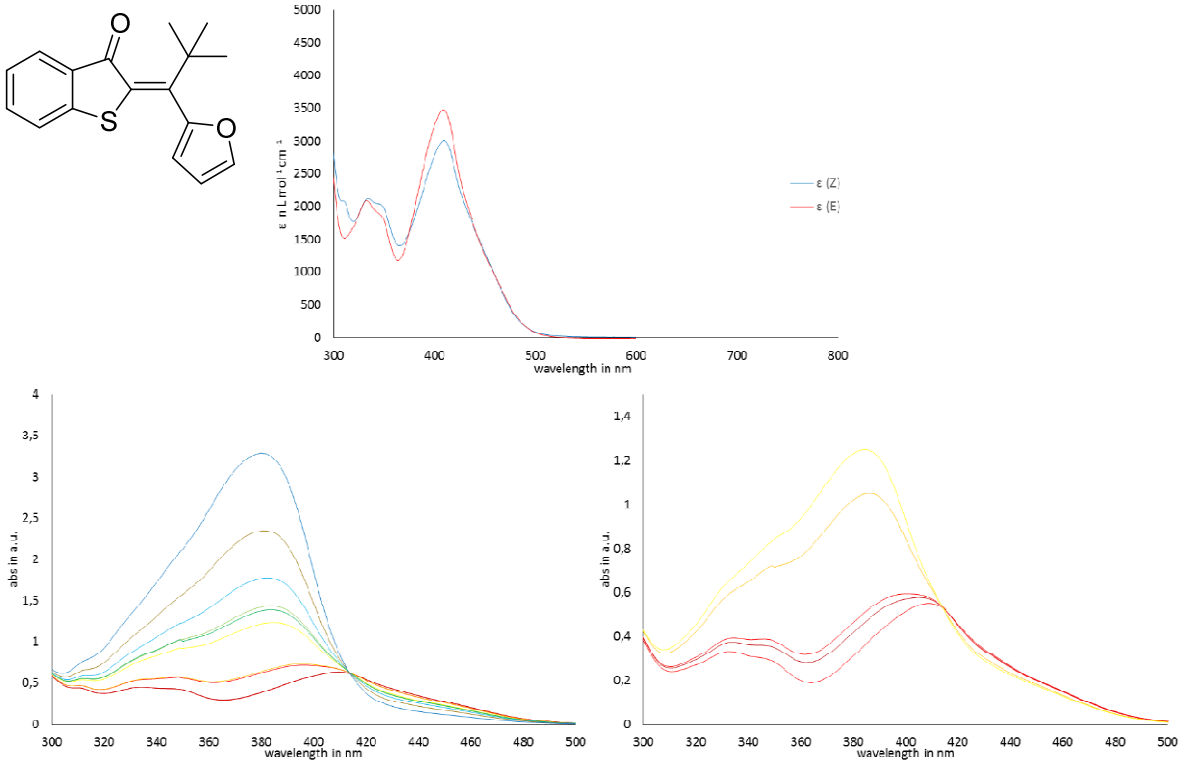

Figure 22: Extinction coefficients for both isomers of HTI **23** (top) and corresponding absorption changes during irradiation with 420 nm of the *Z*-isomer (bottom left) and the *E*-isomer (bottom right) of **23** in toluene. Both isomers are decomposing during irradiation in an unknown product.

2-(4,4-dimethyl-1-(triisopropylsilyl)pent-1-yn-3-ylidene)benzo[*b*]thiophen-3(2*H*)-one (**25**)

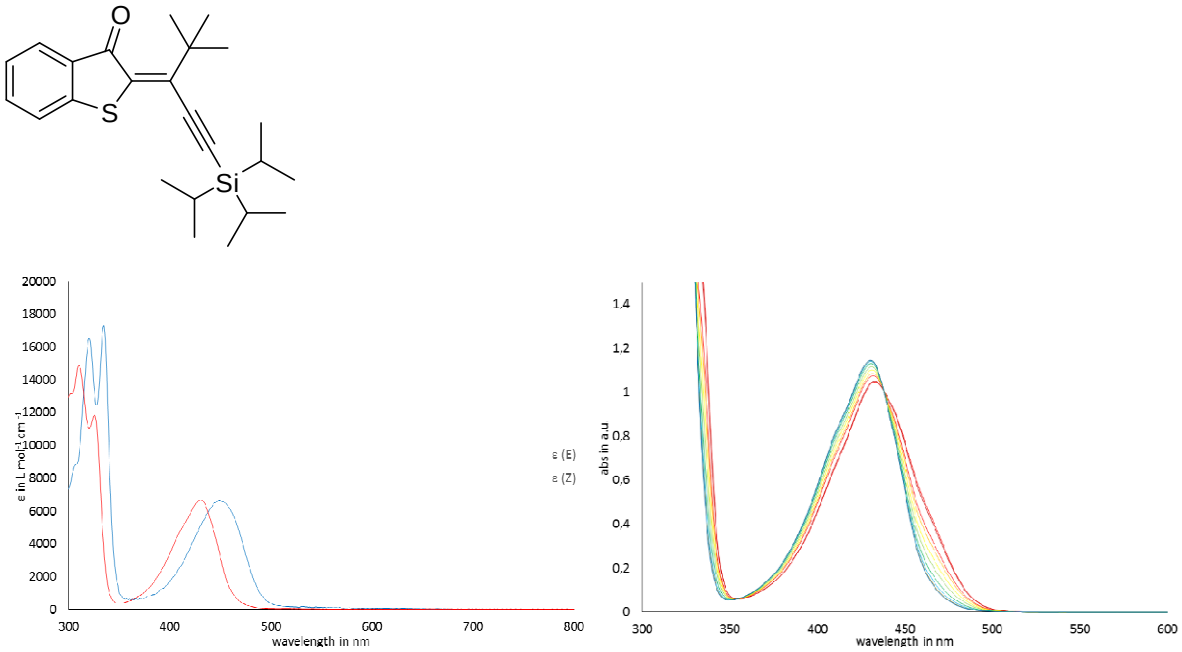

Figure 23: Calculated extinction coefficients for both isomers of HTI **25** (left) and corresponding absorption changes during irradiation with 435 nm and 470 nm (right) of **25** in toluene.

4-((3-oxobenzo[*b*]thiophen-2(3*H*)-ylidene)(*p*-tolyl)methyl)benzonitrile (**26**)

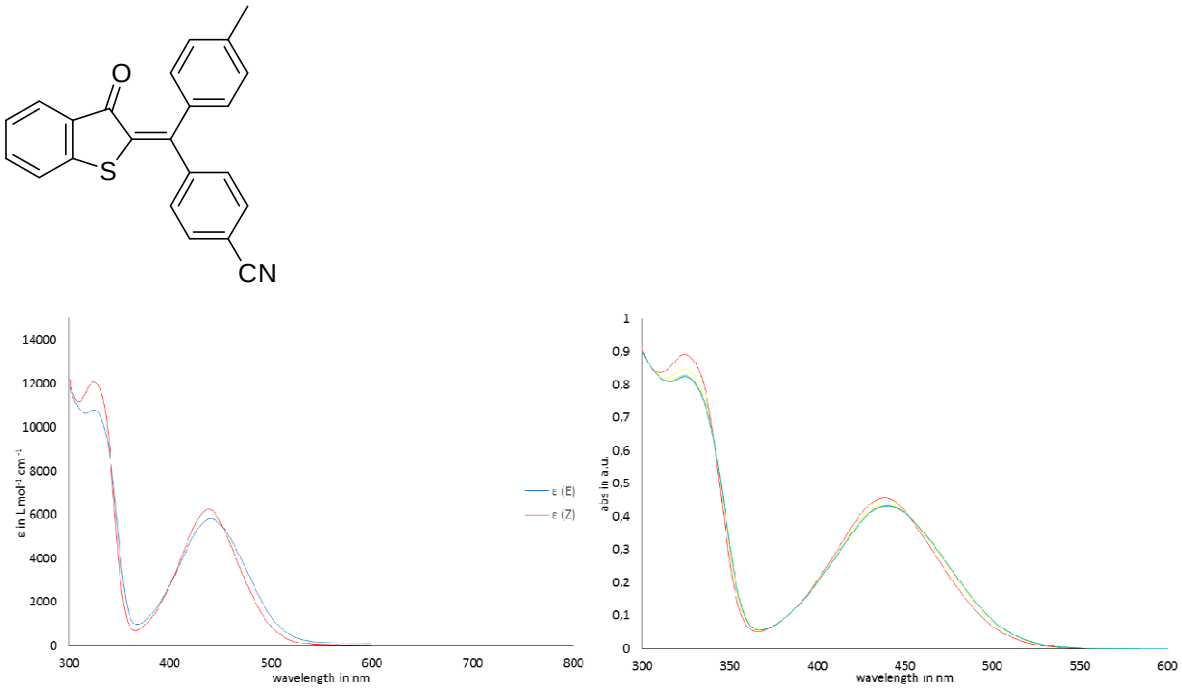

Figure 24: Calculated extinction coefficients for both isomers of HTI **26** (left) and corresponding absorption changes during irradiation with 420, 435 nm (right) of **26** in toluene.

2-((4-(Dimethylamino)phenyl)(*p*-tolyl)methylene)benzo[*b*]thiophen-3(2*H*)-one (**27**)

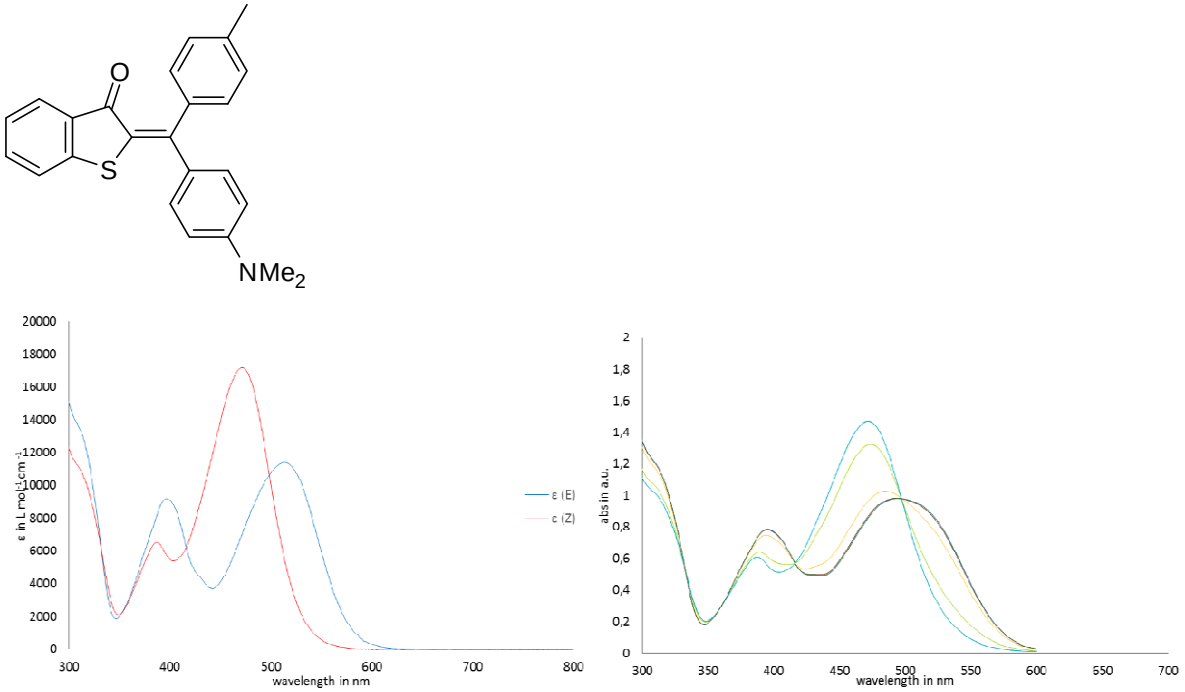

Figure 25: Calculated extinction coefficients for both isomers of HTI **27** (left) and corresponding absorption changes during irradiation with 435, 450, 530, 595 nm (right) of **27** in toluene.

2-((4-methoxy-2,6-dimethylphenyl)(*p*-tolyl)methylene)benzo[*b*]thiophen-3(2*H*)-one (**28**)

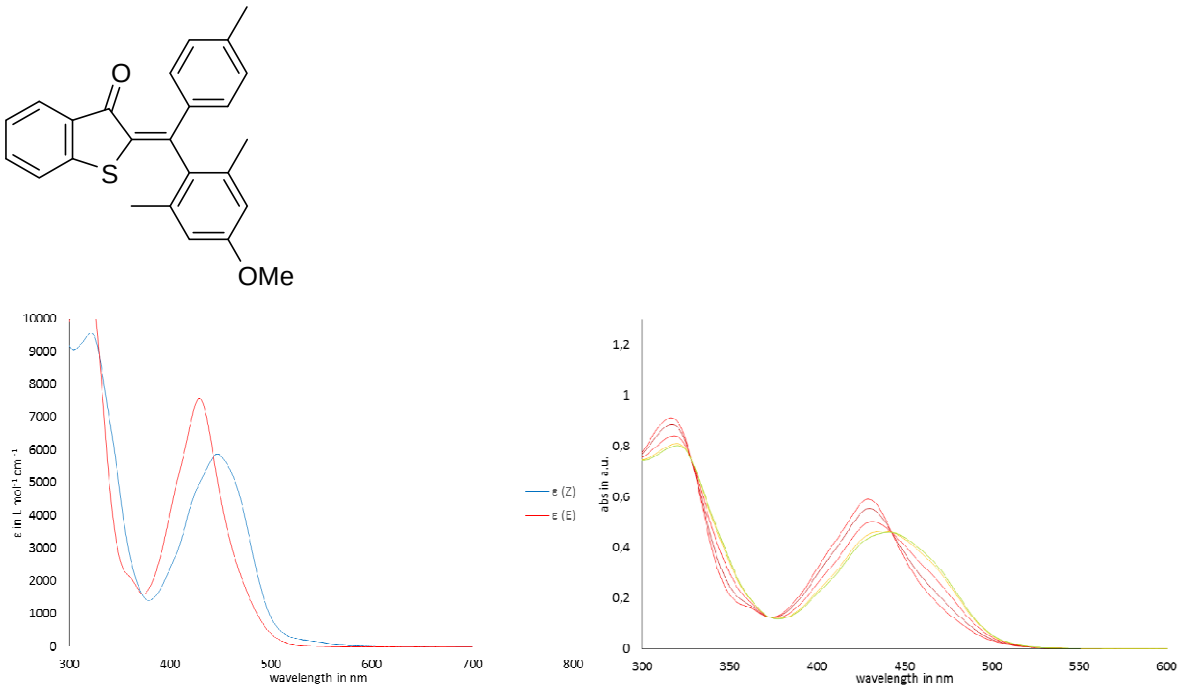

Figure 26: Calculated extinction coefficients for both isomers of HTI **28** (left) and corresponding absorption changes during irradiation with 435 and 470 nm (right) of **28** in toluene.

2-(pyridin-4-yl(*p*-tolyl)methylene)benzo[*b*]thiophen-3(2*H*)-one (**29**)

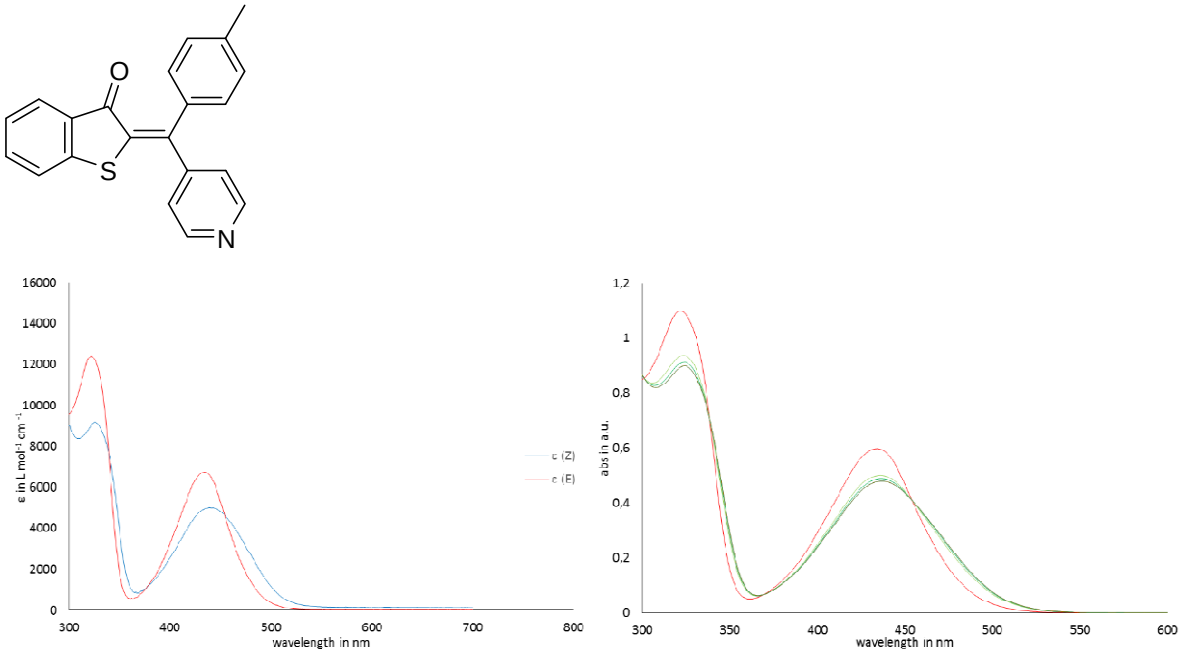

Figure 27: Calculated extinction coefficients for both isomers of HTI **29** (left) and corresponding absorption changes during irradiation with 420 and 435 nm (right) of **29** in toluene.

2-(1-(*p*-tolyl)-3-(triisopropylsilyl)prop-2-yn-1-ylidene)benzo[*b*]thiophen-3(2*H*)-one (**30**)

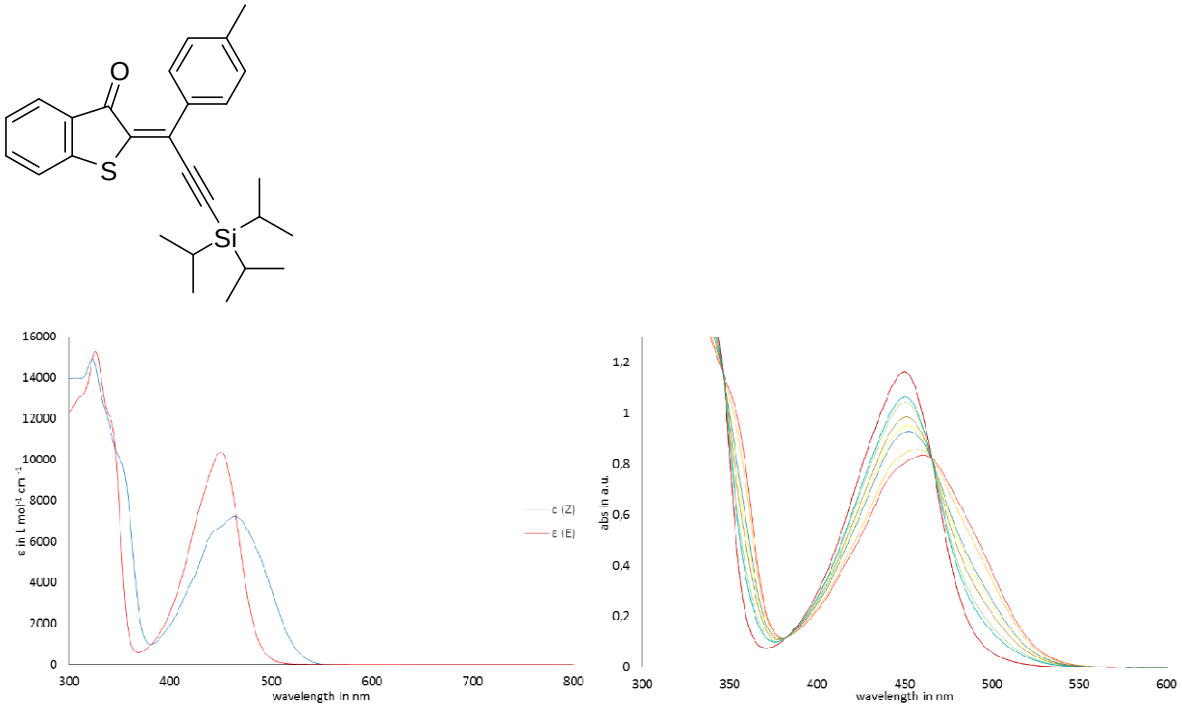

Figure 28: Calculated extinction coefficients for both isomers of HTI **30** (left) and corresponding absorption changes during irradiation with 435 and 530 nm (right) of **30** in toluene.

2-(1-(*p*-tolyl)ethylidene)benzo[*b*]thiophen-3(2*H*)-one (**31**)

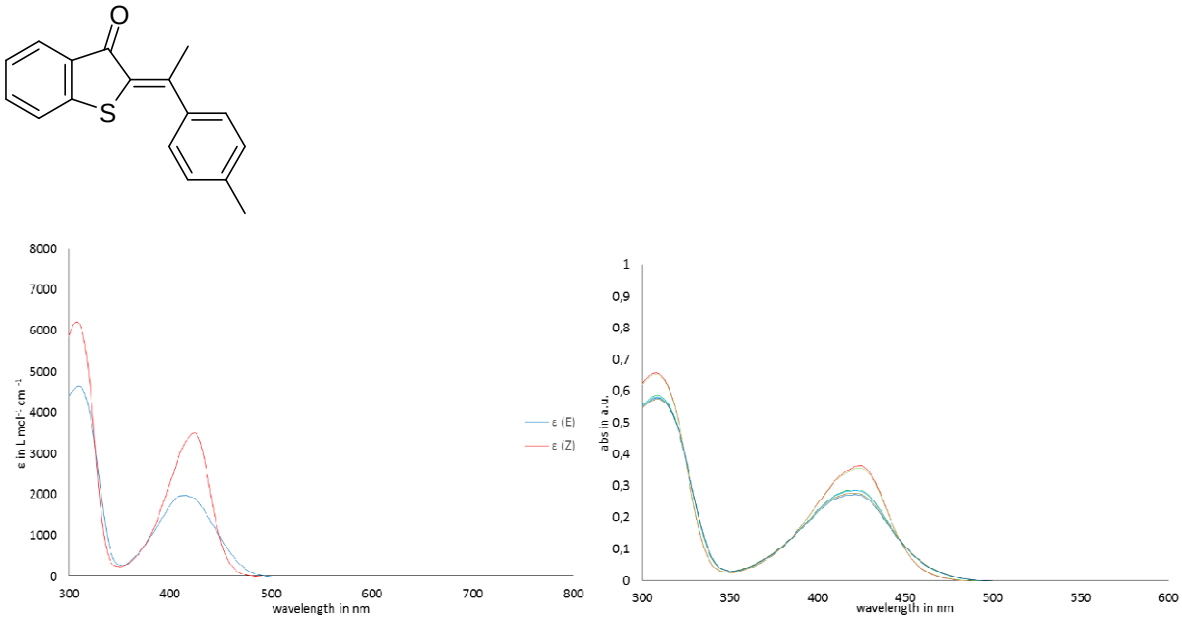

Figure 29: Calculated extinction coefficients for both isomers of HTI **31** (left) and corresponding absorption changes during irradiation with 435 nm (right) of **31** in toluene.

4-((3-oxobenzo[*b*]thiophen-2(3*H*)-ylidene)(pyridin-4-yl)methyl)benzonitrile (**32**)

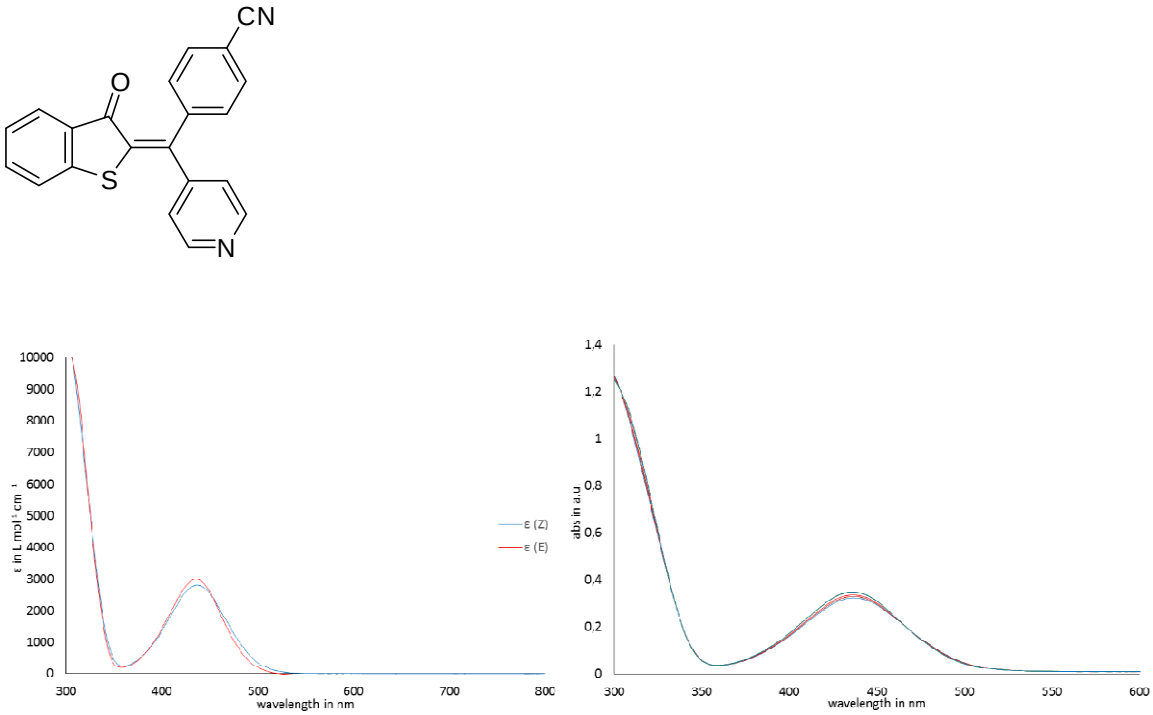

Figure 30: Extinction coefficients for both isomers of HTI **32** (left) and corresponding absorption changes during irradiation with 435 nm (right) of **32** in toluene.

2-((4-(dimethylamino)phenyl)(pyridin-4-yl)methylene)benzo[*b*]thiophen-3(2*H*)-one (**33**)

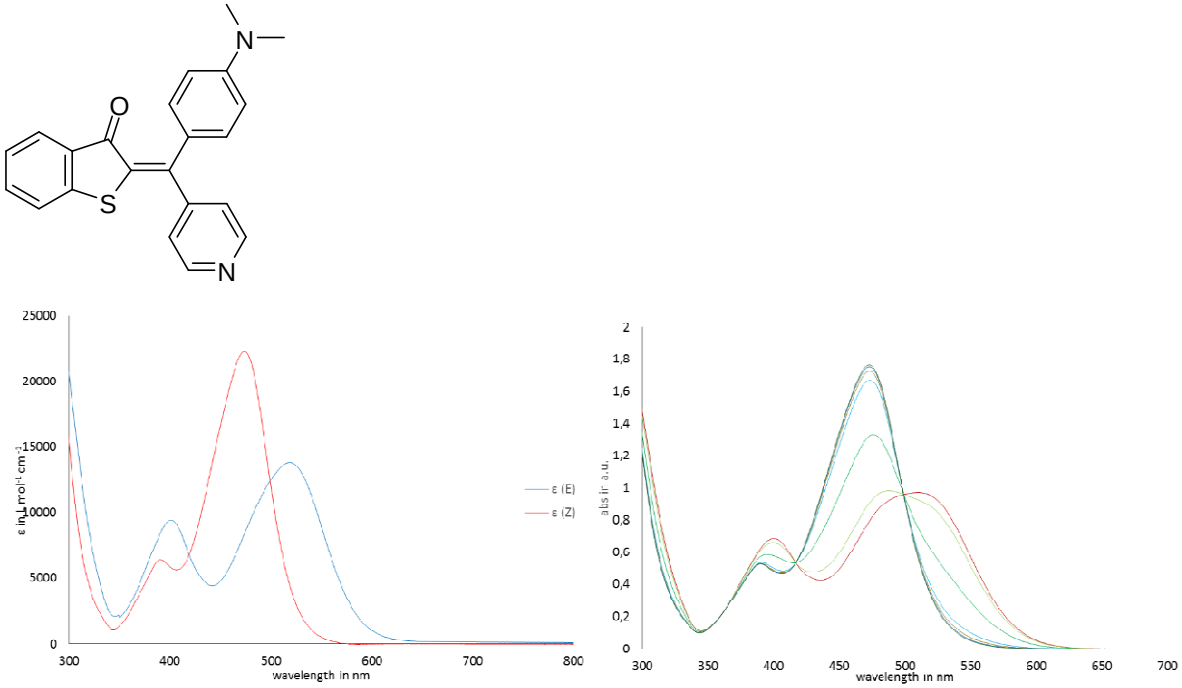

Figure 31: Calculated extinction coefficients for both isomers of HTI **33** (left) and corresponding absorption changes during irradiation with 435, 450, 530, 595 nm (right) of **33** in toluene.

2-(1-(pyridin-4-yl)-3-(triisopropylsilyl)prop-2-yn-1-ylidene)benzo[*b*]thiophen-3(2*H*)-one (**34**)

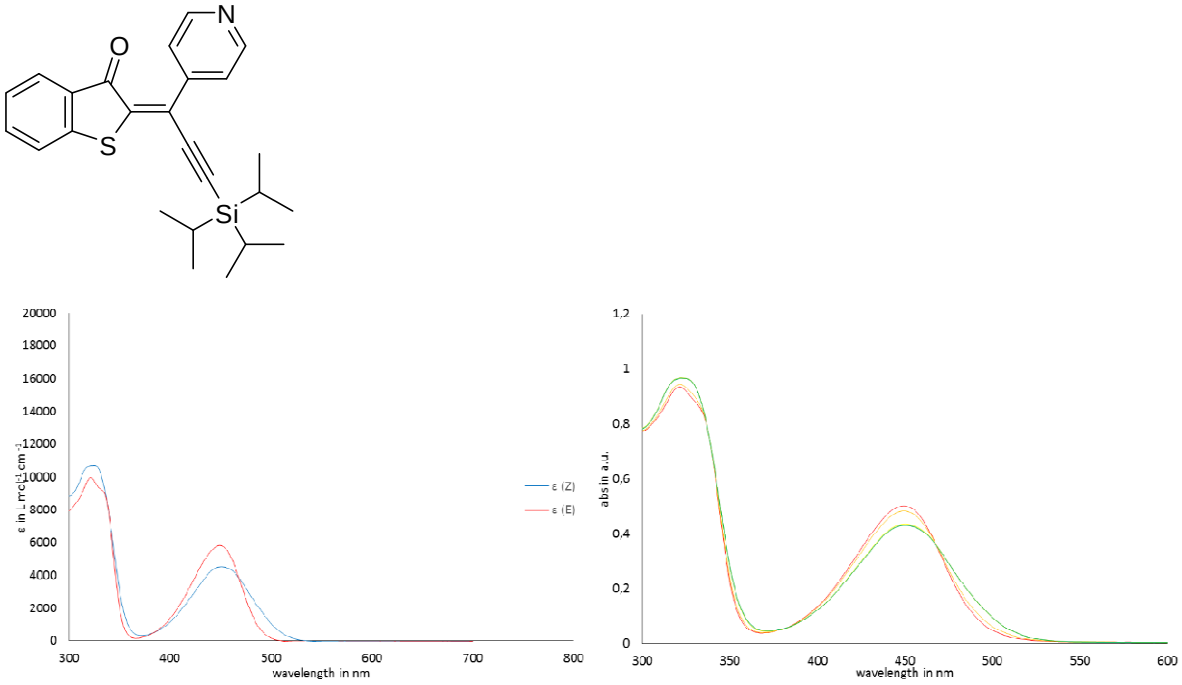

Figure 32: Calculated extinction coefficients for both isomers of HTI **34** (left) and corresponding absorption changes during irradiation with 450 nm (right) of **34** in toluene.

2-(1-(3,5-dimethoxyphenyl)ethylidene)benzo[*b*]thiophen-3(2*H*)-one (**36**)

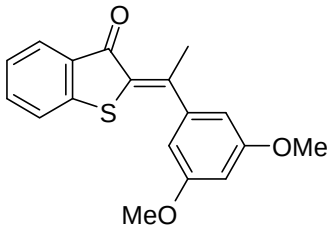

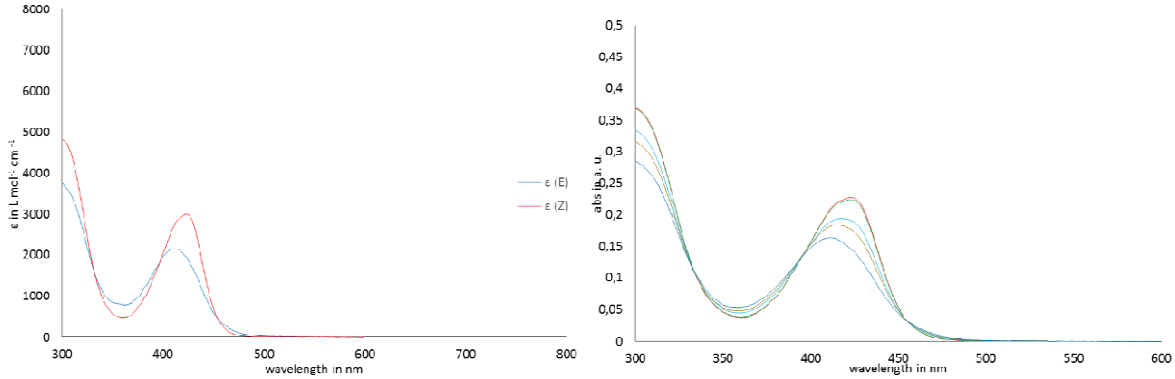

Figure 33: Calculated extinction coefficients for both isomers of HTI **36** (left) and corresponding absorption changes during irradiation with 435 nm (right) of **36** in toluene.

4-(2,2-dimethyl-1-(3-oxothieno[2,3-*b*]pyridin-2(3*H*)-ylidene)propyl)benzonitrile (**37**)

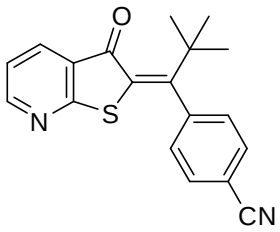

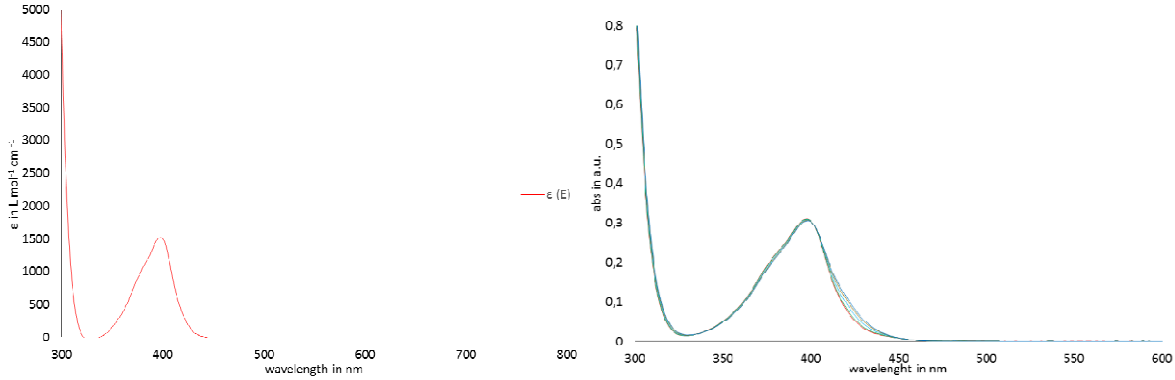

Figure 34: Extinction coefficients for the *E*-isomer of HTI **37** (left) and corresponding absorption changes during irradiation with 405 nm (right) of **37** in toluene. Although no decomposition could be observed in the UV-Vis experiments, upon irradiation of the *E*-isomer in the NMR-Experiment small decomposition product peaks could be observed. Therefore, it was impossible to obtain a clean UV-Vis spectrum of the *Z*-isomer.

2-(1-(4-(dimethylamino)phenyl)-2,2-dimethylpropylidene)benzo[*b*]thiophen-3(2*H*)-one (**38**)

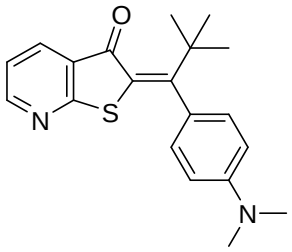

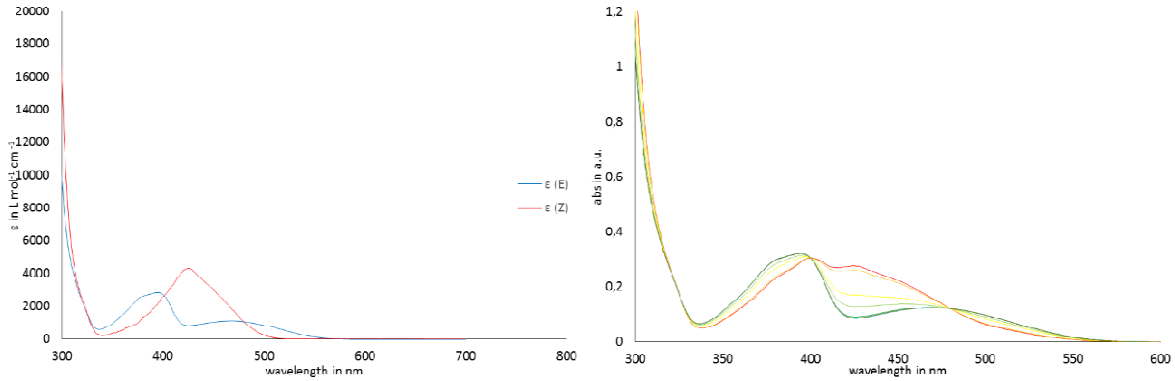

Figure 35: Calculated extinction coefficients for both isomers of HTI **38** (left) and corresponding absorption changes during irradiation with 435, 530 nm (right) of **38** in toluene.

2-(4,4-dimethyl-1-(triisopropylsilyl)pent-1-yn-3-ylidene)thieno[2,3-*b*]pyridin-3(2*H*)-one (**39**)

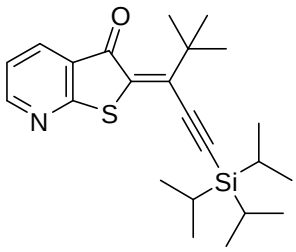

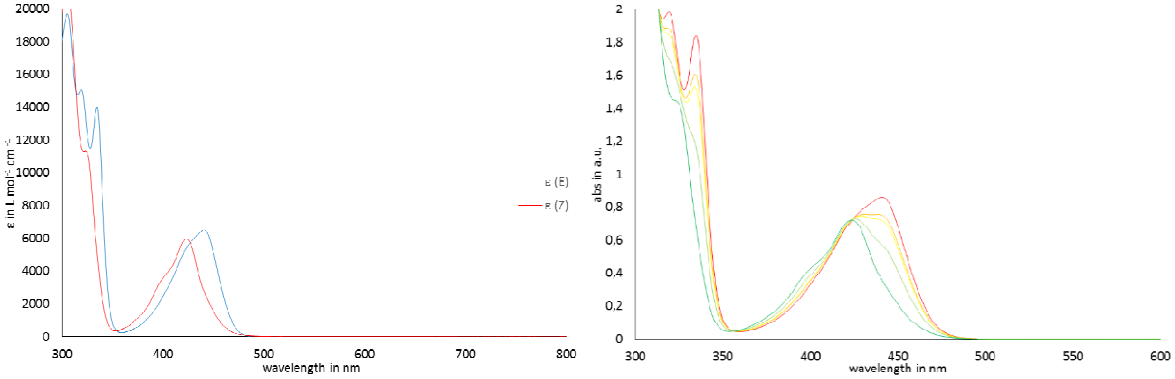

Figure 36: Calculated extinction coefficients for both isomers of HTI **39** (left) and corresponding absorption changes during irradiation with 450 nm (right) of **39** in toluene.

2-(pyrrolidin-1-yl(*p*-tolyl)methylene)benzo[*b*]thiophen-3(2*H*)-one (**40**)

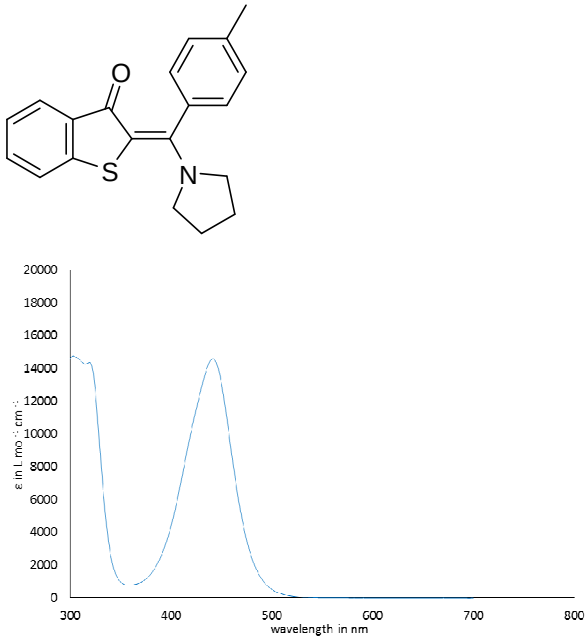

Figure 37: Extinction coefficients for a *Z*:*E* mixture (1:5.6) of the isomers of HTI **40**. Upon irradiation with a 435 nm light source no absorption changes could be measured. It can be assumed that no photo isomerization takes place, so the *Z*- or *E*-spectra cannot be calculated.

2-(ethoxy(*p*-tolyl)methylene)benzo[*b*]thiophen-3(2*H*)-one (**41**)

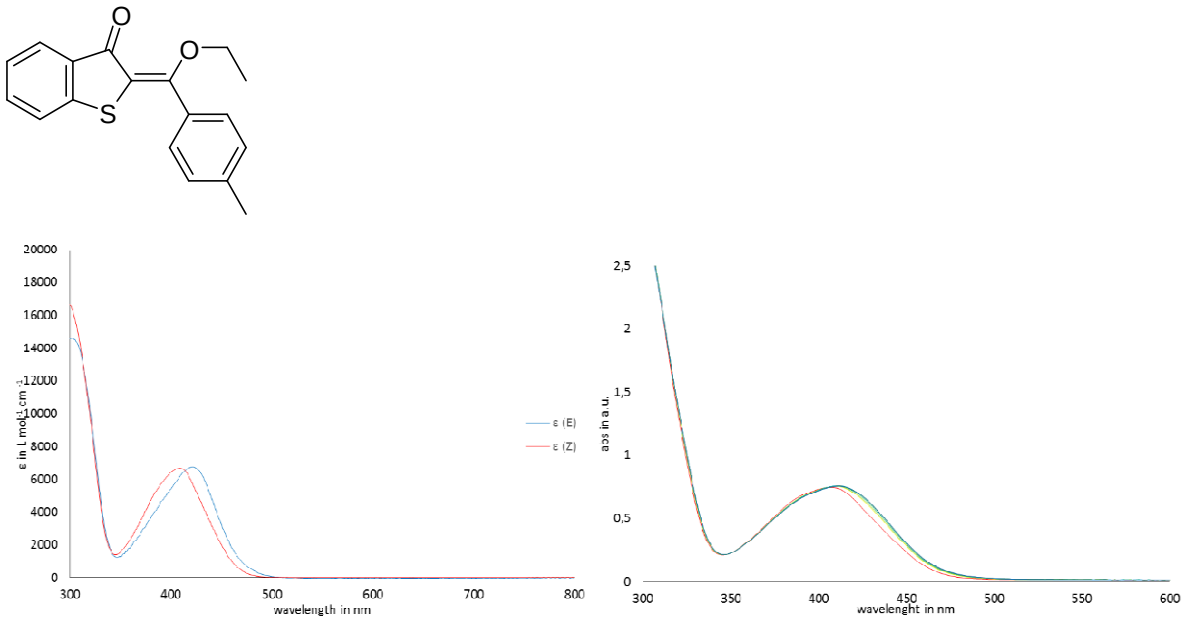

Figure 38: Calculated extinction coefficients for both isomers of HTI **41** (left) and corresponding absorption changes during irradiation with 385, 405, 470 and 490 nm (right) of **39** in toluene.

2-((pyridin-4-ylthio)(*p*-tolyl)methylene)benzo[*b*]thiophen-3(2*H*)-one (**42**)

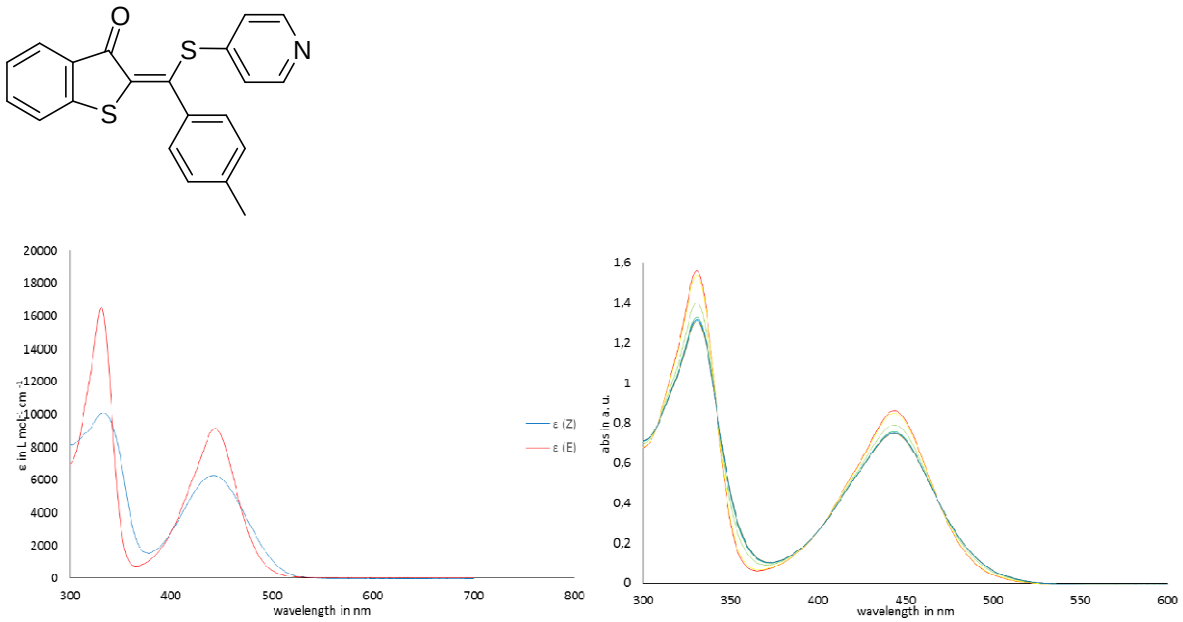

Figure 39: Calculated extinction coefficients for both isomers of HTI **42** (left) and corresponding absorption changes during irradiation with 450 nm (right) of **42** in toluene.

2-(pyridin-4-yl(pyrrolidin-1-yl)methylene)benzo[*b*]thiophen-3(2*H*)-one (**43**)

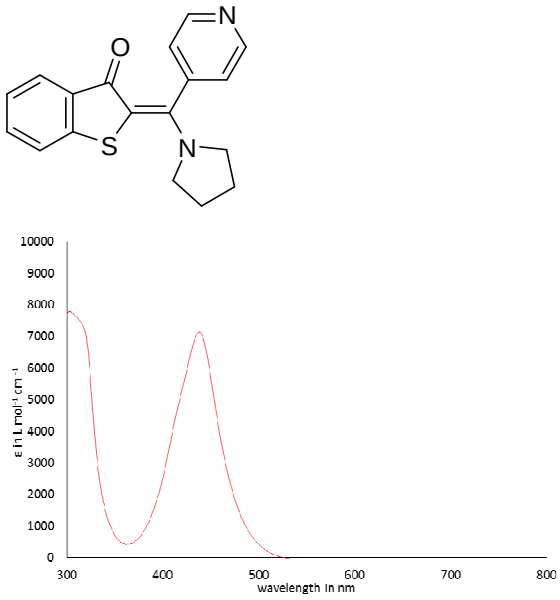

Figure 40: Extinction coefficients for a *Z*:*E* mixture (1.2:1) of the isomers of HTI **43**. Upon irradiation with a 435 nm light source no absorption changes could be measured. It can be assumed that no photo isomerization takes place, so the *Z*- or *E*-spectra cannot be calculated.

2-(1-(pyrrolidin-1-yl)ethylidene)benzo[*b*]thiophen-3(2*H*)-one (**44**)

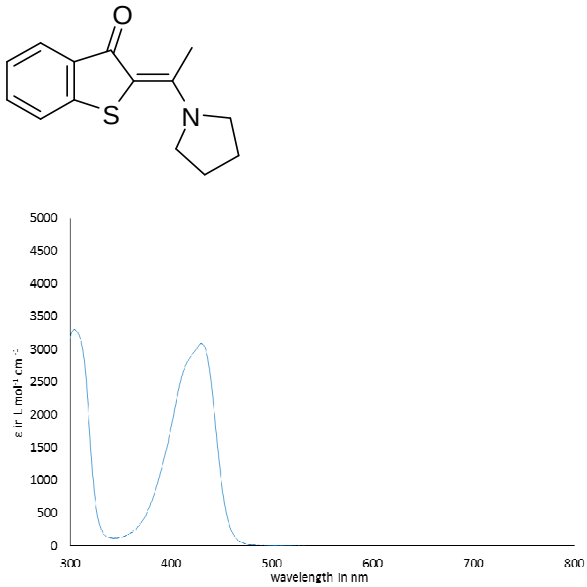

Figure 41: Extinction coefficients for a *Z*:*E* mixture (20:1) of the isomers of HTI **44**. Upon irradiation with a 435 nm light source no absorption changes could be measured. It can be assumed that no photo isomerization takes place, so the *Z*- or *E*-spectra could not be calculated.

Appendix

NMR-Spectra

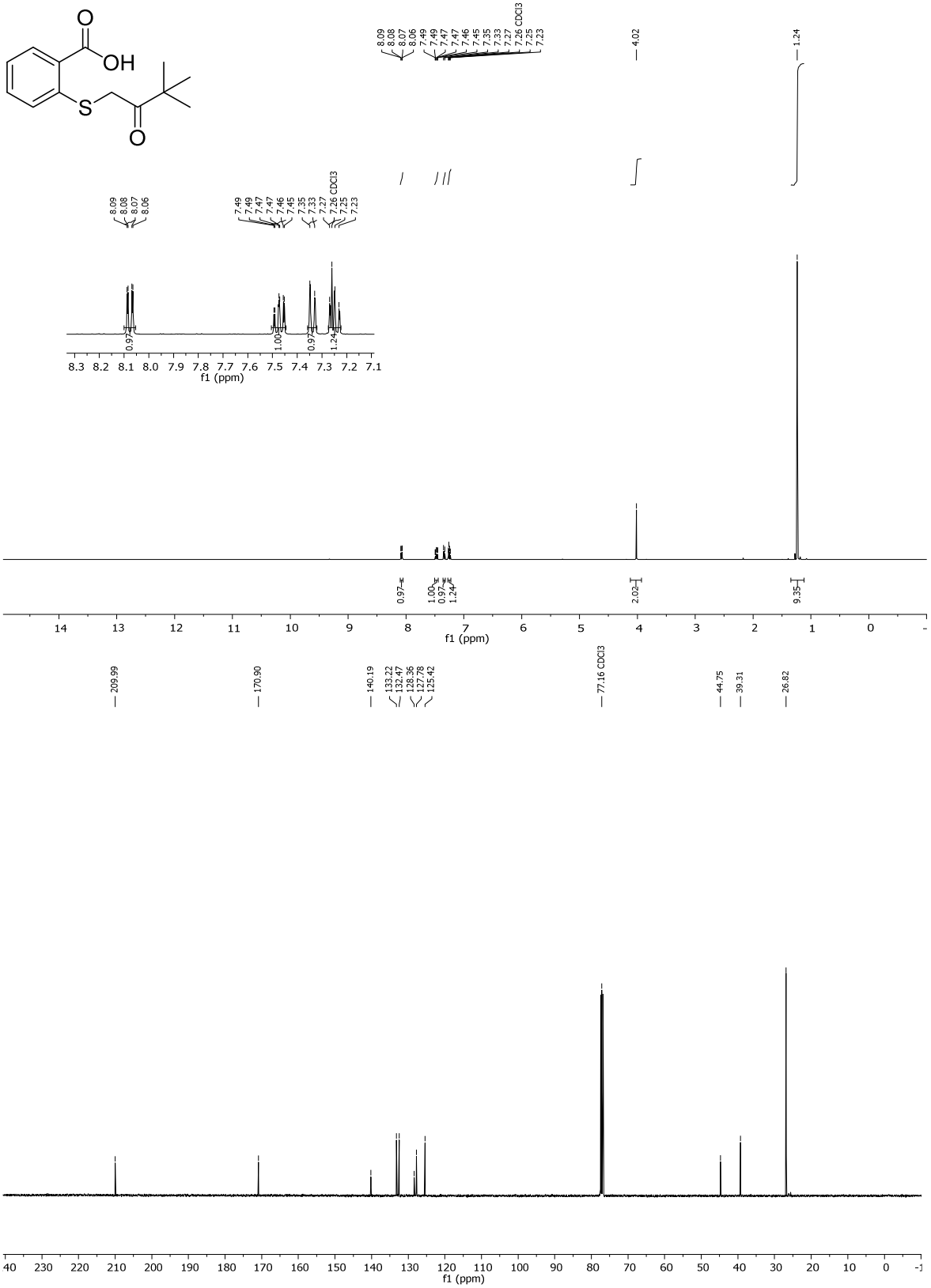

Figure 42: 400 MHz ^{1}H-NMR spectrum (top) and 100 MHz ^{13}C-NMR-spectrum (bottom) of 2-((3,3-dimethyl-2-oxobutyl)thio)benzoic acid (**1**).

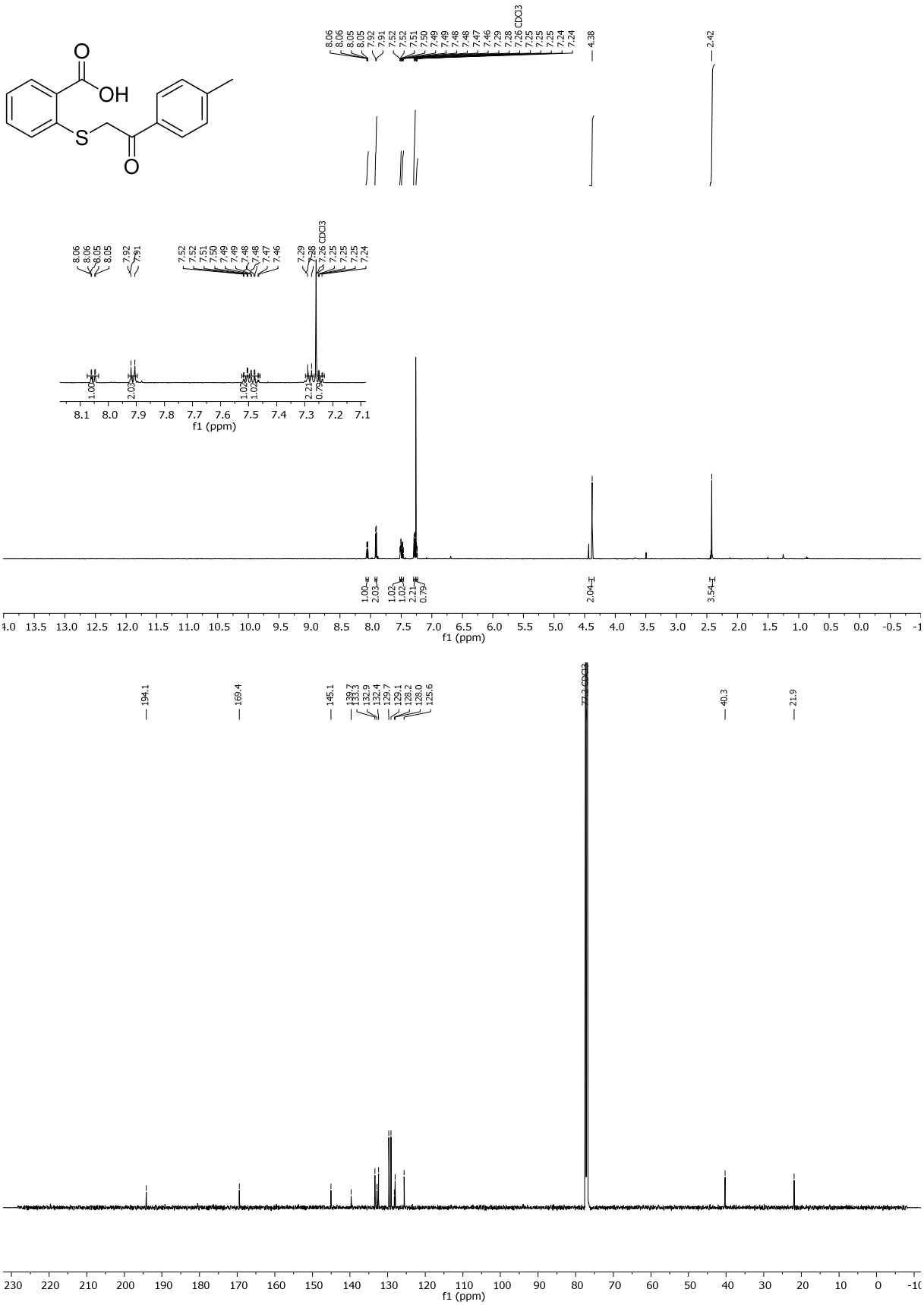

Figure 43: 600 MHz ^{1}H-NMR spectrum (top) and 150 MHz ^{13}C-NMR-spectrum (bottom) of 2-((2-oxo-2-(*p*-tolyl)ethyl)thio)benzoic acid (**2**).

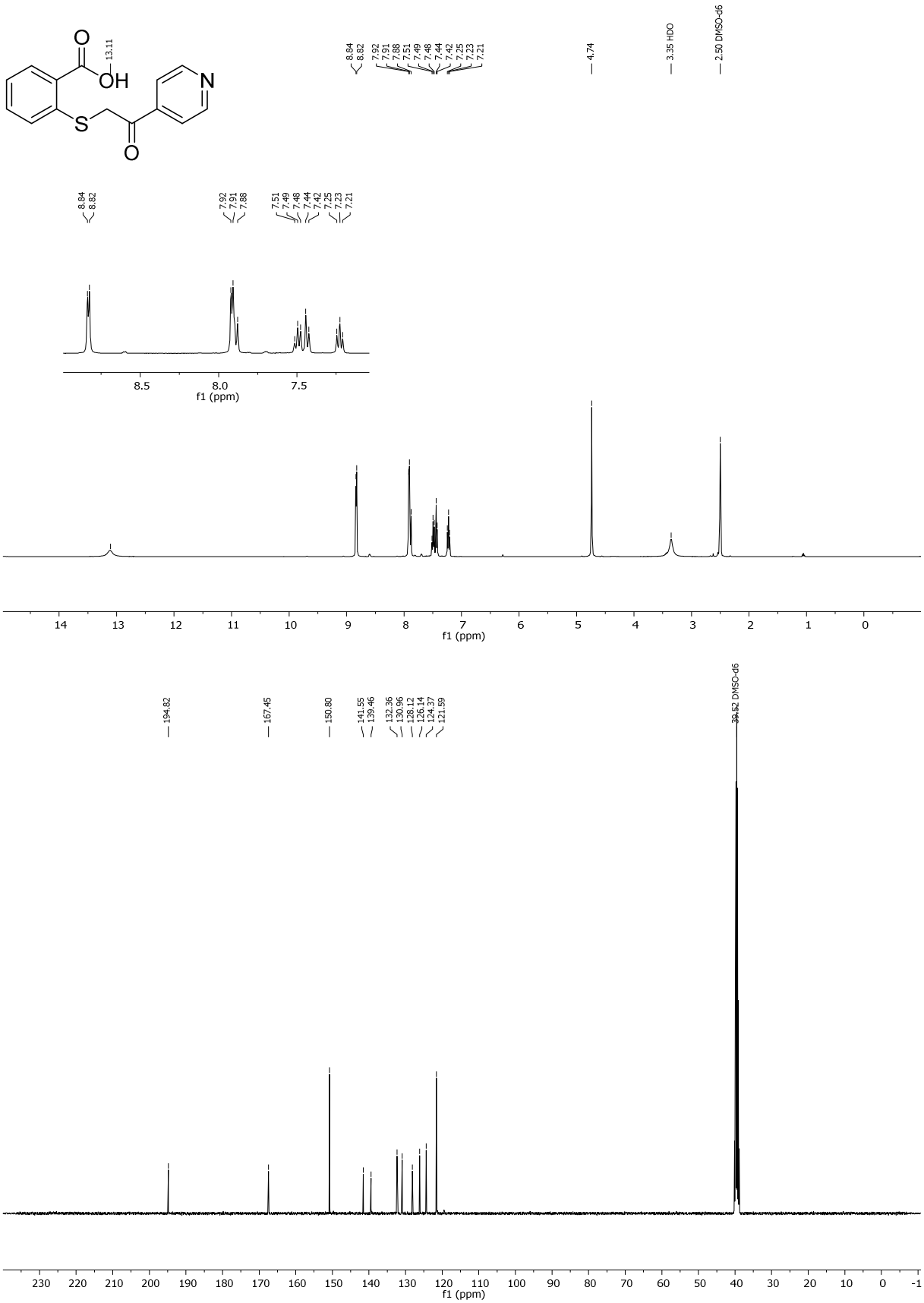

Figure 44: 400 MHz ^{1}H-NMR spectrum (top) and 100 MHz ^{13}C-NMR-spectrum (bottom) of 2-((2-oxo-2-(pyridin-4-yl)ethyl)thio)benzoic acid (**3**).

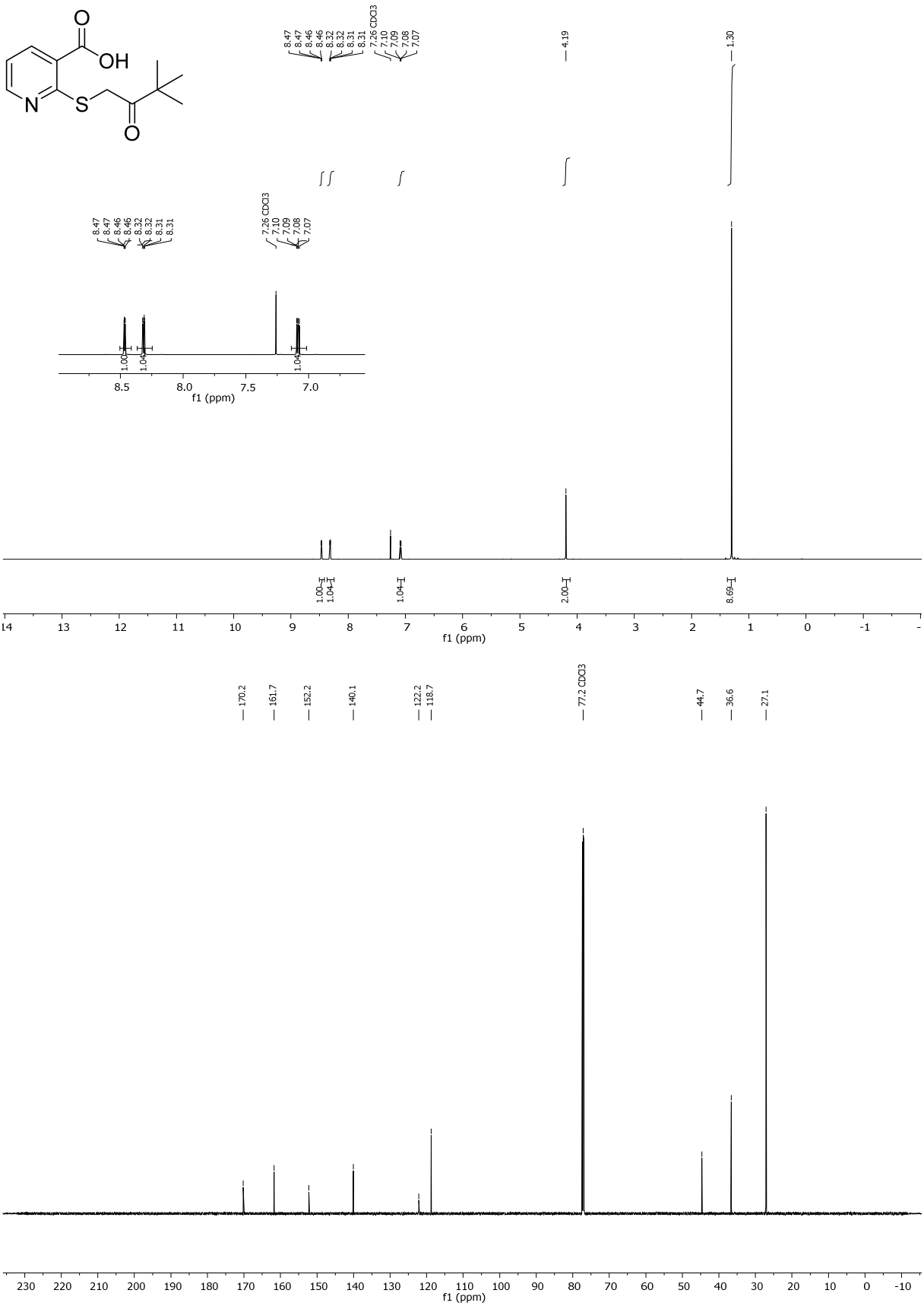

Figure 45: 600 MHz ^{1}H-NMR spectrum (top) and 150 MHz ^{13}C-NMR-spectrum (bottom) of 2-((3,3-dimethyl-2-oxobutyl)thio)nicotinic acid (**4**).

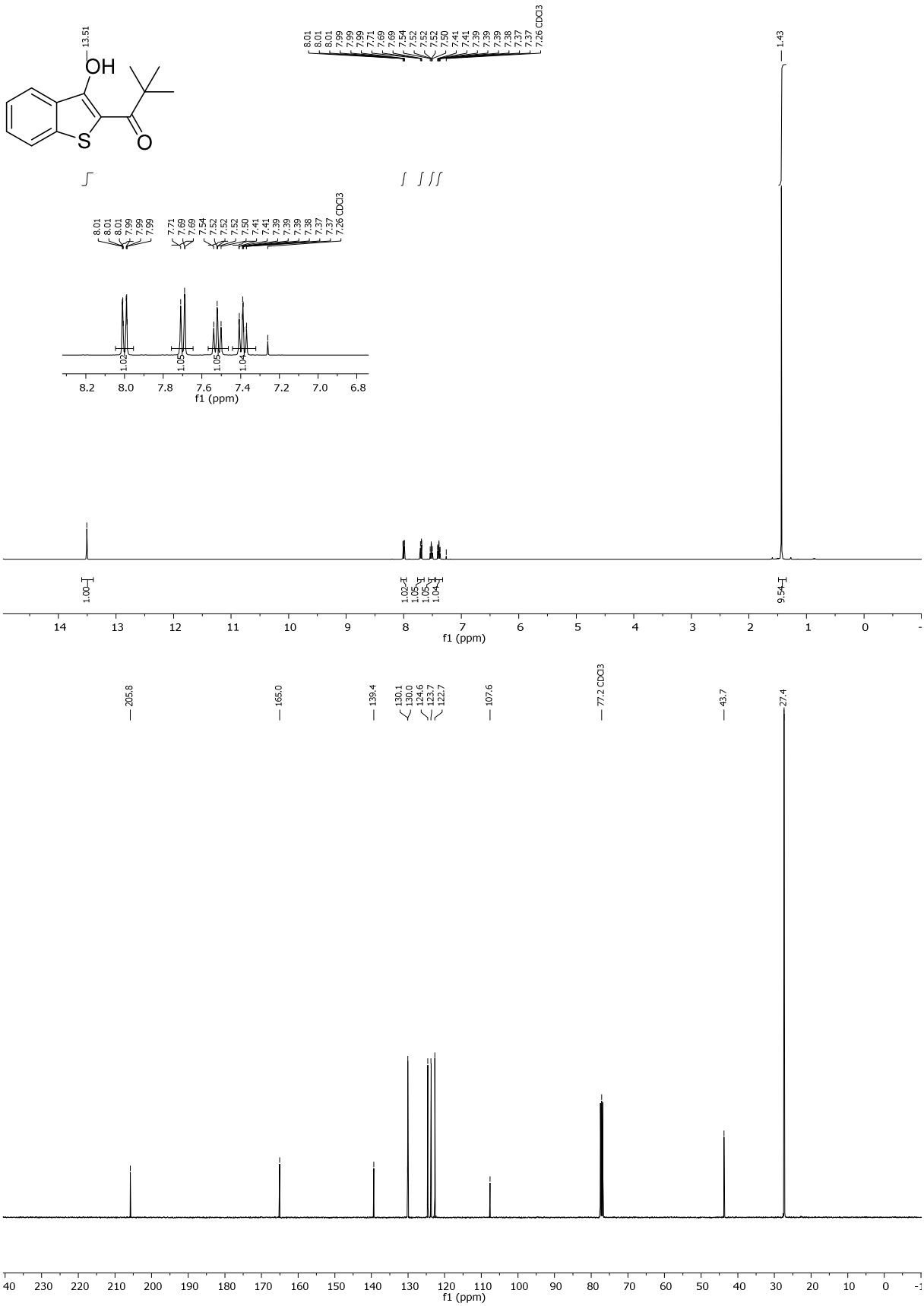

Figure 46: 400 MHz ^{1}H-NMR spectrum (top) and 100 MHz ^{13}C-NMR-spectrum (bottom) of 1-(3-hydroxybenzo[*b*]thiophen-2-yl)-2,2-dimethylpropan-1-one (**5**).

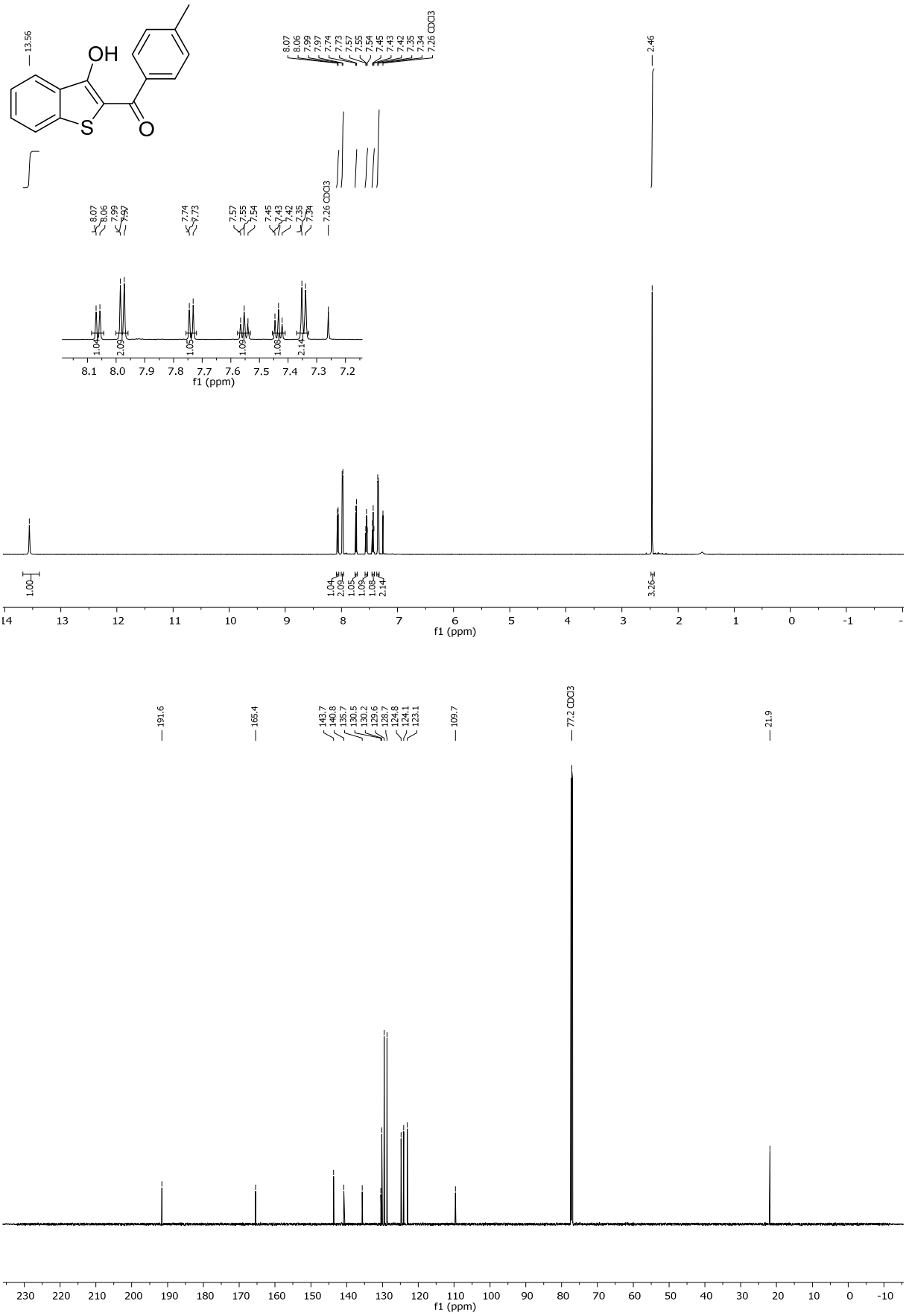

Figure 47: 600 MHz ^{1}H-NMR spectrum (top) and 150 MHz ^{13}C-NMR-spectrum (bottom) of (3-hydroxybenzo[*b*]thiophen-2-yl)(*p*-tolyl)methanone. (**6**).

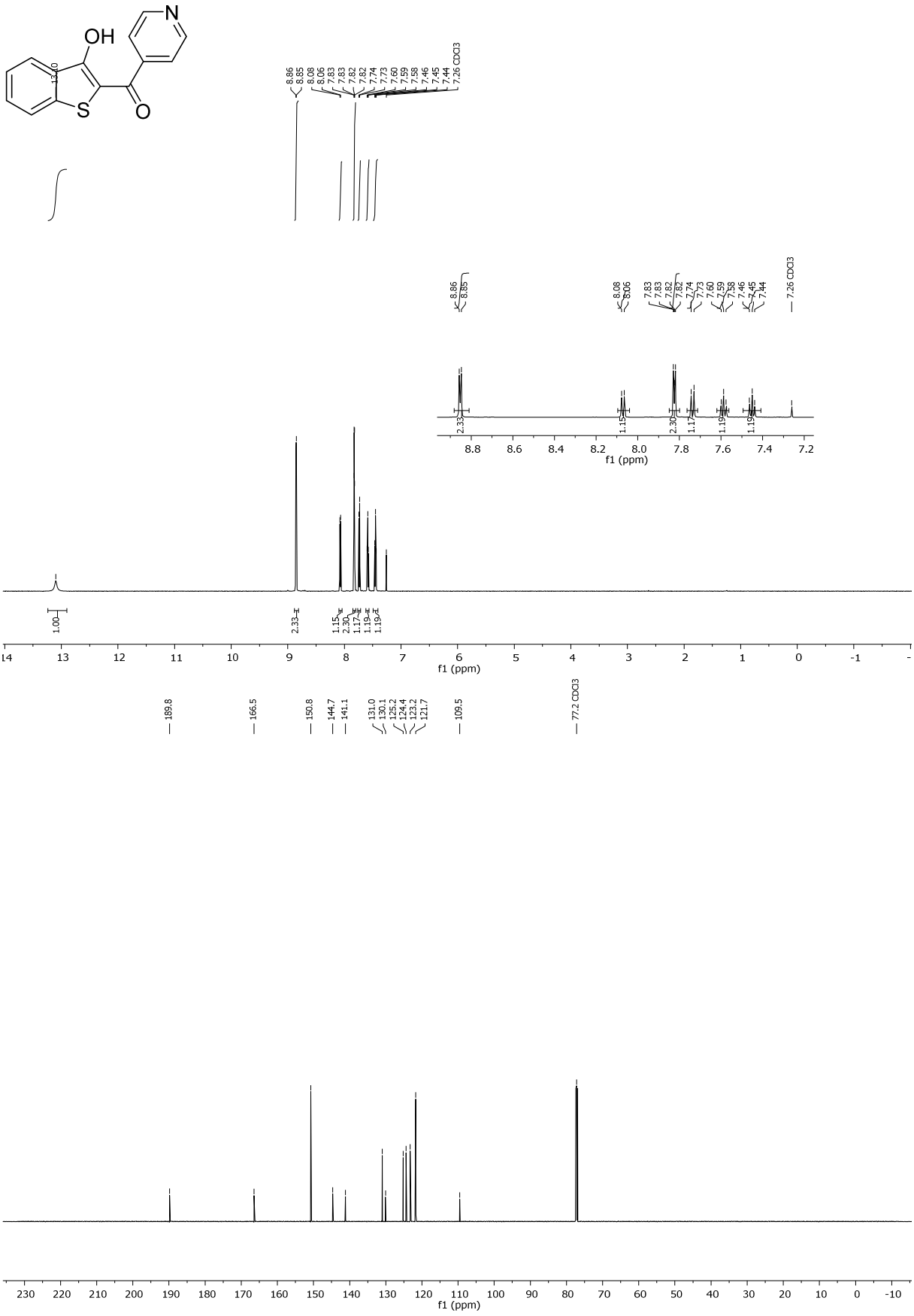

Figure 48: 600 MHz ^{1}H-NMR spectrum (top) and 150 MHz ^{13}C-NMR-spectrum (bottom) of (3-hydroxybenzo[*b*]thiophen-2-yl)(pyridin-4-yl)methanone (**7**).

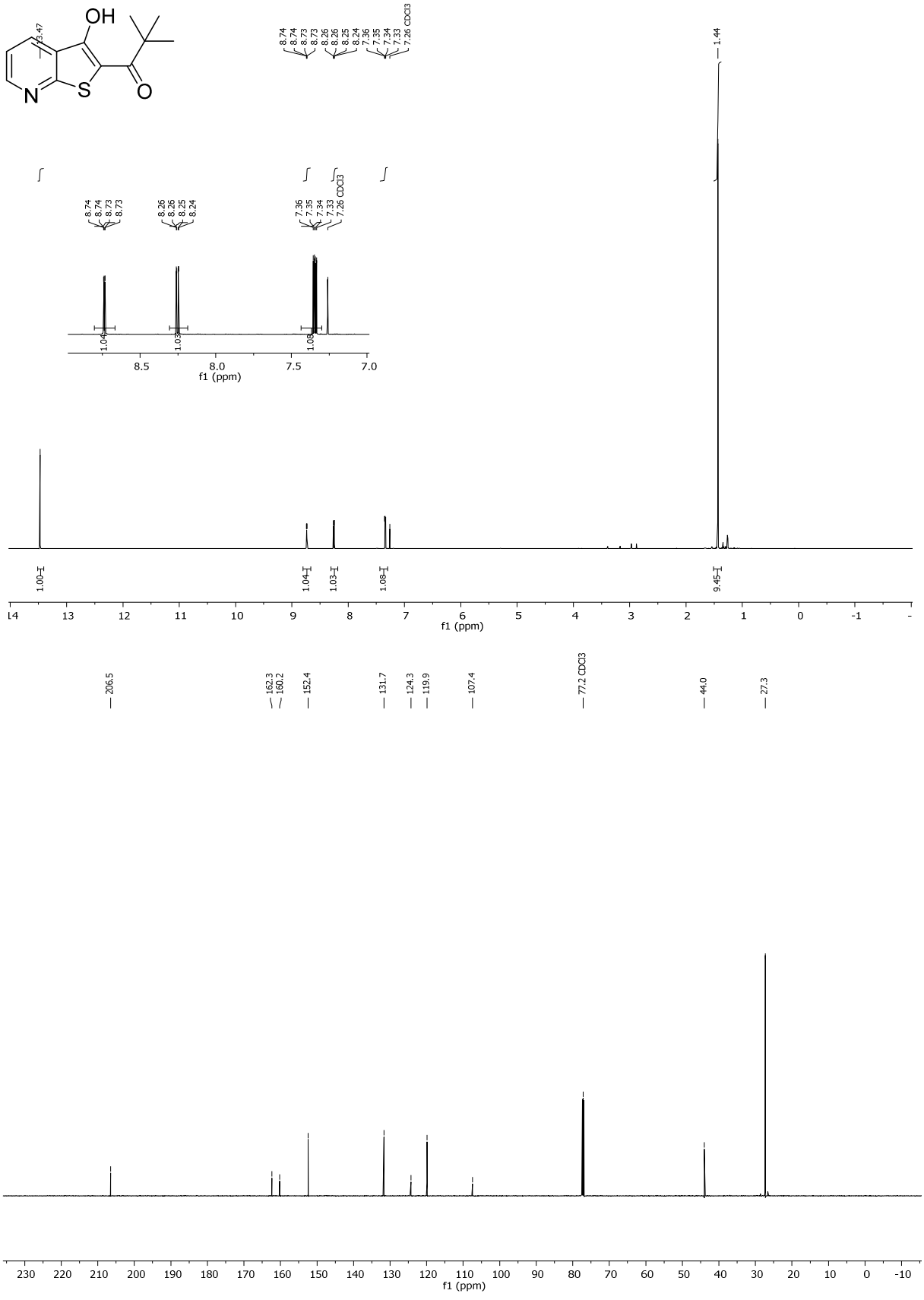

Figure 49: 600 MHz ^{1}H-NMR spectrum (top) and 150 MHz ^{13}C-NMR-spectrum (bottom) of 1-(3-hydroxythieno[2,3-*b*]pyridin-2-yl)-2,2-dimethylpropan-1-one (**9**).

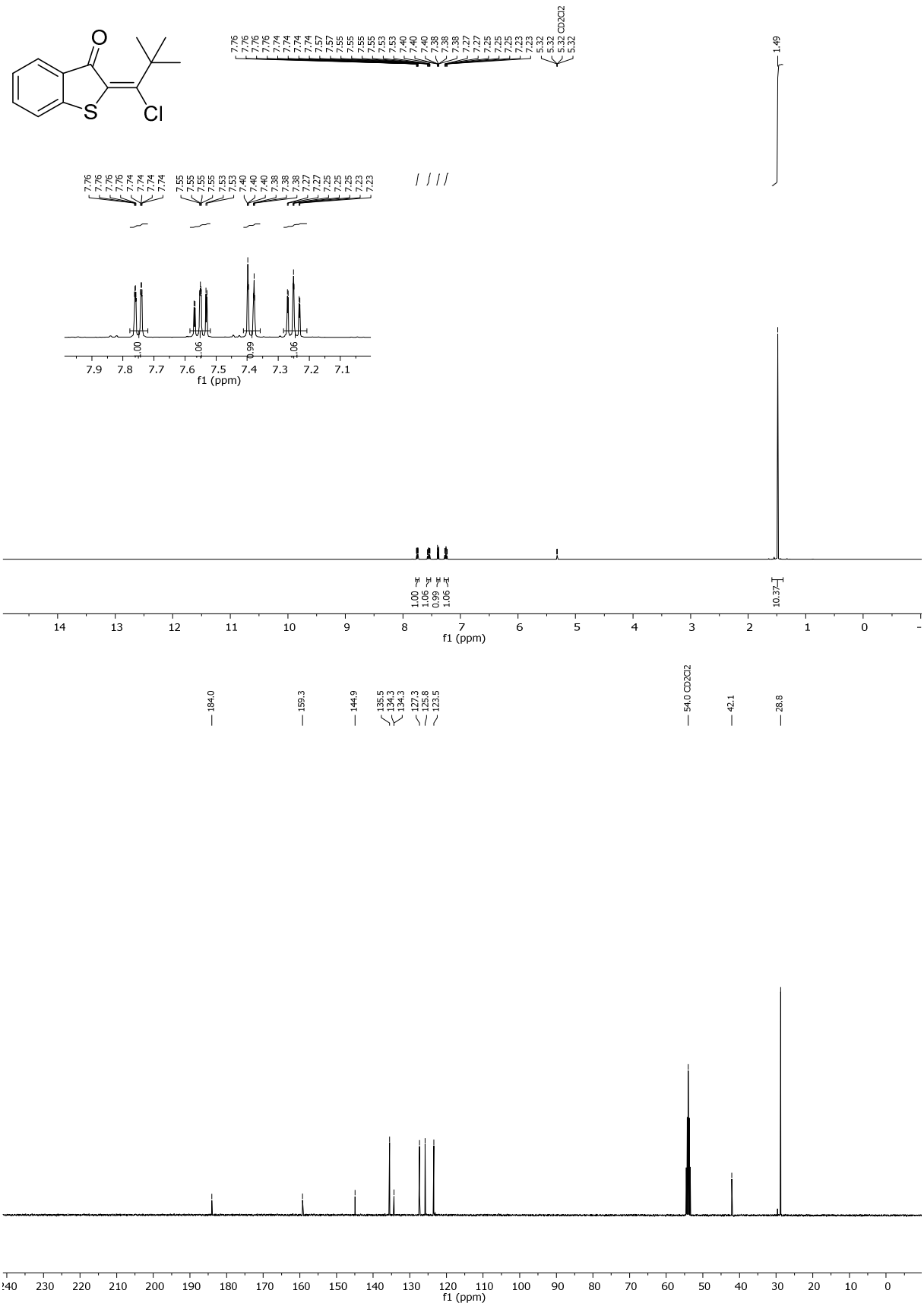

Figure 50: 400 MHz ^{1}H-NMR spectrum (top) and 100 MHz ^{13}C-NMR-spectrum (bottom) of 2-(1-chloro-2,2-dimethylpropylidene)benzo[*b*]thiophen-3(2*H*)-one (**10**).

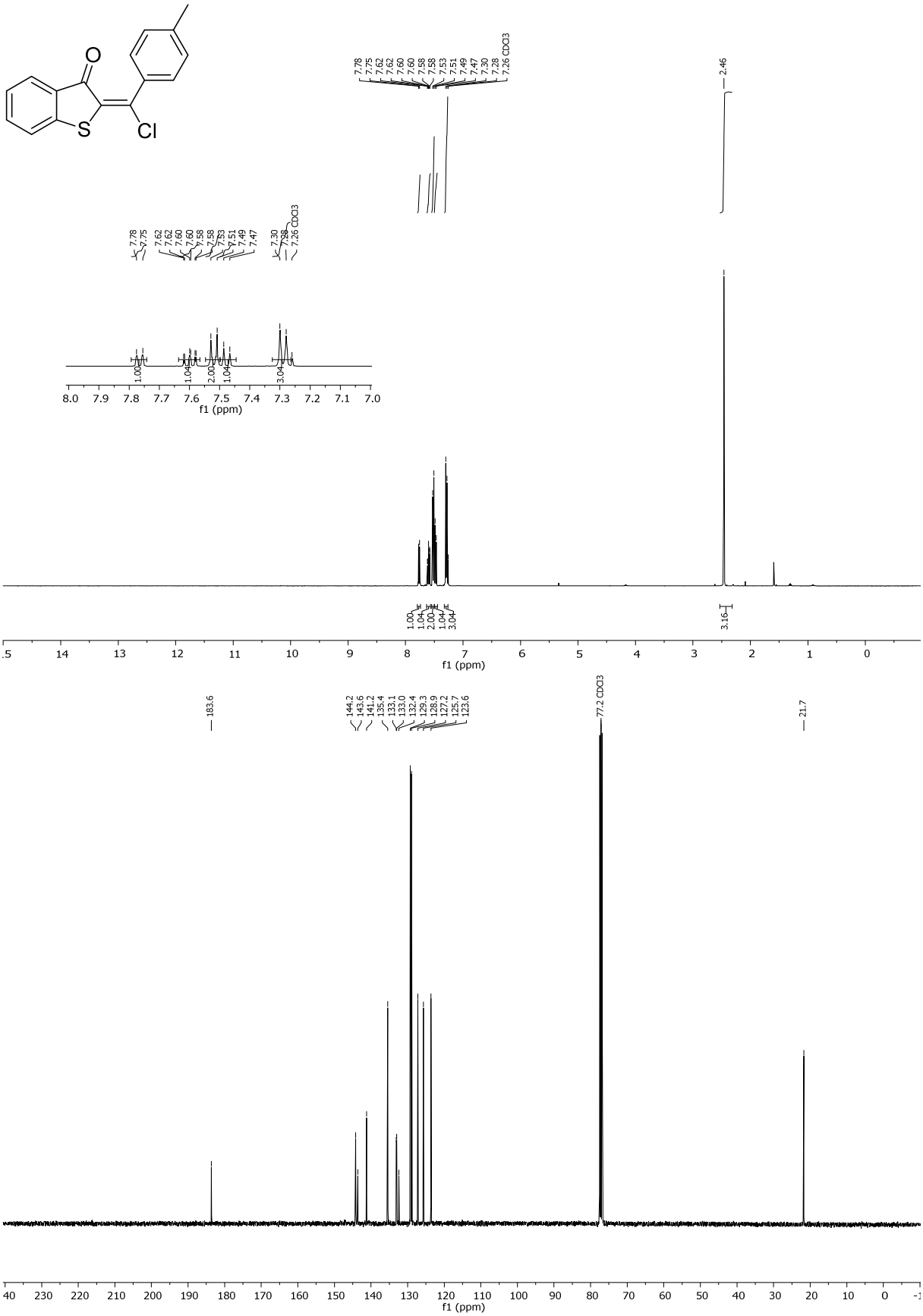

Figure 51: 600 MHz ^{1}H-NMR spectrum (top) and 150 MHz ^{13}C-NMR-spectrum (bottom) of 2-(chloro(*p*-tolyl)methylene)benzo[*b*]thiophen-3(2*H*)-one (**11**).

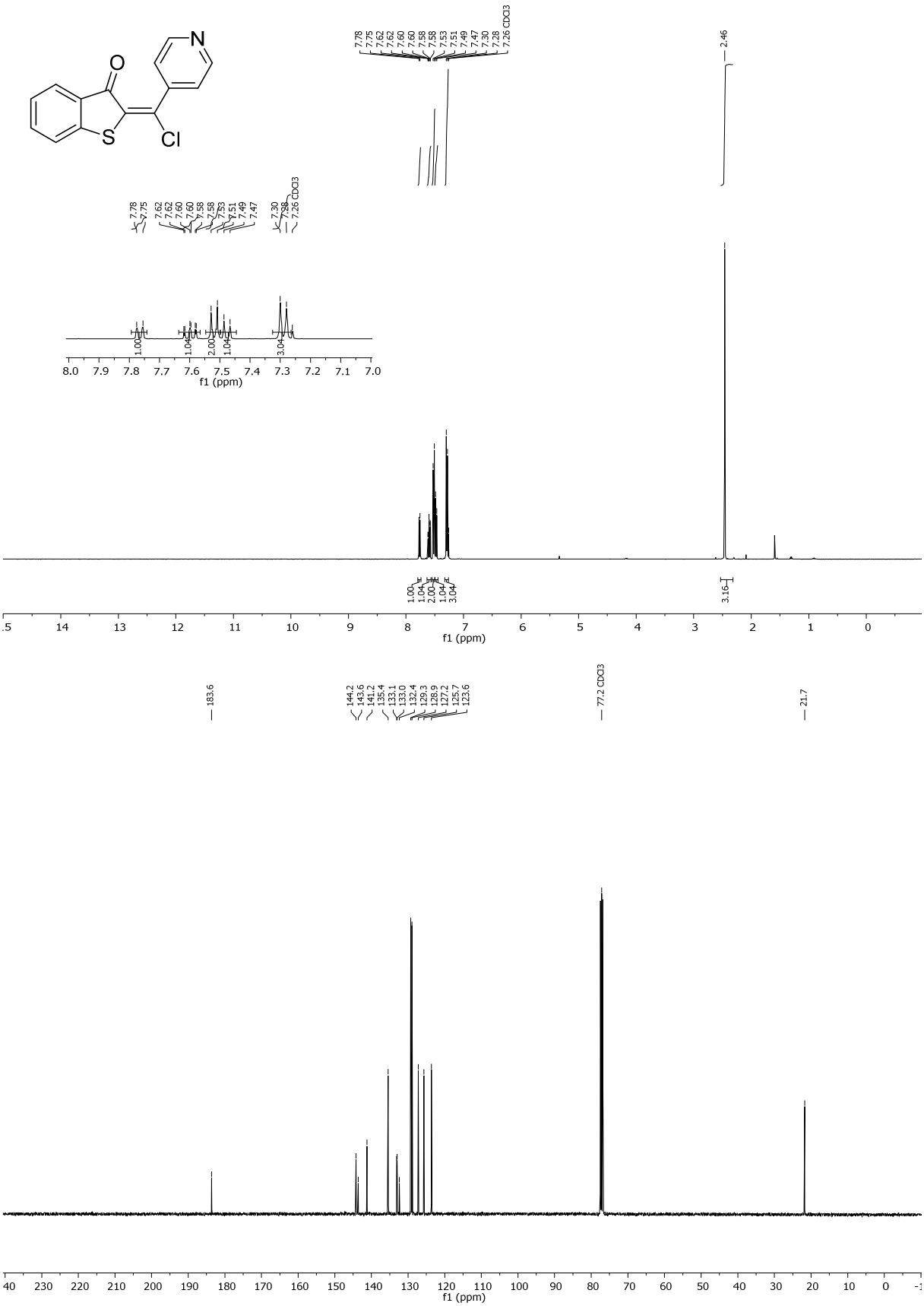

Figure 52: 400 MHz ^{1}H-NMR spectrum (top) and 100 MHz ^{13}C-NMR-spectrum (bottom) of 2-(chloro(pyridine-4-yl)methylene)benzo[*b*]thiophen-3(2*H*)-one (**12**).

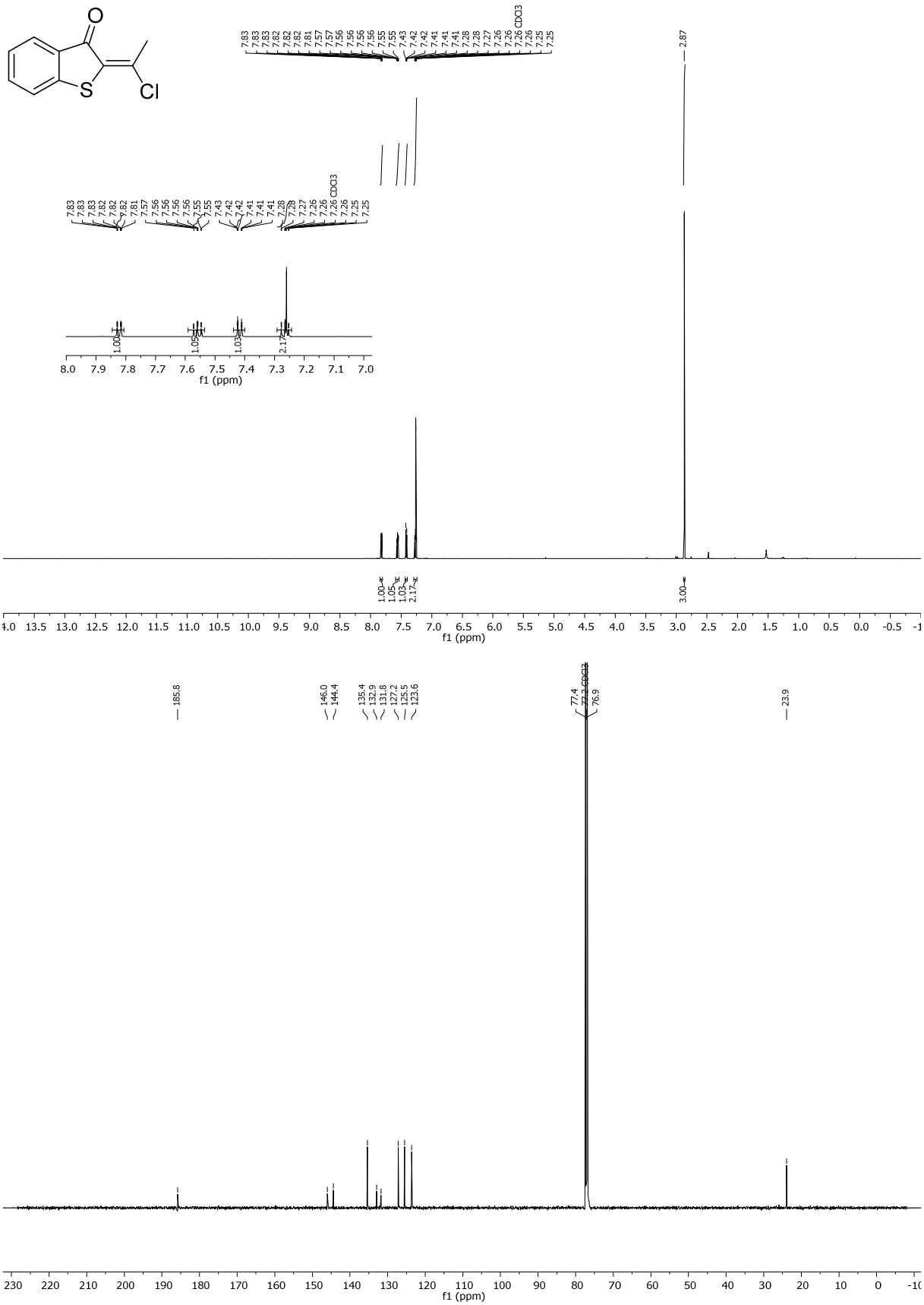

Figure 53: 600 MHz ^{1}H-NMR spectrum (top) and 150 MHz ^{13}C-NMR-spectrum (bottom) of 2-(1-chloroethylidene)benzo[*b*]thiophen-3(2*H*)-one (**13**).

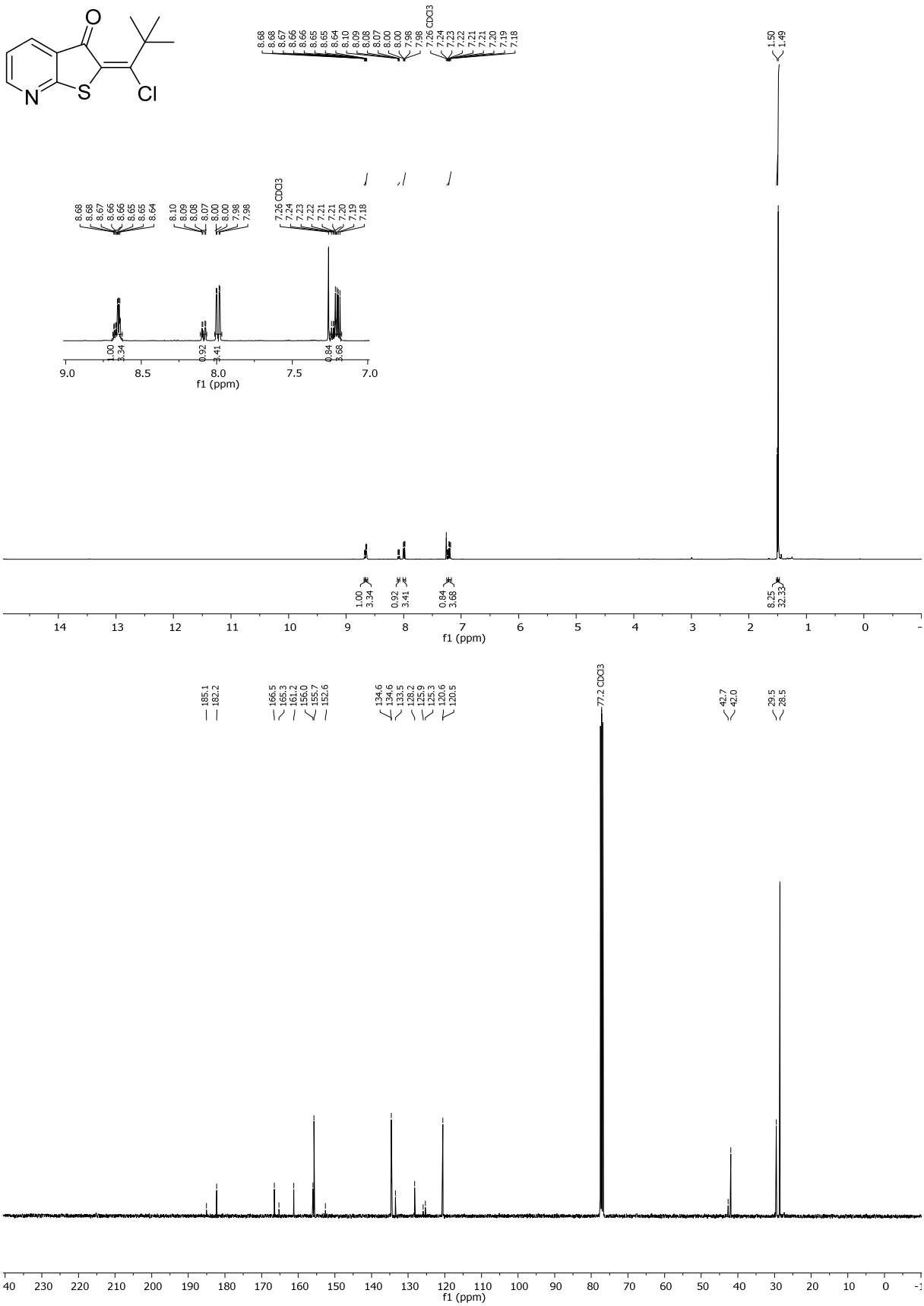

Figure 54: 400 MHz ^{1}H-NMR spectrum (top) and 100 MHz ^{13}C-NMR-spectrum (bottom) of 2-(1-chloro-2,2-dimethylpropylidene)thieno[2,3-*b*]pyridin-3(2*H*)-one (***14***).

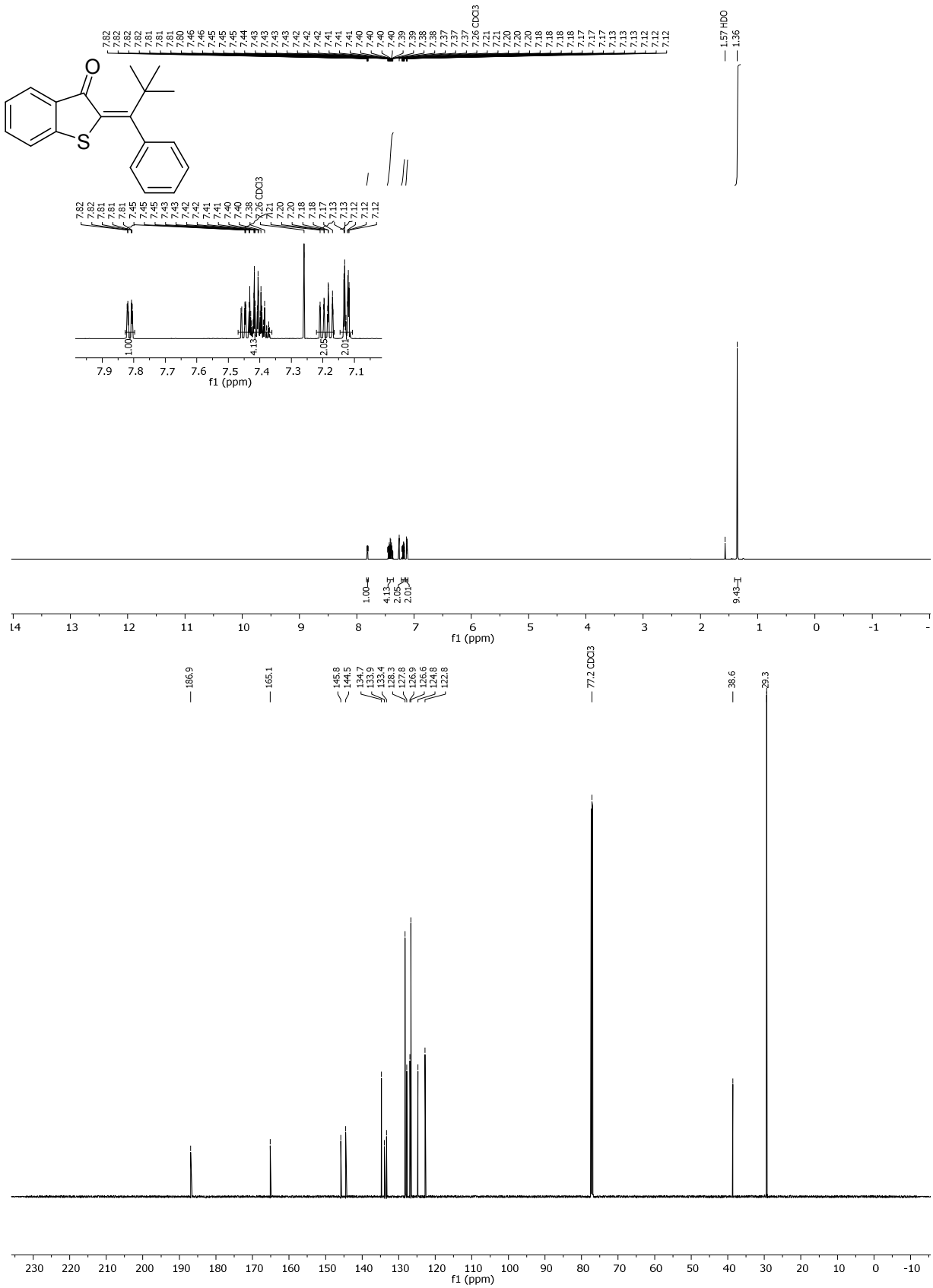

Figure 55: 400 MHz ^{1}H-NMR spectrum (top) and 100 MHz ^{13}C-NMR-spectrum (bottom) of (*Z*)-2-(2,2-dimethyl-1-phenylpropylidene)benzo[*b*]thiophen-3(2*H*)-one (***15***).

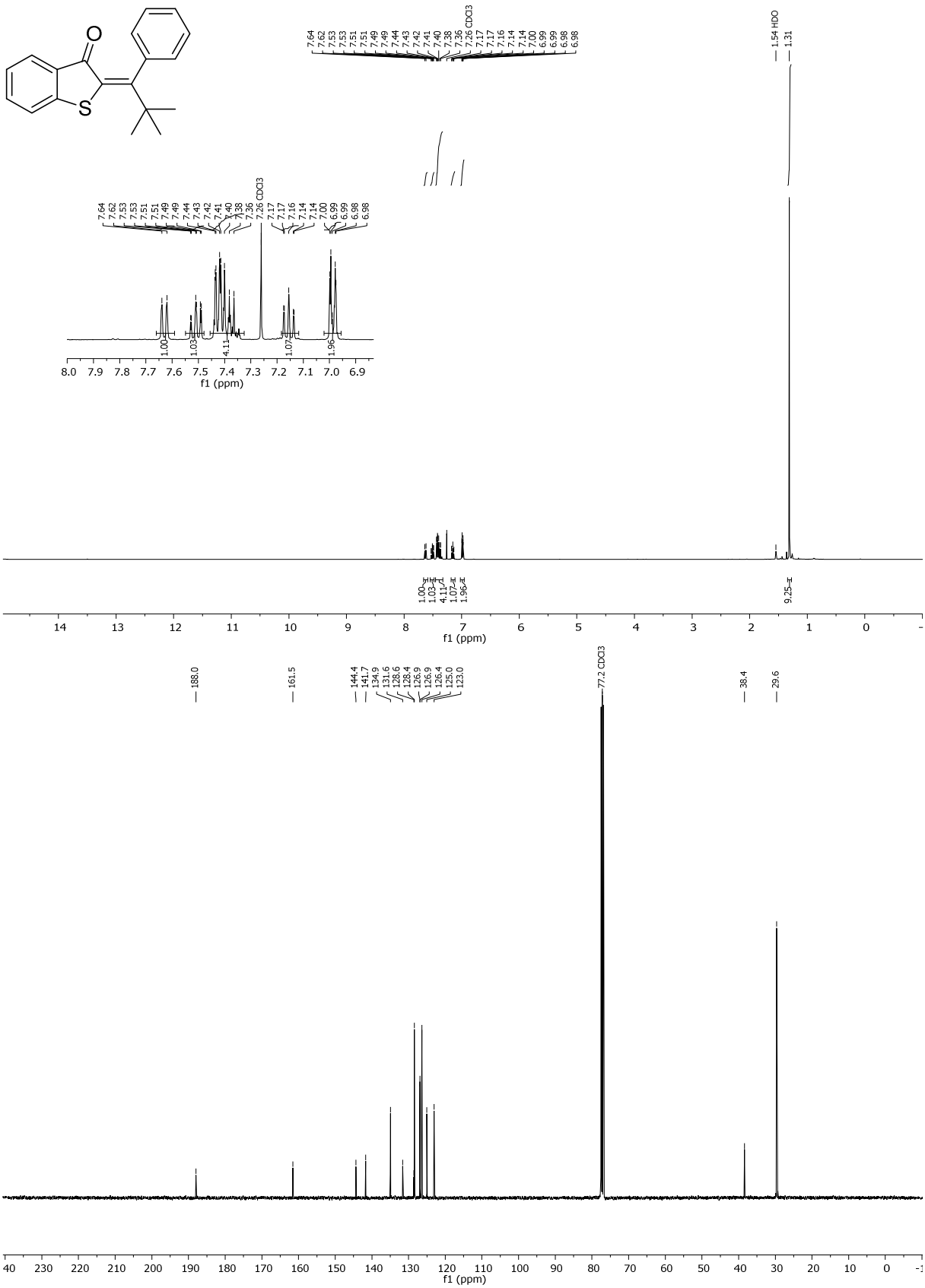

Figure 56: 400 MHz ^{1}H-NMR spectrum (top) and 100 MHz ^{13}C-NMR-spectrum (bottom) of (*E*)-2-(2,2-dimethyl-1-phenylpropylidene)benzo[*b*]thiophen-3(2*H*)-one (***15***).

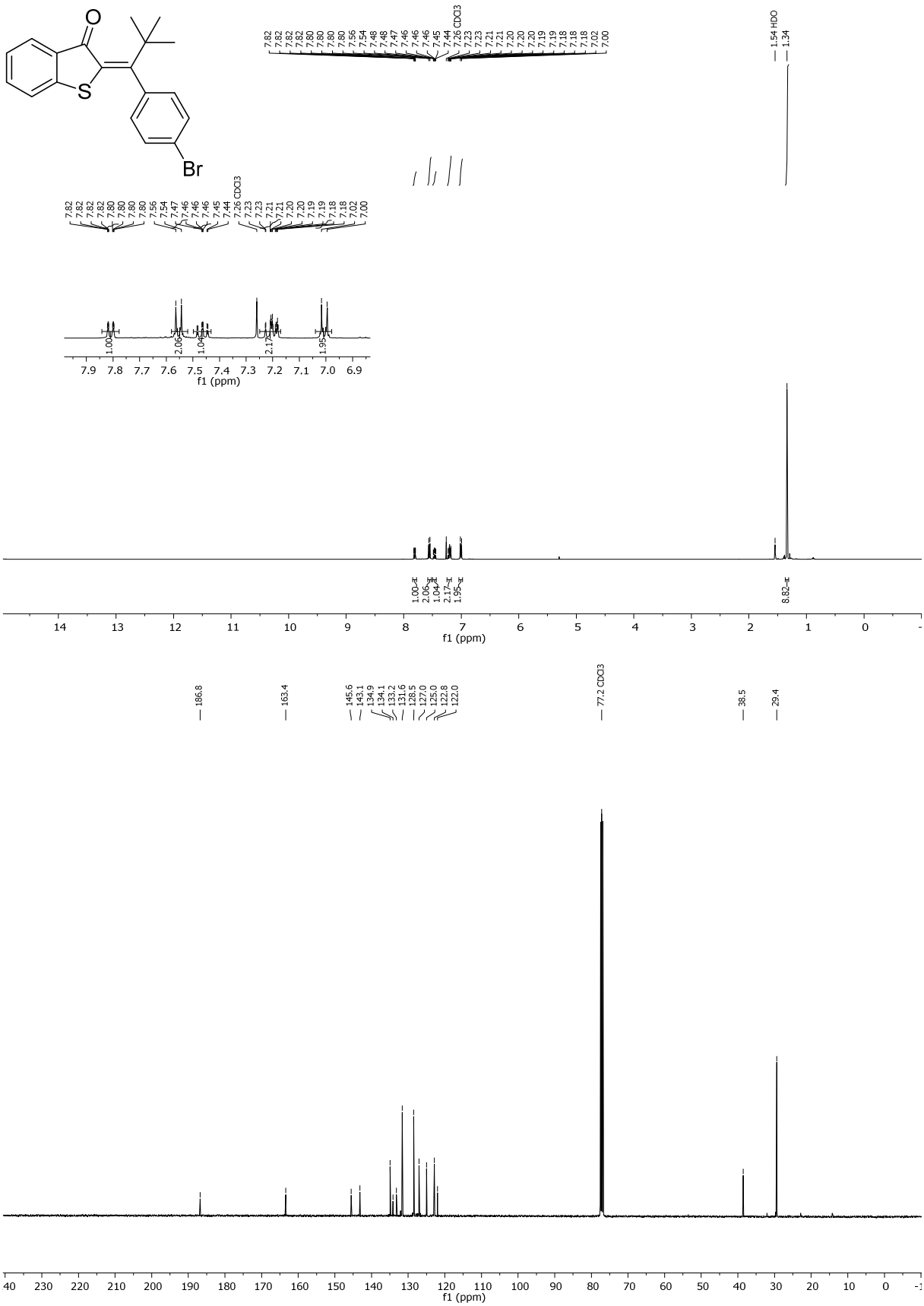

Figure 57: 400 MHz ^{1}H-NMR spectrum (top) and 100 MHz ^{13}C-NMR-spectrum (bottom) of (*Z*)- 2-(1-(4-bromophenyl)-2,2-dimethylpropylidene)benzo[*b*]thiophen-3(2*H*)-one (***16***).

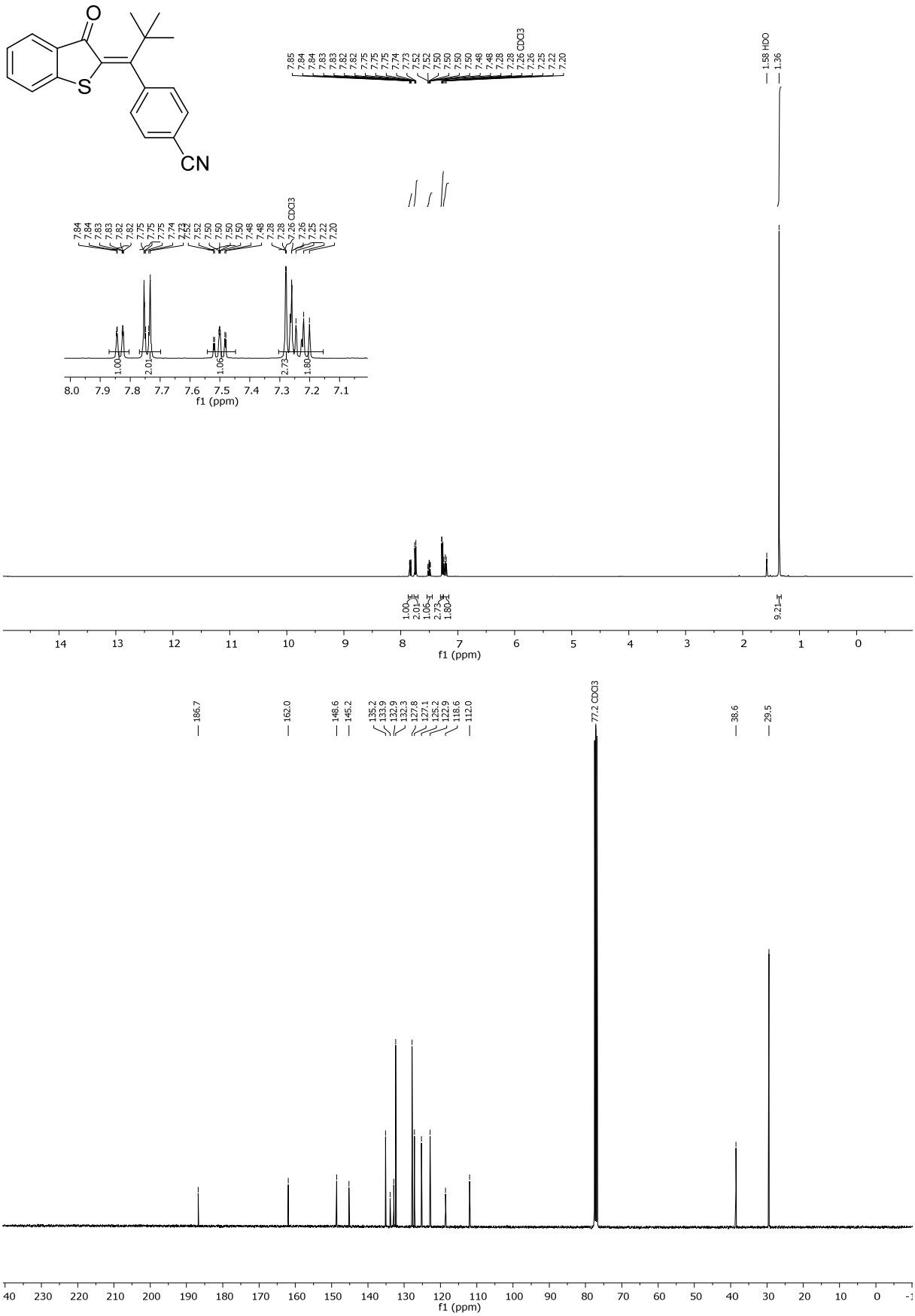

Figure 58: 400 MHz ^{1}H-NMR spectrum (top) and 100 MHz ^{13}C-NMR-spectrum (bottom) of (*Z*)-4-(2,2-Dimethyl-1-(3-oxobenzo[*b*]thiophen-2(3*H*)-ylidene)propyl)benzonitrile (***17***).

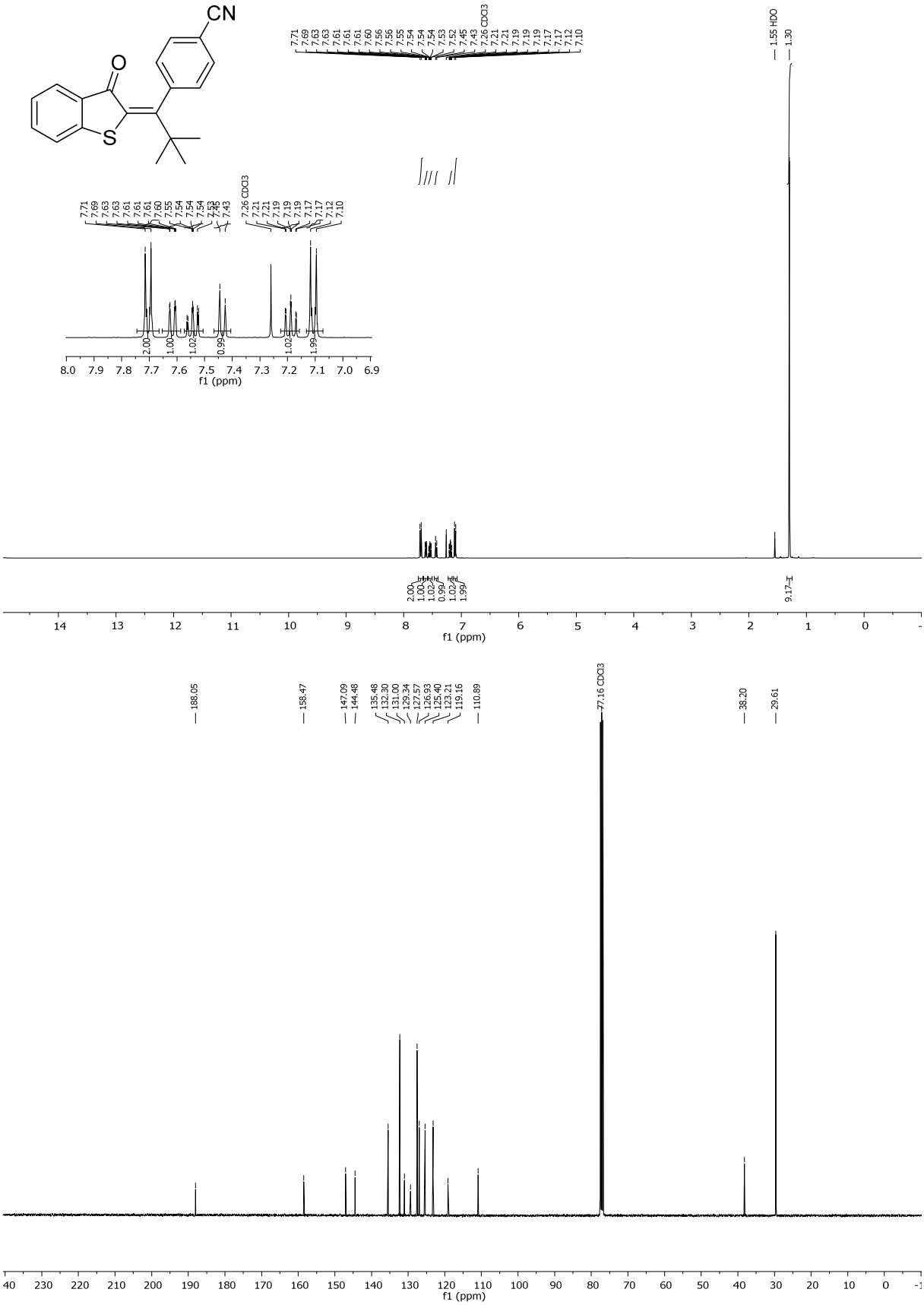

Figure 59: 400 MHz ^{1}H-NMR spectrum (top) and 100 MHz ^{13}C-NMR-spectrum (bottom) of (*E*)-4-(2,2-Dimethyl-1-(3-oxobenzo[*b*]thiophen-2(3*H*)-ylidene)propyl)benzonitrile (***17***).

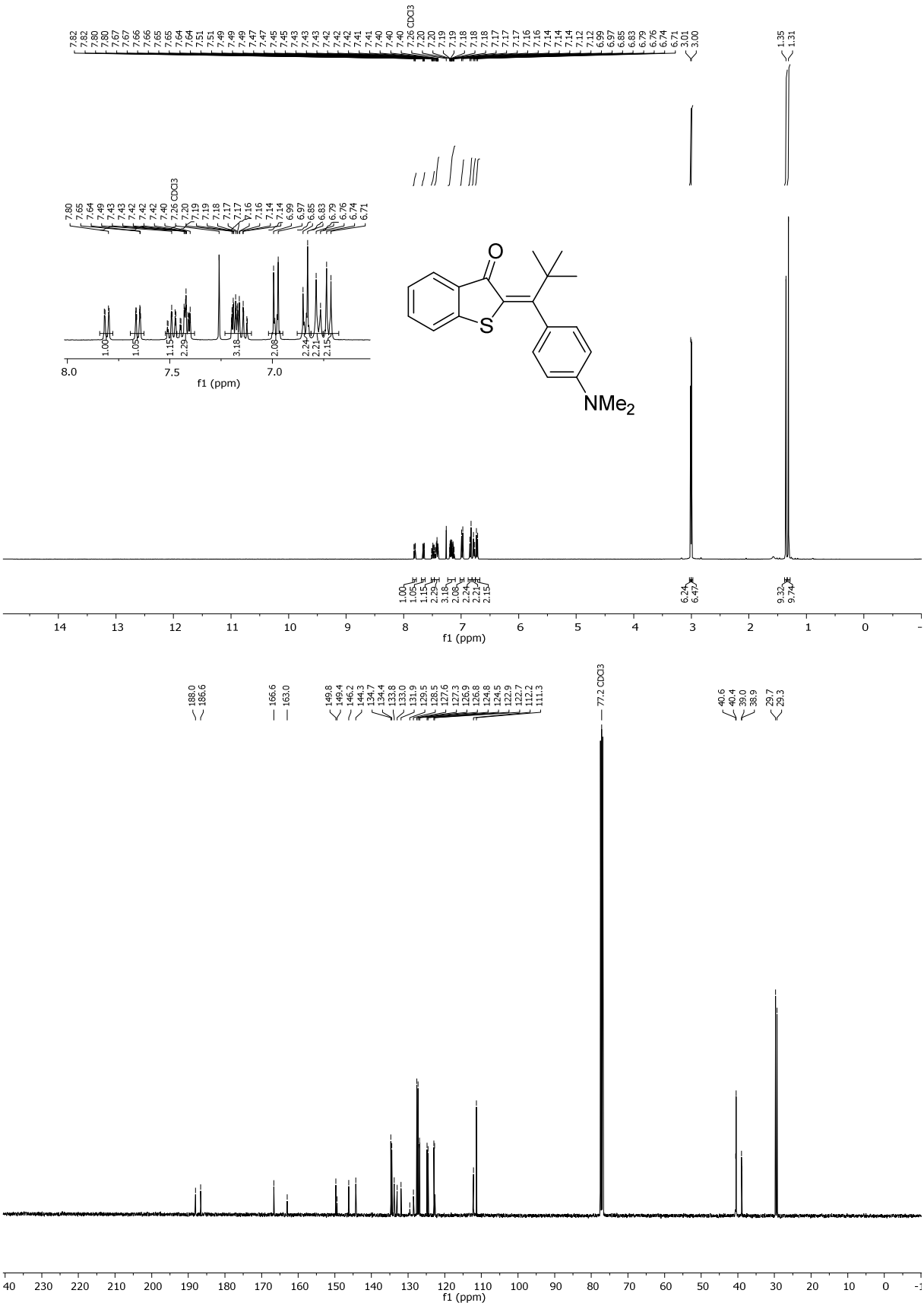

Figure 60: 400 MHz ^{1}H-NMR spectrum (top) and 100 MHz ^{13}C-NMR-spectrum (bottom) of (*E/Z*)-2-(1-(4-(dimethylamino)phenyl)-2,2-dimethylpropylidene)benzo[*b*]thiophen-3(2*H*)-one (***18***).

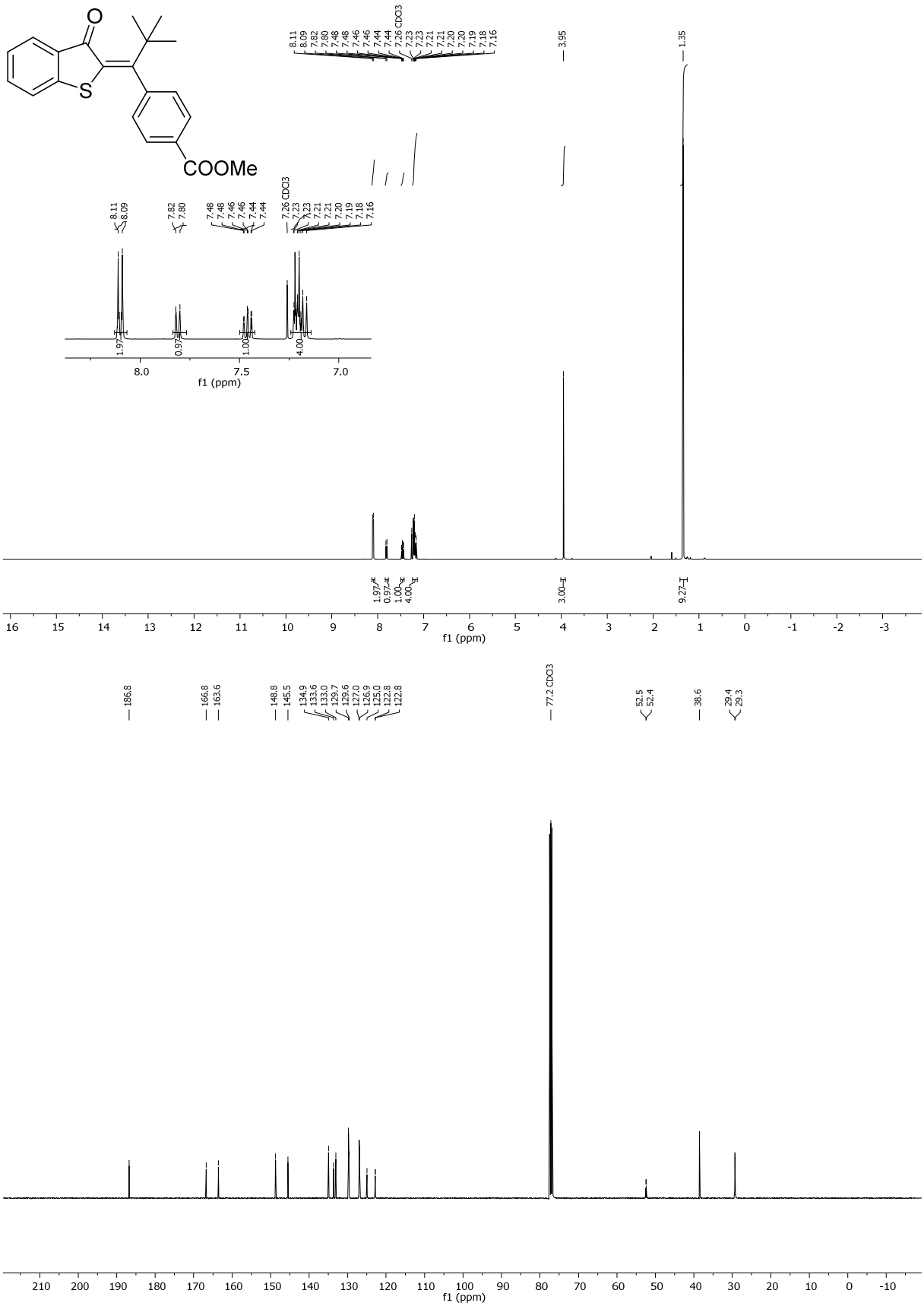

Figure 61: 400 MHz ^{1}H-NMR spectrum (top) and 100 MHz ^{13}C-NMR-spectrum (bottom) of (*Z*)-methyl 4-(2,2-dimethyl-1-(3-oxobenzo[*b*]thiophen-2(3*H*)-ylidene)propyl)benzoate (***19***).

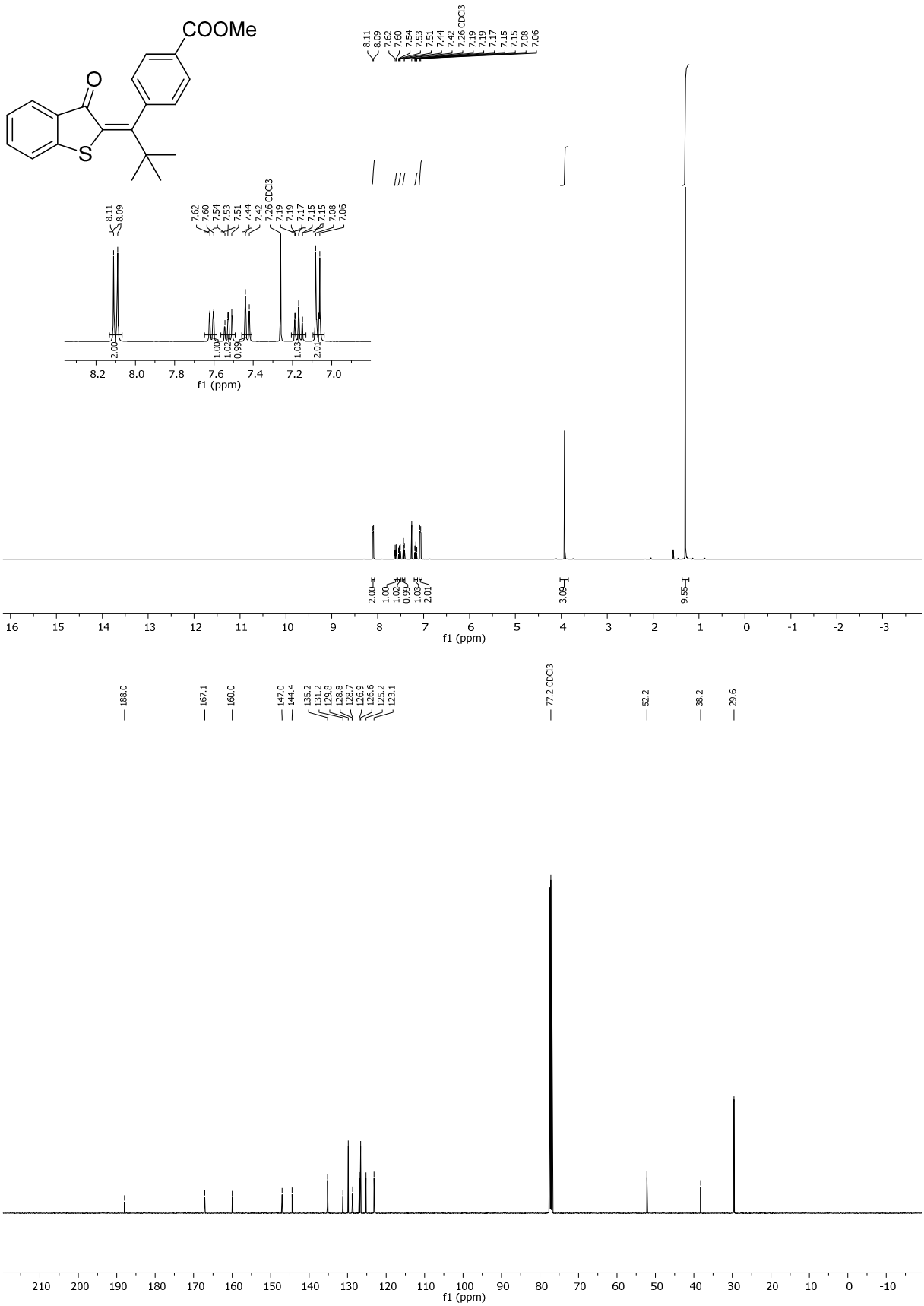

Figure 62: 400 MHz ^{1}H-NMR spectrum (top) and 100 MHz ^{13}C-NMR-spectrum (bottom) of (*E*)-methyl 4-(2,2-dimethyl-1-(3-oxobenzo[*b*]thiophen-2(3*H*)-ylidene)propyl)benzoate (***19***).

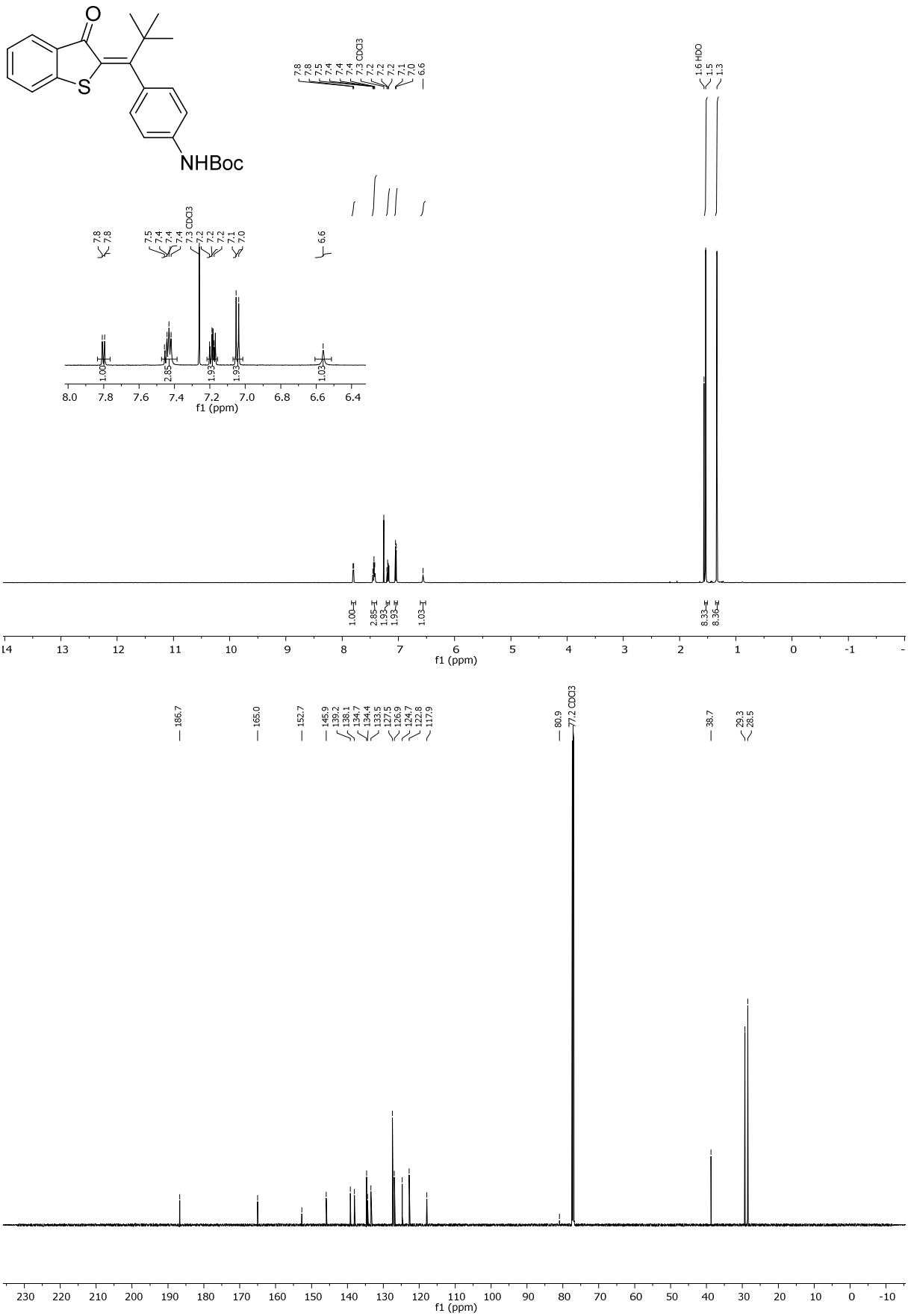

Figure 63: 600 MHz ^{1}H-NMR spectrum (top) and 150 MHz ^{13}C-NMR-spectrum (bottom) of (*Z*)-*tert*-butyl(4-(2,2-dimethyl-1-(3-oxobenzo[*b*]thiophen-2(3*H*)-ylidene)propyl)phenyl)carbamate (***20***).

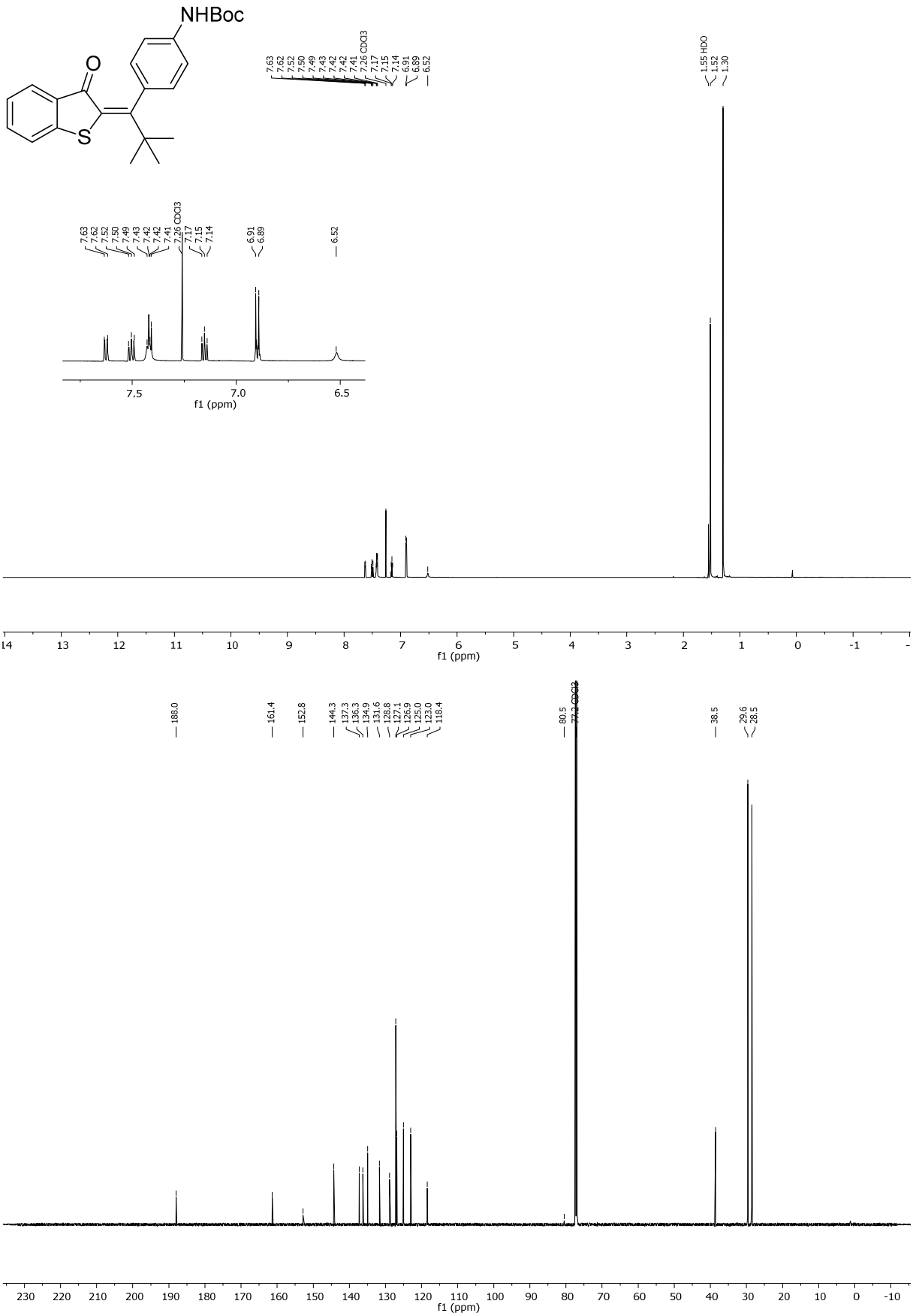

Figure 64: 600 MHz ^{1}H-NMR spectrum (top) and 150 MHz ^{13}C-NMR-spectrum (bottom) of (*E*)-*tert*-butyl(4-(2,2-dimethyl-1-(3-oxobenzo[*b*]thiophen-2(3*H*)-ylidene)propyl)phenyl)carbamate (**20**).

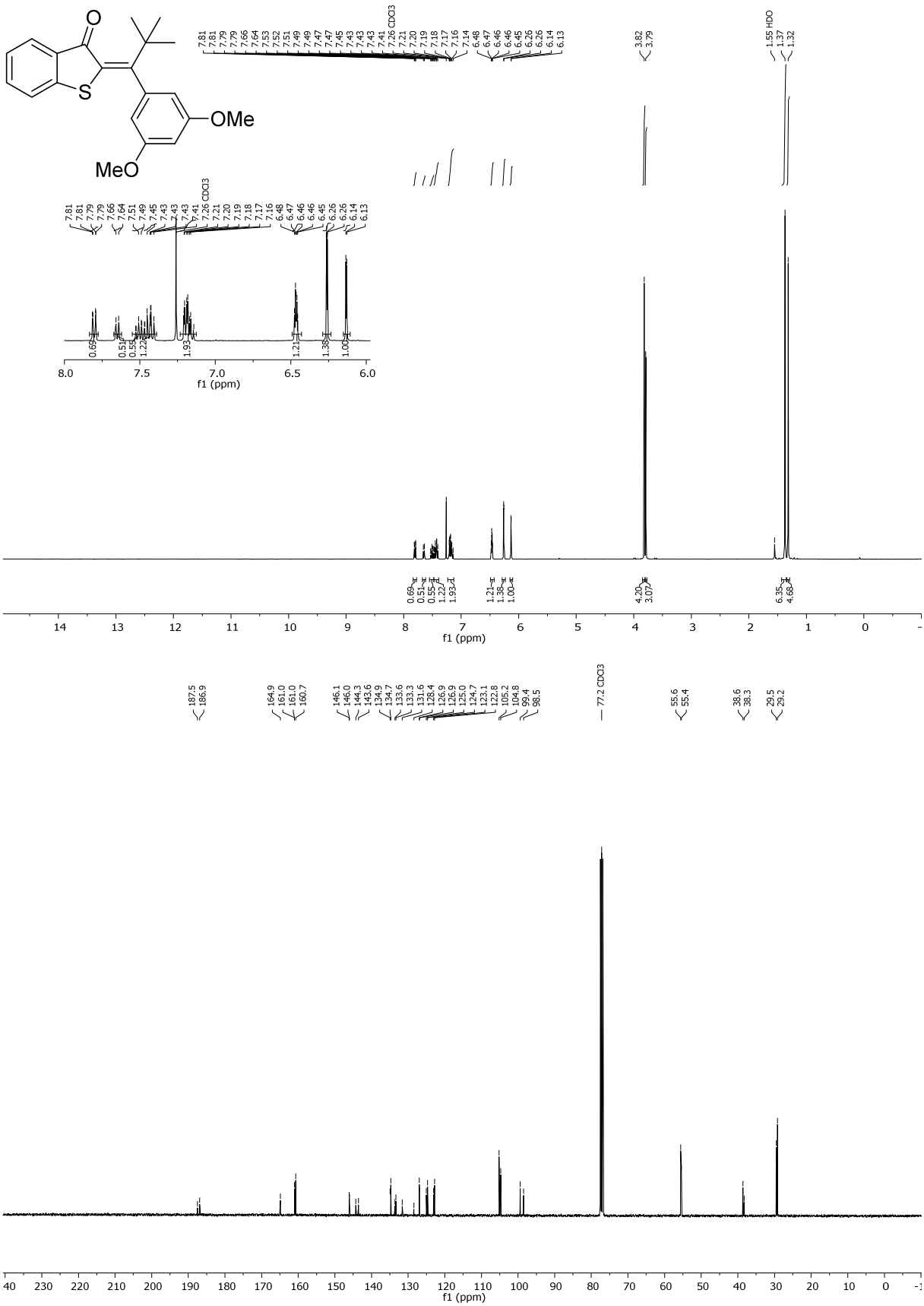

Figure 65: 400 MHz ^{1}H-NMR spectrum (top) and 100 MHz ^{13}C-NMR-spectrum (bottom) of (*E/Z*) 2-(1-(3,5-dimethoxyphenyl)-2,2-dimethylpropylidene)benzo[*b*]thiophen-3(2*H*)-one (**21**).

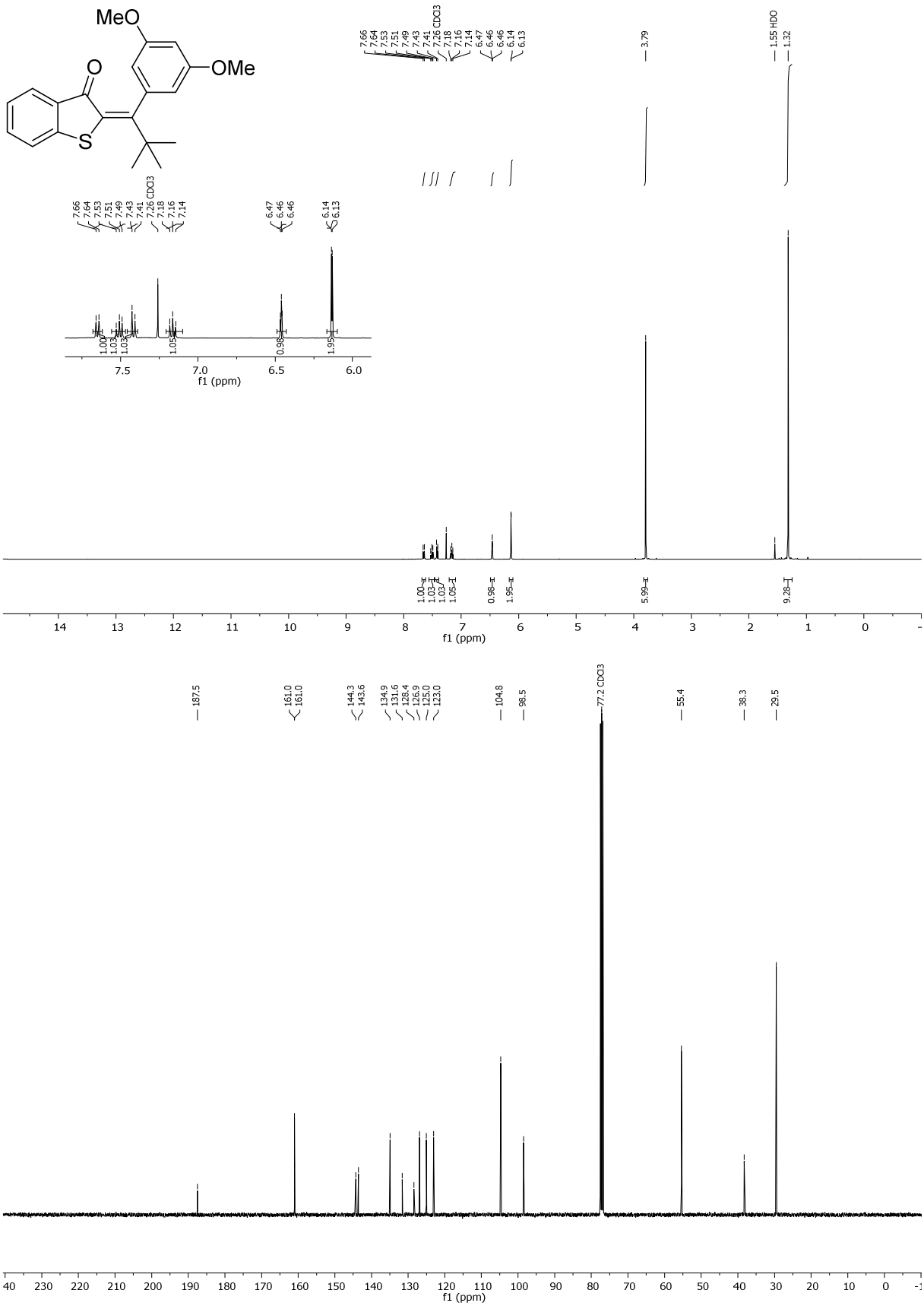

Figure 66: 400 MHz ^{1}H-NMR spectrum (top) and 100 MHz ^{13}C-NMR-spectrum (bottom) of (*E*)-2-(1-(3,5-dimethoxyphenyl)-2,2-dimethylpropylidene)benzo[*b*]thiophen-3(2*H*)-one (**21**).

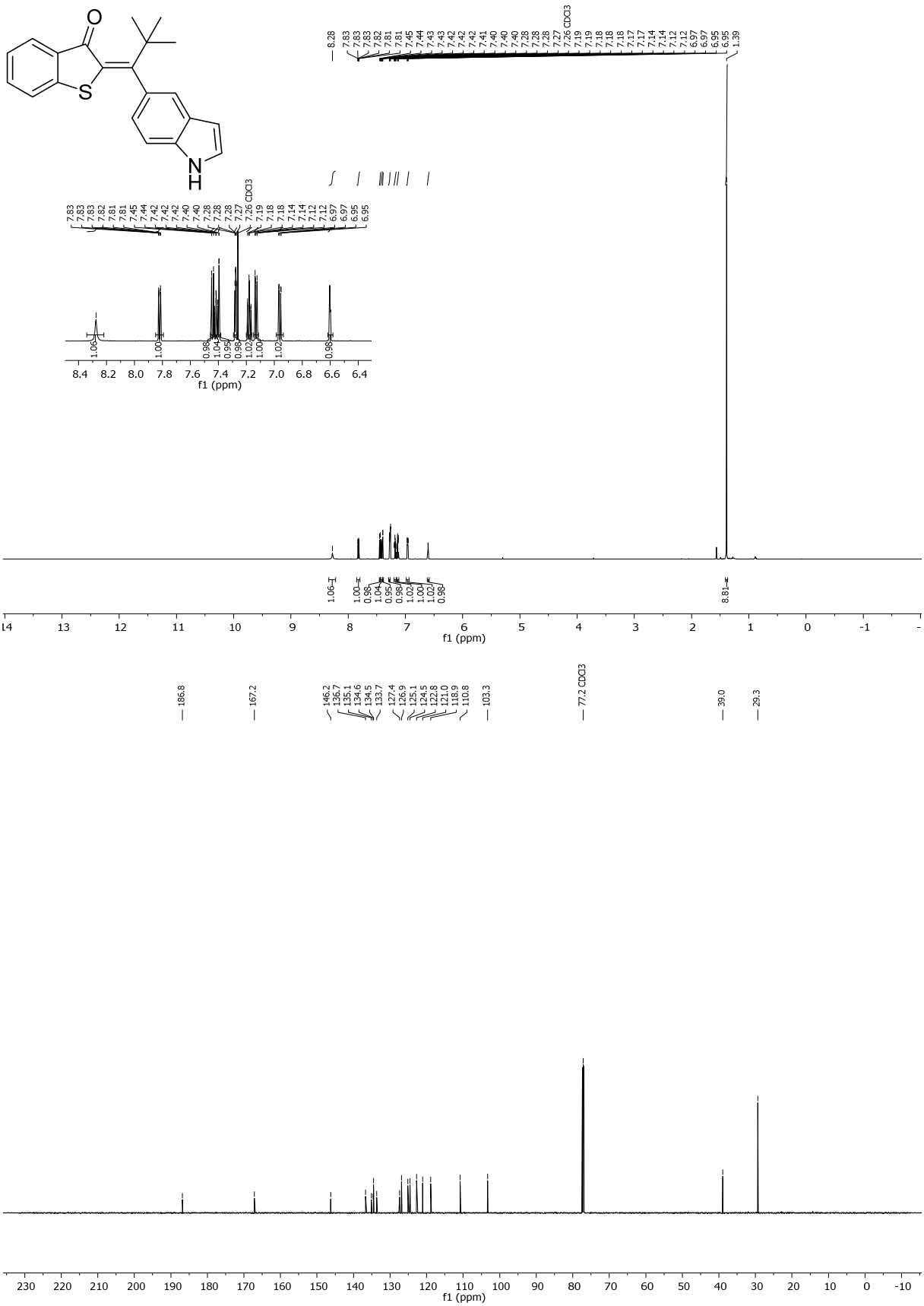

Figure 67: 400 MHz ^{1}H-NMR spectrum (top) and 100 MHz ^{13}C-NMR-spectrum (bottom) of (*Z*)-2-(1-(1*H*-indol-5-yl)-2,2-dimethylpropylidene)benzo[*b*]thiophen-3(2*H*)-one (**22**).

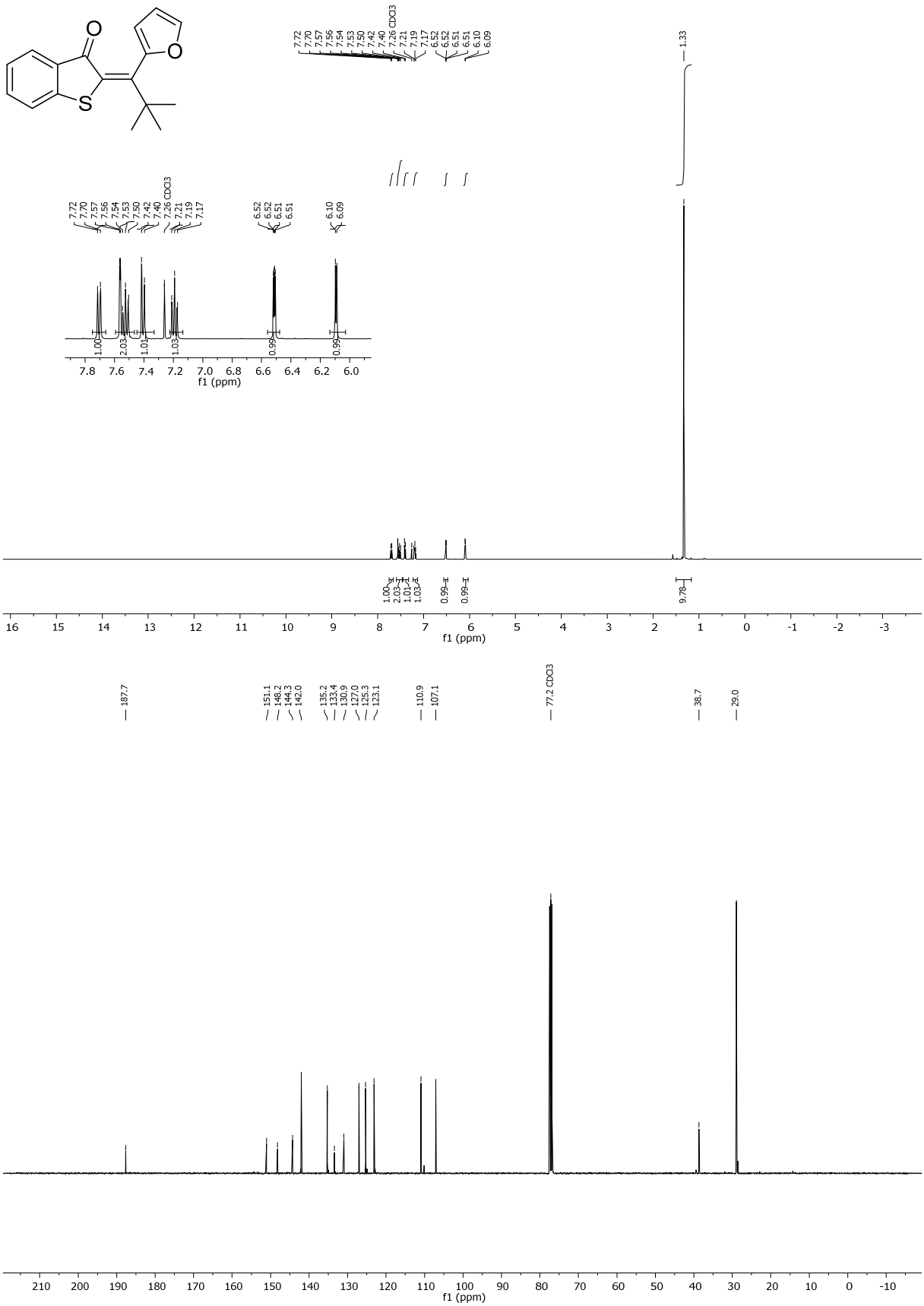

Figure 68: 400 MHz ^{1}H-NMR spectrum (top) and 100 MHz ^{13}C-NMR-spectrum (bottom) of (*E*)-2-(1-(furan-2-yl)-2,2-dimethylpropylidene)benzo[*b*]thiophen-3(2*H*)-one (**23**).

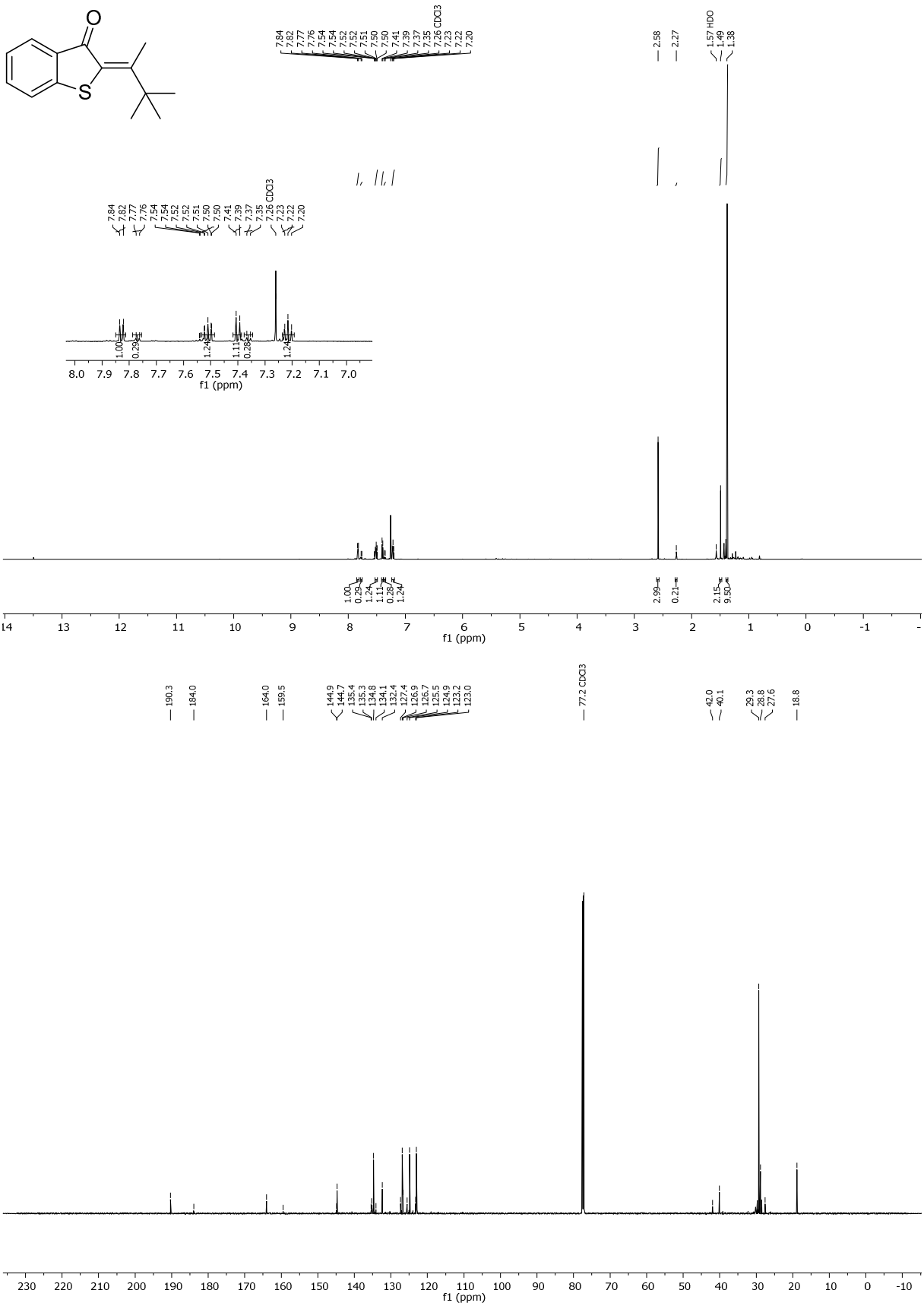

Figure 69: 400 MHz ^{1}H-NMR spectrum (top) and 100 MHz ^{13}C-NMR-spectrum (bottom) of (*Z*/*E*)-2-(3,3-dimethylbutan-2-ylidene)benzo[*b*]thiophen-3(2*H*)-one (5:1) (**24**).

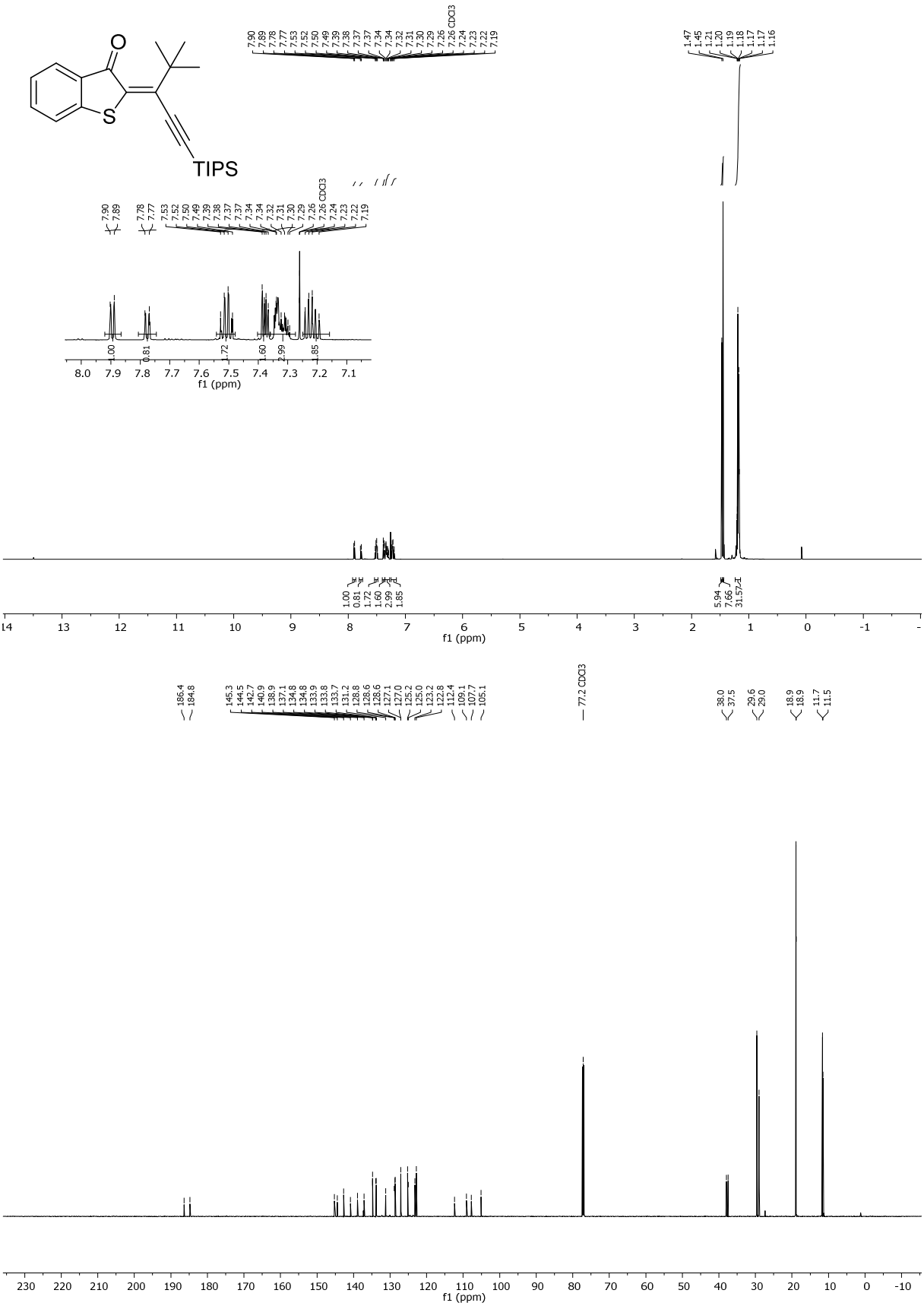

Figure 70: 600 MHz ^{1}H-NMR spectrum (top) and 150 MHz ^{13}C-NMR-spectrum (bottom) of (*Z*/*E*)-2-(4,4-dimethyl-1-(triisopropylsilyl)pent-1-yn-3-ylidene)benzo[*b*]thiophen-3(2*H*)-one (**25**).

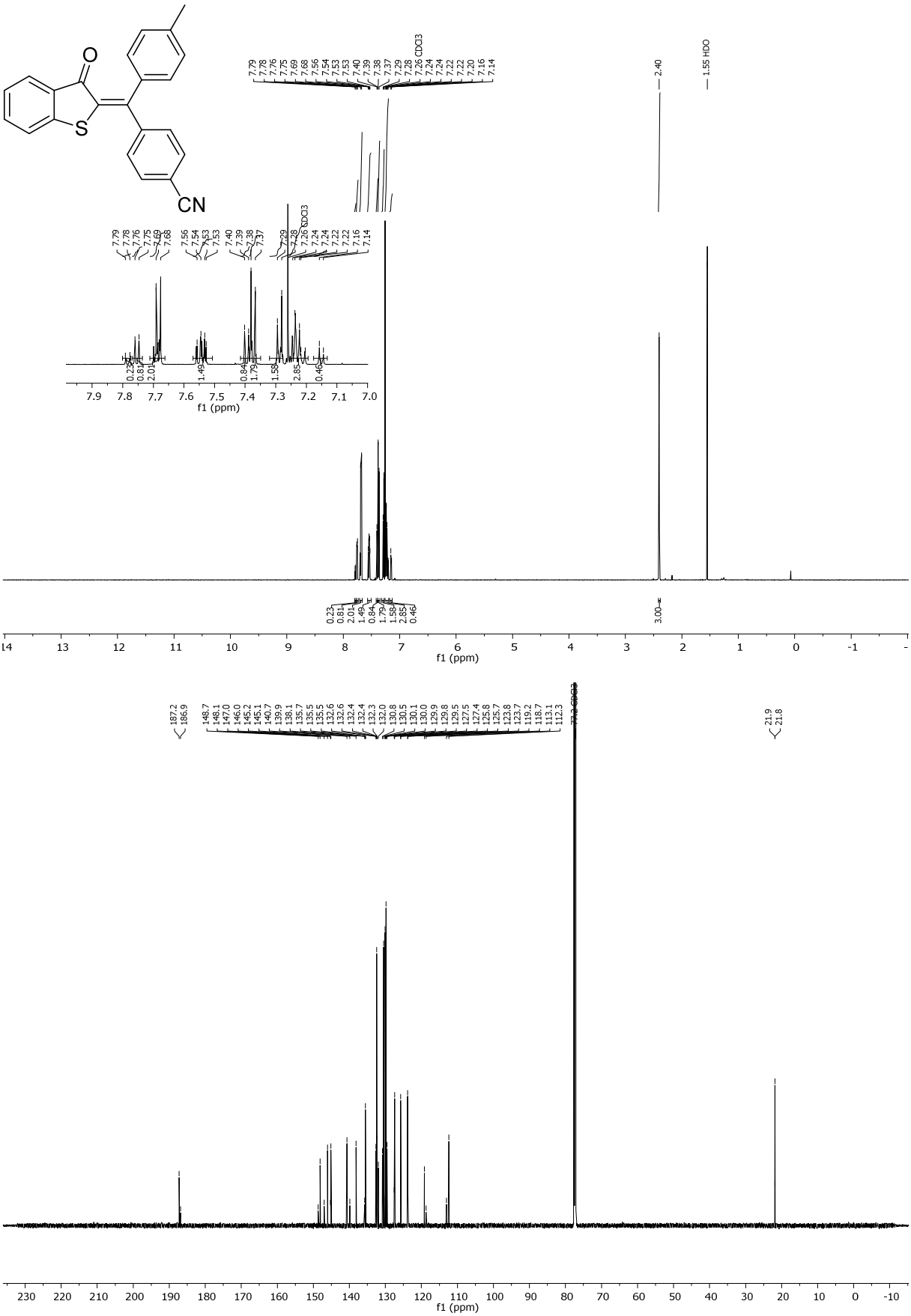

Figure 71: 600 MHz ^{1}H-NMR spectrum (top) and 150 MHz ^{13}C-NMR-spectrum (bottom) of (*Z*/*E*)-4-((3-oxobenzo[*b*]thiophen-2(3*H*)-ylidene)(*p*-tolyl)methyl)benzonitrile (**26**).

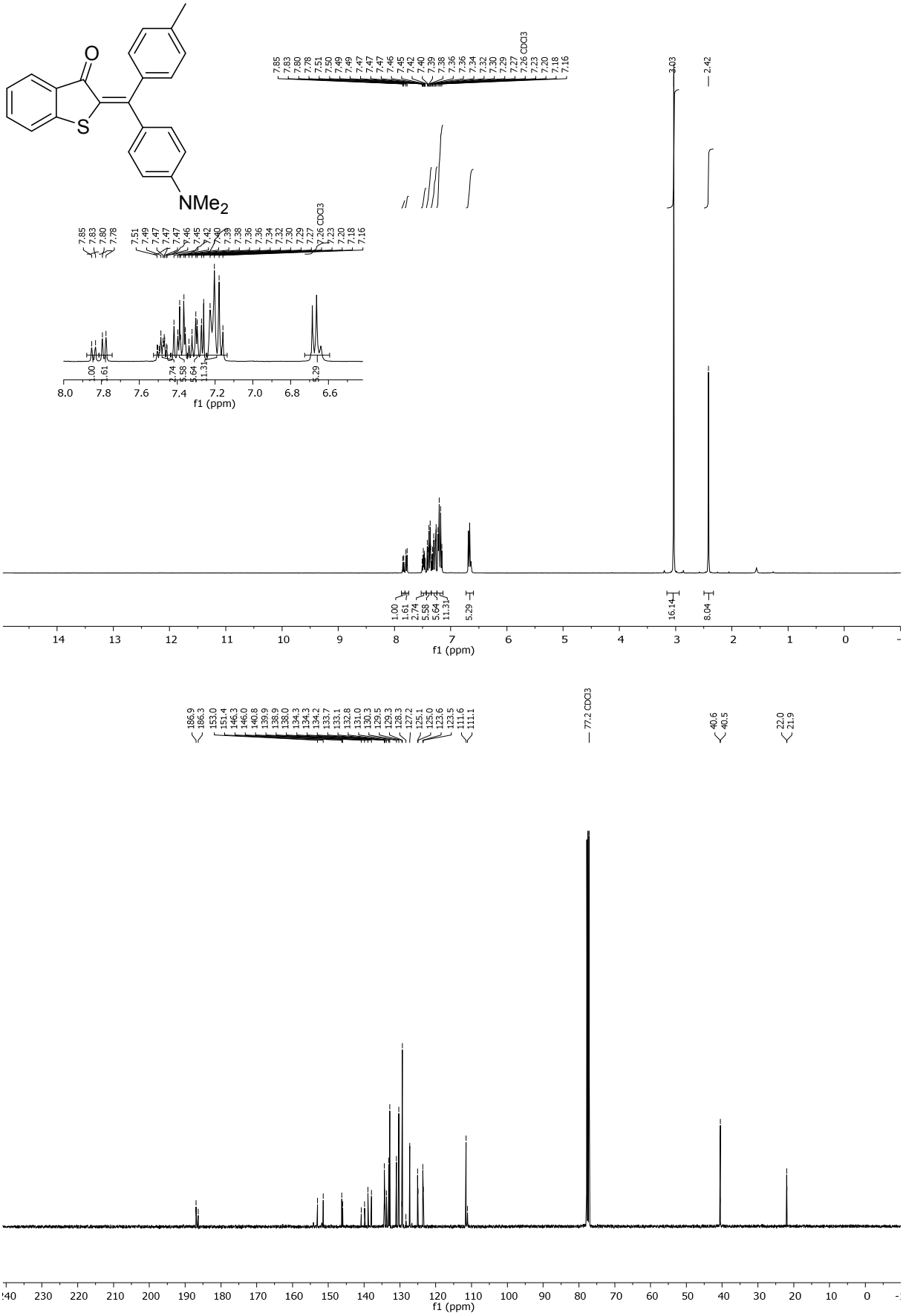

Figure 72: 400 MHz ^{1}H-NMR spectrum (top) and 100 MHz ^{13}C-NMR-spectrum (bottom) of (*Z*/*E*)-2-((4-(dimethylamino)phenyl)(*p*-tolyl)methylene)benzo[*b*]thiophen-3(2*H*)-one (**27**).

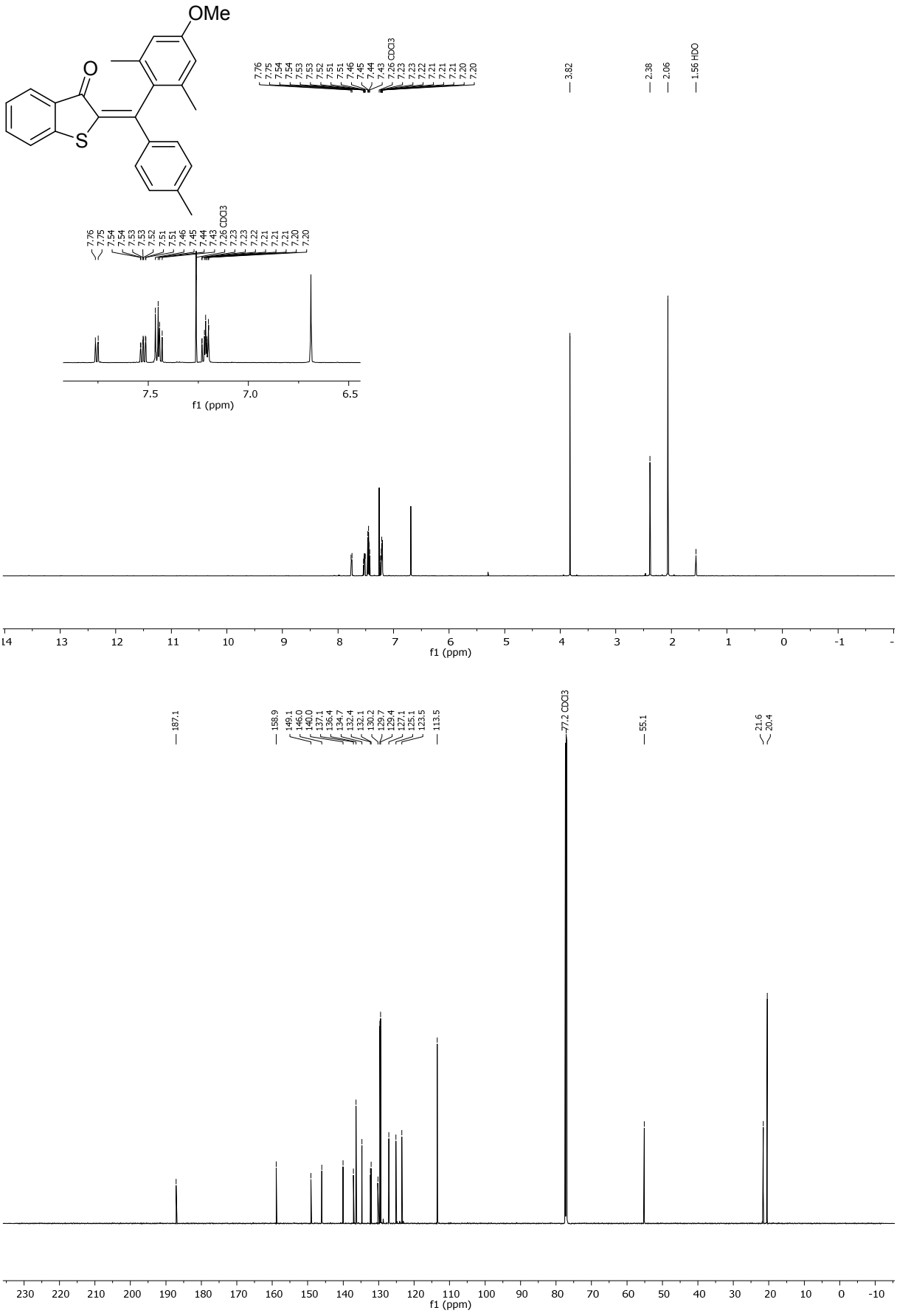

Figure 73: 600 MHz ^{1}H-NMR spectrum (top) and 150 MHz ^{13}C-NMR-spectrum (bottom) of (*E*)-2-((4-methoxy-2,6-dimethylphenyl)(*p*-tolyl)methylene)benzo[*b*]thiophen-3(2*H*)-one (**28**).

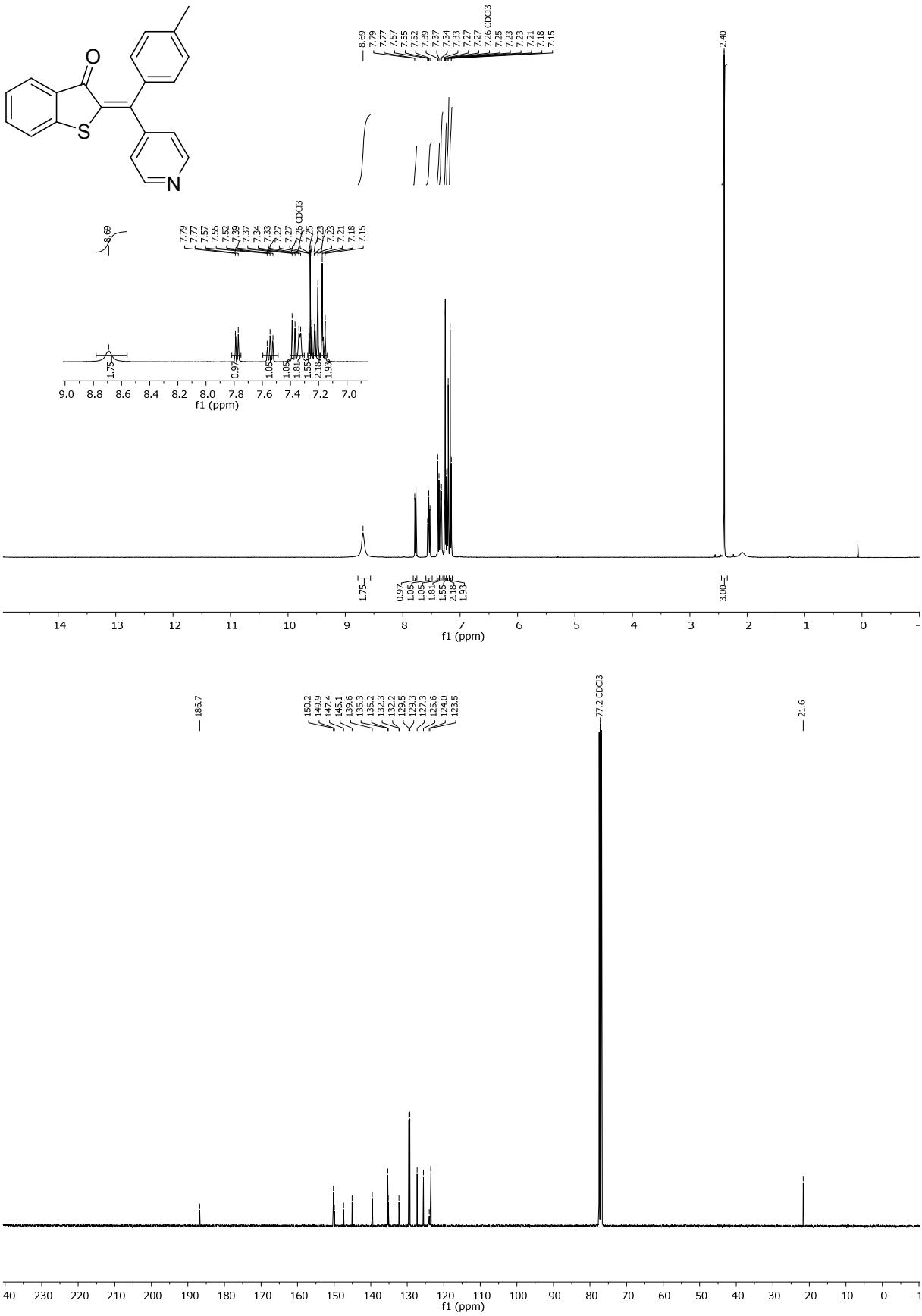

Figure 74: 400 MHz ^{1}H-NMR spectrum (top) and 100 MHz ^{13}C-NMR-spectrum (bottom) of (*Z*)-2-(pyridin-4-yl(*p*-tolyl)methylene)benzo[*b*]thiophen-3(2*H*)-one (**29**)

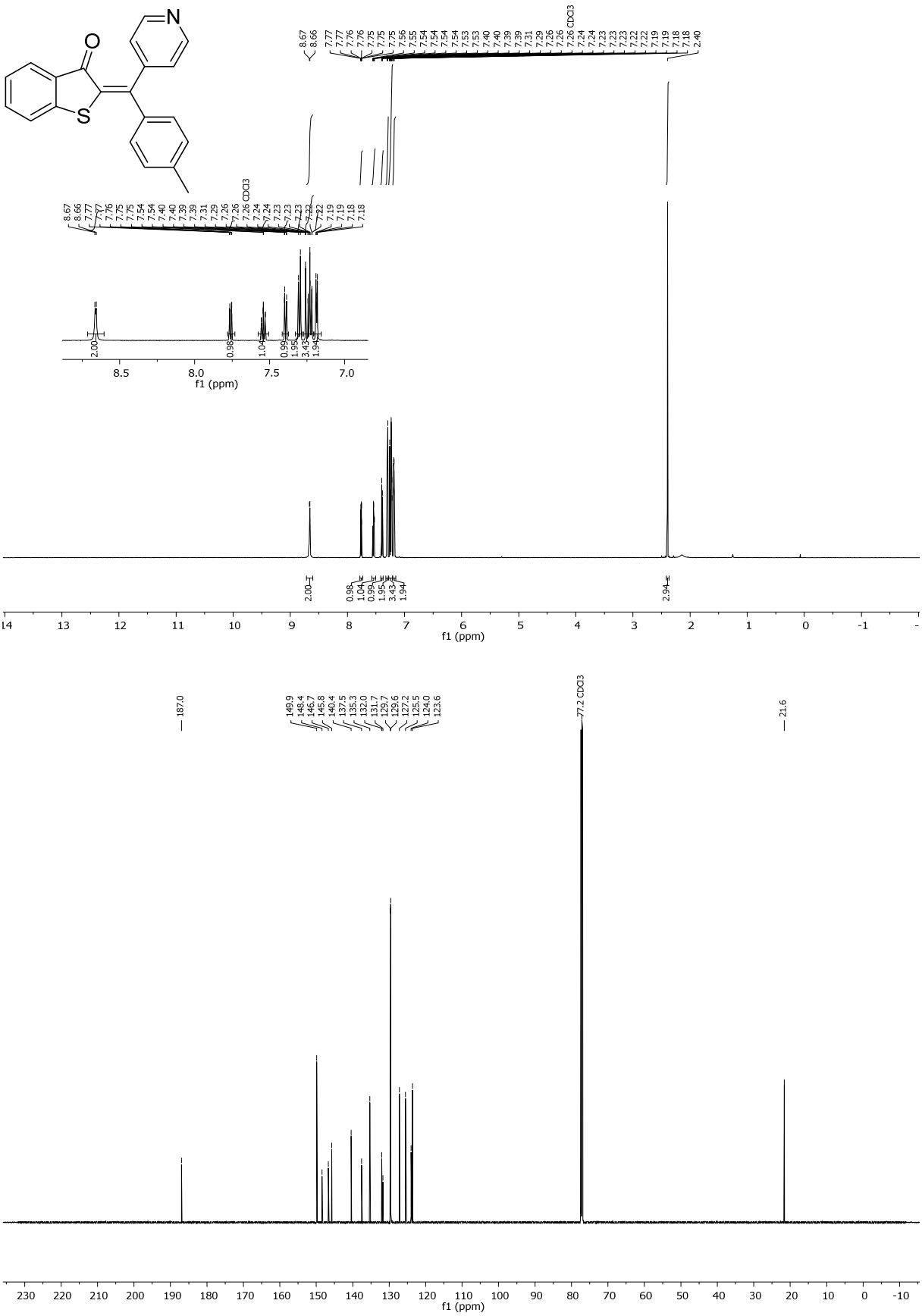

Figure 75: 600 MHz ^{1}H-NMR spectrum (top) and 150 MHz ^{13}C-NMR-spectrum (bottom) of (*E*)-2-(pyridin-4-yl(*p*-tolyl)methylene)benzo[*b*]thiophen-3(2*H*)-one (**29**).

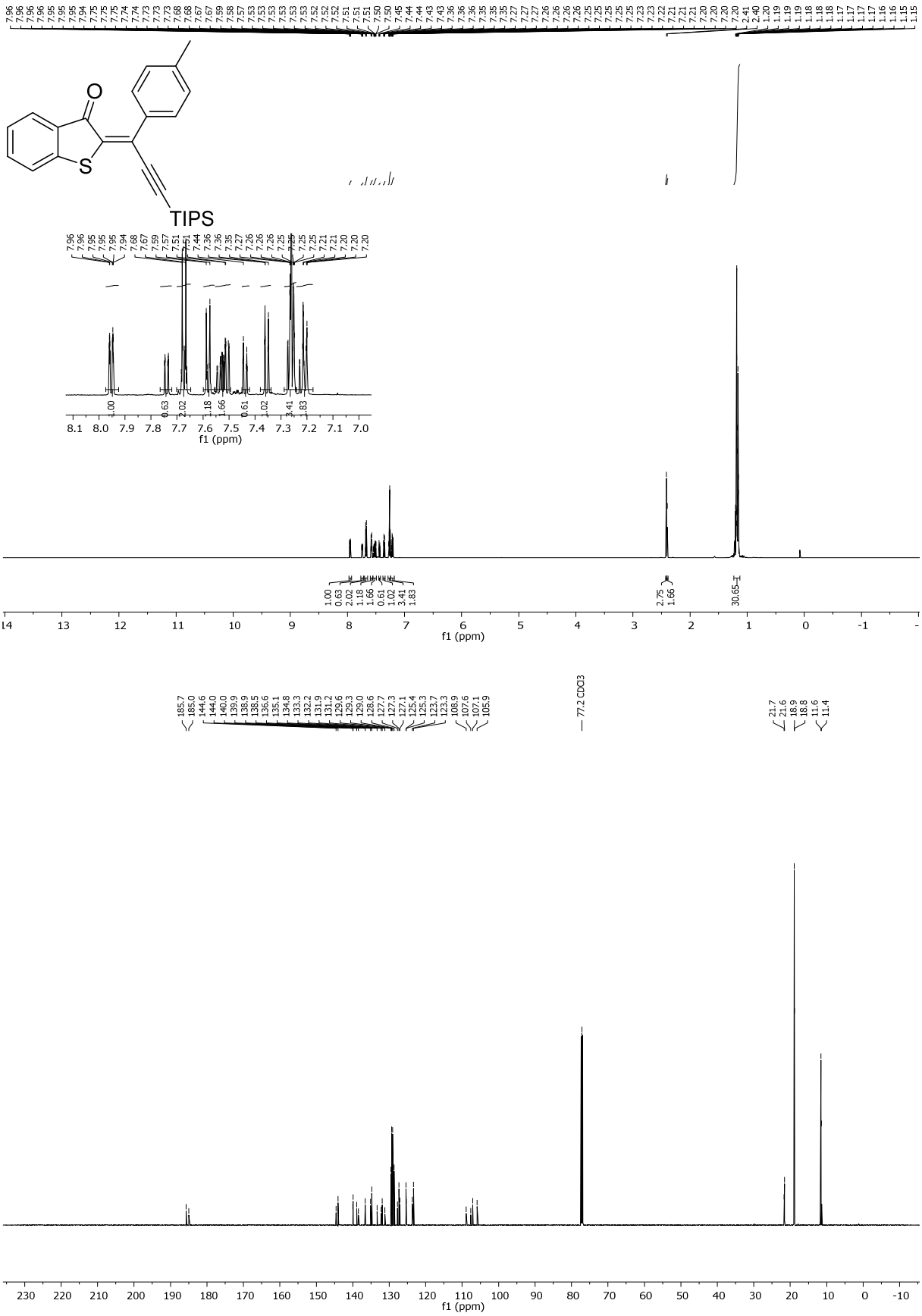

Figure 76: 600 MHz ^{1}H-NMR spectrum (top) and 150 MHz ^{13}C-NMR-spectrum (bottom) of (*E/Z*)-2-(1-(*p*-tolyl)-3-(triisopropylsilyl)prop-2-yn-1-ylidene)benzo[*b*]thiophen-3(2*H*)-one (**30**).

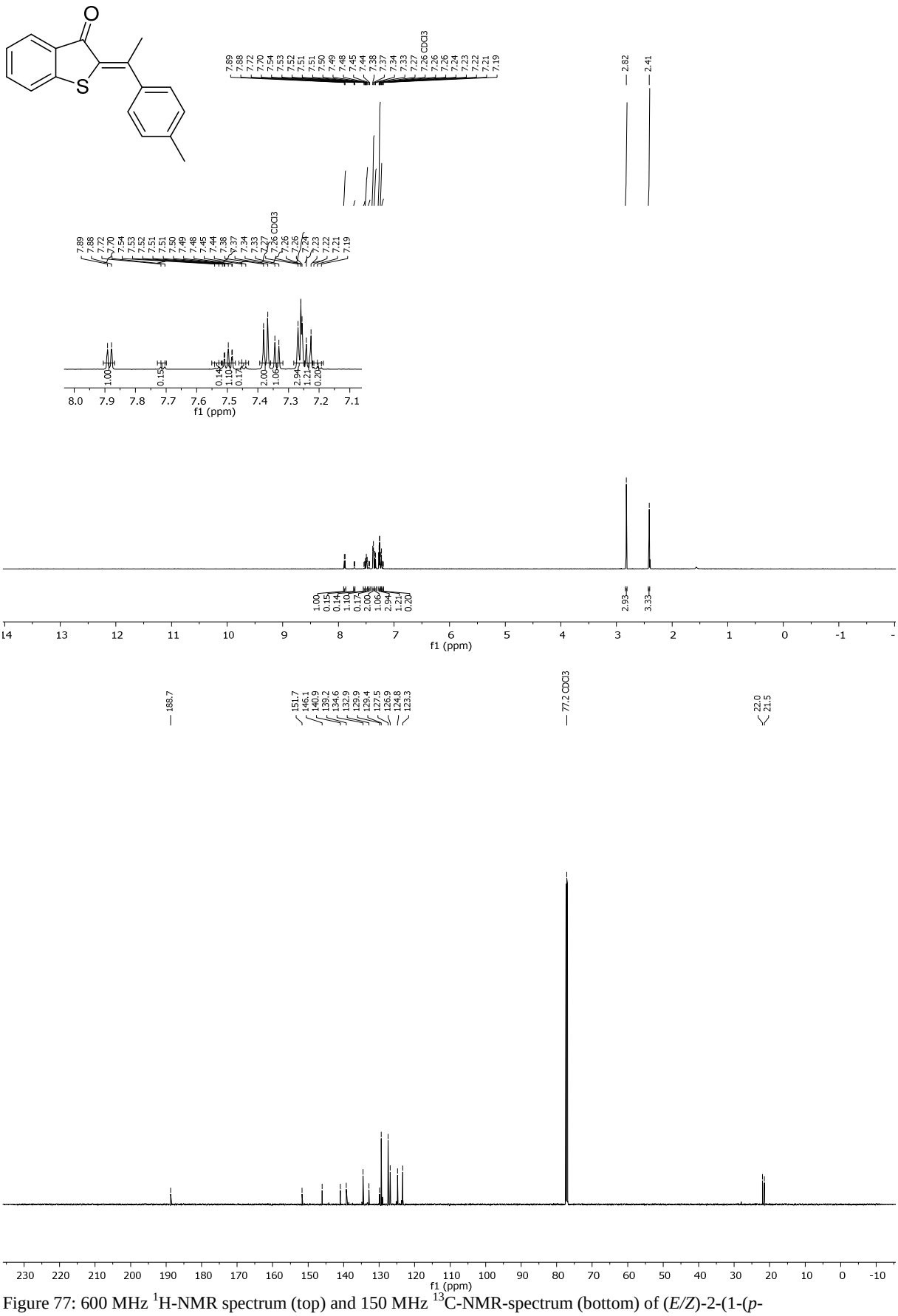

Figure 77: 600 MHz ^{1}H-NMR spectrum (top) and 150 MHz ^{13}C-NMR-spectrum (bottom) of (*E/Z*)-2-(1-(*p*-tolyl)ethylidene)benzo[*b*]thiophen-3(2*H*)-one (**31**).

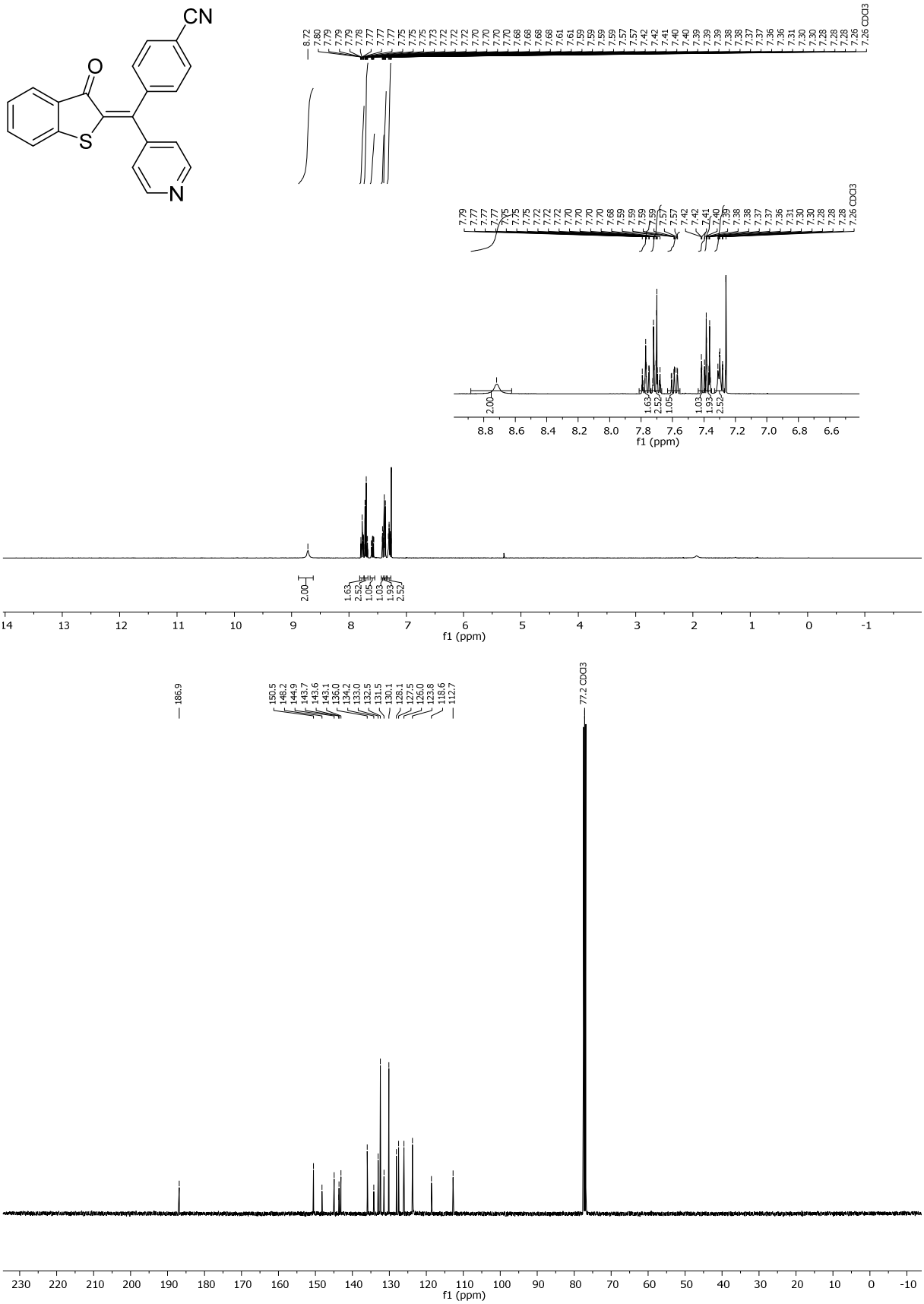

Figure 78: 600 MHz ^{1}H-NMR spectrum (top) and 150 MHz ^{13}C-NMR-spectrum (bottom) of (*Z*)-4-((3-oxobenzo[*b*]thiophen-2(3*H*)-ylidene)(pyridin-4-yl)methyl)benzonitrile (**32**).

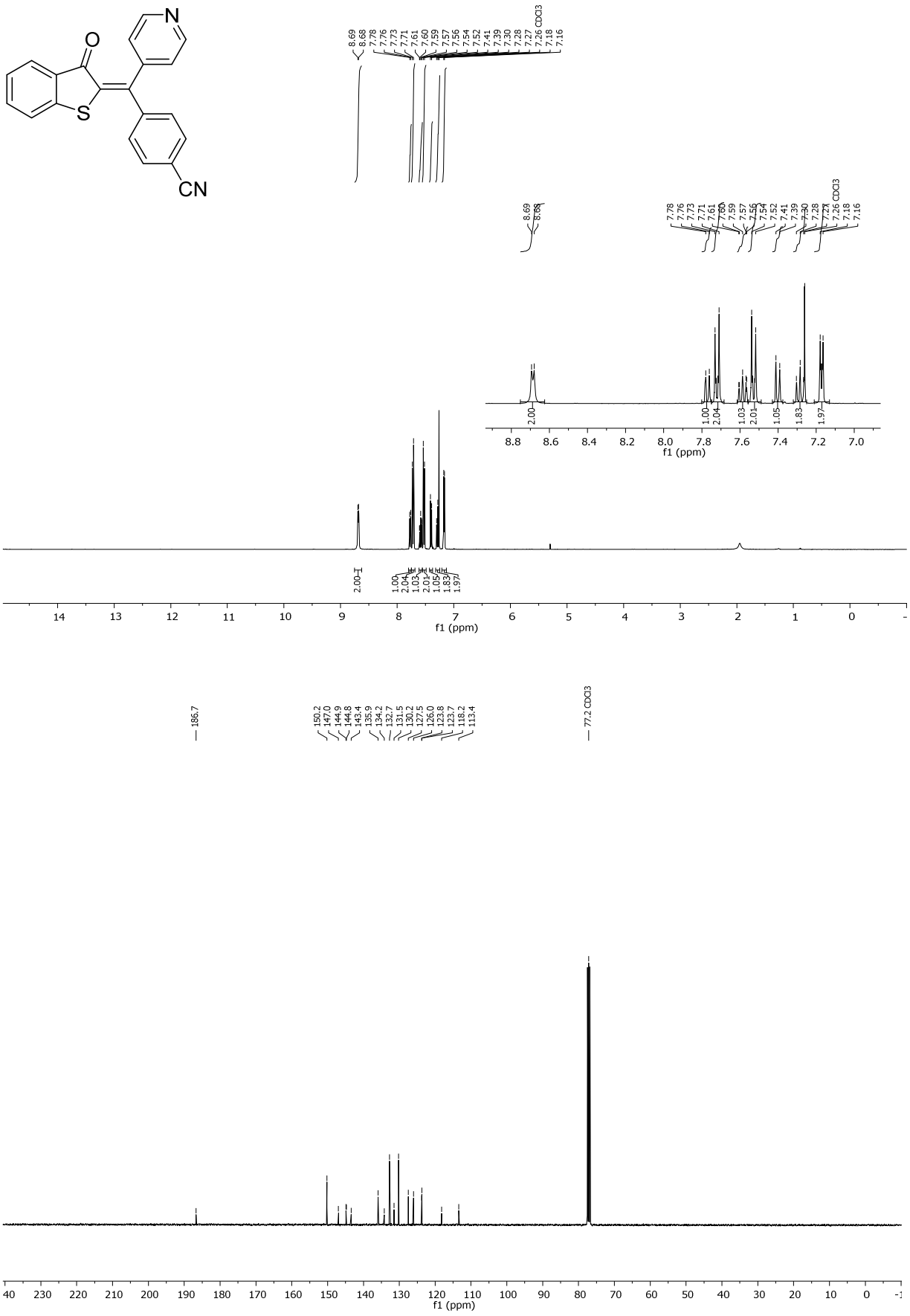

Figure 79: 400 MHz ^{1}H-NMR spectrum (top) and 100 MHz ^{13}C-NMR-spectrum (bottom) of (*E*)-4-((3-oxobenzo[*b*]thiophen-2(3*H*)-ylidene)(pyridin-4-yl)methyl)benzonitrile (32).

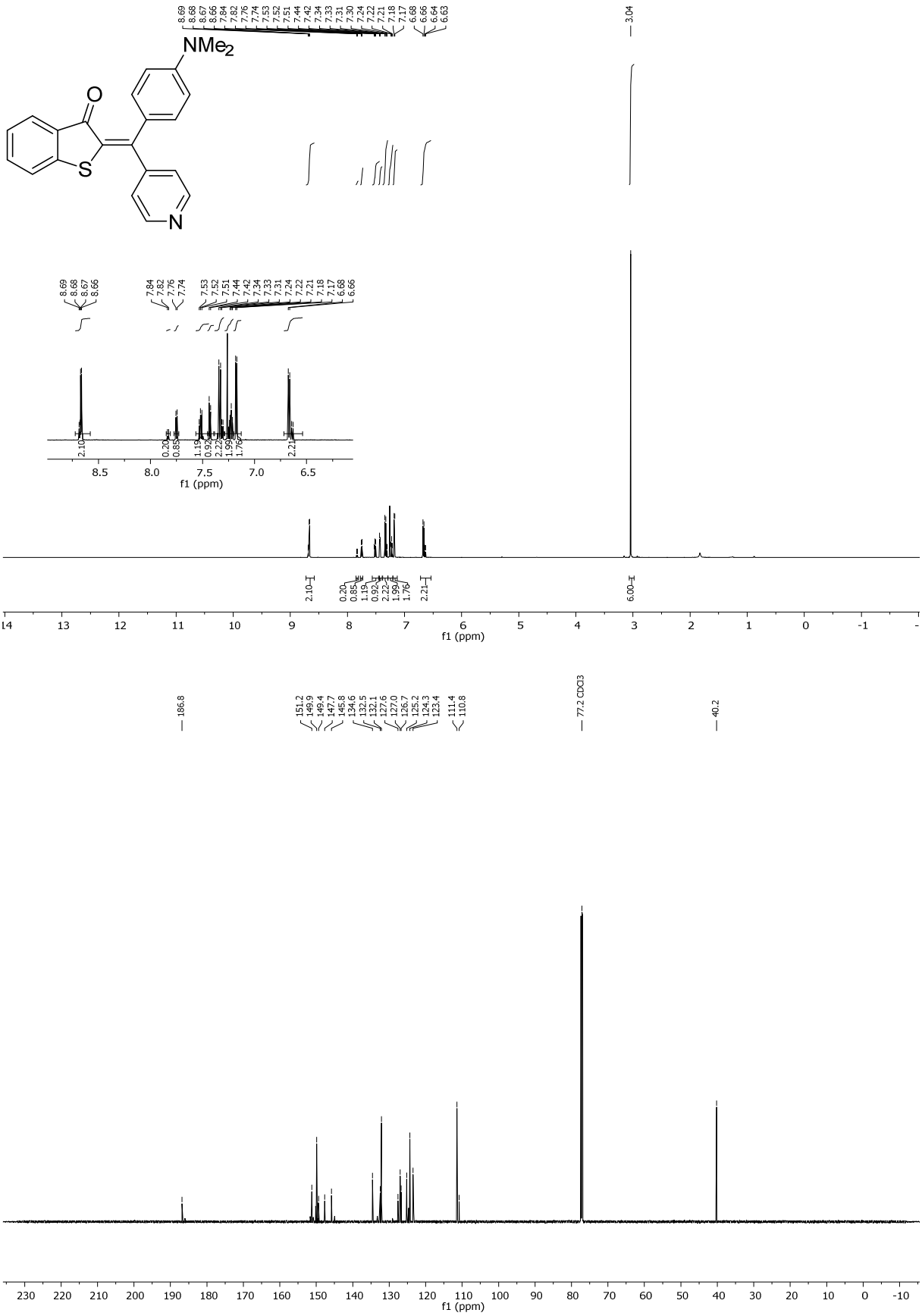

Figure 80: 600 MHz ^{1}H-NMR spectrum (top) and 150 MHz ^{13}C-NMR-spectrum (bottom) of (*E/Z*)-2-((4-(dimethylamino)phenyl)(pyridin-4-yl)methylene)benzo[*b*]thiophen-3(2*H*)-one (**33**).

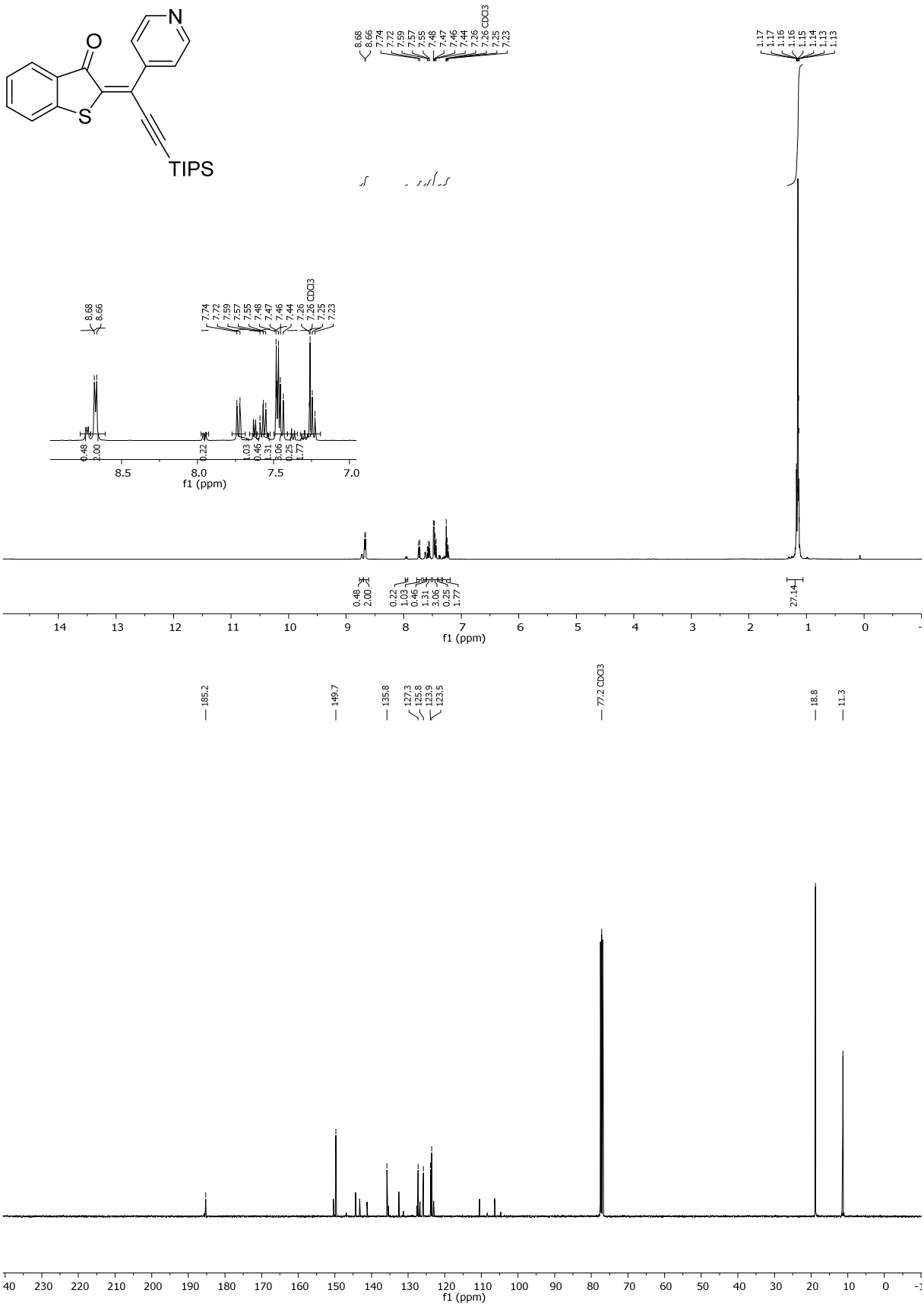

Figure 81: 400 MHz ^{1}H-NMR spectrum (top) and 100 MHz ^{13}C-NMR-spectrum (bottom) of (*E/Z*)-2-(1-(pyridin-4-yl)-3-(triisopropylsilyl)prop-2-yn-1-ylidene)benzo[*b*]thiophen-3(2*H*)-one (1 : 5) (**34**).

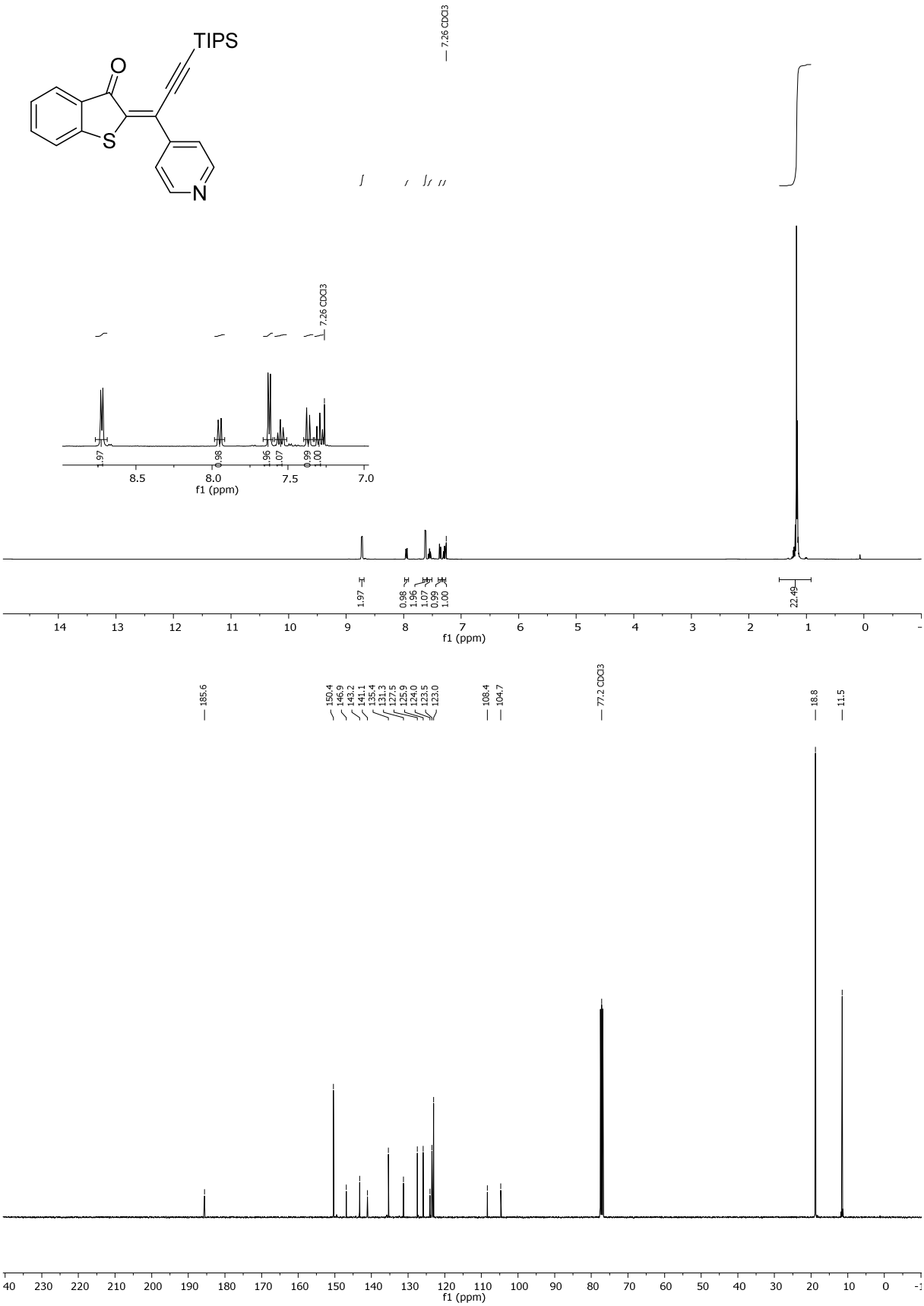

Figure 82: 400 MHz ^{1}H-NMR spectrum (top) and 100 MHz ^{13}C-NMR-spectrum (bottom) of (*E*)-2-(1-(pyridin-4-yl)-3-(triisopropylsilyl)prop-2-yn-1-ylidene)benzo[*b*]thiophen-3(2*H*)-one (**34**).

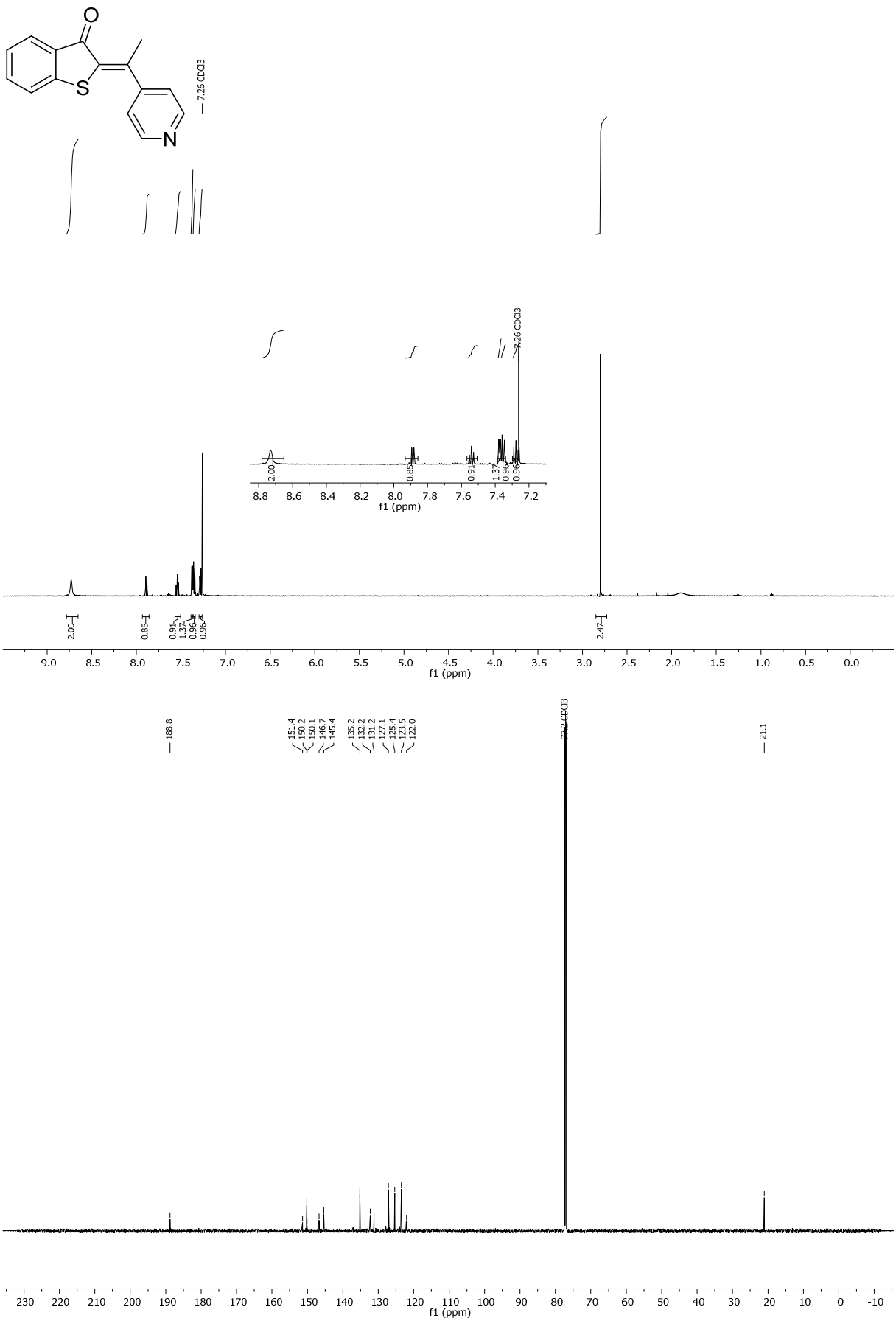

Figure 83: 600 MHz ^{1}H-NMR spectrum (top) and 150 MHz ^{13}C-NMR-spectrum (bottom) of (*Z*)-2-(1-(pyridin-4-yl)ethylidene)benzo[*b*]thiophen-3(2*H*)-one (**35**).

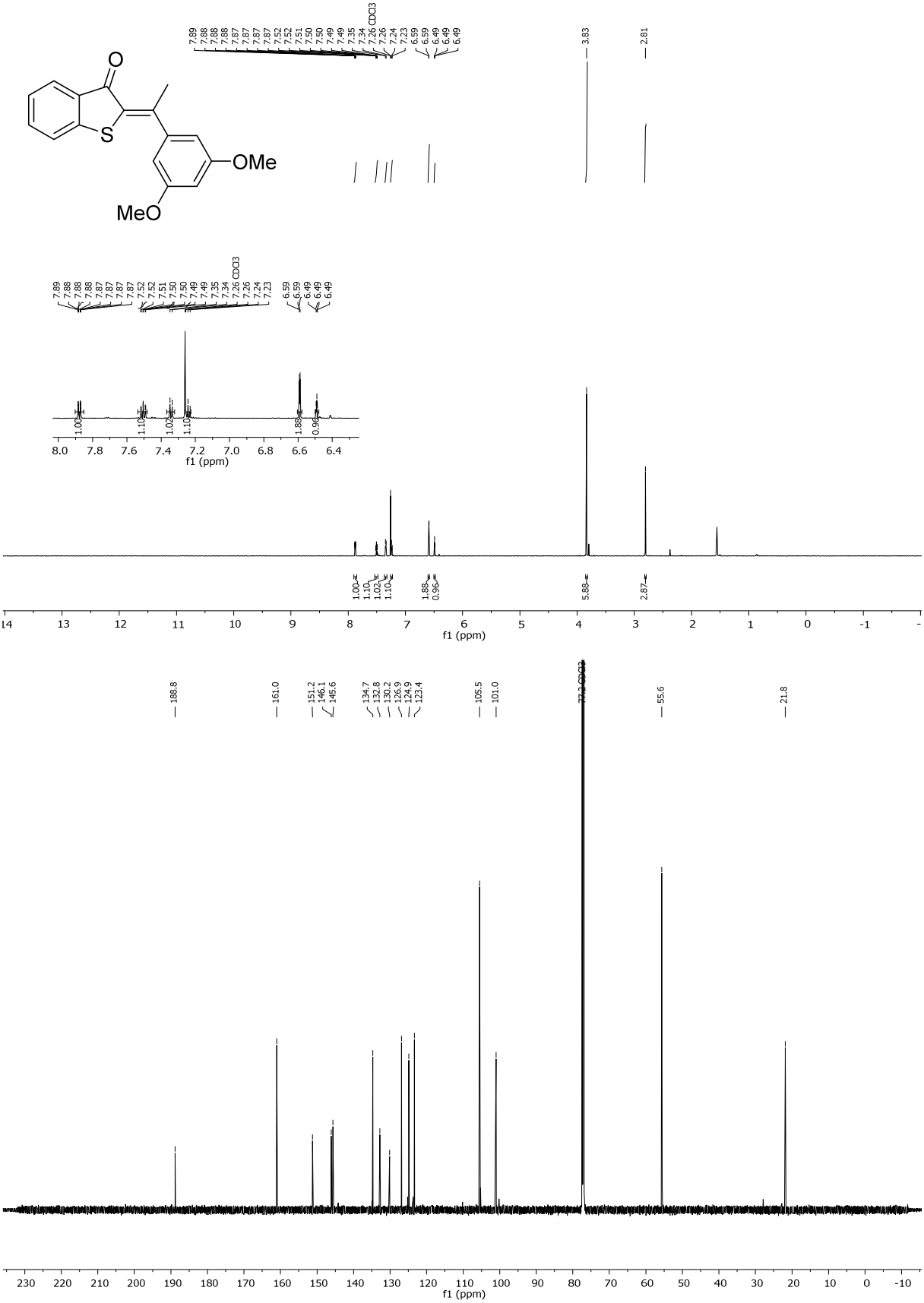

Figure 84: 600 MHz ^{1}H-NMR spectrum (top) and 150 MHz ^{13}C-NMR-spectrum (bottom) of (*Z*/*E*)-2-(1-(3,5-dimethoxyphenyl)ethylidene)benzo[*b*]thiophen-3(2*H*)-one (8 : 1) (**36**).

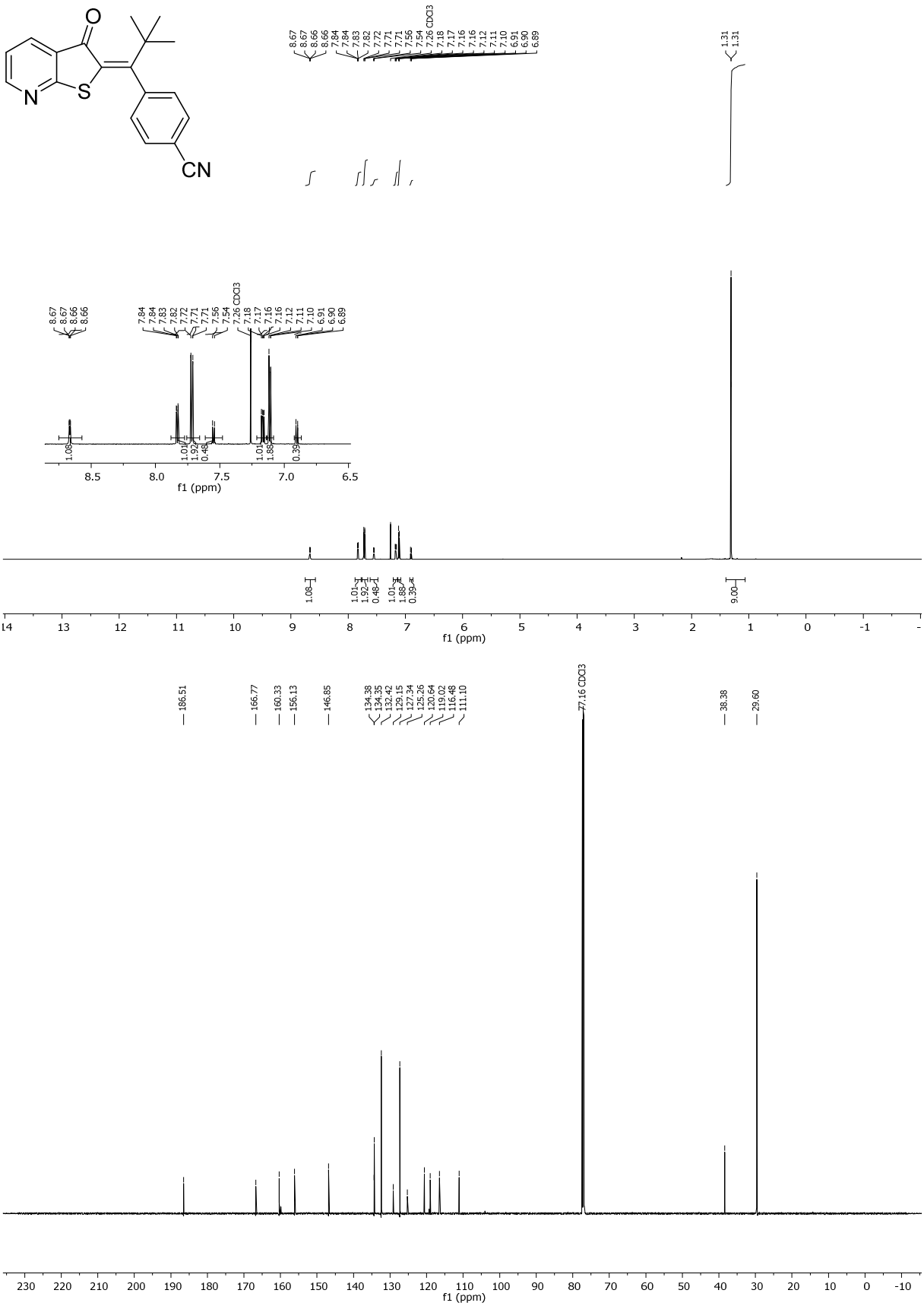

Figure 85: 600 MHz ^{1}H-NMR spectrum (top) and 150 MHz ^{13}C-NMR-spectrum (bottom) of (*Z*/*E*)-4-(2,2-dimethyl-1-(3-oxothieno[2,3-*b*]pyridin-2(3*H*)-ylidene)propyl)benzonitrile (1 : 3) (**37**).

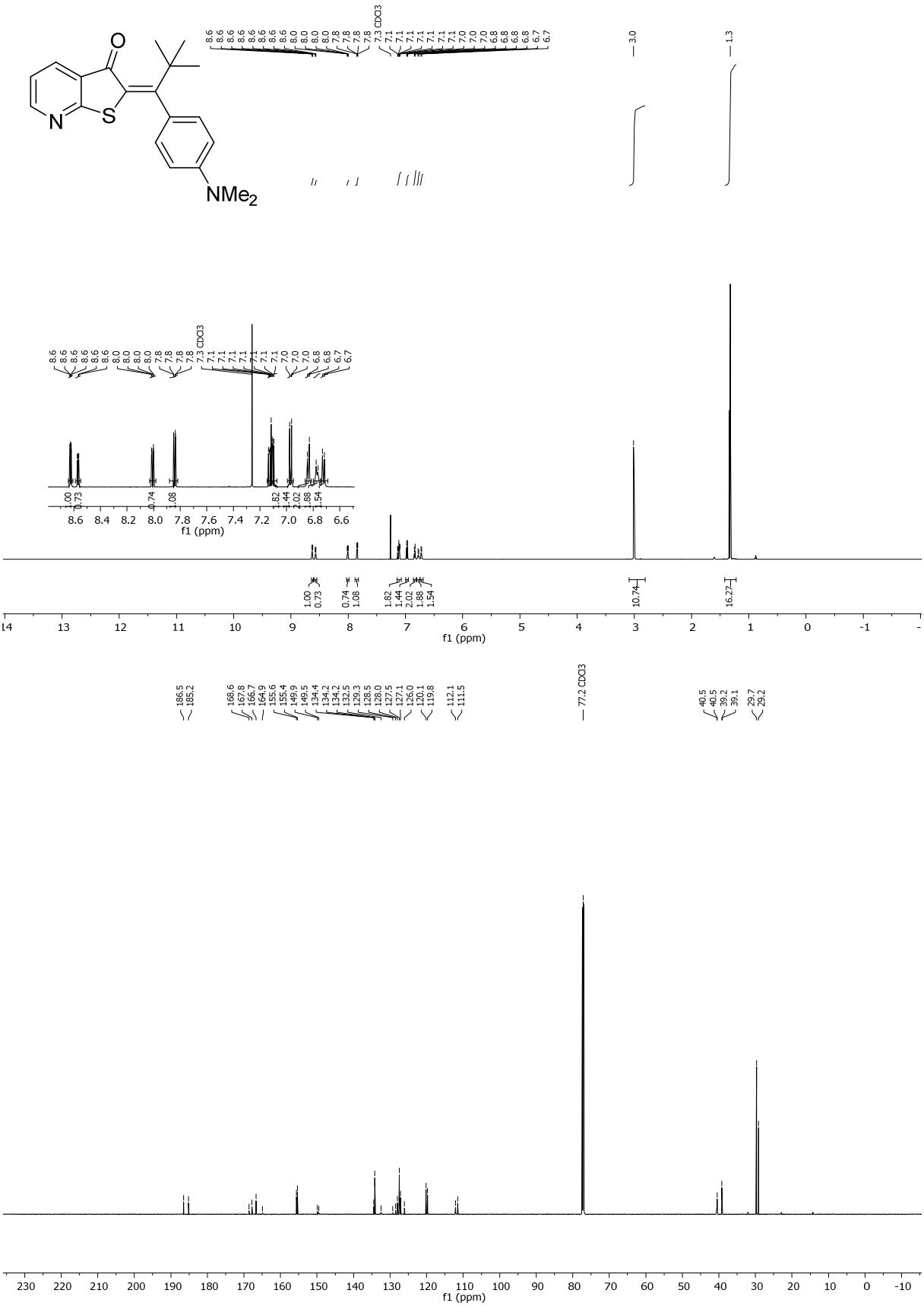

Figure 86: 600 MHz ^{1}H-NMR spectrum (top) and 150 MHz ^{13}C-NMR-spectrum (bottom) of (*Z*/*E*)-2-(1-(4-(dimethylamino)phenyl)-2,2-dimethylpropylidene)thieno[2,3-*b*]pyridin-3(2*H*)-one (1 : 1.5) (**38**).

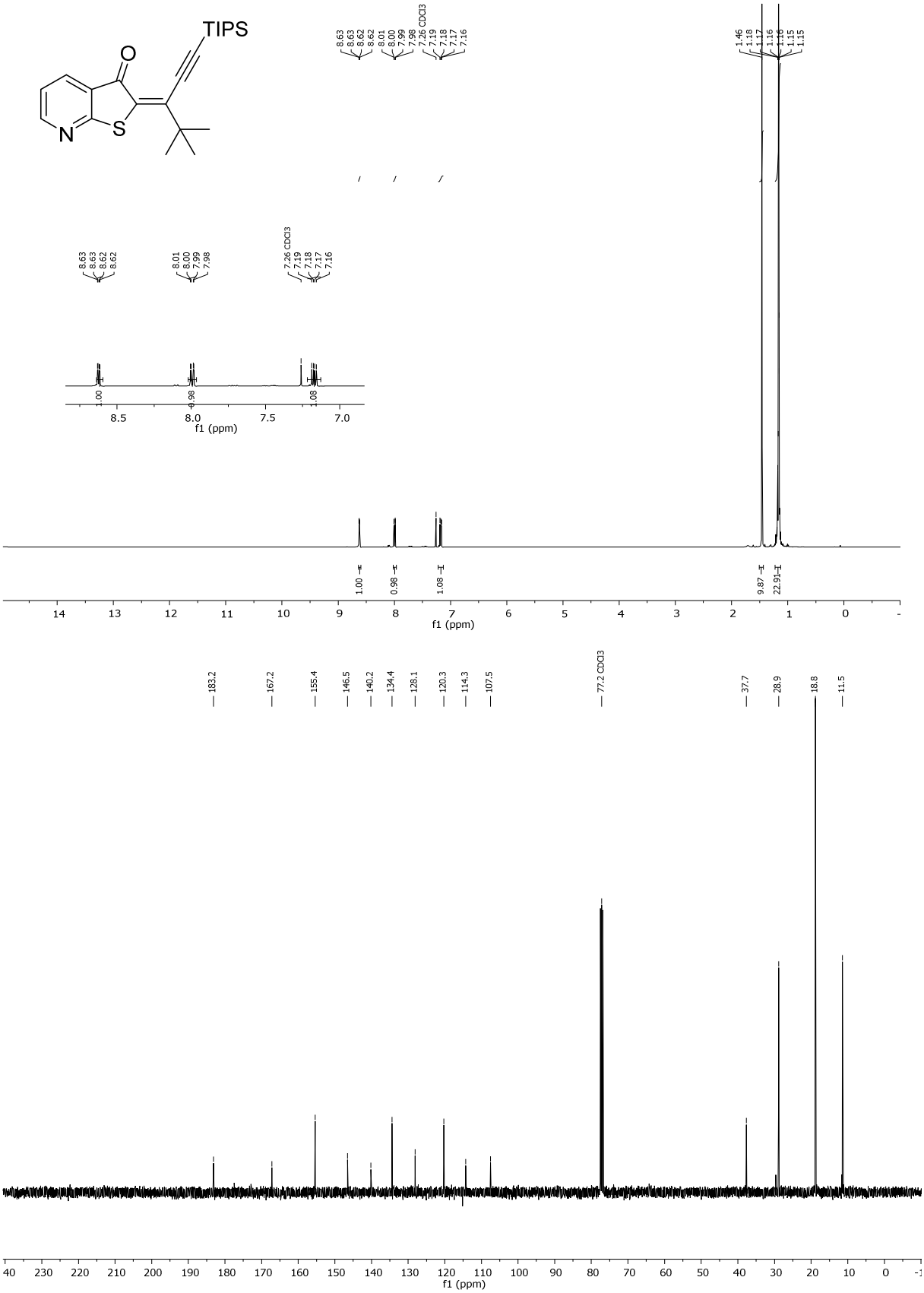

Figure 87: 400 MHz ^{1}H-NMR spectrum (top) and 100 MHz ^{13}C-NMR-spectrum (bottom) of (*E*)-2-(4,4-dimethyl-1-(triisopropylsilyl)pent-1-yn-3-ylidene)thieno[2,3-*b*]pyridin-3(2*H*)-one (**39**).

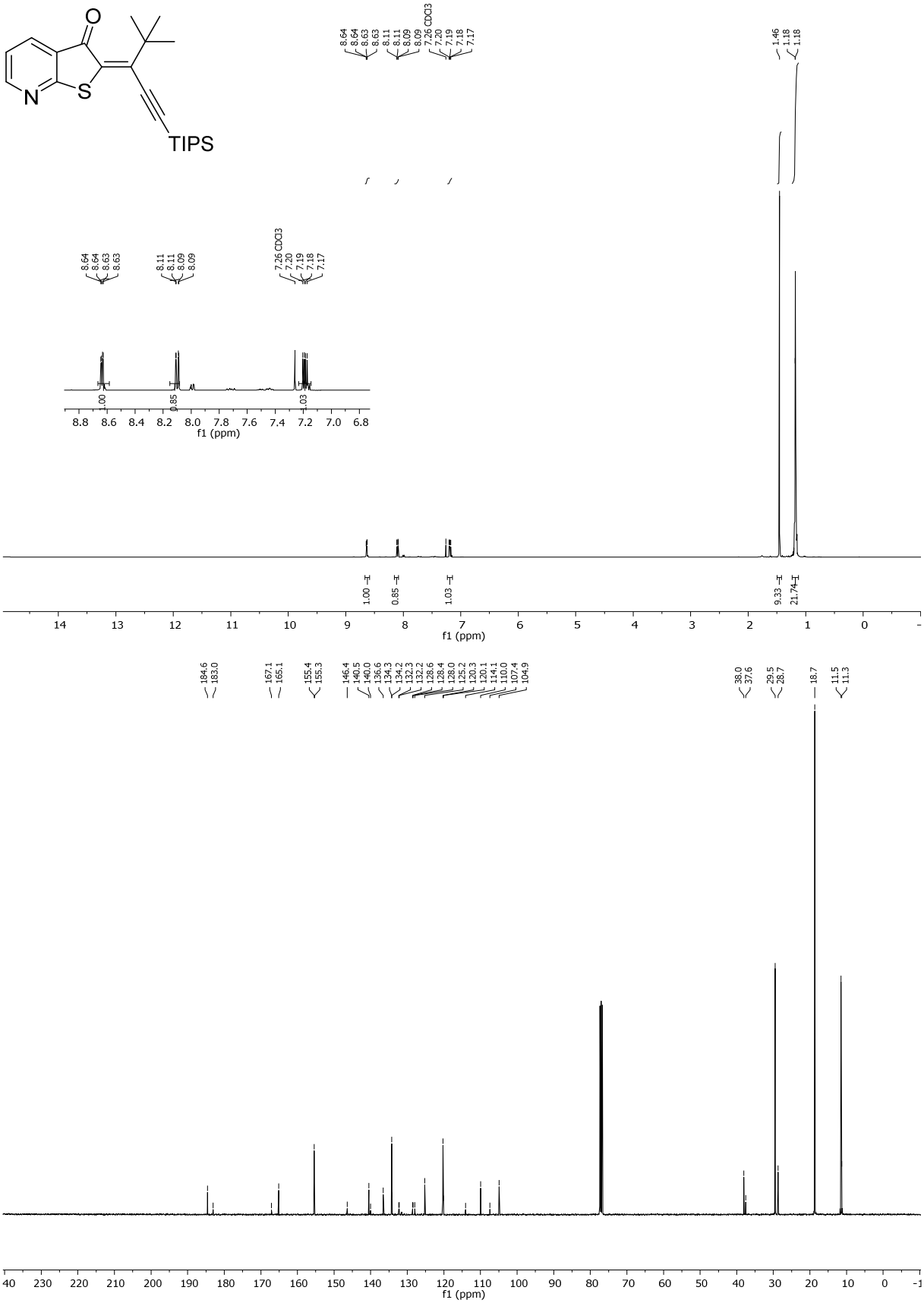

Figure 88: 400 MHz ^{1}H-NMR spectrum (top) and 100 MHz ^{13}C-NMR-spectrum (bottom) of (*E/Z*)-2-(4,4-dimethyl-1-(triisopropylsilyl)pent-1-yn-3-ylidene)thieno[2,3-*b*]pyridin-3(2*H*)-one (1 : 9) (**39**).

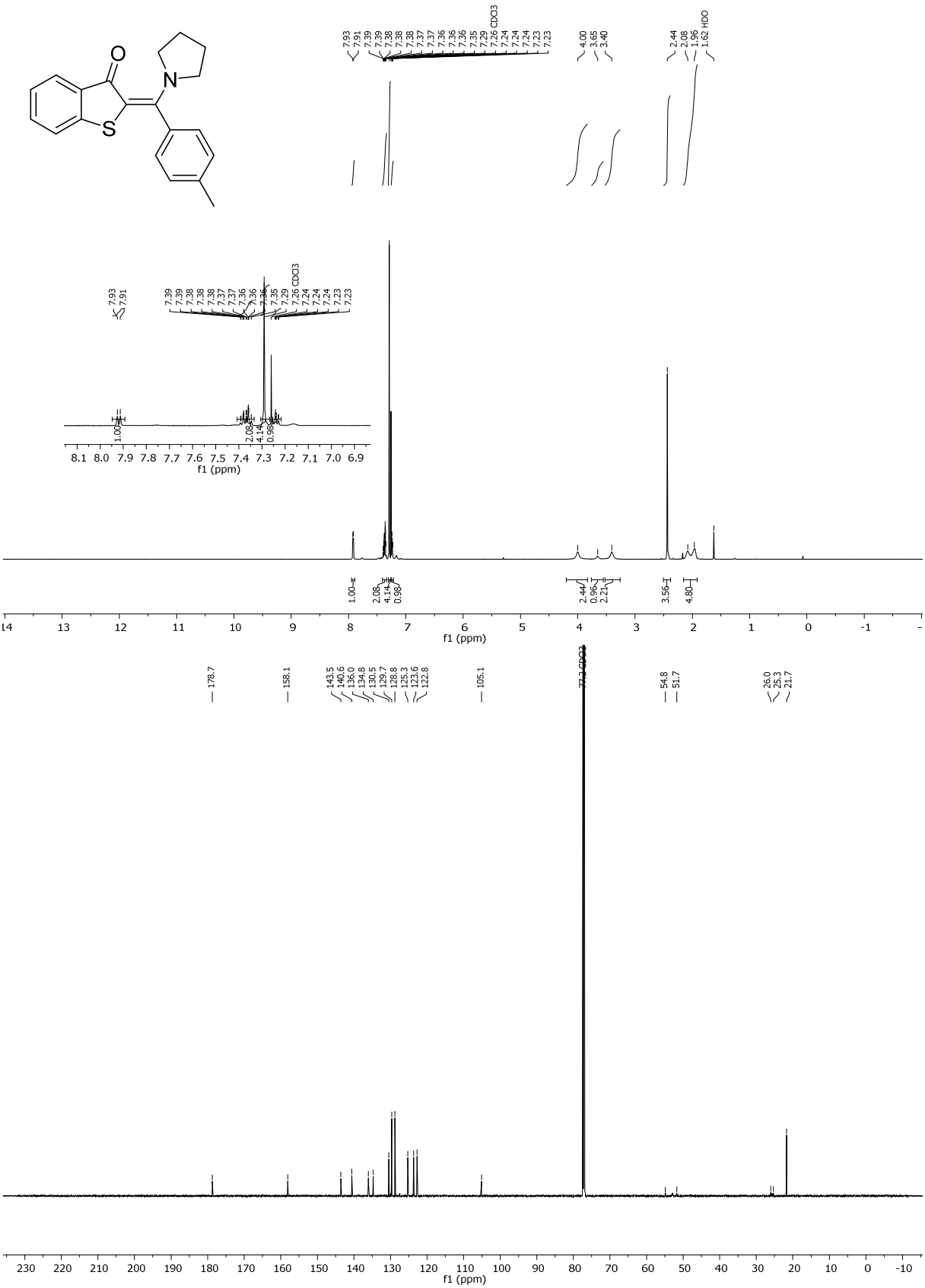

Figure 89: 600 MHz ^{1}H-NMR spectrum (top) and 150 MHz ^{13}C-NMR-spectrum (bottom) of (*E*/*Z*)-2-(pyrrolidin-1-yl(*p*-tolyl)methylene)benzo[*b*]thiophen-3(2*H*)-one (1 : 6) (**40**).

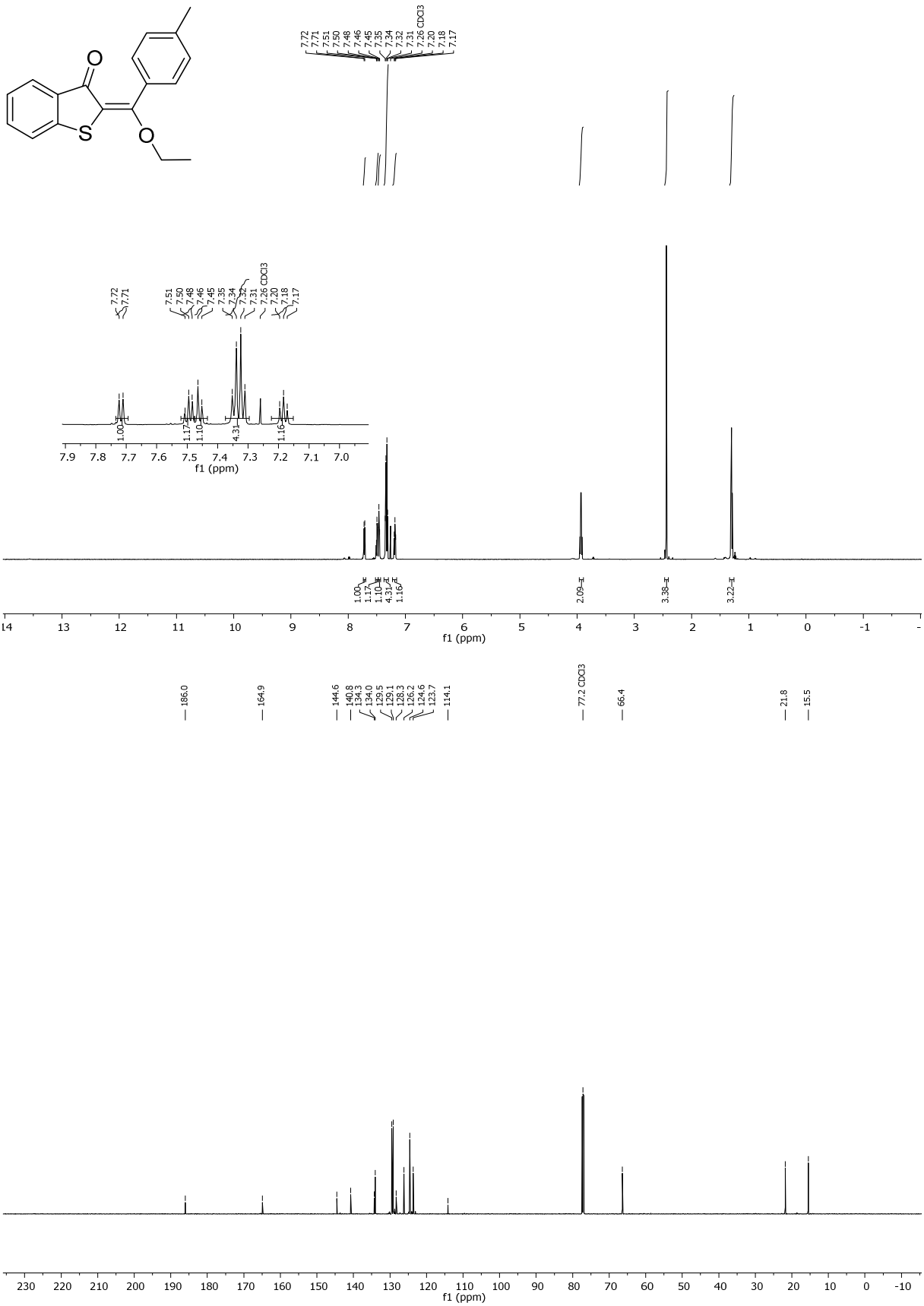

Figure 90: 600 MHz ^{1}H-NMR spectrum (top) and 150 MHz ^{13}C-NMR-spectrum (bottom) of (*Z*)-2-(ethoxy(*p*-tolyl)methylene)benzo[*b*]thiophen-3(2*H*)-one (**41**).

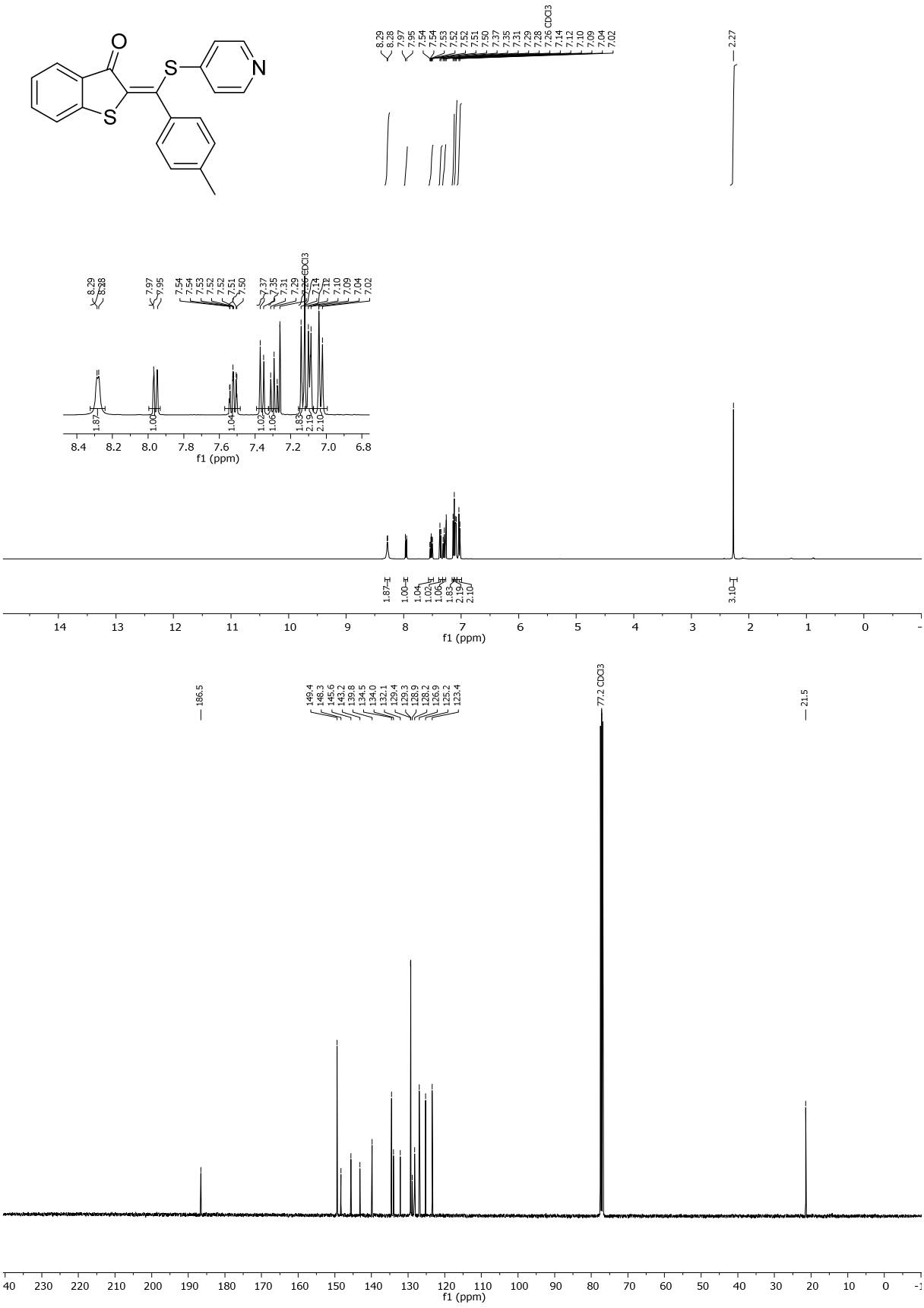

Figure 91: 400 MHz ^{1}H-NMR spectrum (top) and 100 MHz ^{13}C-NMR-spectrum (bottom) of (*E*)-2-((pyridin-4-ylthio)(*p*-tolyl)methylene)benzo[*b*]thiophen-3(2*H*)-one (**42**).

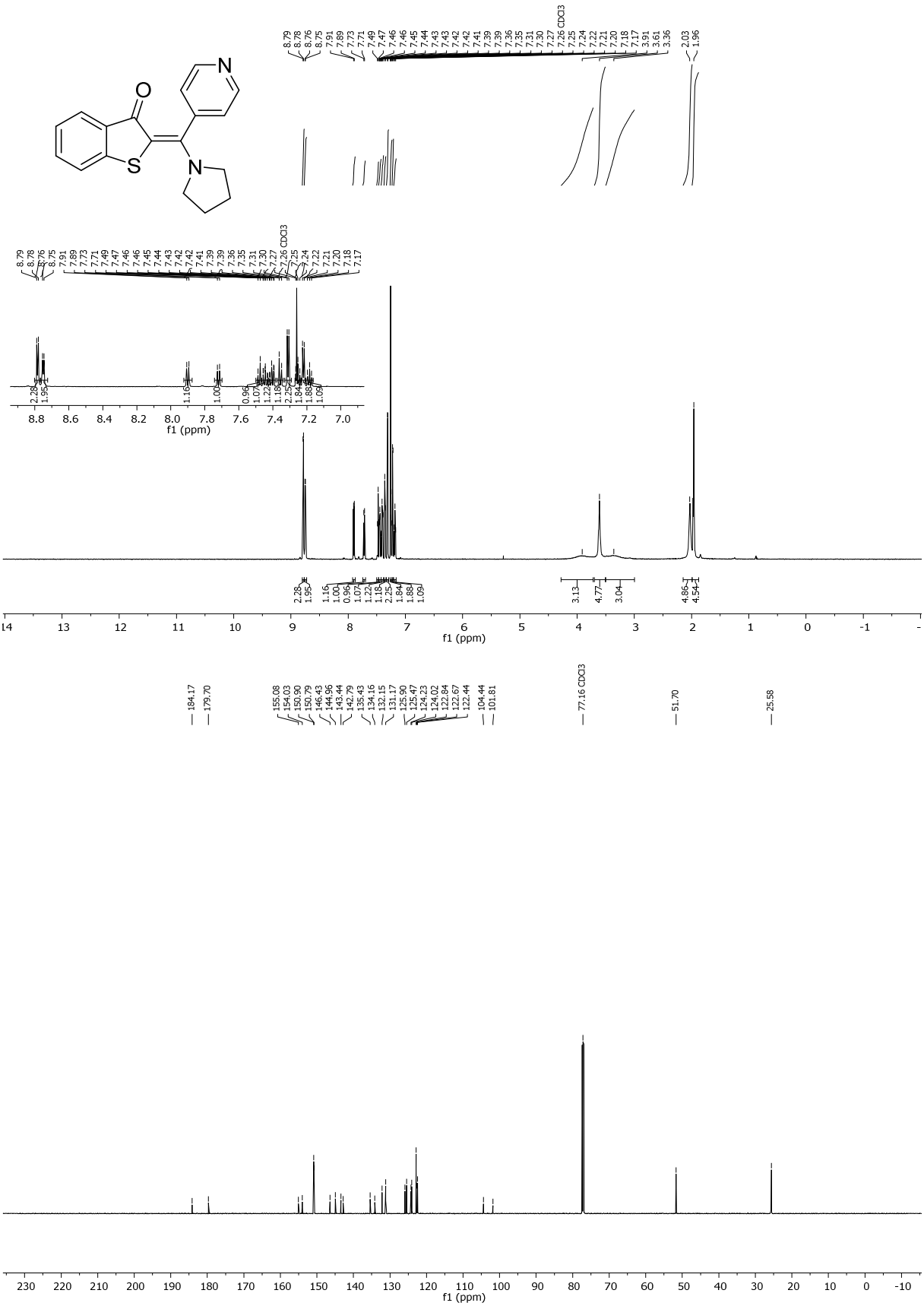

Figure 92: 400 MHz ^{1}H-NMR spectrum (top) and 100 MHz ^{13}C-NMR-spectrum (bottom) of (*E/Z*)-2-(pyridin-4-yl(pyrrolidin-1-yl)methylene)benzo[*b*]thiophen-3(2*H*)-one (1.2:1) (**43**).

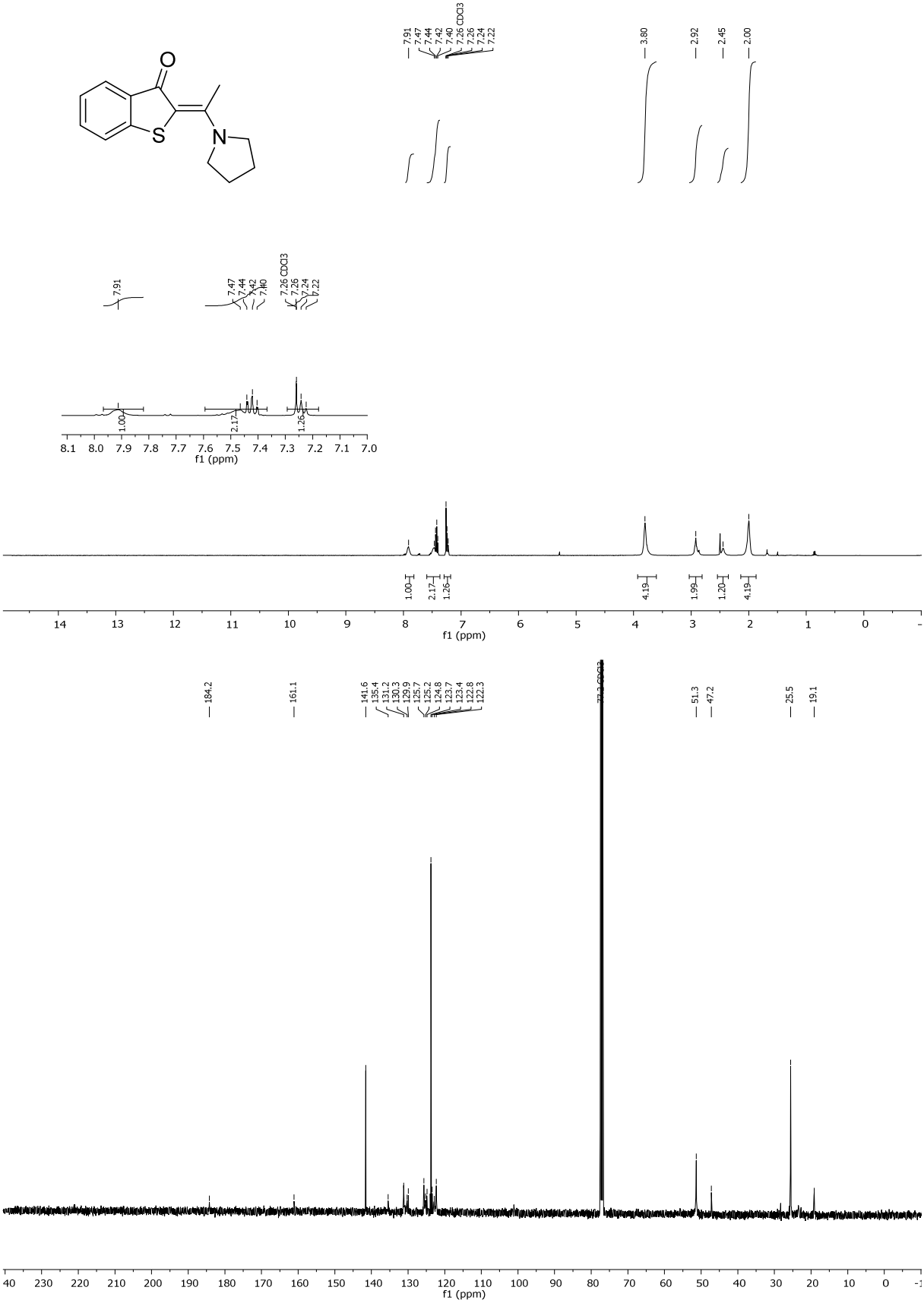

Figure 93: 400 MHz ^{1}H-NMR spectrum (top) and 100 MHz ^{13}C-NMR-spectrum (bottom) of (*E*/*Z*)-2-(1-(pyrrolidin-1-yl)ethylidene)benzo[*b*]thiophen-3(2*H*)-one (1:20) (**44**).

Crystal Structure Analysis

HTI	***Z*-10** CCDC 1586002	***E*-19** CCDC 1586003
net formula	$C_{13}H_{13}ClOS$	$C_{21}H_{20}O_3S$
M_r/g mol^{-1}	252.74	352.43
crystal size/mm	0.080 × 0.060 × 0.030	0.100 × 0.060 × 0.050
T/K	100.(2)	293.(2)
radiation	MoKα	MoKα
diffractometer	'Bruker D8 Venture TXS'	'Bruker D8 Venture TXS'
crystal system	monoclinic	orthorhombic
space group	'P 1 21/m 1'	'P b c a'
a/Å	8.1794(2)	14.6407(7)
b/Å	6.8622(2)	13.6465(5)
c/Å	11.0015(4)	18.1800(9)
α/°	90	90
β/°	105.9480(10)	90
γ/°	90	90
V/Å^3	593.73(3)	3632.3(3)
Z	2	8
calc. density/g cm^{-3}	1.414	1.289
μ/mm^{-1}	0.472	0.195
absorption correction	Multi-Scan	Multi-Scan
transmission factor range	0.9132–0.9705	0.9150–0.9705
refls. measured	7011	40063
R_{int}	0.0287	0.0613
mean σ(*I*)/*I*	0.0248	0.0246
θ range	3.539–26.351	3.158–25.348
observed refls.	1228	2690
x, *y* (weighting scheme)	0.0155, 0.4842	0.0458, 2.2455
hydrogen refinement	constr	constr
Flack parameter	0	-
refls in refinement	1311	3315
parameters	95	231
restraints	-	0
$R(F_{obs})$	0.0264	0.0506
$R_w(F^2)$	0.0649	0.1219
S	1.088	1.086
shift/error$_{max}$	0.001	0.001
max electron density/e Å^{-3}	0.419	0.259
min electron density/e Å^{-3}	−0.280	−0.332

HTI	*Z*-**19** CCDC 1586004	*E*-**29** CCDC 1586005
net formula	$C_{21}H_{20}O_3S$	$C_{21}H_{15}NOS$
M_r/g mol^{-1}	352.43	329.40
crystal size/mm	0.100 × 0.090 × 0.080	0.100 × 0.020 × 0.020
T/K	293.(2)	293.(2)
radiation	MoKα	MoKα
diffractometer	'Bruker D8 Venture TXS'	'Bruker D8 Venture TXS'
crystal system	monoclinic	monoclinic
space group	'P 1 21/n 1'	'P 1 21/c 1'
a/Å	6.0193(6)	8.8488(3)
b/Å	38.495(4)	18.4461(6)
c/Å	8.0246(6)	20.4155(8)
α/°	90	90
β/°	94.679(3)	92.5030(10)
γ/°	90	90
V/Å^3	1853.2(3)	3329.2(2)
Z	4	8
calc. density/g cm^{-3}	1.263	1.314
μ/mm^{-1}	0.191	0.201
absorption correction	Multi-Scan	Multi-Scan
transmission factor range	0.9047–0.9705	0.9087–0.9705
refls. measured	9312	26352
R_{int}	0.0223	0.0416
mean σ(*I*)/*I*	0.0271	0.0333
θ range	3.175–25.349	3.181–25.027
observed refls.	2890	4172
x, *y* (weighting scheme)	0.0444, 0.7167	0.0760, 2.7006
hydrogen refinement	constr	constr
Flack parameter	-	-
refls in refinement	3379	5856
parameters	230	435
restraints	0	0
$R(F_{obs})$	0.0453	0.0569
$R_w(F^2)$	0.1143	0.1711
S	1.112	1.022
shift/error$_{max}$	0.001	0.002
max electron density/e Å^{-3}	0.183	1.045
min electron density/e Å^{-3}	−0.220	−0.378

HTI	*E*-**33** CCDC 1586006	*E*-**37** CCDC 1586007
net formula	$C_{22}H_{18}N_2OS$	$C_{19}H_{16}N_2OS$
M_r/g mol^{-1}	358.44	320.40
crystal size/mm	0.070 × 0.040 × 0.030	0.070 × 0.050 × 0.040
T/K	103.(2)	293.(2)
radiation	MoKα	MoKα
diffractometer	'Bruker D8 Venture TXS'	'Bruker D8 Venture TXS'
crystal system	monoclinic	monoclinic
space group	'P 1 21/c 1'	'P 1 21/c 1'
a/Å	12.0501(6)	16.9913(18)
b/Å	15.3570(7)	10.1443(11)
c/Å	9.7770(4)	9.5628(9)
α/°	90	90
β/°	100.2150(10)	92.085(3)
γ/°	90	90
V/Å^3	1780.59(14)	1647.2(3)
Z	4	4
calc. density/g cm^{-3}	1.337	1.292
μ/mm^{-1}	0.195	0.202
absorption correction	Multi-Scan	Multi-Scan
transmission factor range	0.9289–0.9705	0.93–0.99
refls. measured	22787	20899
R_{int}	0.0315	0.0409
mean σ(*I*)/*I*	0.0209	0.0265
θ range	3.161–26.371	3.129–26.400
observed refls.	3252	2726
x, *y* (weighting scheme)	0.0346, 1.2316	0.0343, 0.8169
hydrogen refinement	constr	constr
Flack parameter	-	-
refls in refinement	3621	3340
parameters	237	211
restraints	0	0
$R(F_{obs})$	0.0327	0.0380
$R_w(F^2)$	0.0844	0.0986
S	1.026	1.042
shift/error$_{max}$	0.001	0.001
max electron density/e Å^{-3}	0.293	0.211
min electron density/e Å^{-3}	−0.314	−0.216

HTI	***E*-40** CCDC 1586008	***E*-42** CCDC 1586009
net formula	$C_{20}H_{19}NOS$	$C_{21}H_{15}NOS_2$
M_r/g mol^{-1}	321.42	361.46
crystal size/mm	0.090 × 0.030 × 0.030	0.070 × 0.050 × 0.030
T/K	103.(2)	103.(2)
radiation	MoKα	MoKα
diffractometer	'Bruker D8 Venture TXS'	'Bruker D8 Venture TXS'
crystal system	monoclinic	triclinic
space group	'P 1 21/c 1'	'P -1'
a/Å	7.9580(4)	7.8529(3)
b/Å	20.4688(10)	9.8991(4)
c/Å	9.8123(4)	12.2197(5)
α/°	90	66.2530(10)
β/°	90.942(2)	88.0560(10)
γ/°	90	88.3490(10)
V/Å^3	1598.12(13)	868.87(6)
Z	4	2
calc. density/g cm^{-3}	1.336	1.382
μ/mm^{-1}	0.207	0.315
absorption correction	Multi-Scan	Multi-Scan
transmission factor range	0.9043–0.9705	0.9227–0.9705
refls. measured	13502	16474
R_{int}	0.0400	0.0274
mean σ(I)/I	0.0341	0.0234
θ range	3.243–26.369	3.135–27.103
observed refls.	2722	3358
x, y (weighting scheme)	0.0228, 1.1372	0.0263, 0.5858
hydrogen refinement	constr	constr
Flack parameter	-	-
refls in refinement	3231	3823
parameters	209	227
restraints	0	0
$R(F_{obs})$	0.0369	0.0295
$R_w(F^2)$	0.0821	0.0753
S	1.060	1.048
shift/error$_{max}$	0.001	0.001
max electron density/e Å^{-3}	0.256	0.327
min electron density/e Å^{-3}	−0.254	−0.246

HTI	***Z*-44** CCDC 1586010
net formula	$C_{14}H_{15}NOS$
M_r/g mol^{-1}	245.33
crystal size/mm	0.050 × 0.040 × 0.030
T/K	103.(2)
radiation	MoKα
diffractometer	'Bruker D8 Venture TXS'
crystal system	orthorhombic
space group	'P b c a'
a/Å	7.1678(3)
b/Å	13.8297(5)
c/Å	23.6682(9)
α/°	90
β/°	90
γ/°	90
V/Å^3	2346.19(16)
Z	8
calc. density/g cm^{-3}	1.389
μ/mm^{-1}	0.257
absorption correction	Multi-Scan
transmission factor range	0.8975–0.9705
refls. measured	14685
R_{int}	0.0382
mean σ(*I*)/*I*	0.0236
θ range	3.315–26.368
observed refls.	2007
x, *y* (weighting scheme)	0.0301, 1.6391
hydrogen refinement	constr
Flack parameter	-
refls in refinement	2394
parameters	155
restraints	0
$R(F_{obs})$	0.0297
$R_w(F^2)$	0.0796
S	1.060
shift/error$_{max}$	0.001
max electron density/e Å^{-3}	0.278
min electron density/e Å^{-3}	−0.222

References

1. Chan, S. L.-F.; Low, K.-H.; Yang, C.; Cheung, S. H.-F.; Che, C.-M., Iron-Ligand Coordination in Tandem Radical Cyclizations: Synthesis of Benzo[b]thiophenes by a One-pot Reaction of Iron 1,3-Diketone Complexes with 2-Thiosalicylic Acids. *Chem. - Eur. J.* **2011,** *17*, 4709-4714, S4709/1-S4709/12.
2. Molander, G. A.; Canturk, B.; Kennedy, L. E., Scope of the Suzuki-Miyaura Cross-Coupling Reactions of Potassium Heteroaryltrifluoroborates. *J. Org. Chem.* **2009,** *74*, 973-980.
3. Molander, G. A.; Trice, S. L. J.; Kennedy, S. M.; Dreher, S. D.; Tudge, M. T., Scope of the Palladium-Catalyzed Aryl Borylation Utilizing Bis-Boronic Acid. *J. Am. Chem. Soc.* **2012,** *134*, 11667-11673.
4. Moinet, G.; Leriche, C.; Kergoat, M. Preparation of benzofuran and benzothiophene derivatives as antidiabetic agents. FR2862646A1, 2005.

5. Direct evidence for Hula-Twist and single-bond rotation photoproducts

As presented in the introduction, the Hula-Twist (HT) photoreaction was discussed for various naturally occurring photoswitches as a possible photoswitching mechanism. However, the existence of this photoreaction could never be unambiguously proven, as the energy barriers for thermal follow-up isomerization reactions that lead to exchange of the HT to the double-bond isomerization (DBI) product are generally very low and the primary photoproduct could therefore not be evidenced unambiguously. Also, photochemical single-bond isomerizations were discussed as photoreactions but are not used in photoswitches to obtain different states. By the above presented synthesis, it was possible to obtain sterically overcrowded HTI photoswitches bearing a chiral stilbene part resulting in stable atropisomers at ambient temperatures. By introducing a chiral sulfoxide, the atropisomers were distinguishable as diastereomers allowing their individual observation by NMR spectroscopy. All four states could be separated and crystallized individually enabling unambiguous structural proof. Afterwards, the photochemistry of each isomer could be investigated individually revealing the existence of the Hula-Twist photoreaction as well as the photochemical single-bond rotation. Furthermore, the preference for the specific photoreactions could be controlled by changing the temperature, the polarity, and the viscosity of the surrounding medium.

License

nature COMMUNICATIONS

ARTICLE

DOI: 10.1038/s41467-018-04928-9 OPEN

Direct evidence for hula twist and single-bond rotation photoproducts

Aaron Gerwien[1], Monika Schildhauer[1], Stefan Thumser[1], Peter Mayer[1] & Henry Dube[1]

Photoisomerization reactions are quintessential processes driving molecular machines and motors, govern smart materials, catalytic processes, and photopharmacology, and lie at the heart of vision, phototaxis, or vitamin production. Despite this plethora of applications fundamental photoisomerization mechanisms are not well understood at present. The famous hula-twist motion—a coupled single and double-bond rotation—was proposed to explain proficient photoswitching in restricted environments but fast thermal follow-up reactions hamper identification of primary photo products. Herein we describe an asymmetric chromophore possessing four geometrically distinct diastereomeric states that do not interconvert thermally and can be crystallized separately. Employing this molecular setup direct and unequivocal evidence for the hula-twist photoreaction and for photoinduced single-bond rotation is obtained. The influences of the surrounding medium and temperature are quantified and used to favor unusual photoreactions. Based on our findings molecular engineers will be able to implement photo control of complex molecular motions more consciously.

[1] Department of Chemistry, Ludwig-Maximilians-Universität München and Munich Center for Integrated Protein Science CIPSM, Butenandtstrasse 5-13, 81377 München, Germany. Correspondence and requests for materials should be addressed to H.D. (email: henry.dube@cup.uni-muenchen.de)

Light-induced motions of molecules play a fundamental role for sensing and responsiveness in nature and have become similarly important in the construction of artificial nanoscale machinery[1], molecular motors[2–6], smart materials[7–11], or photopharmacophores[12,13]. In crucial cases however, the geometrical changes induced by light irradiation are not known and even the most fundamental photoreaction mechanisms are still under dispute[14–23]. This uncertainty not only hampers the conscious and rational design of synthetic systems with predictable responsive functions but at the same time prevents mechanistic and atomistic understanding of central photochemical processes in living systems.

One central problem concerns the photoisomerization of carbon–carbon double bonds with adjacent carbon–carbon single bonds (Fig. 1a)—a configuration that is found in the vast class of polyenes[24], styrenes, and stilbene dye compounds[18,25–27], and in the biological most relevant retinal[28,29], *p*-coumaric acid[16,30,31], previtamine D_3[17,19,20], or GFP chromophores[32,33]. For this bonding situation the photoreaction has essentially been described as either a sole double-bond isomerization (DBI)[17,34], a combination of double bond and single-bond rotations i.e., the famous hula twist (HT) initially proposed by Liu[18,19,25,35–38], or in extended conjugated systems as bipedal motions as proposed by Warshel[21,22] and later experimentally shown by Saltiel[39–41]. Additionally, sole single-bond rotations (SBR) are also described as viable photoreactions[42–45]. The main problem to differentiate between these mechanisms is the short lived nature of primary products of the photoreaction, which are high-energy intermediates undergoing rapid thermal conversion to more stable structures in solution (Fig. 1a). Due to their fleeting character an unambiguous assignment of their molecular and electronic structure has not been possible so far, as time resolved methods[14–16,28,31,46,47] or isolation of these intermediates under extremely cold[17,19,20] or rigid-medium conditions[25,39,48,49] provide still too little direct structural information. In rigid matrices (i.e., solvent glasses) and at very low temperatures intermediates have frequently been observed with absorption or fluorescence spectroscopy but the assignment of similar spectra to a particular isomeric structure is not straight forward. Consequently, Saltiel and co-workers have recently refuted earlier claims of HT evidences and identified the intermediate photoproducts as the result of simple DBIs[17,50,51]. The question whether a possible HT mechanism is an intrinsic property of the molecule itself[18] or on the contrary is dictated mainly by outside restrictions[52,53] (e.g., imposing volume conservation[16,54] during the motion) is even less resolved.

To overcome this dilemma we have designed a geometrically strongly restricted asymmetric molecule **1** (Fig. 1b), which can assume only four stable diastereomeric states in the ground state (Fig. 2a). Different to the systems studied so far the barriers for thermal interconversion between the intermediate states are very high, which effectively decouples geometry changes during the photoreaction from thermal processes. With this molecular setup it is possible to track the formed photoproducts at ambient temperatures in solution directly and without interference of thermal follow-up reactions. After studying the photochemistry of **1** we provide direct experimental evidence for the presence of photoinduced HT, SBR, as well as the well-known sole DBI products. We are now able to isolate all these different photoproducts at ambient conditions and characterize them with high resolution techniques (NMR spectroscopy and crystal structural analysis). At the same time we are able to conveniently study the influences of polarity and rigidity of the surrounding medium, as well as temperature and give insights into how they affect the outcome of the photoreactions. Our findings give quantitative (photoquantum yields ϕ for each process) insights into the nature of photoinduced intramolecular motions, establish the exact influences of the surrounding medium, and clarify that light-induced HT, as well as SBR are viable and prominent photoreactions. We further give prospects of how these complex motions can be used for advanced photoresponsive tools and molecular machinery.

Results

Ground state energy profile of 1. Photoresponsive compound **1** is based on the hemithioindigo (HTI) chromophore[55–57] and was synthesized according to a protocol previously developed in our group[58]. HTI **1** is rendered asymmetric via the introduction of a sulfoxide stereocenter and an adjacent chiral axis. This molecule can therefore exist in four geometrically and energetically different ground states, which we term **A**, **B**, **C**, and **D**. The stereo assignments of these states are given in Fig. 2a. We have obtained exact molecular structures from the crystalline state (Fig. 2b) for each isomer **A**, **B**, **C**, and **D** and could therefore unambiguously assign the corresponding high-resolution ^{1}H NMR solution spectra to a particular geometry in each case (see Supplementary Figs. 1–4). **A** and **B** share the same *Z* configuration of the double bond but possess opposite axial chirality. Likewise **C** and **D** are atropisomers of each other in the *E* isomeric state. The atropisomers are thermally very stable, which is manifested in their extremely long solution half-lives of at least 1.7 years at 27 °C (see Fig. 2c, d for the kinetic measurements of their interconversion at >80 °C, see also Supplementary Figs. 5–8 and Supplementary

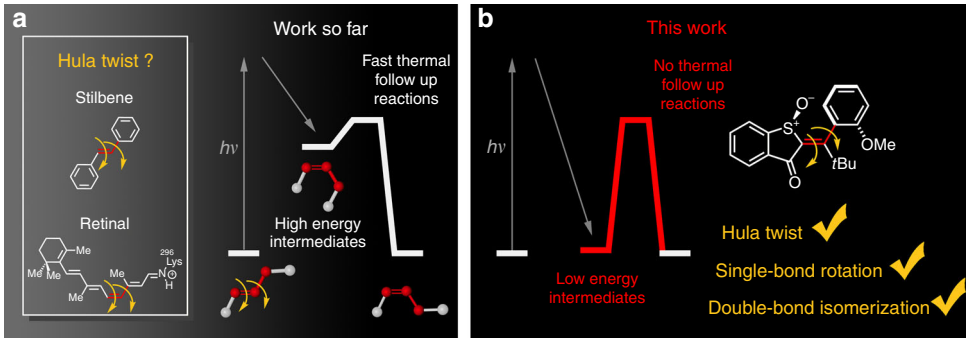

Fig. 1 Complex light-induced motions in chromophores. **a** Proposed hula-twist (HT) motion for the photoisomerization of stilbene dyes or retinal in rhodopsin. Population of high-energy intermediates after the photoreaction leads to fast thermal decay and hampers a precise elucidation of their structural and electronic properties. **b** Chromophore **1** possesses only four possible, thermally highly stable, and geometrically distinct intermediate states and therefore enables unambiguous assignment of the photoproducts at ambient conditions. Three different geometrical changes could directly be observed as photoreactions: hula twist (HT), single-bond rotation (SBR), and double-bond isomerization (DBI)

Table 1). The thermal double bond rotation was not observed for any of the four isomers even after prolonged heating at 100 °C for 25 h, which gives a lower limit for the corresponding barrier to be at least 30 kcal/mol high (Fig. 2e, see also Supplementary Fig. 9 and Supplementary Table 1).

Photochemistry of 1. The established high barriers for thermal interconversion render the individual isomers **A**, **B**, **C**, and **D** completely stable at ambient temperatures. It is therefore possible to study their photochemistry individually and without the complication of an intervening fast thermal decay after the photoreaction (for molar absorption coefficients see Supplementary Figs. 10–13). To this end we have irradiated solutions of either pure **A**, **B**, **C**, or **D** in benzene-d_6 at 23 °C while counting the number of photons that led to photoproducts. This experiment established quantum yields (ϕ) for every photoconversion individually (Fig. 3a, see also Supplementary Figs. 14–18 and Supplementary Table 2). In a second independent experiment, the changes in isomer composition of the solution were measured for different time points during prolonged irradiation at 27 °C. To disentangle the different photo processes at later stages of the irradiation wholesome simulations of the different photokinetics of **A**, **B**, **C**, and **D** were conducted (Fig. 3b, c, see also Supplementary Figs. 19–43). As we kept the irradiation conditions constant in all experiments these latter kinetic measurements could be used to obtain relative probabilities for the individual photo-transformations (see Supplementary Fig. 44 and Supplementary Table 2). Fitting the experimental data to a Markov-matrix derived kinetic model provided excellent agreement between measured quantum yield ratios and the kinetic experiments. For a further assignment of the photoproducts' identities the starting points of the photoconversions were examined more closely (Fig. 3d–g). At this time point the concentration of the different photoproducts is low enough to prevent them from light absorption in the presence of a far higher concentration of the starting material. As the photoconversions progress photoproducts are accumulating and enter their respective photoequilibria as well. All three approaches, determination of quantum yields for individual phototransformations in benzene, fitting kinetic data of the whole photoconversion process to a kinetic model, and independent identification of the photoproducts at early stages of the irradiation provided the same conclusions.

As shown in Fig. 3 each isomer **A**, **B**, **C**, or **D** converts directly into more than one photoproduct after irradiation. The efficiencies of these transformations differ dramatically but it is

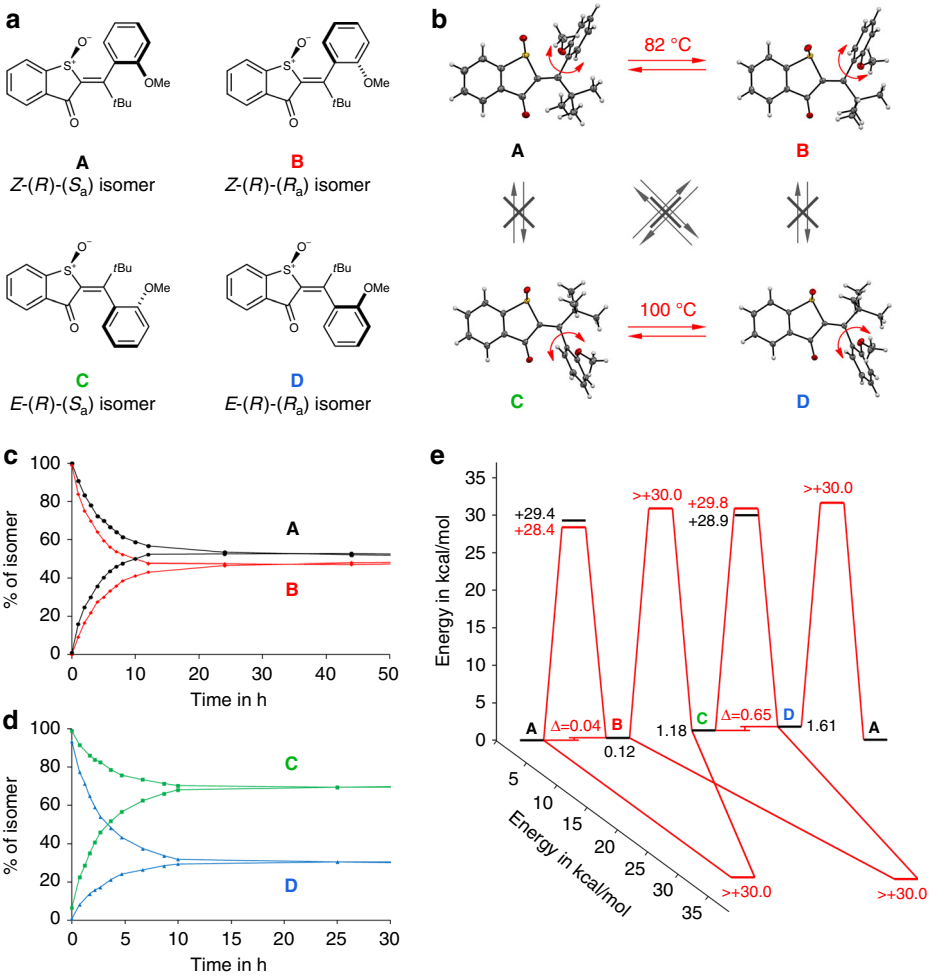

Fig. 2 Ground state energy profile of HTI **1**. **a** Molecular geometries of the four stable isomeric states **A** to **D** of **1**. **b** Molecular structures of all four isomers of **1** obtained from crystal structural analysis and their slow thermal interconversions at high temperature (>80 °C). **c** Experimental first order kinetics for thermal interconversion of atropisomers **A** and **B** (82 °C) in $(CDCl_2)_2$ solution. **d** Experimental first order kinetics for thermal interconversion of atropisomers **C** and **D** (100 °C) in $(CDCl_2)_2$ solution. No thermal DBI occurs at elevated temperatures. The interconversion was quantified using ^{1}H NMR spectroscopy. **e** Ground-state energy profile for **1**. Thermal conversion between the four different isomers at ambient temperature is prevented by very high kinetic barriers. Values in black are derived from quantum chemical calculations (B3LYP/6-311 G(d,p), PCM(DCM)), values in red were determined experimentally

clearly evident that very different types of motions are generated by light irradiation of different isomers.

Irradiation of **A** at 405 nm in benzene-d_6 at 27 °C leads to three photoproducts with **B** and **C** being the main products formed in $\phi = 9\%$ and 31%, respectively (Fig. 3a). Isomer **D** is formed with only 0.8% quantum yield and thus represents a minor channel of the photoreaction. Irradiation of **B** leads to **C** ($\phi = 8\%$) and **D** ($\phi = 9\%$) in almost the same efficiencies while formation of **A** presents just a minor channel ($\phi = 0.9\%$). The photoreactions of **C** and **D** are much less effective in comparison but are also branching in each case. Irradiation of **C** leads to inefficient transformation to **A** ($\phi = 0.09\%$), **B** ($\phi = 0.1\%$), and **D** ($\phi = 0.07\%$). Photoconversion of **D** leads to slow population of **A** ($\phi = 0.3\%$), **B** ($\phi = 0.06\%$), and **C** ($\phi = 0.01\%$).

With these measurements we could unambiguously show that all three possibilities of light-induced bond rotations are actually realized in **1**. The simple DBI is most prominent in the light-induced transition of **A** to **C**. Highly efficient is also the hitherto elusive HT, which couples double bond and SBRs, as seen by the transformation of **B** to **C**. Interestingly the HT for **B** is almost as efficient as the DBI from **B** to **D**. For isomer **D** the HT leading to **A** is actually the most prominent pathway. A sole SBR could also directly be demonstrated as dominant photoreaction—exemplified by the prolific photoconversion of atropisomer **A** into **B**. With the term HT we emphasize the causal connection of double and SBRs occurring after photoexcitation. This does however not mean that both motions must occur in a concerted way as originally proposed by Liu and Hammond[52]. A sequential motion as proposed by Saltiel[52] is also a possibility as discussed below in the Discussion section.

Medium and temperature effects on the photoreactions of 1. After quantifying the different photoconversion pathways between **A**, **B**, **C**, and **D** in benzene-d_6 solution the influences of the surrounding medium were of primary interest. With the experiments described above it became already clear that even in a nonrestrictive solution environment there is an intrinsic propensity to undergo coupled motions as opposed to just simple DBI after photoexcitation of **1**. With the term coupled motions we again emphasize the causal connection of double and single-bond rotations occurring after photoexcitation without specific mechanistic implications. As different motions appear concomitantly after photoexcitation of **1** it is of utmost importance to understand the influence of the surrounding environment on a particular motion. Only then these motions can be used in a conscious way for advanced functions such as complex light driven molecular machinery or smart nanosystems. In the following we present possible ways in which such selectivity for particular motions via the surrounding medium can be achieved. We focus on the light-induced motions of **A** and **B** (Fig. 4a) since they display the most efficient photoreactions and experimental errors are therefore very small.

Photoirradiation of **A** in benzene-d_6 solution results mainly in DBI to **C** and SBR to **B**. The relative ratio of these processes is roughly 80%:20% (Fig. 4a). Increasing the polarity of the solvent changes this ratio to a value of 60%:40% in MeOH-d_4, thus enhancing the SBR considerably (Fig. 4b). If the polarity of the solvent is kept constant but the viscosity is increased drastically (MeOH-d_4 to ethylene glycol (EG)) the DBI is becoming more pronounced again and a decrease of the SBR is observed. The inefficient HT motion from **A** to **D** is increased slightly at high viscosity conditions (see also Supplementary Figs. 19–44).

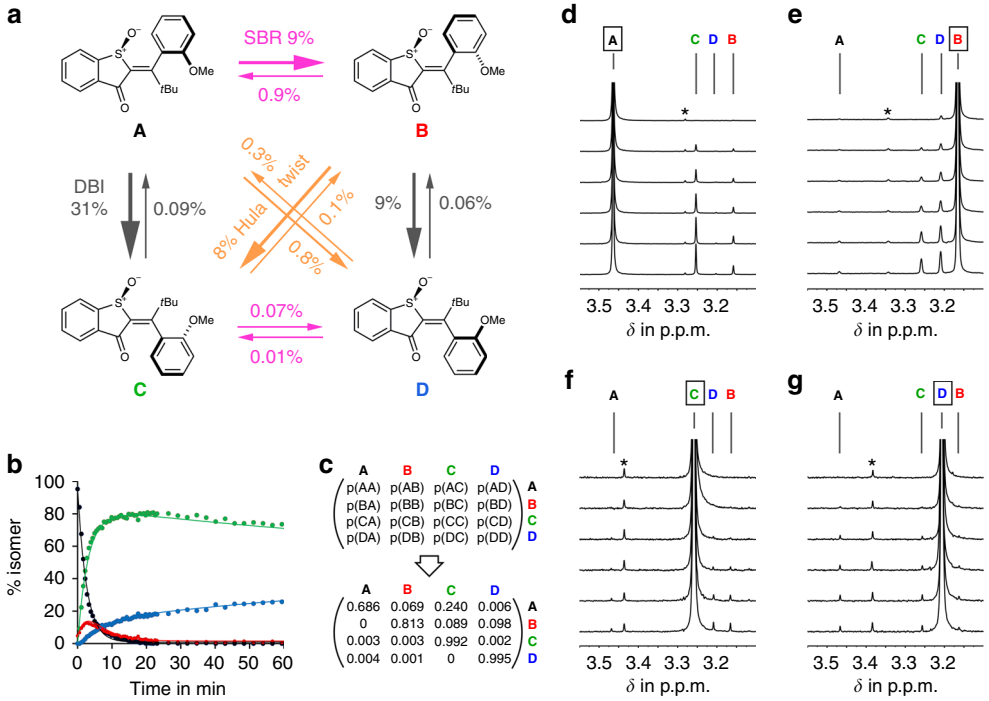

Fig. 3 Photochemistry of **1** in benzene-d_6 solution. **a** Individual photoconversions between the four isomers of **1** in benzene-d_6 under 405 nm irradiation experimentally determined by quantum yield measurements. **b** Fitting of experimental data obtained at 27 °C in benzene-d_6 (dots) to a global kinetic model (lines) for the photoconversion of individual isomers starting from pure **A**. **c** Markov matrix describing the phototransition probability between individual isomers (starting isomer to product isomer) within one minute of irradiation in benzene-d_6. Numeric values were obtained from the best global fit to the experimental data. The ratios between off-diagonal elements mirror the ratios of the measured quantum yields for individual phototransitions. The diagonal elements describe the percentage of remaining starting isomer after one minute of irradiation. **d**–**g** Indicative sections of ^{1}H NMR spectra (400 MHz, 27 °C, benzene-d_6) recorded during irradiation of each pure isomer **A** (**d**), **B** (**e**), **C** (**f**), and **D** (**g**) at 23 °C. Different photoproducts are generated at different rates. * ^{13}C carbon coupling satellites

The light-induced motions of **B** are also very sensitive to the solvent nature. In benzene-d_6 the SBR and HT motions are similarly efficient. An increase of solvent polarity induces the most pronounced changes and clearly favors the HT motion. In the most polar MeOH-d_4 a 70%:30% ratio is observed for the relative propensities to undergo HT versus DBI. Viscosity changes produce smaller, yet discernible trends showing an increase in the propensity for simple DBI with increasing viscosity (Fig. 4b, see also Supplementary Figs. 19–44 and Supplementary Table 2).

Additionally we have tested the influence of temperature in liquid and in solid media on the different photoinduced motions of **A** and **B** (Fig. 4c–e, see also Supplementary Figs. 45–53 and Supplementary Table 3). Irradiation of **A** in toluene-d_8 and CD_2Cl_2 showed no significant changes in the photoreactions at elevated (60 °C in toluene-d_8), ambient (20 or 27 °C), and low

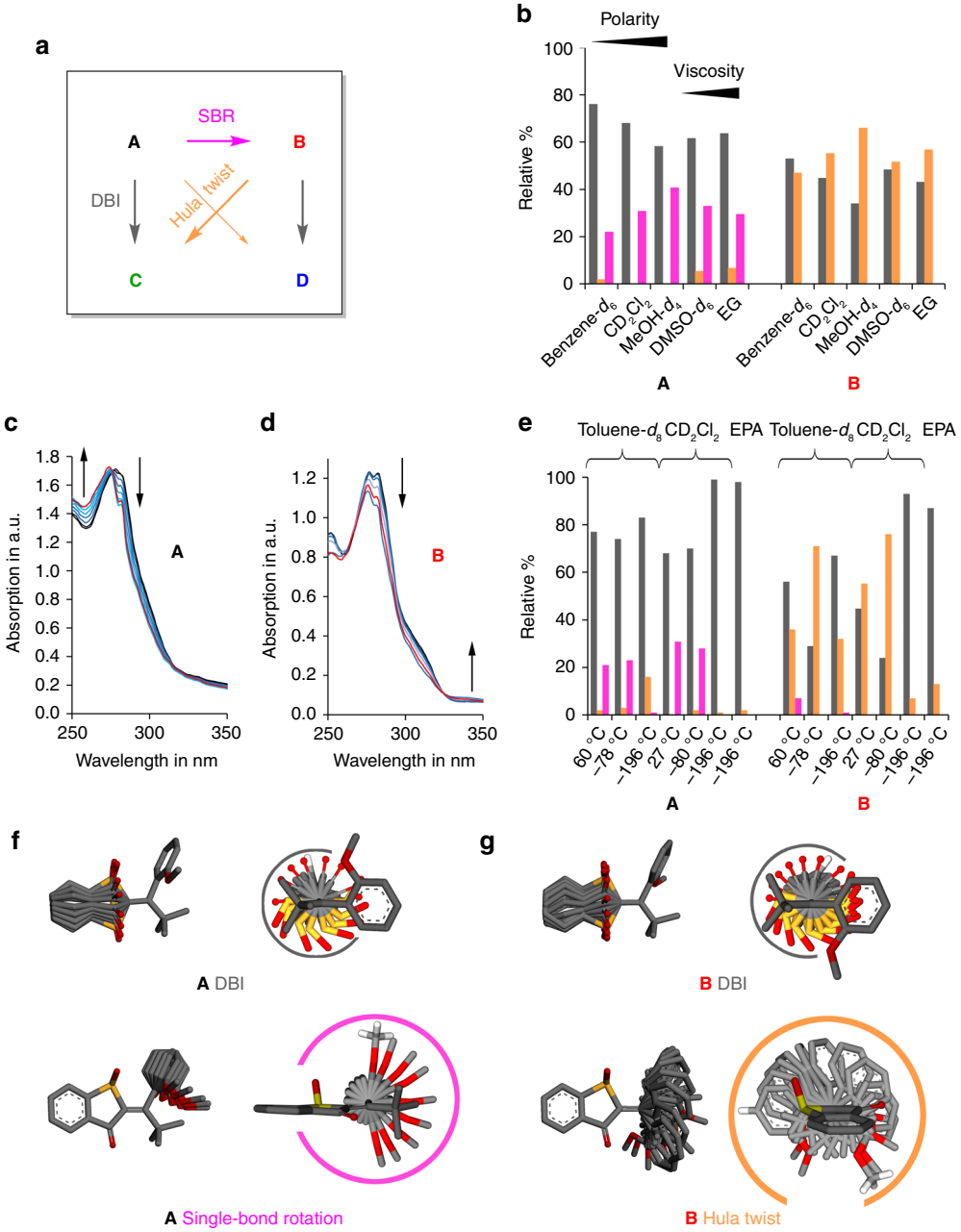

Fig. 4 Photoreactions of **A** and **B** under different conditions. **a** The different photo processes are color coded: SBR in purple, DBI in gray, and HT in orange. **b** Dependence of the photoinduced motions on solvent polarity and viscosity. The relative efficiencies of different processes are derived from a Markov-matrix analysis of the corresponding ^{1}H NMR data. **c** Ultraviolet/vis absorption changes (arrows) observed during irradiation of **A** at −183 °C within an EPA matrix. No significant spectral changes are observed after warming the sample to −80 °C and recooling to −183 °C (red spectrum). **d** Ultraviolet/vis absorption changes observed during irradiation of **B** at −183 °C within an EPA matrix. No significant spectral changes are observed after warming the sample to −80 °C and recooling to −183 °C (red spectrum). **e** Dependence of the photoinduced motions on temperature and rigidity of the medium. The relative efficiencies of different processes are derived from a Markov-matrix analysis of the corresponding ^{1}H NMR data. **f** Approximated volume changes of **A** during DBI (top) and SBR (bottom). Two different views are shown. The required volumes for individual motions are emphasized by color coded circles, perspectives are at the same scale. **g** Approximated volume changes of **B** during DBI (top) and HT motion (bottom)

(−78 or −80 °C) temperatures (Fig. 4e, see also Supplementary Figs. 49 and 50). The situation is quite different for **B** for which temperature effects are very pronounced. At 60 °C in toluene-d_8 solution DBI is clearly the favored photoreaction (56% versus 36% HT) and also 7% of the SBR is observed. At 20 °C DBI is still favored with 54% but the HT motion is now more pronounced with 43% at the expense of the SBR. This selectivity changes dramatically at −78 °C, where the HT photoreaction is now strongly favored with 71% versus 29% DBI. In CD_2Cl_2 the changes are similarly dramatic. At 27 °C HT is slightly favored with 55% over DBI with 45%. At −80 °C the HT is strongly favored with 76% (see also Supplementary Figs. 45–46).

When freezing toluene-d_8 or CD_2Cl_2 solutions of **A** and **B** to ice at −196 °C irradiation still leads to photoreactions. Irradiation of **A** in toluene-d_8 ice results in strongly preferred formation of the DBI product **C** (83%) and almost complete suppression of the SBR product **B** (1%). Instead the HT pathway clearly gains in efficiency with 16%. In CD_2Cl_2 the trend is even more pronounced with almost exclusive selectivity for the DBI product **C** (99%). Irradiation of **B** in toluene-d_8 ice also leads to preference of the DBI, however in this case the HT is still very pronounced with 32%. The situation is different in CD_2Cl_2 where almost exclusive DBI is observed. Therefore, in CD_2Cl_2 it is possible to strongly favor either HT (76% of all photoreactions) at low temperature in liquid solution or DBI (93%) at even lower temperature in solvent glass, which is a remarkable control over photoreactions (see also Supplementary Figs. 45–53). Photoisomerization experiments were also conducted during irradiation with different wavelengths. Only marginal changes in photoproduct composition could be observed by varying the wavelength from 305 to 405 nm (see also Supplementary Figs. 54–55 and Supplementary Table 4).

We also conducted low temperature irradiation experiments of **A** and **B** in diethyl ether/*iso*-pentane/ethanol (EPA) glass at −183 °C and followed the photoreactions with ultraviolet/visible absorption spectroscopy (see also Supplementary Figs. 13, 56–59). Isomers **C** and **D** were found not to undergo photoreactions under these conditions (i.e., within 2 h of irradiation). Irradiation of **A** in EPA glass proceeds with clear isosbestic points leading to the absorption spectrum of **C**. After 30 min of 405 nm illumination the sample was allowed to warm to −80 °C and then recooled to −183 °C. Only marginal spectral changes are observed after the warming and cooling procedure indicating no thermally labile intermediates being formed during irradiation in the EPA matrix (Fig. 4c, see also Supplementary Fig. 56). The isomer composition obtained from irradiation of **A** in the EPA matrix at low temperature was determined directly afterwards by NMR spectroscopy and showed only formation of **C**. An independent Markov analysis of the isomer composition changes occurring during photoirradiation of **A** in EPA glass at −196 °C showed almost exclusive formation of the DBI product **C**. Irradiation of **B** in the EPA glass at −183 °C leads to clear isosbestic points during the irradiation, and no significant changes upon warming and re-cooling (Fig. 4d, see also Supplementary Fig. 57). Again, the isomer composition obtained from irradiation of **B** in the EPA matrix at −183 °C was determined directly afterwards by NMR spectroscopy and showed formation of **C** and **D** in almost equal amounts. Photoirradiation of **B** in EPA glass at −196 °C was scrutinized by Markov analysis revealing almost exclusive formation of the DBI product and about 13% of the HT product at these conditions. There seems to be a significant temperature effect also in rigid matrix surroundings. Overall, at −196 °C the propensities for a particular photoreaction in EPA are similar to the ones found in CD_2Cl_2 ice, i.e., strongly favoring DBI. For comparison we tested also the corresponding photoreactions of **A** and **B** in liquid EPA solution at 22 °C, as well as −80 °C. The same trends are seen as for the other liquid solvents: no temperature effects on the photoreactions of **A** but significant effects for **B**. For the latter at ambient temperature the HT is slightly favored and becomes strongly favored (82%) at lower temperature in solution. For comparison of all relative quantum yields at different temperature in different solvents see Fig. 4e and Supplementary Fig. 60.

Discussion

From our experiments it becomes clear that more polar solvents and the capacity for hydrogen bonding favor the unusual SBR and coupled HT motions against the well-known simple DBI. Decreasing the temperature in solution leads to no significant changes for the SBR compared to DBI in **A**. However, for **B** dramatic changes are observed when lowering the temperature. A significant increase of the HT product is detected in this case regardless of the solvent, but most dramatically in CD_2Cl_2 and EPA where 76% and 82% HT is observed at −80 and −78 °C, respectively. Irradiation in low temperature solvent ices or glasses strongly emphasizes the trends observed when increasing solvent viscosities. In these rigid media almost exclusive DBI is observed for **A** and likewise also a very strong preference for DBI of **B**. In the latter case HT is nevertheless still present to appreciable degree. The decrease of the SBR for **A** in more viscous solvents can be explained by the more space-demanding nature of this motion compared to the DBI in **1** (Fig. 4f). It was previously suggested that external volume restrictions and high viscosity evoke the HT motion, but we clearly did not observe such an influence in our experiments with **B**. On the contrary, we found the DBI is actually strongly favored at higher viscosity and rigidity of the surrounding medium. Our explanation for these seemingly contradictory findings is rooted in the special setup of HTI **1**. When tracing the geometry changes of DBI versus HT motion in a simple bond-rotation model (as we do not know the exact light-induced motions the simple bond-rotation model should however be regarded as just a crude visualization) the latter seems to be even more space-demanding than the competing DBI (Fig. 4g). Because in rigid glasses viscosity effects are strongly amplified it is possible to almost exclusively favor DBI for **A** and **B** e.g., in CD_2Cl_2 ice.

The clear influence of temperature, polarity, hydrogen bonding capacity, as well as viscosity/rigidity of the environment hints at main factors governing complex and unusual light-induced motions in molecules. With the herein presented molecular setup these different influences could be quantified directly and allowed us to either strongly favor the HT motion or the simple DBI against competing photoreactions. Likewise the propensity to undergo SBR could be increased by simple changes in the nature of the solvent at ambient temperatures.

From the data obtained in this work some indications with regard to the mechanism of HT photoproduct formation could be obtained. First, the energy barriers between all four isomeric states **A**–**D** are very high and thermal equilibration occurs both, slowly even at temperatures >80 °C and selectively between **A** and **B** and separated between **C** and **D**. The observed HT photoproducts therefore cannot be formed by first DBI in the excited state, relaxation to the ground state minima and subsequent thermal SBRs. A high-energy ground state intermediate that is populated after the photoreaction and from which a branching towards HT and DBI products occurs is also highly unlikely. The strongest evidence against the presence of such an intermediate is found in the temperature dependence of the photoreaction selectivity in toluene-d_8 solution. At high and ambient temperatures a clear selectivity favoring DBI is observed. This selectivity is turned upside down at low temperatures where HT products are formed with

high preference. Such temperature sensitivity cannot be the result of thermal branching from a common intermediate state, because in such a case the initial trend should be augmented at lower temperature where energy-barrier differences are more important. The only other option for a common ground-state intermediate process—thermodynamic product formation at high and ambient temperatures and kinetic product formation at low temperatures—can also be ruled out, since at ambient temperature there is no thermal equilibrium between the isomers **A**–**D** established.

The absence of any discernible fluorescence in solution also disfavors an adiabatic mechanism. To distinguish between the remaining possibilities, a mechanism involving hot-ground states or a diabatic photoreaction requires more detailed studies and time-resolved measurements, which we will pursue in the near future. To speculate, the observed strong temperature dependence of the photoreactions of **B** could be interpreted in terms of a hot-ground state mechanism[59]. On the other hand, a diabatic process where the product distribution is determined earlier by a conical intersection[60–62] is also possible. In line with this interpretation is the observed formation of all three possible photoproducts (although in varying efficiencies) after irradiation of **A**, **B**, **C**, and **D**, which is indicative for a kinked conical intersection[60,61,63,64]. As solvent polarity increase favors the HT product in our case, a polar ionic conical intersection leading to sole DBI (usually observed in permanently charged systems[62,65]) is likely to be absent in our system. Here the found solvent dependence could be explained by the involvement of an ionic charge-transfer state perturbing the photochemically active state and its decay to the ground state[65,66]. Other options involving further reaction coordinates, and thus more complex conical intersections[67], or the existence of an extended crossing space are also possible[68]. The insensitivity of the photoreactions of **A** towards temperature disfavors a hot ground state in this case and instead hint at a photoreaction directly via conical intersections.

In summary, hitherto ephemeral light-induced motions were directly and unambiguously proven to exist. The exact influences of the surrounding medium and temperature were quantified directly and enabled us to favor unusual photoreactions and complex motions against the long known simple DBI. Just by changing temperature and rigidity of the outside medium we were able to favor HT photoproducts with up to 82% or the simple DBI products by up to 99%. Using the herein presented molecular setup it is now possible to rationally design HTI photoswitches with unusual motions, complex molecular machines, or responsive and functional materials and nanosystems. Likewise molecular engineers will be able to test for the presence of hula-twist photoreactions in other classes of chromophores by applying the herein established design principles: reduction of conformational space, introduction of asymmetry into the molecule via stable stereogenic centers in conjunction with chiral axes, and inhibition of thermal single bond rotation by increased sterical hindrance. It did not escape our attention that the combination of all the different photoinduced motions for **A**–**1** to **D**–**1** under constant illumination are very likely to lead to a netto-directional motion around a virtual axis. Therefore, HTI **1** could actually constitute a completely different type of light-driven molecular motor with unique rotation mechanism. Our future efforts are inter alia aimed in this exciting new direction.

Methods

General experimental. The synthesis and spectroscopic characterization of **A**–**1**, **B**–**1**, **C**–**1**, and **D**–**1** is given in the Supplementary Methods. Reagents and solvents were obtained from abcr, Acros, Fluka, Merck, Sigma-Aldrich, or TCI in the qualities puriss., p.a., or purum and used as recieved. Technical solvents were distilled before use for column chromatography and extraction on a rotary evaporator (Heidolph Hei-VAP Value, vacuubrand CVC 3000). Reactions were monitored on Merck Silica 60 F254 TLC plates. Detection was done by irradiation with UV light (254 nm or 366 nm). Column chromatography was performed with silica gel 60 (Merck, particle size 0.063–0.200 mm) and distilled technical solvents. ^{1}H NMR and ^{13}C NMR spectra were measured on a Varian Mercury 200 VX, Varian 300, Inova 400, Varian 600 NMR, or Bruker Avance III HD 800 MHz spectrometer at 23 °C. Chemical shifts (δ) are given relative to tetramethylsilane as external standard. Residual solvent signals in the ^{1}H and ^{13}C NMR spectra were used as internal reference. Deuterated solvents were obtained from Cambridge Isotope Laboratories or Eurisotop and used without further purification. For ^{1}H NMR: $CDCl_3$ = 7.26 p.p.m., CD_2Cl_2 = 5.32 p.p.m., benzene-d_6 = 7.16 p.p.m., toluene-d_8 = 2.08 p.p.m., $(CDCl_2)_2$ = 6.00 p.p.m., cyclohexane-d_{12} = 1.38 p.p.m., $(CD_3)_2SO$ = 2.50 p.p.m., THF-d_8 = 1.72, 3.58 p.p.m., MeOH-d_4 = 3.31 p.p.m. For ^{13}C NMR: $CDCl_3$ = 77.16 p.p.m., CD_2Cl_2 = 53.84 p.p.m., benzene-d_6 = 128.06 p.p.m., toluene-d_8 = 20.43, cyclohexane-d_{12} = 26.43 p.p.m., THF-d_8 = 67.57, 23.37 p.p.m., MeOH-d_4 = 49.00 p.p.m. The resonance multiplicity is indicated as s (singlet), d (doublet), t (triplet), q (quartet), and m (multiplet). The chemical shifts are given in parts per million (p.p.m.) on the delta scale (δ). The coupling constant values (J) are given in hertz (Hz). Electron Impact (EI) mass spectra were measured on a Finnigan MAT95Q or on a Finnigan MAT90 mass spectrometer. Electronspray ionization (ESI) mass spectra were measured on a Thermo Finnigan LTQ-FT. The most important signals are reported in m/z units with M as the molecular ion. Elemental analysis were performed in the micro analytical laboratory of the LMU department of chemistry on an Elementar Vario EL apparatus. Infrared spectra were recorded on a Perkin Elmer Spectrum BX-FT-IR instrument equipped with a Smith DuraSamplIR II ATR-device. Transmittance values are qualitatively described by wavenumber (cm^{-1}) as very strong (vs), strong (s), medium (m), and weak (w). UV/Vis spectra were measured on a Varian Cary 5000 spectrophotometer. The spectra were recorded in a quartz cuvette (1 cm). Solvents for spectroscopy were obtained from VWR and Merck. Absorption wavelength (λ) are reported in nm and the molar absorption coefficients (ε) in L mol^{-1} cm^{-1}. Low temperature UV/vis spectra in EPA glass (diethylether/isopentane/ethanol 5:5:2) at 90 K (−183 °C) were measured on a Varian Cary® 50 spectrophotometer with an Oxford DN 1704 optical cryostat controlled by an Oxford ITC 4 device. Low temperatures were reached by cooling slowly with liquid nitrogen. The spectra were recorded in a quartz cuvette (1 cm). Solvents for spectroscopy were obtained from VWR, Merck and Sigma Aldrich and were dried, degassed and filtrated prior use. For irradiation studies a Mightex FCS-0405-200 LED (405 nm) was used as light source. Absorption wavelength (λ) are reported in nm and the molar absorption coefficients (ε) in L·mol^{-1}·cm^{-1}. Melting points (M. p.) were measured on a Stuart SMP10 melting point apparatus in open capillaries and are not corrected.

Photoisomerization experiments. Continuous irradiations of the solutions were conducted in NMR tubes in different solvents (CD_2Cl_2, $(CDCl_2)_2$, benzene-d_6, toluene-d_8, MeOH-d_4, DMSO-d_6, EPA, EG). Irradiations were conducted using LEDs from Roithner Lasertechnik GmbH (305 nm, 365 nm, 405 nm). For low temperature studies a Mightex FCS-0405-200 LED (405 nm) was used as light source and the light beam was guided by a fiber-optic cable (0.39 NA, one SMA, one blank end) and pointed directly into the NMR tube during NMR measurements. For quantum yield measurements see Supplementary Methods.

Data availability. All data that support the findings of this study are available from the corresponding author upon reasonable request. The X-ray crystallographic coordinates for the structures **A**–**1** to **D**–**1** reported in this study have been deposited at the Cambridge Crystallographic Data Centre (CCDC), under CCDC numbers 1586011 (**A**–**1**), 1586012 (**B**–**1**), 1586013 (**C**–**1**), 1586014 (**D**–**1**). These data can be obtained free of charge from the Cambridge Crystallographic Data Centre via www.ccdc.cam.ac.uk/data_request/cif.

Received: 21 December 2017 Accepted: 3 May 2018
Published online: 28 June 2018

References

1. Erbas-Cakmak, S., Leigh, D. A., McTernan, C. T. & Nussbaumer, A. L. Artificial molecular machines. *Chem. Rev.* **115**, 10081–10206 (2015).
2. Koumura, N., Zijlstra, R. W. J., van Delden, R. A. & Feringa, B. L. Light-driven monodirectional molecular rotor. *Nature* **401**, 152–155 (1999).
3. Greb, L. & Lehn, J. M. Light-driven molecular motors: imines as four-step or two-step unidirectional rotors. *J. Am. Chem. Soc.* **136**, 13114–13117 (2014).
4. Hernandez, J. V., Kay, E. R. & Leigh, D. A. A reversible synthetic rotary molecular motor. *Science* **306**, 1532–1537 (2004).
5. Guentner, M. et al. Sunlight-powered kHz rotation of a hemithioindigo-based molecular motor. *Nat. Commun.* **6**, 8406 (2015).
6. Huber, L. A. et al. Direct observation of hemithioindigo-motor unidirectionality. *Angew. Chem. Int. Ed.* **56**, 14536–14539 (2017).

7. Foy, J. T. et al. Dual-light control of nanomachines that integrate motor and modulator subunits. *Nat. Nanotechnol.* **12**, 540–545 (2017).
8. Li, H. et al. Relative unidirectional translation in an artificial molecular assembly fueled by light. *J. Am. Chem. Soc.* **135**, 18609–18620 (2013).
9. Kundu, P. K. et al. Light-controlled self-assembly of non-photoresponsive nanoparticles. *Nat. Chem.* **7**, 646–652 (2015).
10. Fuhrmann, A. et al. Conditional repair by locally switching the thermal healing capability of dynamic covalent polymers with light. *Nat. Commun.* **7**, 13623 (2016).
11. Iamsaard, S. et al. Conversion of light into macroscopic helical motion. *Nat. Chem.* **6**, 229–235 (2014).
12. Frank, J. A. et al. Photoswitchable diacylglycerols enable optical control of protein kinase C. *Nat. Chem. Biol.* **12**, 755–762 (2016).
13. Velema, W. A., Szymanski, W. & Feringa, B. L. Photopharmacology: beyond proof of principle. *J. Am. Chem. Soc.* **136**, 2178–2191 (2014).
14. Jung, Y. O. et al. Reply to 'contradictions in X-ray structures of intermediates in the photocycle of photoactive yellow protein'. *Nat. Chem.* **6**, 259–260 (2014).
15. Kaila, V. R. I., Schotte, F., Cho, H. S., Hummer, G. & Anfinrud, P. A. Contradictions in X-ray structures of intermediates in the photocycle of photoactive yellow protein. *Nat. Chem.* **6**, 258–259 (2014).
16. Jung, Y. O. et al. Volume-conserving trans-cis isomerization pathways in photoactive yellow protein visualized by picosecond X-ray crystallography. *Nat. Chem.* **5**, 212–220 (2013).
17. Redwood, C., Bayda, M. & Saltiel, J. Photoisomerization of pre- and provitamin D3 in EPA at 77 K: one-bond-twist, not hula-twist. *J. Phys. Chem. Lett.* **4**, 716–721 (2013).
18. Fuß, W., Kosmidis, C., Schmid, W. E. & Trushin, S. A. The photochemical cis-trans isomerization of free stilbene molecules follows a hula-twist pathway. *Angew. Chem. Int. Ed.* **43**, 4178–4182 (2004).
19. Müller, A. M., Lochbrunner, S., Schmid, W. E. & Fuß, W. Low-temperature photochemistry of previtamin d: a hula-twist isomerization of a triene. *Angew. Chem. Int. Ed.* **37**, 505–507 (1998).
20. Maessen, P. A., Jacobs, H. J. C., Cornelisse, J. & Havinga, E. Photochemistry of previtamin D3 at 92 K; formation of an unstable tachysterol3 rotamer. *Angew. Chem. Int. Ed.* **22**, 718–719 (1983).
21. Warshel, A. Bicycle-pedal model for the first step in the vision process. *Nature* **260**, 679–683 (1976).
22. Schapiro, I., Weingart, O. & Buss, V. Bicycle-pedal isomerization in a rhodopsin chromophore model. *J. Am. Chem. Soc.* **131**, 16–17 (2009).
23. Liu, R. S. H. & Hammond, G. S. Photochemical reactivity of polyenes: from dienes to rhodopsin, from microseconds to femtoseconds. *Photochem. Photobiol. Sci.* **2**, 835–844 (2003).
24. Ramamurthy, V. & Liu, R. S. H. Photochemistry of polyenes. IX. Excitation, relaxation, and deactivation of dienes, trienes, and higher polyenes in the vitamin A series in the sensitized isomerization reaction. *J. Am. Chem. Soc.* **98**, 2935–2942 (1976).
25. Imamoto, Y. et al. Photoisomerization by Hula Twist: 2,2'-dimethylstilbene and a ring-fused analogue. *Angew. Chem., Int. Ed.* **42**, 3630–3633 (2003).
26. Waldeck, D. H. Photoisomerization dynamics of stilbenes in polar solvents. *J. Mol. Liq.* **57**, 127–148 (1993).
27. Görner, H. & Kuhn, H. J. In *Advances in Photochemistry* (eds Neckers, D. C. et al.) Ch 1 (John Wiley & Sons, Inc., 2007).
28. Kukura, P., McCamant, D. W., Yoon, S., Wandschneider, D. B. & Mathies, R. A. Structural observation of the primary isomerization in vision with femtosecond-stimulated Raman. *Science* **310**, 1006–1009 (2005).
29. Ernst, O. P. et al. Microbial and animal rhodopsins: structures, functions, and molecular mechanisms. *Chem. Rev.* **114**, 126–163 (2014).
30. Wei, L., Wang, H., Chen, X., Fang, W. & Wang, H. A comprehensive study of isomerization and protonation reactions in the photocycle of the photoactive yellow protein. *Phys. Chem. Chem. Phys.* **16**, 25263–25272 (2014).
31. Pande, K. et al. Femtosecond structural dynamics drives the trans/cis isomerization in photoactive yellow protein. *Science* **352**, 725–729 (2016).
32. Zhang, Q., Chen, X., Cui, G., Fang, W.-H. & Thiel, W. Concerted asynchronous hula-twist photoisomerization in the S65T/H148D mutant of green fluorescent protein. *Angew. Chem. Int. Ed.* **53**, 8649–8653 (2014).
33. Andresen, M. et al. Structure and mechanism of the reversible photoswitch of a fluorescent protein. *Proc. Natl Acad. Sci. USA* **102**, 13070–13074 (2005).
34. Saltiel, J., Megarity, E. D. & Kneipp, K. G. The mechanism of direct *cis-trans* photoisomerization of the stilbenes. *J. Am. Chem. Soc.* **88**, 2336–2338 (1966).
35. Liu, R. S. & Asato, A. E. The primary process of vision and the structure of bathorhodopsin: a mechanism for photoisomerization of polyenes. *Proc. Natl Acad. Sci. USA* **82**, 259–263 (1985).
36. Liu, R. S. & Hammond, G. S. Examples of hula-twist in photochemical cis-trans isomerization. *Chem. Eur. J.* **7**, 4537–4544 (2001).
37. Fuß, W. Hula-twist cis–trans isomerization: the role of internal forces and the origin of regioselectivity. *J. Photochem. Photobiol., A* **237**, 53–63 (2012).
38. Röhrig, U. F., Guidoni, L., Laio, A., Frank, I. & Rothlisberger, U. A molecular spring for vision. *J. Am. Chem. Soc.* **126**, 15328–15329 (2004).
39. Saltiel, J., Bremer, M. A., Laohhasurayotin, S. & Krishna, T. S. Photoisomerization of cis,cis- and cis,trans-1,4-Di-o-tolyl-1,3-butadiene in glassy media at 77 K: one-bond-twist and bicycle-pedal mechanisms. *Angew. Chem. Int. Ed.* **47**, 1237–1240 (2008).
40. Saltiel, J. et al. Photoisomerization of all-cis-1,6-diphenyl-1,3,5-hexatriene in the solid state and in solution: a simultaneous three-bond twist process. *Angew. Chem. Int. Ed.* **48**, 8082–8085 (2009).
41. Saltiel, J., Krishna, T. S., Turek, A. M. & Clark, R. J. Photoisomerization of cis, cis-1,4-diphenyl-1,3-butadiene in glassy media at 77 K: the bicycle-pedal mechanism. *Chem. Commun.* **0**, 1506–1508 (2006).
42. Squillacote, M. E., Sheridan, R. S., Chapman, O. L. & Anet, F. A. L. Planar s-cis-1,3-butadiene. *J. Am. Chem. Soc.* **101**, 3657–3659 (1979).
43. Werst, D. W., Londo, W. F., Smith, J. L. & Barbara, P. F. The excited-state torsional potentials of substituted 9-phenylanthracenes. *Chem. Phys. Lett.* **118**, 367–374 (1985).
44. Brouwer, A. M. & Jacobs, H. J. C. Photochemistry of 2,5-dimethyl-1,3,5-hexatrienes in argon matrices. Formation of isomers and rotamers. *Recl. Trav. Chim. Pays-Bas* **114**, 449–458 (1995).
45. Furukawa, Y., Takeuchi, H., Harada, I. & Tasumi, M. Matrix-isolation infrared and ultraviolet spectroscopic studies of less stable conformers of 1,3,5-hexatriene. *J. Mol. Struct.* **100**, 341–350 (1983).
46. Schoenlein, R., Peteanu, L., Mathies, R. & Shank, C. The first step in vision: femtosecond isomerization of rhodopsin. *Science* **254**, 412–415 (1991).
47. van Wilderen, L. J. et al. Ultrafast infrared spectroscopy reveals a key step for successful entry into the photocycle for photoactive yellow protein. *Proc. Natl Acad. Sci. USA* **103**, 15050–15055 (2006).
48. Yang, L.-Y. & Liu, R. S. H. Mechanism of photoisomerization of 1-naphthyl-2-phenylethylenes in organic glasses. *Photochem. Photobiol.* **83**, 1436–1440 (2007).
49. Liu, R. S. H., Yang, L.-Y. & Liu, J. Mechanisms of photoisomerization of polyenes in confined media: from organic glasses to protein binding cavities. *Photochem. Photobiol.* **83**, 2–10 (2007).
50. Bayda, M., Redwood, C. E., Gupta, S., Dmitrenko, O. & Saltiel, J. Lumisterol to tachysterol photoisomerization in EPA glass at 77 K. A comparative study. *J. Phys. Chem. A* **121**, 2331–2342 (2017).
51. Redwood, C. et al. Photoisomerization of cis-1,2-di(1-Methyl-2-naphthyl) ethene at 77 K in glassy media. *Photochem. Photobiol.* **91**, 607–615 (2015).
52. Liu, R. S. H. & Hammond, G. S. The case of medium-dependent dual mechanisms for photoisomerization: one-bond-flip and hula-twist. *Proc. Natl Acad. Sci. USA* **97**, 11153–11158 (2000).
53. Liu, R. S. H. & Hammond, G. S. Reflection on medium effects on photochemical reactivity. *Acc. Chem. Res.* **38**, 396–403 (2005).
54. Balomenou, I. & Pistolis, G. Torsional photoisomerization proceeding adiabatically through a volume-conserving pathway in uninhibited fluid media. *Chem. Eur. J.* **15**, 4228–4232 (2009).
55. Wiedbrauk, S. & Dube, H. Hemithioindigo—an emerging photoswitch. *Tetrahedron Lett.* **56**, 4266–4274 (2015).
56. Kitzig, S., Thilemann, M., Cordes, T. & Rück-Braun, K. Light-switchable peptides with a hemithioindigo unit: peptide design, photochromism, and optical spectroscopy. *Chemphyschem* **17**, 1252–1263 (2016).
57. Wiedbrauk, S. et al. Twisted hemithioindigo photoswitches: solvent polarity determines the type of light-induced rotations. *J. Am. Chem. Soc.* **138**, 12219–12227 (2016).
58. Gerwien, A., Reinhardt, T., Mayer, P. & Dube, H. Synthesis of double-bond substituted hemithioindigo photoswitches. *Org. Lett.* **1**, 232–235 (2018).
59. Arruda, B. C. & Sension, R. J. Ultrafast polyene dynamics: the ring opening of 1,3-cyclohexadiene derivatives. *Phys. Chem. Chem. Phys.* **16**, 4439–4455 (2014).
60. Robb, M. A., Garavelli, M., Olivucci, M. & Bernardi, F. In *Reviews of Computational Chemistry* (eds Lipkowitz, K. B. et al.) 87–146 (John Wiley & Sons, Inc., 2007).
61. Olivucci, M. *Computational Photochemistry* 1st edn (Elsevier, 2005).
62. Sampedro Ruiz, D., Cembran, A., Garavelli, M., Olivucci, M. & Fuß, W. Structure of the conical intersections driving the cis–trans photoisomerization of conjugated molecules. *Photochem. Photobiol.* **76**, 622–633 (2002).
63. Levine, B. G. & Martinez, T. J. Isomerization through conical intersections. *Annu. Rev. Phys. Chem.* **58**, 613–634 (2007).
64. Celani, P. et al. Molecular "Trigger" for radiationless deactivation of photoexcited conjugated hydrocarbons. *J. Am. Chem. Soc.* **117**, 11584–11585 (1995).
65. Gonzalez-Luque, R. et al. Computational evidence in favor of a two-state, two-mode model of the retinal chromophore photoisomerization. *Proc. Natl Acad. Sci. USA* **97**, 9379–9384 (2000).
66. Cembran, A., Bernardi, F., Olivucci, M. & Garavelli, M. The retinal chromophore/chloride ion pair: Structure of the photoisomerization path and interplay of charge transfer and covalent states. *Proc. Natl Acad. Sci. USA* **102**, 6255–6260 (2005).

67. Polli, D. et al. Conical intersection dynamics of the primary photoisomerization event in vision. *Nature* **467**, 440–443 (2010).
68. Conti, I., Garavelli, M. & Orlandi, G. The different photoisomerization efficiency of azobenzene in the lowest nπ* and ππ* singlets: the role of a phantom state. *J. Am. Chem. Soc.* **130**, 5216–5230 (2008).

Acknowledgements

H.D. thanks the "Fonds der Chemischen Industrie" for a Liebig fellowship (Li 188/05) and the DFG for an Emmy Noether fellowship (DU 1414/1-1). We further thank the collaborative research center SFB749/3, A12 and the Cluster of Excellence "Center for Integrated Protein Science Munich (CiPS^{M})" for financial support.

Author contributions

A.G., M.S., and H.D. designed the molecular setup and experiments. A.G. synthesized and characterized HTI **1** and conducted the kinetic experiments. M.S. conducted low temperature measurements in EPA matrices. M.S. and S.T. participated in designing experiments and analyzing data. S.T. provided the theoretical description of HTI **1**. P.M. determined the crystal structures. H.D. coordinated the study and wrote the manuscript. All authors read and approved the manuscript.

Additional information

Supplementary Information accompanies this paper at https://doi.org/10.1038/s41467-018-04928-9.

Competing interests: The authors declare no competing interests.

Supplementary Information

Direct Evidence for Hula Twist and Single-Bond Rotation Photoproducts

A. Gerwien et al.

Supplementary Methods

Synthesis

General experimental

Reagents and solvents were obtained from *abcr*, *Acros, Fluka, Merck, Sigma-Aldrich* or *TCI* in the qualities *puriss., p.a., or purum* and used as recieved. Technical solvents were distilled before use for column chromatography and extraction on a rotary evaporator (*Heidolph Hei-VAP Value*, *vacuubrand* CVC 3000). Reactions were monitored on *Merck* Silica 60 F254 TLC plates. Detection was done by irradiation with UV light (254 nm or 366 nm).

Column chromatography was performed with silica gel 60 (*Merck*, particle size 0.063- 0.200 mm) and distilled technical solvents.

^{1}H NMR and ^{13}C NMR spectra were measured on a *Varian Mercury 200 VX, Varian 300, Inova 400, Varian 600 NMR* or *Bruker Avance III HD 800 MHz* spectrometer at different temperatures. Chemical shifts (δ) are given relative to tetramethylsilane as external standard. Residual solvent signals in the ^{1}H and ^{13}C NMR spectra were used as internal reference. Deuterated solvents were obtained from *Cambridge Isotope Laboratories* or *Eurisotop* and used without further purification. ^{1}H NMR: $CDCl_3$ = 7.26 ppm, CD_2Cl_2 = 5.32 ppm, benzene-d_6 = 7.16 ppm, toluene-d_8 = 2.08 ppm, $(CDCl_2)_2$ = 6.00 ppm, cyclohexane-d_{12} = 1.38 ppm, $(CD_3)_2SO$ = 2.50 ppm, THF-d_8 = 1.72, 3.58 ppm, MeOH-d_4 = 3.31 ppm. For ^{13}C NMR: $CDCl_3$ = 77.16 ppm, CD_2Cl_2 = 53.84 ppm, benzene-d_6 = 128.06 ppm, toluene-d_8 = 20.43, cyclohexane-d_{12} = 26.43 ppm, THF-d_8 = 67.57, 23.37 ppm, MeOH-d_4 = 49.00 ppm The resonance multiplicity is indicated as *s* (singlet), *d* (doublet), *t* (triplet), *q* (quartet) and *m* (multiplet). The chemical shifts are given in parts per million (ppm) on the delta scale (δ). The coupling constant values (*J*) are given in hertz (Hz).

Electron Impact (EI) mass spectra were measured on a *Finnigan MAT95Q* or on a *Finnigan MAT90* mass spectrometer. **Electronspray ionisation (ESI) mass spectra were** measured on a *Thermo Finnigan LTQ-FT*. The most important signals are reported in *m/z* units with *M* as the molecular ion.

Elemental analysis were performed in the micro analytical laboratory of the LMU department of chemistry on an *Elementar Vario EL* apparatus.

Infrared spectra were recorded on a *Perkin Elmer Spectrum BX-FT-IR* instrument equipped with a *Smith DuraSamplIR II ATR*-device. Transmittance values are qualitatively described by wavenumber (cm^{-1}) as very strong (vs), strong (s), medium (m) and weak (w).

UV/Vis spectra were measured on a *Varian Cary 5000* spectrophotometer. The spectra were recorded in a quartz cuvette (1 cm). Solvents for spectroscopy were obtained from *VWR* and *Merck*. Absorption

wavelength (λ) are reported in nm and the molar absorption coefficients (ε) in L mol^{-1} cm^{-1}. Shoulders are declared as sh.

Low temperature UV/vis spectra in EPA glass (ether/isopentane/ethanol 5:5:2) at 90 K were measured on a *Varian Cary® 50* spectrophotometer with an *Oxford DN 1704* optical cryostat controlled by an *Oxford ITC 4* device. Low temperatures were reached by cooling slowly with liquid nitrogen. The spectra were recorded in a quartz cuvette (1 cm). Solvents for spectroscopy were obtained from *VWR*, *Merck* and *Sigma Aldrich* and were dried, degassed and filtrated prior use. For irradiation studies a *Mightex FCS-0405-200 LED* (405 nm) was used as light source. Absorption wavelength (λ) are reported in nm and the molar absorption coefficients (ε) in $L \cdot mol^{-1} \cdot cm^{-1}$.

Melting points (M.p.) were measured on a *Stuart* SMP10 melting point apparatus in open capillaries and are not corrected.

Photoisomerization experiments. Continuous irradiations of the solutions were conducted in NMR tubes in different solvents (CD_2Cl_2, $(CDCl_2)_2$, benzene-d_6, toluene-d_8, MeOH-d_4, DMSO-d_6, EPA, EG). Irradiations were conducted using LEDs from Roithner Lasertechnik GmbH (305 nm, 365 nm, 405 nm). For low temperature studies a *Mightex FCS-0405-200 LED* (405 nm) was used as light source and the light beam was guided by a fiber-optic cable (0.39 NA, one SMA, one blank end) and pointed directly into the NMR tube during NMR measurements.

HTI Synthesis

2-((3,3-Dimethyl-2-oxobutyl)thio)benzoic acid (**2**)

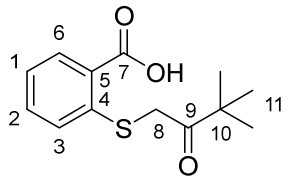

Thiosalicylic acid (50 mmol, 1.0 equiv.) and sodium acetate (100 mmol, 2.0 equiv.) were added to the *in situ* generated 1-bromo-3, 3-dimethyl-2-butanone (50 mmol, 1.0 equiv., based on used ketone) in methanol (1 M solution) and the solution was stirred for 30 min at 23 °C. Afterwards the reaction suspension was poured on ice water and the reaction product was filtered off, washed with water and hexanes and dried *in vacuo*. The title compound (**2**) was isolated as colorless solid (12.4 g, 49 mmol, 98%).[1]

^{1}H NMR (400 MHz, $CDCl_3$) δ = 8.08 (dd, ^{3}J(H,H) = 8.0 Hz, ^{4}J(H,H) = 1.6 Hz, 1H, H-C(6)), 7.47 (ddd, ^{3}J(H,H) = 8.0 Hz, ^{3}J(H,H) = 7.8 Hz, ^{4}J(H,H) = 1.6 Hz, 1H, H-C(2)), 7,34 (dd, ^{3}J(H,H) = 7.8 Hz, ^{4}J(H,H) = 1.6 Hz, 1H, H-C(3)), 7.25 (td, ^{3}J(H,H) = 8.0 Hz, ^{4}J(H,H) = 1.6 Hz, 1H, H-C(1)), 4.02 (s, 2H, H-C(8)), 1.24 (s, 9H, H-C(11)) ppm.

^{13}C NMR (101 MHz, $CDCl_3$) δ = 209.9 (C(9)), 170.9 (C(7)), 140.1 (C(4)), 133.2 (C(2)), 132.4 (C(6)), 128.3 (C(5)), 127.7 (C(3)), 125.4 (C(1)), 44.7 (C(8)), 39.3 (C(10)), 26.8 (C(11)) ppm.

IR $\tilde{\nu}$ (cm^{-1}) = 2969 (w), 2643 (w), 1684 (vs), 1583 (w), 1561 (w), 1472 (w), 1460 (m), 1404 (m), 1395 (m), 1367 (w), 1314 (m), 1289 (m), 1255 (vs), 1151 (w), 1058 (m), 1050 (m), 1044 (s), 917 (s), 815 (w), 803 (w), 793 (w), 734 (vs), 703 (m), 686 (w).

Melting point: 161°C.

HRMS (EI^+), [M^+]: *m/z* calcd. 252.0815 für $[C_{13}H_{16}O_3S]^+$, found 252.0815.

R_f (SiO_2, *i*Hex/EtOAc = 50/50) = 0.12.

1-(3-Hydroxybenzo[*b*]thiophen-2-yl)-2,2-dimethylpropan-1-one (**3**)

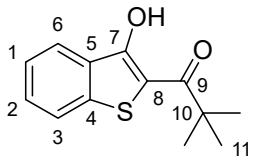

2-((3,3-Dimethyl-2-oxobutyl)thio)benzoic acid (**2**, 40 mmol, 1 equiv.) was dissolved in DMF to receive a 1 M solution, sodium acetate (120 mmol, 3.0 equiv.) was added and the solution was heated to 140 °C for 4 h under continuous stirring. After the mixture was cooled down to room temperature, water (50 ml) was added, the product was extracted with dichloromethane (3 x 50 ml) and dried over Na_2SO_4. The combined organic phases were removed *in vacuo* and the title compound (**3**) was isolated after crystallization from hexanes/dichloromethane as light yellow crystals (9.1 g, 39 mmol, 97%).[1]

^{1}H NMR (400 MHz, $CDCl_3$) δ = 13.51 (s, 1H, H-O), 8.06 (d, ^3J(H,H) = 9.1 Hz, 1H, H-C(6)), 7.70 (d, ^3J(H,H) = 8.1 Hz, 1H, H-C(3)), 7.52 (t, ^3J(H,H) = 8.1 Hz, 1H, H-C(2)), 7.38 (t, ^3J(H,H) = 8.1 Hz, 1H, H-C(1)), 1.43 (s, 9H, H-C(11)) ppm.

^{13}C NMR (101 MHz, $CDCl_3$) δ = 206.1 (C(9)), 165.3 (C(7)), 139.6 (C(4)), 130.4 (C(5)), 130.3 (C(2)), 124.9 (C(1)), 124.0 (C(6)), 123.0 (C(3)), 107.9 (C(8)), 44.0 (C(10)), 27.6 (C(11)) ppm.

IR $\tilde{\nu}$ (cm^{-1}) = 2969 (w), 2643 (w), 1684 (vs), 1583 (w), 1561 (w), 1472 (w), 1460 (m), 1404 (m), 1395 (m), 1367 (w), 1314 (m), 1289 (m), 1255 (vs), 1151 (w), 1058 (m), 1050 (m), 1044 (s), 917 (s), 815 (w), 803 (w), 793 (w), 734 (vs), 703 (m), 686 (w).

Melting point: 161°C.

HRMS (EI^+), [M^+]: *m/z* calcd. 234.0715 für $[C_{13}H_{14}O_2S]^+$, found 234.0716.

R_f (SiO_2, *i*Hex/EtOAc = 98/2) = 0.56.

(*Z*)-2-(1-Chloro-2,2-dimethylpropylidene)benzo[*b*]thiophen-3(2*H*)-one (**4**)

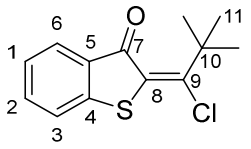

1-(3-Hydroxybenzo[*b*]thiophen-2-yl)-2,2-dimethylpropan-1-one (**3**, 8.5 mmol, 1 equiv.) was dissolved in toluene to receive a 1 M solution. Thionylchloride (2.0 equiv.) and DMF (0.1 equiv.) were added and the solution was stirred at 50 °C for 3 h. Saturated sodium carbonate solution was added until the solution was neutralized, the product was extracted with dichloromethane (3 x 50 mL) and the combined organic phases were dried over Na_2SO_4. The solvent was removed *in vacuo*. The product was purified by column chromatography over a short plug of silica (SiO_2, *i*Hex/EtOAc = 99/1 → 95/5) and further by crystallization from *n*heptane as light yellow solid (2.15 g, 8.5 mmol, quant., only the *Z* isomer was obtained after crystallization).[1]

^{1}H NMR (400 MHz, CD_2Cl_2) δ = 7.75 (dd, ^3J(H,H) = 7.8, ^4J(H,H) = 1.4, 1H, H-C(6)), 7.55 (ddd, ^3J(H,H) = 7.9, ^3J(H,H) = 7.2, ^4J(H,H) = 1.3 Hz, 1H, H-C(2)), 7.39 (dd, ^3J(H,H) = 7.9, ^4J(H,H) = 0.9 Hz, 1H, H-C(3)), 7.25 (ddd, ^3J(H,H) = 8.1, ^3J(H,H) = 7.3, ^4J(H,H) = 1.0 Hz, 1H, H-C(1)), 1.49 (s, 9H, H-C(11)) ppm.

^{13}C NMR (101 MHz, CD_2Cl_2) δ = 184.0 (C(7)), 159.3 (C(9)), 144.9 (C(4)), 135.5 (C(2)), 134.3 (C(8)), 134.3 (C(5)), 127.3 (C(6)), 125.8 (C(1)), 123.5 (C(3)), 42.1 (C(10)), 28.8 (C(11)) ppm.

IR $\tilde{\nu}$ (cm^{-1}) = 2975 (w), 1583 (vs), 1509 (s), 1477 (m), 1461 (w), 1400 (w), 1390 (w), 1366 (m), 1334 (m), 1304 (s), 1288 (m), 1275 (m), 1239 (m), 1205 (vs), 1172 (m), 1129 (w), 1095 (s), 1063 (m), 999 (vs), 940 (w), 856 (w), 821 (m), 774 (s), 750 (s), 735 (vs).

Melting point: 51°C.

HRMS (EI$^+$), [M$^+$]: *m/z* calcd. 252.0370 für $[C_{13}H_{13}OClS]^+$, found 252.0361.

R_f (SiO_2, *i*Hex/EtOAc = 98/2) = 0.51.

(Z)-2-(1-(2-Methoxyphenyl)-2,2-dimethylpropylidene)benzo[*b*]thiophen-3(2*H*)-one (**5**)

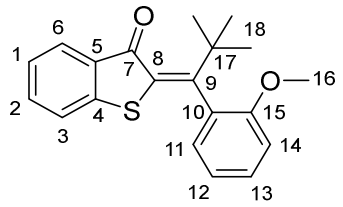

(*Z*)-2-(1-Chloro-2,2-dimethylpropylidene)benzo[*b*]thiophen-3(2*H*)-one (**4**, 1.1 mmol 1.0 equiv.) was dissolved in toluene (18 mL). (2-Methoxyphenyl)boronic acid (1.65 mmol, 1.5 equiv.), potassium carbonate (2.2 mmol, 2.0 equiv.) and water (2 mL) were added. After degassing with argon, $Pd(PPh_3)_4$ (5 mol%) was added and the reaction mixture was stirred for 24 h at 80 °C. Subsequently, saturated sodium carbonate solution (5 mL) was added, the aqueous phase was extracted with dichloromethane (3 x 20 mL) and the combined organic phases were dried over Na_2SO_4. After removing the solvent *in vacuo*, the crude product was purified by column chromatography (SiO_2, *i*Hex/EtOAc = 95/5) and further by crystallization from *n*heptane. The title compound was isolated as yellow crystals (341 mg, 1.05 mmol, 96%, only the *Z* isomer was obtained after crystallization).

^{1}H NMR (400 MHz, $CDCl_3$) δ = 7.81 (dd, ^3J(H,H) = 8.3 Hz, ^4J(H,H) = 1.3 Hz, 1H, H-C(6)), 7.43 (ddd, ^3J(H,H) = 7.9 Hz, ^3J(H,H) = 7.2 Hz, ^4J(H,H) = 1.4 Hz, 1H, H-C(2)), 7.37 (ddd, ^3J(H,H) = 8.5 Hz, ^3J(H,H) = 7.2 Hz, ^4J(H,H) = 1.4 Hz, 1H, H-C(13)), 7.21 – 7.15 (m, 2H, H-C(1), H-C(3)), 7.04 – 7.00 (m, 2H, H-C(11), H-C(12)), 6.99 – 6.94 (m, 1H, H-C(14)), 3.82 (s, 3H, H-C(16)), 1.36 (s, 9H, H-C(18)) ppm.

^{13}C NMR (101 MHz, $CDCl_3$) δ = 186.4 (C(7)), 163.93 (C(9)), 155.4 (C(15)), 145.9 (C(4)), 134.5 (C(2)), 3x 133.7 (C(5,8,12)), 129.4 (C(13)), 128.4 (C(11)), 126.8 (C(6)), 124.5 (C(3)), 122.8 (C(1)), 120.6 (C(12)), 111.0 (C(14)), 55.7 (C(16)), 38.7 (C(17)), 28.6 (C(18)) ppm.

IR $\tilde{\nu}$ (cm^{-1}) = 2960 (w), 2910 (w), 1667 (vs), 1588 (s), 1536 (m), 1487 (m), 1451 (s), 1433 (w), 1390 (w), 1359 (w), 1313 (w), 1280 (s), 1257 (m), 1239 (m), 1218 (m), 1178 (w), 1160 (w), 1116 (m), 1069 (s), 1047 (w), 1024 (m), 953 (w), 929 (w), 899 (w), 821 (w), 743 (vs), 670 (w).

Melting point: 109 °C.

HRMS (EI^+), [M^+]: *m/z* calcd: 324.1179 for $[C_{20}H_{20}O_2S]^+$, found: 324.1179.

R_f (SiO_2, *i*Hex/EtOAc = 98/2) = 0.42.

2-(1-(2-Methoxyphenyl)-2,2-dimethylpropylidene)benzo[*b*]thiophen-3(2*H*)-one-1-oxide (**1**)

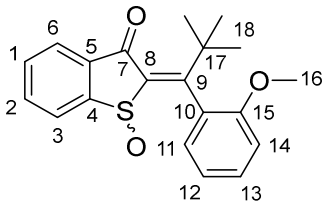

2-(1-(2-Methoxyphenyl)-2,2-dimethylpropylidene)benzo[*b*]thiophen-3(2*H*)-one (**5**, 0.55 mmol 1.0 equiv.) was dissolved in acetic acid (10 mL). Sodium perborate (0.60 mmol, 1.1 equiv.) was added and the reaction mixture was stirred for 12 h at 23 °C. Subsequently, saturated sodium carbonate solution (15 mL) was added, the aqueous phase was extracted with dichloromethane (3 x 20 mL) and the combined organic phases were dried over Na_2SO_4. After removing the solvent *in vacuo*, the crude product was purified by column chromatography (SiO_2, *i*Hex/EtOAc = 1/1) as yellow solid (182 mg, 0.53 mmol, 97%) as a mixture of four isomers. These isomers could be separated by column chromatography in the dark (SiO_2, *i*Hex/EtOAc = 6/4) and were subsequently purified further by individual crystallization from *n*heptane/dichloromethane.

A-1

^{1}H NMR (600 MHz, CD_2Cl_2) δ = 7.97 (dt, ^3J(H,H) = 7.7, ^4J(H,H) = 1.0 Hz, 1H, H-C(6)), 7.83 – 7.77 (m, 2H, H-C(2), H-C(3)), 7.71 (ddd, ^3J(H,H) = 7.7, ^3J(H,H) = 6.4, ^4J(H,H) = 2.0 Hz, 1H, H-C(1)), 7.44 (ddd, ^3J(H,H) = 8.4, ^3J(H,H) = 7.2, ^4J(H,H) = 2.0 Hz, 1H, H-C(13)), 7.08 – 7.01 (m, 2H, H-C(11), H-C(12)), 6.99 (d, ^3J(H,H) = 8.4 Hz, 1H, H-C(14)), 3.81 (s, 3H, H-C(16)), 1.37 (s, 9H, H-C(18)) ppm.

^{13}C NMR (150 MHz, CD_2Cl_2) δ = 185.1 (C(7)), 180.2 (C(9)), 157.6 (C(15)), 149.0 (C(4)), 143.6 (C(8)), 136.7 (C(5)), 136.1 (C(2)), 133.1 (C(1)), 130.8 (C(10)), 130.6 (C(13)), 128.0 (C(11)), 127.5 (C(3)), 126.4 (C(6)), 120.7 (C(12)), 111.5 (C(14)), 56.0 (C(16)), 40.1 (C(17)), 28.8 (C(18)) ppm.

IR $\tilde{\nu}$ (cm^{-1}) = 1683 (vs), 1653 (w), 1591 (m), 1580 (m), 1551 (s), 1488 (s), 1457 (m), 1433 (m), 1392 (w), 1360 (w), 1274 (m), 1258 (s), 1221 (s), 1161 (w), 1117 (m), 1072 (m), 1044 (s), 1023 (m), 955 (m), 930 (w), 820 (w), 752 (vs), 703 (w), 678 (m), 609 (m).

Melting point: 134 °C.

R_f (SiO_2, *i*Hex/EtOAc = 1/1) = 0.15.

B-1

^{1}H NMR (600 MHz, CD_2Cl_2) δ = 7.96 (dt, ^{3}J(H,H) = 7.7, 1.0 Hz, 1H, H-C(6)), 7.81 – 7.76 (m, 2H, H-C(2), H-C(3)), 7.71 (ddd, ^{3}J(H,H) = 7.7, ^{3}J(H,H) = 6.3, ^{4}J(H,H) = 2.1 Hz, 1H, H-C(1)), 7.44 (ddd, ^{3}J(H,H) = 8.4, ^{3}J(H,H) = 7.4, ^{4}J(H,H) = 1.8 Hz, 1H, H-C(13)), 7.13 (dd, ^{3}J(H,H) = 7.4, ^{4}J(H,H) = 1.8 Hz, 1H, H-C(11)), 7.07 (td, ^{3}J(H,H) = 7.4, ^{4}J(H,H) = 1.0 Hz, 1H, H-C(12)), 7.01 (dd, ^{3}J(H,H) = 8.4, ^{4}J(H,H) = 0.9 Hz, 1H, H-C(14)), 3.78 (s, 3H, H-C(16)), 1.33 (s, 9H, H-C(18)) ppm.

^{13}C NMR (150 MHz, CD_2Cl_2) δ = 186.6 (C(7)), 179.0 (C(9)), 155.6 (C(15)), 148.8 (C(4)), 142.9 (C(8)), 136.6 (C(5)), 136.3 (C(2)), 133.2 (C(1)), 130.7 (C(11)), 130.6 (C(13)), 129.3 (C(10)), 127.6 (C(3)), 126.7 (C(6)), 120.2 (C(12)), 111.0 (C(14)), 55.9 (C(16)), 39.8 (C(17)), 29.3 (C(18)) ppm.

IR $\tilde{\nu}$ (cm^{-1}) = 1686 (vs), 1653 (w), 1616 (w), 1592 (m), 1580 (m), 1557 (m), 1521 (w), 1506 (w), 1487 (m), 1457 (m), 1435 (w), 1419 (w), 1393 (w), 1361 (w), 1321 (w), 1274 (m), 1255 (m), 1236 (m), 1220 (s), 1162 (w), 1118 (m), 1067 (m), 1038 (s), 955 (m), 930 (w), 851 (w), 820 (w), 800 (w), 752 (vs), 720 (w), 704 (m), 679 (m), 667 (w), 607 (w).

Melting point: 183 °C.

R_f (SiO_2, *i*Hex/EtOAc = 1/1) = 0.21.

C-1

^{1}H NMR (600 MHz, CD_2Cl_2) δ = 8.02 (dt, ^{3}J(H,H) = 7.8, ^{4}J(H,H) = 0.8 Hz, 1H, H-C(3)), 7.84 (t, ^{3}J(H,H) = 8.4 Hz, 1H, H-C(2)), 7.75 (dt, ^{3}J(H,H) = 8.0, ^{4}J(H,H) = 0.9 Hz, 1H, H-C(6)), 7.67 (td, ^{3}J(H,H) = 7.5, ^{4}J(H,H) = 1.0 Hz, 1H, H-C(1)), 7.37 (ddd, ^{3}J(H,H) = 8.3, ^{3}J(H,H) = 7.4, ^{4}J(H,H) = 1.7 Hz, 1H, H-C(13)), 7.00 (td, ^{3}J(H,H) = 7.5, ^{4}J(H,H) = 1.0 Hz, 1H, H-C(12)), 6.95 (dd, ^{3}J(H,H) = 8.3, ^{4}J(H,H) = 1.0 Hz, 1H, H-C(14)), 6.90 (dd, ^{3}J(H,H) = 7.4, ^{4}J(H,H) = 1.7 Hz, 1H, H-C(11)), 3.73 (s, 3H, H-C(16)), 1.46 (s, 9H, H-C(18)) ppm.

^{13}C NMR (150 MHz, CD_2Cl_2) δ = 185.5 (C(7)), 175.1 (C(9)), 156.3 (C(15)), 148.4 (C(4)), 140.0 (C(8)), 136.3 (C(2)), 134.7 (C(5)), 133.2 (C(1)), 130.1 (C(10)), 129.2 (C(13)), 127.5 (C(3)), 126.9 (C(11)), 126.2 (C(6)), 120.9 (C(14)), 110.7 (C(12)), 55.8 (C(16)), 41.1 (C(17)), 30.2 (C(18)) ppm.

IR $\tilde{\nu}$ (cm^{-1}) = 1691 (s), 1593 (w), 1551 (m), 1487 (m), 1463 (m), 1451 (m), 1433 (m), 1393 (w), 1360 (w), 1274 (m), 1256 (w), 1227 (m), 1115 (s), 1072 (m), 1057 (m), 1023 (s), 933 (w), 863 (w), 828 (w), 801 (w), 777 (w), 753 (vs), 700 (m), 675 (m).

Melting point: 145 °C.

R_f (SiO_2, *i*Hex/EtOAc = 1/1) = 0.42.

D-1

^{1}H NMR (800 MHz, CD_2Cl_2) δ = 8.00 (d, ^{3}J(H,H) = 7.7 Hz, 1H, H-C(3)), 7.84 (t, ^{3}J(H,H) = 7.8 Hz, 1H, H-C(2)), 7.74 (d, ^{3}J(H,H) = 7.6 Hz, 1H, H-C(1)), 7.68 (t, ^{3}J(H,H) = 7.4 Hz, 1H, H-C(6)), 7.36 (t, ^{3}J(H,H) = 7.5 Hz, 1H, H-C(13)), 7.00 (d, ^{3}J(H,H) = 8.1 Hz, 1H, H-C(14)), 6.94 (t, ^{3}J(H,H) = 7.5 Hz, 1H, H-C(12)), 6.68 (d, ^{3}J(H,H) = 8.8 Hz, 1H, H-C(11)), 3.82 (s, 3H, H-C(16)), 1.45 (s, 9H, H-C(18)) ppm.

^{13}C NMR (200 MHz, CD_2Cl_2) δ = 187.5 (C(7)), 174.6 (C(9)), 156.5 (C(15)), 148.4 (C(4)), 139.5 (C(8)), 136.4 (C(2)), 134.3 (C(5)), 133.4 (C(6)), 130.1 (C(10)), 129.3 (C(13)), 127.5 (C(3)), 126.5 (C(11)), 126.4 (C(1)), 120.8 (C(12)), 111.0 (C(14)), 56.0 (C(16)), 40.9 (C(17)), 31.4 (C(18)) ppm.

IR $\tilde{\nu}$ (cm^{-1}) = 1693 (s), 1580 (w), 1556 (m), 1488 (m), 1451 (m), 1430 (w), 1364 (w), 1325 (w), 1276 (m), 1253 (m), 1221 (s), 1200 (w), 1176 (w), 1156 (w), 1116 (m), 1057 (w), 1044 (w), 1026 (vs), 996 (m), 928 (w), 865 (w), 848 (w), 829 (w), 801 (w), 779 (w), 755 (vs), 722 (w), 702 (m), 677 (m), 655 (m).

Melting point: 192 °C.

R_f (SiO_2, *i*Hex/EtOAc = 1/1) = 0.31.

For all isomers:

HRMS (EI^+), [M^+]: *m/z* calcd: 340.1122 for $[C_{20}H_{20}O_3S]^+$, found: 340.1126.

Elemental analysis: calcd (%) for $C_{20}H_{20}O_3S$: C 70.56, H 5.92, S 9.42; found: C 70.26, H 5.85, S 9.49.

Physical and photophysical properties

Thermal atropisomerizations A to B and C to D

NMR tubes were charged with 0.8 mg to 2.5 mg of respective isomer **A**, **B**, **C**, or **D** and 0.7 mL of deuterated solvent. Subsequent heating was carried out in amberized NMR tubes at 82 °C or 100 °C. Kinetics were followed by ^{1}H NMR measurements at defined time intervals. The equilibrium concentrations of isomers after prolonged heating were obtained from integration of the corresponding signals in the ^{1}H NMR spectrum.

At 82 °C or 100 °C only the atropisomerizations between **A** and **B** and between **C** and **D** proceed. The thermal atropisomerizations follow unimolecular first order reactions and proceed towards an equilibrium composition with both atropisomers present, according to Supplementary Equation 1 and Supplementary Equation 2, respectively:

$$\ln\left(\frac{[\mathbf{A}]_{t_0}-[\mathbf{A}]_{eq}}{[\mathbf{A}]_t-[\mathbf{A}]_{eq}}\right) = (k_{\mathbf{A/B}} + k_{\mathbf{B/A}})t \qquad \text{(Supplementary Equation 1)}$$

$$\ln\left(\frac{[\mathbf{C}]_{t_0}-[\mathbf{C}]_{eq}}{[\mathbf{C}]_t-[\mathbf{C}]_{eq}}\right) = (k_{\mathbf{C/D}} + k_{\mathbf{D/C}})t \qquad \text{(Supplementary Equation 2)}$$

with [**A** or **C**]$_{t_0}$ being the initial concentration of the isomers **A** or **C** at the time t = 0, [**A** or **C**]$_{eq}$ being the concentration of the isomers **A** or **C** at equilibrium, [**A** or **C**]$_t$ representing the concentration of the isomers **A** or **C** at specific times in the measurement t, $k_{\mathbf{A/B}}$ being the rate constant k of the **A** to **B** conversion, $k_{\mathbf{B/A}}$ being the rate constant k of the **B** to **A** conversion, $k_{\mathbf{C/D}}$ being the rate constant k of the **C** to **D** conversion, $k_{\mathbf{D/C}}$ being the rate constant k of the **D** to **C** conversion, and t being the elapsed time. When plotting the logarithmic left part of Supplementary Equation 1 or Supplementary Equation 2 versus time t, the obtained slope m contains rate constants for both proceeding atropisomerization reactions. The rate constants $k_{\mathbf{A/B}}$ and $k_{\mathbf{C/D}}$ can be calculated according to Supplementary Equation 3 and Supplementary Equation 4:

$$k_{\mathbf{A/B}} = \frac{m}{1+\frac{[\mathbf{A}]_{eq}}{[\mathbf{B}]_{eq}}} \qquad \text{(Supplementary Equation 3)}$$

$$k_{\mathbf{C/D}} = \frac{m}{1+\frac{[\mathbf{C}]_{eq}}{[\mathbf{D}]_{eq}}} \qquad \text{(Supplementary Equation 4)}$$

If the corresponding laws of mass action (Supplementary Equation 5 and Supplementary Equation 6) are taken into account:

$$\frac{[\mathbf{A}]_{eq}}{[\mathbf{B}]_{eq}} = \frac{k_{\mathbf{B/A}}}{k_{\mathbf{A/B}}} \qquad \text{(Supplementary Equation 5)}$$

$$\frac{[\mathbf{C}]_{eq}}{[\mathbf{D}]_{eq}} = \frac{k_{\mathbf{D/C}}}{k_{\mathbf{C/D}}} \qquad \text{(Supplementary Equation 6)}$$

Likewise the reverse rate constants are defined and could be determined from separate measurements starting from the opposite pure isomers **B** and **D** and application of Supplementary Equation 7 to Supplementary Equation 10, respectively.

$$\ln\left(\frac{[\mathbf{B}]_{t_0} - [\mathbf{B}]_{eq}}{[\mathbf{B}]_t - [\mathbf{B}]_{eq}}\right) = (k_{\mathbf{A/B}} + k_{\mathbf{B/A}})t \qquad \text{(Supplementary Equation 7)}$$

$$\ln\left(\frac{[\mathbf{D}]_{t_0} - [\mathbf{D}]_{eq}}{[\mathbf{D}]_t - [\mathbf{D}]_{eq}}\right) = (k_{\mathbf{C/D}} + k_{\mathbf{D/C}})t \qquad \text{(Supplementary Equation 8)}$$

$$k_{\mathbf{B/A}} = \frac{m}{1 + \frac{[\mathbf{B}]_{eq}}{[\mathbf{A}]_{eq}}} \qquad \text{(Supplementary Equation 9)}$$

$$k_{\mathbf{D/C}} = \frac{m}{1 + \frac{[\mathbf{D}]_{eq}}{[\mathbf{C}]_{eq}}} \qquad \text{(Supplementary Equation 10)}$$

$$\Delta G^{\ddagger} = \ln\left(\frac{k * h}{k_{\mathbf{B}} * T}\right) * R * T \qquad \text{(Supplementary Equation 11)}$$

By using the *Eyring* equation (Supplementary Equation 11) the free activation enthalpies ΔG^{*} can be calculated from the rate constants $k_{\mathbf{A/B}}$ to $k_{\mathbf{D/C}}$ for the corresponding reaction. The obtained free activation enthalpies ΔG^{*} for the thermal atropisomerizations between **A** to **B** as well as **C** to **D** and *vice versa* in $(CDCl_2)_2$ and the corresponding half-lives at 25 °C are given in Supplementary Table 1 together with the equilibrium atropisomer compositions obtained at high temperatures.

From these measurements we could quantify the ground state energy profile of hemithioindigo **1**. As we did not observe any thermal double-bond isomerizations over the course of several hours at temperatures >100 °C a lower limit for the energy barriers could be given, which are at least 30 kcal/mol high for each double-bond isomerization. The equilibrium atropisomer compositions at high temperatures deliver the thermodynamic energy differences between the corresponding states (red Δ values in Supplementary Figure 9) according to the relation of the change of *Gibbs* free energy and the equilibrium constant $-\Delta G = R \cdot T \cdot \ln K$

(see also Supplementary Table 1). The theoretical values are in good agreement with the experimentally determined ones.

Photoconversion of A, B, C, and D determined by quantum yield measurements

The photochemical quantum yield of the different photoconversion reactions ϕ were calculated as the ratio between the numbers of isomerized molecules *n*(molecules isomerized) and the number of absorbed photons *n*(*hv*) according to Supplementary Equation 12:

$$\phi = \frac{n(\text{molecules isomerized})}{n(hv)} \qquad \text{(Supplementary Equation 12)}$$

To determine the quantum yields ϕ, a sample with known concentration (3.0 mM) of each pure isomer **A**, **B**, **C**, or **D** in benzene-d_6 was irradiated with a focused light beam of a 405 nm LED within the published instrumental setup from the group of *E. Riedle*.[2] The number of absorbed photons over time *n*(*hv*) was measured directly at the thermal photometer of the instrument according to Supplementary Equation 13:

$$n(hv) = \frac{\Delta P \cdot \lambda_{ex} \cdot t}{c \cdot h} \qquad \text{(Supplementary Equation 13)}$$

Where c is the speed of light ($2.99792 \cdot 10^8$ m·s^{-1}), h is Planck's constant ($6.62607 \cdot 10^{-34}$ J·s), λ_{ex} is the excitation wavelength in m, t is the elapsed time during irradiation, and ΔP is the difference in power read-outs at the thermal photometer between a solvent filled cuvette (P_0) and a cuvette containing the sample solution (P_t) during the irradiation period in Watt (Supplementary Equation 14). The power read out during irradiation did not change substantially (<5%) over the irradiation periods.

$$\Delta P = P_t - P_0 \qquad \text{(Supplementary Equation 14)}$$

Since more than one photoproduct is formed during irradiation, the number of each type of photoconverted molecules *n*(molecules isomerized) was determined by ^{1}H NMR spectroscopy directly after the irradiation step. Multiple measurements with increasing time of irradiation were conducted and the obtained ϕ values were averaged. The amount of isomerized molecules was also plotted against irradiation time showing linear

behavior over measurement periods up to 30 min in case of **A**, **B**, and **C** (Supplementary Figure 14 - 16). Therefore, the quantum yield measurements conform to initial-slope behavior, where only the initial isomer is photoconverted but not the photoproducts. The photoconversion of **D** did not conform very well to linear behavior (Supplementary Figure 17). Nevertheless, the initial slope assumption gave good starting points for the comprehensive analysis of all quantum yields ϕ using a rate matrix as described below.

For hemithioindigo **1** the rate of an individual phototransition e.g. **A** to **B**, depends on all other absorbing species present at the same time and is described by the corresponding rate matrix element $r_{\mathbf{A/B}}$ (Supplementary Equation 15):

$$r_{\mathbf{A/B}} = \phi_{\mathbf{A/B}} \cdot I_0 \cdot \varepsilon_{\mathbf{A}} \cdot d \cdot [\mathbf{A}] \cdot \left(\frac{1 - e^{-d \sum_i \varepsilon_i \cdot [i]}}{d \sum_i \varepsilon_i \cdot [i]} \right) \qquad \text{(Supplementary Equation 15)}$$

Likewise every phototransition from isomer **i** to isomer **j** can be written as:

$$r_{\mathbf{i/j}} = \phi_{\mathbf{i/j}} \cdot I_0 \cdot \varepsilon_{\mathbf{i}} \cdot d \cdot [\mathbf{i}] \cdot \left(\frac{1 - e^{-d \sum_i \varepsilon_i \cdot [i]}}{d \sum_i \varepsilon_i \cdot [i]} \right) \qquad \text{(Supplementary Equation 16)}$$

with $\phi_{\mathbf{i/j}}$ = photoisomerization quantum yield for the phototransition of **i** to **j**, I_0 the photon flux (Einstein L^{-1} s^{-1}) of the light, $\varepsilon_{\mathbf{i}}$ the molar absorption coefficient of **i** at the wavelength of irradiation, d the pathlength of the light through the sample, [**i**] the concentration of **i**, $\varepsilon_{\mathbf{i}}$ the molar absorption coefficient of species **i**. The corresponding rate matrix containing all possible rates $r_{\mathbf{i/j}}$ for the transitions of isomers **i** into isomers **j** for hemithioindigo **1** is therefore written as:

$$M_1 = \begin{array}{c} \begin{matrix} \mathbf{A} & \mathbf{B} & \mathbf{C} & \mathbf{D} \end{matrix} \\ \begin{pmatrix} r_{A/A} & r_{A/B} & r_{A/C} & r_{A/D} \\ r_{B/A} & r_{B/B} & r_{B/C} & r_{B/D} \\ r_{C/A} & r_{C/B} & r_{C/C} & r_{C/D} \\ r_{D/A} & r_{D/B} & r_{D/C} & r_{D/D} \end{pmatrix} \end{array} \begin{matrix} \mathbf{A} \\ \mathbf{B} \\ \mathbf{C} \\ \mathbf{D} \end{matrix} \qquad \text{(Supplementary Equation 17)}$$

Matrix M_1 (Supplementary Equation 17) describes all possible photoconversions quantitatively, but each element is a nonlinear differential equation dependent on the other elements at a given time, which makes an analytical solution impossible.

We have used the different rate elements $r_{i/j}$ in the rate matrix M_1 to simulate our quantum yield measurements. For every incremental irradiation step (Δt) we have used the following expressions (Supplementary Equation 18 - 21) to achieve the corresponding next concentration of the respective isomer:

$$[A]_{t+1} = [A]_t - r_{A/B}\Delta t - r_{A/C}\Delta t - r_{A/D}\Delta t + r_{B/A}\Delta t + r_{C/A}\Delta t + r_{D/A}\Delta t \quad \text{(Supplementary Equation 18)}$$

$$[B]_{t+1} = [B]_t - r_{B/A}\Delta t - r_{B/C}\Delta t - r_{B/D}\Delta t + r_{A/B}\Delta t + r_{C/B}\Delta t + r_{D/B}\Delta t \quad \text{(Supplementary Equation 19)}$$

$$[C]_{t+1} = [C]_t - r_{C/A}\Delta t - r_{C/B}\Delta t - r_{C/D}\Delta t + r_{A/C}\Delta t + r_{B/C}\Delta t + r_{D/C}\Delta t \quad \text{(Supplementary Equation 20)}$$

$$[D]_{t+1} = [D]_t - r_{D/A}\Delta t - r_{D/B}\Delta t - r_{D/C}\Delta t + r_{A/D}\Delta t + r_{B/D}\Delta t + r_{C/D}\Delta t \quad \text{(Supplementary Equation 21)}$$

Since every component of $r_{i/j}$ (Supplementary Equation 16) is known from our experiment except for the quantum yields ϕ_{ij} the latter can be obtained from the best fit to the rate model M_1 (Supplementary Equation 17). To this end we have started the simulation with experimental quantum yield values obtained from the initial slope analyses described above. 10,000 incremental time points were used in the simulations and the quantum yields were adjusted manually until an adequate match of experimental and simulated data were obtained. While the quantum yields of **A** and **B** obtained from the simulation were very similar to the ones obtained from the initial slope method (maximum ±2% deviation), the quantum yields of **C** and **D** were considerably improved by the simulation. This can clearly be seen by the much better description of the nonlinear photoconversions of **C** and **D** using the optimized quantum yields from the fitting simulation (Supplementary Figure 18).

Markov matrix analysis of the photoconversion of A, B, C, and D in different solvents

The photoconversions of pure **A**, **B**, **C**, and **D** in different solvents were determined by *in situ* irradiations within the NMR spectrometer at ambient temperature (exact temperatures are given in Supplementary Figures 20 - 43 for each experiment) while recording a ^{1}H NMR spectrum in short time intervals (typically several seconds) for prolonged overall times. For the *in situ* irradiations, a fiber-coupled LED setup from *Mightex* (UHP 405 nm LED) was used. To ensure very high reproducibility and comparability between individual experiments, the glass fiber was fixed to the NMR tubes in the same position for each irradiation and its light intensity kept constant. With this setup it is however not possible to determine the light pathlength *d*. The same concentrations (3 mM) of the pure initial isomer and the same solvent volumes were used as well.

The relative percentage of each isomer **A**, **B**, **C**, and **D** was then plotted against irradiation time for each pure starting isomer. These kinetic data were then simulated using an adjusted Markov matrix accounting for the different conversion probabilities per time increment (1 min in this case).

In general a Markov matrix describes the probabilities for different transitions of different states p(**ij**) within a given time increment. For a photoreaction the probabilities are directly proportional to the rate $r_{i/j}$ of the transition if all molar absorption coefficients are the same and therefore the kinetics are first order:

$$\mathrm{p}(\mathbf{ij}) = k_{\mathbf{i/j}} \cdot \Delta t = \frac{r_{i/j}}{[\mathbf{i}]} \cdot \Delta t = \frac{\phi_{i/j} \cdot I_0 \cdot \varepsilon_i \cdot d \cdot [\mathbf{i}] \cdot \left(\frac{1-e^{-d \sum_i \varepsilon_i \cdot [i]}}{d \sum_i \varepsilon_i \cdot [i]}\right)}{[\mathbf{i}]} \cdot \Delta t \qquad \text{(Supplementary Equation 22)}$$

Additionally we have to include the diagonal elements p(**ii**) describing the probability that no conversion occurs:

$$\mathrm{p}(\mathbf{ii}) = 1 - \sum_j \mathrm{p}(\mathbf{ij}) \qquad \text{(Supplementary Equation 23)}$$

Therefore, a Markov matrix can be written for hemithioindigo **1** in which the transition probabilities p(**ij**) are given:

$$M_2 = \begin{array}{c} \begin{array}{cccc} \mathbf{A} & \mathbf{B} & \mathbf{C} & \mathbf{D} \end{array} \\ \begin{pmatrix} \mathrm{p}(\mathbf{AA}) & \mathrm{p}(\mathbf{AB}) & \mathrm{p}(\mathbf{AC}) & \mathrm{p}(\mathbf{AD}) \\ \mathrm{p}(\mathbf{BA}) & \mathrm{p}(\mathbf{BB}) & \mathrm{p}(\mathbf{BC}) & \mathrm{p}(\mathbf{BD}) \\ \mathrm{p}(\mathbf{CA}) & \mathrm{p}(\mathbf{CB}) & \mathrm{p}(\mathbf{CC}) & \mathrm{p}(\mathbf{CD}) \\ \mathrm{p}(\mathbf{DA}) & \mathrm{p}(\mathbf{DB}) & \mathrm{p}(\mathbf{DC}) & \mathrm{p}(\mathbf{DD}) \end{pmatrix} \begin{array}{c} \mathbf{A} \\ \mathbf{B} \\ \mathbf{C} \\ \mathbf{D} \end{array} \end{array} \qquad \text{(Supplementary Equation 24)}$$

By plotting the relative isomer percentage against the elapsed time during irradiation, four different kinetic plots (starting from either pure **A**, **B**, **C**, or **D**) were obtained from the experiments. These plots show the changes in isomer composition over time during the irradiation. These experimental kinetics were then simulated via an iterative process in which a Markov matrix M_2 (Supplementary Equation 24) is multiplied with the corresponding isomer percentage vector for each time point (Supplementary Equation 25). The

product vector is then multiplied by the same Markov matrix to give the corresponding vector of the next time point:

$$\begin{pmatrix} \%\mathbf{A} \\ \%\mathbf{B} \\ \%\mathbf{C} \\ \%\mathbf{D} \end{pmatrix}_{t_{x+1}} = \begin{pmatrix} p(\mathbf{AA}) & p(\mathbf{AB}) & p(\mathbf{AC}) & p(\mathbf{AD}) \\ p(\mathbf{BA}) & p(\mathbf{BB}) & p(\mathbf{BC}) & p(\mathbf{BD}) \\ p(\mathbf{CA}) & p(\mathbf{CB}) & p(\mathbf{CC}) & p(\mathbf{CD}) \\ p(\mathbf{DA}) & p(\mathbf{DB}) & p(\mathbf{DC}) & p(\mathbf{DD}) \end{pmatrix} \cdot \begin{pmatrix} \%\mathbf{A} \\ \%\mathbf{B} \\ \%\mathbf{C} \\ \%\mathbf{D} \end{pmatrix}_{t_x}$$

(Supplementary Equation 25)

The elements of the Markov matrix in Supplementary Equation 24 were adjusted manually until the best match with the experimental data was obtained.

We conducted four independent irradiation experiments for each solvent starting from either pure **A**, **B**, **C**, or **D**. If it is possible to keep I_0, d, and the initial concentration of the pure isomer [**i**] constant and the same in every experiment and if also the molar absorption coefficients of all different isomers are the same at the irradiation wavelength the same Markov matrix can be used to describe all experiments. In this case Supplementary Equation 22 transforms into:

$$p(\mathbf{ij}) = \frac{\phi_{\mathbf{i/j}} \cdot I_0 \cdot \varepsilon_{\mathbf{i}} \cdot d \cdot [\mathbf{i}] \cdot \left(\frac{1-e^{-d\sum_i \varepsilon_i \cdot [i]}}{d\sum_i \varepsilon_i \cdot [i]}\right)}{[\mathbf{i}]} \cdot \Delta t = \phi_{\mathbf{i/j}} \cdot I_0 \cdot \varepsilon_{\mathbf{i}} \cdot d \cdot \left(\frac{1-e^{-d\sum_i \varepsilon_i \cdot [i]}}{d\sum_i \varepsilon_i \cdot [i]}\right) \cdot \Delta t = \phi_{\mathbf{i/j}} \cdot const \cdot \Delta t$$

(Supplementary Equation 26)

and only depends on the individual quantum yields $\phi_{\mathbf{i/j}}$.For benzene as solvent we were able to achieve a consistency high enough to be able to describe all four different isomers conversions with the same Markov matrix (see Supplementary Figure 20 - 23).

For all other solvents, different Markov matrices had to be used for each irradiation experiment of a different starting isomer **A**, **B**, **C**, or **D**. However, the relative ratios of off-diagonal elements in each row of the Markov matrix reproduce the relative ratios of the corresponding quantum yields ϕ according to Supplementary Equation 27 (exemplarily for the photoconversions of **A** to **B** and **C**):

$$\frac{p(\mathbf{AB})}{p(\mathbf{AC})} = \frac{\phi_{\mathbf{A/B}} \cdot I_0 \cdot \varepsilon_{\mathbf{A}} \cdot d \cdot \left(\frac{1-e^{-d\sum_i \varepsilon_i \cdot [i]}}{d\sum_i \varepsilon_i \cdot [i]}\right) \cdot \Delta t}{\phi_{\mathbf{A/C}} \cdot I_0 \cdot \varepsilon_{\mathbf{A}} \cdot d \cdot \left(\frac{1-e^{-d\sum_i \varepsilon_i \cdot [i]}}{d\sum_i \varepsilon_i \cdot [i]}\right) \cdot \Delta t} = \frac{\phi_{\mathbf{A/B}}}{\phi_{\mathbf{A/C}}}$$

(Supplementary Equation 27)

As can be seen from Supplementary Equation 26 the relative ratios of off-diagonal elements in each row of a Markov matrix directly correspond to the respective quantum yield ratios even if the molar absorption coefficients of different present isomers are different to each other (the sum expressions cancel each other out). As the matrix elements of one row correspond to one and the same experiment I_0, d, and the initial concentration of the pure isomer [**i**] are constant per se. Therefore, the relative ratios within one row of each Markov matrix have to be the same for all matrices.

Likewise the ratio of one off-diagonal probability to the sum of all off-diagonal probabilities within one row of the Markov matrix is related to the corresponding ratio of the quantum yields (exemplarily for the photoconversions of **A** to **B**, **C**, and **D**) giving the relative percentage of each process:

$$\text{rel. } \% = \frac{\mathrm{p}(\mathbf{AB})}{\mathrm{p}(\mathbf{AB})+\mathrm{p}(\mathbf{AC})+\mathrm{p}(\mathbf{AD})} = \frac{\phi_{\mathbf{A/B}}}{\phi_{\mathbf{A/B}}+\phi_{\mathbf{A/C}}+\phi_{\mathbf{A/D}}} \qquad \text{(Supplementary Equation 28)}$$

Additionally, the diagonal elements in the same Markov matrix can be compared at least qualitatively if the different molar absorptions coefficients ε_i are similar enough. This gives a qualitative assessment of the relative efficiencies of the overall photoconversions for each starting isomer. In the case of HTI **1** it is clear that isomers **A** and **B** are much more efficiently photoconverted than the isomers **C** and **D**, independent of the solvent.

All ratios determined from the irradiation experiments in different solvents are summarized in Supplementary Table 2.

In the solvent benzene-d_6 we could use the same Markov matrix for all four individual measurements (each corresponding to one individual row in the Markov matrix), which means that also ratios of quantum yields in different rows can be determined. The obtained ratios are in very good agreement with the ratios of the direct quantum yield measurements (see Supplementary Table 2). Absolute quantum yield values cannot be determined from the Markov matrix analysis since the exact values of I_0 and d are not known.

Calculated Ground State Energy Profile of Compound 1

A relaxed optimization of the four isomeric states and all four transition state structures of compound **1** at the B3LYP level of theory with the 6-311G(d,p) basis set has been conducted using the Gaussian09 Revision A.02 program package.[3] To account for solvent effects, the calculations have been carried out using the Polarizable Continuum Model (PCM) with dichloromethane parameters. The convergence criteria have been set tight and an ultrafine integration grid has been used. A following frequency analysis confirmed all four structures **A**-**1** (*Z*-(*S*)-(R_a)), **B**-**1** (*Z*-(*S*)-(S_a)), **C**-**1** (*E*-(*S*)-(R_a)), and **D**-**1** (*E*-(*S*)-(S_a)) to be minimum structures since no imaginary frequencies have been found. All other structures were shown to be first order saddle points on the potential energy surface since only one imaginary vibrational mode has been found, which confirmed them to be transition state structures.

Supplementary Figures

Determination of constitution and conformation in the crystalline state and in solution

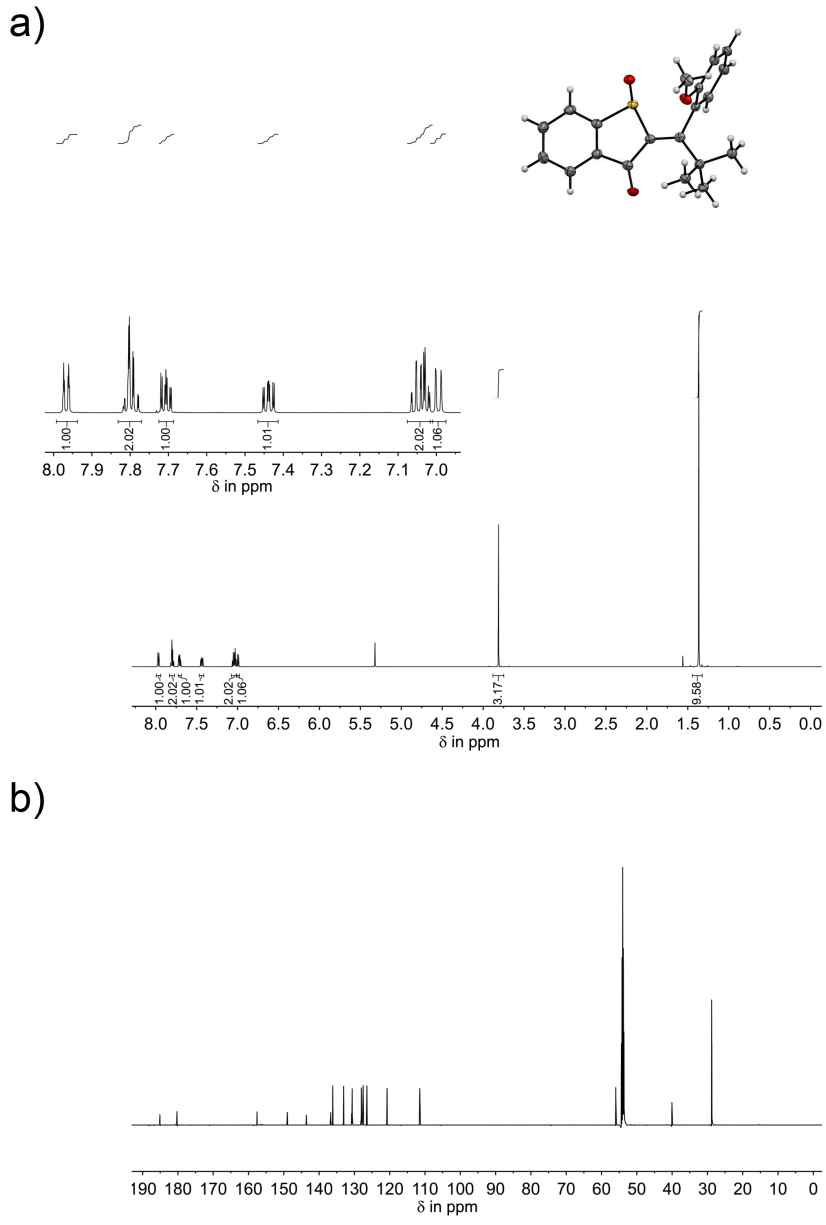

Supplementary Figure 1 | Structure assignment of A-1. a) Crystal structure of **A**-**1** and the corresponding ^{1}H NMR spectrum (CD_2Cl_2, 600 MHz, 27 °C) of the same crystal batch. The aromatic part of the spectrum is enlarged. The signals of only one single species are observed in the ^{1}H NMR spectrum, which could thus be directly assigned to the **A**-**1**. b) Corresponding ^{13}C NMR spectrum (CD_2Cl_2, 150 MHz, 27 °C).

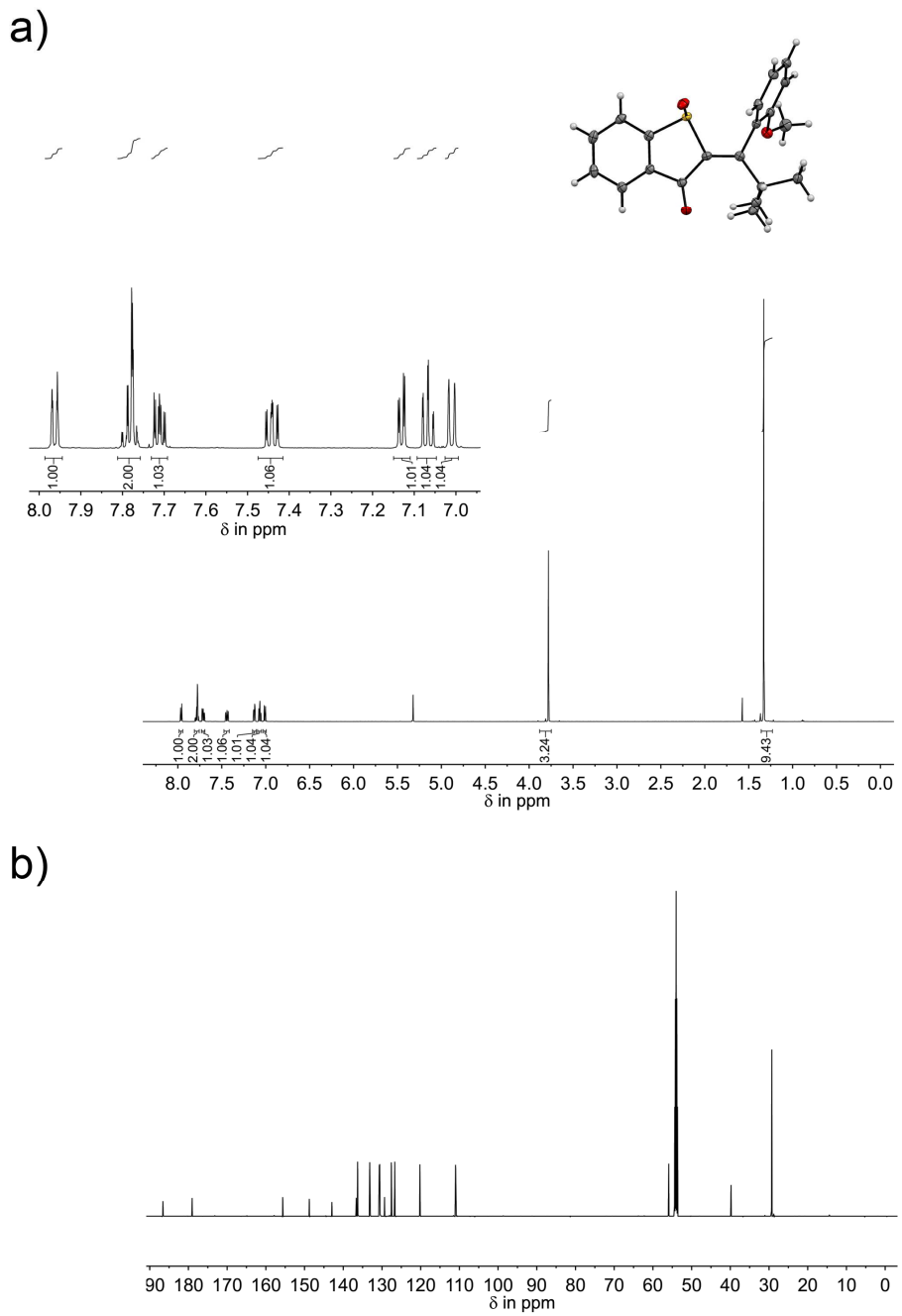

Supplementary Figure 2 | Structure assignment of B-1. a) Crystal structure of **B-1** and the corresponding ^{1}H NMR spectrum (CD_2Cl_2, 600 MHz, 27 °C) of the same crystal batch. The aromatic part of the spectrum is enlarged. The signals of only one single species are observed in the ^{1}H NMR spectrum, which could thus be directly assigned to the **B-1**. b) Corresponding ^{13}C NMR spectrum (CD_2Cl_2, 150 MHz, 27 °C).

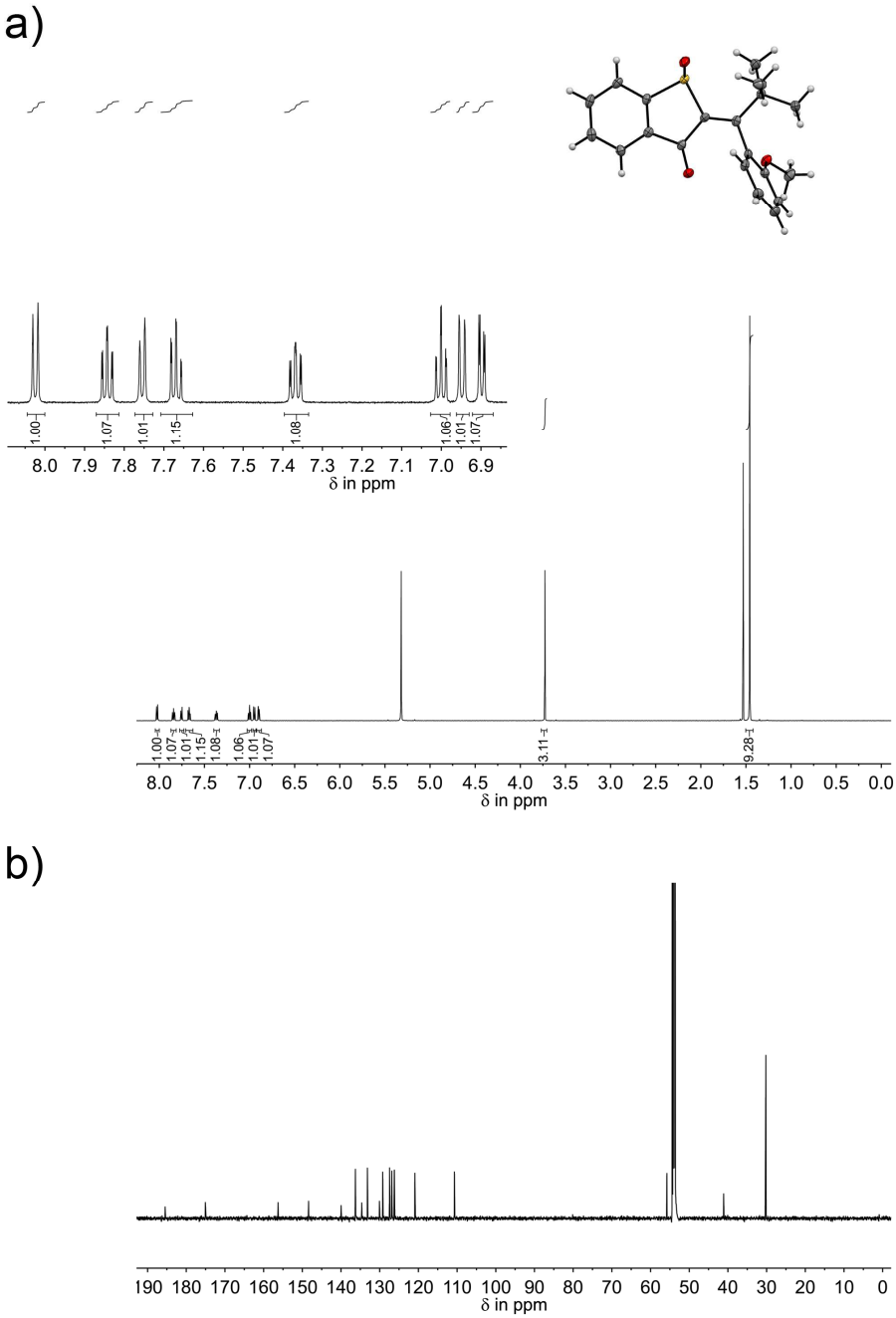

Supplementary Figure 3 | Structure assignment of C-1. a) Crystal structure of **C-1** and the corresponding ^{1}H NMR spectrum (CD_2Cl_2, 600 MHz, 27 °C) of the same crystal batch. The aromatic part of the spectrum is enlarged. The signals of only one single species are observed in the ^{1}H NMR spectrum, which could thus be directly assigned to the **C-1**. b) Corresponding ^{13}C NMR spectrum (CD_2Cl_2, 150 MHz, 27 °C).

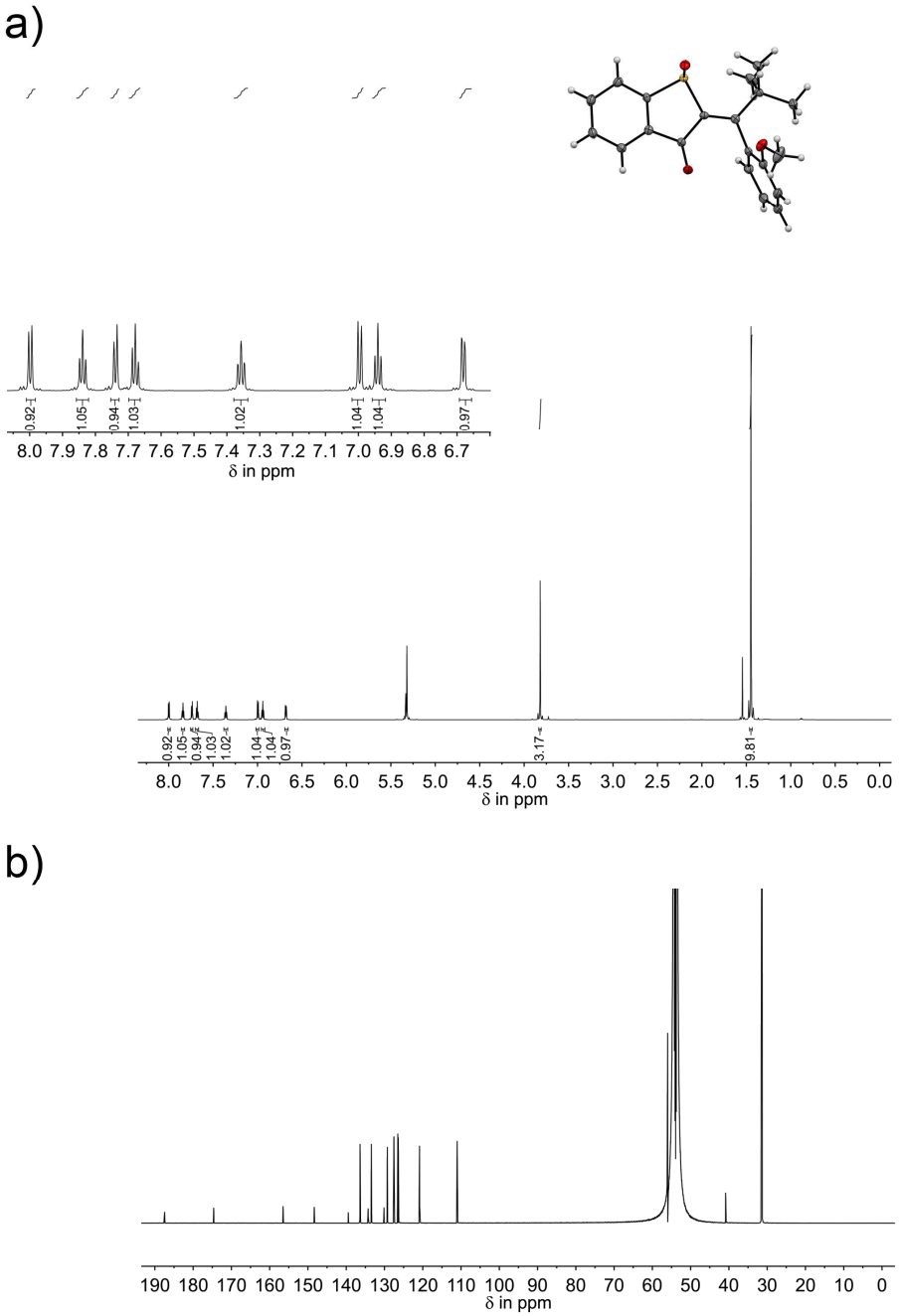

Supplementary Figure 4 | Structure assignment of D-1. a) Crystal structure of **D-1** and the corresponding ^{1}H NMR spectrum (CD_2Cl_2, 800 MHz, 25 °C) of the same crystal batch. The aromatic part of the spectrum is enlarged. The signals of only one single species are observed in the ^{1}H NMR spectrum, which could thus be directly assigned to the **D-1**. b) Corresponding ^{13}C NMR spectrum (CD_2Cl_2, 200 MHz, 25 °C).

Thermal atropisomerizations

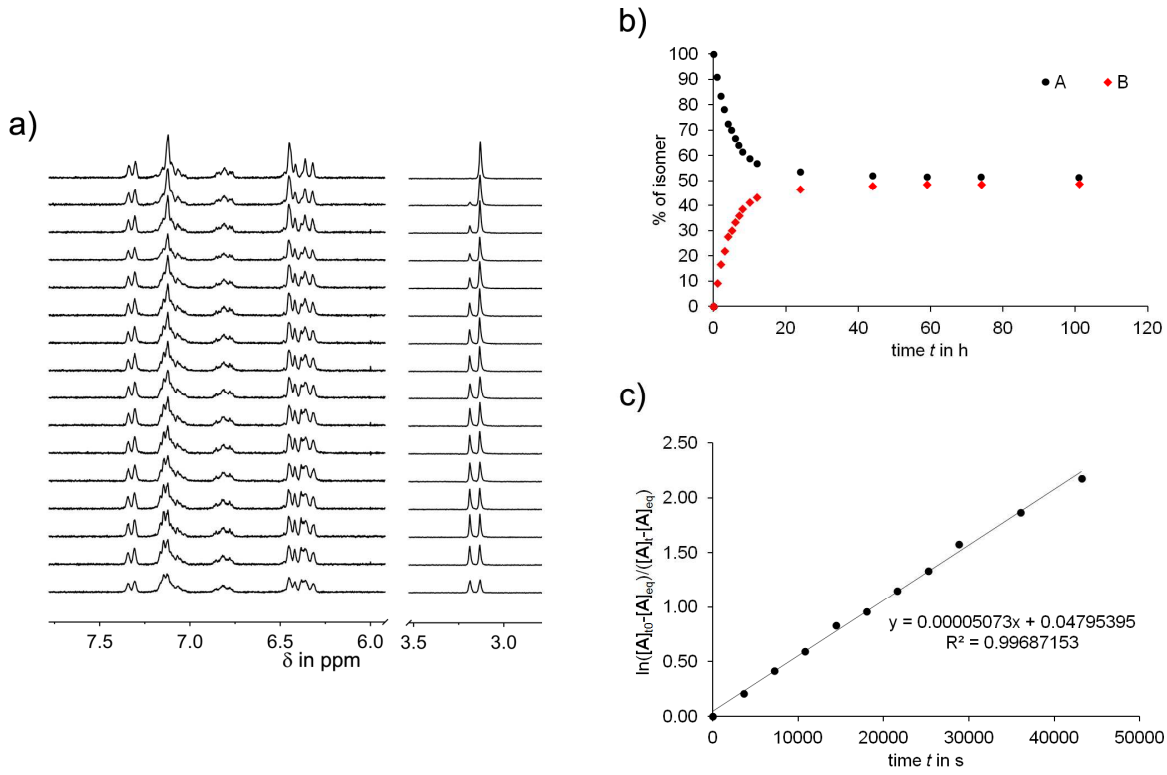

Supplementary Figure 5 | Thermal atropisomerization of A to B. a) Thermal atropisomerization of **A** to **B** in $(CDCl_2)_2$ at 82 °C followed by ^1H NMR spectroscopy (200 MHz, 25 °C) in regular time intervals . b) Atropisomer conversion over time. c) First order kinetic analysis of the thermal atropisomerization of **A** to **B**. Taking into account the dynamic equilibrium by plotting according to Supplementary Equation 1 gives a linear relationship. The slope *m* can be translated into the rate constants $k_{(\mathbf{A/B})}$ according to Supplementary Equation 3. The corresponding Gibbs energy of activation for the thermal **A** to **B** isomerization are given in Supplementary Table 1.

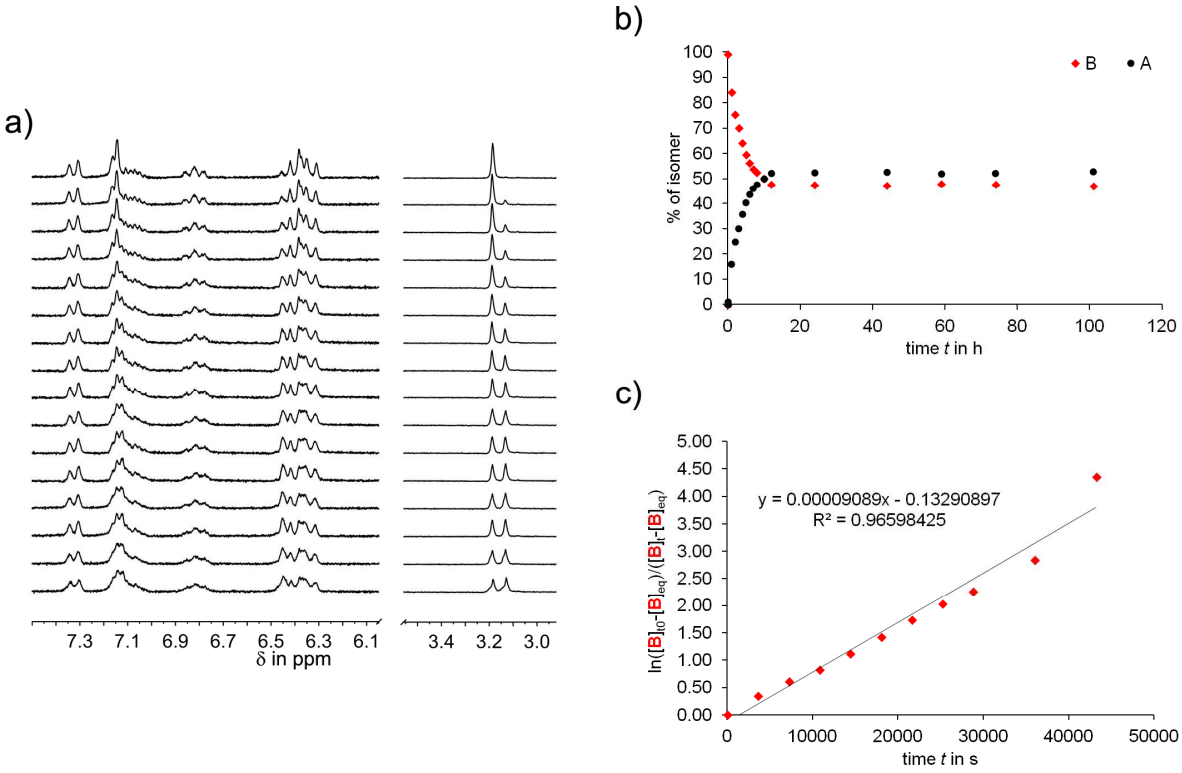

Supplementary Figure 6 | Thermal atropisomerization of B to A. a) Thermal atropisomerization of **B** to **A** in $(CDCl_2)_2$ at 82 °C followed by ^{1}H NMR spectroscopy (200 MHz, 25 °C) in regular time intervals. b) Atropisomer conversion over time. c) First order kinetic analysis of the thermal atropisomerization of **B** to **A**. Taking into account the dynamic equilibrium by plotting according to Supplementary Equation 7 gives a linear relationship. The slope *m* can be translated into the rate constants $k_{(\mathbf{B/A})}$ according to Supplementary Equation 9. The corresponding Gibbs energy of activation for the thermal **B** to **A** isomerization are given in Supplementary table 1.

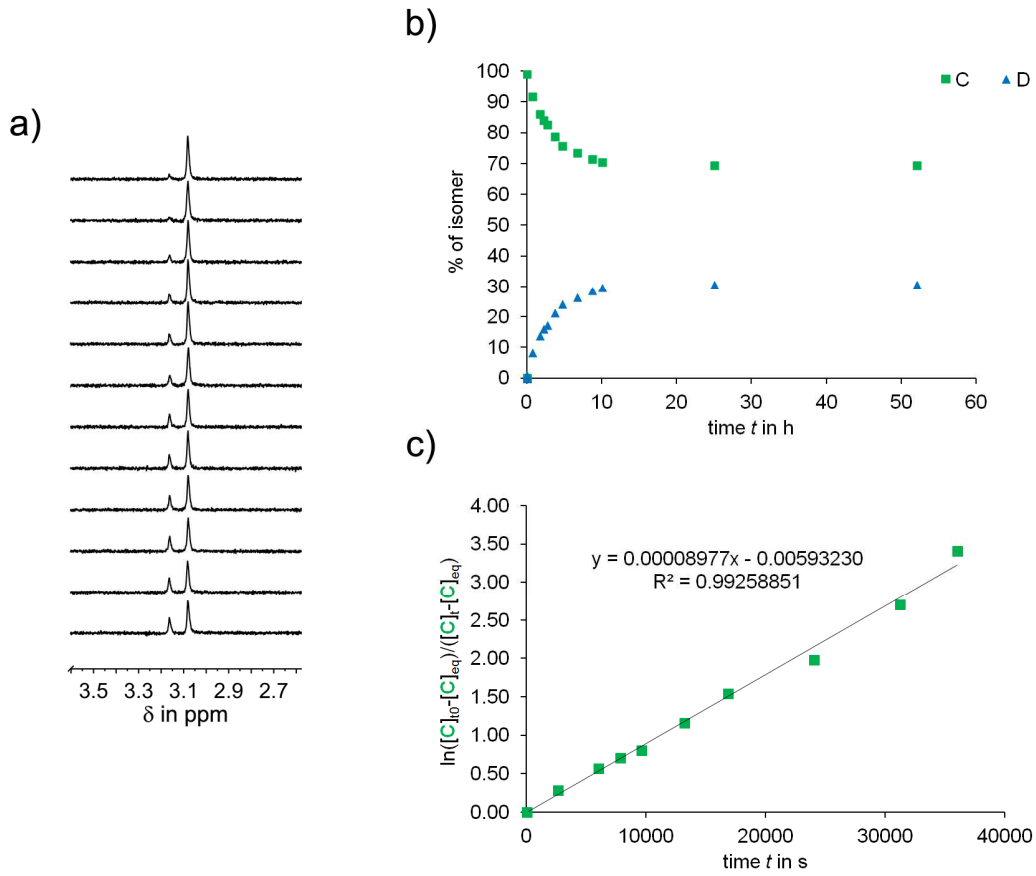

Supplementary Figure 7 | Thermal atropisomerization of C to D. a) Thermal atropisomerization of **C** to **D** in $(CDCl_2)_2$ at 100 °C followed by ^{1}H NMR spectroscopy (200 MHz, 25 °C) in regular time intervals. b) Atropisomer conversion over time. c) First order kinetic analysis of the thermal atropisomerization of **C** to **D**. Taking into account the dynamic equilibrium by plotting according to Supplementary Equation 2 gives a linear relationship. The slope *m* can be translated into the rate constants $k_{(\mathbf{C}/\mathbf{D})}$ according to Supplementary Equation 4. The corresponding Gibbs energy of activation for the thermal **C** to **D** isomerization are given in Supplementary Table 1.

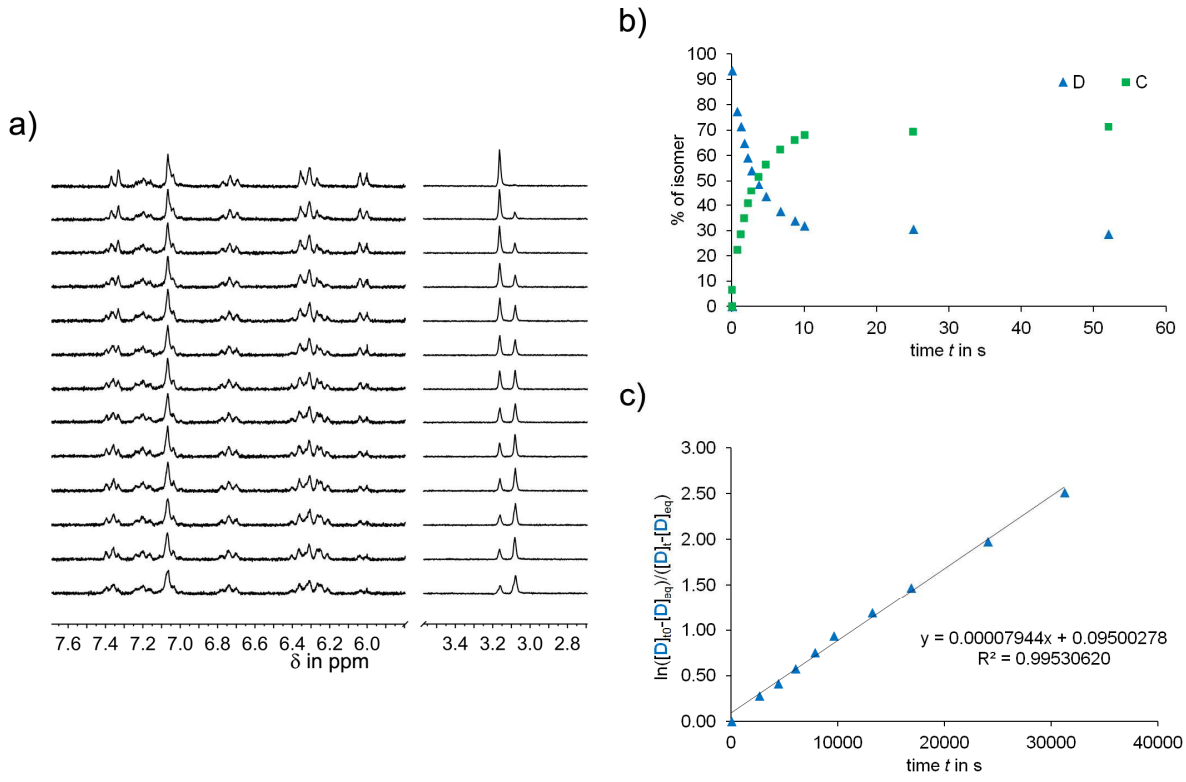

Supplementary Figure 8 | Thermal atropisomerization of D to C. a) Thermal atropisomerization of **D** to **C** in $(CDCl_2)_2$ at 100 °C followed by ^{1}H NMR spectroscopy (200 MHz, 25 °C) in regular time intervals. b) Atropisomer conversion over time. c) First order kinetic analysis of the thermal atropisomerization of **D** to **C**. Taking into account the dynamic equilibrium by plotting according to Supplementary Equation 8 gives a linear relationship. The slope *m* can be translated into the rate constants $k_{(\mathbf{D/C})}$ according to Supplementary Equation 10. The corresponding Gibbs energy of activation for the thermal **D** to **C** isomerization are given in Supplementary Table 1.

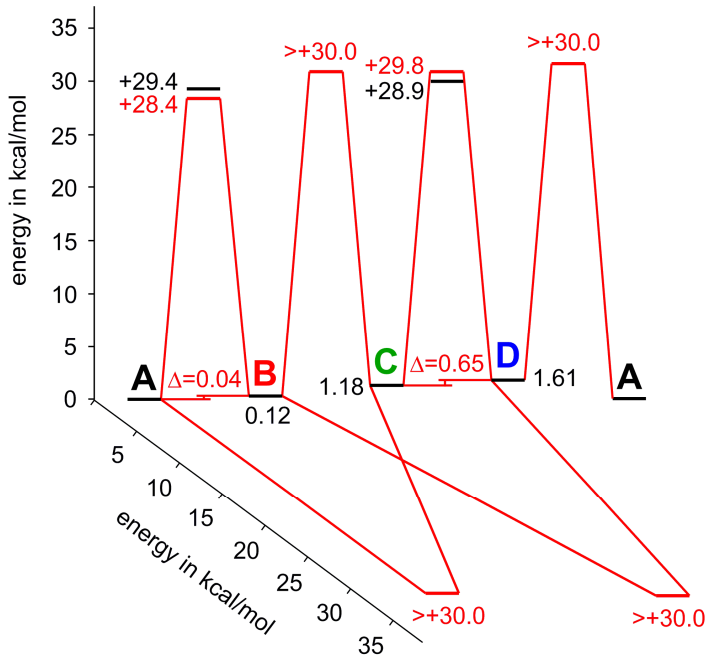

Supplementary Figure 9 | Ground state energy profile for 1. Thermal interconversion between the four different isomers **A** to **D** at ambient temperature is completely prevented by very high kinetic barriers. Black values are derived from quantum chemical calculations (B3LYP/6-311G(d,p)), red values were determined experimentally. The Δ values correspond to the experimentally determined $\Delta\Delta G^0$ values.

Molar absorption coefficients at room temperature

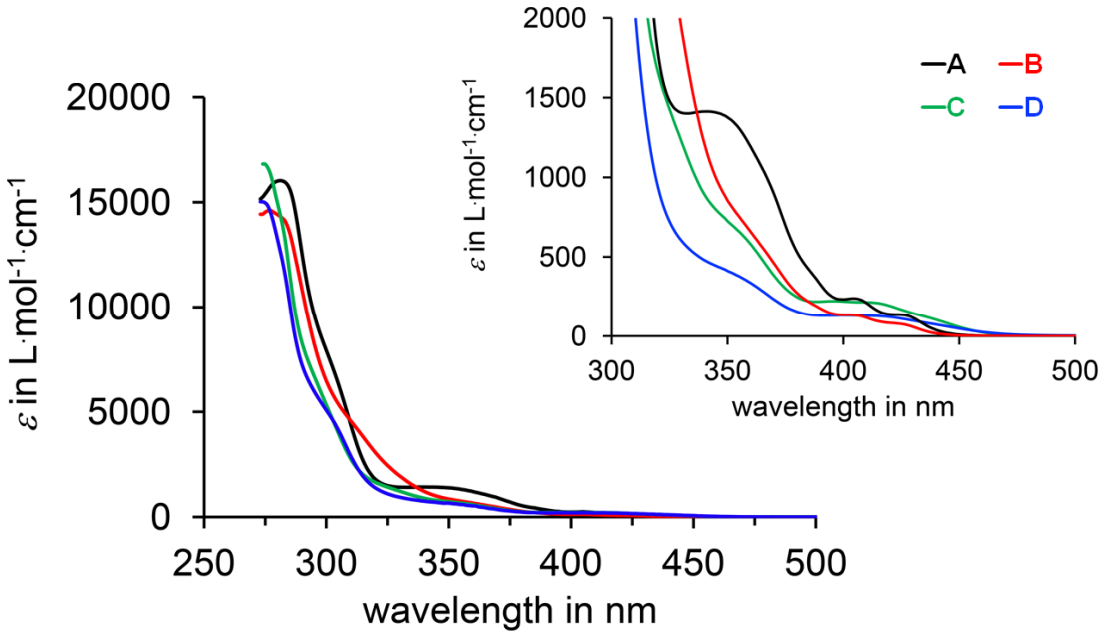

Supplementary Figure 10 | Molar absorption coefficients of 1. Molar absorption coefficients ε of **A** (black), **B** (red), **C** (green), and **D** (blue) at 23 °C in benzene solution.

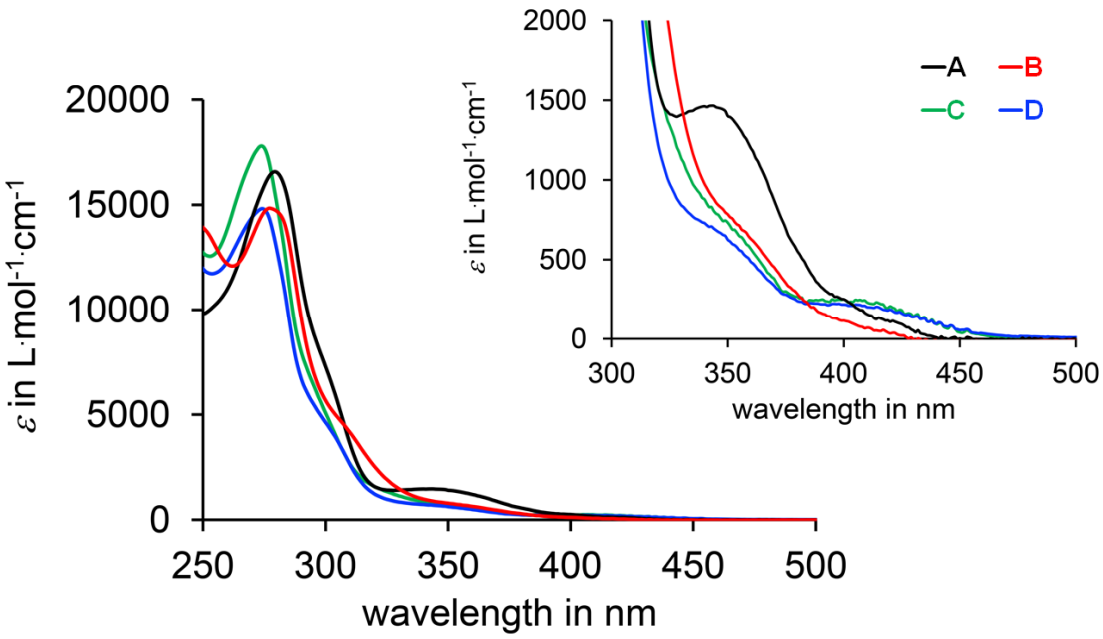

Supplementary Figure 11 | Molar absorption coefficients of 1. Molar absorption coefficients ε of **A** (black), **B** (red), **C** (green), and **D** (blue) at 23 °C in CH_2Cl_2 solution.

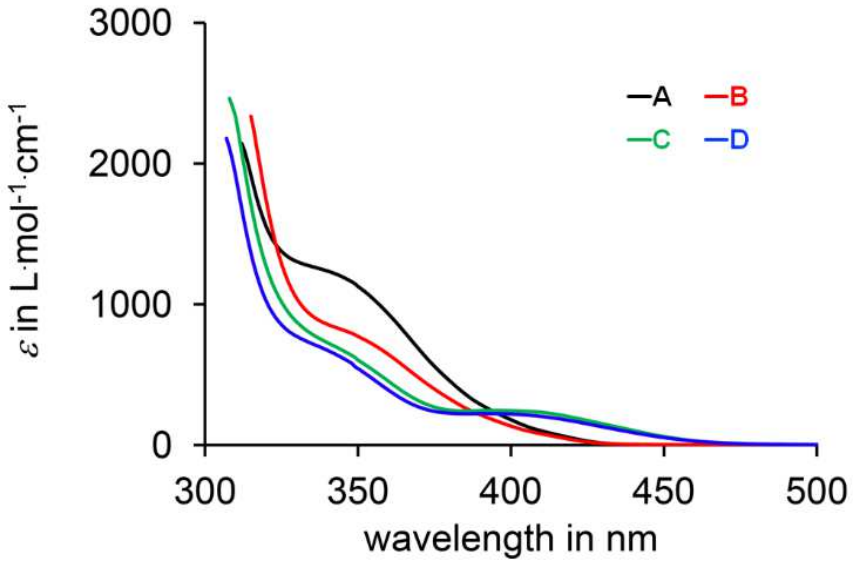

Supplementary Figure 12 | Molar absorption coefficients of 1. Molar absorption coefficients ε of **A** (black), **B** (red), **C** (green), and **D** (blue) at 23 °C in MeOH solution.

Molar absorption coefficients in EPA glass at 90 K

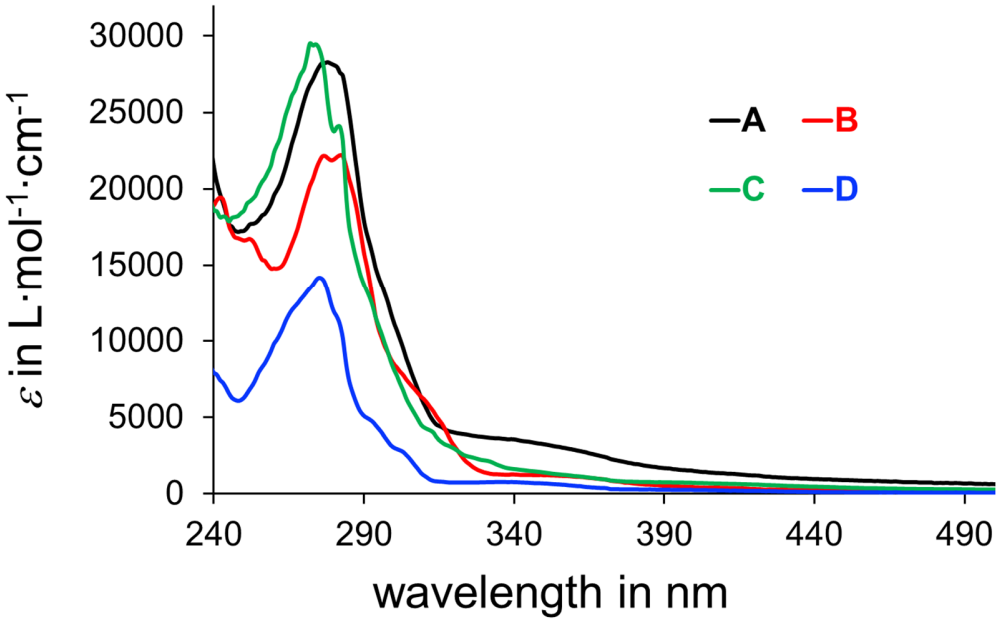

Supplementary Figure 13 | Molar absorption coefficients of 1. Molar absorption coefficients ε of **A** (black), **B** (red), **C** (green), and **D** (blue) in EPA glass (diethyl ether/*iso*pentane/ethanol 5:5:2) at 90 K.

Photoconversion of A, B, C, and D determined by quantum yield measurements

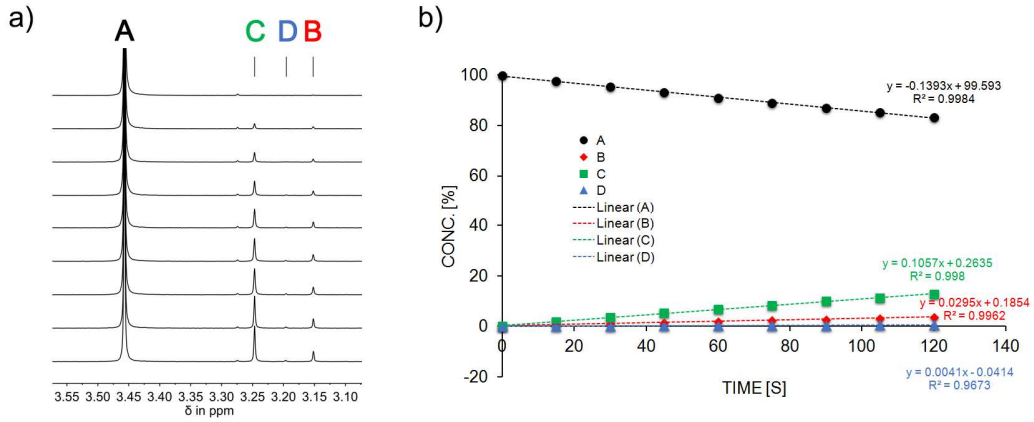

Supplementary Figure 14 | Quantum yields of A. Quantum yield ϕ measurement for the photoconversion of **A**-**1** at 23 °C in benzene-d_6 solution (3.04 mM) using a focused 405 nm LED. a) ^{1}H NMR spectra (400 MHz, 18 °C) recorded after different irradiation durations. Signals of individual isomers are indicated. b) The relative changes of the isomer composition is plotted against different duration times of irradiation. Each point represents an individual measurement, the relative isomer ratios were determined by ^{1}H NMR spectroscopy. Linear behavior is observed showing that only **A**-**1** undergoes photoreactions. Quantum yields were determined by averaging over all experiments (see Supplementary Table 2).

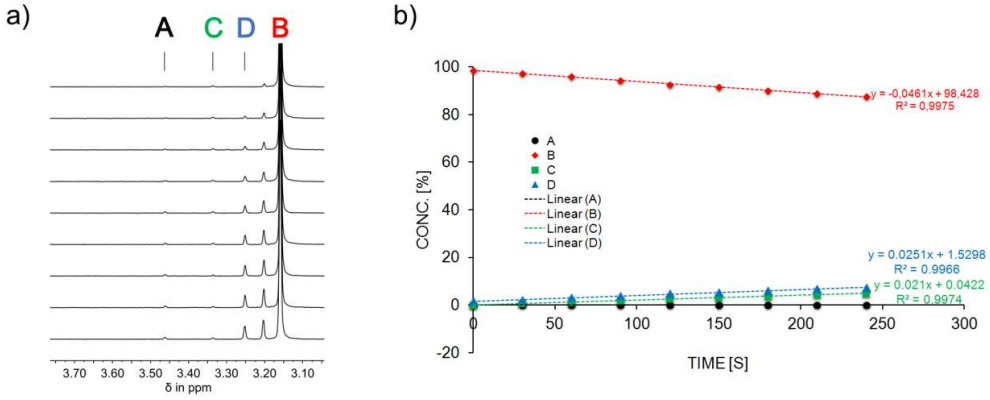

Supplementary Figure 15 | Quantum yields of B. Quantum yield ϕ measurement for the photoconversion of **B**-**1** at 23 °C in benzene-d_6 solution (3.04 mM) using a focused 405 nm LED. a) ^{1}H NMR spectra (400 MHz, 22 °C) recorded after different irradiation durations. Signals of individual isomers are indicated. b) The relative changes of the isomer composition is plotted against different duration times of irradiation. Each point represents an individual measurement, the relative isomer ratios were determined by ^{1}H NMR spectroscopy. Linear behavior is observed showing that only **B**-**1** undergoes photoreactions. Quantum yields were determined by averaging over all experiments (see Supplementary Table 2).

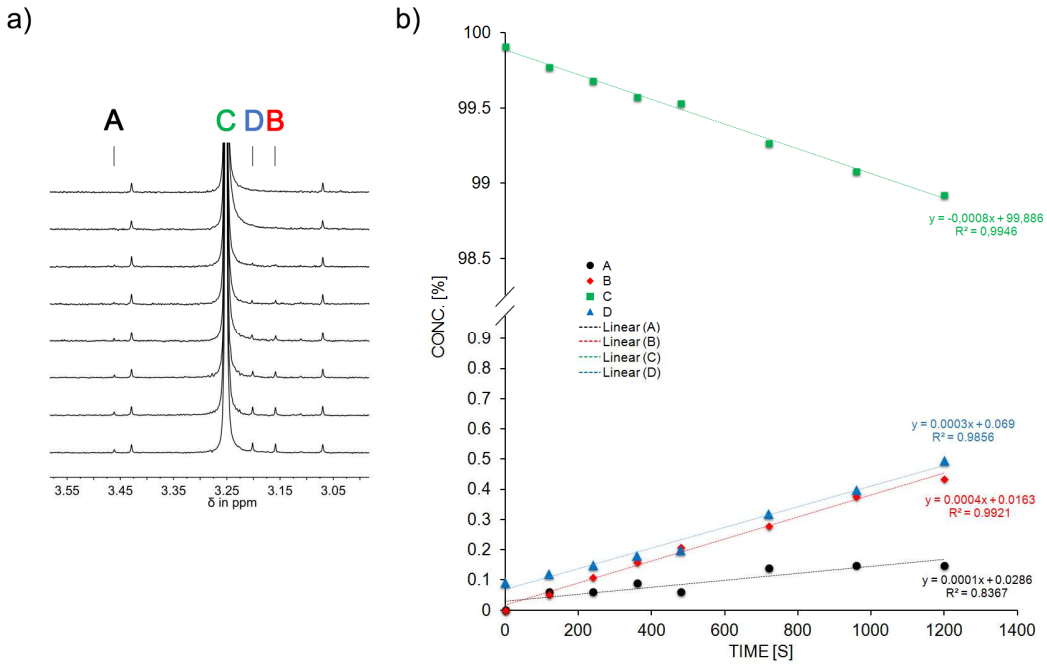

Supplementary Figure 16 | Quantum yields of C. Quantum yield ϕ measurement for the photoconversion of **C-1** at 23 °C in benzene-d_6 solution (3.04 mM) using a focused 405 nm LED. a) ^{1}H NMR spectra (400 MHz, 22 °C) recorded after different irradiation durations. Signals of individual isomers are indicated. b) The relative changes of the isomer composition is plotted against different duration times of irradiation. Each point represents an individual measurement, the relative isomer ratios were determined by ^{1}H NMR spectroscopy. Linear behavior is observed showing that only **C-1** undergoes photoreactions. Quantum yields were determined by averaging over all experiments (see Supplementary Table 2).

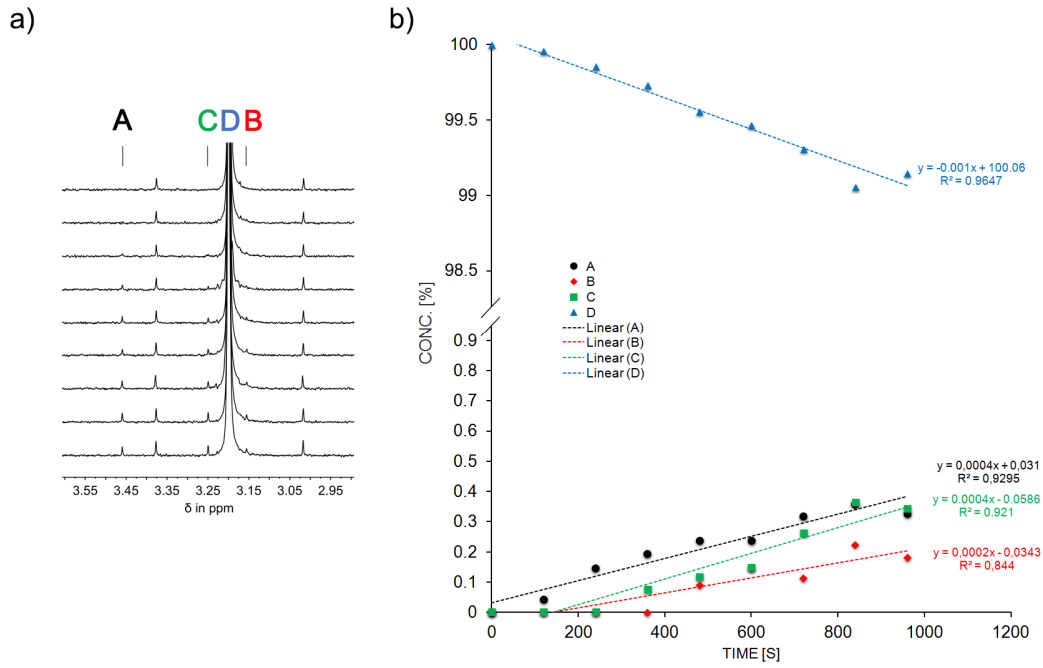

Supplementary Figure 17 | Quantum yields of D. Quantum yield ϕ measurement for the photoconversion of **D-1** at 23 °C in benzene-d_6 solution (3.04 mM) using a 405 nm LED. a) ^{1}H NMR spectra (400 MHz, 20 °C) recorded after different irradiation durations. Signals of individual isomers are indicated. b) The relative changes of the isomer composition is plotted against different duration times of irradiation. Each point represents an individual measurement, the relative isomer ratios were determined by ^{1}H NMR spectroscopy. Quantum yields were determined by averaging over all experiments (see Supplementary Table 2).

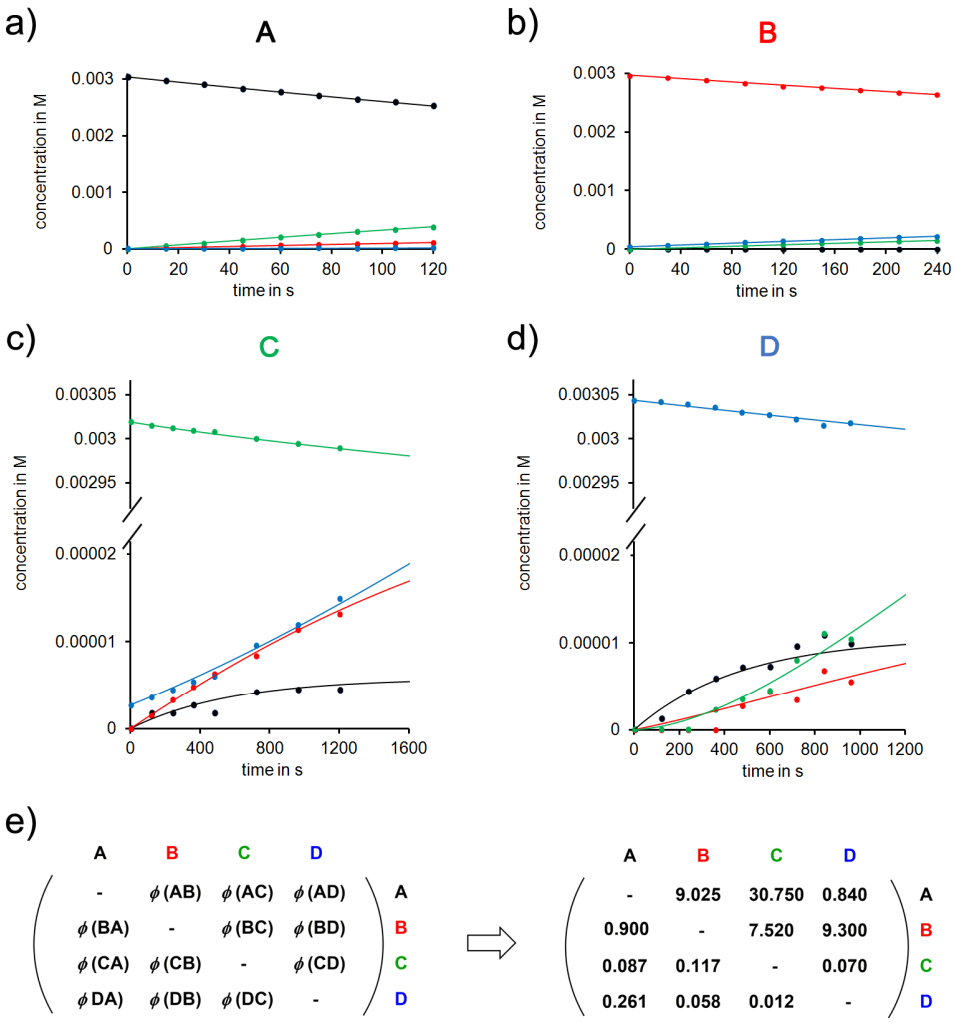

Supplementary Figure 18 | Quantum yields of 1. Quantum yield ϕ measurements for the photoconversions of **1** at 23 °C in benzene-d_6 solution. a) Photoconversion of **A**. b) Photoconversion of **B**. c) Photoconversion of **C**. d) Photoconversion of **D**. e) Optimized fitted quantum yields for all photoconversion processes.

Markov matrix analysis of the photoconversion of A, B, C, and D in different solvents

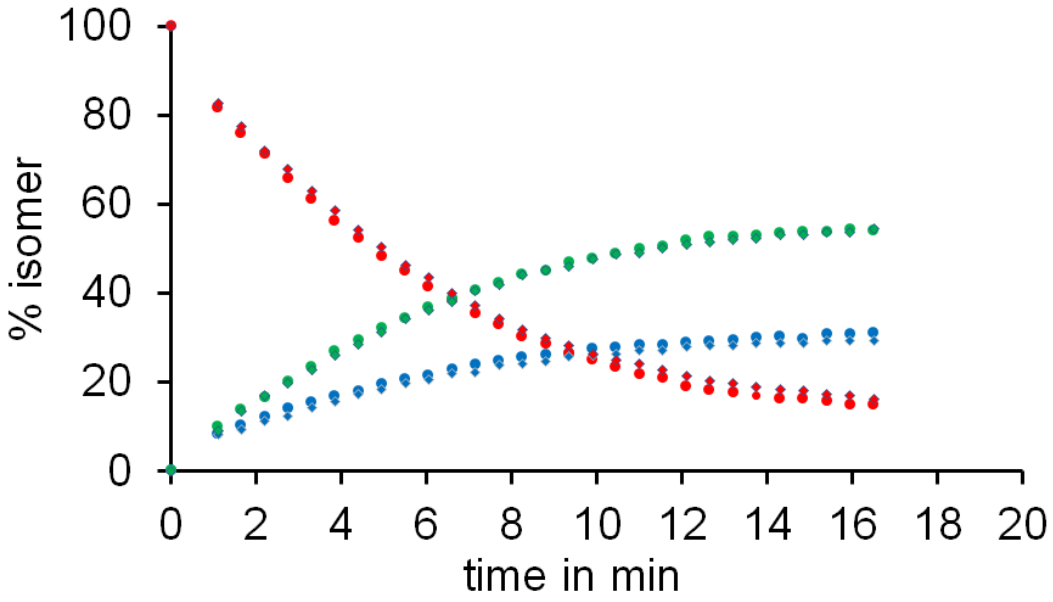

Supplementary Figure 19 | Accuracy of Markov matrix analysis. Changes in the relative concentrations of isomers **A**, **B**, **C**, and **D** during illumination of isomer **B** in tetrachloroethane-d_2 solution at 27 °C with 405 nm light. Data points were obtained via integration of indicative signals from ^{1}H NMR spectra (400 MHz) recorded during irradiation. Diamonds and circles represents two independent measurements using a freshly prepared solution of isomer **B** in a different NMR tube with newly attached optical fiber in each case. The deviation is commonly lower than 1% showing that all the external parameters I_0, d, and initial concentration of the pure isomer [**i**] were kept constant and in every independent experiment.

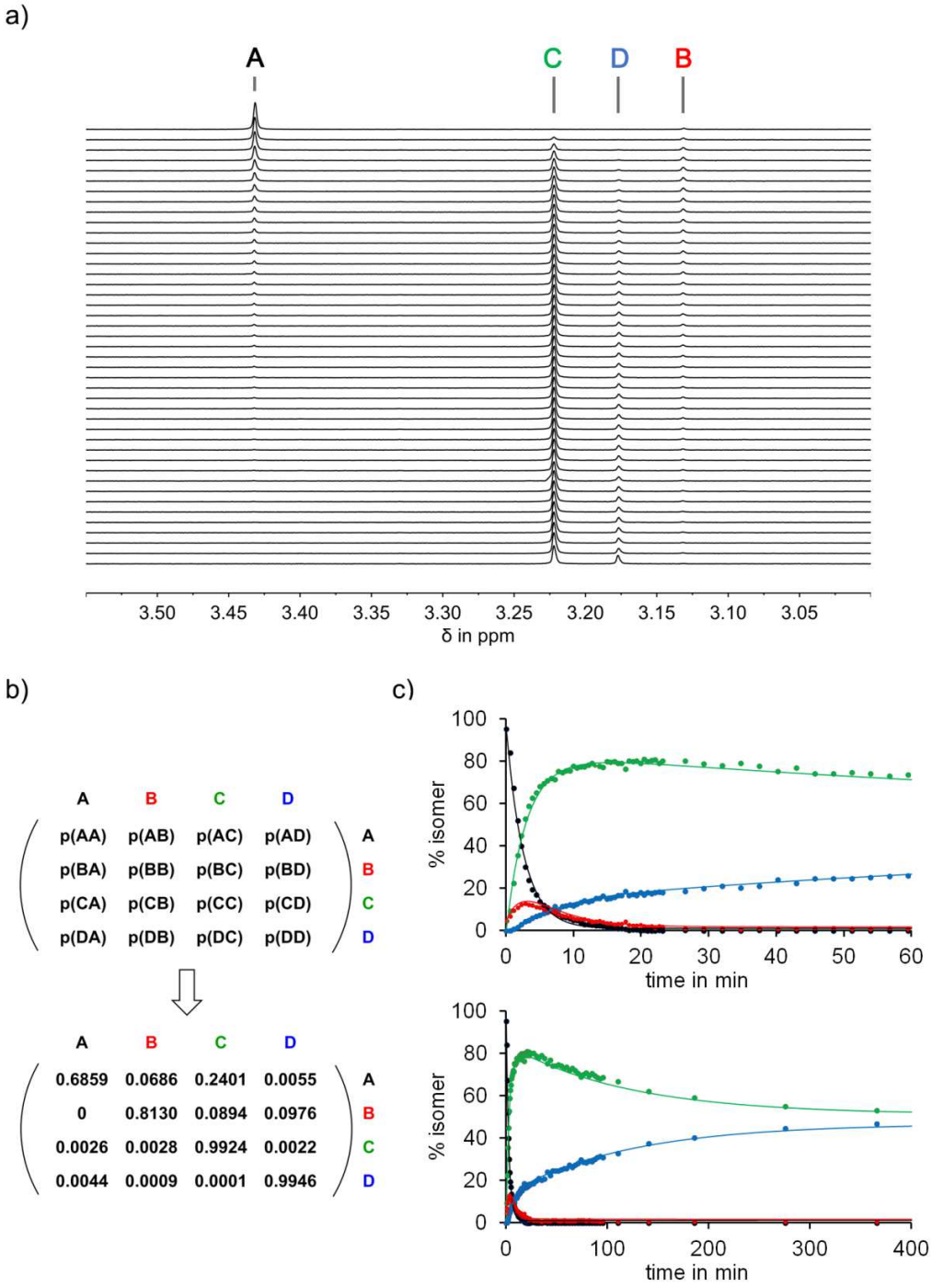

Supplementary Figure 20 | Markov matrix analysis of A in benzene-d_6. Markov matrix analysis of the photoreactions of **1** starting from isomer **A** in benzene-d_6 solution at 27 °C under 405 nm illumination. a) Section of the ^{1}H NMR spectra (400 MHz) recorded during irradiation of **A**-**1**. Spectra were recorded in 33 s intervals. The bottom spectrum was recorded after 365 min. b) Markov matrix describing the different phototransition probabilities p(**ij**) per minute for **1**. c) Kinetic plots of the experimentally determined changes in isomer composition during irradiation of **A**-**1** (dots) and fitted values derived from the Markov matrix (lines).

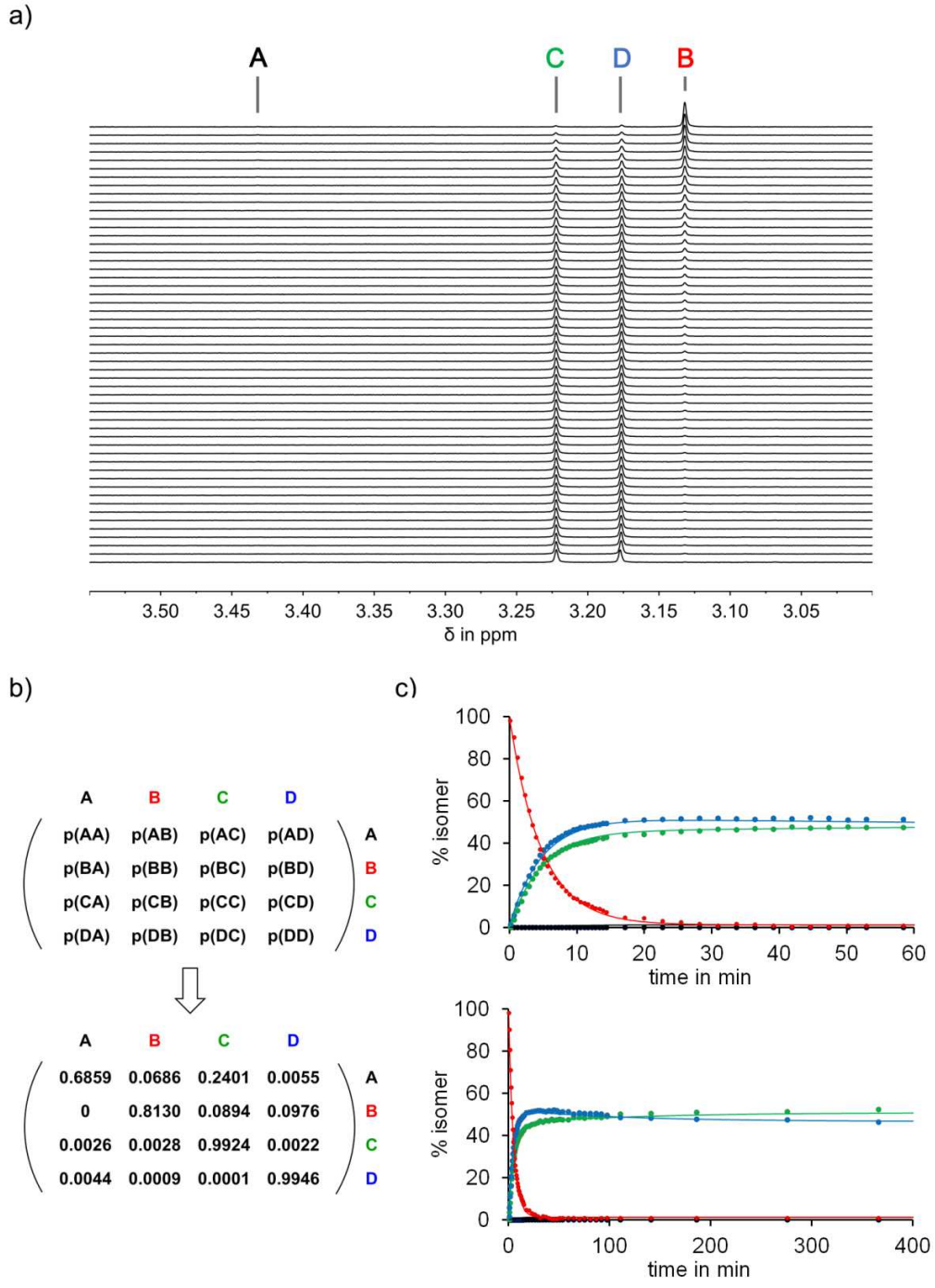

Supplementary Figure 21 | Markov matrix analysis of B in benzene-d_6. Markov matrix analysis of the photoreactions of **1** starting from isomer **B** in benzene-d_6 solution at 27 °C under 405 nm illumination. a) Section of the ^{1}H NMR spectra (400 MHz) recorded during irradiation of **B**-**1**. Spectra were recorded in 33 s intervals. The bottom spectrum was recorded after 365 min. b) Markov matrix describing the phototransition probabilities p(**ij**) per minute for **1**. c) Kinetic plots of the experimentally determined changes in isomer composition during irradiation of **B**-**1** (dots) and fitted values derived from the Markov matrix (lines).

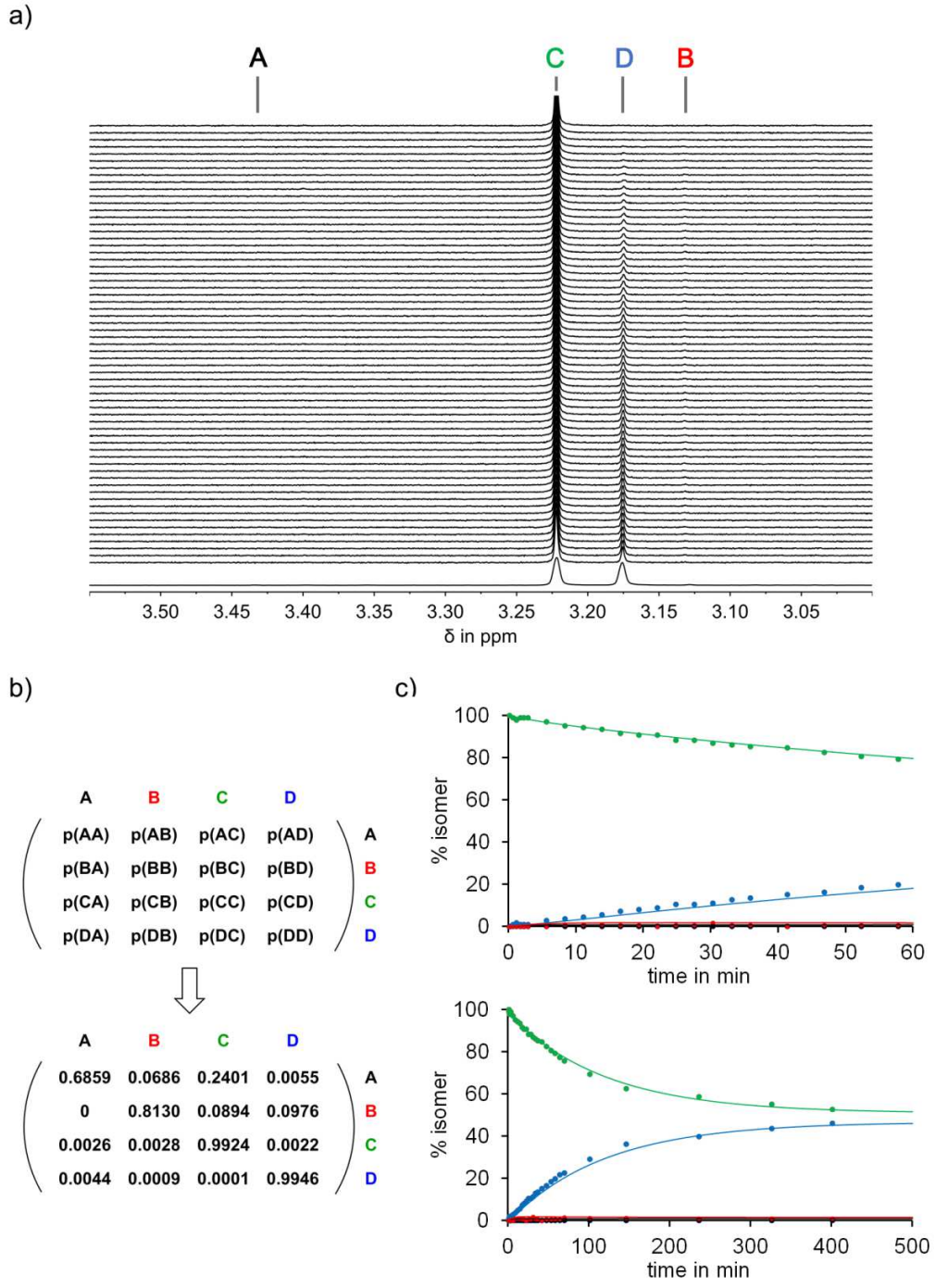

Supplementary Figure 22 | Markov matrix analysis of C in benzene-d_6. Markov matrix analysis of the photoreactions of **1** starting from isomer **C** in benzene-d_6 solution at 27 °C under 405 nm illumination. a) Section of the ^{1}H NMR spectra (400 MHz) recorded during irradiation of **C**-**1**. Spectra were recorded in 66 s intervals. The bottom spectrum was recorded after 12 h. b) Markov matrix describing the phototransition probabilities p(**ij**) per minute for **1**. c) Kinetic plots of the experimentally determined changes in isomer composition during irradiation of **C**-**1** (dots) and fitted values derived from the Markov matrix (lines).

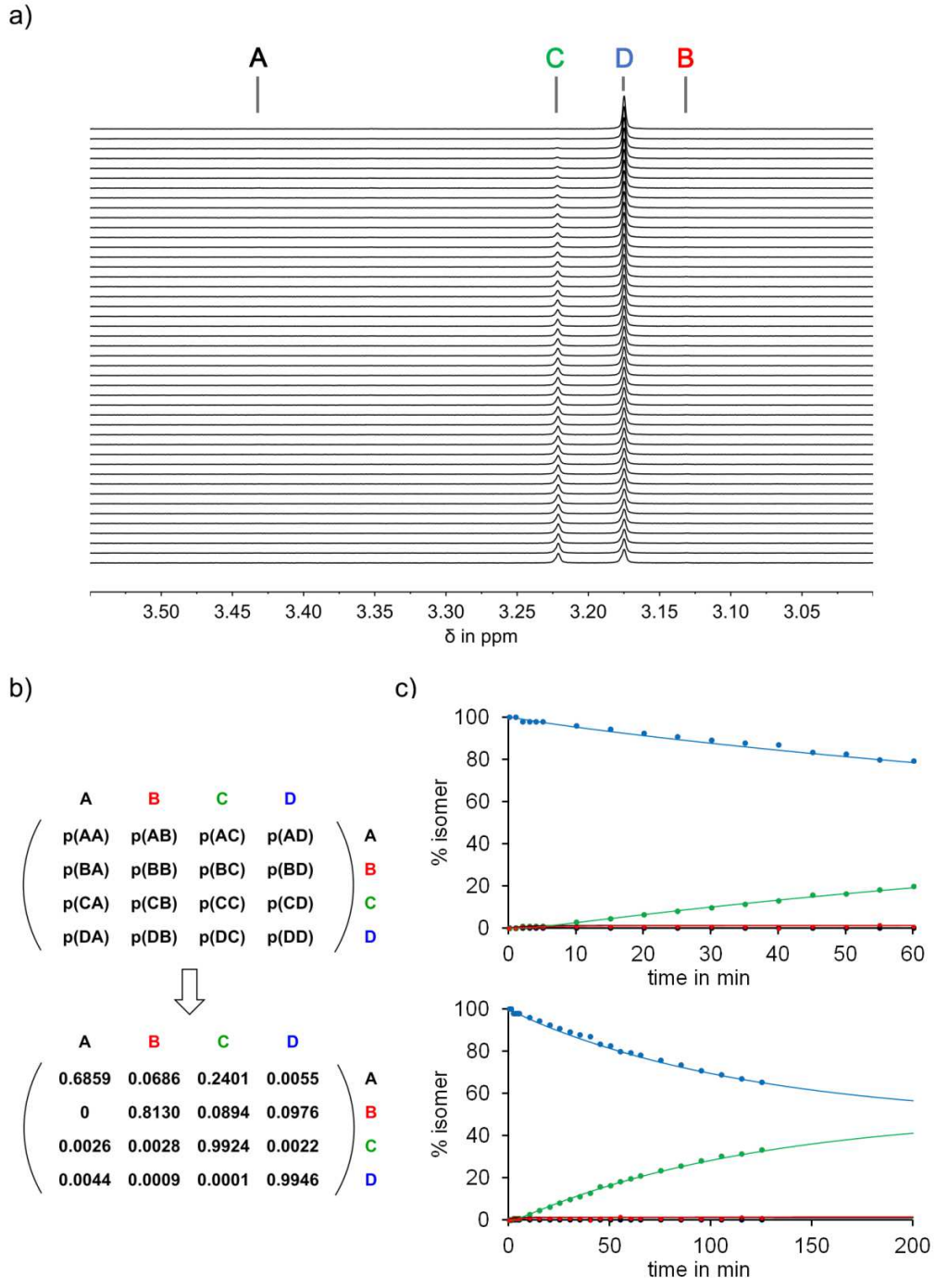

Supplementary Figure 23 | Markov matrix analysis of D in benzene-d_6. Markov matrix analysis of the photoreactions of **1** starting from isomer **D** in benzene-d_6 solution at 27 °C under 405 nm illumination. a) Section of the ^{1}H NMR spectra (400 MHz) recorded during irradiation of **D**-**1**. Spectra were recorded in 132 s intervals. b) Markov matrix describing the phototransition probabilities p(**ij**) per minute for **1**. c) Kinetic plots of the experimentally determined changes in isomer composition during irradiation of **D**-**1** (dots) and fitted values derived from the Markov matrix (lines).

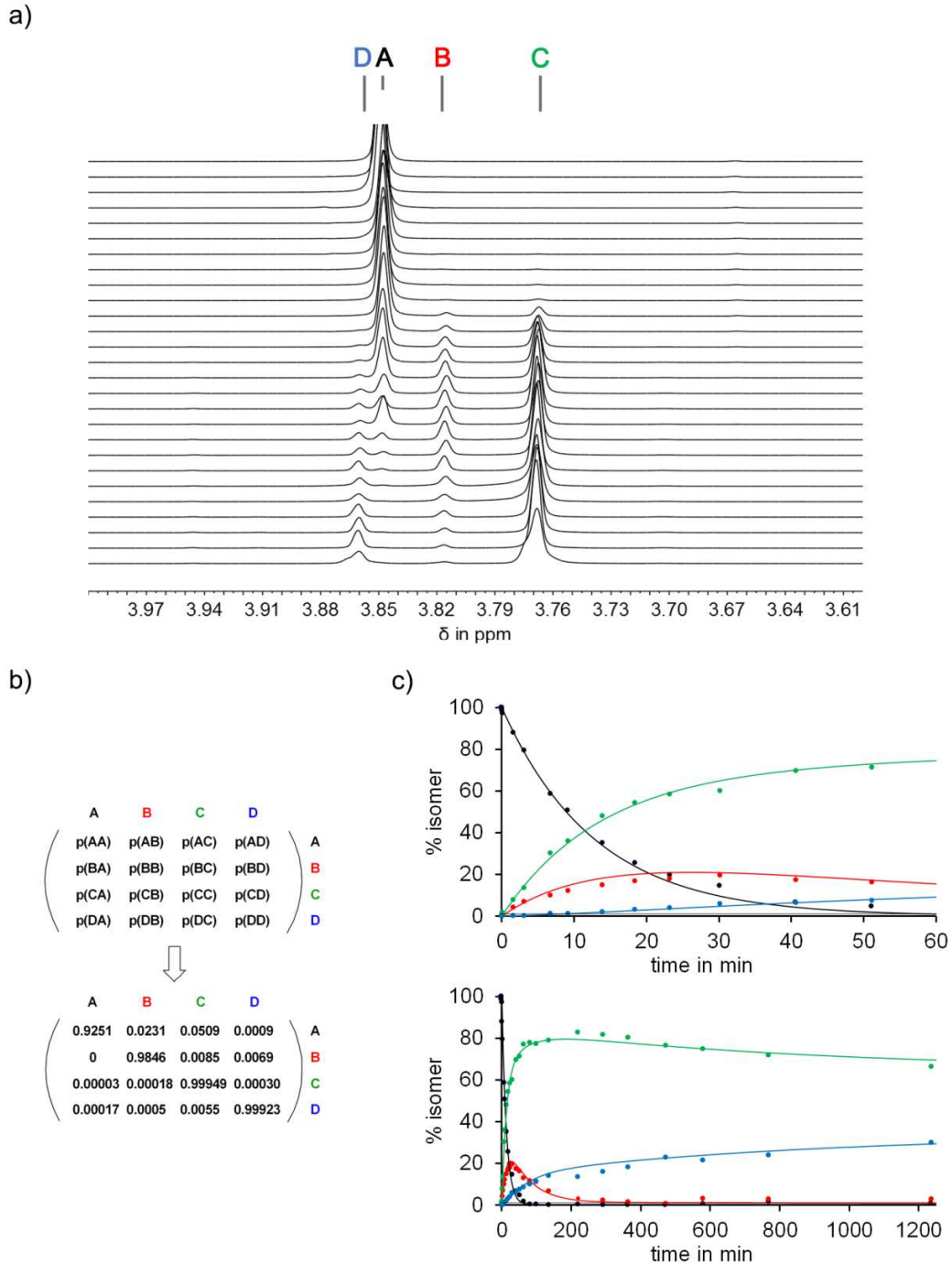

Supplementary Figure 24 | Markov matrix analysis of A in CD_2Cl_2. Markov matrix analysis of the photoreactions of **1** starting from isomer **A** in CD_2Cl_2 solution at 22 °C under 405 nm illumination. a) Section of the ^1H NMR spectra (400 MHz) recorded during irradiation of **A**-**1**. Each spectrum represents a set of data points in the kinetic plot. b) Markov matrix describing the phototransition probabilities p(**ij**) per minute for **1**. c) Kinetic plots of the experimentally determined changes in isomer composition during irradiation of **A**-**1** (dots) and fitted values derived from the Markov matrix (lines).

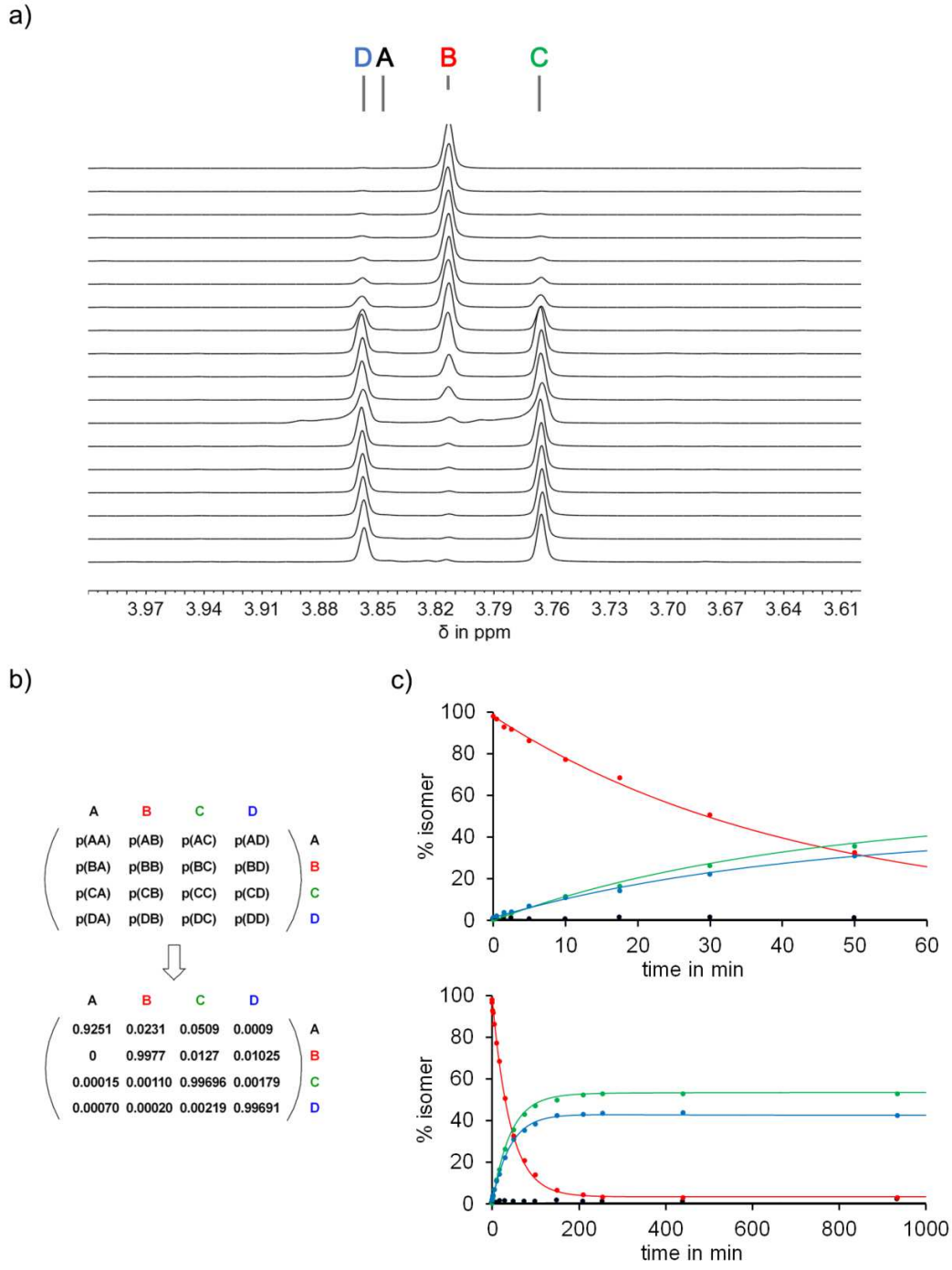

Supplementary Figure 25 | Markov matrix analysis of B in CD_2Cl_2. Markov matrix analysis of the photoreactions of **1** starting from isomer **B** in CD_2Cl_2 solution at 22 °C under 405 nm illumination. a) Section of the ^1H NMR spectra (400 MHz) recorded during irradiation of **B**-**1**. Each spectrum represents a set of data points in the kinetic plot. b) Markov matrix describing the phototransition probabilities p(**ij**) per minute for **1**. c) Kinetic plots of the experimentally determined changes in isomer composition during irradiation of **B**-**1** (dots) and fitted values derived from the Markov matrix (lines).

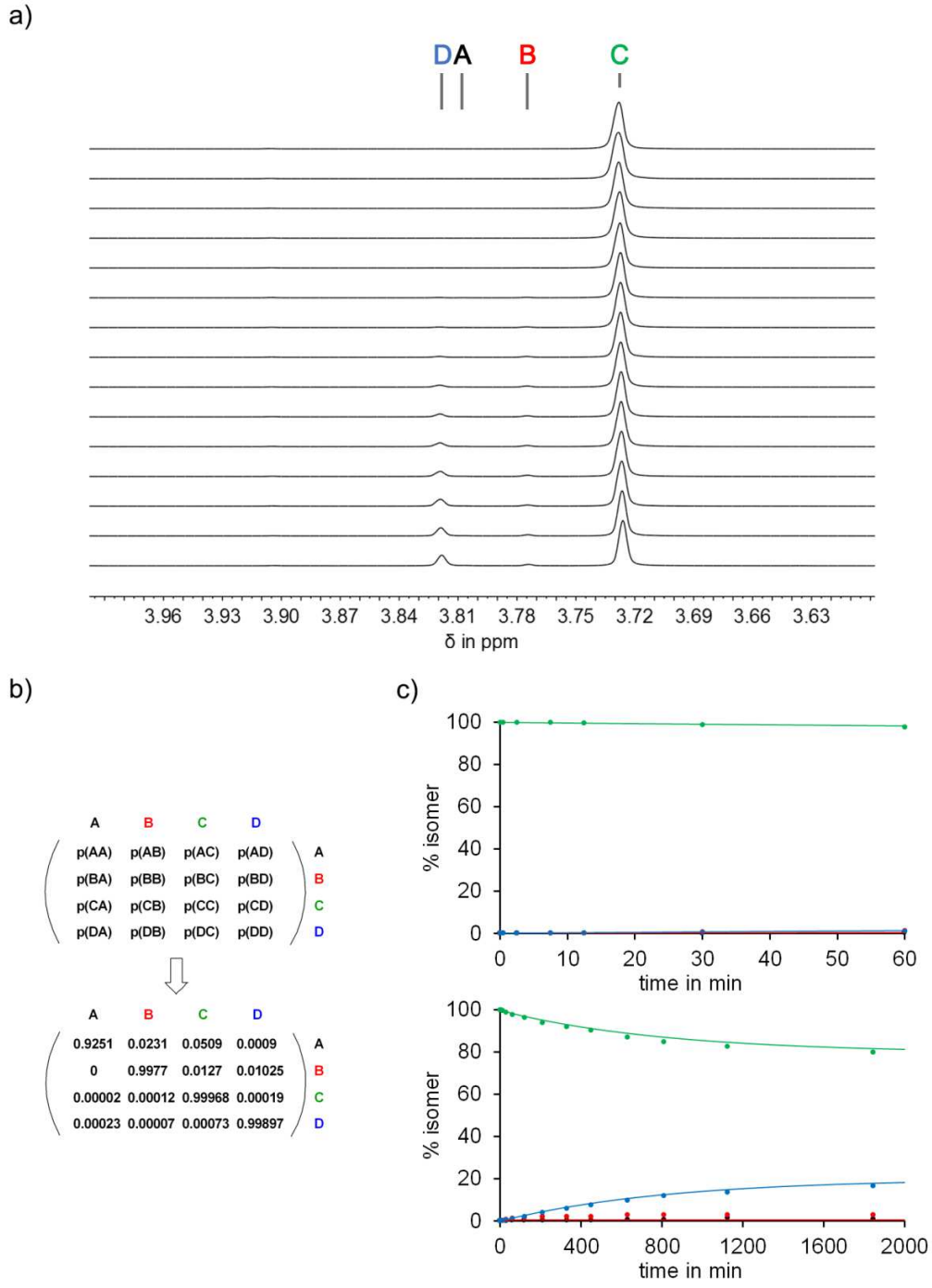

Supplementary Figure 26 | Markov matrix analysis of C in CD_2Cl_2. Markov matrix analysis of the photoreactions of **1** starting from isomer **C** in CD_2Cl_2 solution at 22 °C under 405 nm illumination. a) Section of the ^1H NMR spectra (400 MHz) recorded during irradiation of **C**-**1**. Each spectrum represents a set of data points in the kinetic plot. b) Markov matrix describing the phototransition probabilities p(**ij**) per minute for **1**. c) Kinetic plots of the experimentally determined changes in isomer composition during irradiation of **C**-**1** (dots) and fitted values derived from the Markov matrix (lines).

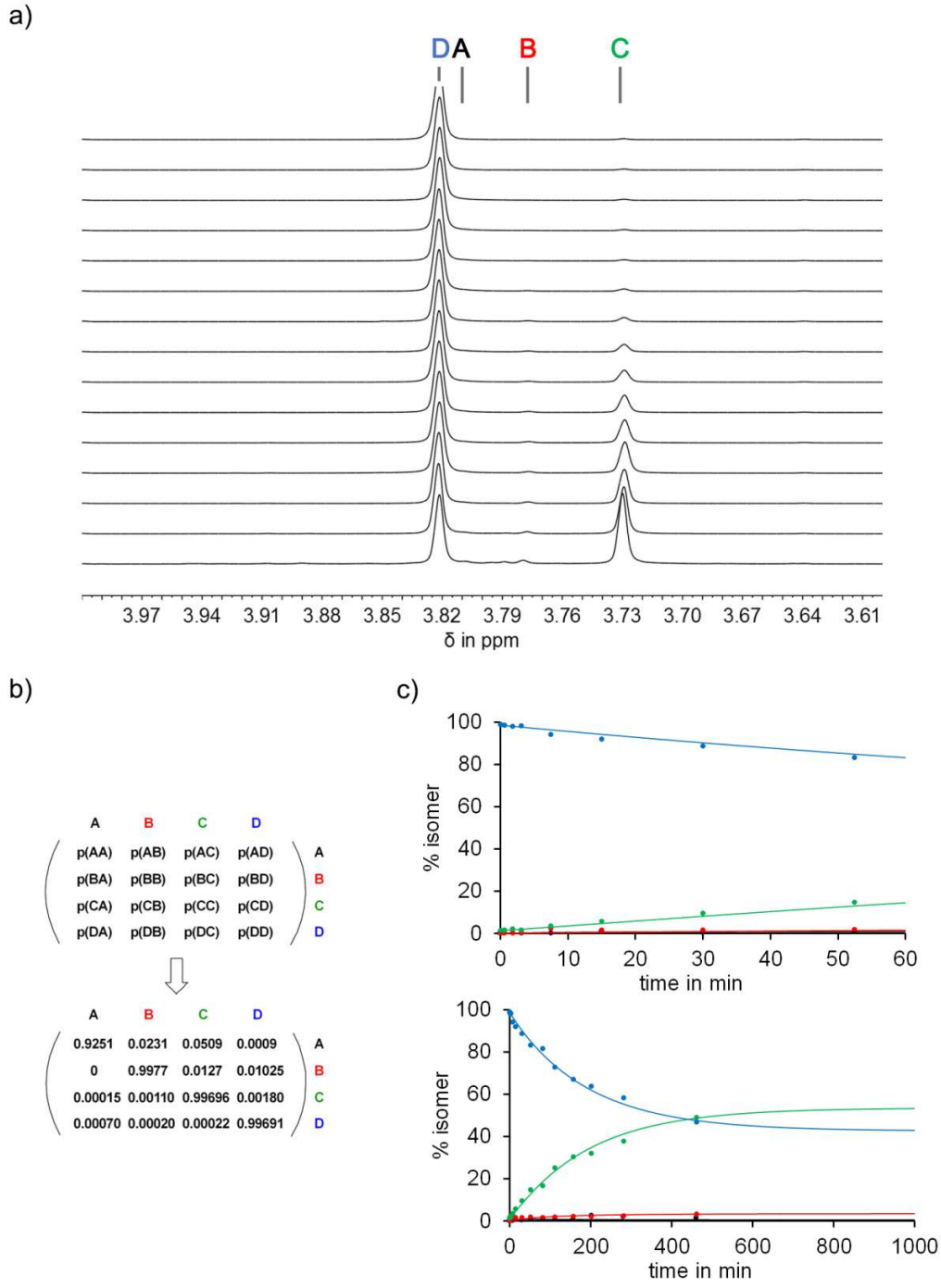

Supplementary Figure 27 | Markov matrix analysis of D in CD_2Cl_2. Markov matrix analysis of the photoreactions of **1** starting from isomer **D** in CD_2Cl_2 solution at 22 °C under 405 nm illumination. a) Section of the ^{1}H NMR spectra (400 MHz) recorded during irradiation of **D**-**1**. Each spectrum represents a set of data points in the kinetic plot. b) Markov matrix describing the phototransition probabilities p(**ij**) per minute for **1**. c) Kinetic plots of the experimentally determined changes in isomer composition during irradiation of **D**-**1** (dots) and fitted values derived from the Markov matrix (lines).

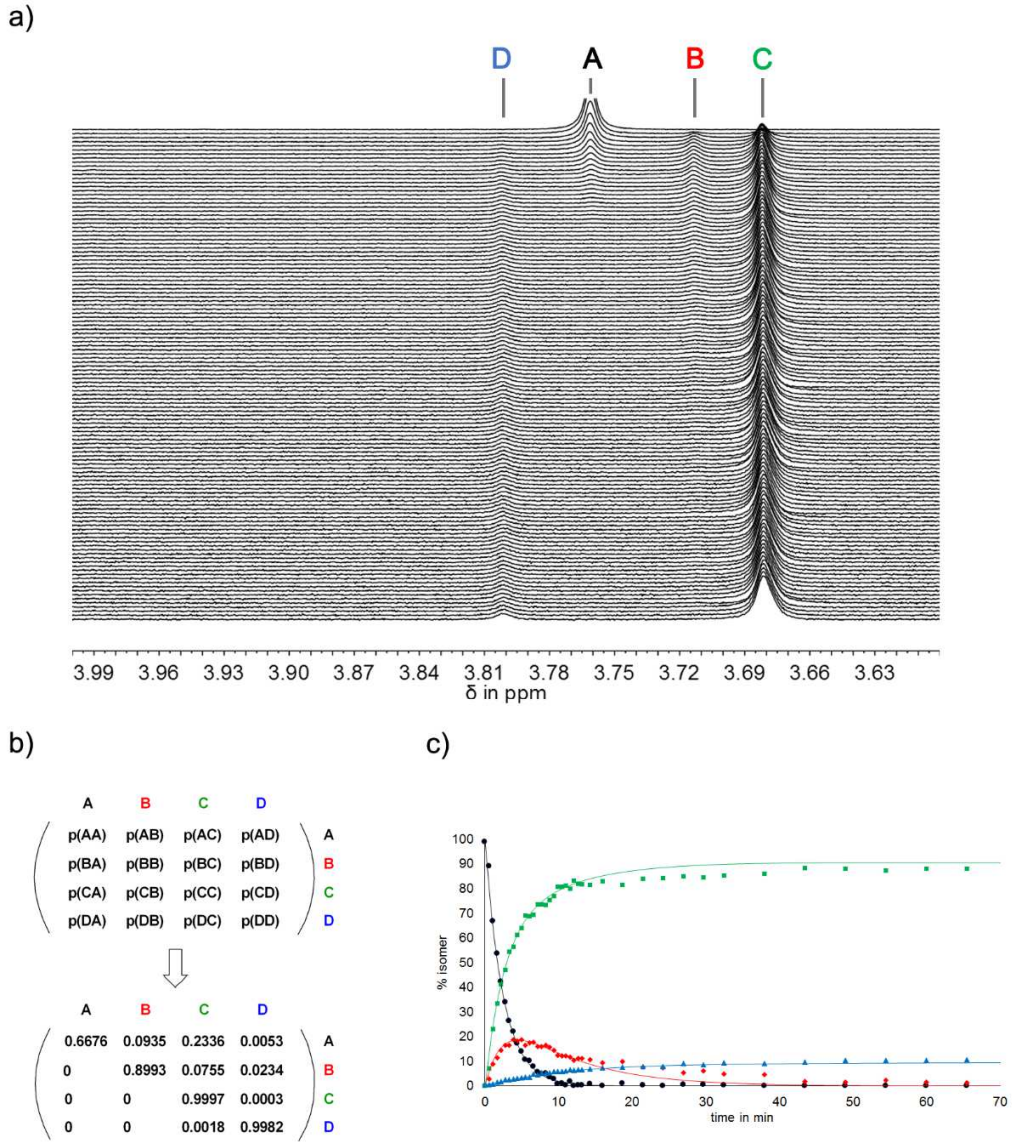

Supplementary Figure 28 | Markov matrix analysis of A in CD_2Cl_2 at -80 °C. Markov matrix analysis of the photoreactions of **1** starting from isomer **A** in CD_2Cl_2 solution at -80 °C under 405 nm illumination. a) Section of the ^{1}H NMR spectra (400 MHz) recorded during irradiation of **A**-**1**. Each spectrum represents a set of data points in the kinetic plot. b) Markov matrix describing the phototransition probabilities p(**ij**) per minute for **1**. c) Kinetic plots of the experimentally determined changes in isomer composition during irradiation of **A**-**1** (dots) and fitted values derived from the Markov matrix (lines).

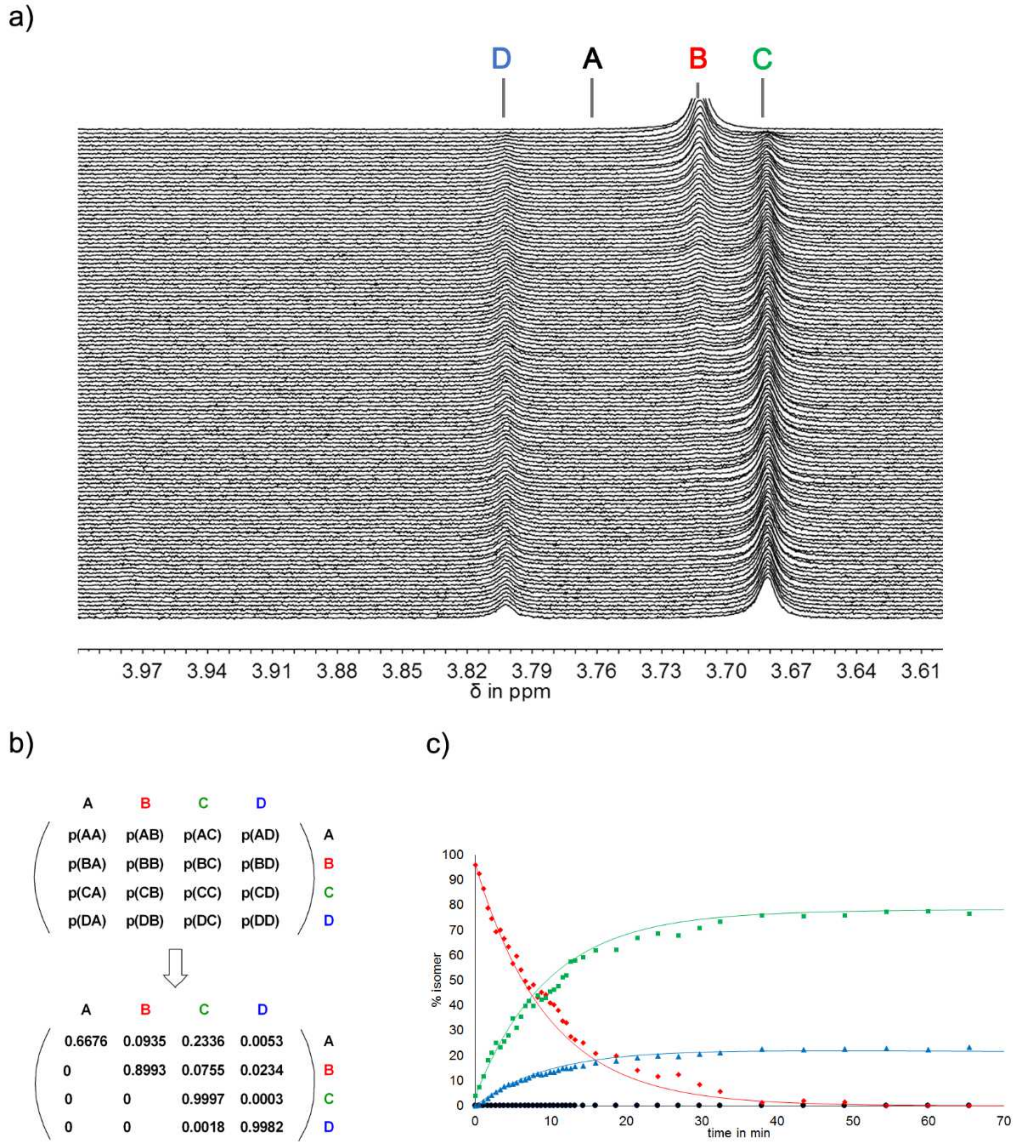

Supplementary Figure 29 | Markov matrix analysis of B in CD_2Cl_2 at -80 °C. Markov matrix analysis of the photoreactions of **1** starting from isomer **B** in CD_2Cl_2 solution at -80 °C under 405 nm illumination. a) Section of the ^{1}H NMR spectra (400 MHz) recorded during irradiation of **B**-**1**. Each spectrum represents a set of data points in the kinetic plot. b) Markov matrix describing the phototransition probabilities p(**ij**) per minute for **1**. c) Kinetic plots of the experimentally determined changes in isomer composition during irradiation of **B**-**1** (dots) and fitted values derived from the Markov matrix (lines).

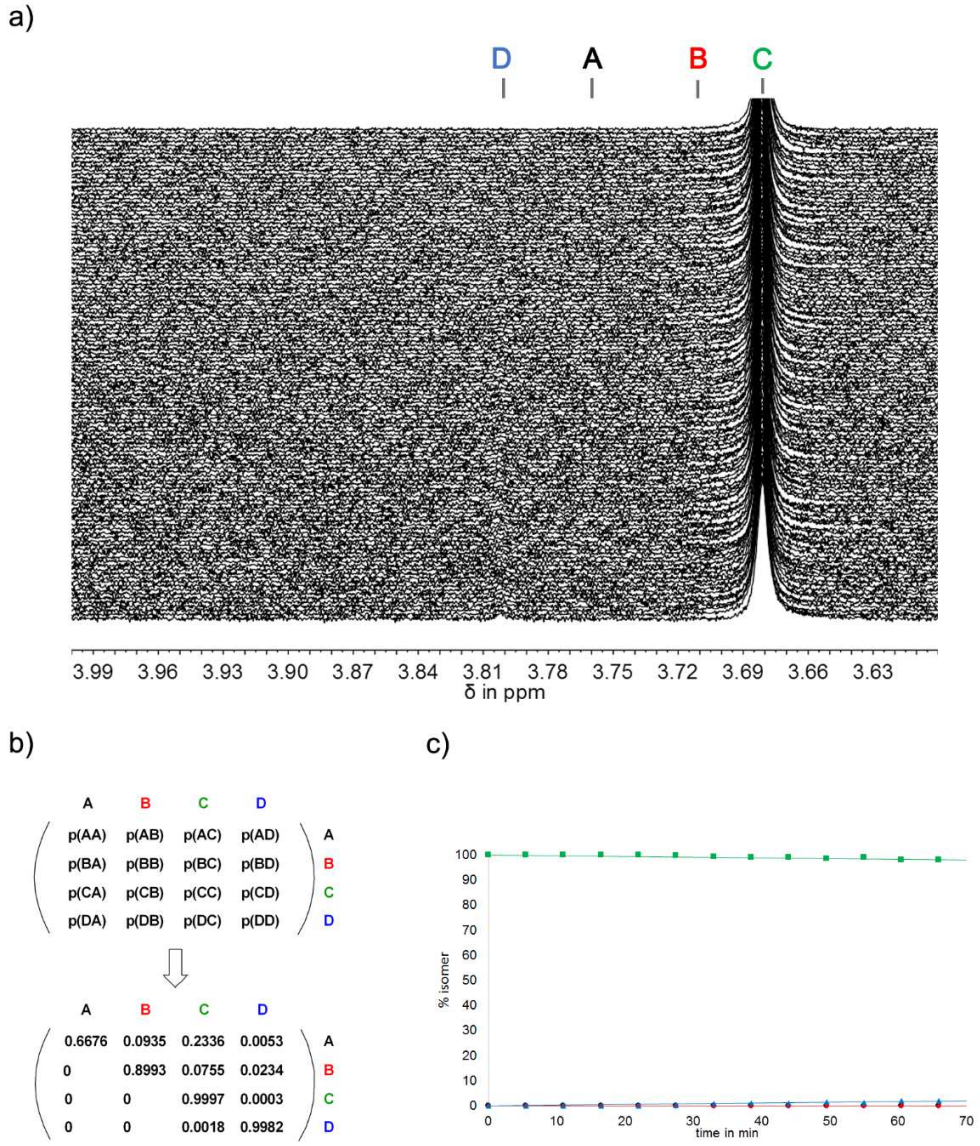

Supplementary Figure 30 | Markov matrix analysis of C in CD_2Cl_2 at -80 °C. Markov matrix analysis of the photoreactions of **1** starting from isomer **C** in CD_2Cl_2 solution at -80 °C under 405 nm illumination. a) Section of the ^{1}H NMR spectra (400 MHz) recorded during irradiation of **C**-**1**. Each spectrum represents a set of data points in the kinetic plot. b) Markov matrix describing the phototransition probabilities p(**ij**) per minute for **1**. c) Kinetic plots of the experimentally determined changes in isomer composition during irradiation of **C**-**1** (dots) and fitted values derived from the Markov matrix (lines).

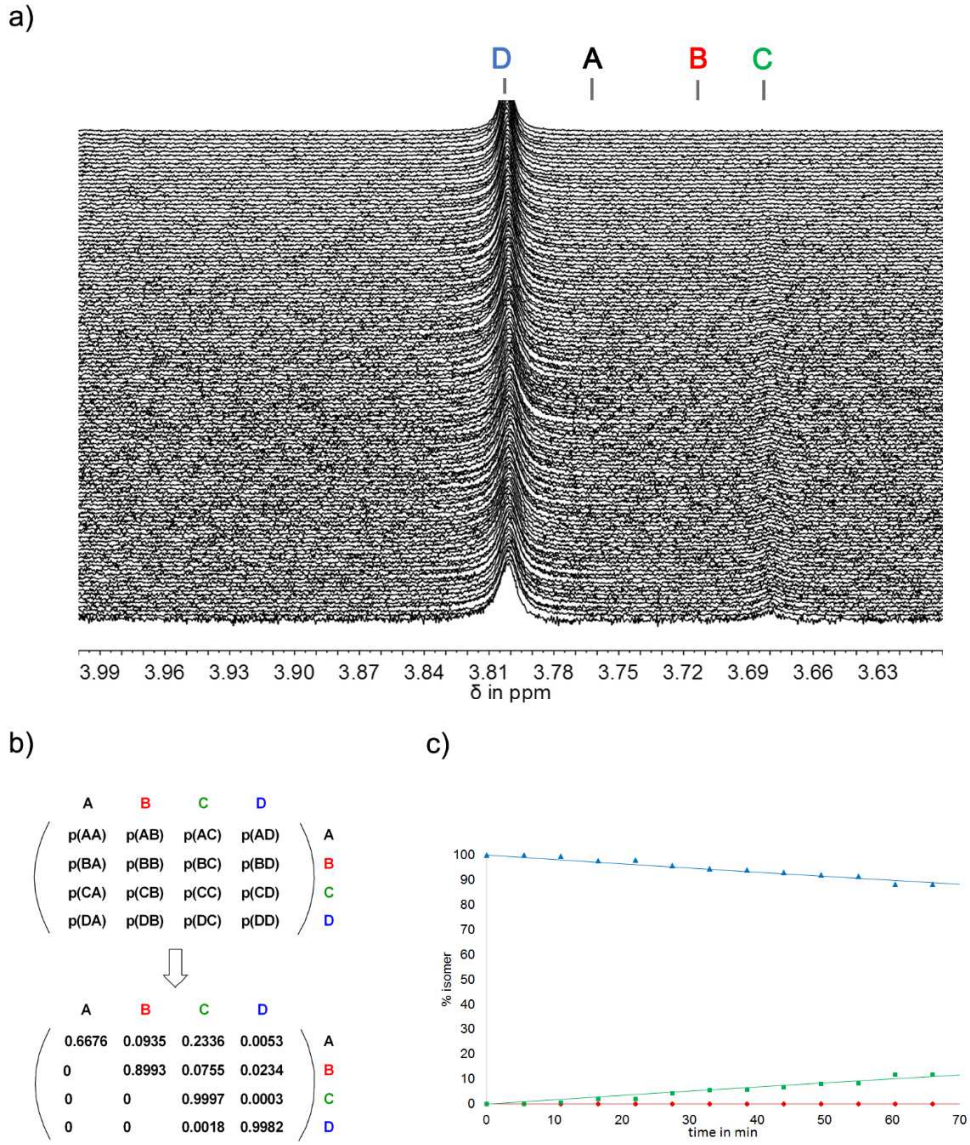

Supplementary Figure 31 | Markov matrix analysis of D in CD_2Cl_2 at -80 °C. Markov matrix analysis of the photoreactions of **1** starting from isomer **D** in CD_2Cl_2 solution at -80 °C under 405 nm illumination. a) Section of the ^{1}H NMR spectra (400 MHz) recorded during irradiation of **D**-**1**. Each spectrum represents a set of data points in the kinetic plot. b) Markov matrix describing the phototransition probabilities p(**ij**) per minute for **1**. c) Kinetic plots of the experimentally determined changes in isomer composition during irradiation of **D**-**1** (dots) and fitted values derived from the Markov matrix (lines).

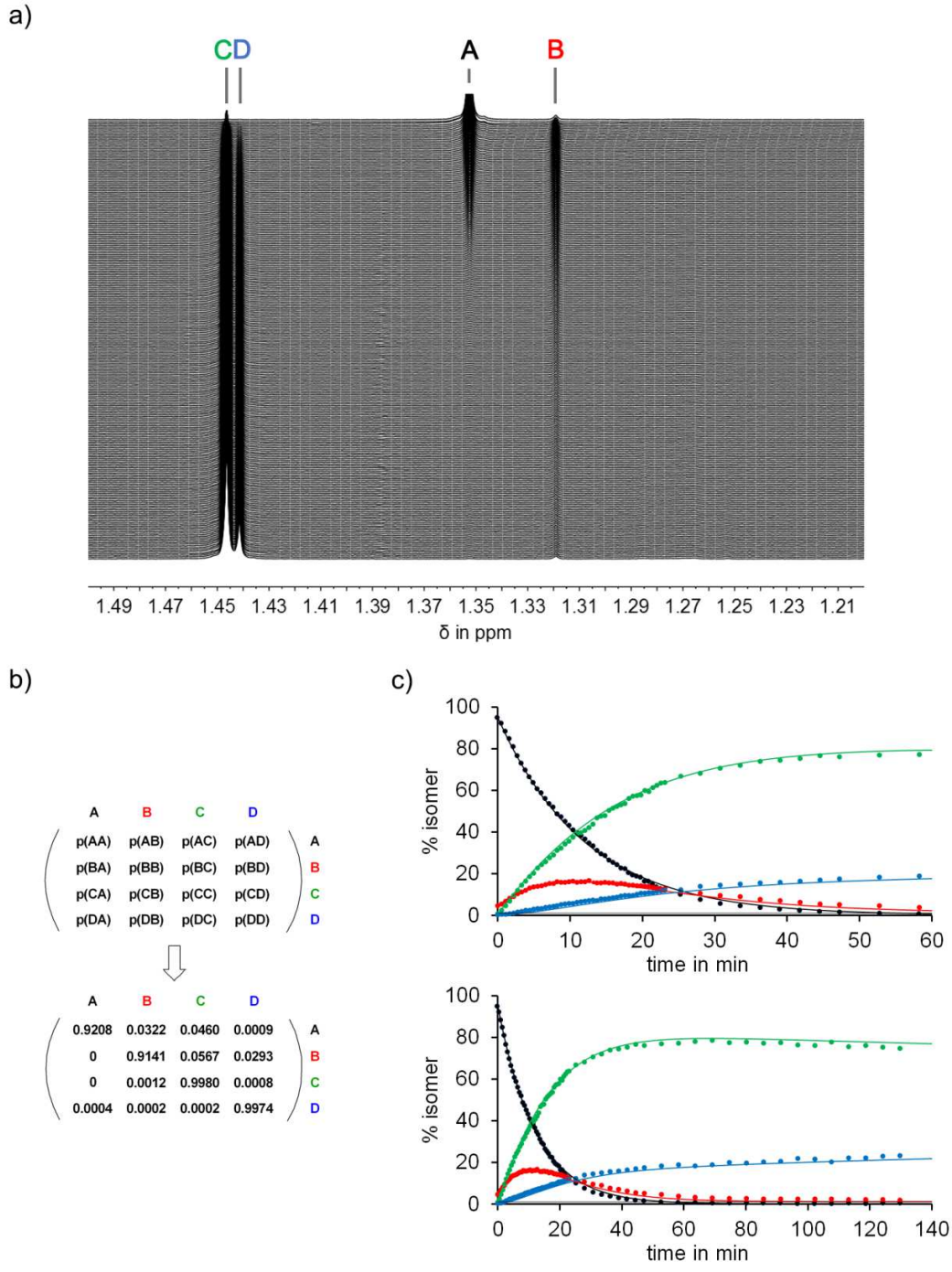

Supplementary Figure 32 | Markov matrix analysis of A in MeOH-d_4. Markov matrix analysis of the photoreactions of **1** starting from isomer **A** in MeOH-d_4 solution at 27 °C under 405 nm illumination. a) Section of the ^{1}H NMR spectra (400 MHz) recorded during irradiation of **A**-**1**. Spectra were recorded in 63 s intervals. b) Markov matrix describing the phototransition probabilities p(**ij**) per minute for **1**. c) Kinetic plots of the experimentally determined changes in isomer composition during irradiation of **A**-**1** (dots) and fitted values derived from the Markov matrix (lines).

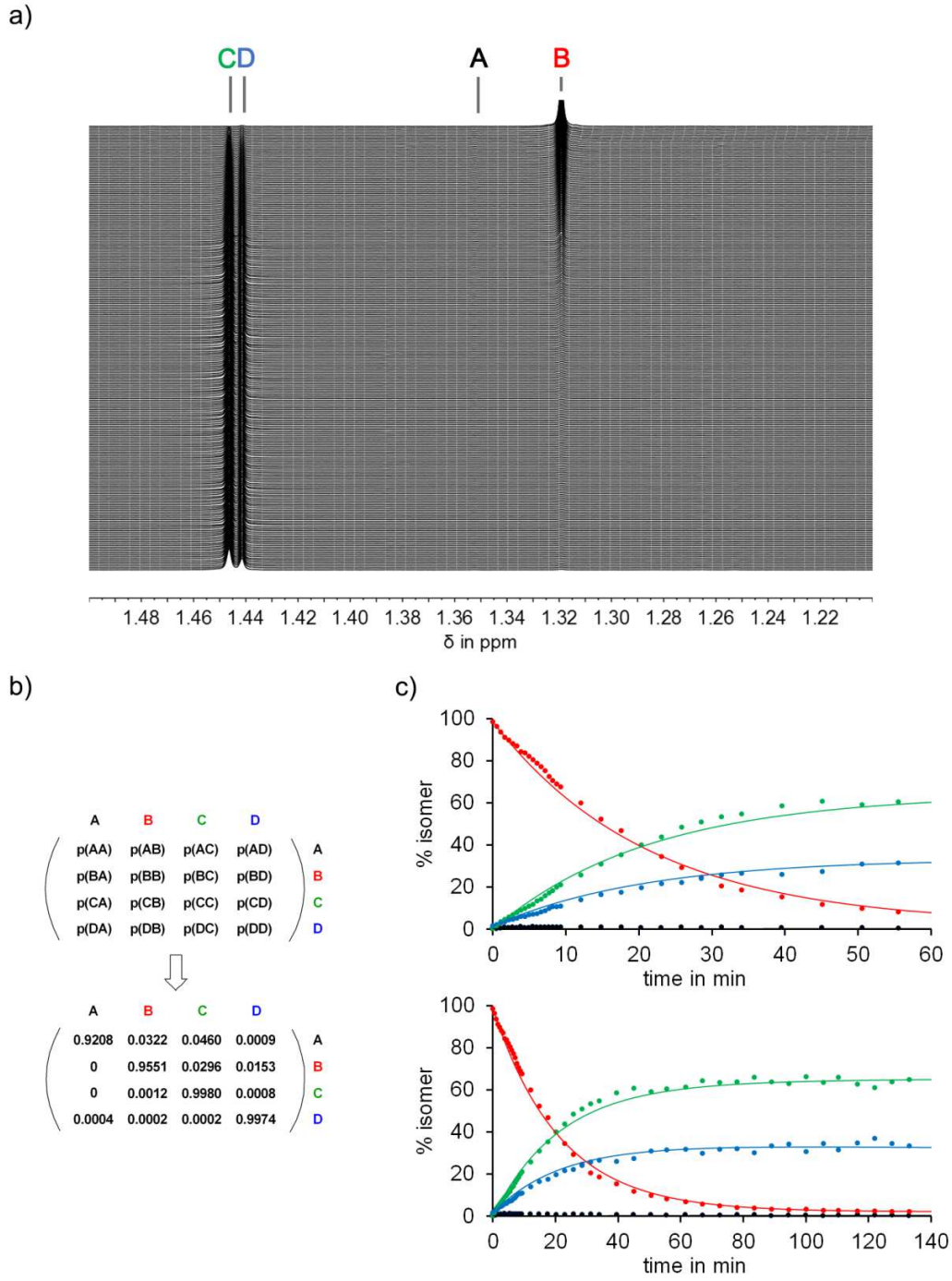

Supplementary Figure 33 | Markov matrix analysis of B in MeOH-d_4. Markov matrix analysis of the photoreactions of **1** starting from isomer **B** in MeOH-d_4 solution at 27 °C under 405 nm illumination. a) Section of the ^{1}H NMR spectra (400 MHz) recorded during irradiation of **B**-**1**. Spectra were recorded in 63 s intervals. b) Markov matrix describing the phototransition probabilities p(**ij**) per minute for **1**. c) Kinetic plots of the experimentally determined changes in isomer composition during irradiation of **B**-**1** (dots) and fitted values derived from the Markov matrix (lines).

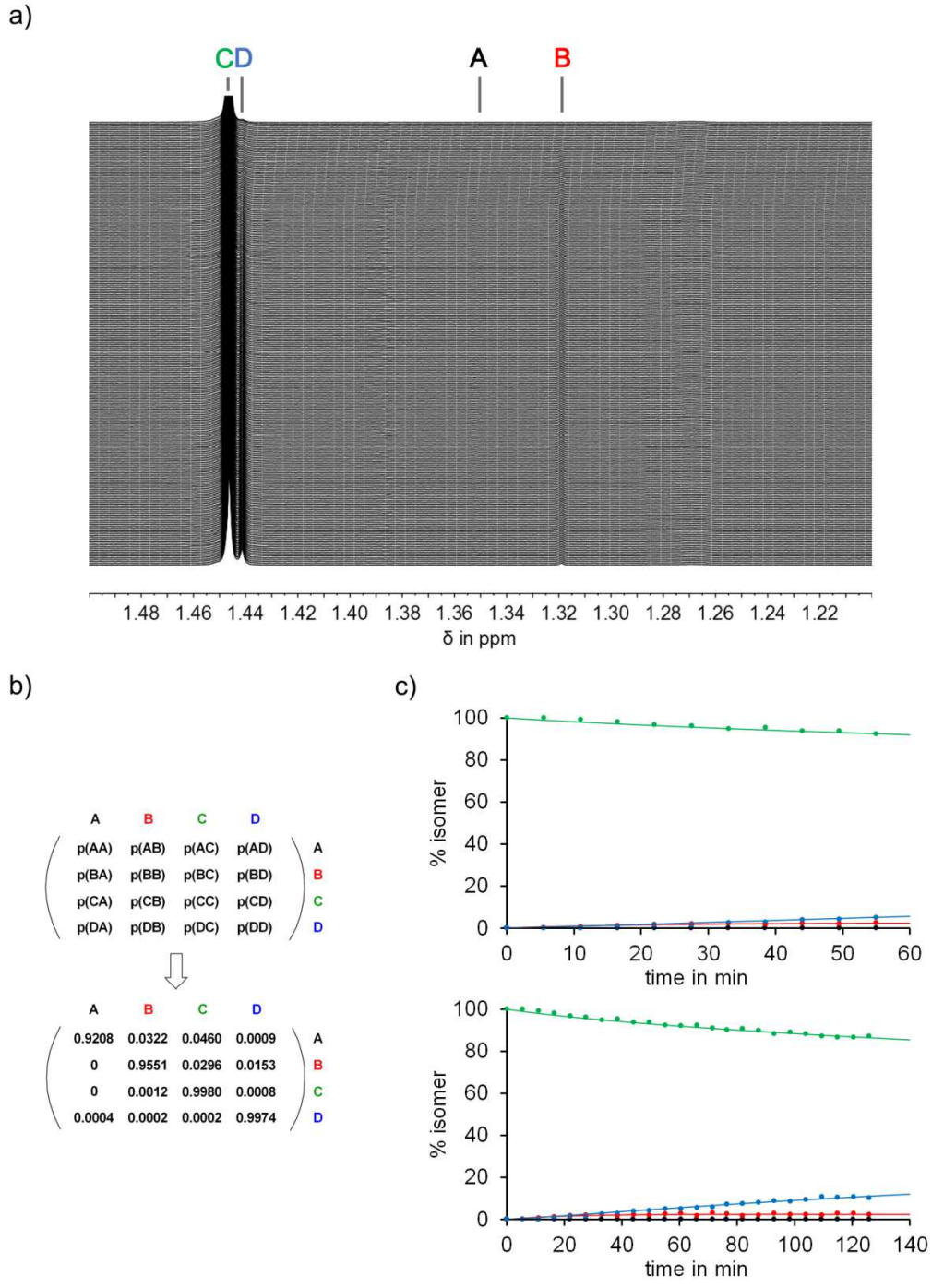

Supplementary Figure 34 | Markov matrix analysis of C in MeOH-d_4. Markov matrix analysis of the photoreactions of **1** starting from isomer **C** in MeOH-d_4 solution at 27 °C under 405 nm illumination. a) Section of the ^{1}H NMR spectra (400 MHz) recorded during irradiation of **C**-**1**. Spectra were recorded in 63 s intervals. b) Markov matrix describing the phototransition probabilities p(**ij**) per minute for **1**. c) Kinetic plots of the experimentally determined changes in isomer composition during irradiation of **C**-**1** (dots) and fitted values derived from the Markov matrix (lines).

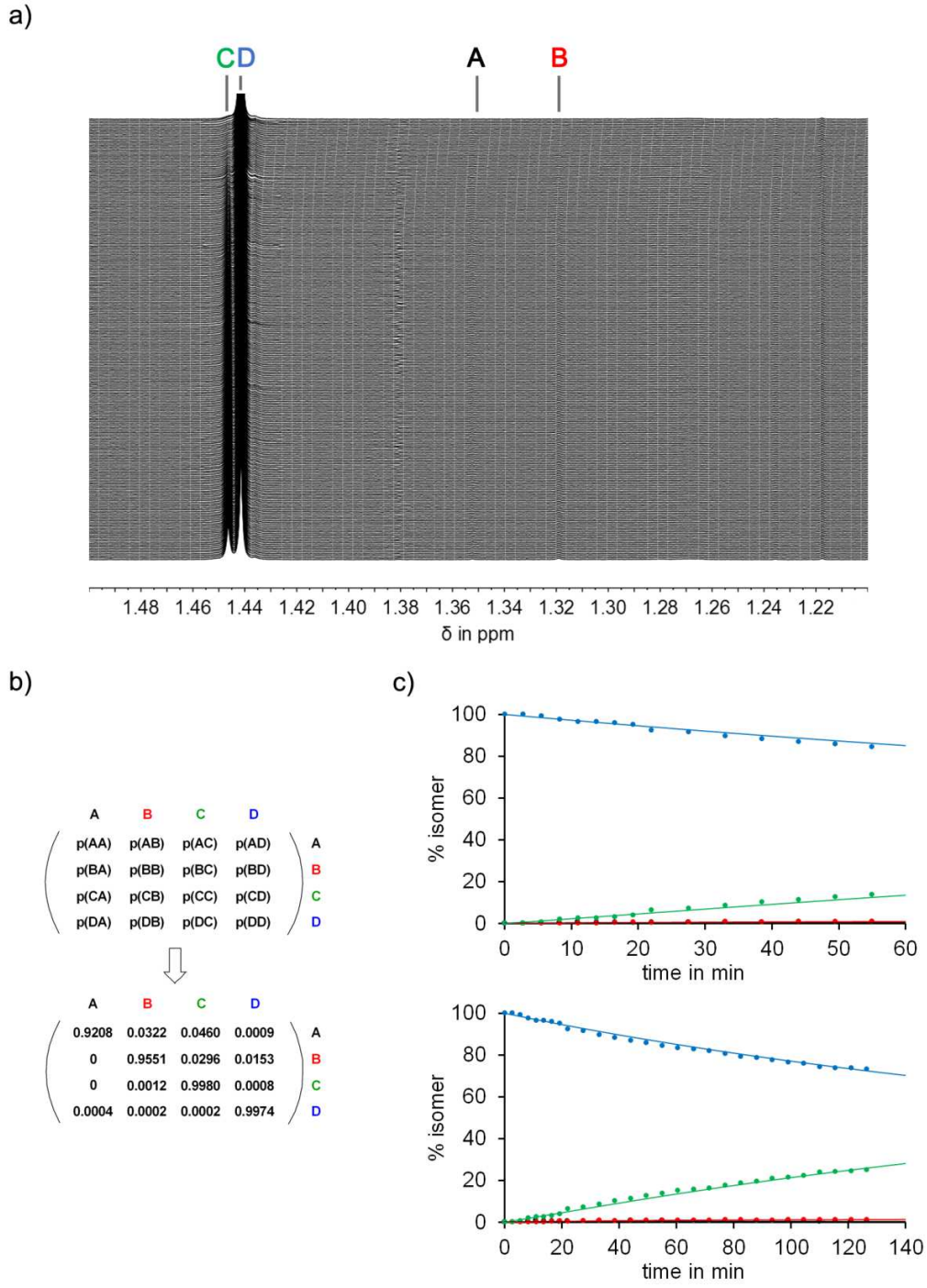

Supplementary Figure 35 | Markov matrix analysis of D in MeOH-d_4. Markov matrix analysis of the photoreactions of **1** starting from isomer **D** in MeOH-d_4 solution at 27 °C under 405 nm illumination. a) Section of the ^{1}H NMR spectra (400 MHz) recorded during irradiation of **D**-**1**. Spectra were recorded in 63 s intervals. b) Markov matrix describing the phototransition probabilities p(**ij**) per minute for **1**. c) Kinetic plots of the experimentally determined changes in isomer composition during irradiation of **D**-**1** (dots) and fitted values derived from the Markov matrix (lines).

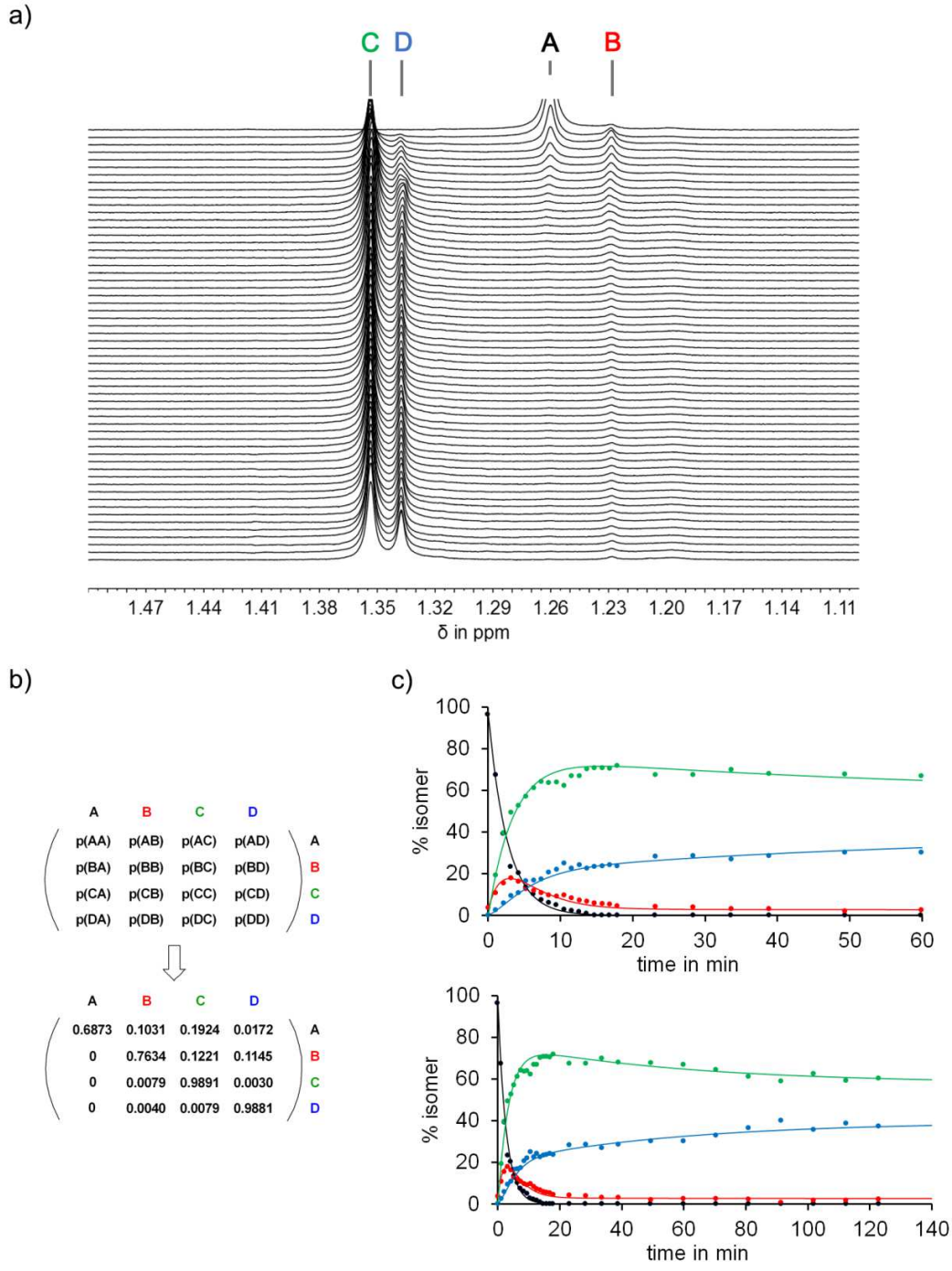

Supplementary Figure 36 | Markov matrix analysis of A in DMSO-d_6. Markov matrix analysis of the photoreactions of **1** starting from isomer **A** in DMSO-d_6 solution at 22 °C under 405 nm illumination. a) Section of the ^{1}H NMR spectra (400 MHz) recorded during irradiation of **A**-**1**. Spectra were recorded in 63 s intervals. b) Markov matrix describing the phototransition probabilities p(**ij**) per minute for **1**. c) Kinetic plots of the experimentally determined changes in isomer composition during irradiation of **A**-**1** (dots) and fitted values derived from the Markov matrix (lines).

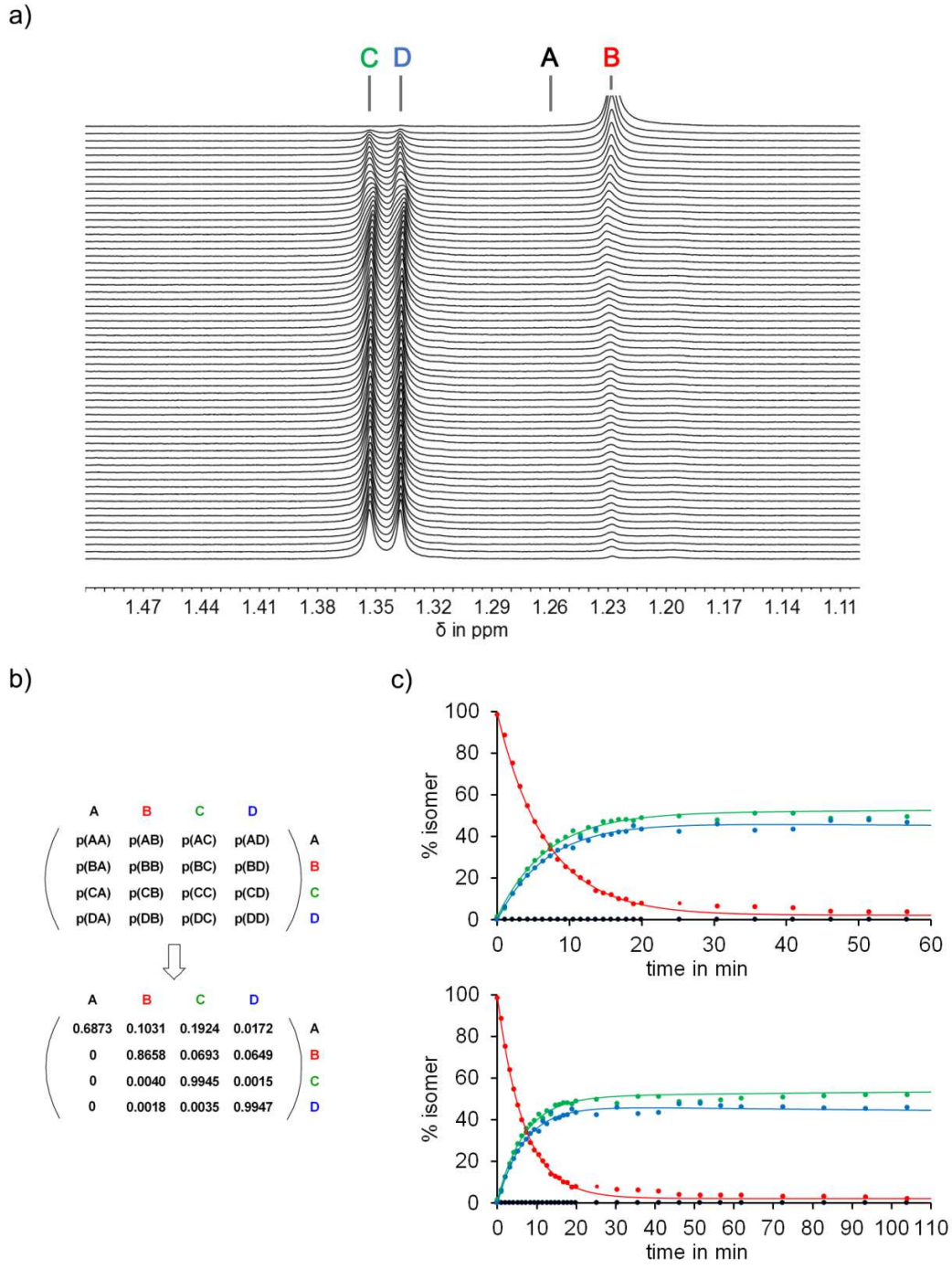

Supplementary Figure 37 | Markov matrix analysis of B in DMSO-d_6. Markov matrix analysis of the photoreactions of **1** starting from isomer **B** in DMSO-d_6 solution at 22 °C under 405 nm illumination. a) Section of the ^{1}H NMR spectra (400 MHz) recorded during irradiation of **B**-**1**. Spectra were recorded in 63 s intervals. b) Markov matrix describing the phototransition probabilities p(**ij**) per minute for **1**. c) Kinetic plots of the experimentally determined changes in isomer composition during irradiation of **B**-**1** (dots) and fitted values derived from the Markov matrix (lines).

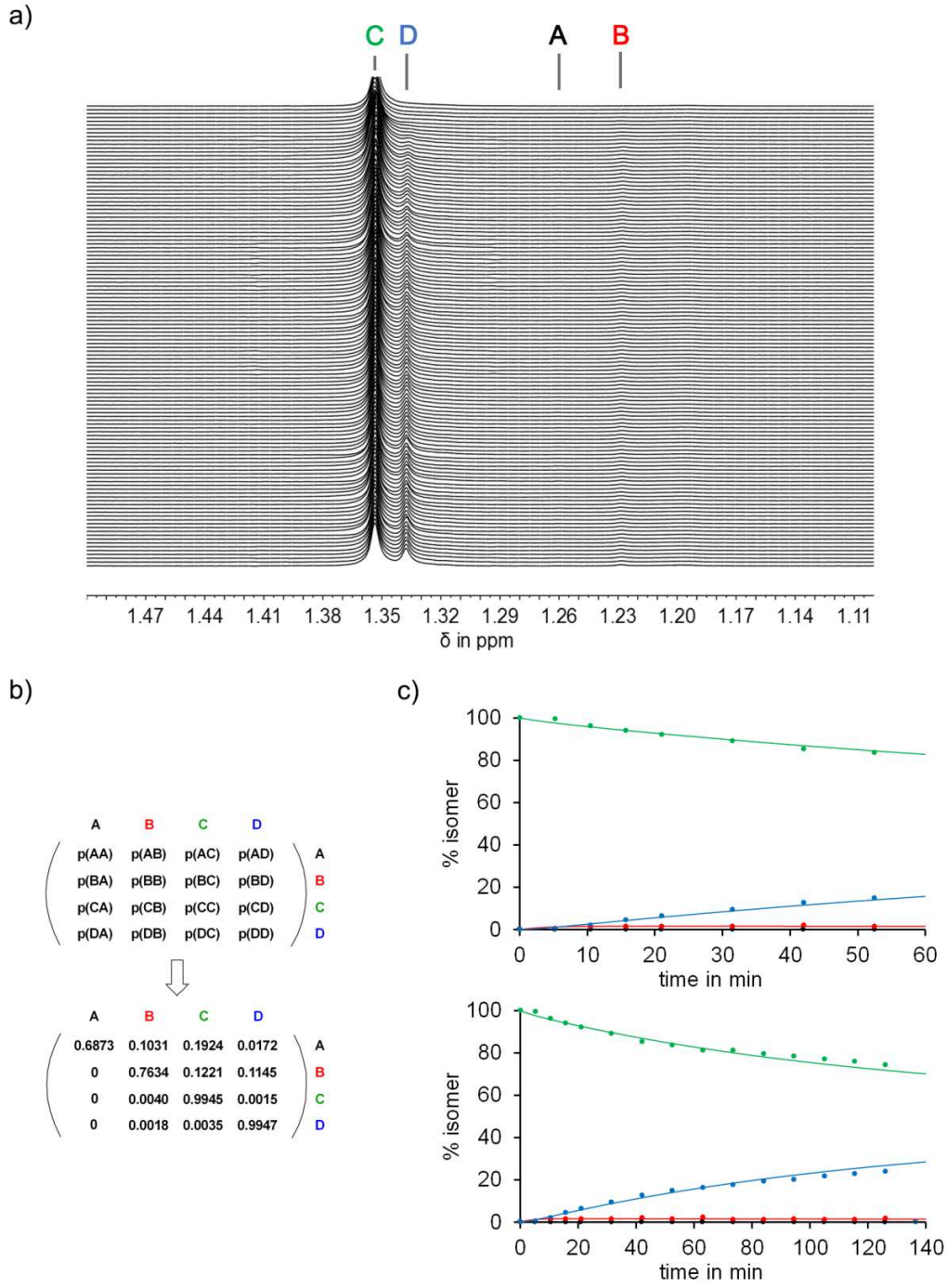

Supplementary Figure 38 | Markov matrix analysis of C in DMSO-d_6. Markov matrix analysis of the photoreactions of **1** starting from isomer **C** in DMSO-d_6 solution at 22 °C under 405 nm illumination. a) Section of the ^{1}H NMR spectra (400 MHz) recorded during irradiation of **C**-**1**. Spectra were recorded in 63 s intervals. b) Markov matrix describing the phototransition probabilities p(**ij**) per minute for **1**. c) Kinetic plots of the experimentally determined changes in isomer composition during irradiation of **C**-**1** (dots) and fitted values derived from the Markov matrix (lines).

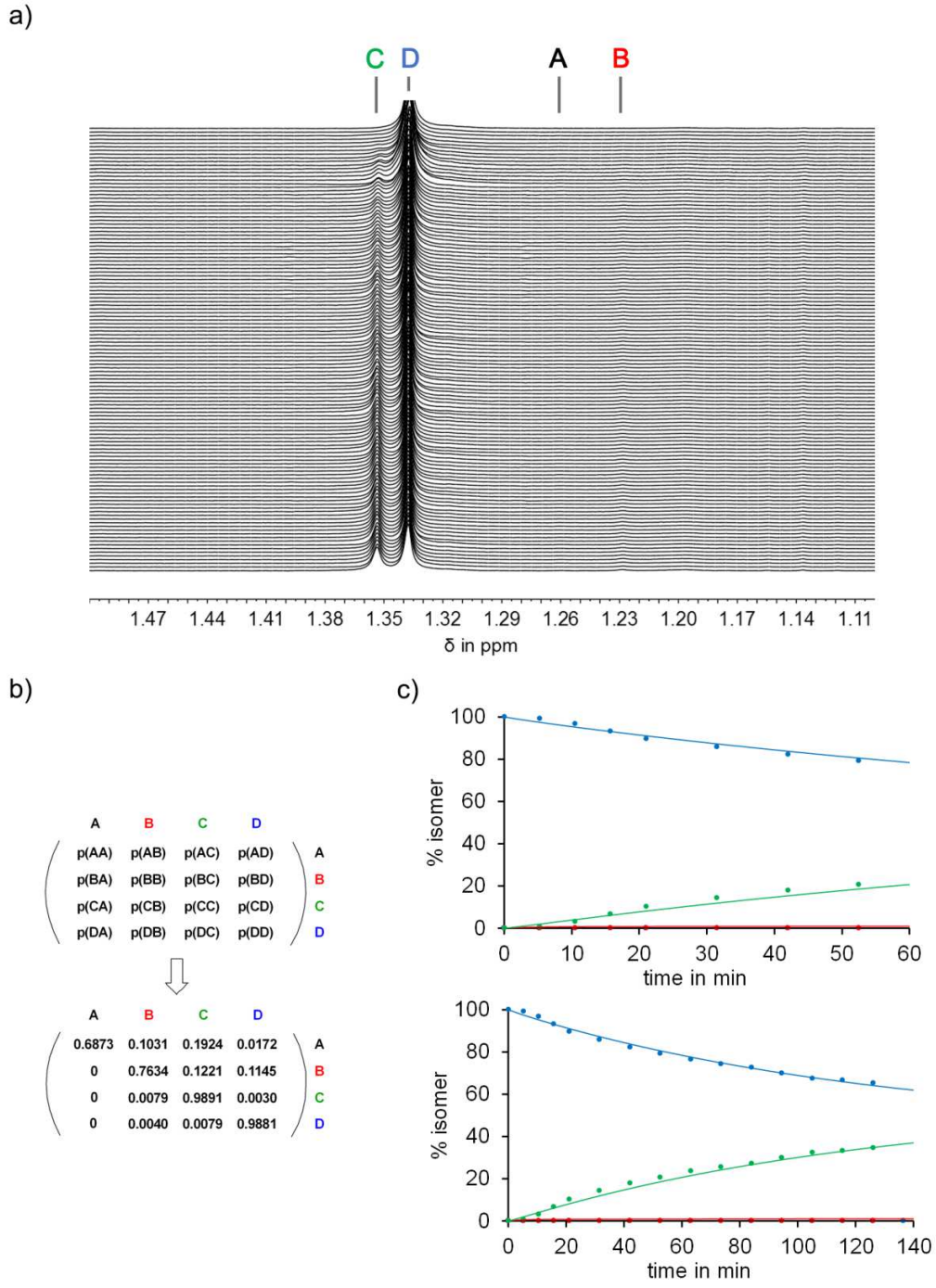

Supplementary Figure 39 | Markov matrix analysis of D in DMSO-d_6. Markov matrix analysis of the photoreactions of **1** starting from isomer **D** in DMSO-d_6 solution at 22 °C under 405 nm illumination. a) Section of the ^{1}H NMR spectra (400 MHz) recorded during irradiation of **D**-**1**. Spectra were recorded in 63 s intervals. b) Markov matrix describing the phototransition probabilities p(**ij**) per minute for **1**. c) Kinetic plots of the experimentally determined changes in isomer composition during irradiation of **D**-**1** (dots) and fitted values derived from the Markov matrix (lines).

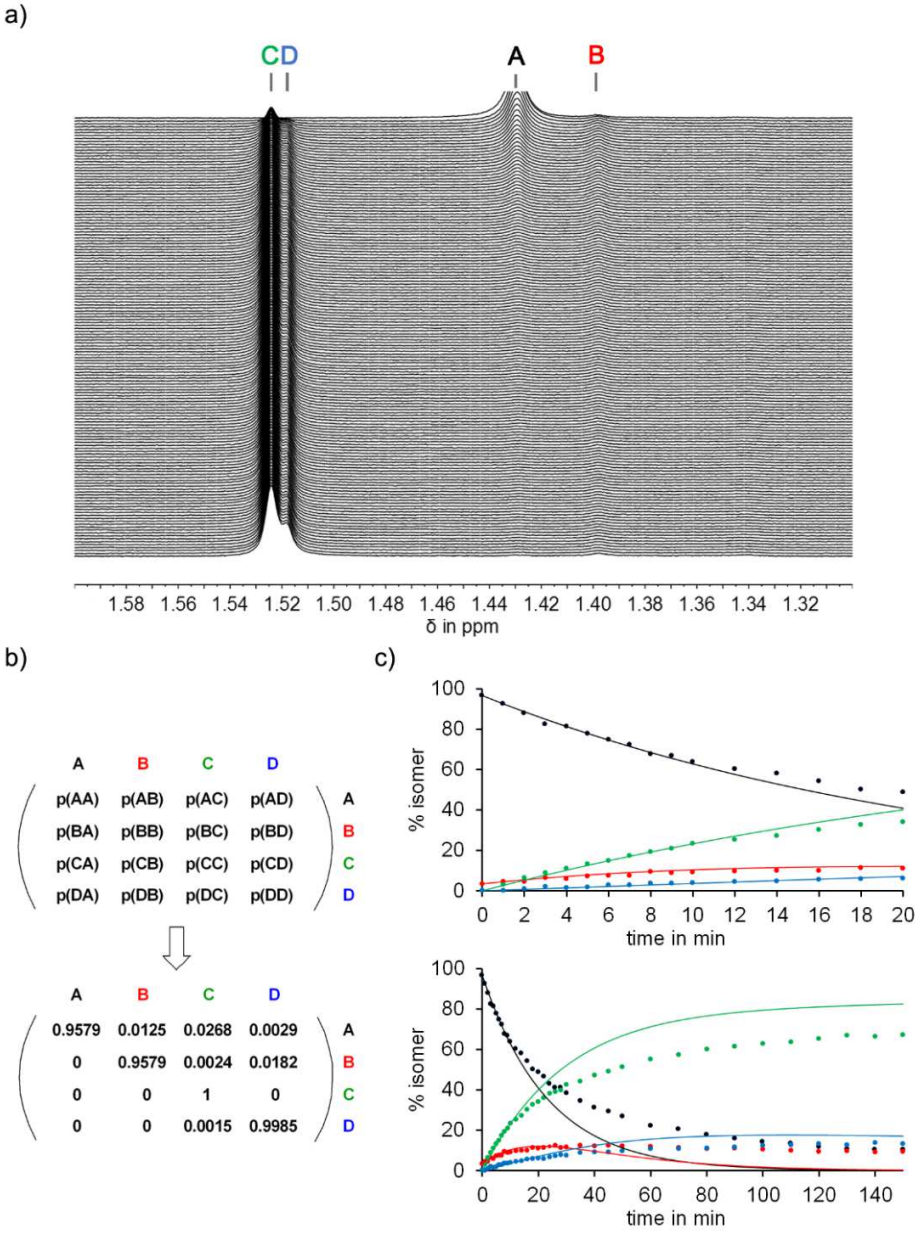

Supplementary Figure 40 | Markov matrix analysis of A in ethylene glycol. Markov matrix analysis of the photoreactions of **1** starting from isomer **A** in ethylene glycol solution at 22 °C under 405 nm illumination. The spectra were recorded with PRESAT solvent suppression and a benzene-d_6 capillary. a) Section of the ^{1}H NMR spectra (400 MHz) recorded during irradiation of **A**-**1**. Spectra were recorded in 60 s intervals. b) Markov matrix describing the phototransition probabilities p(**ij**) per minute for **1**. c) Kinetic plots of the experimentally determined changes in isomer composition during irradiation of **A**-**1** (dots) and fitted values derived from the Markov matrix (lines). As ethylene glycol is a very viscous liquid the diffusion inside the NMR-tube is very slow. Therefore unreacted **A**-1 from above the glass fiber or from the bottom of the NMR-tube diffuse slowly inside the measuring area and the kinetics slow down. This effect cannot be simulated by the Markov Matrix. Hence we used only the first minutes to fit the Markov Matrix as the diffusion should be negligible in this section.

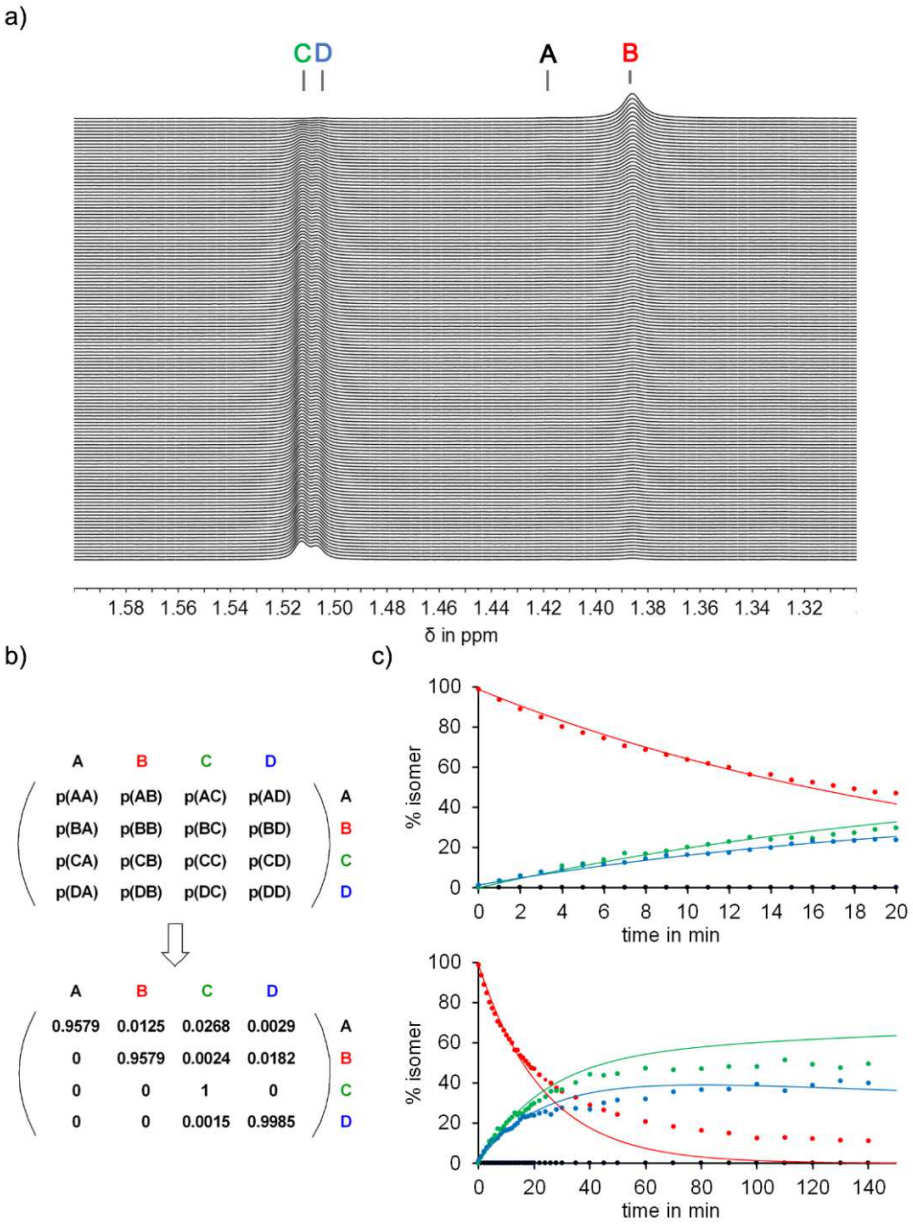

Supplementary Figure 41 | Markov matrix analysis of B in ethylene glycol. Markov matrix analysis of the photoreactions of **1** starting from isomer **B** in ethylene glycol solution at 22 °C under 405 nm illumination. The spectra were recorded with PRESAT solvent suppression and a benzene-d_6 capillary. a) Section of the ^{1}H NMR spectra (400 MHz) recorded during irradiation of **B**-**1**. Spectra were recorded in 60 s intervals. b) Markov matrix describing the phototransition probabilities p(**ij**) per minute for **1**. c) Kinetic plots of the experimentally determined changes in isomer composition during irradiation of **B**-**1** (dots) and fitted values derived from the Markov matrix (lines). As ethylene glycol is a very viscous liquid the diffusion inside the NMR-tube is very slow. Therefore unreacted **B**-1 from above the glass fiber or from the bottom of the NMR-tube diffuse slowly inside the measuring area and the kinetics slow down. This effect cannot be simulated by the Markov Matrix. Hence we used only the first minutes to fit the Markov Matrix as the diffusion should be negligible in this section.

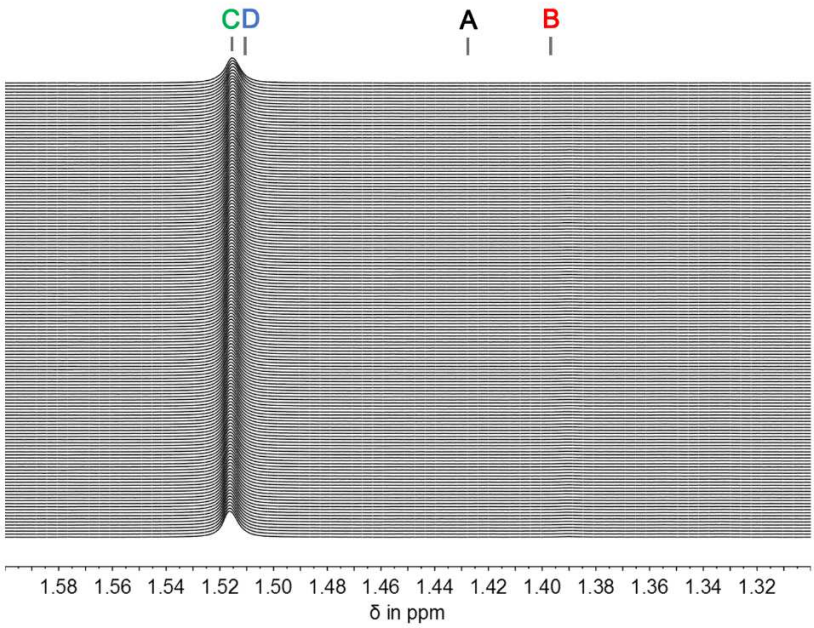

Supplementary Figure 42 | Markov matrix analysis of C in ethylene glycol. Markov matrix analysis of the photoreactions of **1** starting from isomer **C** in ethylene glycol solution at 22 °C under 405 nm illumination. The spectra were recorded with PRESAT solvent suppression and a benzene-d_6 capillary. a) Section of the ^{1}H NMR spectra (400 MHz) recorded during irradiation of **C**-**1**. Spectra were recorded in 60 s intervals. No changes in isomer concentration could be measured although the experiment was conducted twice. Probably the weak signal of upcoming isomer **D** could not be detected because it's overlapping with the signal of **C.** Nevertheless this experiment shows that the photo isomerization of **C** is very slow in comparison with those of **A** and **B** and therefore does not affect the kinetics of **A** and **B**.

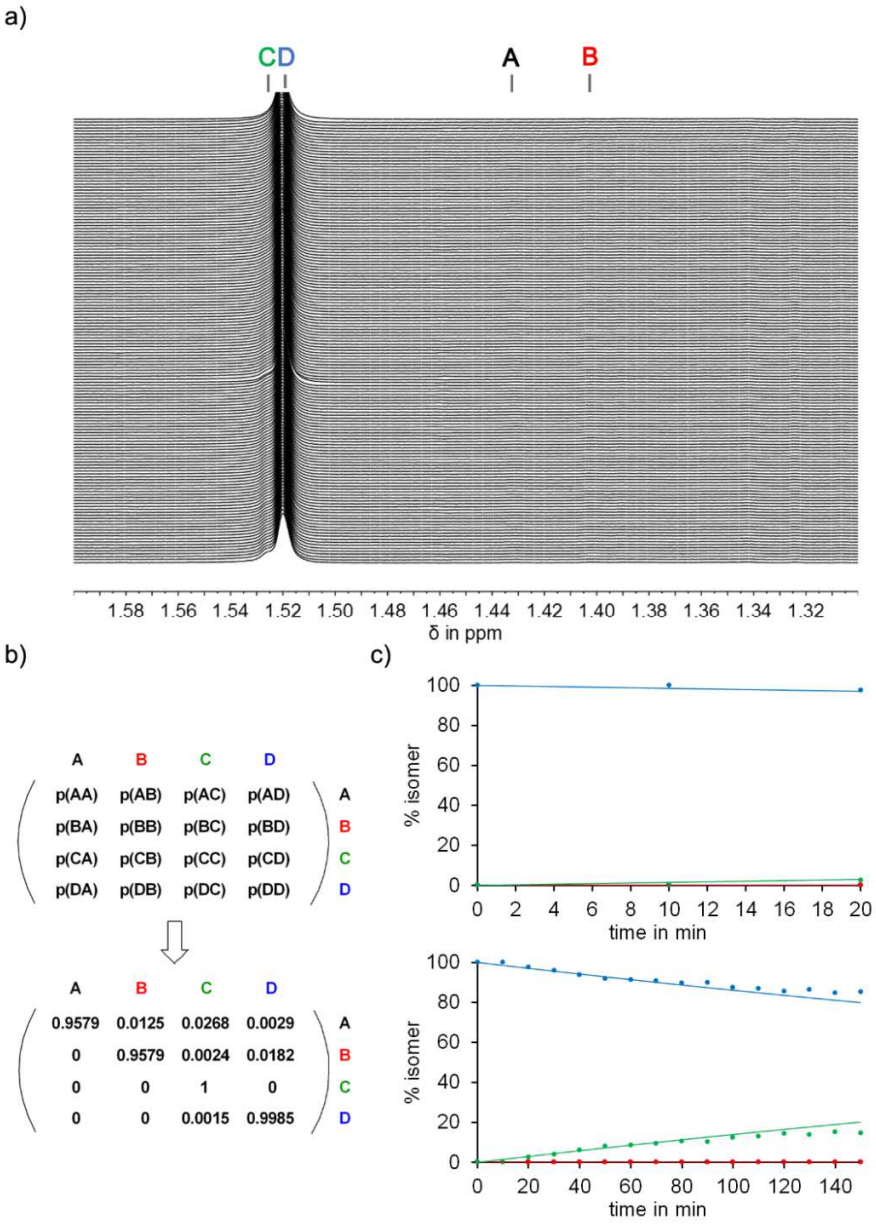

Supplementary Figure 43 | Markov matrix analysis of D in ethylene glycol. Markov matrix analysis of the photoreactions of **1** starting from isomer **D** in ethylene glycol solution at 22 °C under 405 nm illumination. The spectra were recorded with PRESAT solvent suppression and a benzene-d_6 capillary. a) Section of the ^{1}H NMR spectra (400 MHz) recorded during irradiation of **D**-**1**. Spectra were recorded in 60 s intervals. b) Markov matrix describing the phototransition probabilities p(**ij**) per minute for **1**. c) Kinetic plots of the experimentally determined changes in isomer composition during irradiation of **D**-**1** (dots) and fitted values derived from the Markov matrix (lines). As ethylene glycol is a very viscous liquid the diffusion inside the NMR-tube is very slow. Therefore unreacted **D**-1 from above the glass fiber or from the bottom of the NMR-tube diffuse slowly inside the measuring area and the kinetics slow down. This effect cannot be simulated by the Markov Matrix. Hence we used only the first minutes to fit the Markov Matrix as the diffusion should be negligible in this section.

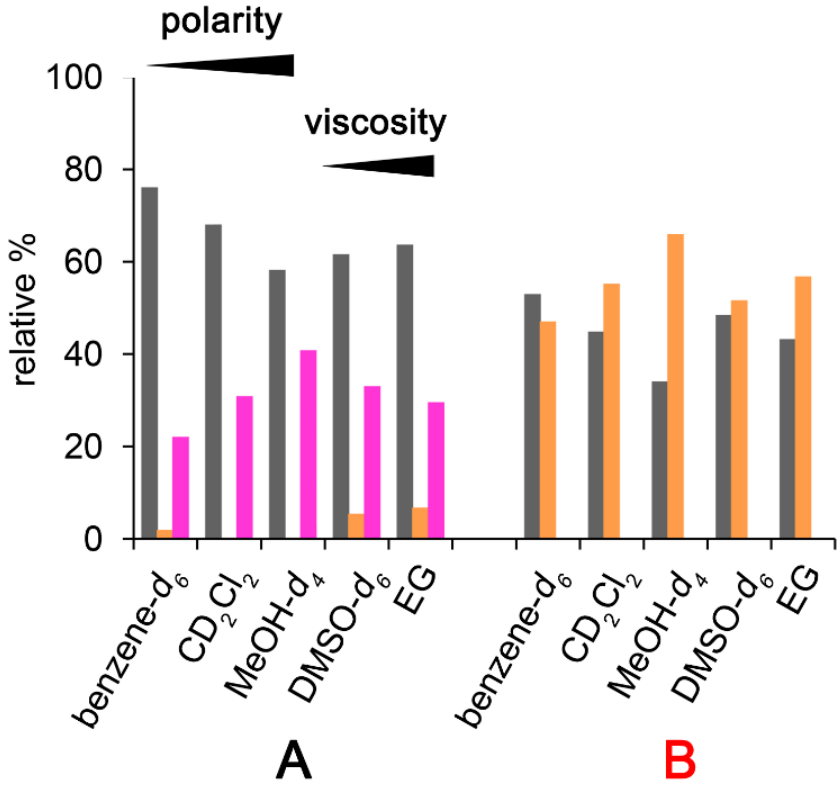

Supplementary Figure 44 | Relative quantum yields for 1 in different solvents. Markov matrix analysis of the photoreactions of **1** in different solvents at 27 °C under 405 nm illumination. The relative efficiency of different processes is given when solvent polarity and viscosity are varied independently from each other. The different photoprocesses are color coded: single-bond rotation (SBR) in purple, double-bond isomerization (DBI) in grey, and hula twist (HT) in orange.

Comparison of the photoconversion of A and B at different temperatures

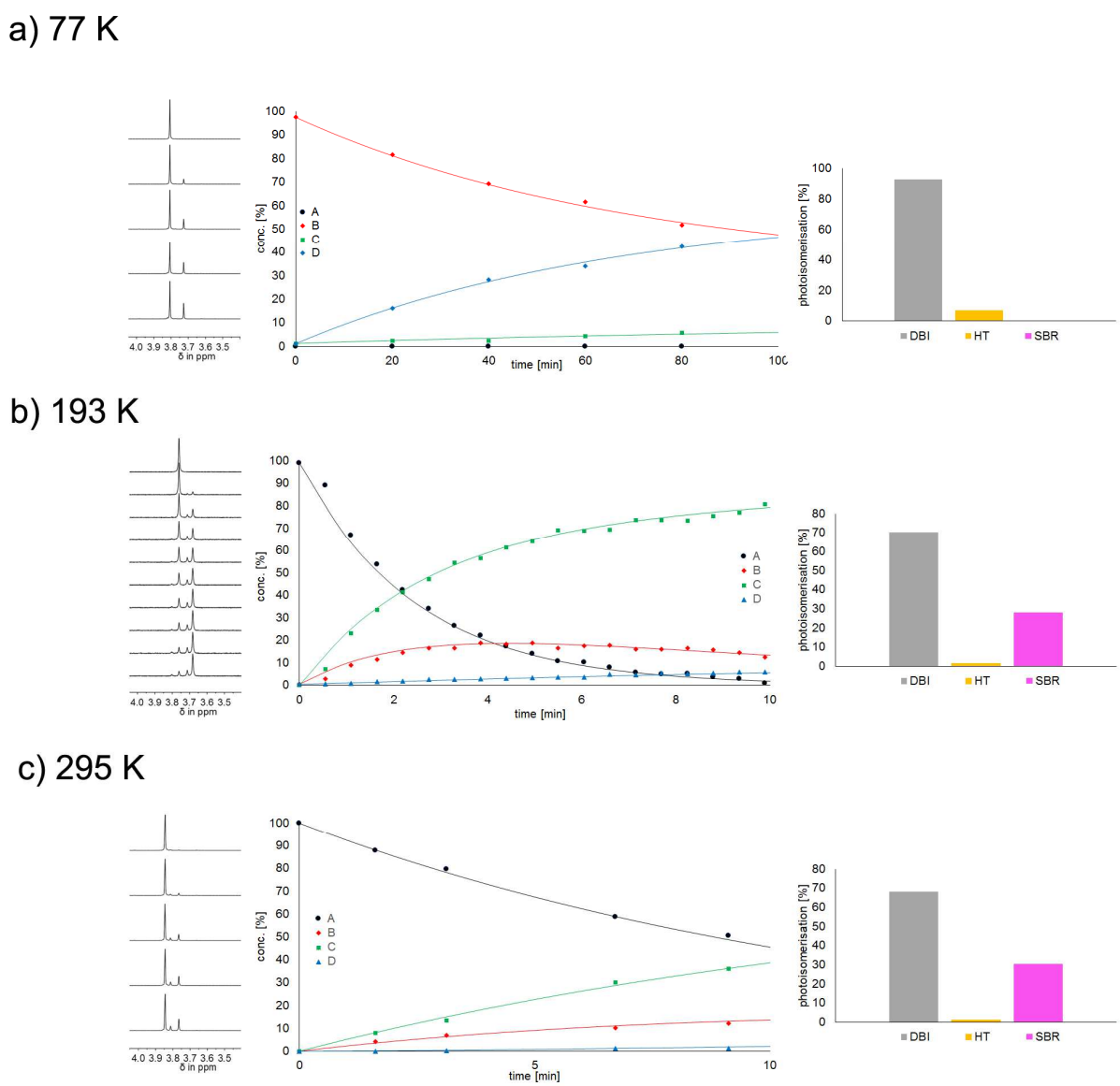

Supplementary Figure 45 | Photoreactions of A in CD_2Cl_2 at different temperatures. ^{1}H NMR spectra, Markov matrix analysis, and comparison of the different photoreactions (double-bond isomerization (DBI), hula twist (HT), single-bond rotation (SBR)) at a) 77 K (ice), b) 193 K (liquid), and c) 295 K (liquid) under 405 nm illumination. The rates of the photoreactions at different temperatures cannot be compared with each other as the illumination conditions are not comparable at different temperatures. Kinetic plots of the experimentally determined changes in isomer composition during irradiation of **A-1** (dots) are fitted by a simplified Markov matrix (lines) using phototransition probabilities of **C-1** = 0 and **D-1** = 0 since these transitions are much slower and therefore negligible in the experiments.

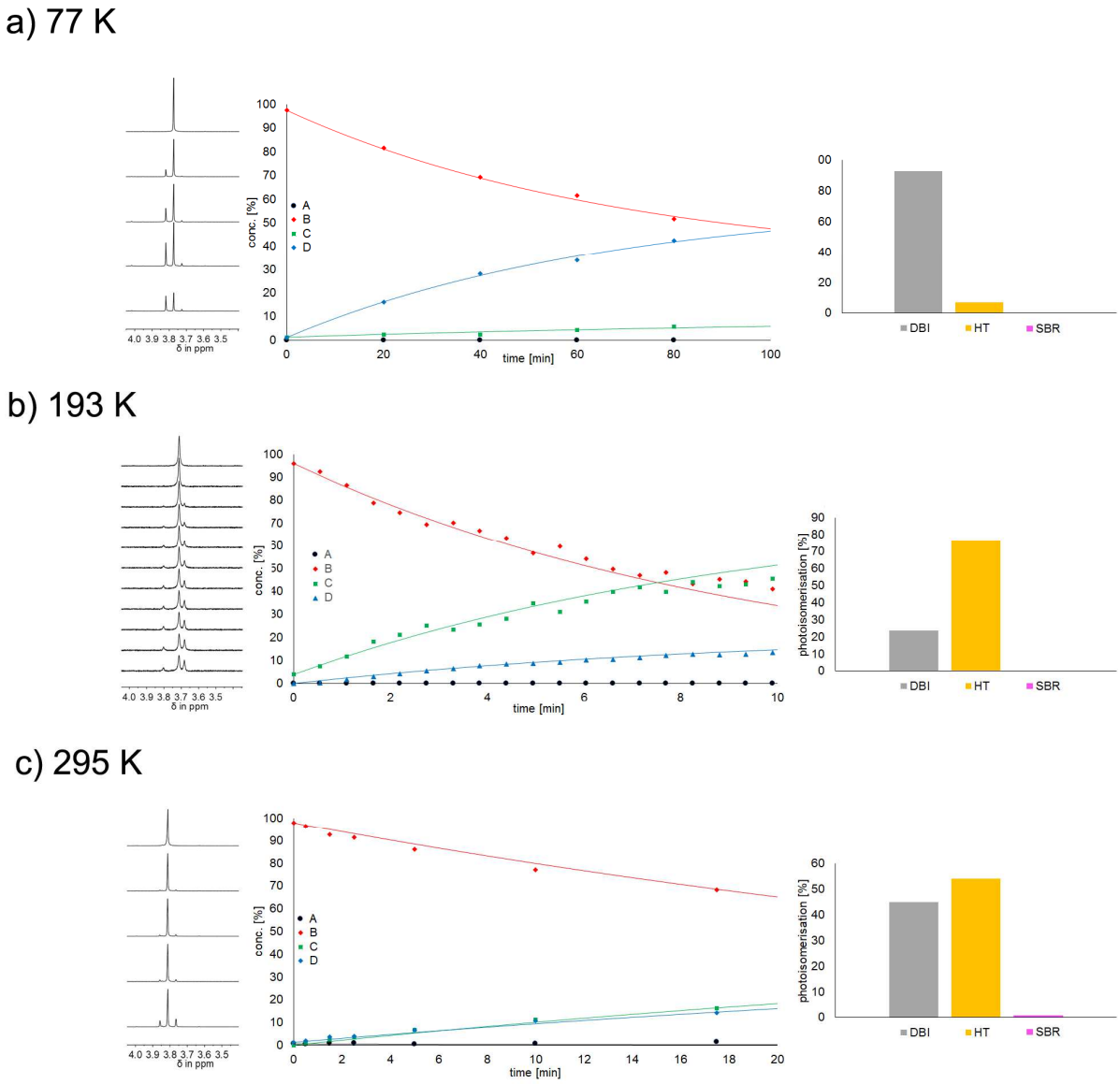

Supplementary Figure 46 | Photoreactions of B in CD_2Cl_2 at different temperatures. ^{1}H NMR spectra, Markov matrix analysis, and comparison of the different photoreactions (double-bond isomerization (DBI), hula twist (HT), single-bond rotation (SBR)) at a) 77 K (ice), b) 193 K (liquid), and c) 295 K (liquid) under 405 nm illumination. The rates of the photoreactions at different temperatures cannot be compared with each other as the illumination conditions are not comparable at different temperatures. Kinetic plots of the experimentally determined changes in isomer composition during irradiation of **B-1** (dots) are fitted by a simplified Markov matrix (lines) using phototransition probabilities of **C-1** = 0 and **D-1** = 0 since these transitions are much slower and therefore negligible in the experiments.

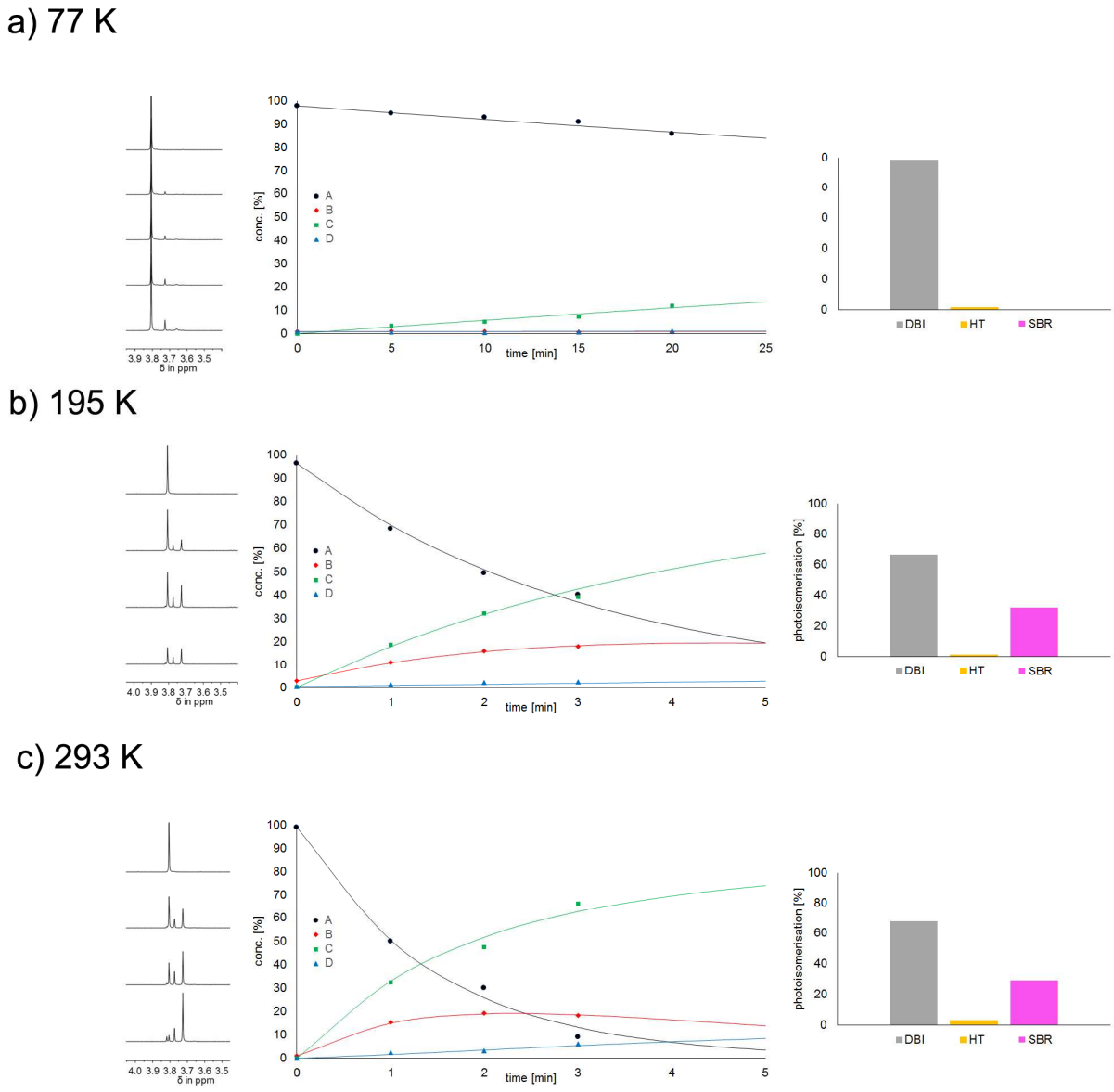

Supplementary Figure 47 | Photoreactions of A in EPA at different temperatures. ^{1}H NMR spectra in CD_2Cl_2, Markov matrix analysis, and comparison of the different photoreactions (double-bond isomerization (DBI), hula twist (HT), single-bond rotation (SBR)) at a) 77 K (ice), b) 193 K (liquid), and c) 295 K (liquid) under 405 nm illumination. The rates of the photoreactions at different temperatures cannot be compared with each other as the illumination conditions are not comparable at different temperatures. Kinetic plots of the experimentally determined changes in isomer composition during irradiation of **A-1** (dots) are fitted by a simplified Markov matrix (lines) using phototransition probabilities of **C-1** = 0 and **D-1** = 0 since these transitions are much slower and therefore negligible in the experiments.

a) 77 K

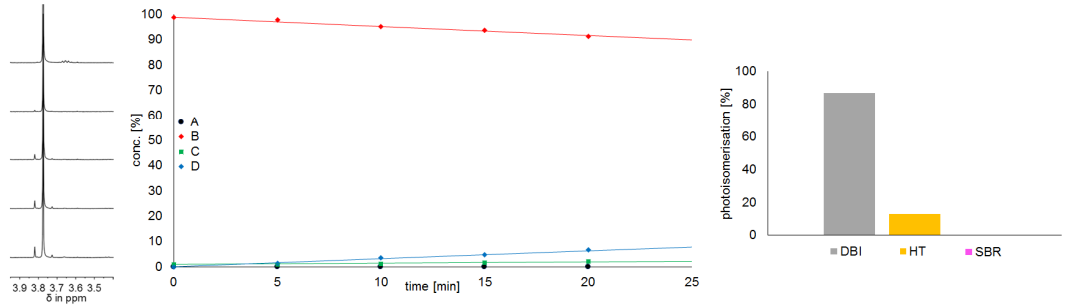

b) 195 K

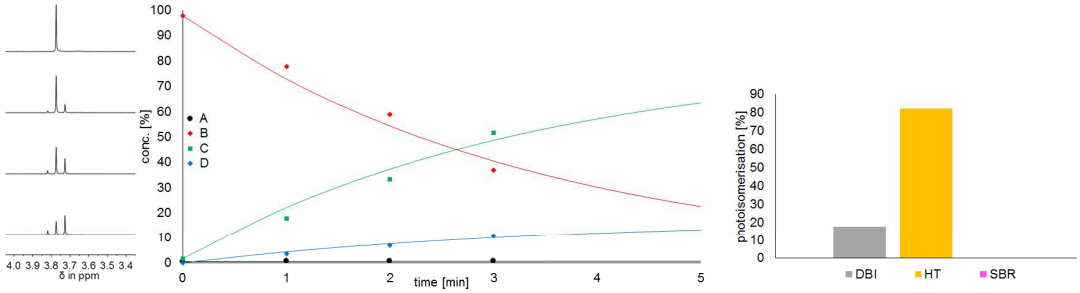

c) 293 K

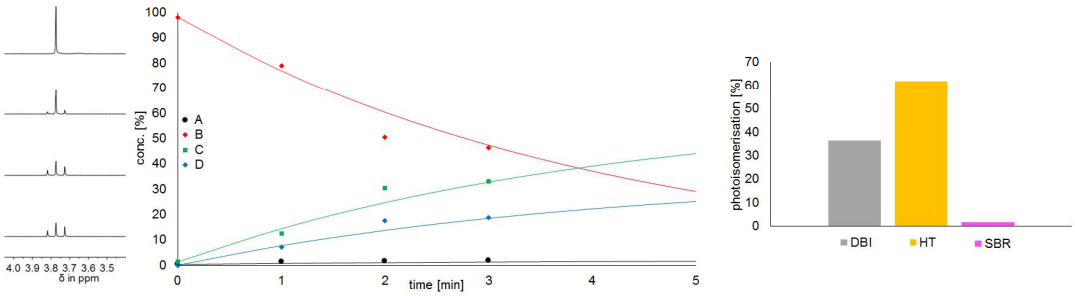

Supplementary Figure 48 | Photoreactions of B in EPA at different temperatures. Photoreactions of **B-1** in EPA at different temperatures. ^{1}H NMR spectra in CD_2Cl_2, Markov matrix analysis, and comparison of the different photoreactions (double-bond isomerization (DBI), hula twist (HT), single-bond rotation (SBR)) at a) 77 K (ice), b) 193 K (liquid), and c) 295 K (liquid) under 405 nm illumination. The rates of the photoreactions at different temperatures cannot be compared with each other as the illumination conditions are not comparable at different temperatures. Kinetic plots of the experimentally determined changes in isomer composition during irradiation of **B-1** (dots) are fitted by a simplified Markov matrix (lines) using phototransition probabilities of **C-1** = 0 and **D-1** = 0 since these transitions are much slower and therefore negligible in the experiments.

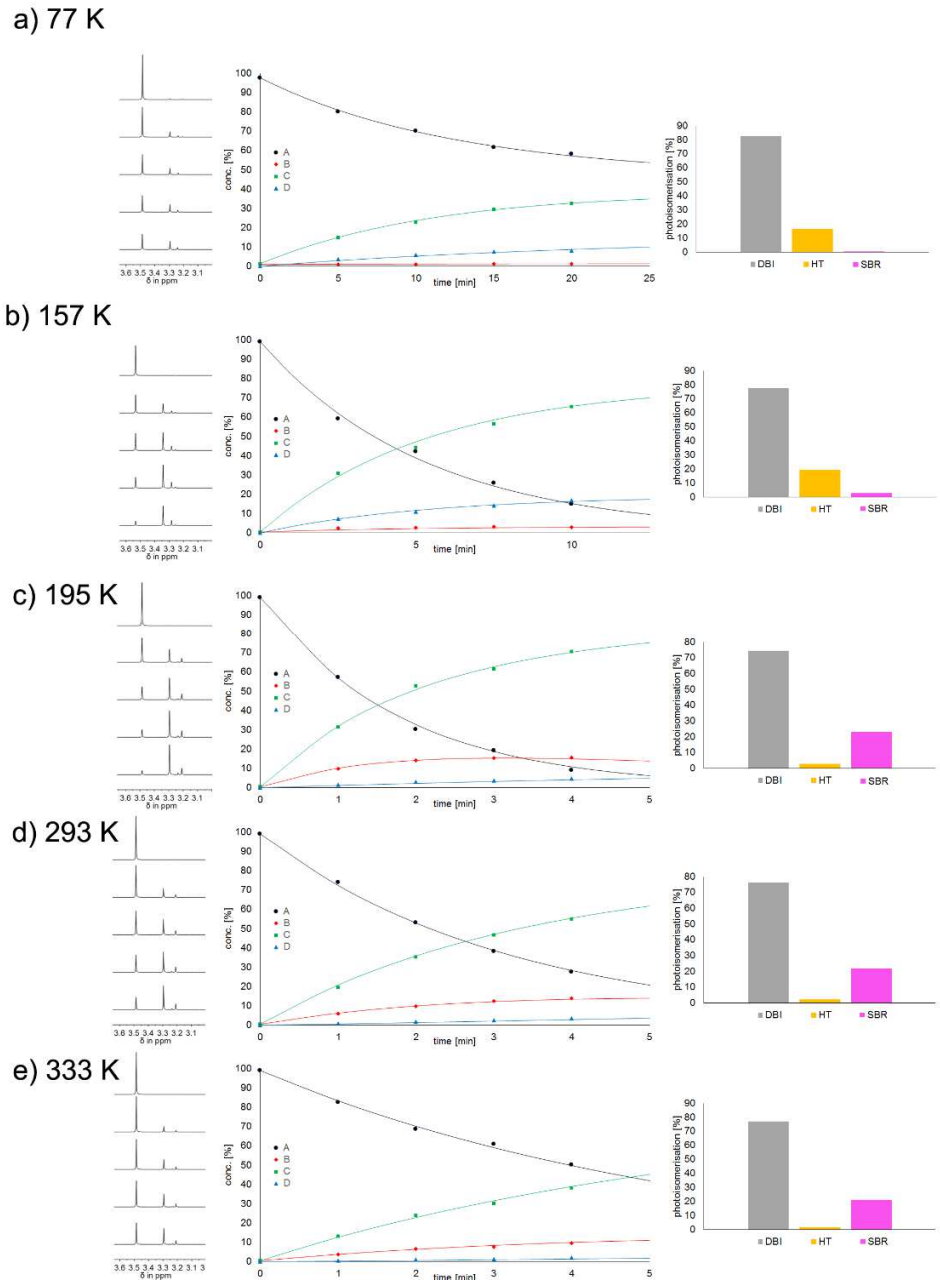

Supplementary Figure 49 | Photoreactions of A in toluene-d_8 at different temperatures. ^{1}H NMR spectra, Markov matrix analysis, and comparison of the different photoreactions (double-bond isomerization (DBI), hula twist (HT), single-bond rotation (SBR)) at a) 77 K (ice), b) 157 K (ice), c) 195 K (liquid), d) 293 K (liquid), and e) 333 K (liquid) under 405 nm illumination. The rates of the photoreactions at different temperatures cannot be compared with each other as the illumination conditions are not comparable at different temperatures. Kinetic plots of the experimentally determined changes in isomer composition during irradiation of **A**-**1** (dots) are fitted by a simplified Markov matrix (lines) using phototransition probabilities of **C-1 =** 0 and **D-1** = 0 since these transitions are much slower and therefore negligible in the experiments.

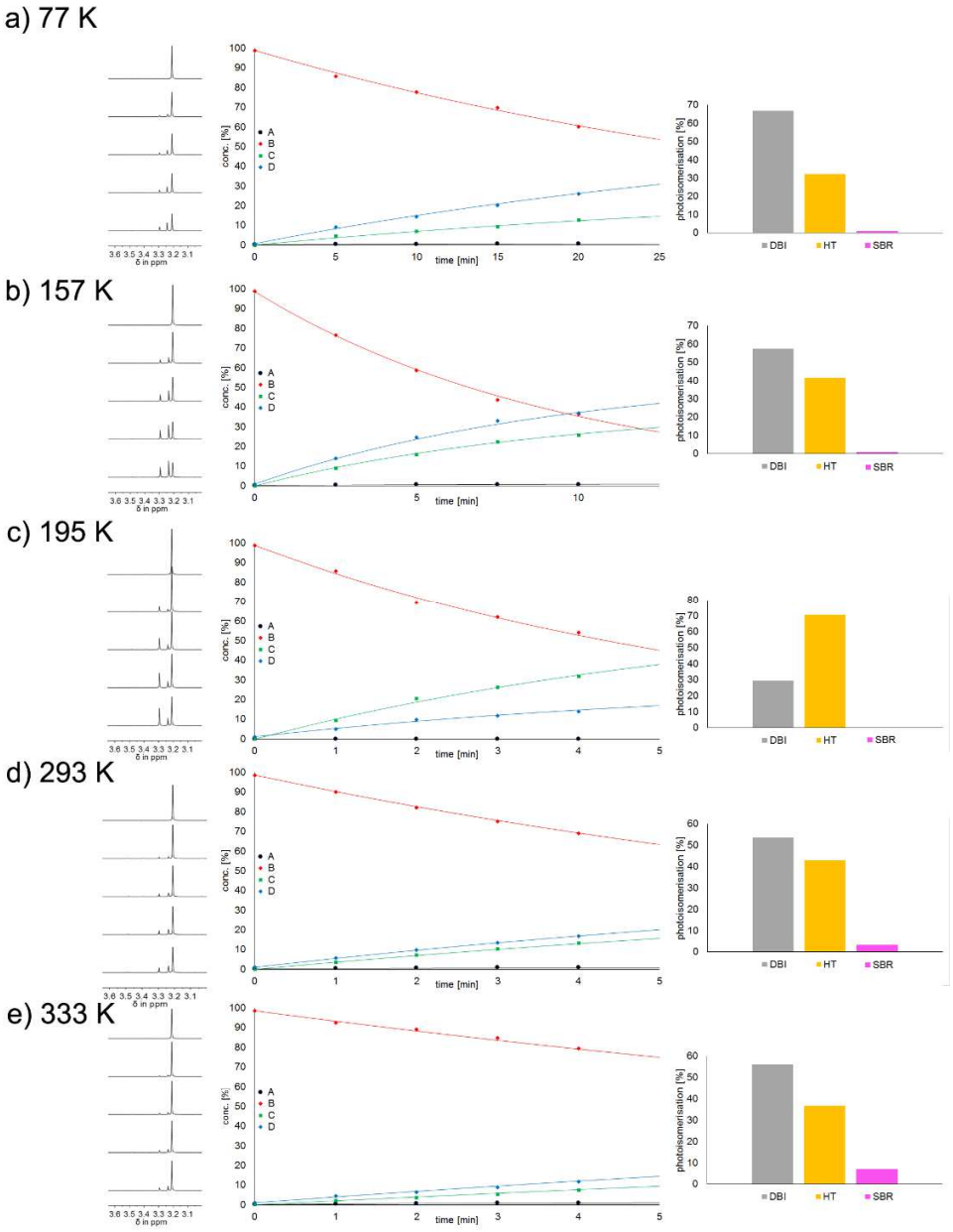

Supplementary Figure 50 | Photoreactions of B in toluene-*d*$_8$ at different temperatures. ^{1}H NMR spectra, Markov matrix analysis, and comparison of the different photoreactions (double-bond isomerization (DBI), hula twist (HT), single-bond rotation (SBR)) at a) 77 K (ice), b) 157 K (ice), c) 195 K (liquid), d) 293 K (liquid), and e) 333 K (liquid) under 405 nm illumination. The rates of the photoreactions at different temperatures cannot be compared with each other as the illumination conditions are not comparable at different temperatures. Kinetic plots of the experimentally determined changes in isomer composition during irradiation of **B-1** (dots) are fitted by a simplified Markov matrix (lines) using phototransition probabilities of **C-1** = 0 and **D-1** = 0 since these transitions are much slower and therefore negligible in the experiments.

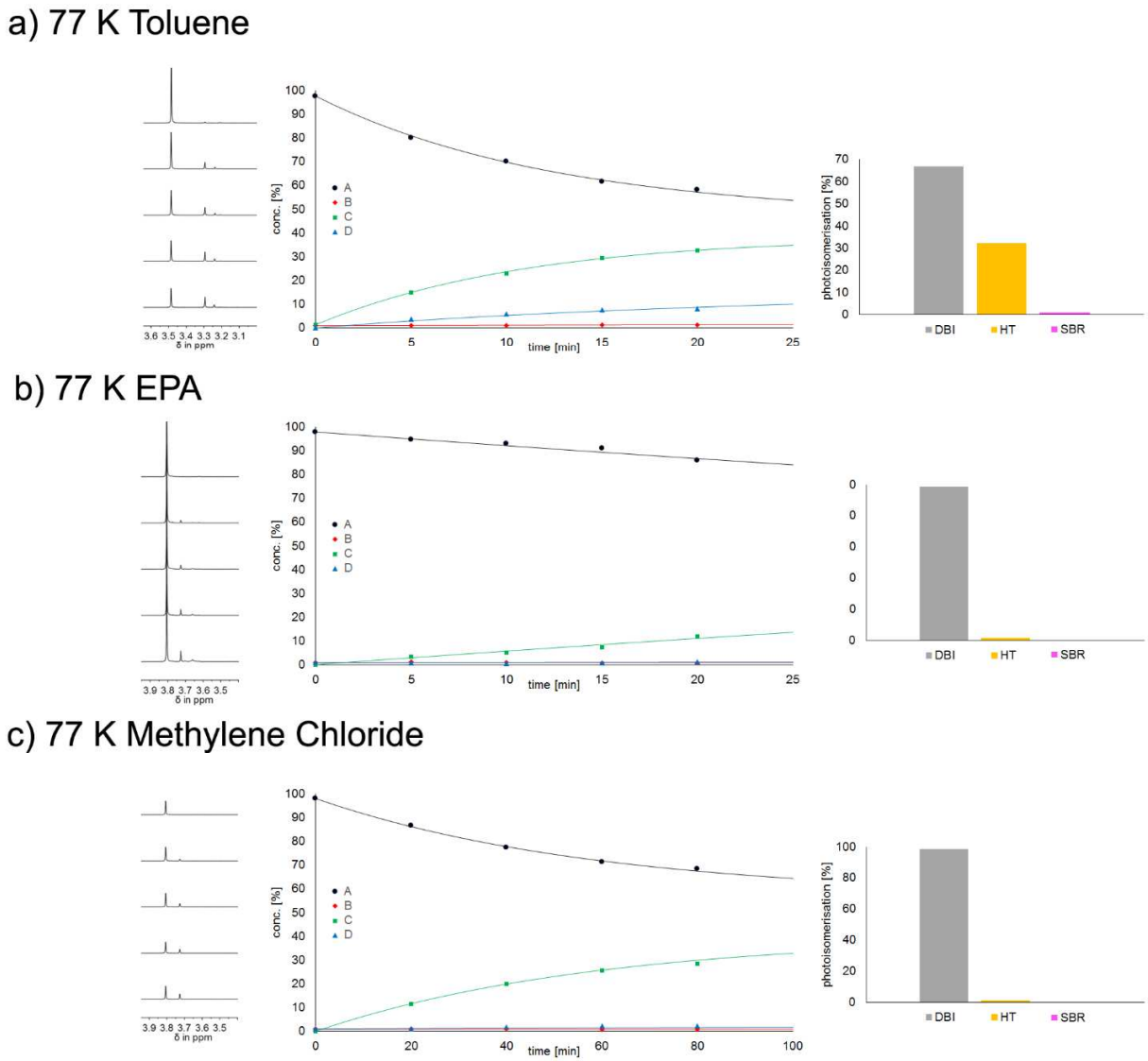

Supplementary Figure 51 | Photoreactions of A in different solvent ices at 77 K. ^{1}H NMR spectra, Markov matrix analysis, and comparison of the different photoreactions (double-bond isomerization (DBI), hula twist (HT), single-bond rotation (SBR)) at in a) toluene-d_8 (ice) at 77 K, b) EPA (glas) at 77 K, and c) CD_2Cl_2 (ice) at 77 K under 405 nm illumination. The EPA-solvent mixture was evaporated and the ^{1}H NMR spectra were recorded in CD_2Cl_2 after illumination. The rates of the photoreactions in different media cannot be compared with each other as the illumination conditions are not comparable. Kinetic plots of the experimentally determined changes in isomer composition during irradiation of **A**-**1** (dots) are fitted by a simplified Markov matrix (lines) with phototransition probabilities of **C-1** = 0 and **D-1** = 0 since these transitions are much slower and therefore negligible.

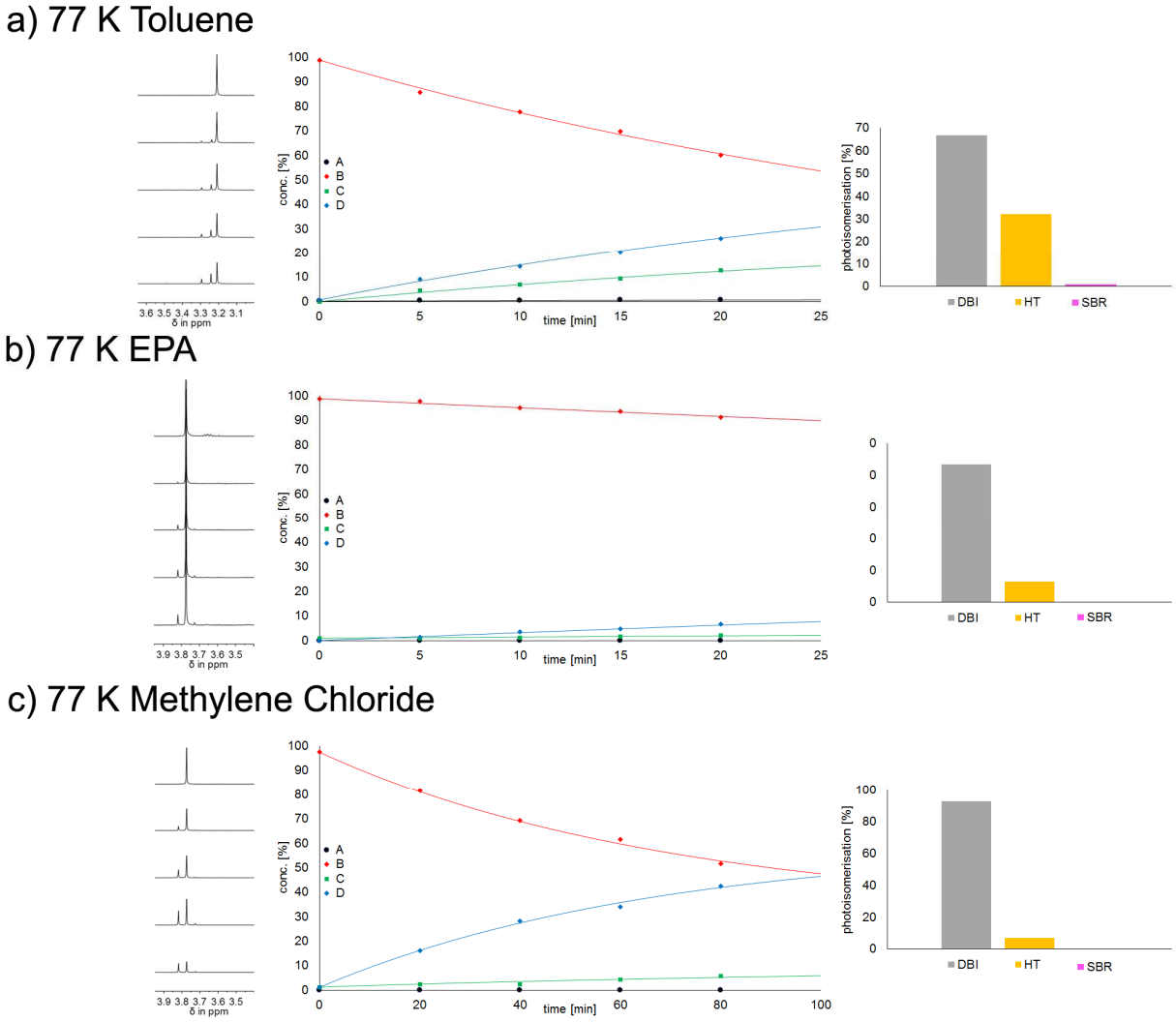

Supplementary Figure 52 | Photoreactions of B in different solvent ices at 77 K. ^{1}H NMR spectra, Markov matrix analysis, and comparison of the different photoreactions (double-bond isomerization (DBI), hula twist (HT), single-bond rotation (SBR)) at in a) toluene-d_8 (ice) at 77 K, b) EPA (glas) at 77 K, and c) CD_2Cl_2 (ice) at 77 K under 405 nm illumination. The EPA-solvent mixture was evaporated and the ^{1}H NMR spectra were recorded in CD_2Cl_2 after illumination. The rates of the photoreactions in different media cannot be compared with each other as the illumination conditions are not comparable. Kinetic plots of the experimentally determined changes in isomer composition during irradiation of **B**-**1** (dots) are fitted by a simplified Markov matrix (lines) with phototransition probabilities of **C-1** = 0 and **D-1** = 0 since these transitions are much slower and therefore negligible.

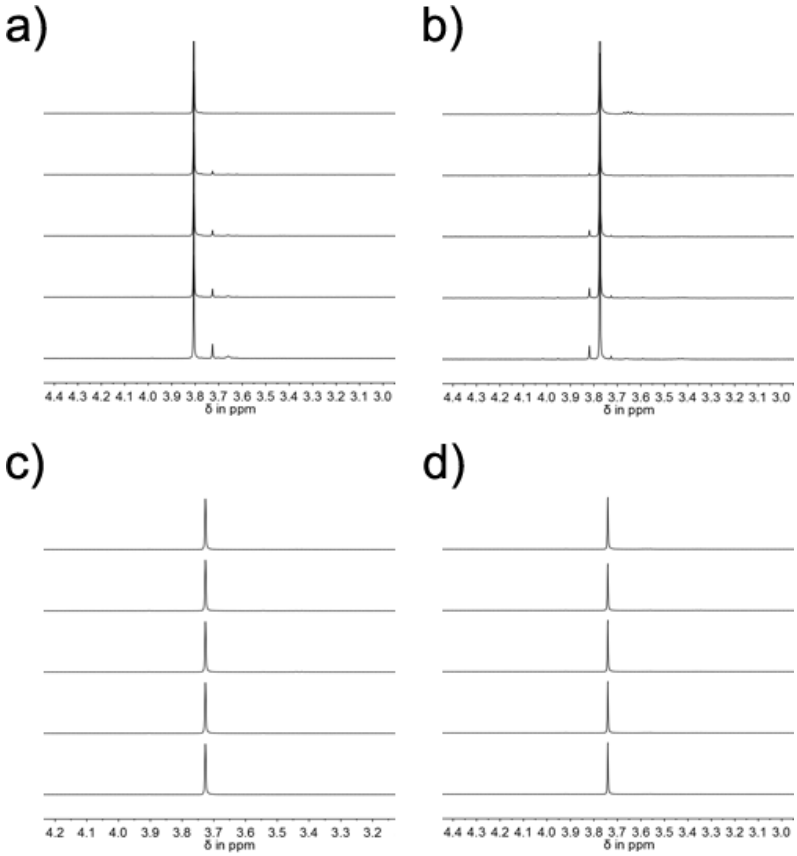

Supplementary Figure 53 | Comparison of the photoreaction kinetics of 1 in EPA matrices at 77 K. ^{1}H NMR spectra recorded after 405 nm irradiation of a) **A-1** (5 min intervals), (b) **B-1** (5 min intervals), c) **C-1** (20 min intervals), and d) **D-1** (20 min intervals). After illumination the EPA-solvent mixture was evaporated and the spectra were recorded in CD_2Cl_2. Similar illumination conditions were ensured by a hand-build setup with fixed sample and LED positions. For **C-1** and **D-1** no photoreaction was observed.

Comparison of the photoconversion of A and B under illumination with different wavelengths

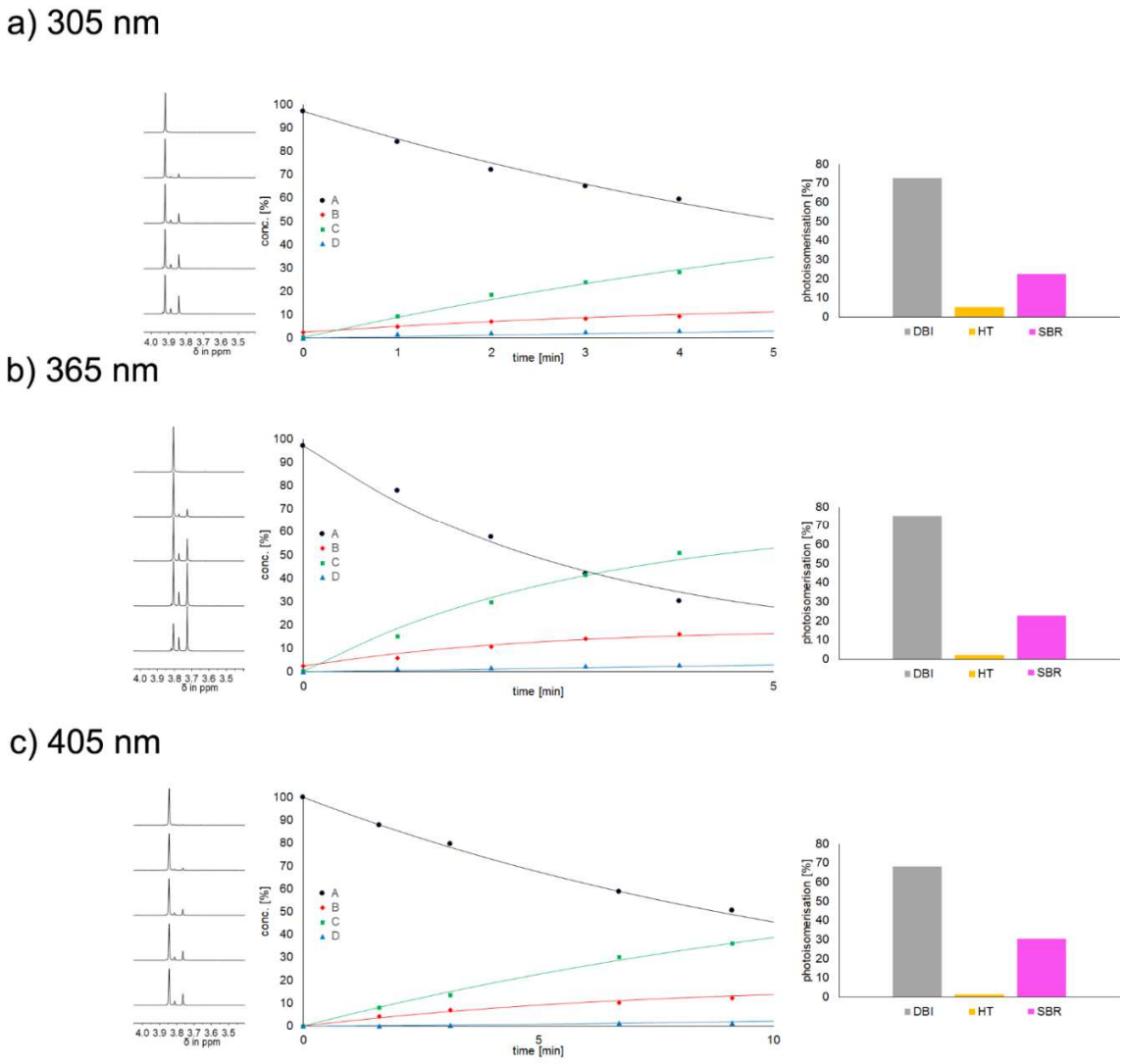

Supplementary Figure 54 | Photoreactions of A under illumination with different wavelength. Photoreactions (double-bond isomerization (DBI), hula twist (HT), single-bond rotation (SBR)) of **A-1** in CD_2Cl_2 at 20 °C using different irradiation wavelengths. ^{1}H NMR spectra, Markov matrix analysis, and comparison of the different photoreactions under a) 305 nm illumination, b) 365 nm illumination, and c) 405 nm illumination. Kinetic plots of the experimentally determined changes in isomer composition during irradiation of **A**-**1** (dots) are fitted by a simplified Markov matrix (lines) with phototransition probabilities of **C-1 =** 0 and **D-1** = 0 since these transitions are much slower and therefore negligible.

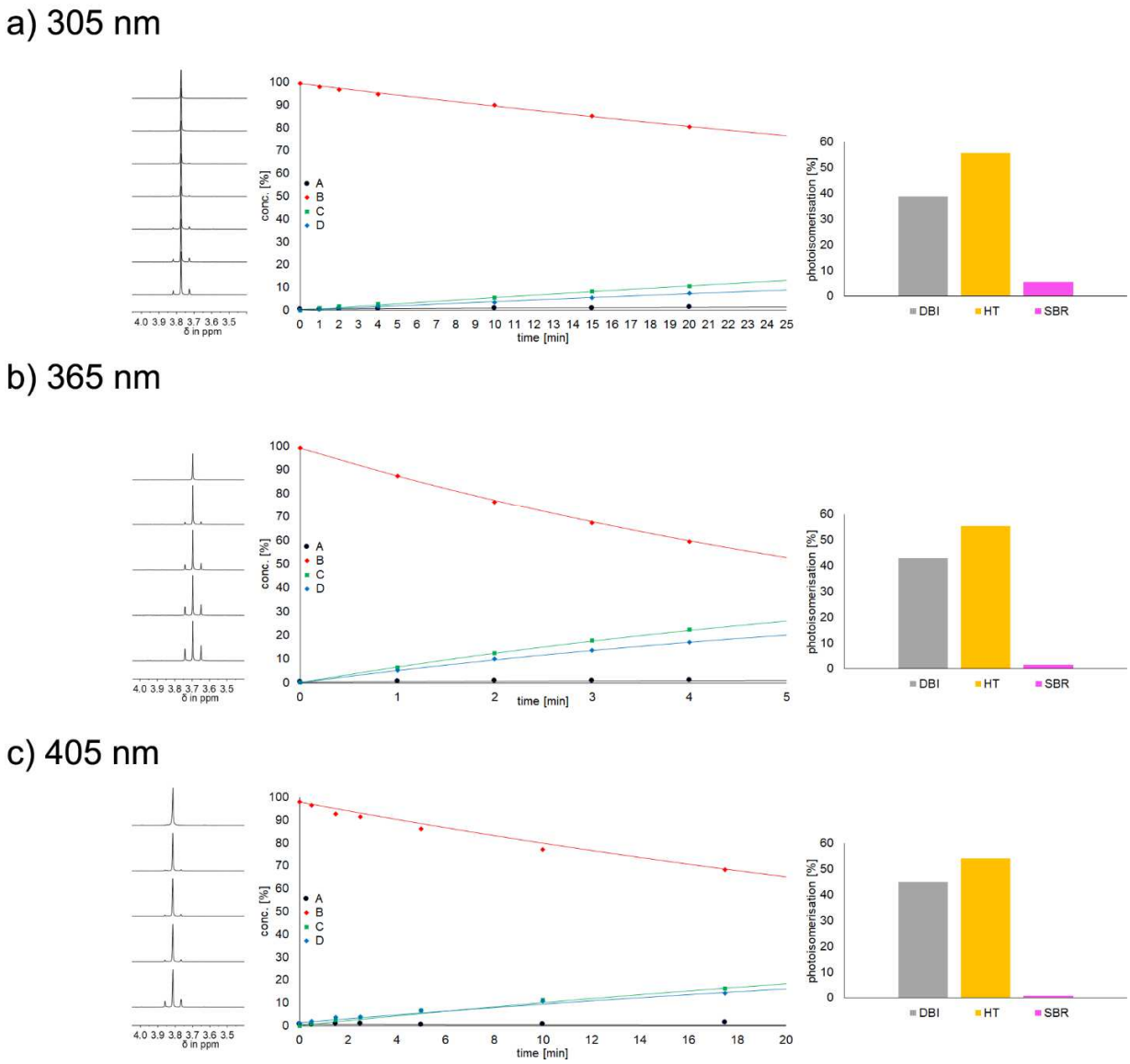

Supplementary Figure 55 | Photoreactions of B under illumination with different wavelength. Photoreactions (double-bond isomerization (DBI), hula twist (HT), single-bond rotation (SBR)) of **B-1** in CD_2Cl_2 at20 °C using different irradiation wavelengths. ^{1}H NMR spectra, Markov matrix analysis, and comparison of the different photoreactions under a) 305 nm illumination, b) 365 nm illumination, and c) 405 nm illumination. Kinetic plots of the experimentally determined changes in isomer composition during irradiation of **B-1** (dots) are fitted by a simplified Markov matrix (lines) with phototransition probabilities of **C-1** = 0 and **D-1** = 0 since these transitions are much slower and therefore negligible.

Photoconversion of A, B, C and D in EPA glass at 90 K

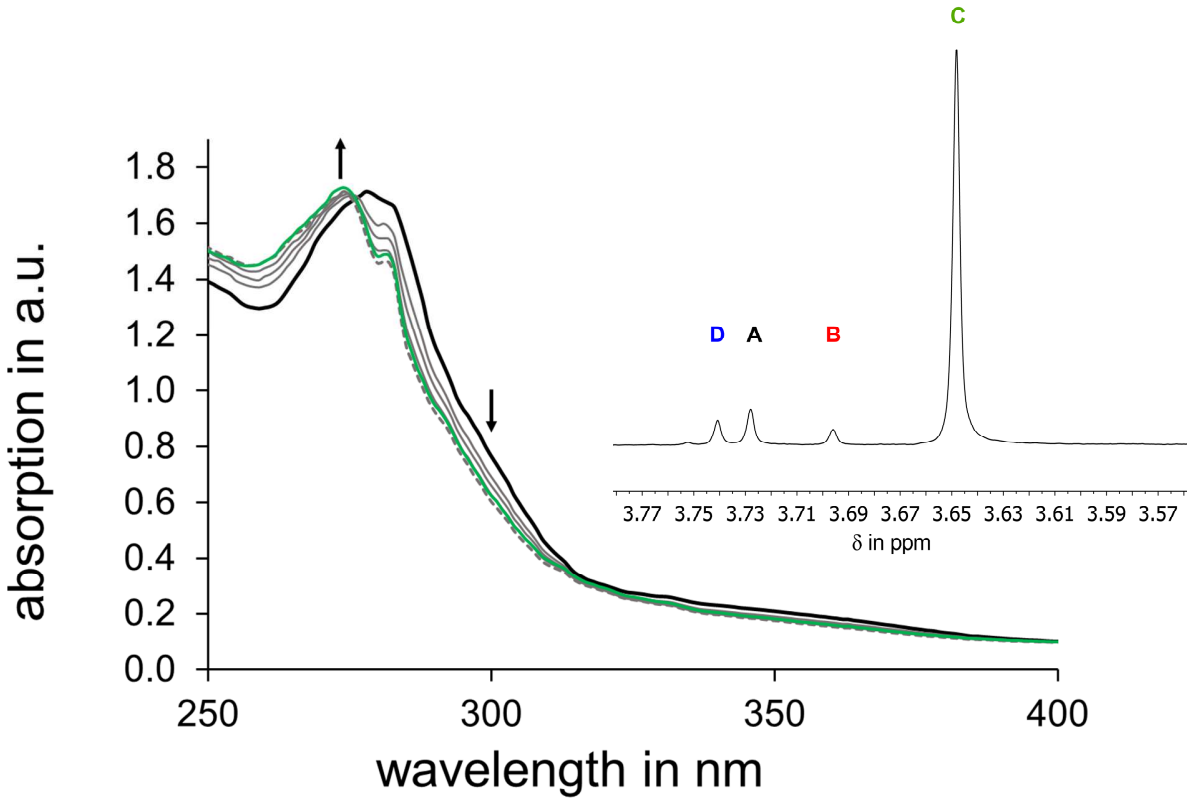

Supplementary Figure 56 | Photoconversion of A in EPA. UV/vis absorption spectra showing the photoconversion of **A** in EPA glass (diethyl ether/*iso*-pentane/ethanol 5:5:2) at 90 K. Starting from pure **A** (black) spectra were measured after 5, 10, 20 (grey lines), and 50 min (grey dashed line) of irradiation with a 405 nm ultra high power LED. After irradiation, the EPA glass was warmed to 195 K and cooled down again to 90 K (green). To determine the product distribution after irradiation the EPA solvent was evaporated, the resulting residue was dissolved in CD_2Cl_2 and a ^1H NMR spectrum (400 MHz, 27 °C) was recorded (inset). The main photoisomerization product can be assigned to **C** as shown in the NMR inset.

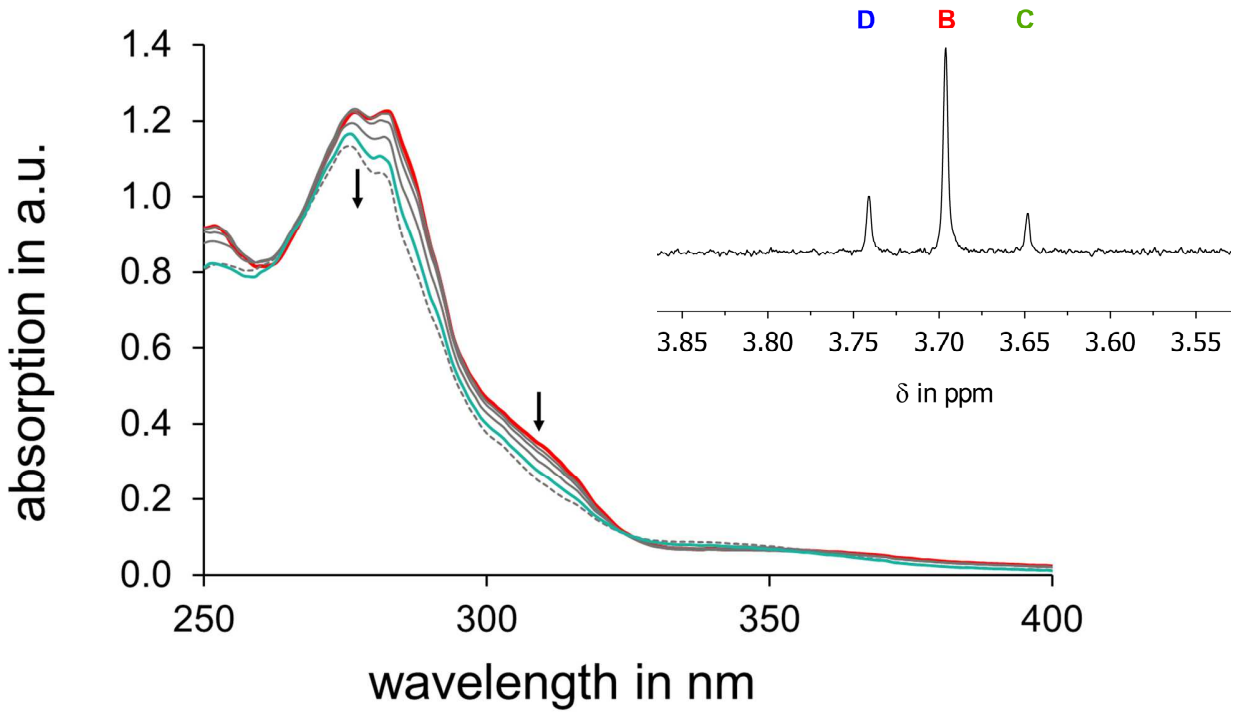

Supplementary Figure 57 | Photoconversion of B in EPA. UV/vis absorption spectra showing the photoconversion of **B** in EPA glass (diethyl ether/*iso*-pentane/ethanol 5:5:2) at 90 K. Starting from pure **B** (red) spectra were measured after 5, 10, 20 (grey lines), and 50 min (grey dashed line) of irradiation with a 405 nm ultra high power LED. After irradiation, the EPA glass was warmed to 195 K and cooled down again to 90 K (cyan). Changes in the UV/vis spectrum after warming and recooling can be assigned to diffusion effects and dilution of the spectum with unreacted **B**. To determine the product distribution after irradiation the EPA solvent was evaporated and the resulting residue was dissolved in CD_2Cl_2 and a ^1H NMR spectrum (400 MHz, 27 °C) was recorded (inset). The two photoisomerization products can be assigned to **C** and **D**, as shown in the NMR inset.

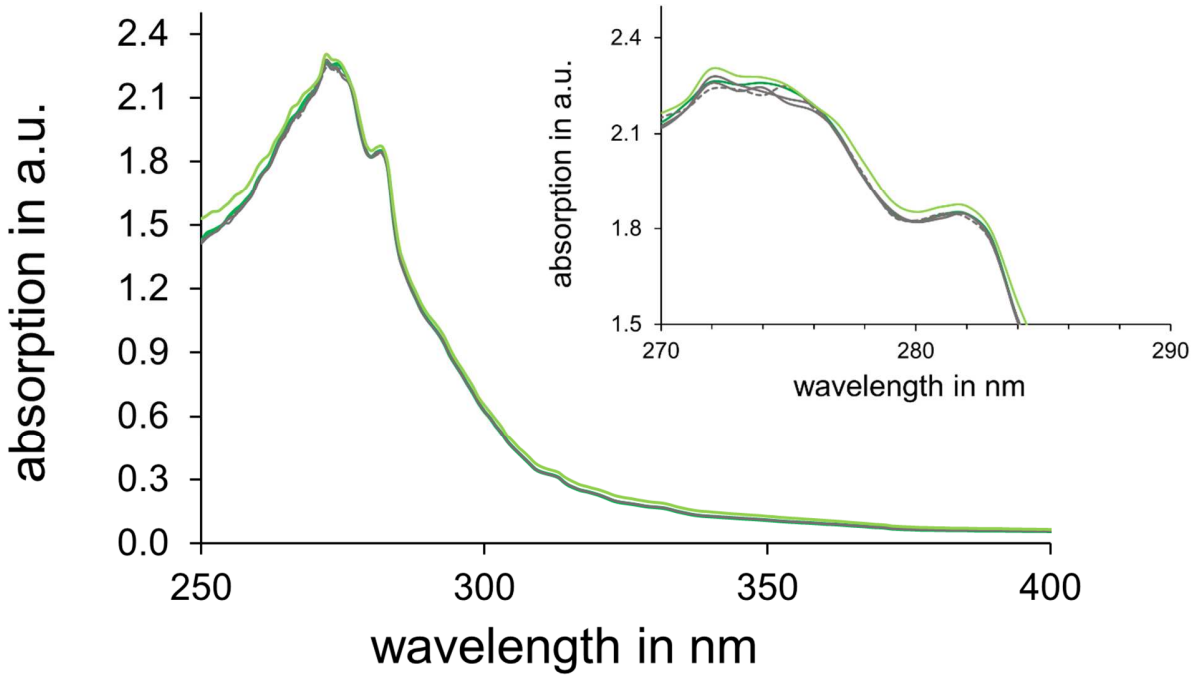

Supplementary Figure 58 | Photoconversion of C in EPA. UV/vis absorption spectra recorded during irradiation of **C** in EPA glass (diethyl ether/*iso*-pentane/ethanol 5:5:2) at 90 K. Starting from pure **C** (dark green) measurements were made after 30, 60, (grey lines), and 120 min (grey dashed line) of irradiation with a 405 nm ultra high power LED. After irradiation, the EPA glass was warmed to 195 K and cooled down again to 90 K (light green). As shown in the enlarged UV/vis absorption spectrum inset, no significant photoisomerization could be observed.

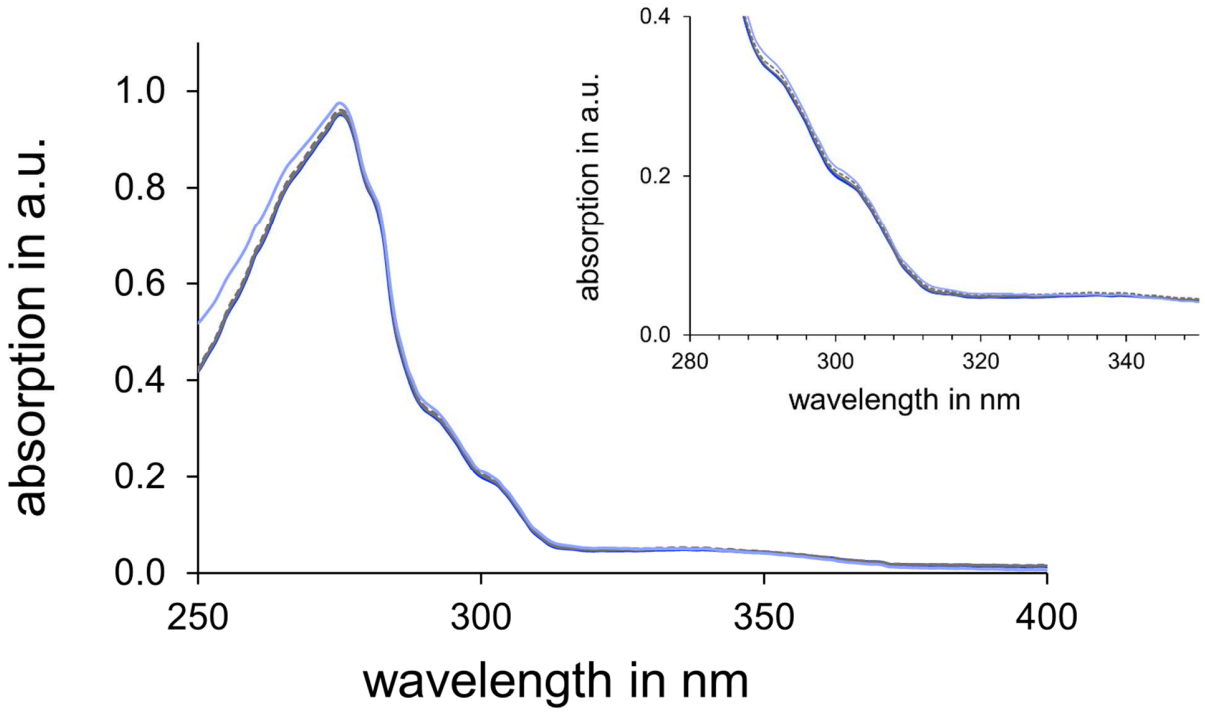

Supplementary Figure 59 | Photoconversion of D in EPA. UV/vis absorption spectra recorded during irradiation of **D** in EPA glass (diethyl ether/*iso*-pentane/ethanol 5:5:2) at 90 K. Starting from pure **D** (dark blue) measurements were made after 30, 60, (grey lines), and 120 min (grey dashed line) of irradiation with a 405 nm ultra high power LED. After irradiation, the EPA glass was warmed to 195 K and cooled down again to 90 K (light blue). As shown in the enlarged UV/vis absorption spectrum inset, no significant photoisomerization could be observed.

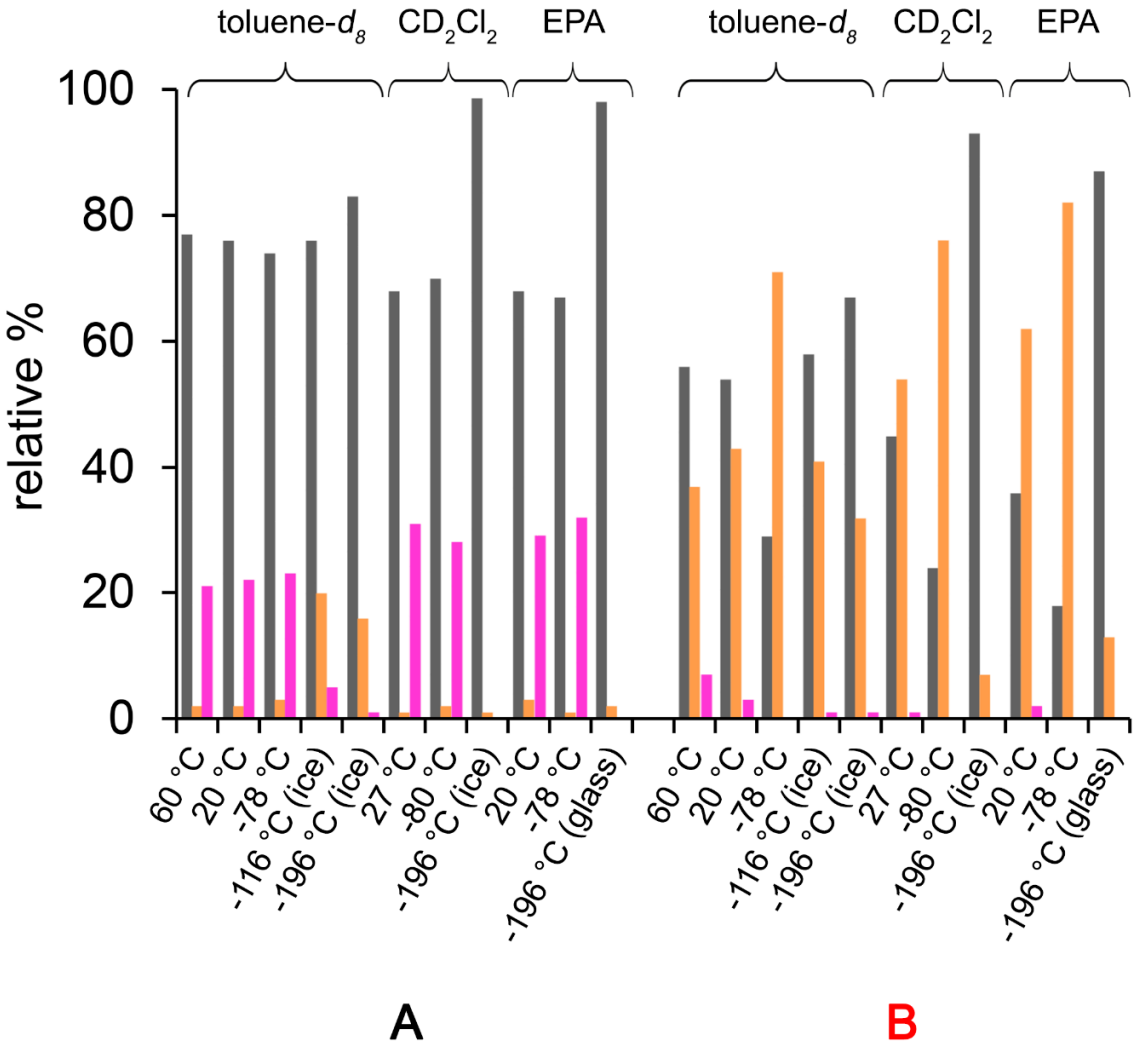

Supplementary Figure 60 | Relative quantum yields of 1 in different solvents and temperatures. Markov matrix analysis of the photoreactions of **1** in different solvents at different temperatures under 405 nm illumination. The relative efficiency of different processes is given. Measurements are conducted in liquid solutions at the indicated temperatures or in frozen solvent glasses or ices as indicated in brackets. The different photoprocesses are color coded: single-bond rotation (SBR) in purple, double-bond isomerization (DBI) in grey, and hula twist (HT) in orange.

NMR-Spectra

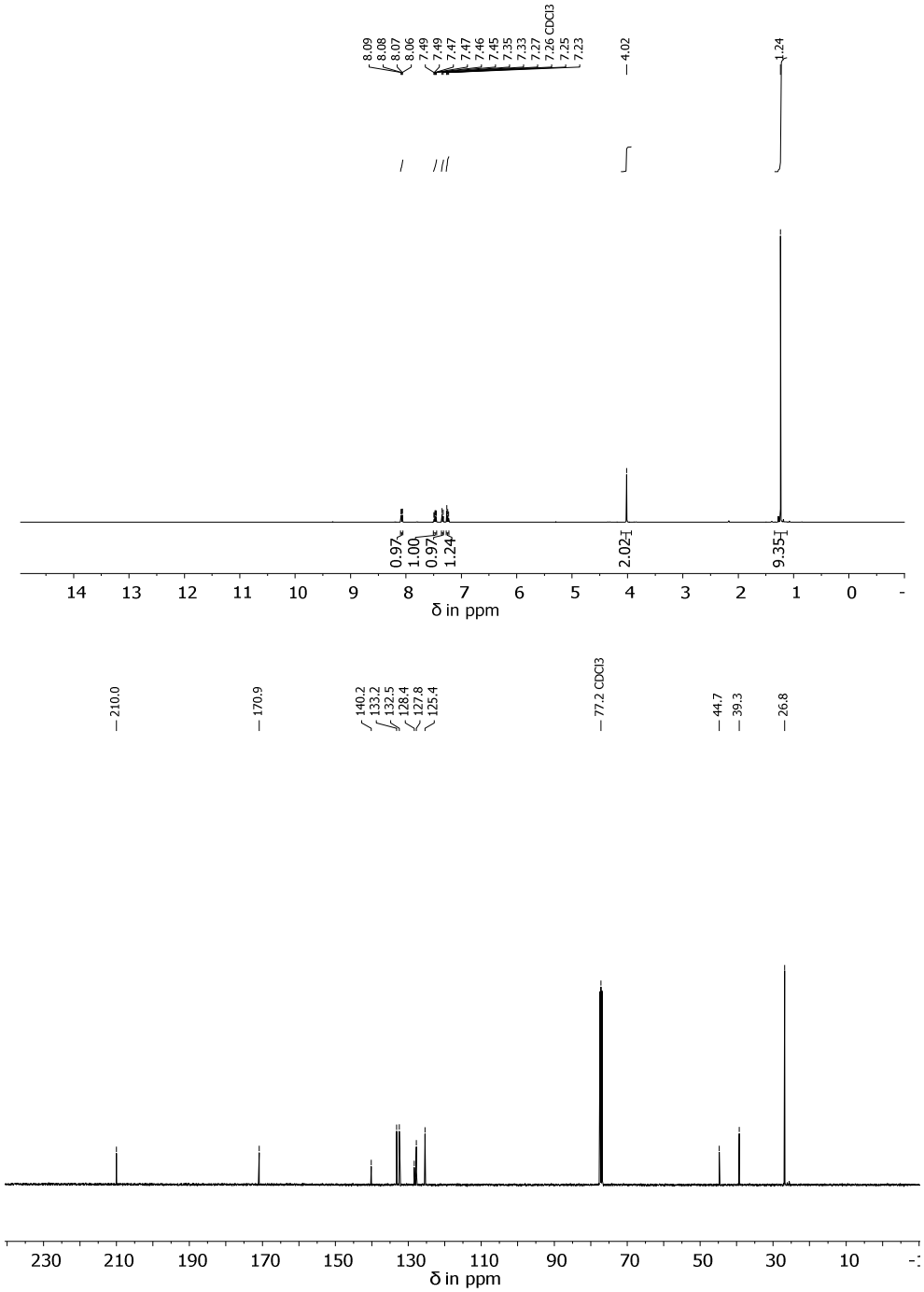

Supplementary Figure 61 | NMR spectra of 2. 400 MHz ^{1}H-NMR Spectrum (top) and 100 MHz ^{13}C-NMR Spectrum (bottom) of 2-((3,3-dimethyl-2-oxobutyl)thio)benzoic acid (**2**) in $CDCl_3$.

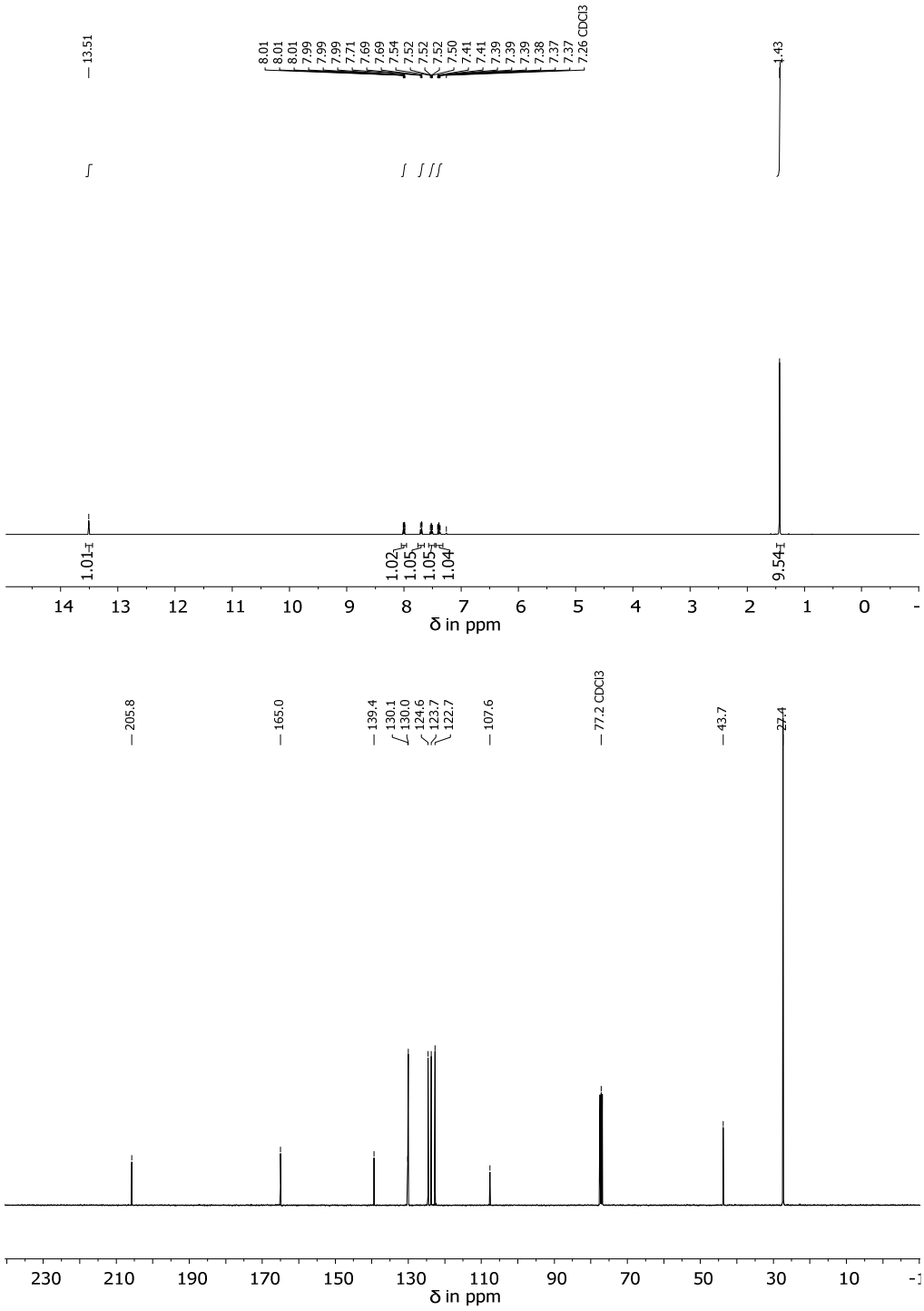

Supplementary Figure 62 | NMR spectra of 3. 400 MHz ^{1}H-NMR Spectrum (top) and 100 MHz ^{13}C-NMR Spectrum (bottom) of 1-(3-hydroxybenzo[b]thiophen-2-yl)-2,2-dimethylpropan-1-one (**3**) in $CDCl_3$.

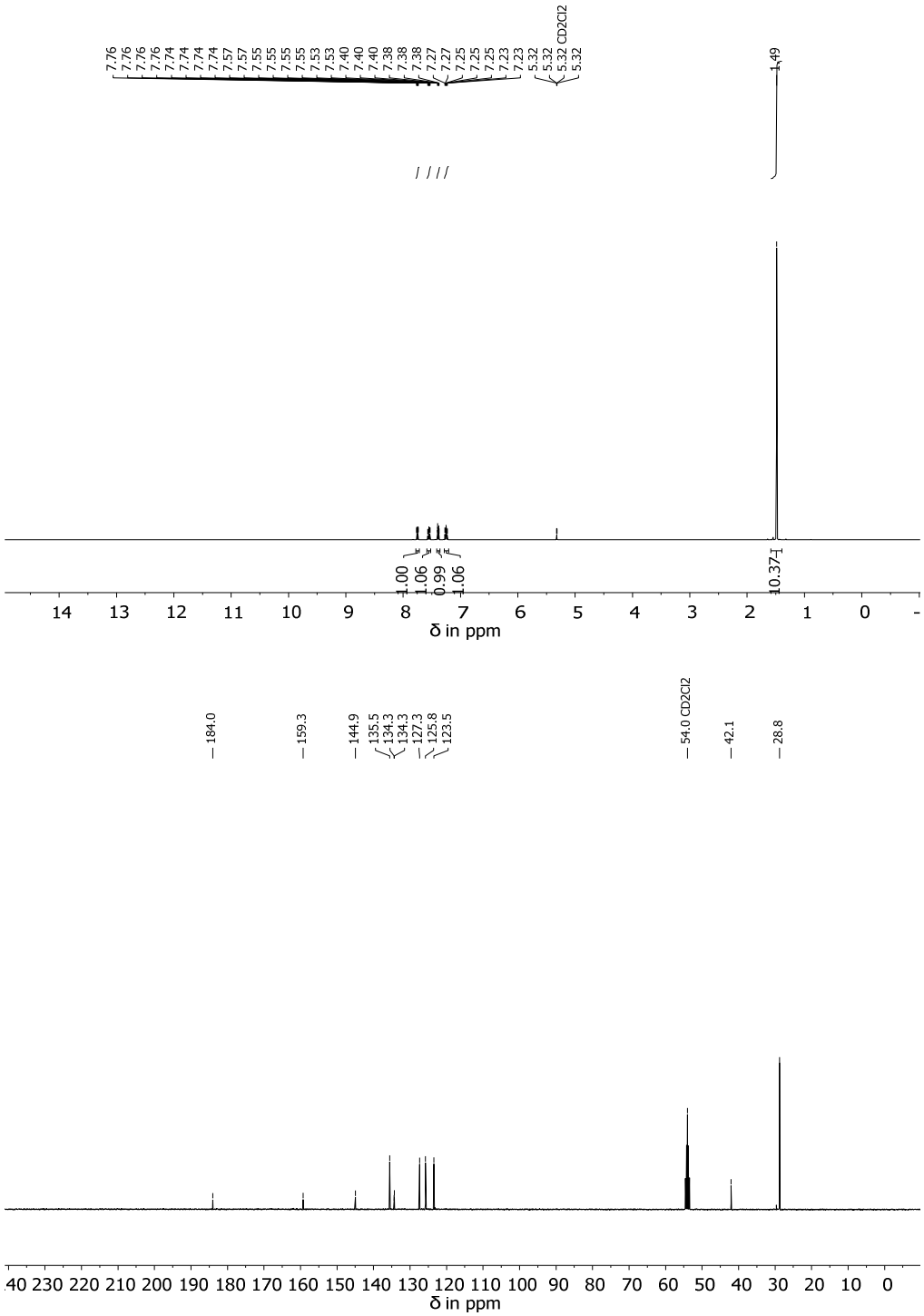

Supplementary Figure 63 | NMR spectra of 4. 400 MHz ^{1}H-NMR Spectrum (top) and 100 MHz ^{13}C-NMR Spectrum (bottom) of (*Z*)-2-(1-chloro-2,2-dimethylpropylidene)benzo[*b*]thiophen-3(2*H*)-one (**4**) in CD_2Cl_2.

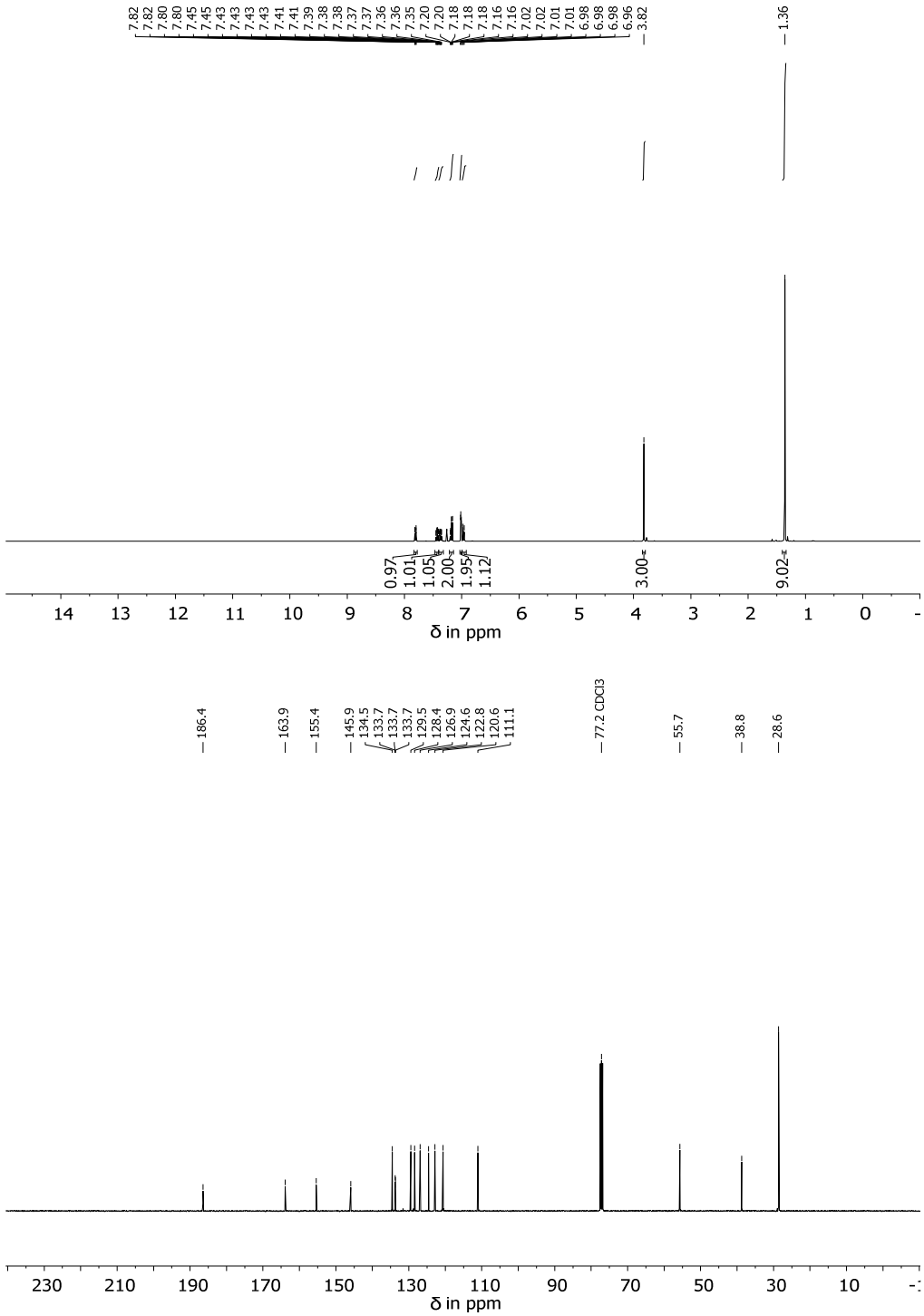

Supplementary Figure 64 | NMR spectra of 5. 400 MHz ^{1}H-NMR Spectrum (top) and 100 MHz ^{13}C-NMR Spectrum (bottom) of (*Z*)-2-(1-(2-Methoxyphenyl)-2,2-dimethylpropylidene)benzo[*b*]thiophen-3(2*H*)-one (**5**) in $CDCl_3$.

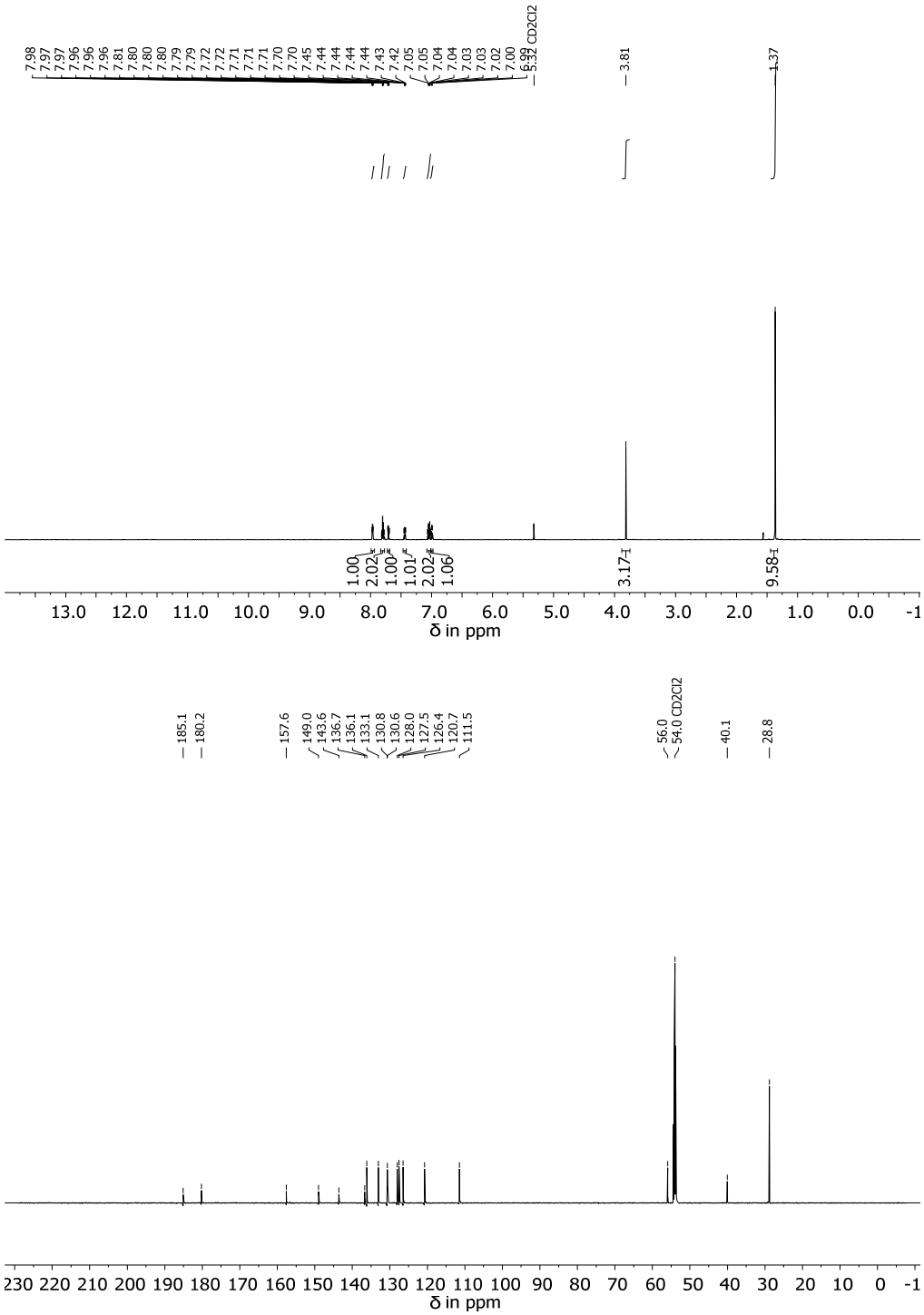

Supplementary Figure 65 | NMR spectra of A. 600 MHz ^{1}H-NMR Spectrum (top) and 150 MHz ^{13}C-NMR Spectrum (bottom) of the **A** isomer of 2-(1-(2-methoxyphenyl)-2,2-dimethylpropylidene)benzo[*b*]thiophen-3(2*H*)-one 1-oxide (**1**) in CD_2Cl_2.

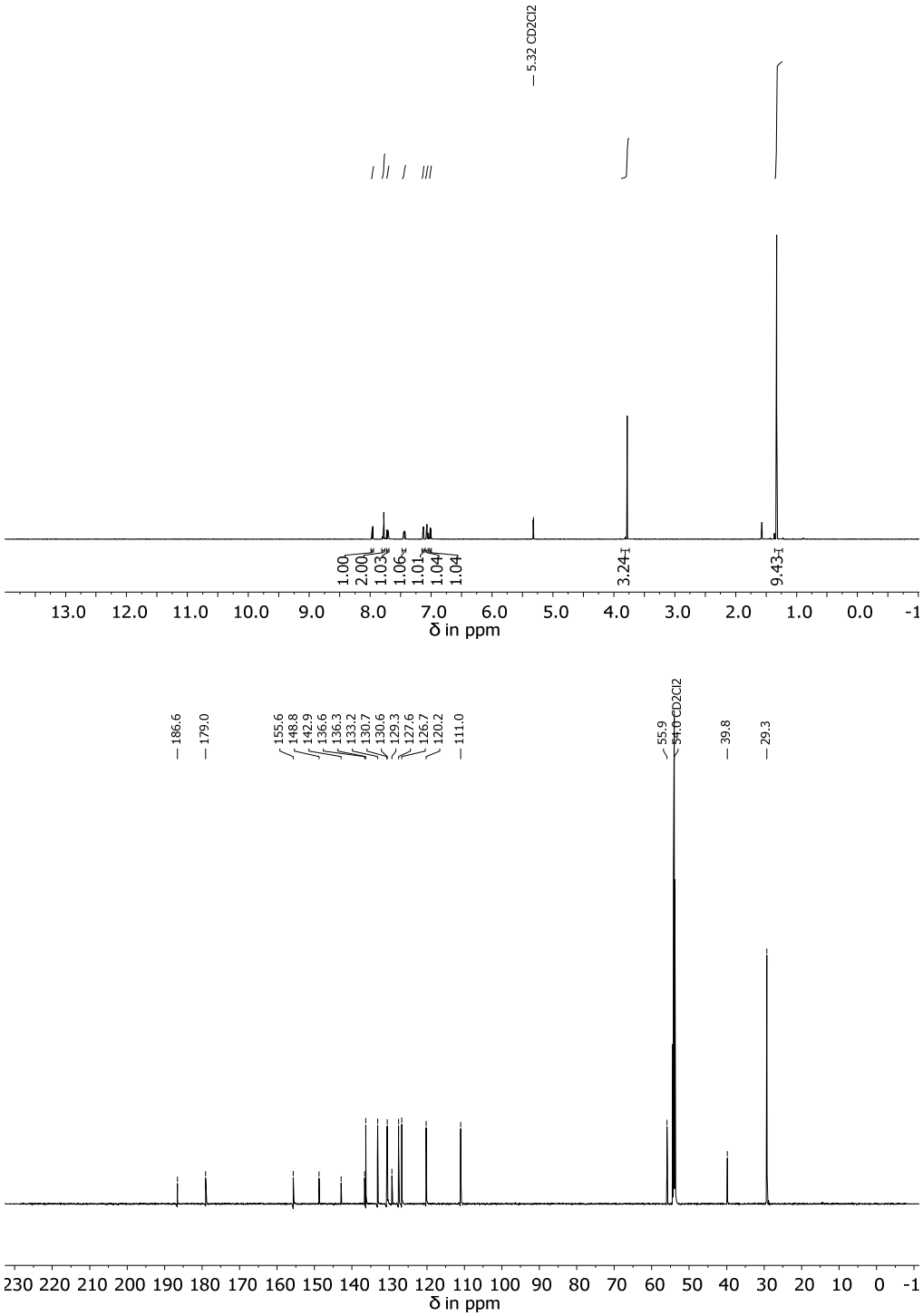

Supplementary Figure 66 | NMR spectra of B. 600 MHz ^{1}H-NMR Spectrum (top) and 150 MHz ^{13}C-NMR Spectrum (bottom) of the **B** isomer of 2-(1-(2-methoxyphenyl)-2,2-dimethylpropylidene)benzo[*b*]thiophen-3(2*H*)-one 1-oxide in CD_2Cl_2.

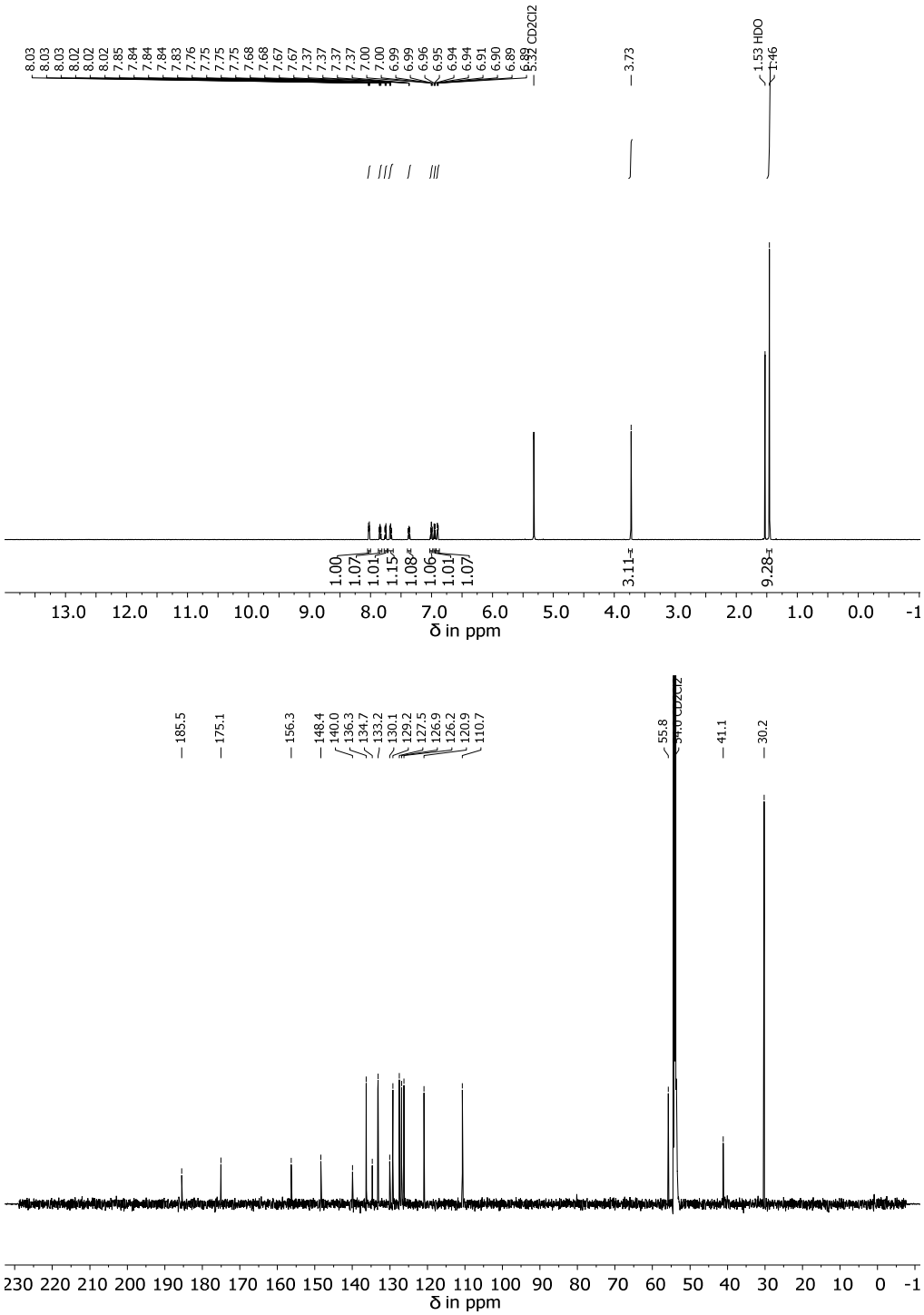

Supplementary Figure 67 | NMR spectra of C. 600 MHz ^{1}H-NMR Spectrum (top) and 150 MHz ^{13}C-NMR Spectrum (bottom) of the **C** isomer of 2-(1-(2-methoxyphenyl)-2,2-dimethylpropylidene)benzo[*b*]thiophen-3(2*H*)-one 1-oxide in CD_2Cl_2.

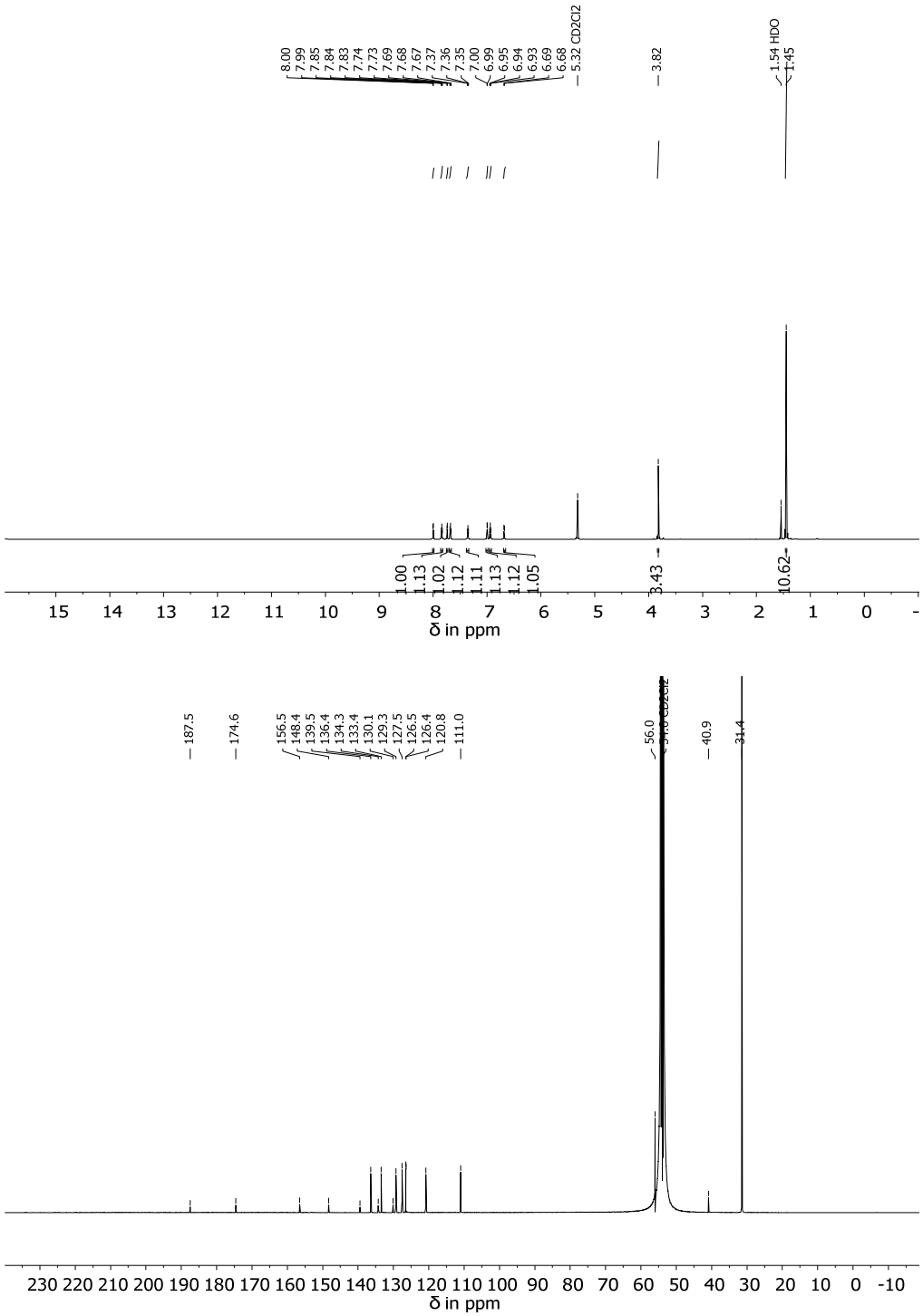

Supplementary Figure 68 | NMR spectra of D. 800 MHz ^{1}H-NMR Spectrum (top) and 200 MHz ^{13}C-NMR Spectrum (bottom) of the **D** isomer of 2-(1-(2-methoxyphenyl)-2,2-dimethylpropylidene)benzo[*b*]thiophen-3(2*H*)-one 1-oxide in CD_2Cl_2.

Supplementary Tables

Supplementary Table 1 | Thermal isomerization of 1. Thermal isomerization behavior of hemithioindigo 1 in $(CDCl_2)_2$ at high temperature.

Isomer	$k_{(\text{isom. 1/isom. 2})}$ / s^{-1} (at T / °C)	ΔG^* (therm. isomer equilibration) /kcal mol^{-1}	Equilibration half-life of pure isomer at 27 °C	Thermo-dynamic isomer 1/isomer 2 equilibrium in the dark (at T / °C)	$\Delta\Delta G^0$(isomer 1 / isomer 2) / kcal mol^{-1}	Slope m / s^{-1} (at T / °C)
A	$k_{(\mathbf{A/B})}$ = 2.47x10^{-5} (82 °C)	ΔG^*(**A/B**) = 28.40	1.7 a	**A/B** = 49/51 (82 °C)	$\Delta\Delta G^0$(**A/B**) = -0.04	5.07x10^{-5} (82 °C)
B	$k_{(\mathbf{B/A})}$ = 2.82x10^{-5} (82 °C)	ΔG^*(**B/A**) = 27.93	0.8 a	**B/A** = 52/48 (82 °C)	$\Delta\Delta G^0$(**B/A**) = 0.04	9.09x10^{-5} (82 °C)
C	$k_{(\mathbf{C/D})}$ = 2.74x10^{-5} (100 °C)	ΔG^*(**C/D**) = 29.80	18 a	**C/D** = 69/31 (100 °C)	$\Delta\Delta G^0$(**C/D**) = -0.65	8.98x10^{-5} (100 °C)
D	$k_{(\mathbf{D/C})}$ = 5.67x10^{-5} (100 °C)	ΔG^*(**D/C**) = 29.26	7.3 a	**D/C** = 29/71 (100 °C)	$\Delta\Delta G^0$(**D/C**) = 0.65	7.94x10^{-5} (100 °C)

Supplementary Table 2 | Relative quantum yields of 1. Relative percentage of different photoconversions of **1** in different solvents *obtained from Markov matrix analysis according to Supplementary Equation 28 or **from direct quantum yield measurements. SBR = single-bond rotation, DBI = double-bond isomerization, HT = hula twist, EG = ethylene glycol.

Pathway %	ϕ Measurement	Markov Matrix Analysis				
		Solvent				
	Benzene**	Benzene*	CH_2Cl_2*	MeOH*	DMSO*	EG*
A to B SBR	22	22	31	42	33	30
A to C DBI	76	76	68	58	62	63
A to D HT	2	2	0	0	5	7
B to A SBR	5	0	0	0	0	0
B to C HT	42	47	55	66	52	57
B to D DBI	51	53	45	34	48	43

Supplementary Table 3 | Relative quantum yields of A and B at different temperatures. Relative percentage of different photoconversions of **1** in different solvents and temperatures obtained from Markov matrix analysis according to Supplementary Equation 28. SBR = single-bond rotation, DBI = double-bond isomerization, HT = hula twist.

Solvent	Toluene-d_8					CD_2Cl_2			EPA		
T in °C	60	20	- 78	- 116	- 196	27	- 80	- 196	20	- 78	- 196
A to B SBR	21	22	23	5	1	31	28	0	29	32	0
A to C DBI	77	76	74	76	83	68	70	99	68	67	98
A to D HT	2	2	3	20	16	1	2	1	3	1	2
B to A SBR	7	3	0	1	1	1	0	0	2	0	0
B to C HT	37	43	71	41	32	54	76	7	62	82	13
B to D DBI	56	54	29	58	67	45	24	93	36	18	87

Supplementary Table 4 | Relative quantum yields of A and B under illumination with different wavelengths. Relative percentage of different photoconversions of **1** under different illumination conditions in CD_2Cl_2 at 20 °C obtained from Markov matrix analysis according to Supplementary Equation 28. SBR = single-bond rotation, DBI = double-bond isomerization, HT = hula twist.

Wavelength	305 nm	365 nm	405 nm
A to B SBR	22	23	31
A to C DBI	72	75	68
A to D HT	5	2	1
B to A SBR	6	1	1
B to C HT	56	56	54
B to D DBI	39	53	45

Calculated ground state geometries - xyz coordinates

Supplementary Table 5 | Calculated ground state geometries of *E*-(*S*)-(R_a)-1 and *E*-(*S*)-(S_a)-1.

E-(*S*)-(R_a)-**1**			*E*-(*S*)-(S_a)-**1**		
S	-1.9046	1.4644	0.3482	S	1.8785	1.5237	0.0476
O	-0.2507	-2.0933	0.0158	O	0.3187	-2.0622	0.4225
O	-2.1220	2.4021	-0.8335	O	1.9911	2.0752	1.4666
C	-3.0529	0.0798	0.1656	C	3.0568	0.1481	-0.0552
C	-4.4357	0.2157	0.1697	C	4.4305	0.3107	-0.1712
H	-4.9070	1.1871	0.2579	H	4.8764	1.2932	-0.2707
C	-5.2007	-0.9441	0.0548	C	5.2237	-0.8375	-0.1538
H	-6.2819	-0.8714	0.0516	H	6.2990	-0.7445	-0.2493
C	-4.5910	-2.2016	-0.0506	C	4.6479	-2.1060	-0.0140
H	-5.2078	-3.0884	-0.1324	H	5.2842	-2.9828	-0.0041
C	-3.2058	-2.3177	-0.0537	C	3.2693	-2.2487	0.1102
H	-2.7158	-3.2800	-0.1417	H	2.8067	-3.2222	0.2213
C	-2.4358	-1.1571	0.0454	C	2.4731	-1.1040	0.0862
C	-0.9550	-1.1020	0.0214	C	0.9918	-1.0786	0.1881
C	-0.4802	0.3265	0.0480	C	0.4839	0.3177	-0.0547
C	0.8026	0.7324	-0.1135	C	-0.7938	0.6519	-0.3588
C	1.8104	-0.3055	-0.5178	C	-1.7880	-0.4617	-0.5119
C	2.6008	-0.9531	0.4501	C	-2.6465	-0.8054	0.5477
C	3.5632	-1.8829	0.0580	C	-3.5884	-1.8213	0.3830
C	3.7359	-2.1772	-1.2963	C	-3.6788	-2.4945	-0.8366
C	2.9534	-1.5530	-2.2591	C	-2.8374	-2.1612	-1.8910
H	3.0803	-1.7856	-3.3096	H	-2.9057	-2.6835	-2.8377
C	1.9912	-0.6226	-1.8614	C	-1.8948	-1.1466	-1.7198
C	1.3312	2.1871	-0.0425	C	-1.3161	2.0910	-0.6289
H	1.3655	-0.1425	-2.6047	H	-4.2487	-2.0961	1.1941
H	4.1741	-2.3865	0.7945	H	-1.2271	-0.8865	-2.5336
C	1.0678	2.8486	-1.4227	C	-1.1212	2.9740	0.6280
H	1.4454	3.8753	-1.4016	H	-1.5103	3.9756	0.4233
H	1.5951	2.3169	-2.2186	H	-1.6767	2.5541	1.4690
H	0.0023	2.8669	-1.6507	H	-0.0796	3.0660	0.9315
C	2.8557	2.2171	0.2163	C	-2.8235	2.0985	-0.9625
H	3.1827	3.2594	0.2310	H	-3.0514	1.5189	-1.8587
H	3.1070	1.7676	1.1783	H	-3.4231	1.7098	-0.1384
H	3.4168	1.7026	-0.5642	H	-3.1325	3.1313	-1.1424
C	0.6696	3.0212	1.0775	C	-0.5773	2.6996	-1.8476
H	-0.3557	3.3080	0.8501	H	0.4904	2.8171	-1.6718
H	0.6865	2.4900	2.0321	H	-0.7121	2.0767	-2.7359
H	1.2318	3.9505	1.1990	H	-0.9949	3.6868	-2.0624
O	2.3442	-0.6100	1.7449	O	-2.4800	-0.0868	1.6946
C	3.0804	-1.2556	2.7839	C	-3.2847	-0.4087	2.8293
H	2.7004	-0.8415	3.7157	H	-3.1186	-1.4412	3.1502
H	2.9146	-2.3368	2.7716	H	-2.9679	0.2708	3.6178
H	4.1513	-1.0463	2.7028	H	-4.3476	-0.2543	2.6206
H	4.4864	-2.9032	-1.5878	H	-4.4142	-3.2827	-0.9520

Supplementary Table 6 | Calculated ground state geometries of Z-(*S*)-(R_a)-1 and *Z*-(*S*)-(S_a)-1.

Z-(*S*)-(R_a)-**1**			*Z*-(*S*)-(S_a)-**1**		
S	-0.9028	-1.3331	-0.2487	S	0.8714	-1.3220	-0.4538
O	-1.8798	2.4954	0.0350	O	1.8563	2.4923	-0.3566
O	-0.4838	-2.0189	1.0438	O	0.9245	-1.7464	-1.9165
C	-2.6710	-0.9676	-0.1081	C	2.5876	-0.9654	0.0252
C	-3.6671	-1.9359	-0.0873	C	3.5505	-1.9348	0.2703
H	-3.4291	-2.9900	-0.1655	H	3.3059	-2.9901	0.2501
C	-4.9888	-1.5089	0.0357	C	4.8501	-1.5081	0.5480
H	-5.7868	-2.2418	0.0540	H	5.6209	-2.2424	0.7503
C	-5.2983	-0.1457	0.1319	C	5.1703	-0.1452	0.5676
H	-6.3332	0.1618	0.2226	H	6.1860	0.1620	0.7858
C	-4.2899	0.8107	0.1131	C	4.1960	0.8139	0.3103
H	-4.5081	1.8691	0.1905	H	4.4249	1.8728	0.3187
C	-2.9644	0.3857	0.0003	C	2.8952	0.3900	0.0361
C	-1.7826	1.2803	-0.0213	C	1.7441	1.2839	-0.2432
C	-0.5257	0.4833	-0.1678	C	0.4841	0.4816	-0.3374
C	0.7793	0.8476	-0.2693	C	-0.8260	0.8305	-0.2875
C	1.7590	-0.2481	-0.5757	C	-1.8260	-0.2843	-0.4077
C	2.5465	-0.8194	0.4425	C	-2.3821	-0.8666	0.7484
C	3.4527	-1.8363	0.1348	C	-3.3362	-1.8785	0.6323
C	3.5837	-2.2778	-1.1818	C	-3.7417	-2.3082	-0.6321
C	2.8141	-1.7196	-2.1963	C	-3.1978	-1.7441	-1.7798
H	2.9126	-2.0649	-3.2182	H	-3.5060	-2.0840	-2.7610
C	1.9012	-0.7127	-1.8843	C	-2.2380	-0.7389	-1.6605
C	1.3485	2.2854	-0.1553	C	-1.3943	2.2657	-0.1470
H	1.2853	-0.2793	-2.6638	H	-3.7656	-2.3339	1.5140
H	4.0542	-2.2885	0.9113	H	-1.7953	-0.3042	-2.5482
C	2.8914	2.2975	-0.2359	C	-1.0395	3.0693	-1.4230
H	3.3456	1.7542	0.5932	H	-1.4627	2.5937	-2.3121
H	3.2597	1.8766	-1.1733	H	-1.4710	4.0716	-1.3435
H	3.2294	3.3355	-0.1807	H	0.0367	3.1641	-1.5488
C	0.8245	3.1274	-1.3461	C	-0.8332	2.9577	1.1172
H	1.2547	4.1314	-1.2850	H	0.2428	3.1019	1.0666
H	1.1378	2.6885	-2.2976	H	-1.3006	3.9413	1.2194
H	-0.2588	3.2183	-1.3345	H	-1.0751	2.3723	2.0069
C	0.9518	2.9214	1.1969	C	-2.9335	2.2562	-0.0163
H	-0.1251	3.0309	1.2959	H	-3.4204	1.8076	-0.8838
H	1.3287	2.3145	2.0227	H	-3.2622	1.7250	0.8786
H	1.4043	3.9149	1.2689	H	-3.2788	3.2901	0.0635
O	2.3559	-0.3125	1.6893	O	-1.9202	-0.3755	1.9330
C	2.9998	-0.9461	2.7959	C	-2.4281	-0.9263	3.1499
H	2.6543	-0.4153	3.6804	H	-2.2034	-1.9942	3.2236
H	2.7108	-1.9982	2.8650	H	-1.9191	-0.3926	3.9496
H	4.0883	-0.8631	2.7247	H	-3.5073	-0.7698	3.2359
H	4.2927	-3.0666	-1.4061	H	-4.4850	-3.0934	-0.7094

Supplementary Table 7 | Calculated ground state geometries of the transition states of *E*-1.

Transition state *E*-**1** (OMe over *t*Bu)				Transition state *E*-**1** (OMe over carbonyl)			
S	1.6330	-1.3348	-0.7356	S	1.5129	-1.7614	-0.2274
O	1.1124	1.8125	1.5764	O	0.9530	1.1491	2.1031
O	1.2845	-1.1952	-2.2123	O	1.0871	-2.2107	-1.6126
C	3.1147	-0.3570	-0.4105	C	2.7546	-0.4652	-0.4204
C	4.3783	-0.6586	-0.9020	C	3.9205	-0.5996	-1.1643
H	4.5445	-1.5134	-1.5466	H	4.1125	-1.4861	-1.7566
C	5.4339	0.1724	-0.5258	C	4.8366	0.4496	-1.1173
H	6.4336	-0.0368	-0.8880	H	5.7522	0.3855	-1.6934
C	5.2178	1.2659	0.3220	C	4.5953	1.5788	-0.3227
H	6.0539	1.8941	0.6057	H	5.3288	2.3759	-0.2944
C	3.9424	1.5542	0.7988	C	3.4286	1.6864	0.4274
H	3.7558	2.4001	1.4493	H	3.2346	2.5534	1.0472
C	2.8815	0.7369	0.4083	C	2.4873	0.6590	0.3477
C	1.4555	0.9475	0.7747	C	1.1750	0.5959	1.0385
C	0.6035	-0.0989	0.1857	C	0.3084	-0.4476	0.4201
C	-0.7688	-0.3541	0.2832	C	-1.0397	-0.6898	0.2985
C	-1.7376	0.7393	0.0022	C	-2.0115	0.3304	-0.2043
C	-1.2310	2.0556	-0.1672	C	-1.9191	1.7446	-0.0633
C	-2.0141	3.1709	-0.3846	C	-2.8456	2.5975	-0.6763
C	-3.3943	3.0244	-0.5045	C	-3.8575	2.0911	-1.4804
C	-3.9453	1.7560	-0.4553	C	-3.9483	0.7185	-1.6818
C	-3.1509	0.6185	-0.2470	C	-3.0474	-0.1254	-1.0477
C	-1.2022	-1.7845	0.7647	C	-1.6058	-2.1252	0.6696
H	-1.5485	4.1443	-0.4758	H	-4.7101	0.3002	-2.3281
H	-0.1726	2.2130	-0.1054	H	-2.7656	3.6653	-0.5311
H	-5.0084	1.6394	-0.6027	H	-3.1314	-1.1784	-1.2489
C	-1.7058	-2.7006	-0.3765	C	-0.6903	-2.7854	1.7375
H	-2.4960	-2.2490	-0.9656	H	0.2511	-3.1573	1.3374
H	-0.8791	-2.9529	-1.0450	H	-0.4648	-2.0900	2.5492
H	-2.0822	-3.6337	0.0535	H	-1.2142	-3.6455	2.1601
C	-2.2383	-1.5898	1.9153	C	-1.7786	-3.1447	-0.4854
H	-2.5519	-2.5797	2.2571	H	-1.9934	-4.1252	-0.0505
H	-1.7579	-1.0864	2.7587	H	-2.6072	-2.9089	-1.1530
H	-3.1269	-1.0386	1.6418	H	-0.8733	-3.2216	-1.0856
C	-0.0589	-2.5584	1.4835	C	-2.9612	-1.9259	1.4065
H	0.4622	-1.9290	2.2083	H	-2.8569	-1.2185	2.2336
H	-0.5109	-3.3908	2.0279	H	-3.7633	-1.5735	0.7628
H	0.6724	-2.9852	0.8041	H	-3.2663	-2.8877	1.8259
O	-3.7040	-0.6089	-0.3305	O	-0.9064	2.2128	0.6831
C	-5.0967	-0.7698	-0.6203	C	-0.7482	3.6131	0.9025
H	-5.7173	-0.3295	0.1641	H	-0.5932	4.1490	-0.0383
H	-5.3502	-0.3329	-1.5891	H	-1.6121	4.0290	1.4285
H	-5.2581	-1.8451	-0.6511	H	0.1357	3.7017	1.5298
H	-4.0349	3.8829	-0.6696	H	-4.5593	2.7695	-1.9517

Supplementary Table 8 | Calculated ground state geometries of the transition states of *Z*-1.

Transition state *Z*-**1** (OMe over *t*Bu)				Transition state *Z*-**1** (OMe over sulfoxide)		
S	1.4223	1.4954	0.4255	S	0.9301	-1.4973	0.3991
O	1.3607	-1.9008	-1.5193	O	1.3405	1.4827	-1.9728
O	1.2028	1.5894	1.9277	O	1.1030	-2.5678	-0.6720
C	3.0440	0.7732	0.1066	C	2.6092	-0.7755	0.4312
C	4.2507	1.3747	0.4430	C	3.6918	-1.3228	1.1016
H	4.2836	2.3131	0.9833	H	3.5707	-2.1467	1.7951
C	5.4235	0.7287	0.0541	C	4.9553	-0.7802	0.8481
H	6.3824	1.1668	0.3046	H	5.8200	-1.1772	1.3670
C	5.3768	-0.4721	-0.6668	C	5.1192	0.2589	-0.0736
H	6.3021	-0.9499	-0.9661	H	6.1094	0.6582	-0.2582
C	4.1582	-1.0542	-0.9997	C	4.0207	0.7864	-0.7508
H	4.1047	-1.9825	-1.5555	H	4.1311	1.5938	-1.4652
C	2.9819	-0.4265	-0.5869	C	2.7590	0.2663	-0.4750
C	1.6059	-0.9386	-0.7988	C	1.4606	0.7461	-1.0074
C	0.6015	-0.0674	-0.1600	C	0.3181	0.1395	-0.2605
C	-0.7412	-0.3788	0.0281	C	-0.8628	0.7949	0.0309
C	-1.8214	0.6377	-0.1732	C	-2.2279	0.1844	0.0962
C	-1.4592	1.9867	-0.4209	C	-2.5355	-1.2100	0.0059
C	-2.3519	3.0293	-0.5792	C	-3.8577	-1.6699	-0.0602
C	-3.7178	2.7665	-0.5465	C	-4.9272	-0.7896	-0.0679
C	-4.1442	1.4572	-0.4108	C	-4.6759	0.5759	-0.0199
C	-3.2374	0.3960	-0.2653	H	-5.4861	1.2939	-0.0503
C	-1.0212	-1.8124	0.6182	C	-3.3686	1.0263	0.0630
H	-1.9793	4.0330	-0.7412	C	-0.7463	2.3499	0.3514
H	-5.2027	1.2460	-0.4353	H	-4.0483	-2.7316	-0.1041
H	-0.4198	2.2465	-0.5080	H	-3.2403	2.0896	0.0746
C	-1.9218	-1.5996	1.8767	C	0.6991	2.8339	0.6561
H	-1.3891	-0.9869	2.6090	H	1.2217	2.1601	1.3382
H	-2.8833	-1.1461	1.6779	H	1.3036	2.9846	-0.2325
H	-2.1013	-2.5776	2.3307	H	0.6258	3.8047	1.1510
C	0.2409	-2.4823	1.2306	C	-1.4496	2.6033	1.7279
H	-0.0954	-3.3270	1.8368	H	-1.3796	3.6696	1.9556
H	0.9217	-2.8786	0.4839	H	-2.4926	2.3168	1.7959
H	0.7836	-1.7983	1.8865	H	-0.9135	2.0631	2.5134
C	-1.5944	-2.8217	-0.4044	C	-1.2561	3.2679	-0.7887
H	-2.4456	-2.4379	-0.9552	H	-0.6099	3.1387	-1.6583
H	-0.8084	-3.0885	-1.1113	H	-2.2779	3.0831	-1.1123
H	-1.9075	-3.7278	0.1241	H	-1.1928	4.3115	-0.4665
O	-3.6933	-0.8737	-0.2551	O	-1.5126	-2.0843	-0.0161
C	-5.0913	-1.1555	-0.3697	C	-1.7527	-3.4803	-0.2540
H	-5.6497	-0.7392	0.4724	H	-2.2931	-3.9274	0.5839
H	-5.4951	-0.7761	-1.3116	H	-2.3117	-3.6218	-1.1818
H	-5.1643	-2.2408	-0.3529	H	-0.7614	-3.9109	-0.3509
H	-4.4447	3.5626	-0.6563	H	-5.9402	-1.1716	-0.1171

Crystal structure analysis

Supplementary Table 9 | Crystal structure analysis of A and B.

Compound	**A-1** CCDC 1586011	**B-1** CCDC 1586012
net formula	$C_{20}H_{20}O_3S$	$C_{20}H_{20}O_3S$
M_r/g mol^{-1}	340.42	340.42
crystal size/mm	0.100 × 0.080 × 0.050	0.100 × 0.060 × 0.030
T/K	100.(2)	100.(2)
radiation	MoKα	MoKα
diffractometer	'Bruker D8 Venture TXS'	'Bruker D8 Venture TXS'
crystal system	triclinic	orthorhombic
space group	'P -1'	'P b c a'
a/Å	8.3514(4)	13.0489(3)
b/Å	13.3861(6)	15.1168(4)
c/Å	15.2817(7)	16.9239(4)
α/°	83.607(2)	90
β/°	86.533(2)	90
γ/°	87.048(2)	90
V/Å^3	1692.92(14)	3338.37(14)
Z	4	8
calc. density/g cm^{-3}	1.336	1.355
μ/mm^{-1}	0.206	0.209
absorption correction	Multi-Scan	Multi-Scan
transmission factor range	0.8916–0.9705	0.9044–0.9705
refls. measured	19349	31719
R_{int}	0.0387	0.0534
mean σ(I)/I	0.0448	0.0266
θ range	3.211–26.372	3.170–26.373
observed refls.	5350	2779
x, y (weighting scheme)	0.0312, 1.4998	0.0324, 2.8521
hydrogen refinement	constr	constr
Flack parameter	-	-
refls in refinement	6838	3406
parameters	441	221
restraints	0	0
$R(F_{obs})$	0.0420	0.0347
$R_w(F^2)$	0.1041	0.0920
S	1.039	1.070
shift/error$_{max}$	0.001	0.001
max electron density/e Å^{-3}	0.391	0.345
min electron density/e Å^{-3}	−0.446	−0.374

Supplementary Table 10 | Crystal structure analysis of C and D.

Compound	**C-1** CCDC 1586013	**D-1** CCDC 1586014
net formula	$C_{20}H_{20}O_3S$	$C_{20}H_{20}O_3S$
M_r/g mol^{-1}	340.42	340.42
crystal size/mm	0.080 × 0.070 × 0.030	0.100 × 0.090 × 0.060
T/K	100.(2)	100.(2)
radiation	MoKα	MoKα
diffractometer	'Bruker D8 Venture TXS'	'Bruker D8 Venture TXS'
crystal system	triclinic	orthorhombic
space group	'P -1'	'P 21 21 21'
a/Å	10.0205(3)	10.3115(3)
b/Å	10.8597(3)	12.0645(3)
c/Å	16.2287(5)	13.9574(3)
α/°	81.7640(10)	90
β/°	80.7990(10)	90
γ/°	85.3530(10)	90
V/Å^3	1722.24(9)	1736.34(8)
Z	4	4
calc. density/g cm^{-3}	1.313	1.302
μ/mm^{-1}	0.203	0.201
absorption correction	Multi-Scan	Multi-Scan
transmission factor range	0.9339–0.9705	0.9059–0.9705
refls. measured	32659	15544
R_{int}	0.0536	0.0386
mean σ(I)/I	0.0406	0.0311
θ range	3.134–26.372	3.372–26.367
observed refls.	5647	3365
x, y (weighting scheme)	0.0304, 1.7686	0.0167, 0.6551
hydrogen refinement	constr	constr
Flack parameter	-	0.21(8)
refls in refinement	7025	3527
parameters	441	222
restraints	0	0
$R(F_{obs})$	0.0417	0.0271
$R_w(F^2)$	0.1012	0.0644
S	1.023	1.080
shift/error$_{max}$	0.001	0.001
max electron density/e Å^{-3}	0.891	0.222
min electron density/e Å^{-3}	−0.430	−0.217

Supplementary References

1. A. Gerwien, T. Reinhardt, P. Mayer, H. Dube, Versatile Synthesis of Double-Bond Substituted Hemithioindigo Photoswitches. *Org. Lett.* **1**, 232-235 (2018).

2. U. Megerle, R. Lechner, B. König, E. Riedle, Laboratory apparatus for the accurate, facile and rapid determination of visible light photoreaction quantum yields. *Photochem. Photobiol. Sci.* **9**, 1400-1406 (2010).

3. Gaussian 09, Revision A.02, M. J. Frisch, G. W. Trucks, H. B. Schlegel, G. E. Scuseria, M. A. Robb, J. R. Cheeseman, G. Scalmani, V. Barone, G. A. Petersson, H. Nakatsuji, X. Li, M. Caricato, A. Marenich, J. Bloino, B. G. Janesko, R. Gomperts, B. Mennucci, H. P. Hratchian, J. V. Ortiz, A. F. Izmaylov, J. L. Sonnenberg, D. Williams-Young, F. Ding, F. Lipparini, F. Egidi, J. Goings, B. Peng, A. Petrone, T. Henderson, D. Ranasinghe, V. G. Zakrzewski, J. Gao, N. Rega, G. Zheng, W. Liang, M. Hada, M. Ehara, K. Toyota, R. Fukuda, J. Hasegawa, M. Ishida, T. Nakajima, Y. Honda, O. Kitao, H. Nakai, T. Vreven, K. Throssell, J. A. Montgomery, Jr., J. E. Peralta, F. Ogliaro, M. Bearpark, J. J. Heyd, E. Brothers, K. N. Kudin, V. N. Staroverov, T. Keith, R. Kobayashi, J. Normand, K. Raghavachari, A. Rendell, J. C. Burant, S. S. Iyengar, J. Tomasi, M. Cossi, J. M. Millam, M. Klene, C. Adamo, R. Cammi, J. W. Ochterski, R. L. Martin, K. Morokuma, O. Farkas, J. B. Foresman, and D. J. Fox, Gaussian, Inc., Wallingford CT, 2016.

6. Photon-only molecular motor

The photoreactions of the HTI presented in the previous chapter point to an idea of a photon only molecular motor in which every rotation step is driven by a photoreaction. This idea is based on the single-bond rotation (SBR) photoreaction of **A** to **B** for which the reverse photoisomerization reaction (**B** to **A** photoreaction) is significantly less efficient. Instead, **B** reacts further to **C** or **D**. However, the photoreactions of the *E* configured isomers **C** and **D**, which are needed to return to the starting isomer **A**, have very low quantum yields and are not very selective making a rotation pathway not unambiguously determinable. From previous studies on HTI photoswitches by Sandra Wiedbrauk[149], it is known that electron donating groups increase the quantum yield of the *E* to *Z* photoisomerization and improve the photochromism of the switch. Therefore, a four-state switch with an additional methoxy group in *para*-position was synthesized. This small change was sufficient to confidently determine the photoreactions of the *E* configured isomers, revealing that isomer **C** reacts in a DBI photoreaction back to the starting point **A**. Therefore, a photon-only molecular motor is obtained without thermal ratcheting steps present in the Feringa-type motors. As no thermal steps are included the speed of the motor is not lowered with decreasing temperature like it was observed in all previous motor systems but instead it is even increased as the selectivity for the **B** to **C** transition is improved with lower temperature.

License

JACS
JOURNAL OF THE AMERICAN CHEMICAL SOCIETY
Cite This: J. Am. Chem. Soc. 2018, 140, 16442−16445
Communication
pubs.acs.org/JACS

Photon-Only Molecular Motor with Reverse Temperature-Dependent Efficiency

Aaron Gerwien, Peter Mayer, and Henry Dube*

Department für Chemie and Munich Center for Integrated Protein Science CIPSM, Ludwig-Maximilians-Universität München, D-81377 Munich, Germany

Supporting Information

ABSTRACT: Light-driven molecular motors are archetypal molecular machines and enable fast and efficient unidirectional motions under photoirradiation. Their common working mechanism contains thermal ratcheting steps leading to slowed-down and even halted directional movement at lower temperatures. In this work, an alternative type of molecular motor is presented, which operates without thermal ratcheting in the ground state. Instead, three consecutive and different photoreactions lead to a directional stepwise rotation of one molecular fragment with respect to the other. This motion is increased in speed and directionality at lower temperatures and at the same time allows a considerably larger fraction of the supplied photon energy to be used for performing work.

The development of artificial molecular machines has become one of the most prominent research topics in the chemical sciences.[1−4] Archetypal such machines are molecular motors providing continuous directional motions upon external energy input at the nanoscale.[5−10] Light-driven motors have risen to particular distinction enabling efficient and instant fueling without creation of waste products[11−16] and have been used for a variety of unique applications already.[17−21] Their rotation mechanisms necessarily include thermal ratcheting steps converting instable isomers into more stable ones in the electronic ground state, which then undergo the next photoreaction (Figure 1). As these thermal steps proceed between relatively low lying energy levels and over significant energy barriers, rotation speed, directionality, and energy transmittance of such motors is limited by the thermal energy of the surrounding medium. As temperature decreases, thermal ratcheting steps are frozen out and molecular motors become simple photoswitches without directional motion.

In this work, we present a different type of light-driven molecular motor **1**, which uses exclusively photon-energy for all its rotation steps and does not lose directionality upon cooling but instead enhances it. At the same time, the overall speed of rotation is also increased instead of decreased at lower temperatures. With up to 98% preference for one rotation pathway, motor **1** is virtually fully monodirectional and can be powered with nondamaging visible light. As the working mechanism is not halted by thermal ground-state steps but comprises three consecutive photoreactions, a considerably larger fraction of the photonic energy can be used for its motion (Figure 1b). Derivative **1** therefore constitutes the first member of an entirely new class of light-only driven molecular motors operating with a distinct mechanism to establish a repetitive three-step unidirectional rotation.

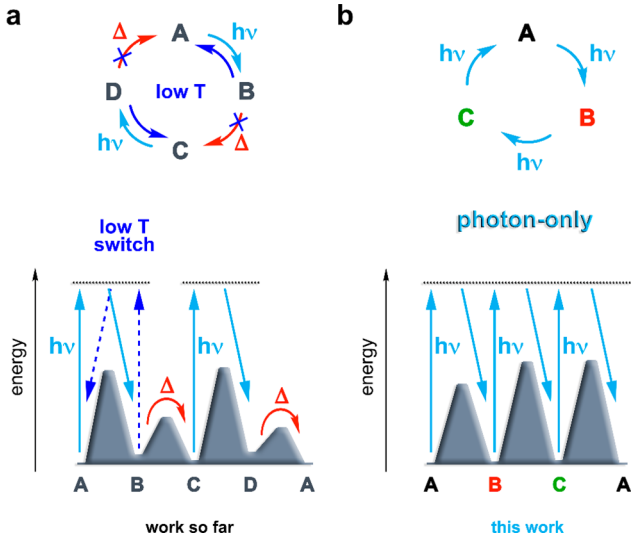

Figure 1. Comparison between classical light-driven molecular motors and hemithioindigo **1**. (a) Working mechanism of a classical four-step motor. Photoreactions (hν, light blue) are intercepted by thermal ratcheting steps (D, red) in the ground state. At lower temperature *T*, the energy barriers of thermal steps are not overcome and the backward photoreaction (dark blue) is entered exclusively. (b) Working mechanism of motor **1**. Three consecutive photoreactions lead to directional structural interconversions without invoking thermal ratcheting steps in the ground state.

Molecular motor **1** is derived from the parent hemithioindigo (HTI) chromophore[22−24] and bears a sulfur-based stereogenic center as well as an adjacent, thermally stable chiral axis. Because of these stereo elements, **1** can exist in four diastereomeric forms: **A**, **B**, **C**, and **D**. The complete stereo assignments of these isomers are given in Figure 2a. All four different isomers of **1** could be separated by column chromatography and crystallized individually. After crystal structural analysis (Figure 3a), the corresponding high-resolution ^{1}H NMR solution spectra could be assigned unambiguously to a particular and well-defined structure. **A** and **B** share the same *Z* configuration of the double bond but

Received: October 3, 2018
Published: November 18, 2018

DOI: 10.1021/jacs.8b10660
J. Am. Chem. Soc. 2018, 140, 16442−16445

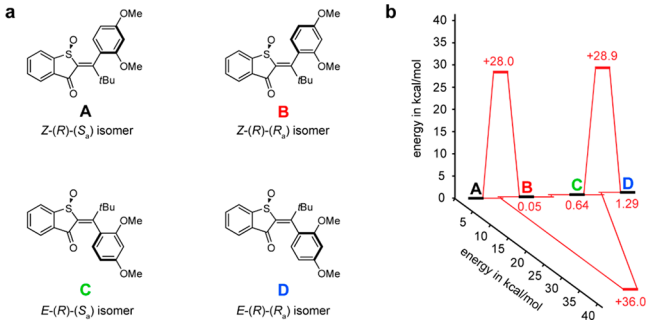

Figure 2. Ground state energy pofile of HTI **1**. (a) The four stable diastereoisomers **A** to **D** of **1**. (b) Experimentally determined ground state energy profile of **1**. Thermal conversion between the four different isomers **A** to **D** is prevented kinetically at ambient temperatures because of very high energy barriers.

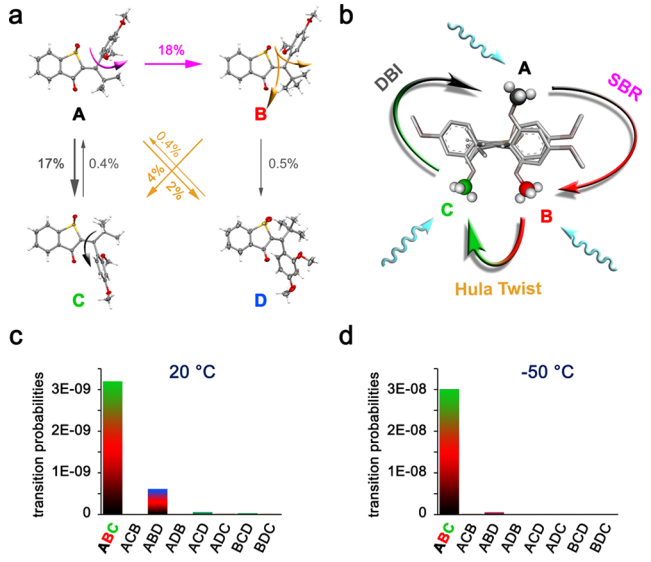

Figure 3. Photoreactions of **1** and resulting directional movements. (a) Quantum yields of the individual photoreactions of all isomers **A** to **D** (structures in the crystalline state) in CD_2Cl_2 at −50 °C. The different types of photoreactions are shown by color coded bent arrows. (b) Front view of a superposition of isomers **A**, **B**, and **C** assuming a static benzothiophenone fragment (in the back). Isomer interconversion in the sequence **ABC** leads to directional rotation of the *ortho*-methoxy group (colored spheres). (c) Total probabilities for all light powered three-step isomer interconversion cycles at 20 °C. (d) Total probabilities for all three-step cycles at −50 °C.

possess opposite axial chirality. Likewise, **C** and **D** are atropisomers of each other in the *E* isomeric state. The atropisomers are thermally very stable, which is manifested in their very long solution half-lives of at least 0.7 years at 27 °C (Figure 2b and Supporting Information). The barrier for the thermal double bound isomerization is even higher (at least 35.5 kcal mol^{-1}) and cannot be overcome at 27 °C on reasonable time scales (see Supporting Information).

Because of the high thermal stability of all four isomers of **1**, their individual photoreactions could be studied at ambient conditions without interference of thermal follow-up processes. In total, 16 different photoreactions are possible including nonproductive reactions, e.g., **A** returning to **A** after photoexcitation. Using the high spectral resolution power of ^1H NMR spectroscopy in conjunction with photon counting, we investigated the photoreactions of each individual isomer in CD_2Cl_2 solution under illumination with a 442 nm laser. In this way, the quantum yields for each productive transformation could be determined directly allowing us to distinguish three different photoreactions for each isomer quantitatively. All measured quantum yields are summarized in Table 1. Similar to an earlier HTI system developed in our group,[25] each isomer of **1** undergoes more than one photoreaction after excitation leading to single-bond rotation (SBR), double-bond isomerization (DBI), and hula twist (HT) photoproducts. As we discussed in our previous work about the HT, it is not unambiguously proven for this system whether the reaction proceeds mechanistically in a fully concerted way via a "kinked" conical intersection or in a sequential way via a "hot ground state" reaction.[25] In the older system, no clear net-sequence of isomer population during illumination could be observed because of very inefficient photoreactions of the two *E* configured isomers. For HTI **1** ,the *E* to *Z* photoreactions are significantly amplified allowing us to identify a clearly preferred sequence of isomer interconversions under irradiation conditions.

At 20 °C, the photoreactions of **A** are the most efficient of all four isomers with quantum yields reaching up to 17% (for the DBI of **A** to **C**). The SBR of **A** to **B** is also quite effective with 10%. For **B**, the HT photoreaction to **C** is the most important and proceeds with 2.3% quantum yield. The photoreactions of **C** and **D** are less efficient but still sizable enough to enable precise measurements. The most prominent photoreactions are DBI of **C** to **A** (0.27%) and the HT of **D** to **A** (0.20%). Importantly, the back-reactions **B** to **A** (SBR) and **C** to **B** (HT) are either not observed or orders of magnitude less efficient, respectively. The general errors in the quantum yield measurements (Table 1) were found to be at maximum 15% when taking into account the combined errors arising from integration of the NMR spectra, sample weighing in, and photometer accuracy. Accounting for these errors does, however, not change the findings reported.

Cooling to −50 °C (Figure 2a) leads to significant changes in the quantum yields of individual photoreactions. At this temperature, **A** still undergoes the most efficient photoreactions but now the SBR leading to **B** is much more enhanced to 18% and thus slightly preferred over DBI. Likewise, the preferred photoreactions of **B** to **C** (HT) and **C** to **A** (DBI) are considerably improved and almost twice as efficient as at 20 °C.

With the quantum yields for each photoreaction measured, all possible sequences of isomer interconversions could be compared and their probabilities calculated. To create an overall directional process, and therefore constitute a molecular step motor, at least three transformations have to occur without reversal of a single step. There are eight such different three-step cycles denoted by their three member repeat sequences. Four of these are the exact backward cycles, e.g., **ACB** is the backward cycle of **ABC**. As many of the determined quantum yields are below percent range, the overall probabilities for cycles involving more than three steps are so small that they can be considered insignificant.

To calculate, which cycle is performed by **1** upon illumination it is not enough to simply multiply quantum yields of each step because all four isomers have different extinctions at 442 nm and their individual concentrations are not the same. We therefore calculated the probability for each step in the cycle in the photostationary state (pss) at 442 nm and then multiplied these probabilities for the corresponding

DOI: 10.1021/jacs.8b10660
J. Am. Chem. Soc. 2018, 140, 16442−16445

Table 1. Experimentally determined quantum yields and calculated probabilities for all cycle processes of 1 in CD_2Cl_2

	quantum yields [%]			relative probability [%]	
reaction	20 °C	−50 °C	cycle	20 °C	−50 °C
A to **B** SBR	10 ± 2	18 ± 3	**ABC**	81 ± 7	98 ± 2
A to **C** DBI	17 ± 3	17 ± 3	**ACB**	<0.1	0.6 ± 0.4
A to **D** HT	1.8 ± 0. 3	2.3 ± 0.4	**ABD**	16 ± 6	1.8 ± 0.9
B to **A** SBR	0 ± 0.001	0.007 ± 0.001	**ADB**	<0.1	0.1 ± 0.1
B to **C** HT	2.3 ± 0.3	3.6 ± 0.5	**ACD**	1.5 ± 0.8	<0.1
B to **D** DBI	1.3 ± 0.2	0.54 ± 0.08	**ADC**	0.4 ± 0.3	<0.1
C to **A** DBI	0.27 ± 0.04	0.41 ± 0.06	**BCD**	0.9 ± 0.4	<0.1
C to **B** HT	0.01 ± 0.002	0.01 ± 0.02	**BDC**	0.4 ± 0.3	<0.1
C to **D** SBR	0.009 ± 0.001	0 ± 0.001			
D to **A** HT	0.20 ± 0.03	0.36 ± 0.05			
D to **B** DBI	0.040 ± 0.006	0.059 ± 0.009			
D to **C** SBR	0.019 ± 0.003	0 ± 0.001			

three step cycles (see Supporting Information for details). Additionally, there are three possible permutations resulting in the same overall cycle, e.g., **ABC**, **BCA**, and **CAB**. To account for this starting point dependency, the overall probability of every three-step cycle was multiplied by three.

To discuss the cyclic processes in the photoreaction of **1**, it is important to distinguish between the terms monodirectional and unidirectional. We define monodirectionality as preference for one cycle against all others and unidirectionality as preference for one cycle against the corresponding cycle in opposite direction. At 20 °C, **1** has a monodirectionality of 81% with the cycle **ABC** as most dominant pathway for a full rotation. Additionally, this cycle is 100% unidirectional as the backward cycle **ACB** is not performed. The next most probable cycles are **ABD** with 16% and **ACD** with 1.5%. To visualize the stepwise directional motion of HTI **1**, the benzothiophenon fragment can be assumed as static, while the dimethoxybenzene ring rotates around a virtual axis, which is coaligned with the central double bond. In Figure 3b, all three states **A**, **B**, and **C** are superimposed and depicted as front view along the virtual axis. In this way, the three different positions of the *ortho*-methoxy group relative to the benzothiophene fragment, and consequently its directional rotation in space, are clearly visible during the rotation cycle.

To improve monodirectionality of **1**, it was necessary to favor the **ABC** cycle, especially against **ABD**. The branching point of these two cycles is the photoreaction of **B** and, consequently, its HT photoreaction to **C** needs to be increased against the DBI to **D**. Exactly this behavior is observed at −50 °C where the quantum yield of the **B** to **C** (HT) transition roughly doubled to 3.6% while the quantum yield of **B** to **D** (DBI) is lowered to 0.54%. As a result monodirectionality of **1** increases at the lower temperature to a value of 98% for the cycle **ABC** while unidirectionality is still 99%. Apart from this highly desirable increase in directionality upon lowering the temperature, the overall efficiency of the **ABC** cycle is also improved at the same time. While on average 3400 absorbed photons are necessary to drive one complete rotation at 20 °C, only 1900 photons are necessary at −50 °C (see Supporting Information for details on the calculation). Therefore, rotation speed increases by a factor of ∼2 when decreasing the temperature by 70 °C, a phenomenon that is unprecedented in the history of molecular motors. So far, light as well as chemically driven motors significantly decrease in speed, if not coming to a complete halt, with lower temperature as their thermal ratcheting steps and/or chemical reactions become more sluggish. The presented system avoids thermal ratcheting in the ground state as each of its operational steps is light powered. allowing to generate an entirely different mode of operation.

In summary, a new molecular three-step motor is presented, which interconverts three different isomeric states in a fixed sequence upon visible light irradiation. This is possible because each step is the result of a different photoreaction: SBR, HT, and DBI preventing any backward reaction. Overall, the cyclic isomer interconversion results in a mono- and unidirectional rotation of one molecular fragment against the other with up to 98% directionality. In contrast to known molecular motors, the speed and efficiency of this molecular machine increases with lowering the temperature and no thermal ratcheting step in the ground state hampers full use of the supplied photonic energy.

■ ASSOCIATED CONTENT

Supporting Information

The Supporting Information is available free of charge on the ACS Publications website at DOI: 10.1021/jacs.8b10660.

Synthetic procedures for **1**, characterization including m.p., ^{1}H NMR, ^{13}C NMR, IR, (HR)MS, elemental analysis, X-ray crystallography, conformational analysis, photophysical data including molar absorption coefficients, isomer compositions in the pss, quantum yields, kinetic analyses of the interconversion of isomers at different temperatures, and computational details (PDF)

Data for $C_{20}H_{20}O_3S$ (CIF)

■ AUTHOR INFORMATION

Corresponding Author

*henry.dube@cup.uni-muenchen.de

ORCID

Aaron Gerwien: 0000-0001-5639-1774

Peter Mayer: 0000-0002-1847-8032

Henry Dube: 0000-0002-5055-9924

Notes

The authors declare no competing financial interest.

■ ACKNOWLEDGMENTS

We thank the Deutsche Forschungsgemeinschaft (DFG) for an Emmy Noether fellowship (DU 1414/1-1). We further thank the Deutsche Forschungsgemeinschaft (SFB 749, A12) and the

Cluster of Excellence 'Center for Integrated Protein Science Munich' (CIPSM) for financial support.

REFERENCES

(1) Erbas-Cakmak, S.; Leigh, D. A.; McTernan, C. T.; Nussbaumer, A. L. Artificial Molecular Machines. *Chem. Rev.* **2015**, *115* (18), 10081−10206.
(2) Stoddart, J. F. Mechanically Interlocked Molecules (MIMs)-Molecular Shuttles, Switches, and Machines (Nobel Lecture). *Angew. Chem., Int. Ed.* **2017**, *56* (37), 11094−11125.
(3) Cheng, C.; McGonigal, P. R.; Schneebeli, S. T.; Li, H.; Vermeulen, N. A.; Ke, C.; Stoddart, J. F. An artificial molecular pump. *Nat. Nanotechnol.* **2015**, *10* (6), 547−553.
(4) Sauvage, J. P. From Chemical Topology to Molecular Machines (Nobel Lecture). *Angew. Chem., Int. Ed.* **2017**, *56* (37), 11080−11093.
(5) Kassem, S.; van Leeuwen, T.; Lubbe, A. S.; Wilson, M. R.; Feringa, B. L.; Leigh, D. A. Artificial molecular motors. *Chem. Soc. Rev.* **2017**, *46* (9), 2592−2621.
(6) Koumura, N.; Zijlstra, R. W. J.; van Delden, R. A.; Harada, N.; Feringa, B. L. Light-driven monodirectional molecular rotor. *Nature* **1999**, *401*, 152−155.
(7) Hernandez, J. V.; Kay, E. R.; Leigh, D. A. A Reversible Synthetic Rotary Molecular Motor. *Science* **2004**, *306*, 1532−1537.
(8) Erbas-Cakmak, S.; Fielden, S. D. P.; Karaca, U.; Leigh, D. A.; McTernan, C. T.; Tetlow, D. J.; Wilson, M. R. Rotary and linear molecular motors driven by pulses of a chemical fuel. *Science* **2017**, *358* (6361), 340−343.
(9) Wilson, M. R.; Sola, J.; Carlone, A.; Goldup, S. M.; Lebrasseur, N.; Leigh, D. A. An autonomous chemically fuelled small-molecule motor. *Nature* **2016**, *534* (7606), 235−240.
(10) Fletcher, S. P.; Dumur, F.; Pollard, M. M.; Feringa, B. L. A Reversible, Unidirectional Molecular Rotary Motor Driven by Chemical Energy. *Science* **2005**, *310*, 80−82.
(11) Kistemaker, H. A.; Stacko, P.; Visser, J.; Feringa, B. L. Unidirectional rotary motion in achiral molecular motors. *Nat. Chem.* **2015**, *7*, 890−896.
(12) Stacko, P.; Kistemaker, J. C. M.; van Leeuwen, T.; Chang, M.-C.; Otten, E.; Feringa, B. L. Locked synchronous rotor motion in a molecular motor. *Science* **2017**, *356* (6341), 964−968.
(13) Greb, L.; Lehn, J. M. Light-driven molecular motors: imines as four-step or two-step unidirectional rotors. *J. Am. Chem. Soc.* **2014**, *136* (38), 13114−13117.
(14) Guentner, M.; Schildhauer, M.; Thumser, S.; Mayer, P.; Stephenson, D.; Mayer, P. J.; Dube, H. Sunlight-powered kHz rotation of a hemithioindigo-based molecular motor. *Nat. Commun.* **2015**, *6*, 8406.
(15) Huber, L. A.; Hoffmann, K.; Thumser, S.; Böcher, N.; Mayer, P.; Dube, H. Direct Observation of Hemithioindigo-Motor Unidirectionality. *Angew. Chem., Int. Ed.* **2017**, *56*, 14536−14539.
(16) Wilcken, R.; Schildhauer, M.; Rott, F.; Huber, L. A.; Guentner, M.; Thumser, S.; Hoffmann, K.; Oesterling, S.; de Vivie-Riedle, R.; Riedle, E.; Dube, H. The Complete Mechanism of Hemithioindigo Motor Rotation. *J. Am. Chem. Soc.* **2018**, *140*, 5311−5318.
(17) Eelkema, R.; Pollard, M. M.; Vicario, J.; Katsonis, N.; Ramon, B. S.; Bastiaansen, C. W.; Broer, D. J.; Feringa, B. L. Molecular machines: nanomotor rotates microscale objects. *Nature* **2006**, *440* (7081), 163.
(18) Foy, J. T.; Li, Q.; Goujon, A.; Colard-Itte, J.-R.; Fuks, G.; Moulin, E.; Schiffmann, O.; Dattler, D.; Funeriu, D. P.; Giuseppone, N. Dual-light control of nanomachines that integrate motor and modulator subunits. *Nat. Nanotechnol.* **2017**, *12*, 540−545.
(19) Garcia-Lopez, V.; Chen, F.; Nilewski, L. G.; Duret, G.; Aliyan, A.; Kolomeisky, A. B.; Robinson, J. T.; Wang, G.; Pal, R.; Tour, J. M. Molecular machines open cell membranes. *Nature* **2017**, *548* (7669), 567−572.
(20) Chen, J.; Leung, F. K.; Stuart, M. C. A.; Kajitani, T.; Fukushima, T.; van der Giessen, E.; Feringa, B. L. Artificial muscle-like function from hierarchical supramolecular assembly of photoresponsive molecular motors. *Nat. Chem.* **2018**, *10* (2), 132−138.
(21) Wang, J.; Feringa, B. L. Dynamic control of chiral space in a catalytic asymmetric reaction using a molecular motor. *Science* **2011**, *331* (6023), 1429−32.
(22) Friedländer, P. Ueber schwefelhaltige Analoga der Indigogruppe. *Ber. Dtsch. Chem. Ges.* **1906**, *39*, 1060−1066.
(23) Wiedbrauk, S.; Dube, H. Hemithioindigo—an emerging photoswitch. *Tetrahedron Lett.* **2015**, *56* (29), 4266−4274.
(24) Gerwien, A.; Reinhardt, T.; Mayer, P.; Dube, H. Synthesis of Double-Bond Substituted Hemithioindigo Photoswitches. *Org. Lett.* **2018**, *20* (1), 232−235.
(25) Gerwien, A.; Schildhauer, M.; Thumser, S.; Mayer, P.; Dube, H., Direct evidence for hula twist and single-bond rotation photoproducts. *Nat. Commun.* **2018**, *9*, DOI: 10.1038/s41467-018-04928-9

DOI: 10.1021/jacs.8b10660
J. Am. Chem. Soc. 2018, 140, 16445−16445

Supplementary Information

Photon-Only Molecular Motor with Reverse Temperature-Dependent Efficiency

Aaron Gerwien, Peter Mayer, and Henry Dube*

Department für Chemie and Munich Center for Integrated Protein Science CIPSM, Ludwig-Maximilians-Universität München, D-81377 Munich, Germany.

henry.dube@cup.uni-muenchen.de

Table of Contents

Supplementary materials and methods

General experimental methods

Reagents and solvents were obtained from *abcr*, *Acros, Fluka, Merck, Sigma-Aldrich* or *TCI* in the qualities *puriss., p.a., or purum* and used as received. Technical solvents were distilled before use for column chromatography and extraction on a rotary evaporator (*Heidolph Hei-VAP Value*, *vacuubrand* CVC 3000). Reactions were monitored on *Merck* Silica 60 F254 TLC plates. Detection was done by irradiation with UV light (254 nm or 366 nm).

Column chromatography was performed with silica gel 60 (*Merck*, particle size 0.063- 0.200 mm) and distilled technical solvents.

^{1}H NMR and ^{13}C NMR spectra were measured on a *Varian Mercury 200 VX, Varian 300, Inova 400, Varian 600 NMR*, or *Bruker Avance III HD 800 MHz* spectrometer at different temperatures. Deuterated solvents were obtained from *Cambridge Isotope Laboratories* or *Eurisotop* and used without further purification. Chemical shifts (δ) are given in parts per million (ppm) on the delta scale (δ) relative to tetramethylsilane as external standard. Residual solvent signals in the ^{1}H and ^{13}C NMR spectra were used as internal reference. ^{1}H NMR: $CDCl_3$ = 7.26 ppm, CD_2Cl_2 = 5.32 ppm, $(CDCl_2)_2$ = 6.00 ppm. For ^{13}C NMR: $CDCl_3$ = 77.16 ppm, CD_2Cl_2 = 53.84 ppm. Resonance multiplicity is indicated as *s* (singlet), *d* (doublet), *t* (triplet), *q* (quartet) and *m* (multiplet). Coupling constant values (*J*) are given in hertz (Hz).

Electron Impact (EI) mass spectra were measured on a *Finnigan MAT95Q* or on a *Finnigan MAT90* mass spectrometer. **Electronspray ionisation (ESI) mass spectra were** measured on a *Thermo Finnigan LTQ-FT*. The most important signals are reported in *m/z* units with *M* as the molecular ion.

Elemental analysis were performed in the micro analytical laboratory of the LMU department of chemistry on an *Elementar Vario EL* apparatus.

Infrared spectra were recorded on a *Perkin Elmer Spectrum BX-FT-IR* instrument equipped with a *Smith DuraSamplIR II ATR*-device. Transmittance values are described by wavenumber (cm^{-1}) as very strong (vs), strong (s), medium (m) and weak (w).

UV/vis spectra were measured on a *Varian Cary 5000* spectrophotometer. The spectra were recorded in a quartz cuvette (1 cm). Solvents for spectroscopy were obtained from *VWR* and

Merck. Absorption wavelength (λ) are reported in nm and the molar absorption coefficients (ε) in L mol^{-1} cm^{-1}. Shoulders are declared as sh.

Low temperature UV/vis spectra and quantum yields of the photoreactions at –50 °C were measured on a *Varian Cary® 50* spectrophotometer with an *Oxford DN 1704* optical cryostat controlled by an *Oxford ITC 4* device. Low temperatures were reached by cooling slowly with liquid nitrogen. The spectra were recorded in a quartz cuvette (1 cm). Solvents for spectroscopy were obtained from *VWR*, *Merck* and *Sigma Aldrich* and were dried, degassed, and filtrated prior use. For irradiation studies a *CNI MDL-III-445* Blue Diode Laser (442 nm) was used as light source. Absorption wavelengths (λ) are reported in nm and the molar absorption coefficients (ε) in $L \cdot mol^{-1} \cdot cm^{-1}$.

Melting points (M.p.) were measured on a *Stuart* SMP10 melting point apparatus in open capillaries and are not corrected.

Synthesis

Precursors **2** and **3** were prepared following literature procedures[1] according to the following scheme.

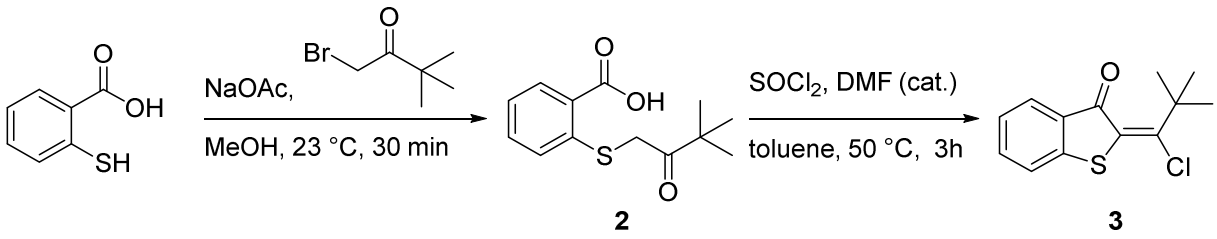

2-(1-(2,4-Dimethoxyphenyl)-2,2-dimethylpropylidene)benzo[*b*]thiophen-3(2*H*)-one (**4**)

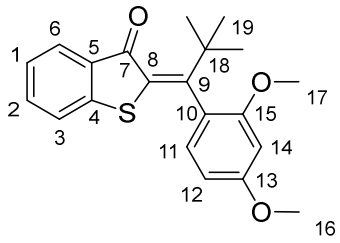

2-(1-Chloro-2,2-dimethylpropylidene)benzo[*b*]thiophen-3(2*H*)-one (**3**, 3.96 mmol 1.0 equiv.) was dissolved in THF (18 mL). (2,4-Dimethoxyphenyl)boronic acid (5.93 mmol, 1.5 equiv.), potassium carbonate (7.91 mmol, 2.0 equiv.) and water (2 mL) were added. After bubbling argon through the solution for 10 min, $Pd(PPh_3)_4$ (0.20 mmol, 5 mol%) was added and the reaction mixture was stirred at 60 °C for 24 h. Subsequently, a saturated sodium carbonate solution (20 mL) was added, the aqueous phase was extracted with CH_2Cl_2 (3 x 50 mL), and the combined organic phases were dried over Na_2SO_4. After removing the solvent i*n vacuo* the crude product was purified by column chromatography (SiO_2, *i*Hex/EtOAc = 95/5) and further by crystallization from *n*heptane/EtOAc. The title compound was isolated as yellow crystals (1360 mg, 3.84 mmol, 97%, only the Z-isomer was obtained after crystallization).

^{1}H NMR (400 MHz, $CDCl_3$) δ = 7.80 (dd, ^3J(H,H) = 8.1 Hz, ^4J(H,H) = 1.1 Hz, 1H, H-C(6)), 7.42 (app td, ^3J(H,H) = 7.7 Hz, ^4J(H,H) = 1.3 Hz, 1H, H-C(2)), 7.21 – 7.14 (m, 2H, H-C(1), H-C(3)), 6.94 – 6.89 (m, 1H, H-C(16), 6.56 – 6.49 (m, 2H, H-C(13), H-C(14)), 3.86 (s, 3H, H-C(17)), 3.79 (s, 3H, H-C(16)), 1.34 (s, 9H, H-C(19)) ppm.

^{13}C NMR (101 MHz, $CDCl_3$) δ = 186.3 (C(7)), 164.0 (C(9)), 160.9 (C(15)), 156.6 (C(13)), 146.0 (C(4)), 134.5 (C(5)), 134.5 (C(2)), 133.9 (C(8)), 128.8 (C(11)), 126.8 (C(6)), 126.8 (C(10)), 124.5 (C(1)), 122.8 (C(6)), 104.2 (C(12)), 98.8 (C(14)), 55.7 (C(16)), 55.5 (C(17)), 38.9 (C(18)), 28.5 (C(19)).

IR $\tilde{\nu}$ (cm^{-1}) = 2952 (w), 2866 (w), 1652 (s), 1603 (m), 1585 (m), 1578 (m), 1534 (m), 1500 (m), 1482 (w), 1462 (w), 1449 (m), 1435 (w), 1414 (m), 1387 (w), 1353 (w), 1303 (m), 1281 (m), 1271 (m), 1243 (w), 1218 (w), 1207 (vs), 1155 (s), 1132 (s), 1069 (m), 1043 (m), 1029 (m), 1021 (m), 982 (w), 954 (w), 912 (m), 896 (m), 846 (s), 807 (m), 798 (m), 769 (m), 743 (vs), 711 (w), 704 (w), 676 (m), 658 (m).

Melting point: 176 °C.

HRMS (EI^+), [$M^{+\bullet}$]: *m/z* calcd: 354.1284 for $[C_{21}H_{22}O_3S]^{+\bullet}$, found: 354.1288.

R_f (SiO_2, *i*Hex/EtOAc = 98/2) = 0.42.

2-(1-(2,4-Dimethoxyphenyl)-2,2-dimethylpropylidene)benzo[*b*]thiophen-3(2*H*)-one 1-oxide (**1**)

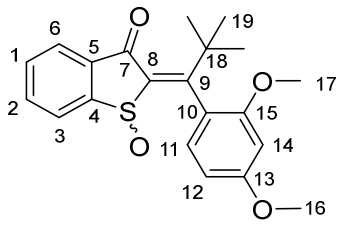

2-(1-(2,4-Dimethoxyphenyl)-2,2-dimethylpropylidene)benzo[*b*]thiophen-3(2*H*)-one (**4**, 2.91 mmol 1.0 equiv.) was dissolved in acetic acid (10 mL). Sodium perborate (3.20 mmol, 1.1 equiv.) was added and the reaction mixture was stirred at 23 °C for 12 h. Subsequently, a saturated sodium carbonate solution (15 mL) was added, the aqueous phase was extracted with CH_2Cl_2 (3 x 20 mL), and the combined organic phases were dried over Na_2SO_4. After removing the solvent i*n vacuo* the crude product was purified by column chromatography (SiO_2, *i*Hex/EtOAc = 1/1) as yellow solid (852.3 mg, 2.38 mmol, 82%) as a mixture of four isomers. These isomers could be separated by column chromatography in the dark (SiO_2, *i*Hex/EtOAc = 6/4) and crystallized separately from *n*heptane/CH_2Cl_2.

A-1

^{1}H NMR (600 MHz, $CDCl_3$) δ = 7.96 (d, ^3J(H,H) = 7.7 Hz, 1H, H-C(6)), 7.82 (d, ^3J(H,H) = 7.7 Hz, 1H, H-C(3)), 7.75 (t, ^3J(H,H) = 7.5 Hz, 1H, H-C(2)), 7.67 (t, ^3J(H,H) = 7.5 Hz, 1H, H-C(2)), 6.90 (d, ^3J(H,H) = 8.2 Hz, 1H, H-C(11)), 6.56 (dd, ^3J(H,H) = 8.2, 2.3 Hz, 1H, H-C(12)), 6.53 (d, ^3J(H,H) = 2.2 Hz, 1H, H-C(14)), 3.86 (s, 3H, H-C(16)), 3.82 (s, 3H, H-C(17)), 1.37 (s, 9H, H-C(19)) ppm.

^{13}C NMR (150 MHz, $CDCl_3$) δ = 184.4 (C(7)), 181.2 (C(9)), 161.7 (C(13)), 158.4 (C(15)), 148.4 (C(4)), 143.6 (C(8)), 136.5 (C(5)), 135.6 (C(2)), 132.6 (C(1)), 127.8 (C(11)), 127.3 (C(3)), 126.2 (C(6)), 123.3 (C(10)), 104.6 (C(12)), 98.5 (C(14)), 55.7 (C(17)), 55.5 (C(16)), 40.1 (C(18)), 28.6 (C(19)) ppm.

IR $\tilde{\nu}$ (cm^{-1}) = 3096 (w), 3005 (w), 2969 (w), 1674 (s), 1604 (m), 1579 (m), 1558 (m), 1503 (m), 1456 (m), 1416 (m), 1389 (w), 1358 (w), 1321 (w), 1298 (m), 1272 (m), 1221 (m), 1206 (s), 1181 (m), 1153 (m), 1138 (s), 1066 (m), 1037 (vs), 1024 (s), 954 (m), 911 (m), 886 (w), 847 (s), 819 (m), 801 (m), 753 (vs), 729 (m), 700 (w), 685 (m), 657 (m).

Melting point: 136 °C.

R_f (SiO_2, *i*Hex/EtOAc = 1/1) = 0.09.

B-1

^{1}H NMR (600 MHz, $CDCl_3$) δ = 7.95 (d, ^3J(H,H) = 7.7 Hz, 1H, H-C(6)), 7.77 (d, ^3J(H,H) =7.2 Hz, 1H, H-C(3)), 7.75 (td, ^3J(H,H) =7.4, ^4J(H,H) =1.3 Hz, 1H, H-C(2)), 7.67 (td, ^3J(H,H) =7.4, ^4J(H,H) =1.3 Hz, 1H, H-C(1)), 7.09 (d, ^3J(H,H) = 8.3 Hz, 1H, H-C(11)), 6.60 (dd, ^3J(H,H) = 8.3, ^4J(H,H) = 2.2 Hz, 1H, H-C(12)), 6.52 (d, ^4J(H,H) = 2.2 Hz, 1H, H-C(14)), 3.86 (s, 3H, H-C(16)), 3.75 (s, 3H, H-C(17)), 1.32 (s, 9H, H-C(19)) ppm.

^{13}C NMR (150 MHz, $CDCl_3$) δ = 185.9 (C(7)), 179.9 (C(9)), 161.5 (C(13)), 156.3 (C(15)), 148.2 (C(4)), 142.9 (C(8)), 136.3 (C(5)), 135.7 (C(2)), 132.7 (C(1)), 131.0 (C(11)), 127.3 (C(3)), 126.4 (C(6)), 121.8 (C(10)), 103.2 (C(12)), 98.7 (C(14)), 2 x 55.5 (C(16)), 39.8 (C(18)), 29.0 (C(19)) ppm.

IR $\tilde{\nu}$ (cm^{-1}) = 3096 (w), 3005 (w), 2969 (w), 1674 (s), 1604 (m), 1579 (m), 1558 (m), 1503 (m), 1456 (m), 1416 (m), 1389 (w), 1358 (w), 1321 (w), 1298 (m), 1272 (m), 1221 (m), 1206 (s), 1181 (w), 1153 (m), 1138 (s), 1066 (m), 1037 (vs), 1024 (s), 954 (m), 911 (m), 886 (w), 847 (s), 819 (w), 801 (m), 753 (s), 729 (w), 700 (w), 685 (s), 657 (m).

Melting point: 188 °C.

R_f (SiO_2, *i*Hex/EtOAc = 1/1) = 0.17.

C-1

^{1}H NMR (600 MHz, $CDCl_3$) δ = 8.03 (d, *J* = 7.7 Hz, 1H, H-C(3)), 7.84 – 7.77 (m, 2H, H-C(2), H-C(6)), 7.64 (t, *J* = 7.5 Hz, 1H, H-C(1)), 6.79 (d, *J* = 7.8 Hz, 1H, H-C(11)), 6.56 – 6.52 (m, 2H, H-C(12), H-C(14)), 3.85 (s, 3H, H-C(16)), 3.72 (s, 3H, H-C(17)), 1.48 (s, 9H, H-C(19)) ppm.

^{13}C NMR (150 MHz, $CDCl_3$) δ = 185.2 (C(7)), 175.7 (C(9)), 160.7 (C(13)), 156.8 (C(15)), 147.6 (C(4)), 139.5 (C(8)), 135.8 (C(2)), 134.4 (C(5)), 132.8 (C(1)), 127.2 (C(3)), 126.7 (C(11)), 126.1 (C(6)), 122.0 (C(10)), 104.0 (C(12)), 98.6 (C(14)), 55.5 (C(17)), 55.4 (C(16)), 41.2 (C(18)), 30.0 (C(19)) ppm.

IR $\tilde{\nu}$ (cm^{-1}) = 3057 (w), 2972 (w), 2952 (w), 1692 (s), 1606 (m), 1591 (w), 1580 (m), 1542 (m), 1500 (w), 1481 (w), 1463 (w), 1449 (m), 1431 (w), 1414 (m), 1395 (w), 1367 (w), 1361 (w), 1308 (m), 1283 (m), 1274 (m), 1263 (m), 1220 (s), 1205 (vs), 1152 (s), 1125 (s), 1073 (m), 1053 (m), 1038 (s), 1028 (vs), 1008 (m), 992 (m), 964 (w), 939 (w), 915 (w), 856 (s), 793 (m), 765 (m), 753 (vs), 726 (w), 699 (m), 676 (s).

Melting point: 198 °C.

R_f (SiO_2, *i*Hex/EtOAc = 1/1) = 0.33.

D-1

^{1}H NMR (600 MHz, $CDCl_3$) δ = 8.00 (d, ^3J(H,H) = 7.7 Hz, 1H, H-C(3)), 7.81 (td, ^3J(H,H) = 7.6, ^4J(H,H) = 1.2 Hz, 1H, H-C(2)), 7.78 (d, ^3J(H,H) = 7.7 Hz, 1H, H-C(6)), 7.65 (t, ^3J(H,H) = 7.1 Hz, 1H, H-C(1)), 6.59 (d, ^3J(H,H) = 8.2 Hz, 1H, H-C(11)), 6.55 (d, ^4J(H,H) = 2.3 Hz, 1H, H-C(14)), 6.49 (dd, ^3J(H,H) = 8.3, ^4J(H,H) =2.3 Hz, 1H, H-C(12)), 3.85 (s, 3H, H-C(16)), 3.77 (s, 3H, H-C(17)), 1.48 (s, 9H, H-C(19)) ppm.

^{13}C NMR (150 MHz, $CDCl_3$) δ = 186.9 (C(7)), 175.2 (C(9)), 160.7 (C(13)), 157.1 (C(15)), 147.6 (C(4)), 138.9 (C(8)), 135.8 (C(2)), 134.1 (C(5)), 133.0 (C(1)), 127.3 (C(3)), 126.5 (C(11)), 126.2 (C(6)), 122.1 (C(10)), 104.3 (C(12)), 98.5 (C(14)), 55.6 (C(17)), 55.4 (C(16)), 41.0 (C(18)), 31.2 (C(19)) ppm.

IR $\tilde{\nu}$ (cm^{-1}) = 2970 (w), 2934 (w), 2838 (w), 1696 (s), 1604 (m), 1583 (m), 1558 (m), 1502 (m), 1455 (m), 1448 (m), 1437 (m), 1419 (m), 1396 (w), 1369 (w), 1361 (w), 1323 (w), 1303 (m), 1284 (m), 1266 (m), 1208 (s), 1155 (s), 1138 (vs), 1119 (w), 1062 (w), 1055 (w), 1025 (vs), 993 (m), 966 (w), 935 (w), 918 (w), 859 (w), 841 (s), 824 (w), 809 (w), 797 (m), 756 (vs), 700 (w), 681 (m).

Melting point: 172 °C.

R_f (SiO_2, *i*Hex/EtOAc = 1/1) = 0.27.

For all isomers:

HRMS (EI$^+$), [$M^{+\bullet}$]: *m/z* calcd: 370.1233 for $[C_{21}H_{22}O_4S]^{+\bullet}$, found: 370.1233.

Elemental analysis: calcd (%) for $C_{21}H_{22}O_4S$: C 68.09, H 5.99, S 8.65; found: C 68.06, H 5.93, S 8.41.

Physical and photophysical properties

Thermal isomerization of 1

Amberized NMR tubes were charged with 0.8 mg to 2.5 mg of the respective isomer **A**, **B**, **C**, or **D** and 0.7 mL of deuterated solvent. Subsequently the NMR tubes were heated to 90 °C and the kinetics of thermal isomerizations were followed by ^{1}H NMR measurements in defined time intervals. The unchanging equilibrium concentrations of isomers after prolonged heating were obtained from integration of the corresponding signals in the ^{1}H NMR spectrum.

At 90 °C only the atropisomerizations between **A** and **B** and between **C** and **D** are taking place. These thermal atropisomerizations are unimolecular first order reactions and proceed towards an equilibrium composition with both atropisomers present according to eq. 1 and eq. 2, respectively. At 140 °C the thermal isomerization of the double bond takes place, while the atropisomers are in rapid exchange with each other. Correspondingly, the concentration of *Z* is the sum of the concentrations of **A** and **B** and the concentration of *E* is the sum of the concentrations **C** and **D** under these conditions. The thermal double bond isomerization can therefore also be considered as an unimolecular first order reaction, which proceeds towards an equilibrium composition with both *Z* and *E* isomers present according to eq. 3.

$$\ln\left(\frac{[\mathbf{A}]_{t_0}-[\mathbf{A}]_{eq}}{[\mathbf{A}]_t-[\mathbf{A}]_{eq}}\right) = (k_{\mathbf{A/B}} + k_{\mathbf{B/A}})t \qquad \text{(eq. 1)}$$

$$\ln\left(\frac{[\mathbf{C}]_{t_0}-[\mathbf{C}]_{eq}}{[\mathbf{C}]_t-[\mathbf{C}]_{eq}}\right) = (k_{\mathbf{C/D}} + k_{\mathbf{D/C}})t \qquad \text{(eq. 2)}$$

$$\ln\left(\frac{[\mathrm{E}]_{t_0}-[\mathrm{E}]_{eq}}{[\mathrm{E}]_t-[\mathrm{E}]_{eq}}\right) = (k_{\mathrm{E/Z}} + k_{\mathrm{Z/E}})t \qquad \text{(eq. 3)}$$

With [**A**, **C** or *E*]$_{t_0}$ being the initial concentration of the isomers **A**, **C** or *E* (i.e. the sum of the concentration of **C** and **D**) at the time $t = 0$, [**A**, **C** or *E*]$_{eq}$ being the concentration of the isomers **A**, **C** or *E* at equilibrium, [**A**, **C** or *E*]$_t$ representing the concentration of the isomers **A**, **C** or *E* at specific times in the measurement *t*, $k_{\mathbf{A/B}}$ being the rate constant *k* of the **A** to **B** conversion, $k_{\mathbf{B/A}}$ being the rate constant *k* of the **B** to **A** conversion, $k_{\mathbf{C/D}}$ being the rate constant *k* of the **C** to **D** conversion, $k_{\mathbf{D/C}}$ being the rate constant *k* of the **D** to **C** conversion, $k_{E/Z}$ being the rate constant *k* of the *E* to *Z* conversion, $k_{Z/E}$ being the rate constant *k* of the *Z* to *E* conversion, and *t* being the elapsed time. When plotting the logarithmic left part of eq. 1 or eq. 2 versus time *t* the obtained

slope *m* contains the rate constants for the isomerization reactions taking place. The rate constants $k_{\mathbf{A/B}}$, $k_{\mathbf{C/D}}$, and $k_{E/Z}$ can then be calculated according to eq. 4, eq. 5, and eq. 6:

$$k_{\mathbf{A/B}} = \frac{m}{1+\frac{[\mathbf{A}]_{eq}}{[\mathbf{B}]_{eq}}} \quad \text{(eq. 4)}$$

$$k_{\mathbf{C/D}} = \frac{m}{1+\frac{[\mathbf{C}]_{eq}}{[\mathbf{D}]_{eq}}} \quad \text{(eq. 5)}$$

$$k_{E/Z} = \frac{m}{1+\frac{[E]_{eq}}{[Z]_{eq}}} \quad \text{(eq. 6)}$$

when taking into account the corresponding laws of mass action (eq. 7, eq. 8, and eq. 9):

$$\frac{[\mathbf{A}]_{eq}}{[\mathbf{B}]_{eq}} = \frac{k_{\mathbf{B/A}}}{k_{\mathbf{A/B}}} \quad \text{(eq. 7)}$$

$$\frac{[\mathbf{C}]_{eq}}{[\mathbf{D}]_{eq}} = \frac{k_{\mathbf{D/C}}}{k_{\mathbf{C/D}}} \quad \text{(eq. 8)}$$

$$\frac{[E]_{eq}}{[Z]_{eq}} = \frac{k_{Z/E}}{k_{E/Z}} \quad \text{(eq. 9)}$$

Likewise the reverse rate constants are defined and could be determined from separate measurements starting from the opposite pure isomers **B**, **D** and *Z* and application of eq. 10 to eq. 15, respectively.

$$\ln\left(\frac{[\mathbf{B}]_{t_0}-[\mathbf{B}]_{eq}}{[\mathbf{B}]_{t}-[\mathbf{B}]_{eq}}\right) = (k_{\mathbf{A/B}} + k_{\mathbf{B/A}})t \quad \text{(eq. 10)}$$

$$\ln\left(\frac{[\mathbf{D}]_{t_0}-[\mathbf{D}]_{eq}}{[\mathbf{D}]_{t}-[\mathbf{D}]_{eq}}\right) = (k_{\mathbf{C/D}} + k_{\mathbf{D/C}})t \quad \text{(eq. 11)}$$

$$\ln\left(\frac{[Z]_{t_0}-[Z]_{eq}}{[\mathrm{Z}]_{t}-[Z]_{eq}}\right) = (k_{\mathrm{E/Z}} + k_{Z/E})t \quad \text{(eq. 12)}$$

$$k_{\mathbf{B/A}} = \frac{m}{1+\frac{[\mathbf{B}]_{eq}}{[\mathbf{A}]_{eq}}} \quad \text{(eq. 13)}$$

$$k_{\mathbf{D/C}} = \frac{m}{1+\frac{[\mathbf{D}]_{eq}}{[\mathbf{C}]_{eq}}} \quad \text{(eq. 14)}$$

$$k_{\mathrm{Z/E}} = \frac{m}{1+\frac{[\mathrm{Z}]_{eq}}{[\mathrm{E}]_{eq}}} \quad \text{(eq. 15)}$$

$$\Delta G^{\ddagger} = \ln\left(\frac{k*h}{k_B*T}\right) * R * T \quad \text{(eq. 16)}$$

By using the *Eyring* equation (eq. 16) the free activation enthalpies ΔG^* can be calculated from the rate constants of the corresponding reaction. The obtained free activation enthalpies ΔG^* for the thermal isomerizations between **A** to **B**, **C** to **D** as well as *E* to *Z* and *vice versa* in $(CDCl_2)_2$ and the corresponding extrapolated half-lives at 25 °C are given in Table S1 together with the equilibrium compositions obtained at high temperatures.

From these measurements we could quantify the full ground state energy profile of hemithioindigo **1**. The equilibrium compositions at high temperatures deliver the energy differences between the corresponding states (red Δ values in Fig. S15) according to the relation of the change of *Gibbs* free energy and the equilibrium constant $-\Delta G = R \cdot T \cdot \ln K$ (see also Table S1). The theoretical values were found to be in good agreement with the experimentally determined ones.

Photoconversions of 1 determined by quantum yield measurements

The photochemical quantum yields of the different photoconversion reactions ϕ were calculated as the ratio between the numbers of isomerized molecules *n*(molecules isomerized) and the number of absorbed photons *n*(*hv*) according to eq. 17:

$$\phi = \frac{n(\text{molecules isomerized})}{n(hv)} \qquad \text{(eq. 17)}$$

To determine the quantum yields ϕ a sample with known concentration (3.0 mM) of each pure isomer **A**, **B**, **C**, or **D** in CD_2Cl_2 was irradiated with a 442 nm *CNI MDL-III-445* Blue Diode Laser within an *Oxford DN 1704* optical cryostat controlled by an *Oxford ITC 4* device to adjust the temperature during measurement. For counting the photons the instrumental setup published by the group of *E. Riedle*[2] was used and the number of absorbed photons over time *n*(*hv*) was measured directly at the thermal photometer of the instrument according to eq. 18:

$$n(hv) = \frac{\Delta P \cdot \lambda_{ex} \cdot t}{c \cdot h} \qquad \text{(eq. 18)}$$

where c is the speed of light ($2.99792 \cdot 10^8$ m$\cdot$s^{-1}), h is Planck's constant ($6.62607 \cdot 10^{-34}$ J$\cdot$s), λ_{ex} is the excitation wavelength in m, t is the elapsed time during irradiation, and ΔP is the difference in power read-outs at the thermal photometer between a solvent filled kuvette (P_0) and a kuvette containing the sample solution (P_t) during the irradiation period in Watt (eq. 19). The power readout during irradiation did not change substantially (<5%) over the irradiation periods.

$$\Delta P = P_t - P_0 \qquad \text{(eq. 19)}$$

Since more than one photoproduct is formed during irradiation the number of each type of photoconverted molecules n(molecules isomerized) was determined by ^{1}H NMR spectroscopy directly after each irradiation step. Multiple measurements with increasing time of irradiation were conducted and the obtained ϕ values were averaged. The amount of isomerized molecules was also plotted against irradiation time showing linear behavior over measurement periods up to 30 min in case of **A**, **B**, **C**, and **D** (Figs. S18 – S25). Therefore, the quantum yield measurements conform to initial-slope behavior, where only the initial isomer is photoconverted but not the photoproducts.

Probabilities of cycle processes in the photoisomerization of 1

To determine the cycle processes in the photoisomerizations of **1** quantum yields of each phototransition, the molar absorption coefficients of each isomer, and the concentrations of each isomer in the photostationary state (PSS) are needed. From these data the probability of each possible phototransition $p_{(x,y)}$ after absorption of one photon can be calculated under the assumption that the solution of **1** resides in the PSS:

$$p_{(x,y)} = \phi_{(x,y)} \cdot pEx_x \qquad \text{(eq. 20)}$$

with $\phi_{(x,y)}$ being the quantum yield of the phototransition from isomer x to isomer y and pEx_x the excitation probability of isomer x. pE_x can be calculated using eq. 21.

$$pEx_x = \frac{\frac{[x]}{\sum[x]} \cdot \frac{\varepsilon_x}{\sum \varepsilon_x}}{\sum \frac{[x]}{\sum[x]} \cdot \frac{\varepsilon_x}{\sum \varepsilon_x}} \quad \text{(eq. 21)}$$

with [x] being the concentration of isomer x in the PSS, and ε_x the molar absorption of isomer x at the wavelength of irradiation.

The probability for any process is therefore the product of each transition probability $p_{(x,y)}$ involved in this process. For example the possibility of the single cycle process **A** to **B** to **C** and back to **A** is given by eq. 22:

$$p_{(\boldsymbol{A\rightarrow B\rightarrow C\rightarrow A})} = p_{(\boldsymbol{A,B})} \cdot p_{(\boldsymbol{B,C})} \cdot p_{(\boldsymbol{C,A})} \quad \text{(eq. 22)}$$

There are three possible permutations resulting in the overall cycle **ABC**, namely **A→B→C→A**, **B→C→A→B**, and **C→A→B→C**. Therefore the possibility of the process **A→B→C→A** has to be multiplied by 3 to account for the different starting points (eq. 23). This must also be applied to all other cycle processes containing three steps. Cycle processes containing four steps must be multiplied by 4 since four possible permutations are possible for these processes. The probabilities $p_{\boldsymbol{cycle}}$ for all possible 3 and 4-step cycles are summarized in Table S5.

$$p_{(\boldsymbol{ABC})} = p_{(\boldsymbol{A\rightarrow B\rightarrow C\rightarrow A})} + p_{(\boldsymbol{B\rightarrow C\rightarrow A\rightarrow B})} + p_{(\boldsymbol{C\rightarrow A\rightarrow B\rightarrow C})} = p_{(\boldsymbol{A\rightarrow B\rightarrow C\rightarrow A})} \cdot 3 \quad \text{(eq. 23)}$$

Efficiencies of cycle processes in the photoisomerization of 1

To determine the number of photons needed for one full revolution in a particular cyclic process we first have to know the probability of one photon to be productive in that cycle. To aid understanding we discuss first a very simple model, wherein only three isomers **A**, **B**, **C** interconvert and only one interconversion is also occurring backwards (Scheme S1). The system does not have to be in the photostationary state (PSS) and the molar absorption of each isomer can also be different. However, in the PSS the efficiency of operation is highest.

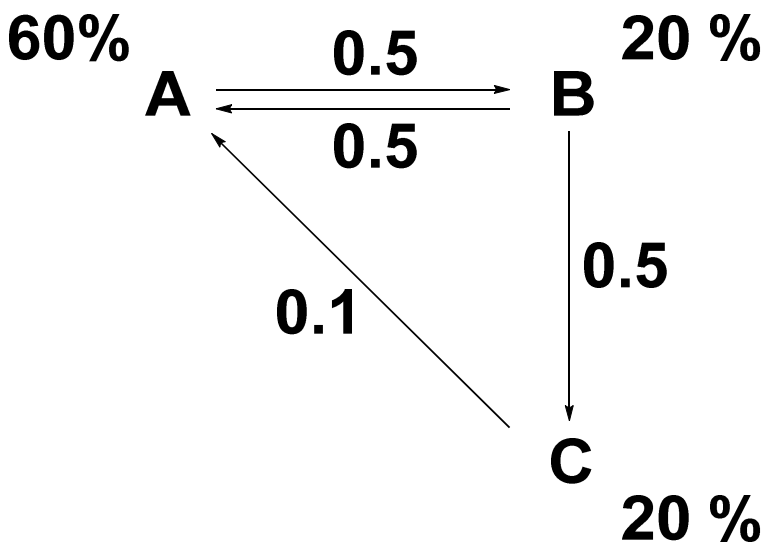

Scheme S1: Simple model system to explain the calculation of efficiencies of cycle processes.

In Scheme S1 the quantum yields ϕ for individual transformations are arbitrarily chosen to be $\phi_{(\mathbf{A}\rightarrow\mathbf{B})} = 0.5$ (i.e. 50%), $\phi_{(\mathbf{B}\rightarrow\mathbf{A})} = 0.5$, $\phi_{(\mathbf{B}\rightarrow\mathbf{C})} = 0.5$, and $\phi_{(\mathbf{C}\rightarrow\mathbf{A})} = 0.1$ and the system is not in the PSS but 60% **A**, 20% **B**, and 20% **C** is present. For simplicity molar absorptions of the three isomers are set to be identical.

First, the quantum yields for the identity photoreactions $\phi_{(\mathbf{A}\rightarrow\mathbf{A})}$, $\phi_{(\mathbf{B}\rightarrow\mathbf{B})}$, and $\phi_{(\mathbf{C}\rightarrow\mathbf{C})}$ have to be determined. This is simply done by subtracting all productive photoreaction quantum yields of each individual isomer from 1, e.g.:

$$\phi_{(\boldsymbol{A}\rightarrow\boldsymbol{A})} = 1 - \left(\phi_{(\boldsymbol{A}\rightarrow\boldsymbol{B})} + \phi_{(\boldsymbol{A}\rightarrow\boldsymbol{C})}\right) = 0.5 \qquad \text{(eq. 24)}$$

Next the probability of an incident photon being absorbed by either isomer (with its particular molar absorption and at the particular concentration) and leading to transformation into itself or a different isomer, is calculated according to eq. 20. Thus, the probability for the transformation of **A** to **B** in our example is:

$$p_{(\boldsymbol{A}\rightarrow\boldsymbol{B})} = \phi_{(\boldsymbol{A}\rightarrow\boldsymbol{B})} \cdot pEx_{\boldsymbol{A}} = 0.3 \qquad \text{(eq. 25)}$$

This probability is now calculated for each transformation that is present in the system including the identity reactions giving $p_{(\boldsymbol{A\rightarrow A})} = 0.3,\ p_{(\boldsymbol{B\rightarrow B})} = 0,\ p_{(\boldsymbol{C\rightarrow C})} = 0.18, p_{(\boldsymbol{A\rightarrow B})} = 0.3,\ p_{(\boldsymbol{B\rightarrow A})} = 0.1,\ p_{(\boldsymbol{B\rightarrow C})} = 0.1,$ and $p_{(\boldsymbol{C\rightarrow A})} = 0.02$ in our example. The sum of all these probabilities must be 1, since every photon that is absorbed by either of the isomers leads to one of the described photoreactions.

Next the probability of an incident photon to be productive in a particular transformation cycle is calculated. In our example the probability $p_{(\boldsymbol{A\rightarrow B})}$ is involved in two different transformation cycles, namely **AB** and **ABC**. Therefore it has to be dissected what percentage of the overall probability $p_{(\boldsymbol{A\rightarrow B})}$ is actually contributing to a particular cycle. If only molecules reacting from **A** to **B** are taken into consideration it is impossible to judge, which of them are part of the cycle **AB** or **ABC**. This cannot be distinguished until a second event is happening, i.e. a second photoreaction, which has to be productive: **B→A** or **B→C**. If the unproductive photoreaction **B→B** takes place instead, the dissection can still not be done. On average it takes exactly the same amount of identity reactions **B→B** until the decision between the **B→A** and **B→C** photoreaction is made since isomer **B** is the branching point. The branching at **B** is quantitatively described by the quantum yields of the different **B** photo-transformations without counting the quantum yield of the identity reaction. Thus a normalized quantum yield nϕ for each productive transformation can be written as exemplified for the photoreaction of **B** to **A** (eq. 26):

$$n\phi_{(\boldsymbol{B\rightarrow A})} = \frac{\phi_{(\boldsymbol{B\rightarrow A})}}{\phi_{(\boldsymbol{B\rightarrow A})} + \phi_{(\boldsymbol{B\rightarrow C})}} \qquad \text{(eq. 26)}$$

Analogously the normalized quantum yield for the other transformations can be formulated. The normalized quantum yields in our example are $n\phi_{(\boldsymbol{A\rightarrow B})} = 1,\ n\phi_{(\boldsymbol{B\rightarrow A})} = 0.5,\ n\phi_{(\boldsymbol{B\rightarrow C})} = 0.5,$ and $n\phi_{(\boldsymbol{C\rightarrow A})} = 1$. With the normalized quantum yields nϕ the probability of one absorbed photon to participate in the photoreaction **A→B** within the particular cycle **AB** ($p_{\boldsymbol{AB}_{(\boldsymbol{A\rightarrow B})}}$) can now be calculated according to eq. 27:

$$p_{\mathbf{AB}_{(A\rightarrow B)}} = p_{(A\rightarrow B)} \cdot \frac{n\phi_{(A\rightarrow B)} \cdot n\phi_{(B\rightarrow A)}}{n\phi_{(A\rightarrow B)} \cdot n\phi_{(B\rightarrow A)} + n\phi_{(A\rightarrow B)} \cdot n\phi_{(B\rightarrow C)} \cdot n\phi_{(C\rightarrow A)}} \quad \text{(eq. 27)}$$

The resulting probabilities of one absorbed photon to participate in a specific photoreaction **X→Y** within a particular cycle **XY** or **XYZ** in our example are: $p_{\mathbf{AB}_{(A\rightarrow B)}} = 0.15$, $p_{\mathbf{ABC}_{(A\rightarrow B)}} = 0.15$, $p_{\mathbf{AB}_{(B\rightarrow A)}} = 0.1$, $p_{\mathbf{ABC}_{(B\rightarrow C)}} = 0.1$, and $p_{\mathbf{ABC}_{(C\rightarrow A)}} = 0.02$.

Within the cycle **AB** the probability of $p_{\mathbf{AB}_{(B\rightarrow A)}} = 0.1$ is smaller then $p_{\mathbf{AB}_{(A\rightarrow B)}} = 0.15$, therefore more molecules move from **A** to **B** then from **B** to **A**. This shows that the system is at the moment not yet in the PSS.

To calculate the efficiency of one absorbed photon to drive the particular cycle **AB** ($E_{\mathbf{AB}}$) we have to sum up all probabilities within this cycle and subtract all unproductive probabilities leading to net photoreactions:

$$E_{\mathbf{AB}} = (p_{\mathbf{AB}_{(B\rightarrow A)}} + p_{\mathbf{AB}_{(A\rightarrow B)}}) - \left(p_{\mathbf{AB}_{(A\rightarrow B)}} - p_{\mathbf{AB}_{(B\rightarrow A)}}\right) = 2 \cdot p_{\mathbf{AB}_{(B\rightarrow A)}} \quad \text{(eq. 28)}$$

As shown in eq. 28 the efficiency $E_{\mathbf{AB}}$ can simply be written as two times the lowest probability in the cycle.

In our example the efficiency $E_{\mathbf{AB}}$ of one absorbed photon to drive cycle **AB** is 20%. To calculate the number of photons needed to drive one full cycle **AB** the reciprocal value of $E_{\mathbf{AB}}$ is taken and multiplied by a factor of 2 since two photons are needed in reality to complete one full cycle:

$$\#\text{photons}_{(\mathbf{AB})} = (1/E_{\mathbf{AB}}) \cdot 2 = 10 \quad \text{(eq. 29)}$$

The corresponding probability values for the cycle **ABC** can be obtained by the same approach. The probabilities of one absorbed photon to participate in each photoreaction **X→Y** within a particular cycle **XY** or **XYZ** were already calculated using eq. 27: To reiterate, they are: $p_{\mathbf{AB}_{(A\rightarrow B)}} = 0.125$, $p_{\mathbf{ABC}_{(A\rightarrow B)}} = 0.125$, $p_{\mathbf{AB}_{(B\rightarrow A)}} = 0.15$, $p_{\mathbf{ABC}_{(B\rightarrow C)}} = 0.15$, and $p_{\mathbf{ABC}_{(C\rightarrow A)}} = 0.02$.

The probability $p_{\mathbf{ABC}_{(C\rightarrow A)}}$ = 0.02 has the smallest value within the cycle **ABC** and is therefore the rate limiting step in this cycle. As **ABC** is a three step cycle this probability has to be multiplied by 3 to determine the overall efficiency of the cycle **ABC**:

$$E_{\mathbf{ABC}} = 3 \cdot p_{\mathbf{ABC}_{(C\rightarrow A)}} = 0.06 \quad \text{(eq. 30)}$$

As mentioned above the system is not in the PSS. It is possible to calculate how many photons are not used to drive either cycle **AB** or **ABC** but are used instead to drive net photoreactions to reach the PSS. To this end the efficiencies for all possible cycles ($E_{\mathbf{AB}}$ and $E_{\mathbf{ABC}}$ in our example) are each divided by the number of steps in the particular cycle and then both are subtracted from the overall probability of a particular photoreaction (e.g. $p_{(\mathbf{A}\rightarrow\mathbf{B})}$). The efficiencies of the net photoreactions are thus calculated with eq. 31-34:

$$E_{\mathbf{A}\rightarrow\mathbf{B}(\mathbf{net})} = p_{(\mathbf{A}\rightarrow\mathbf{B})} - \left(\frac{E_{\mathbf{AB}}}{2} + \frac{E_{\mathbf{ABC}}}{3}\right) = 0.18 \quad \text{(eq. 31)}$$

$$E_{\mathbf{B}\rightarrow\mathbf{A}(\mathbf{net})} = p_{(\mathbf{B}\rightarrow\mathbf{A})} - \frac{E_{\mathbf{AB}}}{2} = 0 \quad \text{(eq. 32)}$$

$$E_{\mathbf{B}\rightarrow\mathbf{C}(\mathbf{net})} = p_{(\mathbf{B}\rightarrow\mathbf{C})} - \frac{E_{\mathbf{ABC}}}{3} = 0.08 \quad \text{(eq. 33)}$$

$$E_{\mathbf{C}\rightarrow\mathbf{A}(\mathbf{net})} = p_{(\mathbf{C}\rightarrow\mathbf{A})} - \frac{E_{\mathbf{ABC}}}{3} = 0 \quad \text{(eq. 34)}$$

The efficiencies for the identity cycles **A** and **C** are simply the probabilities $p_{(\mathbf{A}\rightarrow\mathbf{A})}$ and $p_{(\mathbf{C}\rightarrow\mathbf{C})}$. All obtained efficiencies and the corresponding number of photons needed for a particular cycle in our example are summarized in Table S1.

If the reactions of our simple example are simulated until the PSS is reached concentrations of 25% **A**; 12.5% **B**, and 62.5% **C** are obtained. The calculated probabilities/efficiencies at the PSS for each cycle were then again calculated according to eq. 24-34 and are also given in Table S1. In the PSS all photons are contributing to a cycle and none are used to reach the PSS as it should be expected. However, in reality the calculated and measured PSS will differ slightly because of measurement errors. For the description of our system we nevertheless used the experimentally determined PSS isomer composition to calculate photon efficiencies because the isomer composition in the PSS can be measured experimentally with higher precision than individual quantum yields or molar absorptions.

Table S1: Calculated efficiencies of the above mentioned example

Cycle	**A**	**C**	**AB**	**ABC**	**A→B** (net)	**B→A** (net)	**B→C** (net)	∑
Example $E_{cycle/net}$	0.3	0.18	0.2	0.06	0.18	0	0.08	1
Example $\#photons_{cycle}$	3.3	5.6	10	50	-	-	-	-
Example in PSS $E_{cycle/net}$	0.125	0.5625	0.125	0.1875	0	0	0	1
Example in PSS $\#photons_{cycle}$	8	1.8	16	16	-	-	-	-

For the more complex photochemistry of HTI motor **1** the mathematical treatment is similar to the above described simpler system. Below we provide the general equations that were used to calculate the efficiencies for motor **1**. In addition to the floating variables **X**, **Y**, and **Z** we introduce also **W** to account for the presence of four isomers in HTI motor **1**.

The quantum yields for the identity reactions $\phi_{(W\rightarrow W)}$ were calculated using eq. 35.

$$\phi_{(W\rightarrow W)} = 1 - \left(\phi_{(W\rightarrow X)} + \phi_{(W\rightarrow Y)} + \phi_{(X\rightarrow Z)}\right) \quad \text{(eq. 35)}$$

The probabilities for individual transformations $p_{(W\rightarrow X)}$ in our motor system are calculated with eq. 36.

$$p_{(W\rightarrow X)} = \phi_{(W\rightarrow X)} \cdot pEx_{W} \quad \text{(eq. 36)}$$

The general equation to determine the normalized quantum yields nϕ for each productive transformation can be written according to eq. 37:

$$n\phi_{(W\rightarrow X)} = \frac{\phi_{(W\rightarrow X)}}{\phi_{(W\rightarrow X)} + \phi_{(W\rightarrow Y)} + \phi_{(W\rightarrow Z)}} \quad \text{(eq. 37)}$$

Each transformation is part of five possible cycles in case of motor **1**. In our motor system 12 different photoreactions or transformations can take place and each of them is part of five cycles. Therefore, in total 60 equations are obtained to calculate all probabilities of each photoreaction to

take place in each cycle. The probability of one absorbed photon to participate in the photoreaction **W→X** within the particular cycles **WX** ($p_{WX_{(W\rightarrow X)}}$), **WXY** ($p_{WXY_{(W\rightarrow X)}}$), **WXZ** ($p_{WXZ_{(W\rightarrow X)}}$), **WXYZ** ($p_{WXYZ_{(W\rightarrow X)}}$), or **WXZY** ($p_{WXZY_{(W\rightarrow X)}}$) can be calculated according to eq. 38-42:

$$p_{WX_{(W\rightarrow X)}} = p_{(W\rightarrow X)} \cdot \frac{n\phi_{(W\rightarrow X)} \cdot n\phi_{(X\rightarrow W)}}{n\phi_{(W\rightarrow X)} \cdot n\phi_{(X\rightarrow W)} + n\phi_{(W\rightarrow X)} \cdot n\phi_{(X\rightarrow Y)} \cdot n\phi_{(Y\rightarrow W)} + n\phi_{(W\rightarrow X)} \cdot n\phi_{(X\rightarrow Z)} \cdot n\phi_{(Z\rightarrow W)} + n\phi_{(W\rightarrow X)} \cdot n\phi_{(X\rightarrow Y)} \cdot n\phi_{(Y\rightarrow Z)} \cdot n\phi_{(Z\rightarrow W)} + n\phi_{(W\rightarrow X)} \cdot n\phi_{(X\rightarrow Z)} \cdot n\phi_{(Z\rightarrow Y)} \cdot n\phi_{(Y\rightarrow W)}} \quad \text{(eq. 38)}$$

$$p_{WXY_{(W\rightarrow X)}} = p_{(W\rightarrow X)} \cdot \frac{n\phi_{(W\rightarrow X)} \cdot n\phi_{(X\rightarrow Y)} \cdot n\phi_{(Y\rightarrow W)}}{n\phi_{(W\rightarrow X)} \cdot n\phi_{(X\rightarrow W)} + n\phi_{(W\rightarrow X)} \cdot n\phi_{(X\rightarrow Y)} \cdot n\phi_{(Y\rightarrow W)} + n\phi_{(W\rightarrow X)} \cdot n\phi_{(X\rightarrow Z)} \cdot n\phi_{(Z\rightarrow W)} + n\phi_{(W\rightarrow X)} \cdot n\phi_{(X\rightarrow Y)} \cdot n\phi_{(Y\rightarrow Z)} \cdot n\phi_{(Z\rightarrow W)} + n\phi_{(W\rightarrow X)} \cdot n\phi_{(X\rightarrow Z)} \cdot n\phi_{(Z\rightarrow Y)} \cdot n\phi_{(Y\rightarrow W)}} \quad \text{(eq. 39)}$$

$$p_{WXZ_{(W\rightarrow X)}} = p_{(W\rightarrow X)} \cdot \frac{n\phi_{(W\rightarrow X)} \cdot n\phi_{(X\rightarrow Z)} \cdot n\phi_{(Z\rightarrow W)}}{n\phi_{(W\rightarrow X)} \cdot n\phi_{(X\rightarrow W)} + n\phi_{(W\rightarrow X)} \cdot n\phi_{(X\rightarrow Y)} \cdot n\phi_{(Y\rightarrow W)} + n\phi_{(W\rightarrow X)} \cdot n\phi_{(X\rightarrow Z)} \cdot n\phi_{(Z\rightarrow W)} + n\phi_{(W\rightarrow X)} \cdot n\phi_{(X\rightarrow Y)} \cdot n\phi_{(Y\rightarrow Z)} \cdot n\phi_{(Z\rightarrow W)} + n\phi_{(W\rightarrow X)} \cdot n\phi_{(X\rightarrow Z)} \cdot n\phi_{(Z\rightarrow Y)} \cdot n\phi_{(Y\rightarrow W)}} \quad \text{(eq. 40)}$$

$$p_{WXYZ_{(W\rightarrow X)}} = p_{(W\rightarrow X)} \cdot \frac{n\phi_{(W\rightarrow X)} \cdot n\phi_{(X\rightarrow Y)} \cdot n\phi_{(Y\rightarrow Z)} \cdot n\phi_{(Z\rightarrow W)}}{n\phi_{(W\rightarrow X)} \cdot n\phi_{(X\rightarrow W)} + n\phi_{(W\rightarrow X)} \cdot n\phi_{(X\rightarrow Y)} \cdot n\phi_{(Y\rightarrow W)} + n\phi_{(W\rightarrow X)} \cdot n\phi_{(X\rightarrow Z)} \cdot n\phi_{(Z\rightarrow W)} + n\phi_{(W\rightarrow X)} \cdot n\phi_{(X\rightarrow Y)} \cdot n\phi_{(Y\rightarrow Z)} \cdot n\phi_{(Z\rightarrow W)} + n\phi_{(W\rightarrow X)} \cdot n\phi_{(X\rightarrow Z)} \cdot n\phi_{(Z\rightarrow Y)} \cdot n\phi_{(Y\rightarrow W)}} \quad \text{(eq. 41)}$$

$$p_{WXZY_{(W\rightarrow X)}} = p_{(W\rightarrow X)} \cdot \frac{n\phi_{(W\rightarrow X)} \cdot n\phi_{(X\rightarrow Z)} \cdot n\phi_{(Z\rightarrow Y)} \cdot n\phi_{(Y\rightarrow W)}}{n\phi_{(W\rightarrow X)} \cdot n\phi_{(X\rightarrow W)} + n\phi_{(W\rightarrow X)} \cdot n\phi_{(X\rightarrow Y)} \cdot n\phi_{(Y\rightarrow W)} + n\phi_{(W\rightarrow X)} \cdot n\phi_{(X\rightarrow Z)} \cdot n\phi_{(Z\rightarrow W)} + n\phi_{(W\rightarrow X)} \cdot n\phi_{(X\rightarrow Y)} \cdot n\phi_{(Y\rightarrow Z)} \cdot n\phi_{(Z\rightarrow W)} + n\phi_{(W\rightarrow X)} \cdot n\phi_{(X\rightarrow Z)} \cdot n\phi_{(Z\rightarrow Y)} \cdot n\phi_{(Y\rightarrow W)}} \quad \text{(eq. 42)}$$

First the probability of a photon to be productive in the identity cycles **W**, **X**, **Y**, **Z** were calculated using eq. 43-46.

$$E_W = p_{(W\rightarrow W)} \quad \text{(eq. 43)}$$

$$E_X = p_{(X\rightarrow X)} \quad \text{(eq. 44)}$$

$$E_Y = p_{(Y\rightarrow Y)} \quad \text{(eq. 45)}$$

$$E_Z = p_{(Z\rightarrow Z)} \quad \text{(eq. 46)}$$

To calculate the efficiency E_{WX} of one photon to drive a 2 step cycle **WX** it is necessary to determine the rate limiting step in this cycle if the system is not in the PSS. If the system is in the PSS both transformation steps have the same probability and therefore the same speed ($p_{WX_{(W\rightarrow X)}} = p_{WX_{(X\rightarrow W)}}$). E_{WX} is calculated

by multiplying the rate limiting step by 2 (if the system is not in the PSS) or by summing up the probabilities of both reactions (in the PSS) according to (eq. 47-49). In total there are 6 different 2 step cycles for motor **1** and therefore 18 different equations describing them.

$$E_{WX} = p_{WX_{(W\to X)}} \cdot 2 \quad \text{if } p_{WX_{(W\to X)}} < p_{WX_{(X\to W)}} \quad \text{(eq. 47)}$$

$$E_{WX} = p_{WX_{(X\to W)}} \cdot 2 \quad \text{if } p_{WX_{(W\to X)}} > p_{WX_{(X\to W)}} \quad \text{(eq. 48)}$$

$$E_{WX} = p_{WX_{(W\to X)}} + p_{WX_{(X\to W)}} \quad \text{if } p_{WX_{(W\to X)}} = p_{WX_{(X\to W)}} \quad \text{(eq. 49)}$$

To calculate the efficiency E_{WXY} of one photon to drive a 3 step cycle **WXY** it is necessary to determine the rate limiting step in this cycle if the system is not in the PSS. If the system is in the PSS all three reaction steps have the same probability and therefore the same speed ($p_{WXY_{(W\to X)}} = p_{WXY_{(X\to Y)}} = p_{WXY_{(Y\to W)}}$). E_{WXY} is calculated by multiplying the rate limiting step by 3 (if the system is not in the PSS) or by summing up the probabilities of all three reactions (in the PSS) according to (eq. 50-53). In total there are 8 different 3 step cycles for motor **1** and therefore 32 different equations describing them.

$$E_{WXY} = p_{WXY_{(W\to X)}} \cdot 3 \quad \text{if } (p_{WXY_{(W\to X)}} < p_{WXY_{(X\to Y)}} \text{ and } p_{WXY_{(W\to X)}} < p_{WXY_{(Y\to W)}}) \text{ (eq. 50)}$$

$$E_{WXY} = p_{WXY_{(X\to Y)}} \cdot 3 \quad \text{if } (p_{WXY_{(X\to Y)}} < p_{WXY_{(W\to X)}} \text{ and } p_{WXY_{(X\to Y)}} < p_{WXY_{(Y\to W)}}) \text{ (eq. 51)}$$

$$E_{WXY} = p_{WXY_{(Y\to W)}} \cdot 3 \quad \text{if } (p_{WXY_{(Y\to W)}} < p_{WXY_{(W\to X)}} \text{ and } p_{WXY_{(Y\to W)}} < p_{WXY_{(X\to Y)}}) \text{ (eq. 52)}$$

$$E_{WXY} = p_{WXY_{(W\to X)}} + p_{WXY_{(X\to Y)}} + p_{WXY_{(Y\to W)}} \quad \text{if } p_{WXY_{(W\to X)}} = p_{WXY_{(X\to Y)}} = p_{WXY_{(Y\to W)}} \quad \text{(eq. 53)}$$

To calculate the efficiency E_{WXYZ} of one photon to drive a 4 step cycle **WXYZ** it is necessary to determine the rate limiting step in this cycle if the system is not in the PSS. If the system is in the PSS all four reaction steps have the same probability and therefore the same speed ($p_{WXYZ_{(W\to X)}} = p_{WXYZ_{(X\to Y)}} = p_{WXYZ_{(Y\to Z)}} = p_{WXYZ_{(Z\to W)}}$). E_{WXYZ} is calculated by multiplying the rate limiting step by 4 (if the system

is not in the PSS) or by summing up the probabilities of all four reactions (in the PSS) according to (eq. 54-58). In total there are 6 different 4 step cycles for motor **1** and therefore 30 different equations describing them.

$$E_{WXYZ} = p_{WXYZ_{(W\to X)}} \cdot 4 \quad \text{if } (p_{WXYZ_{(W\to X)}} < p_{WXYZ_{(X\to Y)}} \text{ and } p_{WXYZ_{(W\to X)}} < p_{WXYZ_{(Y\to Z)}} \text{ and } p_{WXYZ_{(W\to X)}} < p_{WXYZ_{(Z\to W)}}) \quad \text{(eq. 54)}$$

$$E_{WXYZ} = p_{WXYZ_{(X\to Y)}} \cdot 4 \quad \text{if } (p_{WXYZ_{(X\to Y)}} < p_{WXYZ_{(W\to X)}} \text{ and } p_{WXYZ_{(X\to Y)}} < p_{WXYZ_{(Y\to Z)}} \text{ and } p_{WXYZ_{(X\to Y)}} < p_{WXYZ_{(Z\to W)}}) \quad \text{(eq. 55)}$$

$$E_{WXYZ} = p_{WXYZ_{(Y\to Z)}} \cdot 4 \quad \text{if } (p_{WXYZ_{(Y\to Z)}} < p_{WXYZ_{(W\to X)}} \text{ and } p_{WXYZ_{(Y\to Z)}} < p_{WXYZ_{(X\to Y)}} \text{ and } p_{WXYZ_{(Y\to Z)}} < p_{WXYZ_{(Z\to W)}}) \quad \text{(eq. 56)}$$

$$E_{WXYZ} = p_{WXYZ_{(Z\to W)}} \cdot 4 \quad \text{if } (p_{WXYZ_{(Z\to W)}} < p_{WXYZ_{(W\to X)}} \text{ and } p_{WXYZ_{(Z\to W)}} < p_{WXYZ_{(X\to Y)}} \text{ and } p_{WXYZ_{(Z\to W)}} < p_{WXYZ_{(Y\to Z)}}) \quad \text{(eq. 57)}$$

$$E_{WXYZ} = p_{WXYZ_{(W\to X)}} + p_{WXYZ_{(X\to Y)}} + p_{WXYZ_{(Y\to Z)}} + p_{WXYZ_{(Z\to W)}} \quad \text{if } p_{WXYZ_{(W\to X)}} = p_{WXYZ_{(X\to Y)}} = p_{WXYZ_{(Y\to Z)}} = p_{WXYZ_{(Z\to Y)}} \quad \text{(eq. 58)}$$

Next it is calculated how many photons are not used to drive any cycle but are used instead to drive net photoreactions to reach the PSS. To this end the efficiencies for all possible cycles (E_{WX}, E_{WXY}, and E_{WXYZ}) are each divided by the number of steps in the particular cycle and then are subtracted from the overall probability of a particular photoreaction ($p_{(X \rightarrow W)}$). The efficiencies of the net photoreactions are thus calculated with eq. 59:

$$E_{W \rightarrow X(net)} = p_{(W \rightarrow X)} - \left(\frac{E_{WX}}{2} + \frac{E_{WXY}}{3} + \frac{E_{WXZ}}{3} + \frac{E_{WXYZ}}{4} + \frac{E_{WXZY}}{4}\right) \qquad \text{(eq. 59)}$$

To calculate how many photons are on average needed to drive one full rotation of a particular cycle the number of steps in this cycle has to be divided by the efficiencies of that cycle according to eq. 60:

$$\#\text{photons}_{cycle} = \frac{steps\ in\ cycle}{E_{cycle}} \qquad \text{(eq. 60)}$$

All obtained efficiencies and number of photons needed for one particular full cycle are summarized in Table S6.

Determination of constitution and conformation in the crystalline state and in solution

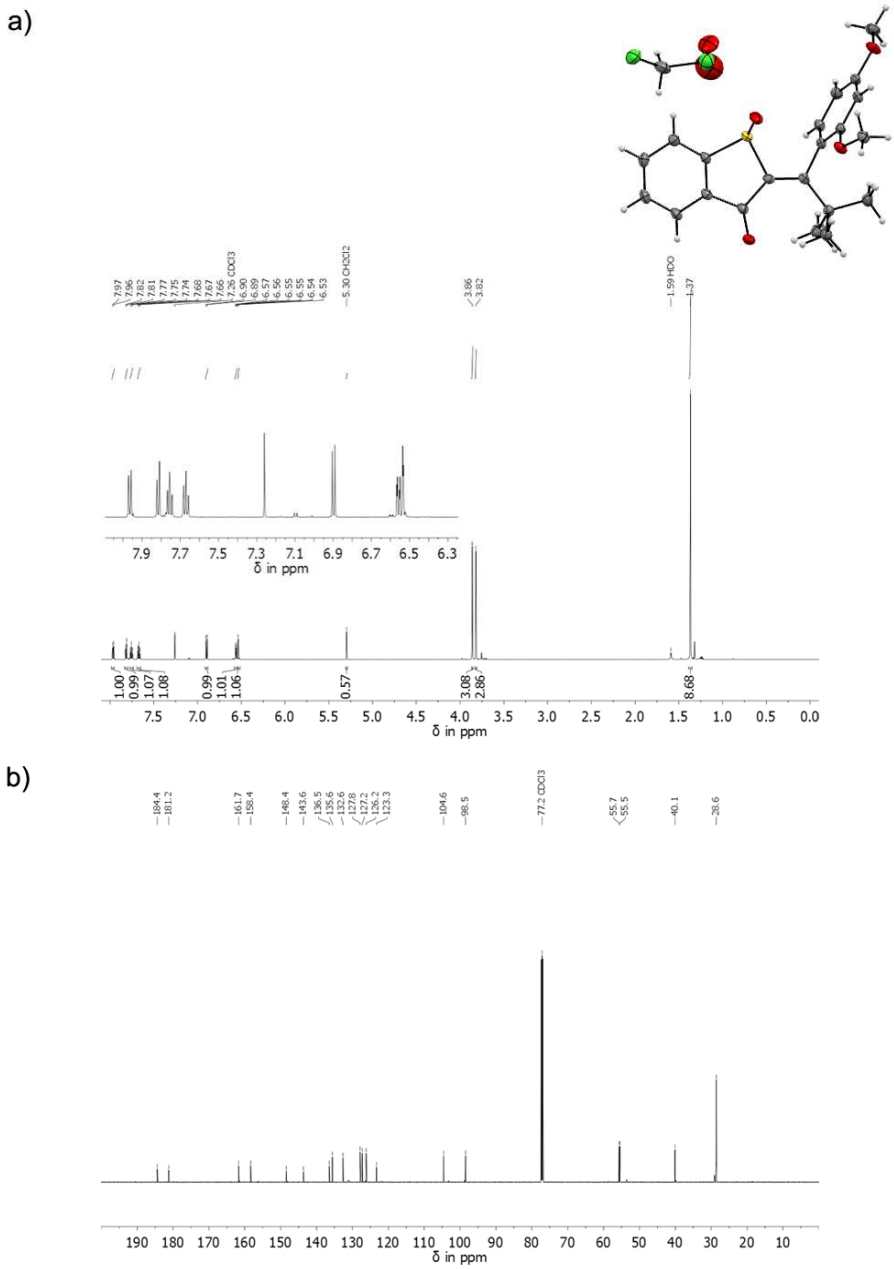

Figure S1. a) Crystal structure of **A-1** and the corresponding ^{1}H NMR spectrum ($CDCl_3$, 600 MHz, 27 °C) of the same crystal batch. The aromatic part of the spectrum is enlarged. The signals of only one single species are observed in the ^{1}H NMR spectrum, which could thus be directly assigned to **A-1**. b) Corresponding ^{13}C NMR spectrum ($CDCl_3$, 150 MHz, 27 °C).

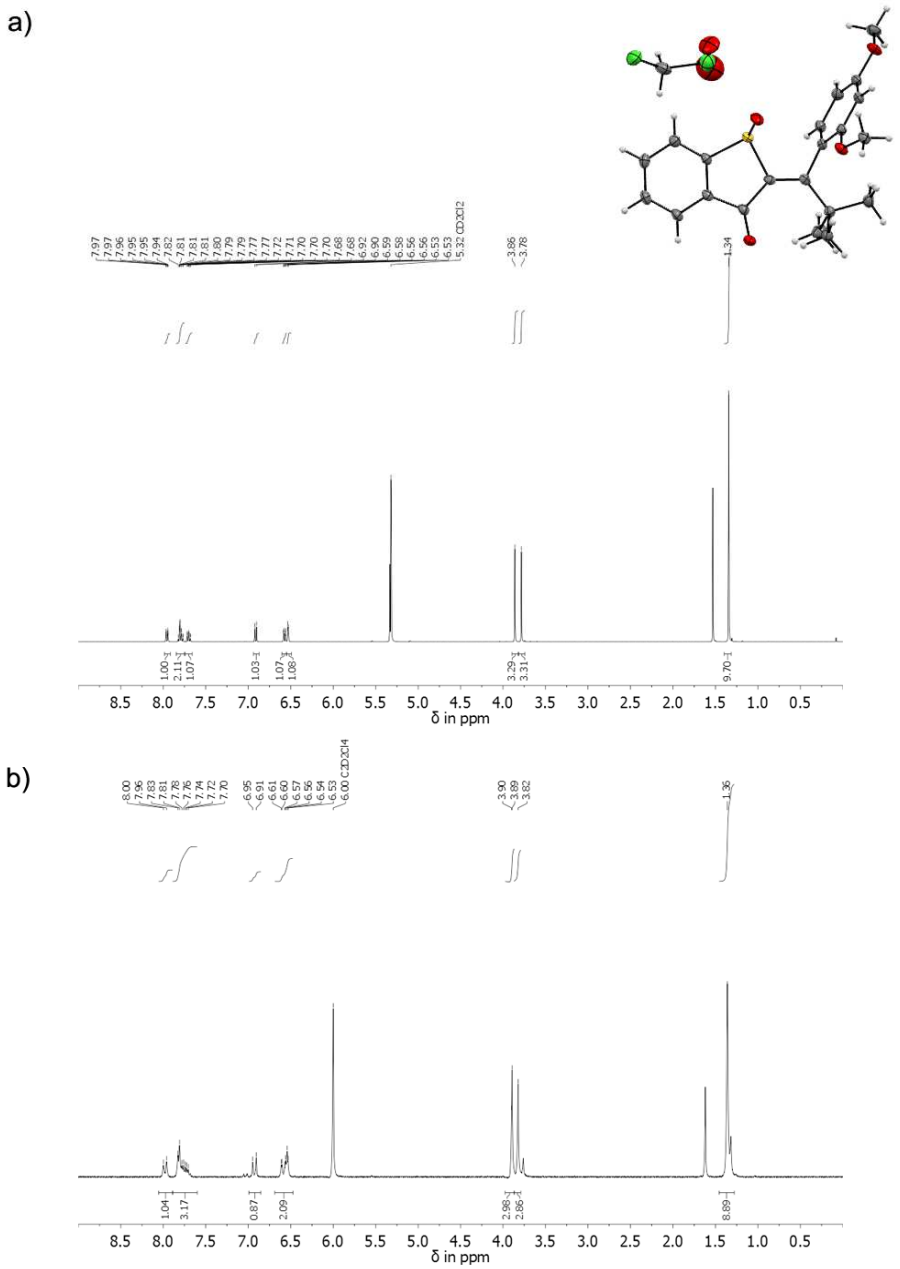

Figure S2. a) Crystal structure of **A-1** and the corresponding ^{1}H NMR spectrum (CD_2Cl_2, 400 MHz, 23 °C) of the same crystal batch. b) Corresponding ^{1}H NMR spectrum ($(CDCl_2)_2$, 200 MHz, 25 °C) of the same crystal batch after removing co-crystallized CH_2Cl_2 *in vacuo*.

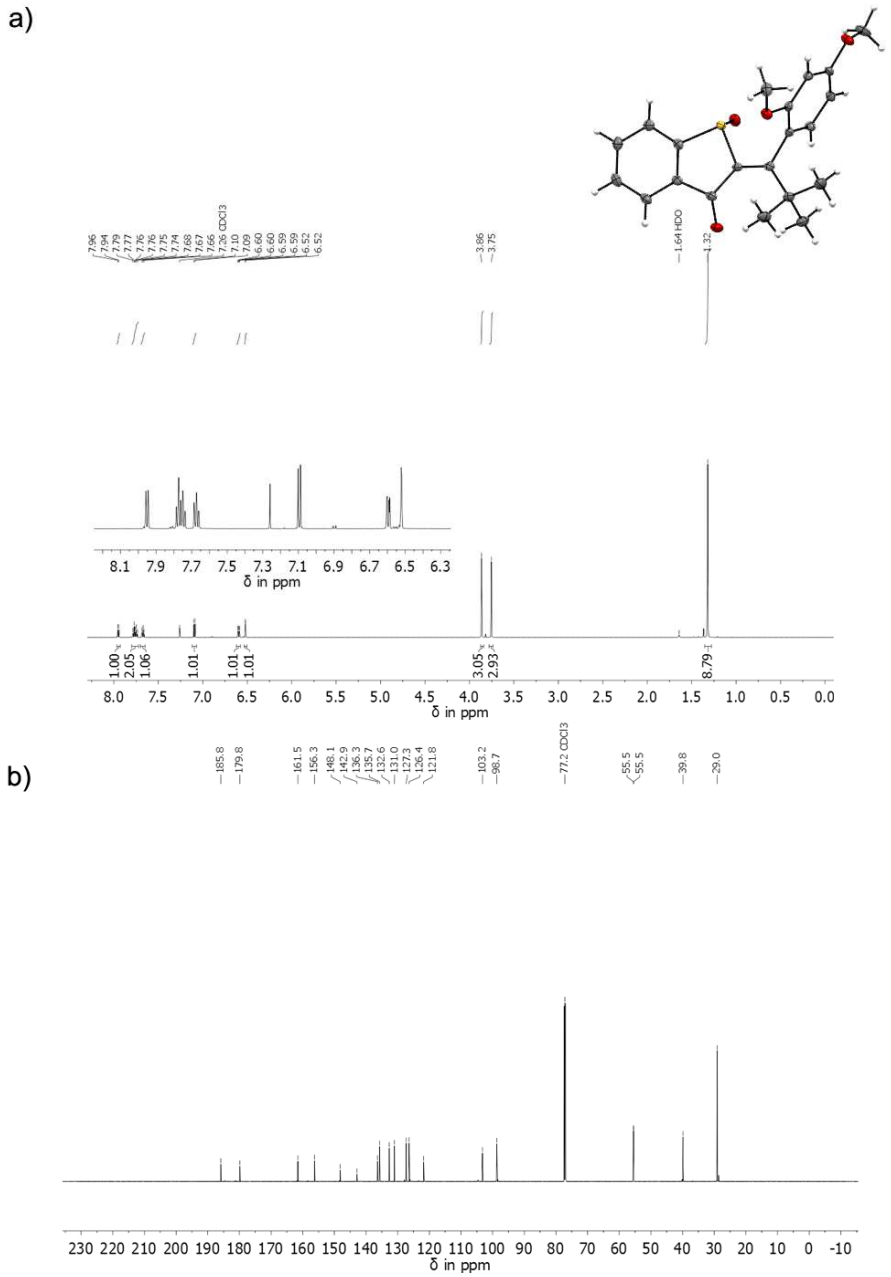

Figure S3. a) Crystal structure of **B**-**1** and the corresponding ^{1}H NMR spectrum ($CDCl_3$, 600 MHz, 27 °C) of the same crystal batch. The aromatic part of the spectrum is enlarged. The signals of only one single species are observed in the ^{1}H NMR spectrum, which could thus be directly assigned to **B**-**1**. b) Corresponding ^{13}C NMR spectrum ($CDCl_3$, 150 MHz, 27 °C).

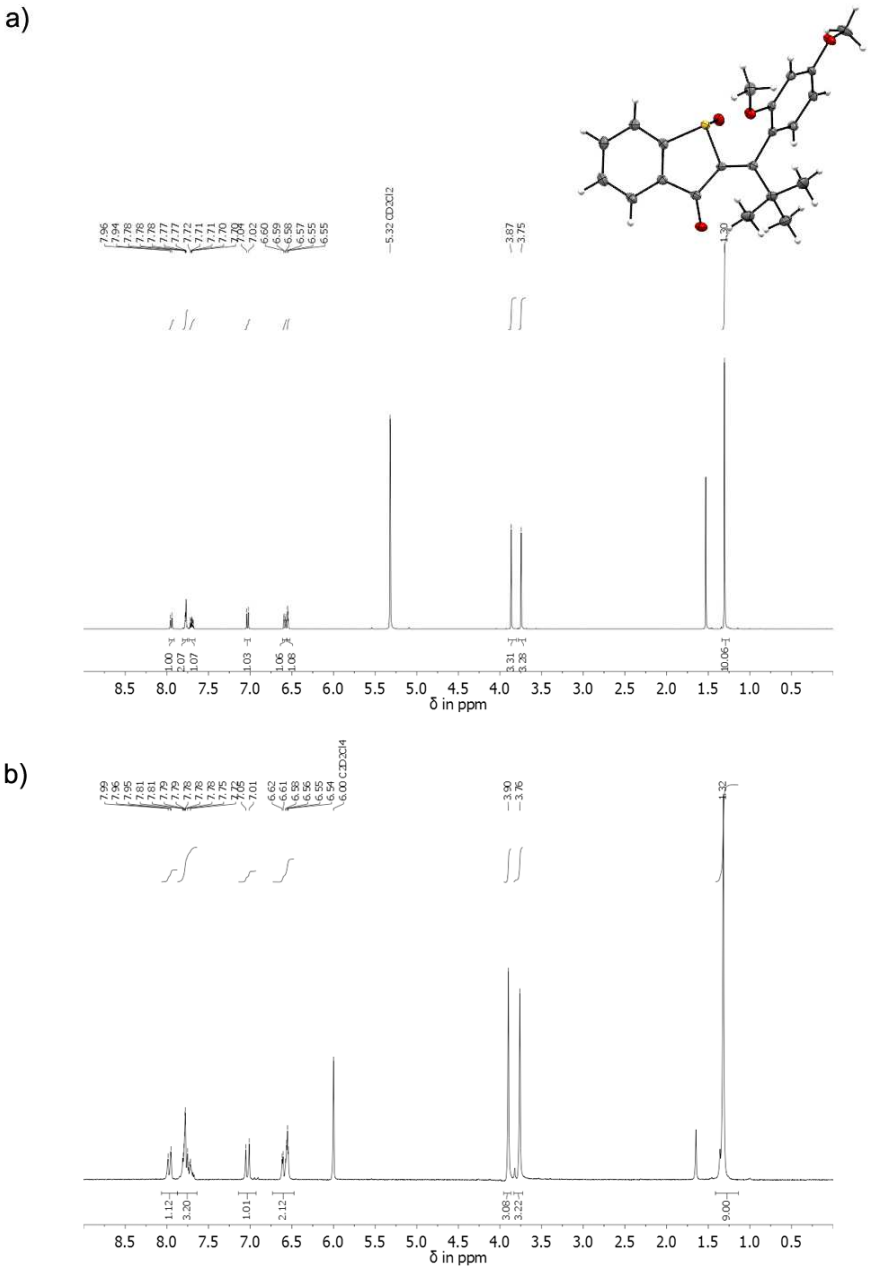

Figure S4. a) Crystal structure of **B-1** and the corresponding ^{1}H NMR spectrum (CD_2Cl_2, 400 MHz, 23 °C) of the same crystal batch. b) Corresponding ^{1}H NMR spectrum ($(CDCl_2)_2$, 200 MHz, 25 °C) of the same crystal batch.

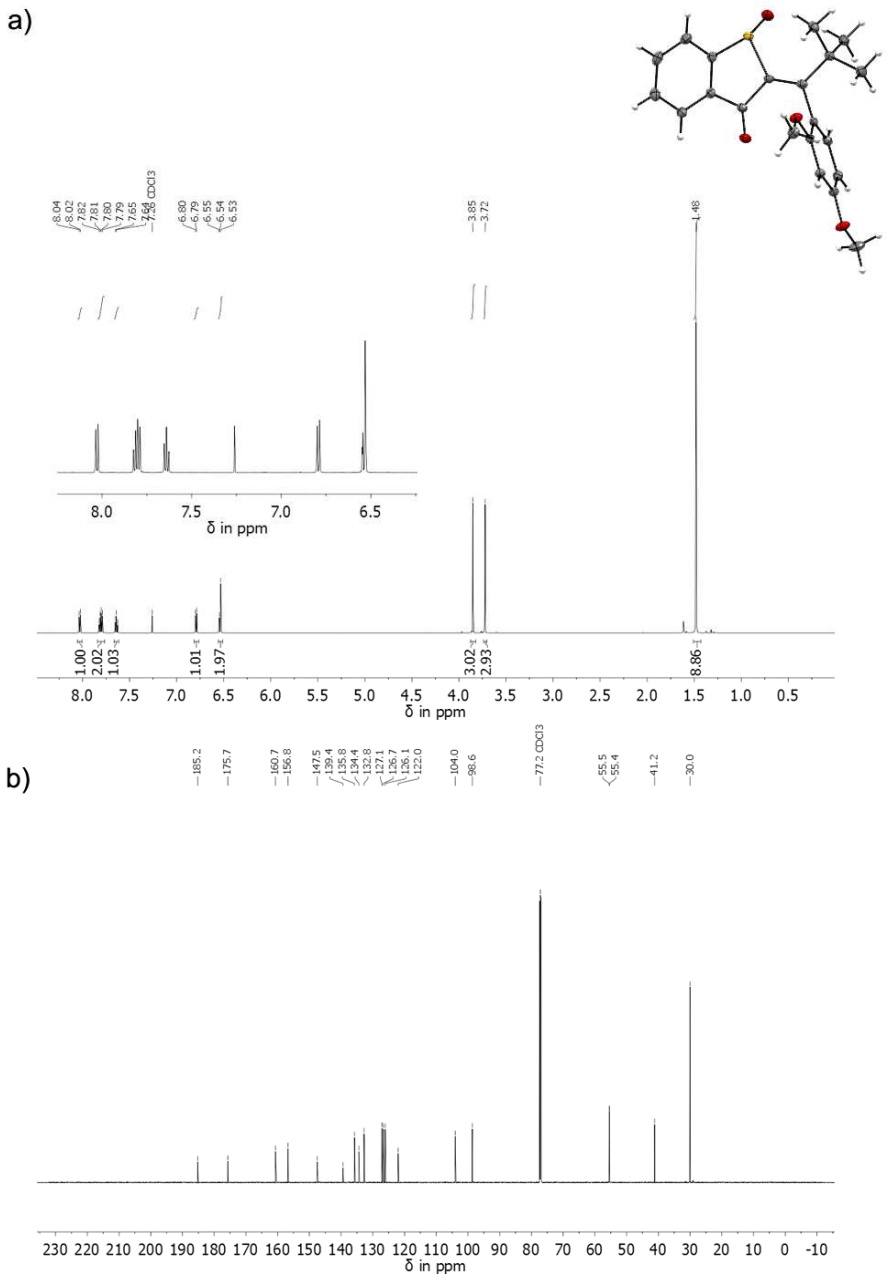

Figure S5. a) Crystal structure of **C-1** and the corresponding ^{1}H NMR spectrum ($CDCl_3$, 600 MHz, 27 °C) of the same crystal batch. The aromatic part of the spectrum is enlarged. The signals of only one single species are observed in the ^{1}H NMR spectrum, which could thus be directly assigned to **C-1**. b) Corresponding ^{13}C NMR spectrum ($CDCl_3$, 150 MHz, 27 °C).

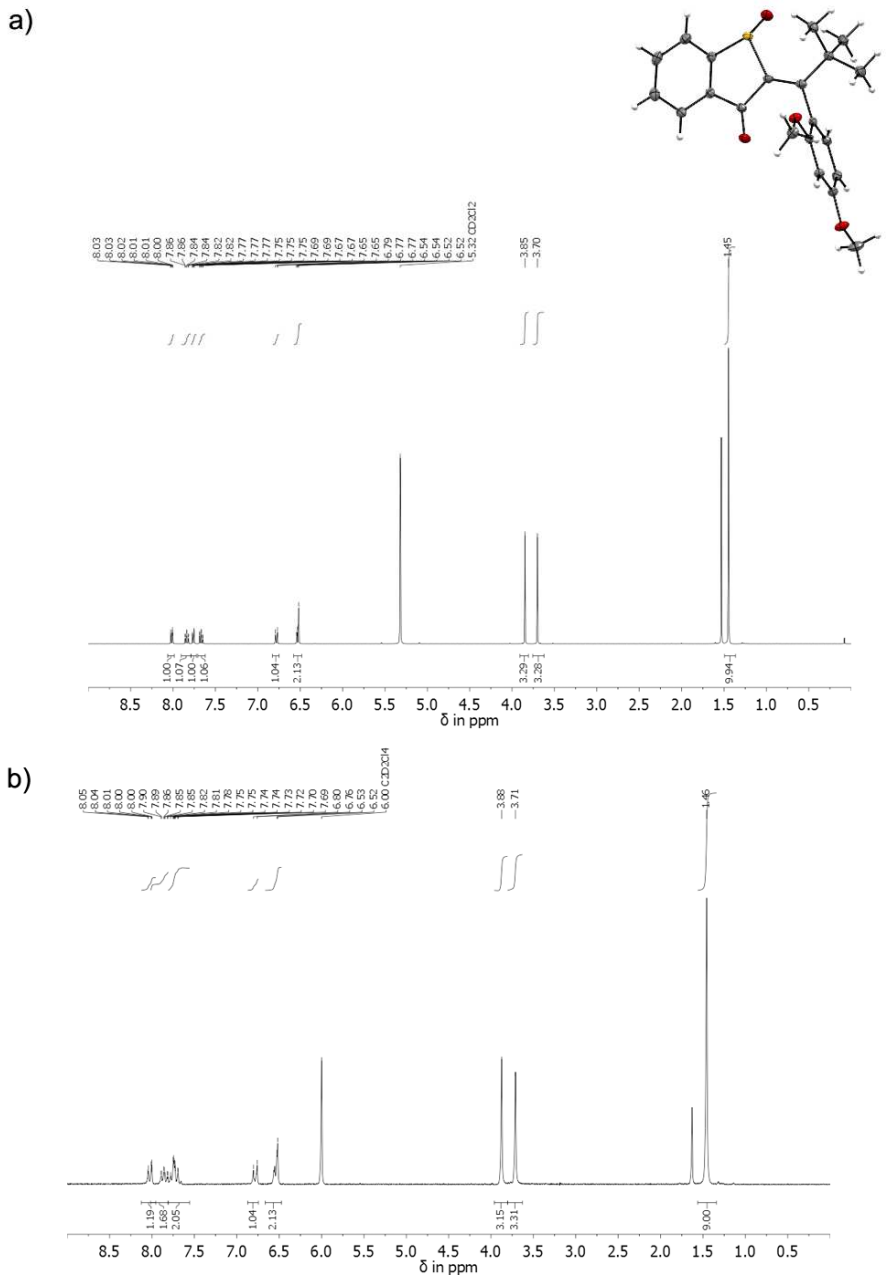

Figure S6. a) Crystal structure of **C-1** and the corresponding ^{1}H NMR spectrum (CD_2Cl_2, 400 MHz, 23 °C) of the same crystal batch. b) Corresponding ^{1}H NMR spectrum ($(CDCl_2)_2$, 200 MHz, 25 °C) of the same crystal batch.

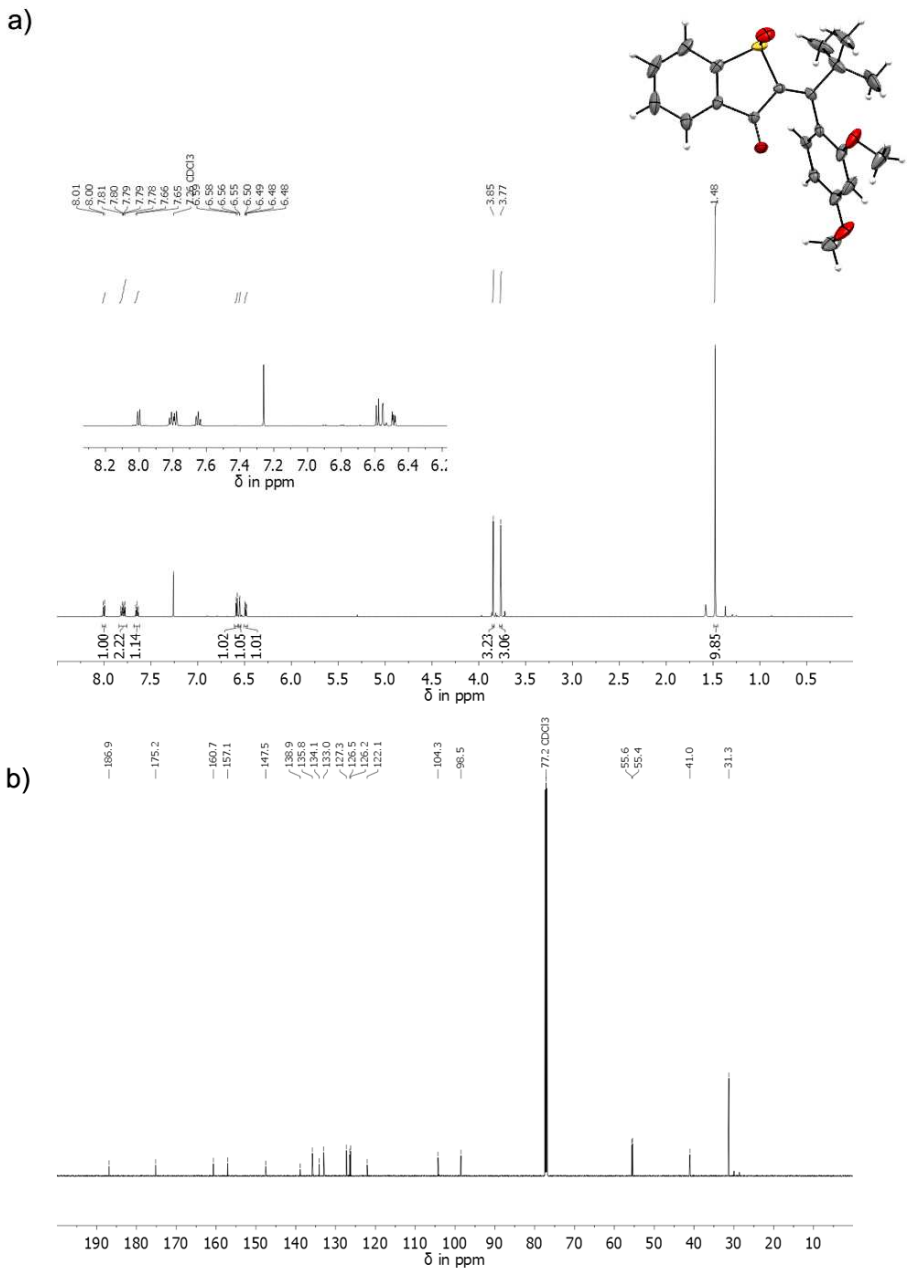

Figure S7. a) Crystal structure of **D-1** and the corresponding ^{1}H NMR spectrum ($CDCl_3$, 600 MHz, 27 °C) of the same crystal batch. The aromatic part of the spectrum is enlarged. The signals of only one single species are observed in the ^{1}H NMR spectrum, which could thus be directly assigned to **D-1**. b) Corresponding ^{13}C NMR spectrum ($CDCl_3$, 150 MHz, 27 °C).

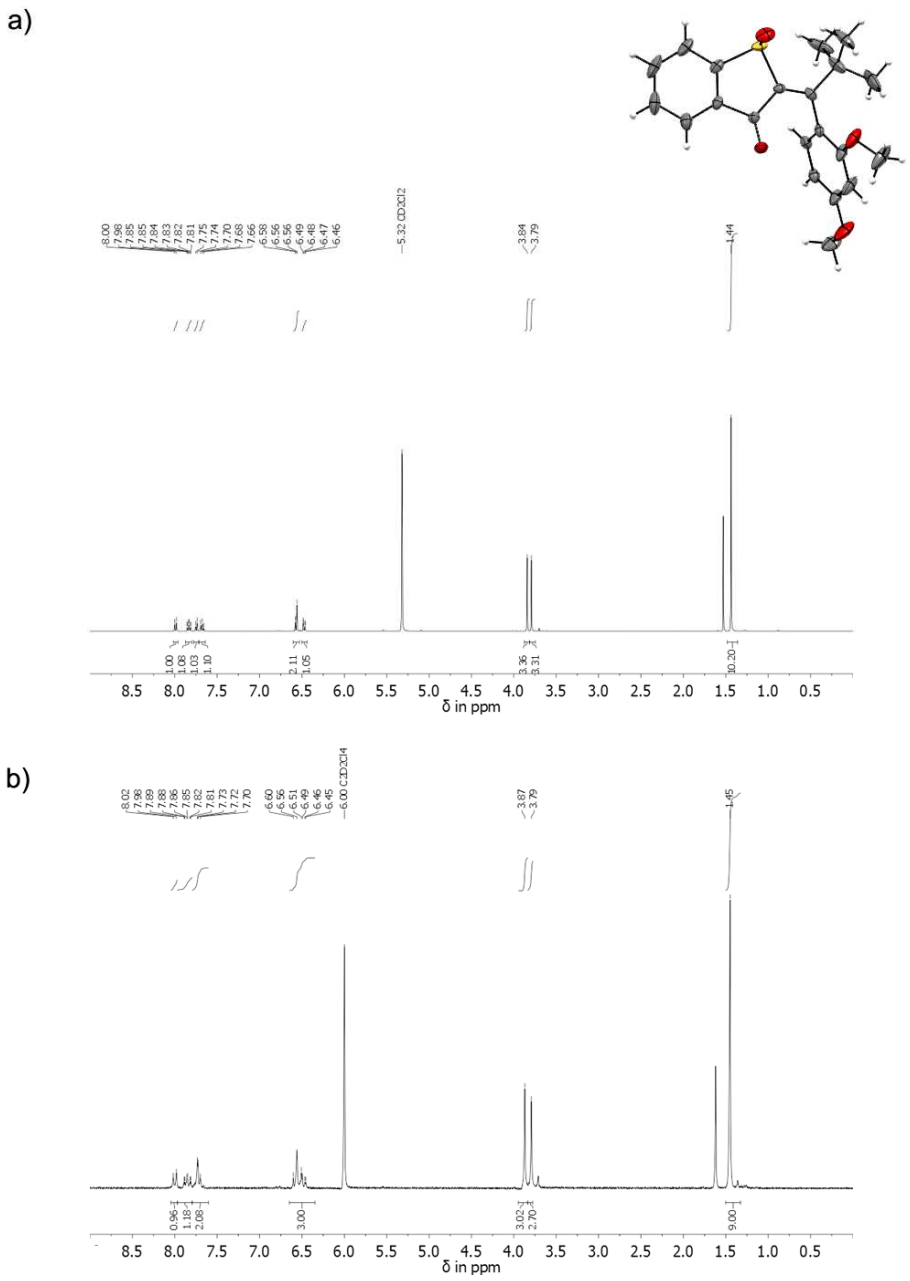

Figure S8. a) Crystal structure of **D-1** and the corresponding ^{1}H NMR spectrum (CD_2Cl_2, 400 MHz, 23 °C) of the same crystal batch. b) Corresponding ^{1}H NMR spectrum ($(CDCl_2)_2$, 200 MHz, 25 °C) of the same crystal batch.

Data for the thermal isomerization of 1

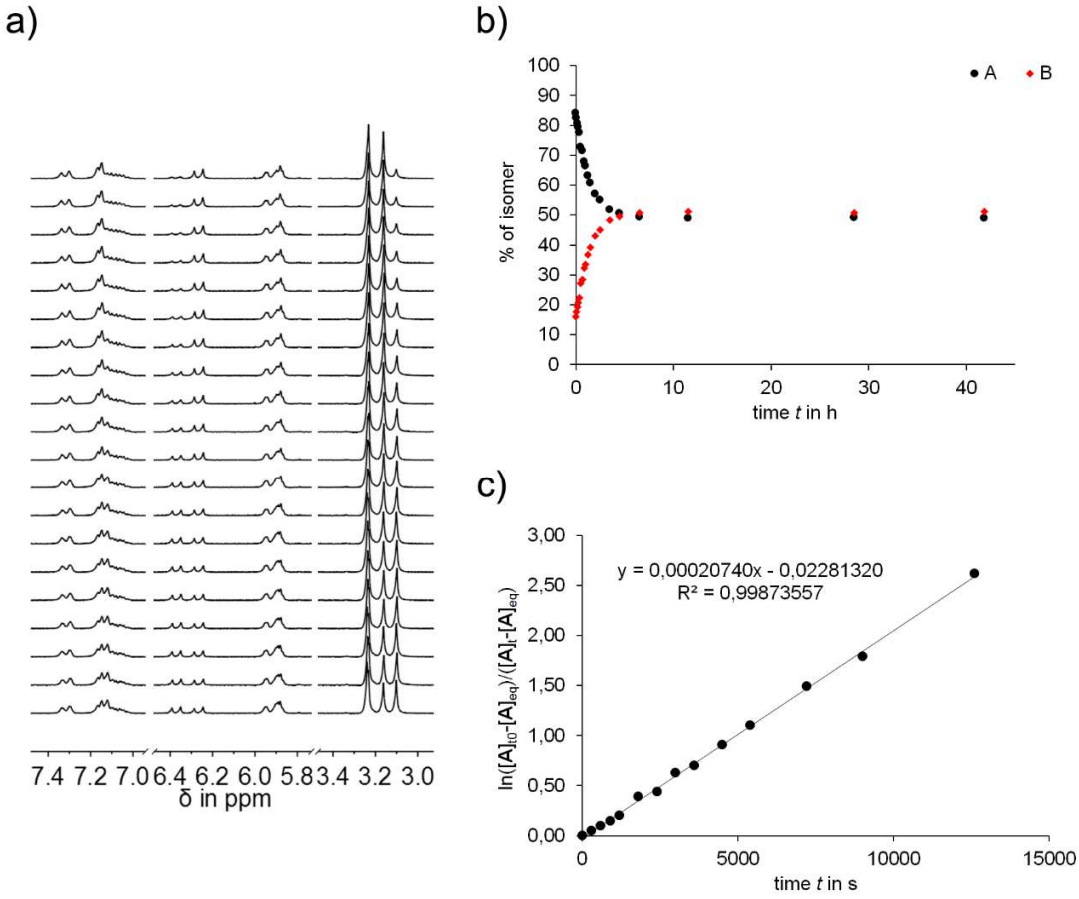

Figure S9. a) Thermal atropisomerization of **A** to **B** in $(CDCl_2)_2$ at 90 °C followed by ^{1}H NMR spectroscopy (200 MHz, 25 °C) in regular time intervals. b) Atropisomer conversion over time. c) First order kinetic analysis of the thermal atropisomerization of **A** to **B**. Taking into account the dynamic equilibrium by plotting according to eq. 1 gives a linear relationship. The slope *m* can be translated into the rate constants $k_{(\mathbf{A/B})}$ according to eq. 4. The corresponding Gibbs energy of activation for the thermal **A** to **B** isomerization is given in Table S2.

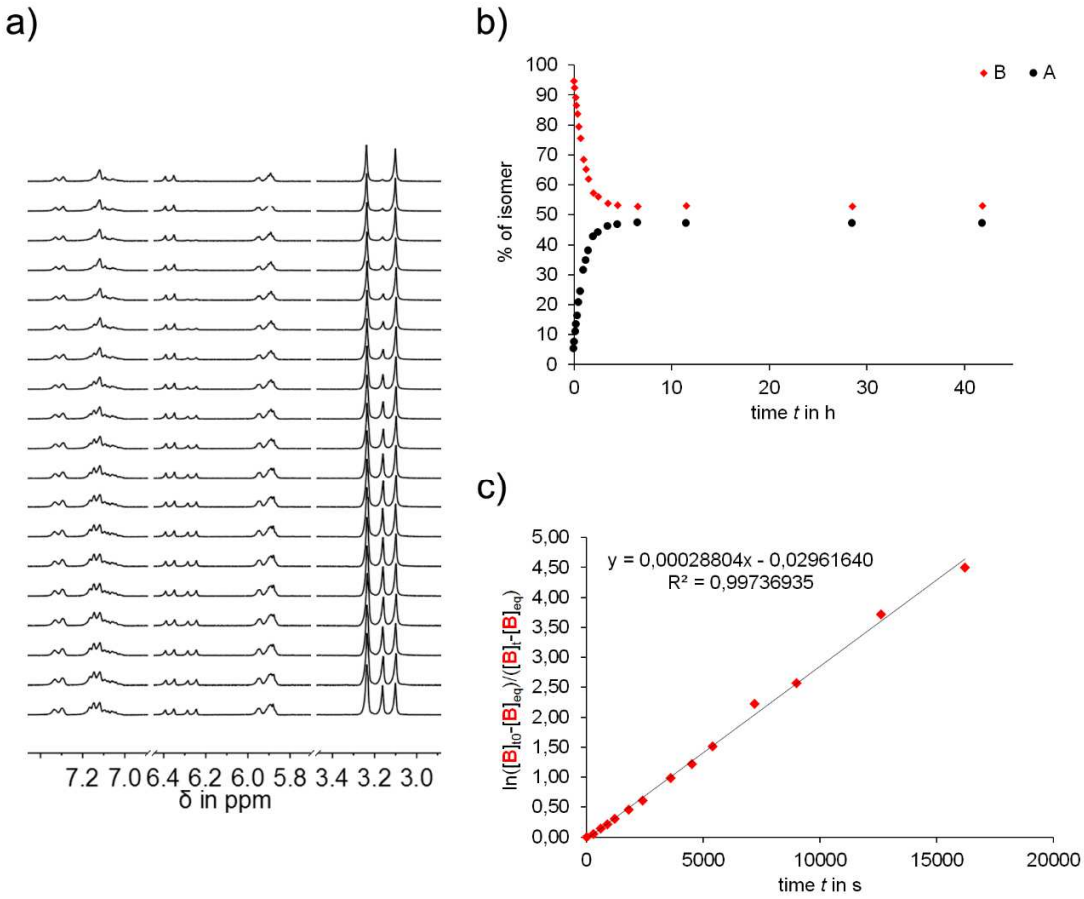

Figure S10. a) Thermal atropisomerization of **B** to **A** in $(CDCl_2)_2$ at 90 °C followed by ^{1}H NMR spectroscopy (200 MHz, 25 °C) in regular time intervals. b) Atropisomer conversion over time. c) First order kinetic analysis of the thermal atropisomerization of **B** to **A**. Taking into account the dynamic equilibrium by plotting according to eq. 10 gives a linear relationship. The slope *m* can be translated into the rate constants $k_{(\mathbf{B/A})}$ according to eq. 13. The corresponding Gibbs energy of activation for the thermal **B** to **A** isomerization is given in Table S2.

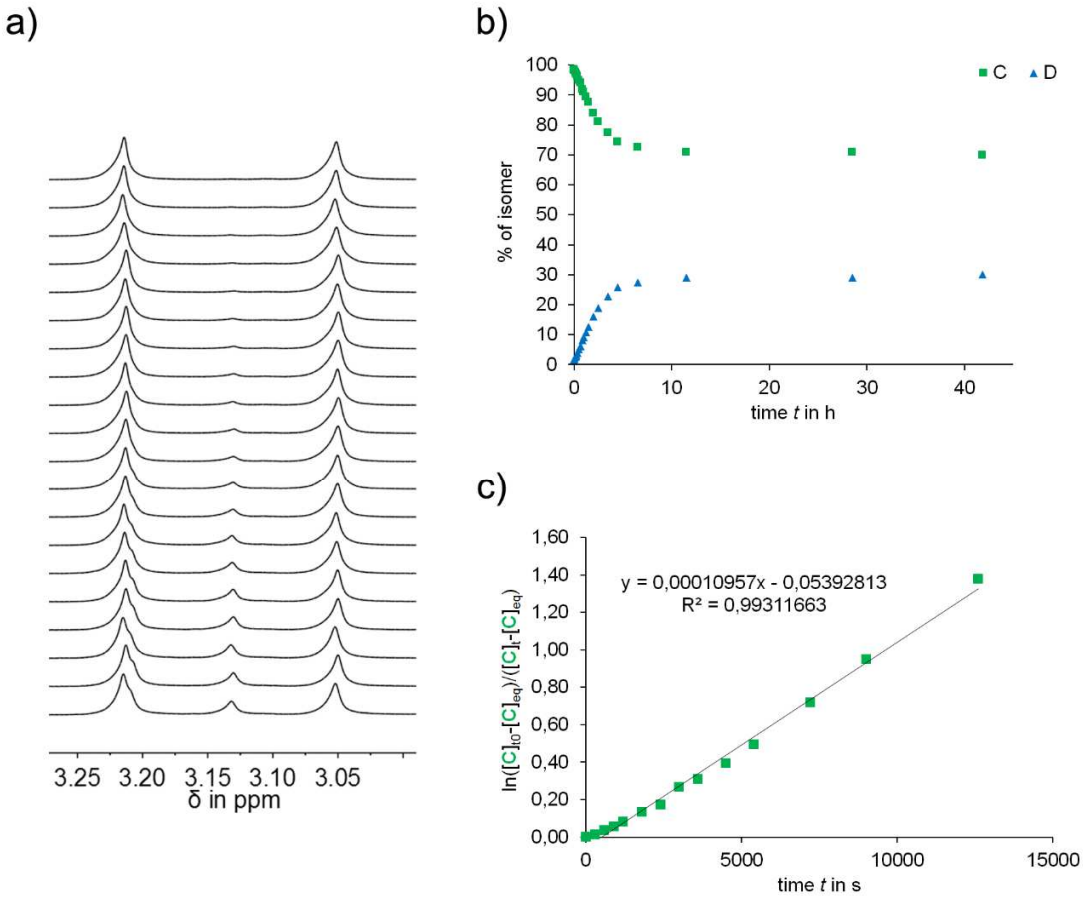

Figure S11. a) Thermal atropisomerization of **C** to **D** in $(CDCl_2)_2$ at 90 °C followed by ^{1}H NMR spectroscopy (200 MHz, 25 °C) in regular time intervals. b) Atropisomer conversion over time. c) First order kinetic analysis of the thermal atropisomerization of **C** to **D**. Taking into account the dynamic equilibrium by plotting according to eq. 2 gives a linear relationship. The slope *m* can be translated into the rate constants $k_{(\mathbf{C/D})}$ according to eq. 5. The corresponding Gibbs energy of activation for the thermal **C** to **D** isomerization is given in Table S2.

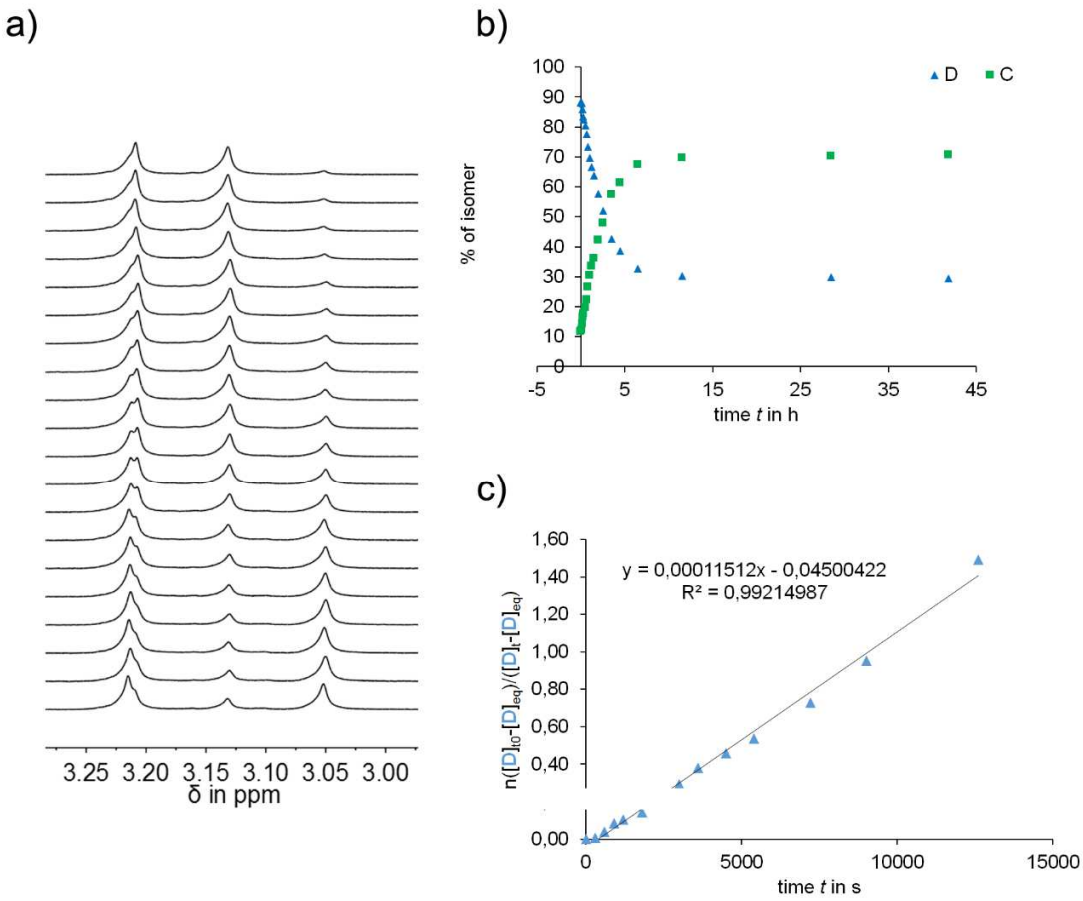

Figure S12. a) Thermal atropisomerization of **D** to **C** in $(CDCl_2)_2$ at 90 °C followed by ^{1}H NMR spectroscopy (200 MHz, 25 °C) in regular time intervals. b) Atropisomer conversion over time. c) First order kinetic analysis of the thermal atropisomerization of **D** to **C**. Taking into account the dynamic equilibrium by plotting according to eq. 11 gives a linear relationship. The slope *m* can be translated into the rate constants $k_{(\mathbf{D/C})}$ according to eq. 14. The corresponding Gibbs energy of activation for the thermal **D** to **C** isomerization is given in Table S2.

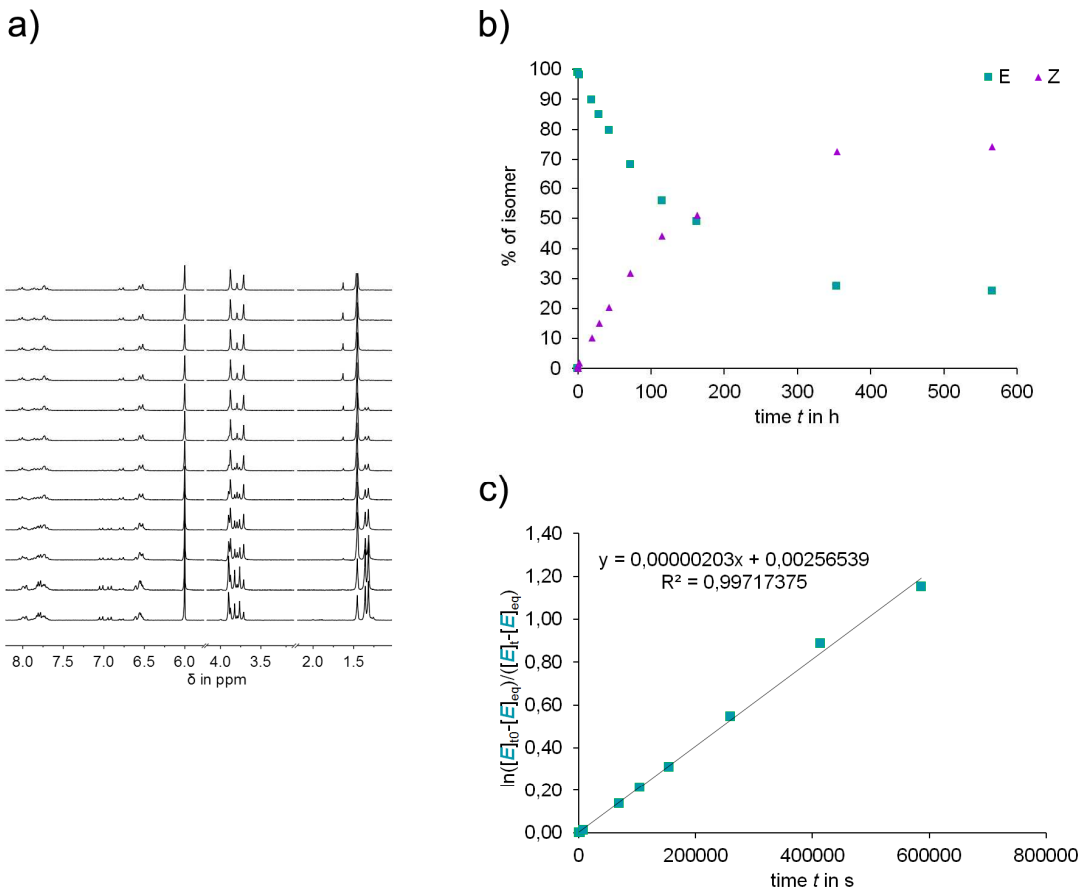

Figure S13. a) Thermal isomerization of ***E*** to ***Z*** isomers in $(CDCl_2)_2$ at 140 °C followed by ^1H NMR spectroscopy (200 MHz, 25 °C) in regular time intervals. b) Isomer conversion over time. c) First order kinetic analysis of the thermal isomerization of ***E*** to ***Z***. Taking into account the dynamic equilibrium by plotting according to eq. 3 gives a linear relationship. The slope *m* can be translated into the rate constants $k_{(E/Z)}$ according to eq. 6. The corresponding Gibbs energy of activation for the thermal ***E*** to ***Z*** isomerization is given in Table S2.

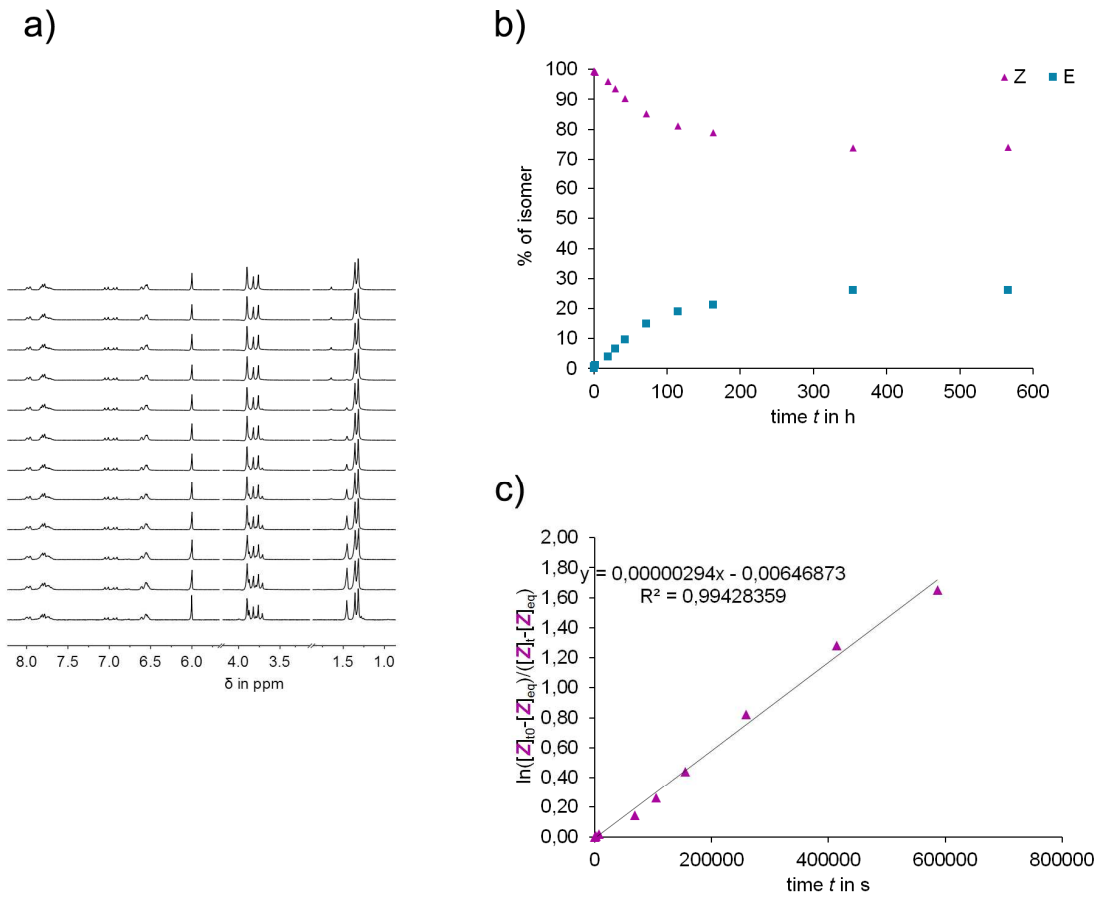

Figure S14. a) Thermal isomerization of ***Z*** to ***E*** isomers in $(CDCl_2)_2$ at 140 °C followed by ^1H NMR spectroscopy (200 MHz, 25 °C) in regular time intervals. b) Isomer conversion over time. c) First order kinetic analysis of the thermal isomerization of ***Z*** to ***E***. Taking into account the dynamic equilibrium by plotting according to eq. 12 gives a linear relationship. The slope *m* can be translated into the rate constants $k_{(Z/E)}$ according to eq. 15. The corresponding Gibbs energy of activation for the thermal ***Z*** to ***E*** isomerization is given in Table S2.

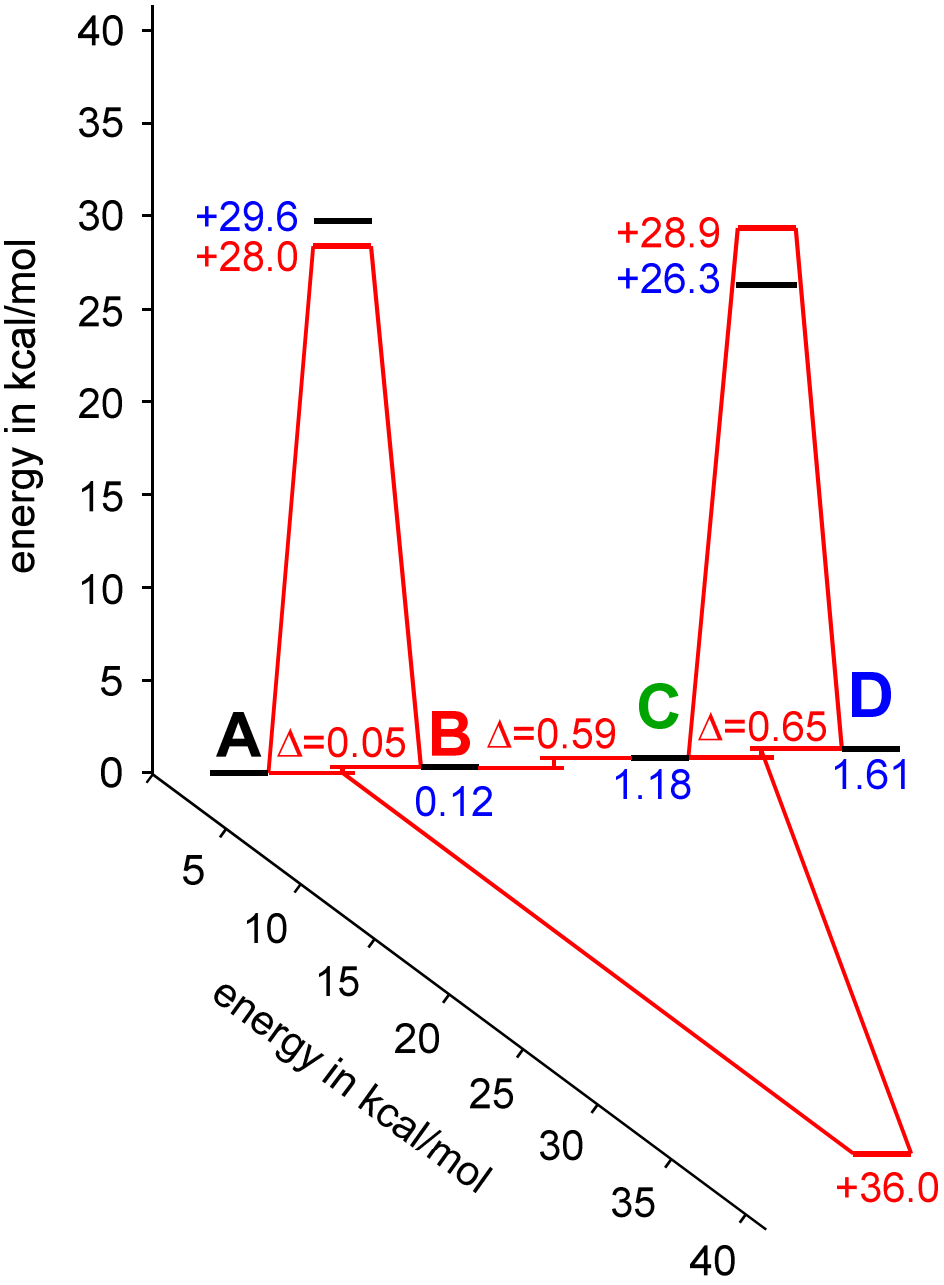

Figure S15. Ground state energy profile for **1**. Thermal interconversion between the four different isomers **A** to **D** at ambient temperature is completely prevented by very high kinetic barriers. Blue values are derived from quantum chemical calculations (B3LYP/6-311G(d,p)), red values were determined experimentally. The Δ values correspond to the experimentally determined $\Delta\Delta G^0$ values.

Molar absorption coefficients of 1

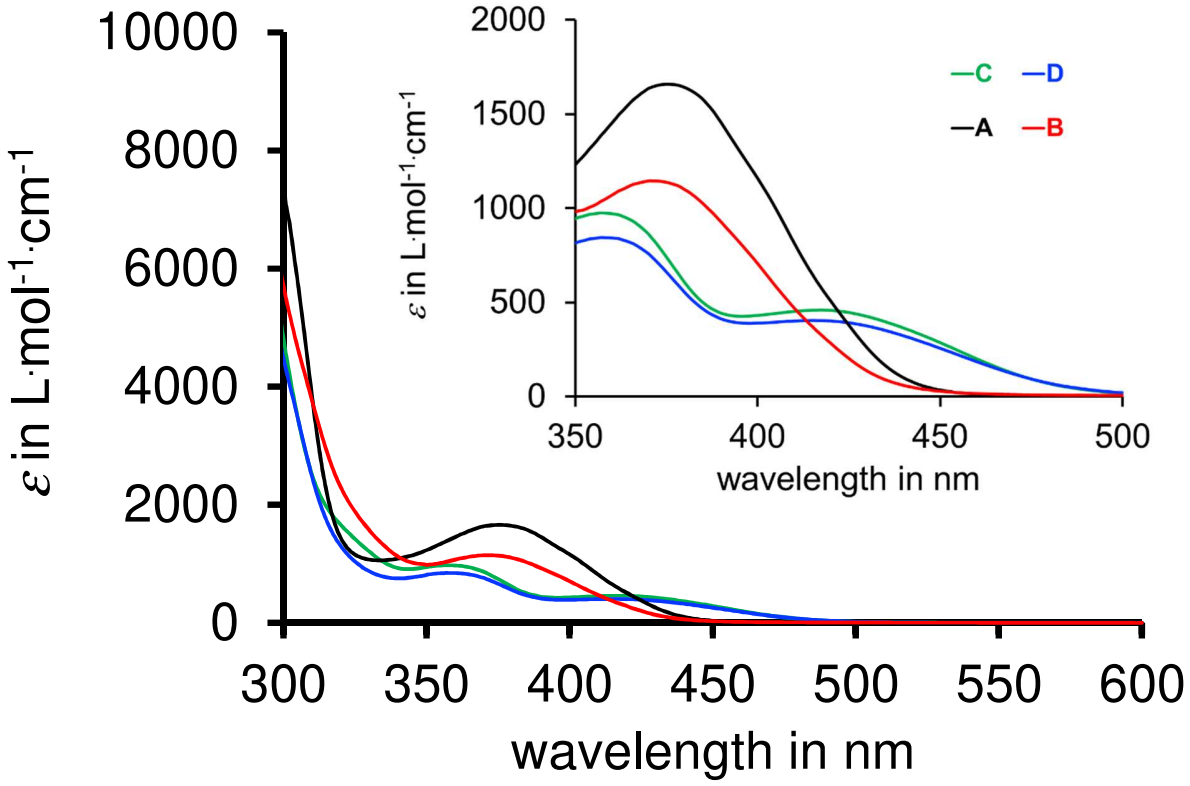

Figure S16. Molar absorption coefficients of **A** (black), **B** (red), **C** (green), and **D** (blue) at 20 °C in CD_2Cl_2 solution.

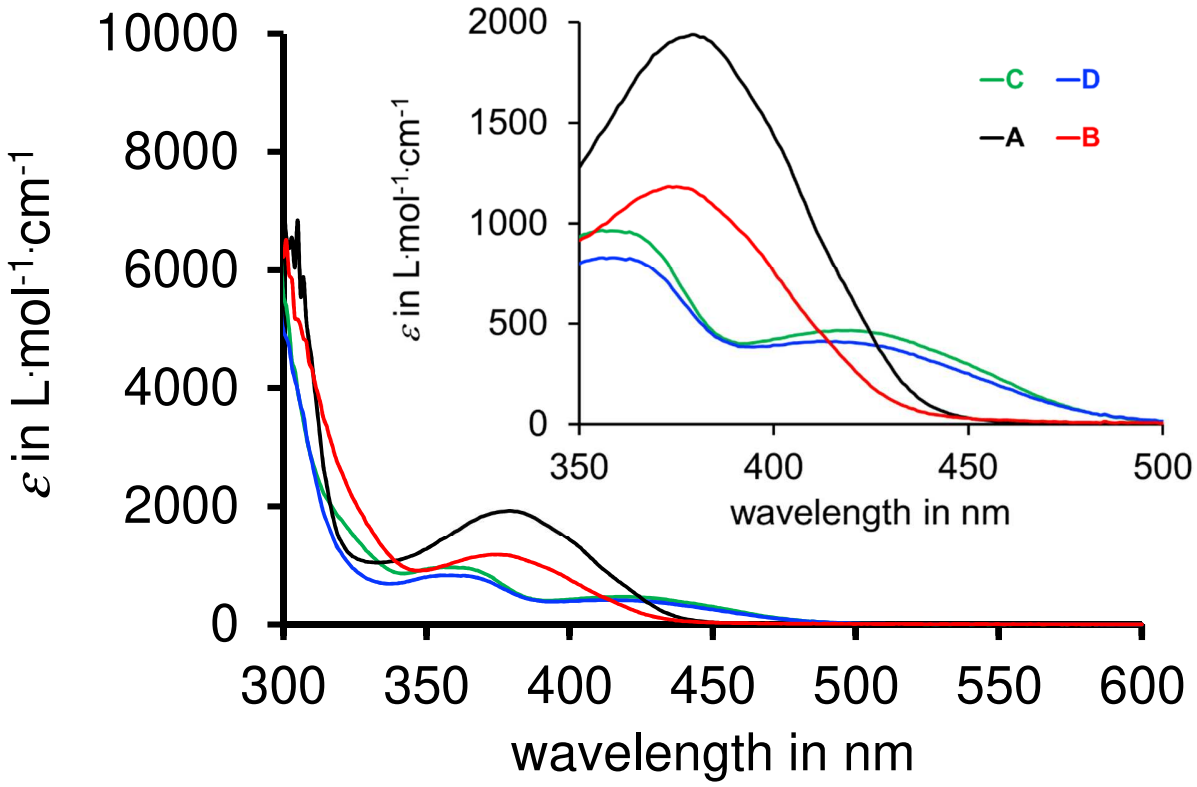

Figure S17. Molar absorption coefficients of **A** (black), **B** (red), **C** (green), and **D** (blue) at -50 °C in CD_2Cl_2 solution.

Data for the photoconversion of 1

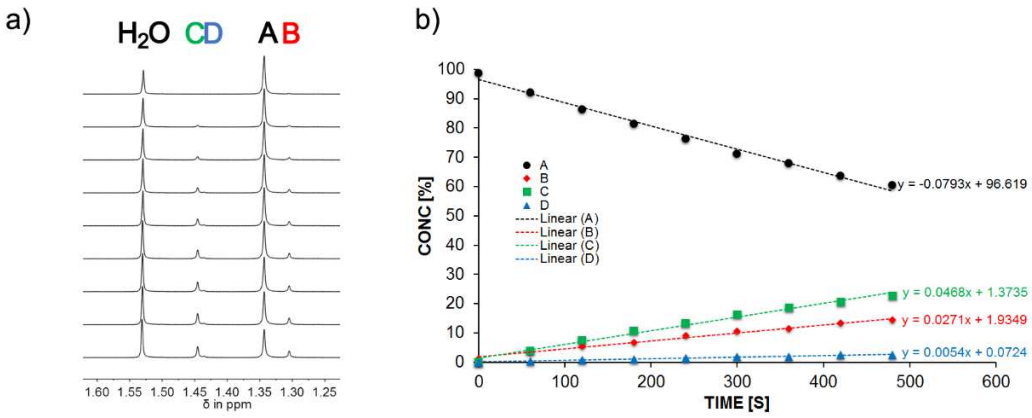

Figure S18. Quantum yield ϕ measurement for the photoconversion of **A-1** at 20 °C in CD_2Cl_2 solution (3.10 mM) using a 442 nm cw laser for irradiation. a) ^{1}H NMR spectra (400 MHz, 18 °C) recorded after different irradiation durations. Signals of individual isomers are indicated. b) The relative changes of the isomer composition is plotted against different duration times of irradiation. Each point represents an individual measurement, the relative isomer ratios were determined by ^{1}H NMR spectroscopy. Linear behavior is observed showing that only **A-1** undergoes significant photoreactions. Quantum yields were determined by averaging over all experiments (see Table S3).

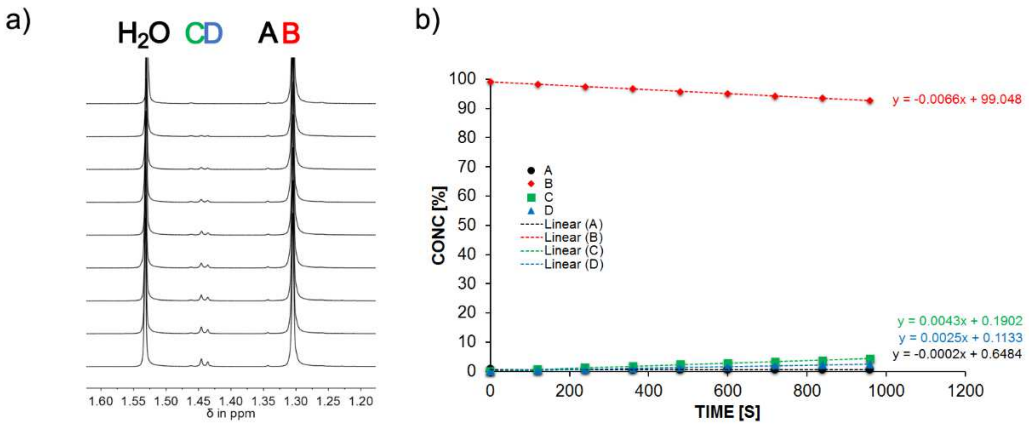

Figure S19. Quantum yield ϕ measurement for the photoconversion of **B-1** at 20 °C in CD_2Cl_2 solution (3.10 mM) using a 442 nm cw laser for irradiation. a) ^{1}H NMR spectra (400 MHz, 18 °C) recorded after different irradiation durations. Signals of individual isomers are indicated. b) The relative changes of the isomer composition is plotted against different duration times of irradiation. Each point represents an individual measurement, the relative isomer ratios were determined by ^{1}H NMR spectroscopy. Linear behavior is observed showing that only **B-1** undergoes significant photoreactions. Quantum yields were determined by averaging over all experiments (see Table S3).

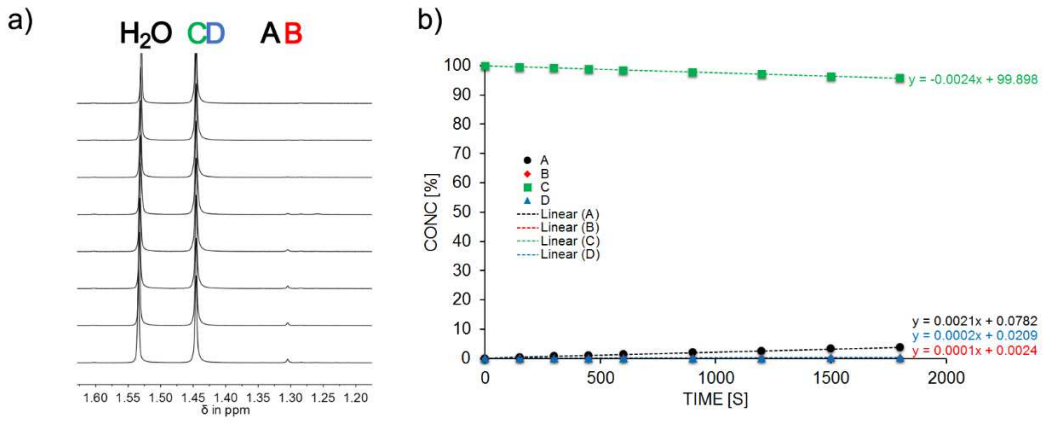

Figure S20. Quantum yield ϕ measurement for the photoconversion of **C-1** at 20 °C in CD_2Cl_2 solution (3.01 mM) using a 442 nm cw laser for irradiation. a) ^{1}H NMR spectra (400 MHz, 18 °C) recorded after different irradiation durations. Signals of individual isomers are indicated. b) The relative changes of the isomer composition is plotted against different duration times of irradiation. Each point represents an individual measurement, the relative isomer ratios were determined by ^{1}H NMR spectroscopy. Linear behavior is observed showing that only **C-1** undergoes significant photoreactions. Quantum yields were determined by averaging over all experiments (see Table S3).

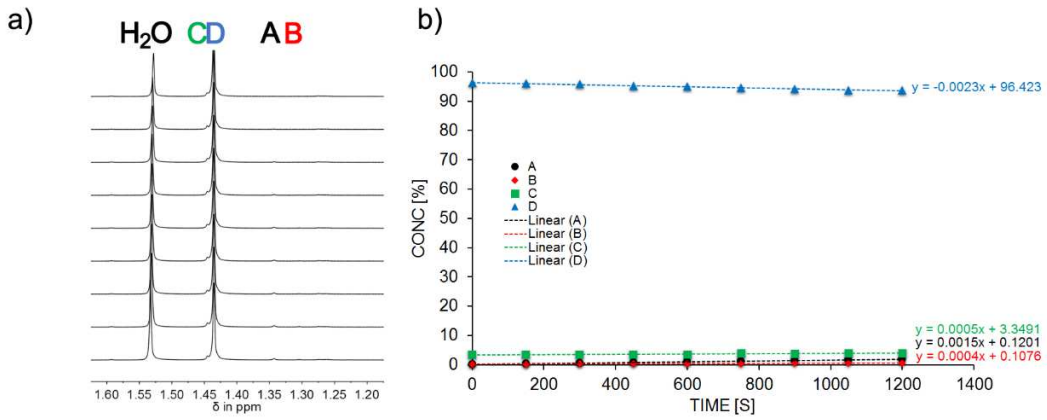

Figure S21. Quantum yield ϕ measurement for the photoconversion of **D-1** at 20 °C in CD_2Cl_2 solution (2.74 mM) using a 442 nm cw laser for irradiation. a) ^{1}H NMR spectra (400 MHz, 18 °C) recorded after different irradiation durations. Signals of individual isomers are indicated. b) The relative changes of the isomer composition is plotted against different duration times of irradiation. Each point represents an individual measurement, the relative isomer ratios were determined by ^{1}H NMR spectroscopy. Linear behavior is observed showing that only **D-1** undergoes significant photoreactions. Quantum yields were determined by averaging over all experiments (see Table S3).

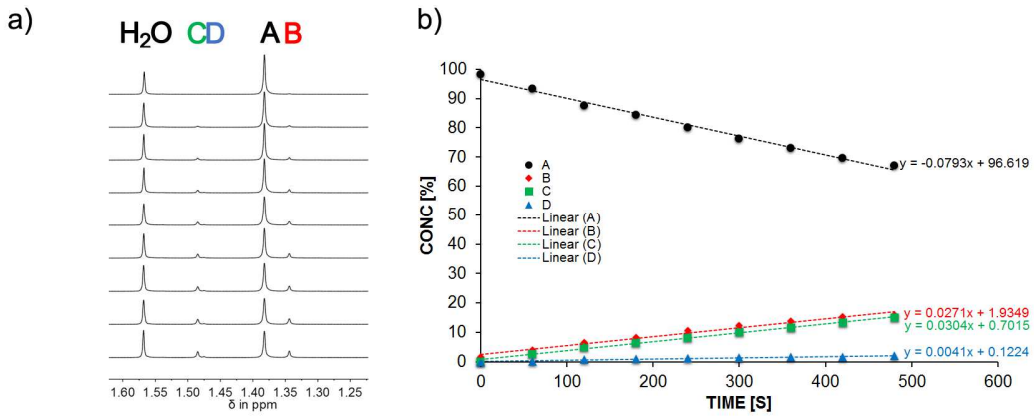

Figure S22. Quantum yield ϕ measurement for the photoconversion of **A**-**1** at -50 °C in CD_2Cl_2 solution (3.10 mM) using a 442 nm cw laser for irradiation. a) ^{1}H NMR spectra (400 MHz, 18 °C) recorded after different irradiation durations. Signals of individual isomers are indicated. b) The relative changes of the isomer composition is plotted against different duration times of irradiation. Each point represents an individual measurement, the relative isomer ratios were determined by ^{1}H NMR spectroscopy. Linear behavior is observed showing that only **A**-**1** undergoes significant photoreactions. Quantum yields were determined by averaging over all experiments (see Table S3).

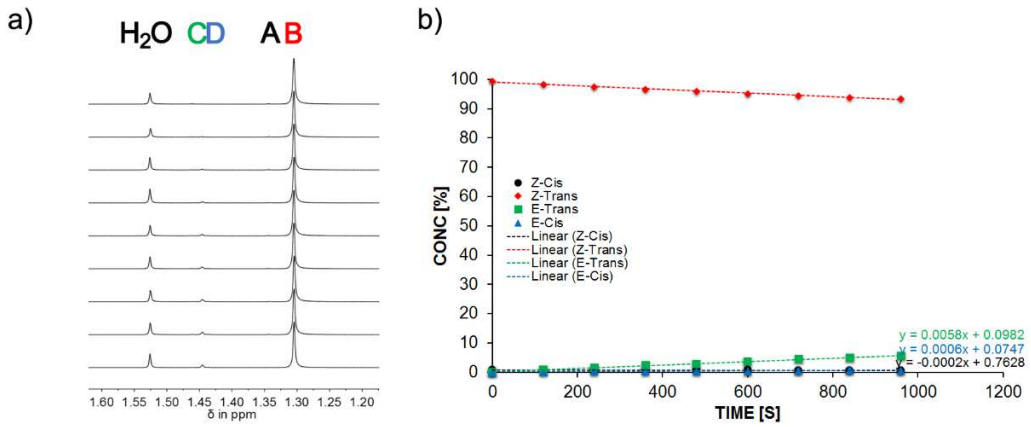

Figure S23. Quantum yield ϕ measurement for the photoconversion of **B-1** at 20 °C in CD_2Cl_2 solution (3.10 mM) using a 442 nm cw laser for irradiation. a) ^{1}H NMR spectra (400 MHz, 18 °C) recorded after different irradiation durations. Signals of individual isomers are indicated. b) The relative changes of the isomer composition is plotted against different duration times of irradiation. Each point represents an individual measurement, the relative isomer ratios were determined by ^{1}H NMR spectroscopy. Linear behavior is observed showing that only **B-1** undergoes significant photoreactions. Quantum yields were determined by averaging over all experiments (see Table S3).

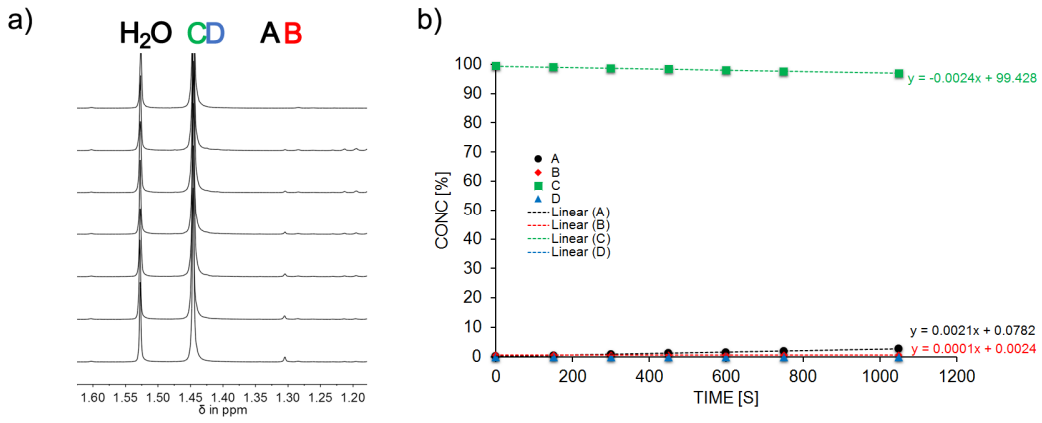

Figure S24. Quantum yield ϕ measurement for the photoconversion of **C-1** at -50 °C in CD_2Cl_2 solution (3.01 mM) using a 442 nm cw laser for irradiation. a) ^{1}H NMR spectra (400 MHz, 18 °C) recorded after different irradiation durations. Signals of individual isomers are indicated. b) The relative changes of the isomer composition is plotted against different duration times of irradiation. Each point represents an individual measurement, the relative isomer ratios were determined by ^{1}H NMR spectroscopy. Linear behavior is observed showing that only **C-1** undergoes significant photoreactions. Quantum yields were determined by averaging over all experiments (see Table S3).

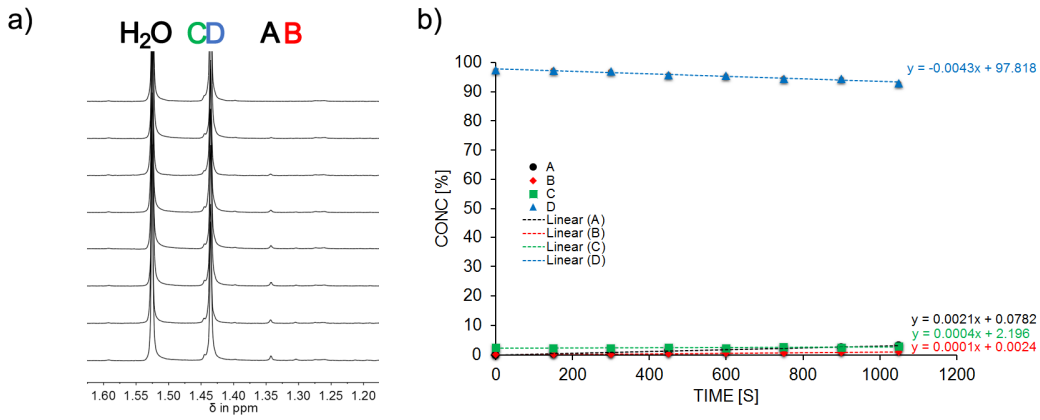

Figure S25. Quantum yield ϕ measurement for the photoconversion of **D-1** at -50 °C in CD_2Cl_2 solution (2.74 mM) using a 442 nm cw laser for irradiation. a) ^{1}H NMR spectra (400 MHz, 18 °C) recorded after different irradiation durations. Signals of individual isomers are indicated. b) The relative changes of the isomer composition is plotted against different duration times of irradiation. Each point represents an individual measurement, the relative isomer ratios were determined by ^{1}H NMR spectroscopy. Linear behavior is observed showing that only **D-1** undergoes significant photoreactions. Quantum yields were determined by averaging over all experiments (see Table S3).

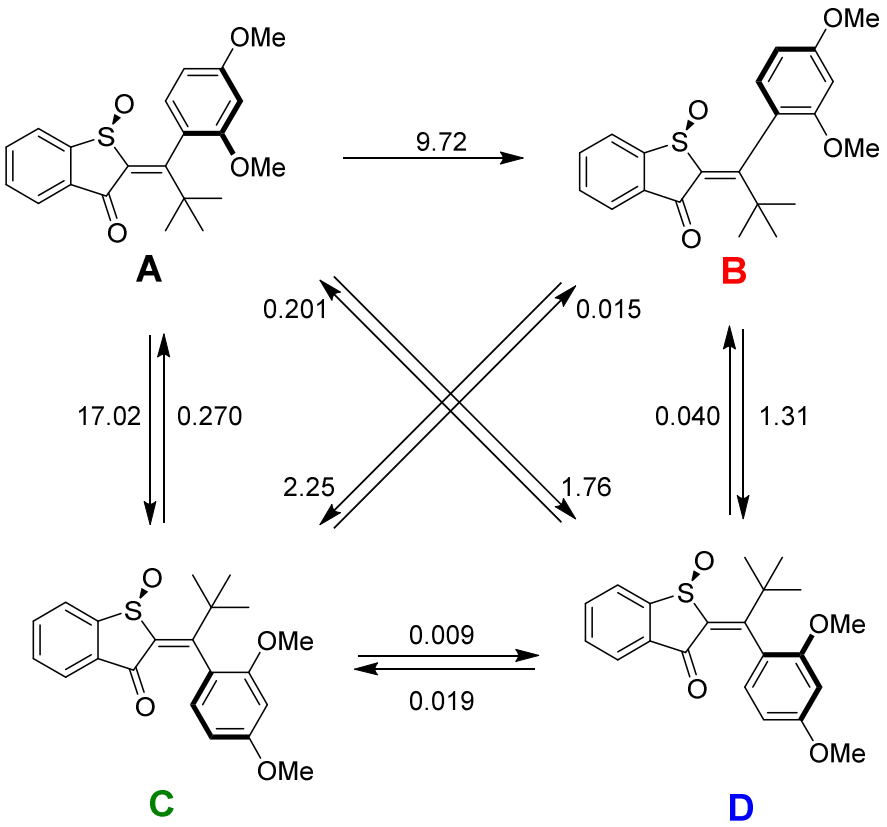

Figure S26. Photoreactions of **1** in CD_2Cl_2 at 20 °C. Every productive photoreaction is shown with the corresponding quantum yield.

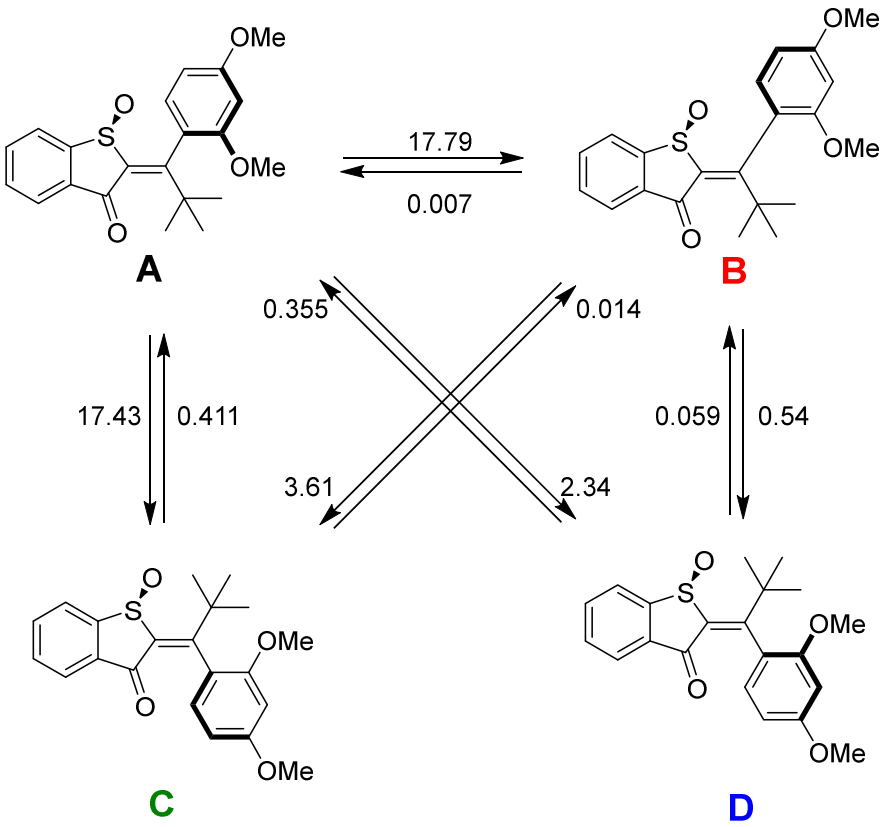

Figure S27. Photoreactions of **1** in CD_2Cl_2 at - 50 °C. Every productive photoreaction is shown with the corresponding quantum yield.

Photostationary states of 1

a)

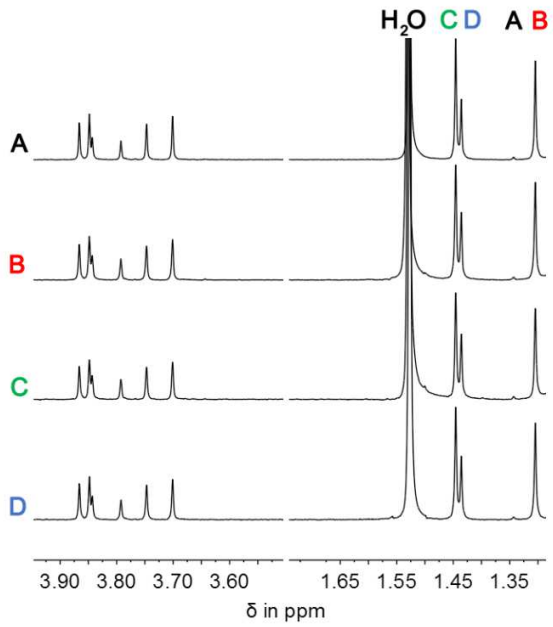

b)

	A	B	C	D
	1	36	43	20
	1	36	42	21
	1	36	41	22
	1	36	41	22
Ø =	1	36	42	21

Figure S28. Isomer composition in the photostationary state reached at 20 °C in CD_2Cl_2 solution after illumination of pure **A**-**1**, **B**-**1**, **C**-**1**, and **D**-**1** with a 442 nm cw laser. a) ^{1}H NMR spectra (400 MHz, 18 °C) recorded after 12 h of irradiation. Signals of individual isomers are indicated. b) Relative ratio in % of **A**-**1**, **B**-**1**, **C**-**1**, and **D**-**1** in the photostationary state obtained by line fitting and integration of the *t*Bu-Group signals. The mean value of these ratios was used to minimize integration errors.

a)

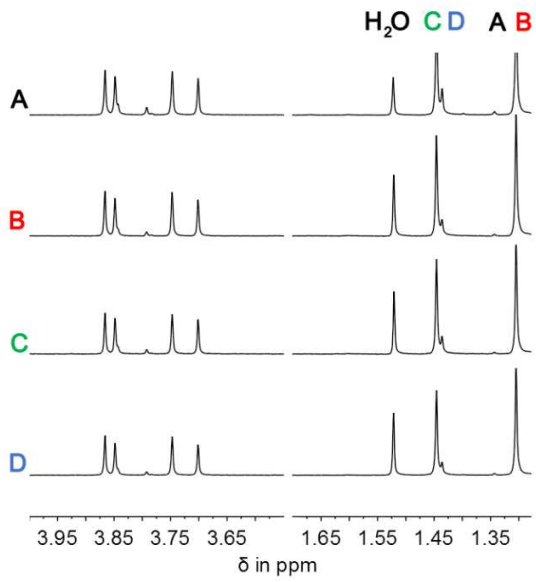

b)

	A	B	C	D
	1	53	41	5
	1	50	42	7
	1	54	40	6
	1	50	40	9
Ø =	1	51	41	7

Figure S29. Isomer composition in the photostationary state reached at -50 °C in CD_2Cl_2 solution after illumination of pure **A**-**1**, **B**-**1**, **C**-**1**, and **D**-**1** with a 442 nm cw laser. a) ^{1}H NMR spectra (400 MHz, 18 °C) recorded after 12 h of irradiation. Signals of individual isomers are indicated. b) Relative ratio in % of **A**-**1**, **B**-**1**, **C**-**1**, and **D**-**1** in the photostationary state obtained by line fitting and integration of the *t*Bu-Group signals. The mean of these ratios was used to minimize the integration errors.

Supplementary Tables

Table S2. Thermal isomerization behavior of hemithioindigo **1** in $(CDCl_2)_2$ at high temperature.

Isomer	$k_{(\text{isom. 1/isom. 2})}$ / s^{-1} (at T / °C)	ΔG^* (therm. isomer equilibration) /kcal mol^{-1}	Equilibration half-life of pure isomer at 27 °C	Thermo-dynamic isomer 1/isomer 2 equilibrium in the dark (at T / °C)	$\Delta\Delta G^0$(isomer 1 / isomer 2) / kcal mol^{-1}	Slope m / s^{-1} (at T / °C)
A	$k_{(\mathbf{A/B})}$ = 1.05x10^{-4} (90 °C)	ΔG^*(**A/B**) = 28.01	0.9 a	**A/B** = 49/51 (90 °C)	$\Delta\Delta G^0$(**A/B**) = -0.03	5.07x10^{-5} (90 °C)
B	$k_{(\mathbf{B/A})}$ = 1.36x10^{-4} (90 °C)	ΔG^*(**B/A**) = 27.82	0.7 a	**B/A** = 52/48 (90 °C)	$\Delta\Delta G^0$(**B/A**) = 0.08	2.88x10^{-5} (90 °C)
C	$k_{(\mathbf{C/D})}$ = 3.27x10^{-5} (90 °C)	ΔG^*(**C/D**) = 28.85	3.7 a	**C/D** = 70/30 (90 °C)	$\Delta\Delta G^0$(**C/D**) = -0.63	1.10x10^{-4} (90 °C)
D	$k_{(\mathbf{D/C})}$ = 8.13x10^{-5} (90 °C)	ΔG^*(**D/C**) = 28.19	1.2 a	**D/C** = 29/71 (90 °C)	$\Delta\Delta G^0$(**D/C**) = 0.63	1.15x10^{-4} (90 °C)
E	$k_{(E/Z)}$ = 1.51x10^{-6} (140 °C)	ΔG^*(*E*/*Z*) = 35.46	242 x10^3 a	*E*/*Z* = 26/74 (140 °C)	$\Delta\Delta G^0$(*E*/*Z*) = 0.86	2.03x10^{-5} (140 °C)
Z	$k_{(Z/E)}$ = 7.65x10^{-7} (140 °C)	ΔG^*(*Z*/*E*) = 36.01	609 x10^3 a	*Z*/*E* = 74/26 (140 °C)	$\Delta\Delta G^0$(*Z*/*E*) = -0.86	2.94x10^{-5} (140 °C)

Table S3. Quantum yields ϕ in % for different photoconversions of **1** in CD_2Cl_2 at different temperatures. SBR = single-bond rotation, DBI = double-bond isomerization, HT = hula twist. Following error margins are included: 5% integration error in the ^1H NMR spectra, 5% error in weighing in of the samples, and 5% error in light intensity during irradiations. This amounts to a maximum of 15% total error for the obtained experimental values.

	ϕ in % T = 20 °C	ϕ in % T = -50 °C
A to B SBR	9.7 ± 1.5	17.8 ± 2.7
A to C DBI	17.0 ± 2.6	17.4 ± 2.6
A to D HT	1.76 ± 0.26	2.34 ± 0.35
B to A SBR	0 ± 0.001	0.007 ± 0.001
B to C HT	2.25 ± 0.34	3.61 ± 0.54
B to D DBI	1.31 ± 0.20	0.540 ± 0.081
C to A DBI	0.27 ± 0.04	0.411 ± 0.061
C to B HT	0.015 ± 0.002	0.014 ± 0.021
C to D SBR	0.009 ± 0.001	0 ± 0.001
D to A HT	0.20 ± 0.03	0.355 ± 0.053
D to B DBI	0.040 ± 0.006	0.059 ± 0.009
D to C SBR	0.019 ± 0.003	0 ± 0.001

Table S4. Molar absorption coefficients (442 nm) in $L \cdot mol^{-1} \cdot cm^{-1}$ in the photostationary state (PSS) and relative ratio of **A**, **B**, **C,** and **D** in % at 20 °C and -50 °C. Following error margins are included: 5% integration error in the ^1H NMR spectra and 5% error in weighing in of the samples. This amounts to a maximum of 10% total error for the obtained experimental values.

	Ratio in PSS [%]		Molar absorption coefficient at 442 nm [$L \cdot mol^{-1} \cdot cm^{-1}$]	
	T = 20 °C	T = - 50 °C	T = 20 °C	T = -50 °C
A	1 ± 0	1 ± 0	82 ± 4	77 ± 4
B	36 ± 2	51 ± 3	52 ± 3	48 ± 2
C	42 ± 2	41 ± 2	351 ± 18	360 ± 18
D	21 ± 1	7 ± 0	311 ± 16	305 ± 15

Table S5. Probabilities for all possible 3- and 4-step isomer interconversion cycles occurring during illumination of **1** in the PSS in CD_2Cl_2 at different temperatures in relation to all possible photo-transitions (65536 possibilities after 4 transitions) or in relation to all possible cycles. Error margins were obtained by calculating the probability of each cycle using random permutations of the upper and lower error limits given in Table S3 and S4 (typically ±5-15%). The 99th percentile of values obtained in 10,000 such permutations were then used to determine the upper and lower limits for these values.

	T = 20 °C		T = -50 °C	
	Absolute cycle probability (p_{cycle})	Relative probability of the cycle versus all possible cycles [%]	Absolute cycle probability (p_{cycle})	Relative probability of the cycle versus all possible cycles [%]
ABC	$3 \pm 1 \cdot 10^{-9}$	81 ± 7	$3 \pm 1 \cdot 10^{-8}$	98 ± 2
ACB	$0 \pm 2 \cdot 10^{-13}$	$0 \pm 6 \cdot 10^{-3}$	$2 \pm 1 \cdot 10^{-10}$	0.6 ± 0.4
ABD	$6 \pm 2 \cdot 10^{-10}$	16 ± 6	$6 \pm 3 \cdot 10^{-10}$	1.8 ± 0.9
ADB	$0 \pm 3 \cdot 10^{-13}$	$0 \pm 7 \cdot 10^{-4}$	$2 \pm 1 \cdot 10^{-11}$	0.05 ± 0.03
ACD	$6 \pm 2 \cdot 10^{-11}$	1.5 ± 0.8	$0 \pm 1 \cdot 10^{-11}$	0 ± 0.03
ADC	$2 \pm 1 \cdot 10^{-11}$	0.4 ± 0.2	$0 \pm 2 \cdot 10^{-12}$	$0 \pm 5 \cdot 10^{-3}$
BCD	$4 \pm 1 \cdot 10^{-11}$	0.9 ± 0.4	$0 \pm 1 \cdot 10^{-11}$	0 ± 0.03
BDC	$2 \pm 1 \cdot 10^{-11}$	0.4 ± 0.2	$0 \pm 4 \cdot 10^{-13}$	0 ± 0.01
ABCD	$8 \pm 3 \cdot 10^{-14}$	$2.0 \pm 0.7 \cdot 10^{-3}$	$0 \pm 7 \cdot 10^{-14}$	$0 \pm 2 \cdot 10^{-4}$
ADCB	$0 \pm 2 \cdot 10^{-18}$	$0 \pm 4 \cdot 10^{-8}$	$0 \pm 1 \cdot 10^{-11}$	$0 \pm 2 \cdot 10^{-7}$
ACBD	$1 \pm 1 \cdot 10^{-13}$	$3.5 \pm 2.0 \cdot 10^{-3}$	$8 \pm 3 \cdot 10^{-14}$	$2 \pm 2 \cdot 10^{-4}$
ADBC	$9 \pm 4 \cdot 10^{-14}$	$2.2 \pm 0.9 \cdot 10^{-3}$	$3 \pm 2 \cdot 10^{-13}$	$1 \pm 1 \cdot 10^{-3}$
ABDC	$1 \pm 1 \cdot 10^{-13}$	$3.3 \pm 1.2 \cdot 10^{-3}$	$0 \pm 1 \cdot 10^{-14}$	$0 \pm 4 \cdot 10^{-5}$
ACDB	$0 \pm 2 \cdot 10^{-17}$	$0 \pm 5 \cdot 10^{-7}$	$0 \pm 2 \cdot 10^{-15}$	$0 \pm 7 \cdot 10^{-6}$

Table S6. Efficiencies of all possible processes and cycles and number of photons, which are needed on average to drive one particular process in motor **1** at 20 °C and -50 °C. Values were calculated using eq. 35-60. Error margins were obtained by calculating the efficiency of each process or cycle using random permutations of the upper and lower error limits given in Table S3 and S4 (typically ±5-15%). The 99th percentile of values obtained in 10,000 such permutations were then used to determine the upper and lower limits for these values.

	T = 20 °C		T = -50 °C	
	Efficiency ($E_{\mathbf{cycle}}$)	Number of photons (#photons$_{\mathbf{cycle}}$)	Efficiency ($E_{\mathbf{cycle}}$)	Number of photons (#photons$_{\mathbf{cycle}}$)
A	$2.5 \pm 0.3 \cdot 10^{-3}$	400 ± 60	$2.5 \pm 0.4 \cdot 10^{-3}$	400 ± 60
B	$7.8 \pm 0.8 \cdot 10^{-2}$	13 ± 2	0.12 ± 0.02	8 ± 2
C	0.63 ± 0.03	1.6 ± 0.1	0.76 ± 0.03	1.3 ± 0.1
D	0.26 ± 0.03	3.8 ± 0.4	0.11 ± 0.02	9 ± 2
AB	$0 \pm 0.4 \cdot 10^{-6}$	-	$2.1 \pm 0.8 \cdot 10^{-4}$	$0.9 \pm 0.4 \cdot 10^{4}$
AC	$1.2 \pm 0.3 \cdot 10^{-3}$	$1.6 \pm 0.5 \cdot 10^{3}$	$1.4 \pm 0.3 \cdot 10^{-3}$	$1.4 \pm 0.4 \cdot 10^{3}$
AD	$5.7 \pm 0.2 \cdot 10^{-6}$	$3.5 \pm 1.5 \cdot 10^{5}$	$1.6 \pm 0.4 \cdot 10^{-4}$	$1.2 \pm 0.3 \cdot 10^{4}$
BC	$1.6 \pm 0.3 \cdot 10^{-4}$	$1.2 \pm 0.2 \cdot 10^{4}$	$1.9 \pm 0.3 \cdot 10^{-4}$	$1.1 \pm 0.2 \cdot 10^{3}$
BD	$1.8 \pm 0.4 \cdot 10^{-3}$	$1.1 \pm 0.3 \cdot 10^{3}$	$3.4 \pm 1.2 \cdot 10^{-4}$	$5.8 \pm 2.2 \cdot 10^{3}$
CD	$4.6 \pm 1.2 \cdot 10^{-5}$	$4.3 \pm 1.4 \cdot 10^{4}$	$0 \pm 0.8 \cdot 10^{-10}$	-
ABC	$8.7 \pm 2.0 \cdot 10^{-4}$	$3.4 \pm 0.8 \cdot 10^{3}$	$1.6 \pm 0.4 \cdot 10^{-3}$	$1.9 \pm 0.4 \cdot 10^{3}$
ACB	$0 \pm 0.5 \cdot 10^{-6}$	-	$1.0 \pm 0.5 \cdot 10^{-5}$	$3.0 \pm 1.6 \cdot 10^{5}$
ABD	$1.6 \pm 0.8 \cdot 10^{-5}$	$1.8 \pm 0.9 \cdot 10^{5}$	$2.1 \pm 0.8 \cdot 10^{-4}$	$1.4 \pm 0.5 \cdot 10^{4}$
ADB	$0 \pm 0.7 \cdot 10^{-8}$	-	$5.8 \pm 2.9 \cdot 10^{-6}$	$5.1 \pm 2.6 \cdot 10^{5}$
ACD	$2.0 \pm 1.0 \cdot 10^{-6}$	$1.5 \pm 0.9 \cdot 10^{6}$	$0 \pm 0.7 \cdot 10^{-6}$	-
ADC	$7.5 \pm 2.1 \cdot 10^{-5}$	$4.0 \pm 1.4 \cdot 10^{4}$	$0 \pm 0.1 \cdot 10^{-6}$	-
BCD	$9.6 \pm 2.1 \cdot 10^{-5}$	$3.1 \pm 0.8 \cdot 10^{4}$	$0 \pm 0.4 \cdot 10^{-6}$	-
BDC	$4.0 \pm 1.6 \cdot 10^{-5}$	$7.5 \pm 3.0 \cdot 10^{4}$	$0 \pm 0.2 \cdot 10^{-7}$	-
ABCD	$1.3 \pm 0.6 \cdot 10^{-6}$	$3.2 \pm 1.6 \cdot 10^{6}$	$0 \pm 0.7 \cdot 10^{-6}$	-
ADCB	$0 \pm 0.3 \cdot 10^{-6}$	-	$0 \pm 0.8 \cdot 10^{-9}$	-
ACBD	$1.5 \pm 0.9 \cdot 10^{-6}$	$2.7 \pm 1.5 \cdot 10^{6}$	$0.9 \pm 0.4 \cdot 10^{-5}$	$4.5 \pm 2.5 \cdot 10^{5}$
ADBC	$1.4 \pm 0.4 \cdot 10^{-4}$	$2.9 \pm 1.9 \cdot 10^{4}$	$3.9 \pm 1.5 \cdot 10^{-5}$	$1.0 \pm 0.5 \cdot 10^{5}$
ABDC	$1.9 \pm 0.8 \cdot 10^{-4}$	$2.1 \pm 0.9 \cdot 10^{4}$	$0 \pm 1.3 \cdot 10^{-7}$	-
ACDB	$0 \pm 0.2 \cdot 10^{-6}$	-	$0 \pm 2.4 \cdot 10^{-7}$	-

NMR-spectra

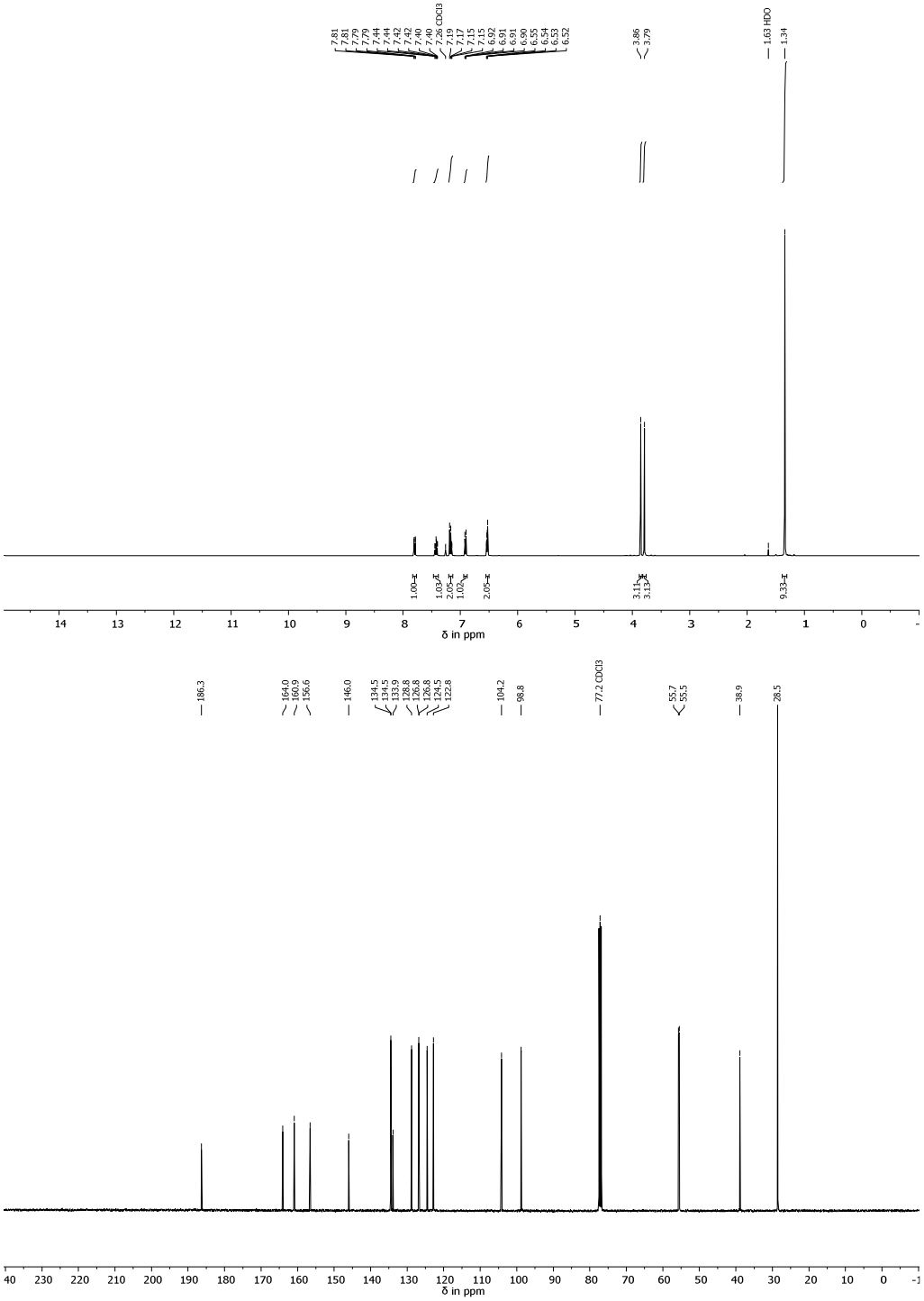

Figure S30. 400 MHz ^{1}H NMR spectrum (top) and 100 MHz ^{13}C NMR spectrum (bottom) of **4** in $CDCl_3$.

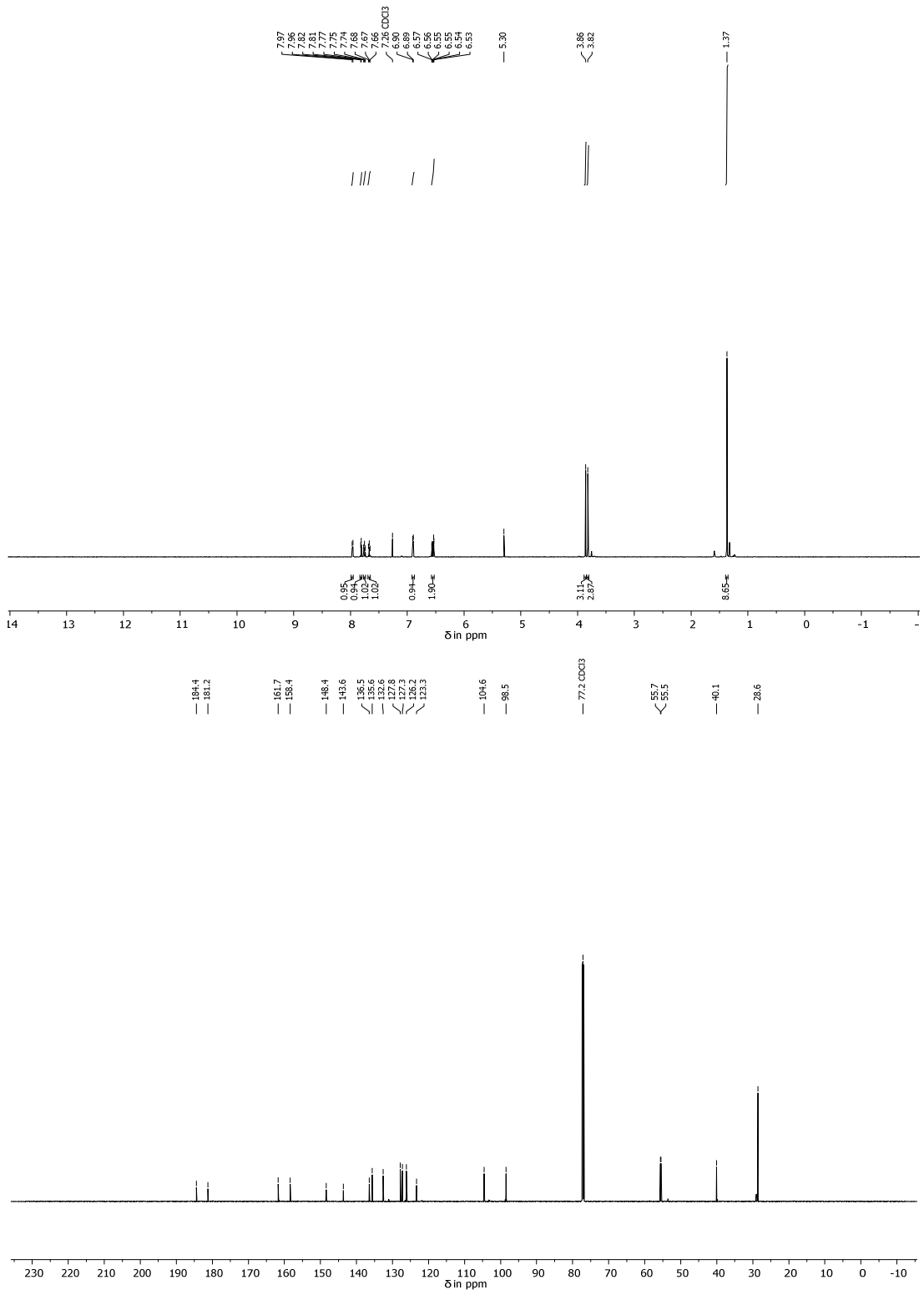

Figure S31. 600 MHz ^{1}H NMR spectrum (top) and 150 MHz ^{13}C NMR spectrum (bottom) of **1-A** in $CDCl_3$.

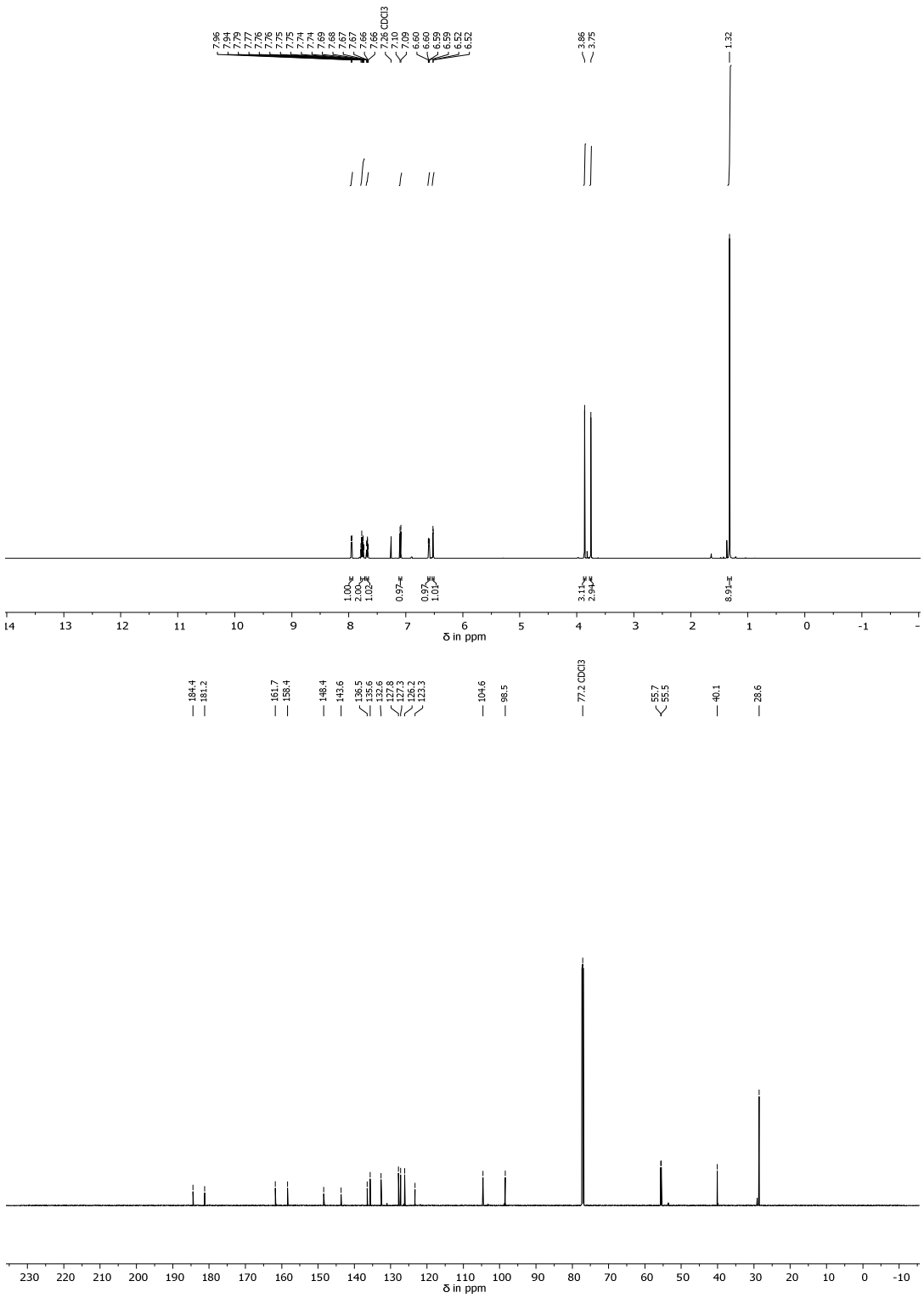

Figure S32. 600 MHz ^{1}H NMR spectrum (top) and 150 MHz ^{13}C NMR spectrum (bottom) of **1-B** in $CDCl_3$.

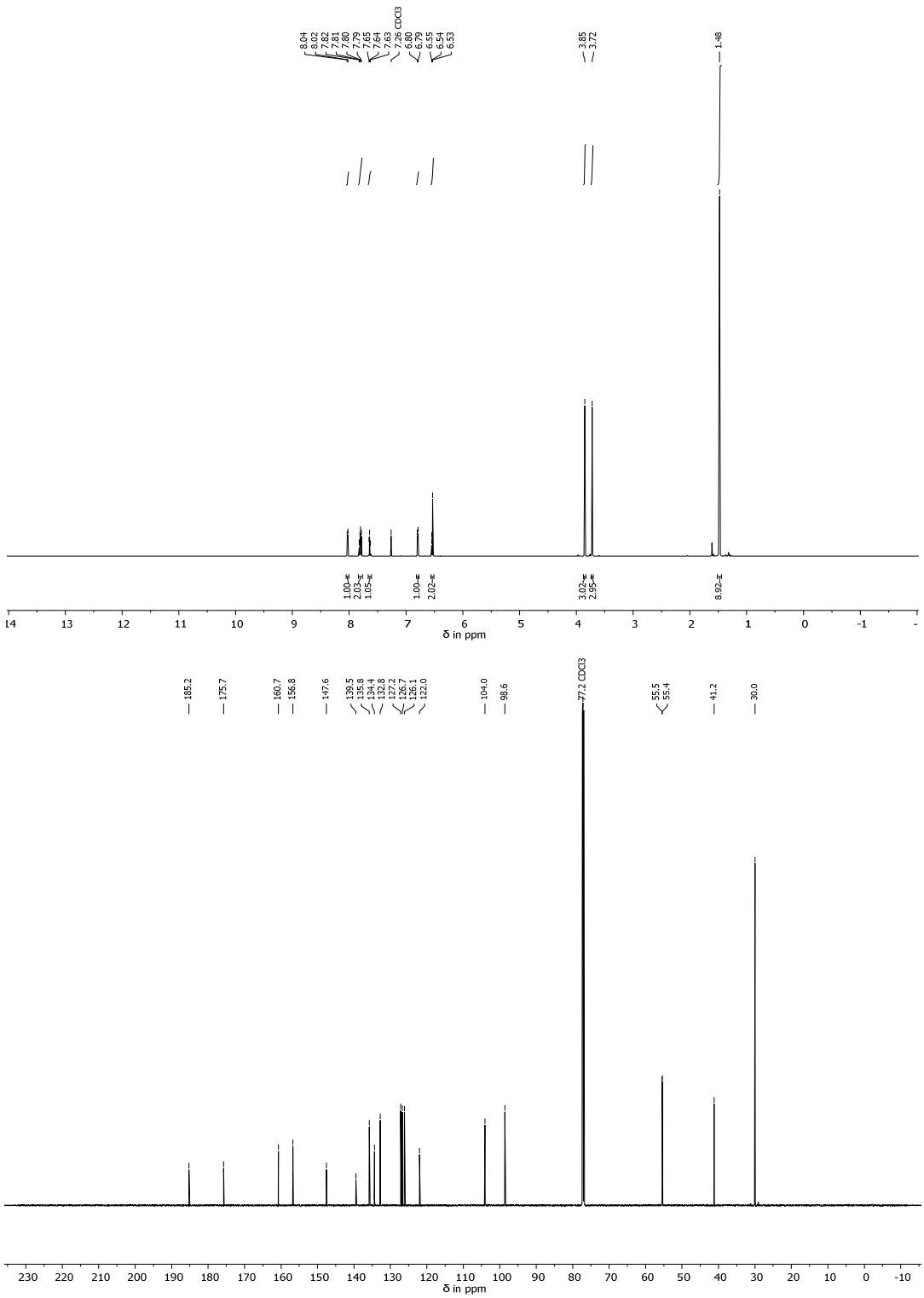

Figure S33. 600 MHz ^{1}H NMR spectrum (top) and 150 MHz ^{13}C NMR spectrum (bottom) of **1-C** in $CDCl_3$.

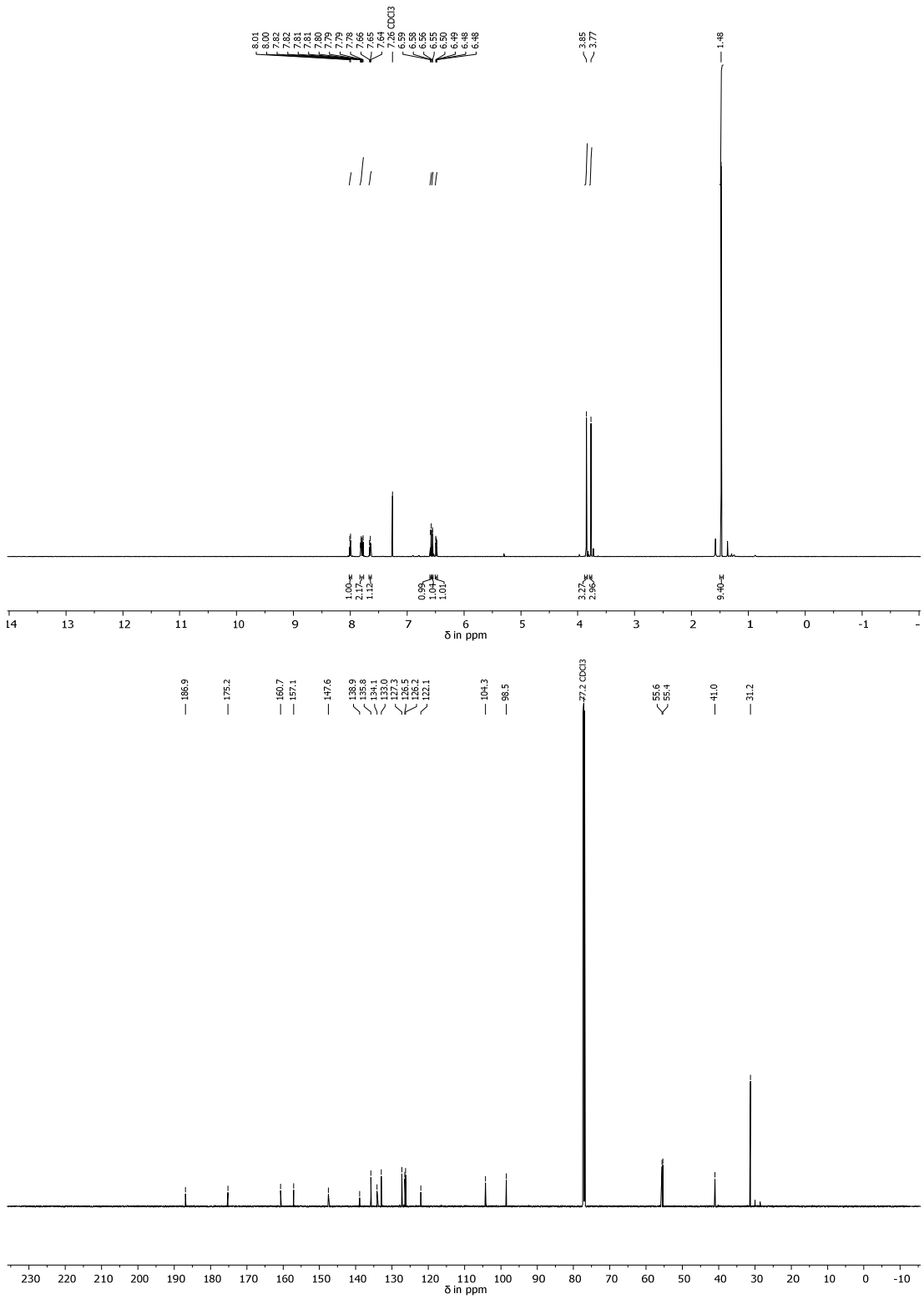

Figure S34. 600 MHz ^{1}H NMR spectrum (top) and 150 MHz ^{13}C NMR spectrum (bottom) of **1-D** in $CDCl_3$.

Crystal structure analysis

All X-ray intensity data were measured on a Bruker D8 Venture TXS system equipped with a multilayer mirror optics monochromator and a Mo Kα rotating-anode X-ray tube (λ = 0.71073 Å). The data collections were performed at 103 K. The frames were integrated with the Bruker SAINT Software package[3]. Data were corrected for absorption effects using the Multi-Scan method (SADABS).[4] The structures were solved and refined using the Bruker SHELXTL Software Package.[5] In **A**-**1** there is a disorder, which has been described by a split model. A CH_2Cl_2 molecule (site occupation factor 0.83) shares the void with two water molecules (site occupation factors 0.17). The temperature factors of one of the water-O atoms has been improved by applying the ISOR restraint. All C-bound hydrogen atoms were calculated in positions having ideal geometry riding on their parent atoms while the water-O-bound hydrogen atoms in **A**-**1** could not be located and hence have not been considered in the refinement. The data have been deposited with the Cambridge Crystallographic Data Centre (CCDC) and can be obtained free of charge from: https://www.ccdc.cam.ac.uk/structures/. The deposition numbers are: CCDC 1853632 (**A**-**1**), CCDC 1853633 (**B**-**1**), CCDC 1853634 (**C**-**1**) and CCDC 1853635 (**D**-**1**).

Compound	**A-1** CCDC 1853632	**B-1** CCDC 1853633
net formula	$C_{21.83}H_{24.35}Cl_{1.66}O_{4.34}S$	$C_{21}H_{22}O_4S$
M_r/g mol^{-1}	446.95	370.44
crystal size/mm	0.100 × 0.090 × 0.060	0.050 × 0.040 × 0.030
T/K	103.(2)	103.(2)
radiation	MoKα	MoKα
diffractometer	'Bruker D8 Venture TXS'	'Bruker D8 Venture TXS'
crystal system	triclinic	monoclinic
space group	'P -1'	'P 1 21/n 1'
a/Å	10.6575(6)	7.9027(3)
b/Å	10.7639(6)	14.2042(4)
c/Å	10.8491(6)	16.7672(5)
α/°	108.347(2)	90
β/°	109.185(2)	97.5650(10)
γ/°	97.167(2)	90
V/Å^3	1078.94(11)	1865.76(10)
Z	2	4
calc. density/g cm^{-3}	1.374	1.319
μ/mm^{-1}	0.382	0.197
absorption correction	Multi-Scan	Multi-Scan
transmission factor range	0.86–0.98	0.95–0.99
refls. measured	11294	12557
R_{int}	0.0319	0.0375
mean σ(I)/I	0.0395	0.0426
θ range	3.291–26.370	3.341–26.373
observed refls.	3638	3095
x, y (weighting scheme)	0.0557, 0.7935	0.0334, 0.9221
hydrogen refinement	constr	constr
Flack parameter	-	-
refls in refinement	4401	3797
parameters	286	240
restraints	6	0
$R(F_{obs})$	0.0425	0.0377
$R_w(F^2)$	0.1187	0.0906
S	1.029	1.042
shift/error$_{max}$	0.001	0.001
max electron density/e Å^{-3}	0.561	0.310
min electron density/e Å^{-3}	−0.507	−0.408

Compound	**C-1** CCDC 1853634	**D-1** CCDC 1853635
net formula	$C_{21}H_{22}O_4S$	$C_{21}H_{22}O_4S$
M_r/g mol^{-1}	370.44	370.44
crystal size/mm	0.100 × 0.060 × 0.050	0.080 × 0.060 × 0.020
T/K	103.(2)	103.(2)
radiation	MoKα	MoKα
diffractometer	'Bruker D8 Venture TXS'	'Bruker D8 Venture TXS'
crystal system	monoclinic	monoclinic
space group	'P 1 21/n 1'	'P 1 21/n 1'
a/Å	8.3322(2)	13.9708(5)
b/Å	12.5124(3)	9.2553(3)
c/Å	17.6900(4)	16.1152(6)
α/°	90	90
β/°	91.6560(10)	115.0830(10)
γ/°	90	90
V/Å^3	1843.52(8)	1887.25(12)
Z	4	4
calc. density/g cm^{-3}	1.335	1.304
μ/mm^{-1}	0.199	0.194
absorption correction	Multi-Scan	Multi-Scan
transmission factor range	0.96–0.99	0.93–1.00
refls. measured	16617	11652
R_{int}	0.0402	0.0443
mean σ(I)/I	0.0361	0.0576
θ range	3.182–26.370	3.220–26.366
observed refls.	3073	3000
x, y (weighting scheme)	0.0296, 1.3194	0.0349, 1.4439
hydrogen refinement	constr	constr
Flack parameter	-	-
refls in refinement	3756	3841
parameters	240	240
restraints	0	0
$R(F_{obs})$	0.0375	0.0492
$R_w(F^2)$	0.0872	0.1236
S	1.023	1.035
shift/error$_{max}$	0.001	0.001
max electron density/e Å^{-3}	0.281	0.413
min electron density/e Å^{-3}	−0.347	−0.599

Calculated ground-state energy profile of compound 1

A relaxed optimization of the four isomeric states and all four transition state structures of compound **1** at the B3LYP/6-311G(d,p) level of theory has been conducted using the Gaussian09 Revision A.02 program package.[6] To account for solvent effects, the calculations have been carried out using the Polarizable Continuum Model (PCM) with Dichloromethane parameters. The convergence criteria have been set tight and an ultrafine integration grid was employed. A subsequent frequency analysis confirmed four structures (**A**, **B**, **C**, **D**) to be minimum structures since no imaginary frequencies have been found. All other structures were shown to be first order saddle points on the potential energy surface possessing only one imaginary vibrational mode confirming them to be transition state structures.

Isomer	G_0 (Hartree)	ΔG (Hartree)	ΔG (kcal mol^{-1})
A	-1512.468144	0.00038	0.238454
B	-1512.468524	0	0
C	-1512.466737	0.001787	1.121359
D	-1512.46594	0.002584	1.621484
TS *Z*1	-1512.421336	0.047188	29.61092
TS *Z*2	-1512.417849	0.050675	31.79904
TS *E*1	-1512.424794	0.041943	26.31963
TS *E*2	-1512.419919	0.046818	29.37874

Calculated ground state geometries - xyz coordinates

A-1				B-1			
S	-0.34224412	-0.85955564	-0.15676243	S	0.37202042	-0.85468678	0.0464537
O	-2.35891879	2.54308518	-0.37919151	O	2.38851011	2.30173794	-1.17802566
O	-0.01443832	-1.35470259	1.24509017	O	0.25514321	-1.79394325	-1.14865512
C	-2.13546864	-1.0048411	-0.36484509	C	2.13507311	-0.82915376	0.4861123
C	-2.81616603	-2.21384126	-0.43933137	C	2.79581875	-1.86175613	1.13722297
H	-2.29062517	-3.15978098	-0.38504021	H	2.26458232	-2.74020331	1.48400568
C	-4.20196733	-2.17391874	-0.58855635	C	4.17123633	-1.73361586	1.33646922
H	-4.75925168	-3.10130241	-0.64962412	H	4.71201986	-2.52099713	1.84826755
C	-4.88226798	-0.95125691	-0.66419933	C	4.86058196	-0.60229254	0.88327413
H	-5.9589926	-0.94571098	-0.78422492	H	5.92830458	-0.52487922	1.04973376
C	-4.1872535	0.24994063	-0.58554641	C	4.18565871	0.41993763	0.22372363
H	-4.69491857	1.20553733	-0.63847419	H	4.70206549	1.30178534	-0.13622945
C	-2.80033823	0.21310822	-0.42560217	C	2.80993681	0.29563967	0.02657041
C	-1.92432994	1.40408675	-0.31617925	C	1.94601594	1.29942859	-0.6434194
C	-0.49480329	0.99121471	-0.17186785	C	0.5100497	0.89304584	-0.53484819
C	0.65834714	1.70483727	-0.0709981	C	-0.65058766	1.57486477	-0.71155125
C	1.93640474	0.92167704	-0.098165	C	-1.92170191	0.80569575	-0.50001623
C	2.66744877	0.67017352	1.08371881	C	-2.61769624	0.88795262	0.72599653
C	3.85470548	-0.04938013	1.03501971	C	-3.81401618	0.20565739	0.90445444
C	4.34228191	-0.52631882	-0.19043324	C	-4.34541473	-0.56785026	-0.13884633
C	3.63387589	-0.28829602	-1.36854946	C	-3.67017418	-0.66462291	-1.35505261
H	3.98510813	-0.64850539	-2.32466158	H	-4.05273275	-1.26189649	-2.1699862
C	2.43657909	0.42606864	-1.29906333	C	-2.46329805	0.02001126	-1.51254882
C	0.77854929	3.24916983	0.00909952	C	-0.78856584	3.05754416	-1.14204933
H	1.87873078	0.60324681	-2.21126486	H	-4.36225307	0.24695631	1.83479813
H	4.42652864	-0.26611524	1.9259589	H	-1.92994593	-0.06594064	-2.45098602
C	2.24477336	3.70230609	0.18757411	C	-0.26251181	3.20256679	-2.59218361
H	2.66635474	3.35392354	1.13052724	H	-0.82971653	2.56500423	-3.2761942
H	2.88413476	3.36109169	-0.62873478	H	-0.39352494	4.23934645	-2.91640239
H	2.26701201	4.79513872	0.19497134	H	0.79268589	2.94824773	-2.66172284
C	0.2791961	3.85651573	-1.32680316	C	-0.01751021	3.98837637	-0.17756557
H	0.39757477	4.94339055	-1.28689866	H	1.05343121	3.80345806	-0.19190681
H	0.87640531	3.48721019	-2.16538319	H	-0.18390472	5.02699288	-0.47787682
H	-0.76888978	3.63349625	-1.50944455	H	-0.38870996	3.86611539	0.84230904
C	-0.025653	3.79928551	1.20918911	C	-2.26388787	3.51494494	-1.13714507
H	-1.08965722	3.59906301	1.11327559	H	-2.88234224	2.92272821	-1.81376228
H	0.34025512	3.35998855	2.13959499	H	-2.70054789	3.46834089	-0.13830494
H	0.11438217	4.8829549	1.26514138	H	-2.30360842	4.55510553	-1.4706213
O	2.12917223	1.16959711	2.22692234	C	-2.66957368	1.78076185	2.95522703
C	2.73929462	0.84036047	3.47625821	H	-2.7585696	0.80785766	3.44673021
H	2.11694948	1.30362099	4.23877357	H	-2.02676365	2.42915957	3.54664526
H	2.75801264	-0.24234409	3.6266984	H	-3.65894066	2.23680518	2.85773024
H	3.75467067	1.24216174	3.54113232	O	-2.02974426	1.65769808	1.68313689
O	1.39691128	-0.9621221	-2.121921	O	-5.52327927	-1.18532468	0.14559487
C	1.73523268	-0.79314744	-3.49803094	C	-6.12825025	-1.99537287	-0.86345885
H	0.88069522	-1.1642483	-4.0604415	H	-5.47978779	-2.830929	-1.14303672
H	1.90006555	0.26114943	-3.74054371	H	-7.04519558	-2.38023495	-0.42188224
H	2.62463884	-1.37313234	-3.76332565	H	-6.37156475	-1.40553763	-1.75228167

C-1				D-1			
S	6.1432501	2.48992564	3.69007428	S	-4.26606281	2.73862098	4.63869429
O	2.96845629	2.69647663	1.36735769	O	-1.80584007	2.53951125	1.58587816
O	7.5655751	2.44918763	3.14277592	O	-3.471515	2.20996181	5.83051111
C	5.49123802	4.15055247	3.39674146	C	-3.48435167	4.30696168	4.16708115
C	6.02500564	5.30296487	3.96051483	C	-3.64574779	5.49591642	4.8652412
H	6.89698471	5.2656935	4.60232838	H	-4.31480195	5.56585958	5.71454876
C	5.39931802	6.51498277	3.67236021	C	-2.91371402	6.60448864	4.437459
H	5.79316239	7.43186137	4.09483208	H	-3.02323252	7.54890493	4.95731426
C	4.26573515	6.56247477	2.84974496	C	-2.04029513	6.51116115	3.3473176
H	3.79394565	7.516212	2.64586668	H	-1.48319676	7.3856721	3.03323475
C	3.74617131	5.39903192	2.29430915	C	-1.88413944	5.3079983	2.66561856
H	2.87448935	5.41556233	1.65120535	H	-1.21120948	5.21654854	1.82138867
C	4.37885487	4.18479346	2.56823239	C	-2.62015838	4.200501	3.08535403
C	3.97247298	2.86342374	2.03296056	C	-2.58733728	2.85297938	2.46121849
C	4.94079463	1.7966444	2.47113369	C	-3.64953066	1.97787423	3.07254034
C	4.93615825	0.5069139	2.05312512	C	-4.12632136	0.82489201	2.54168958
C	4.00491802	0.14864125	0.93229178	C	-3.61573808	0.42264919	1.19122717
C	2.73215972	-0.40030342	1.19413067	C	-2.60327964	-0.54842413	1.05610937
C	1.8928801	-0.76081702	0.14873798	C	-2.15620091	-0.92935569	-0.20234602
C	2.30157764	-0.57242158	-1.18046404	C	-2.71222764	-0.34932114	-1.35225869
C	3.54956374	-0.01902427	-1.45766589	C	-3.71548935	0.61140473	-1.23765475
H	3.88523227	0.14458071	-2.47163122	H	-4.15945828	1.07398658	-2.10743383
C	4.38025819	0.33736693	-0.39059286	C	-4.14672166	0.98501603	0.0381169
C	5.88149494	-0.62372774	2.53128657	C	-5.20950893	-0.08738361	3.18227248
H	5.3442542	0.78325538	-0.60587613	H	-1.3756565	-1.66535076	-0.33278016
H	0.91195317	-1.18011682	0.32194015	H	-4.91835975	1.74121038	0.12869674
C	7.20686182	-0.49064002	1.73269234	C	-4.71246069	-0.62678076	4.54589193
H	7.88910167	-1.28844737	2.0414383	H	-5.48129356	-1.27567784	4.97537188
H	7.02975003	-0.60119973	0.65993373	H	-3.80463836	-1.21665209	4.40368604
H	7.68049888	0.47316429	1.91865671	H	-4.48794316	0.16135457	5.26322534
C	5.28250858	-2.01721801	2.22992462	C	-5.5236033	-1.30964317	2.29305503
H	5.99641083	-2.77775407	2.55490059	H	-5.9043542	-1.01892967	1.31244187
H	4.34717224	-2.17536421	2.76913923	H	-4.64688336	-1.94225085	2.14944354
H	5.09792332	-2.16467046	1.1656416	H	-6.29120058	-1.90979539	2.78830694
C	6.17330562	-0.57963795	4.0481998	C	-6.53316154	0.70079736	3.3514464
H	6.85289292	0.22224647	4.33200907	H	-6.43619554	1.54012593	4.03738522
H	5.25221469	-0.48579867	4.62839468	H	-6.88342183	1.08369654	2.38908495
H	6.65958416	-1.51470328	4.33739823	H	-7.30093475	0.0297373	3.74586871
O	2.40618098	-0.53004106	2.51073844	C	-1.06084692	-2.01459531	2.16860896
C	1.11834936	-1.04457519	2.85036344	O	-2.11839493	-1.05647441	2.22337645
H	1.07795097	-1.0449086	3.93767831	O	-2.19776065	-0.7988434	-2.53090029
H	0.32285732	-0.40588496	2.45581705	C	-2.70645447	-0.25014904	-3.74615633
H	0.98814292	-2.06594724	2.48027737	H	-2.53287998	0.82902584	-3.79839434
O	1.39691128	-0.9621221	-2.121921	H	-2.15802111	-0.74387366	-4.54594974
C	1.73523268	-0.79314744	-3.49803094	H	-3.77568448	-0.45499554	-3.85825002
H	0.88069522	-1.1642483	-4.0604415	H	-1.37212433	-2.92004584	1.63915071
H	1.90006555	0.26114943	-3.74054371	H	-0.17329265	-1.59341911	1.68784444
H	2.62463884	-1.37313234	-3.76332565	H	-0.83109228	-2.25989742	3.20334046

TS *Z*1				TS *Z*2			
S	1.473505	-1.54456	0.436279	S	1.420954	-1.49201	0.425891
O	2.230019	1.752004	-1.502653	O	1.961569	1.467762	-1.959731
O	1.262717	-2.682558	-0.567593	O	1.516083	-2.594815	-0.624194
C	3.235143	-1.149265	0.267346	C	3.140347	-0.874409	0.41467
C	4.263592	-1.982641	0.679426	C	4.203543	-1.481798	1.063577
H	4.067628	-2.906017	1.211102	H	4.049832	-2.293912	1.764524
C	5.57148	-1.592125	0.379771	C	5.490982	-1.015248	0.779537
H	6.399466	-2.21543	0.696369	H	6.342259	-1.45966	1.282048
C	5.822962	-0.412859	-0.328785	C	5.694331	0.008205	-0.151331
H	6.845162	-0.131578	-0.552456	H	6.701695	0.348418	-0.360176
C	4.771865	0.399868	-0.749637	C	4.613014	0.5957	-0.807368
H	4.947641	1.31179	-1.307766	H	4.754126	1.3918	-1.529062
C	3.468991	0.022385	-0.433625	C	3.329627	0.151762	-0.501229
C	2.230691	0.776649	-0.761888	C	2.049083	0.70813	-1.006268
C	1.035563	0.151617	-0.158223	C	0.891597	0.161892	-0.247386
C	-0.181253	0.807888	0.061392	C	-0.259424	0.878678	0.047199
C	-1.482939	0.110533	-0.051761	C	-1.64394	0.34589	0.11885
C	-2.785183	0.721133	-0.19046	C	-2.034728	-1.033964	0.033326
C	-3.949275	-0.038172	-0.145647	C	-3.369943	-1.420892	-0.03097
C	-3.912976	-1.430972	-0.054262	C	-4.401909	-0.482995	-0.043502
C	-2.671732	-2.072746	-0.081755	C	-4.075524	0.873821	0.000318
H	-2.585095	-3.149354	-0.111577	H	-4.831609	1.644695	-0.037934
C	-1.523279	-1.303661	-0.112716	C	-2.743095	1.239028	0.083984
C	-0.080281	2.285273	0.622886	C	-0.057449	2.425048	0.37732
H	-0.616591	-1.868926	-0.235649	H	-3.642535	-2.464151	-0.071576
H	-4.918915	0.429914	-0.220772	H	-2.562509	2.294969	0.088223
C	-0.2928	3.393843	-0.436079	C	1.412708	2.823752	0.686914
H	0.5598	3.40943	-1.113811	H	1.891773	2.119819	1.370498
H	-1.198276	3.25395	-1.015914	H	2.027813	2.936628	-0.199823
H	-0.354437	4.362121	0.071048	H	1.395433	3.797742	1.180742
C	-1.070506	2.403867	1.822883	C	-0.749355	2.713497	1.752084
H	-0.940832	3.393046	2.269025	H	-0.602433	3.768838	1.994133
H	-2.114756	2.299178	1.561061	H	-1.811573	2.505064	1.809038
H	-0.824393	1.663248	2.589044	H	-0.261741	2.125221	2.53468
C	1.290897	2.572924	1.298221	C	-0.513931	3.377255	-0.757177
H	1.568435	1.786025	2.003185	H	0.12245	3.216144	-1.628362
H	2.101305	2.720761	0.591761	H	-1.545523	3.253805	-1.079776
H	1.194113	3.50323	1.863126	H	-0.390668	4.413625	-0.428861
O	-2.854595	2.047027	-0.430759	O	-1.062473	-1.961911	0.018819
C	-4.120789	2.688795	-0.606805	C	-1.381893	-3.344856	-0.199027
H	-3.88772	3.734201	-0.796924	H	-1.949802	-3.746569	0.643765
H	-4.65774	2.270923	-1.461834	H	-1.947153	-3.466537	-1.125814
H	-4.733599	2.608731	0.294963	H	-0.416813	-3.832927	-0.286994
O	-5.108838	-2.049968	-0.001212	C	-6.759168	-0.070531	-0.116829
C	-5.143213	-3.481888	0.05929	H	-7.650389	-0.692231	-0.161127
H	-6.196279	-3.745346	0.123714	H	-6.779652	0.53499	0.793156
H	-4.70974	-3.922489	-0.842062	H	-6.722036	0.578884	-0.995428
H	-4.617408	-3.849167	0.944197	O	-5.65461	-0.982323	-0.103679

TS *E*1				TS *E*2			
S	2.26581	-1.047169	-0.922515	S	-2.31697	1.405964	-0.550446
O	1.057293	1.725343	1.603998	O	-1.47041	-1.099952	2.169193
O	1.872861	-0.786118	-2.373685	O	-1.790912	1.77734	-1.926098
C	3.515554	0.173529	-0.458551	C	-3.218884	-0.147739	-0.710449
C	4.818318	0.193395	-0.937098	C	-4.27335	-0.355848	-1.591329
H	5.174636	-0.5531	-1.637105	H	-4.570968	0.403294	-2.304455
C	5.664439	1.201964	-0.471897	C	-4.937087	-1.579346	-1.520797
H	6.69053	1.240911	-0.818229	H	-5.757816	-1.781852	-2.19875
C	5.203408	2.155747	0.442462	C	-4.5653	-2.544024	-0.57424
H	5.878213	2.927269	0.794388	H	-5.104016	-3.483345	-0.53222
C	3.888247	2.124423	0.900797	C	-3.516063	-2.308837	0.308536
H	3.512937	2.858956	1.603337	H	-3.223124	-3.045513	1.046857
C	3.037653	1.127181	0.42687	C	-2.820116	-1.102859	0.211968
C	1.59456	0.985499	0.777906	C	-1.660798	-0.678978	1.038705
C	1.025949	-0.197328	0.137843	C	-0.977933	0.491249	0.424249
C	-0.228625	-0.827923	0.276774	C	0.279397	1.057456	0.459528
C	-1.457223	-0.051989	0.087018	C	1.535559	0.293403	0.224299
C	-2.800305	-0.547869	-0.125242	C	1.807956	-1.062856	0.576577
C	-3.882217	0.320807	-0.216965	C	2.986403	-1.692669	0.186557
C	-3.713071	1.706201	-0.185028	C	3.93143	-1.031576	-0.601835
C	-2.415195	2.231527	-0.114299	C	3.685024	0.283211	-1.001701
H	-2.230057	3.295102	-0.155072	C	2.519233	0.905208	-0.576161
C	-1.351909	1.362498	-0.014426	C	0.419219	2.618061	0.722843
C	-0.21255	-2.333827	0.727845	H	4.371407	0.824447	-1.636757
H	-4.884898	-0.053623	-0.35569	H	3.195373	-2.711529	0.477851
H	-0.376057	1.806351	0.022278	H	2.351771	1.907033	-0.9314
C	-0.451437	-3.331824	-0.430286	C	-0.771671	3.100183	1.597094
H	-0.543848	-4.341842	-0.019531	H	-1.711924	3.166389	1.053166
H	-1.347067	-3.107803	-0.999962	H	-0.920579	2.442877	2.456685
H	0.402541	-3.330399	-1.112278	H	-0.547679	4.102847	1.968054
C	-1.234333	-2.497896	1.893071	C	0.498043	3.547495	-0.515808
H	-0.955303	-1.84567	2.724985	H	0.374415	4.58128	-0.18008
H	-2.26259	-2.299717	1.623199	H	1.458647	3.497814	-1.029191
H	-1.176666	-3.529547	2.249907	H	-0.283256	3.320926	-1.23945
C	1.131217	-2.733854	1.402579	C	1.667651	2.844442	1.621185
H	1.952722	-2.842783	0.700635	H	1.634694	2.206314	2.508327
H	1.421327	-2.017733	2.174232	H	2.610641	2.661963	1.111256
H	0.99001	-3.705382	1.882422	H	1.663693	3.884646	1.956552
C	-4.284461	-2.397701	-0.579305	O	0.878592	-1.688868	1.313105
O	-2.982029	-1.871023	-0.302287	C	1.062169	-3.044411	1.714093
O	-4.838119	2.43702	-0.272058	H	1.16639	-3.704764	0.848216
C	-4.741381	3.868821	-0.272305	H	1.935165	-3.147726	2.364994
H	-4.17994	4.221945	-1.140602	H	0.161478	-3.298474	2.267865
H	-5.765976	4.228182	-0.328764	O	5.033532	-1.749322	-0.924824
H	-4.275046	4.228809	0.647793	C	6.03967	-1.132732	-1.733534
H	-4.139351	-3.468836	-0.699778	H	6.81802	-1.882744	-1.855815
H	-4.969639	-2.211738	0.251386	H	5.642713	-0.855538	-2.714094
H	-4.689288	-1.974702	-1.501641	H	6.456731	-0.250349	-1.240155

References

1. A. Gerwien, T. Reinhardt, P. Mayer, H. Dube, Synthesis of Double-Bond Substituted Hemithioindigo Photoswitches. *Org. Lett.* **2018**, *1*, 232-235.

2. U. Megerle, R. Lechner, B. König, E. Riedle, Laboratory apparatus for the accurate, facile and rapid determination of visible light photoreaction quantum yields. *Photochem. Photobiol. Sci.* **2010**, *9*, 1400-1406.

3. Bruker, *SAINT*. Bruker AXS Inc., Madison, Wisconsin, USA, (2012).

4. G. M. Sheldrick, *SADABS*. University of Göttingen, Germany, (1996).

5. G. M. Sheldrick, *SHELXT* – Integrated space-group and crystal-structure determination. *Acta Cryst.* **2015**, *A71*, 3-8.

6. Gaussian 09, Revision A.02, M. J. Frisch, G. W. Trucks, H. B. Schlegel, G. E. Scuseria, M. A. Robb, J. R. Cheeseman, G. Scalmani, V. Barone, G. A. Petersson, H. Nakatsuji, X. Li, M. Caricato, A. Marenich, J. Bloino, B. G. Janesko, R. Gomperts, B. Mennucci, H. P. Hratchian, J. V. Ortiz, A. F. Izmaylov, J. L. Sonnenberg, D. Williams-Young, F. Ding, F. Lipparini, F. Egidi, J. Goings, B. Peng, A. Petrone, T. Henderson, D. Ranasinghe, V. G. Zakrzewski, J. Gao, N. Rega, G. Zheng, W. Liang, M. Hada, M. Ehara, K. Toyota, R. Fukuda, J. Hasegawa, M. Ishida, T. Nakajima, Y. Honda, O. Kitao, H. Nakai, T. Vreven, K. Throssell, J. A. Montgomery, Jr., J. E. Peralta, F. Ogliaro, M. Bearpark, J. J. Heyd, E. Brothers, K. N. Kudin, V. N. Staroverov, T. Keith, R. Kobayashi, J. Normand, K. Raghavachari, A. Rendell, J. C. Burant, S. S. Iyengar, J. Tomasi, M. Cossi, J. M. Millam, M. Klene, C. Adamo, R. Cammi, J. W. Ochterski, R. L. Martin, K. Morokuma, O. Farkas, J. B. Foresman, and D. J. Fox, Gaussian, Inc., Wallingford CT, (2016).

7. Green light powered molecular state motor enabling eight-shaped unidirectional rotation

Studies of various four state HTIs revealed, that increasing the energy barrier associated with thermal SBR, which can be done by increasing the steric demand of the *ortho*-substituent at the stilbene part of the HTI, leads to a preference of DBI and suppression of HT and SBR photoreactions. However, by introducing strong electron donating groups the energy barrier associated with thermal DBI is lowered resulting in a hitherto not described new coupled isomerization, i.e. a thermal Hula-Twist (HT) in polar solvents. By introducing the strong electron donating group julolidine and a methyl substituent at *ortho*-position of the stilbene part, it was thus possible to design an HTI motor operating via alternating photochemical DBI and thermal HT steps. The rotation cycle consists of DBI from **A** to **C**, thermal HT from **C** to **B** followed by DBI to **D** and subsequent thermal HT to the starting point **A**. In a complete rotation cycle the double-bond rotates two times by 360° and the motion of one methyl substituent at the stilbene part against the thioindigo part follows the path of an eight shape.

License

nature COMMUNICATIONS

ARTICLE

https://doi.org/10.1038/s41467-019-12463-4 OPEN

Green light powered molecular state motor enabling eight-shaped unidirectional rotation

Aaron Gerwien[1], Peter Mayer[1] & Henry Dube[1*]

Molecular motors convert external energy into directional motions at the nano-scales. To date unidirectional circular rotations and linear motions have been realized but more complex directional trajectories remain unexplored on the molecular level. In this work we present a molecular motor powered by green light allowing to produce an eight-shaped geometry change during its unidirectional rotation around the central molecular axis. Motor motion proceeds in four different steps, which alternate between light powered double bond isomerizations and thermal hula-twist isomerizations. The result is a fixed sequence of populating four different isomers in a fully unidirectional trajectory possessing one crossing point. This motor system opens up unexplored avenues for the construction and mechanisms of molecular machines and will therefore not only significantly expand the toolbox of responsive molecular devices but also enable very different applications in the field of miniaturized technology than currently possible.

[1] Department of Chemistry and Center for Integrated Protein Science CIPSM, Ludwig Maximilians-Universität München, Butenandtstrasse 5-13, 81377 München, Germany. *email: henry.dube@cup.uni-muenchen.de

Synthetic molecular motors are miniaturized versions of macroscopic motors and convert external energy input into directional motions at the molecular level. Since the first examples have been developed by the groups of Feringa[1] and Leigh[2] in the late 1990s and early 2000s, a growing number of different systems have been established. These include chemically driven motors as well as light-driven ones[3–16]. We have contributed to the field with visible light-driven molecular motors[17–21], which are based on the hemithioindigo (HTI) chromophore[22–32]. Most recently we have introduced a light-only powered molecular motor enabling stepwise directional motions without thermal ratcheting in the ground state[33]. To this end, the hula-twist (HT) photoreaction[34–38], as recently experimentally evidenced by our group[38], was employed in combination with simple double-bond isomerization (DBI) and single bond rotation (SBR) photoreactions. The HT motion was originally proposed as volume conserving photoreaction for the isomerization of retinal inside the opsin protein framework and proceeding as fully concerted process wherein a double bond and adjacent single bond rotate at the same time after photoexcitation[34–38]. According to Saltiel the HT photoreaction proceeds stepwise with the double-bond photoisomerizing first in the excited state and the single bond rotating afterwards in a hot ground-state reaction[37]. The term "double-bond isomerization (DBI)" refers here to the sole *E*–*Z* isomerization of the central double bond. This reaction is also called one-bond-flip (OBF) or one-bond-twist (OBT) in the literature[35,37].

Despite this great progress in the development of molecular motors, the types of directional geometry changes available at present are almost exclusively simple circular rotations or linear locomotions. More complex directional molecular motions have only been realized in a combinatorial multi-switch fashion resulting in flexible and thus less defined geometrical changes in each motion step[39,40]. Herein, we present a simple molecular setup **1** that allows realization of a very precise and repetitive eight-shaped geometry change during unidirectional rotation of one molecular fragment around the other within a single switch architecture. To this end, an unusual type of thermal HT motion is employed alternating with photoinduced DBI. The term "thermal hula-twist (HT)" motion refers here to a 180° rotation of both the double bond and the adjacent single bond in the ground state leading to concomitant *E*–*Z* isomerization, as well as atropisomerization without observable intermediates.

Results

Ground-state properties of motor 1. Motor **1** is derived from the parent HTI chromophore, and is equipped with a permanent sulfoxide stereocenter. In addition, a chiral axis is established via introduction of a nonsymmetric julolidine unit, the atropisomerization of which is slowed down by increased sterical hindrance in the molecule. Therefore, all four different diastereomeric states of **1** — denoted **A** to **D** as shown in Fig. 1a — can be isolated, characterized, and their photoreactions as well as thermal reactions can be scrutinized individually. Synthesis of **1** follows an established protocol for the generation of sterically hindered, fourfold double-bond substituted HTI photoswitches[30]. Isolation of all individual racemic isomers **A** to **D** was achieved using HPLC separation, and their structures in the crystalline state were determined (Fig. 1b) to enable assignment of the corresponding solution spectra (Supplementary Figs. 1–4).

When heating solutions of pure isomers **A**, **B**, **C**, and **D** in different solvents, their thermal interconversions could be monitored directly. Interestingly, these isomers do not randomly interconvert at elevated temperatures but undergo a HT-like combined 180° rotation of both the central double bond and the adjacent single bond, which establishes the chiral axis. This behavior is unknown to the best of our knowledge, and also distinctively different to related HTI molecules reported earlier, showing first only SBR at elevated temperatures and after further temperature increase interconversion between all isomers[33,38]. In this case, isomer **D** thermally interconverts predominantly to **A** (e.g., in 93% at 27 °C in acetonitrile-d_3/D_2O (8/2) solution) in the thermal equilibrium. Likewise, **C** predominantly converts to **B** (e.g., in 87% at 60 °C in acetonitrile-d_3/D_2O (8/2) solution) in the thermal equilibrium. Again, this behavior is different to related oxidized HTI systems, where thermal equilibria with substantial fractions of different isomers being present are established[17,33,38]. From first-order kinetic analyses of thermal isomer interconversions and observed thermal equilibria, the ground-state energy profiles of **1** could experimentally be quantified in acetonitrile-d_3/D_2O (8/2), 1,2-dichlorobenzene-d_4 (12DCB-d_4), and DMSO-d_6 solutions (Fig. 1c, d). In 12DCB-d_4, it could be established that isomer **A** is the global minimum structure. In more apolar solvents such as cyclohexane or 12DCB-d_4 energy barriers for thermal HT-bond rotations are considerably increased (by about 6 kcal/mol in 12DCB-d_4) and more similar to the energy barriers for the simpler one-bond rotations. As a result higher temperatures are required for isomer interconversion and a mixture of mainly **A** and **B** isomers are obtained in thermal equilibrium (Supplementary Figs. 5–14 and Supplementary Tables 1–3).

The theoretical description on the ω-B97XD/6-311G(d,p) level of theory (Fig. 1d; Supplementary Fig. 26, Supplementary Tables 5–9) was found to be in good agreement with these experiments. However, the calculated energy barriers are in general higher than in the experiments. The calculations predict four possible transition states for the thermal HT reaction, showing only one imaginary vibrational mode. In all of them, the double bond is twisted by 90° and is now orthogonal to the thioindigo part of the molecule. At the same time, the adjacent single bond is also twisted by 90° and receives a large double-bond character. Given the similar degree of rotation of both adjacent bonds in the transition states, a fully concerted thermal HT-like rotation is predicted from the theoretical description. From the four possibilities, two transition states with the methyl group facing away from the tertiary butyl group are energetically significantly favored. As the experiments established two distinct and non-crossing thermal HT isomerizations (**C** to **B** with the larger energy barrier and **D** to **A** with the lower energy barrier), the two theoretically found transition states could be assigned to a particular process (Supplementary Fig. 26). In the transition state reached from isomer **C**, the julolidine rotated with its methyl group below the thioindigo fragment residing on the opposite face of the sulfoxide oxygen. This motion is then continued by further 90° rotation around the single and double bond leading to isomer **B**. The thermal HT reaction of isomer **D** leads to a transition state with the julolidine rotated with its methyl group above the thioindigo part residing on the same face of the sulfoxide oxygen. Again, this motion is completed by further 90° rotation around the former single and double bonds leading to isomer **A** (see also Supplementary Movies 1–4).

Photoreactions of motor 1. After establishing the thermal reactions of **1**, its photoreactions were analyzed separately for each isomer **A**, **B**, **C**, and **D** at 25 °C in cyclohexane-d_{12} (Fig. 2a–d) and 12DCB solutions. In more polar solvents, the photoreactions are strongly reduced rendering them impractical. Three different photoreactions are possible for each isomer: a simple DBI, a SBR around the chiral axis, and a combined HT photoreaction where both adjacent bonds are rotated. Since

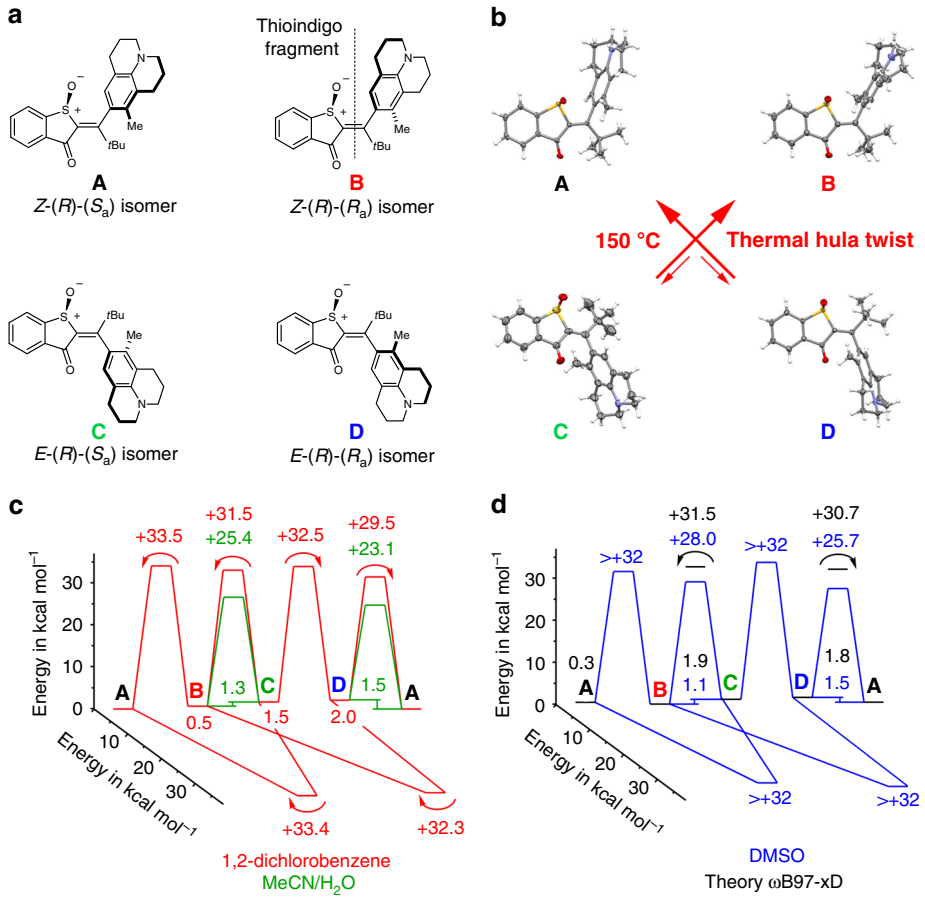

Fig. 1 Structures of isomers **A** to **D** of motor **1** and ground-state properties. **a** Schematic representation of the molecular structures of **A** to **D**. **b** Structures of isomers **A** to **D** in the crystalline state and thermal interconversion in solution. **c** Ground-state energy profile of **1** experimentally determined in 12DCB-d_4 (red) and in acetonitrile-d_3/D_2O (8/2, green). **d** Ground-state energy profile of **1** calculated at the ω-B97XD/6-311 G(d,p) PCM(DMSO) level of theory (black) and experimentally determined in DMSO-d_6 (blue)

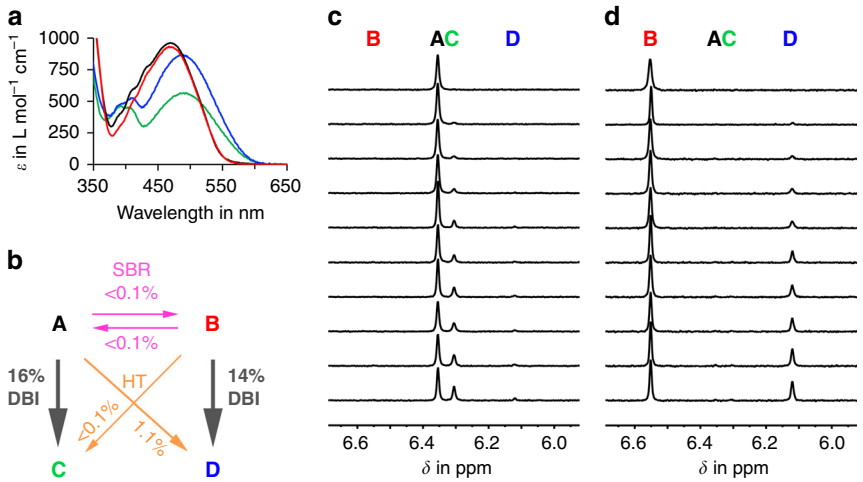

Fig. 2 Photoreactions of HTI **1** during 520 nm irradiation. **a** Molar absorption coefficients in cyclohexane solution. **b** Experimental quantum yields determined for the photoreactions of isomers **A** and **B** in cyclohexane-d_{12} solution at 27 °C under 520 nm irradiation. **c** Beginning of the photoreaction of isomer **A** in cyclohexane-d_{12} at 27 °C. **d** Beginning of the photoreaction of isomer **B** in cyclohexane-d_{12} at 27 °C

thermal isomer interconversion is halted completely at 25 °C, the primary photoproducts are directly observed in the irradiation experiments and are not obscured by fast thermal follow-up isomerizations. Quantum yields for individual transformations during 520 nm irradiation were measured in cyclohexane-d_{12} and 12DCB (see Fig. 2b; Supplementary Figs. 18–21, Supplementary Table 4). Again, stark differences to previously reported related HTIs, which do in fact undergo all three photoreactions for each isomer[33,40], are observed. In this case, DBI is performed with very high selectivity leading to efficient photoconversion of **A** to **C** as

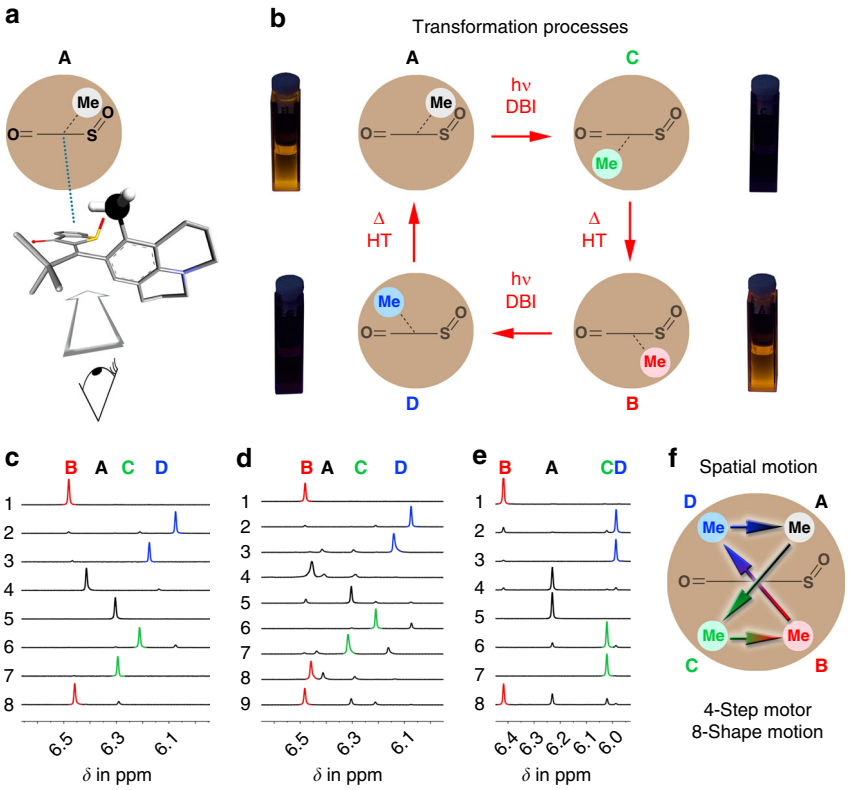

Fig. 3 Molecular motor properties of **1**. **a** Schematic representation of the geometry of **A**. **b** Four-step process of the motor motion and associated fluorescence changes. **c** Individual steps of motor operation followed by ^{1}H NMR spectroscopy, (1) **B** in cyclohexane-d_{12}, (2) after 520 nm irradiation, (3) **D** in acetonitrile-d_3/D_2O (8/2), (4) after heating to 27 °C, (5) **A** in cyclohexane-d_{12}, (6) after 520 nm irradiation, (7) **C** in acetonitrile-d_3/D_2O (8/2), (8) after heating to 60 °C. **d** One full cycle of motor operation followed by ^{1}H NMR spectroscopy, (1) **B** in cyclohexane-d_{12}, (2) after 520 nm irradiation, (3) after solvent change to acetonitrile-d_3/D_2O (8/2), (4) after heating to 60 °C, (5) after solvent change to cyclohexane-d_{12}, (6) after irradiation with 520 nm, (7) after solvent change to acetonitrile-d_3/D_2O (8/2), (8) after heating to 60 °C, (9) after solvent change to cyclohexane-d_{12}. **e** Individual steps of autonomous motor operation followed by ^{1}H NMR spectroscopy in 12DCB-d_4, (1) pure **B**, (2) after 520 nm irradiation, (3) pure **D**, (4) after heating to 130 °C, (5) pure **A**, (6) after 520 nm irradiation, (7) pure **C**, (8) after heating to 130 °C. **f** Positional changes of the methyl group with respect to the static thioindigo fragment during one full cycle of directional motion

well as of **B** to **D** while all other photoreactions are at least one order of magnitude less efficient. The corresponding backward photoreactions of **C** and **D** are even less efficient as neither **A** or **B** photoproducts were observed when irradiating pure **C** or **D** and can thus be regarded as non-interfering. Consequently, strong photoenrichment of **C** and **D** is possible in the photostationary state (pss, see Fig. 3; Supplementary Figs. 18–21, Supplementary Table 4).

Discussion

Taking both thermal interconversions and photoreactions into account, a repetitive unidirectional motion of HTI **1** can be established in four distinct steps (Fig. 3a, b). Every individual step was first conducted separately starting from the respective pure isomer to determine its completeness (see Fig. 3c and Supplementary Fig. 23). Afterward, the whole sequence was conducted in a row starting from pure isomer **B** (see Fig. 3d and Supplementary Fig. 22). The first step consists of irradiation of isomer **B** in cyclohexane-d_{12} with 520 nm light resulting in DBI and enrichment of isomer **D** to 86% in the pss. Second a solvent change to acetonitrile-d_3/D_2O (8/2) solution and subsequent heating to 60 °C for 3 min leads to population of isomer **A** in 94% via thermal HT. Another solvent change back to cyclohexane-d_{12} and irradiation with 520 nm results in DBI of **A** to yield 86% of **C**. A final solvent change to acetonitrile-d_3/D_2O (8/2) solution and subsequent heating to 60 °C for 120 min results again in thermal HT to populate the starting isomer **B** in 88%. The overall process therefore interconverts all four isomers of **1** into each other in a fixed sequence that does not contain "backwards motions". When this sequence is done within one experiment in a row enrichment of individual isomers in each step is slightly less complete as the minor isomers produced add up (see Supplementary Fig. 22). In this case, 63% of the molecules performed a full rotation while the other molecules did not complete the cycle as every step proceeds only with conversions of about 90% on average. Repetitive solvent changes were employed to maximize the efficiencies of each individual step in the sequence. However, using 12DCB as solvent allows to continuously power the directional motion at high temperatures of 130 °C without the need of solvent changes (Fig. 3e). 12DCB represents a good compromise between solvent polarity and high boiling point rendering photoisomerizations as well as thermal HT reactions selective and efficient enough to warrant full motor operation (Supplementary Figs. 24, 25).

To quantify unidirectionality, the selectivity of each thermal and photoreaction has to be determined. The selectivity for the thermal steps in acetonitrile-d_3/D_2O (8/2) solution can be considered as 100%, as the barriers for the other rotations are much higher and only one product isomer is formed. The photoreaction of **B** in cyclohexane-d_{12} occurs with 92% selectivity to the **D** isomer, while also 8% **C** is formed in the pss. The photoreaction of **A** proceeds with 89% selectivity leading to the **C** isomer, while also 11% **D** is formed. The total degree of unidirectionality is therefore 82% when changing solvents. In 12DCB, thermal steps

become less selective and the degree of unidirectionality is lowered to 47%.

Next, we visualize the geometry changes occurring during this four-step process of the directional motion. HTI motor **1** establishes the fixed isomer sequence **ACBD** as shown in Fig. 3b. The clearest picture emerges when regarding the thioindigo fragment as static while the julolidine moiety represents the revolving unit. The most obvious changes are then seen for the *ortho*-methyl group of the julolidine moiety, which follows an eight-shaped spatial change during the full directional motion with respect to the static fragment (Fig. 3f). At present, it is not possible to elucidate the exact full trajectory of the directional motion as the DBI steps can either occur clockwise or counterclockwise in the photoisomerization steps. It seems, however, likely that one trajectory will be favored given the asymmetry of the molecule. For the thermal HT motions, our quantum chemical calculations clearly show that these combined rotations occur on opposite faces of the thioindigo fragment when starting from either **C** or **D** (see Supplementary Fig. 26). Only four possible trajectories remain in total, which are presented in Supplementary Movies 1–4. It is clear that all of them are in no case simple circular rotations but follow more complex directional pathways that unequivocally include one crossing point and therefore form a directional eight-shaped path. Furthermore, the remaining possibilities do not cancel each other out ensuring overall directionality if the motor is driven continuously and one-directional cycle **ACBD** is followed by another and so on. Currently, it is not possible to make a clear assertion whether one eight shape is preferred over the others.

An additional benefit of HTI motor **1** is the possibility of photonic readout for its operational state. Only isomers **A** and **B** show yellow fluorescence, while isomers **C** and **D** remain non-emissive in cyclohexane (Fig. 3b). Therefore, the stepwise motion can be followed via appearing and disappearing fluorescence offering interesting possibilities for i.a. online-monitoring of molecular motor operation (e.g., determination of the endpoint of the irradiation step) or photonic device building[41–47].

In summary, we present herein a molecular motor allowing the realization of a well-defined repetitive eight-shaped geometry change during its directional motion. Motor **1** is based on the HTI chromophore endowed with a sulfoxide stereocenter and a sterically hindered chiral axis. The unidirectional motion is powered by green light and proceeds in four distinct steps alternating two DBI photoreactions with two thermal HT reactions. Isomer interconversion can be followed visually by associated fluorescence changes. In 12DCB solution, the directional motion can be driven continuously at high temperatures. With this type of molecular machine, more complex unidirectional trajectories than purely circular or linear motions can now be generated at the molecular level offering unique potential for future nanomachinery and controllable molecular behavior.

Methods

Synthesis. The synthesis of **1** from commercially available reagents took place over five linear steps (seven in total) with an overall yield of 10%. All synthetic procedures and spectroscopic characterizations of **A**-**1**, **B**-**1**, **C**-**1**, and **D**-**1** as well as of synthetic intermediates are given in the Supplementary Methods. Reagents and solvents were obtained from abcr, Acros, Fluka, Merck, Sigma-Aldrich, or TCI in the qualities puriss., p.a., or purum and used as received. Technical solvents were distilled before use for column chromatography and extraction on a rotary evaporator (Heidolph Hei VAP Value, vacuubrand CVC 3000). Reactions were monitored on Merck Silica 60 F254 TLC plates. Detection was done by irradiation with UV light (254 nm or 366 nm). Column chromatography was performed with silica gel 60 (Merck, particle size 0.063–0.200 mm) and distilled technical solvents. ^{1}H NMR and ^{13}C NMR spectra were measured on a Varian Mercury 200 VX, Varian 300, Inova 400, Varian 600 NMR, or Bruker Avance III HD 800 MHz spectrometer at 23 °C. Deuterated solvents were obtained from Cambridge Isotope Laboratories or Eurisotop and used without further purification. Residual solvent signals in the ^{1}H and ^{13}C NMR spectra were used as internal reference. For ^{1}H NMR, $CDCl_3$ = 7.26 ppm, CD_2Cl_2 = 5.32 ppm, benzene-d_6 = 7.16 ppm, $(CD_3)_2SO$ = 2.50 ppm, 1,2-dichlorobenzene-d_4 = 6.93. For ^{13}C NMR, $CDCl_3$ = 77.16 ppm. The resonance multiplicity is indicated as s (singlet), d (doublet), t (triplet), q (quartet), and m (multiplet). The chemical shifts are given in parts per million (ppm) on the delta scale (δ). The coupling constant values (J) are given in hertz (Hz). Electron impact (EI) mass spectra were measured on a Finnigan MAT95Q or on a Finnigan MAT90 mass spectrometer. Electronspray ionization (ESI) mass spectra were measured on a Thermo Finnigan LTQ-FT. The most important signals are reported in m/z units with M as the molecular ion. Elemental analysis were performed in the micro analytical laboratory of the LMU department of chemistry on an Elementar Vario EL apparatus. Infrared spectra were recorded on a Perkin Elmer Spectrum BX-FT-IR instrument equipped with a Smith DuraSamplIR II ATR-device. Transmittance values are qualitatively described by wavenumber (cm^{-1}) as very strong (vs), strong (s), medium (m) and weak (w). UV/Vis spectra were measured on a Varian Cary 5000 spectrophotometer. Fluorescence spectra were measured on a Varian Eclipse spectrophotometer. The spectra were recorded in a quartz cuvette (1 cm). Solvents for spectroscopy were obtained from VWR and Merck. Absorption wavelength (λ) are reported in nm, and the molar absorption coefficients (ε) in L mol^{-1} cm^{-1}. Melting points (M.p.) were measured on a Stuart SMP10 melting point apparatus in open capillaries, and are not corrected.

Thermal isomerizations. Amberized NMR tubes were charged with 1 mg to 2.5 mg of the respective isomer of **A**-**1**, **B**-**1**, **C**-**1**, and **D**-**1** and 0.7 mL of 1,2-dichlorobenzene-d_4, DMSO-d_6, or MeCN-d_4/D_2O: 8/2. Subsequently the NMR tubes were heated to the appropriate temperatures in a stirred oil bath for isomerization reactions to occur, and the kinetics were followed by integration of the corresponding signals in the ^{1}H NMR measurements in defined time intervals. The equilibrium ratio of isomers was obtained after prolonged heating until the integration values did not change anymore. The obtained experimental data, required equations, and the resulting energy barriers are shown in Supplementary Methods, Supplementary Figs. 5–14, and Supplementary Tables 1–3.

Quantum yield measurements. A stock solution of the respective isomer **A**-**1** and **B**-**1** in 12DCB or cyclohexane (10 mL, 0.87 mM–1.01 mM) was prepared. One milliliter of the stock solutions was transferred into a quartz cuvette (1 cm) and irradiated with a focused light beam of a 520 nm LED within the published instrumental setup from the group of E. Riedle[48]. The number of absorbed photons over time $n(h\nu)$ was measured directly at the thermal photometer of the instrument. After defined time intervals, the solutions were transferred form the quartz cuvette into an amberized NMR tube, the solvent was removed in vacuo and replaced with CD_2Cl_2 or benzene-d_6. The concentrations of photoproducts were obtained by integrations of the corresponding signals in the ^{1}H NMR spectra. This procedure was repeated up to ten times with different irradiation times allowing to average over all measurements. The obtained experimental data, required equations, and the resulting quantum yields are shown in the Supplementary Methods, Supplementary Figs. 18–21, and Supplementary Table 4.

Motor operation followed by NMR spectroscopy. With changing solvents: Isomer **B**-**1** (1 mg) was dissolved in cylcohexane-d_{12} and a ^{1}H NMR spectrum was recorded (starting point, **B** isomer). Afterward, the NMR tube was irradiated with a 520 nm LED until the fluorescence vanished and again a ^{1}H NMR spectrum was recorded (motor step 1, mainly **D** isomer was obtained). Cylcohexane-d_{12} was removed in vacuo, and replaced with acetonitrile-d_3/D_2O (8/2) and immediately a ^{1}H NMR spectrum was recorded (motor step 1, mainly **D** isomer present). After heating to 60 °C for a few minutes, another ^{1}H NMR spectrum was recorded (motor step 2, mainly **A** isomer was obtained). Acetonitrile-d_3/D_2O (8/2) was removed in vacuo and replaced with cylcohexane-d_{12} and a ^{1}H NMR spectrum was recorded (motor step 2, mainly **A** isomer present). The NMR tube was irradiated with a 520 nm LED until the fluorescence vanished and a ^{1}H NMR spectrum was recorded (motor step 3, mainly **C** isomer was obtained). Cylcohexane-d_{12} was removed in vacuo and replaced with acetonitrile-d_3/D_2O (8/2), and immediately a ^{1}H NMR spectrum was recorded (motor step 3, mainly **C** isomer present). After heating to 60 °C for a few minutes, another ^{1}H NMR spectrum was recorded (motor step 4, mainly **B** isomer was obtained, starting point was reached again). Without changing solvent for autonomous operation: Isomer **B**-**1** (1 mg) was dissolved in 12DCB and one drop of benzene-d_6 for easier locking and shimming was added and a ^{1}H NMR spectrum was recorded (starting point, **B** isomer). Afterward, the NMR tube was irradiated with a 520 nm LED, and again a ^{1}H NMR spectrum was recorded (motor step 1, mainly **D** isomer was obtained). After heating to 150 °C, another ^{1}H NMR spectrum was recorded (motor step 2, mainly **A** isomer was obtained). The NMR tube was irradiated again with a 520 nm LED and a ^{1}H NMR spectrum was recorded (motor step 3, mainly **C** isomer was obtained). After heating to 150 °C, another ^{1}H NMR spectrum was recorded (motor step 4, mainly **B** isomer was obtained, the starting point was reached again). The obtained ^{1}H NMR spectra after all steps and the corresponding ratios of the isomers are shown in Supplementary Figs. 22–25.

Data availability

All data that support the findings of this study are available from the Supplementary Information or from the corresponding author H. D. upon reasonable request. The X-ray crystallographic coordinates for the structures **A-1** to **D-1** reported in this study have been deposited at the Cambridge Crystallographic Data Centre (CCDC), under CCDC numbers 1910546 (**A-1**), 1910547 (**B-1**), 1910548 (**C-1**), and 1910549 (**D-1**). These data can be obtained free of charge from the Cambridge Crystallographic Data Centre via www.ccdc.cam.ac.uk/data_request/cif.

Received: 12 July 2019; Accepted: 10 September 2019;
Published online: 01 October 2019

References

1. Koumura, N., Zijlstra, R. W. J., van Delden, R. A. & Feringa, B. L. Light-driven monodirectional molecular rotor. *Nature* **401**, 152–155 (1999).
2. Hernandez, J. V., Kay, E. R. & Leigh, D. A. A reversible synthetic rotary molecular motor. *Science* **306**, 1532–1537 (2004).
3. Fletcher, S. P., Dumur, F., Pollard, M. M. & Feringa, B. L. A reversible, unidirectional molecular rotary motor driven by chemical energy. *Science* **310**, 80–82 (2005).
4. Kistemaker, H. A., Stacko, P., Visser, J. & Feringa, B. L. Unidirectional rotary motion in achiral molecular motors. *Nat. Chem.* **7**, 890–896 (2015).
5. Kassem, S. et al. Artificial molecular motors. *Chem. Soc. Rev.* **46**, 2592–2621 (2017).
6. Roke, D., Wezenberg, S. J. & Feringa, B. L. Molecular rotary motors: Unidirectional motion around double bonds. *Proc. Natl Acad. Sci. USA* **115**, 9423–9431 (2018).
7. Kay, E. R., Leigh, D. A. & Zerbetto, F. Synthetic molecular motors and mechanical machines. *Angew. Chem. Int. Ed.* **46**, 72–191 (2007).
8. Barrell, M. J., Campana, A. G., von Delius, M., Geertsema, E. M. & Leigh, D. A. Light-driven transport of a molecular walker in either direction along a molecular track. *Angew. Chem. Int. Ed.* **50**, 285–290 (2011).
9. Erbas-Cakmak, S., Leigh, D. A., McTernan, C. T. & Nussbaumer, A. L. Artificial molecular machines. *Chem. Rev.* **115**, 10081–10206 (2015).
10. Wilson, M. R. et al. An autonomous chemically fuelled small-molecule motor. *Nature* **534**, 235–240 (2016).
11. Erbas-Cakmak, S. et al. Rotary and linear molecular motors driven by pulses of a chemical fuel. *Science* **358**, 340–343 (2017).
12. Harris, J. D., Moran, M. J. & Aprahamian, I. New molecular switch architectures. *Proc. Natl Acad. Sci. USA* **115**, 9414–9422 (2018).
13. Tierney, H. L. et al. Experimental demonstration of a single-molecule electric motor. *Nat. Nanotechnol.* **6**, 625–629 (2011).
14. Greb, L. & Lehn, J. M. Light-driven molecular motors: imines as four-step or two-step unidirectional rotors. *J. Am. Chem. Soc.* **136**, 13114–13117 (2014).
15. Greb, L., Eichhofer, A. & Lehn, J. M. Synthetic molecular motors: thermal N inversion and directional photoinduced CN bond rotation of camphorquinone imines. *Angew. Chem. Int. Ed.* **54**, 14345–14348 (2015).
16. Ragazzon, G., Baroncini, M., Silvi, S., Venturi, M. & Credi, A. Light-powered autonomous and directional molecular motion of a dissipative self-assembling system. *Nat. Nanotechnol.* **10**, 70–75 (2015).
17. Guentner, M. et al. Sunlight-powered kHz rotation of a hemithioindigo-based molecular motor. *Nat. Commun.* **6**, 8406 (2015).
18. Huber, L. A. et al. Direct observation of hemithioindigo-motor unidirectionality. *Angew. Chem. Int. Ed.* **56**, 14536–14539 (2017).
19. Wilcken, R. et al. Complete mechanism of hemithioindigo motor rotation. *J. Am. Chem. Soc.* **140**, 5311–5318 (2018).
20. Hoffmann, K., Mayer, P. & Dube, H. A hemithioindigo molecular motor for metal surface attachment. *Org. Biomol. Chem.* **17**, 1979–1983 (2019).
21. Uhl, E., Thumser, S., Mayer, P. & Dube, H. Transmission of unidirectional molecular motor rotation to a remote biaryl axis. *Angew. Chem. Int. Ed.* **57**, 11064–11068 (2018).
22. Friedländer, P. Ueber schwefelhaltige Analoga der Indigogruppe. *Chem. Ber.* **39**, 1060–1066 (1906).
23. Izmail'skii, V. A. & Mostoslavskii, M. A. Absorption spectra of 3-oxo-2,3-dihydrothianaphthene and its derivatives. II. Isomerism of 2-benzylidene-3-oxo-2,3-dihydrothionaphthene. *Ukr. Khem. Zh.* **27**, 234–237 (1961).
24. Nenov, A., Cordes, T., Herzog, T. T., Zinth, W. & de Vivie-Riedle, R. Molecular driving forces for Z/E isomerization mediated by heteroatoms: the example hemithioindigo. *J. Phys. Chem. A* **114**, 13016–13030 (2010).
25. Cordes, T., Schadendorf, T., Rück-Braun, K. & Zinth, W. Chemical control of hemithioindigo-photoisomerization—substituent-effects on different molecular parts. *Chem. Phys. Lett.* **455**, 197–201 (2008).
26. Graupner, F. F. et al. Photoisomerization of hemithioindigo compounds: combining solvent- and substituent-effects into an advanced reaction model. *Chem. Phys.* **515**, 614–621(2018).
27. Kitzig, S., Thilemann, M., Cordes, T. & Ruck-Braun, K. Light-switchable peptides with a hemithioindigo unit: peptide design, photochromism, and optical spectroscopy. *ChemPhysChem* **17**, 1252–1263 (2016).
28. Wiedbrauk, S. & Dube, H. Hemithioindigo—an emerging photoswitch. *Tetrahedron Lett.* **56**, 4266–4274 (2015).
29. Petermayer, C. & Dube, H. Indigoid photoswitches: visible light responsive molecular tools. *Acc. Chem. Res.* **51**, 1153–1163 (2018).
30. Gerwien, A., Reinhardt, T., Mayer, P. & Dube, H. Synthesis of double-bond substituted hemithioindigo photoswitches. *Org. Lett.* **1**, 232–235 (2018).
31. Zweig, J. E. & Newhouse, T. R. Isomer-specific hydrogen bonding as a design principle for bidirectionally quantitative and redshifted hemithioindigo photoswitches. *J. Am. Chem. Soc.* **139**, 10956–10959 (2017).
32. Wiedbrauk, S., Bartelmann, T., Thumser, S., Mayer, P. & Dube, H. Simultaneous complementary photoswitching of hemithioindigo tweezers for dynamic guest relocalization. *Nat. Commun.* **9**, 1456 (2018).
33. Gerwien, A., Mayer, P. & Dube, H. Photon-only molecular motor with reverse temperature-dependent efficiency. *J. Am. Chem. Soc.* **140**, 16442–16445 (2018).
34. Liu, R. S. & Asato, A. E. The primary process of vision and the structure of bathorhodopsin: a mechanism for photoisomerization of polyenes. *Proc. Natl Acad. Sci. USA* **82**, 259–263 (1985).
35. Redwood, C., Bayda, M. & Saltiel, J. Photoisomerization of pre- and provitamin D3 in EPA at 77 K: one-bond-twist, not hula-twist. *J. Phys. Chem. Lett.* **4**, 716–721 (2013).
36. Fuss, W. & Previtamin, D. Z-E photoisomerization via a Hula-twist conical intersection. *Phys. Chem. Chem. Phys.* **21**, 6776–6789 (2019).
37. Liu, R. S. H. & Hammond, G. S. The case of medium-dependent dual mechanisms for photoisomerization: one-bond-flip and Hula-Twist. *Proc. Natl Acad. Sci. USA* **97**, 11153–11158 (2000).
38. Gerwien, A., Schildhauer, M., Thumser, S., Mayer, P. & Dube, H. Direct evidence for hula twist and single-bond rotation photoproducts. *Nature Commun.* **9**, 2510 (2018).
39. Haberhauer, G. A molecular four-stroke motor. *Angew. Chem. Int. Ed.* **50**, 6415–6418 (2011).
40. Haberhauer, G., Burkhart, C., Woitschetzki, S. & Wölper, C. Light and chemically driven molecularmachines showing a unidirectional four-state switching cycle. *J. Org. Chem.* **80**, 1887–1895 (2015).
41. Andreasson, J. & Pischel, U. Molecules for security measures: from keypad locks to advanced communication protocols. *Chem. Soc. Rev.* **47**, 2266–2279 (2018).
42. Andreasson, J. & Pischel, U. Molecules with a sense of logic: a progress report. *Chem. Soc. Rev.* **44**, 1053–1069 (2015).
43. Balter, M., Li, S., Nilsson, J. R., Andreasson, J. & Pischel, U. An all-photonic molecule-based parity generator/checker for error detection in data transmission. *J. Am. Chem. Soc.* **135**, 10230–10233 (2013).
44. Gust, D., Andreasson, J., Pischel, U., Moore, T. A. & Moore, A. L. Data and signal processing using photochromic molecules. *Chem. Commun.* **48**, 1947–1957 (2012).
45. Kink, F., Collado, M. P., Wiedbrauk, S., Mayer, P. & Dube, H. Bistable photoswitching of hemithioindigo with green and red light: entry point to advanced molecular digital information processing. *Chem. Eur. J.* **23**, 6237–6243 (2017).
46. de Silva, A. P., Gunaratne, N. & McCoy, C. P. A molecular photoionic AND gate based on fluorescent signalling. *Nature* **364**, 42–44 (1993).
47. De Silva, A. P. *Molecular logic-based computation* (PSC Publishing, 2013).
48. Megerle, U., Lechner, R., König, B. & Riedle, E. Laboratory apparatus for the accurate, facile and rapid determination of visible light photoreaction quantum yields. *Photochem. Photobiol. Sci.* **9**, 1400–1406 (2010).

Acknowledgements

H. Dube thanks the Deutsche Forschungsgemeinschaft (DFG) for an Emmy Noether fellowship (DU 1414/1-1). We further thank the Deutsche Forschungsgemeinschaft (SFB 749, A12) and the Cluster of Excellence "Center for Integrated Protein Science Munich" (CIPS^{M}) for financial support.

Author contributions

A.G. and H.D. designed the molecular setup and experiments. A.G. synthesized and characterized HTI **1** and conducted the kinetic experiments. A.G. provided the theoretical description of HTI **1**. P.M. determined the crystal structures. H.D. coordinated the study and wrote the paper. All authors read and approved the paper.

Competing interests

The authors declare no competing interests.

Additional information

Supplementary information is available for this paper at https://doi.org/10.1038/s41467-019-12463-4.

Correspondence and requests for materials should be addressed to H.D.

Peer review information *Nature Communications* thanks Jack Saltiel and the other, anonymous, reviewer(s) for their contribution to the peer review of this work.

Reprints and permission information is available at http://www.nature.com/reprints

Publisher's note Springer Nature remains neutral with regard to jurisdictional claims in published maps and institutional affiliations.

Supplementary Information

Green Light Powered Molecular State Motor Enabling Eight-Shaped Unidirectional Rotation

A. Gerwien et al.

Supplementary Methods

Synthesis

General experimental

Reagents and solvents were obtained from *abcr*, *Acros, Fluka, Merck, Sigma-Aldrich* or *TCI* in the qualities *puriss., p.a., or purum* and used as received. Technical solvents were distilled on a rotary evaporator (*Heidolph Hei-VAP Value*, *vacuubrand* CVC 3000) before use for column chromatography and extraction. Reactions were monitored on *Merck* Silica 60 F254 TLC plates. Detection was done by irradiation with UV light (254 nm or 366 nm).

Column chromatography was performed with silica gel 60 (*Merck*, particle size 0.063- 0.200 mm) and distilled technical solvents.

^{1}H NMR and ^{13}C NMR spectra were measured on a *Varian Mercury 200 VX, Varian 300, Inova 400, Varian 600 NMR*, or *Bruker Avance III HD 800 MHz* spectrometer. Chemical shifts (δ) are reported relative to tetramethylsilane as external standard. Residual solvent signals in the ^{1}H and ^{13}C NMR spectra were used as internal reference. Deuterated solvents were obtained from *Cambridge Isotope Laboratories* or *Eurisotop* and used without further purification. Deuterated solvents were obtained from Cambridge Isotope Laboratories or Eurisotop and used without further purification. For ^{1}H NMR: $CDCl_3$ = 7.26 ppm, CD_2Cl_2 = 5.32 ppm, benzene-d_6 = 7.16 ppm, $(CD_3)_2SO$ = 2.50 ppm, 1,2-dichlorobenzene-d_4 = 6.93. For ^{13}C NMR: $CDCl_3$= 77.16 ppm. Resonance multiplicity is indicated as *s* (singlet), *d* (doublet), *t* (triplet), *q* (quartet) and *m* (multiplet). The chemical shifts are given in parts per million (ppm) on the delta scale (δ). The coupling constant values (*J*) are given in hertz (Hz).

Electron Impact (EI) mass spectra were measured on a *Finnigan MAT95Q* or on a *Finnigan MAT90* mass spectrometer. **Electrospray ionisation (ESI) mass spectra were** measured on a *Thermo Finnigan LTQ-FT* mass spectrometer. The most important signals are reported in *m/z* units with *M* as the molecular ion.

Elemental analysis was performed in the micro analytical laboratory of the LMU department of chemistry on an *Elementar Vario EL* apparatus.

Infrared spectra were recorded on a *Perkin Elmer Spectrum BX-FT-IR* instrument equipped with a *Smith DuraSamplIR II ATR*-device. Transmittance values are qualitatively described by wavenumber (cm^{-1}) as very strong (vs), strong (s), medium (m) and weak (w).

UV/Vis and fluorescence spectra were measured on a *Varian Cary 5000* spectrophotometer. Fluorescence spectra were measured on a Varian Eclipse spectrophotometer. The spectra were recorded in a quartz cuvette (1 cm). Solvents for spectroscopy were obtained from *VWR* and *Merck*. Absorption wavelength (λ) are reported in nm and the molar absorption coefficients (ε) in L mol^{-1} cm^{-1}. Shoulders are declared as sh.

Melting points (M.p.) were measured on a *Stuart* SMP10 melting point apparatus in open capillaries and are not corrected.

Photoisomerization experiments. Continuous irradiations of the solutions were conducted in NMR tubes in different solvents (cyclohexane-d_{12}, 12DCB-d_4). Irradiations were conducted using a *Prizmatix UHP-T-520-DI LED* (520 nm) as light source.

HTI Synthesis

Precursors **2** and **3** were prepared following a previously reported protocol according to the following scheme.[1]

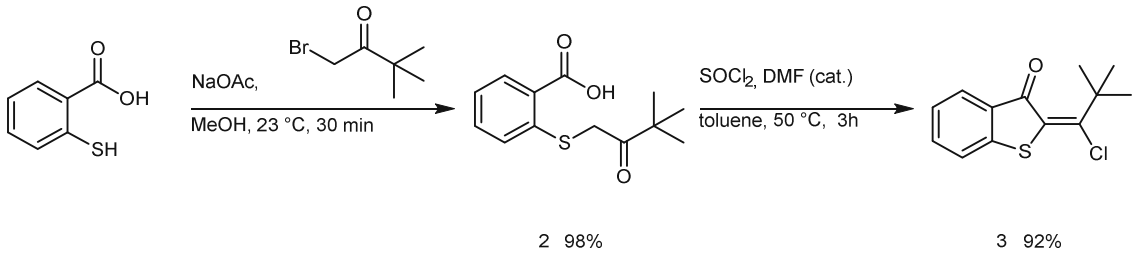

2 98%

3 92%

8-Methyl-2,3,6,7-tetrahydro-1*H*,5*H*-pyrido[3,2,1-*ij*]quinoline (4)

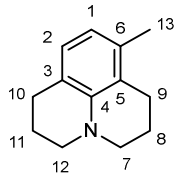

3-Toluidine (4.00 mL, 3.96 g, 37.0 mmol, 1 equiv.), 1-bromo-3-chloropropane (40.0 mL, 63.7 g, 404 mmol, 11 equiv.), sodium carbonate (15.0 g, 142 mmol, 3.8 equiv., oven dried at 300 °C *in vacuo* for 1 hour) and 4 Å molecular sieves (3.5 g, activated at 300 °C *in vacuo* for 1 hour) were added to a flame-dried 250 mL round bottom flask equipped with a reflux condenser. The reaction was heated stepwise: 1 h at 80 °C, 2 h at 100 °C and 12 h at 160 °C. Afterwards the reaction mixture was cooled to room temperature and 200 mL CH_2Cl_2 were added. The organic phase was washed successively with: HCl (2 M aqueous solution, 1 x 200 mL), H_2O (2 x 200 mL), NaOH (2 M aqueous solution, 1 x 200 mL), and again H_2O (2 x 200 mL). The organic phase was dried over sodium sulfate and after removing the solvent i*n vacuo* the crude product was purified by column chromatography (SiO_2, *i*Hex/EtOAc = 98/2 → 9/1). The title compound was isolated as colorless liquid (5.97 g, 31.9 mmol, 86%).

HR-MS (EI) for $C_{13}H_{17}N^{\cdot+}$, $[M]^{\cdot+}$, calcd. 187.1356, found 187.1352.

^{1}H NMR ($CDCl_3$, 400 MHz): δ (ppm) = 6.75 (d, J = 7.5 Hz, 1H, H-C(2)), 6.46 (d, J = 7.5 Hz, 1H, H-C(1)), 3.23 – 3.06 (m, 4H, H-C(7), H-C(12)), 2.78 (t, J = 6.6 Hz, 2H, H-C(10)), 2.67 (t, J = 6.7 Hz, 2H, H-C(9)), 2.17 (s, 3H, H-C(13)), 2.08 – 1.95 (m, 4H, H-C(8), H-C(11)).

^{13}C NMR ($CDCl_3$, 100 MHz): δ (ppm) = 143.4 (C(4)), 134.4 (C(6)), 126.6 (C(2)), 120.5 (C(5)), 119.8 (C(3)), 118.1 (C(1)), 50.6 (C(12)), 49.9 (C(7)), 27.8 (C(10)), 24.9 (C(9)), 22.5(C(11)), 22.4 (C(8)), 19.8 (C(13)).

IR: $\tilde{\upsilon}$/cm^{-1} = 2929 (s), 2836 (m), 2771 (m), 1672 (w), 1599 (m), 1578 (m), 1489 (vs), 1453 (s), 1439 (s), 1422 (m), 1392 (m), 1352 (m), 1327 (m), 1304 (vs), 1240 (w), 1208 (m), 1194 (s), 1186 (s), 1154 (m), 1120 (s), 1075 (w), 1047 (w), 1002 (w), 920 (m), 887 (w), 867 (w), 785 (vs), 737 (m), 718 (m).

R_f (SiO_2, *i*hex/EtOAc = 95/5) = 0.56.

9-Bromo-8-methyl-2,3,6,7-tetrahydro-1*H*,5*H*-pyrido[3,2,1-*ij*]quinoline (5)

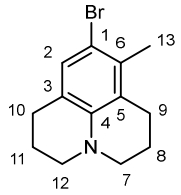

Compound **4** (3.58 g, 19.1 mmol, 1 equiv.) was dissolved in CH_2Cl_2 (10 mL) and cooled to -78 °C. Bromine (1.03 mL, 3.21 g, 20.1 mmol, 1.05 equiv.) was added over 10 min. After addition the reaction was immediately warmed to 22 °C and sodium thiosulfate solution (2 mL) and saturated sodium carbonate solution (10 mL) were added. The aqueous phase was extracted with CH_2Cl_2 (3 x 20 mL), and the combined organic phases were dried over Na_2SO_4. After removing the solvent i*n vacuo* the crude product was purified by column chromatography (SiO_2, *i*Hex/EtOAc = 98/2). The title compound was isolated as white solid (4.426 mg, 16.7 mmol, 87 %).

HR-MS (EI) for $C_{13}H_{16}{}^{79}BrN^{\cdot+}$, $[M]^{\cdot+}$, calcd. 265.0461, found 265.0464.

^{1}H NMR ($CDCl_3$, 400 MHz): δ (ppm) = 7.02 (s, 1H, H-C(2)), 3.13 – 3.03 (m, 4H, H-C(7), H-C(12)), 2.75 – 2.65 (m, 4H, H-C(9), H-C(10)), 2.25 (s, 3H, H-C(13)), 2.04 – 1.91 (m, 4H, 9 H-C(8), H-C(11)).

^{13}C NMR ($CDCl_3$, 100 MHz): δ (ppm) = 142.8 (C(4)), 133.2 (C(6)), 130.0 (C(2)), 122.1 (C(5)), 121.6 (C(3)), 111.8 (C(1)), 50.4 (C(12)), 49.4 (C(7)), 27.5 (C(10)), 26.3 (C(9)), 22.4 (C(8)), 22.2 (C(11)), 19.2 (C(13)).

IR: $\tilde{\upsilon}/cm^{-1}$ = 2921 (m), 2792 (m), 1585 (w), 1558 (m), 1478 (s), 1458 (s), 1443 (m), 1415 (s), 1387 (m), 1348 (m), 1339 (w), 1323 (m), 1300 (vs), 1203 (s), 1185 (vs), 1158 (s), 1118 (m), 1081 (m), 1052 (m), 1015 (m), 1003 (m), 894 (w), 881 (vs), 859 (m), 844 (w), 825 (w), 738 (s), 726 (m).

Melting point: 49 °C.

R_f (SiO_2, *i*hex/EtOAc = 95/5) = 0.56.

8-Methyl-9-(4,4,5,5-tetramethyl-1,3,2-dioxaborolan-2-yl)-2,3,6,7-tetrahydro-1*H*,5*H*-pyrido[3,2,1-*ij*]quinoline (6)

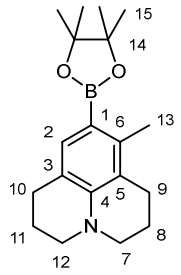

Compound **5** (1.00 g, 3.76 mmol, 1 equiv.) was dissolved in dry THF (20 mL) and cooled to -78 °C. *n*-BuLi (1.8 M in cyclohexane, 2.50 mL, 4.51 mmol, 1.2 equiv.) was added dropwise and the mixture was stirred at -78 °C for 30 min. Then, 2-isopropoxy-4,4,5,5-tetramethyl-1,3,2-dioxaborolane (0.92 mL, 4.51 mmol, 1.2 equiv.) was added and the mixture was warmed to 22 °C. H_2O (20 mL) was added, the mixture was extracted with CH_2Cl_2 (3 x 20 mL) and the combined organic phases were dried over Na_2SO_4. After removing the solvent i*n vacuo* the crude product was purified by column chromatography (SiO_2, *i*Hex/EtOAc = 99/1 → 97/3). The title compound was isolated as white solid (1.020 g, 3.27 mmol, 87 %).

HR-MS (EI) for $C_{19}H_{28}BNO^{\cdot+}$, $[M]^{\cdot+}$, calcd. 313.2208, found 313.2210.

^{1}H NMR ($CDCl_3$, 600 MHz): δ (ppm) = 7.30 (s, 1H, H-C(2)), 3.15 (t, J = 5.7 Hz, 2H, H-C(12)), 3.12 (t, J = 5.5 Hz, 2H, H-C(7)), 2.75 (t, J = 6.5 Hz, 2H, H-C(10)), 2.66 (t, J = 6.6 Hz, 2H, H-C(9)), 2.39 (s, 3H, H-C(13)), 2.02 – 1.97 (m, 2H, H-C(8)), 1.97 – 1.92 (m, 2H, H-C(11)), 1.32 (s, 12H, H-C(15)).

^{13}C NMR ($CDCl_3$, 100 MHz): δ (ppm) = 145.5 (C(4)), 141.9 (C(6)), 135.0 (C(2)), 119.9 (C(5)), 118.3 (C(3)), 82.8 (C(14)), 50.6 (C(12)), 49.6 (C(7)), 27.7 (C(10)), 25.1 (C(9)), 24.9 (C(15)), 22.3 (C(8), C(11)), 18.2 (C(13)). The signal of C(1) was not found, due to quadrupolar relaxation of the adjacent ^{11}B.

IR: $\tilde{\upsilon}$/cm^{-1} = 2972 (w), 2930 (w), 2837 (w), 2782 (w), 1593 (m), 1557 (m), 1499 (w), 1461 (w), 1434 (w), 1404 (m), 1387 (w), 1369 (m), 1357 (s), 1336 (vs), 1357 (vs), 1304 (vs), 1271 (s), 1238 (m), 1212 (m), 1182 (s), 1142 (vs), 1108 (m), 1075 (w), 1055 (m), 1028 (m), 1005 (m), 874 (m), 951 (w), 918 (w), 872 (w), 860 (m), 839 (w), 746 (m), 725 (w), 705 (w), 689 (m).

Melting point: 103 °C.

R_f (SiO_2, *i*hex/EtOAc = 95/5) = 0.44.

2-(2,2-dimethyl-1-(8-methyl-2,3,6,7-tetrahydro-1*H*,5*H*-pyrido[3,2,1-*ij*]quinolin-9-yl)propylidene)benzo[*b*]thiophen-3(2*H*)-one (7)

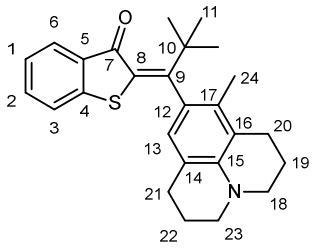

2-(1-Chloro-2,2-dimethylpropylidene)benzo[*b*]thiophen-3(2*H*)-one (**3**, 1.57 g, 6.22 mmol 1.0 equiv.) was dissolved in dioxane (18 mL). 8-Methyl-9-(4,4,5,5-tetramethyl-1,3,2-dioxaborolan-2-yl)-2,3,6,7-tetrahydro-1*H*,5*H*-pyrido[3,2,1-*ij*]quinoline (**6**, 1.95 g, 6.22 mmol, 1.0 equiv.), KO*t*Bu (1.72 g, 12.5 mmol, 2.0 equiv.) and H_2O (2 mL) were added. After bubbling argon through the solution for 10 min, $Pd(PPh_3)_4$ (360 mg, 0.31 mmol, 5 mol%) was added and the reaction mixture was stirred at 90 °C for 6 h. Subsequently, a saturated sodium carbonate solution (20 mL) was added, the aqueous phase was extracted with CH_2Cl_2 (3 x 50 mL), and the combined organic phases were dried over Na_2SO_4. After removing the solvent i*n vacuo* the crude product was purified by column chromatography (SiO_2, *i*Hex/EtOAc = 99/1 → 9/1). The title compound was isolated as red resin (550 mg, 0.22 mmol, 22 %).

HR-MS (EI) for $C_{26}H_{29}NO^{32}S^{\cdot+}$, $[M]^{\cdot+}$, calcd. 403.1964, found 403.1960.

^{1}H NMR ($CDCl_3$, 400 MHz): δ (ppm) = 7.80 (dd, J = 7.8, 1.4 Hz, 1H, H-C(6)), 7.45 – 7.39 (m, 1H, H-C(2)), 7.22 – 7.13 (m, 2H, H-C(1), H-C(3)), 6.41 (s, 1H, H-C(13)), 3.19 – 3.08 (m, 4H, H-C(18), H-C(23)), 2.80 – 2.70 (m, 2H, H-C(21)), 2.70 – 2.60 (m, 2H, H-C(20)), 2.11 – 1.94 (m, 7H, H-C(20), H-C(22), H-C(24)), 1.34 (s, 9H, H-C(11)).

^{13}C NMR ($CDCl_3$, 100 MHz): δ (ppm) = 186.4 (C(7)), 167.8 (C(9)), 146.4 (C(4)), 142.7 (C(15)), 134.7 (C(8)), 134.4 (C(0)), 134.1 (C(5)), 133.5 (C(12)), 129.8 (C(17)), 126.8 (C(6)), 124.5 (C(13)), 124.4 (C(1)), 122.8 (C(3)), 119.9 (C(16)), 119.1 (C(14)), 50.6 (C(23)), 49.7 (C(18)), 39.3 (C(10)), 29.1 (C(11)), 27.8 (C(21)), 25.1 (C(20)), 22.4 (C(22)), 22.3 (C(19)), 17.3 (C(24)).

IR: $\tilde{\upsilon}/cm^{-1}$ = 2927 (s), 2856 (m), 1664 (vs), 1588 (s), 1531 (m), 1491 (m), 1642 (s), 1450 (vs), 1391 (w), 1376 (w), 1360 (m), 1326 (m), 1306 (s), 1279 (vs), 1213 (s), 1188 (w), 1157 (w), 1135 (w), 1073 (s), 1062 (m), 1042 (w), 1019 (w), 995 (w), 924 (w), 907 (w), 887 (w), 862 (w), 797 (w), 774 (w), 744 (s), 734 (s), 681 (w).

R_f (SiO_2, *i*hex/EtOAc = 95/5) = 0.44.

2-(2,2-Dimethyl-1-(8-methyl-2,3,6,7-tetrahydro-1*H*,5*H*-pyrido[3,2,1-*ij*]quinolin-9-yl)propylidene)benzo[*b*]thiophen-3(2*H*)-one 1-oxide (1)

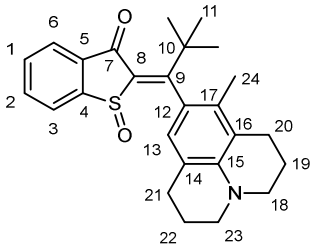

Compound **7** (550 mg, 1.36 mmol, 1 equiv.) was dissolved in a mixture of 4 mL CH_2Cl_2 and 2 mL TFA. *Meta*-chloroperoxybenzoic acid (235 mg, 1.36 mmol, 1 equiv.) was added at 0 °C in portions and the solution was further stirred for 10 min at 0 °C. Subsequently, a saturated sodium carbonate solution was added until the pH was adjusted to 7, the aqueous phase was extracted with CH_2Cl_2 (3 x 50 mL), and the combined organic phases were dried over Na_2SO_4. After removing the solvent i*n vacuo* the crude product was purified by column chromatography (SiO_2, *i*hex/EtOAc = 7/3 → 1/1). The isomers **1-A** and **1-D** were further purified by HPLC (<u>*Chiralpak*</u> IC Semiprep column, *n*heptane/EtOAc = 7/3). All isomers were separately crystallized from *n*heptane/EtOAc. The four isomers of the title compound were isolated as orange to red crystals (405 mg, 0.97 mmol, 71 %, sum of all isomers).

1-A

^{1}H NMR ($CDCl_3$, 400 MHz): δ (ppm) = 7.96 (dt, *J* = 7.6, 1.0 Hz, 1H, H-C(6)), 7.81 (dt, *J* = 7.7, 0.9 Hz, 1H, H-C(3)), 7.75 (td, *J* = 7.4, 1.3 Hz, 1H, H-C(2)), 7.66 (td, *J* = 7.4, 1.2 Hz, 1H, H-C(1)), 6.35 (s, 1H, H-C(13)), 3.19 – 3.08 (m, 4H, H-C(18), H-C(23)), 2.77 – 2.57 (m, 4H, H-C(20), H-C(21)), 2.10 – 1.93 (m, 7H, H-C(19), H-C(22), H-C(24)), 1.35 (s, 9H, H-C(11)).

^{13}C NMR ($CDCl_3$, 100 MHz): δ (ppm) = 185.1 (C(9)), 184.8 (C(7)), 148.7 (C(4)), 143.4 (C(15)), 143.1 (C(8)), 136.4 (C(5)), 135.5 (C(2)), 132.5 (C(1)), 132.2 (C(17)), 129.7 (C(12)), 127.1 (C(3)), 126.2 (C(6)), 124.4 (C(13)), 119.9 (C(16)), 118.9 (C(14)), 50.5 (C(23)), 49.6 (C(18)), 40.5 (C(13)), 29.1 (C(11)), 27.9 (C(21)), 24.9 (C(20)), 22.4 (C(22)), 22.2 (C(19)), 19.7 (C(24)).

IR: $\tilde{\upsilon}$/cm^{-1} = 2942 (m), 2858 (w), 1679 (vs), 1587 (m), 1548 (s), 1490 (s), 1459 (s), 1448 (m), 1392 (w), 1374 (w), 1353 (w), 1325 (w), 1305 (vs), 1273 (s), 1214 (vs), 1188 (m), 1157 (w), 1134 (w), 1119 (w), 1059 (m), 1028 (vs), 926 (m), 906 (w), 860 (w), 799 (w), 767 (m), 748 (vs), 739 (s), 699 (m), 684 (s), 663 (m).

Melting point: 190 °C.

R_f (SiO_2, *i*hex/EtOAc = 6/4) = 0.35.

1-B

^{1}H NMR ($CDCl_3$, 599 MHz): δ (ppm) = 7.95 (dt, J = 7.6, 1.0 Hz, 1H, H-C(6)), 7.79 (dt, J = 7.7, 1.0 Hz, 1H, H-C(3)), 7.75 (td, J = 7.4, 1.2 Hz, 1H, H-C(2)), 7.67 (td, J = 7.4, 1.2 Hz, 1H, H-C(1)), 6.55 (s, 1H, H-C(13)), 3.22 – 3.08 (m, 4H, H-C(18), H-C(13)), 2.87 – 2.79 (m, 1H, H-C(21)), 2.75 – 2.68 (m, 1H, H-C(21)), 2.64 (t, J = 6.7 Hz, 2H, H-C(20)), 2.07 – 1.95 (m, 4H, H-C(19), H-C(22)), 1.94 (s, 3H, H-C(24)), 1.34 (s, 9H, H-C(11)).

^{13}C NMR ($CDCl_3$, 151 MHz): δ (ppm) = 185.9 (C(7)), 183.7 (C(9)), 148.8 (C(4)), 143.4 (C(15)), 142.5 (C(8)), 136.5 (C(5)), 135.6 (C(2)), 132.5 (C(1)), 129.0 (C(17)), 128.1 (C(12)), 127.2 (C(3)), 127.0 (C(13)), 126.3 (C(6)), 119.8 (C(16)), 118.3 (C(14)), 50.5 (C(23)), 49.6 (C(18)), 40.3 (C(10)), 29.5 (C(11)), 27.8 (C(21)), 25.1 (C(20)), 22.3 (C(19), C(22)), 17.9 (C(24)).

IR: $\tilde{\upsilon}/cm^{-1}$ = 2942 (w), 1683 (vs), 1589 (s), 1554 (s), 1493 (s), 1462 (s), 1393 (m), 1360 (m), 1323 (s), 1305 (vs), 1272 (s), 1214 (vs), 1185 (s), 1156 (w), 1134 (m), 1119 (m), 1060 (m), 1034 (vs), 994 (w), 924 (m), 902 (w), 845 (w), 801 (w), 755 (vs), 729 (vs), 697 (s), 688 (vs), 661 (m).

Melting point: 123 °C.

R_f (SiO_2, *i*hex/EtOAc = 6/4) = 0.26.

1-C

^{1}H NMR ($CDCl_3$, 599 MHz): δ (ppm) = 8.03 (dt, J = 7.3, 1.0 Hz, 1H, H-C(3)), 7.83 – 7.79 (m, 2H, H-C(2), H-C(6)), 7.64 (td, J = 7.5, 1.0 Hz, 1H, H-C(1)), 6.31 (s, 1H, H-C(13)), 3.18 – 3.04 (m, 4H, H-C(18), H-C(23)), 2.80 – 2.59 (m, 4H, H-C(20), H-C(21)), 2.11 – 1.94 (m, 4H, H-C(19), H-C(22)), 1.87 (s, 3H, H-C(24)), 1.47 (s, 9H, H-C(11)).

^{13}C NMR ($CDCl_3$, 151 MHz): δ (ppm) = 184.9 (C(7)), 180.3 (C(11)), 147.6 (C(4)), 142.6 (C(15)), 139.4 (C(8)), 135.6 (C(2)), 134.6 (C(5)), 132.7 (C(1)), 130.1 (C(17)), 128.3 (C(12)), 127.1 (C(3)), 126.0 (C(6)), 122.9 (C(13)), 119.9 (C(16)), 118.9 (C(14)), 50.6 (C(23)), 49.7 (C(18)), 41.9 (C(10)), 30.3 (C(11)), 27.7 (C(21)), 25.0 (C(20)), 22.5 (C(25), C(28)), 18.0 (C(24)).

IR: $\tilde{\upsilon}/cm^{-1}$ = 2928 (m), 2803 (w), 2773 (w), 1693 (s), 1591 (m), 1580 (m), 1545 (s), 1488 (s), 1454 (s), 1391 (w), 1373 (w), 1358 (w), 1326 (m), 1304 (s), 1272 (vs), 1189 (s), 1157 (s), 1120 (s), 1107 (m), 1070 (m), 1055 (w), 1033 (vs), 997 (s), 962 (w), 891 (w), 874 (w), 852 (w), 796 (w), 756 (vs), 735 (m), 713 (m), 701 (w), 682 (s), 655 (s).

Melting point: 184 °C.

R_f (SiO_2, *i*hex/EtOAc = 6/4) = 0.50.

1-D

^{1}H NMR ($CDCl_3$, 400 MHz): δ (ppm) = 7.99 (dd, J = 8.1, 1.1 Hz, 1H, H-C(3)), 7.82 – 7.77 (m, 2H, H-C(2), H-C(6)), 7.65 (td, J = 7.4, 1.0 Hz, 1H, H-C(1)), 6.12 (s, 1H, H-C(13)), 3.19 – 3.05 (m, 4H, H-C(18), H-C(23)), 2.76 – 2.59 (m, 4H, H-C(20), H-C(21)), 2.09 – 1.92 (m, 7H, H-C(19), H-C(22), H-C(24)), 1.46 (s, 9H, H-C(11)).

^{13}C NMR ($CDCl_3$, 101 MHz): δ (ppm) = 187.0 (C(7)), 178.7 (C(11)), 147.5 (C(4)), 142.6 (C(15)), 139.0 (C(8)), 135.6 (C(2)), 134.2 (C(5)), 133.0 (C(1)), 130.8 (C(17)), 127.9 (C(12)), 127.3 (C(3)), 126.3 (C(6)), 122.4 (C(13)), 120.0 (C(16)), 118.7 (C(14)), 50.6 (C(23)), 49.7 (C(18)), 41.5 (C(10)), 31.7 (C(11)), 27.8 (C(20)), 25.0 (C(21)), 22.4 (C(19), C(22)), 17.4 (C(24)).

IR: $\tilde{\upsilon}/cm^{-1}$ = 2923 (m), 1694 (vs), 1592 (m), 1528 (m), 1495 (m), 1463 (s), 1450 (m), 1396 (w), 1357 (w), 1325 (m), 1307 (s), 1277 (s), 1215 (vs), 1188 (m), 1156 (m), 1134 (m), 1123 (m), 1109 (m), 1071 (m), 1034 (vs), 997 (m), 889 (w), 850 (w), 797 (w), 759 (vs), 733 (m), 712 (w), 700 /m), 681 (s), 681 (m).

Melting point: 176 °C.

R_f (SiO_2, *i*hex/EtOAc = 6/4) = 0.38.

For all isomers:

HR-MS (EI) for $C_{26}H_{29}NO_2{}^{32}S^{\cdot+}$, $[M]^{\cdot+}$, calcd. 419.1914, found 419.1898.

Physical and photophysical properties

Thermal isomerizations

Amberized NMR tubes were charged with 1 mg to 2.5 mg of the respective isomer **A**, **B**, **C**, or **D** and 0.7 mL of 1,2-dichlorobenzene-d_4, DMSO-d_6, or MeCN-d_4/D_2O: 8/2. Subsequently the NMR tubes were heated to the appropriate temperatures for isomerization reactions to occur and the kinetics were followed by ^{1}H NMR measurements in defined time intervals. The unchanging equilibrium ratio of isomers after prolonged heating were obtained from integration of the corresponding signals in the ^{1}H NMR spectrum.

The kinetics of thermal isomer interconversions differ strongly in the different solvents, however the most prominent isomerization is the thermal Hula-Twist isomerization of *E* configured **C** and **D** to *Z* configured **B** and **A**, respectively in all solvents. These isomerizations are unimolecular first order reactions and proceed towards an equilibrium composition with only the two interconverting isomers present. The kinetics can therefore generally expressed for the reaction **X→Y** according to Supplementary Equation 1.

$$\ln\left(\frac{[\mathbf{X}]_{t_0}-[\mathbf{X}]_{\mathrm{eq}}}{[\mathbf{X}]_t-[\mathbf{X}]_{\mathrm{eq}}}\right) = (k_{\mathbf{X/Y}} + k_{\mathbf{Y/X}})t \qquad \text{(Supplementary Equation 1)}$$

With $[\mathbf{X}]_{t_0}$ being the initial concentration of the starting isomer **X** at the time t = 0, $[\mathbf{X}]_{\mathrm{eq}}$ being the concentration of the isomer **X** at equilibrium, $[\mathbf{X}]_t$ representing the concentration of the isomer **X** at a specific time t during the measurement, $k_{\mathbf{X/Y}}$ being the rate constant k of the **X** to **Y** conversion, $k_{\mathbf{Y/X}}$ being the rate constant k of the **Y** to **X** conversion, and t being the elapsed time. When plotting the logarithmic left part of Supplementary Equation 1 versus time t the obtained slope m contains the rate constants for both isomerization reactions taking place. The rate constant can then be calculated according to Supplementary Equation 2:

$$k_{\mathbf{X/Y}} = \frac{m}{1+\frac{[\mathbf{X}]_{\mathrm{eq}}}{[\mathbf{Y}]_{\mathrm{eq}}}} \qquad \text{(Supplementary Equation 2)}$$

when taking into account the corresponding law of mass action (Supplementary Equation 3):

$$\frac{[\mathbf{X}]_{\mathrm{eq}}}{[\mathbf{Y}]_{\mathrm{eq}}} = \frac{k_{\mathbf{Y/X}}}{k_{\mathbf{X/Y}}} \qquad \text{(Supplementary Equation 3)}$$

Likewise the reverse rate constant is defined and can be determined from separate measurements starting from the opposite isomer Y.

By using the *Eyring* equation (Supplementary Equation 4) the free activation enthalpies ΔG^* can be calculated from the rate constants of the corresponding reaction.

$$\Delta G^* = \ln\left(\frac{k*h}{k_B*T}\right) * R * T \qquad \text{(Supplementary Equation 4)}$$

The obtained free activation enthalpies ΔG^* for the thermal isomerizations between **A** to **B**, **C** to **D**, and *vice versa* in the different solvents as well as the corresponding extrapolated half-lives at 25 °C are given in Table S1 together with the equilibrium compositions obtained at high temperatures.

However in nonpolar solvents like 1,2-dichlorobenzene-d_4 not only the thermal hula twist reaction occurs but also single bond rotations and double bond isomerizations. To model the kinetics of this more complicated scenario the Markov matrix approach from our previous publication[2] was used by replacing the probability elements of the matrix with the converted *Eyring* equation (Supplementary Equation5).

$$M_1 = \begin{pmatrix} k_{AA} & k_{AB} & k_{AC} & k_{AD} \\ k_{BA} & k_{BB} & k_{BC} & k_{BD} \\ k_{CA} & k_{CB} & k_{CC} & k_{CD} \\ k_{DA} & k_{DB} & k_{DC} & k_{DD} \end{pmatrix} \quad \text{with } k_{AA} = 1 - (k_{AB} + k_{AC} + k_{AD}) \quad \ldots \quad \text{and } k_{AB} = \frac{k_B \bullet T}{h} \bullet e^{\frac{-\Delta G^{\ddagger}_{AB}}{R \bullet T}} \quad \ldots$$

(Supplementary Equation 5)

The kinetics were then modelled by multiplication of M_1 with the concentrations of the isomers **A**, **B**, **C**, **D** to give the corresponding concentration vector of the next time point (Supplementary Equation6). The sum of the concentrations of the isomers were previously normalized to 100 to enable an easier presentation of the data.

$$\begin{pmatrix} [A] \\ [B] \\ [C] \\ [D] \end{pmatrix}_{t_{x+1}} = \begin{pmatrix} k_{AA} & k_{AB} & k_{AC} & k_{AD} \\ k_{BA} & k_{BB} & k_{BC} & k_{BD} \\ k_{CA} & k_{CB} & k_{CC} & k_{CD} \\ k_{DA} & k_{DB} & k_{DC} & k_{DD} \end{pmatrix} \bullet \begin{pmatrix} [A] \\ [B] \\ [C] \\ [D] \end{pmatrix}_{t_x}$$

(Supplementary Equation 6)

The different ΔG^{*} values for each isomerization were optimized against a refinement factor R, which was calculated according to Supplementary Equation 7.

$$R = \frac{\sum \frac{[\mathbf{X}\mathrm{m}]_t}{[\mathbf{X}\mathrm{c}]_t}}{x} \qquad \text{(Supplementary Equation7)}$$

With $[\mathbf{X}\mathrm{m}]_t$ being the measured concentration of **X** at time *t*, $[\mathbf{X}\mathrm{c}]_t$ being the calculated concentration of **X** at time *t*, and *x* being the total amount of acquired measurement points. The closer *R* becomes to 1 the better is the obtained fit of the data. Measurement points below a concentration of 0.01 were not taken into account for the calculation of the *R* factor as the error of integration might be very high at low concentrations.
From these measurements we could quantify the full ground state energy profile of HTI **1** in 12DCB. The equilibrium isomer composition at high temperatures delivers the energy differences between the corresponding states according to the relation of the change of *Gibbs* free energy and the equilibrium constant.

Quantum yield measurements in different solvents

The photochemical quantum yields of the different photoconversion reactions ϕ were calculated as the ratio between the numbers of isomerized molecules *n*(molecules isomerized) and the number of absorbed photons *n*(*hv*) according to Supplementary Equation 8:

$$\phi = \frac{n(\text{molecules isomerized})}{n(hv)} \qquad \text{(Supplementary Equation 8)}$$

To determine the quantum yields ϕ, a sample with known concentration of each pure isomer **A**, **B**, **C**, or **D** in different solvents was irradiated with a focused light beam of a 520 nm LED within the published instrumental setup from the group of *E. Riedle*.[3] The number of absorbed photons over time *n*(*hv*) was measured directly at the thermal photometer of the instrument according to Supplementary Equation 9:

$$n(hv) = \frac{\Delta P \cdot \lambda_{ex} \cdot t}{c \cdot h} \qquad \text{(Supplementary Equation 9)}$$

Where *c* is the speed of light ($2.99792 \cdot 10^{8}$ m·s^{-1}), *h* is Planck's constant ($6.62607 \cdot 10^{-34}$ J·s), λ_{ex} is the excitation wavelength in m, *t* is the elapsed time during irradiation, and ΔP is the difference in power read-outs at the thermal photometer between a solvent filled cuvette (P_0) and a cuvette containing the sample solution (P_t) during the irradiation period in Watt (Supplementary Equation 10). The power read out during

irradiation did not change substantially (<5%) over the irradiation periods in the control experiment with the solvent filled cuvette.

$$\Delta P = P_t - P_0 \qquad \text{(Supplementary Equation 10)}$$

Since more than one photoproduct can be formed during irradiation, the number of each type of photoconverted molecules *n*(molecules isomerized) was determined by ^{1}H NMR spectroscopy directly after the irradiation step. Multiple measurements with increasing time of irradiation were conducted and the obtained ϕ values were averaged.

Theoretical description of the ground state of 1

A relaxed optimization of the four isomeric states and all four transition state structures of compound **1** at the ω–B97XD/6-311G(d,p) level of theory has been conducted using the Gaussian16 Revision A.03 program package.[4] To account for solvent effects, the calculations have been carried out using the Polarizable Continuum Model (PCM) with DMSO parameters. The convergence criteria have been set tight and an ultrafine integration grid has been used. Frequency analysis confirmed four structures (**A**, **B**, **C**, **D**) to be minimum structures since no imaginary frequencies have been found. All other structures were shown to be first order saddle points on the potential energy surface since only one imaginary vibrational mode has been found confirming them to be transition state structures.

Crystal structure analysis

All X-ray intensity data were measured on a Bruker D8 Venture TXS system equipped with a multilayer mirror optics monochromator and a Mo Kα rotating-anode X-ray tube (λ = 0.71073 Å). The data collections were performed at 103 K. The frames were integrated with the Bruker SAINT Software package [5]. Data were corrected for absorption effects using the Multi-Scan method (SADABS) [6]. The structures were solved and refined using the Bruker SHELXTL Software Package [7]. All C-bound hydrogen atoms were calculated in positions having ideal geometry riding on their parent atoms. The data have been deposited with the Cambridge Crystallographic Data Centre (CCDC) and can be obtained free of charge from: https://www.ccdc.cam.ac.uk/structures/. The deposition numbers are: CCDC 1910546 (**A**-**1**), CCDC 1910547 (**B**-**1**), CCDC 1910548 (**C**-**1**) and CCDC 1910549 (**D**-**1**).

Supplementary Figures

Determination of constitutions and conformations in the crystalline state and in solution

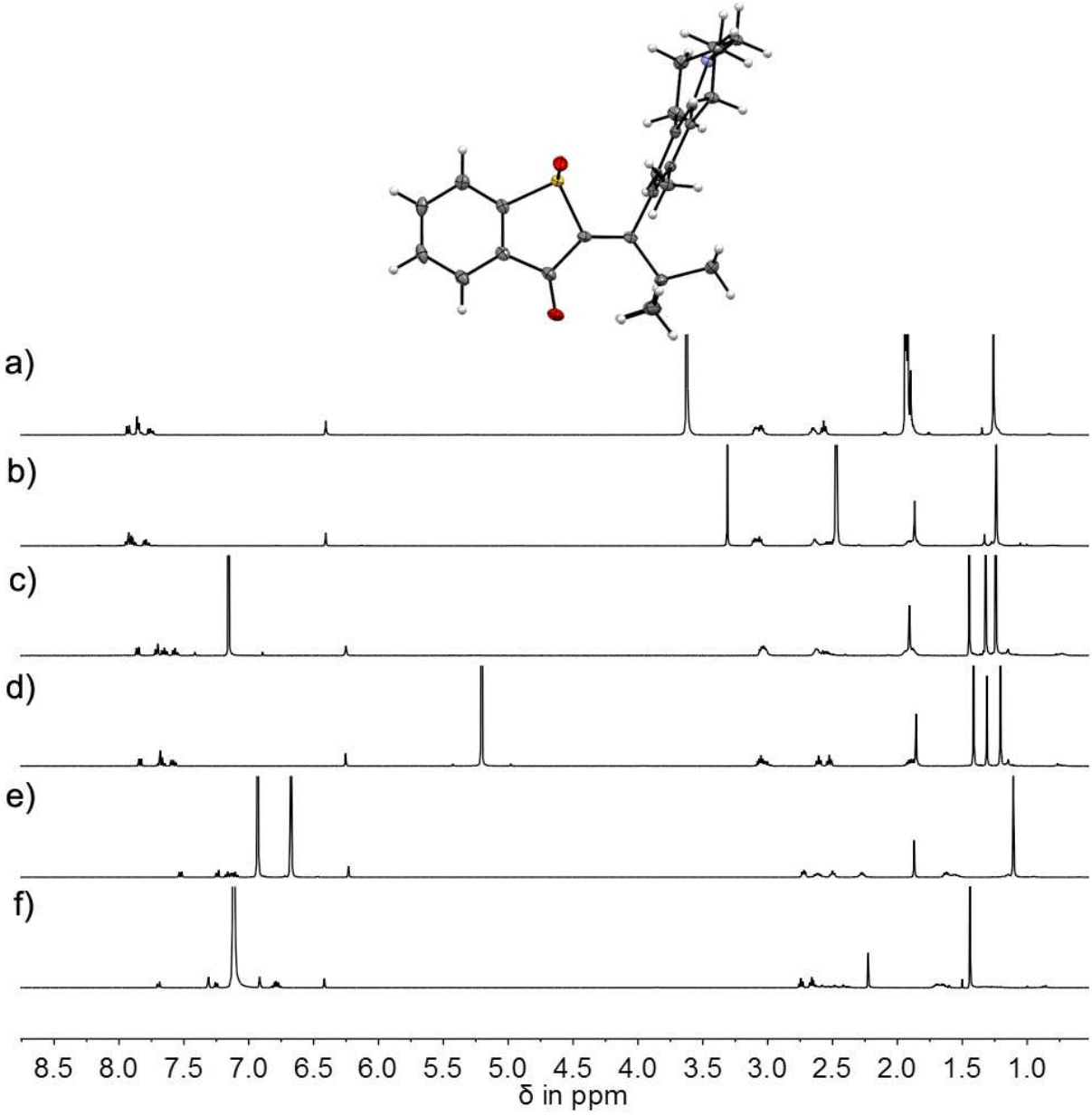

Supplementary Figure 1 | Structure assignment of A-1. Structure of **A-1** in the crystalline state and the corresponding ^{1}H NMR solution spectra (400 MHz, 20 °C) obtained from the same crystal batch in: a) MeCN-d_4/D_2O: 8/2, b) DMSO-d_6, c) $CDCl_3$, d) CD_2Cl_2, e) 1,2-dichlorobenzene-d_4, f) benzene-d_6.

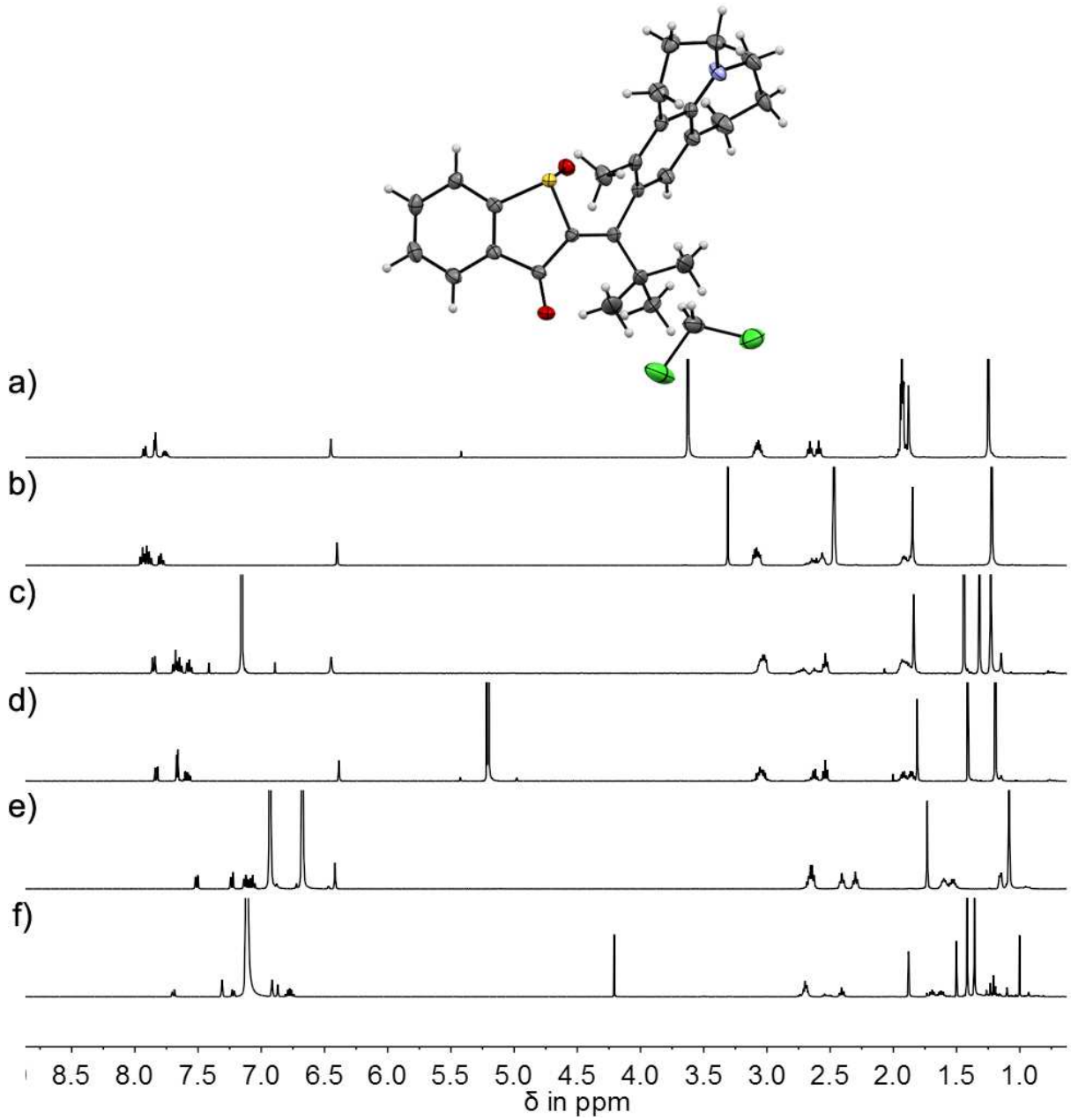

Supplementary Figure 2 | Structure assignment of B-1. Structure of **B-1** in the crystalline state and the corresponding ^{1}H NMR solution spectra (400 MHz, 20 °C) obtained from the same crystal batch in: a) MeCN-d_4/D_2O: 8/2, b) DMSO-d_6 (co-crystallized CH_2Cl_2 was removed by evaporation), c) $CDCl_3$ (co-crystallized CH_2Cl_2 was removed by evaporation), d) CD_2Cl_2, e) 1,2-dichlorobenzene-d_4 (co-crystallized CH_2Cl_2 was removed by evaporation), f) benzene-d_6.

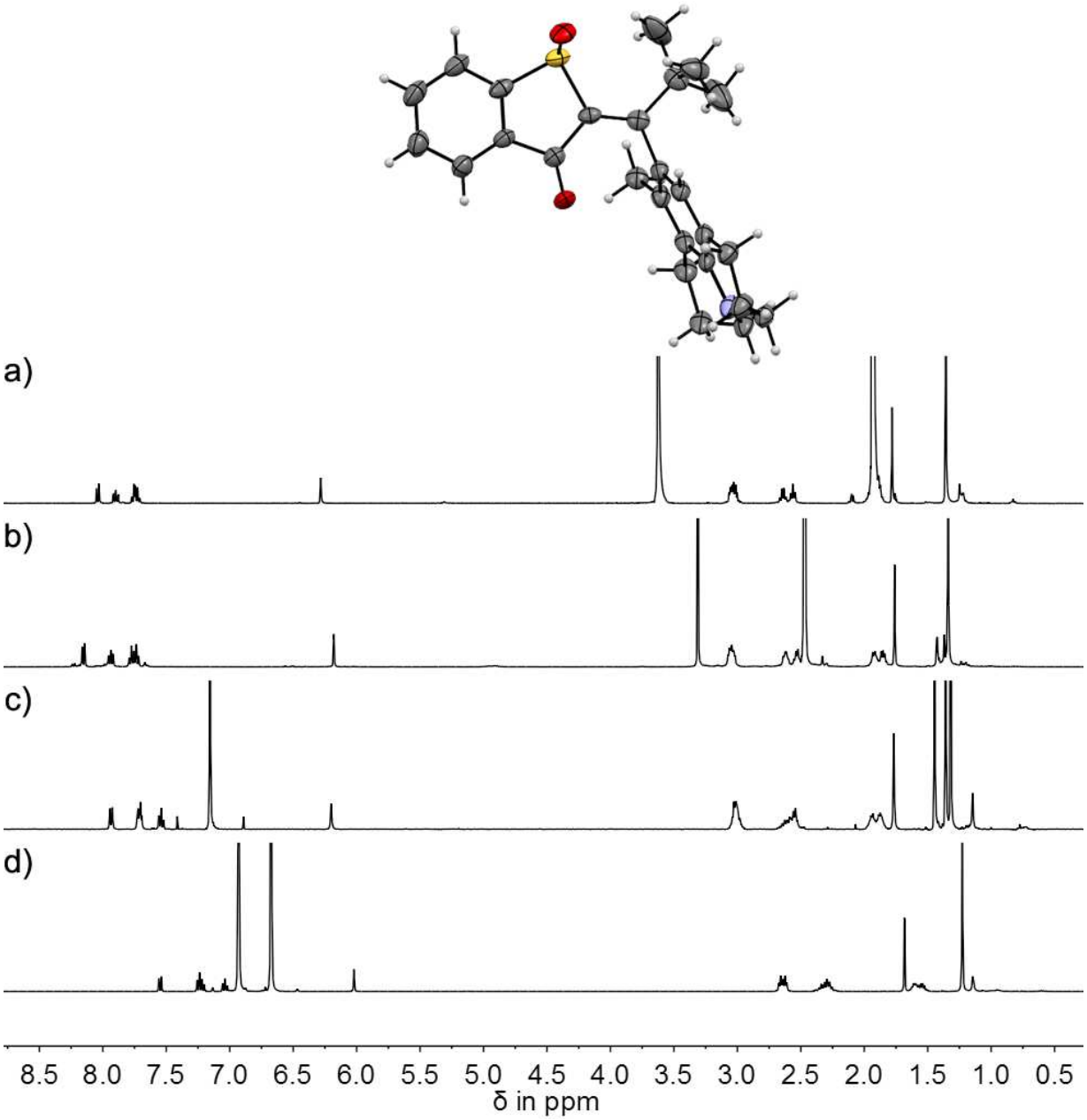

Supplementary Figure 3 | Structure assignment of C-1. Structure of **C-1** in the crystalline state and the corresponding ^{1}H NMR solution spectra (400 MHz, 20 °C) obtained from the same crystal batch in: a) MeCN-d_4/D_2O: 8/2, b) DMSO-d_6, c) $CDCl_3$, d) 1,2-dichlorobenzene-d_4.

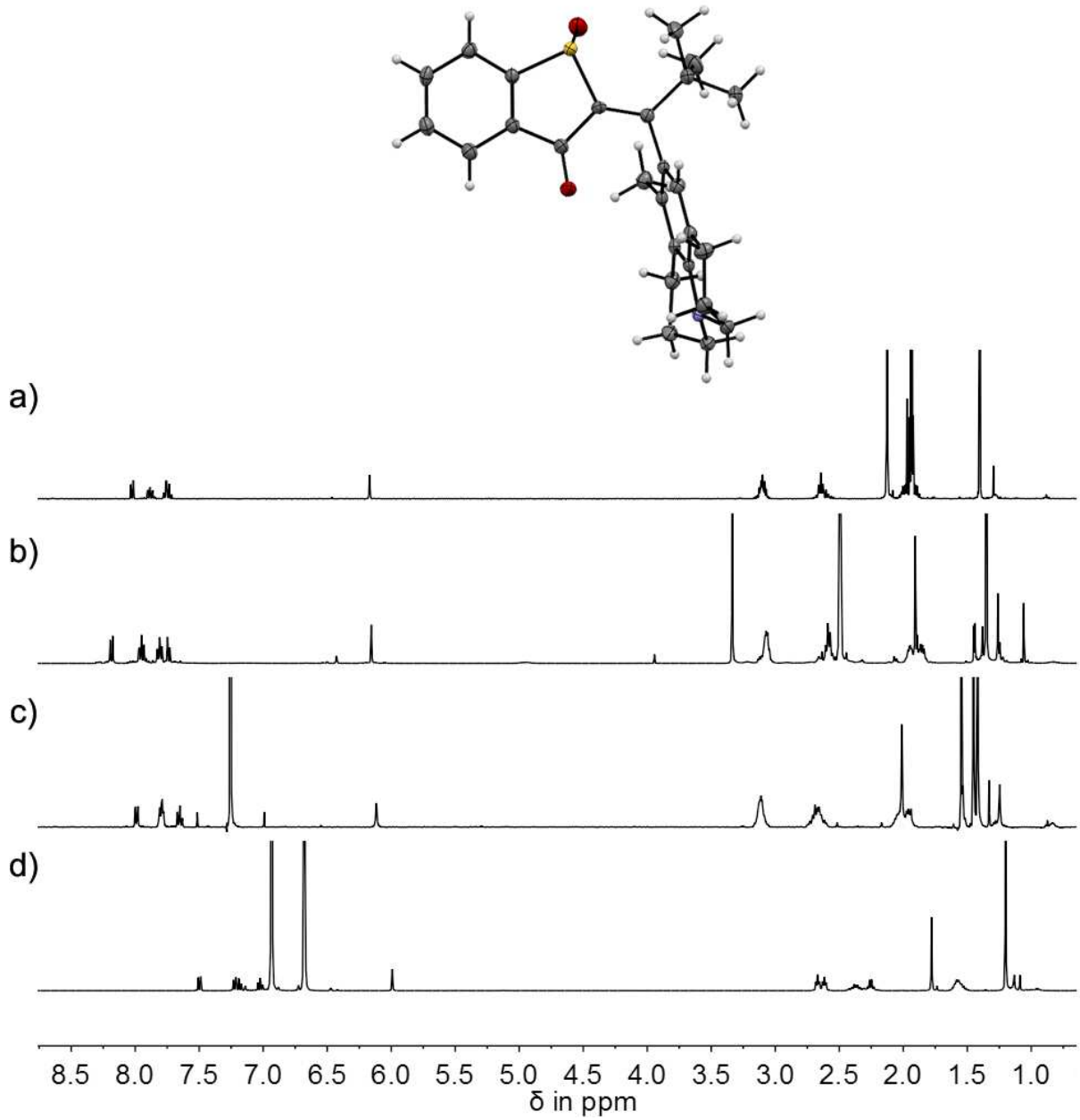

Supplementary Figure 4 | Structure assignment of D-1. Structure of **D-1** in the crystalline state and the corresponding ^{1}H NMR solution spectra (400 MHz) obtained from the same crystal batch in: a) MeCN-d_4 (27 °C), b) DMSO-d_6 (20 °C), c) $CDCl_3$ (20 °C), d) 1,2-dichlorobenzene-d_4 (20 °C).

Thermal isomerizations

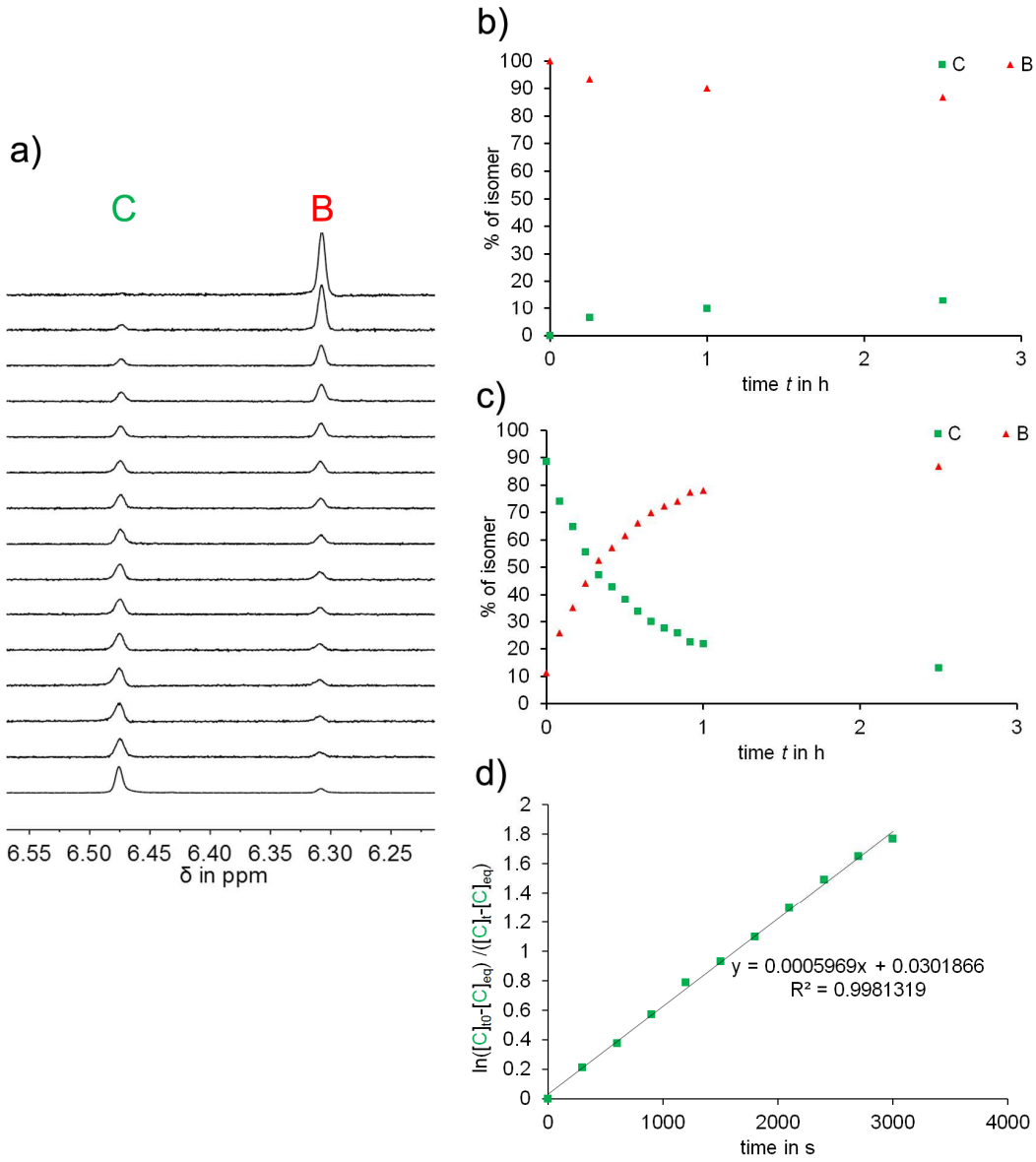

Supplementary Figure 5 | Thermal isomerization between C and B in the dark. a) Thermal isomerization of **C** to **B** in MeCN-d_4/D_2O: 8/2 at 60 °C followed by ^{1}H NMR spectroscopy (400 MHz, 60 °C) in regular time intervals. b) Thermal isomer conversion from **B** to **C** used as control experiment for determination of the isomer composition in thermal equilibrium. These data were not used to determine ΔG^* values as the changes in concentration are very smallc) Thermal isomer conversion from **C** to **B**. d) First order kinetic analysis of the thermal isomerization of **C** to **B**. Taking into account the dynamic equilibrium by plotting according to Supplementary Equation 1 gives a linear relationship. The slope m can be translated into the rate constant $k_{(\mathbf{C/B})}$ according to Supplementary Equation 2. The corresponding Gibbs free energy of activation ΔG^* for thermal **C** to **B** isomerization is given in Supplementary Table 1.

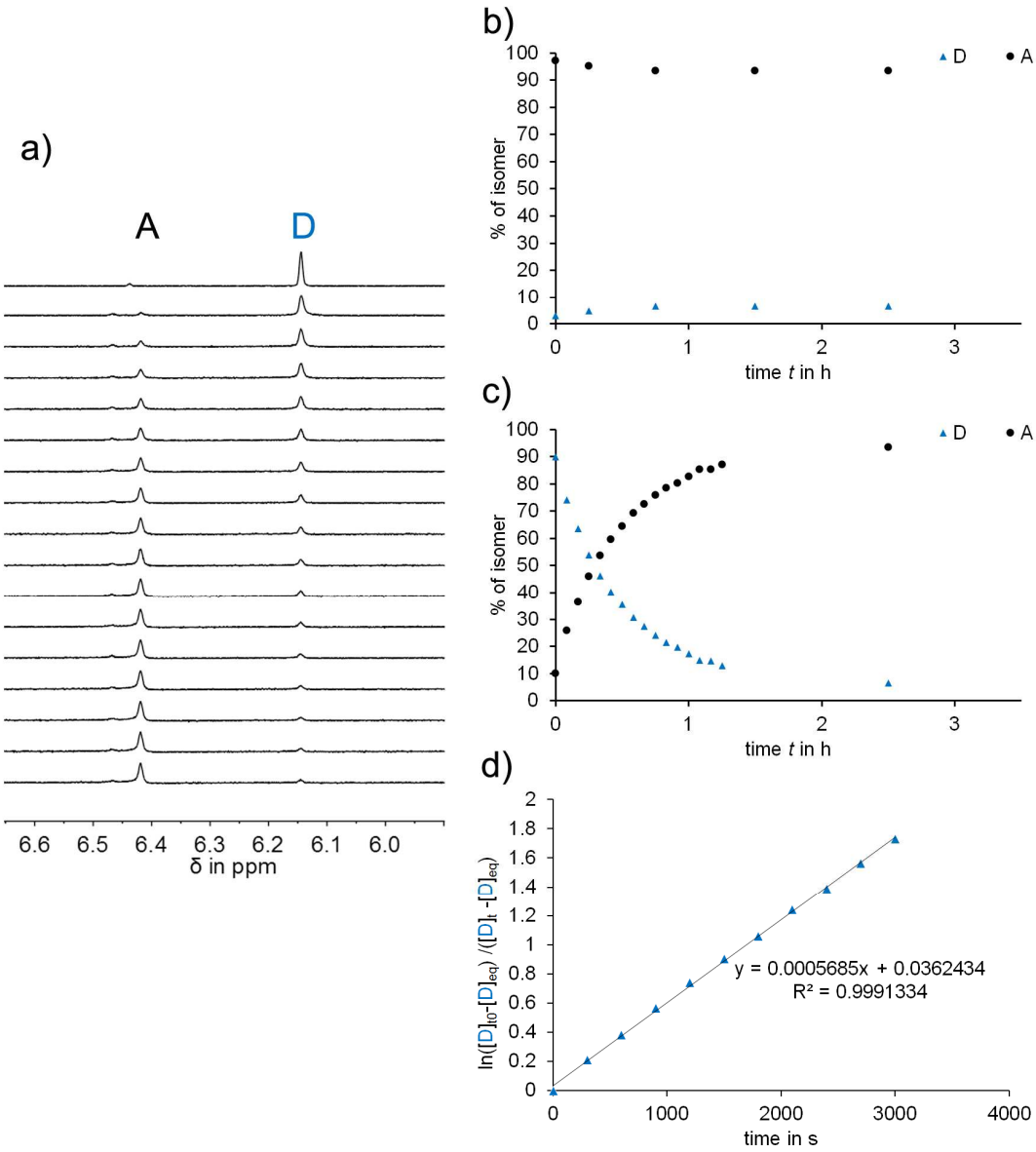

Supplementary Figure 6 | Thermal isomerization between D and A in the dark. a) Thermal isomerization of **D** to **A** in MeCN-d_4/D_2O: 8/2 at 27 °C followed by ^{1}H NMR spectroscopy (400 MHz, 27 °C) in regular time intervals. b) Thermal isomer conversion from **A** to **D** used as control experiment for determination of the isomer composition in thermal equilibrium. These data were not used to determine ΔG^* values as the changes in concentration are very small. c) Thermal isomer conversion from **D** to **A**. d) First order kinetic analysis of the thermal isomerization of **D** to **A**. Taking into account the dynamic equilibrium by plotting according to Supplementary Equation 1 gives a linear relationship. The slope m can be translated into the rate constant $k_{(\mathbf{D/A})}$ according to Supplementary Equation 2. The corresponding Gibbs free energy of activation ΔG^* for thermal **D** to **A** isomerizations is given in Supplementary Table 1.

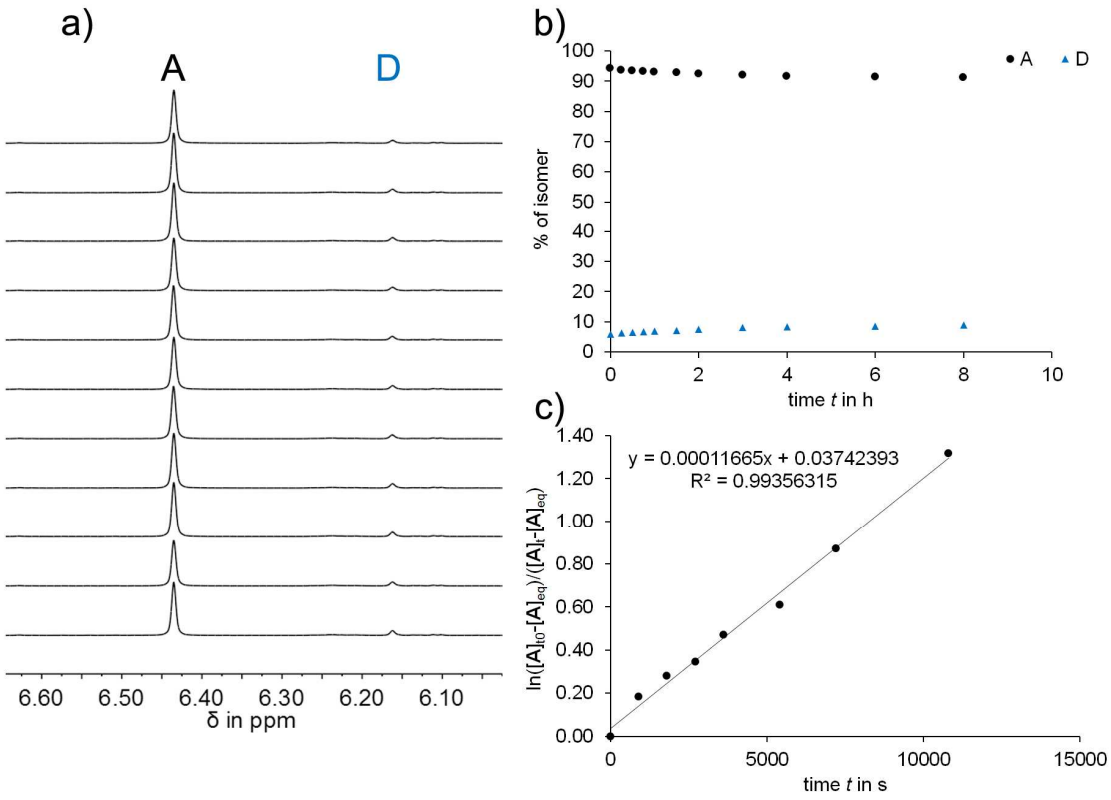

Supplementary Figure 7 | Thermal isomerization from A to D in the dark. a) Thermal isomerization of **A** to **D** in DMSO-d_6 at 60 °C followed by ^{1}H NMR spectroscopy (400 MHz, 20 °C) in regular time intervals. b) Thermal isomer conversion from **A** to **D**. c) First order kinetic analysis of the thermal isomerization of **A** to **D**. Taking into account the dynamic equilibrium by plotting according to Supplementary Equation 1 gives a linear relationship. The slope m can be translated into the rate constant $k_{(\mathbf{A/D})}$ according to Supplementary Equation 2. The corresponding Gibbs free energy of activation ΔG^* for the thermal **A** to **D** isomerization is given in Supplementary Table 2.

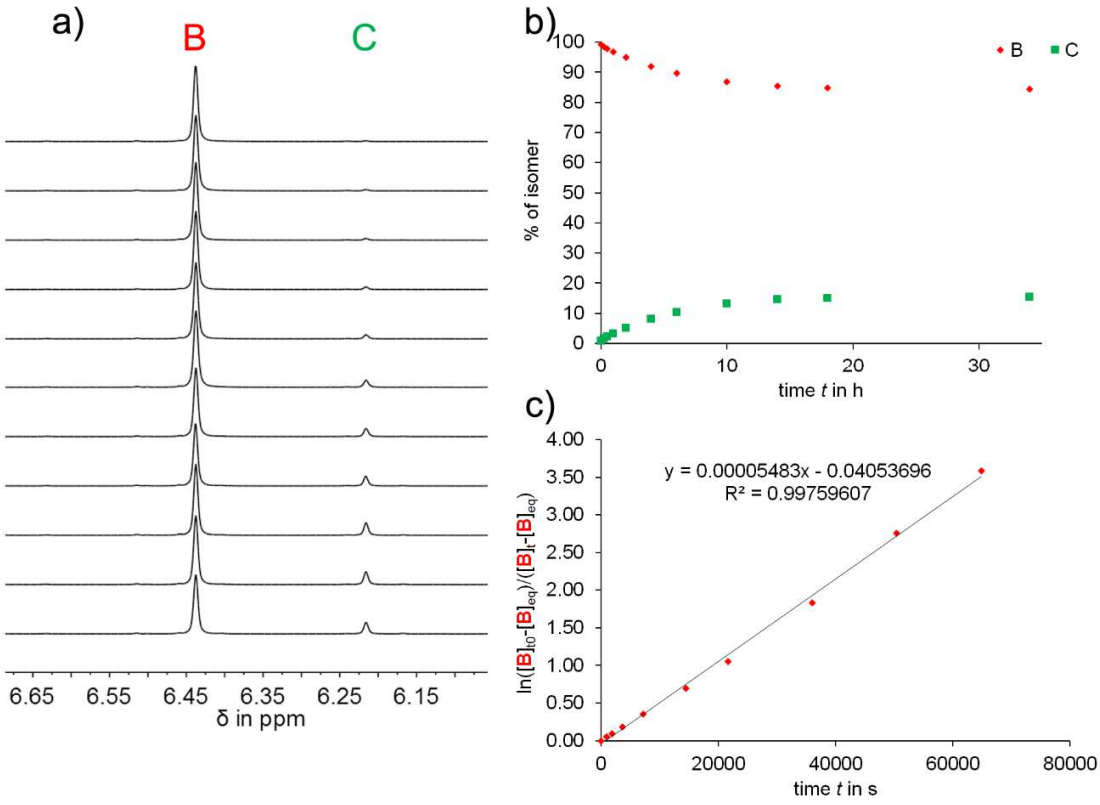

Supplementary Figure 8 | Thermal isomerization from B to C in the dark. a) Thermal isomerization of **B** to **C** in DMSO-d_6 at 80 °C followed by ^{1}H NMR spectroscopy (400 MHz, 20 °C) in regular time intervals. b) Thermal isomer conversion from **B** to **C**. c) First order kinetic analysis of the thermal isomerization of **B** to **C**. Taking into account the dynamic equilibrium by plotting according to Supplementary Equation 1 gives a linear relationship. The slope m can be translated into the rate constant $k_{(B/C)}$ according to Supplementary Equation 2. The corresponding Gibbs free energy of activation ΔG^{*} for the thermal **B** to **C** isomerization is given in Supplementary Table 2.

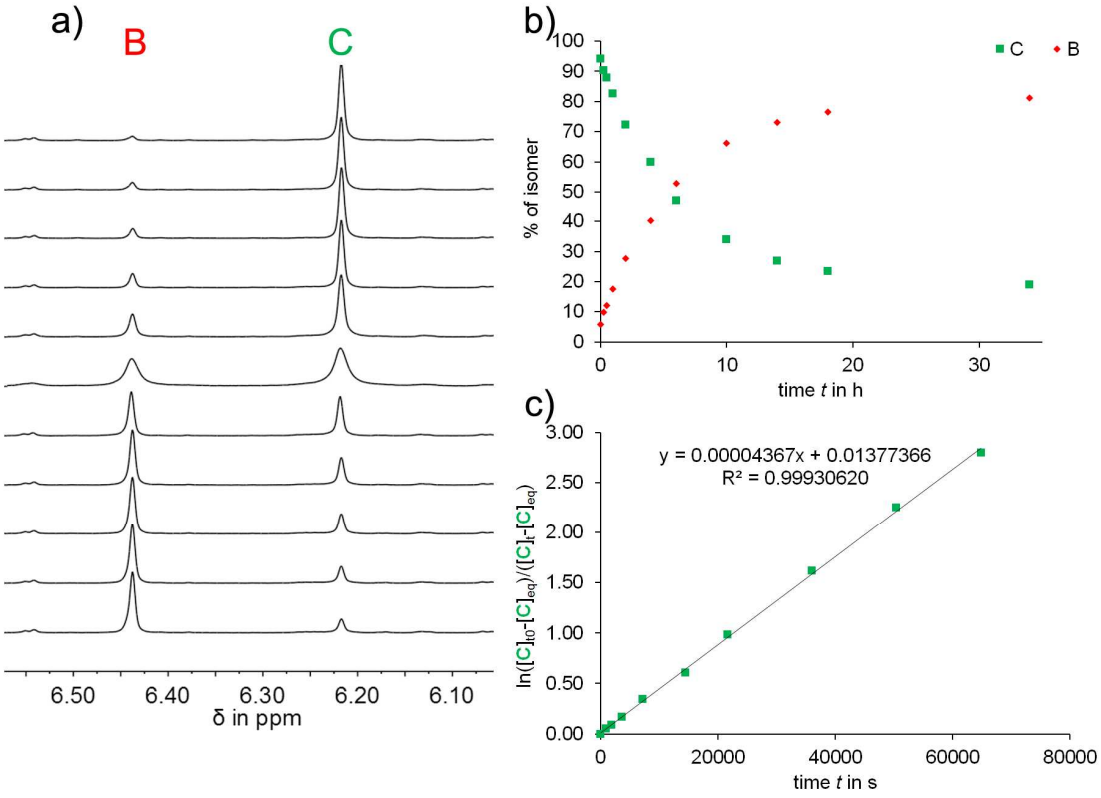

Supplementary Figure 9 | Thermal isomerization from C to B in the dark. a) Thermal isomerization of **C** to **B** in DMSO-d_6 at 80 °C followed by ^{1}H NMR spectroscopy (400 MHz, 20 °C) in regular time intervals. b) Thermal isomer conversion from **C** to **B**. c) First order kinetic analysis of the thermal isomerization of **C** to **B**. Taking into account the dynamic equilibrium by plotting according to Supplementary Equation 1 gives a linear relationship. The slope m can be translated into the rate constant $k_{(\mathbf{C}/\mathbf{B})}$ according to Supplementary Equation 2. The corresponding Gibbs free energy of activation $\Delta G^{\ddagger}$ for the thermal **C** to **B** isomerization is given in Supplementary Table 2.

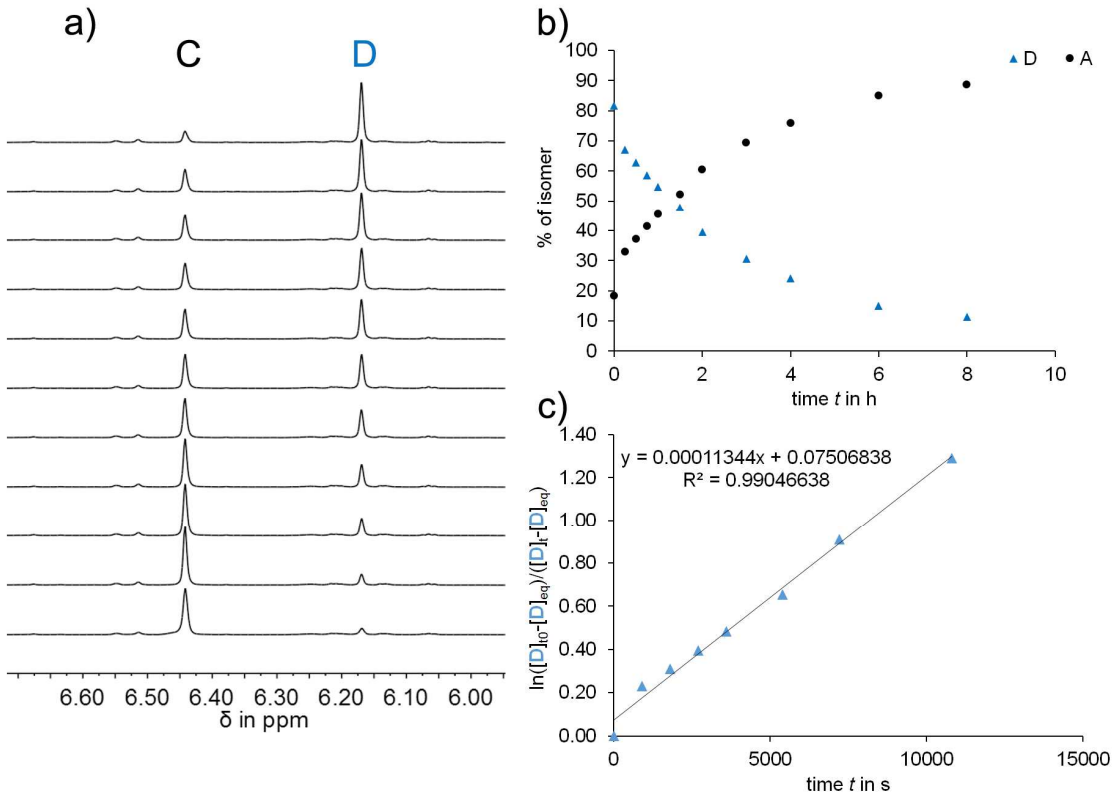

Supplementary Figure 10 | Thermal isomerization from D to A in the dark. a) Thermal isomerization of **D** to **A** in DMSO-d_6 at 60 °C followed by ^{1}H NMR spectroscopy (400 MHz, 20 °C) in regular time intervals. b) Thermal isomer conversion from **D** to **A**. c) First order kinetic analysis of the thermal isomerization of **D** to **A**. Taking into account the dynamic equilibrium by plotting according to Supplementary Equation 1 gives a linear relationship. The slope m can be translated into the rate constant $k_{(\mathbf{D/A})}$ according to Supplementary Equation 2. The corresponding Gibbs free energy of activation ΔG^{*} for the thermal **D** to **A** isomerization is given in Supplementary Table 2.

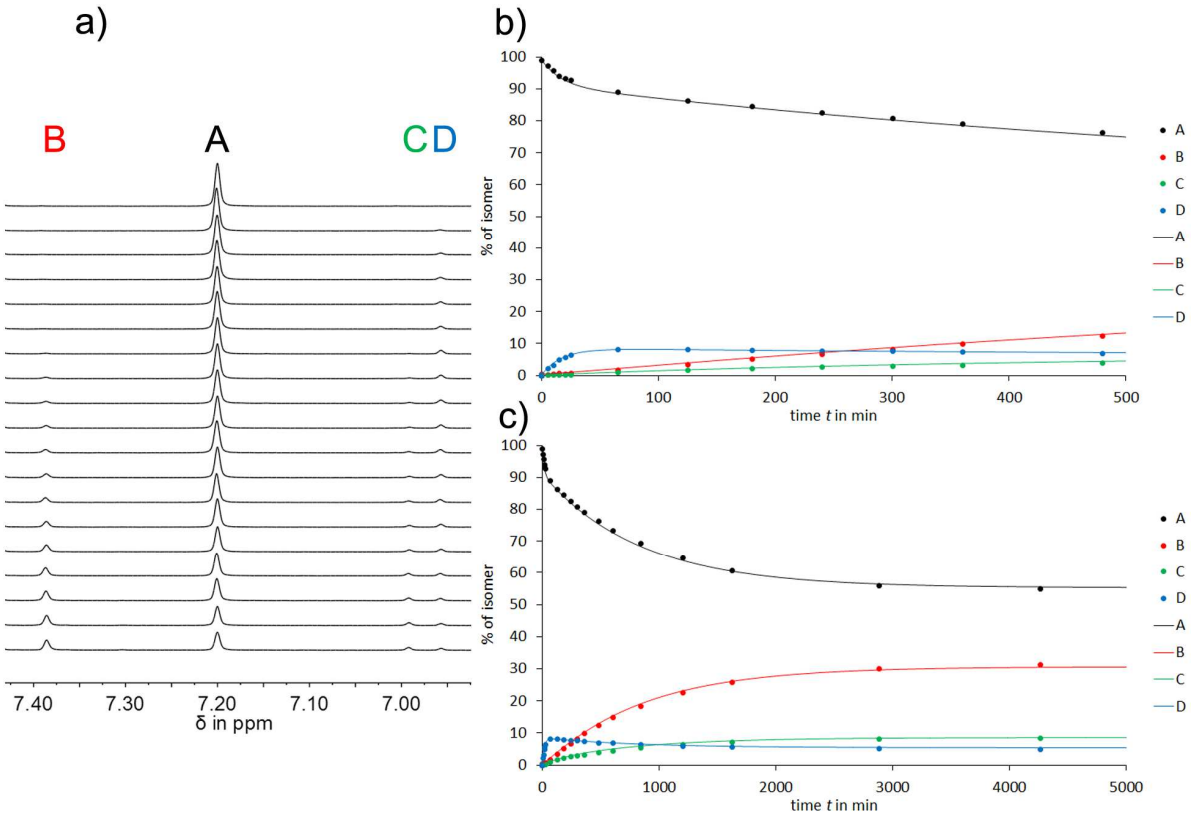

Supplementary Figure 11 | Thermal isomerization of A in 12DCB in the dark. a) Thermal isomerization of **A** in 12DCB-d_4 at 130 °C followed by ^{1}H NMR spectroscopy (400 MHz, 20 °C) in regular time intervals. b) Isomer conversion at the start of the thermal reaction of **A**. c) Isomer conversion over the whole thermal reaction of **A**. The corresponding Gibbs free energies of activation ΔG^* for the thermal reactions of **A** were obtained by fitting the experimental data according to Supplementary Equation 6. A refinement factor of 0.98 was obtained for the best fit. The values are given in Supplementary Table 3.

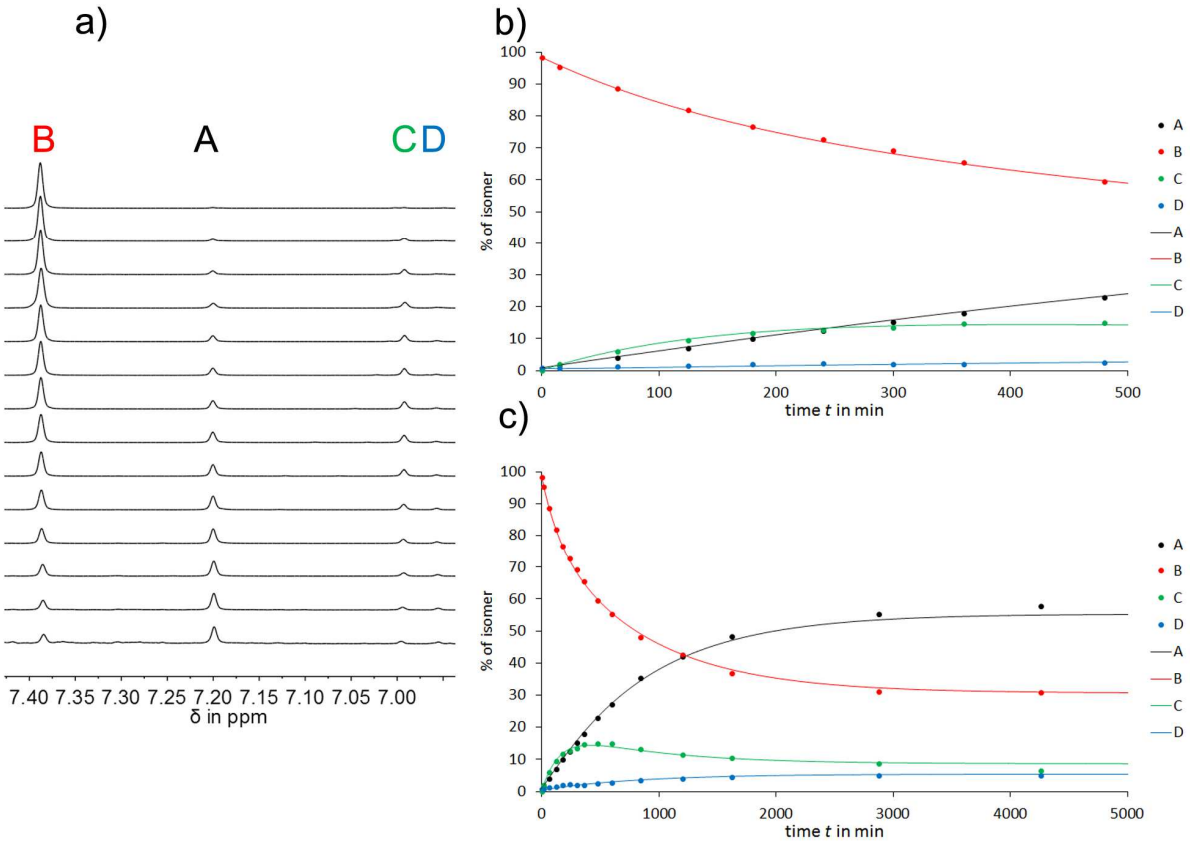

Supplementary Figure 12 | Thermal isomerization of B in 12DCB in the dark. a) Thermal isomerization of **B** in 12DCB -d_4 at 130 °C followed by ^{1}H NMR spectroscopy (400 MHz, 20 °C) in regular time intervals. b) Isomer conversion at the start of the thermal reaction of **B**. c) Isomer conversion over the whole thermal reaction of **B**. The corresponding Gibbs free energies of activation ΔG^* for the thermal reactions of **B** were obtained by fitting the experimental data according to Supplementary Equation 6. A refinement factor of 0.98 was obtained for the best fit. The values are given in Supplementary Table 3.

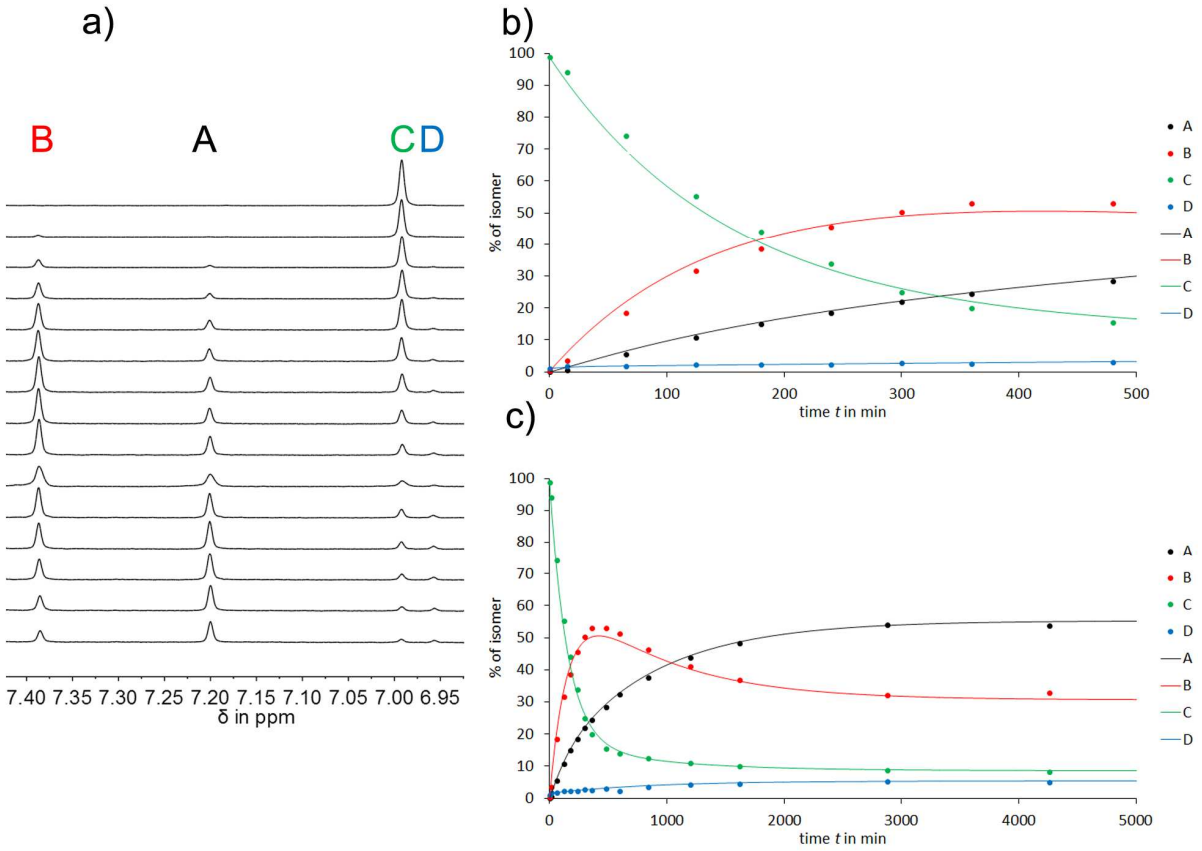

Supplementary Figure 13 | Thermal isomerization of C in 12DCB. a) Thermal isomerization of **C** in 12DCB-d_4 at 130 °C followed by ^{1}H NMR spectroscopy (400 MHz, 20 °C) in regular time intervals. b) Isomer conversion at the start of the thermal reaction of **C**. c) Isomer conversion over the whole thermal reaction of **C**. The corresponding Gibbs free energies of activation $\Delta G^{\ddagger}$ for the thermal reactions of **C** were obtained by fitting the experimental data according to Supplementary Equation 6. A refinement factor of 0.98 was obtained for the best fit. The values are given in Supplementary Table 3.

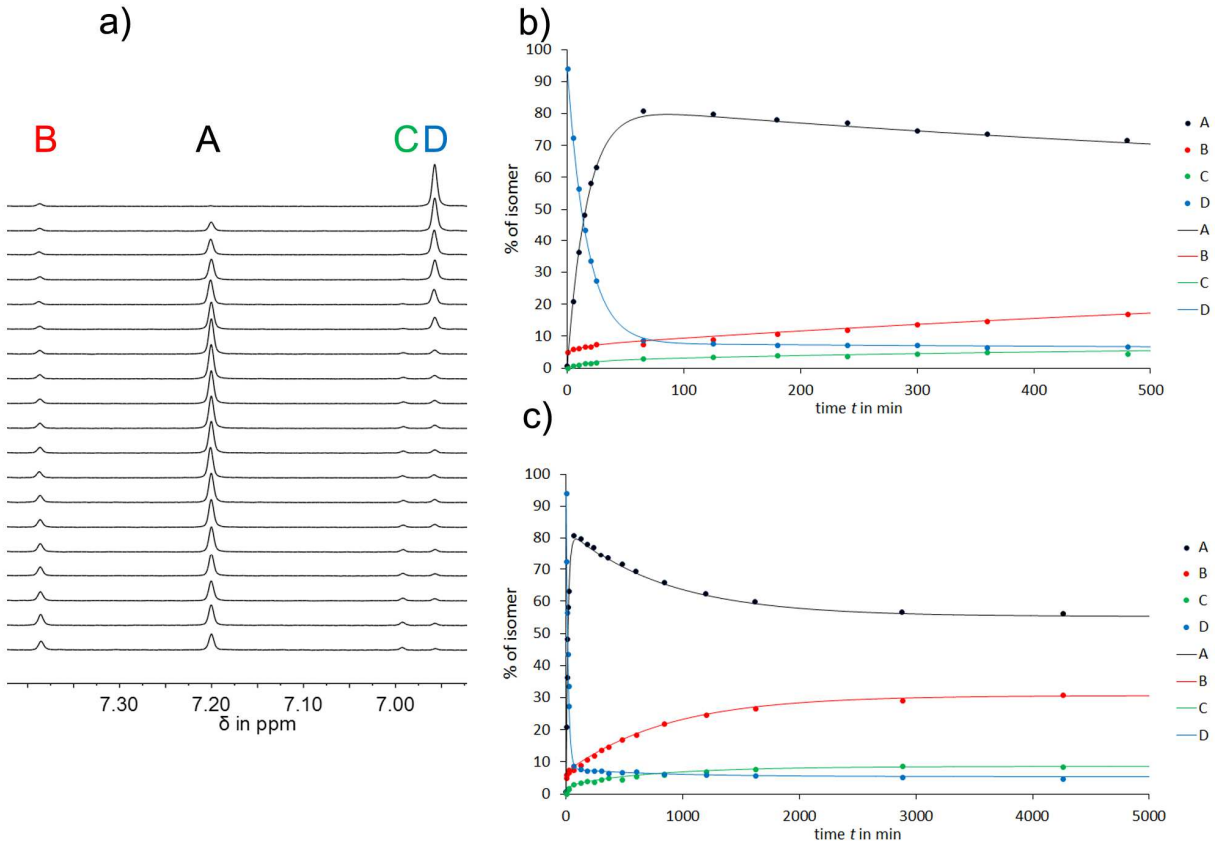

Supplementary Figure 14 | Thermal isomerization of D in 12DCB in the dark. a) Thermal isomerization of **D** in ODCB-d_4 at 130 °C followed by ^{1}H NMR spectroscopy (400 MHz, 20 °C) in regular time intervals. b) Isomer conversion at the start of the thermal reaction of **D**. c) Isomer conversion over the whole thermal reaction of **D**. The corresponding Gibbs free energies of activation ΔG^* for the thermal reactions of **A** were obtained by fitting the experimental data according to Supplementary Equation 6. A refinement factor of 0.98 was obtained for the best fit. The values are given in Supplementary Table 3.

Molar absorption coefficients

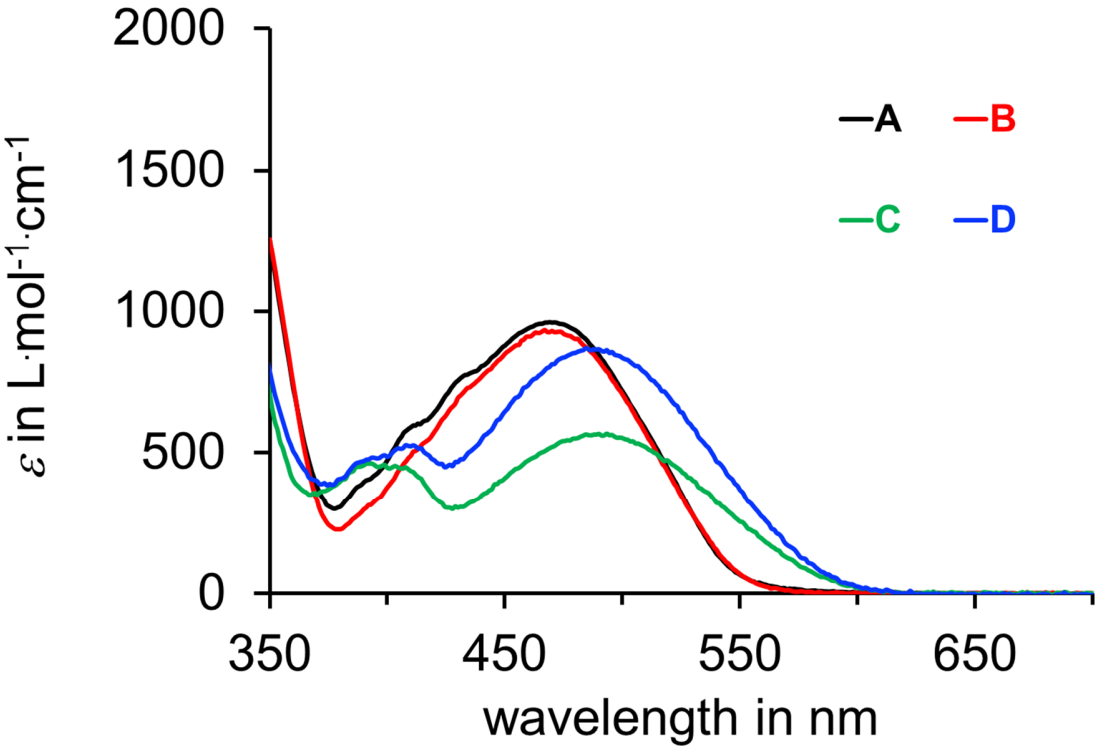

Supplementary Figure 15 | Comparison of molar absorption coefficients of all four isomers of 1 in *c*hexane.

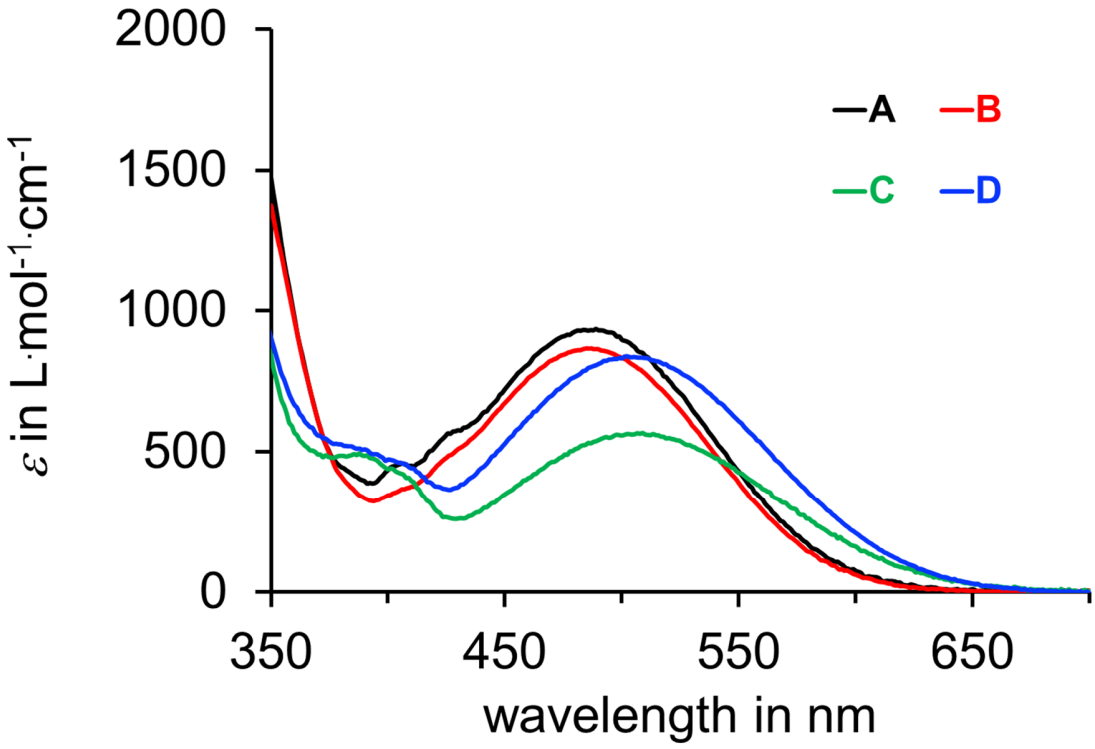

Supplementary Figure 16 | Comparison of molar absorption coefficients of all four isomers of 1 in 12DCB.

Fluorescence spectra in *c*hexane

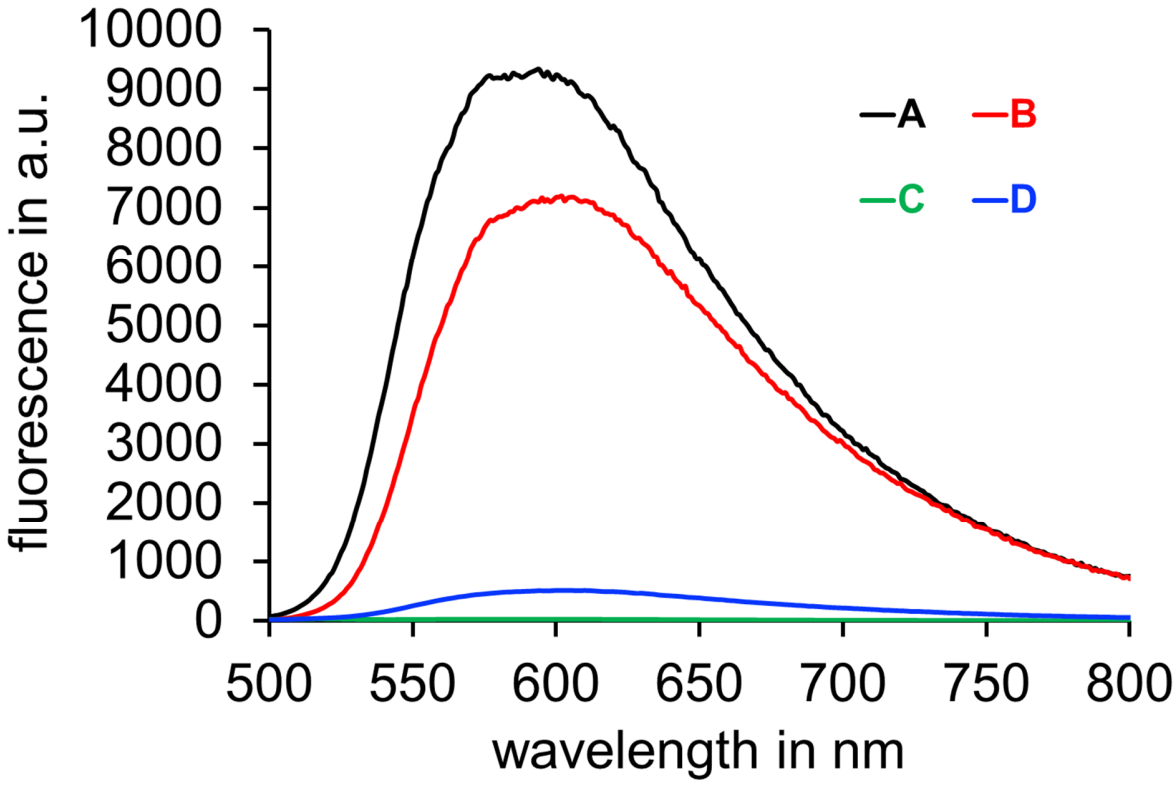

Supplementary Figure 17 | Fluorescence spectra (excitation with 450 nm) of 1 in *c*hexane. The concentration of **1-A** in *c*hexane was 0.26 mM. The fluorescence spectra in the other solvents were multiplied with a factor to account for different concentrations used and to enable quantitative comparison of the spectra with the spectrum of **1-A**.

Quantum yield measurements in different solvents

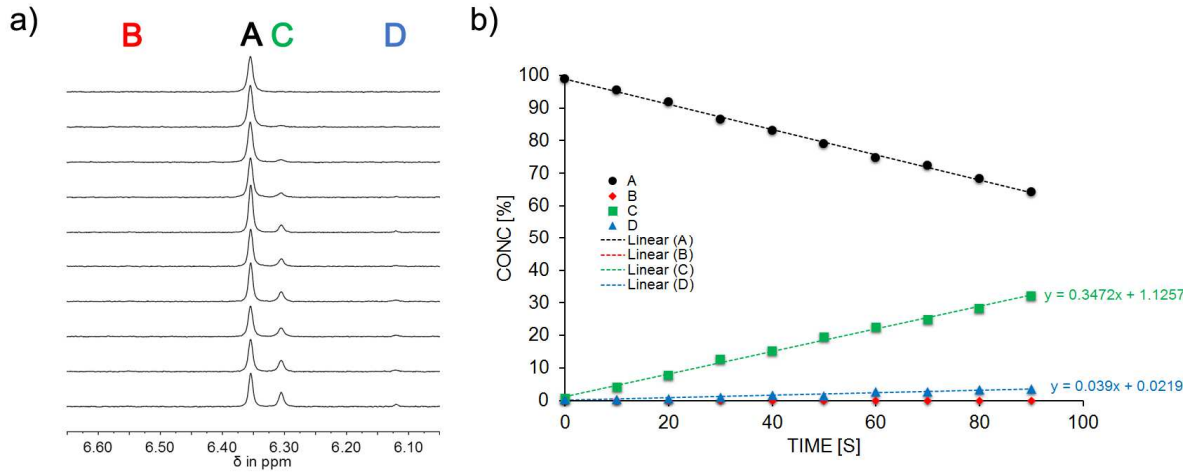

Supplementary Figure 18 | Quantum yields of the photoreactions of A in *c*hexane solution. Quantum yield ϕ measurement for the photoconversion of **A**-**1** at 25 °C in *c*hexane solution (1.01 mM) using a focused 520 nm LED. a) ^{1}H NMR spectra (400 MHz, 18 °C, *c*hexane was removed *in vacuo* and replaced with $CDCl_3$ prior to NMR measurements) recorded after different irradiation durations. Signals of individual isomers are assigned. b) Relative changes of the isomer composition plotted against different duration times of irradiation. Each point represents an individual measurement, the relative isomer ratios were determined by ^{1}H NMR spectroscopy. Quantum yields were determined by averaging over all experiments and are given in Supplementary Table 4.

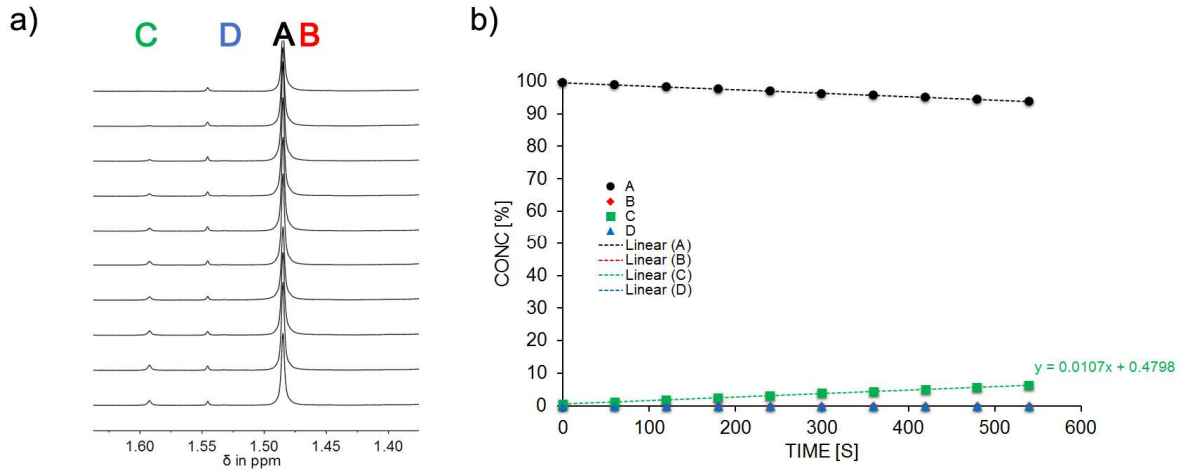

Supplementary Figure 19 | Quantum yields of the photoreactions of A in 12DCB solution. Quantum yield ϕ measurement for the photoconversion of **A**-**1** at 25 °C in 12DCB solution (0.97 mM) using a focused 520 nm LED. a) ^{1}H NMR spectra (400 MHz, 18 °C, 12DCB was removed *in vacuo* and replaced with benzene-d_6 prior to NMR measurements) recorded after different irradiation durations. Signals of individual isomers are assigned. b) Relative changes of the isomer composition plotted against different duration times of irradiation. Each point represents an individual measurement, the relative isomer ratios were determined by ^{1}H NMR spectroscopy. Quantum yields were determined by averaging over all experiments and are given in Supplementary Table 4.

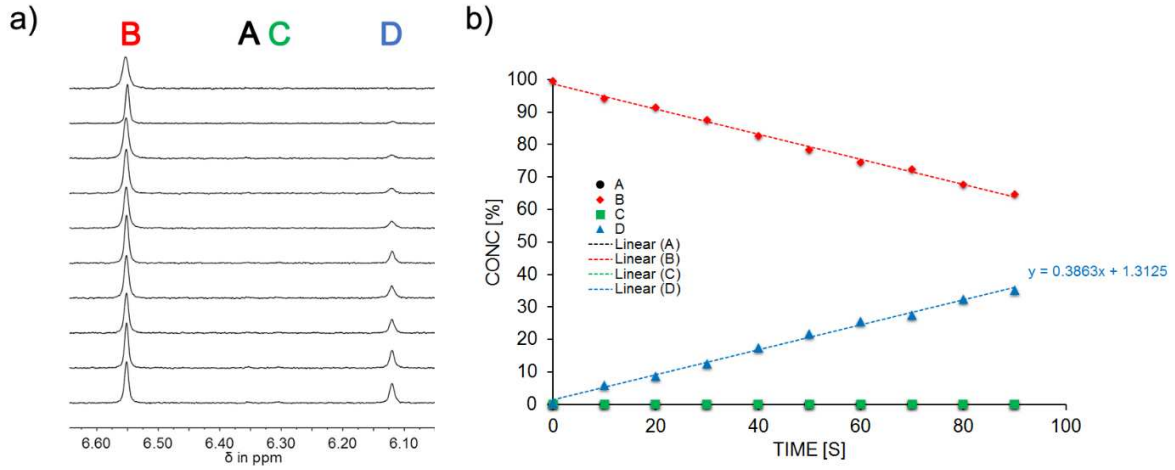

Supplementary Figure 20 | Quantum yields of the photoreactions of B in *c*hexane solution. Quantum yield ϕ measurement for the photoconversion of **B**-**1** at 25 °C in *c*hexane solution (0.87 mM) using a focused 520 nm LED. a) ^{1}H NMR spectra (400 MHz, 18 °C, *c*hexane was removed *in vacuo* and replaced with $CDCl_3$ prior to NMR measurements) recorded after different irradiation durations. Signals of individual isomers are assigned. b) Relative changes of the isomer composition plotted against different duration times of irradiation. Each point represents an individual measurement, the relative isomer ratios were determined by ^{1}H NMR spectroscopy. Quantum yields were determined by averaging over all experiments and are given in Supplementary Table 4.

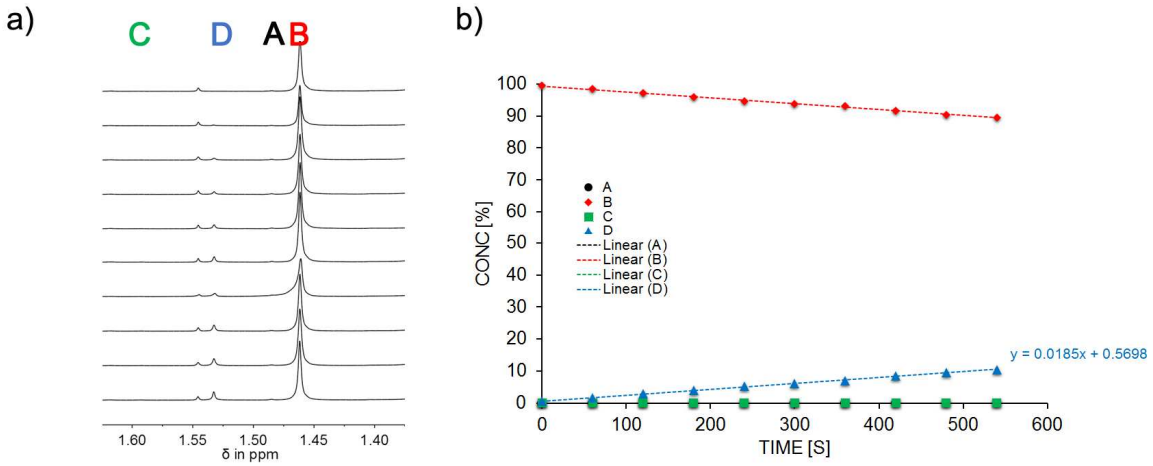

Supplementary Figure 21 | Quantum yields of the photoreactions of B in 12DCB solution. Quantum yield ϕ measurement for the photoconversion of **B**-**1** at 25 °C in 12DCB solution (0.97 mM) using a focused 520 nm LED. a) ^{1}H NMR spectra (400 MHz, 18 °C, 12DCB was removed *in vacuo* and replaced with benzene-d_6 prior to NMR measurements) recorded after different irradiation durations. Signals of individual isomers are assigned. b) Relative changes of the isomer composition plotted against different duration times of irradiation. Each point represents an individual measurement, the relative isomer ratios were determined by ^{1}H NMR spectroscopy. Quantum yields were determined by averaging over all experiments and are given in Supplementary Table 4.

Motor operation followed by NMR-spectroscopy

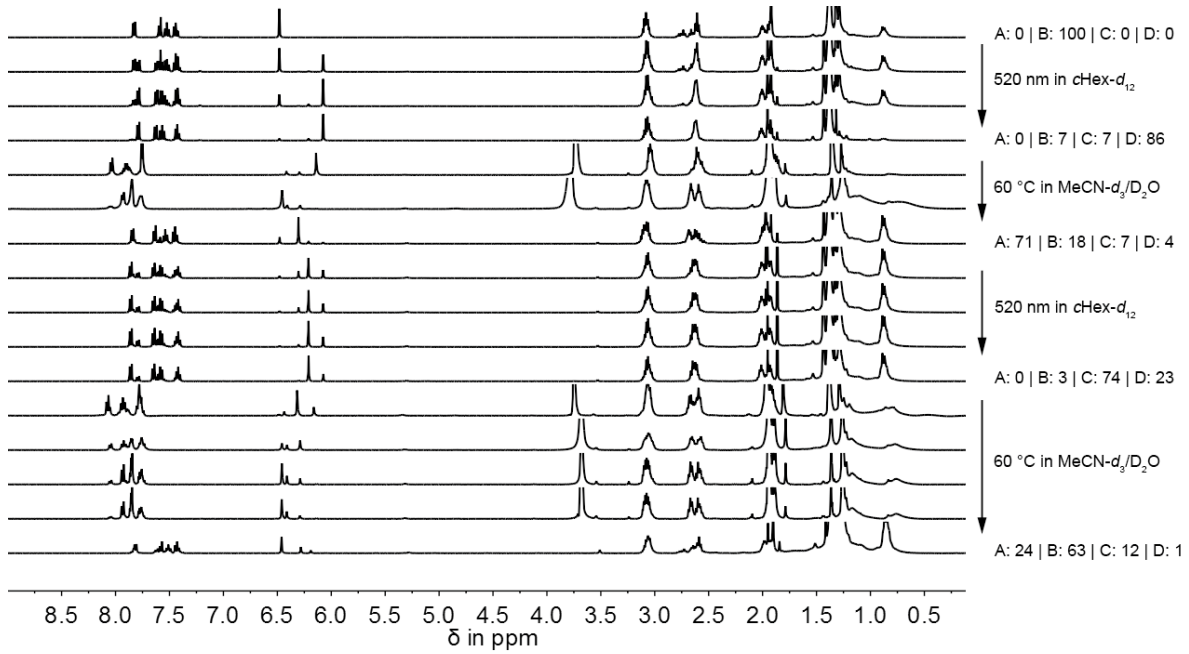

Supplementary Figure 22 | Motor operation of 1 followed by ^{1}H NMR spectroscopy (400 MHz, 18 °C) in different solvents. All steps were recorded for a single sample in a row starting with pure isomer **B**. Solvent changes were done by removing the current solvent *in vacuo* and replacing it with a new one.

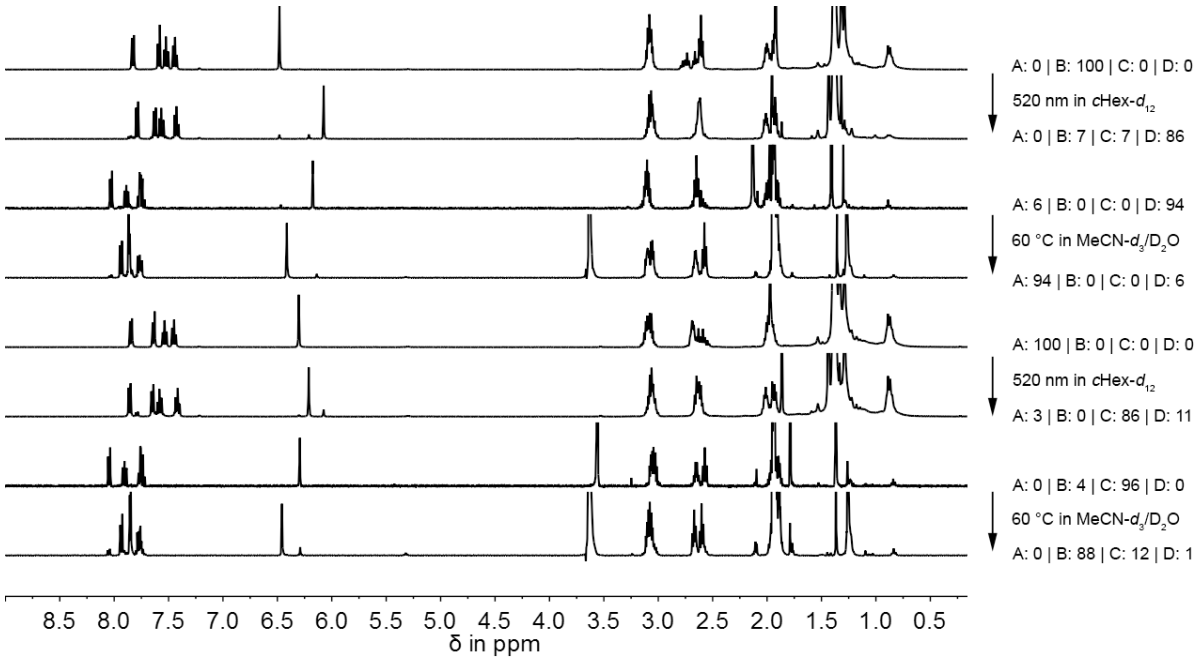

Supplementary Figure 23 | Motor operation of 1 followed by ^{1}H NMR spectroscopy (400 MHz, 18 °C) in different solvents separately for each transformation. A new solution of each respective pure isomer in the respective solvent was used for each step allowing to quantify the corresponding selectivity and degree of completeness individually.

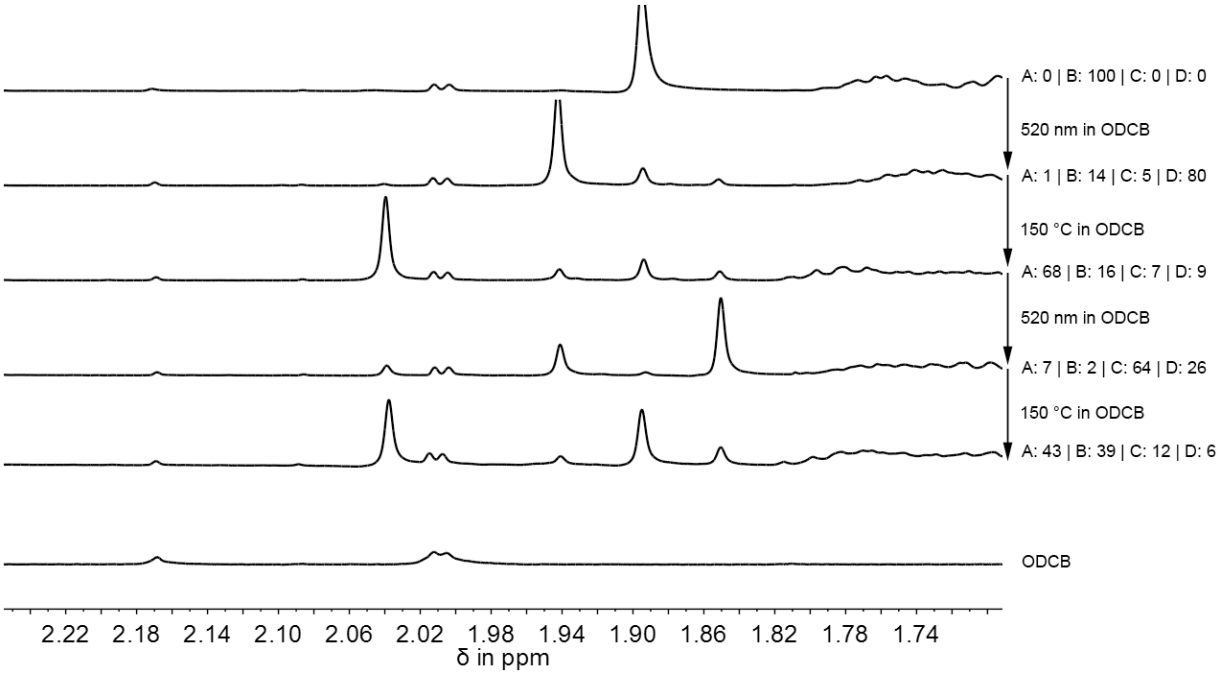

Supplementary Figure 24 | Motor operation of 1 followed by ^{1}H NMR spectroscopy (400 MHz, 18 °C) in non-deuterated 12DCB. All steps were recorded for a single sample in a row starting with pure isomer **B**.

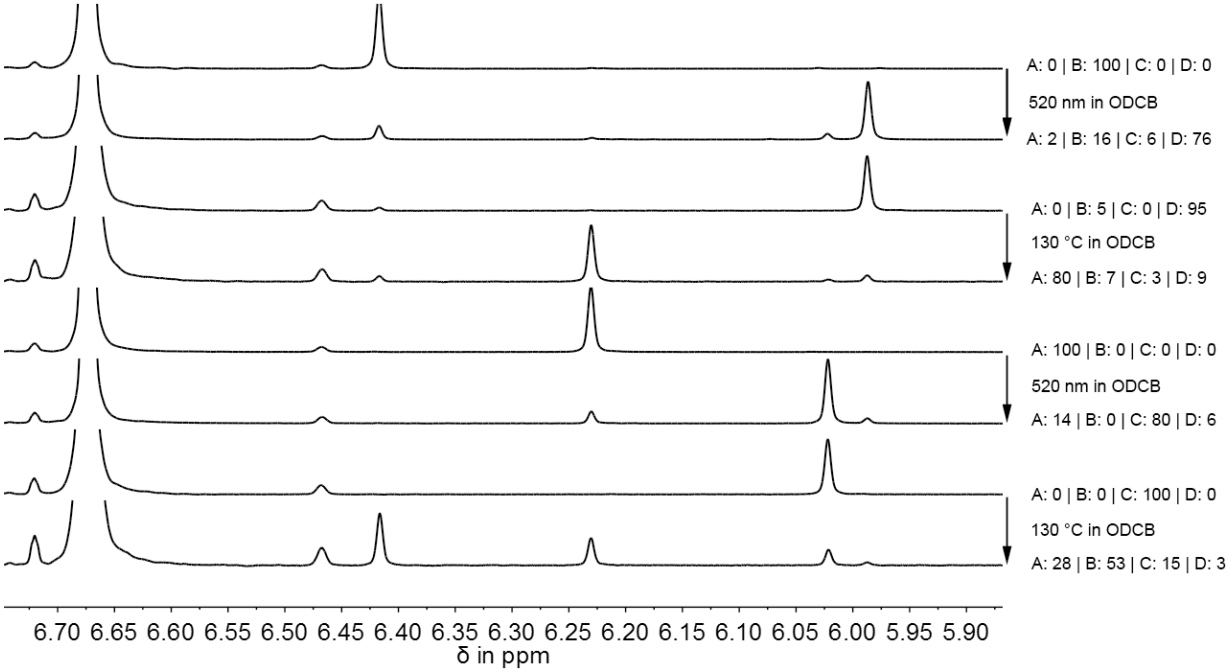

Supplementary Figure 25 | Motor operation of 1 followed by ^{1}H NMR spectroscopy (400 MHz, 18 °C) in 12DCB-d_4 separately for each transformation. A new solution of each respective pure isomer was used for each step allowing to quantify the corresponding selectivity and degree of completeness individually.

Theoretical description of the ground state of 1

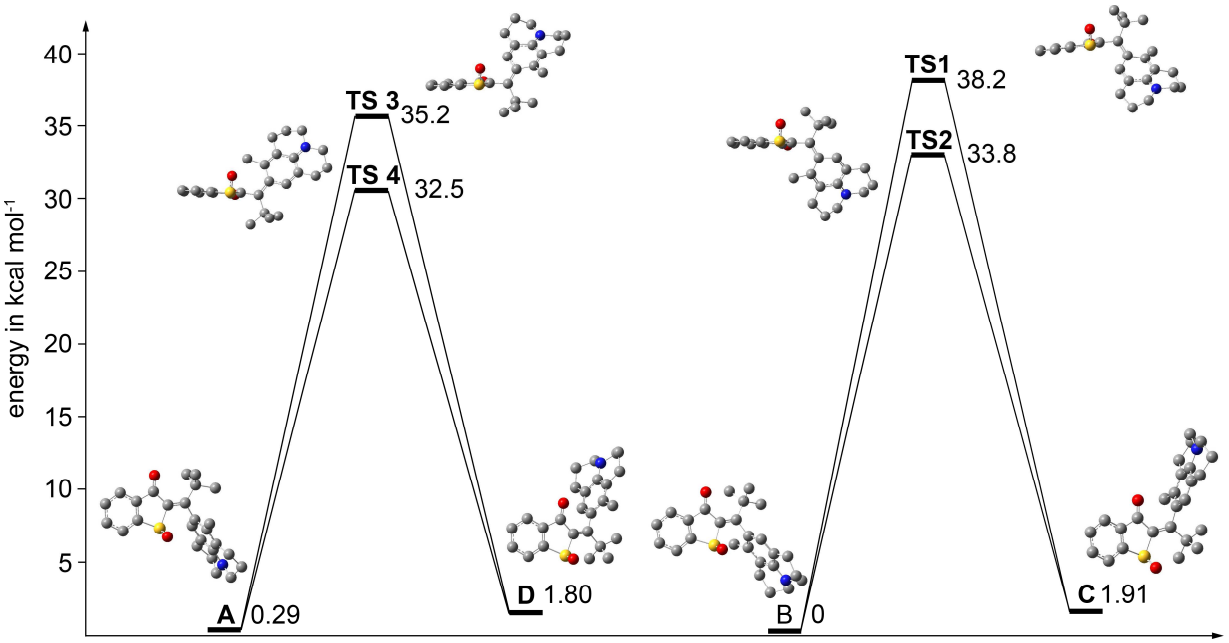

Supplementary Figure 26 | Calculated ground state energy profile of 1 in DMSO solution. All energy values are given in kcal mol^{-1} and were obtained by DFT calculations at the ω–B97XD/6-311G(d,p) level of theory.

NMR Spectra

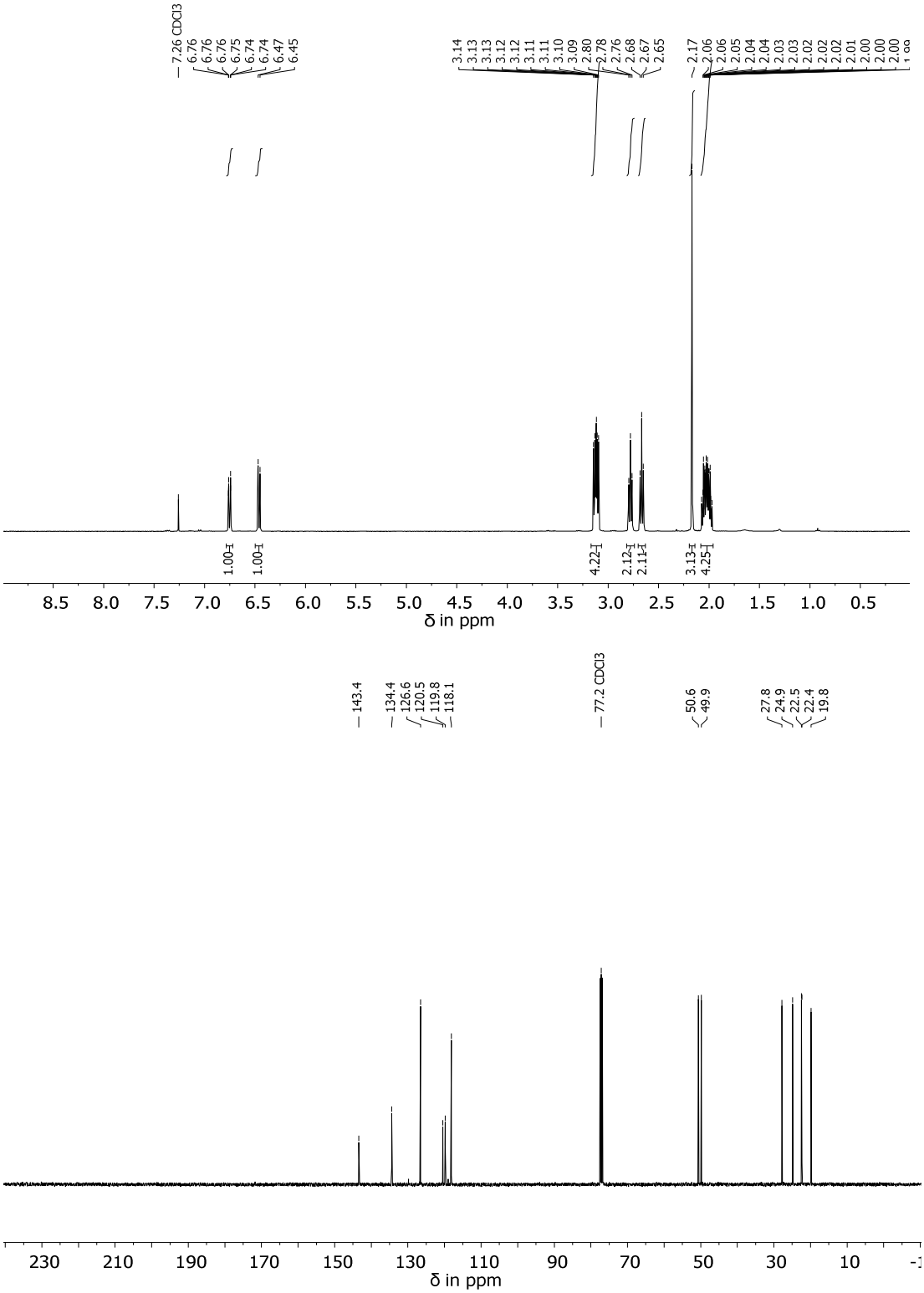

Supplementary Figure 27 | 400 MHz ^{1}H NMR spectrum (top) and 100 MHz ^{13}C NMR spectrum (bottom) of 4 in $CDCl_3$.

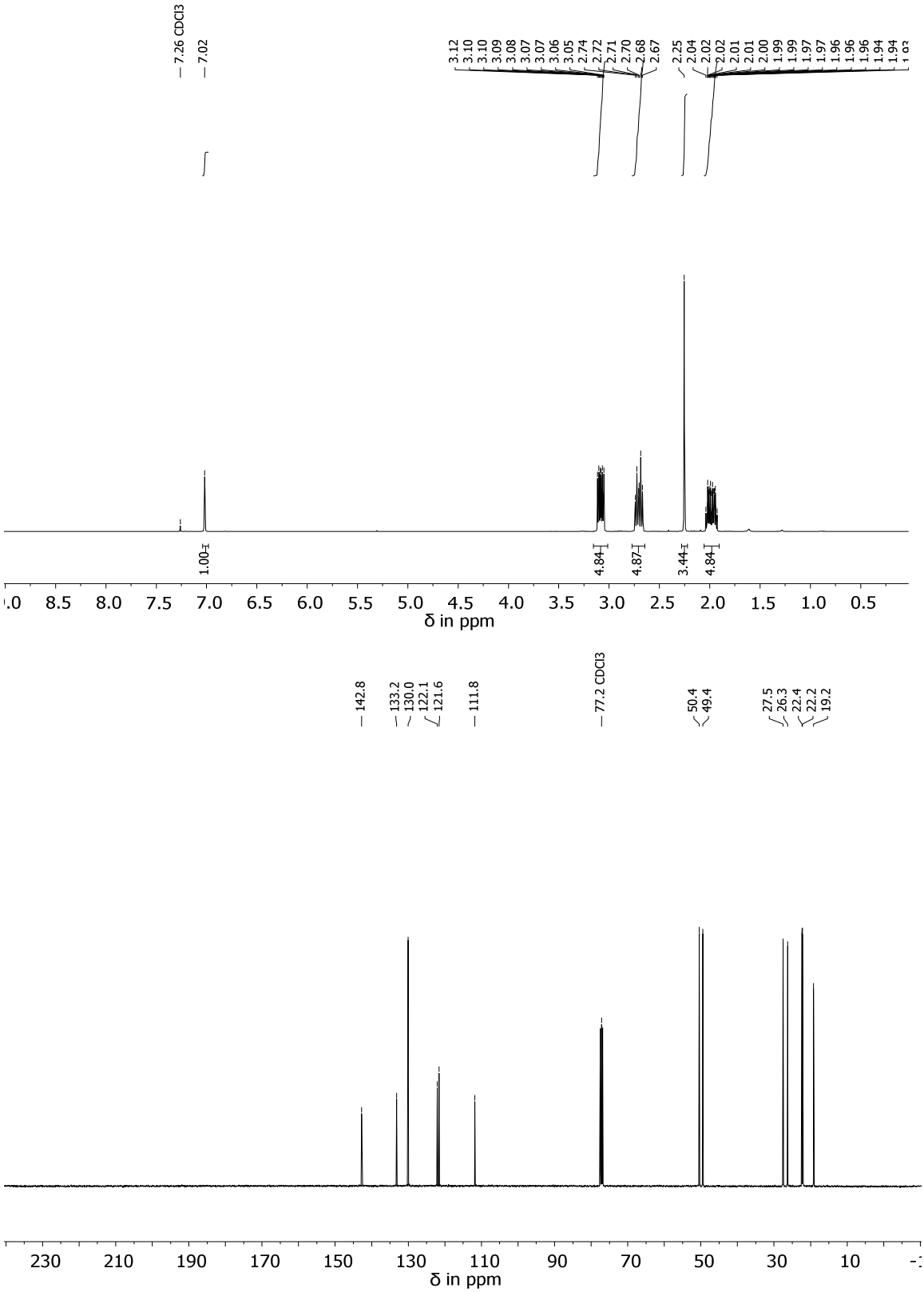

Supplementary Figure 28 | 400 MHz ^{1}H NMR spectrum (top) and 100 MHz ^{13}C NMR spectrum (bottom) of 5 in $CDCl_3$.

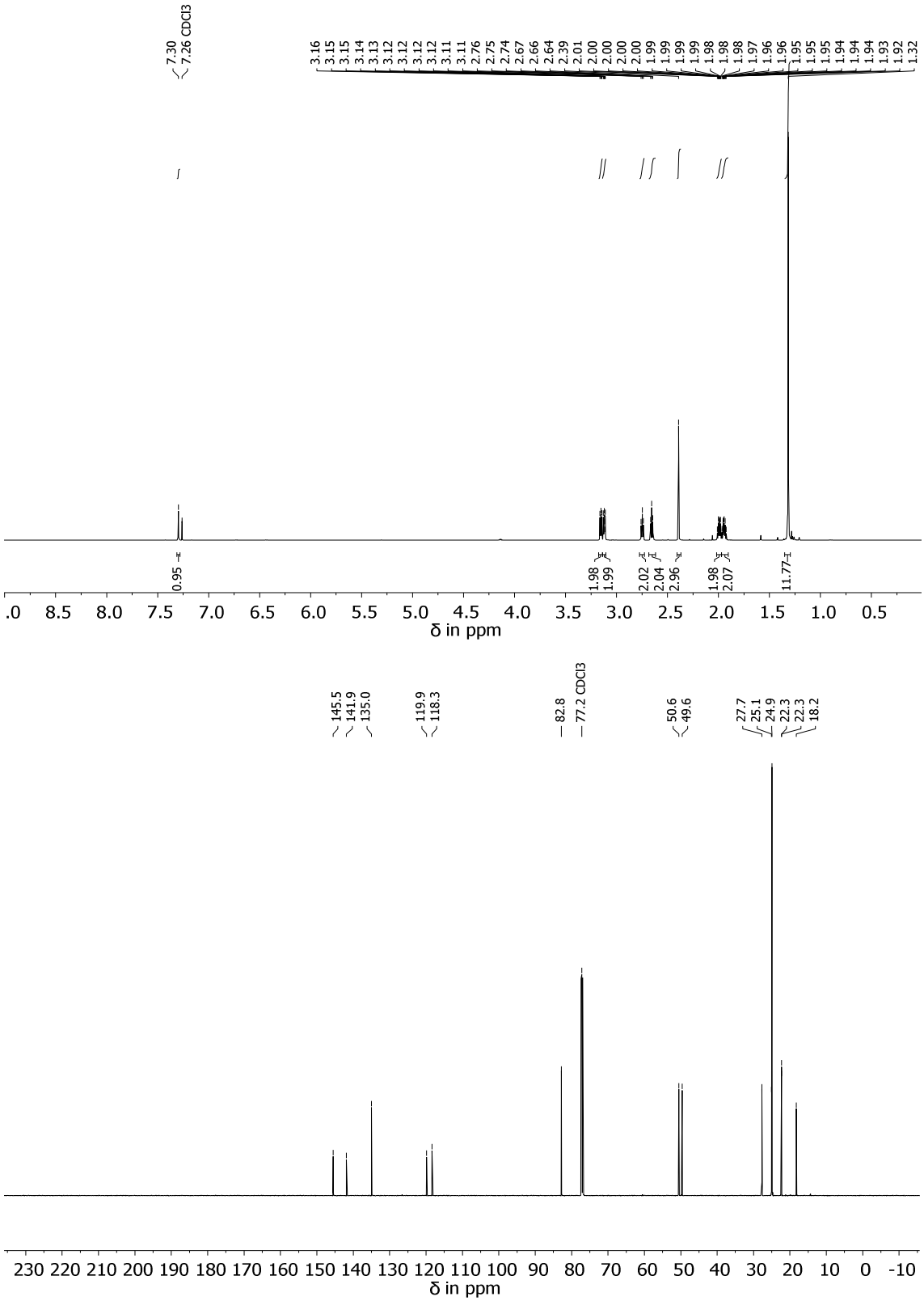

Supplementary Figure 29 | 400 MHz ^{1}H NMR spectrum (top) and 100 MHz ^{13}C NMR spectrum (bottom) of 6 in $CDCl_3$.

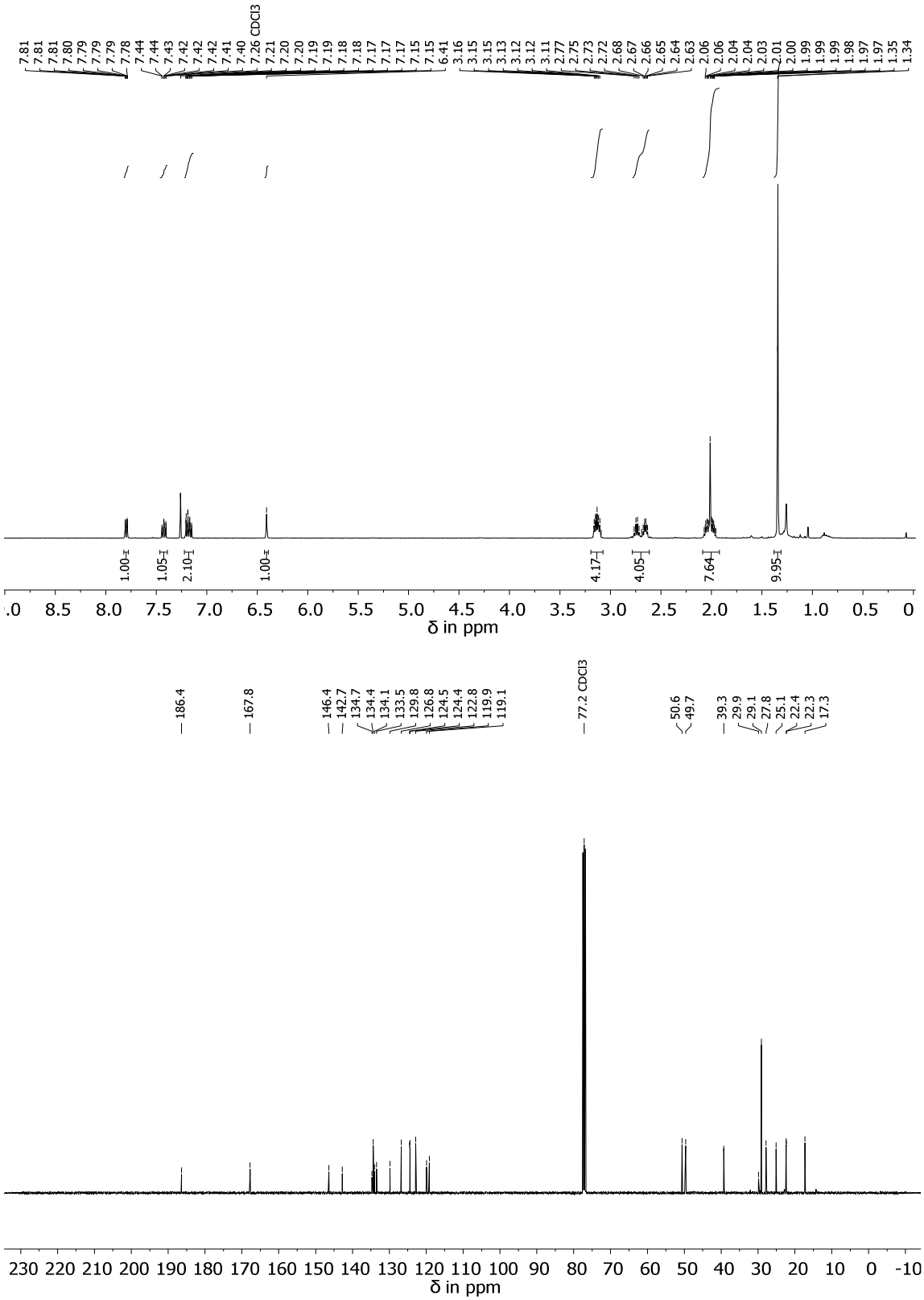

Supplementary Figure 30 | 400 MHz ^{1}H NMR spectrum (top) and 100 MHz ^{13}C NMR spectrum (bottom) of 7 in $CDCl_3$.

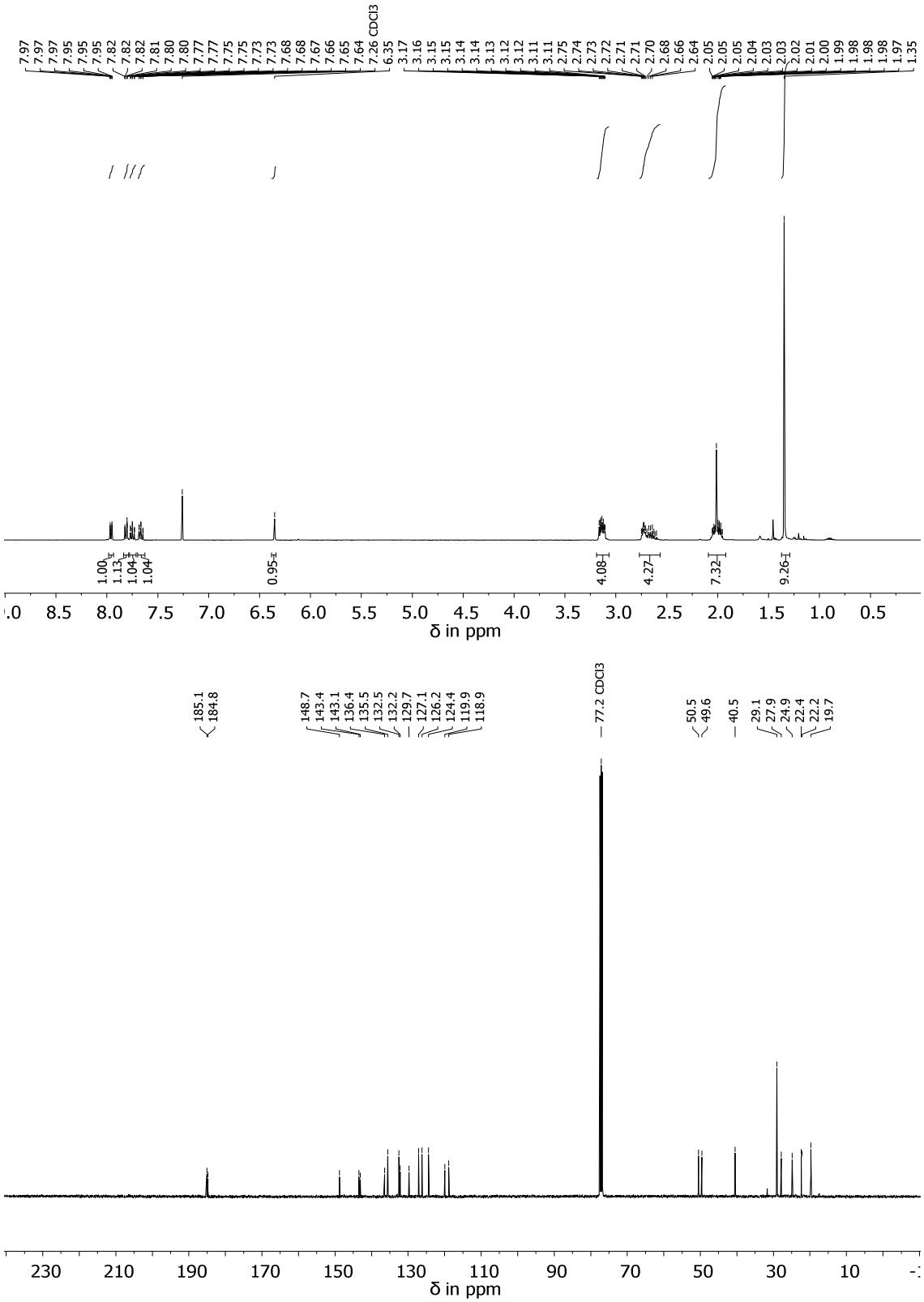

Supplementary Figure 31 | 400 MHz ^{1}H NMR spectrum (top) and 100 MHz ^{13}C NMR spectrum (bottom) of A-1 in $CDCl_3$.

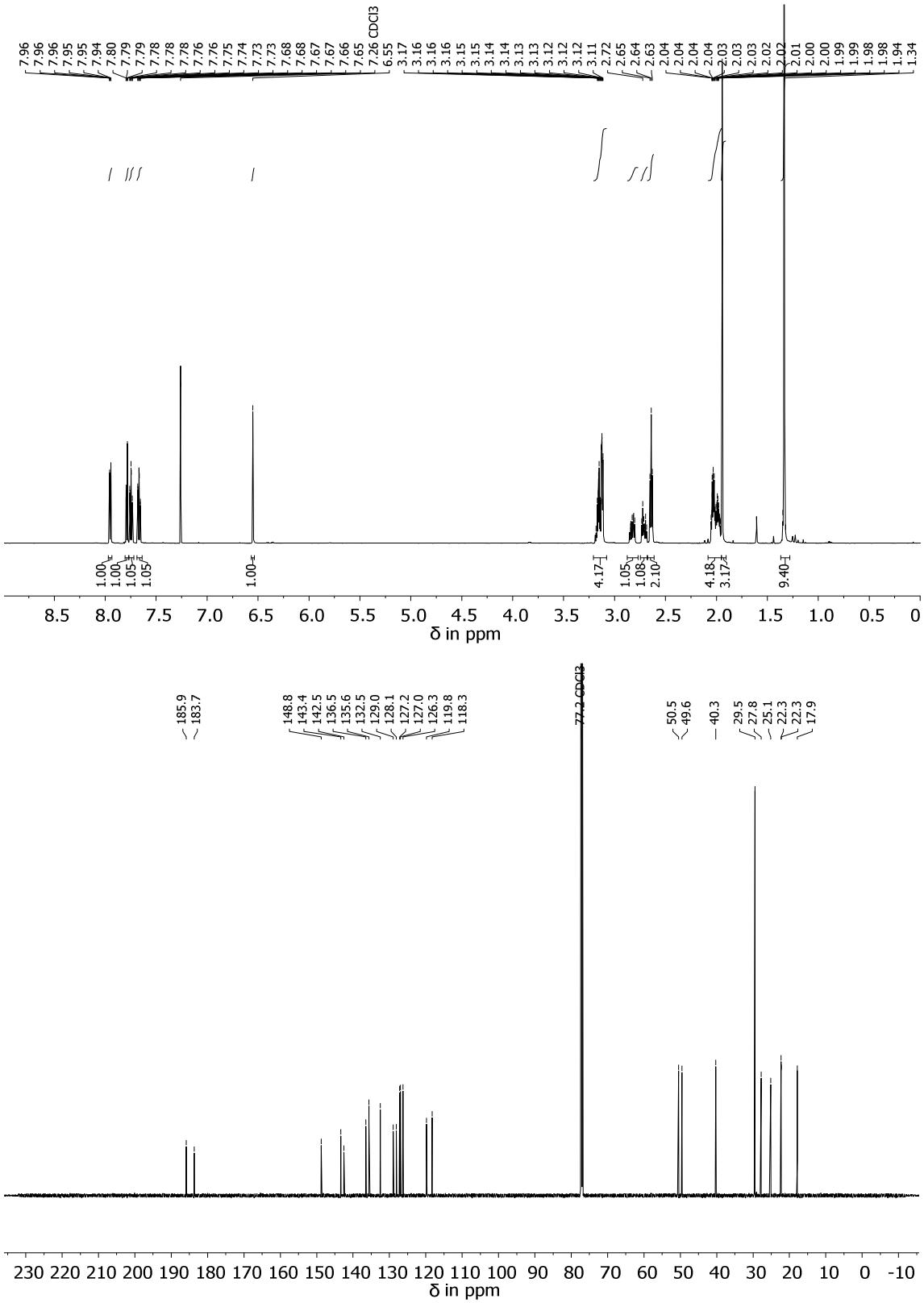

Supplementary Figure 32 | 599 MHz ^{1}H NMR spectrum (top) and 151 MHz ^{13}C NMR spectrum (bottom) of B-1 in $CDCl_3$.

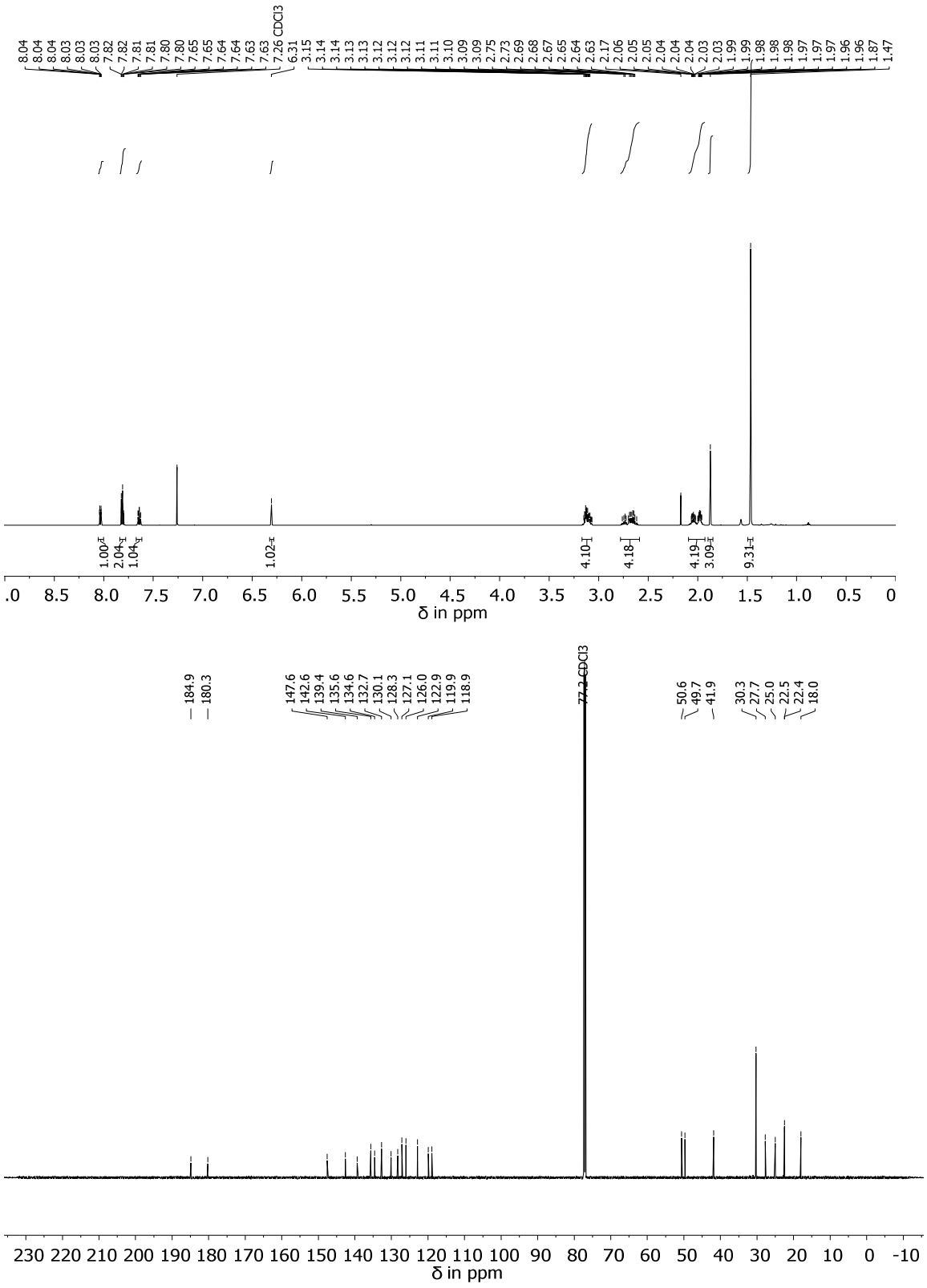

Supplementary Figure 33 | 599 MHz ^{1}H NMR spectrum (top) and 151 MHz ^{13}C NMR spectrum (bottom) of C-1 in $CDCl_3$.

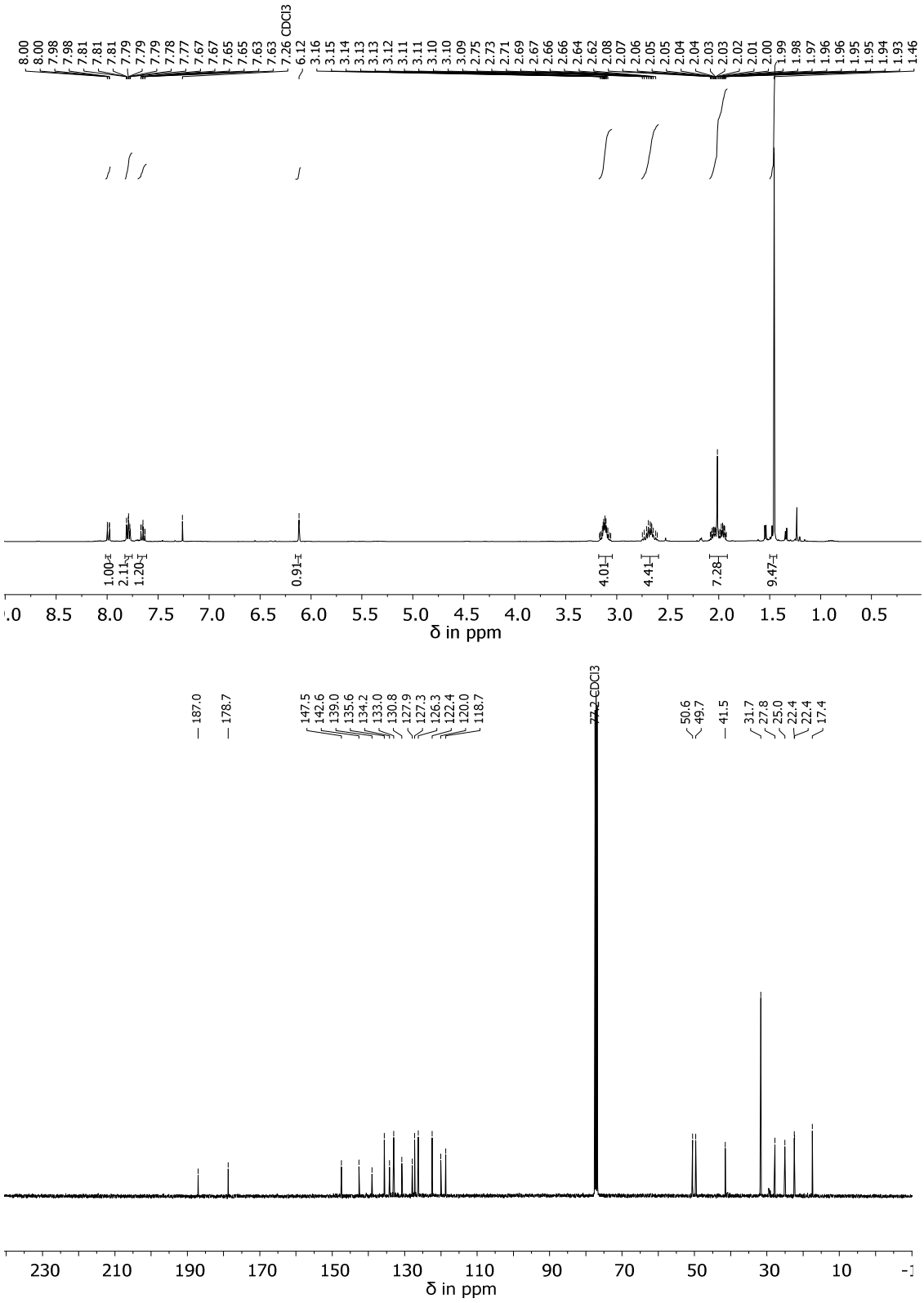

Supplementary Figure 34 | 400 MHz ^{1}H NMR spectrum (top) and 100 MHz ^{13}C NMR spectrum (bottom) of D-1 in $CDCl_3$.

Supplementary Tables

Physical and photophysical properties and theoretical description of the ground state

Supplementary Table 1 | Thermal isomerization behavior of HTI 1. Thermal isomerization behavior of HTI **1** in MeCN-d_3/D_2O (8:2) at elevated temperature.

Isomer	$k_{(\text{isom. 1/isom. 2})}$ / s^{-1} (at T / °C)	ΔG^* (therm. isomer equilibration) /kcal mol^{-1}	Equilibration half-life of pure isomer at 27 °C	Thermo-dynamic isomer 1/isomer 2 equilibrium in the dark (at T / °C)	$\Delta\Delta G^0$(isomer 1 / isomer 2) / kcal mol^{-1}	Slope m / s^{-1} (at T / °C)
C	$k_{(\mathbf{C/B})}$ = 1.46x10^{-4} (60 °C)	ΔG^*(**C/B**) = 25.42	4.2 d	**C/B** = 13/87 (60 °C)	$\Delta\Delta G^0$(**C/B**) = 1.26	5.97x10^{-4} (60 °C)
D	$k_{(\mathbf{D/A})}$ = 9.38x10^{-5} (27 °C)	ΔG^*(**D/A**) = 23.10	125 min	**D/A** = 7/93 (27 °C)	$\Delta\Delta G^0$(**D/A**) = 1.54	5.68x10^{-4} (27 °C)

Supplementary Table 2 | Thermal isomerization behavior of HTI 1. Thermal isomerization behavior of HTI **1** in DMSO-d_6 at elevated temperature.

Isomer	$k_{(\text{isom. 1/isom. 2})}$ / s^{-1} (at T / °C)	ΔG^* (therm. isomer equilibration) /kcal mol^{-1}	Equilibration half-life of pure isomer at 27 °C	Thermo-dynamic isomer 1/isomer 2 equilibrium in the dark (at T / °C)	$\Delta\Delta G^0$(isomer 1 / isomer 2) / kcal mol^{-1}	Slope m / s^{-1} (at T / °C)
A	$k_{(\mathbf{A/D})}$ = 1.03x10^{-5} (60 °C)	ΔG^*(**A/D**) = 27.17	80 d	**A/D** = 91/9 (60 °C)	$\Delta\Delta G^0$(**A/D**) = -1.53	1.17x10^{-4} (60 °C)
B	$k_{(\mathbf{B/C})}$ = 8.50x10^{-6} (80 °C)	ΔG^*(**B/C**) = 28.98	4.6 a	**B/C** = 85/15 (80 °C)	$\Delta\Delta G^0$(**B/C**) = -1.21	5.48x10^{-5} (80 °C)
C	$k_{(\mathbf{C/B})}$ = 3.54x10^{-5} (80 °C)	ΔG^*(**C/B**) = 27.98	0.86 a	**C/B** = 19/81 (80 °C)	$\Delta\Delta G^0$(**C/B**) = 1.02	4.37x10^{-5} (80 °C)
D	$k_{(\mathbf{D/A})}$ = 1.01x10^{-4} (60 °C)	ΔG^*(**D/A**) = 25.67	6.5 d	**D/A** = 11/89 (60 °C)	$\Delta\Delta G^0$(**D/A**) = 1.38	1.13x10^{-4} (60 °C)

Supplementary Table 3 | Thermal isomerization behavior of HTI 1 in 12DCB-d_4 at 130 °C. The values were obtained by fitting the experimental obtained kinetic data to Supplementary Equation 6. A refinement factor of 0.98 was obtained. *High barriers can only be determined with large uncertainty as this reactions were only performed by a small amount of molecules. The given values are therefore only a lower limit for these barriers.

Reaction	ΔG^* /kcal mol^{-1}
A → B	34*
A → C	34.8*
A → D	31.28
B → A	33.5*
B → C	32.5
B → D	33.8*
C → A	33.4*
C → B	31.5
C → D	32.7
D→ A	29.52
D → B	32.3*
D → C	32.45*

Supplementary Table 4 | Quantum yields of HTI 1. Quantum yields ϕ in % for the different photoconversions of isomers **A**-**1** and **B**-**1** after 520 nm illumination in different solvents at 25 °C. SBR = single-bond rotation, DBI = double-bond isomerization, HT = hula twist.

	*c*Hex	ODCB
A to B SBR	<0.1%[a]	<0.01%[a]
A to C DBI	16%[a]	0.10%[a]
A to D HT	1.1%[a]	<0.01%[a]
B to A SBR	<0.1%[a]	<0.01%[a]
B to C HT	<0.1%[a]	<0.01%[a]
B to D DBI	14%[a]	0.18%[a]

Supplementary Table 5 | Ground state energies of HTI 1. Summary of the calculated energies for important stationary points of the ground state energy profile of **1**.

Isomer	G_0 (Hartree)	ΔG (Hartree)	ΔG (kcal mol^{-1})
A	-1611.0717	0.000444	0.2786142
B	-1611.0722	0	0
C	-1611.0691	0.003038	1.90637377
D	-1611.0693	0.002875	1.80408972
TS 1	-1611.0113	0.060863	38.1921088
TS 2	-1611.0183	0.053814	33.7687946
TS 3	-1611.0161	0.056018	35.1518254
TS 4	-1611.0203	0.051834	32.5263258

Calculated ground state geometries - xyz coordinates

Supplementary Table 6 | Calculated ground state geometries of A-1 and B-1.

A-1				B-1			
S	-1.481773	-1.246402	0.2849	S	1.469092	-1.272251	-0.24029
O	-3.849107	1.790765	-0.52053	O	3.817627	1.829947	-0.600104
O	-1.143427	-1.416524	1.748121	O	1.159916	-1.694249	-1.659401
C	-3.227436	-1.63712	0.112206	C	3.223529	-1.606151	0.003942
C	-3.757436	-2.909618	0.258224	C	3.757592	-2.867157	0.21004
H	-3.124147	-3.76316	0.469258	H	3.122142	-3.739785	0.304317
C	-5.132985	-3.058958	0.11982	C	5.142118	-2.979512	0.297532
H	-5.576179	-4.041881	0.226391	H	5.588628	-3.952149	0.466364
C	-5.950121	-1.960719	-0.159298	C	5.962559	-1.857205	0.170561
H	-7.018455	-2.103646	-0.266998	H	7.037399	-1.970152	0.243537
C	-5.404691	-0.693076	-0.299144	C	5.412618	-0.600958	-0.046028
H	-6.022466	0.171006	-0.512927	H	6.033976	0.280873	-0.148283
C	-4.029808	-0.540938	-0.151164	C	4.029899	-0.487616	-0.12859
C	-3.296066	0.742278	-0.260439	C	3.280192	0.774563	-0.341112
C	-1.834454	0.513599	-0.063658	C	1.816881	0.517233	-0.193984
C	-0.764563	1.339678	-0.131923	C	0.761952	1.337814	0.005262
C	0.587838	0.701121	-0.084515	C	-0.593178	0.702983	0.028619
C	1.355051	0.636232	1.080589	C	-1.210954	0.290325	1.211673
C	2.64109	0.086819	1.031777	C	-2.50139	-0.248815	1.168277
C	3.162053	-0.416574	-0.181609	C	-3.194949	-0.349251	-0.058963
C	2.370938	-0.356736	-1.348623	C	-2.558781	0.068684	-1.246761
C	1.109233	0.206636	-1.275734	C	-1.271462	0.571798	-1.177958
C	-0.797423	2.865763	-0.340789	C	0.805688	2.871291	0.142762
C	0.610943	3.479334	-0.249133	C	-0.566019	3.432133	0.558046
H	1.054757	3.343606	0.738928	H	-1.344943	3.195513	-0.168921
H	1.291922	3.057482	-0.990719	H	-0.882866	3.053028	1.532649
H	0.529994	4.553783	-0.433504	H	-0.487066	4.519913	0.630825
C	-1.326818	3.14391	-1.762465	C	1.821319	3.321067	1.207926
H	-2.346468	2.786465	-1.890591	H	2.840383	3.03788	0.958577
H	-1.312582	4.222659	-1.943121	H	1.78555	4.41101	1.289669
H	-0.683677	2.669367	-2.509239	H	1.565703	2.907079	2.187047
C	-1.668633	3.553856	0.724694	C	1.161124	3.459474	-1.237583
H	-1.655348	4.633512	0.549612	H	1.151115	4.551657	-1.175263
H	-2.701245	3.216209	0.689902	H	2.149573	3.136232	-1.560867
H	-1.265474	3.373282	1.724644	H	0.423316	3.158549	-1.986846
H	0.506158	0.252095	-2.17807	H	-0.780457	0.874331	-2.097672
C	0.799673	1.131269	2.390844	C	-0.488526	0.396789	2.530407
H	1.311846	2.03856	2.728441	H	-0.25676	-0.595731	2.930248
H	-0.265066	1.347955	2.311385	H	0.455211	0.93273	2.431916
H	0.917211	0.378242	3.173148	H	-1.094326	0.914225	3.279132
N	4.449715	-0.94604	-0.237359	N	-4.478283	-0.888267	-0.107086

C	4.827715	-1.736304	-1.396525	C	-5.269319	-0.690051	-1.309206
H	4.395491	-2.749913	-1.343267	H	-5.669023	0.337075	-1.357066
H	5.914709	-1.846498	-1.381478	H	-6.124039	-1.368729	-1.25893
C	5.082978	-1.342739	1.006784	C	-5.236011	-0.964549	1.127868
H	4.647816	-2.27996	1.393277	H	-5.591222	0.032259	1.439867
H	6.137783	-1.535791	0.797979	H	-6.118348	-1.581001	0.941462
C	3.460303	0.022878	2.30384	C	-3.150212	-0.708038	2.457457
H	3.059265	-0.769544	2.948642	H	-3.432929	0.172178	3.048868
H	3.34809	0.953595	2.865746	H	-2.425007	-1.25684	3.063972
C	2.864524	-0.912869	-2.665496	C	-3.254574	-0.015227	-2.587108
H	2.410354	-1.896887	-2.832646	H	-3.611253	0.98252	-2.869386
H	2.52724	-0.271844	-3.484344	H	-2.535782	-0.316468	-3.353823
C	4.380388	-1.054344	-2.677595	C	-4.435783	-0.975293	-2.546532
H	4.708385	-1.635305	-3.542344	H	-5.050925	-0.870141	-3.442881
H	4.853694	-0.069192	-2.738781	H	-4.082976	-2.010591	-2.503884
C	4.936461	-0.238936	2.0364	C	-4.37905	-1.575964	2.219997
H	5.416358	0.665572	1.649756	H	-4.077281	-2.579789	1.905297
H	5.448124	-0.515639	2.960898	H	-4.957202	-1.677577	3.141105

Supplementary Table 7 | Calculated ground state geometries of C-1 and D-1.

C-1				D-1			
S	-3.523047	0.92962	0.007782	S	3.522394	0.934465	-0.152384
O	-0.712144	-1.707252	0.702463	O	0.773127	-1.413233	1.28036
O	-3.799199	1.451996	-1.384561	O	4.061788	1.599728	1.095855
C	-4.06003	-0.781009	0.051677	C	3.996908	-0.799157	-0.038381
C	-5.376898	-1.179728	-0.118145	C	5.262957	-1.278743	-0.328369
H	-6.165857	-0.460253	-0.301582	H	6.035518	-0.630713	-0.724808
C	-5.653051	-2.540017	-0.043208	C	5.511249	-2.628446	-0.095254
H	-6.671919	-2.884794	-0.173347	H	6.488992	-3.037262	-0.320313
C	-4.63721	-3.467373	0.203584	C	4.518796	-3.460869	0.424508
H	-4.879888	-4.521389	0.26331	H	4.736521	-4.508062	0.596035
C	-3.325398	-3.049448	0.370591	C	3.257366	-2.959871	0.719562
H	-2.523496	-3.75374	0.557385	H	2.475576	-3.592466	1.123141
C	-3.044697	-1.689828	0.28171	C	3.005532	-1.615273	0.479739
C	-1.701285	-1.076589	0.40684	C	1.715307	-0.916387	0.710293
C	-1.784091	0.403781	0.16289	C	1.788429	0.463254	0.122687
C	-0.726313	1.237507	0.062705	C	0.727805	1.206016	-0.253349
C	0.642285	0.633612	0.03534	C	-0.634576	0.606689	-0.119637
C	1.425802	0.502514	1.183534	C	-1.463983	0.861838	0.971579
C	2.725997	-0.002138	1.080581	C	-2.75775	0.329788	0.997978
C	3.245472	-0.399008	-0.172566	C	-3.235604	-0.445575	-0.082106
C	2.436732	-0.281052	-1.319457	C	-2.384605	-0.700885	-1.176075
C	1.158116	0.238625	-1.190822	C	-1.101526	-0.178093	-1.165698
C	-0.776778	2.76328	-0.154614	C	0.798726	2.588802	-0.941389
C	-0.933888	3.004784	-1.672616	C	-0.600124	3.211442	-1.092007
H	-0.078414	2.603955	-2.221966	H	-1.266036	2.585465	-1.688011
H	-1.849555	2.544119	-2.045281	H	-1.072875	3.385672	-0.122805
H	-0.975943	4.08239	-1.856893	H	-0.498118	4.176775	-1.594227
C	-1.920122	3.456836	0.607045	C	1.652574	3.589459	-0.141159
H	-1.964841	3.130379	1.649411	H	2.697711	3.299715	-0.047575
H	-1.739547	4.53445	0.599988	H	1.622578	4.559627	-0.644193
H	-2.89387	3.304274	0.14313	H	1.252904	3.721899	0.867636
C	0.536652	3.429096	0.297611	C	1.381114	2.393314	-2.356522
H	0.475609	4.496955	0.074157	H	1.370354	3.349345	-2.88707
H	0.69625	3.321356	1.372862	H	2.409462	2.033217	-2.323035
H	1.404388	3.022764	-0.222567	H	0.780708	1.681299	-2.929051
H	0.539741	0.318578	-2.079901	H	-0.448676	-0.385824	-2.008922
C	0.866988	0.855455	2.538627	C	-0.966756	1.683707	2.132935
H	1.419664	1.676898	3.005061	H	-0.902805	1.077889	3.04212
H	-0.180527	1.152312	2.476451	H	0.029069	2.085021	1.944465
H	0.927627	0.000805	3.218571	H	-1.634832	2.522371	2.349532
N	4.552464	-0.882277	-0.281797	N	-4.523893	-0.984905	-0.055699
C	4.922551	-1.590634	-1.495027	C	-5.086259	-1.475128	-1.301957
H	4.506476	-2.612877	-1.500992	H	-5.399123	-0.640848	-1.953269
H	6.011303	-1.684098	-1.504936	H	-5.982949	-2.049834	-1.057864

C	5.198368	-1.36872	0.923143	C	-5.483514	-0.397688	0.860334
H	4.780819	-2.341764	1.234731	H	-5.810753	0.597452	0.5127
H	6.255309	-1.526482	0.69559	H	-6.365548	-1.042009	0.879757
C	3.559968	-0.144642	2.336812	C	-3.64242	0.609678	2.19521
H	3.18085	-0.991639	2.923083	H	-3.958015	1.660476	2.167361
H	3.435285	0.73759	2.969874	H	-3.067593	0.494372	3.117923
C	2.924212	-0.726987	-2.680115	C	-2.846249	-1.515236	-2.364555
H	2.487137	-1.704864	-2.91558	H	-3.082307	-0.837324	-3.193565
H	2.563261	-0.033917	-3.44489	H	-2.029488	-2.154691	-2.710486
C	4.442381	-0.835339	-2.721983	C	-4.078523	-2.345899	-2.032348
H	4.769501	-1.350091	-3.628145	H	-4.526675	-2.753757	-2.941154
H	4.89473	0.161535	-2.723289	H	-3.807305	-3.187968	-1.387732
C	5.038746	-0.354862	2.039483	C	-4.87154	-0.288828	2.243917
H	5.497809	0.587102	1.723327	H	-4.59267	-1.292207	2.580433
H	5.563296	-0.69419	2.935574	H	-5.604006	0.10586	2.951691

Supplementary Table 8 | Calculated ground state geometries of TS-1 and TS-1.

TS-1				TS-2			
S	-2.071138	-0.762011	1.200955	S	2.80863	0.49377	-1.350652
O	-2.577098	1.361012	-2.027297	O	1.428482	-0.560621	2.134576
O	-2.504664	-0.293035	2.581199	O	3.549711	1.815616	-1.520805
C	-3.567249	-1.171359	0.285422	C	3.88923	-0.642218	-0.458371
C	-4.485038	-2.139431	0.647793	C	5.101963	-1.118929	-0.91785
H	-4.349084	-2.742272	1.53871	H	5.493015	-0.830251	-1.887062
C	-5.595233	-2.320833	-0.177681	C	5.810966	-1.99139	-0.090343
H	-6.334521	-3.071919	0.07526	H	6.76668	-2.383326	-0.418341
C	-5.756567	-1.548183	-1.32607	C	5.296317	-2.36499	1.14886
H	-6.621173	-1.709095	-1.960124	H	5.856595	-3.050859	1.77427
C	-4.821316	-0.57216	-1.665569	C	4.072094	-1.866346	1.592558
H	-4.934121	0.037327	-2.555167	H	3.659937	-2.147961	2.555149
C	-3.727494	-0.378837	-0.836992	C	3.375228	-0.986527	0.780441
C	-2.626255	0.626907	-1.019425	C	2.057218	-0.331417	1.080402
C	-1.720008	0.534999	0.046942	C	1.686345	0.47533	0.004488
C	-0.460734	1.323068	0.09077	C	0.437396	1.252237	-0.050998
C	0.70634	0.729483	-0.356779	C	-0.752909	0.673273	-0.438631
C	2.01438	1.338408	-0.617961	C	-0.936174	-0.767111	-0.697416
C	3.15615	0.613192	-0.440729	C	-2.159965	-1.343004	-0.477993
C	3.072296	-0.783815	-0.075526	C	-3.289852	-0.526944	-0.093185
C	1.815612	-1.467877	-0.249126	C	-3.205238	0.904911	-0.261575
C	0.707809	-0.718637	-0.431294	C	-1.982026	1.439917	-0.426342
C	-0.596463	2.726156	0.732765	C	0.549138	2.71561	0.469769
C	-1.160436	3.734487	-0.290438	C	-0.468173	3.011628	1.596781
H	-0.476004	3.944156	-1.112781	H	-1.496931	3.132206	1.263563
H	-2.086639	3.355844	-0.723608	H	-0.44618	2.207855	2.337729
H	-1.363673	4.67848	0.22394	H	-0.179585	3.939125	2.098102
C	-1.632172	2.63858	1.874608	C	1.93457	2.956573	1.101691
H	-1.341029	1.906993	2.630202	H	2.740011	2.777539	0.390045
H	-1.707643	3.620988	2.348513	H	1.984201	3.997255	1.436238
H	-2.614938	2.348341	1.506437	H	2.086395	2.31123	1.970279
C	0.692906	3.250075	1.391534	C	0.42349	3.701024	-0.71125
H	0.439646	4.102999	2.026174	H	0.523092	4.7249	-0.339183
H	1.140605	2.482858	2.029376	H	1.230009	3.522	-1.427252
H	1.444767	3.59669	0.691031	H	-0.523494	3.630041	-1.24752
H	-0.240693	-1.223855	-0.536193	H	-1.926271	2.511881	-0.529077
C	2.121269	2.662386	-1.323486	C	0.167993	-1.639515	-1.227143
H	2.481979	2.470995	-2.340054	H	-0.242035	-2.414162	-1.873999
H	1.164907	3.161822	-1.413852	H	0.88327	-1.06639	-1.806518
H	2.839491	3.337968	-0.854648	H	0.706158	-2.13776	-0.416182
N	4.149642	-1.44372	0.321632	N	-4.406563	-1.072117	0.363807
C	4.116391	-2.886047	0.594581	C	-5.586715	-0.260145	0.688099
H	3.853571	-3.040827	1.646522	H	-5.512529	0.073096	1.728918
H	5.125624	-3.266815	0.442642	H	-6.456719	-0.910134	0.605991

C	5.41288	-0.731652	0.53158	C	-4.480634	-2.510791	0.630762
H	5.364425	-0.187295	1.48056	H	-3.988494	-2.721088	1.586228
H	6.204343	-1.47451	0.609402	H	-5.531658	-2.776331	0.727163
C	4.515554	1.230029	-0.701064	C	-2.361166	-2.840086	-0.62419
H	4.686373	2.022717	0.036096	H	-1.763517	-3.352786	0.137378
H	4.516872	1.714252	-1.680509	H	-1.979375	-3.173673	-1.590451
C	1.748884	-2.97183	-0.144865	C	-4.440237	1.766363	-0.155818
H	1.352472	-3.245032	0.83933	H	-4.428332	2.287069	0.807981
H	1.049072	-3.357459	-0.88903	H	-4.416572	2.53237	-0.933617
C	3.128697	-3.587934	-0.320541	C	-5.701584	0.923164	-0.254973
H	3.113934	-4.651878	-0.080037	H	-6.582984	1.508615	0.009839
H	3.46519	-3.48444	-1.356537	H	-5.839475	0.554711	-1.27586
C	5.649828	0.216121	-0.629396	C	-3.818427	-3.263429	-0.503825
H	5.704356	-0.368757	-1.55194	H	-4.359272	-3.046552	-1.429517
H	6.606508	0.724352	-0.501933	H	-3.886714	-4.337218	-0.324374

Supplementary Table 9 | Calculated ground state geometries of TS-2 and TS-3.

TS-3				TS-4			
S	-2.860656	0.854389	-1.185133	S	-2.644409	0.446149	-1.451629
O	-1.482997	-1.110566	1.877855	O	-2.022594	-0.193953	2.336013
O	-2.376725	0.410957	-2.561239	O	-2.067042	-0.47743	-2.519793
C	-3.992838	-0.405352	-0.566815	C	-3.99653	-0.423435	-0.63664
C	-5.228461	-0.706086	-1.107407	C	-5.156161	-0.854231	-1.252529
H	-5.619195	-0.164208	-1.961437	H	-5.337006	-0.675963	-2.306576
C	-5.965793	-1.72995	-0.510409	C	-6.094381	-1.526498	-0.467984
H	-6.940407	-1.990086	-0.906683	H	-7.014383	-1.880499	-0.91832
C	-5.460295	-2.414461	0.592347	C	-5.858501	-1.741499	0.888168
H	-6.050111	-3.20182	1.047925	H	-6.602839	-2.258208	1.483453
C	-4.206361	-2.099401	1.114188	C	-4.677984	-1.302401	1.485336
H	-3.801045	-2.625951	1.970912	H	-4.48149	-1.463944	2.539335
C	-3.467807	-1.092398	0.514356	C	-3.737332	-0.649728	0.704684
C	-2.097697	-0.619924	0.910552	C	-2.404219	-0.123705	1.148203
C	-1.699445	0.421979	0.063712	C	-1.729007	0.417623	0.055287
C	-0.479651	1.247866	0.191228	C	-0.460878	1.156817	0.101124
C	0.715199	0.707207	-0.251211	C	0.744279	0.547319	-0.202928
C	1.998521	1.369911	-0.477146	C	0.96788	-0.909554	-0.202355
C	3.164177	0.671285	-0.356381	C	2.243653	-1.400411	-0.055006
C	3.128452	-0.742704	-0.050956	C	3.395105	-0.532798	-0.146382
C	1.886797	-1.454376	-0.2053	C	3.189264	0.868916	-0.425996
C	0.753096	-0.735273	-0.355065	C	1.93223	1.346537	-0.395805
C	-0.66055	2.575269	0.970604	C	-0.580144	2.65439	0.509385
C	-1.265871	3.681095	0.082589	C	-0.488482	3.546191	-0.750713
H	-0.599311	3.997709	-0.720478	H	-0.669256	4.58594	-0.463875
H	-2.203065	3.348764	-0.366572	H	0.473001	3.504768	-1.261677
H	-1.479829	4.555818	0.703229	H	-1.259859	3.258194	-1.470101
C	-1.674911	2.301206	2.108529	C	-1.961597	2.939244	1.133102
H	-1.367814	1.443721	2.711566	H	-2.136177	2.315406	2.011036
H	-1.724688	3.182439	2.752938	H	-1.991267	3.987966	1.440792
H	-2.673509	2.101285	1.720518	H	-2.774369	2.77359	0.424861
C	0.618158	3.071445	1.66958	C	0.447851	3.054595	1.589784
H	0.345816	3.854128	2.381849	H	0.227336	4.068208	1.934567
H	1.093614	2.261287	2.228823	H	0.361625	2.380731	2.44658
H	1.351862	3.504082	0.997668	H	1.484092	3.041551	1.258898
H	-0.191229	-1.252998	-0.43842	H	1.813672	2.399918	-0.587823
C	2.048864	2.740467	-1.095289	C	-0.150524	-1.909421	-0.320229
H	2.400735	2.634198	-2.127156	H	-0.672059	-2.032732	0.633102
H	1.072585	3.20875	-1.139639	H	-0.876154	-1.586532	-1.06183
H	2.748063	3.409034	-0.588858	H	0.237345	-2.879005	-0.625551
N	4.238	-1.386929	0.286175	N	4.634107	-1.002228	-0.034467
C	4.25485	-2.83655	0.517434	C	5.830748	-0.164176	-0.207547
H	4.052652	-3.027632	1.577001	H	6.191826	-0.29525	-1.233778
H	5.264327	-3.185723	0.302301	H	6.593688	-0.559003	0.46367

C	5.487367	-0.650071	0.490957	C	4.920768	-2.429526	0.139619
H	5.458488	-0.157222	1.468712	H	5.058794	-2.880085	-0.849678
H	6.300758	-1.373152	0.503123	H	5.866241	-2.508355	0.675814
C	4.497709	1.34436	-0.607857	C	2.485571	-2.877198	0.184919
H	4.663878	2.095175	0.173061	H	2.483331	-3.419915	-0.768015
H	4.460488	1.88824	-1.5548	H	1.679465	-3.291002	0.789659
C	1.857957	-2.959834	-0.11121	C	4.366185	1.755137	-0.725359
H	1.517953	-3.248975	0.889378	H	4.606547	1.693291	-1.793053
H	1.128782	-3.354546	-0.821641	H	4.110405	2.794043	-0.510856
C	3.240078	-3.542546	-0.363634	C	5.566036	1.296953	0.087499
H	3.260148	-4.610952	-0.143782	H	6.45834	1.872942	-0.161916
H	3.523662	-3.412228	-1.412412	H	5.370473	1.428906	1.155764
C	5.661541	0.362756	-0.624661	C	3.80688	-3.111585	0.897289
H	5.702867	-0.171206	-1.578297	H	3.763999	-2.712731	1.915324
H	6.60727	0.891695	-0.499278	H	4.019307	-4.179288	0.968208

Crystal structure analysis

Supplementary Table 10 | Crystal structure analysis of A-1 and B-1.

Compound	**A-1** CCDC 1910546	**B-1** CCDC 1910547
net formula	$C_{26}H_{29}NO_2S$	$C_{27}H_{31}Cl_2NO_2S$
M_r/g mol^{-1}	419.56	504.49
crystal size/mm	0.080 × 0.070 × 0.030	0.070 × 0.030 × 0.030
T/K	110.(2)	110.(2)
radiation	MoKα	MoKα
diffractometer	'Bruker D8 Venture TXS'	'Bruker D8 Venture TXS'
crystal system	triclinic	monoclinic
space group	'P -1'	'P 1 21/n 1'
a/Å	7.0410(5)	15.1748(8)
b/Å	8.5158(6)	10.8807(6)
c/Å	18.4408(15)	15.4174(7)
α/°	81.582(3)	90
β/°	87.739(3)	92.771(2)
γ/°	76.464(2)	90
V/Å^3	1063.40(14)	2542.6(2)
Z	2	4
calc. density/g cm^{-3}	1.310	1.318
μ/mm^{-1}	0.176	0.362
absorption correction	Multi-Scan	Multi-Scan
transmission factor range	0.93–0.99	0.91–0.99
refls. measured	10942	21971
R_{int}	0.0421	0.0404
mean σ(I)/I	0.0540	0.0338
θ range	2.577–26.370	2.304–25.349
observed refls.	3515	3620
x, y (weighting scheme)	0.0364, 0.5689	0.0375, 2.2661
hydrogen refinement	constr	constr
Flack parameter	-	-
refls in refinement	4318	4511
parameters	275	340
restraints	0	30
$R(F_{obs})$	0.0416	0.0412
$R_w(F^2)$	0.1014	0.1054
S	1.017	1.068
shift/error$_{max}$	0.001	0.001
max electron density/e Å^{-3}	0.278	0.276
min electron density/e Å^{-3}	–0.330	–0.262

Supplementary Table 11 | Crystal structure analysis of C-1 and D-1.

Compound	**C-1** CCDC 1910548	**D-1** CCDC 1910549
net formula	$C_{26}H_{29}NO_2S$	$C_{26}H_{29}NO_2S$
M_r/g mol^{-1}	419.56	419.56
crystal size/mm	0.100 × 0.090 × 0.020	0.090 × 0.060 × 0.020
T/K	109.(2)	111.(2)
radiation	MoKα	MoKα
diffractometer	'Bruker D8 Venture TXS'	'Bruker D8 Venture TXS'
crystal system	monoclinic	triclinic
space group	'P 1 21/n 1'	'P -1'
a/Å	14.6022(7)	7.0642(9)
b/Å	7.0310(3)	12.2255(14)
c/Å	21.6607(10)	13.2154(16)
α/°	90	78.599(4)
β/°	103.123(2)	87.959(4)
γ/°	90	75.015(4)
V/Å^3	2165.79(17)	1080.6(2)
Z	4	2
calc. density/g cm^{-3}	1.287	1.289
μ/mm^{-1}	0.172	0.173
absorption correction	Multi-Scan	Multi-Scan
transmission factor range	0.92–1.00	0.89–1.00
refls. measured	31376	11750
R_{int}	0.0485	0.0406
mean σ(I)/I	0.0321	0.0551
θ range	3.070–26.372	2.985–27.101
observed refls.	3564	3692
x, y (weighting scheme)	0.0320, 4.2363	0.0473, 0.6988
hydrogen refinement	constr	constr
Flack parameter	-	-
refls in refinement	4415	4735
parameters	299	275
restraints	36	0
$R(F_{obs})$	0.0747	0.0484
$R_w(F^2)$	0.1649	0.1259
S	1.145	1.045
shift/error$_{max}$	0.001	0.001
max electron density/e Å^{-3}	0.341	0.486
min electron density/e Å^{-3}	−0.397	−0.320

Supplementary References

1. A. Gerwien, T. Reinhardt, P. Mayer, H. Dube, Synthesis of Double-Bond Substituted Hemithioindigo Photoswitches. *Org. Lett.* **1**, 232-235 (2018).

2. A. Gerwien, P. Mayer, H. Dube, Photon-Only Molecular Motor with Reverse Temperature-Dependent Efficiency. *J. Am. Chem. Soc.* **140**, 16442-16445 (2018).

3. U. Megerle, R. Lechner, B. König, E. Riedle, Laboratory apparatus for the accurate, facile and rapid determination of visible light photoreaction quantum yields. *Photochem. Photobiol. Sci.* **9**, 1400-1406 (2010).

4. Gaussian 16, Revision A.03, M. J. Frisch, G. W. Trucks, H. B. Schlegel, G. E. Scuseria, M. A. Robb, J. R. Cheeseman, G. Scalmani, V. Barone, G. A. Petersson, H. Nakatsuji, X. Li, M. Caricato, A. V. Marenich, J. Bloino, B. G. Janesko, R. Gomperts, B. Mennucci, H. P. Hratchian, J. V. Ortiz, A. F. Izmaylov, J. L. Sonnenberg, D. Williams-Young, F. Ding, F. Lipparini, F. Egidi, J. Goings, B. Peng, A. Petrone, T. Henderson, D. Ranasinghe, V. G. Zakrzewski, J. Gao, N. Rega, G. Zheng, W. Liang, M. Hada, M. Ehara, K. Toyota, R. Fukuda, J. Hasegawa, M. Ishida, T. Nakajima, Y. Honda, O. Kitao, H. Nakai, T. Vreven, K. Throssell, J. A. Montgomery, Jr., J. E. Peralta, F. Ogliaro, M. J. Bearpark, J. J. Heyd, E. N. Brothers, K. N. Kudin, V. N. Staroverov, T. A. Keith, R. Kobayashi, J. Normand, K. Raghavachari, A. P. Rendell, J. C. Burant, S. S. Iyengar, J. Tomasi, M. Cossi, J. M. Millam, M. Klene, C. Adamo, R. Cammi, J. W. Ochterski, R. L. Martin, K. Morokuma, O. Farkas, J. B. Foresman, and D. J. Fox, Gaussian, Inc., Wallingford CT, (2016).

5. Bruker, *SAINT*. Bruker AXS Inc., Madison, Wisconsin, USA, (2012).

6. G. M. Sheldrick, *SADABS*. University of Göttingen, Germany, (1996).

7. G. M. Sheldrick, *SHELXT* – Integrated space-group and crystal-structure determination. *Acta Cryst.* A**71**, 3-8 (2015).

8. 8-State molecular sequential switch featuring the unprecedented “dual single bond rotation” photoreaction

HTI photoswitches possessing four diastereomeric states can also be obtained by introducing another stereoinformation than the sulfoxide stereocenter. If this stereoinformation is not permanent as in the sulfoxide, but flexible, it is now possible that the whole stereoinformation in the system can be interchanged resulting in a switch that can alternate between eight states, which are divided into four enantiomeric pairs. The flexible stereoinformation was established by introducing a second chiral aromatic residue to obtain another chiral axis in the molecule. In the case of the presented HTI the photoreactions as well as the thermal reactions of the respective isomers are selective converting only one isomer into another specific isomer, respectively. The exception is isomer **B**, which is converted to isomer **D** by photochemical HT reaction or in a completely new photoreaction in which both single bonds rotate at the same time and isomer **B’** is obtained. From this branching point an eight-step or a five-step sequential transformation cycle can be performed by this system. By changing the temperature and solvent it can be controlled, which cycle is performed. As both enantiomeric halves of the cycles are connected the presented HTI is not a motor but a special kind of switch for which one forward rotation cycle must follow one backward cycle and so on. This is also different from a normal switch performing the forwards and backwards rotations randomly. Therefore, this kind of behavior is described as sequential switching.

An eight-state molecular sequential switch featuring a dual single-bond rotation photoreaction

Aaron Gerwien,[§] *Benjamin Jehle,*[§] *Marvin Irmler,*[§] *Peter Mayer,*[§] *Henry Dube*[†]*

[§] Ludwig-Maximilians Universität München, Department of Chemistry and Center for Integrated Protein Science CIPSM, Butenandtstr. 5–13, 81377 Munich, Germany

[†] Friedrich-Alexander Universität Erlangen-Nürnberg, Department of Chemistry and Pharmacy, Nikolaus-Fiebiger-Str. 10, 91058 Erlangen, Germany

* E-mail: henry.dube@fau.de

Abstract

Typical photowitches interconvert between two different states by simple isomerization reactions, which represents a fundamental limit for applications. To expand the switching capacity usually different photoswitches have to be linked together leading to strong increase in molecular weight, diminished switching function, and less precision and selectivity of switching events. Herein we present an approach for solving this essential problem with a different photoswitching concept. A basic molecular switch architecture provides precision photoswitching between eight different states via controlled rotations around three adjacent covalent bonds. All eight states can be populated one after another in an eight-step cycle by alternating between photochemical Hula-Twist isomerizations and thermal single bond rotations. By simply changing solvent and temperature the same switch can also undergo a different cycle instead interconverting just five isomers in a selective sequence. This behavior is enabled through the discovery of an unprecedented photoreaction, a one photon dual single bond rotation.

Introduction

Molecular photoswitches are at the center of attention in smart nanotechnology research enabling high precision control of events at the smallest scales and instilling bottom-up responsiveness and adaptability into materials, drugs, or catalytic reactions. Consequentially photoswitches are used for switching or gradual modulation of functions in myriads of applications nowadays and developments are ever steeply increasing.[1-16] Roughly two different classes of photoswitches can be distinguished, bond isomerizing switches that undergo significant changes in molecular geometry and switches that provide substantial changes in their electronic structure.[6, 13, 17, 18] The overwhelming majority of light induced bond isomerizations are achieved by simple one-bond rotations such as double bond isomerization (DBI) reactions.[8, 12, 19-21] Direct experimental proof for more complex coupled bond isomerizations, where more than one bond rotates concomitantly, are so far only available for bicycle pedal[22] and Hula Twist photoreactions[23, 24] (Figure 1a) although such simultaneous photochemical processes are proposed frequently in the literature.[25-32]

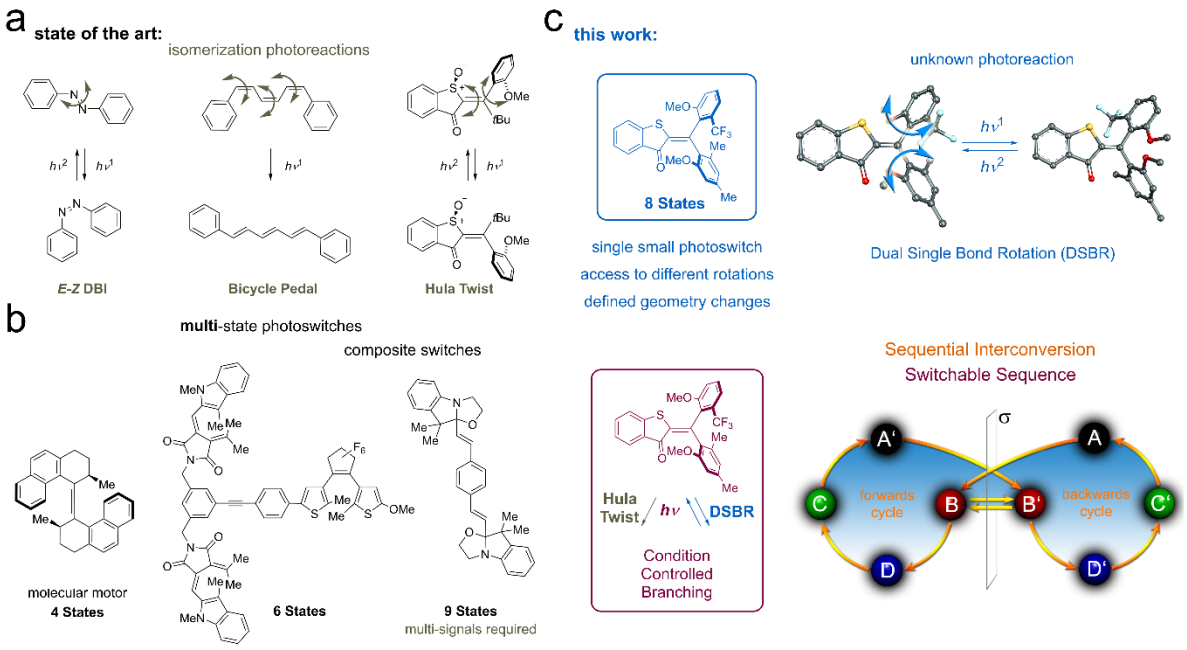

Figure 1 Molecular photoswitching. a) Bond rotations currently evidenced in photoswitching. b) Multi-state switching approaches. c) Simple and compact 8-state photoswitch with switchable sequential interconversion employing a hitherto unknown dual single bond rotation (DSBR) and Hula Twist photoreactions.

At the current state of the art most small molecular photoswitches can undergo reversible changes between two different states upon irradiation with light. To go beyond this binary behavior and open up more fundamental switching possibilities (Figure 1b), multiple photo responsive units can be incorporated into a single larger molecule. This is achieved by linking either the same or different photochromic units together in a covalent fashion or through weaker interactions.[16, 33-38] Many well-

known photoswitches like azobenzene,[37, 39-43] diarylethene,[44-47] or spiropyranes[48] have been interlinked in such a manner but the method can be extended to virtually any photochromic dye[34, 35, 49] or dye-combination.[50-52] An impressive escalation in the number of switching states is thus achievable, for example six different states are possible by connecting three light-responsive units covalently into one structure.[51] Another possibility to enhance the switching state number for a given photochromic molecule is provided by adding chemical signals like protonation and deprotonation.[7, 53-55] Alternatively, photon driven molecular motors can be considered as compact multi-state photoswitches,[56-59] usually operating by alternating four different diastereomeric states.[56, 60-65] The advantage of the latter is their unequivocally more precise geometry control as opposed to the oftentimes rather loose changes obtained in multi-component architectures. We recently contributed different types of visible light driven molecular motors to the field, featuring different rotation mechanisms and alternating between three to four different states.[24, 63, 66] Up to five distinct states could be accessed in macrocyclic integrated hemithioindigo (HTI) motors.[67] Despite this steep progress in molecular photoswitches research, controlling more complex motions and using the full state-density capacity offered by small molecular frameworks remain untackled challenges at present.

Herein we report on a simple and compact molecular setup **1** assuming eight different stable states, which interchange one after another by alternating visible light irradiation and heating steps. The photochemical steps encompass a variant of the Hula Twist photoreaction as well as a hitherto unknown dual single bond rotation (DSBR) photoreaction (Figure 1c). The thermal steps are sole single bond rotations (SBRs). Change of the solvent polarity enables to control the sequence of isomer interconversions and either eight or five states are interchanged under irradiation and heating in specific sequences. With this compact multi-state photoswitch architecture the next level in molecular addressability has been achieved providing exquisite control over precise molecular geometry changes via light signaling. At the same time a so far unknown coupled photoisomerization reaction is discovered, which provides molecular scientists with a novel light-inducible molecular motion type.

Results and discussion

Sequential switch **1** is derived from the parent HTI chromophore but contains two different aryl groups geminally connected to the photoisomerizable double bond. Both aryl groups are nonsymmetrically substituted thus establishing a chiral axis each, which coincides with the respective single bond connecting to the central double bond. Therefore, sequential switch **1** exists in four diastereomeric states and eight enantiomeric states. All states of **1** - denoted **A** (*Z*-(S_a)-(R_a) configuration), enantiomeric **A'** *(Z*-(R_a)-(S_a) configuration), **B** (*Z*-(R_a)-(R_a) configuration), enantiomeric **B'** (*Z*-(S_a)-(S_a) configuration), **C** (*E*-(R_a)-(R_a) configuration), enantiomeric **C'** (*E*-(S_a)-(S_a) configuration), **D** (*E*-(R_a)-(S_a) configuration), and enantiomeric **D'** (*E*-(S_a)-(R_a) configuration) are depicted in Figure 2a.

Synthesis of **1** followed an established protocol for the generation of fourfold double-bond substituted HTIs (see Supporting Information).[68] Because of increased steric hindrance of the two aryl substituents all atropisomers show increased thermal stability facilitating isolation and analysis. Isomers *rac*-**A** and *rac*-**B** are stable enough at 22 °C to enable separation by chromatography methods. Isomers *rac*-**C** and *rac*-**D** are interconverting rapidly at 22 °C making a separation impossible. However, since isomer *rac*-**C** is significantly more stable, it is mainly populated at ambient temperatures as confirmed by NMR spectroscopy. Consequentially it is also the only isomer, which crystallizes from a solution of *rac*-**C** and *rac*-**D** isomers and can thus be obtained in highly enriched form. These results are in good agreement with the theoretical description predicting isomers *rac*-**D** to be 0.63 kcal/mol higher in energy as compared to *rac*-**C** (see Figure 3 and the Supporting Information).

The relative configurations of the different diastereomers were elucidated by 1D and 2D-NMR methods in combination with crystal structure analysis by X-ray diffraction (see Figure 2b and Supporting Information). The absolute configurations could be revealed after separation of the enantiomers by chiral HPLC and comparison of experimentally obtained ECD-spectra with calculated ECD spectra (B3LYP/6-311G(d,p) level of theory using a PCM solvent model for MeCN). The structural assignments were confirmed by X-ray crystal structure analysis of racemic **A**/ **A'**, **B**/ **B'**, and **C**/ **C'** and enantiopure **C'** and **C** isomers (see Figure 2b and c, and Supporting Information).

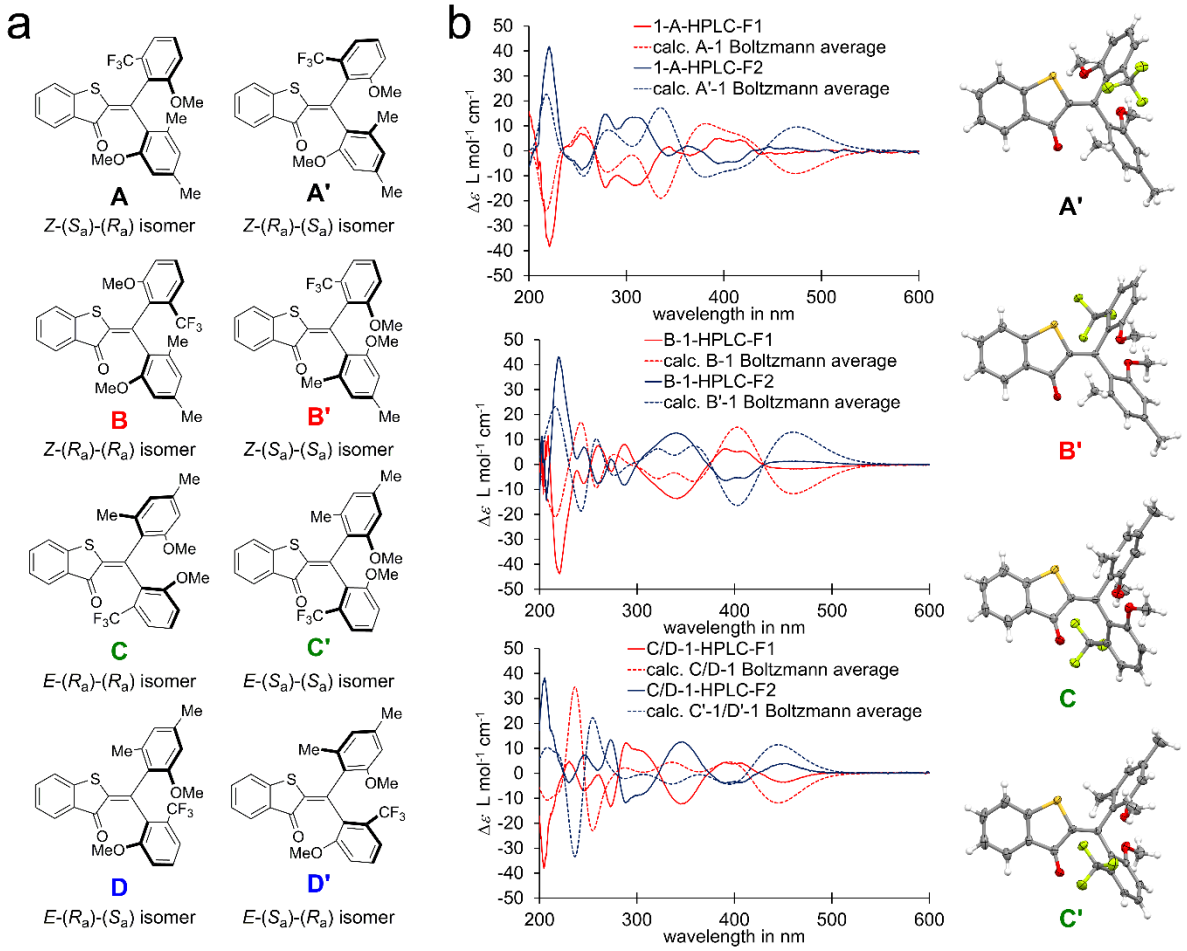

Figure 2 Structures of all eight isomers of sequential HTI switch **1** and corresponding ECD-spectra of enantiomerically pure samples. a) Schematic representation of the molecular structures of **1** with stereo labels. b) Structures of isomers **A'** (from racemic crystals), **B'** (from racemic crystals), **C'**, and **C** in the crystalline state and corresponding ECD-spectra in MeCN at 20 °C of **A**, **A'**, **B**, **B'**, **C/D**, **C'/D'**. Experimental spectra were compared with calculated spectra (B3LYP/6-311G(d,p) level of theory using a PCM solvent model for MeCN).

Thermal isomerization reactions and the ground state energy profile of HTI **1** and its different isomers were determined in a combined theoretical (B3LYP/6-311G(d,p) level of theory using a PCM solvent model for MeCN) and experimental approach as summarized in Figure 3. The relative Gibbs free energies ΔG of the stable isomers were determined experimentally by heating a sample of **1** to 62 °C over prolonged time in MeCN-d_3 solution to establish thermal equilibrium (Figure 3a and b). From the relative abundance of each enantiomeric pair *rac*-**A** to *rac*-**D** the corresponding ΔG value could be obtained (see Supporting Information). The Gibbs energy of activation for thermal atropisomerization of *rac*-**A** to *rac*-**B** was determined to be $\Delta G^{\ddagger}$ = 26.8 kcal mol^{-1} in MeCN-d_3 solution by following its thermal decay at 62 °C with ^{1}H NMR spectroscopy. The theoretical description predicts isomer interconversion by selective rotation of the trifluormethylanisol substituent whereby the methoxy substituent faces the side of the sulfur atom (TS2, Figure 3c). The selective rotation of one aromatic ring was confirmed by following the atropisomerization of enantiomers by chiral HPLC (see Figure 3a and Supporting Information for details). Isomer **A** is thermally converted exclusively into isomer **B** and **A'** is thermally converted exclusively into **B'**. This selectivity is only possible by sole rotation around the trifluormethylanisol substituent. It should be mentioned at this point that a significant energy difference between the two possible transition states TS1 and TS2 is found in the theoretical description. Therefore theory predicts a unidirectional rotation for this atropisomerization, which can however not be proven straightforwardly in an experiment. A strong indication is given by the good agreement between the absolute $\Delta G^{\ddagger}$ values obtained from theory and experiment.

The corresponding Gibbs energy of activation for thermal *rac*-**C**/*rac*-**D** interconversion was found to be $\Delta G^{\ddagger}$ = 18.8 kcal mol^{-1} in MeCN-d_3 solution by following the decay kinetics of a *rac*-**D** enriched sample with low temperature ^{1}H NMR at -20 °C in the dark (see Figure 3b and Supporting Information). The theoretical description predicts that this atropisomerization takes place by sole rotation of the dimethylanisol substituent whereby the methoxy substituent faces the side of the sulfur atom (i.e. via transition state TS5, Figure 3c). The selective rotation could be confirmed experimentally (see Supporting Information). After chiral HPLC separation of the enantiomer pairs **C**/**D** from the pairs **C'**/**D'** at 22 °C thermal interconversion of the enantiopure samples was monitored using chiral HPLC as analytical method. Only thermal conversion of **D** to **C** as well as of **D'** to **C'** is observed after photoinduced enrichment of the **D**/**D'** isomers. Rotation of the trifluormethylanisol substituent would lead to interconversions from **D'** to **C** and **D** to **C'** respectively, which was not observed in the experiments. Again an unidirectional rotation of the single bond is predicted from theory for the

atropisomerization between *rac*-**D** and *rac*-**C**. The thermal isomerization reactions of HTI **1** were thus found to be highly selective and only the aromatic residue with *Z* relation to the sulfur atom rotates in this process. No thermal double bond isomerization was observed even after prolonged heating to 140 °C in tetrachloroethane-d_2 solution and thus the relative stabilities of *Z* and *E* configured isomers could not be determined experimentally.

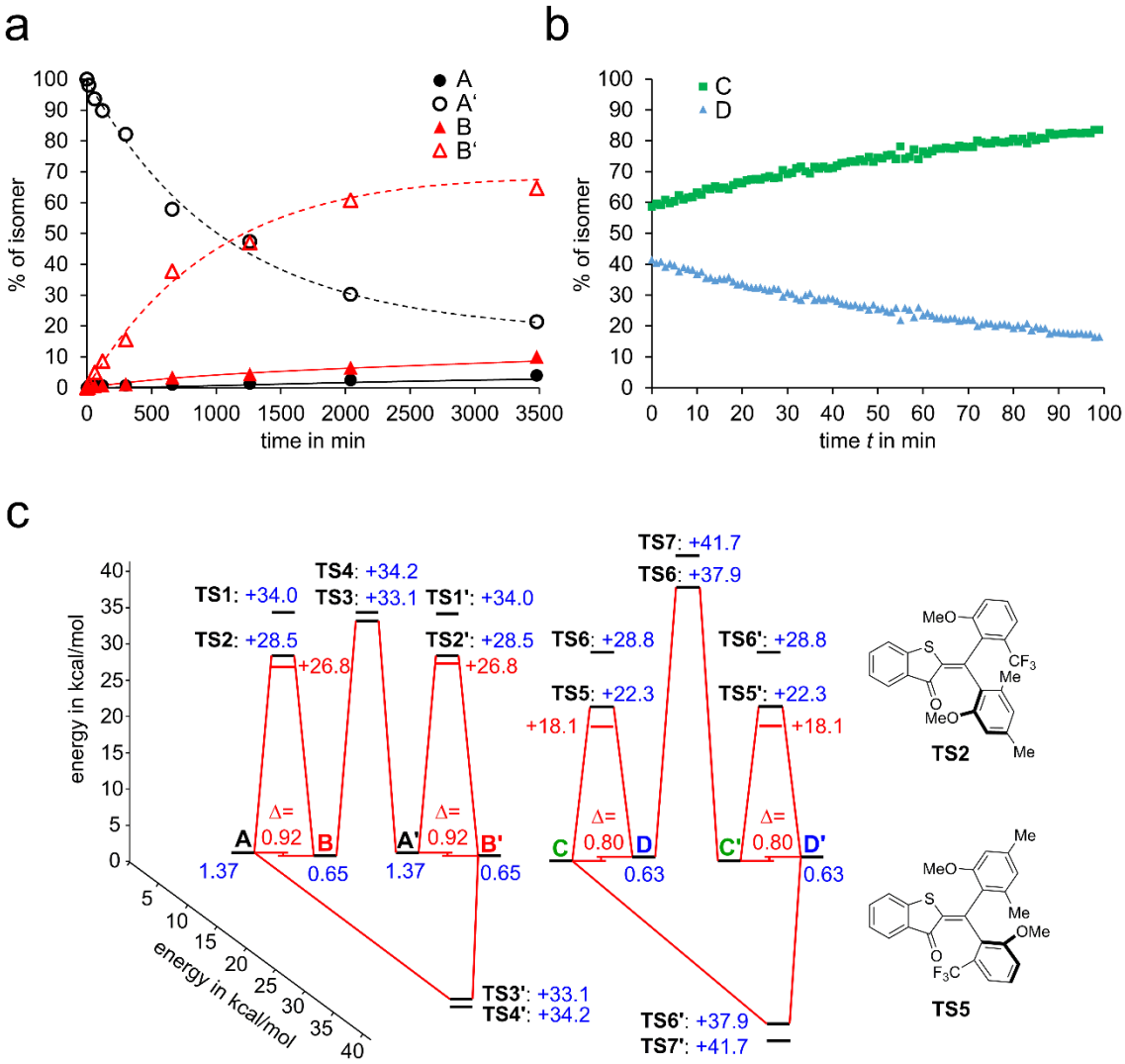

Figure 3 Thermal properties of sequential HTI switch **1**. a) Kinetics of the thermal atropisomerization from **A'** to **B'** in MeCN at 60 °C followed by chiral HPLC. Experimental data were fitted using a Markov matrix kinetic model (see Supporting Information for details). b) Kinetics of the thermal atropisomerization from *rac*-**D** to *rac*-**C** in MeCN-d_3 at -20 °C followed by ^{1}H NMR spectroscopy (400 MHz, -20 °C). c) Ground state energy profile of HTI **1** experimentally determined in MeCN-d_3 solution (red) and calculated at the B3LP/6-311G(d,p) of level of theory with a PCM solvent model for MeCN (blue).

After establishing the thermal behavior of **1** its photochemistry was studied in detail (Figure 4a). Isomers **A**, **A'**, **B**, and **B'** could be isolated in pure form and their photochemical reactions were elucidated individually. Isomers **C/D** and **C'/D'** could only be isolated as enantiomerically pure mixtures of diastereomers at ambient temperatures. Their photochemical properties were thus determined in

thermodynamic equilibrium at 22 °C or separately at low temperatures after selective isomer enrichment. Irradiation of pure *rac*-**A** in MeCN did not lead to significant population of other isomers and therefore productive photochemistry of these enantiomers is strongly subdued. In contrast irradiation of isomers *rac*-**B** in MeCN at -40 °C with 450 nm leads to exclusive formation of *rac*-**D** and a ratio of *rac*-**B** : *rac*-**D** = 52 : 48 is established in the photostationary state (PSS, see Figure 4b and Supporting Information). Because of this PSS composition it was also established that *rac*-**D** only undergoes photoisomerization back to *rac*-**B**. When warming up the solution above -30 °C thermal *rac*-**D** to *rac*-**C** atropisomerization was observed as discussed above. If irradiation was continued at the higher temperature photochemical *rac*-**C** to *rac*-**A** isomerization occurred. In a similar experiment at 22 °C, illumination of an equilibrium *rac*-**D**/*rac*-**C** mixture with 405 nm light resulted in strong accumulation of *rac*-**A** in the PSS with a ratio of *rac*-**A** : *rac*-**B** : *rac*-**C** : *rac*-**D** = 95 : 3 : 2 : 0 (see Figure 4c and Supporting Information). It is thus possible to enrich *rac*-**A** almost quantitatively under irradiation with blue light. Quantum yields for the two photoreactions of *rac*-**B** and *rac*-**C** were obtained using photon counting in conjunction with ^{1}H NMR or UV/vis spectroscopy and chiral HPLC analysis and are discussed further below (also see Supporting Information for more details).

Both photoreactions *rac*-**B** to *rac*-**D** and *rac*-**C** to *rac*-**A** are Hula-Twist reactions, a photoreaction in which the central double bond and one adjacent single bond rotate in the same step.[23, 69] However, the molecular setup of HTI **1** allows for two different Hula-Twist photoreactions for each *rac*-**B** to *rac*-**D** and *rac*-**C** to *rac*-**A** conversion, respectively as such coupled bond rotation can involve either of the two aryl substituents. To elucidate, which single bond is rotated in the Hula-Twist reaction enantiopure samples of **B**, **B'**, **C**/**D**, and **C'**/**D'** were illuminated and the photoreaction kinetics were followed by quantitative ^{1}H NMR or chiral HPLC (see Figure 4b – d, and the Supporting Information). Irradiation of **B** with 450 nm light at -40°C led to formation of **D** in MeCN with a quantum yield of 1.4% while no notable reaction into **D'** was observable (see Figure 4b and d). Thus, the Hula-Twist photoreaction proceeds exclusively by rotation around the central double bond and the single bond connecting to the dimethylanisol substituent. However, another photoreaction was also observed in this experiment leading from **B** to **B'** with a significant quantum yield of 0.9% (Figure 4d). The associated motion is a dual single bond rotation (DSBR) in which two atropisomerization photoreactions occur at the same time, while the central double bond is not isomerized. This reaction is – to the best of our knowledge – not described in the literature. Interestingly, a sole single bond rotation from **B** to **A** or to **A'** was not observed photochemically - if one single bond rotates the other single bond also undergoes rotation. As a result of this dual atropisomerization isomer **B** is converted into its enantiomer **B'**. Isomers **B** and **B'** therefore represent a branching point for the photochemistry of **1**. Full racemization of the sample via DSBR is however prevented since a significant amount of **B** is converted to **D** in the competing Hula Twist photoreaction. As expected, it was found that the enantiomeric isomer **B'** behaves mirror-symmetric and photoisomerizes into **D'** via a Hula-Twist reaction and into **B** via DSBR. Isomer **C** underwent predominantly photoisomerization into **A'** with a quantum yield of 5.2% at 450 nm

irradiation. This corresponds to a Hula-Twist photoreaction involving the central double bond and the adjacent single bond to the dimethylanisol fragment. In this case no DSBR photoreaction or other photoreactions were observed. However, the thermal equilibrium between **C** and **D** accounts for a small population of the **D** isomer in the experiment and therefore photoisomerization of the latter via Hula-Twist to isomer **B** was also detected to some degree. Irradiation of the enantiomeric mixture **C'**/**D'** showed the expected mirror-symmetric behavior and led to population of **A** and small amounts of **B'**, respectively. Finally the photochemistry of both enantiomers **A** and **A'** was scrutinized and (as observed already for the racemic mixture) showed strongly diminished efficiency by at least a factor of 10 compared to photochemical processes that produce **A** and **A'** as products. Some minimal DSBR converting **A** into **A'** and *vice versa* were found together with similarly inefficient conversion to the **C**/**C'** isomers (for details see the Supporting Information).

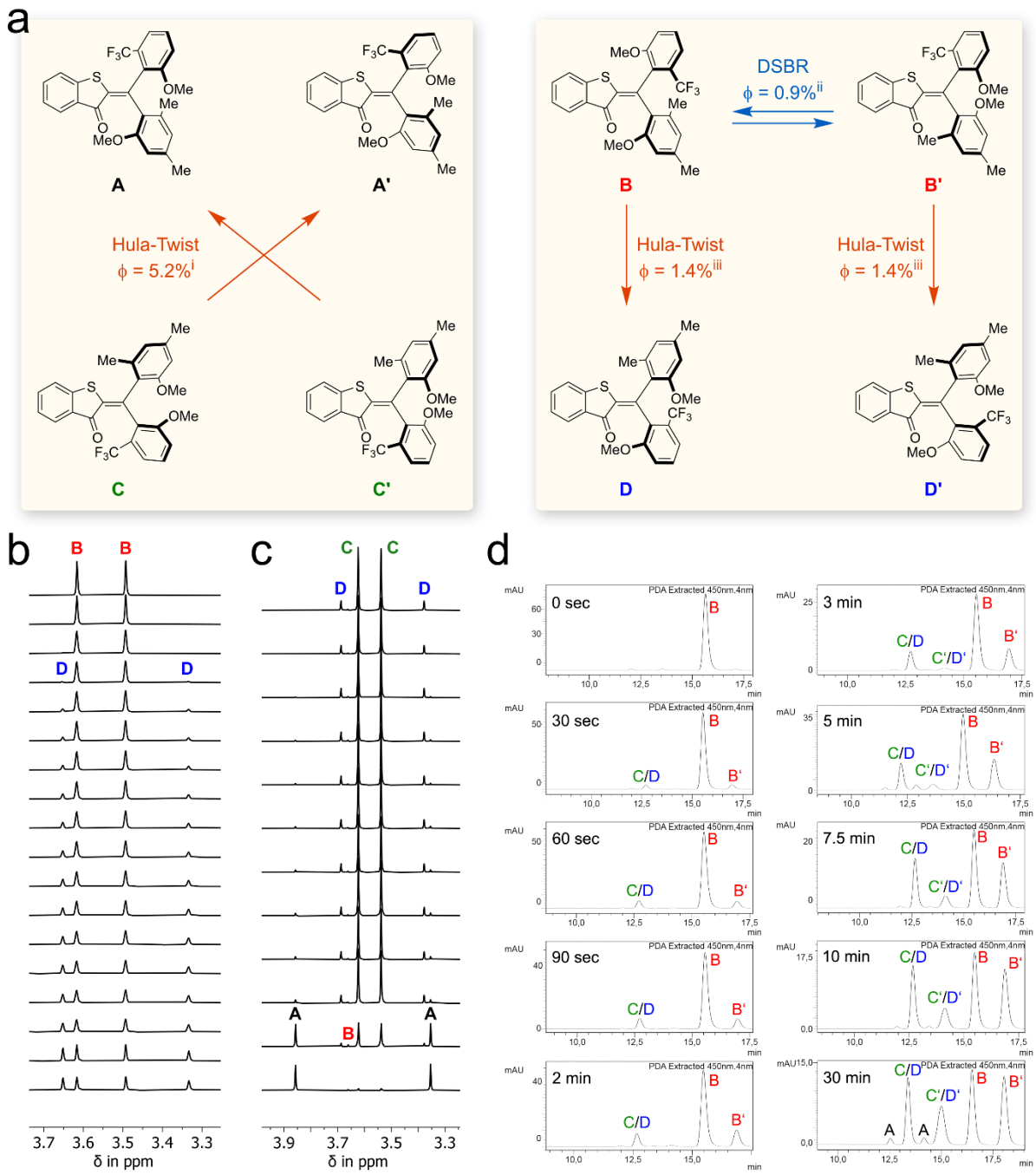

Figure 4 Photoreactions of HTI **1** during 450 nm irradiation. a) Photoreactions of **1** and associated quantum yields measured in MeCN solution. [i] Quantum yield determined taking into account the thermodynamic equilibrium of **C** and **D** at 20 °C. [ii] DSBR = double single bond rotation, quantum yield indirectly determined by multiplying the ratio of the photoproducts determined by chiral HPLC analysis with the quantum yield for the Hula-Twist reaction from *rac*-**B** to *rac*-**D** measured at -40 °C. [iii] Quantum yield determined at -40 °C. b) Photoconversion of isomer *rac*-**B** in MeCN-d_3 solution at -40 °C followed by ^{1}H NMR-spectroscopy (400 MHz). Starting with pure *rac*-**B** (top spectrum) only population of isomer *rac*-**D** is observed (top to bottom spectra). c) Photoconversion of the isomer mixture *rac*-**C**/*rac*-**D** in MeCN-d_3 solution at 22 °C followed by ^{1}H NMR-spectroscopy (400 MHz). Starting with a mixture of *rac*-**C**/*rac*-**D** (top spectrum) almost exclusive population of isomer *rac*-**A** is observed (top to bottom spectra). d)

Photoconversion of isomers **B** in MeCN solution at -40 °C followed by chiral HPLC. Starting with enantiomerically pure **B** (chromatogram 1) HPLC runs were conducted after different times of continuous irradiation at -40 °C monitoring the photoisomerization process (chromatograms 2-10).

Taking the thermal interconversions and the photoreactions together a repetitive isomerization cycle of racemic HTI **1** can be established in four distinct steps (Figure 5a). Starting with isomer *rac*-**B** the *rac*-**D** isomer can be obtained with 48% in the PSS. By thermal SBR *rac*-**D** is converted into the *rac*-**C** isomer with 86%, as the thermal equilibrium ratio between *rac*-**C** and *rac*-**D** is 86:14. By further irradiation at 20 °C isomer *rac*-**A** can be enriched up to 95% (*rac*-**A**: *rac*-**B**: *rac*-**C**: *rac*-**D** = 95:3:2:0). In the next thermal SBR *rac*-**A** is converted to *rac*-**B** with 78% (*rac*-**A**: *rac*-**B**: *rac*-**C**: *rac*-**D** = 20:78:2:0). Therefore, a complete cycle populating one of the four diastereomers selectively after another is performed by HTI **1**. This cycle can be repeated without isolation of one of the diastereomers by "refocussing" the mixture in the isomer *rac*-**A** enriched state. This is achieved by irradiation of the mixture with 405 nm light at 20 °C, which reestablishes reliably the *rac*-**A**: *rac*-**B**: *rac*-**C**: *rac*-**D** = 95:3:2:0 ratio in solution. Consequently, the following heating and photoisomerization steps produce the same isomer ratios as in the first cycle. The fact that this cycle is reproducible when starting from an arbitrary mixture of isomers of HTI **1** was demonstrated by executing the cycle experiment 3 times in a row with the same NMR-sample (see Supplementary Information). Also, after 10 cycles, corresponding to 20 photochemical and 20 thermal steps, only minimal degradation of the performance by about 5% was observed (Figure 5b).

When also taking the enantiomers into account a selective cycle of isomer interconversions **A→B→D→C→A'→B'→D'→C'→A** is constituted from the main photoreactions and thermal reactions. This is possible because each individual isomer transformation is highly selective under well controlled conditions. The **A→B** and **A'→B'** as well as **D→C** and **D'→C'** interconversions proceed thermally and without racemization as sole SBRs and all photochemical steps proceed as Hula-Twist reactions again with high selectivities. After a total of eight steps the starting isomer is obtained again. This eight-step cycle can however be bypassed by the one-photon-DSBR converting isomer **B** into **B'**. In this case HTI **1** performs the two enantiomeric cycles **A→B→B'→D'→C'→A** and **A'→B'→B→D→C→A'**.

By changing the environmental conditions during photoirradiation steps switching between the five- and eight-step cycles is possible (Figure 5c). If isomers **B** and **B'** perform a Hula-Twist photoreaction the eight-step cycle is followed and if the one photon DSBR occurs one of the five-step cycles is pursued. Obviously, the probability of the eight step-cycle is 100% if both **B** isomers perform exclusively the Hula-Twist reaction. This situation is nearly reached in MeOH solution at -80 °C with a preference for the Hula-Twist reaction of 85% corresponding to 72% eight-step cycle overall (see Figure 5c and the

Supporting Information for calculation details). Optimizing the conditions for the five-step cycle is not so obvious, as both the Hula-Twist and DSBR reaction of **B**/ **B'** are required for this cycle. Maximum efficiency for the five-step cycles is therefore reached in a situation where 50% Hula-Twist and 50% DSBR are present. This situation is reached nearly perfectly in MeCN solution at 20 °C where 61% DSBR and 39% Hula-Twist leads to 48% propensity for the five-step cycle (Figure 5c). At the same time 15% of the eight-step cycle are present under these conditions. Similarly irradiation of **B**/ **B'** at -40 °C in MeCN also leads to 48% propensity for the five-step cycle, owed to 61% Hula-Twist and 39% DSBR photoreactions taking place under these conditions. However, now 35% of the eight-step cycle are also present, which makes this situation less selective. When further increasing the overall DSBR probability by strongly reducing solvent polarity and conducting experiments in toluene solution, the efficiency for the five-step cycles decreases again slightly, as more "unproductive" switching back and forwards between **B** and **B'** is taking place. However, the decrease of the Hula-Twist reaction is much more severe in this case and a comfortable situation can be reached in which the latter is almost completely suppressed. Thus, in toluene solution at 20 °C the eight-step cycle is only present to 8% and the five-step cycle is much more likely with 40%. In this way the preferences of HTI **1** to undergo a specific isomer interconversion cycle can be switched upside down by simply changing solvent and temperatures. The eight-step cycle is preferred 5fold over the five-step cycle in MeOH solvent at -80 °C (i.e. 72% total likelihood for eight-step versus 15% total likelihood for the five-step cycle). The five-step cycle is preferred over the eight-step cycle also by a factor of 5 in toluene solution at 20 °C (8% total likelihood for eight-step versus 40% total likelihood for the five-step cycle).

Although performing sequential switching cycles HTI **1** is not a molecular motor. Obviously both five-step cycles are mirror-symmetric to each other and therefore any partial directional motions cancel each other out. The eight-step cycle possesses no enantiomeric counterpart but a mirror plane that mirrors one half of the cycle with the other one. This situation is comparable with a *meso*-compound, which is achiral despite the presence of stereo information. While one half of the rotations within the eight-step cycle of HTI **1** is forward, the other half must be backwards and both motions cancel each other out (see Figure 5d). However, HTI **1** is also not a simple switch as the forward and backwards motions are not random but follow a specific sequence and are isomer selective. Therefore, we refer to HTI **1** as a sequential switch. Interestingly, under observation with achiral techniques like NMR or UV-Vis spectroscopy the five- and eight-step cycles are indistinguishable and both cycles lead to the same apparent conversion in the sequence *rac*-**A**→*rac*-**B**→*rac*-**C**→*rac*-**D**.

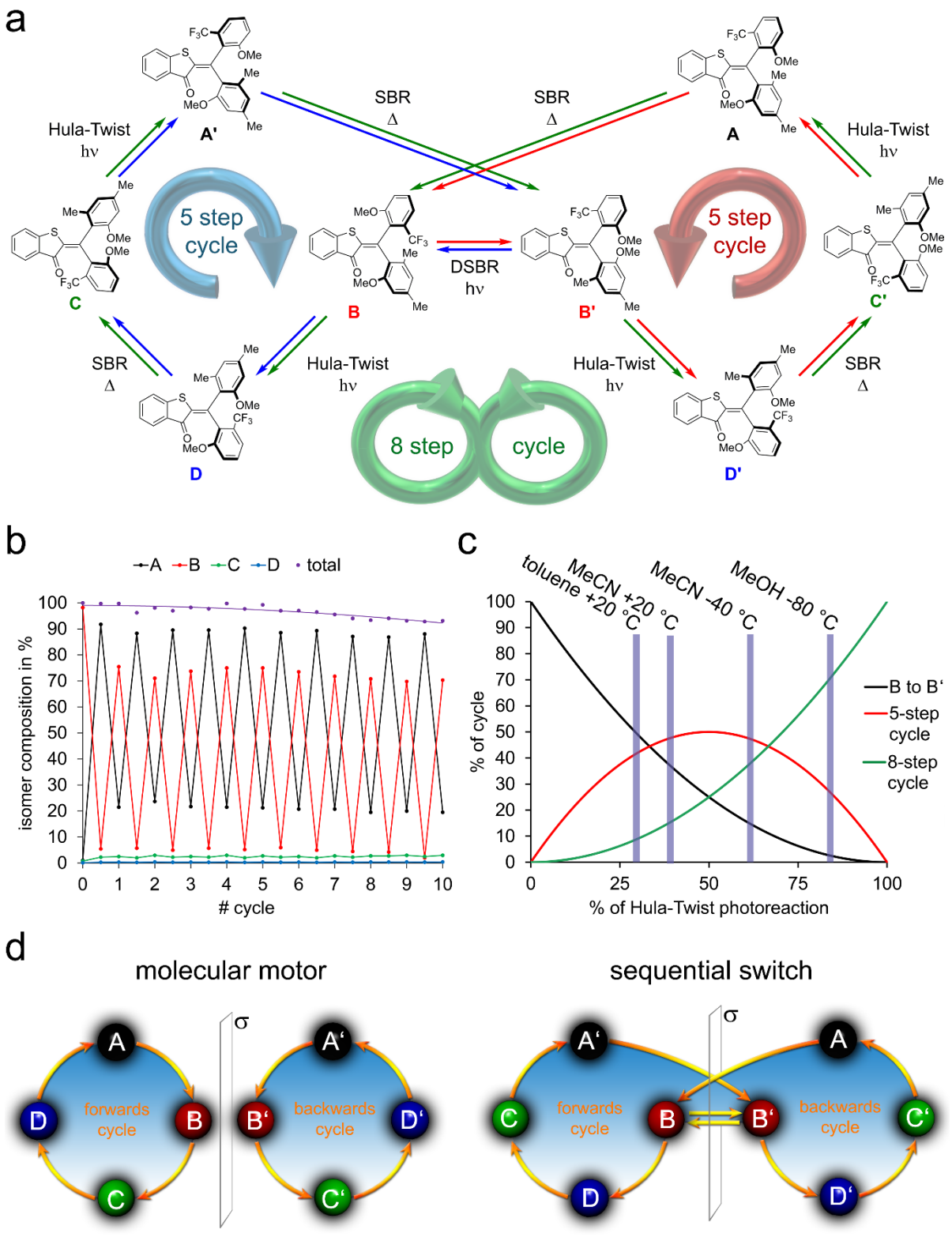

Figure 4 Isomerization properties of the sequential photoswitch **1**. a) Comprehensive scheme showing the selective and sequential switching behavior of HTI **1**. The nature of individual transformations are assigned. b) Repetitive reversible switching cycles of racemic HTI **1**. Minimal loss of performance is observed after 10 full cycles. Refocussing by the same enrichment of isomer *rac*-**A**. c) Propensity for eight- (green trace) or five-step (red trace) sequential switching cycles depending on the ratio of Hula-Twist (x-axis) versus DSBR (black trace) photoreactions of

isomers **B**/**B'**. d) Schematic representation of a molecular motor mechanism as opposed to the herein presented sequential switch mechanism.

In conclusion we herein present an unprecedented type of a sequential molecular switch allowing the interconversion of eight different isomers selectively and in defined sequence. This interconversion can be performed in an eight-step cycle featuring sequential photo activated Hula-Twist reactions and thermal single bond rotations or by two enantiomeric five-step cycles involving an unprecedented one photon DSBR photoreaction. By simply changing solvent and temperature each cycle can be preferred over the other by a factor of five. Furthermore, enrichment of one racemic isomer up to 95% in the PSS is possible enabling a continuous and identical repeatable sequence of isomer interconversions – even when starting with an arbitrary mixture of isomers. This new type of compact molecular tool providing complex sequential movements and eight different accessible states will add new fundamental opportunities for photoswitch applications and future bottom-up building of nanomaterials. In addition, the here discovered one photon DSBR photoreaction enables a new type of light-induced motion at the molecular scale, which should be of great interest for photoswitching applications and especially for future advanced molecular machine building .

Acknowledgements:

H. Dube thanks the Deutsche Forschungsgemeinschaft (DFG) for an Emmy Noether fellowship (DU 1414/1-2). We further thank the European Research Council under the European Union's Horizon 2020 research and innovation program (PHOTOMECH, grant agreement No 101001794, the Deutsche Forschungsgemeinschaft (SFB 749, A12), and the Cluster of Excellence 'Center for Integrated Protein Science Munich' (CIPS^{M}) for further support.

Conflict of interest

The authors declare no conflict of interest.

Keywords: molecular machines • photochemistry • isomerization • hemithioindigo • physical chemistry

References

1. Lubbe, A. S.; Szymanski, W.; Feringa, B. L., Recent developments in reversible photoregulation of oligonucleotide structure and function. *Chem. Soc. Rev.* **2017,** *46* (4), 1052-1079.
2. Lerch, M. M.; Hansen, M. J.; van Dam, G. M.; Szymanski, W.; Feringa, B. L., Emerging Targets in Photopharmacology. *Angew. Chem. Int. Ed.* **2016,** *55* (37), 10978-10999.

3. Velema, W. A.; Szymanski, W.; Feringa, B. L., Photopharmacology: beyond proof of principle. *J. Am. Chem. Soc.* **2014,** *136* (6), 2178-91.
4. Morstein, J.; Trauner, D., New players in phototherapy: photopharmacology and bio-integrated optoelectronics. *Curr. Opin. Chem. Biol.* **2019,** *50*, 145-151.
5. Brieke, C.; Rohrbach, F.; Gottschalk, A.; Mayer, G.; Heckel, A., Light-controlled tools. *Angew. Chem. Int. Ed.* **2012,** *51* (34), 8446-76.
6. Irie, M.; Fukaminato, T.; Matsuda, K.; Kobatake, S., Photochromism of diarylethene molecules and crystals: memories, switches, and actuators. *Chem. Rev.* **2014,** *114* (24), 12174-12277.
7. Andreasson, J.; Pischel, U., Molecules with a sense of logic: a progress report. *Chem. Soc. Rev.* **2015,** *44*, 1053-1069.
8. Shao, B.; Aprahamian, I., Hydrazones as New Molecular Tools. *Chem* **2020,** *6* (9), 2162-2173.
9. Boelke, J.; Hecht, S., Designing Molecular Photoswitches for Soft Materials Applications. *Adv. Optical Mater.* **2019,** *7* (16), 1900404.
10. Göstl, R.; Senf, A.; Hecht, S., Remote-controlling chemical reactions by light: Towards chemistry with high spatio-temporal resolution. *Chem. Soc. Rev.* **2014,** *43* (6), 1982-1996.
11. In *Molecular Switches*, Second ed.; Feringa, B. L.; Browne, W. R., Eds. Wiley-VCH Verlag GmbH & Co. KGaA: 2011.
12. Petermayer, C.; Dube, H., Indigoid Photoswitches: Visible Light Responsive Molecular Tools. *Acc. Chem. Res.* **2018,** *51* (5), 1153-1163.
13. Kortekaas, L.; Browne, W. R., The evolution of spiropyran: fundamentals and progress of an extraordinarily versatile photochrome. *Chem. Soc. Rev.* **2019,** *48* (12), 3406-3424.
14. Hull, K.; Morstein, J.; Trauner, D., In Vivo Photopharmacology. *Chem. Rev.* **2018,** *118* (21), 10710-10747.
15. Klajn, R., Spiropyran-based dynamic materials. *Chem. Soc. Rev.* **2014,** *43* (1), 148-84.
16. Andreasson, J.; Pischel, U., Molecules for security measures: from keypad locks to advanced communication protocols. *Chem. Soc. Rev.* **2018,** *47* (7), 2266-2279.
17. Fischer, E.; Hirshberg, Y., Formation of coloured forms of spirans by low-temperature irradiation. *J. Chem. Soc.* **1952**, 4522-4524.
18. Irie, M.; Mohri, M., Thermally Irreversible Photochromic Systems. Reversible Photocyclization of Diarylethene Derivatives. *J. Org. Chem.* **1987,** *53*, 803-808.
19. Waldeck, D. H., Photoisomerization Dynamics of Stilbenes. *Chem. Rev.* **1991,** *91*, 415-436.
20. Bandara, H. M.; Burdette, S. C., Photoisomerization in different classes of azobenzene. *Chem. Soc. Rev.* **2012,** *41* (5), 1809-25.
21. Weinstein, J.; Wyman, G. M., Spectroscopic Studies on Dyes. II. The Structure of N,N'-Dimethylindigo1. *J. Am. Chem. Soc.* **1956,** *78* (16), 4007-4010.
22. Saltiel, J.; Papadimitriou, D.; Krishna, T. S.; Huang, Z. N.; Krishnamoorthy, G.; Laohhasurayotin, S.; Clark, R. J., Photoisomerization of all-cis-1,6-diphenyl-1,3,5-hexatriene in the solid state and in solution: a simultaneous three-bond twist process. *Angew. Chem. Int. Ed.* **2009,** *48* (43), 8082-5.
23. Gerwien, A.; Schildhauer, M.; Thumser, S.; Mayer, P.; Dube, H., Direct evidence for hula twist and single-bond rotation photoproducts. *Nat. Commun.* **2018,** *9* (1), 2510.
24. Gerwien, A.; Mayer, P.; Dube, H., Photon-Only Molecular Motor with Reverse Temperature-Dependent Efficiency. *J. Am. Chem. Soc.* **2018,** *140*, 16442-16445.
25. Liu, R. S.; Asato, A. E., The primary process of vision and the structure of bathorhodopsin: a mechanism for photoisomerization of polyenes. *Proc. Natl. Acad. Sci. U. S. A.* **1985,** *82* (2), 259-63.
26. Fuß, W.; Kosmidis, C.; Schmid, W. E.; Trushin, S. A., The photochemical cis-trans isomerization of free stilbene molecules follows a hula-twist pathway. *Angew. Chem. Int. Ed.* **2004,** *43* (32), 4178-82.

27. Warshel, A., Bicycle-pedal model for the first step in the vision process. *Nature* **1976,** *260*, 679-683.
28. Schapiro, I.; Weingart, O.; Buss, V., Bicycle-Pedal Isomerization in a Rhodopsin Chromophore Model. *J. Am. Chem. Soc.* **2009,** *131* (1), 16-17.
29. Zhang, Q.; Chen, X.; Cui, G.; Fang, W.-H.; Thiel, W., Concerted Asynchronous Hula-Twist Photoisomerization in the S65T/H148D Mutant of Green Fluorescent Protein. *Angew. Chem., Int. Ed.* **2014,** *53* (33), 8649-8653.
30. Jung, Y. O.; Lee, J. H.; Kim, J.; Schmidt, M.; Moffat, K.; Srajer, V.; Ihee, H., Volume-conserving trans-cis isomerization pathways in photoactive yellow protein visualized by picosecond X-ray crystallography. *Nat. Chem.* **2013,** *5* (3), 212-220.
31. Kaila, V. R. I.; Schotte, F.; Cho, H. S.; Hummer, G.; Anfinrud, P. A., Contradictions in X-ray structures of intermediates in the photocycle of photoactive yellow protein. *Nat. Chem.* **2014,** *6* (4), 258-259.
32. Jung, Y. O.; Lee, J. H.; Kim, J.; Schmidt, M.; Moffat, K.; Šrajer, V.; Ihee, H., Reply to 'contradictions in X-ray structures of intermediates in the photocycle of photoactive yellow protein'. *Nat. Chem.* **2014,** *6*, 259-60.
33. Gust, D.; Andreasson, J.; Pischel, U.; Moore, T. A.; Moore, A. L., Data and signal processing using photochromic molecules. *Chem. Commun.* **2012,** *48* (14), 1947-57.
34. Mutoh, K.; Kobayashi, Y.; Yamane, T.; Ikezawa, T.; Abe, J., Rate-Tunable Stepwise Two-Photon-Gated Photoresponsive Systems Employing a Synergetic Interaction between Transient Biradical Units. *J. Am. Chem. Soc.* **2017,** *139* (12), 4452-4461.
35. Moran, M. J.; Magrini, M.; Walba, D. M.; Aprahamian, I., Driving a Liquid Crystal Phase Transition Using a Photochromic Hydrazone. *J. Am. Chem. Soc.* **2018,** *140* (42), 13623-13627.
36. Fihey, A.; Perrier, A.; Browne, W. R.; Jacquemin, D., Multiphotochromic molecular systems. *Chem. Soc. Rev.* **2015,** *44* (11), 3719-59.
37. Yu, Z.; Weidner, S.; Risse, T.; Hecht, S., The role of statistics and microenvironment for the photoresponse in multi-switch architectures: The case of photoswitchable oligoazobenzene foldamers. *Chem. Sci.* **2013,** *4*, 4156-4167.
38. Zhang, J.; Zou, Q.; Tian, H., Photochromic materials: more than meets the eye. *Adv. Mater.* **2013,** *25* (3), 378-99.
39. Zhao, F.; Grubert, L.; Hecht, S.; Bleger, D., Orthogonal switching in four-state azobenzene mixed-dimers. *Chemical Communications (Cambridge, United Kingdom)* **2017,** *53*, 3323-3326.
40. Bléger, D.; Liebig, T.; Thiermann, R.; Maskos, M.; Rabe, J. P.; Hecht, S., Light-Orchestrated Macromolecular "Accordions": Reversible Photoinduced Shrinking of Rigid-Rod Polymers. *Angew. Chem. Int. Ed.* **2011,** *50* (52), 12559-12563.
41. Heindl, A. H.; Becker, J.; Wegner, H. A., Selective switching of multiple azobenzenes. *Chem. Sci.* **2019,** *10* (31), 7418-7425.
42. Yang, C.; Slavov, C.; Wegner, H. A.; Wachtveitl, J.; Dreuw, A., Computational design of a molecular triple photoswitch for wavelength-selective control. *Chem Sci* **2018,** *9* (46), 8665-8672.
43. Cisnetti, F.; Ballardini, R.; Credi, A.; Gandolfi, M. T.; Masiero, S.; Negri, F.; Pieraccini, S.; Spada, G. P., Photochemical and electronic properties of conjugated bis(azo) compounds: an experimental and computational study. *Chem. Eur. J.* **2004,** *10* (8), 2011-21.
44. Peters, A.; Branda, N. R., Limited photochromism in covalently linked double 1,2-dithienylethenes. *Adv. Mater. Opt. Electron.* **2000,** *10* (6), 245-249.
45. Yagi, K.; Irie, M., Photochromic and Fluorescent Properties of a Diarylethene Dimer. *Chem. Lett.* **2003,** *32* (9), 848-849.
46. Han, M.; Luo, Y.; Damaschke, B.; Gomez, L.; Ribas, X.; Jose, A.; Peretzki, P.; Seibt, M.; Clever, G. H., Light-Controlled Interconversion between a Self-Assembled Triangle and a Rhombicuboctahedral Sphere. *Angew. Chem. Int. Ed.* **2016,** *55* (1), 445-449.

47. Han, M.; Michel, R.; He, B.; Chen, Y. S.; Stalke, D.; John, M.; Clever, G. H., Light-triggered guest uptake and release by a photochromic coordination cage. *Angew. Chem. Int. Ed.* **2013,** *52* (4), 1319-1323.
48. Kortekaas, L.; Ivashenko, O.; van Herpt, J. T.; Browne, W. R., A Remarkable Multitasking Double Spiropyran: Bidirectional Visible-Light Switching of Polymer-Coated Surfaces with Dual Redox and Proton Gating. *J. Am. Chem. Soc.* **2016,** *138* (4), 1301-12.
49. Hoffmann, K.; Guentner, M.; Mayer, P.; Dube, H., Symmetric and nonsymmetric bis-hemithioindigos – precise visible light controlled shape-shifters. *Org. Chem. Front.* **2019,** *6* (8), 1244-1252.
50. Vlasceanu, A.; Koerstz, M.; Skov, A. B.; Mikkelsen, K. V.; Nielsen, M. B., Multistate Photoswitches: Macrocyclic Dihydroazulene/Azobenzene Conjugates. *Angew. Chem. Int. Ed.* **2018,** *57* (21), 6069-6072.
51. Andreasson, J.; Pischel, U.; Straight, S. D.; Moore, T. A.; Moore, A. L.; Gust, D., All-photonic multifunctional molecular logic device. *J. Am. Chem. Soc.* **2011,** *133* (30), 11641-8.
52. Balter, M.; Li, S.; Nilsson, J. R.; Andreasson, J.; Pischel, U., An all-photonic molecule-based parity generator/checker for error detection in data transmission. *J. Am. Chem. Soc.* **2013,** *135* (28), 10230-3.
53. Guerrin, C.; Aidibi, Y.; Sanguinet, L.; Leriche, P.; Aloise, S.; Orio, M.; Delbaere, S., When Light and Acid Play Tic-Tac-Toe with a Nine-State Molecular Switch. *J. Am. Chem. Soc.* **2019,** *141* (48), 19151-19160.
54. Gobbi, L.; Seiler, P.; Diederich, F., A Novel Three-Way Chromophoric Molecular Switch: pH and Light Controllable Switching Cycles. *Angew. Chem. Int. Ed.* **1999,** *38* (5), 674-678.
55. Kink, F.; Collado, M. P.; Wiedbrauk, S.; Mayer, P.; Dube, H., Bistable Photoswitching of Hemithioindigo with Green and Red Light: Entry Point to Advanced Molecular Digital Information Processing. *Chem. Eur. J.* **2017,** *23*, 6237-6243.
56. Koumura, N.; Zijlstra, R. W. J.; van Delden, R. A.; Feringa, B. L., Light-driven monodirectional molecular rotor. *Nature* **1999,** *401*, 152-155.
57. Kassem, S.; van Leeuwen, T.; Lubbe, A. S.; Wilson, M. R.; Feringa, B. L.; Leigh, D. A., Artificial molecular motors. *Chem. Soc. Rev.* **2017,** *46* (9), 2592-2621.
58. Roke, D.; Wezenberg, S. J.; Feringa, B. L., Molecular rotary motors: Unidirectional motion around double bonds. *Proc. Natl. Acad. Sci. U. S. A.* **2018,** *115* (38), 9423-9431.
59. Kistemaker, H. A.; Stacko, P.; Visser, J.; Feringa, B. L., Unidirectional rotary motion in achiral molecular motors. *Nat. Chem.* **2015,** *7*, 890-896.
60. Klok, M.; Boyle, N.; Pryce, M. T.; Meetsma, A.; Browne, W. R.; Feringa, B. L., MHz Unidirectional Rotation of Molecular Rotary Motors. *J. Am. Chem. Soc.* **2008,** *130*, 10484-10485.
61. Štacko, P.; Kistemaker, J. C. M.; van Leeuwen, T.; Chang, M.-C.; Otten, E.; Feringa, B. L., Locked synchronous rotor motion in a molecular motor. *Science* **2017,** *356* (6341), 964-968.
62. Greb, L.; Lehn, J. M., Light-driven molecular motors: imines as four-step or two-step unidirectional rotors. *J. Am. Chem. Soc.* **2014,** *136* (38), 13114-13117.
63. Guentner, M.; Schildhauer, M.; Thumser, S.; Mayer, P.; Stephenson, D.; Mayer, P. J.; Dube, H., Sunlight-powered kHz rotation of a hemithioindigo-based molecular motor. *Nat. Commun.* **2015,** *6*, 8406.
64. Huber, L. A.; Hoffmann, K.; Thumser, S.; Böcher, N.; Mayer, P.; Dube, H., Direct Observation of Hemithioindigo-Motor Unidirectionality. *Angew. Chem. Int. Ed.* **2017,** *56*, 14536-14539.
65. Wilcken, R.; Schildhauer, M.; Rott, F.; Huber, L. A.; Guentner, M.; Thumser, S.; Hoffmann, K.; Oesterling, S.; de Vivie-Riedle, R.; Riedle, E.; Dube, H., Complete Mechanism of Hemithioindigo Motor Rotation. *J. Am. Chem. Soc.* **2018,** *140*, 5311-5318.

66. Gerwien, A.; Mayer, P.; Dube, H., Green light powered molecular state motor enabling eight-shaped unidirectional rotation. *Nat. Commun.* **2019,** *10* (1), 4449.
67. Uhl, E.; Mayer, P.; Dube, H., Active and Unidirectional Acceleration of Biaryl Rotation by a Molecular Motor. *Angew. Chem. Int. Ed.* **2020,** *59* (14), 5730-5737.
68. Gerwien, A.; Reinhardt, T.; Mayer, P.; Dube, H., Synthesis of Double-Bond Substituted Hemithioindigo Photoswitches. *Org. Lett.* **2018,** *1*, 232-235.
69. Liu, R. S. H., Photoisomerization by Hula-Twist: A Fundamental Supramolecular Photochemical Reaction. *Acc. Chem. Res.* **2001,** *34* (7), 555-562.

An eight-state molecular sequential switch featuring a dual single-bond rotation photoreaction

Aaron Gerwien,[§] *Benjamin Jehle,*[§] *Marvin Irmler,*[§] *Peter Mayer,*[§] *Henry Dube*[†]*

[§] Ludwig-Maximilians Universität München, Department of Chemistry and Center for Integrated Protein Science CIPSM, Butenandtstr. 5–13, 81377 Munich, Germany

[†] Friedrich-Alexander Universität Erlangen-Nürnberg, Department of Chemistry and Pharmacy, Nikolaus-Fiebiger-Str. 10, 91058 Erlangen, Germany

* E-mail: henry.dube@fau.de

Supplementary File

Table of contents

Synthesis

General experimental

Reagents and solvents were obtained from *abcr*, *Acros, Fluka, Merck, Sigma-Aldrich* or *TCI* in the qualities *puriss., p.a.,* or *purum* and used as received. Technical solvents were distilled before use for column chromatography and extraction on a rotary evaporator (*Heidolph Hei-VAP Value*, *vacuubrand* CVC 3000). Reactions were monitored on *Merck* Silica 60 F254 TLC plates. Detection was done by irradiation with UV light (254 nm or 366 nm).

Flash column chromatography (FCC) was performed with silica gel 60 (*Merck*, particle size 0.063- 0.200 mm) and distilled technical solvents.

^{1}H NMR and ^{13}C NMR spectra were measured on a *Varian Mercury 200 VX, Varian 300, Inova 400, Varian 600 NMR* or *Bruker Avance III HD 800 MHz* spectrometer at 23 °C. Deuterated solvents were obtained from *Cambridge Isotope Laboratories* or *Eurisotop* and used without further purification. Chemical shifts (δ) are given relative to tetramethylsilane as external standard. Residual solvent signals in the ^{1}H and ^{13}C NMR spectra were used as internal reference. For ^{1}H NMR: $CDCl_3$ = 7.26 ppm, CD_2Cl_2 = 5.32 ppm, toluene-d_8 = 2.08 ppm, MeCN-d_3 = 1.94 ppm. For ^{13}C NMR: $CDCl_3$= 77.16 ppm, CD_2Cl_2= 53.84 ppm, toluene-d_8= 20.43, MeCN-d_3 = 118.26 ppm. The resonance multiplicity is indicated as *s* (singlet), *d* (doublet), *t* (triplet), *q* (quartet) and *m* (multiplet). The chemical shifts are given in parts per million (ppm) on the delta scale (δ). The coupling constant values (*J*) are given in hertz (Hz).

Electron Impact (EI) mass spectra were measured on a *Finnigan MAT95Q* or on a *Finnigan MAT90* mass spectrometer. **Electronspray ionisation (ESI) mass spectra were** measured on a *Thermo Finnigan LTQ-FT*. The most important signals are reported in *m/z* units with *M* as the molecular ion.

Elemental analysis was performed in the micro analytical laboratory of the LMU department of chemistry on an *Elementar Vario EL* apparatus.

Infrared spectra were recorded on a *Perkin Elmer Spectrum BX-FT-IR* instrument equipped with a *Smith DuraSamplIR II ATR*-device. Transmittance values are qualitatively described by wavenumber (cm^{-1}) as very strong (vs), strong (s), medium (m) and weak (w).

Isomerization experiments: Irradiations of the HTI solutions were conducted in NMR tubes at concentrations in the range of $1x10^{-3}$ mol/L in deuterated solvents or in UV/vis cuvettes at concentrations in the range of $1x10^{-5}$ mol/L in *spectroscopic grade* solvents. For irradiation, LEDs from *Roithner Lasertechnik GmbH* (365 nm, 385 nm, 405 nm, 420 nm, 435 nm) were used.

UV/vis spectra were measured on a *Varian Cary 5000* spectrophotometer. The spectra were recorded in a quartz cuvette (l = 1 cm). Solvents for spectroscopy were obtained from *VWR* and *Merck*. Absorption wavelength (λ) are reported in nm and the molar extinction coefficient (ε) L mol^{-1} cm^{-1} in brackets. Shoulders are declared as sh.

Quantum yields at a given temperature were measured on a *Varian Cary® 50* spectrophotometer with an *Oxford DN 1704* optical cryostat controlled by an *Oxford ITC 4* device. Low temperatures were reached by cooling slowly with liquid nitrogen. The spectra were recorded in a quartz cuvette (l = 1 cm). Solvents for spectroscopy were obtained from *VWR*, *Merck* and *Sigma Aldrich* and were dried, degassed prior use. For irradiation studies a *Prizmatix UHP-T-LED-450* (450 nm) was used as light source.

Melting points (M.p.) were measured on a *Stuart* SMP10 melting point apparatus in open capillaries and are not corrected.

High Performance Liquid Chromatography (HPLC) was performed on a Shimadzu HPLC system consisting of a LC-20AP solvent delivery module, a CTO-20A column oven, a SPD-M20A photodiode array UV/vis detector and a CBM-20A system controller using a preparative or analytical CHIRALPAK® ID column (particle size 5 µm) from *Daicel* and HPLC grade solvents (*n*-heptane and ethyl acetate) from *Sigma-Aldrich*, *VWR*, and *ROTH*.

Synthesis of HTI 1

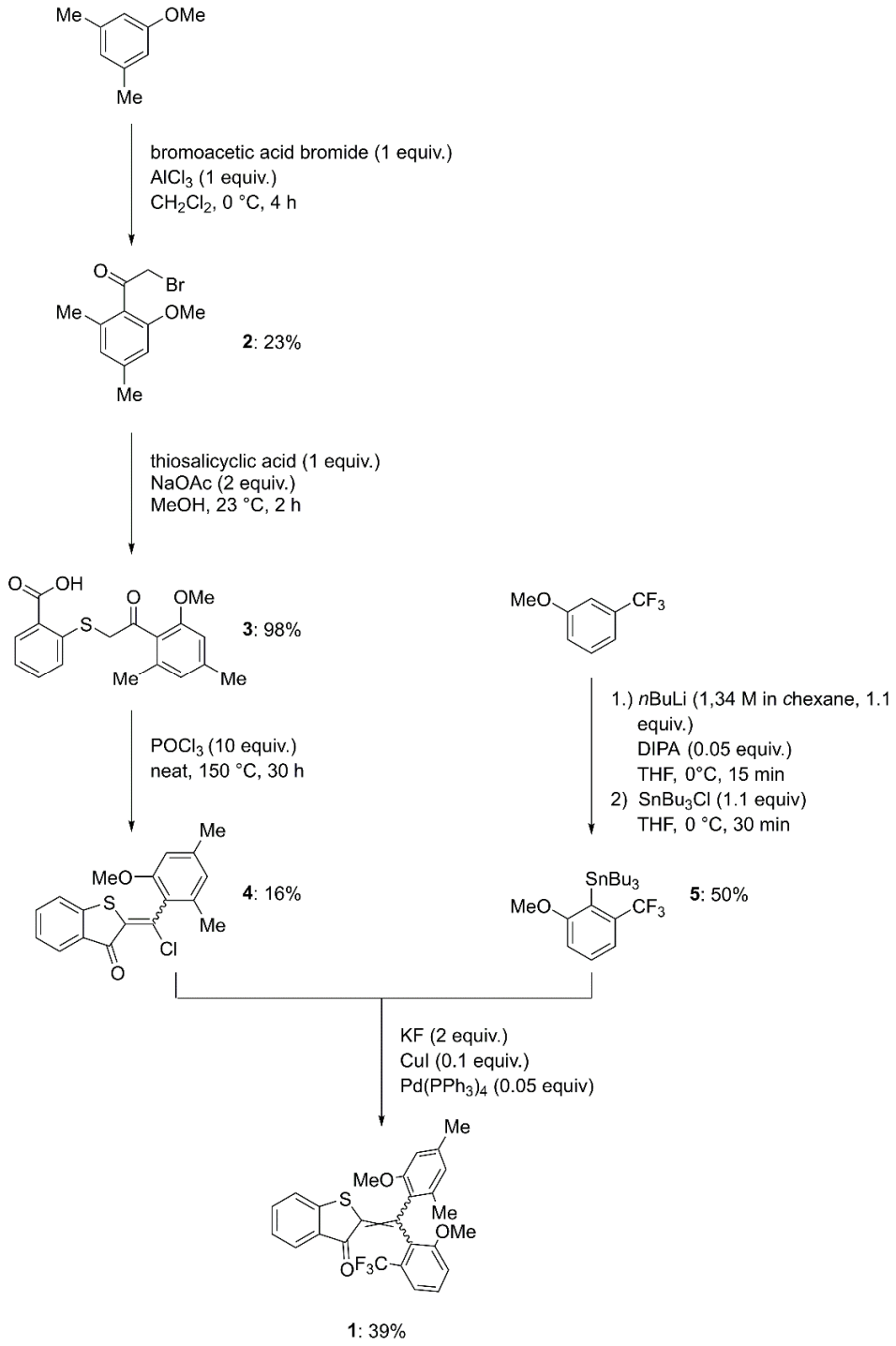

Supplementary Scheme 1. Synthesis of motor **1**. Compounds **2**[1] and **3**[2] were prepared following published procedures.

2-Bromo-1-(2-methoxy-4,6-dimethylphenyl)ethan-1-one (2) [1]

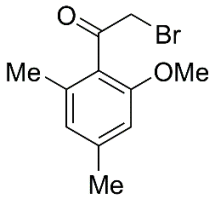

3,5-Dimethylanisole (9.55 mL, 9.20 g, 67.5 mmol, 1 equiv.) and bromoacetyl bromide (5.88 mL, 13.6 g, 67.4 mmol, 1 equiv.) were dissolved in CH_2Cl_2 (50 mL) and $AlCl_3$ (9.00 g, 67.5 mmol, 1 equiv.) was added portion-wise at 0 °C. The reaction mixture was stirred for 4 h while reaching 23 °C and was then completed by adding HCl (2 M aq. solution, 50 mL) carefully under cooling with an ice bath (0 °C). The aqueous phase was extracted with CH_2Cl_2 (3 x 50 mL) the combined organic phases were dried over Na_2SO_4 and the solvent was removed *in vacuo*. The crude product was purified via FCC (SiO_2, *i*Hex:EtOAc = 99:1) yielding the title compound as colorless solid (5.73 g, 22.3 mmol, 33%).

^{1}H NMR (200 MHz, $CDCl_3$) δ (ppm) = 6.67 (s, 1H), 6.59 (s, 1H), 4.36 (s, 2H), 3.83 (s, 3H), 2.33 (s, 3H), 2.25 (s, 3H).

2-((2-(2-Methoxy-4,6-dimethylphenyl)-2-oxoethyl)thio)benzoic acid (3) [2]

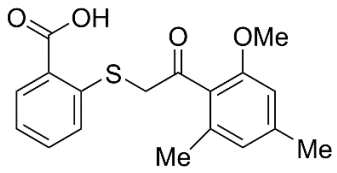

Thiosalicylic acid (7.58 g, 50.9 mmol, 1 equiv.), bromide **2** (13.1 g, 50.9 mmol, 1 equiv.) and sodium acetate (8.56 g, 102 mmol, 2.00 equiv.) were dissolved in MeOH (100 mL) and stirred for 30 min at 60 °C. The reaction was terminated by adding a mixture of HCl (2 M aq. solution) and ice water (100 mL) upon which a precipitate formed. The precipitate was filtered, washed with H_2O and hexanes and dried *in vacuo*. The thus obtained pure compound **3** was isolated as colorless solid (16.5 g, 49.9 mmol, 98 %).

^{1}H NMR (200 MHz, $CDCl_3$) δ (ppm) = 8.07 (dt, J = 7.8, 1.2, 1H), 7.55 – 7.40 (m, 2H), 7.21 (ddd, J = 8.4, 6.1, 2.3, 1H), 6.65 – 6.51 (m, , 2H), 4.27 (s, 2H), 3.83 (s, 3H), 2.31 (s, 3H), 2.06 (s, 3H).

2-(Chloro(2-methoxy-4,6-dimethylphenyl)methylene)benzo[*b*]thiophen-3(2*H*)-one (4) [3]

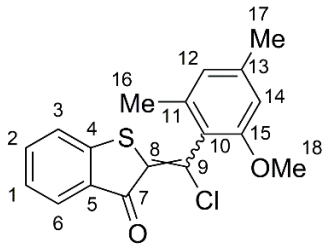

Thioether **3** (15.3 g, 46.3 mmol, 1 equiv.) was dissolved in $POCl_3$ (42.3 mL, 71.9 g, 463 mmol, 10.0 equiv.) and the reaction mixture was immediately heated up to 150 °C. After stirring for 30 min at that temperature the reaction was stopped by carefully adding water (250 mL). The aqueous phase was extracted with CH_2Cl_2 (3 x 80 mL) the combined organic phases were dried over Na_2SO_4 and the solvent was removed *in vacuo*. The crude product was purified via FCC (SiO_2, *i*Hex:EtOAc = 98:2 → 93:7) yielding the title compound as mixture of *E*/*Z* isomers in a ratio of 1:5 as yellow solid (2.40 g, 7.25 mmol, 16%).

HR-MS (EI) for $C_{18}H_{15}ClO_2S^{\bullet+}$, $[M]^{\bullet+}$, calcd. 330.0476, found 330.0474.

^{1}H-NMR (600 MHz, $CDCl_3$) δ = 7.90 (d, J = 7.6 Hz, 1H, H-C(6)$_E$), 7.67 (d, J = 8.3 Hz, 1H, H-C(6)$_Z$), 7.57 – 7.52 (m, 1H, H-C(2)$_Z$), 7.51 (t, J = 7.6 Hz, 1H, H-C(2)$_E$), 7.44 (d, J = 7.9 Hz, 1H, H-C(6)$_Z$), 7.28 – 7.24 (m, 2H, H-C(1)$_E$, H-C(3)$_E$), 7.21 (t, J = 7.8 Hz, 1H, H-C(1)$_Z$), 6.71 (s, 1H, H-C(12)$_Z$), 6.66 (s, 1H, H-C(12)$_E$), 6.63 (s, 1H, H-C(14)$_E$), 6.62 (s, 1H, , H-C(14)$_Z$), 3.79 (s, 3H, H-C(18)$_E$), 3.76 (s, 3H, H-C(18)$_E$), 2.36 (s, 3H, H-C(17)$_E$), 2.36 (s, 3H, H-C(17)$_E$), 2.25 (s, 3H, H-C(17)$_E$), 2.19 (s, 3H, H-C(17)$_Z$) ppm.

^{13}C-NMR (151 MHz, $CDCl_3$) δ = 185.2 (C(7)$_E$), 183.7 (C(7)$_Z$), 156.5 (C(15)$_Z$), 156.1 (C(15)$_E$), 144.5 (C(4)$_Z$), 144.0 (C(4)$_E$), 141.5 (C(13)$_E$), 140.9 (C(13)$_Z$), 140.2 (C(8/9)$_Z$), 140.2 (C(8/9)$_E$), 137.2 (C(11)$_Z$), 136.8 (C(11)$_E$), 135.2 (C(2)$_Z$), 135.1 (C(2)$_E$), 134.2 (C(8/9)$_Z$), 133.7 (C(8/9)$_E$), 132.6 (C(5)$_Z$), 132.5 (C(5)$_E$), 127.1 (C(6)$_E$), 127.0 (C(6)$_Z$), 125.4 (C(1)$_Z$), 125.2 (C(1)$_E$), 124.4 (C(10)$_E$), 123.6 (C(3)$_Z$), 123.4 (C(12)$_Z$), 123.1 (C(3)$_E$), 122.4 (C(10)$_Z$), 109.8 (C(14)$_E$), 109.6 (C(14)$_Z$), 56.0 (C(18)$_E$), 55.8 (C(18)$_Z$), 21.9 (C(17)$_Z$), 21.8 (C(17)$_E$), 19.0 (C(16)$_Z$), 18.8 (C(16)$_E$) ppm.

IR (ATR): $\tilde{\upsilon}$/cm^{-1} = 2915 (w), 2832 (w), 1728 (m), 1679 (vs), 1591 (vs), 1565 (vs), 1446 (vs), 1408 (m),1375 (w), 1311 (vs), 1279 (vs), 1249 (m), 1222 (s), 1185 (m), 1157 (vs), 1093 (vs), 1056 (m), 1020 (m), 1002 (m), 948 (m), 921 (m), 893 (w), 876 (w), 860 (m), 845 (m), 828 (vs), 789 (m), 733 (vs), 702 (m), 687 (m), 663 (m).

R$_f$ (SiO_2, *i*hexane:EtOAc = 95:5) = 0.37.

Tributyl(2-methoxy-6-(trifluoromethyl)phenyl)stannane (5)

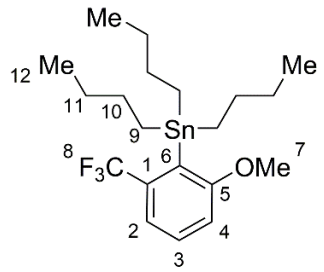

In a flame dried round bottom flask 1-methoxy-3-(trifluoromethyl)benzene (5.00 mL, 4.11 g, 23.3 mmol, 1 equiv.) was dissolved in THF (20 mL) and the solution was cooled to 0 °C. Diisopropylamine (0.16 mL, 118 mg, 1.17 mmol, 0.05 equiv.) and *n*BuLi (1.43 M in *c*hexane, 17.9 mL, 25.7 mmol, 1.1 equiv.) were added at 0 °C and the reaction was stirred for 15 min at that temperature. Tributyltin chloride (6.96 mL, 8.35 g, 25.7 mmol, 1.1 equiv.) was added and stirring was continued for 30 min at 0 °C. After completion the reaction was quenched by adding a sat. aq. $NaHCO_3$ solution (50 mL), the aqueous phase was extracted with CH_2Cl_2 (3 x 50 mL) and the combined organic phases were dried over Na_2SO_4. After removing the solvent *in vacuo* the crude product was purified via FCC (SiO_2, *i*Hex:EtOAc = 99:1) and the product was obtained as colorless liquid (5.45 g, 11.7 mmol, 50%).

HR-MS (EI) for $C_{20}H_{33}F_3O_2Sn^{\bullet+}$, $[M]^{\bullet+}$, calcd. 466.1500, found 466.1456.

^{1}H-NMR (400 MHz, $CDCl_3$) δ = 7.40 (t, J = 7.7 Hz, 1H), 7.34 (d, J = 7.7 Hz, 1H), 6.98 (d, J = 8.0 Hz, 1H), 3.83 (s, 3H), 1.52 – 1.44 (m, 2H), 1.33 (tq, J = 7.3, 7.2 Hz, 2H), 1.14 – 1.08 (m, 2H), 0.89 (t, J = 7.3 Hz, 3H) ppm.

^{13}C-NMR (101 MHz, $CDCl_3$) δ = 164.2 (C(5)), 137.7 (q, J = 30.2 Hz, C(1)), 130.4 (q, J = 3.9 Hz, C(6)), 129.6 (C(3), 124.4 (q, J = 273.4 Hz, C(8), 118.3 (q, J = 5.4 Hz, C(2)), 111.9 (q, J = 1.3 Hz, C(4)), 55.5 (C(7)), 28.9 (C(10)), 27.3 (C(11)), 13.7 (C(12)), 11.9 (q, J = 2.1 Hz, C(9)) ppm.

IR (ATR): $\tilde{\upsilon}$/cm^{-1} = 2955 (w), 2921 (w), 2871 (w), 2853 (w), 1462 (m), 1444 (w), 1425 (m), 1376 (w), 1317 (vs), 1289 (w), 1244 (s), 1188 (m), 1163 (s), 1096 (s), 1071 (w), 1041 (vs), 960 (w), 857 (w), 790 (s), 748 (m), 720 (m), 675 (m).

R_f (SiO_2, *i*hexane:EtOAc = 99:1) = 0.86.

2-((2-Methoxy-4,6-dimethylphenyl)(2-methoxy-6-(trifluoromethyl)phenyl)methylene)benzo[*b*]thiophen-3(2*H*)-one (1)

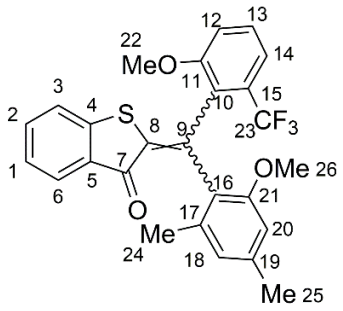

HTI-chloride **4** (750 mg, 2.27 mmol, 1.00 equiv.), tributyl stannane **5** (1.06 g, 2.27 mmol, 1.00 equiv.), potassium fluoride (264 mg, 4.54 mmol, 2.00 equiv.), and copper(I) iodide (43.8 mg, 0.23 mmol, 0.10 equiv.) were added to dioxane (10 mL) and N_2 was bubbled through the suspension for 15 min under continuous stirring. Under N_2 atmosphere $Pd(PPh_3)_4$ (127 mg, 0.11 mmol, 0.05 equiv.) was added and the reaction mixture was heated to 100 °C. After stirring the reaction mixture at that temperature for 12 h N_2 was bubbled through the solution again for 5 min. Subsequently tributyl stannane **5** (528 mg, 1.14 mmol, 0.50 equiv.) and $Pd(PPh_3)_4$ (127 mg, 0.11 mmol, 0.05 equiv.) were added again and the resulting mixture was further stirred for 2 d at 100 °C. The reaction was terminated by addition of a sat. aq. $NaHCO_3$ solution (30 mL), the aqueous phase was extracted with CH_2Cl_2 (3 x 50 mL) and the combined organic phases were dried over Na_2SO_4. After removing the solvent *in vacuo* the crude product was purified via FCC (SiO_2, *i*Hex:EtOAc = 95:5 → 9:1) yielding three fractions containing different diastereoisomers of the title compound: fraction 1 with **1-B** (120 mg, 0.26 mmol, 11%), fraction 2 containing both *E* isomers (**1-C**, **1-D**, 223 mg, 0.48 mmol, 21%) and fraction 3 containing **1-A** (74.4 mg, 0.16 mmol, 7%).; overall yield of **1** = 39%. All isomers were obtained as yellow to orange crystals after crystallization from *n*heptane/CH_2Cl_2.

A-1

^{1}H-NMR (800 MHz, $CDCl_3$) δ = 7.80 (dd, *J* = 7.8, 1.4 Hz, 1H, H-C(6)), 7.50 (ddd, *J* = 8.3, 7.2, 1.3 Hz, 1H, H-C(2)), 7.46 (t, *J* = 8.2 Hz, 1H, H-C(13)), 7.32 (d, *J* = 7.9 Hz, 1H, H-C(3)), 7.27 (dd, *J* = 8.0, 1.1 Hz, 1H, H-C(14)), 7.22 (t, *J* = 7.9 Hz, 1H, H-C(1)), 7.18 (d, *J* = 8.4 Hz, 1H, H-C(12)), 6.75 (s, 1H, H-C(18)), 6.45 (s, 1H, H-C(20)), 3.86 (s, 3H, H-C(22)), 3.38 (s, 3H, H-C(26)), 2.31 (s, 6H, H-C(24), H-C(25)) ppm.

^{13}C-NMR (200 MHz, $CDCl_3$) δ = 185.7 (C(7)), 158.5 (C(11)), 157.8 (C(21)), 145.2 (C(4)), 141.1 (C(19)), 139.7 (C(17)), 137.7 (C(8/9)), 134.5 (C(2)), 132.7 (C(5)), 129.4 (C(13)), 129.3 (C(10)), 128.8 (q, *J* = 30.8 Hz, (C(11))), 126.9 (C(6)), 124.7 (C(1)), 124.2 (C(18)), 123.9 (C(16)), 123.6 (q, *J* = 274.3 Hz, (C(23))), 123.2 (C(3)), 118.0 (q, *J* = 6.6 Hz, (C(14))), 114.2 (C(12)), 109.9 (C(20)), 56.5 (C(22)), 55.5 (C(26)), 21.7 (C(25)), 20.2 (q, *J* = 3.1 Hz, (C(24))) ppm.

IR (ATR): $\tilde{\nu}/cm^{-1}$ = 1669 (m), 1584 (m), 1457 (m), 1315 (vs), 1266 (s), 1171 (s), 1137 (vs), 1094 (s), 1032 (vs), 870 (m), 829 (s), 785 (m), 748 (vs), 735 (vs), 707 (m), 676 (m).

Melting point: 158 – 162 °C.

R_f (SiO_2, *i*Hex/EtOAc = 9/1) = 0.10.

B-1

^{1}H-NMR (600 MHz, $CDCl_3$) δ = 7.76 (d, *J* = 8.3 Hz, 1H, H-C(6)), 7.48 (td, *J* = 7.7, 1.3 Hz, 2H, H-C(2)), 7.43 (t, *J* = 8.1 Hz, 1H, H-C(13)), 7.31 (d, *J* = 4.5 Hz, 1H, H-C(3)), 7.30 (d, *J* = 4.5 Hz, 1H, H-C(14)), 7.20 (t, *J* = 7.5 Hz, 1H, H-C(1)), 7.03 (d, *J* = 8.3 Hz, 1H, H-C(12)), 6.68 (s, 1H, H-C(18)), 6.50 (s, 2H, H-C(20)), 3.67 (s, 3H, H-C(22)), 3.56 (s, 5H, H-C(26)), 2.30 (s, 3H, H-C(25)), 2.29 (s, 3H, H-C(24)) ppm.

^{13}C-NMR (150 MHz, $CDCl_3$) δ = 186.0 (C(7)), 157.6 (C(11)), 157.5 (C(21)), 145.2 (C(4)), 140.6 (C(17)), 140.3 (C(8/9)), 139.5 (C(19)), 136.9 (C(8/9)), 134.8 (C(2)), 132.8 (C(5)), 131.6 (q, *J* = 30.8 Hz, (C(15))), 129.8 (C(13)), 128.3 (C(10)), 127.0 (C(6)), 125.0 (C(1)), 124.4 (q, *J* = 274.5 Hz, (C(23))), 123.8 (C(3)), 123.5 (C(18)), 122.8 (C(16)), 119.9 (C(14)), 114.5 (C(12)), 109.7 (C(20)), 56.2 (C(22)), 55.1 (C(26)), 21.8 (C(25)), 20.0 (C(24)) ppm.

C/D-1

^{1}H-NMR (800 MHz, $CDCl_3$) δ = 7.74 – 7.72 (m, 2H, H-C(6_C), H-C(6_D)), 7.50 – 7.47 (m, 2H, H-C(2_C), H-C(2_D)), 7.39 (t, *J* = 8.2 Hz, 1H, H-C(13_C)), 7.37 (t, *J* = 8.2 Hz, 1H, H-C(13_D)), 7.35 – 7.31 (m, 2H, H-C(3_C), H-C(3_D)), 7.29 (dd, *J* = 8.1, 1.1 Hz, 1H, H-C(14_C)), 7.27 – 7.26 (m, 1H, H-C(14_D)), 7.21 – 7.17 (m, 2H, H-C(1_C), H-C(1_D)), 7.07 (d, *J* = 7.7 Hz, 1H, H-C(12_D)), 6.99 (d, *J* = 8.2 Hz, 1H, H-C(12_C)), 6.75 (s, 1H, H-C(18_D)), 6.72 (s, 1H, H-C(18_C)), 6.50 (s, 1H, H-C(20_C)), 6.44 (s, 1H, H-C(20_D)), 3.72 (s, 3H, H-C(22_D)), 3.61 (s, 3H, H-C(22_C)), 3.57 (s, 3H, H-C(26_C)), 3.36 (s, 3H, H-C(26_D)), 2.45 (s, 3H, H-C(24_C)), 2.43 (s, 3H, H-C(24_D)), 2.32 (s, 3H, H-C(25_C)), 2.30 (s, 3H, H-C(25_D)) ppm.

^{13}C-NMR (200 MHz, $CDCl_3$) δ = 186.7 (C(7_C)), 186.5 (C(7_D)), 158.5 (C(11_D)), 158.1 (C(21_D)), 157.6 (C(21_C)), 157.1 (C(11_C)), 145.9 (C(6_D)), 145.8 (C(4_C)), 140.0 (C(19_D)), 139.8 (C(19_C)), 139.6 (C($8/9_C$)), 139.4 (C(17_C)), 139.2 (C(17_D)), 137.3 (C($8/9_D$)), 136.6 (C($8/9_C$)), 136.4 (C($8/9_D$)), 134.8 (C(2_C)), 134.7 (C(2_D)), 132.3 (C(5_C)), 132.1 (C(5_D)), 131.5 (q, *J* = 31.0 Hz, (C(15_D))), 128.8 (C(13_C)), 128.7 – 128.4 (m, (C(10_D), (C(13_D), (C(15_D))), 126.9 (C(6_C)), 126.8 (C(16_D)), 126.7 (C(6_D)), 126.3 (C(10_C)), 125.1 (C(16_C)), 124.8 (C(1_C)), 124.8 (C(1_D)), 124.8 (C(18_D)), 124.0 (C(18_C)), 123.4 (C(3_C)), 123.3 (C(3_D)), 119.8 (C(14_C)),

118.3 ($C(14_D)$), 114.0 ($C(12_C)$), 113.5 ($C(12_D)$), 110.2 ($C(20_D)$), 109.6 ($C(20_C)$), 56.4 ($C(22_D)$), 55.8 ($C(22_C)$), 55.7 ($C(26_D)$), 55.0 ($C(26_C)$), 21.7 ($C(25_C)$), 21.6 ($C(25_D)$), 21.1 ($C(24_D)$), 20.5 ($C(24_D)$).

For all isomers:

HRMS (EI^+), [M^+]: *m/z* calcd: 470.1158 for $[C_{21}H_{22}O_4S]^+$, found: 470.1158.

Determination of constitution and conformation in the crystalline state and in solution

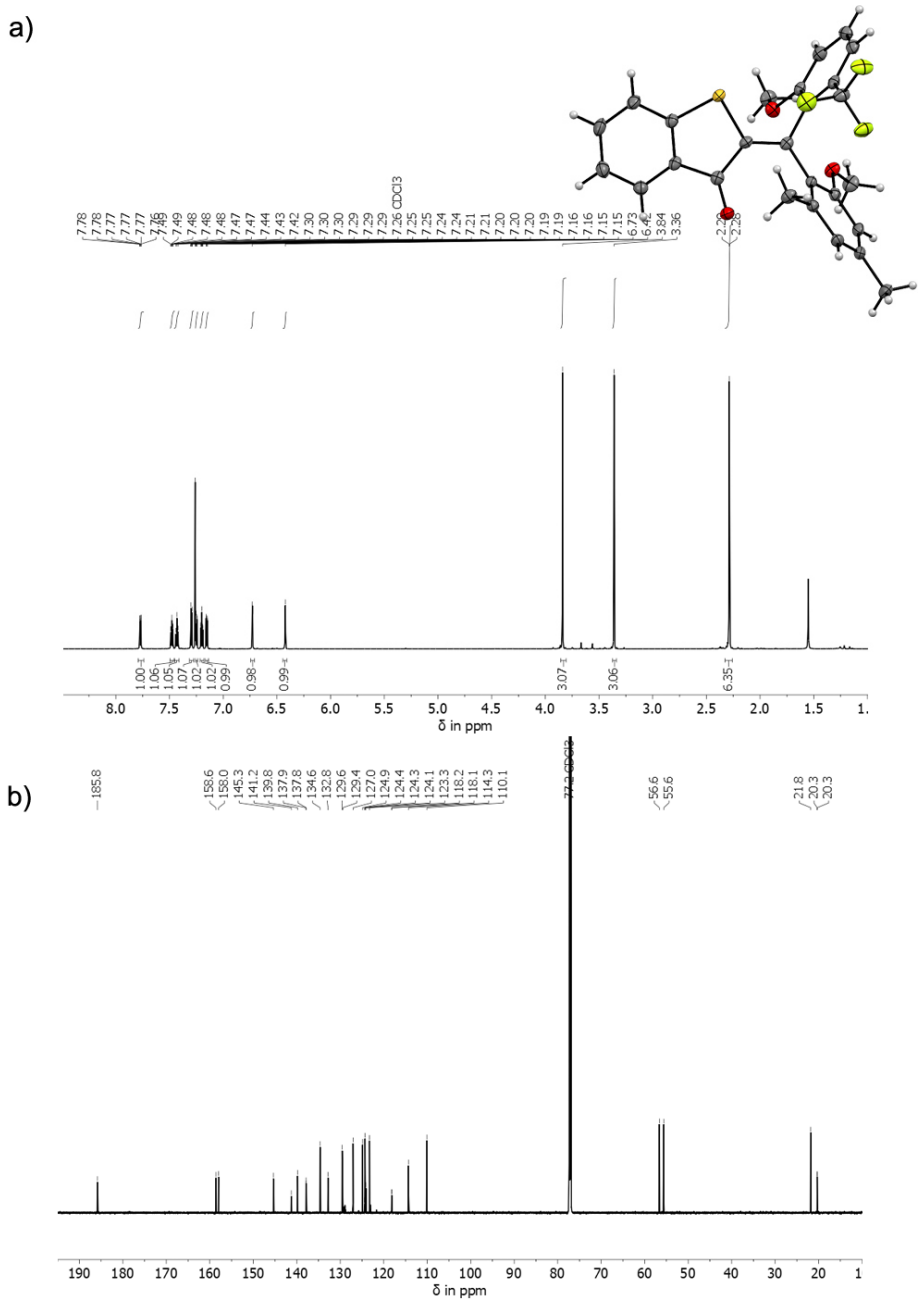

Supplementary Figure 1. a) Structure of **A-1** in the crystalline state and the corresponding ^{1}H NMR spectrum ($CDCl_3$, 800 MHz, 27 °C) of the same crystal batch. The signals of only one single species are observed in the ^{1}H NMR spectrum, which could thus be directly assigned to **A-1**. b) Corresponding ^{13}C NMR spectrum ($CDCl_3$, 200 MHz, 27 °C).

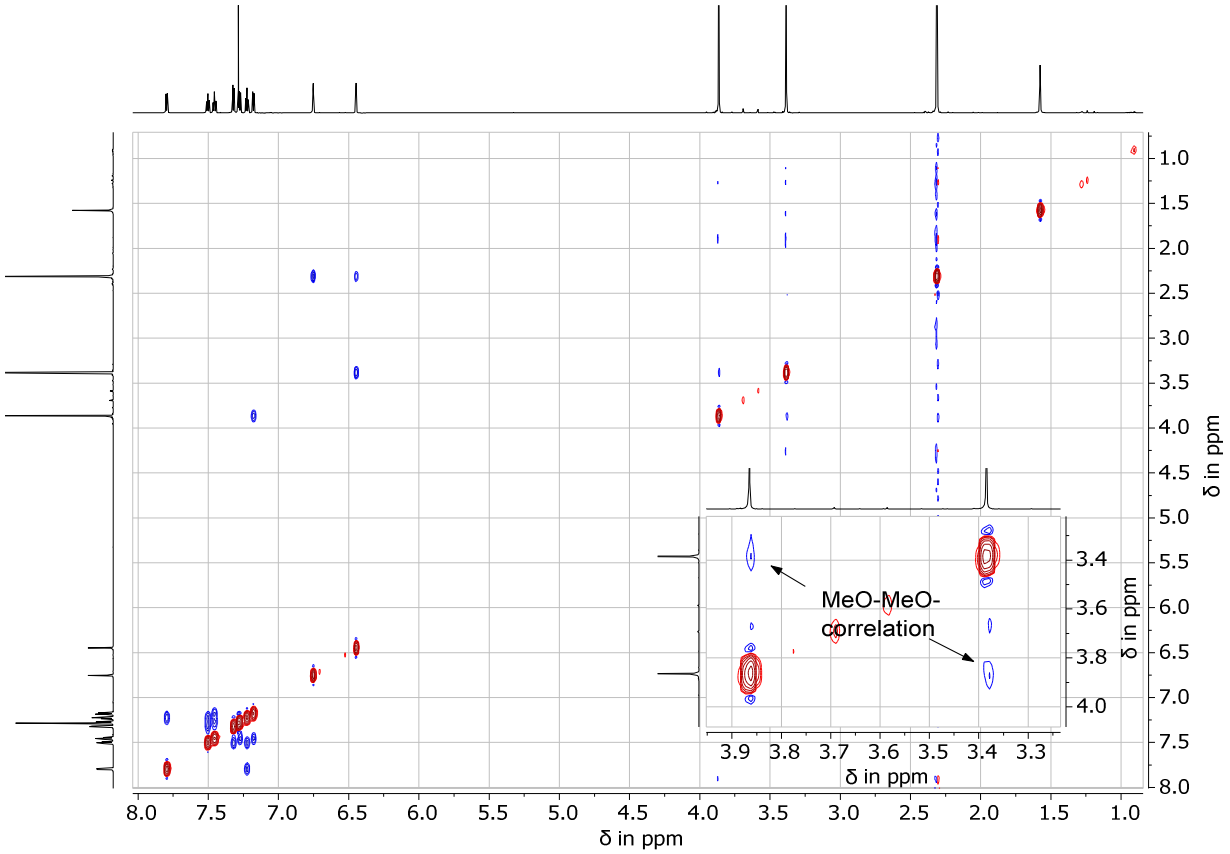

Supplementary Figure 2. NOESY NMR spectrum ($CDCl_3$, 800 MHz, 27 °C) of **A-1**. The inset shows the methoxy part of the spectrum enlarged. A correlation between both methoxy groups can be observed. This is indicative for the **A-1** structure with *syn*-relation of the methoxy groups and is also in agreement with the molecular structure in the crystalline state.

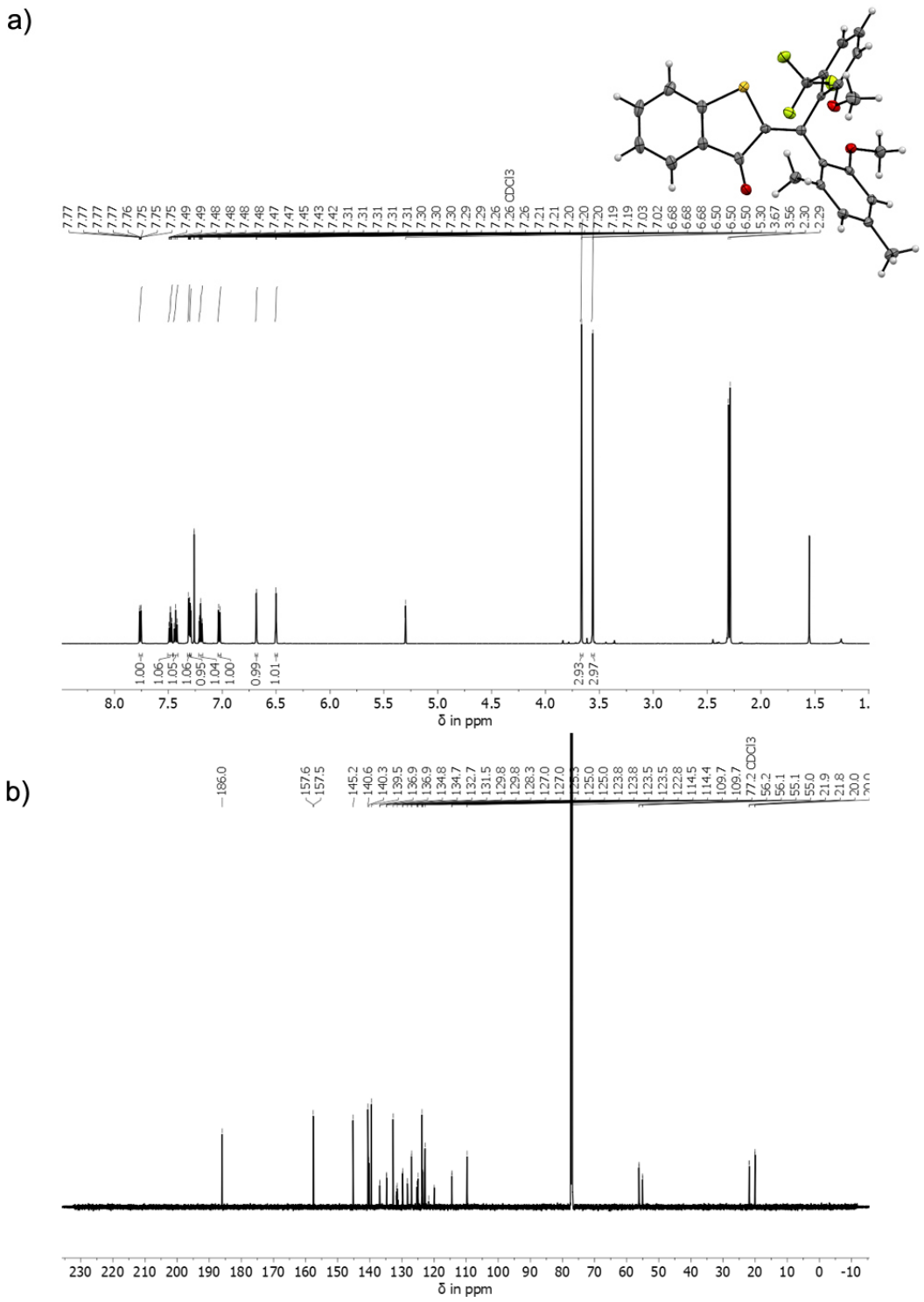

Supplementary Figure 3. a) Structure of **B-1** in the crystalline state and the corresponding ^{1}H NMR spectrum ($CDCl_3$, 600 MHz, 27 °C) of the same crystal batch. The signals of only one single species are observed in the ^{1}H NMR spectrum, which could thus be directly assigned to **B-1**. b) Corresponding ^{13}C NMR spectrum ($CDCl_3$, 150 MHz, 27 °C).

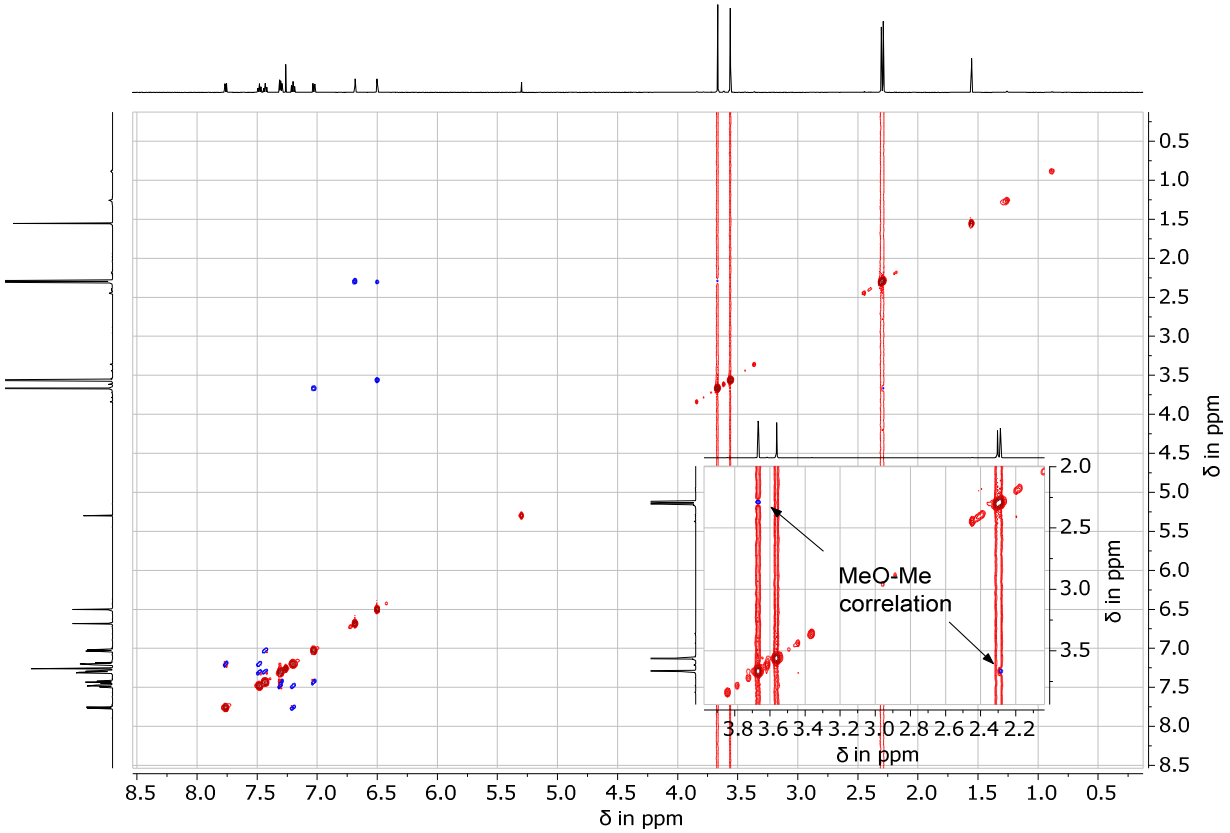

Supplementary Figure 4. NOESY NMR spectrum ($CDCl_3$, 600 MHz, 27 °C) of **B-1**. The aliphatic part of the spectrum is enlarged. A small correlation between a methoxy and a methyl group can be observed. This is indicative for the **B-1** structure with *anti*-relation of the methoxy groups and is also in agreement with the molecular structure in the crystalline state.

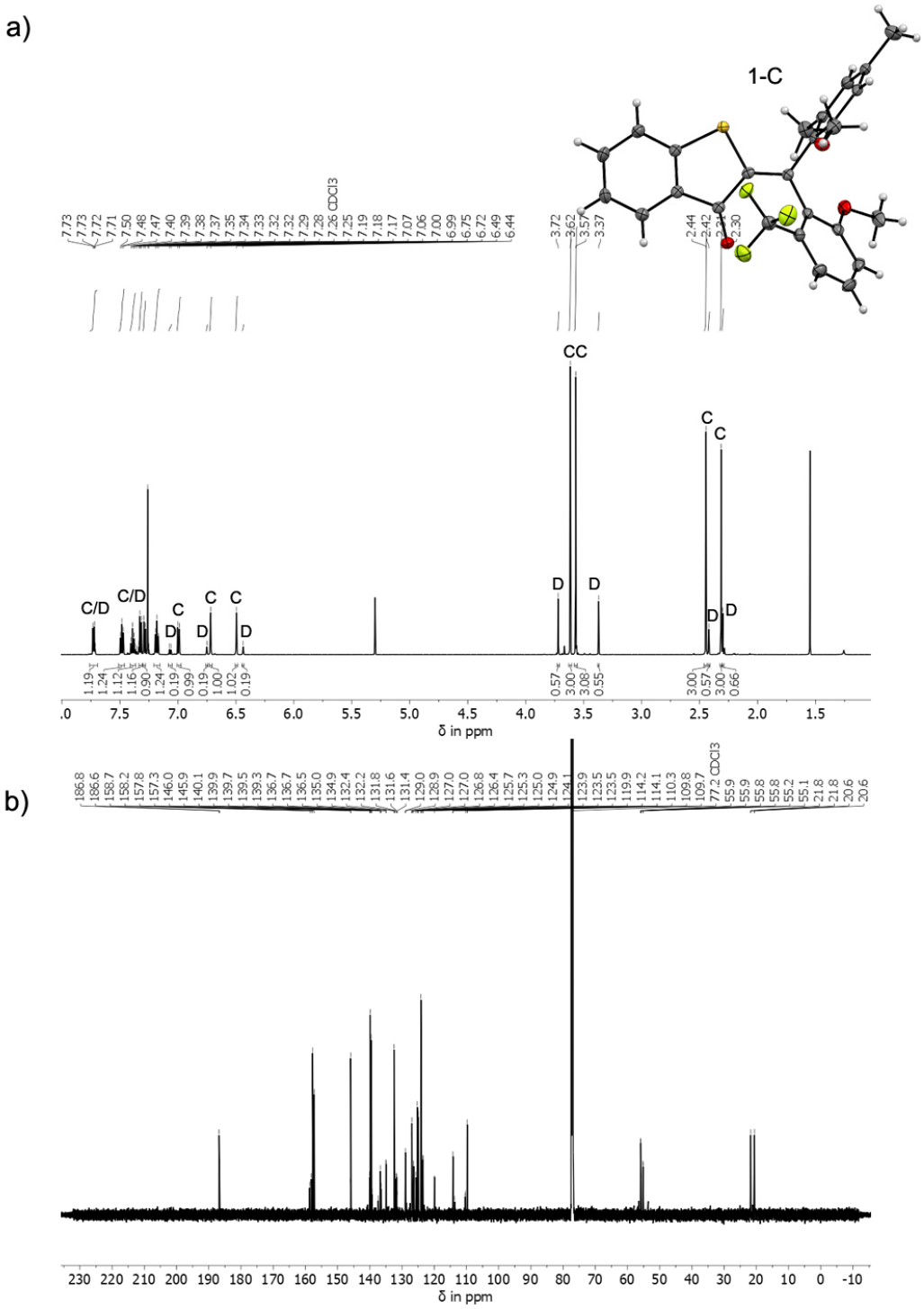

Supplementary Figure 5. a) Structure of **C-1** in the crystalline state and the corresponding ^{1}H NMR spectrum ($CDCl_3$, 600 MHz, 27 °C) of the same crystal batch. **C-1** is not stable at ambient temperatures and atropisomerizes to **D-1**. Therefore, a mixture of both isomers is present. The signals are thus labeled with the corresponding isomer designation. The assignment of signals to a specific isomer is based on the NOESY NMR spectrum as shown below. b) Corresponding ^{13}C NMR spectrum ($CDCl_3$, 150 MHz, 27 °C).

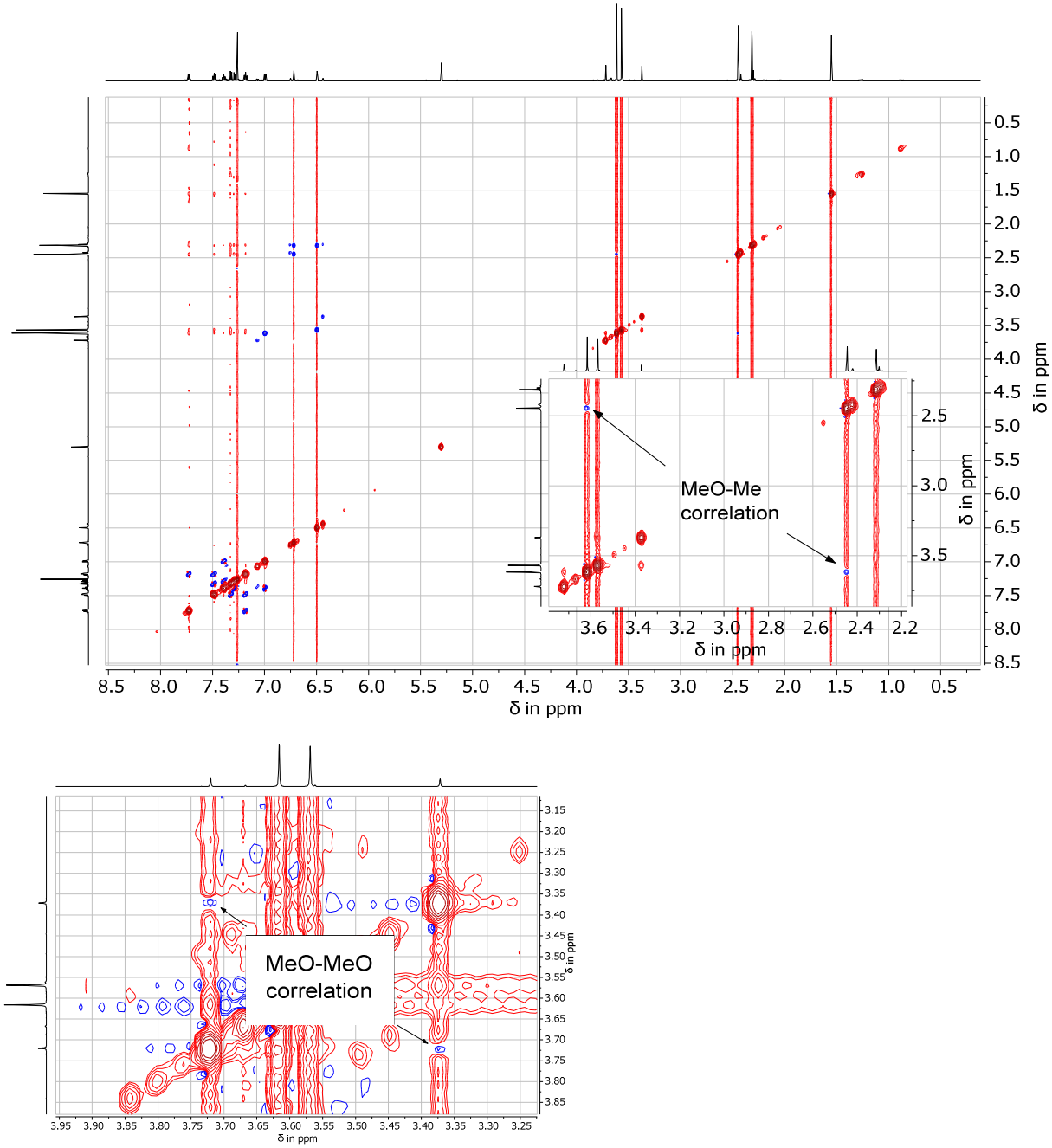

Supplementary Figure 6. NOESY NMR spectrum ($CDCl_3$, 600 MHz, 27 °C) of an isomeric mixture of **C-1** and **D-1** in thermal equilibrium. The aliphatic part of the spectrum is enlarged. A correlation between a methoxy and methyl group can be observed for the more intense set of signals. This correlation is indicative for *anti*-relation of the methoxy groups and therefore the respective set of most intense signals is assigned to the **C-1** isomer. A very small correlation between both methoxy groups is observed for the set of signals with lower intensity. This is indicative for a *syn*-relation of the methoxy groups and therefore the set of less intense signals is assigned to the **D-1** isomer. The NMR-spectra show that **C-1** is thermally more stable than **D-1**. This finding is in agreement with the theoretical description.

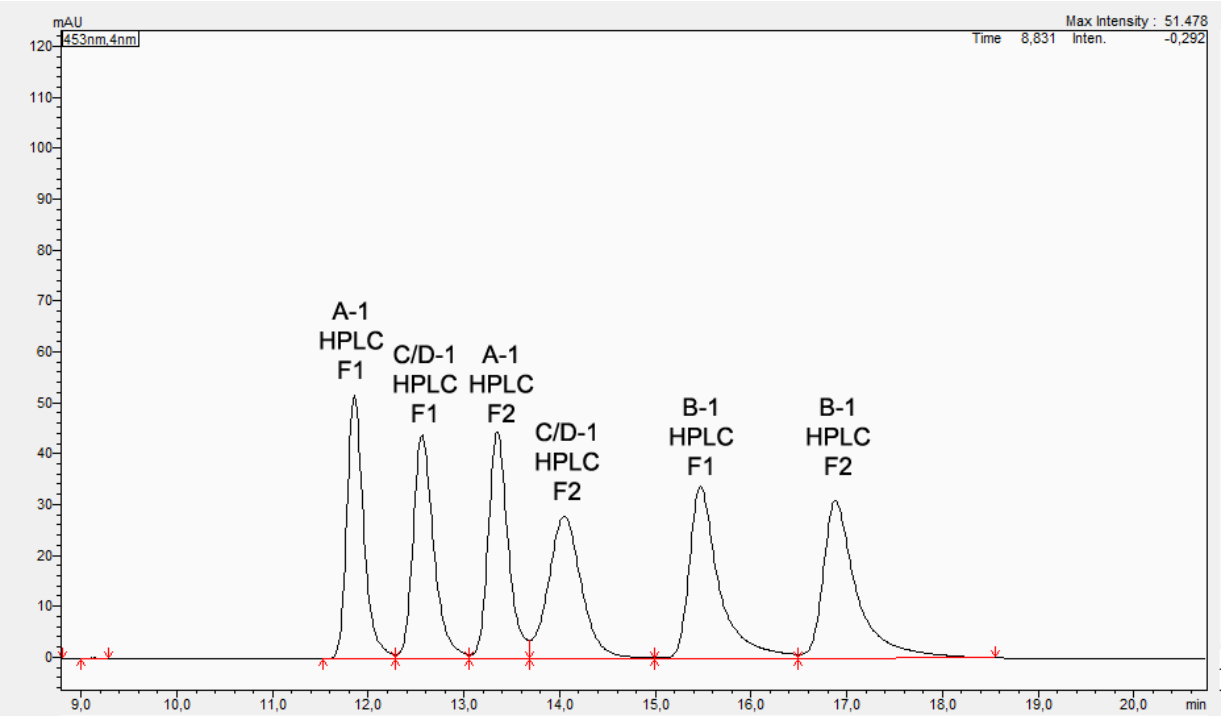

Supplementary Figure 7. HPLC chromatogram trace of all isomers of **1** at 453 nm. Separation was performed on a DAICEL CHIRALPAK ID column (20 mm Ø x 20 mmL) with an eluent of 11% EtoAc in *n*-heptane at 60 °C and a flow of 3 mL. All isomers are separated except **C** and **D**, which are in rapid equilibrium with each other at 22 °C or more elevated temperatures. However, two different fractions for the **C** and **D** isomers are separated in the HPLC run, which evidences that only one single bond (connecting to the dimethyl-methoxy-substituted aryl residue) is rotating in the thermal equilibrium converting either **C** in **D** or **C'** in **D'**. The other single bond (connecting to the trifluoromethyl-methoxy-substituted aryl residue) does not rotate, which would otherwise result in a conversion of all four isomers **C**, **C'**, **D**, and **D'** into each other (e.g. **C** in **C'**, **D** and, **D'**). Therefore, the mixture of **C**/**D** isomers after HPLC separation is expected to give an ECD signal and assignment to an absolute configuration should thus be possible.

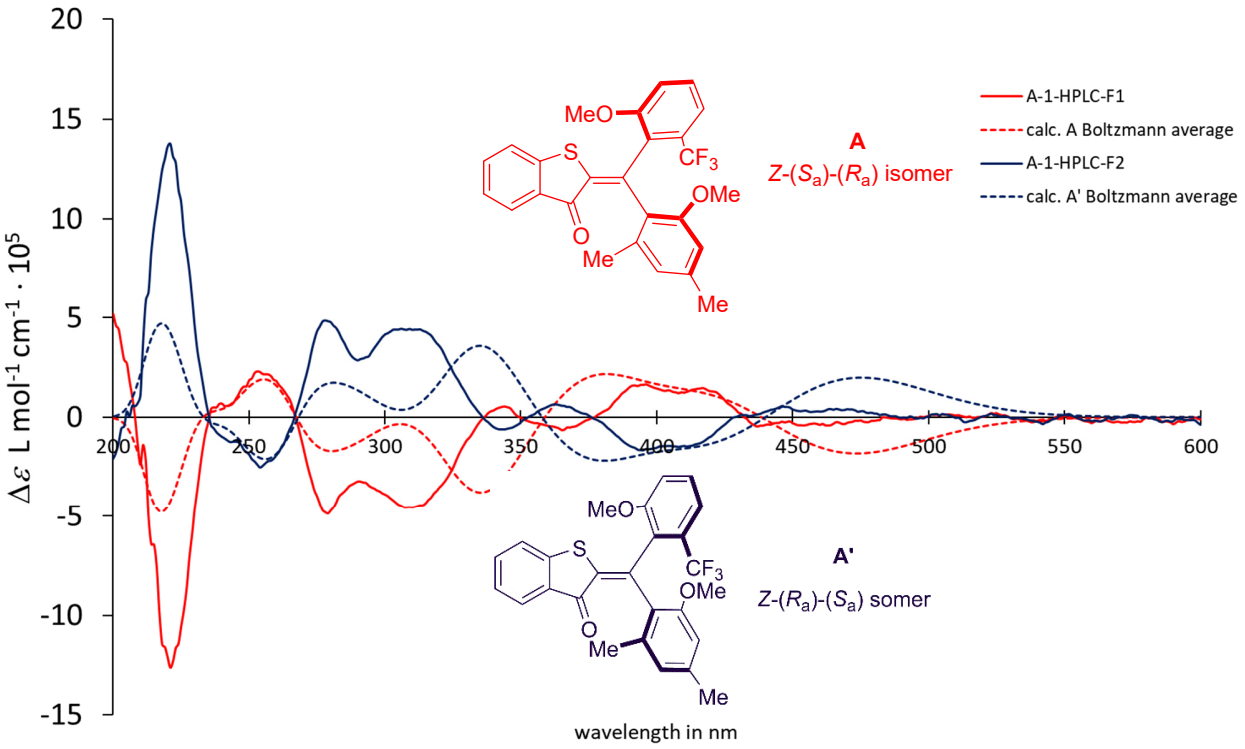

Supplementary Figure 8. Experimental and calculated (see chapter "Calculated Ground State Energy Profile of Compound **1**" for details of the calculations) ECD spectra of both enantiomers of **A-1** in MeCN at 20 °C. The fraction termed "A-HPLC-F1" was assigned to the **A-1** isomer and "A-1-HPLC-F2" was assigned to the **A'-1** isomer.

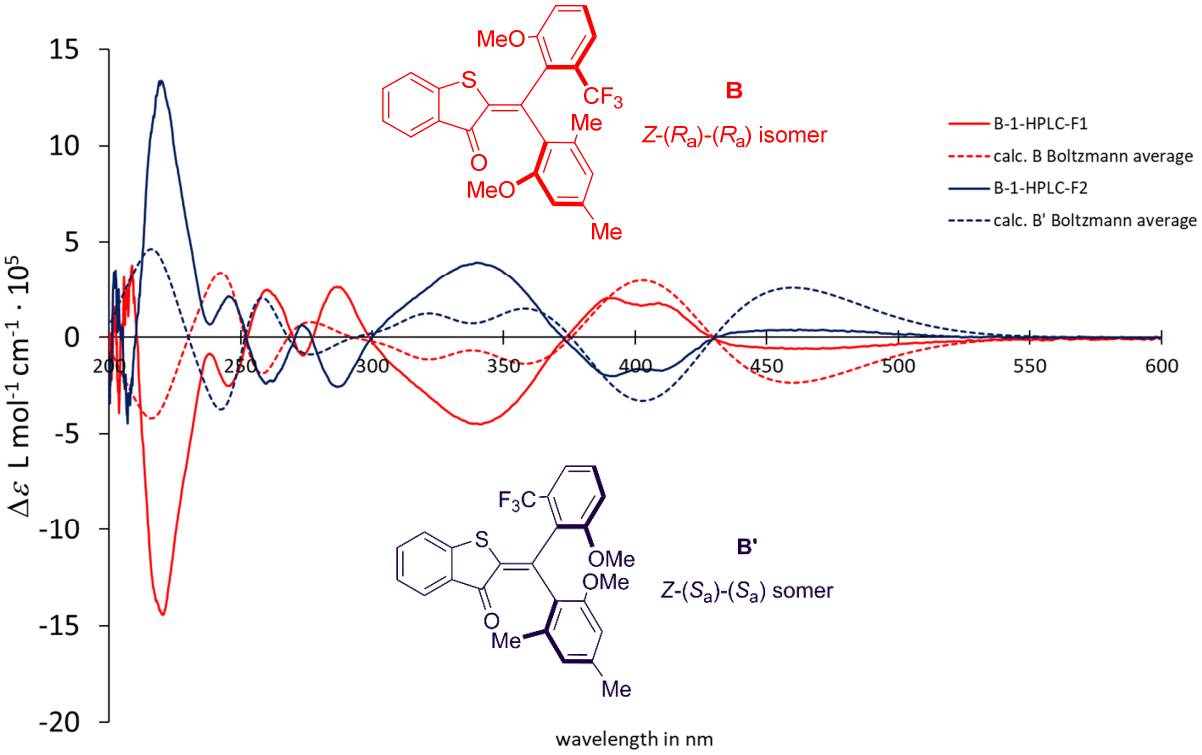

Supplementary Figure 9. Experimental and calculated (see chapter "Calculated Ground State Energy Profile of Compound **1**" for details of the calculations) ECD spectra of both enantiomers of **B-1** in MeCN at 20 °C. The fraction termed "B-HPLC-F1" was assigned to the **B-1** isomer and "B-1-HPLC-F2" was assigned to the **B'-1** isomer.

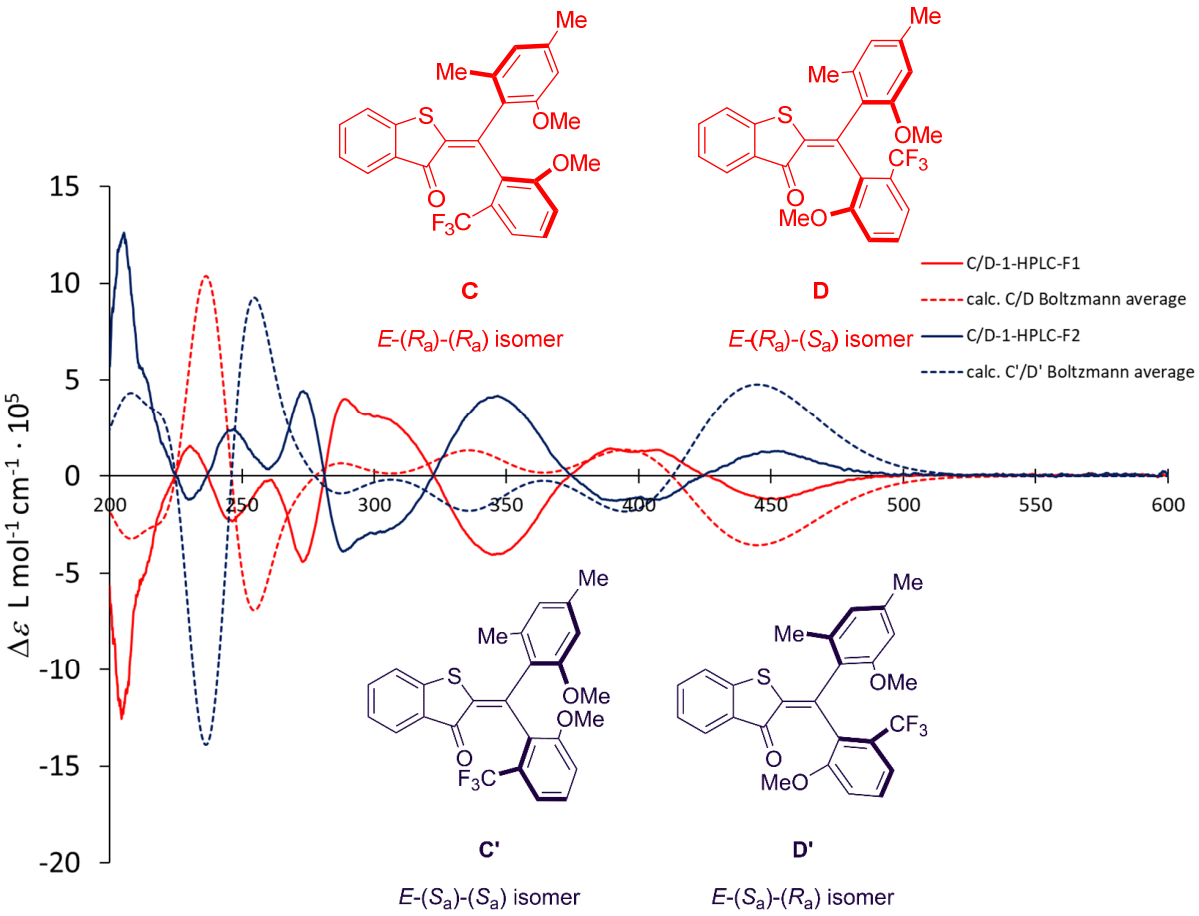

Supplementary Figure 10. Experimental and calculated (see chapter "Calculated Ground State Energy Profile of Compound **1**" for details of the calculations) ECD spectra of both enantiomers of **C**/**D-1** in Me CN at 20 °C. The fraction termed "C/D-HPLC-F1" was assigned to the **C**/**D -1** isomers and "C/D -1-HPLC-F2" was assigned to the **C**/**D'-1** isomer.

Physical and photophysical properties

Thermal atropisomerizations *rac*-A to *rac*-B and *rac*-D to *rac*-C

An amberized NMR tube was charged with 0.5 mg of isomer *rac*-**A** in 0.7 mL of deuterated solvent. Subsequent heating at 62 °C was carried out in an oil bath and kinetics were followed by ^{1}H NMR measurements at defined time intervals. The equilibrium concentrations of isomers after prolonged heating were obtained from integration of the corresponding signals in the ^{1}H NMR spectrum.

The kinetics of thermal atropisomerization of *rac*-**D** to *rac*-**C** were measured starting from an irradiated sample of 0.5 mg *rac*-**B** with 450 nm at -30 °C. An Isomer composition of *rac*-**A**:*rac*-**B**:*rac*-**C**:*rac*-**D** of 16:67:5:12 was achieved after 1 h of irradiation in the NMR-instrument. The irradiation was stopped and after heating to -20 °C the thermal kinetics from *rac*-**D** to *rac*-**C** isomerization were measured over a time of 100 min.

The thermal atropisomerizations are unimolecular first order reactions and proceed towards an equilibrium composition with both atropisomers present according to eq. 1 and eq. 2, respectively.

$$\ln\left(\frac{[\mathbf{A}]_{t_0}-[\mathbf{A}]_{eq}}{[\mathbf{A}]_t-[\mathbf{A}]_{eq}}\right) = (k_{\mathbf{A/B}} + k_{\mathbf{B/A}})t \qquad \text{(eq. 1)}$$

$$\ln\left(\frac{[\mathbf{D}]_{t_0}-[\mathbf{D}]_{eq}}{[\mathbf{D}]_t-[\mathbf{D}]_{eq}}\right) = (k_{\mathbf{D/C}} + k_{\mathbf{C/D}})t \qquad \text{(eq. 2)}$$

with [**A**, **D**]$_{t_0}$ being the initial concentration of the isomers **A** or **D** at the time t = 0, [**A**, **D**]$_{eq}$ being the concentration of the isomers **A** or **D** at equilibrium, [**A** or **D**]$_t$ representing the concentration of the isomers **A** or **D** at specific times in the measurement t, $k_{\mathbf{A/B}}$ being the rate constant k of the **A** to **B** conversion, $k_{\mathbf{B/A}}$ being the rate constant k of the **B** to **A** conversion, $k_{\mathbf{C/D}}$ being the rate constant k of the **C** to **D** conversion, $k_{\mathbf{D/C}}$ being the rate constant k of the **D** to **C** conversion and t being the elapsed time. When plotting the logarithmic left part of eq. 1 or eq. 2 versus time t the obtained slope m contains rate constants for the isomerization reactions taking place. The rate constants $k_{\mathbf{A/B}}$ and $k_{\mathbf{D/C}}$ can then be calculated according to eq. 3 and eq. 4:

$$k_{\mathbf{A/B}} = \frac{m}{1+\frac{[\mathbf{A}]_{eq}}{[\mathbf{B}]_{eq}}} \qquad \text{(eq. 3)}$$

$$k_{\mathbf{D/C}} = \frac{m}{1+\frac{[\mathbf{D}]_{eq}}{[\mathbf{C}]_{eq}}} \qquad \text{(eq. 4)}$$

when taking into account the corresponding laws of mass action (eq. 5 and eq. 6):

$$\frac{[\mathbf{A}]_{eq}}{[\mathbf{B}]_{eq}} = \frac{k_{\mathbf{B/A}}}{k_{\mathbf{A/B}}} \qquad \text{(eq. 5)}$$

$$\frac{[\mathbf{D}]_{eq}}{[\mathbf{C}]_{eq}} = \frac{k_{\mathbf{C/D}}}{k_{\mathbf{D/C}}} \qquad \text{(eq. 6)}$$

By using the *Eyring* equation (eq. 7) the $\Delta G^{\ddagger}$ can be calculated from the rate constants of the corresponding reaction. The obtained Gibbs energies of activation $\Delta G^{\ddagger}$ for the thermal isomerizations between **A** to **B** and **C** to **D** and *vice versa* in MeCN-d_3 and the corresponding half-lives at 25 °C are given in Supplementary Table 1 together with the equilibrium compositions obtained at elevated temperatures.

$$\Delta G^{\ddagger} = \ln\left(\frac{k*h}{k_B*T}\right) * R * T \qquad \text{(eq. 7)}$$

From these measurements we could quantify the ground state energy profile of HTI **1**. The equilibrium compositions at high temperatures deliver the thermodynamic energy differences between the corresponding states (red Δ values in Supplementary Figure 13) according to the relation of the change of *Gibbs* free energy and the equilibrium constant $-\Delta G = R \cdot T \cdot \ln K$ (see also Supplementary Table 1). The theoretical values are in good agreement with the experimentally determined ones.

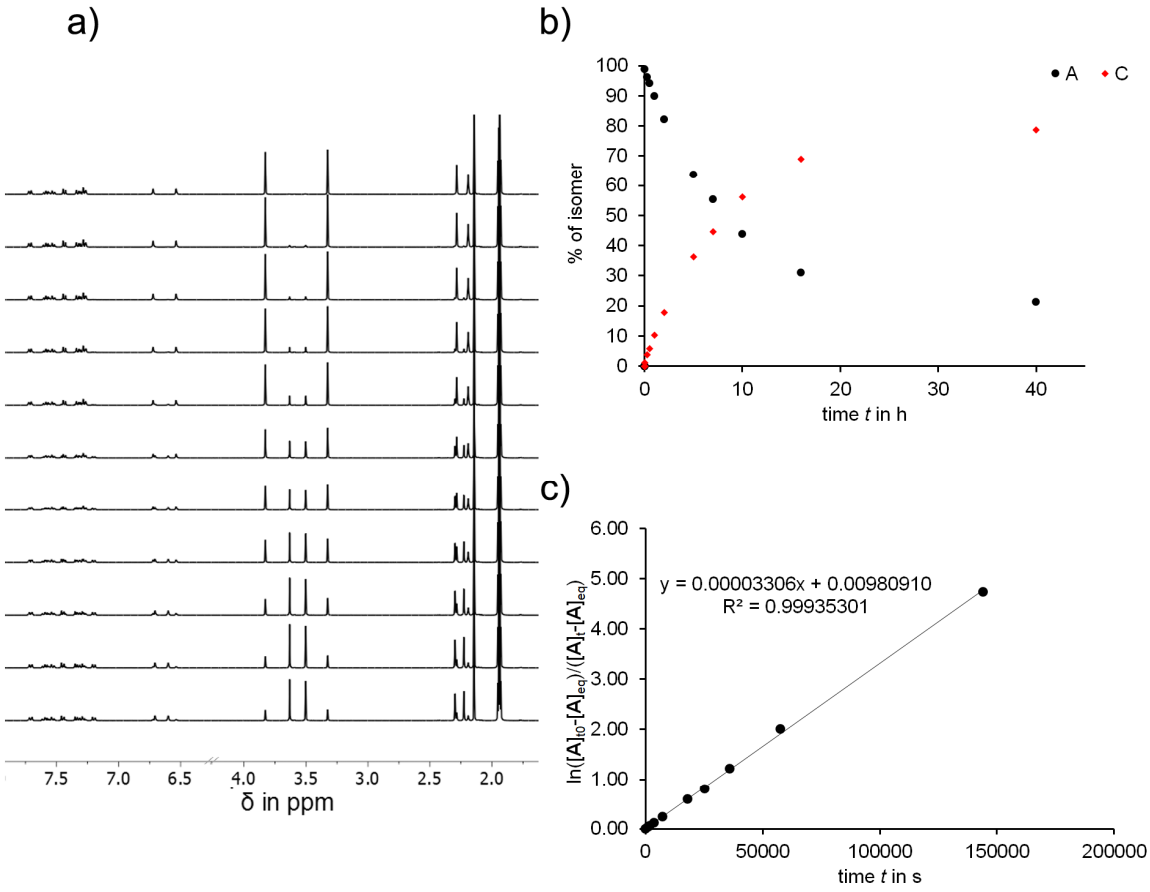

Supplementary Figure 11. a) Thermal atropisomerization of **A** to **B** in MeCN-d_3 at 62 °C followed by ^{1}H NMR spectroscopy (400 MHz, 20 °C) in regular time intervals. b) Atropisomer conversion over time. c) First order kinetic analysis of the thermal atropisomerization of **A** to **B**. Taking into account the dynamic equilibrium by plotting according to eq. 1 gives a linear relationship. The slope *m* can be translated into the rate constants $k_{(\mathbf{A/B})}$ according to eq. 3. The corresponding Gibbs energy of activation for the thermal **A** to **B** isomerization is given in Supplementary Table 1.

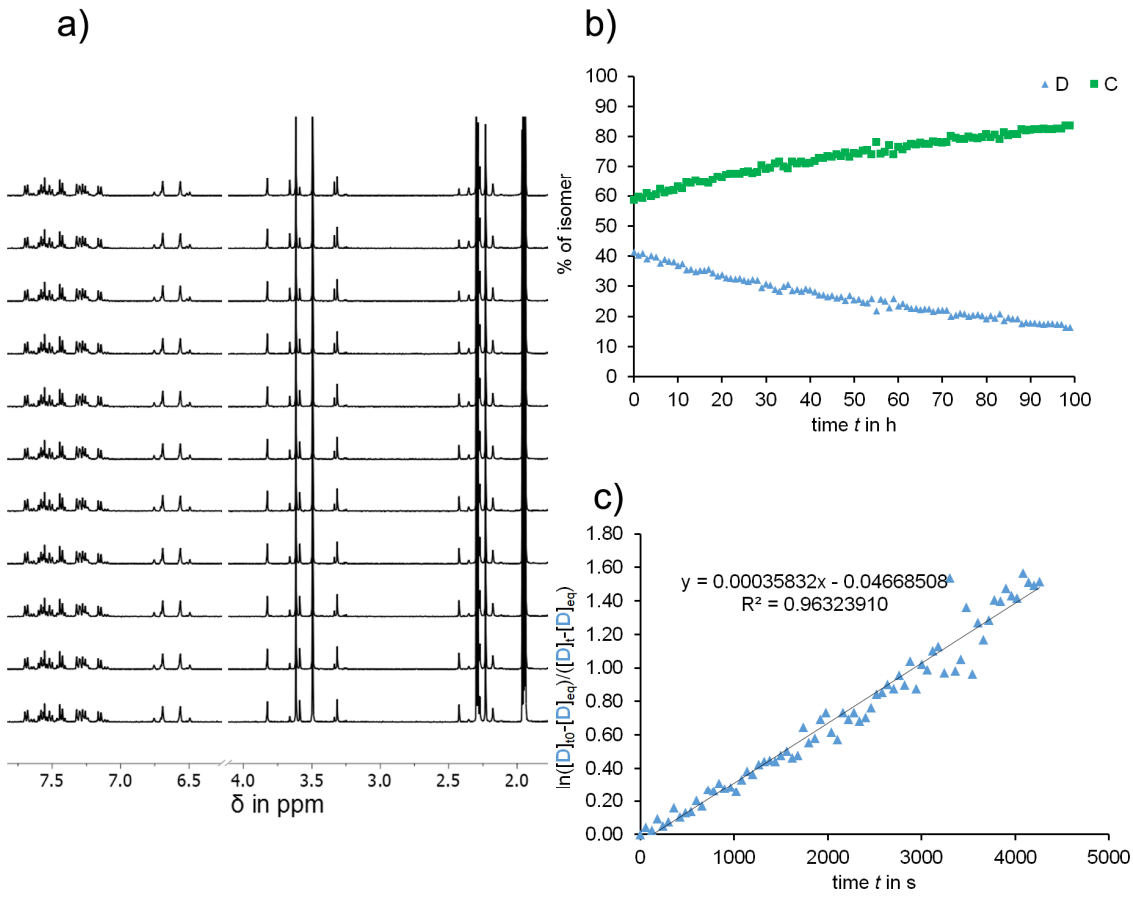

Supplementary Figure 12. a) Thermal atropisomerization of **D** to **C** in MeCN-d_3 at -20 °C followed by ^{1}H NMR spectroscopy (400 MHz, -20 °C) in regular time intervals (only every tenth spectrum is shown. b) Atropisomer conversion over time. c) First order kinetic analysis of the thermal atropisomerization of **D** to **C**. Taking into account the dynamic equilibrium by plotting according to eq. 2 gives a linear relationship. The slope m can be translated into the rate constants $k_{(\mathbf{D/C})}$ according to eq. 4. The corresponding Gibbs energy of activation for the thermal **D** to **C** isomerization are given in Supplementary Table 1.

Supplementary Table 1. Thermal isomerization behavior of HTI **1** in MeCN-d_3 at elevated temperature.

Isomer	$k_{(\text{isom. 1/isom. 2})}$ / s^{-1} (at T / °C)	$\Delta G^{\ddagger}$ (therm. isomer equilibration) /kcal mol^{-1}	Equilibration half-life of pure isomer at 25 °C	Thermodynamic isomer 1/isomer 2 equilibrium in the dark (at T / °C)	ΔG(isomer 1 / isomer 2) / kcal mol^{-1}	Slope m / s^{-1} (at T / °C)
rac-**A**	$k_{(\mathbf{A/B})} = 2.513\text{x}10^{-5}$ (62 °C)	$\Delta G^{\ddagger}$ (**A**/**B**) = 26.75	54 d	**A**/**B** = 20/80 (62 °C)	ΔG(**A**/**B**) = 0.92	$3.16\text{x}10^{-5}$ (62 °C)
rac-**D**	$k_{(\mathbf{D/C})} = 2.992\text{x}10^{-4}$ (-20 °C)	$\Delta G^{\ddagger}$ (**D**/**C**) = 18.8	6.9 s	**D**/**C** = 14/86 (20 °C)	ΔG(**D**/**C**) = 0.80	$3.58\text{x}10^{-4}$ (-20 °C)

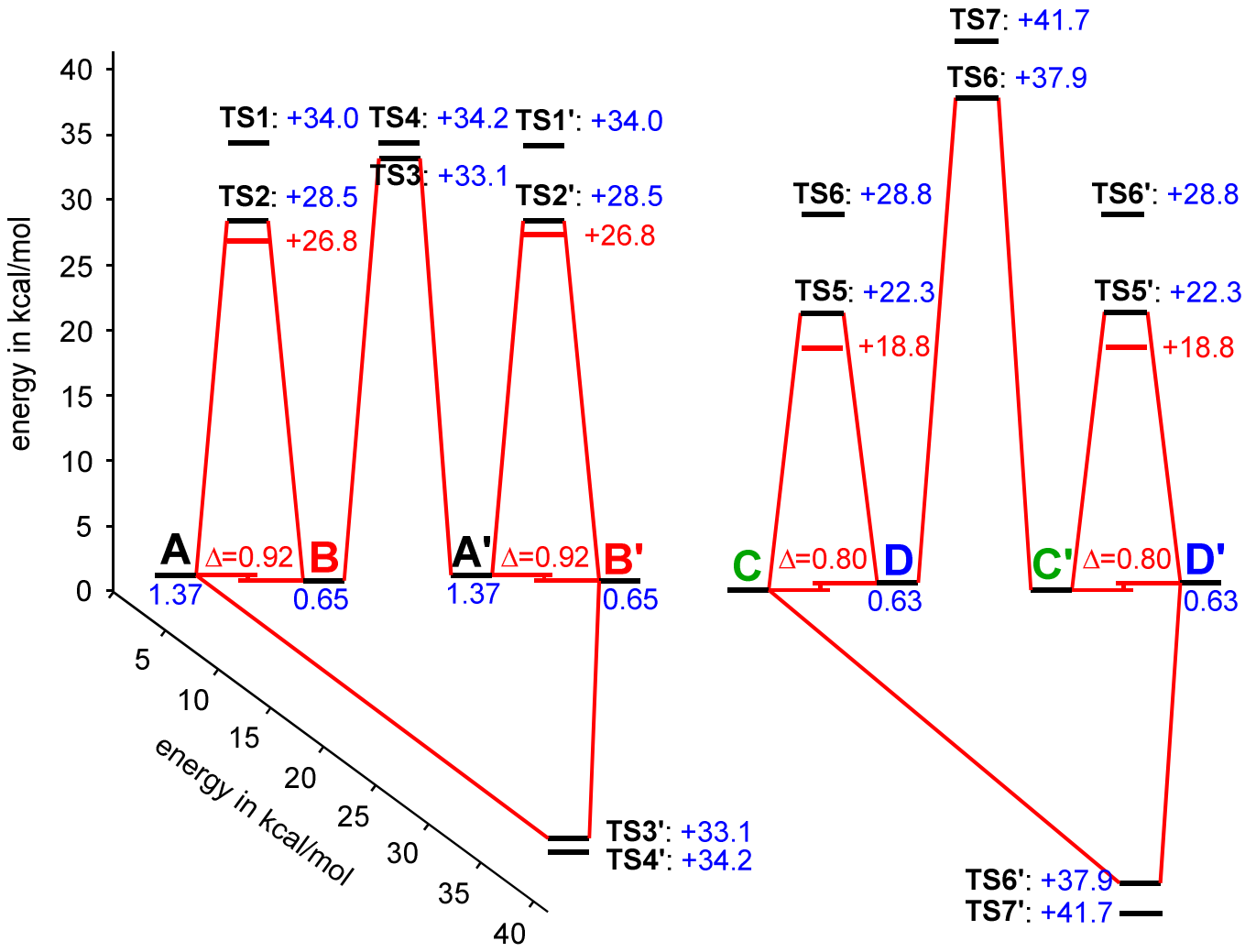

Supplementary Figure 13. Ground state energy profile for **1**. Possible thermal interconversions between the different isomers **A** to **D** by rotating one single bond are shown with red connections. Black values are derived from quantum chemical calculations (B3LYP/6-311G(d,p)), red values were determined experimentally in MeCN-d_3. The Δ values correspond to the experimentally determined ΔG values.

Molar extinction coefficients

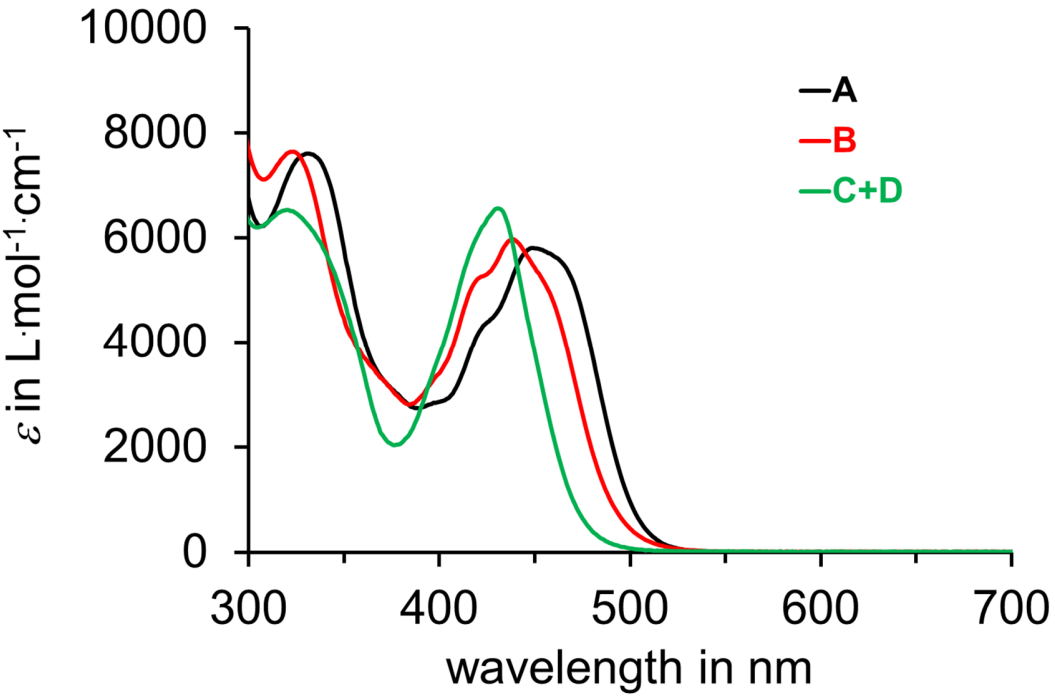

Supplementary Figure 14. Molar extinction coefficients of **A** (black), **B** (red), and **C** + **D** in thermal equilibrium (green) at 20 °C in toluene solution.

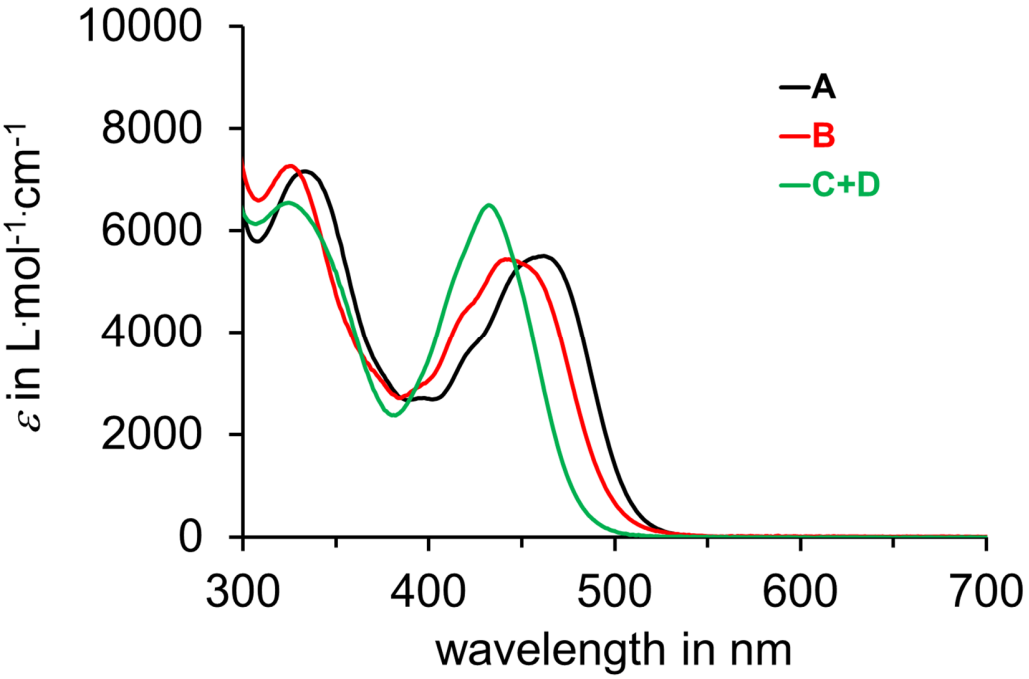

Supplementary Figure 15. Molar extinction coefficients of **A** (black), **B** (red), and **C** + **D** in thermal equilibrium (green) at 20 °C in CH_2Cl_2 solution.

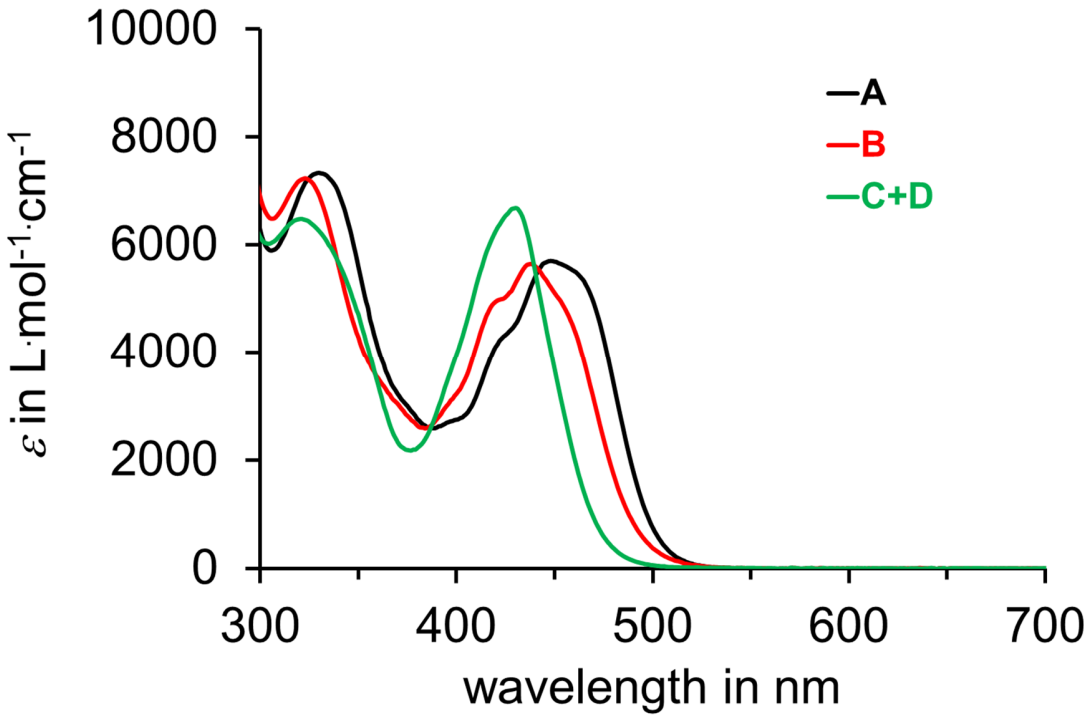

Supplementary Figure 16. Molar extinction coefficients of **A** (black), **B** (red), and **C** + **D** in thermal equilibrium (green) at 20 °C in THF solution.

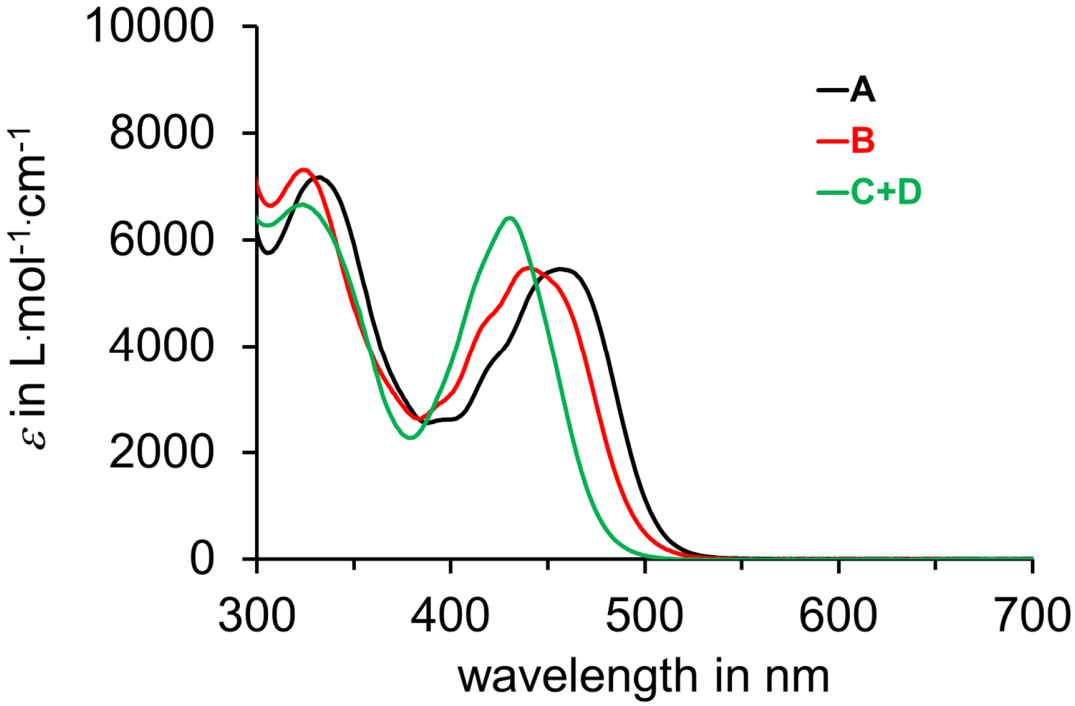

Supplementary Figure 17. Molar extinction coefficients of **A** (black), **B** (red), and **C** + **D** in thermal equilibrium (green) at 20 °C in MeCN solution.

Photoconversion of *rac*-A, *rac*-B, *rac*-C, and *rac*-D followed by NMR-spectroscopy

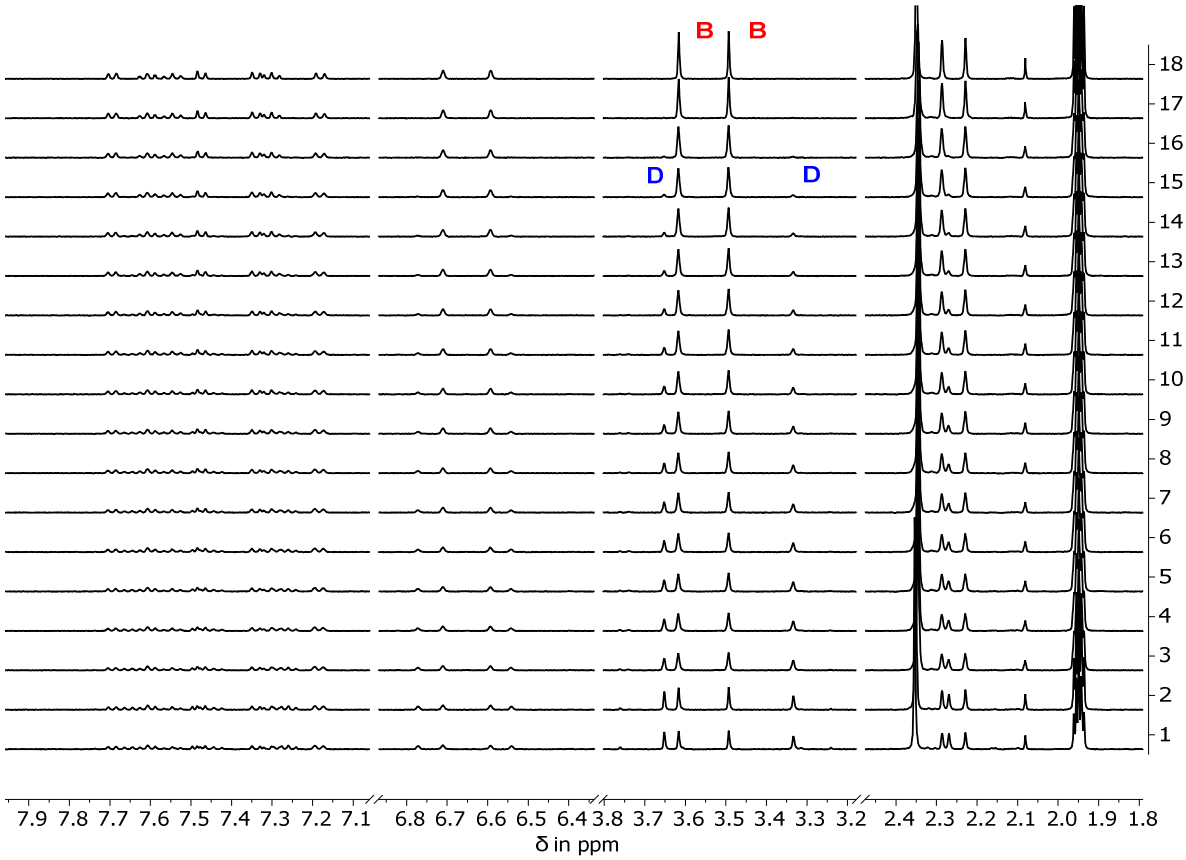

Supplementary Figure 18: Photoconversion of isomer *rac*-**B** to isomer *rac*-**D** followed by ^{1}H NMR spectroscopy in MeCN-d_3 at -40 °C under illumination with 450 nm.

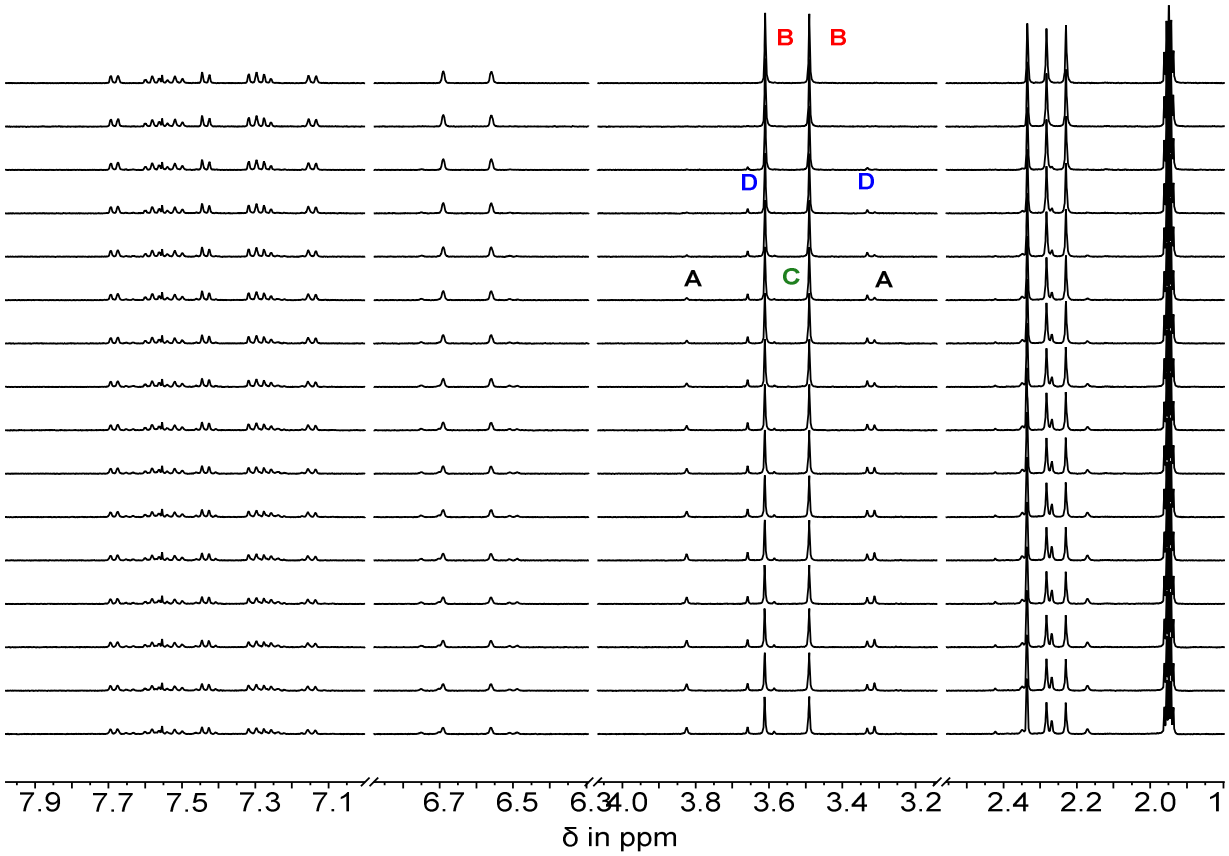

Supplementary Figure 19: Photoconversion of isomer *rac*-**B** to isomer *rac*-**D** followed by NMR spectroscopy in MeCN-d_3 at -30 °C under illumination with 450 nm. At -30 °C a thermal reaction from isomer **D** to isomer **C** can occur. The kinetic for this reaction without illumination is shown in Supplementary Figure 12. Under continued illumination isomer **C** is converted photochemically into isomer **A**.

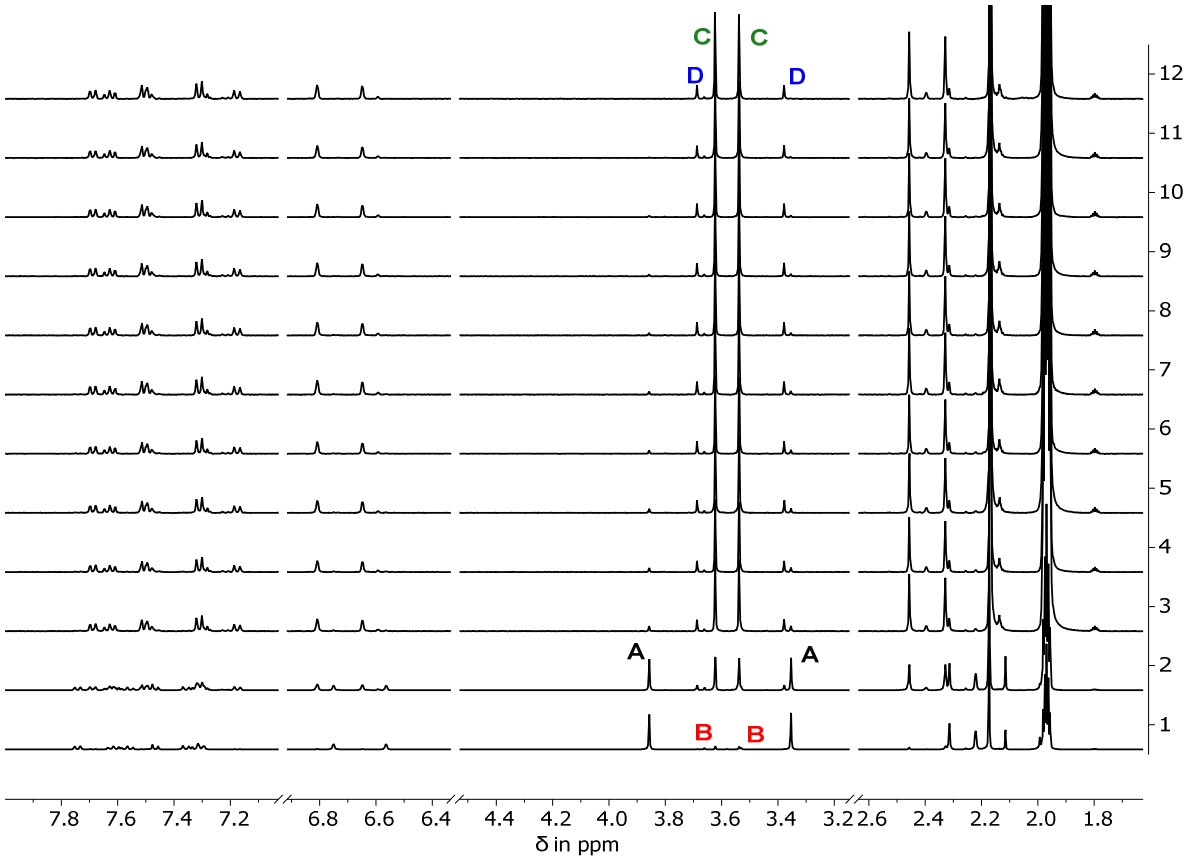

Supplementary Figure 20: Photoconversion of an isomeric mixture of *rac*-**C**/**D** to isomer *rac*-**A** followed by NMR spectroscopy in MeCN-d_3 at 20 °C under illumination with 405 nm. **A** is nearly exclusively formed, resulting in a PSS of **A**:**B**:**C**:**D** = 89:7:3:1.

Photoconversion of *rac*-B, *rac*-C, and *rac*-D determined by quantum yield measurements

The photochemical quantum yield of the different photconversion reactions ϕ were calculated as the ratio between the numbers of isomerized molecules *n*(molecules isomerized) and the number of absorbed photons *n*(*hv*) according to eq. 8:

$$\phi = \frac{n(\text{molecules isomerized})}{n(hv)} \qquad \text{(eq. 8)}$$

To determine the quantum yields ϕ a sample with known concentration of each pure isomer *rac*-**A,** *rac*-**B**, *rac*-**C**, or *rac*-**D** in MeCN-d_3 was irradiated with a 450 nm LED within the published instrumental setup from the group of *E. Riedle*[4] extended with an *Oxford DN 1704* optical cryostat controlled by an *Oxford ITC 4* device to set the temperature during the measurement. The number of absorbed photons over time *n*(*hv*) was measured directly at the thermal photometer of the instrument according to eq. 9:

$$n(hv) = \frac{\Delta P \cdot \lambda_{ex} \cdot t}{c \cdot h} \qquad \text{(eq. 9)}$$

Where c is the speed of light ($2.99792 \cdot 10^8$ m·s^{-1}), h is Planck's constant ($6.62607 \cdot 10^{-34}$ J·s), λ_{ex} is the excitation wavelength in m, t is the elapsed time during irradiation in s, and ΔP is the difference in power read-outs at the thermal photometer between a solvent filled cuvette (P_0) and a cuvette containing the sample solution (P_t) during the irradiation period in Watt (eq. 10). The power read out during irradiation did not change substantially (<5%) over the irradiation periods.

$$\Delta P = P_t - P_0 \qquad \text{(eq.10)}$$

If more than one photoproduct is formed during irradiation the number of each type of photoconverted molecules *n*(molecules isomerized) was determined by ^{1}H NMR spectroscopy directly after the irradiation step. Multiple measurements with increasing time of irradiation were conducted and the obtained ϕ values were averaged. The amount of isomerized molecules was also plotted against irradiation time showing linear behavior over measurement periods up to 30 min in case of *rac*-**B** amd *rac*-**C** (Supplementary Figure 21 and 22). Therefore, the quantum yield measurements conform to initial-slope behavior, where only the initial isomer is photoconverted but not the photoproducts.

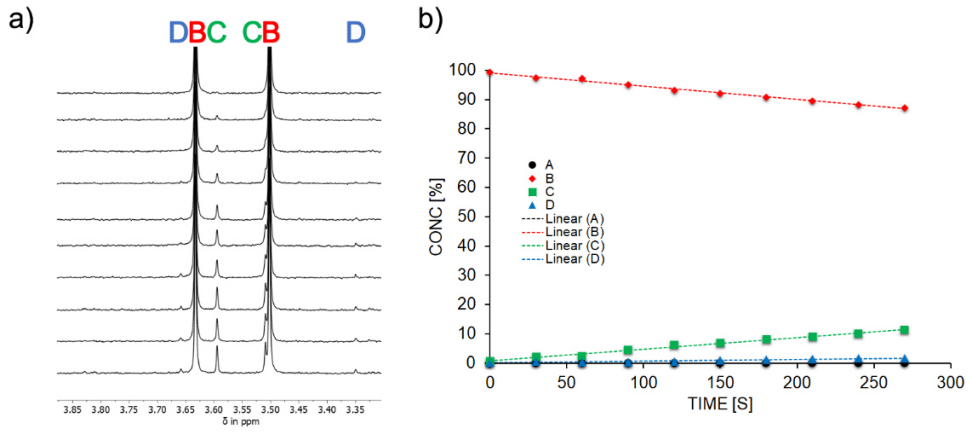

Supplementary Figure 21. Quantum yield ϕ measurement for the photoconversion of *rac*-**B-1** at -40 °C in MeCN-d_3 solution (0.91 mM) using a 450 nm LED for irradiation. a) ^{1}H NMR spectra (400 MHz, 20 °C) recorded after different irradiation durations. Signals of individual isomers are indicated. b) The relative changes of the isomer composition are plotted against different duration times of irradiation. After irradiation the sample was allowed to warm up to 20 °C. Therefore, the initial photoproduct is converted into *rac*-**C-1** and the thermodynamic equilibrium of *rac*-**C-1** and *rac*-**D-1** is formed and observed by NMR spectroscopy at 20 °C. From low temperature measurements it is known that *rac*-**B-1** only converts into *rac*-**D-1**, hence the quantum yield for the reaction *rac*-**B-1** to *rac*-**D-1** is calculated from the sum of the rising isomers *rac*-**C-1** and *rac*-**D-1**. Each point represents an individual measurement, the relative isomer ratios were determined by ^{1}H NMR spectroscopy. Linear behavior is observed showing that only *rac*-**B-1** undergoes significant photoreactions. Quantum yields were determined by averaging over all experiments (see Supplementary Table 2).

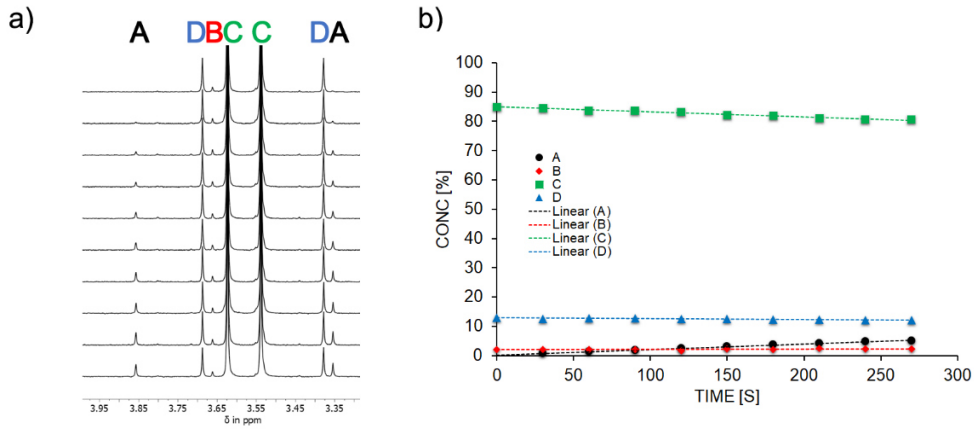

Supplementary Figure 22. Quantum yield ϕ measurement for the photoconversion of *rac*-**C-1** and *rac*-**D-1** at -40 °C in MeCN-d_3 solution (1.12 mM) using a 450 nm LED for irradiation. a) ^{1}H NMR spectra (400 MHz, 20 °C) recorded after different irradiation durations. Signals of individual isomers are indicated. b) The relative changes of the isomer composition are plotted against different duration times of irradiation. Relative isomer ratios were determined by ^{1}H NMR spectroscopy. At 20 °C isomers *rac*-**C-1** and *rac*-**D-1** are in rapid exchange with each other and a thermodynamic equilibrium of 87:13 for the *rac*-**C-1**:*rac*-**D-1** ratio is observed in solution. This ratio is maintained when the samples are cooled quickly to -40 °C for the quantum yield measurement. Therefore, both isomers can undergo photoreactions in this experiment, but the previous low temperature NMR studies show that isomer *rac*-**C-1** is photoreacting only to isomer *rac*-**A-1** and isomer *rac*-**D-1** is only in photoexchange with isomer *rac*-**B-1**. In the quantum yield measurement and in the continuous irradiation inside the NMR device at 20 °C only a photoreaction to *rac*-**A-1** is observable. The formation of *rac*-**A-1** must occur exclusively from *rac*-**C-1** and a photoreaction from *rac*-**C-1** to *rac*-**B-1** is not observed. The photoreaction of *rac*-**D-1** to *rac*-**B-1** is therefore much slower than the photoreaction from *rac*-**C-1** to *rac*-**A-1** and cannot be measured. This may be caused by lower quantum yield or by a lower extinction coefficient of *rac*-**D-1** in relation to isomer *rac*-**C-1** and by the lower concentration of *rac*-**D-1**. The molar extinction coefficients of pure *rac*-**C-1** or *rac*-**D-1** are not measurable individually at 20 °C. A determination of the quantum yield of the isomer *rac*-**D-1** is therefore also not possible as it is not known how much light isomer *rac*-**D-1** is absorbing, overshadowing the photoreaction of *rac*-**C-1**. However, as in practice both isomers cannot be separated and the small overshadowing of the quantum yield of *rac*-**C-1** by *rac*-**D-1** cannot be circumvented, the quantum yield of the formation of *rac*-**A-1** is given from the thermodynamic mixture *rac*-**C-1** and *rac*-**D-1**. Quantum yields were determined by averaging over all experiments (see Supplementary Table 2).

Supplementary Table 2. Quantum yields ϕ in % for different photoconversions of **1** under irradiation with a 450 nm LED in MeCN-d_3 at different temperatures. SBR = single bond rotation, DBI = double bond isomerization, HT = hula twist. [a] values determined at -40 °C, [b] values determined at -40 °C from the thermodynamic equilibrium of *rac*-**C**-**1** and *rac*-**D**-**1** at 20 °C, [c] The dual single bond rotation (DSBR) reaction **B** to **B'** is not observable in the NMR experiment and was determined by multiplication of the quantum yield of **B** to **D** (HT reaction) with the ratio of **B** to **D** (HT reaction) to **B** to **B'** (DSBR reaction) as determined by the Markov matrix studies using chiral HPLC analysis (see the next section for details). All values marked with – were too small to enable a quantitative determination (at least a factor of 10 less than the more productive photoreactions), this was the general case for isomers *rac*-**A**-**1** and *rac*-**D**-**1**.

Photoreaction (all racemic)	ϕ
A to B SBR	-
A to C HT	-
A to D DBI	-
B to A SBR	-[a]
B to C DBI	-[a]
B to D HT	1.4%[a]
C to A HT	5.2%[b]
C to B DBI	-[b]
C to D SBR	-[b]
D to A DBI	-[b]
D to B HT	-[b]
D to C SBR	-[b]
B to B' DSBR	0.9%[c]

Photo and thermal conversions of the enantiomers determined by chiral HPLC and Markov matrix analysis

To determine, which enantiomer converts into which enantiomer upon irradiation or thermally we used a Markov matrix simulation model, which was used previously e.g. by the group of *B. Feringa*[5] or our own[6-8] to elucidate the interconversion of multiple species. The kinetic data for the photoisomerization steps were obtained by preparing a stock solution (10 ml) of every enantiomer of HTI **1** in the respective solvent, transferring an aliquot of 1 ml from this stock solution into an UV-Vis cuvette, which was cooled down to the desired temperature with an *Oxford DN 1704* optical cryostat controlled by an *Oxford ITC 4* device if needed. The cuvette was placed into the published instrumental setup for quantum yield determination from the group of *E. Riedle*[4] to ensure constant illumination conditions and was irradiated for the given time under continuous stirring. Afterwards the solution was allowed to warm up to 20 °C (if cooled down) and transferred into an amberized sample vial and the solvent was evaporated. The sample was dissolved in the HPLC-solvent and separation of the photoproducts was performed on a DAICEL CHIRALPAK ID column (20 mm Ø x 20 mmL) with an eluent of 11 % EtoAc in *n*-heptane at 60 °C and a flow of 3 mL. All isomers could be separated except for **C** and **D**, which are in rapid equilibrium with each other at 20 °C or above that temperature. This procedure was repeated for different irradiation times until the stock solution was consumed.

Kinetic data for the corresponding thermal steps were obtained by a similar method but as the exact number of molecules does not matter for analysis of thermal kinetics the whole stock solution was heated and aliquots were withdrawn after different heating times for HPLC analysis. The resulting HPLC chromatograms are shown in Supplementary Figure 23 exemplarily for the irradiation of isomer **B**-**1**. Kinetic data were quantified by integration of individual chromatogram peaks and dividing through the molar extinction coefficient of the isomers at the recording wavelength of 450 nm. The kinetics were then fitted by a Markov matrix as described earlier,[5-8] but now the simulation was extended to 8 states and included also the rates of the thermal reactions. The derivation is therefore comprehensively explained below.

For HTI **1** the rate of an individual phototransition e.g. **A** to **B**, depends on all other absorbing species present at the same time and is described by the corresponding rate matrix element $r_{P(\mathbf{A/B})}$ (eq. 11):

$$r_{\mathrm{P}(\mathbf{A/B})} = \phi_{\mathbf{A/B}} \cdot I_0 \cdot \varepsilon_{\mathbf{A}} \cdot d \cdot [\mathbf{A}] \cdot \left(\frac{1-e^{-d\sum_i \varepsilon_i \cdot [\mathrm{i}]}}{d\sum_i \varepsilon_i \cdot [\mathrm{i}]}\right) \qquad \text{(eq. 11)}$$

Likewise every phototransition from isomer **i** to isomer **j** can be written as:

$$r_{P(\mathbf{i}/\mathbf{j})} = \phi_{\mathbf{i}/\mathbf{j}} \cdot I_0 \cdot \varepsilon_{\mathbf{i}} \cdot d \cdot [\mathbf{i}] \cdot \left(\frac{1-e^{-d\sum_{\mathbf{i}} \varepsilon_{\mathbf{i}} \cdot [\mathbf{i}]}}{d\sum_{\mathbf{i}} \varepsilon_{\mathbf{i}} \cdot [\mathbf{i}]}\right) \qquad \text{(eq. 12)}$$

with $\phi_{\mathbf{i}/\mathbf{j}}$ = photoisomerization quantum yield for the phototransition of **i** to **j**, I_0 the photon flux (Einstein L^{-1} s^{-1}) of the light, $\varepsilon_{\mathbf{i}}$ the molar extinction coefficient of **i** at the wavelength of irradiation, d the pathlength of the light through the sample, [**i**] the concentration of **i**, $\varepsilon_{\mathbf{i}}$ the molar extinction coefficient of species **i**.

In addition every reaction can occur thermally in which case the Eyring equation expresses the rate of the reaction:

$$r_{T(\mathbf{i}/\mathbf{j})} = \frac{k_B}{h} e^{\frac{-E_a}{RT}} \qquad \text{(eq. 13)}$$

with k_B = Boltzmann constant, h = Planck's constant, E_a activation energy for the reaction **i** to **j**, R = gas constant, T = temperature. The total rate of one reaction is the sum of the rates of the thermal- and photoreaction:

$$r_{(\mathbf{i}/\mathbf{j})} = r_{T(\mathbf{i}/\mathbf{j})} + r_{P(\mathbf{i}/\mathbf{j})} \qquad \text{(eq. 14)}$$

The corresponding rate matrix containing all possible rates $r_{\mathbf{i}/\mathbf{j}}$ for the transitions of isomers **i** into isomers **j** for HTI **1** is therefore written as:

$$M_1 = \begin{array}{c} \begin{array}{cccccccc} \mathbf{A} & \mathbf{A'} & \mathbf{B} & \mathbf{B'} & \mathbf{C} & \mathbf{C'} & \mathbf{D} & \mathbf{D'} \end{array} \\ \begin{pmatrix} r_{A/A} & r_{A/A'} & r_{A/B} & r_{A/B'} & r_{A/C} & r_{A/C'} & r_{A/D} & r_{A/D'} \\ r_{A'/A} & r_{A'/A'} & r_{A'/B} & r_{A'/B'} & r_{A'/C} & r_{A'/C'} & r_{A'/D} & r_{A'/D'} \\ r_{B/A} & r_{B/A'} & r_{B/B} & r_{B/B'} & r_{B/C} & r_{B/C'} & r_{B/D} & r_{B/D'} \\ r_{B'/A} & r_{B'/A'} & r_{B'/B} & r_{B'/B'} & r_{B'/C} & r_{B'/C'} & r_{B'/D} & r_{B'/D'} \\ r_{C/A} & r_{C/A'} & r_{C/B} & r_{C/B'} & r_{C/C} & r_{C/C'} & r_{C/D} & r_{C/D'} \\ r_{C'/A} & r_{C'/A'} & r_{C'/B} & r_{C'/B'} & r_{C'/C} & r_{C'/C'} & r_{C'/D} & r_{C'/D'} \\ r_{D/A} & r_{D/A'} & r_{D/B} & r_{D/B'} & r_{D/C} & r_{D/C'} & r_{D/D} & r_{D/D'} \\ r_{D'/A} & r_{D'/A'} & r_{D'/B} & r_{D'/B'} & r_{D'/C} & r_{D'/C'} & r_{D'/D} & r_{D'/D'} \end{pmatrix} \end{array} \begin{array}{c} \mathbf{A} \\ \mathbf{A'} \\ \mathbf{B} \\ \mathbf{B'} \\ \mathbf{C} \\ \mathbf{C'} \\ \mathbf{D} \\ \mathbf{D'} \end{array} \qquad \text{(eq. 15)}$$

Matrix M_1 (eq. 15) describes all possible photo and thermal conversions quantitatively, but each element for the photoreactions is a nonlinear differential equation dependent on the other elements at a given time, which makes an analytical solution impossible.

We have used the different rate elements $r_{\mathbf{i}/\mathbf{j}}$ in the rate matrix M_1 to simulate our kinetic measurements. For every incremental irradiation step (Δt) we have used the following expressions (eq. 16 - 19) to describe the corresponding next concentration of the respective isomer:

$$[\mathrm{i}]_{t+1} = [\mathrm{i}]_t\text{-}[\mathrm{i}]_{t+1} = -[\mathrm{i}]_t - \sum r_{i/j}\Delta t + \sum r_{j/i}\Delta t \qquad \text{(eq. 16)}$$

While the thermal step elements in the matrix are already known from previous experiments the photo-step elements are not known and not all variables in eq. 12 are determinable in the experiment. However, the relative ratios of the quantum yields of the different photoreactions can still be identified as explained below. In general, a Markov matrix describes the probabilities for different transitions of different states p(**ij**) within a given time increment. For a photoreaction the probabilities are directly proportional to the rate $r_{\mathbf{i/j}}$ of the transition if all molar extinction coefficients are the same (this is to a good approximation the case for HTI **1** at the irradiation wavelength of 450 nm as seen by the molar absorption coefficients):

$$\mathrm{p}(\mathbf{ij}) = k_{\mathbf{p(i/j)}} \cdot \Delta t = \frac{r_{\mathbf{i/j}}}{[\mathbf{i}]} \cdot \Delta t = \frac{\phi_{\mathbf{i/j}} \cdot I_0 \cdot \varepsilon_{\mathbf{i}} \cdot d \cdot [\mathbf{i}] \cdot \left(\frac{1-e^{-d\sum_{\mathrm{i}} \varepsilon_{\mathrm{i}} \cdot [\mathrm{i}]}}{d\sum_{\mathrm{i}} \varepsilon_{\mathrm{i}} \cdot [\mathrm{i}]}\right)}{[\mathbf{i}]} \cdot \Delta t \qquad \text{(eq. 17)}$$

Additionally we have to include the diagonal elements p(**ii**) describing the probability that no conversion occurs:

$$\mathrm{p}(\mathbf{ij}) = 1 - \sum_{\mathrm{j}} p_{P(\boldsymbol{ij})} \qquad \text{(eq. 18)}$$

We conducted independent irradiation experiments for each solvent starting from enantiomerically pure samples. If it is possible to keep I_0, d, and the initial concentration of the pure isomer [**i**] constant and the same in every experiment and if also the molar extinction coefficients of all different isomers are the same at the irradiation wavelength, the same Markov matrix can be used to describe all experiments. In this case eq. 18 transforms into:

$$\mathrm{p}(\mathbf{ij}) = \frac{\phi_{\mathbf{i/j}} \cdot I_0 \cdot \varepsilon_{\mathbf{i}} \cdot d \cdot [\mathbf{i}] \cdot \left(\frac{1-e^{-d\sum_{\mathrm{i}} \varepsilon_{\mathrm{i}} \cdot [\mathrm{i}]}}{d\sum_{\mathrm{i}} \varepsilon_{\mathrm{i}} \cdot [\mathrm{i}]}\right)}{[\mathbf{i}]} \cdot \Delta t = \phi_{\mathbf{i/j}} \cdot I_0 \cdot \varepsilon_{\mathbf{i}} \cdot d \cdot \left(\frac{1-e^{-d\sum_{\mathrm{i}} \varepsilon_{\mathrm{i}} \cdot [\mathrm{i}]}}{d\sum_{\mathrm{i}} \varepsilon_{\mathrm{i}} \cdot [\mathrm{i}]}\right) \cdot \Delta t = \phi_{\mathbf{i/j}} \cdot const \cdot \Delta t \qquad \text{(eq. 19)}$$

and only depends on the individual quantum yields $\phi_{\mathbf{i/j}}$.

Even if the mentioned variables are not constant the relative ratios of off-diagonal elements in each row of the Markov matrix reproduce the relative ratios of the corresponding quantum yields ϕ according to eq. 20 (exemplarily for the photoconversions of **A** to **B** and **C**):

$$\frac{\mathrm{p}(\mathbf{AB})}{\mathrm{p}(\mathbf{AC})} = \frac{\phi_{\mathbf{A/B}} \cdot I_0 \cdot \varepsilon_{\mathbf{A}} \cdot d \cdot \left(\frac{1-e^{-d\sum_i \varepsilon_i \cdot [i]}}{d\sum_i \varepsilon_i \cdot [i]}\right) \cdot \Delta t}{\phi_{\mathbf{A/C}} \cdot I_0 \cdot \varepsilon_{\mathbf{A}} \cdot d \cdot \left(\frac{1-e^{-d\sum_i \varepsilon_i \cdot [i]}}{d\sum_i \varepsilon_i \cdot [i]}\right) \cdot \Delta t} = \frac{\phi_{\mathbf{A/B}}}{\phi_{\mathbf{A/C}}} \qquad \text{(eq. 20)}$$

As can be seen from eq. 20 the relative ratios of off-diagonal elements in each row of a Markov matrix directly correspond to the respective quantum yield ratios even if the molar extinction coefficients of different present isomers are different to each other (the sum expressions cancel each other out). As the matrix elements of one row correspond to one and the same experiment I_0, d, and the initial concentration of the pure isomer [**i**] are constant per se. Therefore, the relative ratios within one row of each Markov matrix have to be the same for all matrices.

Likewise, the ratio of one off-diagonal probability to the sum of all off-diagonal probabilities within one row of the Markov matrix is related to the corresponding ratio of the quantum yields giving the relative percentage of each process:

$$\text{rel. \%} = \frac{\mathrm{p}(\mathbf{ij})}{\sum \mathrm{p}(\mathbf{ij})} = \frac{\phi(\mathbf{ij})}{\sum \phi(\mathbf{ij})} \qquad \text{(eq. 21)}$$

Additionally, the diagonal elements in the same Markov matrix can be compared at least qualitatively if the different molar extinction coefficients ε_i are similar enough. This gives a quantitative assessment of the relative efficiencies of the overall photoconversions for each starting isomer.

By plotting the relative isomer percentage against the elapsed time during irradiation, different kinetic plots (starting from the eight pure isomers) were obtained from the experiments. These plots show the changes in isomer composition over time during the irradiation. This experimental kinetics were then simulated via an iterative process in which a Markov matrix M_1 (eq. 15) is multiplied with the corresponding isomer percentage vector for each time point (eq. 22). The product vector is then multiplied by the same Markov matrix to give the corresponding vector of the next time point:

$$\begin{pmatrix} \%\mathbf{A} \\ \%\mathbf{A'} \\ \%\mathbf{B} \\ \%\mathbf{B'} \\ \%\mathbf{C} \\ \%\mathbf{C'} \\ \%\mathbf{D} \\ \%\mathbf{D'} \end{pmatrix}_{t_{x+1}} = \begin{pmatrix} r_{A/A} & r_{A/A'} & r_{A/B} & r_{A/B'} & r_{A/C} & r_{A/C'} & r_{A/D} & r_{A/D'} \\ r_{A'/A} & r_{A'/A'} & r_{A'/B} & r_{A'/B'} & r_{A'/C} & r_{A'/C'} & r_{A'/D} & r_{A'/D'} \\ r_{B/A} & r_{B/A'} & r_{B/B} & r_{B/B'} & r_{B/C} & r_{B/C'} & r_{B/D} & r_{B/D'} \\ r_{B'/A} & r_{B'/A'} & r_{B'/B} & r_{B'/B'} & r_{B'/C} & r_{B'/C'} & r_{B'/D} & r_{B'/D'} \\ r_{C/A} & r_{C/A'} & r_{C/B} & r_{C/B'} & r_{C/C} & r_{C/C'} & r_{C/D} & r_{C/D'} \\ r_{C'/A} & r_{C'/A'} & r_{C'/B} & r_{C'/B'} & r_{C'/C} & r_{C'/C'} & r_{C'/D} & r_{C'/D'} \\ r_{D/A} & r_{D/A'} & r_{D/B} & r_{D/B'} & r_{D/C} & r_{D/C'} & r_{D/D} & r_{D/D'} \\ r_{D'/A} & r_{D'/A'} & r_{D'/B} & r_{D'/B'} & r_{D'/C} & r_{D'/C'} & r_{D'/D} & r_{D'/D'} \end{pmatrix} \cdot \begin{pmatrix} \%\mathbf{A} \\ \%\mathbf{A'} \\ \%\mathbf{B} \\ \%\mathbf{B'} \\ \%\mathbf{C} \\ \%\mathbf{C'} \\ \%\mathbf{D} \\ \%\mathbf{D'} \end{pmatrix}_{t_x}$$

(eq. 22)

The elements of the Markov matrix in eq. 22 were adjusted manually until the best match with the experimental data was obtained. All ratios determined from the irradiation experiments in different solvents are summarized in Supplementary Table 2 and shown in Supplementary Figures 24-39. Note that column values signify the starting point isomer and the row elements signify the product formed, i.e. the individual elements, e.g. $\mathbf{r_{A/A'}}$ in the matrix read as starting point **A** and product **A´** of the transformation.

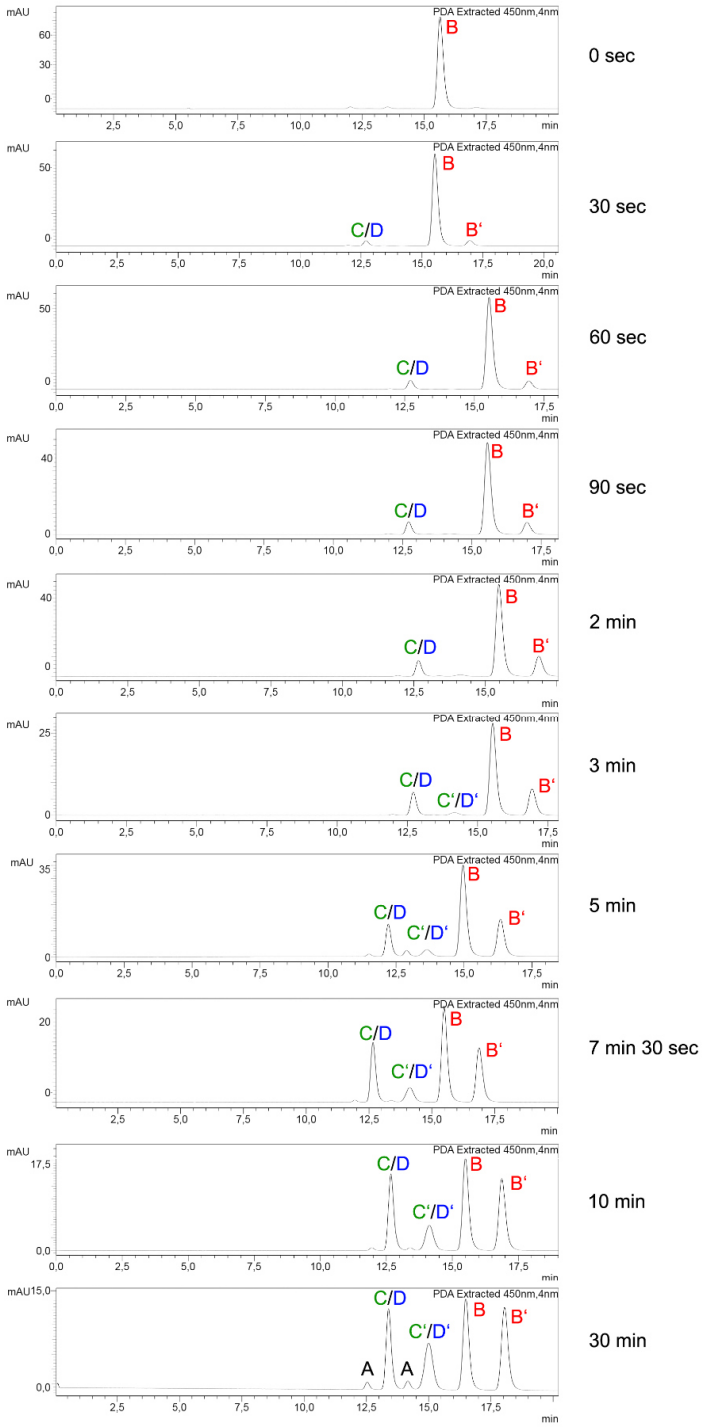

Supplementary Figure 23. Photoconversion of **B-1** at -40 °C in MeCN solution using a 450 nm LED for irradiation. HPLC chromatograms (measured at 450 nm absorption, DAICEL CHIRALPAK ID column (20 mm Ø x 20 mmL) with an eluent of 11 % EtoAc in *n*Heptane at 60 °C and a flow of 3 mL) recorded after different irradiation durations. Signals of individual isomers are indicated. The corresponding integration values and resulting kinetics are shown in Supplementary Figure 24.

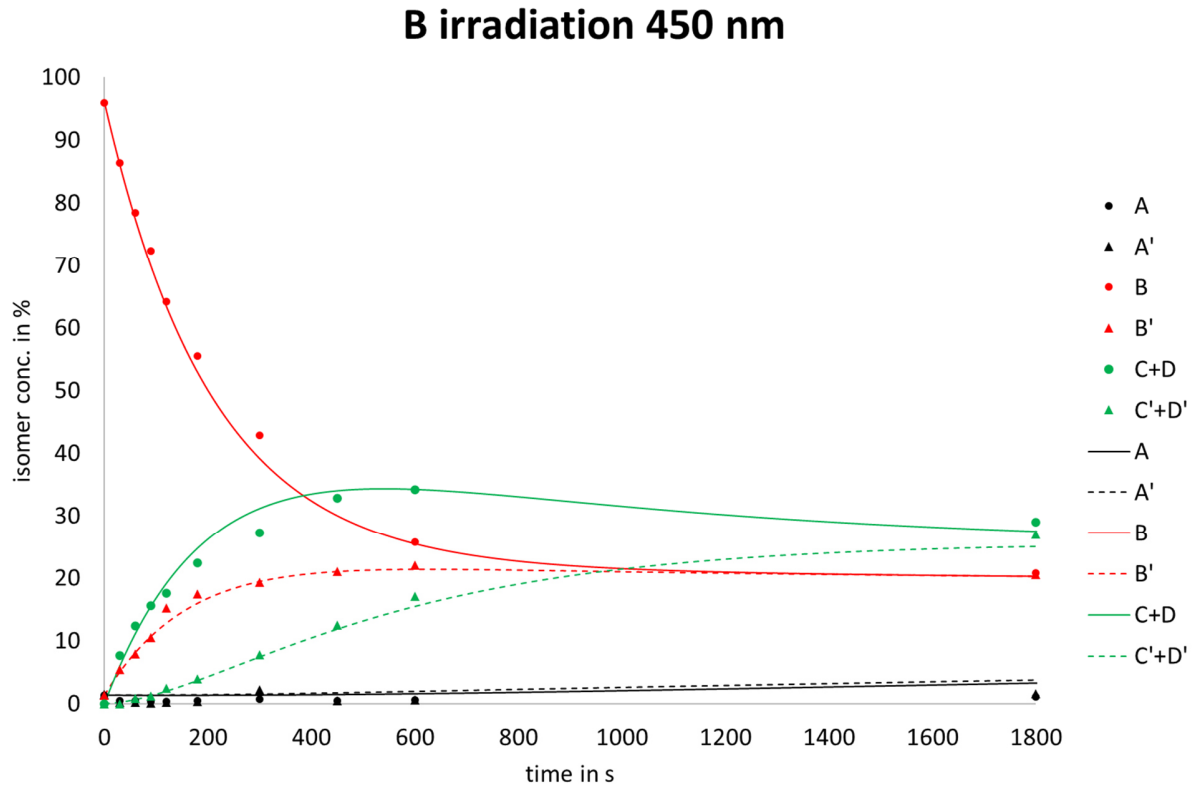

Supplementary Figure 24. Photoconversion of **B-1** at -40 °C in MeCN solution using a 450 nm LED for irradiation. The isomer composition (dots) was determined by integration of the respective HPLC chromatogram peaks (DAICEL CHIRALPAK ID column (20 mm Ø x 20 mmL) with an eluent of 11 % EtoAc in *n*Heptane at 60 °C and a flow of 3 mL). HPLC chromatograms were recorded after different irradiation durations. Kinetics are modeled by the Markov matrix shown in Supplementary Figure 26 (lines).

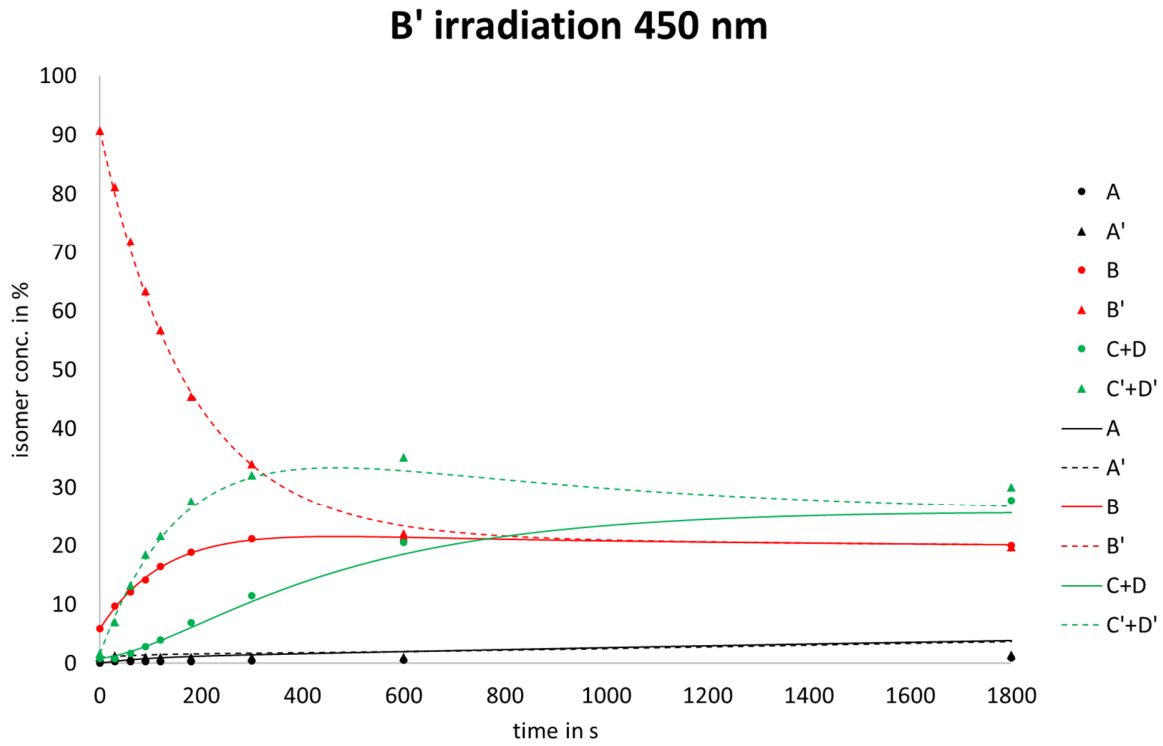

Supplementary Figure 25. Photoconversion of **B'-1** at -40 °C in MeCN solution using a 450 nm LED for irradiation. The isomer composition (dots) was determined by integration of HPLC chromatogram peaks (DAICEL CHIRALPAK ID column (20 mm Ø x 20 mmL) with an eluent of 11 % EtoAc in *n*Heptane at 60 °C and a flow of 3 mL). HPLC chromatograms were recorded after different irradiation durations. Kinetics are modeled by the Markov matrix shown in Supplementary Figure 26 (lines).

A	A'	B	B'	C	C'	D	D'	
-	$1.88 \cdot 10^{-4}$	28.7	27.1	$1.25 \cdot 10^{-4}$	$6.25 \cdot 10^{-5}$	-	-	A
$2.25 \cdot 10^{-4}$	-	27.1	28.7	$6.25 \cdot 10^{-5}$	$1.25 \cdot 10^{-4}$	-	-	A'
29.6	28.0	-	$1.47 \cdot 10^{-3}$	-	-	$2.28 \cdot 10^{-3}$	-	B
28.0	29.6	$1.47 \cdot 10^{-3}$	-	-	-	-	$2.28 \cdot 10^{-3}$	B'
$7.29 \cdot 10^{-4}$	$7.29 \cdot 10^{-3}$	-	-	-	$7.29 \cdot 10^{-4}$	18.85	-	C
$7.29 \cdot 10^{-3}$	$7.29 \cdot 10^{-4}$	-	-	$7.29 \cdot 10^{-4}$	-	-	18.85	C'
-	-	$8.75 \cdot 10^{-4}$	$8.75 \cdot 10^{-5}$	18.1	-	-	-	D
-	-	$8.75 \cdot 10^{-5}$	$8.75 \cdot 10^{-4}$	-	18.1	-	-	D'

Supplementary Figure 26. Markov matrix used for modeling the kinetics of the photoconversion of **1** at -40 °C in MeCN solution using a 450 nm LED for irradiation. Black and blue values indicate photoreactions, which must be multiplied with the relative light intensity. Blue values signify the most dominant photoreaction pathways, which are preferred strongly over the other possibilities giving riser to high photochemical selectivity. Red values indicate thermal reactions and are given in kcal · mol^{-1}, which must be converted into reaction rates using the Eyring equation for the appropriate temperature. Note that the values for the reactions of the **A-1**, **C-1**, and **D-1** enantiomers may not be highly accurate as their reactions were not measured with the pure isomers and are only fitted with the data obtained by the irradiation of the **B-1** enantiomers. These values are therefore not used in further discussions.

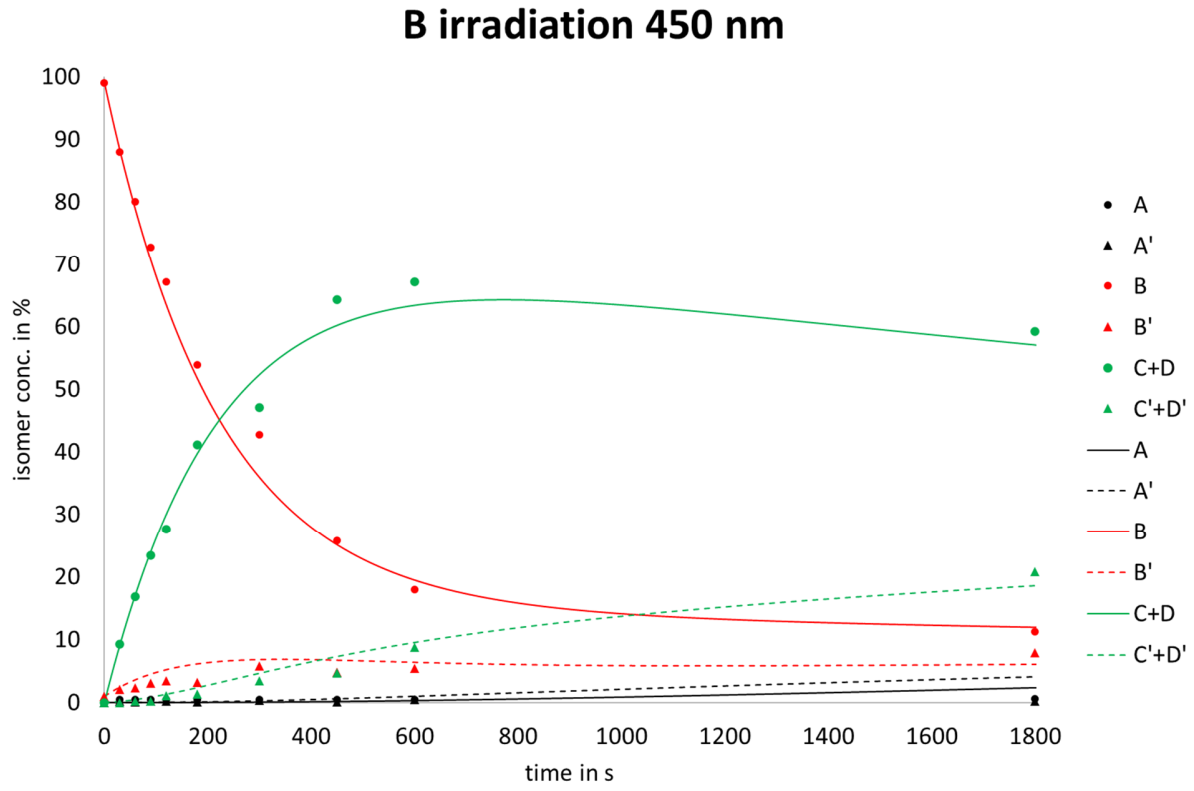

Supplementary Figure 27. Photoconversion of **B-1** at -80 °C in MeOH solution using a 450 nm LED for irradiation. The isomer composition (dots) was determined by integration of HPLC chromatogram peaks (DAICEL CHIRALPAK ID column (20 mm Ø x 20 mmL) with an eluent of 11 % EtoAc in *n*Heptane at 60 °C and a flow of 3 mL). HPLC chromatograms were recorded after different irradiation durations. Kinetics are modeled by the Markov matrix shown in Supplementary Figure 29 (lines).

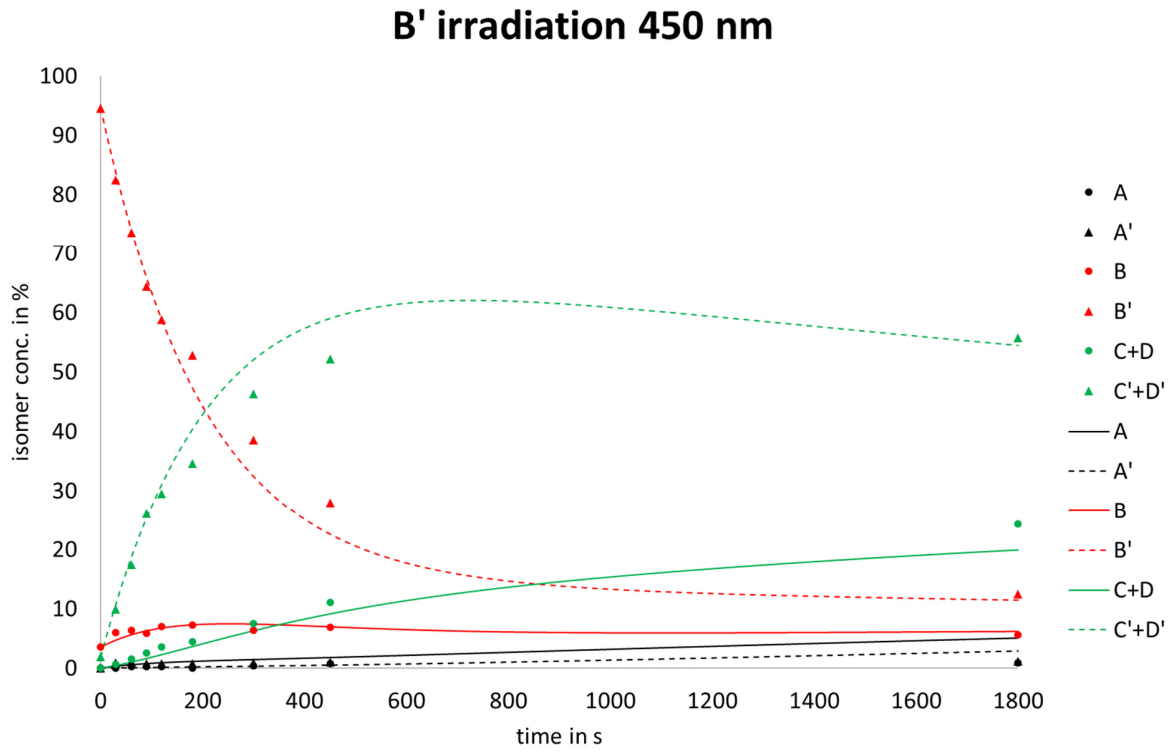

Supplementary Figure 28. Photoconversion of **B'-1** at -80 °C in MeOH solution using a 450 nm LED for irradiation. The isomer composition (dots) was determined by integration of HPLC chromatogram peaks (DAICEL CHIRALPAK ID column (20 mm Ø x 20 mmL) with an eluent of 11 % EtoAc in *n*Heptane at 60 °C and a flow of 3 mL). HPLC chromatograms were recorded after different irradiation durations. Kinetics are modeled by the Markov matrix shown in Supplementary Figure 29 (lines).

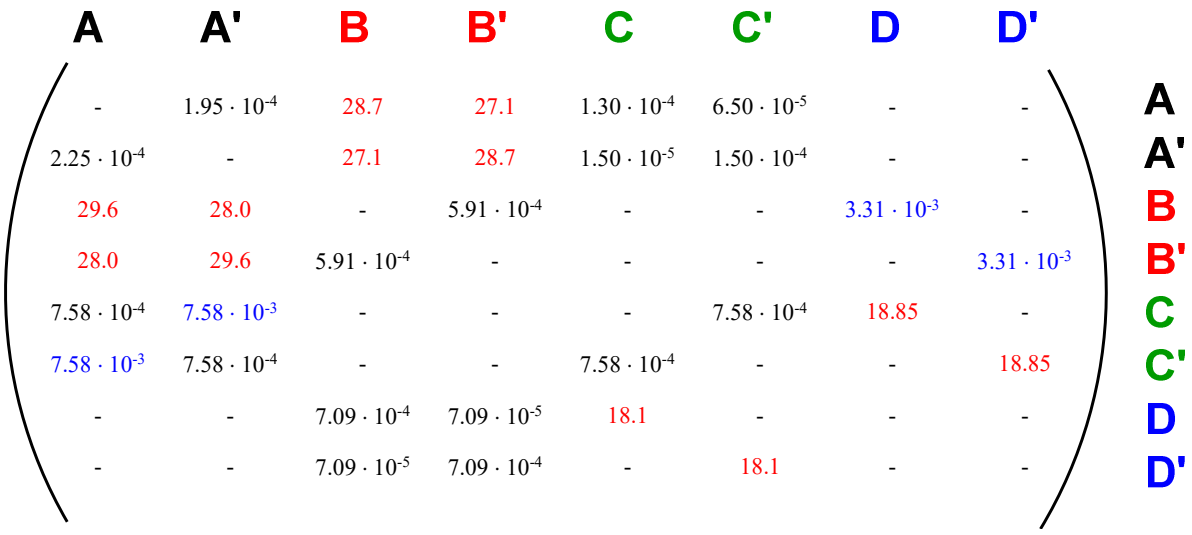

Supplementary Figure 29. Markov matrix used for modeling the kinetics of the photoconversion of **1** at -80 °C in MeOH solution using a 450 nm LED for irradiation. Black and blue values indicate photoreactions, which must be multiplied with the relative light intensity. Blue values signify the most dominant photoreaction pathways, which are preferred strongly over the other possibilities giving riser to high photochemical selectivity. Red values indicate thermal reactions and are given in kcal · mol^{-1}, which must be converted into reaction rates using the Eyring equation for the appropriate temperature. Note that the values for the reactions of the **A-1**, **C-1**, and **D-1** enantiomers are not perfectly accurate as their reactions were not measured starting from the respective pure isomers and are only fitted with the data obtained by irradiation of the **B-1** enantiomers. These values are therefore not used in further discussions.

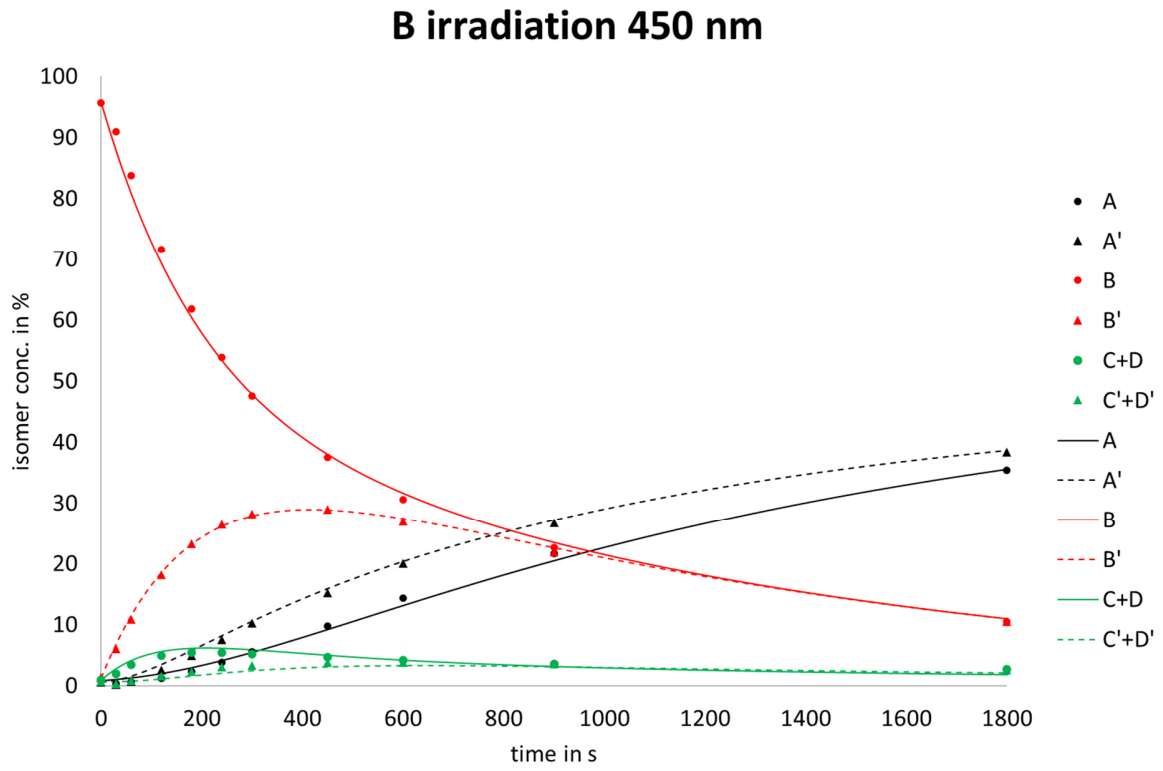

Supplementary Figure 30. Photoconversion of **B-1** at 20 °C in toluene solution using a 450 nm LED for irradiation. The isomer composition (dots) was determined by integration of HPLC chromatogram peaks (DAICEL CHIRALPAK ID column (20 mm Ø x 20 mmL) with an eluent of 11 % EtoAc in *n*Heptane at 60 °C and a flow of 3 mL). HPLC chromatograms were recorded after different irradiation durations. Kinetics are modeled by the Markov matrix shown in Supplementary Figure 32 (lines).

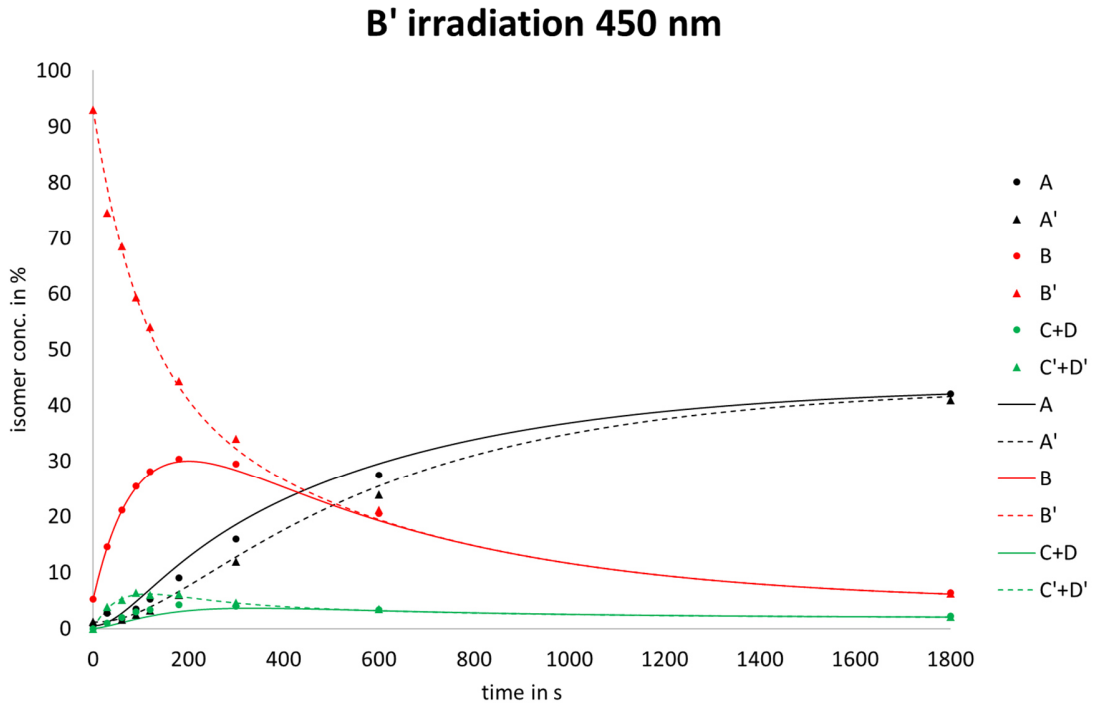

Supplementary Figure 31. Photoconversion of **B'-1** at 20 °C in toluene solution using a 450 nm LED for irradiation. The isomer composition (dots) was determined by integration of HPLC chromatogram peaks (DAICEL CHIRALPAK ID column (20 mm Ø x 20 mmL) with an eluent of 11 % EtoAc in *n*Heptane at 60 °C and a flow of 3 mL). HPLC chromatograms were recorded after different irradiation durations. Kinetics are modeled by the Markov matrix shown in Supplementary Figure 32 (lines).

A	A'	B	B'	C	C'	D	D'	
-	$1.54 \cdot 10^{-4}$	28.7 $+2.57 \cdot 10^{-5}$	27.1 $+2.57 \cdot 10^{-5}$	$1.03 \cdot 10^{-4}$	$5.14 \cdot 10^{-5}$	-	-	A
$1.54 \cdot 10^{-4}$	-	27.1 $+2.57 \cdot 10^{-5}$	28.7 $+2.57 \cdot 10^{-5}$	$5.14 \cdot 10^{-5}$	$1.03 \cdot 10^{-4}$	-	-	A'
29.6	28.0	-	$1.30 \cdot 10^{-3}$	-	-	$4.96 \cdot 10^{-4}$	-	B
28.0	29.6	$1.30 \cdot 10^{-3}$	-	-	-	-	$4.96 \cdot 10^{-4}$	B'
$1.00 \cdot 10^{-3}$	$5.00 \cdot 10^{-3}$	-	-	-	-	18.85	-	C
$5.00 \cdot 10^{-3}$	$1.00 \cdot 10^{-3}$	-	-	-	-	-	18.85	C'
-	-	-	-	18.1	-	-	-	D
-	-	-	-	-	18.1	-	-	D'

Supplementary Figure 32. Markov matrix used for modeling the kinetics of the photoconversion of **1** at 20 °C in toluene solution using a 450 nm LED for irradiation. Black and blue values indicate photoreactions, which must be multiplied with the relative light intensity. Blue values signify the most dominant photoreaction pathways, which are preferred strongly over the other possibilities giving riser to high photochemical selectivity. Red values indicate thermal reactions and are given in kcal · mol^{-1}, which must be converted into reaction rates using the Eyring equation for the appropriate temperature. Note that the values for the reactions of the **A-1** and **C-1** enantiomers may not be accurate as their reactions were not measured starting from pure isomers and are only fitted with the data obtained by the irradiation of the **B-1** enantiomers. These values are therefore not used in further discussions. The thermal reaction of the **D-1** enantiomers to the **C-1** enantiomers is fast at 20 °C and therefore overlaying the photochemistry of the **D-1** enantiomers.

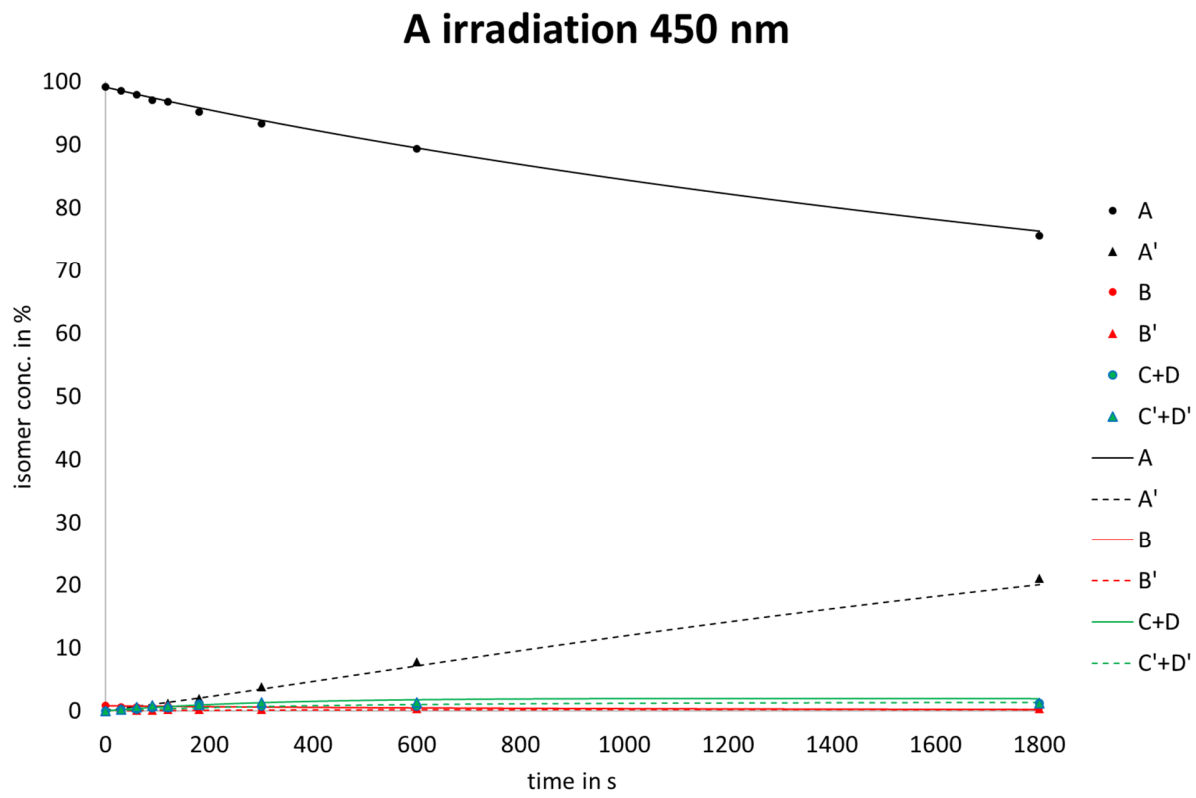

Supplementary Figure 33. Photoconversion of **A-1** at 20 °C in MeCN solution using a 450 nm LED irradiation. The isomer composition (dots) was determined by integration of HPLC chromatogram peaks (DAICEL CHIRALPAK ID column (20 mm Ø x 20 mmL) with an eluent of 11 % EtoAc in *n*Heptane at 60 °C and a flow of 3 mL). HPLC chromatograms were recorded after different irradiation durations. Kinetics are modeled by the Markov matrix shown in Supplementary Figure 39 (lines).

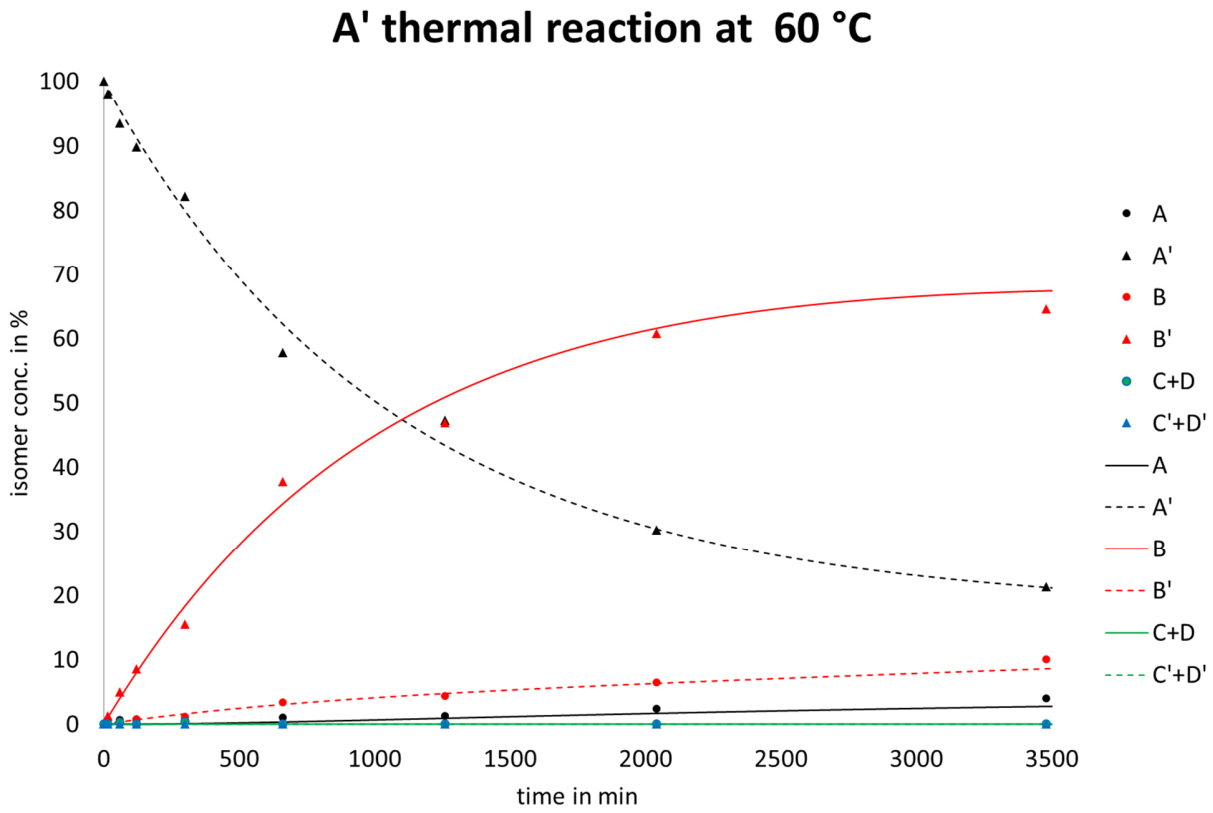

Supplementary Figure 34. Thermal conversion of **A'-1** at 60 °C in MeCN solution. The isomer composition (dots) was determined by integration of HPLC chromatogram peaks (DAICEL CHIRALPAK ID column (20 mm Ø x 20 mmL) with an eluent of 11 % EtoAc in *n*Heptane at 60 °C and a flow of 3 mL). HPLC chromatograms were recorded after different heating durations. Kinetics are modeled by the Markov matrix shown in Supplementary Figure 39 (lines).

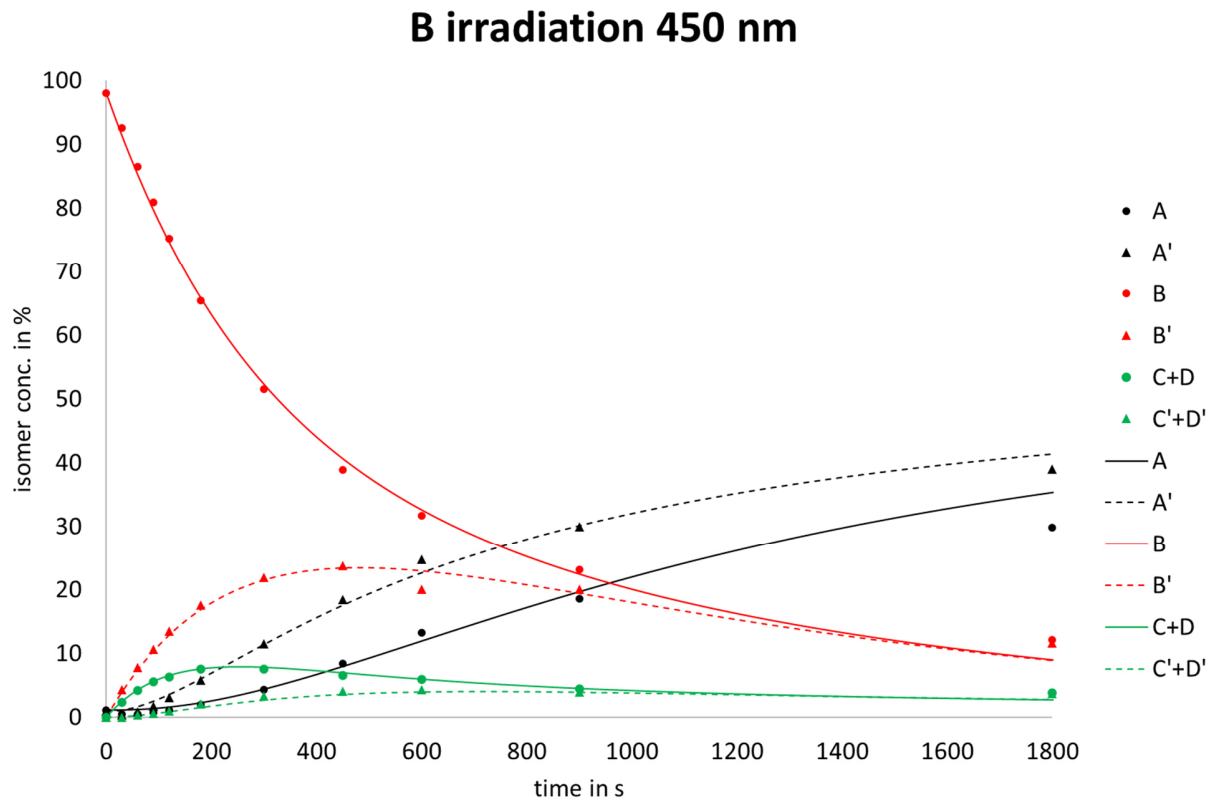

Supplementary Figure 35. Photoconversion of **B-1** at 20 °C in MeCN solution using a 450 nm LED for irradiation. The isomer composition (dots) was determined by integration of HPLC chromatogram peaks (DAICEL CHIRALPAK ID column (20 mm Ø x 20 mmL) with an eluent of 11 % EtoAc in *n*Heptane at 60 °C and a flow of 3 mL). HPLC chromatograms recorded after different irradiation durations. Kinetics are modeled by the Markov matrix shown in Supplementary Figure 39 (lines).

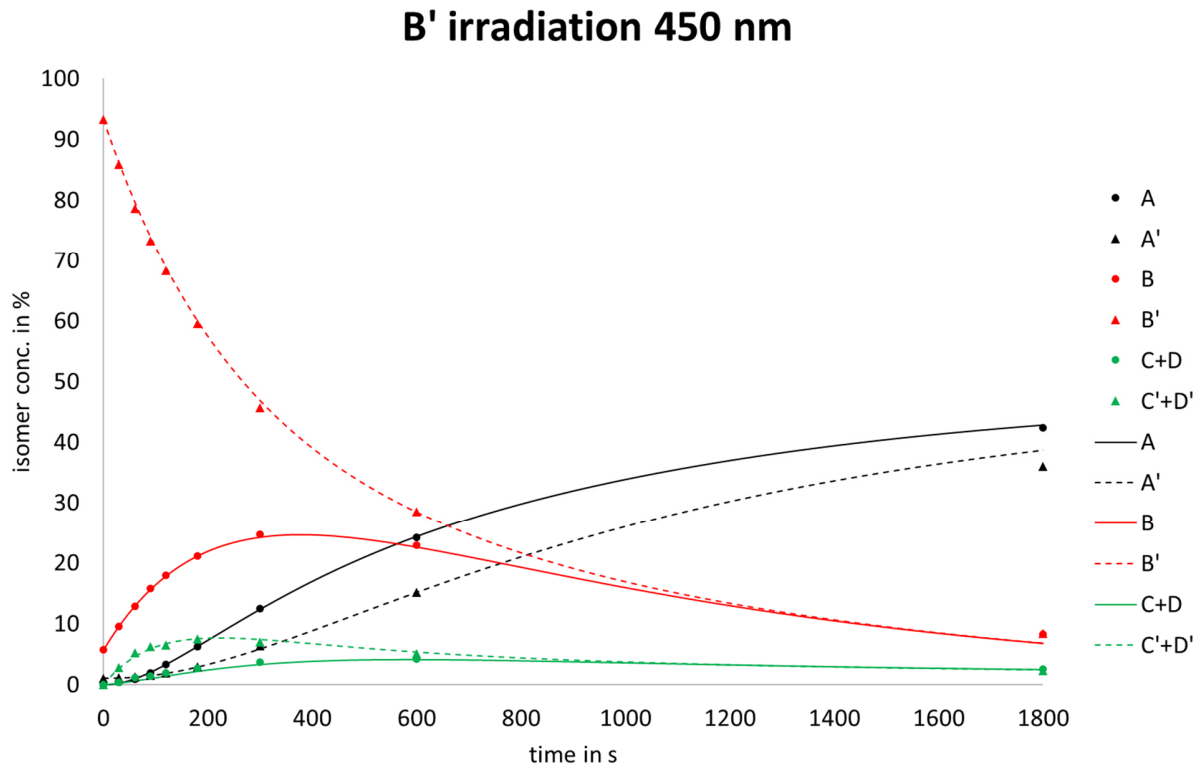

Supplementary Figure 36. Photoconversion of **B'-1** at 20 °C in MeCN solution using a 450 nm LED for irradiation. The isomer composition (dots) was determined by integration of HPLC chromatogram peaks (DAICEL CHIRALPAK ID column (20 mm Ø x 20 mmL) with an eluent of 11 % EtoAc in *n*Heptane at 60 °C and a flow of 3 mL). HPLC chromatograms were recorded after different irradiation durations. Kinetics are modeled by the Markov matrix shown in Supplementary Figure 39 (lines).

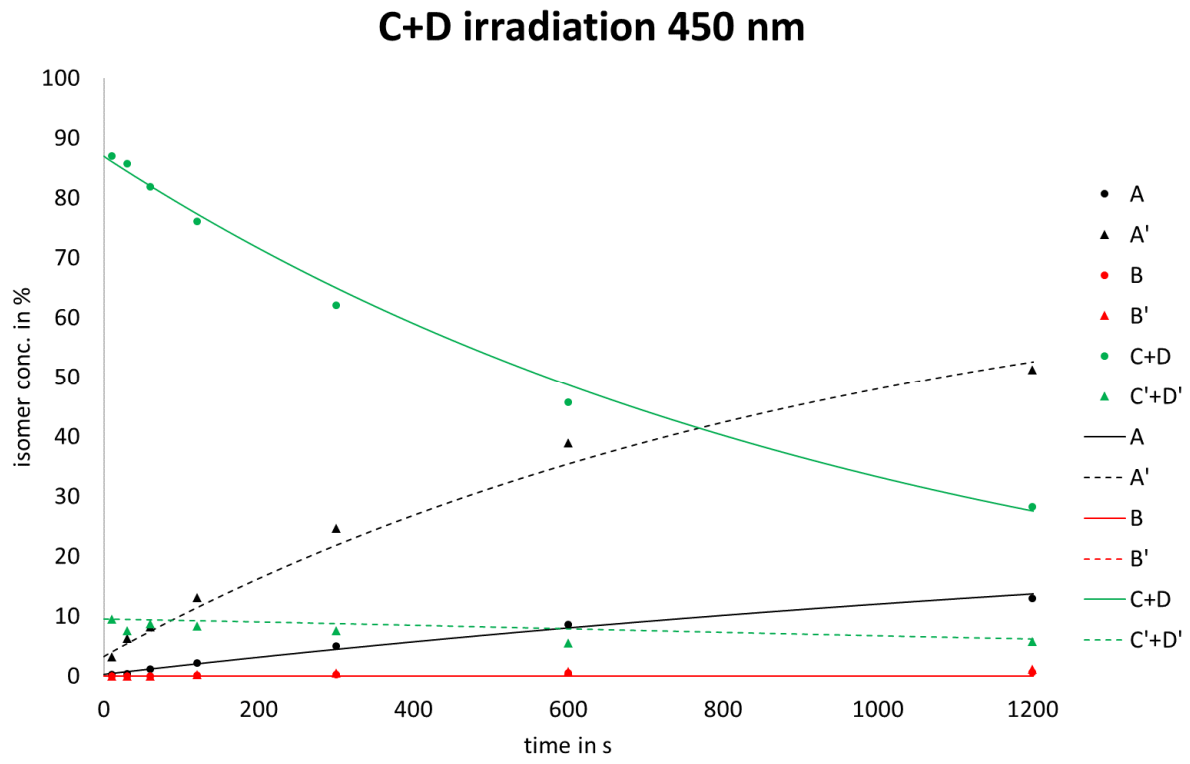

Supplementary Figure 37. Photoconversion of **C-1** and **D-1** at 20 °C in MeCN solution using a 450 nm LED for irradiation. The isomer composition (dots) was determined by integration of HPLC chromatogram peaks (DAICEL CHIRALPAK ID column (20 mm Ø x 20 mmL) with an eluent of 11 % EtoAc in *n*Heptane at 60 °C and a flow of 3 mL). HPLC chromatograms were recorded after different irradiation durations. Kinetics are modeled by the Markov matrix shown in Supplementary Figure 39 (lines).

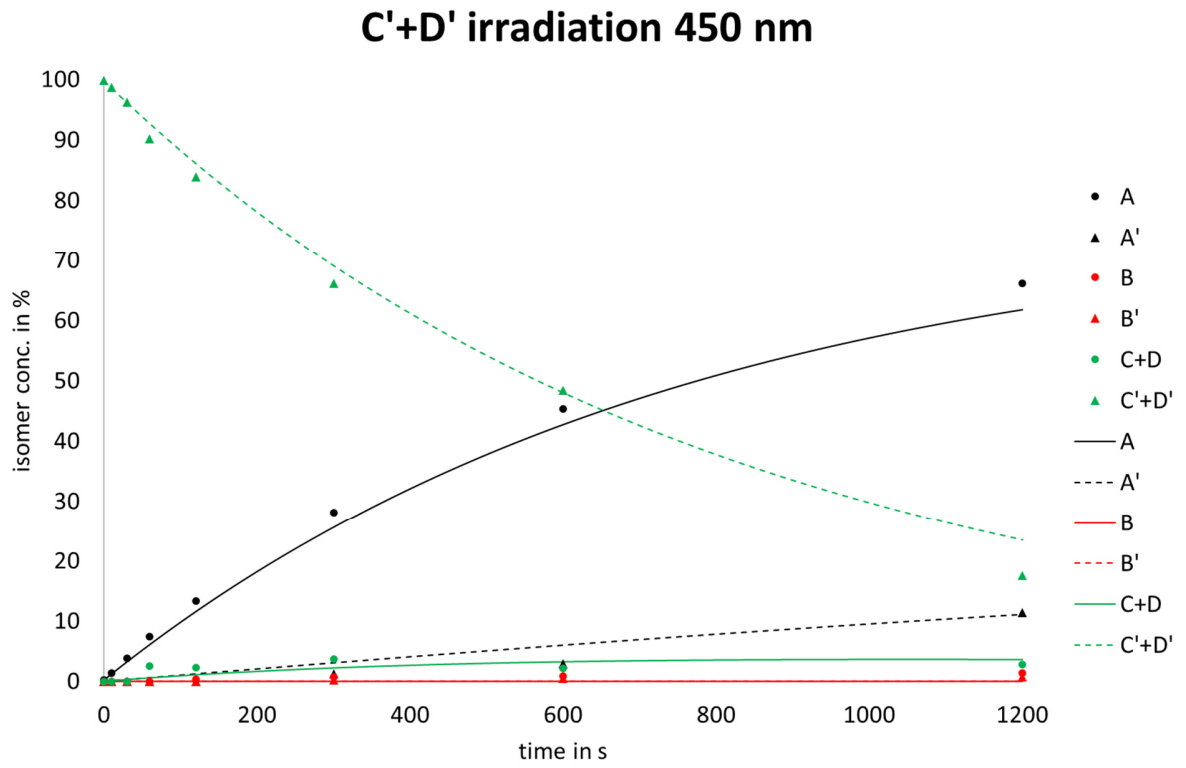

Supplementary Figure 38. Photoconversion of **C'-1** and **D'-1** at 20 °C in MeCN solution using a 450 nm LED for irradiation. The isomer composition (dots) was determined by integration of HPLC chromatogram peaks (DAICEL CHIRALPAK ID column (20 mm Ø x 20 mmL) with an eluent of 11 % EtoAc in *n*Heptane at 60 °C and a flow of 3 mL). HPLC chromatograms were recorded after different irradiation durations. Kinetics are modeled by the Markov matrix shown in Supplementary Figure 39 (lines).

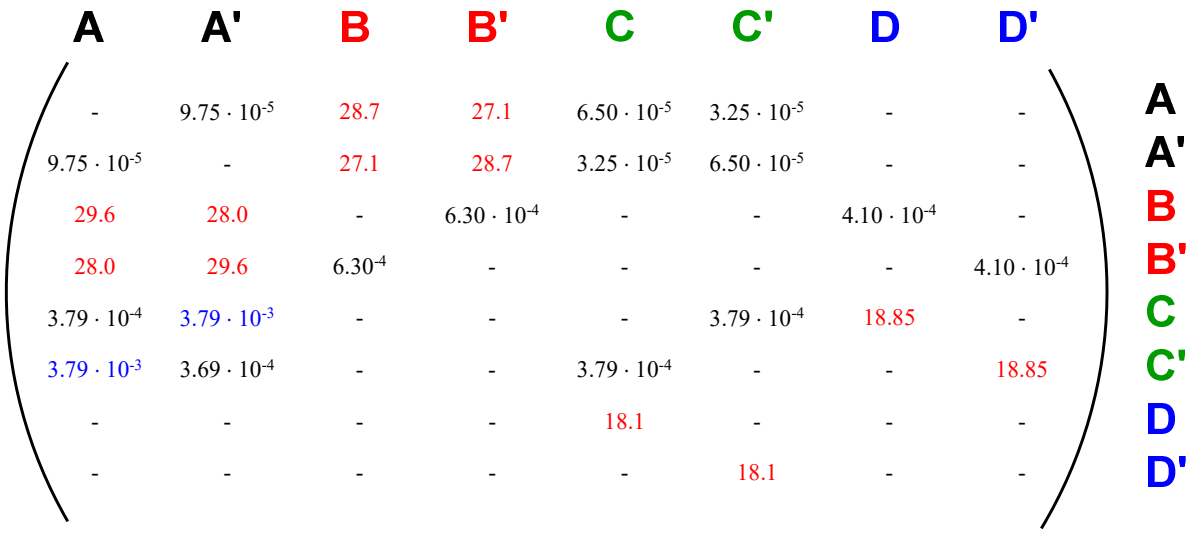

Supplementary Figure 39. Markov matrix used for modeling the kinetics of the photoconversion of **1** at 20 °C using a 450 nm LED for irradiation and thermal reactions at 60 °C in MeCN solution. Black and blue values indicate photoreactions, which must be multiplied with the relative light intensity. Blue values signify the most dominant photoreaction pathways, which are preferred strongly over the other possibilities giving riser to high photochemical selectivity. Red values indicate thermal reactions and are given in kcal · mol^{-1}, which must be converted into reaction rates using the Eyring equation for the appropriate temperature. The thermal reaction of the **D-1** enantiomers to the **C-1** enantiomers is fast at the ambient irradiation temperature and therefore overlaying the photochemistry of the **D-1** enantiomers.

Cycle processes in the photoisomerization of HTI 1

HTI **1** isomerizes following the cycle *rac*-**B**→*rac*-**D**→*rac*-**C**→ *rac*-**A**→ *rac*-**B** (**ABDC**), if racemates were used and observed. In this cycle one isomer can be populated after another in a sequential manner (Supplementary Figure 40). Starting with isomer *rac*-**B** the *rac*-**D** isomer can be obtained with 48% in the PSS. By thermal SBR *rac*-**D** is converted into the *rac*-**C** isomer with 33%, as the thermal equilibrium between *rac*-**C** and *rac*-**D** is 86:14. By further irradiation at 20 °C isomer *rac*-**A** can be enriched up to 95% (**A**:**B**:**C**:**D** = 95:3:2:0). In the next thermal SBR isomer *rac*-**B** is recovered with 78% (**A**:**B**:**C**:**D** = 20:78:2:0). Reproducibility of the cycle **ABDC** is given even when starting from an arbitrary mixture of isomers of HTI **1** because the **A** enriched solution can be obtained as "refocussing step" of the sequence. Full reversibility was demonstrated by executing the cycle experiment three times in a row (Supplementary Figure 40) or 10 times in a row with the same NMR-sample omitting the observation of isomer *rac*-**C** and *rac*-**D** at -40 °C to reduce the overall time needed in the experiment (Supplementary Figure 41).

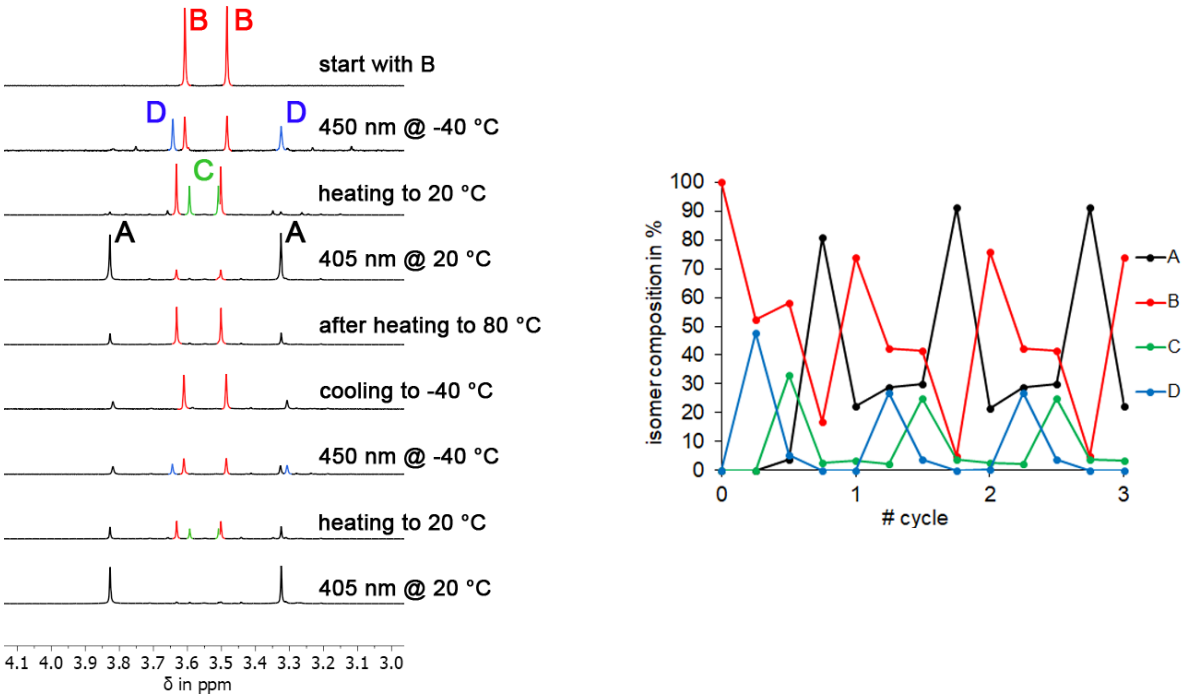

Supplementary Figure 40: Consecutive irradiation and heating steps showing the sequential isomerization cycle in HTI **1** in MeCN-d_3 solution. The ^{1}H NMR spectra of the first 1.75 cycles with assignment to the different isomers are shown on the left and the isomer composition during the cycles is shown on the right. After reaching cycle two the experiment starts always at the same isomer composition as enrichment of isomer **A** by irradiation with 450 nm light at 20 °C leads to the same ratio of **A**:**B**:**C**:**D** = 95:3:2:0.

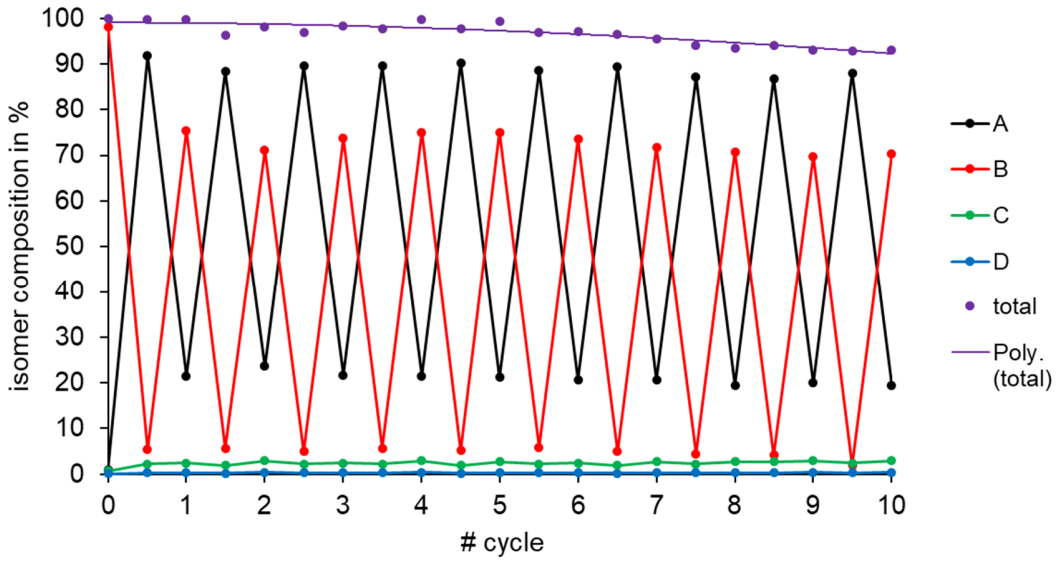

Supplementary Figure 41: Stability of **1** during the sequential isomerization cycle process in MeCN-d_3 solution. The solution of **1** was irradiated with 450 nm until the PSS was reached (enrichment of isomer **A**). Afterwards the solution was heated to 80 °C until a thermal equilibrium was reached (enrichment of isomer **B**). These steps represent a complete *rac*-**B**→*rac*-**D**→*rac*-**C**→ *rac*-**A** cycle but without monitoring the photoreaction from *rac*-**B** to *rac*-**D** followed by thermal reaction to *rac*-**C** individually. The cycle was repeated 10 times and the sum of integrals was compared with an internal standard. Only slight decomposition of about 5% after 10 cycles (20 photoisomerization steps and 20 heating steps) was observed.

Taking the enantiomers into account a cycle of **A→B→D→C→A'→B'→D'→C'→A** is constituted from the main photoreactions and thermal reactions as elucidated by chiral HPLC kinetic analysis and shown in Supplementary Figure 40. In this cycle photochemical Hula-Twist reactions and thermal single bond rotations alternate and after in total eight steps the starting isomer is obtained again. This eight-step cycle can be bypassed by the dual single-bond rotation (DSBR) converting isomer **B** into **B'**. In this case HTI **1** pursues the two enantiomeric cycles **A→B→B'→D'→C'→A** and **A'→B'→B→D→C→A'**. The two cycles with the corresponding reactions are shown in Supplementary Figure 42.

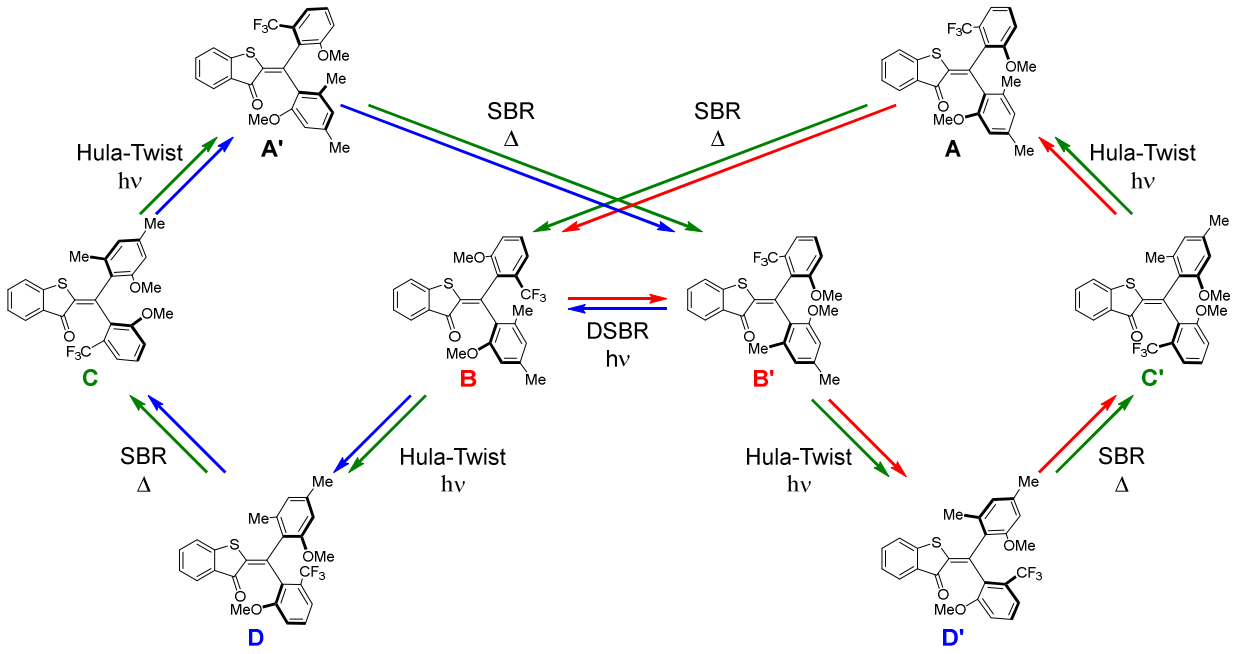

Supplementary Figure 42. Isomerization cycles of HTI **1** with depicted with the color code: **A→B→B'→D'→C'→A** = red, the enantiomeric cycle **A'→B'→B→D→C→A'** = blue, and the eight step cycle **A→B→D→C→A'→B'→D'→C'→A** = green.

To determine the preference for one cycle against the other possibilities the kinetic data obtained by the chiral HPLC Markov matrix analysis (Supplementary Figure 24-39) was used. It is found that every reaction (thermal or photochemical) yields exclusively the respective "next step" isomer in the error margin of the analysis except for the photoreaction of isomer **B** and **B'**. The photoreactions of *rac*-**B** are therefore the branching point for the two possible five-step and eight-step cycles. Which cycle is performed is therefore only dependent on the ratio of the Hula-Twist versus DSBR photoreactions. As this ratio is very dependent on the surrounding medium switching between the five- and eight-step cycle is possible by changing the

irradiation conditions. If isomer **B** and **B'** perform a Hula-Twist photoreaction the eight-step cycle is followed and if the DSBR occurs one of the five-step cycles is pursued. However, if exclusively the DSBR occurs, only photoswitching between **B** and **B'** is observed. The preference for one cycle is therefore given by the three equations:

$$P_{(B\leftrightarrow B')} = P_{(B\rightarrow B')} \cdot P_{(B'\rightarrow B)} \quad \text{(eq. 23)}$$

$$P_{(5\text{-step})} = P_{(B\rightarrow B')} \cdot P_{(B\rightarrow D)} + P_{(B'\rightarrow B)} \cdot P_{(B'\rightarrow D')} \quad \text{(eq. 24)}$$

$$P_{(8\text{-step})} = P_{(B\rightarrow D)} \cdot P_{(B'\rightarrow D')} \quad \text{(eq. 25)}$$

With $P_{(B\leftrightarrow B')}$ = probability of the switching between **B** and **B'**, $P_{(5\text{-step})}$ = probability of the five-step cycle, $P_{(8\text{-step})}$ = probability of the eight-step cycle and $P_{(i\rightarrow j)}$ = probability of the photoreaction from isomer i to j e.g. $P_{(B\rightarrow B')}$ = probability of the photoreaction from isomer **B** to **B'**.

Obviously, the probability of the eight-step cycle is 100% if the both **B** isomers perform exclusively the Hula-Twist reaction and the probability of the photoswitching between **B** and **B'** is 100% if exclusively DSBRs are observed. It is impossible to obtain exclusively the five-step cycle however, it can be favored significantly if conditions are suitable and the highest ratio of the five-step cycle is obtained if the Hula-Twist reaction and DSBR occur with the same probability. The preference of **1** for each cycle depending on the Hula-Twist reaction ratio is shown in Supplementary Figure 43.

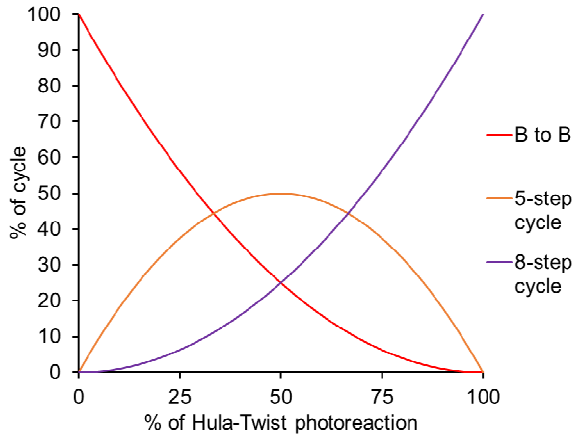

Supplementary Figure 43. Maximum achievable preference for each cycle depending on the amount of the Hula-Twist photoreaction.

NMR-Spectra

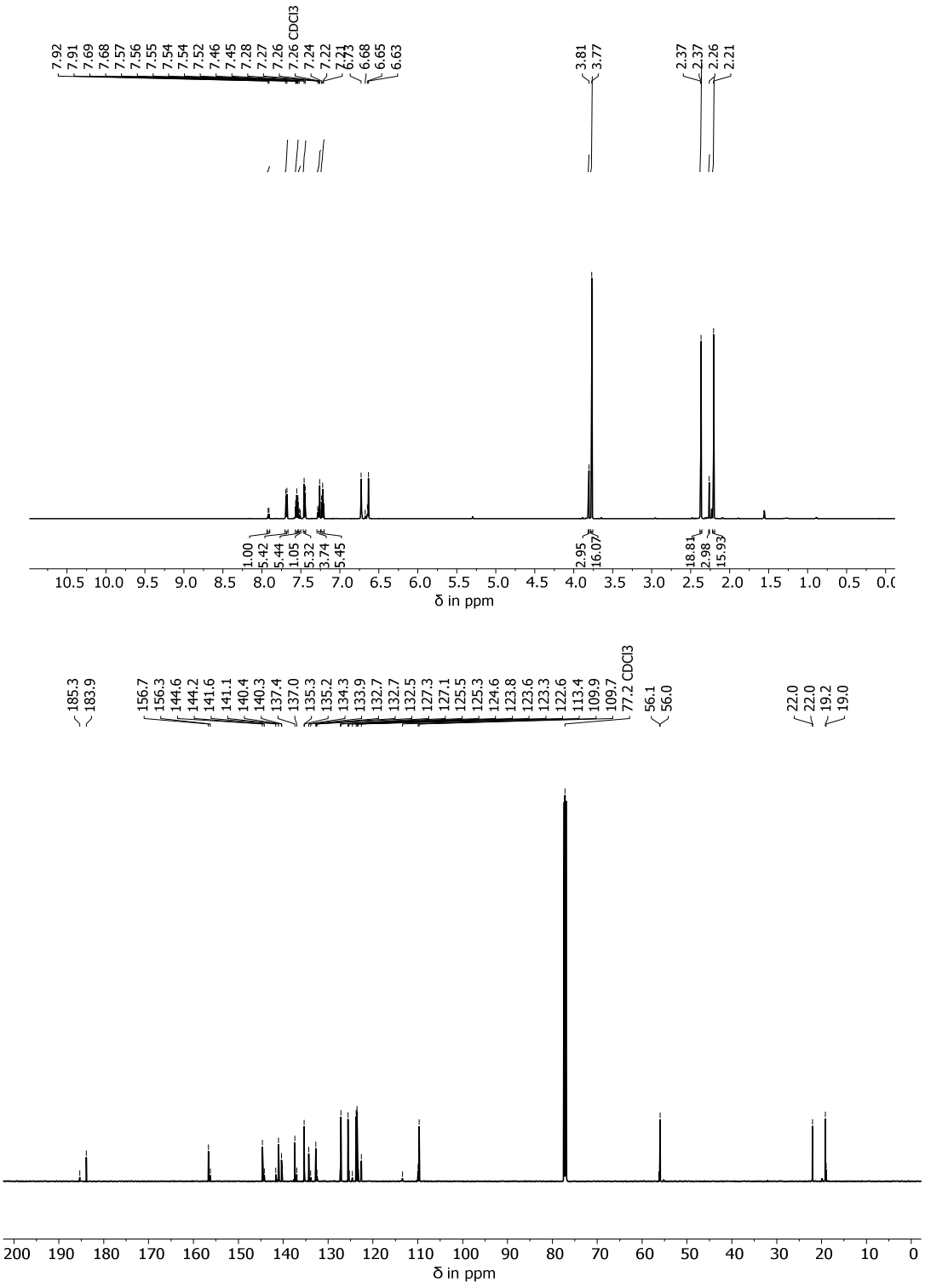

Supplementary Figure 44. 400 MHz ^{1}H-NMR spectrum (top) and 100 MHz ^{13}C-NMR spectrum (bottom) of 2-(chloro(2-methoxy-4,6-dimethylphenyl)methylene)benzo[*b*]thiophen-3(2*H*)-one (**4**) (mix of *E*/*Z* isomers) in $CDCl_3$.

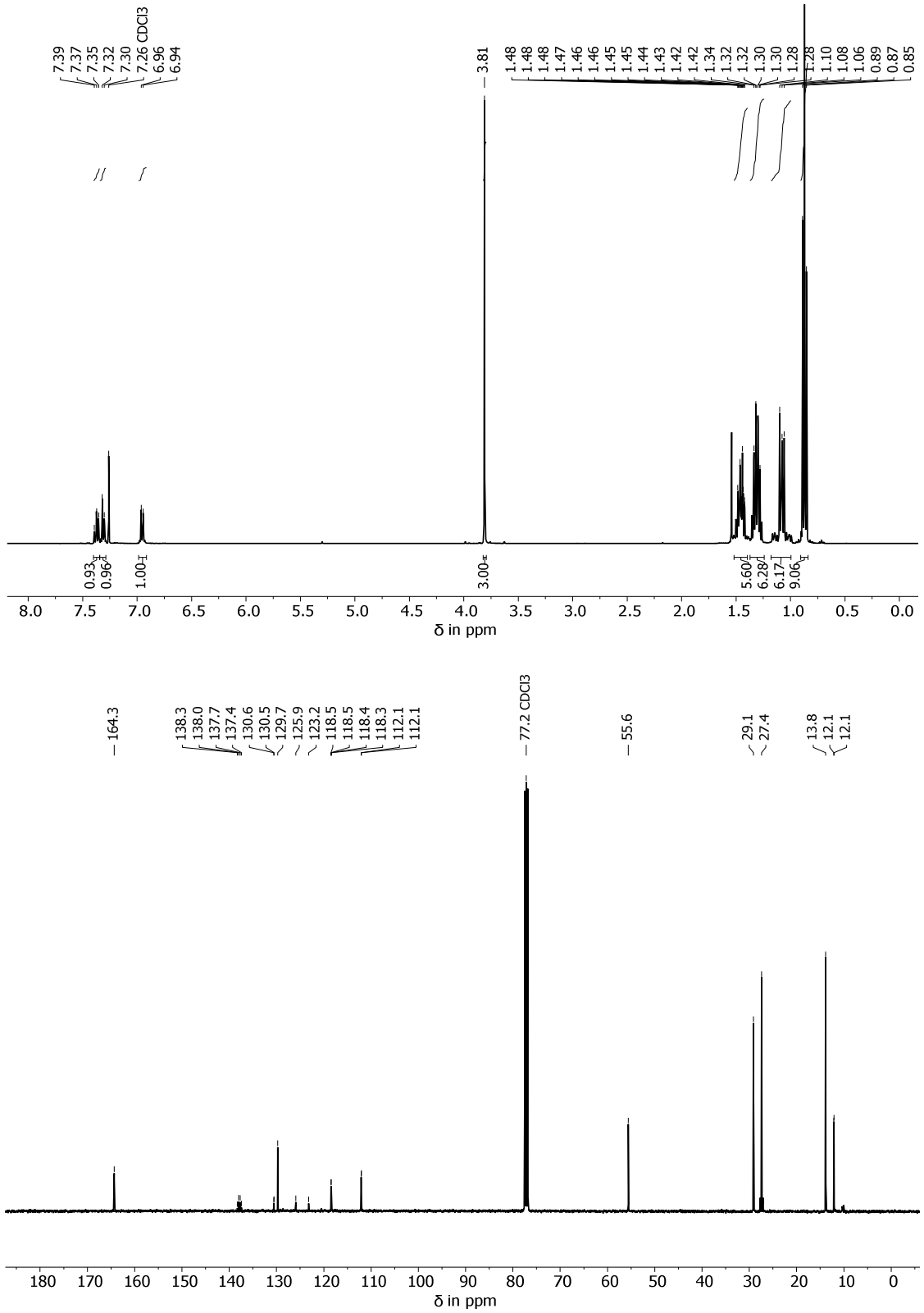

Supplementary Figure 45. 400 MHz ^{1}H-NMR spectrum (top) and 100 MHz ^{13}C-NMR spectrum (bottom) of tributyl(2-methoxy-6-(trifluoromethyl)phenyl)stannane (**5**) in $CDCl_3$.

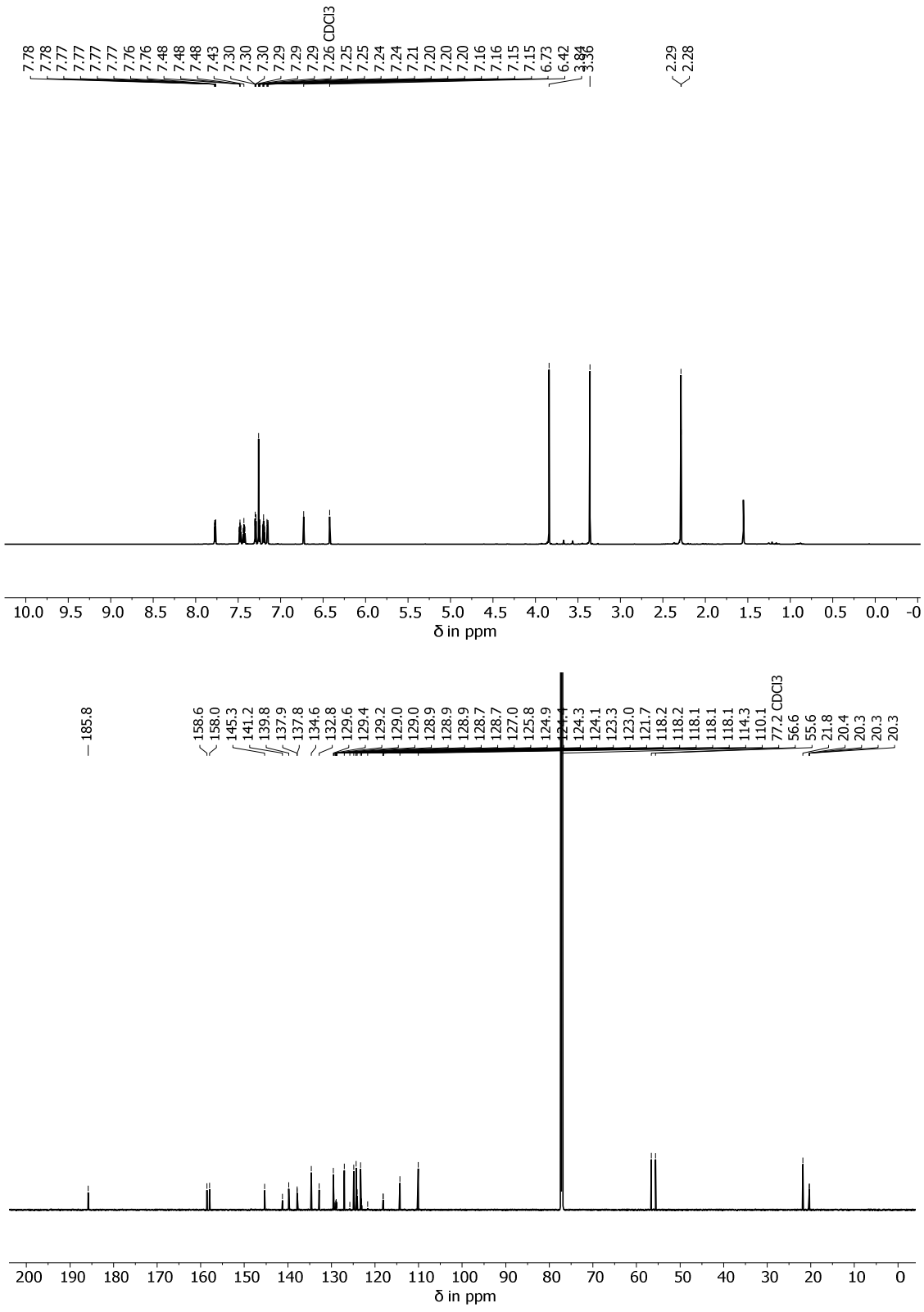

Supplementary Figure 46. 800 MHz ^{1}H-NMR spectrum (top) and 200 MHz ^{13}C-NMR spectrum (bottom) of **A-1** in $CDCl_3$.

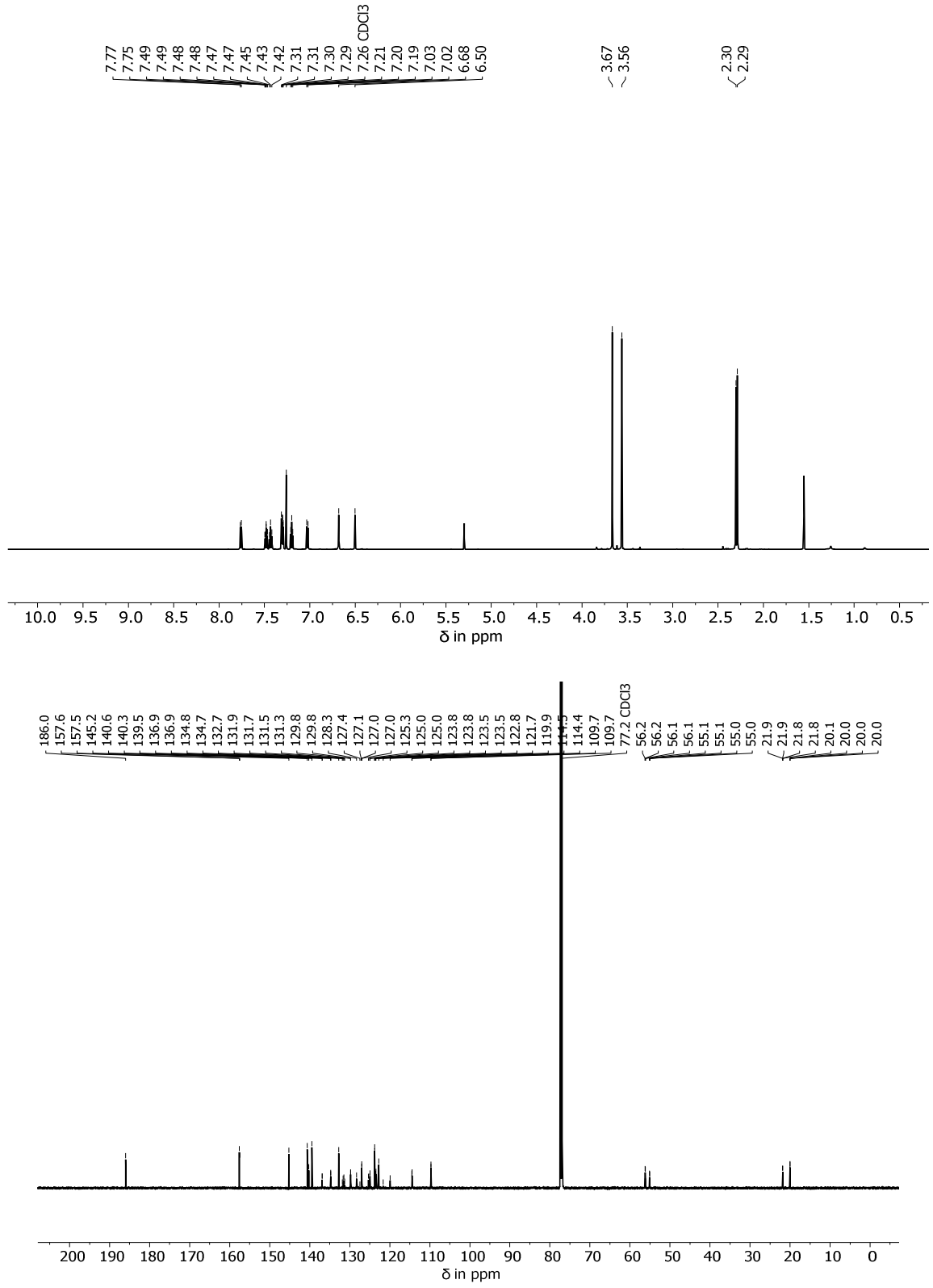

Supplementary Figure 47. 600 MHz ^{1}H-NMR spectrum (top) and 150 MHz ^{13}C-NMR spectrum (bottom) of **B-1** in $CDCl_3$.

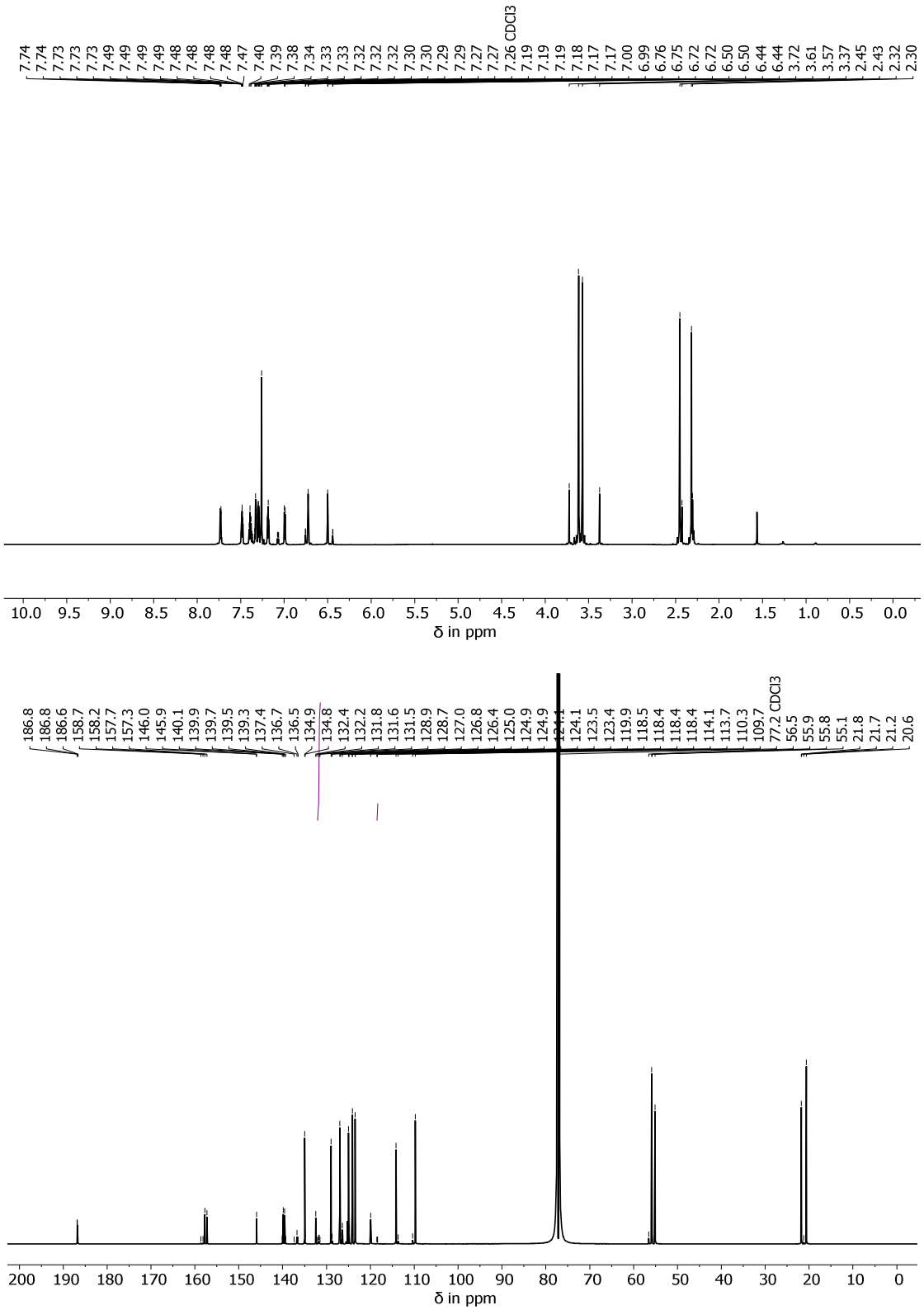

Supplementary Figure 48. 800 MHz ^{1}H-NMR spectrum (top) and 200 MHz ^{13}C-NMR spectrum (bottom) of **-C/D-1** in $CDCl_3$.

Crystal structure analysis

The X-ray intensity data were measured on a Bruker D8 Venture TXS system equipped with a multilayer mirror monochromator and a Mo Kα rotating anode X-ray tube (λ = 0.71073 Å). The frames were integrated with the Bruker SAINT software package.[9] Data were corrected for absorption effects using the Multi-Scan method (SADABS).[10] The structure was solved and refined using the Bruker SHELXTL Software Package.[11] All C-bound hydrogen atoms have been calculated in ideal geometry riding on their parent atoms. The PLATON SQUEEZE program[12] has been applied in order to squeeze-out solvent contents which could not be modelled properly. All figures were drawn at the 50% ellipsoid probability level.[13]

Compound	*rac.* **A-1**/ **A'-1** (wv225) CCDC 2100909	*rac.* **B-1**/ **B'-1** (wv228) CCDC 2100907
net formula	$C_{26}H_{21}F_3O_3S$	$C_{26}H_{21}F_3O_3S$
M_r/g mol^{-1}	470.49	470.49
crystal size/mm	0.100 × 0.060 × 0.040	0.090 × 0.050 × 0.020
T/K	100.(2)	100.(2)
radiation	MoKα	MoKα
diffractometer	'Bruker D8 Venture TXS'	'Bruker D8 Venture TXS'
crystal system	triclinic	monoclinic
space group	'P -1'	'P 1 21/c 1'
a/Å	9.7960(3)	7.8853(3)
b/Å	11.4686(4)	16.4888(6)
c/Å	11.8838(4)	17.2013(7)
α/°	94.3040(10)	90
β/°	105.6660(10)	101.400(2)
γ/°	93.8950(10)	90
V/Å^3	1276.46(7)	2192.37(15)
Z	2	4
calc. density/g cm^{-3}	1.224	1.425
μ/mm^{-1}	0.172	0.200
absorption correction	Multi-Scan	Multi-Scan
transmission factor range	0.95–0.99	0.97–1.00
refls. measured	13332	21847
R_{int}	0.0269	0.0466
mean σ(I)/I	0.0355	0.0341
θ range	3.170–26.372	3.204–25.349
observed refls.	4338	3241
x, y (weighting scheme)	0.0375, 0.6276	0.0279, 1.7845
hydrogen refinement	constr	constr
Flack parameter	-	-
refls in refinement	5180	4009
parameters	302	302
restraints	0	0
$R(F_{obs})$	0.0377	0.0366
$R_w(F^2)$	0.0945	0.0859
S	1.042	1.036
shift/error$_{max}$	0.001	0.001
max electron density/e Å^{-3}	0.274	0.275
min electron density/e Å^{-3}	−0.256	−0.317

Compound	*rac.* **C-1**/ **C'-1** (wv229) CCDC 2100908
net formula	$C_{26}H_{21}F_3O_3S$
M_r/g mol^{-1}	470.49
crystal size/mm	0.090 × 0.050 × 0.040
T/K	100.(2)
radiation	MoKα
diffractometer	'Bruker D8 Venture TXS'
crystal system	triclinic
space group	'P -1'
a/Å	10.9833(3)
b/Å	11.7467(3)
c/Å	17.4631(5)
α/°	91.4340(10)
β/°	93.9910(10)
γ/°	103.9640(10)
V/Å^3	2179.12(10)
Z	4
calc. density/g cm^{-3}	1.434
μ/mm^{-1}	0.201
absorption correction	Multi-Scan
transmission factor range	0.91–0.99
refls. measured	22166
R_{int}	0.0354
mean σ(I)/I	0.0429
θ range	3.216–25.350
observed refls.	6223
x, y (weighting scheme)	0.0329, 1.4449
hydrogen refinement	constr
Flack parameter	-
refls in refinement	7910
parameters	603
restraints	0
$R(F_{obs})$	0.0386
$R_w(F^2)$	0.0927
S	1.027
shift/error$_{max}$	0.001
max electron density/e Å^{-3}	0.425
min electron density/e Å^{-3}	−0.399

Compound	**C-1** (yv157) CCDC 2100910	**C'-1** (yv156) CCDC 2100911
net formula	$C_{53}H_{44}Cl_2F_6O_6S_2$	$C_{53}H_{44}Cl_2F_6O_6S_2$
M_r/g mol^{-1}	1025.90	1025.90
crystal size/mm	0.100 × 0.060 × 0.060	0.100 × 0.030 × 0.030
T/K	102.(2)	102.(2)
radiation	MoKα	MoKα
diffractometer	'Bruker D8 Venture TXS'	'Bruker D8 Venture TXS'
crystal system	orthorhombic	orthorhombic
space group	'P 21 21 21'	'P 21 21 21'
a/Å	13.6458(10)	13.6343(5)
b/Å	18.6506(15)	18.6527(5)
c/Å	18.8599(16)	18.8361(6)
α/°	90	90
β/°	90	90
γ/°	90	90
V/Å^3	4799.9(7)	4790.3(3)
Z	4	4
calc. density/g cm^{-3}	1.420	1.422
μ/mm^{-1}	0.297	0.297
absorption correction	Multi-Scan	Multi-Scan
transmission factor range	0.92–0.98	0.95–0.99
refls. measured	28148	28204
R_{int}	0.0536	0.0367
mean σ(I)/I	0.0623	0.0439
θ range	2.844–26.371	2.846–26.371
observed refls.	8254	8460
x, y (weighting scheme)	0.0315, 1.3791	0.0322, 1.5945
hydrogen refinement	constr	constr
Flack parameter	0.12(3)	0.01(2)
refls in refinement	9729	9745
parameters	630	630
restraints	0	0
$R(F_{obs})$	0.0407	0.0383
$R_w(F^2)$	0.0975	0.0828
S	1.055	1.036
shift/error$_{max}$	0.001	0.001
max electron density/e Å^{-3}	0.343	0.342
min electron density/e Å^{-3}	−0.462	−0.436

Calculated Ground State Energy Profile of Compound 1

A relaxed optimization of the isomeric states and transition state structures of compound **1** has been conducted at the B3LYP level of theory with the 6-311G(d,p) basis set using the Gaussian09 Revision A.02 program package.[14] To account for solvent effects, the calculations have been carried out using the Polarizable Continuum Model (PCM) with acetonitrile parameters. The convergence criteria have been set tight and an ultrafine integration grid has been used. A following frequency analysis confirmed 16 structures to be minimum structures since no imaginary frequencies have been found. Eight of the structures are enantiomeric to the other and were determined to show that the enantiomers (e.g. **A** and **A'**) possess the same energies. In addition, all the expected isomeric minimum structures are present in two different geometries with different helicities, which have different energies. They are denoted with *P* and *M* stereo assignments. All structures are shown schematically in Supporting Figure 49. The helical structures are in rapid equilibrium with each other at 20 °C as well as at lower temperatures since in the low temperature experiments no line broadening or signal splitting could be observed in the NMR spectra. Therefore, the calculated thermodynamic equilibrium between the two helices was used to describe the properties of the isomers. If this thermodynamically equilibrated mixture was used, we omitted the helix stereo labels. All other structures were shown to be first order saddle points on the potential energy surface since only one imaginary vibrational mode has been found and confirmed them to be transition state structures.

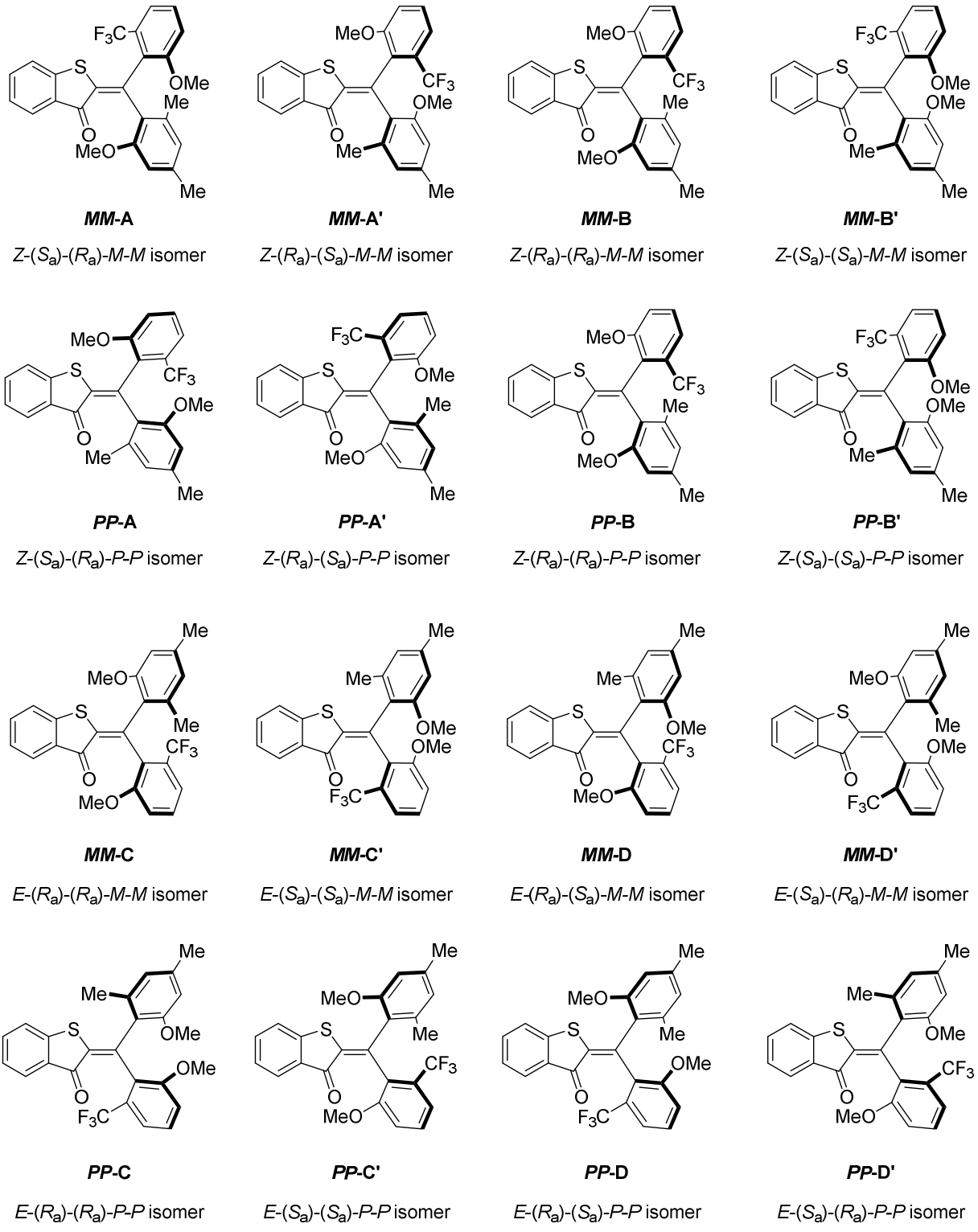

Supplementary Figure 49. All isomeric and enantiomeric states of **1**, which were found to be minimum structures. The corresponding energies are given in Supplementary Table 3.

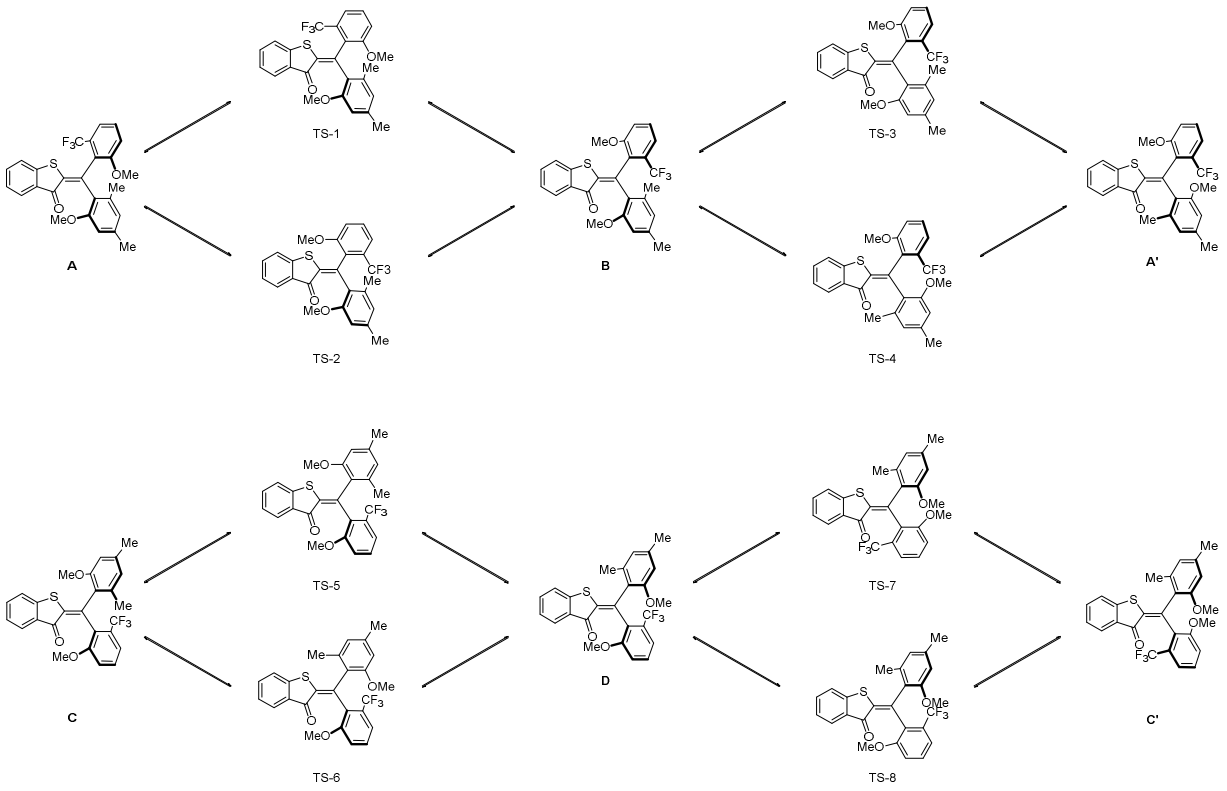

Supplementary Figure 50. Transition state structures between the different isomers of **1.** Only one enantiomeric half of the transition states is shown.

Supplementary Table 3. Calculated minimum and transition state energies for the isomers of HTI **1** and their conversions.

Isomer	G_0 (Hartree)	ΔG (Hartree)	ΔG (kcal mol^{-1})
***M*-A**	-1926.863346	0.004577	2.87211084
***M*-A'**	-1926.8657	0.002185	1.37110819
***P*-A**	-1926.8657	0.002185	1.37110819
***P*-A'**	-1926.863346	0.004577	2.87211084
***M*-B**	-1926.8655	0.002408	1.5110428
***M*-B'**	-1926.8669	0.00103	0.64633475
***P*-B**	-1926.8669	0.00103	0.64633475
***P*-B'**	-1926.8655	0.002408	1.5110428
***M*-C**	-1926.866	0.001936	1.21485833
***M*-C'**	-1926.8679	1E-06	0.00062751
***P*-C**	-1926.8679	0	0
***P*-C'**	-1926.866	0.001936	1.21485833
***M*-D**	-1926.8669	0.001003	0.629392
***M*-D'**	-1926.8645	0.003473	2.17934039
***P*-D**	-1926.8644	0.003476	2.18122291
***P*-D'**	-1926.8669	0.001003	0.629392
TS1	-1926.8115	0.056384	35.3814939
TS2	**-1926.8203**	**0.047614**	**29.8782359**
TS3	-1926.8129	0.055	34.5130208
TS4	-1926.8113	0.056611	35.52393855
TS5	**-1926.8313**	**0.036581**	**22.9549239**
TS6	-1926.8211	0.046818	29.3787383
TS7	-1926.8005	0.067447	42.3236312
TS8	-1926.8065	0.061448	38.5592019

Calculated Ground state geometries - xyz coordinates

***M*-A**				***M*-A'**			
S	-2.199865	0.772639	0.846905	S	2.325543	1.104238	-0.622394
O	-1.034441	-2.251022	-1.322045	O	1.511924	-2.450022	0.764542
C	-3.491379	-0.374401	0.448574	C	3.751193	0.09032	-0.348139
C	-4.828118	-0.257665	0.825353	C	5.074623	0.461003	-0.581556
H	-5.173557	0.583228	1.41448	H	5.322481	1.443268	-0.965231
C	-5.715492	-1.2529	0.421526	C	6.077148	-0.465654	-0.304358
H	-6.758626	-1.176546	0.706408	H	7.111402	-0.191725	-0.478864
C	-5.286261	-2.346076	-0.344666	C	5.774562	-1.740639	0.195308
H	-5.998072	-3.104794	-0.64623	H	6.574146	-2.44112	0.403342
C	-3.952035	-2.451769	-0.714446	C	4.452665	-2.100345	0.421324
H	-3.592339	-3.284716	-1.307584	H	4.188676	-3.078925	0.805574
C	-3.051576	-1.461901	-0.311473	C	3.438181	-1.179423	0.145585
C	-1.609677	-1.436062	-0.618952	C	1.993656	-1.420025	0.315759
C	-0.972047	-0.229298	0.01206	C	1.219609	-0.19916	-0.089784
C	0.332578	0.13056	-0.046158	C	-0.11991	0.008897	0.023913
C	1.418309	-0.810949	-0.458916	C	-1.110757	-1.086435	0.19096
C	2.372963	-0.49183	-1.443724	C	-1.175572	-2.204585	-0.67152
C	3.411916	-1.39037	-1.723323	C	-2.214794	-3.130951	-0.517607
C	3.547102	-2.597032	-1.047365	C	-3.184998	-3.010155	0.470495
C	2.602898	-2.919065	-0.067365	C	-3.118155	-1.915989	1.338841
H	2.697504	-3.855693	0.465508	H	-3.857922	-1.814405	2.121413
C	1.550954	-2.054034	0.221547	C	-2.105285	-0.972394	1.203717
H	4.126863	-1.13218	-2.49722	H	-2.260539	-3.971785	-1.201969
C	0.740366	1.482974	0.473256	C	-0.62116	1.430568	-0.031805
C	1.502541	1.51708	1.672089	C	-0.281131	2.302034	1.037237
C	0.414377	2.717935	-0.118249	C	-1.416913	1.954581	-1.06714
C	1.926593	2.725403	2.226974	C	-0.740984	3.621051	1.056872
C	0.839207	3.926343	0.449315	C	-1.869637	3.277279	-1.041489
C	1.591707	3.926167	1.611284	C	-1.533502	4.101048	0.021468
H	2.506126	2.735468	3.139112	H	-0.486819	4.274691	1.879089
H	0.584691	4.861457	-0.031823	H	-2.469421	3.656158	-1.856074
H	1.920565	4.862492	2.045273	H	-1.883949	5.125816	0.044854
C	-0.367809	2.910549	-1.401001	C	-1.816352	1.126448	-2.263829
C	2.531513	0.249872	3.433806	C	0.874989	2.602285	3.118559
H	2.603408	-0.807782	3.676666	H	1.483764	1.965986	3.757166
H	3.533837	0.657734	3.276392	H	1.469837	3.456209	2.782017
H	2.039865	0.779496	4.254632	H	0.005336	2.955022	3.680221
O	1.752465	0.313673	2.237268	O	0.48395	1.776635	2.020516
F	-0.751259	1.791281	-2.039151	F	-0.784426	0.410381	-2.771141
F	0.360762	3.625888	-2.299535	F	-2.275605	1.890243	-3.281621
F	-1.494119	3.63383	-1.178297	F	-2.805855	0.244077	-1.985353
C	2.307423	0.773915	-2.266795	C	-0.194063	-2.479208	-1.784812
H	2.479166	1.667396	-1.662057	H	0.351807	-1.594775	-2.102274
H	3.071309	0.753681	-3.045097	H	0.538691	-3.221149	-1.455354
H	1.337553	0.886249	-2.752571	H	-0.717327	-2.890303	-2.650786
C	4.676324	-3.549164	-1.355482	C	-4.287353	-4.029045	0.61869
H	5.320786	-3.158274	-2.144601	H	-4.221363	-4.800647	-0.149947
H	5.294266	-3.726893	-0.469853	H	-4.239583	-4.519269	1.596048
H	4.294348	-4.521953	-1.680104	H	-5.271823	-3.55725	0.544516
O	0.617891	-2.33675	1.166347	O	-1.977468	0.08955	2.04068
C	0.692522	-3.571876	1.873541	C	-2.964295	0.314135	3.045833
H	0.607291	-4.426022	1.195042	H	-3.958086	0.444338	2.607552
H	1.621281	-3.650656	2.446873	H	-2.986748	-0.505296	3.77031
H	-0.153589	-3.568533	2.5581	H	-2.666119	1.231913	3.548693

***P*-A**				***P*-A'**			
S	2.325544	-1.104232	-0.622406	S	-2.199865	-0.772637	0.846907
O	1.511922	2.450026	0.764532	O	-1.034438	2.251027	-1.322037
C	3.751193	-0.090315	-0.348147	C	-3.491379	0.374403	0.448575
C	5.074624	-0.460997	-0.581563	C	-4.828119	0.257667	0.825352
H	5.322483	-1.443261	-0.96524	H	-5.173558	-0.583227	1.414479
C	6.077149	0.465659	-0.30436	C	-5.715492	1.252901	0.421523
H	7.111403	0.191731	-0.478865	H	-6.758627	1.176547	0.706402
C	5.774562	1.740643	0.195308	C	-5.286261	2.346077	-0.344668
H	6.574145	2.441123	0.403346	H	-5.998071	3.104794	-0.646235
C	4.452664	2.100348	0.421323	C	-3.952034	2.451771	-0.714445
H	4.188674	3.078927	0.805575	H	-3.592337	3.284718	-1.307582
C	3.438181	1.179427	0.14558	C	-3.051575	1.461903	-0.311471
C	1.993655	1.420028	0.315752	C	-1.609675	1.436065	-0.618947
C	1.21961	0.199162	-0.089793	C	-0.972047	0.2293	0.012064
C	-0.119909	-0.008897	0.023912	C	0.332578	-0.130559	-0.046156
C	-1.110756	1.086433	0.190962	C	1.41831	0.810948	-0.458915
C	-1.175577	2.204582	-0.671518	C	2.372964	0.491827	-1.443723
C	-2.214801	3.130946	-0.517602	C	3.41192	1.390366	-1.72332
C	-3.185003	3.010147	0.470502	C	3.547107	2.597027	-1.047363
C	-3.118154	1.915982	1.338848	C	2.602903	2.919062	-0.067362
H	-3.857918	1.814397	2.121422	H	2.697512	3.855689	0.465511
C	-2.105283	0.97239	1.203721	C	1.550958	2.054034	0.221549
H	-2.260548	3.971781	-1.201964	H	4.126867	1.132174	-2.497217
C	-0.621157	-1.430568	-0.031806	C	0.740366	-1.482975	0.473256
C	-0.281119	-2.302035	1.037233	C	1.502541	-1.517083	1.672088
C	-1.416915	-1.95458	-1.067137	C	0.414372	-2.717935	-0.11825
C	-0.740967	-3.621054	1.056866	C	1.92659	-2.725408	2.226973
C	-1.869636	-3.27728	-1.041487	C	0.839199	-3.926343	0.449314
C	-1.533491	-4.101051	0.021465	C	1.591699	-3.92617	1.611283
H	-0.486795	-4.274697	1.879079	H	2.506121	-2.735474	3.139113
H	-2.469425	-3.656158	-1.856068	H	0.584681	-4.861457	-0.031824
H	-1.883933	-5.125821	0.04485	H	1.920553	-4.862497	2.045271
C	-1.816367	-1.126445	-2.263821	C	-0.367811	-2.910545	-1.401003
C	0.875008	-2.602287	3.11855	C	2.531513	-0.249878	3.433807
H	1.483779	-1.965987	3.757159	H	2.603414	0.807776	3.676666
H	0.005356	-2.955029	3.680211	H	2.039858	-0.779499	4.254631
H	1.469859	-3.456208	2.782006	H	3.533837	-0.657746	3.276399
O	0.483965	-1.776637	2.020508	O	1.752471	-0.313676	2.237265
F	-0.784448	-0.41037	-2.771137	F	-0.751268	-1.791278	-2.03915
F	-2.805872	-0.244082	-1.985335	F	-1.494117	-3.633834	-1.178303
F	-2.275621	-1.89024	-3.281613	F	0.360764	-3.625876	-2.29954
C	-0.19407	2.479208	-1.784811	C	2.307423	-0.773918	-2.266793
H	0.351803	1.594777	-2.102272	H	2.47917	-1.667399	-1.662057
H	-0.717335	2.890301	-2.650784	H	1.33755	-0.886253	-2.752564
H	0.538681	3.221153	-1.455353	H	3.071303	-0.753681	-3.0451
C	-4.287366	4.029029	0.618692	C	4.676326	3.54916	-1.355484
H	-4.221328	4.800679	-0.149891	H	5.320826	3.15824	-2.144557
H	-5.271831	3.557237	0.544424	H	4.294346	4.521926	-1.680173
H	-4.23966	4.519188	1.596086	H	5.294229	3.726948	-0.46984
O	-1.97746	-0.089554	2.040684	O	0.617896	2.336749	1.16635
C	-2.964273	-0.314132	3.045852	C	0.692518	3.571884	1.87353
H	-2.986719	0.505307	3.77032	H	1.621275	3.650674	2.446865
H	-3.95807	-0.444341	2.607585	H	0.607287	4.426022	1.195021
H	-2.666089	-1.231904	3.548717	H	-0.153594	3.568546	2.558086

***M*-B**				***M*-B'**			
S	2.22683	1.136323	-0.631427	S	2.292532	0.847491	-0.81952
O	1.395013	-2.222547	1.161721	O	1.260117	-2.473538	0.952846
C	3.622471	0.066004	-0.416493	C	3.65841	-0.169998	-0.331794
C	4.930728	0.342685	-0.80947	C	5.006154	0.127204	-0.527332
H	5.184391	1.277257	-1.295074	H	5.313005	1.044201	-1.015636
C	5.910689	-0.615403	-0.558326	C	5.954619	-0.786782	-0.074032
H	6.933221	-0.415009	-0.857421	H	7.006923	-0.569547	-0.217542
C	5.599988	-1.82822	0.073051	C	5.57513	-1.977159	0.563122
H	6.38177	-2.554891	0.257711	H	6.334006	-2.669463	0.906696
C	4.292713	-2.092976	0.460069	C	4.229847	-2.2639	0.751052
H	4.023517	-3.021271	0.950856	H	3.906909	-3.176035	1.239516
C	3.300778	-1.141183	0.210014	C	3.268799	-1.355386	0.298547
C	1.872586	-1.278062	0.553384	C	1.809252	-1.525648	0.411871
C	1.118037	-0.057802	0.105888	C	1.106965	-0.345281	-0.197333
C	-0.205357	0.199116	0.270113	C	-0.224218	-0.09266	-0.211596
C	-1.200653	-0.857645	0.609822	C	-1.271285	-1.117922	0.06178
C	-2.138167	-0.706779	1.652793	C	-1.368194	-2.314858	-0.680043
C	-3.099836	-1.69981	1.874344	C	-2.435974	-3.187283	-0.438839
C	-3.180608	-2.840795	1.083454	C	-3.40902	-2.927328	0.521476
C	-2.254759	-2.998472	0.048483	C	-3.317597	-1.74372	1.25836
H	-2.302524	-3.885212	-0.569042	H	-4.066265	-1.528324	2.008507
C	-1.272199	-2.039379	-0.183039	C	-2.272407	-0.85078	1.031663
H	-3.797837	-1.572164	2.694981	H	-2.505892	-4.094465	-1.030185
C	-0.685017	1.612097	0.061107	C	-0.700232	1.271179	-0.638989
C	-0.251414	2.613191	0.970456	C	-1.291453	1.37905	-1.923017
C	-1.541653	2.016926	-0.982908	C	-0.600399	2.441144	0.131115
C	-0.677101	3.937752	0.838889	C	-1.784716	2.597456	-2.392022
C	-1.961111	3.343098	-1.107858	C	-1.09216	3.661862	-0.347408
C	-1.530482	4.295622	-0.195726	C	-1.684941	3.734221	-1.597095
H	-0.349336	4.688698	1.543466	H	-2.237156	2.666774	-3.371062
H	-2.608105	3.626958	-1.924908	H	-1.012952	4.548543	0.267748
H	-1.855879	5.324268	-0.292141	H	-2.068244	4.679331	-1.962025
C	-2.033914	1.049495	-2.03388	C	0.016141	2.537674	1.510199
C	1.080602	3.164907	2.894956	C	-1.931039	0.240557	-3.941057
H	1.72313	2.603349	3.569328	H	-1.845958	-0.779525	-4.308611
H	1.670778	3.925466	2.376941	H	-2.986623	0.516899	-3.871516
H	0.279424	3.64103	3.466777	H	-1.41372	0.918874	-4.625143
O	0.560465	2.200991	1.974843	O	-1.312884	0.235332	-2.651873
F	-3.014841	0.234215	-1.575051	F	0.48822	1.402709	2.03994
F	-1.05229	0.256549	-2.512621	F	-0.878103	3.041358	2.405003
F	-2.557916	1.689786	-3.10603	F	1.054659	3.418511	1.501887
C	-2.138853	0.481929	2.585863	C	-0.378019	-2.712949	-1.747131
H	-2.606823	1.355047	2.120842	H	0.066163	-1.851224	-2.241317
H	-2.70853	0.248365	3.486739	H	0.429255	-3.307877	-1.310865
H	-1.130931	0.771056	2.882322	H	-0.869664	-3.329285	-2.50254
C	-4.231386	-3.895026	1.329547	C	-4.535413	-3.897668	0.779294
H	-4.859097	-3.638249	2.184405	H	-4.57819	-4.669989	0.009449
H	-4.880189	-4.014133	0.45622	H	-4.407883	-4.395787	1.746077
H	-3.774033	-4.869867	1.524293	H	-5.50153	-3.386149	0.806348
O	-0.356129	-2.168316	-1.174367	O	-2.130921	0.306107	1.734094
C	-0.451323	-3.26568	-2.078383	C	-3.112894	0.652395	2.711353
H	-0.308312	-4.221132	-1.564878	H	-4.10442	0.753933	2.260597
H	-1.412889	-3.26925	-2.600477	H	-3.149004	-0.088356	3.515438
H	0.351051	-3.120991	-2.799272	H	-2.794911	1.610683	3.113508

***P*-B**				***P*-B'**			
S	2.292531	-0.847478	-0.819545	S	-2.226831	1.136324	-0.631426
O	1.260118	2.47354	0.952844	O	-1.395015	-2.222546	1.161719
C	3.65841	0.170007	-0.331811	C	-3.622473	0.066006	-0.416492
C	5.006154	-0.127193	-0.527351	C	-4.93073	0.342689	-0.809468
H	5.313005	-1.044186	-1.015665	H	-5.184393	1.277261	-1.295071
C	5.954619	0.786787	-0.074041	C	-5.910691	-0.615398	-0.558323
H	7.006923	0.569552	-0.217553	H	-6.933223	-0.415002	-0.857418
C	5.57513	1.977157	0.563125	C	-5.599992	-1.828216	0.073052
H	6.334007	2.669457	0.906708	H	-6.381774	-2.554886	0.257713
C	4.229848	2.263897	0.751057	C	-4.292717	-2.092973	0.46007
H	3.90691	3.176028	1.239531	H	-4.023521	-3.021269	0.950856
C	3.2688	1.355389	0.298543	C	-3.300781	-1.141181	0.210014
C	1.809253	1.525652	0.411867	C	-1.872589	-1.278061	0.553383
C	1.106966	0.345288	-0.197342	C	-1.118039	-0.057802	0.105886
C	-0.224217	0.092662	-0.211596	C	0.205356	0.199115	0.270111
C	-1.271285	1.117922	0.061787	C	1.200651	-0.857646	0.609822
C	-1.368201	2.314857	-0.680038	C	2.138165	-0.706778	1.652792
C	-2.435985	3.187277	-0.438831	C	3.099836	-1.699807	1.874344
C	-3.409028	2.927316	0.521486	C	3.18061	-2.840792	1.083454
C	-3.317597	1.743709	1.25837	C	2.254762	-2.998471	0.048483
H	-4.066264	1.52831	2.008518	H	2.302529	-3.885211	-0.569043
C	-2.272402	0.850776	1.031673	C	1.272199	-2.03938	-0.183039
H	-2.505911	4.094458	-1.030178	H	3.797838	-1.572158	2.69498
C	-0.700233	-1.271177	-0.638985	C	0.685017	1.612095	0.061106
C	-1.291467	-1.379049	-1.923008	C	0.251416	2.61319	0.970455
C	-0.600388	-2.441143	0.131116	C	1.541654	2.016923	-0.982911
C	-1.78473	-2.597456	-2.392009	C	0.677105	3.937751	0.838888
C	-1.09215	-3.661862	-0.347403	C	1.961113	3.343095	-1.10786
C	-1.684943	-3.734222	-1.597085	C	1.530486	4.295619	-0.195727
H	-2.237181	-2.666774	-3.371044	H	0.34934	4.688697	1.543464
H	-1.012933	-4.548543	0.267751	H	2.608107	3.626955	-1.92491
H	-2.068247	-4.679332	-1.962012	H	1.855884	5.324265	-0.292143
C	0.016163	-2.537672	1.510196	C	2.033912	1.049493	-2.033883
C	-1.931076	-0.240555	-3.941041	C	-1.080585	3.164905	2.894965
H	-1.846	0.779528	-4.308593	H	-1.723106	2.603348	3.569343
H	-1.413762	-0.91887	-4.625131	H	-0.279398	3.641024	3.466776
H	-2.986659	-0.516899	-3.871491	H	-1.670766	3.925467	2.37696
O	-1.31291	-0.235329	-2.651861	O	-0.560463	2.200991	1.974842
F	-0.878068	-3.041366	2.405005	F	1.052289	0.256546	-2.512622
F	0.48824	-1.402705	2.039936	F	3.014842	0.234214	-1.575056
F	1.054689	-3.418502	1.501871	F	2.557912	1.689784	-3.106034
C	-0.378032	2.712952	-1.747129	C	2.138848	0.481931	2.585863
H	0.066145	1.851229	-2.241321	H	2.606808	1.355053	2.120839
H	-0.869681	3.329292	-2.502533	H	1.130926	0.771049	2.882328
H	0.429247	3.307875	-1.310865	H	2.708532	0.248371	3.486735
C	-4.535421	3.897655	0.779309	C	4.231385	-3.895025	1.329552
H	-4.578282	4.669903	0.009395	H	4.859146	-3.638207	2.184362
H	-5.501524	3.386119	0.806498	H	3.774027	-4.869847	1.524382
H	-4.407815	4.395871	1.746032	H	4.880138	-4.014194	0.456197
O	-2.130906	-0.306108	1.734109	O	0.356128	-2.168319	-1.174366
C	-3.1129	-0.652423	2.711336	C	0.451324	-3.265684	-2.07838
H	-3.149034	0.088311	3.515437	H	1.412889	-3.269252	-2.600477
H	-4.104414	-0.753957	2.260554	H	0.308317	-4.221136	-1.564874
H	-2.79492	-1.610717	3.113479	H	-0.351053	-3.120999	-2.799267

***M*-C**				***M*-C'**			
S	1.610025	-1.910654	0.50396	S	-1.575797	-2.021892	-0.510173
O	2.148577	1.690476	-0.881584	O	-2.179781	1.463638	1.132375
C	3.297186	-1.530894	0.112791	C	-3.286769	-1.615489	-0.28051
C	4.379209	-2.399248	0.244901	C	-4.367768	-2.424315	-0.626268
H	4.246674	-3.40767	0.617757	H	-4.21828	-3.397169	-1.078719
C	5.642937	-1.937957	-0.118315	C	-5.653041	-1.949816	-0.373336
H	6.494489	-2.601669	-0.020782	H	-6.50417	-2.56739	-0.63657
C	5.832835	-0.637595	-0.607079	C	-5.865602	-0.694452	0.214296
H	6.826097	-0.305739	-0.883712	H	-6.87588	-0.351313	0.400753
C	4.747365	0.219071	-0.735639	C	-4.781477	0.103186	0.555084
H	4.863539	1.228724	-1.112581	H	-4.915425	1.0774	1.011041
C	3.476264	-0.231087	-0.369716	C	-3.487474	-0.361016	0.303533
C	2.231209	0.553629	-0.444047	C	-2.241178	0.365442	0.600991
C	1.075867	-0.263054	0.068197	C	-1.054002	-0.45819	0.181074
C	-0.205239	0.152532	0.218231	C	0.247008	-0.096354	0.256654
C	-1.283422	-0.820953	0.590792	C	1.343038	-1.076138	-0.019858
C	-2.029759	-0.710255	1.782	C	1.534177	-2.236165	0.759452
C	-3.020941	-1.656521	2.069407	C	2.601434	-3.094842	0.459145
C	-3.312806	-2.709807	1.208556	C	3.483604	-2.847579	-0.585988
C	-2.582911	-2.820891	0.022787	C	3.300352	-1.694577	-1.357061
H	-2.801753	-3.632381	-0.658238	H	3.978889	-1.491546	-2.174597
C	-1.584495	-1.899338	-0.286976	C	2.253663	-0.82021	-1.079387
H	-3.570573	-1.564289	3.000162	H	2.744706	-3.975694	1.076607
C	-0.552508	1.613478	0.106494	C	0.660347	1.29916	0.634726
C	-0.007498	2.514084	1.058675	C	1.309774	1.46889	1.882086
C	-1.420625	2.152338	-0.862841	C	0.500362	2.437488	-0.169683
C	-0.379107	3.85929	1.072477	C	1.803564	2.711109	2.281831
C	-1.776689	3.504367	-0.852203	C	0.992448	3.683349	0.237563
C	-1.267318	4.347743	0.122476	C	1.645054	3.815591	1.452
H	0.025802	4.5295	1.817158	H	2.300765	2.823544	3.234812
H	-2.436923	3.8915	-1.61411	H	0.863911	4.544512	-0.404972
H	-1.549028	5.393603	0.137053	H	2.028584	4.780286	1.761281
C	-1.949552	1.32298	-2.009827	C	-0.207945	2.483244	-1.504981
C	1.493057	2.852472	2.90653	C	2.085939	0.417554	3.899683
H	2.167523	2.216279	3.475405	H	2.040774	-0.588601	4.310479
H	2.065787	3.641906	2.412464	H	3.130612	0.705686	3.753065
H	0.755064	3.295796	3.58096	H	1.602993	1.114361	4.590487
O	0.87318	1.990582	1.948999	O	1.387425	0.355026	2.654693
F	-0.967772	0.652497	-2.651251	F	-1.277926	3.32271	-1.443296
F	-2.558112	2.085544	-2.950193	F	-0.672043	1.321992	-1.987209
F	-2.873899	0.408268	-1.628234	F	0.604571	3.001356	-2.468379
C	-1.79072	0.384241	2.794938	C	0.660701	-2.606523	1.936202
H	-2.222944	1.333514	2.464245	H	0.119893	-1.752756	2.335566
H	-2.258881	0.123959	3.745355	H	-0.07033	-3.368717	1.650613
H	-0.728643	0.556001	2.968155	H	1.275901	-3.028611	2.734234
C	-4.387468	-3.716981	1.5363	C	4.61897	-3.791968	-0.895984
H	-4.852434	-3.502104	2.499751	H	4.668731	-4.60504	-0.17
H	-5.17202	-3.716603	0.773432	H	4.500665	-4.233664	-1.890409
H	-3.978113	-4.730969	1.575154	H	5.579968	-3.269234	-0.889254
O	-0.868256	-1.957698	-1.437887	O	2.017583	0.304451	-1.806876
C	-1.200897	-2.93486	-2.420823	C	2.89643	0.635978	-2.882556
H	-1.040509	-3.950889	-2.047942	H	3.920712	0.783191	-2.527903
H	-2.237215	-2.824414	-2.753656	H	2.882882	-0.136531	-3.656909
H	-0.53014	-2.747941	-3.257033	H	2.513976	1.567953	-3.290666

***P*-C**				***P*-C'**			
S	-1.575796	2.02189	-0.510173	S	1.610023	-1.91066	-0.50396
O	-2.179784	-1.463643	1.132368	O	2.148581	1.69047	0.881578
C	-3.286768	1.615488	-0.280513	C	3.297185	-1.530903	-0.11279
C	-4.367766	2.424315	-0.626271	C	4.379206	-2.39926	-0.244899
H	-4.218278	3.39717	-1.07872	H	4.246668	-3.407682	-0.617751
C	-5.65304	1.949817	-0.37334	C	5.642935	-1.937971	0.118317
H	-6.504169	2.567392	-0.636573	H	6.494485	-2.601686	0.020786
C	-5.865602	0.694452	0.214291	C	5.832835	-0.637609	0.607079
H	-6.875881	0.351314	0.400747	H	6.826098	-0.305754	0.883712
C	-4.781478	-0.103187	0.555077	C	4.747367	0.21906	0.735637
H	-4.915427	-1.077403	1.011033	H	4.863544	1.228713	1.112577
C	-3.487474	0.361014	0.303528	C	3.476266	-0.231095	0.369714
C	-2.241179	-0.365446	0.600985	C	2.231212	0.553623	0.444044
C	-1.054002	0.458186	0.181072	C	1.075868	-0.263061	-0.068198
C	0.247008	0.096352	0.256654	C	-0.205237	0.152529	-0.218233
C	1.343037	1.076138	-0.019854	C	-1.283423	-0.820951	-0.590795
C	1.534174	2.236163	0.759458	C	-2.02976	-0.710248	-1.782003
C	2.60143	3.094844	0.459151	C	-3.020947	-1.656507	-2.069411
C	3.483598	2.847584	-0.585984	C	-3.312817	-2.709794	-1.208562
C	3.300345	1.694585	-1.357062	C	-2.582921	-2.820885	-0.022794
H	3.97888	1.49156	-2.1746	H	-2.801763	-3.632377	0.658227
C	2.253659	0.820215	-1.079388	C	-1.584501	-1.899336	0.28697
H	2.7447	3.975695	1.076614	H	-3.57058	-1.564271	-3.000165
C	0.660347	-1.299162	0.634727	C	-0.552503	1.613476	-0.106495
C	1.309768	-1.468891	1.882091	C	-0.007493	2.514082	-1.058675
C	0.500367	-2.437491	-0.16968	C	-1.420618	2.152335	0.862841
C	1.803556	-2.71111	2.28184	C	-0.379103	3.859287	-1.072478
C	0.992452	-3.683351	0.237569	C	-1.776685	3.504363	0.852203
C	1.64505	-3.815592	1.452009	C	-1.267316	4.34774	-0.122477
H	2.300752	-2.823543	3.234824	H	0.025804	4.529497	-1.817161
H	0.863917	-4.544515	-0.404966	H	-2.436918	3.891496	1.61411
H	2.028579	-4.780287	1.761294	H	-1.549026	5.3936	-0.137055
C	-0.207926	-2.483249	-1.504986	C	-1.949543	1.322978	2.009829
C	2.085913	-0.417555	3.899696	C	1.493082	2.852478	-2.906511
H	2.04074	0.588599	4.310494	H	2.16756	2.216289	-3.475377
H	1.602959	-1.114365	4.590492	H	0.755102	3.295807	-3.580952
H	3.130588	-0.705685	3.753091	H	2.065802	3.641909	-2.412429
O	1.387415	-0.355026	2.654697	O	0.873187	1.990581	-1.948998
F	-0.672041	-1.322	-1.987208	F	-0.967761	0.652491	2.651247
F	-1.277896	-3.322733	-1.443316	F	-2.873895	0.40827	1.628241
F	0.604605	-3.001339	-2.46838	F	-2.558093	2.085545	2.950198
C	0.660701	2.606518	1.936211	C	-1.790716	0.384249	-2.79494
H	0.119871	1.752758	2.335557	H	-2.222941	1.333522	-2.464248
H	1.275908	3.028579	2.734253	H	-0.728639	0.556007	-2.968155
H	-0.07031	3.368735	1.650631	H	-2.258876	0.123968	-3.745358
C	4.618973	3.791966	-0.895969	C	-4.387488	-3.716959	-1.536306
H	4.668642	4.605117	-0.170066	H	-4.852418	-3.502107	-2.49978
H	5.579983	3.269253	-0.889081	H	-3.978152	-4.730957	-1.575109
H	4.500764	4.23355	-1.890454	H	-5.172066	-3.716536	-0.773464
O	2.01758	-0.304444	-1.806879	O	-0.868261	-1.957704	1.437881
C	2.896411	-0.635951	-2.882577	C	-1.200941	-2.934832	2.420836
H	2.882853	0.136572	-3.656915	H	-2.237265	-2.82436	2.753643
H	3.920698	-0.783172	-2.527941	H	-1.040561	-3.950875	2.047989
H	2.513951	-1.567919	-3.2907	H	-0.5302	-2.747901	3.257057

***M*-D**				***M*-D'**			
S	-1.791115	1.946003	0.260081	S	-1.252801	-2.022026	-0.709468
O	-2.165457	-1.788339	-0.790945	O	-2.176655	1.192362	1.291507
C	-3.471476	1.416144	0.055915	C	-2.967063	-1.909692	-0.272467
C	-4.601848	2.214676	0.220032	C	-3.948219	-2.852955	-0.572788
H	-4.515968	3.25819	0.497873	H	-3.70911	-3.75536	-1.122388
C	-5.852666	1.635957	0.015311	C	-5.251393	-2.607792	-0.144944
H	-6.741492	2.243947	0.139605	H	-6.025364	-3.332443	-0.370806
C	-5.982644	0.28812	-0.34896	C	-5.579166	-1.447084	0.570342
H	-6.967534	-0.135314	-0.503573	H	-6.600359	-1.28284	0.891866
C	-4.849495	-0.497852	-0.511292	C	-4.594096	-0.51353	0.86387
H	-4.919286	-1.541771	-0.794758	H	-4.817415	0.392676	1.415093
C	-3.589822	0.070382	-0.303582	C	-3.284343	-0.747288	0.436771
C	-2.299065	-0.627936	-0.435093	C	-2.135286	0.146317	0.66175
C	-1.170569	0.309503	-0.105636	C	-0.898369	-0.437621	0.035616
C	0.147332	-0.003962	-0.043339	C	0.337252	0.115757	0.00465
C	1.178936	1.066216	0.112172	C	1.522943	-0.686926	-0.442028
C	1.338565	2.113757	-0.819923	C	2.314112	-0.324244	-1.550884
C	2.34215	3.071411	-0.612563	C	3.416534	-1.112516	-1.903489
C	3.194268	3.032319	0.483143	C	3.772994	-2.250118	-1.186303
C	3.04167	1.994974	1.410407	C	2.99732	-2.610415	-0.081875
H	3.692669	1.956777	2.273383	H	3.269498	-3.487894	0.489037
C	2.05617	1.030167	1.232411	C	1.889787	-1.849895	0.291274
H	2.459583	3.861272	-1.347454	H	4.003628	-0.825491	-2.769296
C	0.586474	-1.443924	-0.005204	C	0.583701	1.532575	0.442221
C	0.181237	-2.237299	1.101076	C	1.437591	1.72652	1.560207
C	1.424391	-2.048164	-0.95822	C	0.075054	2.68681	-0.181151
C	0.64977	-3.542387	1.255059	C	1.778056	3.005049	2.004823
C	1.877757	-3.363562	-0.805826	C	0.415953	3.966145	0.274271
C	1.499102	-4.09891	0.304812	C	1.264516	4.122267	1.357424
H	0.351774	-4.131385	2.110812	H	2.431269	3.132478	2.856311
H	2.511935	-3.804251	-1.560992	H	0.018652	4.836233	-0.231473
H	1.853732	-5.114816	0.430451	H	1.528116	5.114316	1.703322
C	1.842758	-1.3328	-2.21844	C	-0.86592	2.720545	-1.366187
C	-1.100887	-2.395077	3.123957	C	2.764935	0.690667	3.273341
H	-1.760707	-1.724778	3.670666	H	2.974866	-0.335732	3.565629
H	-1.655148	-3.291096	2.829908	H	3.696266	1.186541	2.985323
H	-0.257863	-2.6752	3.7621	H	2.307359	1.221488	4.11302
O	-0.666395	-1.655733	1.982559	O	1.86428	0.595613	2.169155
F	0.801881	-0.72097	-2.833876	F	-2.058123	3.27032	-1.025501
F	2.372284	-2.176508	-3.13438	F	-1.145912	1.537663	-1.945236
F	2.784466	-0.381231	-2.005753	F	-0.362369	3.50838	-2.354831
C	0.52364	2.261042	-2.085913	C	2.002129	0.873689	-2.417758
H	-0.132696	1.417892	-2.274655	H	2.124447	1.813806	-1.874892
H	-0.089717	3.165195	-2.039472	H	2.673694	0.899037	-3.276769
H	1.195137	2.366847	-2.942019	H	0.978536	0.842525	-2.793215
C	4.263225	4.077319	0.686432	C	4.960453	-3.090677	-1.58704
H	4.284128	4.790139	-0.139384	H	5.518148	-2.62687	-2.402246
H	4.094028	4.636129	1.612139	H	5.643698	-3.235921	-0.745294
H	5.252928	3.617701	0.765461	H	4.643112	-4.084535	-1.918442
O	1.842703	0.022793	2.118381	O	1.124009	-2.158097	1.368671
C	2.699599	-0.104467	3.252016	C	1.418249	-3.332687	2.121483
H	3.740984	-0.249885	2.950275	H	1.348167	-4.232461	1.502835
H	2.625028	0.76915	3.906321	H	2.411427	-3.277487	2.577294
H	2.350403	-0.986064	3.785629	H	0.664381	-3.373365	2.90526

***P*-D**				**P-D'**			
S	1.252804	-2.022022	-0.709476	S	-1.791119	-1.946002	0.260084
O	2.176654	1.192362	1.291507	O	-2.165456	1.78833	-0.79098
C	2.967065	-1.90969	-0.27247	C	-3.471479	-1.416144	0.055911
C	3.948221	-2.852952	-0.572792	C	-4.601852	-2.214671	0.220038
H	3.709113	-3.755355	-1.122395	H	-4.515973	-3.258182	0.49789
C	5.251395	-2.607791	-0.144943	C	-5.852669	-1.635953	0.015311
H	6.025365	-3.332442	-0.370805	H	-6.741497	-2.24394	0.139612
C	5.579166	-1.447086	0.570348	C	-5.982645	-0.288119	-0.348975
H	6.600358	-1.282843	0.891875	H	-6.967536	0.135314	-0.503593
C	4.594095	-0.513532	0.863875	C	-4.849496	0.497849	-0.511316
H	4.817414	0.392673	1.415101	H	-4.919285	1.541764	-0.794794
C	3.284343	-0.747288	0.436771	C	-3.589823	-0.070384	-0.3036
C	2.135287	0.146317	0.661749	C	-2.299065	0.627931	-0.435114
C	0.898371	-0.437621	0.035611	C	-1.170572	-0.309504	-0.105644
C	-0.337251	0.115757	0.004649	C	0.147329	0.003961	-0.043342
C	-1.522942	-0.686926	-0.442029	C	1.178932	-1.066215	0.112178
C	-2.314111	-0.324244	-1.550886	C	1.338563	-2.113761	-0.819911
C	-3.416532	-1.112517	-1.903491	C	2.342149	-3.071413	-0.612544
C	-3.772993	-2.250118	-1.186305	C	3.194265	-3.032313	0.483163
C	-2.997317	-2.610417	-0.081878	C	3.041664	-1.994964	1.410422
H	-3.269492	-3.487898	0.489031	H	3.692661	-1.956762	2.273399
C	-1.889786	-1.849896	0.291272	C	2.056162	-1.03016	1.232419
H	-4.003625	-0.825494	-2.7693	H	2.459583	-3.861278	-1.34743
C	-0.583702	1.532574	0.442222	C	0.586472	1.443923	-0.005208
C	-1.437591	1.726516	1.560208	C	0.181223	2.237304	1.101063
C	-0.075054	2.686811	-0.181147	C	1.424406	2.048155	-0.958214
C	-1.778059	3.005044	2.004826	C	0.649759	3.542391	1.255046
C	-0.415955	3.966144	0.274278	C	1.877774	3.363552	-0.805821
C	-1.264519	4.122263	1.35743	C	1.499106	4.098906	0.304808
H	-2.431272	3.132471	2.856314	H	0.351757	4.131394	2.110793
H	-0.018653	4.836234	-0.231462	H	2.511965	3.804235	-1.56098
H	-1.52812	5.114311	1.70333	H	1.853737	5.114812	0.430447
C	0.865919	2.72055	-1.366183	C	1.842791	1.332783	-2.218424
C	-2.764943	0.690657	3.273334	C	-1.100957	2.395111	3.123906
H	-2.97488	-0.335744	3.565613	H	-1.760806	1.724827	3.670596
H	-2.307375	1.221471	4.113021	H	-0.257959	2.675239	3.762083
H	-3.69627	1.186534	2.985309	H	-1.655196	3.291129	2.829814
O	-1.864277	0.595607	2.169156	O	-0.666417	1.655744	1.982541
F	1.145917	1.537669	-1.945231	F	0.80193	0.720931	-2.833862
F	2.05812	3.270331	-1.025498	F	2.784513	0.38123	-2.005718
F	0.362364	3.508381	-2.354827	F	2.372315	2.176489	-3.134367
C	-2.002127	0.873689	-2.417759	C	0.523641	-2.261054	-2.085903
H	-2.12446	1.813806	-1.874896	H	-0.132706	-1.417912	-2.274643
H	-0.97853	0.842533	-2.793204	H	1.195142	-2.366846	-2.942008
H	-2.673683	0.899029	-3.276778	H	-0.089701	-3.165216	-2.039465
C	-4.960463	-3.090668	-1.587029	C	4.263225	-4.077309	0.686457
H	-5.518043	-2.626959	-2.402369	H	4.284117	-4.790146	-0.139345
H	-4.643154	-4.084603	-1.918229	H	5.252929	-3.617689	0.765462
H	-5.643806	-3.235724	-0.74533	H	4.094042	-4.636101	1.612178
O	-1.124006	-2.158099	1.368667	O	1.842689	-0.022783	2.118384
C	-1.418243	-3.332694	2.121473	C	2.699582	0.104487	3.25202
H	-2.411423	-3.277499	2.577283	H	2.625014	-0.769128	3.90633
H	-1.348158	-4.232465	1.502822	H	3.740966	0.249911	2.950282
H	-0.664377	-3.373373	2.905251	H	2.35038	0.986085	3.785629

TS1				TS2			
S	-2.576824	0.788658	-0.403234	S	-2.624626	1.430337	0.232785
O	-0.826564	-2.628321	0.200921	O	-1.435345	-2.229475	-0.369742
C	-3.674002	-0.543044	-0.046552	C	-3.92039	0.249617	0.032343
C	-5.064193	-0.459908	0.01611	C	-5.286712	0.529635	0.062018
H	-5.579597	0.479857	-0.141346	H	-5.650454	1.538147	0.219282
C	-5.775562	-1.625295	0.292775	C	-6.176301	-0.527017	-0.115927
H	-6.857252	-1.582922	0.350022	H	-7.242268	-0.330522	-0.094254
C	-5.119181	-2.84769	0.4983	C	-5.718695	-1.837403	-0.321679
H	-5.696661	-3.738677	0.712928	H	-6.432149	-2.641019	-0.458473
C	-3.733514	-2.913184	0.42687	C	-4.355405	-2.100075	-0.349698
H	-3.199887	-3.844015	0.579568	H	-3.972645	-3.101385	-0.509047
C	-3.013174	-1.748426	0.150121	C	-3.45812	-1.043554	-0.169147
C	-1.54574	-1.65798	0.036488	C	-1.989981	-1.160198	-0.178688
C	-1.108552	-0.217093	-0.260686	C	-1.319347	0.20032	0.058117
C	0.211268	0.185687	-0.324024	C	0.053772	0.374858	0.054412
C	1.175541	-0.982827	-0.300541	C	0.834039	-0.888691	-0.227339
C	1.757795	-1.363738	0.920679	C	1.078199	-1.817459	0.802863
C	2.643524	-2.439203	0.982956	C	1.777047	-2.992834	0.548984
C	2.949757	-3.167157	-0.171189	C	2.202174	-3.295429	-0.750025
C	2.357946	-2.790382	-1.376029	C	1.905415	-2.404435	-1.776153
H	2.595064	-3.342683	-2.279966	H	2.208651	-2.639919	-2.791205
C	1.471809	-1.711781	-1.455966	C	1.224312	-1.204202	-1.535394
H	3.092643	-2.726687	1.92487	H	1.982887	-3.692502	1.348505
C	1.924072	-0.969266	3.287228	C	0.85072	-2.340399	3.133896
O	1.379519	-0.632817	2.013491	O	0.570747	-1.490561	2.024771
H	1.656076	-1.989386	3.579291	H	0.428111	-3.339698	2.990158
H	3.013243	-0.861157	3.299205	H	1.927648	-2.421137	3.311482
H	1.48472	-0.265232	3.991576	H	0.377103	-1.870113	3.993828
C	0.871311	1.52835	-0.19363	C	0.884002	1.620228	0.034077
C	2.314457	1.551593	-0.241147	C	0.339017	2.943258	-0.040512
C	0.333917	2.79233	0.256103	C	2.318273	1.609547	-0.129775
C	3.067912	2.405059	0.57453	C	0.988594	3.97642	-0.724452
C	1.098984	3.660645	1.030994	C	2.976888	2.663284	-0.759257
C	2.443737	3.413953	1.283313	C	2.292584	3.807285	-1.152516
H	4.141487	2.294141	0.622521	H	0.483442	4.917328	-0.886782
H	0.654536	4.583285	1.378439	H	4.047805	2.612645	-0.89381
H	3.013797	4.069558	1.929357	H	2.800614	4.596174	-1.692632
C	0.870044	-1.33473	-2.787503	C	0.883391	-0.305838	-2.701457
H	1.297722	-1.937897	-3.590275	H	1.227247	-0.747547	-3.637922
H	-0.214042	-1.482741	-2.798336	H	-0.196621	-0.148723	-2.779327
H	1.052984	-0.281234	-3.017197	H	1.343599	0.681493	-2.607998
C	-0.921286	3.459172	-0.260353	C	3.283954	0.635786	0.532789
F	-0.68716	4.774669	-0.515371	F	4.411171	1.302281	0.919331
F	-1.972794	3.456832	0.591778	F	3.733742	-0.36975	-0.2456
F	-1.322394	2.939971	-1.442164	F	2.790464	0.105838	1.667575
C	3.895044	-4.343214	-0.097875	C	2.976283	-4.564181	-1.01703
H	4.134873	-4.721448	-1.093365	H	3.006919	-4.793553	-2.083943
H	4.832051	-4.071208	0.396904	H	4.010459	-4.472433	-0.667681
H	3.45683	-5.16679	0.475473	H	2.53536	-5.418203	-0.49572
C	4.319477	0.504903	-1.075741	C	-1.469125	4.429012	0.542809
H	4.875677	1.415794	-1.310679	H	-0.827647	5.213518	0.948396
H	4.615196	0.123725	-0.095718	H	-1.75565	4.664368	-0.48463
H	4.514257	-0.248777	-1.834499	H	-2.360018	4.328212	1.157659
O	2.906827	0.737647	-1.130237	O	-0.812189	3.156153	0.619751

TS3				TS4			
S	2.171838	0.60136	0.952262	S	-2.237501	-0.797075	0.633812
O	1.243028	-2.900367	1.281799	O	-1.867204	2.838475	1.131047
C	3.424175	-0.481839	0.306932	C	-3.641452	0.110728	0.043163
C	4.748613	-0.152476	0.032263	C	-4.89164	-0.411727	-0.280958
H	5.123598	0.850919	0.194058	H	-5.095468	-1.472787	-0.201684
C	5.581872	-1.154383	-0.465904	C	-5.877499	0.472962	-0.715843
H	6.612649	-0.915695	-0.701827	H	-6.853058	0.085214	-0.986135
C	5.111886	-2.458373	-0.664674	C	-5.632334	1.849766	-0.806769
H	5.779787	-3.217733	-1.053065	H	-6.417081	2.514597	-1.146699
C	3.79338	-2.781483	-0.354099	C	-4.388735	2.362112	-0.451716
H	3.4206	-3.792257	-0.473586	H	-4.187095	3.426371	-0.488507
C	2.948466	-1.775994	0.110872	C	-3.388917	1.477216	-0.048557
C	1.564869	-1.927847	0.635938	C	-2.053814	1.823985	0.487042
C	0.833044	-0.586309	0.512496	C	-1.111257	0.636107	0.375834
C	-0.378192	-0.053958	0.145592	C	0.221849	0.359215	0.182365
C	-1.660722	-0.646969	-0.375268	C	1.426013	1.153878	-0.264837
C	-1.986321	-2.027027	-0.201634	C	2.56367	0.431524	-0.783729
C	-3.241992	-2.559494	-0.498617	C	3.803583	1.03168	-1.003076
C	-4.241235	-1.765834	-1.044469	C	3.992985	2.39277	-0.807116
C	-3.920511	-0.4417	-1.318516	C	2.878813	3.134396	-0.439912
H	-4.664172	0.181117	-1.802241	H	2.97589	4.209742	-0.344164
C	-2.679855	0.132822	-1.018111	C	1.622998	2.568536	-0.194128
H	-3.437615	-3.605346	-0.310864	H	4.627365	0.432985	-1.363066
C	-1.24208	-4.194912	0.514849	C	3.525916	-1.682387	-1.454202
O	-1.004965	-2.808476	0.273878	O	2.3991	-0.87226	-1.11371
H	-2.016096	-4.33657	1.274694	H	3.970624	-1.364237	-2.401174
H	-1.529575	-4.711991	-0.405026	H	4.281225	-1.663096	-0.664379
H	-0.297155	-4.583908	0.880627	H	3.132094	-2.689167	-1.562714
C	-0.459351	1.434545	0.455637	C	0.531667	-1.068272	0.636417
C	-1.104295	1.76735	1.671899	C	0.997401	-1.184314	1.966508
C	0.09126	2.484807	-0.29598	C	0.318794	-2.252443	-0.084845
C	-1.203535	3.094883	2.095694	C	1.238715	-2.437001	2.538109
C	-0.005099	3.811319	0.134459	C	0.549296	-3.503004	0.492864
C	-0.651303	4.111068	1.32369	C	1.007891	-3.59142	1.799179
H	-1.703209	3.339263	3.022437	H	1.598522	-2.515489	3.554294
H	0.418799	4.603297	-0.469063	H	0.377801	-4.401388	-0.08612
H	-0.728569	5.13926	1.655519	H	1.190439	-4.560863	2.246722
C	-2.561235	1.563321	-1.511221	C	0.555855	3.576617	0.112108
H	-2.533259	2.301582	-0.710328	H	-0.256054	3.526661	-0.615188
H	-1.685408	1.709226	-2.137819	H	0.111904	3.43284	1.092243
H	-3.430528	1.790983	-2.128708	H	0.97596	4.581406	0.065081
C	0.797871	2.313724	-1.62205	C	-0.124542	-2.298405	-1.529359
F	0.78759	1.060936	-2.113141	F	-0.329491	-1.103699	-2.106167
F	2.091913	2.708122	-1.56459	F	-1.276637	-3.006069	-1.672342
F	0.223635	3.0996	-2.57659	F	0.787415	-2.950881	-2.301683
C	-5.611356	-2.323046	-1.331837	C	5.342215	3.031816	-1.006227
H	-6.225543	-2.323417	-0.424701	H	5.250249	4.102089	-1.20029
H	-6.133655	-1.727082	-2.082624	H	5.961344	2.910389	-0.110629
H	-5.556042	-3.355226	-1.685713	H	5.88238	2.573421	-1.837927
O	-1.600182	0.719442	2.377197	O	1.182344	-0.01212	2.63017
C	-2.26355	0.968672	3.6191	C	1.641727	-0.046057	3.983057
H	-3.149553	1.593646	3.476559	H	2.630335	-0.508485	4.055044
H	-2.564904	-0.008971	3.988566	H	1.705142	0.994105	4.295117
H	-1.58967	1.439206	4.340536	H	0.93682	-0.577716	4.628612

TS5				TS6			
S	-1.569631	2.157278	-0.209798	S	-2.036437	2.08921	0.479444
O	-1.987051	-1.513358	1.015297	O	-2.064881	-1.747555	-0.161568
C	-3.226917	1.680647	0.156551	C	-3.630623	1.403405	0.189383
C	-4.34803	2.50953	0.08497	C	-4.833239	2.110491	0.17485
H	-4.261627	3.545963	-0.219744	H	-4.859541	3.179703	0.347317
C	-5.587135	1.968166	0.415774	C	-6.004949	1.39931	-0.069048
H	-6.469855	2.595444	0.362738	H	-6.950884	1.928642	-0.085108
C	-5.71401	0.628682	0.816206	C	-5.983356	0.01406	-0.293681
H	-6.690281	0.233087	1.06922	H	-6.910122	-0.51459	-0.481076
C	-4.590047	-0.182839	0.888259	C	-4.777605	-0.673728	-0.275743
H	-4.656003	-1.218825	1.199657	H	-4.729986	-1.742847	-0.446463
C	-3.343968	0.353418	0.549373	C	-3.59656	0.033343	-0.031228
C	-2.064501	-0.370953	0.588024	C	-2.246583	-0.55288	0.014253
C	-0.911989	0.501492	0.08576	C	-1.18583	0.511464	0.304274
C	0.380987	0.026708	-0.057471	C	0.168066	0.245403	0.39416
C	1.701839	0.705021	-0.245237	C	1.388442	1.107686	0.581703
C	1.846754	2.128353	-0.344998	C	2.680849	0.458211	0.649899
C	3.032704	2.793977	-0.046143	C	3.867333	1.098455	0.291148
C	4.19621	2.080385	0.219946	C	3.885531	2.454339	-0.000472
C	4.139344	0.699702	0.060684	C	2.69965	3.153556	0.208204
H	5.06179	0.13307	0.118975	H	2.717894	4.236326	0.148144
C	2.959114	0.000013	-0.20762	C	1.489524	2.542941	0.539186
H	3.06162	3.874021	-0.060115	H	4.792111	0.540013	0.278107
C	0.806745	4.239147	-0.893278	C	3.922499	-1.577609	1.049773
O	0.777805	2.81165	-0.806775	O	2.724163	-0.802997	1.127208
H	0.966615	4.693884	0.087476	H	4.279631	-1.653666	0.019632
H	1.579735	4.567563	-1.591322	H	4.70613	-1.157837	1.686123
H	-0.172342	4.523868	-1.271926	H	3.647712	-2.564917	1.414515
C	0.475605	-1.462575	0.192547	C	0.465286	-1.217645	0.092885
C	0.820208	-1.90697	1.485283	C	0.399703	-2.150271	1.150826
C	0.196275	-2.421145	-0.78695	C	0.760395	-1.68815	-1.188584
C	0.905256	-3.269128	1.770182	C	0.656646	-3.498264	0.931743
C	0.276185	-3.787136	-0.502303	C	1.011016	-3.050908	-1.412492
C	0.633825	-4.201747	0.772474	C	0.963267	-3.942409	-0.355241
H	1.174515	-3.610008	2.760175	H	0.618679	-4.207729	1.746779
H	0.06839	-4.513799	-1.274793	H	1.238171	-3.399398	-2.409634
H	0.702113	-5.259468	0.9971	H	1.161326	-4.994155	-0.525185
C	3.205049	-1.46069	-0.556705	C	0.428025	3.545752	0.941617
H	3.002608	-2.15855	0.25472	H	-0.204087	3.862467	0.112503
H	2.620897	-1.772509	-1.41843	H	-0.201403	3.179916	1.748697
H	4.258296	-1.569042	-0.820304	H	0.931983	4.438315	1.315299
C	-0.228341	-2.014387	-2.174759	C	0.73951	-0.778482	-2.390671
F	0.5462	-1.031486	-2.699534	F	1.534226	0.311627	-2.266793
F	-1.505347	-1.555254	-2.221215	F	-0.506243	-0.306021	-2.662639
F	-0.171126	-3.044795	-3.04887	F	1.148975	-1.409755	-3.516603
C	5.472399	2.781169	0.60151	C	5.142655	3.147595	-0.451182
H	5.490849	2.980539	1.67871	H	5.196094	3.164697	-1.54546
H	6.346942	2.172434	0.364704	H	5.170655	4.183944	-0.108038
H	5.568783	3.742869	0.09245	H	6.03584	2.635204	-0.088109
O	1.043575	-0.927342	2.399205	C	0.006423	-2.495603	3.491078
C	1.388125	-1.295781	3.736225	H	-0.259777	-1.86165	4.33441
H	2.325888	-1.858104	3.764634	H	-0.763676	-3.260556	3.354006
H	1.511547	-0.358802	4.27504	H	0.970219	-2.975153	3.686304
H	0.591341	-1.882224	4.202721	O	0.079089	-1.625338	2.361936

TS7				TS8			
S	-1.501893	-1.823295	0.496143	S	1.882929	-1.309213	-0.909554
O	-2.530518	1.756427	0.88429	O	2.751964	2.262541	-0.936335
C	-3.211817	-1.554574	0.112252	C	3.477646	-0.991315	-0.199961
C	-4.185424	-2.535657	-0.06235	C	4.482126	-1.925108	0.042915
H	-3.943314	-3.588612	0.017688	H	4.345802	-2.972735	-0.197438
C	-5.486984	-2.12417	-0.347136	C	5.672955	-1.473649	0.611942
H	-6.256419	-2.872912	-0.497319	H	6.46146	-2.186999	0.823037
C	-5.818119	-0.76577	-0.439661	C	5.867584	-0.119775	0.912952
H	-6.837363	-0.47406	-0.661964	H	6.801385	0.204504	1.356089
C	-4.84154	0.204174	-0.238583	C	4.868174	0.808124	0.633136
H	-5.078285	1.260993	-0.282559	H	5.01164	1.864248	0.830349
C	-3.532477	-0.202592	0.018879	C	3.664038	0.356814	0.095897
C	-2.390666	0.670874	0.363234	C	2.543743	1.18913	-0.414722
C	-1.076775	-0.070759	0.210997	C	1.259522	0.34953	-0.438565
C	0.247599	0.229535	0.010293	C	-0.091102	0.446406	-0.19061
C	1.131018	-0.969921	0.349266	C	-0.833069	-0.842308	-0.499741
C	1.295866	-2.066212	-0.530252	C	-0.758996	-1.966342	0.35811
C	2.050813	-3.172127	-0.147339	C	-1.415759	-3.150236	0.029984
C	2.66168	-3.219962	1.111727	C	-2.141799	-3.257649	-1.160133
C	2.491544	-2.14372	1.975611	C	-2.181751	-2.163702	-2.019632
H	2.94832	-2.171418	2.95943	H	-2.719461	-2.242624	-2.958774
C	1.731922	-1.020304	1.616177	C	-1.538418	-0.959438	-1.710002
H	2.176377	-4.006098	-0.825403	H	-1.362732	-4.003378	0.693188
C	0.661044	-3.104218	-2.598436	C	0.073861	-2.899837	2.405319
O	0.679446	-1.96778	-1.73787	O	-0.003018	-1.821794	1.477183
H	1.667441	-3.372092	-2.934543	H	-0.913715	-3.155324	2.80137
H	0.197967	-3.96675	-2.109307	H	0.528521	-3.786796	1.95337
H	0.062994	-2.811477	-3.459408	H	0.707058	-2.544713	3.216189
C	1.063671	1.471857	-0.299758	C	-1.003999	1.599609	0.135972
C	2.372497	1.217489	-0.850363	C	-0.658358	2.958918	-0.134735
C	0.87575	2.856393	0.032545	C	-2.370209	1.43509	0.556473
C	3.457815	2.075472	-0.648148	C	-1.625446	3.948616	-0.361627
C	1.963841	3.714906	0.204886	C	-3.31725	2.44141	0.371559
C	3.263386	3.306179	-0.051327	C	-2.962886	3.674191	-0.159228
H	4.443327	1.785865	-0.982216	H	-1.319157	4.934176	-0.679508
H	1.779126	4.737456	0.499539	H	-4.336667	2.271626	0.685355
H	4.097968	3.971842	0.129738	H	-3.714492	4.43201	-0.342099
C	1.572511	0.103719	2.615327	C	-1.607874	0.180266	-2.700295
H	0.530776	0.421609	2.704418	H	-2.271997	0.975889	-2.349542
H	1.918274	-0.21121	3.600914	H	-0.626871	0.631534	-2.867984
H	2.151431	0.985529	2.325072	H	-1.989636	-0.17213	-3.659579
C	-0.437899	3.605203	0.066341	C	-2.919486	0.27947	1.375907
F	-0.981254	3.717865	1.292702	F	-1.992363	-0.282126	2.170683
F	-1.32842	3.088798	-0.801207	F	-3.510259	-0.701126	0.655755
F	-0.266267	4.895191	-0.352188	F	-3.892767	0.718672	2.224272
C	3.480369	-4.424413	1.510072	C	-2.872278	-4.536839	-1.490293
H	2.880987	-5.339186	1.473765	H	-3.143786	-4.577933	-2.546757
H	4.326549	-4.568213	0.831028	H	-2.264325	-5.414891	-1.257382
H	3.87459	-4.318749	2.522183	H	-3.795636	-4.61929	-0.906939
O	2.499561	0.113221	-1.606381	O	0.644885	3.23922	-0.166917
C	3.789825	-0.324679	-2.040625	C	1.091343	4.556086	-0.504925
H	4.24209	0.401488	-2.720868	H	0.797297	4.82203	-1.523591
H	4.453795	-0.506975	-1.19198	H	0.699018	5.291294	0.202148

References

1. Lee, W.-H.; Zhu, J.; Hu, C.-M. Small molecule modifiers of the HEC1-NEK2 interaction in G2/M. 2016.
2. Moinet, G.; Leriche, C.; Kergoat, M. New 2-acyl-3-alkoxybenzo-furan or -thiophene derivatives, useful as hypoglycemics, particularly for treating diabetes and its complications, stimulate secretion of insulin. 2015.
3. Jehle, B. G. Synthesis and Characterization of HTI Photoswitches with Eight States. Bachelor thesis, Ludwig-Maximilians-Universität, Munich, 2018.
4. Megerle, U.; Lechner, R.; König, B.; Riedle, E., Laboratory apparatus for the accurate, facile and rapid determination of visible light photoreaction quantum yields. *Photochem. Photobiol. Sci.* **2010,** *9* (10), 1400-1406.
5. Geertsema, E. M.; van der Molen, S. J.; Martens, M.; Feringa, B. L., Optimizing rotary processes in synthetic molecular motors. *Proc. Natl. Acad. Sci. U. S. A.* **2009,** *106* (40), 16919-16924.
6. Gerwien, A.; Schildhauer, M.; Thumser, S.; Mayer, P.; Dube, H., Direct evidence for hula twist and single-bond rotation photoproducts. *Nat. Commun.* **2018,** *9* (1), 2510.
7. Gerwien, A.; Mayer, P.; Dube, H., Photon-Only Molecular Motor with Reverse Temperature-Dependent Efficiency. *J. Am. Chem. Soc.* **2018,** *140*, 16442-16445.
8. Gerwien, A.; Mayer, P.; Dube, H., Green light powered molecular state motor enabling eight-shaped unidirectional rotation. *Nat. Commun.* **2019,** *10* (1), 4449.
9. Bruker (2012), SAINT. Bruker-AXS Inc., Madison, Wisconsin, USA.
10. Sheldrick, G. M. (1996), SADABS, University of Göttingen, Germany.
11. Sheldrick, G., Crystal structure refinement with SHELXL. *Acta Crystallogr., Sect. C: Cryst. Struct. Commun.* **2015,** *71* (1), 3-8.
12. Spek, A. L., *Acta Cryst.* **2015,** *C71*, 9-18.
13. Farrugia, L. J., *J. Appl. Cryst.* **2012,** *45*, 849-854.
14. Frisch, M. J.; Trucks, G. W.; Schlegel, H. B.; Scuseria, G. E.; Robb, M. A.; Cheeseman, J. R.; Scalmani, G.; Barone, V.; Mennucci, B.; Petersson, G. A.; Nakatsuji, H.; Caricato, M.; Li, X.; Hratchian, H. P.; Izmaylov, A. F.; Bloino, J.; Zheng, G.; Sonnenberg, J. L.; Hada, M.; Ehara, M.; Toyota, K.; Fukuda, R.; Hasegawa, J.; Ishida, M.; Nakajima, T.; Honda, Y.; Kitao, O.; Nakai, H.; Vreven, T.; Montgomery, J., J. A.; Peralta, J. E.; Ogliaro, F.; Bearpark, M.; Heyd, J. J.; Brothers, E.; Kudin, K. N.; Staroverov, V. N.; Kobayashi, R.; Normand, J.; Raghavachari, K.; Rendell, A.; Burant, J. C.; Iyengar, S. S.; Tomasi, J.; Cossi, M.; Rega, N.; Millam, J. M.;

Klene, M.; Knox, J. E.; Cross, J. B.; Bakken, V.; Adamo, C.; Jaramillo, J.; Gomperts, R.; Stratmann, R. E.; Yazyev, O.; Austin, A. J.; Cammi, R.; Pomelli, C.; Ochterski, J. W.; Martin, R. L.; Morokuma, K.; Zakrzewski, V. G.; Voth, G. A.; Salvador, P.; Dannenberg, J. J.; Dapprich, S.; Daniels, A. D.; Farkas, Ö.; Foresman, J. B.; Ortiz, J. V.; Cioslowski, J.; Fox, D. J. *Gaussian 09, Revision A.02*, Gaussian, Inc.: Wallingford CT, 2009.

9. References

1. Gerwien, A.; Reinhardt, T.; Mayer, P.; Dube, H., Synthesis of Double-Bond-Substituted Hemithioindigo Photoswitches. *Org. Lett.* **2018,** *20* (1), 232-235.
2. Gerwien, A.; Schildhauer, M.; Thumser, S.; Mayer, P.; Dube, H., Direct evidence for hula twist and single-bond rotation photoproducts. *Nat. Commun.* **2018,** *9* (1), 2510.
3. Gerwien, A.; Mayer, P.; Dube, H., Photon-Only Molecular Motor with Reverse Temperature-Dependent Efficiency. *J. Am. Chem. Soc.* **2018,** *140* (48), 16442-16445.
4. Gerwien, A.; Mayer, P.; Dube, H., Green light powered molecular state motor enabling eight-shaped unidirectional rotation. *Nat. Commun.* **2019,** *10* (1), 4449.
5. Feringa, B. L., Molecular Switches. Wiley-VCH: Weinheim, **2011**.
6. Balzani, V.; Venturi, M.; Credi, A., Molecular devices and machines. Wiley-VCH: Weinheim, **2003**.
7. Dürr, H.; Bouas-Laurent, H., Photochromism: Molecules and Systems. Elsevier Science: Amsterdam, **2003**.
8. Ward, C. L.; Elles, C. G., Cycloreversion Dynamics of a Photochromic Molecular Switch via One-Photon and Sequential Two-Photon Excitation. *J. Phys. Chem. A* **2014,** *118* (43), 10011-10019.
9. Renth, F.; Foca, M.; Petter, A.; Temps, F., Ultrafast transient absorption spectroscopy of the photo-induced Z–E isomerization of a photochromic furylfulgide. *Chem. Phys. Lett.* **2006,** *428* (1), 62-67.
10. Klajn, R., Spiropyran-based dynamic materials. *Chem. Soc. Rev.* **2014,** *43* (1), 148-184.
11. Vetráková, Ľ.; Ladányi, V.; Al Anshori, J.; Dvořák, P.; Wirz, J.; Heger, D., The absorption spectrum of cis-azobenzene. *Photochem. Photobiol. Sci.* **2017,** *16* (12), 1749-1756.
12. Irie, M., Diarylethenes for memories and switches. *Chem. Rev.* **2000,** *100* (5), 1685-1716.
13. Matsuda, K.; Irie, M., Diarylethene as a photoswitching unit. *J. Photochem. Photobiol. C* **2004,** *5* (2), 169-182.
14. Uchida, K.; Irie, M., A photochromic dithienylethene that turns yellow by UV irradiation. *Chem. Lett.* **1995,** *24* (11), 969-970.
15. Irie, M., Photochromism of diarylethene molecules and crystals. *Proc. Jpn. Acad., Ser. B, Phys.* **2010,** *86* (5), 472-483.
16. Irie, M.; Fukaminato, T.; Matsuda, K.; Kobatake, S., Photochromism of diarylethene molecules and crystals: memories, switches, and actuators. *Chem. Rev.* **2014,** *114* (24), 12174-12277.
17. Yokoyama, Y., Fulgides for memories and switches. *Chem. Rev.* **2000,** *100* (5), 1717-1740.
18. Islamova, N. I.; Chen, X.; DiGirolamo, J. A.; Silva, Y.; Lees, W. J., Thermal stability and photochromic properties of a fluorinated indolylfulgimide in a protic and aprotic solvent. *J. Photochem. Photobiol. C* **2008,** *199* (1), 85-91.
19. Irie, M.; Lifka, T.; Kobatake, S.; Kato, N., Photochromism of 1, 2-bis (2-methyl-5-phenyl-3-thienyl) perfluorocyclopentene in a single-crystalline phase. *J. Am. Chem. Soc.* **2000,** *122* (20), 4871-4876.
20. Kießwetter, R.; Pustet, N.; Brandl, F.; Mannschreck, A., 1′, 3′, 3′-Trimethyl-6-nitrospiro [2H-1-benzopyran-2, 2′-indoline]: its thermal enantiomerization and the equilibration with its merocyanine. *Tetrahedron: Asymmetry* **1999,** *10* (24), 4677-4687.
21. Gehrtz, M.; Bräuchle, C.; Voitlaender, J., Photochromic forms of 6-nitrobenzospiropyran. Emission spectroscopic and ODMR investigations. *J. Am. Chem. Soc.* **1982,** *104* (8), 2094-2101.
22. Feeney, M. J.; Thomas III, S. W., Tuning the negative photochromism of water-soluble spiropyran polymers. *Macromolecules* **2018,** *51* (20), 8027-8037.
23. Bergmann, E. D.; Weizmann, A.; Fischer, E., Structure and polarity of some polycyclic spirans. *J. Am. Chem. Soc.* **1950,** *72* (11), 5009-5012.
24. Berkovic, G.; Krongauz, V.; Weiss, V., Spiropyrans and spirooxazines for memories and switches. *Chem. Rev.* **2000,** *100* (5), 1741-1754.
25. Cabrera, I.; Krongauz, V.; Ringsdorf, H., Photo-and Thermochromic Liquid Crystal Polysiloxanes. *Angew. Chem. Int. Ed. Engl.* **1987,** *26* (11), 1178-1180.
26. Krongauz, V.; Fishman, S.; Goldburt, E., Quasi-crystals. Growth from photochromic spiropyrans on irradiation in a constant electric field. *J. Phys. Chem. Lett.* **1978,** *82* (23), 2469-2474.

27. Inouye, M.; Noguchi, Y.; Isagawa, K., Sensitive and Selective Coloration of Cryptand-Type Crown Spirobenzopyrans for Alkaline-Earth Metal Cations. *Angew. Chem. Int. Ed. Engl.* **1994,** *33* (11), 1163-1166.
28. Inouye, M.; Akamatsu, K.; Nakazumi, H., New crown spirobenzopyrans as light-and ion-responsive dual-mode signal transducers. *J. Am. Chem. Soc.* **1997,** *119* (39), 9160-9165.
29. Lutsyk, P.; Janus, K.; Sworakowski, J.; Generali, G.; Capelli, R.; Muccini, M., Photoswitching of an n-type organic field effect transistor by a reversible photochromic reaction in the dielectric film. *J. Phys. Chem. Lett. C* **2011,** *115* (7), 3106-3114.
30. Kanj, A. B.; Chandresh, A.; Gerwien, A.; Grosjean, S.; Bräse, S.; Wang, Y.; Dube, H.; Heinke, L., Proton-conduction photomodulation in spiropyran-functionalized MOFs with large on–off ratio. *Chem. Sci.* **2020,** *11* (5), 1404-1410.
31. Romani, A.; Chidichimo, G.; Formoso, P.; Manfredi, S.; Favaro, G.; Mazzucato, U., Photochromic behavior of a spiro-indolino-oxazine in reverse-mode polymer-dispersed liquid crystal films. *J. Phys. Chem. Lett. B* **2002,** *106* (37), 9490-9495.
32. Macchione, M.; De Filpo, G.; Nicoletta, F. P.; Chidichimo, G., Photochromic reverse mode polymer dispersed liquid crystals. *Liq. Cryst.* **2005,** *32* (3), 315-319.
33. Dreos, A.; Wang, Z.; Udmark, J.; Ström, A.; Erhart, P.; Börjesson, K.; Nielsen, M. B.; Moth-Poulsen, K., Solar Energy Storage: Liquid Norbornadiene Photoswitches for Solar Energy Storage. *Adv. Energy Mater.* **2018,** *8* (18), 1703401.
34. Mansø, M.; Petersen, A. U.; Wang, Z.; Erhart, P.; Nielsen, M. B.; Moth-Poulsen, K., Molecular solar thermal energy storage in photoswitch oligomers increases energy densities and storage times. *Nat. Commun.* **2018,** *9* (1), 1-7.
35. Lennartson, A.; Roffey, A.; Moth-Poulsen, K., Designing photoswitches for molecular solar thermal energy storage. *Tetrahedron Lett.* **2015,** *56* (12), 1457-1465.
36. Goerner, H.; Fischer, C.; Gierisch, S.; Daub, J., Dihydroazulene/vinylheptafulvene photochromism: Effects of substituents, solvent, and temperature in the photorearrangement of dihydroazulenes to vinylheptafulvenes. *J. Phys. Chem. Lett.* **1993,** *97* (16), 4110-4117.
37. Petersen, A. U.; Jevric, M.; Elm, J.; Olsen, S. T.; Tortzen, C. G.; Kadziola, A.; Mikkelsen, K. V.; Nielsen, M. B., Azulenium chemistry: towards new derivatives of photochromic dihydroazulenes. *Org. Biomol. Chem.* **2016,** *14* (8), 2403-2412.
38. Broman, S. L.; Petersen, M. Å.; Tortzen, C. G.; Kadziola, A.; Kilså, K.; Nielsen, M. B., Arylethynyl derivatives of the dihydroazulene/vinylheptafulvene photo/thermoswitch: tuning the switching event. *J. Am. Chem. Soc.* **2010,** *132* (26), 9165-9174.
39. Alves, J.; Wiedbrauk, S.; Gräfe, D.; Walden, S. L.; Blinco, J. P.; Barner-Kowollik, C., It's a Trap: Thiol-Michael Chemistry on a DASA Photoswitch. *Chem. Eur. J.* **2020,** *26* (4), 809-813.
40. Lerch, M. M.; Szymański, W.; Feringa, B. L., The (photo) chemistry of Stenhouse photoswitches: guiding principles and system design. *Chem. Soc. Rev.* **2018,** *47* (6), 1910-1937.
41. Seshadri, S.; Gockowski, L. F.; Lee, J.; Sroda, M.; Helgeson, M. E.; de Alaniz, J. R.; Valentine, M. T., Self-regulating photochemical Rayleigh-Bénard convection using a highly-absorbing organic photoswitch. *Nat. Commun.* **2020,** *11* (1), 1-8.
42. Hemmer, J. R.; Poelma, S. O.; Treat, N.; Page, Z. A.; Dolinski, N. D.; Diaz, Y. J.; Tomlinson, W.; Clark, K. D.; Hooper, J. P.; Hawker, C., Tunable visible and near infrared photoswitches. *J. Am. Chem. Soc.* **2016,** *138* (42), 13960-13966.
43. Villarón, D.; Wezenberg, S., Stiff-Stilbene Photoswitches: From Fundamental Studies to Emergent Applications. *Angew. Chem. Int. Ed. Engl.* **2020**, *59*, 13192
44. Dong, M.; Babalhavaeji, A.; Samanta, S.; Beharry, A. A.; Woolley, G. A., Red-Shifting Azobenzene Photoswitches for in Vivo Use. *Acc. Chem. Res.* **2015,** *48* (10), 2662-2670.
45. Beharry, A. A.; Woolley, G. A., Azobenzene photoswitches for biomolecules. *Chem. Soc. Rev.* **2011,** *40* (8), 4422-4437.
46. Smith, A. M.; Mancini, M. C.; Nie, S., Second window for in vivo imaging. *Nature Nanotechnol.* **2009,** *4* (11), 710-711.

47. Koumura, N.; Zijlstra, R. W. J.; van Delden, R. A.; Harada, N.; Feringa, B. L., Light-drivenmonodirectional molecular rotor. *Nature* **1999,** *1999*, 152 - 155.
48. Feringa, B. L., The Art of Building Small: From Molecular Switches to Motors (Nobel Lecture). *Angew. Chem. Int. Ed. Engl.* **2017,** *56* (37), 11060-11078.
49. Petermayer, C.; Dube, H., Indigoid Photoswitches: Visible Light Responsive Molecular Tools. *Acc. Chem. Res.* **2018,** *51* (5), 1153-1163.
50. Wiedbrauk, S.; Dube, H., Hemithioindigo-An emerging photoswitch. *Tetrahedron Lett.* **2015,** *56*.
51. Qian, H.; Pramanik, S.; Aprahamian, I., Photochromic hydrazone switches with extremely long thermal half-lives. *J. Am. Chem. Soc.* **2017,** *139* (27), 9140-9143.
52. Nogly, P.; Weinert, T.; James, D.; Carbajo, S.; Ozerov, D.; Furrer, A.; Gashi, D.; Borin, V.; Skopintsev, P.; Jaeger, K.; Nass, K.; Båth, P.; Bosman, R.; Koglin, J.; Seaberg, M.; Lane, T.; Kekilli, D.; Brünle, S.; Tanaka, T.; Wu, W.; Milne, C.; White, T.; Barty, A.; Weierstall, U.; Panneels, V.; Nango, E.; Iwata, S.; Hunter, M.; Schapiro, I.; Schertler, G.; Neutze, R.; Standfuss, J., Retinal isomerization in bacteriorhodopsin captured by a femtosecond x-ray laser. *Science* **2018,** *361* (6398).
53. Fuß, W., Previtamin D: Z–E photoisomerization via a Hula-twist conical intersection. *Phys. Chem. Chem. Phys.* **2019,** *21* (13), 6776-6789.
54. Kay, E. R.; Leigh, D. A., Beyond switches: Rotaxane-and catenane-based synthetic molecular motors. *Pure and Appl. Chem.* **2008,** *80* (1), 17-29.
55. Fletcher, S. P.; Dumur, F.; Pollard, M. M.; Feringa, B. L., A reversible, unidirectional molecular rotary motor driven by chemical energy. *Science* **2005,** *310* (5745), 80-82.
56. Stoddart, J. F., Mechanically Interlocked Molecules (MIMs)—Molecular Shuttles, Switches, and Machines (Nobel Lecture). *Angew. Chem. Int. Ed. Engl.* **2017,** *56* (37), 11094-11125.
57. Sauvage, J.-P., From Chemical Topology to Molecular Machines (Nobel Lecture). *Angew. Chem. Int. Ed. Engl.* **2017,** *56* (37), 11080-11093.
58. Balzani, V.; Juris, A, Photochemistry and Photophysics, Vol. 1. Wiley-VCH: Weinheim, **2014**.
59. Shankar, R., Principles of Quantum Mechanics, Vol 2. Springer Science+Business Media S.A.: Berlin, **1994**.
60. Born, M.; Oppenheimer, R., Zur Quantentheorie der Molekeln. *Ann. Phys.* **1927,** *389* (20), 457-484.
61. Condon, E., A Theory of Intensity Distribution in Band Systems. *Phys. Rev.***1926,** *28* (6), 1182-1201.
62. Franck, J.; Dymond, E. G., Elementary processes of photochemical reactions. *J. Chem. Soc. Faraday Trans.* **1926,** *21*, 536-542.
63. Klan; J. W., Photochemistry of organic compounds. Wiley-VCH: Weinheim. **2009**.
64. Turro, N. J.; McVey, J.; Ramamurthy, V.; Lechtken, P., Adiabatic Photoreactions of Organic Molecules. *Angew. Chem. Int. Ed. Engl.* **1979,** *18* (8), 572-586.
65. Turro, N. J.; Ramamurthy, V.; Katz, T. J., Energy Storage and Release: Direct and Sensitized Photoreactions of Dewar Benzene and Prismane. *Nouv. J. Chim.* **1977,** *1*.
66. Carr, R. V.; Kim, B.; McVey, J. K.; Yang, N.; Gerhartz, W.; Michl, J., Photochemistry and photophysics of 1, 4-dewarnaphthalene. *Chem. Phys. Lett.* **1976,** *39* (1), 57-60.
67. Ingham, K.; El-Bayoumi, M. A., Photoinduced double proton transfer in a model hydrogen bonded base pair. Effects of temperature and deuterium substitution. *J. Am. Chem. Soc.* **1974,** *96* (6), 1674-1682.
68. Ingham, K. C.; Abu-Elgheit, M.; El-Bayoumi, M. A., Confirmation of biprotonic phototautomerism in 7-azaindole hydrogen-bonded dimers. *J. Am. Chem. Soc.* **1971,** *93* (20), 5023-5025.
69. Whitesell, J. K.; Minton, M. A.; Tran, V. D., The non-equilibration of excited rotamers (NEER) principle. Ground-state conformational bias in triene photocyclizations. *J. Am. Chem. Soc.* **1989,** *111* (4), 1473-1476.
70. Martinez, T. J., Seaming is believing. *Nature* **2010,** *467* (7314), 412-413.
71. Goldberg, A.; Murakami, A.; Kanda, K.; Kobayashi, T.; Nakamura, S.; Uchida, K.; Sekiya, H.; Fukaminato, T.; Kawai, T.; Kobatake, S.; Irie, M., Rotational Isomerization of Dithienylethenes: A Study on the Mechanism Determining Quantum Yield of Cyclization Reaction. *J. Phys. Chem. A* **2003,** *107* (25), 4982-4988.

72. Crecca, C. R.; Roitberg, A. E., Theoretical study of the isomerization mechanism of azobenzene and disubstituted azobenzene derivatives. *J. Phys. Chem. A* **2006,** *110* (26), 8188-8203.
73. Bandara, H. D.; Burdette, S. C., Photoisomerization in different classes of azobenzene. *Chem. Soc. Rev.* **2012,** *41* (5), 1809-1825.
74. Cordes, T.; Schadendorf, T.; Rück-Braun, K.; Zinth, W., Chemical control of Hemithioindigo-photoisomerization–Substituent-effects on different molecular parts. *Chem. Phys. Lett.* **2008,** *455* (4-6), 197-201.
75. Plotner, J.; Dreuw, A., Molecular Mechanism of the Z/E-Photoisomerization of Hemithioindigo Hemistilbene. *J. Phys. Chem. A* **2009,** *113* (43), 11882-11887.
76. Wilcken, R.; Schildhauer, M.; Rott, F.; Huber, L. A.; Guentner, M.; Thumser, S.; Hoffmann, K.; Oesterling, S.; de Vivie-Riedle, R.; Riedle, E., Complete mechanism of hemithioindigo motor rotation. *J. Am. Chem. Soc.* **2018,** *140* (15), 5311-5318.
77. Ruan, C.-Y.; Lobastov, V. A.; Srinivasan, R.; Goodson, B. M.; Ihee, H.; Zewail, A. H., Ultrafast diffraction and structural dynamics: The nature of complex molecules far from equilibrium. *Proc. Natl. Acad. Sci. USA* **2001,** *98* (13), 7117-7122.
78. Velema, W. A.; Van Der Berg, J. P.; Hansen, M. J.; Szymanski, W.; Driessen, A. J.; Feringa, B. L., Optical control of antibacterial activity. *Nat. Chem.* **2013,** *5* (11), 924-928.
79. Tochitsky, I.; Polosukhina, A.; Degtyar, V. E.; Gallerani, N.; Smith, C. M.; Friedman, A.; Van Gelder, R. N.; Trauner, D.; Kaufer, D.; Kramer, R. H., Restoring visual function to blind mice with a photoswitch that exploits electrophysiological remodeling of retinal ganglion cells. *Neuron* **2014,** *81* (4), 800-813.
80. Bléger, D.; Schwarz, J.; Brouwer, A. M.; Hecht, S., o-Fluoroazobenzenes as Readily Synthesized Photoswitches Offering Nearly Quantitative Two-Way Isomerization with Visible Light. *J. Am. Chem. Soc.* **2012,** *134* (51), 20597-20600.
81. Konrad, D. B.; Savasci, G.; Allmendinger, L.; Trauner, D.; Ochsenfeld, C.; Ali, A. M., Computational Design and Synthesis of a Deeply Red-Shifted and Bistable Azobenzene. *J. Am. Chem. Soc.* **2020,** *142* (14), 6538-6547.
82. Hansen, M. J.; Lerch, M. M.; Szymanski, W.; Feringa, B. L., Direct and Versatile Synthesis of Red-Shifted Azobenzenes. *Angew. Chem. Int. Ed. Engl.* **2016,** *55* (43), 13514-13518.
83. Siewertsen, R.; Neumann, H.; Buchheim-Stehn, B.; Herges, R.; Näther, C.; Renth, F.; Temps, F., Highly Efficient Reversible Z−E Photoisomerization of a Bridged Azobenzene with Visible Light through Resolved S1(nπ*) Absorption Bands. *J. Am. Chem. Soc.* **2009,** *131* (43), 15594-15595.
84. Sell, H.; Näther, C.; Herges, R., Amino-substituted diazocines as pincer-type photochromic switches. *Beilstein J. Org. Chem.* **2013,** *9* (1), 1-7.
85. Moormann, W.; Tellkamp, T.; Stadler, E.; Röhricht, F.; Näther, C.; Puttreddy, R.; Rissanen, K.; Gescheidt, G.; Herges, R., Efficient Conversion of Light to Chemical Energy: Directional, Chiral Photoswitches with Very High Quantum Yields. *Angew. Chem. Int. Ed. Engl.* **2020,** *59* (35), 15081-15086.
86. Yang, Y.; Hughes, R. P.; Aprahamian, I., Near-Infrared Light Activated Azo-BF2 Switches. *J. Am. Chem. Soc.* **2014,** *136* (38), 13190-13193.
87. Salvador, M. A.; Almeida, P.; Reis, L.; Santos, P., Near-infrared absorbing delocalized cationic azo dyes. *Dyes Pigm.* **2009,** *82* (2), 118-123.
88. Samanta, S.; Babalhavaeji, A.; Dong, M. x.; Woolley, G. A., Photoswitching of ortho-Substituted Azonium Ions by Red Light in Whole Blood. *Angew. Chem. Int. Ed. Engl.* **2013,** *125* (52), 14377-14380.
89. Tellkamp, T.; Shen, J.; Okamoto, Y.; Herges, R., Diazocines on molecular platforms. *Eur. J. Org. Chem.* **2014,** *2014* (25), 5456-5461.
90. Joshi, D. K.; Mitchell, M. J.; Bruce, D.; Lough, A. J.; Yan, H., Synthesis of cyclic azobenzene analogues. *Tetrahedron* **2012,** *68* (41), 8670-8676.
91. Bureš, F., Fundamental aspects of property tuning in push–pull molecules. *RSC Adv.* **2014,** *4* (102), 58826-58851.

92. Åstrand, P.-O.; Sommer-Larsen, P.; Hvilsted, S.; Ramanujam, P. S.; Bak, K. L.; Sauer, S. P. A., Five-membered rings as diazo components in optical data storage devices: an ab initio investigation of the lowest singlet excitation energies. *Chem. Phys. Lett.* **2000,** *325* (1), 115-119.
93. Peng, B.; Li, H.; Li, Y.; Lv, Z.; Wu, M.; Zhao, C., A photoresponsive azopyridine-based supramolecular elastomer for self-healing strain sensors. *Chem. Eng. J.* **2020,** *395*, 125079.
94. Qiu, F.; Chen, C.; Zhou, Q.; Cao, Z.; Cao, G.; Guan, Y.; Yang, D., Synthesis, physical properties and simulation of thermo-optic switch based on azo benzothiazole heterocyclic polymer. *Opt. Mater.* **2014,** *36* (7), 1153-1159.
95. Vela, S.; Krüger, C.; Corminboeuf, C., Exploring chemical space in the search for improved azoheteroarene-based photoswitches. *Phys. Chem. Chem. Phys.* **2019,** *21* (37), 20782-20790.
96. Kitaev, Y. P.; Arbuzov, A. E., Tautomerism and geometric isomerism of nitrogen containing derivatives of carbonyl compounds. *Bull. Acad. Sci. USSR, Div. Chem. Sci.* **1960,** *9* (8), 1306-1311.
97. Schmittel, M.; Ruechardt, C., Aliphatic azo compounds. XVI. Stereoisomerization and homolytic decomposition of cis and trans bridgehead diazenes. *J. Am. Chem. Soc.* **1987,** *109* (9), 2750-2759.
98. Wolf, R. A.; Grosso, P. V.; Platt, A. E.; Staples, T. L.; White, J. E., Thermally stable, photoactive polymerizable diazenes. Applications in polymer technology.J. Polym. Sci. Pol. Chem. **1999,** *37* (16), 3203-3213.
99. Baeyer, A., Ueber die Verbindungen der Indigogruppe. *Ber. Dtsch. Chem. Ges.* **1883,** *16* (2), 2188-2204.
100. Izmail'skii, V. A. Mostoslavskii, M. A, Absorption spectra of 3-oxo-2,3-dihydrothianaphthene and its derivatives. II. Isomerism of 2-benzylidene-3-oxo-2,3-dihydrothionaphthene. *Ukr. Khem. Zh.* **1961,** *27*, 234-237.
101. Huang, C.-Y.; Bonasera, A.; Hristov, L.; Garmshausen, Y.; Schmidt, B. M.; Jacquemin, D.; Hecht, S., N, N′-disubstituted indigos as readily available red-light photoswitches with tunable thermal half-Lives. *J. Am. Chem. Soc.* **2017,** *139* (42), 15205-15211.
102. Matsumoto, Y.; Tanaka, H., A simple preparative method of N-arylindigos and substitution effect in uv/visible absorption. *Heterocycles* **2003,** *60* (8), 1805-1810.
103. Wyman, G. M., The interaction of excited thioindigo with hydroxylic compounds and its implications on the photostability of indigo. *J. Chem. Soc. Chem. Commun.* **1971,** (21), 1332-1334.
104. Yamazaki, S.; Sobolewski, A. L.; Domcke, W., Molecular mechanisms of the photostability of indigo. *Phys. Chem. Chem. Phys.* **2011,** *13* (4), 1618-1628.
105. Moreno, M.; Ortiz-Sánchez, J. M.; Gelabert, R.; Lluch, J. M., A theoretical study of the photochemistry of indigo in its neutral and dianionic (leucoindigo) forms. *Phys. Chem. Chem. Phys.* **2013,** *15* (46), 20236-20246.
106. Cui, G.; Thiel, W., Nonadiabatic dynamics of a truncated indigo model. *Phys. Chem. Chem. Phys.* **2012,** *14* (35), 12378-12384.
107. Kobayashi, T.; Rentzepis, P., On the picosecond kinetics and photostability of indigo and 6, 6′-dimethoxyindigo. *J. Chem. Phys.* **1979,** *70* (2), 886-892.
108. Iwakura, I.; Yabushita, A.; Kobayashi, T., Kinetic isotope effect on the proton-transfer in indigo carmine. *Chem. Phys. Lett.* **2010,** *484* (4-6), 354-357.
109. Dittmann, M.; Graupner, F. F.; Maerz, B.; Oesterling, S.; de Vivie-Riedle, R.; Zinth, W.; Engelhard, M.; Lüttke, W., Photostability of 4,4′-Dihydroxythioindigo, a Mimetic of Indigo. *Angew. Chem. Int. Ed. Engl.* **2014,** *53* (2), 591-594.
110. Friedländer, P.; Kunz, K., Über N, N′-Diphenyl-indigo. *Ber. Dtsch. Chem. Ges.* **1922,** *55* (6), 1597-1607.
111. Farka, D.; Scharber, M.; Głowacki, E. D.; Sariciftci, N. S., Reversible Photochemical Isomerization of N, N′-Di (t-butoxycarbonyl) indigos. *J. Phys. Chem. A* **2015,** *119* (15), 3563-3568.
112. Giuliano, C.; Hess, L.; Margerum, J., Cis-trans isomerization and pulsed laser studies of substituted indigo dyes. *J. Am. Chem. Soc.* **1968,** *90* (3), 587-594.
113. Weinstein, J.; Wyman, G. M., Spectroscopic Studies on Dyes. II. The Structure of N,N'-Dimethylindigo1. *J. Am. Chem. Soc.* **1956,** *78* (16), 4007-4010.

114. Weinstein, J.; Wyman, G. M., Spectroscopic Studies on Dyes. II. The Structure of N, N'-Dimethylindigo1. *J. Am. Chem. Soc.* **1956,** *78* (16), 4007-4010.
115. Huber, L. A.; Mayer, P.; Dube, H., Photoisomerization of Mono-Arylated Indigo and Water-Induced Acceleration of Thermal cis-to-trans Isomerization. *ChemPhotoChem* **2018,** *2* (6), 458-464.
116. Wyman, G. M.; Brode, W. R., The Relation between the Absorption Spectra and the Chemical Constitution of Dyes XXII. cis-trans Isomerism in Thioindigo Dyes1. *J. Am. Chem. Soc.* **1951,** *73* (4), 1487-1493.
117. Wyman, G. M.; Zarnegar, B. M., Excited state chemistry of indigoid dyes. II. Interaction of thio-and selenoindigo dyes with hydroxylic compounds and its implications on the photostability of indigo. *J. Phys. Chem. Lett.* **1973,** *77* (10), 1204-1207.
118. Wyman, G. M.; Zarnegar, B. M.; Whitten, D. G., Excited-state chemistry of indigoid dyes. III. Interaction of indigo and thioindigo with tin (IV) tetraphenyltetrahydroporphyrin triplets. Photosensitized isomerization of thioindigo. *J. Phys. Chem. Lett.* **1973,** *77* (21), 2584-2586.
119. Wyman, G. M.; Zarnegar, B. M., Excited state chemistry of indigoid dyes. I. Fluorescence versus cis-trans isomerization. *J. Phys. Chem. Lett.* **1973,** *77* (6), 831-837.
120. Kirsch, A. D.; Wyman, G. M., Excited state chemistry of indigoid dyes. 5. The intermediacy of the triplet state in the direct photoisomerization and the effect of substituents. *J. Phys. Chem. Lett.* **1977,** *81* (5), 413-420.
121. Lüttke, W.; Klessinger, M., Theoretische und spektroskopische Untersuchungen an Indigofarbstoffen, I. Infrarot-und Lichtabsorptionsspektren einfacher Indigofarbstoffe. *Chem. Ber.* **1964,** *97* (8), 2342-2357.
122. Erler, M.; Haucke, G.; Paetzold, R., Untersuchungen zur trans-cis-Isomerisierung indigoider Verbindungen. *Z. Phys. Chem.* **1977,** *258* (1), 315-320.
123. Koeppe, B.; Römpp, F., Reversible Spatial Control in Aqueous Media by Visible Light: A Thioindigo Photoswitch that is Soluble and Operates Efficiently in Water. *Chem. Eur. J.* **2018,** *24* (54), 14382-14386.
124. Hooper, M.; Pitkethly, W., 2-Arylmethylideneindolin-3-ones: stereochemistry and reduction with sodium borohydride. *J. Chem. Soc., Perkin Trans. 1* **1972**, 1607-1613.
125. Hooper, M.; Pitkethly, W. N., 2-Arylmethyleneindolin-3-ones: photodimerisation to cyclobutane derivatives. *J. Chem. Soc., Perkin Trans. 1* **1973**, 2804-2808.
126. M. A. Mostoslavskii, M. D. K., I. N. Shevchuk, *Zh. Fiz. Khim.* **1970,** *44* (44), 1008-1012.
127. Arai, T.; Ikegami, M., Novel photochromic dye based on hydrogen bonding. *Chem. Lett.* **1999,** *28* (9), 965-966.
128. Petermayer, C.; Thumser, S.; Kink, F.; Mayer, P.; Dube, H., Hemiindigo: Highly Bistable Photoswitching at the Biooptical Window. *J. Am. Chem. Soc.* **2017,** *139* (42), 15060-15067.
129. Petermayer, C.; Dube, H., Circular Dichroism Photoswitching with a Twist: Axially Chiral Hemiindigo. *J. Am. Chem. Soc.* **2018,** *140* (42), 13558-13561.
130. Friedländer, P., Ueber schwefelhaltige Analoga der Indigogruppe. *Ber. Dtsch. Chem. Ges.* **1906,** *39* (1), 1060-1066.
131. Friedländer, P.; Woroshzow, N., Über Thioindigofarbstoffe der Naphthalinreihe. *Liebigs Ann.* **1912,** *388* (1), 1-23.
132. Dalgliesh, C. E.; Mann, F. G., 124. The preparation and properties of thionaphthindoles. *J. Chem. Soc.* **1947**, 653-658.
133. Mukherjee, C.; De, A., Application of directed metallation in synthesis, Part 2: An expedient synthesis of methoxybenzo [b] thiophenes. *Synlett* **2002,** *2002* (02), 0325-0327.
134. Zheng, G.; Ma, X.; Liu, B.; Dong, Y.; Wang, M., Iodine-Catalyzed Intramolecular Oxidative Thiolation of Vinylic Carbon-Hydrogen Bonds via Tandem Iodocyclization and Dehydroiodination: Construction of 2-Methylene-3-thiophenones. *Adv. Synth. Catal.* **2014,** *356* (4), 743-748.
135. Huber, L. A.; Hoffmann, K.; Thumser, S.; Böcher, N.; Mayer, P.; Dube, H., Direct Observation of Hemithioindigo-Motor Unidirectionality. *Angew. Chem. Int. Ed. Engl.* **2017,** *129* (46), 14728-14731.

136. Konieczny, M. T.; Konieczny, W.; Wolniewicz, S.; Wierzba, K.; Suda, Y.; Sowiński, P., New domino reaction. One pot synthesis of 4,7-dihydroxythioaurone derivatives from benzaldehydes and 4-acetyl-2-oxo-benz[1,3]oxathiole. *Tetrahedron* **2005,** *61* (36), 8648-8655.
137. Fraleoni, A.; Zanirato, P., Boron Trifluoride-assisted Reactions of 1-Benzothiophen-3 (2 H)-one with Various Ketones: a Convenient Entry to 2-Methylene-1-benzothiophen-3 (2 H)-one and/or 6 H-Di [1] benzothieno [3, 2-b: 2, 3-e] pyran Derivatives. *J. Chem. Res.* **1999,** *23* (9), 542-543.
138. Schönberg, A.; Junghans, K., Versuche mit Epoxiden, V. Untersuchungen in der Benzthiophenreihe. *Chem. Ber.* **1966,** *99* (4), 1241-1244.
139. Brooker, L. G.; White, F. L., Non-ionized cyanine dyes. Google Patents, **1956**.
140. Mostoslavskii, M.; Izmailskii, V.; Shevchuk, I., O prirode fototronykh izmeneii spektrov pogloshcheniya tioinogenidov. Zh. Obshch. Khim. 1962, 32 (2), 660-660.
141. Boykin, D. W.; Parham, W. E., Reactions of lithio derivatives of carboxylic acids. 2. Alkylations and cyclizations of substituted acrylic acids. *J. Org. Chem.* **1979,** *44* (3), 424-428.
142. Gabbutt, C. D.; Hepworth, J. D.; Heron, B. M.; Kanjia, M., Ring contraction of sulfenamides derived from thiochroman-4-ones. *Tetrahedron* **1994,** *50* (3), 827-834.
143. Tamura, Y.; Takebe, Y.; Bayomi, S.; Mukai, C.; Ikeda, M., Murase M. andKise M.,"Conversions of Thiochroman-4-ones into 1, Z-Benzothiazepine, Benzo-[b] thiophen, and 1, 2-Benzisothiarole Systems via Sulphimide Intermediates". *J. Chem. Soc. Perkin Trans.* **1981,** *1*, 1037-1040.
144. Still, I. W.; Thomas, M., Photochemical rearrangements of substituted thiochromanone sulfoxides. *Tetrahedron Lett.* **1970,** *11* (48), 4225-4228.
145. Lévai, A.; Patonay, T., Reaction of E-2-arylidene-1-indanones, Z-aurones, Z-1-thioaurones and Z-2-arylidene-2, 3-dihydro-1H-indol-3-ones with diazomethane. *J. Heterocycl. Chem.* **1999,** *36* (3), 747-753.
146. Awad, S. B.; Abdul-Malik, N. F., Studies on Benzo [b] thiophen derivatives. Synthesis and reactions of 2-p-substituted Benzoylbenzo [b] thiophen-3 (2H) ones. *Aust. J. Chem.* **1975,** *28* (3), 601-605.
147. Konieczny, M. T.; Konieczny, W., Synthesis and reactivity of thioaurones over the past one hundred years. *Heterocycles* **2005,** *65* (2), 451-464.
148. Kink, F.; Collado, M. P.; Wiedbrauk, S.; Mayer, P.; Dube, H., Bistable Photoswitching of Hemithioindigo with Green and Red Light: Entry Point to Advanced Molecular Digital Information Processing. *Chem. Eur. J.* **2017,** *23* (26), 6237-6243.
149. Wiedbrauk, S.; Maerz, B.; Samoylova, E.; Reiner, A.; Trommer, F.; Mayer, P.; Zinth, W.; Dube, H., Twisted Hemithioindigo Photoswitches: Solvent Polarity Determines the Type of Light-Induced Rotations. *J. Am. Chem. Soc.* **2016,** *138* (37), 12219-12227.
150. Zweig, J. E.; Newhouse, T. R., Isomer-Specific Hydrogen Bonding as a Design Principle for Bidirectionally Quantitative and Redshifted Hemithioindigo Photoswitches. *J. Am. Chem. Soc.* **2017,** *139* (32), 10956-10959.
151. Herre, S.; Schadendorf, T.; Ivanov, I.; Herrberger, C.; Steinle, W.; Rück-Braun, K.; Preissner, R.; Kuhn, H., Photoactivation of an Inhibitor of the 12/15-Lipoxygenase Pathway. *ChemBioChem* **2006,** *7* (7), 1089-1095.
152. Sailer, A.; Ermer, F.; Kraus, Y.; Lutter, F. H.; Donau, C.; Bremerich, M.; Ahlfeld, J.; Thorn-Seshold, O., Hemithioindigos for Cellular Photopharmacology: Desymmetrised Molecular Switch Scaffolds Enabling Design Control over the Isomer-Dependency of Potent Antimitotic Bioactivity. *ChemBioChem* **2019,** *20* (10), 1305-1314.
153. Sailer, A.; Ermer, F.; Kraus, Y.; Bingham, R.; Lutter, F. H.; Ahlfeld, J.; Thorn-Seshold, O., Potent hemithioindigo-based antimitotics photocontrol the microtubule cytoskeleton in cellulo. *Beilstein J. Org. Chem.* **2020,** *16* (1), 125-134.
154. Regner, N.; Herzog, T. T.; Haiser, K.; Hoppmann, C.; Beyermann, M.; Sauermann, J.; Engelhard, M.; Cordes, T.; Rück-Braun, K.; Zinth, W., Light-switchable hemithioindigo–hemistilbene-containing peptides: ultrafast spectroscopy of the Z→ E isomerization of the chromophore and the structural dynamics of the peptide moiety. *J. Phys. Chem. Lett. B* **2012,** *116* (14), 4181-4191.
155. Tanaka, K.; Kohayakawa, K.; Iwata, S.; Irie, T., Application of 2-pyridyl-substituted hemithioindigo as a molecular switch in hydrogen-bonded porphyrins. *J. Org. Chem.* **2008,** *73* (10), 3768-3774.

156. Dube, H.; Rebek Jr, J., Selective guest exchange in encapsulation complexes using light of different wavelenghts. *Angew. Chem. Int. Ed. Engl.* **2012,** *51* (13), 3207-3210.
157. Moncelsi, G.; Escobar, L.; Dube, H.; Ballester, P., 2-(4′-Pyridyl-N-oxide)-Substituted Hemithioindigos as Photoresponsive Guests for a Super Aryl-Extended Calix[4]pyrrole Receptor. *Chem. Asian J.* **2018,** *13* (12), 1632-1639.
158. Guentner, M.; Uhl, E.; Mayer, P.; Dube, H., Photocontrol of Polar Aromatic Interactions by a Bis-Hemithioindigo Based Helical Receptor. *Chem. Eur. J.* **2016,** *22* (46), 16433-16436.
159. Wiedbrauk, S.; Bartelmann, T.; Thumser, S.; Mayer, P.; Dube, H., Simultaneous complementary photoswitching of hemithioindigo tweezers for dynamic guest relocalization. *Nat. Commun.* **2018,** *9* (1), 1-9.
160. Nakamichi, H.; Okada, T., Crystallographic Analysis of Primary Visual Photochemistry. *Angew. Chem. Int. Ed. Engl.* **2006,** *45* (26), 4270-4273.
161. Weingart, O., The Twisted C11C12 Bond of the Rhodopsin ChromophoreA Photochemical Hot Spot. *J. Am. Chem. Soc.* **2007,** *129* (35), 10618-10619.
162. Scheerer, P.; Park, J. H.; Hildebrand, P. W.; Kim, Y. J.; Krauß, N.; Choe, H.-W.; Hofmann, K. P.; Ernst, O. P., Crystal structure of opsin in its G-protein-interacting conformation. *Nature* **2008,** *455* (7212), 497-502.
163. Palczewski, K.; Kumasaka, T.; Hori, T.; Behnke, C. A.; Motoshima, H.; Fox, B. A.; Trong, I. L.; Teller, D. C.; Okada, T.; Stenkamp, R. E.; Yamamoto, M.; Miyano, M., Crystal Structure of Rhodopsin: A G Protein-Coupled Receptor. *Science* **2000,** *289* (5480), 739-745.
164. Choe, H.-W.; Kim, Y. J.; Park, J. H.; Morizumi, T.; Pai, E. F.; Krauß, N.; Hofmann, K. P.; Scheerer, P.; Ernst, O. P., Crystal structure of metarhodopsin II. *Nature* **2011,** *471* (7340), 651-655.
165. Redwood, C.; Bayda, M.; Saltiel, J., Photoisomerization of pre-and provitamin D3 in EPA at 77 K: one-bond-twist, not hula-twist. *J. Phys. Chem. Lett.* **2013,** *4* (5), 716-721.
166. Müller, A. M.; Lochbrunner, S.; Schmid, W. E.; Fuß, W., Low-temperature photochemistry of previtamin D: a hula-twist isomerization of a triene. *Angew. Chem. Int. Ed. Engl.* **1998,** *37* (4), 505-507.
167. Maessen, P. A.; Jacobs, H. J.; Cornelisse, J.; Havinga, E., Photochemistry of previtamin D3 at 92 K; formation of an unstable tachysterol3 rotamer. *Angew. Chem. Int. Ed. Engl.* **1983,** *22* (9), 718-719.
168. Wei, L.; Wang, H.; Chen, X.; Fang, W.; Wang, H., A comprehensive study of isomerization and protonation reactions in the photocycle of the photoactive yellow protein. *Phys. Chem. Chem. Phys.* **2014,** *16* (46), 25263-25272.
169. Pande, K.; Hutchison, C. D.; Groenhof, G.; Aquila, A.; Robinson, J. S.; Tenboer, J.; Basu, S.; Boutet, S.; DePonte, D. P.; Liang, M., Femtosecond structural dynamics drives the trans/cis isomerization in photoactive yellow protein. *Science* **2016,** *352* (6286), 725-729.
170. Gulati, S.; Jastrzebska, B.; Banerjee, S.; Placeres, Á. L.; Miszta, P.; Gao, S.; Gunderson, K.; Tochtrop, G. P.; Filipek, S.; Katayama, K.; Kiser, P. D.; Mogi, M.; Stewart, P. L.; Palczewski, K., Photocyclic behavior of rhodopsin induced by an atypical isomerization mechanism. *Proc. Natl. Acad. Sci. USA* **2017,** *114* (13), 2608-2615.
171. Palczewski, K., Chemistry and biology of the initial steps in vision: the Friedenwald lecture. *Invest. Ophthalmol. Vis. Sci.* **2014,** *55* (10), 6651-6672.
172. Ernst, O. P.; Lodowski, D. T.; Elstner, M.; Hegemann, P.; Brown, L. S.; Kandori, H., Microbial and animal rhodopsins: structures, functions, and molecular mechanisms. *Chem. Rev.* **2014,** *114* (1), 126-163.
173. Shichida, Y.; Imai, H., Visual pigment: G-protein-coupled receptor for light signals. *Cell. Mol. Life Sci.* **1998,** *54* (12), 1299-1315.
174. Palczewski, K., G protein–coupled receptor rhodopsin. *Annu. Rev. Biochem.* **2006,** *75*, 743-767.
175. Kubatova, N.; Mao, J.; Eckert, C. E.; Saxena, K.; Gande, S. L.; Wachtveitl, J.; Glaubitz, C.; Schwalbe, H., Light dynamics of retinal disease-relevant G90D bovine rhodopsin mutant. *Angew. Chem. Int. Ed. Engl.* **2020**, *59*, 15656.

176. Ghanbarpour, A.; Nairat, M.; Nosrati, M.; Santos, E. M.; Vasileiou, C.; Dantus, M.; Borhan, B.; Geiger, J. H., Mimicking Microbial Rhodopsin Isomerization in a Single Crystal. *J. Am. Chem. Soc.* **2019,** *141* (4), 1735-1741.
177. Luk, H. L.; Melaccio, F.; Rinaldi, S.; Gozem, S.; Olivucci, M., Molecular bases for the selection of the chromophore of animal rhodopsins. *Proc. Natl. Acad. Sci. USA* **2015,** *112* (50), 15297-15302.
178. Rinaldi, S.; Melaccio, F.; Gozem, S.; Fanelli, F.; Olivucci, M., Comparison of the isomerization mechanisms of human melanopsin and invertebrate and vertebrate rhodopsins. *Proc. Natl. Acad. Sci. USA* **2014,** *111* (5), 1714-1719.
179. Liu, R.; Asato, A. E., The primary process of vision and the structure of bathorhodopsin: a mechanism for photoisomerization of polyenes. *Proc. Natl. Acad. Sci. USA* **1985,** *82* (2), 259-263.
180. Fuß, W.; Kosmidis, C.; Schmid, W. E.; Trushin, S. A., The Photochemical cis–trans Isomerization of Free Stilbene Molecules Follows a Hula-Twist Pathway. *Angew. Chem. Int. Ed. Engl.* **2004,** *43* (32), 4178-4182.
181. Imamoto, Y.; Kuroda, T.; Kataoka, M.; Shevyakov, S.; Krishnamoorthy, G.; Liu, R. S., Photoisomerization by Hula Twist: 2, 2′-Dimethylstilbene and a Ring-Fused Analogue. *Angew. Chem. Int. Ed. Engl.* **2003,** *42* (31), 3630-3633.
182. Liu, R. S.; Hammond, G. S., Examples of Hula-Twist in Photochemical cis–trans Isomerization. *Chem. Eur. J.* **2001,** *7* (21), 4536-4545.
183. Fuß, W., Hula-twist cis–trans isomerization: the role of internal forces and the origin of regioselectivity. *J. Photochem. Photobiol. C* **2012,** *237*, 53-63.
184. Röhrig, U. F.; Guidoni, L.; Laio, A.; Frank, I.; Rothlisberger, U., A molecular spring for vision. *J. Am. Chem. Soc.* **2004,** *126* (47), 15328-15329.
185. Jung, Y. O.; Lee, J. H.; Kim, J.; Schmidt, M.; Moffat, K.; Šrajer, V.; Ihee, H., Volume-conserving trans–cis isomerization pathways in photoactive yellow protein visualized by picosecond X-ray crystallography. *Nat. Chem.* **2013,** *5* (3), 212-220.
186. Kaila, V. R.; Schotte, F.; Cho, H. S.; Hummer, G.; Anfinrud, P. A., Contradictions in X-ray structures of intermediates in the photocycle of photoactive yellow protein. *Nat. Chem.* **2014,** *6* (4), 258-259.
187. Saltiel, J.; Bremer, M. A.; Laohhasurayotin, S.; Krishna, T. S., Photoisomerization of cis, cis-and cis, trans-1, 4-Di-o-tolyl-1, 3-butadiene in Glassy Media at 77 K: One-Bond-Twist and Bicycle-Pedal Mechanisms. *Angew. Chem. Int. Ed. Engl.* **2008,** *47* (7), 1237-1240.
188. Kukura, P.; McCamant, D. W.; Yoon, S.; Wandschneider, D. B.; Mathies, R. A., Structural observation of the primary isomerization in vision with femtosecond-stimulated Raman. *Science* **2005,** *310* (5750), 1006-1009.
189. Schnedermann, C.; Yang, X.; Liebel, M.; Spillane, K. M.; Lugtenburg, J.; Fernández, I.; Valentini, A.; Schapiro, I.; Olivucci, M.; Kukura, P.; Mathies, R. A., Evidence for a vibrational phase-dependent isotope effect on the photochemistry of vision. *Nat. Chem.* **2018,** *10* (4), 449-455.
190. Gozem, S.; Luk, H. L.; Schapiro, I.; Olivucci, M., Theory and Simulation of the Ultrafast Double-Bond Isomerization of Biological Chromophores. *Chem. Rev.* **2017,** *117* (22), 13502-13565.
191. Gueye, M.; Manathunga, M.; Agathangelou, D.; Orozco, Y.; Paolino, M.; Fusi, S.; Haacke, S.; Olivucci, M.; Léonard, J., Engineering the vibrational coherence of vision into a synthetic molecular device. *Nat. Commun.* **2018,** *9* (1), 313.
192. Squillacote, M.; Sheridan, R.; Chapman, O.; Anet, F., Planar s-cis-1, 3-butadiene. *J. Am. Chem. Soc.* **1979,** *101* (13), 3657-3659.
193. Werst, D. W.; Londo, W. F.; Smith, J. L.; Barbara, P. F., The excited-state torsional potentials of substituted 9-phenylanthracenes. *Chem. Phys. Lett.* **1985,** *118* (4), 367-374.
194. Brouwer, A.; Jacobs, H., Photochemistry of 2, 5-dimethyl-1, 3, 5-hexatrienes in argon matrices. Formation of isomers and rotamers. *Recl. Trav. Chim. Pays-Bas* **1995,** *114* (11-12), 449-458.
195. Furukawa, Y.; Takeuchi, H.; Harada, I.; Tasumi, M., Matrix-isolation infrared and ultraviolet spectroscopic studies of less stable conformers of 1, 3, 5-hexatriene. *J. Mol. Struct.* **1983,** *100*, 341-350.
196. Ikeda, T.; Tsutsumi, O., Optical Switching and Image Storage by Means of Azobenzene Liquid-Crystal Films. *Science* **1995,** *268*, 1873 - 1875.

197. Liu, Z. F.; Hashimoto, K.; Fujishima, A., Photoelectrochemical information storage using an azobenzene derivative. *Nature* **1990,** *347*, 658 -660.
198. Wiedbrauk, S.; Dube, H., Hemithioindigo—an emerging photoswitch. *Tetrahedron Lett.* **2015,** *56* (29), 4266-4274.
199. Kortekaas, L.; Browne, W. R., The evolution of spiropyran: fundamentals and progress of an extraordinarily versatile photochrome. *Chem. Soc. Rev.* **2019,** *48* (12), 3406-3424.
200. Irie, M.; Fukaminato, T.; Matsuda, K.; Kobatake, S., Photochromism of diarylethene molecules and crystals: memories, switches, and actuators. *Chem. Rev.* **2014,** *114* (24), 12174-277.
201. Dong, L.; Feng, Y.; Wang, L.; Feng, W., Azobenzene-based solar thermal fuels: design, properties, and applications. *Chem. Soc. Rev.* **2018,** *47* (19), 7339-7368.
202. Beharry, A. A.; Woolley, G. A., Azobenzene photoswitches for biomolecules. *Chem. Soc. Rev.* **2011,** *40* (8), 4422-37.
203. Bandara, H. M.; Burdette, S. C., Photoisomerization in different classes of azobenzene. *Chem. Soc. Rev.* **2012,** *41* (5), 1809-25.
204. Szymanski, W.; Beierle, J. M.; Kistemaker, H. A.; Velema, W. A.; Feringa, B. L., Reversible photocontrol of biological systems by the incorporation of molecular photoswitches. *Chem. Rev.* **2013,** *113* (8), 6114-78.
205. Russew, M. M.; Hecht, S., Photoswitches: from molecules to materials. *Adv. Mater.* **2010,** *22* (31), 3348-60.
206. Gust, D.; Andreasson, J.; Pischel, U.; Moore, T. A.; Moore, A. L., Data and signal processing using photochromic molecules. *Chem. Commun.* **2012,** *48* (14), 1947-57.
207. Andreasson, J.; Pischel, U., Molecules for security measures: from keypad locks to advanced communication protocols. *Chem. Soc. Rev.* **2018,** *47* (7), 2266-2279.
208. Mutoh, K.; Kobayashi, Y.; Yamane, T.; Ikezawa, T.; Abe, J., Rate-Tunable Stepwise Two-Photon-Gated Photoresponsive Systems Employing a Synergetic Interaction between Transient Biradical Units. *J. Am. Chem. Soc.* **2017,** *139* (12), 4452-4461.
209. Moran, M. J.; Magrini, M.; Walba, D. M.; Aprahamian, I., Driving a Liquid Crystal Phase Transition Using a Photochromic Hydrazone. *J. Am. Chem. Soc.* **2018,** *140* (42), 13623-13627.
210. Fihey, A.; Perrier, A.; Browne, W. R.; Jacquemin, D., Multiphotochromic molecular systems. *Chem Soc Rev* **2015,** *44* (11), 3719-59.
211. Zhang, J.; Zou, Q.; Tian, H., Photochromic materials: more than meets the eye. *Adv. Mater.* **2013,** *25* (3), 378-99.
212. Zhao, F.; Grubert, L.; Hecht, S.; Bleger, D., Orthogonal switching in four-state azobenzene mixed-dimers. *Chem. Commun.* **2017,** *53* (23), 3323-3326.
213. Yu, Z.; Weidner, S.; Risse, T.; Hecht, S., The role of statistics and microenvironment for the photoresponse in multi-switch architectures: The case of photoswitchable oligoazobenzene foldamers. *Chem. Sci.* **2013,** *4* (11).
214. Bleger, D.; Liebig, T.; Thiermann, R.; Maskos, M.; Rabe, J. P.; Hecht, S., Light-orchestrated macromolecular "accordions": reversible photoinduced shrinking of rigid-rod polymers. *Angew. Chem. Int. Ed. Engl.* **2011,** *50* (52), 12559-63.
215. Bleger, D.; Dokic, J.; Peters, M. V.; Grubert, L.; Saalfrank, P.; Hecht, S., Electronic decoupling approach to quantitative photoswitching in linear multiazobenzene architectures. *J. Phys. Chem. B* **2011,** *115* (33), 9930-40.
216. Yang, C.; Slavov, C.; Wegner, H. A.; Wachtveitl, J.; Dreuw, A., Computational design of a molecular triple photoswitch for wavelength-selective control. *Chem. Sci.* **2018,** *9* (46), 8665-8672.
217. Slavov, C.; Yang, C.; Schweighauser, L.; Boumrifak, C.; Dreuw, A.; Wegner, H. A.; Wachtveitl, J., Connectivity matters - ultrafast isomerization dynamics of bisazobenzene photoswitches. *Phys. Chem. Chem. Phys.* **2016,** *18* (22), 14795-804.
218. Cisnetti, F.; Ballardini, R.; Credi, A.; Gandolfi, M. T.; Masiero, S.; Negri, F.; Pieraccini, S.; Spada, G. P., Photochemical and electronic properties of conjugated bis(azo) compounds: an experimental and computational study. *Chem. Eur. J.* **2004,** *10* (8), 2011-21.

219. Heindl, A. H.; Becker, J.; Wegner, H. A., Selective switching of multiple azobenzenes. *Chem. Sci.* **2019,** *10* (31), 7418-7425.
220. Vlasceanu, A.; Koerstz, M.; Skov, A. B.; Mikkelsen, K. V.; Nielsen, M. B., Multistate Photoswitches: Macrocyclic Dihydroazulene/Azobenzene Conjugates. *Angew. Chem. Int. Ed. Engl.* **2018,** *57* (21), 6069-6072.
221. Peters, A.; Branda, N. R., Limited photochromism in covalently linked double 1,2-dithienylethenes. *Adv. Mater. Opt. Electron.* **2000,** *10* (10), 245 - 249.
222. Yagi, K.; Irie, M., Photochromic and Fluorescent Properties of a Diarylethene Dimer. *Chem. Lett.* **2003,** *32* (9), 848-849.
223. Li, R. J.; Holstein, J. J.; Hiller, W. G.; Andreasson, J.; Clever, G. H., Mechanistic Interplay between Light Switching and Guest Binding in Photochromic [Pd2Dithienylethene4] Coordination Cages. *J. Am. Chem. Soc.* **2019,** *141* (5), 2097-2103.
224. Han, M.; Luo, Y.; Damaschke, B.; Gomez, L.; Ribas, X.; Jose, A.; Peretzki, P.; Seibt, M.; Clever, G. H., Light-Controlled Interconversion between a Self-Assembled Triangle and a Rhombicuboctahedral Sphere. *Angew. Chem. Int. Ed. Engl.* **2016,** *55* (1), 445-9.
225. Han, M.; Michel, R.; He, B.; Chen, Y. S.; Stalke, D.; John, M.; Clever, G. H., Light-triggered guest uptake and release by a photochromic coordination cage. *Angew. Chem. Int. Ed. Engl.* **2013,** *52* (4), 1319-23.
226. Balter, M.; Li, S.; Nilsson, J. R.; Andreasson, J.; Pischel, U., An all-photonic molecule-based parity generator/checker for error detection in data transmission. *J. Am. Chem. Soc.* **2013,** *135* (28), 10230-3.
227. Andreasson, J.; Pischel, U.; Straight, S. D.; Moore, T. A.; Moore, A. L.; Gust, D., All-photonic multifunctional molecular logic device. *J. Am. Chem. Soc.* **2011,** *133* (30), 11641-8.
228. Kortekaas, L.; Ivashenko, O.; van Herpt, J. T.; Browne, W. R., A Remarkable Multitasking Double Spiropyran: Bidirectional Visible-Light Switching of Polymer-Coated Surfaces with Dual Redox and Proton Gating. *J. Am. Chem. Soc.* **2016,** *138* (4), 1301-12.
229. Hoffmann, K.; Guentner, M.; Mayer, P.; Dube, H., Symmetric and nonsymmetric bis-hemithioindigos – precise visible light controlled shape-shifters. *Org. Chem. Front.* **2019,** *6* (8), 1244-1252.
230. Kink, F.; Collado, M. P.; Wiedbrauk, S.; Mayer, P.; Dube, H., Bistable Photoswitching of Hemithioindigo with Green and Red Light: Entry Point to Advanced Molecular Digital Information Processing. *Chem. Eur. J.* **2017,** *23* (26), 6237-6243.
231. Kortekaas, L.; Chen, J.; Jacquemin, D.; Browne, W. R., Proton-Stabilized Photochemically Reversible E/ Z Isomerization of Spiropyrans. *J. Phys. Chem. B* **2018,** *122* (24), 6423-6430.
232. van Leeuwen, T.; Heideman, G. H.; Zhao, D.; Wezenberg, S. J.; Feringa, B. L., In situ control of polymer helicity with a non-covalently bound photoresponsive molecular motor dopant. *Chem. Commun.* **2017,** *53* (48), 6393-6396.
233. Yu, J. J.; Zhao, L. Y.; Shi, Z. T.; Zhang, Q.; London, G.; Liang, W. J.; Gao, C.; Li, M. M.; Cao, X. M.; Tian, H.; Feringa, B. L.; Qu, D. H., Pumping a Ring-Sliding Molecular Motion by a Light-Powered Molecular Motor. *J. Org. Chem.* **2019,** *84* (9), 5790-5802.
234. Dorel, R.; Feringa, B. L., Stereodivergent Anion Binding Catalysis with Molecular Motors. *Angew. Chem. Int. Ed. Engl.* **2020,** *59* (2), 785-789.
235. Serreli, V.; Lee, C.-F.; Kay, E. R.; Leigh, D. A., A molecular information ratchet. *Nature* **2007,** *445* (7127), 523-527.
236. Dietrich-Buchecker, C.; Jimenez-Molero, M. C.; Sartor, V.; Sauvage, J.-P., Rotaxanes and Catenanes as Prototypes of Molecular Machines and Motors. *ChemInform* **2004,** *35* (10).
237. Credi, A.; Ballardini, R.; Balzani, V.; Ferrer, B.; Gandolfi, M. T.; Silvi, S.; Venturia, M., Rotaxane- and catenane-based molecular machines and motors.
238. Kassem, S.; van Leeuwen, T.; Lubbe, A. S.; Wilson, M. R.; Feringa, B. L.; Leigh, D. A., Artificial molecular motors. *Chem. Soc. Rev.* **2017,** *46* (9), 2592-2621.
239. Feringa, B. L., The Art of Building Small: From Molecular Switches to Motors (Nobel Lecture). *Angew. Chem. Int. Ed. Engl.* **2017,** *56* (37), 11060-11078.
240. Feynman, R. P., There's plenty of room at the bottom. *California Institute of Technology, Engineering and Science magazine* **1960**.

241. Feynman, R. P.; Leighton, R. B.; Sands, M., The Feynman lectures on physics, Vol. I: The new millennium edition: mainly mechanics, radiation, and heat. Basic books, New York, **2011**.
242. Smoluchowski, M., *Phys. Z.* **1912,** *13*, 1069 - 1080.
243. Kelly, T. R.; Sestelo, J. P.; Tellitu, I., New molecular devices: in search of a molecular ratchet. *J. Org. Chem.* **1998,** *63* (11), 3655-3665.
244. Wedler, G., *Lehrbuch der Physikalischen Chemie*, Vol. 4. Wiley-VCH: Weinheim, **1997**.
245. Vicario, J.; Walko, M.; Meetsma, A.; Feringa, B. L., Fine tuning of the rotary motion by structural modification in light-driven unidirectional molecular motors. *J. Am. Chem. Soc.* **2006,** *128* (15), 5127-5135.
246. Klok, M.; Boyle, N.; Pryce, M. T.; Meetsma, A.; Browne, W. R.; Feringa, B. L., MHz unidirectional rotation of molecular rotary motors. *J. Am. Chem. Soc.* **2008,** *130* (32), 10484-10485.
247. van Delden, R. A.; Koumura, N.; Schoevaars, A.; Meetsma, A.; Feringa, B. L., A donor–acceptor substituted molecular motor: unidirectional rotation driven by visible light. *Org. Biomol. Chem.* **2003,** *1* (1), 33-35.
248. Roke, D.; Sen, M.; Danowski, W.; Wezenberg, S. J.; Feringa, B. L., Visible-Light-Driven Tunable Molecular Motors Based on Oxindole. *J. Am. Chem. Soc.* **2019,** *141* (18), 7622-7627.
249. Kistemaker, J. C. M.; Štacko, P.; Roke, D.; Wolters, A. T.; Heideman, G. H.; Chang, M.-C.; van der Meulen, P.; Visser, J.; Otten, E.; Feringa, B. L., Third-Generation Light-Driven Symmetric Molecular Motors. *J. Am. Chem. Soc.* **2017,** *139* (28), 9650-9661.
250. Kistemaker, J. C. M.; Štacko, P.; Visser, J.; Feringa, B. L., Unidirectional rotary motion in achiral molecular motors. *Nat. Chem.* **2015,** *7* (11), 890-896.
251. Roke, D.; Wezenberg, S. J.; Feringa, B. L., Molecular rotary motors: Unidirectional motion around double bonds. *Proc. Natl. Acad. Sci. USA* **2018,** *115* (38), 9423-9431.
252. Wilcken, R.; Schildhauer, M.; Rott, F.; Huber, L. A.; Guentner, M.; Thumser, S.; Hoffmann, K.; Oesterling, S.; de Vivie-Riedle, R.; Riedle, E.; Dube, H., Complete Mechanism of Hemithioindigo Motor Rotation. *J. Am. Chem. Soc.* **2018,** *140* (15), 5311-5318.
253. Wezenberg, S. J.; Chen, K. Y.; Feringa, B. L., Visible-Light-Driven Photoisomerization and Increased Rotation Speed of a Molecular Motor Acting as a Ligand in a Ruthenium (II) Complex. *Angew. Chem. Int. Ed. Engl.* **2015,** *54* (39), 11457-11461.
254. Faulkner, A.; van Leeuwen, T.; Feringa, B. L.; Wezenberg, S. J., Allosteric regulation of the rotational speed in a light-driven molecular motor. *J. Am. Chem. Soc.* **2016,** *138* (41), 13597-13603.
255. Qu, D. H.; Feringa, B. L., Controlling Molecular Rotary Motion with a Self-Complexing Lock. *Angew. Chem. Int. Ed. Engl.* **2010,** *122* (6), 1125-1128.
256. Ruangsupapichat, N.; Pollard, M. M.; Harutyunyan, S. R.; Feringa, B. L., Reversing the direction in a light-driven rotary molecular motor. *Nat. Chem.* **2011,** *3* (1), 53-60.
257. Wezenberg, S. J.; Feringa, B. L., Supramolecularly directed rotary motion in a photoresponsive receptor. *Nat. Commun.* **2018,** *9* (1), 1-7.
258. Štacko, P.; Kistemaker, J. C.; Van Leeuwen, T.; Chang, M.-C.; Otten, E.; Feringa, B. L., Locked synchronous rotor motion in a molecular motor. *Science* **2017,** *356* (6341), 964-968.
259. Eelkema, R.; Pollard, M. M.; Katsonis, N.; Vicario, J.; Broer, D. J.; Feringa, B. L., Rotational reorganization of doped cholesteric liquid crystalline films. *J. Am. Chem. Soc.* **2006,** *128* (44), 14397-14407.
260. Eelkema, R.; Pollard, M. M.; Vicario, J.; Katsonis, N.; Ramon, B. S.; Bastiaansen, C. W.; Broer, D. J.; Feringa, B. L., Nanomotor rotates microscale objects. *Nature* **2006,** *440* (7081), 163-163.
261. Colard-Itté, J.-R.; Li, Q.; Collin, D.; Mariani, G.; Fuks, G.; Moulin, E.; Buhler, E.; Giuseppone, N., Mechanical behaviour of contractile gels based on light-driven molecular motors. *Nanoscale* **2019,** *11* (12), 5197-5202.
262. Li, Q.; Fuks, G.; Moulin, E.; Maaloum, M.; Rawiso, M.; Kulic, I.; Foy, J. T.; Giuseppone, N., Macroscopic contraction of a gel induced by the integrated motion of light-driven molecular motors. *Nature Nanotechnol.* **2015,** *10* (2), 161-165.

263. Foy, J. T.; Li, Q.; Goujon, A.; Colard-Itté, J.-R.; Fuks, G.; Moulin, E.; Schiffmann, O.; Dattler, D.; Funeriu, D. P.; Giuseppone, N., Dual-light control of nanomachines that integrate motor and modulator subunits. *Nature Nanotechnol.* **2017,** *12* (6), 540-545.
264. Greb, L.; Lehn, J.-M., Light-Driven Molecular Motors: Imines as Four-Step or Two-Step Unidirectional Rotors. *J. Am. Chem. Soc.* **2014,** *136* (38), 13114-13117.
265. Greb, L.; Eichhöfer, A.; Lehn, J.-M., Synthetic Molecular Motors: Thermal N Inversion and Directional Photoinduced CN Bond Rotation of Camphorquinone Imines. *Angew. Chem. Int. Ed. Engl.* **2015,** *54* (48), 14345-14348.
266. Guentner, M.; Schildhauer, M.; Thumser, S.; Mayer, P.; Stephenson, D.; Mayer, P. J.; Dube, H., Sunlight-powered kHz rotation of a hemithioindigo-based molecular motor. *Nat. Commun.* **2015,** *6*, 8406.
267. Hoffmann, K.; Mayer, P.; Dube, H., A hemithioindigo molecular motor for metal surface attachment. *Org. Biomol. Chem.* **2019,** *17* (7), 1979-1983.
268. Uhl, E.; Mayer, P.; Dube, H., Active and Unidirectional Acceleration of Biaryl Rotation by a Molecular Motor. *Angew. Chem. Int. Ed. Engl.* **2020,** *59* (14), 5730-5737.
269. Uhl, E.; Thumser, S.; Mayer, P.; Dube, H., Transmission of Unidirectional Molecular Motor Rotation to a Remote Biaryl Axis. *Angew. Chem. Int. Ed. Engl.* **2018,** *57* (34), 11064-11068.